HAI2026

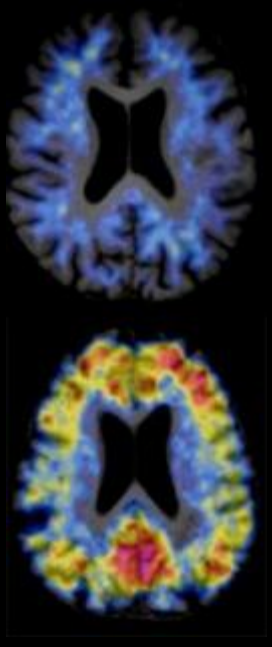


TABLE OF CONTENTS

TABLE OF CONTENTS **2**
WELCOME! **15**
SUPPORTERS **16**
HAI COMMITTEES **17**
POSTER INDEX (by board number) **18**
POSTER INDEX (by presenter's last name) **31**
HAI 2026 PROGRAM **44**
HAI 2026 ABSTRACTS **51**
Monday, January 12, 2026 ..... **52**
Podium Session **52**
SESSION I: Amyloid-beta pathology: PET imaging **52**
Xiao, Yu 53
Auto-rADiology: Toward automated and explainable amyloid-PET interpretation using deep learning 53
Hall, Brandon 57
Choroidal-ventricular remodeling is associated with amyloid aggregation in Alzheimer's disease 57
McLachlan, Max 61
Updated evaluation of the baseline distribution of amyloid positivity and cognitive impairment among adults with Down syndrome in the ABC-DS project 61
La Joie, Renaud 65
Heterogeneous patterns of off target signal with [18F]flutafuranol PET in ADNI4 65
Monday, January 12, 2026 - 10:25 am - 10:30 am 68
Podium Session **68**
B1 - A: Blitz Session **68**
Monday, January 12, 2026 - 10:30 am - 11:30 am 69
Poster Session **69**
Poster Session 1A **69**
Ren, Yuxin 75
1 Longitudinal harmonization effects on tau-PET SUVRs trajectories in ADNI study 75
Fu, Jessie Fang-Lu 78
2 Integrating digital cognitive metrics with PET biomarkers to identify individuals at imminent risk of tau accumulation 78
Roemer-Cassiano, Sebastian 81
3 Amyloid-induced neuronal hyperactivity and metabolism are associated with faster tau accumulation in Alzheimer's Disease 81
Giudicessi, Averi 85
4 Sex differences in white matter microstructure and associations with amyloid and tau pathology in autosomal dominant Alzheimer's disease 85
Bermudez, Camilo 89
5 Concordance between amyloid PET and biomarkers of Alzheimer's disease in plasma and cerebrospinal fluid in cognitively unimpaired individuals 89
Honhar, Praveen 91
6 Comparing performance of different amyloid PET markers of spatial extent in their ability to predict future amyloid conversion 91
Cuppels, Madison 95

7 Elevated ptau217 is more strongly associated with tau accumulation and cognitive decline in younger adults 95

Thal, Dietmar 99

8 Quantitative relationship between Lumipulse G measures of pTau217 in plasma and in brain 99

Salvadó, Gemma 100

9 Distinct mechanisms underlying APOE-ε4 and sex effects on medial temporal tau pathology: A neuropathology study..... 100

Tonietto, Matteo 103

10 Harmonizing amyloid PET tracers at the regional level: evaluation of regional centiloid equations 103

Corriveau-Lecavalier, Nick..... 105

11 A case series of lecanemab treatment response in patients across the clinical phenotypic spectrum of AD 105

Finn, Quentin 106

12 Validation of a pseudo-reference region for [11C]-ER176 in healthy volunteers and Alzheimer's disease patients 106

Finn, Quentin 107

13 β-amyloid PET signal reduction is higher in regions with ARIA-E due to anti-amyloid therapy 107

Hu, Mingzhao 108

14 Lifetime and 10-year absolute risk of cognitive impairment associated with amyloid PET severity: a retrospective, longitudinal cohort study..... 108

Zhang, Mengna 111

15 Trajectory of neurodegeneration and brain aging in relation to amyloid timing and duration 111

Vogt, Nicholas..... 115

16 Associations between tau pathology and cortical microstructure are modulated by amyloid burden independent of cortical atrophy in cognitively unimpaired older adults ... 115

Schott, Jonathan 117

17 Predicting tau PET burden using brain-derived plasma p-tau measures in the British 1946 birth cohort..... 117

Ourry, Valentin 118

18 Association of combined cardiovascular risk factors and treatments with longitudinal amyloid and tau PET in cognitively normal older adults 118

Schaffer Aguzzoli, Cristiano..... 120

19 Amyloid-pet substantiates clinical decision-making in real-life clinical settings in Brazil 120

La Joie, Renaud 123

20 Neuropathological validation of Tau-PET CenTauR units: Preliminary data from a multicenter study 123

Gatto, Rodolfo..... 127

21 Molecular evaluation of a tau-PET analog and pathological TAR DNA-binding protein 43 docking in a cellular model of frontotemporal lobar degeneration ... 127

Maboudian, Samira..... 129

22 Anterior cingulate sulcal pattern is associated with successful cognitive aging..... 129

Lee, Seunghoon 133

23 Microstructural white matter injury mediates the association between vascular risk and plasma biomarkers: Preliminary findings from the Diverse VCID study 133

Hanseeuw, Bernard 135

24 VeraBIND Tau: a novel plasma assay reflecting tau aggregation increases over time in individuals with positive tau-PET signal 135

Tunali, Ilke 139

25 Amyloid PET quantitation using skewness: Autopsy validation and test–retest performance 139

Mundada, Nidhi 143

26 Stratifying preclinical Alzheimer's disease by hippocampal volume to detect concomitant LATE 143

Deng, Han 147

27 Differential sensitivity of [^{18}F]MK6240 and [^{18}F]FTP to measure tau before and after anti-amyloid therapy 147

Ma, Xiao-Jun 148

28 Development of a highly sensitive and automated immunoassay for Brain-Derived pTau-217: Analytical performance in human plasma samples 148

Wooten, Dustin 149

29 Network-based mechanistic modeling of Alzheimer's disease for evaluating diverse therapeutic mechanisms of action 149

Houlihan, Hannah 151

30 Neuroimaging compendium of microglia, amyloid, tau, and neurodegeneration across clinical variants of Alzheimer's disease 151

Fonseca, Corrina 154

31 Predictors of longitudinal atrophy across NIA-AA biological PET stages . 154

Bollack, Ariane 158

32 Effect of uptake time on [18F]-flutemetamol visual interpretation and Centiloid quantification 158

Zammit, Matt 160

33 Episodic memory decline and tau biomarkers progress earlier along the amyloid timeline in Down syndrome compared to neurotypical adults 160

Moon, Hasom 164

34 Relationship between p-tau217 and PET in preclinical AD: The moderating effect of white matter hyperintensity 164

Monto, Abdul Razak 167

35 Systemic inflammation–tau interaction: Insights from CRP modulation of p-tau217 association with tau PET positivity 167

Marin, Anna 168

36 Examining elevated choroid plexus binding of tau PET tracers in aging and Alzheimer's disease 168

Satoh, Ryota 170

37 The influence of β-amyloid on neuroinflammatory 11C-ER176 uptake in progressive apraxia of speech 170

Satoh, Ryota 173

38 Subtracting first principal component may improve detectability of subtle 4R tau signals in 18F flortaucipir tau PET imaging 173

Duggan, Michael 177

39 OMG: a proteomic determinant of neurodegenerative resiliency.....177

Medina Guerra, Lucah.....180

40 Frequency and consequences of extreme PET based pathological profiles in preclinical Alzheimer's disease.....180

Chen, Chang-Le.....184

41 Periventricular diffusivity moderates the relationship between astrocyte reactivity and amyloid deposition in non-demented older adults.....184

Haque, Miraal.....186

42 Disentangling the effects of age and Alzheimer's disease pathology on longitudinal atrophy in cognitively normal older adults.....186

Franzmeier, Nicolai.....188

43 Stronger amyloid-tau coupling explains faster tau progression in early-onset Alzheimer's disease.....188

Zhang, Vivian.....192

44 Harmonization methods to mitigate batch effects in blood biomarker analysis.....192

Cohen, Ann.....195

45 IGFR1, but not BDNF, acts as a suppressive neuroprotective factor between astrogliosis and visuospatial function among non-demented individuals.....195

Cohen, Ann.....197

46 The relation of psychosocial coping mechanisms to ATN pathophysiology differ across demographics.....197

Eldaief, Mark.....198

47 Evaluation of the Clinical IMpact of Blood-Based Biomarker Assays on dementia specialists' decision-making (CIMBBBA): Preliminary report from a real-world dementia subspecialty clinic study.....198

Ottoy, Julie.....199

48 Dynamic interplay of vascular injury and inflammation on Alzheimer's disease pathophysiology.....199

Monday, January 12, 2026 - 11:30 am - 01:00 pm.....202

Podium Session.....202

SESSION II: Tau pathology: In vivo and postmortem measurements.....202

Chen, Charles.....203

The effects of 18F-MK-6240 PET extracerebellar off-target signal on the cerebellum and its substructures.....203

Gatto, Rodolfo.....207

Examining spatial relationships between ex-vivo flortaucipir retention and TMEM106b protein expression in a subset of neuropathologically confirmed frontotemporal lobar degeneration cases with TAR DNA-binding protein 43 pathology.....207

Silva-Rodríguez, Jesús.....209

Hypometabolism and atrophy patterns associated with advanced primary age-related tauopathy mimicking early-stage AD.....209

Tissot, Cécile.....210

Differential age- and Aβ-related tau-PET patterns between [18F]FTP and [18F]MK6240.....210

Monday, January 12, 2026 - 02:45 pm - 04:15 pm.....213

Podium Session.....213

KEYNOTE: The neuropathological basis of current AD biomarkers: Sensitivity and pathogenetic implications 213

The neuropathological basis of current AD biomarkers: Sensitivity and pathogenetic implications 213

Monday, January 12, 2026 - 02:45 pm - 04:15 pm 214

Podium Session 214

SESSION III: Alzheimer's disease biological staging and applications 214

Rabinovici, Gil 215

Combining quantitative and visual read approaches to tau-PET positivity and staging: The Tau-PET Working Group 215

Johnson, Derek 219

Association between PET-based Alzheimer's disease biological stage and autopsy findings 219

Sperling, Reisa 221

Associations among plasma p-tau217, amyloid PET, tau PET, and cognitive testing in the screening cohort for the AHEAD 3-45 Study 221

Wang, Ting-Chen 225

Genetic predictors of multimodal brain tau pathology in older adults 225

Monday, January 12, 2026 - 04:15 pm - 04:20 pm 228

Podium Session 228

B1 - B: Blitz Session 228

Monday, January 12, 2026 - 04:15 pm - 04:20 pm 229

[Special] Podium Session 229

Christopher Schwarz, Mayo Clinic, Rochester, MN, USA 229

Tuesday, January 13, 2026 230

Podium Session 230

ISTAART Collaborations: Neuroimaging in clinical decision making: presentation and interactive discussion of real-world cases to identify evolving research needs 230

Podium Session 231

B2 - A: Blitz Session 231

Tuesday, January 13, 2026 - 09:50 am - 10:50 am 232

Poster Session 232

Poster Session 2A 232

Santos Machado, Luiza 238

49 CSF oligodendrocyte biomarkers are associated with amyloid burden in Alzheimer's disease 238

Yau, Wai-Ying Wendy 242

50 Associations between systolic blood pressure and amyloid burden on cross-sectional inferior temporal tau across mid- to late-life 242

Cogswell, Petrice 245

51 Associations of ER176 TSPO PET with blood-based AD and neuroinflammation biomarkers 245

Tiss, Amal 249

52 Evaluation of [18F]MK6240 test-retest reproducibility for different processing pipelines 249

Kwon, Tae Youn 252

53 Temporal dynamics of tau PET subtypes and its association with heterogeneous neurodegeneration in Alzheimer's disease 252

Kwon, Tae Youn 256

54 A-T-N-C generative model for predicting and simulating patient-tailored cognitive decline trajectories in Alzheimer's disease 256

Salman, Yasmine.....260

55 High-resolution ex-vivo MRI reveals layer-specific atrophy of hippocampal subregions to earliest tau pathology...260

Burns, Kelsey.....264

56 Blood volume influences the association between baseline plasma biomarker values and amyloid PET outcomes over time 264

Pascoal, Tharick 266

57 Visual interpretation methods for tau-PET imaging with Flortaucipir and MK-6240: Insights from the HEAD study ...266

Smith, Anna.....270

58 Associations between TSPO PET and CSF and blood-based biomarkers.....270

Royse, Sarah.....272

59 Regional white matter injury modifies the association between ß-amyloid and cognition.....272

Guzman, Diana.....275

60 Sex differences in neuroinflammation, amyloid, tau, and neurodegeneration 275

Whittington, Alex 276

61 Evaluation of the tau PET ligand [18F]florzolotau in frontotemporal dementia.....276

Reese, Alexandria 279

62 Intersections of gender/sex and neighborhood deprivation on cognition: Are there mediation effects of Alzheimer's disease biomarkers? 279

Smith, Viktorija 282

63 Disentangling cognitive severity and phenotype across dementia syndromes 282

Lopresti, Brian 284

64 Standardized indices of tau burden using the CenTauR universal scale predict distinct cognitive trajectories across Alzheimer's disease biological stages 284

Dong, Mengjin 286

65 SPARE-SVD: An integrated machine-learning metric for cerebral small vessel disease within the ATN(V) framework. 286

Fajardo Valdez, Alfonso..... 290

66 Risk factors and AD prevention: a multivariate and multimodal study..... 290

Bellaver, Bruna..... 293

67 MK6240 and Tauvid positivity, cognitive decline, and their relationship to Aβ PET deposition across the Alzheimer's spectrum 293

Povala, Guilherme..... 296

68 Differential tau-PET load predominance along shared progression trajectories determines clinical variability in Alzheimer's disease 296

Povala, Guilherme..... 299

69 Head-to-head comparison of tau PET tracers across the Alzheimer's disease spectrum: baseline results from the HEAD study..... 299

Bruzzone, Hailey..... 302

70 Comparison of Sampled Iterative Local Approximation (SILA) implemented in R and MATLAB 302

Wolz, Robin..... 306

71 Agreement between amyloid status prediction from visual read, SUVR

thresholding, and AI-based interpretation of amyloid PET 306

DelBene, Alexander 308

72 CenTauR thresholds generated using Gaussian Mixture Models for biological staging of amyloid positive ADNI participants 308

Kim, Min Jung 311

73 Progression to tau-PET positivity by plasma P-tau217 levels and its association with clinical decline in preclinical Alzheimer's disease: data from A4 study 311

Sanchez, Thairi 314

74 Neuroimaging correlates of loneliness 314

Parker, Dana 316

75 Age-dependent associations between salivary inflammatory cytokines and amyloid-beta in cognitively unimpaired older adults 316

Markova, Teodora 318

76 Tau accumulation drives worsening depressive symptoms in cognitively normal older adults 318

Markova, Teodora 321

77 Dorsal raphe nucleus and locus coeruleus differentially relate to depressive symptoms in cognitively normal older adults 321

Schwarz, Christopher 324

78 Evaluating occipital-to-global amyloid PET as a predictor of CAA at autopsy in Mayo Clinic cohorts 324

Schwarz, Christopher 328

79 SCAN: Standardized Centralized Alzheimer's and related dementias Neuroimaging 328

Slade, Elliott 329

80 Differential contributions of amyloid spatial extent and tau burden to domain-specific cognitive decline in early Alzheimer's disease 329

Bettcher, Brecca 333

81 PET-measured amyloid accumulation rate modulates tau accumulation rate in individuals with Down syndrome 333

Thibault, Emma 336

82 Elevated medial temporal lobe tau predicts cross-sectional association between neocortical tau and global amyloid burden 336

McLachlan, Max 339

83 Assessing the effect of amyloid status on the relationship between glucose metabolism and synaptic density in the aging population 339

Brown, Jane 343

84 Associations between p-tau217 and brain atrophy are amplified by Aβ burden and APOEε4 343

Sinclair, Stephanie 347

85 Early cortical thickness change in preclinical AD development 347

Wood Alexander, Madeline 350

86 Immuno-vascular crosstalk drives tau pathology preferentially in women 350

Wood Alexander, Madeline 352

87 Midlife physical activity attenuates the association of earlier menopause

with tau pathology and cognitive decline 352

Young, Christina.....355

88 Improved tau PET signal detection with total-body PET compared to conventional PET: A preliminary study355

Young, Christina.....358

89 Demographic associations with plasma biomarkers in the oldest-old: The LifeAfter90 Study 358

Silva-Rodríguez, Jesús 361

90 Differential sensitivity of T1-MRI and FDG-PET for tracking neurodegeneration across progressive stages of tau pathology in Alzheimer's disease.....361

Wang, David 363

91 SPARE-Tau, a machine-learning derived tau-PET index, correlates with Alzheimer's disease and related dementias biomarkers 363

Liu, Tianshu.....366

92 Assessing the generalizability of plasma p-tau217 cutpoints for amyloid-β detection across clinical and preclinical cohorts 366

Liu, Tianshu.....368

93 Evaluating the transferability of dual cutpoints for plasma p-tau217 in detecting brain amyloid-β across diverse cohorts 368

Sathe, Aditi 370

94 Free-water interacts with amyloid positivity to predict regional tau pathology in both early and late Braak stages.....370

Kuchenbecker, Lindsey.....373

95 Integration of data-driven biomarker discovery with established Alzheimer's disease biomarkers in an African American cohort 373

Farrell, Michelle..... 375

96 Early concordance between Aβ PET spatial extent and plasma %ptau217 .. 375

Tuesday, January 13, 2026 - 10:50 am - 12:20 pm..... 379

Podium Session..... 379

SESSION IV: Longitudinal biomarker measurements of tau pathology.....379

Bauer-Negrini, Guilherme..... 380

Preliminary comparative longitudinal performance of Flortaucipir and MK6240: rates of change, effect sizes, and power estimates in the HEAD Study..... 380

Lopresti, Brian J 383

Standardized expression of longitudinal tau accumulation using the CenTauR scale 383

Coath, William..... 385

TauPace as a novel, time-based metric to investigate accelerated tau and clinical progression in preclinical AD..... 385

Macedo, Arthur C...... 388

Proteomic signatures track tau spread in Alzheimer's disease..... 388

Podium Session..... 392

KEYNOTE: The role of AI in neuroimaging for Alzheimer's disease diagnosis and staging 392

The role of AI in neuroimaging for Alzheimer's disease diagnosis and staging 392

Tuesday, January 13, 2026 - 02:05 pm - 03:35 pm 393

Podium Session..... 393

SESSION V: Alpha-synuclein in PD and MSA: PET imaging 393

Grotegerd, Ann-Kathrin 394

Preclinical and early clinical assessment of [11C]MODAG-005, a novel PET tracer for imaging alpha-synuclein aggregates 394

Hostetler, Eric 397

Clinical evaluation of [11C]MK-7337: insights into the distribution of a-synuclein pathology in Parkinson's disease 397

Hsieh, Chia-Ju 398

[11C]M503-1619 alpha synuclein PET imaging in Parkinson's disease and multiple system atrophy 398

Gunn, Roger.....400

Quantitative analysis of human ^{18}F-FD4 α-synuclein PET imaging data in Parkinson's Disease and Multiple System Atrophy subtypes 400

Tuesday, January 13, 2026 - 03:35 pm - 03:40 pm.....403

Podium Session..... 403

B2 - B: Blitz Session 403

Tuesday, January 13, 2026 - 04:40 pm - 06:10 pm 404

Podium Session..... 404

SESSION VI: Neuroinflammation..... 404

Shi, Ruyu 405

Deep mass spectrometry-based plasma proteomics reveals signatures of reactive astrocytes in Alzheimer's disease.....405

Chan, Tevy.....406

Microglia-Astrocyte interplay modulates tau phosphorylation in Alzheimer's disease 406

Villemagne, Victor 408

Astrogliosis mediates the effects of amyloid, moderated by CVD, on tau and cognition in non-demented individuals 408

Moloney, Christina 411

TSPO expression patterns in the postmortem brain: relevance to neuroinflammation imaging 411

Tuesday, January 14, 2026 - 06:10 pm - 06:15 pm..... 414

[Special] Podium Session 414

Wednesday, January 14, 2026 415

Podium Session..... 415

SESSION VII: Early and intermediate signals and prognostic value..... 415

Heston, Margo..... 416

Discordance between amyloid PET visual read and quantitation: false positives or early pathology detection?..... 416

Rissman, Robert..... 420

Considerations for repeat testing of amyloid PET-validated plasma pTau217 diagnostic assays in the screening cohort for the AHEAD 3-45 study 420

Buckley, Rachel..... 424

The prognostic value of p-tau217 levels on progression to clinical impairment over 2, 5 and 10 years..... 424

Grinberg, Lea 427

Distribution of tau and amyloid pathology across cognitive states in a population-based, admixed autopsy cohort..... 427

Wednesday, January 14, 2026 - 10:30 am - 10:35 am 430

Podium Session..... 430

B3 - A: Blitz Session 430

Wednesday, January 14, 2026 - 10:35 am - 11:35 am 431

PosterSession 431

Poster Session 3A 431

Shekari, Mahnaz.....438

97 Longitudinal trajectories of plasma p-tau217 across multiple assays in relation to amyloid and tau PET and cognition .438

Williams, Lilcelia 442

98 The relation of psychosocial coping mechanisms to ATN pathophysiology differ across demographics. 442

Ziontz, Jacob.....443

99 Intermediate blood-based biomarker status clarified by PET and CSF in cognitively impaired individuals 443

Cuppels, Madison 447

100 Operationalizing clinical criteria for LATE using cognitive, MRI, and AD biomarker (biofluid or PET) data 447

Povala, Guilherme 450

101 CT-based processing is equivalent to MR-based processing for tau PET regional quantification 450

Arowolo, Olatunbosun.....452

102 A pilot study on the association of plasma proteins with neuroimaging biomarkers of Alzheimer's disease in African Americans 452

Rocha, Salma 453

103 Amyloid-PET and white matter hyperintensities but not military service duration nor combat exposure are associated with neurodegeneration and cognitive impairment in older veterans 453

Edison, Paul.....456

104 The influence of cardiovascular risk on white matter integrity along the Alzheimer's disease trajectory: Early impact in preclinical stages 456

Martersteck, Adam 457

105 Longitudinal tau PET progression follows language network spread in primary progressive aphasia 457

Reilhac, Anthonin 459

106 The adjusted Centiloid: Improving reliability by correcting for white matter uptake variability..... 459

Low, Audrey 463

107 Perivascular spaces: Predictors of longitudinal amyloid, tau, cerebrovascular biomarkers?..... 463

Lim, Seokbeen 466

108 Longitudinal evaluation of neuroinflammation using 11C-ER176 TSPO PET 466

Lim, Seokbeen 468

109 Comparison of meningeal signal between [^{18}F]AV-1451 and [^{18}F]MK-6240 tau PET using a distance-based meningeal mask 468

Kapadia, Dhruv..... 472

110 Effects of regional tau accumulation on visual discrimination of novel objects in clinically unimpaired older adults... 472

Dore, Vincent **Error! Bookmark not defined.**

111 Key quantitative benchmarks with CenTauR in cross-sectional and longitudinal large datasets..... 476

Adams, Jenna..... 478

112 Astrocytic reactivity is related to synchronization of regional amyloid-beta deposition 478

Adams, Jenna 480

113 Synergistic effects of amyloid-beta and hyperexcitability on tau pathology and cognitive decline 480

Blazhenets, Ganna 483

114 Amyloid does not discriminate: a meta-analysis of sex differences in Centiloids from 35,468 participants across 33 cohorts 483

Pintucci, Eva 486

115 Preliminary associations of plasma phosphorylated tau217 with regional tau deposition and accumulation in medial temporal and neocortical regions 486

Evelhoch, Jeffrey 489

116 Contrasting neuropathology- and tau PET-based Braak stage associations with dementia severity to clarify differences between radiologic and pathologic findings 489

Tiemann Powles, Savannah 493

117 Novel pet tracer [11C]-CS1P1 uptake reflects decreased sphingosine-1-phosphate receptor 1 activity in vivo in Alzheimer's disease and related dementias 493

Robinson, Talia 496

118 Digital maze test reveals features related to cortical tau in cognitively normal Aβ+ older adults 496

Jacobson, David 497

119 Associations of regional neuroinflammation by ER176 PET SUVR with cognitive scores 497

Varghese, Leah 499

120 Cluster-based metric of early tau-PET aggregation is associated with plasma p-tau217 in cognitively unimpaired older adults with subthreshold amyloid-beta 499

Yi, Emily 502

121 Sex differences in regional Aβ burden are associated with decreased cingulum integrity uniquely in older cognitively unimpaired women 502

Huang, Yuanzhe 506

122 Cerebral vessel morphology is associated with white matter lesions burden 506

Sheng, Jintao 510

123 Early ventral temporal tau burden marks functional vulnerability in aging 510

Coath, William 514

124 Alignment of antemortem images to postmortem fixed hemibrains using standard neuroimaging tools 514

Coath, William 516

125 Towards a harmonized amyloid clock: centralized image processing and temporal modeling with multiple cohorts and tracers 516

Thompson, Jackson 519

126 Cluster-based MK-6240 PET detects early neocortical temporal tau spread 519

Luo, Weiquan 523

127 Gaussian smoothing and partial volume correction modify relationships of tau burden with biological variables in longitudinal multi-site studies of 18F-Flortaucipir PET 523

Han, Yushui 527

128 No detectable association between BDNF Val66Met and hippocampal volume or regional tau PET in ADNI after propensity score matching and ComBat harmonization 527

Han, Yushui 529

129 Centiloid and SUVR amyloid harmonization techniques comparisons for head-to-head unequally spaced data 529

Duran, Tugce 531

130 Plasma amyloid beta 42/40 modifies the associations between MRI biomarkers and subsequent cognitive impairment: a neuroimaging-wide longitudinal study in the BLSA 531

Rowe, Christopher 533

131 High-resolution NAV template using the Siemens Biograph Vision 533

Rowe, Christopher 536

132 Higher clinical throughput quantitative amyloid-β PET using abbreviated acquisition windows 536

Tissot, Cécile 540

133 Tracer-specific effects of hormone replacement therapy on age-related tau accumulation 540

Tissot, Cécile 543

134 Cognitive and age-related differences in low-tau individuals assessed with [18F]FTP and [18F]MK6240 543

Hurst, Cheyenne 546

135 Integration of network analysis of the plasma proteome with Alzheimer's disease neuroimaging outcomes in an African American cohort 546

Pascoal, Tharick 547

137 MK6240 and Flortaucipir Braak staging agreement in a head-to-head cohort 547

Pascoal, Tharick 551

138 Comparing neuropathologic and tau-PET Braak staging across clinical progression using MK6240 and flortaucipir 551

Flores, Shaney 555

139 Predictors of data exclusion in MR-dependent imaging analyses of Alzheimer's disease 555

Frontzkowski, Lukas 559

140 Brain network architecture shapes the pattern of tau-induced neuronal dysfunction in Alzheimer's disease, while tau load drives local damage 559

Mitchell, Stuart 563

141 Cortical thickness and female sex confer resilience to tau-related cognitive decline: A large multi-cohort study 563

Qing, Liang 565

142 Structure-guided design of 18F-FD4—a PET tracer of α-synuclein fibrils 565

Shi, Ruyu 568

143 NULISAseq CNS proteomic signatures of astrocytic reactivity in Alzheimer's disease 568

Shi, Ruyu 569

144 High p-tau217 levels nullify the slower cognitive progression in younger older adults 569

Podium Session 571

KEYNOTE: Integrated Proteomics for Target and Biomarker Discovery in Alzheimer's Disease 571

Integrated Proteomics for Target and Biomarker Discovery in Alzheimer's Disease 571

Wednesday, January 14, 2026 - 01:10 pm - 02:40 pm 572

Podium Session 572

SESSION VIII: Moderators and co-pathologies 572

Ovaici, Nazanin 573

Investigating the role of socioeconomic status on AD biomarker relationships 573

Wang, Tina 575

Blood LDL cholesterol synergistically amplifies tau pathology and cognitive outcome in an APOE4-dependent manner 575

Brown, Christopher 578

Mismatch between tau burden and cognitive domain performance identifies sub-groups with specific co-pathologies 578

Grothe, Michel 582

Characterizing the brain-wide atrophy pattern of LATE-NC-associated hippocampal sclerosis: an imaging-pathologic association study 582

Wednesday, January 14, 2026 - 02:40 pm - 02:45 pm 584

Podium Session 584

B3 - B: Short Poster Presentations 584

Wednesday, January 14, 2026 - 03:45 pm - 05:30 pm 585

Podium Session 585

SESSION IX: Therapeutics: Anti-abeta and anti-tau effects 585

Tonietto, Matteo 586

Tau pathology interferes with amyloid removal by gantenerumab 586

Chiotis, Konstantinos 590

Clinical and PET outcomes following Aβ-targeting therapies in sporadic early-onset Alzheimer's disease: Trial emulation using the LEADS cohort 590

Mercier, Joël 594

Tau positron emission tomography data from the open-label extension study of TOGETHER: a double-blind, placebo-controlled Phase II study of bepranemab in prodromal–mild Alzheimer's disease (AD) 594

Boon, Baayla 596

Cortical laminar and Aβ species-specific correspondence between antemortem Aβ-PET and postmortem pathology in aducanumab-treated Alzheimer's disease 596

Wolk, David 597

In vivo and post-mortem evidence of downstream pathophysiologic effects of treatment-related amyloid clearance 597

WELCOME!

Welcome to Human Amyloid Imaging 2026!

It is a pleasure to welcome you to the Human Amyloid Imaging meeting and to thank you for being part of this community.

Since HAI was first convened nearly two decades ago, its purpose has been clear: to provide a focused forum where new data can be presented succinctly, examined critically, and discussed openly by colleagues who care deeply about rigor, methodology, and meaning. That purpose remains unchanged.

Over the years, many of you have told us — through conversations, correspondence, and post-meeting surveys — that what distinguishes HAI is its commitment to imaging as a scientific discipline in its own right, not as a supporting act. We listened carefully. This meeting continues to stay the course on imaging, while embracing the essential connections to biofluid biomarkers, neuropathology, genetics, and clinical science that now shape the field. The result is a program that remains focused without being narrow, and integrative without losing its center.

The scientific landscape is increasingly crowded, with many excellent meetings addressing Alzheimer's disease from broad perspectives. HAI has never tried to be everything to everyone. Instead, it has remained intentionally structured to allow space for real discussion — not just presentation — and for careful scrutiny of data that challenge assumptions, refine methods, or open new directions. In a field where replication and adaptation are common, HAI continues to value originality of thought, depth of analysis, and candor of exchange.

This meeting exists because of the collective effort of many: the investigators who submitted their latest work, the reviewers who devoted time and expertise to careful evaluation, the session chairs who guide discussion, and the attendees whose questions and insights give the meeting its character. I am deeply grateful to all of you.

I also wish to acknowledge the Executive Committee, the Theme Co-Chairs, the Program Committee, our Award Judges and our generous supporters whose sustained commitment and attention to detail allow HAI to function as the meeting it was intended to be: rigorous, collegial, and focused on science.

I hope you find this year's program stimulating, challenging, and useful. Most of all, I hope the conversations you have here in sessions—at posters, and in the spaces between--continue to advance our understanding and strengthen the collaborations that move the field forward.

Thank you for being part of Human Amyloid Imaging.



Keith A. Johnson, MD
Human Amyloid Imaging Conference

SUPPORTERS

DIAMOND ELITE

PALLADIUM

GOLD

SILVER/ SCHOLARSHIP

SILVER

BRONZE

ALZHEIMER'S® ASSOCIATION

LANTHEUS™

Lilly
A MEDICINE COMPANY

Eisai

ENIGMA
BIOMEDICAL GROUP

Biogen

Bristol Myers Squibb™

Johnson & Johnson

MERCK

RAINWATER
Charitable Foundation

XingImaging
Radiopharmaceutical Production and PET Acquisition

abbvie

ALAMAR BIOSCIENCES

GE HealthCare

HAI COMMITTEES

EXECUTIVE COMMITTEE

Keith Johnson, MD, *Massachusetts General Hospital*
Maria Carrillo, PhD, *Alzheimer's Association*
Milos Ikonomovic, MD, *University of Pittsburgh*
Thomas Karikari, PhD, *University of Gothenburg*
Beth Mormino, PhD, *Stanford University*
Julie Price, PhD, *Massachusetts General Hospital*

THEME CO-CHAIRS

Suzanne Baker, PhD, *Lawrence Berkeley National Laboratory*
Tobey Betthauser, PhD, *University of Wisconsin*
Anne Cohen, PhD, *University of Pittsburgh*
Brad Christian, PhD, *University of Wisconsin*
Teresa Gomez-Isla, MD, *Massachusetts General Hospital*
Lea Grinberg, MD, *Mayo Clinic*
Ansel Hillmer, PhD, *University of Michigan*
Milos Ikonomovic, MD, *University of Pittsburgh*
Heidi Jacobs, PhD, *Massachusetts General Hospital*
Thomas Karikari, PhD, *University of Pittsburgh*
Susan Landau, PhD, *University of California, Berkeley*
Laetitia Lemoine, PhD, *Perceptive*
Beth Mormino, PhD, *Stanford University*
Melissa Murray, PhD, *Mayo Clinic*
Julie Price, PhD, *Harvard Medical School*
Gil Rabinovici, MD, *University of California, San Francisco*
Pedro Rosa-Neto, PhD, *McGill University*
Suzanne Schindler, MD, PhD, *Washington University in St Louis*
Henrik Zetterberg, MD, *University of Gothenburg*

YOUNG INVESTIGATOR AWARD JUDGES

Hartmuth Kolb, PhD, *Janssen R&D*
Michael Pontecorvo, PhD, *Avid Radiopharmaceuticals*
Christopher Rowe, PhD, *Austin Health*
Sandra Sanabria, PhD, *Genentech*

PROGRAM COMMITTEE

Eric Abrahamson, *University of Pittsburgh*
Suzanne Baker, PhD, *Lawrence Berkeley National Laboratory*
Tobey Betthauser, PhD, *University of Wisconsin*
Rachel Buckley, PhD, *Massachusetts General Hospital*
Marianne Chapleau, PhD, *Life Molecular Imaging*
Brad Christian, PhD, *University of Wisconsin*
Anne Cohen, PhD, *University of Pittsburgh*
Tessa Harrison, PhD, *University of California, Berkeley*
Ansel Hillmer, PhD, *University of Michigan*
Kenji Ishii, MD, *Tokyo Metropolitan Inst. of Gerontology*
Milos Ikonomovic, MD, *University of Pittsburgh*
Clifford R. Jack, MD, *Mayo Clinic*
Heidi Jacobs, PhD, *Massachusetts General Hospital*
Renaud La Joie, PhD, *University of California, San Francisco*
Susan Landau, PhD, *University of California, Berkeley*
Laetitia Lemoine, PhD, *Perceptive*
Beth Mormino, PhD, *Stanford University*
Melissa Murray, PhD, *Mayo Clinic*
Agneta Nordberg, MD, PhD, *Karolinska Institute*
Rik Ossenkoppele, PhD, *VU University Medical Center*
Julie Ottoy, PhD, *University of Toronto*
Julie Price, PhD, *Harvard Medical School*
Gil Rabinovici, MD, *University of California, San Francisco*
Dorene Rentz, PsyD, *Brigham and Women's Hospital*
Elena Rodriguez-Vieitez, PhD, *Karolinska Institutet*
Pedro Rosa-Neto, MD, PhD, *McGill University*
Stephen Salloway, MD, *Brown University*
Sandra Sanabria, PhD, *Genentech*
Suzanne Schindler, MD, PhD, *Washington University in St Louis*
Christopher Schwarz, PhD, *Mayo Clinic*
Reisa Sperling, MD, *Brigham and Women's Hospital*
Rik Vandenberghe, MD, PhD, *KU Leuven*
Victor Villemagne, MD, *University of Pittsburgh*
Sylvia Villeneuve, PhD, *McGill University*
Joseph Winer, PhD, *Stanford University*
Christina Young, PhD, *Stanford University*
Henrik Zetterberg, MD, *University of Gothenburg*

POSTER INDEX (by board number)

Board #	Poster Title	Authors	Presenter
MONDAY, JANUARY 12, 2026			
01	**Longitudinal harmonization effects on tau-PET SUVRs trajectories in ADNI study**	Ren | Luo | Laymon | Minhas | Cohen | Wu | Tudorascu	**Ren, Yuxin**
02	**Integrating digital cognitive metrics with PET biomarkers to identify individuals at imminent risk of tau accumulation**	Fu | Robinson | Farrell | Jutten | Thibault | Thompson | Tiss | Chen | Becker | Healy | Penney | Davis | Sperling | Price | Rentz | Johnson	**Fu, Jessie Fang-Lu**
03	**Amyloid-induced neuronal hyperactivity and metabolism are associated with faster tau accumulation in Alzheimer's Disease**	Roemer-Cassiano | Zhang | Evangelista | Klonowski | Hirsch | Frontzkowski | Steward | Dewenter | Biel | Zhu | Gnoerich | Jaekel | Hoeglinger | Brendel | Yeo | Franzmeier	**Roemer-Cassiano, Sebastian**
04	**Sex differences in white matter microstructure and associations with amyloid and tau pathology in autosomal dominant Alzheimer's disease**	Giudicessi | Koops, PhD | Baena | Alvarez | Vidal | Martinez | Gonzalez | Tristão-Pereira | Malotaux | He | Aguillon | Jacobs | Cronin-Golomb | Quiroz	**Giudicessi, Averi**
05	**Concordance between amyloid PET and biomarkers of Alzheimer's disease in plasma and cerebrospinal fluid in cognitively unimpaired individuals**	Bermudez | Fought | Hofrenning | Lowe | Petersen | Vemuri | Jack, Jr. | Algeciral-Schimnich | Bornhorst | Graff-Radford	**Bermudez, Camilo**
06	**Comparing performance of different amyloid PET markers of spatial extent in their ability to predict future amyloid conversion**	Honhar | Farrell | Properzi | Thibault | Schultz | Becker | Fu | Sperling | Price | Johnson	**Honhar, Praveen**
07	**Elevated ptau217 is more strongly associated with tau accumulation and cognitive decline in younger adults**	Coughlan | Townsend | Li | Seto | Birkenbihl | Cody | Klinger | Healy | Farrell | Thibault | Rissman | Properzi | Schultz | Chhatwal | Yang | Donohue | Betthauser | Johnson | Johnson | Sperling | Buckley	**Cuppels, Madison**
08	**Quantitative relationship between Lumipulse G measures of pTau217 in plasma and in brain**	Vandenberghe | Tomé | De Meyer | Goossens | Lambrechts | Poesen | Vanbrabant | Vanmechelen | Thal	**Thal, Dietmar**
09	**Distinct mechanisms underlying APOE-ε4 and sex effects on medial temporal tau pathology: A neuropathology study**	Salvadó | Groot | Wisse | Vogel | Beach | Serrano | Reiman | Schneider | Bennett | Ossenkoppele | Hansson	**Salvadó, Gemma**
10	**Harmonizing amyloid PET tracers at the regional level: evaluation of regional centiloid equations**	Silvestri | Chaggar | Gobbi | Aldea | Klein | Tonietto	**Tonietto, Matteo**
11	**A case series of lecanemab treatment response in patients across the clinical phenotypic spectrum of AD**	Corriveau-Lecavalier | Machulda | Fields | Boots | Whitwell | Day | Aduen | Frank | Kremers | Ramanan | Graff-Radford | Lowe | Boeve | Knopman | Petersen | Jack | Stricker | Jones	**Corriveau-Lecavalier, Nick**

Board #	Poster Title	Authors	Presenter
MONDAY, JANUARY 12, 2026			
12	**Validation of a pseudo-reference region for [11C]-ER176 in healthy volunteers and Alzheimer's disease patients**	Finn | Zanotti-Fregonara | Yu | Masdeu | Pascual	**Finn, Quentin**
13	**β-amyloid PET signal reduction is higher in regions with ARIA-E due to anti-amyloid therapy**	Finn | Pascual | Toledo | Schulz | Masdeu	**Finn, Quentin**
14	**Lifetime and 10-year absolute risk of cognitive impairment associated with amyloid PET severity: a retrospective, longitudinal cohort study**	Hu | Therneau | Wiste | Knopman | Vemuri | Graff-Radford | Lowe | Vassilaki | Cogswell | Schwarz | Algeciras-Schimnich | Petersen | Jack Jr.	**Hu, Mingzhao**
15	**Trajectory of neurodegeneration and brain aging in relation to amyloid timing and duration**	Zhang | Robb | Erus | Castellano | Cui | Cody | Harrison | Engelman | Albert | Resnick | Sperling | Bilgel | Vardarajan | Mayeux | Risacher | Arfanakis | Tosun | Habes | Wang | Toga | Thompson | Kukull | Biber | Landman | Bendlin | Johnson | Schneider | Barnes | Bennett | Saykin | De Jager | Menon | Harrison | Mormino | Cuccaro | Davatzikos | Betthauser | Archer | Hohman | Dumitrescu | Koran	**Zhang, Mengna**
16	**Associations between tau pathology and cortical microstructure are modulated by amyloid burden independent of cortical atrophy in cognitively unimpaired older adults**	Vogt | Koops | Schultz | Properzi | Salat | Pascual-Leone | Huang | Buckley | Rentz | Johnson | Sperling | Jacobs	**Vogt, Nicholas**
17	**Predicting tau PET burden using brain-derived plasma p-tau measures in the British 1946 birth cohort**	Schott | Coath | Wiltshire | Brown | Cash | Whittington | Heslegrave | Zetterberg | Keshavan	**Schott, Jonathan**
18	**Association of combined cardiovascular risk factors and treatments with longitudinal amyloid and tau PET in cognitively normal older adults**	Ourry | Thériault-Dubé | Breitner | Poirier | Villeneuve	**Ourry, Valentin**
19	**Amyloid-pet substantiates clinical decision-making in real-life clinical settings in Brazil**	Schaffer Aguzzoli | Flach | Alves Da Silva | C.L Ferreira | Povala | Ferrari-Souza | Bieger | Teixeira Leffa | Bellaver | Guevara Werlang | Teribele Venturin | Wetters Portuguez | Possa Marroni | Irigoyen da Costa | Bernardi Soder | Sebastião Matushita | Juarez Amorim | Pasquotto Souza | Dario Ramos | Leite | Hygino | Amorim Nogueira | Sturzeneker Tres | Okada de Oliveira | Moriguchi Jeckel | Cortes Domingues | Mosci | Rosado de Castro | Buchpiguel | Paiva Proença Lobo Lopes | Carvalho Campos Neto | Figueiredo Balthazar | Tovar Moll | Martins Novaes Coutinho | Pascoal | Zimmer | Schilling | Costa da Costa	**Schaffer Aguzzoli, Cristiano**

Board #	Poster Title	Authors	Presenter
MONDAY, JANUARY 12, 2026			
20	**Neuropathological validation of Tau-PET CenTauR units: Preliminary data from a multicenter study**	Iaccarino | Chiotis | Grinberg | Kotari | La Joie | Leuzy | Lowe | Lu | Moscoso | Nguyen | Schwarz | Seeley | Jack | Rabinovici | Shcherbinin	**La Joie, Renaud**
21	**Molecular evaluation of a tau-PET analog and pathological TAR DNA-binding protein 43 docking in a cellular model of frontotemporal lobar degeneration**	Gatto | Weissmann | Salinas Castellanos | Montes | Uruk | Youssef | Reichard | Josephs	**Gatto, Rodolfo**
22	**Anterior cingulate sulcal pattern is associated with successful cognitive aging**	Maboudian | Kellerman | Willbrand | Pezzoli | Weiner | Jagust	**Maboudian, Samira**
23	**Microstructural white matter injury mediates the association between vascular risk and plasma biomarkers: Preliminary findings from the Diverse VCID study**	Lee | Sapkota | Rajan | Jin | Hinman | Johnson | Harvey | Maillard | Fornage | DeCarli	**Lee, Seunghoon**
24	**VeraBIND Tau: a novel plasma assay reflecting tau aggregation increases over time in individuals with positive tau-PET signal**	Hanseeuw | Quenon | Bayart | Salman | Pak | Shamsundar | Soldo | Iqbal	**Hanseeuw, Bernard**
25	**Amyloid PET quantitation using skewness: Autopsy validation and test-retest performance**	Tunali | Iaccarino | Wang | Kennedy | Lu | Shcherbinin	**Tunali, Ilke**
26	**Stratifying preclinical Alzheimer's disease by hippocampal volume to detect concomitant LATE**	Mundada | Lyu | Sadeghpour | Brown | McGrew | Yushkevich | Das | Wolk	**Mundada, Nidhi**
27	**Differential sensitivity of [^{18}F]MK6240 and [^{18}F]FTP to measure tau before and after anti-amyloid therapy**	Deng | Finn | Pando | Matutue | Lussier | Fortea | Tudorascu | Soleimani-Meigooni | Lowe | Oh | Gordon | Rosa-Neto | Baker | Pascoal | Masdeu | Pascual	**Deng, Han**
28	**Development of a highly sensitive and automated immunoassay for Brain-Derived pTau-217: Analytical performance in human plasma samples**	Ma | Wang | Danthanarayana | Kim | Ji | Jhaveri | Zhang | Qiu | Mudumba | Luo	**Ma, Xiao-Jun**
29	**Network-based mechanistic modeling of Alzheimer's disease for evaluating diverse therapeutic mechanisms of action**	Wooten | Stage | Mazer | Townsend | Comley | Guo	**Wooten, Dustin**
30	**Neuroimaging compendium of microglia, amyloid, tau, and neurodegeneration across clinical variants of Alzheimer's disease**	Houlihan | Guzman | Smith | Sanchez | Kreisl | Cosentino | Noble | Lao	**Houlihan, Hannah**
31	**Predictors of longitudinal atrophy across NIA-AA biological PET stages**	Fonseca | Maboudian | Chao | Jagust | Harrison	**Fonseca, Corrina**
32	**Effect of uptake time on [18F]-flutemetamol visual interpretation and Centiloid quantification**	Bollack | Buckley | Schwarz | Battle | Smith | Stromrud | Hansson | Palmqvist | Matttsson-Carlgren | La Joie | Farrar	**Bollack, Ariane**

Board #	Poster Title	Authors	Presenter
MONDAY, JANUARY 12, 2026			
33	**Episodic memory decline and tau biomarkers progress earlier along the amyloid timeline in Down syndrome compared to neurotypical adults**	Zammit | Bruzzone | Morse | Batchelar | Bettcher | McLachlan | McVea | Carey | Tudorascu | Hartley | Clark | Ances | Caldwell | Johnson | Handen | Head | Mapstone | Christian | Investigators | Betthauser	**Zammit, Matt**
34	**Relationship between p-tau217 and PET in preclinical AD: The moderating effect of white matter hyperintensity**	Moon | Chen	**Moon, Hasom**
35	**Systemic inflammation–tau interaction: Insights from CRP modulation of p-tau217 association with tau PET positivity**	Monto | Boots | Zeng | Farinas | Sehrawat | Saeed | Cohen | Reis | Lopez | Snitz | Karikari	**Monto, Abdul Razak**
36	**Examining elevated choroid plexus binding of tau PET tracers in aging and Alzheimer's disease**	Marin | Wales | Ruais | Richard | Hedden	**Marin, Anna**
37	**The influence of β-amyloid on neuroinflammatory 11C-ER176 uptake in progressive apraxia of speech**	Satoh | Utianski | Duffy | Clark | Botha | Lowe | Josephs | Whitwell	**Satoh, Ryota**
38	**Subtracting first principal component may improve detectability of subtle 4R tau signals in 18F flortaucipir tau PET imaging**	Satoh | Ali | Clark | Dickson | Lowe | Josephs | Whitwell	**Satoh, Ryota**
39	**OMG: a proteomic determinant of neurodegenerative resiliency**	Duggan | Oh | Frank | Gomez | Zweibaum | Cui | Chen | Surapaneni | Blew | Dark | Joynes | Kandala | Bilgel | Farinas | Erus | Tian | Candia | Pucha | Landman | Dumitrescu | Hohman | Lewis | Moghekar | Siavoshi | Ali | Liu | Xu | Western | Kaneko | Kato | Furuichi | Shibayama | Katsuno | Nishita | Otsuka | Gottesman | Dammer | Seyfried | Levey | Johnson | Mormino | Wagner | Poston | Kapogiannis | Grams | Bhargava | Waga | Davatzikos | Resnick | Ferrucci | Bennett | Cruchaga | Wyss-Coray | Kivimäki | Coresh | Walker	**Duggan, Michael**
40	**Frequency and consequences of extreme PET based pathological profiles in preclinical Alzheimer's disease**	Medina Guerra | Cody | Young | Sheng | Sokolowski | Younes | Trelle | Tosun | Hohman | Mormino	**Medina Guerra, Lucah**
41	**Periventricular diffusivity moderates the relationship between astrocyte reactivity and amyloid deposition in non-demented older adults**	Chen | Wu | Yang | Gogola | Luo | Villemagne | Laymon | Lopresti | Cohen | Ikonomovic | Snitz | Wilckens | Lopez | Tudorascu | Aizenstein | Minhas	**Chen, Chang-Le**
42	**Disentangling the effects of age and Alzheimer's disease pathology on longitudinal atrophy in cognitively normal older adults**	Haque | Fonseca | Maboudian | La Joie | Jagust	**Haque, Miraal**

Board #	Poster Title	Authors	Presenter
MONDAY, JANUARY 12, 2026			
43	**Stronger amyloid–tau coupling explains faster tau progression in early-onset Alzheimer's disease**	Franzmeier	Frontzkowski	Steward	Klonowski	Dewenter	Hirsch	Biel	Zhu	Gnörich	Höglinger	Brendel	Roemer-Cassiano	**Franzmeier, Nicolai**
44	**Harmonization methods to mitigate batch effects in blood biomarker analysis**	Zhang	Lukasewicz Ferreira	Minhas	Pascoal	Zeng	Karikari	Cohen	Tudorascu	**Zhang, Vivian**
45	**IGFR1, but not BDNF, acts as a suppressive neuroprotective factor between astrogliosis and visuospatial function among non-demented individuals**	Ramirez Tirado	Cohen	Lopresti	Ikonomovic	Gogola	Matan	Zeng	Karikari	Lopez	Shaaban	Villemagne	**Cohen, Ann**
46	**The relation of psychosocial coping mechanisms to ATN pathophysiology differ across demographics**	Schatz	Snitz	Roush	Lopresti	Villemagne	Lopez	Williams	Cohen	**Cohen, Ann**
47	**Evaluation of the Clinical IMpact of Blood-Based Biomarker Assays on dementia specialists' decision-making (CIMBBBA): Preliminary report from a real-world dementia subspecialty clinic study**	Eldaief	Krahn	Murdock	Rezaii	Chan	Arnold	Avetisyan	Ramirez Gomez	Gale	McGinnis	Dickerson	**Eldaief, Mark**
48	**Dynamic interplay of vascular injury and inflammation on Alzheimer's disease pathophysiology**	Rusdi	Kang	Yin	Gibson	Rahmouni	Benedet	Zetterberg	Blennow	Karikari	Ashton	Black	Rosa-Neto	Goubran	Ottoy	**Ottoy, Julie**

Board #	Poster Title	Authors	Presenter
TUESDAY, JANUARY 13, 2026			
49	**CSF oligodendrocyte biomarkers are associated with amyloid burden in Alzheimer's disease**	Santos Machado	De Bastiani	Lebrun	Povala	Pola	Vizlin-Hodzic	Rosa-Neto	Zimmer	Blennow	Zetterberg	Benedet	Ashton	**Santos Machado, Luiza**
50	**Associations between systolic blood pressure and amyloid burden on cross-sectional inferior temporal tau across mid- to late-life**	Yau	Scott	Palmgren	Coughlan	Kirn	Properzi	Schultz	Ghosh	Buckley	Amariglio	Rentz	Johnson	Sperling	Beiser	Seshadri	Chhatwal	**Yau, Wai-Ying Wendy**
51	**Associations of ER176 TSPO PET with blood-based AD and neuroinflammation biomarkers**	Cogswell	Lundt	Ou	Algeciras-Schimnich	Zekeridou	Lim	Graff-Radford	Schwarz	Vemuri	Petersen	Jack Jr	Lowe	**Cogswell, Petrice**
52	**Evaluation of [18F]MK6240 test-retest reproducibility for different processing pipelines**	Tiss	Thibault	Fu	Becker	Price	Johnson	**Tiss, Amal**
53	**Temporal dynamics of tau PET subtypes and its association with**	Kwon	Song	Lee	Seong	**Kwon, Tae Youn**

Board #	Poster Title	Authors	Presenter
	TUESDAY, JANUARY 13, 2026		
	heterogeneous neurodegeneration in Alzheimer's disease		
54	**A-T-N-C generative model for predicting and simulating patient-tailored cognitive decline trajectories in Alzheimer's disease**	Lee | Song | Kwon | Lee | Seong	**Kwon, Tae Youn**
55	**High-resolution ex-vivo MRI reveals layer-specific atrophy of hippocampal subregions to earliest tau pathology**	Salman | Tomé | Joudiou | Thal | Annettesdotter | Khandelwal | Yushkevich | Gallez | Wisse | Hanseeuw	**Salman, Yasmine**
56	**Blood volume influences the association between baseline plasma biomarker values and amyloid PET outcomes over time**	Burns | Gogola | Zeng | Karikari | Jacobs | Lopresti | Osorio	**Burns, Kelsey**
57	**Visual interpretation methods for tau-PET imaging with Flortaucipir and MK-6240: Insights from the HEAD study**	Ruppert | Vermeiren | Scop Medeiros | Povala | Rocha | Soares | Ferreira | Amaral | Bauer-Negrini | Lussier | Scarpatto Rodrigues | Oliveira Jr. | Mroue | Bellaver | Moscoso | Ossenkoppele | van de Giessen | Masdeu | Tudorascu | Soleimani-Meigooni | Fortea | Lowe | Oh | Pascual | Gordon | Rosa-Neto | Baker | Pascoal	**Pascoal, Tharick**
58	**Associations between TSPO PET and CSF and blood-based biomarkers**	Smith | Guzman | Houlihan | Sanchez | Kreisl | Talmasov | De Jager | Herman | Simoes | Small | Lao	**Smith, Anna**
59	**Regional white matter injury modifies the association between ß-amyloid and cognition**	Royse | Reese | Snitz | Hengenius | Crane | Mukherjee | Choi | Willie-Permor | Felix | Huppert | Roush | Cisneros | Potopenko | Lopresti | Cohen | Shaaban	**Royse, Sarah**
60	**Sex differences in neuroinflammation, amyloid, tau, and neurodegeneration**	Guzman | Smith | Houlihan | Sanchez | Akinci | Luchsinger | Lao	**Guzman, Diana**
61	**Evaluation of the tau PET ligand [18F]florzolotau in frontotemporal dementia**	Clarke | Whittington | Sholaja | Hield | Huiban | van den Berg | Margolin | Rowe | Rohrer | Salinas | Rabiner	**Whittington, Alex**
62	**Intersections of gender/sex and neighborhood deprivation on cognition: Are there mediation effects of Alzheimer's disease biomarkers?**	Reese | Royse | Snitz | Crane | Mukherjee | Choi | Hengenius | Huppert | Roush | Cisneros | Lopresti | Rameriz Tirado | Willie-Permor | Felix | Cohen | Shaaban	**Reese, Alexandria**
63	**Disentangling cognitive severity and phenotype across dementia syndromes**	Smith | Coyle-Gilchrist | Murley | Rouse | Stockton | Naessens | Savulich | Wiggins | Malpetti | Bowns | Perquin | Lanskey | Karadag | Kocagoncu | Quinn | Pitt | Alcock | O'Brien | Rittman | Rowe | Lambon-Ralph	**Smith, Viktorija**
64	**Standardized indices of tau burden using the CenTauR universal scale predict distinct cognitive trajectories across Alzheimer's disease biological stages**	Lopresti | DelBene | Leuzy | Gogola | Harrison | Landau | Jagust | Villemagne	**Lopresti, Brian**

Board #	Poster Title	Authors	Presenter
TUESDAY, JANUARY 13, 2026			
65	**SPARE-SVD: An integrated machine-learning metric for cerebral small vessel disease within the ATN(V) framework**	Dong | Zhang | Zeng | Wang | Wang | Toledo | Gonzales | Charisis | Rashid | Seshadri | Crane | Archer | Jefferson | Hohman | Habes	**Dong, Mengjin**
66	**Risk factors and AD prevention: a multivariate and multimodal study**	Fajardo Valdez | Qiu | Ourry | Yakoub | Villeneuve | Research Group	**Fajardo Valdez, Alfonso**
67	**MK6240 and Tauvid positivity, cognitive decline, and their relationship to Aβ PET deposition across the Alzheimer's spectrum**	Bellaver | Povala | Lussier | Amaral | Bauer-Negrini | Ferreira | Jagust | Masdeu | Fortea | Tudorascu | Soleimani-Meigooni | Lowe | Oh | Pascual | Gordon | Rosa-Neto | Baker | Pascoal	**Bellaver, Bruna**
68	**Differential tau-PET load predominance along shared progression trajectories determines clinical variability in Alzheimer's disease**	Mroué | Povala | Bellaver | Lukasewicz Ferreira | Bauer-Negrini | Lussier | Amaral | Scop Medeiros | Ruppert | Silva da Rocha | Scarpatto Rodrigues | Silva Oliveira | Soares Katz | Teixeira Leffa | Saha | Masdeu | Soleimani-Meigooni | Fortea | Lowe | Oh | Pascual | Gordon | Rosa-Neto | Baker | Pascoal	**Povala, Guilherme**
69	**Head-to-head comparison of tau PET tracers across the Alzheimer's disease spectrum: baseline results from the HEAD study**	Povala | Bellaver | Lussier | Amaral | Bauer-Negrini | Ferreira | Jagust | Masdeu | Fortea | Tudorascu | Soleimani-Meigooni | Lowe | Oh | Pascual | Gordon | Rosa-Neto | Baker | Pascoal	**Povala, Guilherme**
70	**Comparison of Sampled Iterative Local Approximation (SILA) implemented in R and MATLAB**	Bruzzone | Coath | Navaratna | Carey | Morse | Bilgel | Betthauser	**Bruzzone, Hailey**
71	**Agreement between amyloid status prediction from visual read, SUVR thresholding, and AI-based interpretation of amyloid PET**	Peraza | Joules | Mohs | Beauregard | Dwyer | Hughes | Wolz	**Wolz, Robin**
72	**CenTauR thresholds generated using Gaussian Mixture Models for biological staging of amyloid positive ADNI participants**	DelBene | Villemagne | Gogola | Leuzy | Harrison | Landau | Jagust | Lopresti	**DelBene, Alexander**
73	**Progression to tau-PET positivity by plasma P-tau217 levels and its association with clinical decline in preclinical Alzheimer's disease: data from A4 study**	Kim | Kotari | Morris | Shcherbinin | Yaari | Holdridge | Sims | Ossenkoppele | Collins | Hansson | Lu	**Kim, Min Jung**
74	**Neuroimaging correlates of loneliness**	Sanchez | Guzman | Smith | Houlihan | Stern | Bockting | Lao	**Sanchez, Thairi**
75	**Age-dependent associations between salivary inflammatory cytokines and amyloid-beta in cognitively unimpaired older adults**	Parker | Tang | Taylor | Bock | Meza | Tuteja | Avila | Chang | Simmons | Bamford | Yi | Mcmillan | Kim | Thomas | Adams | Yassa	**Parker, Dana**
76	**Tau accumulation drives worsening depressive symptoms in cognitively normal older adults**	Markova | Berry	**Markova, Teodora**

Board #	Poster Title	Authors	Presenter
TUESDAY, JANUARY 13, 2026			
77	**Dorsal raphe nucleus and locus coeruleus differentially relate to depressive symptoms in cognitively normal older adults**	Markova | Chen | Carlson | Cao | Ciampa | Marcus | Adornato | Matulonis | Morin | Hooker | Berry	**Markova, Teodora**
78	**Evaluating occipital-to-global amyloid PET as a predictor of CAA at autopsy in Mayo Clinic cohorts**	Schwarz | Hu | Cogswell | Graff-Radford | Vemuri | Przybelski | Wiste | Nguyen | Reichard | Dickson | Lowe | Ramanan | Knopman | Petersen | Jack	**Schwarz, Christopher**
79	**SCAN: Standardized Centralized Alzheimer's and related dementias Neuroimaging**	Schwarz | Harrison | DeCarli | Kantarci | Baker | La Joie | Maillard | Rabinovici | Toga | Jack | Jagust	**Schwarz, Christopher**
80	**Differential contributions of amyloid spatial extent and tau burden to domain-specific cognitive decline in early Alzheimer's disease**	Slade | Thibault | Thompson | Fanglu Fu | Price | Rentz | Sperling | Johnson | Farrell	**Slade, Elliott**
81	**PET-measured amyloid accumulation rate modulates tau accumulation rate in individuals with Down syndrome**	Bettcher | McLachlan | Zammit | McVea | Betthauser | Laymon | Tudorascu | Cohen | Price | Head | Mapstone | Lao | Johnson | Ances | Handen | Christian	**Bettcher, Brecca**
82	**Elevated medial temporal lobe tau predicts cross-sectional association between neocortical tau and global amyloid burden**	Thibault | Reilhac-Laborde | Charil | Irizarry | Johnson	**Thibault, Emma**
83	**Assessing the effect of amyloid status on the relationship between glucose metabolism and synaptic density in the aging population**	McLachlan | Bettcher | DiFilippo | LeMerise | McVea | Zammit | Langhough | Johnson | Bendlin | Christian	**McLachlan, Max**
84	**Associations between p-tau217 and brain atrophy are amplified by Aβ burden and APOEε4**	Brown | Properzi | Cuppels | Birkenbihl | Coughlin | Seto | Townsend | Betthauser | Schultz | Chhatwal | Yang | Jacobs | Farrell | Johnson | Johnson | Li | Sperling | Hohman | Donohue | Buckley	**Brown, Jane**
85	**Early cortical thickness change in preclinical AD development**	Sinclair | Chen	**Sinclair, Stephanie**
86	**Immuno-vascular crosstalk drives tau pathology preferentially in women**	Wood Alexander | Kang | Rusdi | Yin | Rahmouni | Wang | Benedet | Zetterberg | Blennow | Karikari | Ashton | Black | Goubran | Rabin | Ottoy	**Wood Alexander, Madeline**
87	**Midlife physical activity attenuates the association of earlier menopause with tau pathology and cognitive decline**	Wood Alexander | Cadwallader | Johnson | Casaletto | Rabin	**Wood Alexander, Madeline**
88	**Improved tau PET signal detection with total-body PET compared to conventional PET: A preliminary study**	Young | Bayerlein | Bhattarai | DeCarli | Badawi | Fan	**Young, Christina**
89	**Demographic associations with plasma biomarkers in the oldest-old: The LifeAfter90 Study**	Young | Colbeth | Gilsanz | Corrada | Rizvi | Zhou | di Lucente | DeCarli | Jin | Whitmer	**Young, Christina**

Board #	Poster Title	Authors	Presenter
TUESDAY, JANUARY 13, 2026			
90	**Differential sensitivity of T1-MRI and FDG-PET for tracking neurodegeneration across progressive stages of tau pathology in Alzheimer's disease**	Vourkas | Karagianni | Moscoso | Zhang | Sanchez-Juan | Schöll | Grothe | Silva-Rodríguez	**Silva-Rodríguez, Jesús**
91	**SPARE-Tau, a machine-learning derived tau-PET index, correlates with Alzheimer's disease and related dementias biomarkers**	Wang | Zeng | Toledo | Gonzales | Honnorat | Charisis | Dong | Ho | Rashid | Kutty | Salman | Vroman | Seshadri | Habes	**Wang, David**
92	**Assessing the generalizability of plasma p-tau217 cutpoints for amyloid-β detection across clinical and preclinical cohorts**	Liu | Zeng | Nafash | Sehrawat | Choity | Gu | Farinas | Bedison | Matan | Gogola | Huang | Sewell | McAuley | Hillman | Kramer | Burns | Kang | Vidoni | Nadkarni | Aizenstein | Kofler | Tudorascu | Shaaban | Lingler | Pascoal | Villemagne | Berman | Sweet | Snitz | Ikonomovic | Kamboh | Erickson | Cohen | Lopez | Deek | Karikari	**Liu, Tianshu**
93	**Evaluating the transferability of dual cutpoints for plasma p-tau217 in detecting brain amyloid-β across diverse cohorts**	Liu | Zeng | Nafash | Sehrawat | Choity | Gu | Farinas | Bedison | Matan | Gogola | Huang | Sewell | McAuley | Hillman | Kramer | Burns | Kang | Vidoni | Nadkarni | Aizenstein | Kofler | Tudorascu | Shaaban | Lingler | Pascoal | Villemagne | Berman | Sweet | Snitz | Ikonomovic | Kamboh | Erickson | Cohen | Lopez | Deek | Karikari	**Liu, Tianshu**
94	**Free-water interacts with amyloid positivity to predict regional tau pathology in both early and late Braak stages**	Sathe | Durant | Koran | Dumitrescu | Cody | Sokołowski | Kim | Mez | Saykin | Toga | Cuccaro | Tosun | Johnson | Barber | O'Bryant | Landman | Mormino | Hohman | Archer	**Sathe, Aditi**
95	**Integration of data-driven biomarker discovery with established Alzheimer's disease biomarkers in an African American cohort**	Kuchenbecker | Heckman | Nguyen | Casellas | Sotelo | Schwarz | Senjem | Jain | Lucas | Willis | Ertekin-Taner | Graff-Radford | Kantarci | Lowe | Lachner | Day | Carrasquillo	**Kuchenbecker, Lindsey**
96	**Early concordance between Aβ PET spatial extent and plasma %ptau217**	Farrell | Thibault | Yang | Price | Chhatwal | Coughlan | Buckley | Sperling | Johnson	**Farrell, Michelle**

Board #	Poster Title	Authors	Presenter
WEDNESDAY, JANUARY 14, 2026			
97	**Longitudinal trajectories of plasma p-tau217 across multiple assays in relation to amyloid and tau PET and cognition**	Shekari | Tosun | Dage | Schindler | Shaw | Jagust | Landau	**Shekari, Mahnaz**
98	**The relation of psychosocial coping mechanisms to ATN pathophysiology differ across demographics.**	Schatz | Snitz | Roush | Lopresti | Villemagne | Lopez | Williams | Cohen	**Williams, Lilcelia**

Board #	Poster Title	Authors	Presenter
WEDNESDAY, JANUARY 14, 2026			
99	**Intermediate blood-based biomarker status clarified by PET and CSF in cognitively impaired individuals**	Ziontz | Blazhenets | Lin | Landau | Shaw | Dage | Hammers | Eloyan | Koeppe | Carillo | Dickerson | Rabinovici | La Joie	**Ziontz, Jacob**
100	**Operationalizing clinical criteria for LATE using cognitive, MRI, and AD biomarker (biofluid or PET) data**	Cuppels | Birkenbihl | Schneider | Bennett | Brown | Seto | Coughlan | Li | Townsend | Properzi | James | Arfanakis | Sperling | Yang | Chhatwal | Amariglio | Hohman | Donohue | Buckley	**Cuppels, Madison**
101	**CT-based processing is equivalent to MR-based processing for tau PET regional quantification**	Povala | Bellaver | Amaral | Lussier | Ferreira | Bauer-Negrini | Tudorascu | Masdeu | Fortea | Soleimani-Meigooni | Lowe | Oh | Pascual | Gordon | Rosa-Neto | Baker | Pascoal	**Povala, Guilherme**
102	**A pilot study on the association of plasma proteins with neuroimaging biomarkers of Alzheimer's disease in African Americans**	Arowolo | Kuchenbecker | Heckman | Nguyen | Casellas | Sotelo | Schwarz | Senjem | Jain | Lucas | Willis | Ertekin-Taner | Graff-Radford | Kantarci | Lowe | Lachner | Day | Carrasquillo	**Arowolo, Olatunbosun**
103	**Amyloid-PET and white matter hyperintensities but not military service duration nor combat exposure are associated with neurodegeneration and cognitive impairment in older veterans**	Rocha | Pasternak | Lesman Segev | Schwartz | Blazhenets | Maiti | Rosen Lang | Hantke | Livny-Ezer | Yaffe | Shaw | Weiner | Hills | Kritikos | Soleimani-Meigooni | Silbert | La Joie | Gardner	**Rocha, Salma**
104	**The influence of cardiovascular risk on white matter integrity along the Alzheimer's disease trajectory: Early impact in preclinical stages**	Edison | Arnold	**Edison, Paul**
105	**Longitudinal tau PET progression follows language network spread in primary progressive aphasia**	Martersteck | Rogalski	**Martersteck, Adam**
106	**The adjusted Centiloid: Improving reliability by correcting for white matter uptake variability**	Reilhac | Irizarry | Reyderman | Charil	**Reilhac, Anthonin**
107	**Perivascular spaces: Predictors of longitudinal amyloid, tau, cerebrovascular biomarkers?**	Low | Gunter | Hu | Raghavan | Przybelski | Schwarz | Kantarci | Lowe | Graff-Radford | Petersen | Jack | Vemuri	**Low, Audrey**
108	**Longitudinal evaluation of neuroinflammation using 11C-ER176 TSPO PET**	Lim | Cogswell | Min | Lee | Brunn | Kandimalla | Jacobson | Nycklemoe | Lee | Lundt | Botha | Graff-Radford | Jones | Vemuri | Kantarci | Jack | Petersen | Lowe	**Lim, Seokbeen**
109	**Comparison of meningeal signal between [^{18}F]AV-1451 and [^{18}F]MK-6240 tau PET using a distance-based meningeal mask**	Lim | Gunter | Baker | Tissot | Brunn | Soleimani-Meigooni | Oh | Fortea | Pascual | Gordon | Rosa-Neto | Pascoal | Klunk | Jagust | Senjem | Botha | Knopman | McCarter | Ramanan | Graff-Radford | Schwarz | Kantarci | Boeve | Vemuri | Jones | Jack | Petersen | Lowe	**Lim, Seokbeen**

Board #	Poster Title	Authors	Presenter
WEDNESDAY, JANUARY 14, 2026			
110	**Effects of regional tau accumulation on visual discrimination of novel objects in clinically unimpaired older adults**	Kapadia | Medina Guerra | Sai | Bonnen | Wagner | Mormino | Trelle	**Kapadia, Dhruv**
111	**Key quantitative benchmarks with CenTauR in cross-sectional and longitudinal large datasets**	Dore | Bourgeat | Betthauser | Feizpour | Moscoso | Leuzy | Fripp | Johnson | Rowe | Villemagne	**Rowe, Christopher**
112	**Astrocytic reactivity is related to synchronization of regional amyloid-beta deposition**	Adams | Parker | Taylor | Tang | Meza | Tuteja | Avila | Chang | Simmons | Malhas | Kim | McMillan | Mapstone | Yassa	**Adams, Jenna**
113	**Synergistic effects of amyloid-beta and hyperexcitability on tau pathology and cognitive decline**	Vanderlip | Adams	**Adams, Jenna**
114	**Amyloid does not discriminate: a meta-analysis of sex differences in Centiloids from 35,468 participants across 33 cohorts**	Blazhenets | Pezzoli | Casaletto | Soleimani-Meigooni | Chiotis | Allen | Rabinovici | La Joie | Study Group	**Blazhenets, Ganna**
115	**Preliminary associations of plasma phosphorylated tau217 with regional tau deposition and accumulation in medial temporal and neocortical regions**	Pintucci | Thibault | Farrell | Yang | Chhatwal | Properzi | Becker | Price | Sperling | Johnson	**Pintucci, Eva**
116	**Contrasting neuropathology- and tau PET-based Braak stage associations with dementia severity to clarify differences between radiologic and pathologic findings**	Evelhoch | Bruzzone | Rocha | Asthana | Nirschl | Johnson | Schneider | Hyman | Pascoal | Betthauser	**Evelhoch, Jeffrey**
117	**Novel pet tracer [11C]-CS1P1 uptake reflects decreased sphingosine-1-phosphate receptor 1 activity in vivo in Alzheimer's disease and related dementias**	Tiemann Powles | Friedrichsen | Flores | Rajamanickam | Keefe | Simmons | Doering | McKay | Hoagey | Sabaredzovic | Ibanez | Morris | An | Brier | Tu | Benzinger	**Tiemann Powles, Savannah**
118	**Digital maze test reveals features related to cortical tau in cognitively normal Aβ+ older adults**	Robinson | Fu | Amariglio | Sperling | Johnson | Davis | Penney | Rentz	**Robinson, Talia**
119	**Associations of regional neuroinflammation by ER176 PET SUVR with cognitive scores**	Jacobson | Lim | Lundt | Nycklemoe | Min | Botha | Graff-Radford | Jones | Vemuri | Kantarci | Knopman | Jack | Petersen | Lowe	**Jacobson, David**
120	**Cluster-based metric of early tau-PET aggregation is associated with plasma p-tau217 in cognitively unimpaired older adults with subthreshold amyloid-beta**	Varghese | Brock | Taylor | Thomas | Yassa | Adams	**Varghese, Leah**
121	**Sex differences in regional Aβ burden are associated with decreased cingulum integrity uniquely in older cognitively unimpaired women**	Yi | Parker | Tang | Taylor | Tuteja | Meza | Avila | Chang | Simmons | Bamford | McMillan | Kim | Thomas | Adams | Yassa	**Yi, Emily**
122	**Cerebral vessel morphology is associated with white matter lesions burden**	Huang | Li | Rocha | Stetten | Yang | Ibrahim | Wu | Aizenstein	**Huang, Yuanzhe**

Board #	Poster Title	Authors	Presenter
WEDNESDAY, JANUARY 14, 2026			
123	**Early ventral temporal tau burden marks functional vulnerability in aging**	Sheng | Trelle | Sai | Young | Romero | Park | Vossler | Younes | Davidzon | Wagner | Mormino	**Sheng, Jintao**
124	**Alignment of antemortem images to postmortem fixed hemibrains using standard neuroimaging tools**	Coath | Staruck | Carey | de Chavez | Karas | Abrahamson | Asthana | Johnson | Ikonomovic | Nirschl | Betthauser	**Coath, William**
125	**Towards a harmonized amyloid clock: centralized image processing and temporal modeling with multiple cohorts and tracers**	Coath | Bruzzone | Morse | Navaratna | Hammond | Staruck | Nowinski | Palmer | Kelley | Schwartz | Carey | Betthauser	**Coath, William**
126	**Cluster-based MK-6240 PET detects early neocortical temporal tau spread**	Thompson | Becker | Fanglu Fu | Farrell | Thibault | Slade | Sperling | Price | Johnson	**Thompson, Jackson**
127	**Gaussian smoothing and partial volume correction modify relationships of tau burden with biological variables in longitudinal multi-site studies of 18F-Flortaucipir PET**	Luo | Laymon | Baker | Cohen | Villemagne | Lopresti | Aizenstein | Tudorascu | Minhas	**Luo, Weiquan**
128	**No detectable association between BDNF Val66Met and hippocampal volume or regional tau PET in ADNI after propensity score matching and ComBat harmonization**	Han | Minhas | Laymon | Villemagne | Tudorascu	**Han, Yushui**
129	**Centiloid and SUVR amyloid harmonization techniques comparisons for head-to-head unequally spaced data**	Han | Lopresti | Bourgea | Laymon | Villemagne | Tafti | Minhas | Tudorascu	**Han, Yushui**
130	**Plasma amyloid beta 42/40 modifies the associations between MRI biomarkers and subsequent cognitive impairment: a neuroimaging-wide longitudinal study in the BLSA**	Duran | Bilgel | An | Kandala | Davatzikos | Landman | Erus | Ferrucci | Moghekar | Walker | Resnick	**Duran, Tugce**
131	**High-resolution NAV template using the Siemens Biograph Vision**	Bourgeat | Rowe | Paranawithana | Feizpour | Huang | Villemagne | Fripp | Dore	**Rowe, Christopher**
132	**Higher clinical throughput quantitative amyloid-β PET using abbreviated acquisition windows**	Paranawithana | Gillman | Bourgeat | Fripp | Villemagne | O'Keefe | Huang | Benzinger | LaMontagne | Morris | Doré | Rowe	**Rowe, Christopher**
133	**Tracer-specific effects of hormone replacement therapy on age-related tau accumulation**	Tissot | Shi | Tsai | Maboudian | Fonseca | Rahmouni | Lussier | Therriault | Trudel | Cassa Macedo | Stevenson | Bellaver | Ferreira | Povala | Gordon | Pascual | Lowe | Soleimani-Meigooni | Oh | Klunk | Rosa-Neto | Jagust | Buckley | Pascoal | Baker	**Tissot, Cécile**
134	**Cognitive and age-related differences in low-tau individuals assessed with [18F]FTP and [18F]MK6240**	Tissot | Shankar | Tsai | Rahmouni | Lussier | Therriault | Trudel | Cassa Macedo | Stevenson | Bellaver | Ferreira | Povala | Gordon | Pascual | Lowe |	**Tissot, Cécile**

Board #	Poster Title	Authors	Presenter
WEDNESDAY, JANUARY 14, 2026			
		Soleimani-Meigooni | Oh | Klunk | Rosa-Neto | Jagust | Landau | Pascoal | Baker	
135	**Integration of network analysis of the plasma proteome with Alzheimer's disease neuroimaging outcomes in an African American cohort**	Hurst | Kuchenbecker | Heckman | Nguyen | Casellas | Sotelo | Shwarz | Senjem | Jain | Lucas | Willis | Ertekin-Taner | Graff-Radford | Kantarci | Lowe | Lachner | Day | Carrasquillo	**Hurst, Cheyenne**
137	**MK6240 and Flortaucipir Braak staging agreement in a head-to-head cohort**	Rocha | Soares | Ruppert | Medeiros | Bellaver | Povala | Ferreira | Bauer-Negrini | Lussier | Tudorascu | Masdeu | Soleimani-Meigooni | Fortea | Lowe | Oh | Pascual | Gordon | Rosa-Neto | Baker | Pascoal	**Pascoal, Tharick**
138	**Comparing neuropathologic and tau-PET Braak staging across clinical progression using MK6240 and flortaucipir**	Rocha | Bruzzone | Ruppert | Medeiros | Soares | Bellaver | Povala | Ferreira | Lussier | Masdeu | Soleimani-Meigooni | Fortea | Lowe | Oh | Pascual | Gordon | Rosa-Neto | Baker | Johnson | Evelhoch | Betthauser | Pascoal	**Pascoal, Tharick**
139	**Predictors of data exclusion in MR-dependent imaging analyses of Alzheimer's disease**	Flores | Scott | Lu | Su | Keefe | Smith | Hornbeck | McKay | Strain | Simmons | Dombrowski | Rizzo | Shimony | Bateman | Babulal | Landau | Jagust | Wolk | Lah | Gleason | Johnson | Roberson | Sperling | Johnson | Morris | Xiong | Gordon | Benzinger	**Flores, Shaney**
140	**Brain network architecture shapes the pattern of tau-induced neuronal dysfunction in Alzheimer's disease, while tau load drives local damage**	Frontzkowski | Roemer-Cassiano | Gnörich | Dewenter | Steward | Zhu | Klonowski | Hirsch | Biel | Palleis | Höglinger | Brendel | Franzmeier	**Frontzkowski, Lukas**
141	**Cortical thickness and female sex confer resilience to tau-related cognitive decline: A large multi-cohort study**	Mitchell	**Mitchell, Stuart**
142	**Structure-guided design of 18F-FD4—a PET tracer of α-synuclein fibrils**	Liu | Li | Wang | Zuo | Tan | Bian | Fan | Liang	**Qing, Liang**
143	**NULISAseq CNS proteomic signatures of astrocytic reactivity in Alzheimer's disease**	Shi | Zeng | Balogun | Farinas | Lopresti | Gogola | Ikonomovic | Aizenstein | Villemagne | Cohen | Karikari	**Shi, Ruyu**
144	**High p-tau217 levels nullify the slower cognitive progression in younger older adults**	Shi | Choity | Brodman | Zeng | Deek | Gu | Farinas | Nafash | Bedison | Mercurio | Matan | Gogola | Kofler | Tudorascu | Nadkarni | Aizenstein | Shaaban | Lingler | Pascoal | Villemagne | Berman | Sweet | Snitz | Ikonomovic | Cohen | Kamboh | Lopez | Karikari	**Shi, Ruyu**

POSTER INDEX (by presenter's last name)

Board #	Poster Title	Authors	Presenter	Day
112	Astrocytic reactivity is related to synchronization of regional amyloid-beta deposition	Adams | Parker | Taylor | Tang | Meza | Tuteja | Avila | Chang | Simmons | Malhas | Kim | McMillan | Mapstone | Yassa	**Adams, Jenna**	3
113	Synergistic effects of amyloid-beta and hyperexcitability on tau pathology and cognitive decline	Vanderlip | Adams	**Adams, Jenna**	3
102	A pilot study on the association of plasma proteins with neuroimaging biomarkers of Alzheimer's disease in African Americans	Arowolo | Kuchenbecker | Heckman | Nguyen | Casellas | Sotelo | Schwarz | Senjem | Jain | Lucas | Willis | Ertekin-Taner | Graff-Radford | Kantarci | Lowe | Lachner | Day | Carrasquillo	**Arowolo, Olatunbosun**	3
67	MK6240 and Tauvid positivity, cognitive decline, and their relationship to Aβ PET deposition across the Alzheimer's spectrum	Bellaver | Povala | Lussier | Amaral | Bauer-Negrini | Ferreira | Jagust | Masdeu | Fortea | Tudorascu | Soleimani-Meigooni | Lowe | Oh | Pascual | Gordon | Rosa-Neto | Baker | Pascoal	**Bellaver, Bruna**	2
05	Concordance between amyloid PET and biomarkers of Alzheimer's disease in plasma and cerebrospinal fluid in cognitively unimpaired individuals	Bermudez | Fought | Hofrenning | Lowe | Petersen | Vemuri | Jack, Jr. | Algeciral-Schimnich | Bornhorst | Graff-Radford	**Bermudez, Camilo**	1
81	PET-measured amyloid accumulation rate modulates tau accumulation rate in individuals with Down syndrome	Bettcher | McLachlan | Zammit | McVea | Betthauser | Laymon | Tudorascu | Cohen | Price | Head | Mapstone | Lao | Johnson | Ances | Handen | Christian	**Bettcher, Brecca**	2
114	Amyloid does not discriminate: a meta-analysis of sex differences in Centiloids from 35,468 participants across 33 cohorts	Blazhenets | Pezzoli | Casaletto | Soleimani-Meigooni | Chiotis | Allen | Rabinovici | La Joie | Study Group	**Blazhenets, Ganna**	3
32	Effect of uptake time on [18F]-flutemetamol visual interpretation and Centiloid quantification	Bollack | Buckley | Schwarz | Battle | Smith | Stromrud | Hansson | Palmqvist | Matttsson-Carlgren | La Joie | Farrar	**Bollack, Ariane**	1
84	Associations between p-tau217 and brain atrophy are amplified by Aβ burden and APOEε4	Brown | Properzi | Cuppels | Birkenbihl | Coughlin | Seto | Townsend | Betthauser | Schultz | Chhatwal | Yang | Jacobs | Farrell | Johnson | Johnson | Li | Sperling | Hohman | Donohue | Buckley	**Brown, Jane**	2
70	Comparison of Sampled Iterative Local Approximation (SILA) implemented in R and MATLAB	Bruzzone | Coath | Navaratna | Carey | Morse | Bilgel | Betthauser	**Bruzzone, Hailey**	2
56	Blood volume influences the association between baseline plasma biomarker values and amyloid PET outcomes over time	Burns | Gogola | Zeng | Karikari | Jacobs | Lopresti | Osorio	**Burns, Kelsey**	2
41	Periventricular diffusivity moderates the relationship between astrocyte reactivity and amyloid deposition in non-demented older adults	Chen | Wu | Yang | Gogola | Luo | Villemagne | Laymon | Lopresti | Cohen | Ikonomovic | Snitz | Wilckens | Lopez | Tudorascu | Aizenstein | Minhas	**Chen, Chang-Le**	1

Board #	Poster Title	Authors	Presenter	Day
124	Alignment of antemortem images to postmortem fixed hemibrains using standard neuroimaging tools	Coath | Staruck | Carey | de Chavez | Karas | Abrahamson | Asthana | Johnson | Ikonomovic | Nirschl | Betthauser	**Coath, William**	3
125	Towards a harmonized amyloid clock: centralized image processing and temporal modeling with multiple cohorts and tracers	Coath | Bruzzone | Morse | Navaratna | Hammond | Staruck | Nowinski | Palmer | Kelley | Schwartz | Carey | Betthauser	**Coath, William**	3
51	Associations of ER176 TSPO PET with blood-based AD and neuroinflammation biomarkers	Cogswell | Lundt | Ou | Algeciras-Schimnich | Zekeridou | Lim | Graff-Radford | Schwarz | Vemuri | Petersen | Jack Jr | Lowe	**Cogswell, Petrice**	2
46	The relation of psychosocial coping mechanisms to ATN pathophysiology differ across demographics	Schatz | Snitz | Roush | Lopresti | Villemagne | Lopez | Williams | Cohen	**Cohen, Ann**	1
45	IGFR1, but not BDNF, acts as a suppressive neuroprotective factor between astrogliosis and visuospatial function among non-demented individuals	Ramirez Tirado | Cohen | Lopresti | Ikonomovic | Gogola | Matan | Zeng | Karikari | Lopez | Shaaban | Villemagne	**Cohen, Ann**	1
11	A case series of lecanemab treatment response in patients across the clinical phenotypic spectrum of AD	Corriveau-Lecavalier | Machulda | Fields | Boots | Whitwell | Day | Aduen | Frank | Kremers | Ramanan | Graff-Radford | Lowe | Boeve | Knopman | Petersen | Jack | Stricker | Jones	**Corriveau-Lecavalier, Nick**	1
07	Elevated ptau217 is more strongly associated with tau accumulation and cognitive decline in younger adults	Coughlan | Townsend | Li | Seto | Birkenbihl | Cody | Klinger | Healy | Farrell | Thibault | Rissman | Properzi | Schultz | Chhatwal | Yang | Donohue | Betthauser | Johnson | Johnson | Sperling | Buckley	**Cuppels, Madison**	1
100	Operationalizing clinical criteria for LATE using cognitive, MRI, and AD biomarker (biofluid or PET) data	Cuppels | Birkenbihl | Schneider | Bennett | Brown | Seto | Coughlan | Li | Townsend | Properzi | James | Arfanakis | Sperling | Yang | Chhatwal | Amariglio | Hohman | Donohue | Buckley	**Cuppels, Madison**	3
72	CenTauR thresholds generated using Gaussian Mixture Models for biological staging of amyloid positive ADNI participants	DelBene | Villemagne | Gogola | Leuzy | Harrison | Landau | Jagust | Lopresti	**DelBene, Alexander**	2
27	Differential sensitivity of [^{18}F]MK6240 and [^{18}F]FTP to measure tau before and after anti-amyloid therapy	Deng | Finn | Pando | Matutue | Lussier | Fortea | Tudorascu | Soleimani-Meigooni | Lowe | Oh | Gordon | Rosa-Neto | Baker | Pascoal | Masdeu | Pascual	**Deng, Han**	1
65	SPARE-SVD: An integrated machine-learning metric for cerebral small vessel disease within the ATN(V) framework	Dong | Zhang | Zeng | Wang | Wang | Toledo | Gonzales | Charisis | Rashid | Seshadri | Crane | Archer | Jefferson | Hohman | Habes	**Dong, Mengjin**	2
39	OMG: a proteomic determinant of neurodegenerative resiliency	Duggan | Oh | Frank | Gomez | Zweibaum | Cui | Chen | Surapaneni | Blew | Dark | Joynes | Kandala | Bilgel | Farinas | Erus | Tian | Candia | Pucha | Landman | Dumitrescu | Hohman | Lewis |	**Duggan, Michael**	1

Board #	Poster Title	Authors	Presenter	Day
		Moghekar | Siavoshi | Ali | Liu | Xu | Western | Kaneko | Kato | Furuichi | Shibayama | Katsuno | Nishita | Otsuka | Gottesman | Dammer | Seyfried | Levey | Johnson | Mormino | Wagner | Poston | Kapogiannis | Grams | Bhargava | Waga | Davatzikos | Resnick | Ferrucci | Bennett | Cruchaga | Wyss-Coray | Kivimäki | Coresh | Walker		
130	Plasma amyloid beta 42/40 modifies the associations between MRI biomarkers and subsequent cognitive impairment: a neuroimaging-wide longitudinal study in the BLSA	Duran | Bilgel | An | Kandala | Davatzikos | Landman | Erus | Ferrucci | Moghekar | Walker | Resnick	**Duran, Tugce**	3
104	The influence of cardiovascular risk on white matter integrity along the Alzheimer's disease trajectory: Early impact in preclinical stages	Edison | Arnold	**Edison, Paul**	3
47	Evaluation of the Clinical IMpact of Blood-Based Biomarker Assays on dementia specialists' decision-making (CIMBBBA): Preliminary report from a real-world dementia subspecialty clinic study	Eldaief | Krahn | Murdock | Rezaii | Chan | Arnold | Avetisyan | Ramirez Gomez | Gale | McGinnis | Dickerson	**Eldaief, Mark**	1
116	Contrasting neuropathology- and tau PET-based Braak stage associations with dementia severity to clarify differences between radiologic and pathologic findings	Evelhoch | Bruzzone | Rocha | Asthana | Nirschl | Johnson | Schneider | Hyman | Pascoal | Betthauser	**Evelhoch, Jeffrey**	3
66	Risk factors and AD prevention: a multivariate and multimodal study	Fajardo Valdez | Qiu | Ourry | Yakoub | Villeneuve | Research Group	**Fajardo Valdez, Alfonso**	2
96	Early concordance between Aβ PET spatial extent and plasma %ptau217	Farrell | Thibault | Yang | Price | Chhatwal | Coughlan | Buckley | Sperling | Johnson	**Farrell, Michelle**	2
12	Validation of a pseudo-reference region for [11C]-ER176 in healthy volunteers and Alzheimer's disease patients	Finn | Zanotti-Fregonara | Yu | Masdeu | Pascual	**Finn, Quentin**	1
13	β-amyloid PET signal reduction is higher in regions with ARIA-E due to anti-amyloid therapy	Finn | Pascual | Toledo | Schulz | Masdeu	**Finn, Quentin**	1
139	Predictors of data exclusion in MR-dependent imaging analyses of Alzheimer's disease	Flores | Scott | Lu | Su | Keefe | Smith | Hornbeck | McKay | Strain | Simmons | Dombrowski | Rizzo | Shimony | Bateman | Babulal | Landau | Jagust | Wolk | Lah | Gleason | Johnson | Roberson | Sperling | Johnson | Morris | Xiong | Gordon | Benzinger	**Flores, Shaney**	3
31	Predictors of longitudinal atrophy across NIA-AA biological PET stages	Fonseca | Maboudian | Chao | Jagust | Harrison	**Fonseca, Corrina**	1

Board #	Poster Title	Authors	Presenter	Day
43	Stronger amyloid–tau coupling explains faster tau progression in early-onset Alzheimer's disease	Franzmeier	Frontzkowski	Steward	Klonowski	Dewenter	Hirsch	Biel	Zhu	Gnörich	Höglinger	Brendel	Roemer-Cassiano	**Franzmeier, Nicolai**	1
140	Brain network architecture shapes the pattern of tau-induced neuronal dysfunction in Alzheimer's disease, while tau load drives local damage	Frontzkowski	Roemer-Cassiano	Gnörich	Dewenter	Steward	Zhu	Klonowski	Hirsch	Biel	Palleis	Höglinger	Brendel	Franzmeier	**Frontzkowski, Lukas**	3
02	Integrating digital cognitive metrics with PET biomarkers to identify individuals at imminent risk of tau accumulation	Fu	Robinson	Farrell	Jutten	Thibault	Thompson	Tiss	Chen	Becker	Healy	Penney	Davis	Sperling	Price	Rentz	Johnson	**Fu, Jessie Fang-Lu**	1
21	Molecular evaluation of a tau-PET analog and pathological TAR DNA-binding protein 43 docking in a cellular model of frontotemporal lobar degeneration	Gatto	Weissmann	Salinas Castellanos	Montes	Uruk	Youssef	Reichard	Josephs	**Gatto, Rodolfo**	1
04	Sex differences in white matter microstructure and associations with amyloid and tau pathology in autosomal dominant Alzheimer's disease	Giudicessi	Koops, PhD	Baena	Alvarez	Vidal	Martinez	Gonzalez	Tristão-Pereira	Malotaux	He	Aguillon	Jacobs	Cronin-Golomb	Quiroz	**Giudicessi, Averi**	1
60	Sex differences in neuroinflammation, amyloid, tau, and neurodegeneration	Guzman	Smith	Houlihan	Sanchez	Akinci	Luchsinger	Lao	**Guzman, Diana**	2
128	No detectable association between BDNF Val66Met and hippocampal volume or regional tau PET in ADNI after propensity score matching and ComBat harmonization	Han	Minhas	Laymon	Villemagne	Tudorascu	**Han, Yushui**	3
129	Centiloid and SUVR amyloid harmonization techniques comparisons for head-to-head unequally spaced data	Han	Lopresti	Bourgea	Laymon	Villemagne	Tafti	Minhas	Tudorascu	**Han, Yushui**	3
24	VeraBIND Tau: a novel plasma assay reflecting tau aggregation increases over time in individuals with positive tau-PET signal	Hanseeuw	Quenon	Bayart	Salman	Pak	Shamsundar	Soldo	Iqbal	**Hanseeuw, Bernard**	1
42	Disentangling the effects of age and Alzheimer's disease pathology on longitudinal atrophy in cognitively normal older adults	Haque	Fonseca	Maboudian	La Joie	Jagust	**Haque, Miraal**	1
06	Comparing performance of different amyloid PET markers of spatial extent in their ability to predict future amyloid conversion	Honhar	Farrell	Properzi	Thibault	Schultz	Becker	Fu	Sperling	Price	Johnson	**Honhar, Praveen**	1
30	Neuroimaging compendium of microglia, amyloid, tau, and neurodegeneration across clinical variants of Alzheimer's disease	Houlihan	Guzman	Smith	Sanchez	Kreisl	Cosentino	Noble	Lao	**Houlihan, Hannah**	1
14	Lifetime and 10-year absolute risk of cognitive impairment associated with	Hu	Therneau	Wiste	Knopman	Vemuri	Graff-Radford	Lowe	Vassilaki	Cogswell	Schwarz	**Hu, Mingzhao**	1

Board #	Poster Title	Authors	Presenter	Day
	amyloid PET severity: a retrospective, longitudinal cohort study	Algeciras-Schimnich | Petersen | Jack Jr.		
122	Cerebral vessel morphology is associated with white matter lesions burden	Huang | Li | Rocha | Stetten | Yang | Ibrahim | Wu | Aizenstein	**Huang, Yuanzhe**	3
135	Integration of network analysis of the plasma proteome with Alzheimer's disease neuroimaging outcomes in an African American cohort	Hurst | Kuchenbecker | Heckman | Nguyen | Casellas | Sotelo | Shwarz | Senjem | Jain | Lucas | Willis | Ertekin-Taner | Graff-Radford | Kantarci | Lowe | Lachner | Day | Carrasquillo	**Hurst, Cheyenne**	3
119	Associations of regional neuroinflammation by ER176 PET SUVR with cognitive scores	Jacobson | Lim | Lundt | Nycklemoe | Min | Botha | Graff-Radford | Jones | Vemuri | Kantarci | Knopman | Jack | Petersen | Lowe	**Jacobson, David**	3
110	Effects of regional tau accumulation on visual discrimination of novel objects in clinically unimpaired older adults	Kapadia | Medina Guerra | Sai | Bonnen | Wagner | Mormino | Trelle	**Kapadia, Dhruv**	3
73	Progression to tau-PET positivity by plasma P-tau217 levels and its association with clinical decline in preclinical Alzheimer's disease: data from A4 study	Kim | Kotari | Morris | Shcherbinin | Yaari | Holdridge | Sims | Ossenkoppele | Collins | Hansson | Lu	**Kim, Min Jung**	2
95	Integration of data-driven biomarker discovery with established Alzheimer's disease biomarkers in an African American cohort	Kuchenbecker | Heckman | Nguyen | Casellas | Sotelo | Schwarz | Senjem | Jain | Lucas | Willis | Ertekin-Taner | Graff-Radford | Kantarci | Lowe | Lachner | Day | Carrasquillo	**Kuchenbecker, Lindsey**	2
53	Temporal dynamics of tau PET subtypes and its association with heterogeneous neurodegeneration in Alzheimer's disease	Kwon | Song | Lee | Seong	**Kwon, Tae Youn**	2
54	A-T-N-C generative model for predicting and simulating patient-tailored cognitive decline trajectories in Alzheimer's disease	Lee | Song | Kwon | Lee | Seong	**Kwon, Tae Youn**	2
20	Neuropathological validation of Tau-PET CenTauR units: Preliminary data from a multicenter study	Iaccarino | Chiotis | Grinberg | Kotari | La Joie | Leuzy | Lowe | Lu | Moscoso | Nguyen | Schwarz | Seeley | Jack | Rabinovici | Shcherbinin	**La Joie, Renaud**	1
23	Microstructural white matter injury mediates the association between vascular risk and plasma biomarkers: Preliminary findings from the Diverse VCID study	Lee | Sapkota | Rajan | Jin | Hinman | Johnson | Harvey | Maillard | Fornage | DeCarli	**Lee, Seunghoon**	1
108	Longitudinal evaluation of neuroinflammation using 11C-ER176 TSPO PET	Lim | Cogswell | Min | Lee | Brunn | Kandimalla | Jacobson | Nycklemoe | Lee | Lundt | Botha | Graff-Radford | Jones | Vemuri | Kantarci | Jack | Petersen | Lowe	**Lim, Seokbeen**	3
109	Comparison of meningeal signal between [^{18}F]AV-1451 and [^{18}F]MK-	Lim | Gunter | Baker | Tissot | Brunn | Soleimani-Meigooni | Oh | Fortea |	**Lim, Seokbeen**	3

Board #	Poster Title	Authors	Presenter	Day
	6240 tau PET using a distance-based meningeal mask	Pascual | Gordon | Rosa-Neto | Pascoal | Klunk | Jagust | Senjem | Botha | Knopman | McCarter | Ramanan | Graff-Radford | Schwarz | Kantarci | Boeve | Vemuri | Jones | Jack | Petersen | Lowe		
92	Assessing the generalizability of plasma p-tau217 cutpoints for amyloid-β detection across clinical and preclinical cohorts	Liu | Zeng | Nafash | Sehrawat | Choity | Gu | Farinas | Bedison | Matan | Gogola | Huang | Sewell | McAuley | Hillman | Kramer | Burns | Kang | Vidoni | Nadkarni | Aizenstein | Kofler | Tudorascu | Shaaban | Lingler | Pascoal | Villemagne | Berman | Sweet | Snitz | Ikonomovic | Kamboh | Erickson | Cohen | Lopez | Deek | Karikari	**Liu, Tianshu**	2
93	Evaluating the transferability of dual cutpoints for plasma p-tau217 in detecting brain amyloid-β across diverse cohorts	Liu | Zeng | Nafash | Sehrawat | Choity | Gu | Farinas | Bedison | Matan | Gogola | Huang | Sewell | McAuley | Hillman | Kramer | Burns | Kang | Vidoni | Nadkarni | Aizenstein | Kofler | Tudorascu | Shaaban | Lingler | Pascoal | Villemagne | Berman | Sweet | Snitz | Ikonomovic | Kamboh | Erickson | Cohen | Lopez | Deek | Karikari	**Liu, Tianshu**	2
64	Standardized indices of tau burden using the CenTauR universal scale predict distinct cognitive trajectories across Alzheimer's disease biological stages	Lopresti | DelBene | Leuzy | Gogola | Harrison | Landau | Jagust | Villemagne	**Lopresti, Brian**	2
107	Perivascular spaces: Predictors of longitudinal amyloid, tau, cerebrovascular biomarkers?	Low | Gunter | Hu | Raghavan | Przybelski | Schwarz | Kantarci | Lowe | Graff-Radford | Petersen | Jack | Vemuri	**Low, Audrey**	3
127	Gaussian smoothing and partial volume correction modify relationships of tau burden with biological variables in longitudinal multi-site studies of 18F-Flortaucipir PET	Luo | Laymon | Baker | Cohen | Villemagne | Lopresti | Aizenstein | Tudorascu | Minhas	**Luo, Weiquan**	3
28	Development of a highly sensitive and automated immunoassay for Brain-Derived pTau-217: Analytical performance in human plasma samples	Ma | Wang | Danthanarayana | Kim | Ji | Jhaveri | Zhang | Qiu | Mudumba | Luo	**Ma, Xiao-Jun**	1
22	Anterior cingulate sulcal pattern is associated with successful cognitive aging	Maboudian | Kellerman | Willbrand | Pezzoli | Weiner | Jagust	**Maboudian, Samira**	1
36	Examining elevated choroid plexus binding of tau PET tracers in aging and Alzheimer's disease	Marin | Wales | Ruais | Richard | Hedden	**Marin, Anna**	1
76	Tau accumulation drives worsening depressive symptoms in cognitively normal older adults	Markova | Berry	**Markova, Teodora**	2

Board #	Poster Title	Authors	Presenter	Day
77	Dorsal raphe nucleus and locus coeruleus differentially relate to depressive symptoms in cognitively normal older adults	Markova | Chen | Carlson | Cao | Ciampa | Marcus | Adornato | Matulonis | Morin | Hooker | Berry	**Markova, Teodora**	2
105	Longitudinal tau PET progression follows language network spread in primary progressive aphasia	Martersteck | Rogalski	**Martersteck, Adam**	3
83	Assessing the effect of amyloid status on the relationship between glucose metabolism and synaptic density in the aging population	McLachlan | Bettcher | DiFilippo | LeMerise | McVea | Zammit | Langhough | Johnson | Bendlin | Christian	**McLachlan, Max**	2
40	Frequency and consequences of extreme PET based pathological profiles in preclinical Alzheimer's disease	Medina Guerra | Cody | Young | Sheng | Sokolowski | Younes | Trelle | Tosun | Hohman | Mormino	**Medina Guerra, Lucah**	1
141	Cortical thickness and female sex confer resilience to tau-related cognitive decline: A large multi-cohort study	Mitchell	**Mitchell, Stuart**	3
35	Systemic inflammation–tau interaction: Insights from CRP modulation of p-tau217 association with tau PET positivity	Monto | Boots | Zeng | Farinas | Sehrawat | Saeed | Cohen | Reis | Lopez | Snitz | Karikari	**Monto, Abdul Razak**	1
34	Relationship between p-tau217 and PET in preclinical AD: The moderating effect of white matter hyperintensity	Moon | Chen	**Moon, Hasom**	1
26	Stratifying preclinical Alzheimer's disease by hippocampal volume to detect concomitant LATE	Mundada | Lyu | Sadeghpour | Brown | McGrew | Yushkevich | Das | Wolk	**Mundada, Nidhi**	1
48	Dynamic interplay of vascular injury and inflammation on Alzheimer's disease pathophysiology	Rusdi | Kang | Yin | Gibson | Rahmouni | Benedet | Zetterberg | Blennow | Karikari | Ashton | Black | Rosa-Neto | Goubran | Ottoy	**Ottoy, Julie**	1
18	Association of combined cardiovascular risk factors and treatments with longitudinal amyloid and tau PET in cognitively normal older adults	Ourry | Thériault-Dubé | Breitner | Poirier | Villeneuve	**Ourry, Valentin**	1
75	Age-dependent associations between salivary inflammatory cytokines and amyloid-beta in cognitively unimpaired older adults	Parker | Tang | Taylor | Bock | Meza | Tuteja | Avila | Chang | Simmons | Bamford | Yi | Mcmillan | Kim | Thomas | Adams | Yassa	**Parker, Dana**	2
57	Visual interpretation methods for tau-PET imaging with Flortaucipir and MK-6240: Insights from the HEAD study	Ruppert | Vermeiren | Scop Medeiros | Povala | Rocha | Soares | Ferreira | Amaral | Bauer-Negrini | Lussier | Scarpatto Rodrigues | Oliveira Jr. | Mroue | Bellaver | Moscoso | Ossenkoppele | van de Giessen | Masdeu | Tudorascu | Soleimani-Meigooni | Fortea | Lowe | Oh | Pascual | Gordon | Rosa-Neto | Baker | Pascoal	**Pascoal, Tharick**	2

Board #	Poster Title	Authors	Presenter	Day
137	MK6240 and Flortaucipir Braak staging agreement in a head-to-head cohort	Rocha | Soares | Ruppert | Medeiros | Bellaver | Povala | Ferreira | Bauer-Negrini | Lussier | Tudorascu | Masdeu | Soleimani-Meigooni | Fortea | Lowe | Oh | Pascual | Gordon | Rosa-Neto | Baker | Pascoal	**Pascoal, Tharick**	3
138	Comparing neuropathologic and tau-PET Braak staging across clinical progression using MK6240 and flortaucipir	Rocha | Bruzzone | Ruppert | Medeiros | Soares | Bellaver | Povala | Ferreira | Lussier | Masdeu | Soleimani-Meigooni | Fortea | Lowe | Oh | Pascual | Gordon | Rosa-Neto | Baker | Johnson | Evelhoch | Betthauser | Pascoal	**Pascoal, Tharick**	3
115	Preliminary associations of plasma phosphorylated tau217 with regional tau deposition and accumulation in medial temporal and neocortical regions	Pintucci | Thibault | Farrell | Yang | Chhatwal | Properzi | Becker | Price | Sperling | Johnson	**Pintucci, Eva**	3
68	Differential tau-PET load predominance along shared progression trajectories determines clinical variability in Alzheimer's disease	Mroué | Povala | Bellaver | Lukasewicz Ferreira | Bauer-Negrini | Lussier | Amaral | Scop Medeiros | Ruppert | Silva da Rocha | Scarpatto Rodrigues | Silva Oliveira | Soares Katz | Teixeira Leffa | Saha | Masdeu | Soleimani-Meigooni | Fortea | Lowe | Oh | Pascual | Gordon | Rosa-Neto | Baker | Pascoal	**Povala, Guilherme**	2
69	Head-to-head comparison of tau PET tracers across the Alzheimer's disease spectrum: baseline results from the HEAD study	Povala | Bellaver | Lussier | Amaral | Bauer-Negrini | Ferreira | Jagust | Masdeu | Fortea | Tudorascu | Soleimani-Meigooni | Lowe | Oh | Pascual | Gordon | Rosa-Neto | Baker | Pascoal	**Povala, Guilherme**	2
101	CT-based processing is equivalent to MR-based processing for tau PET regional quantification	Povala | Bellaver | Amaral | Lussier | Ferreira | Bauer-Negrini | Tudorascu | Masdeu | Fortea | Soleimani-Meigooni | Lowe | Oh | Pascual | Gordon | Rosa-Neto | Baker | Pascoal	**Povala, Guilherme**	3
142	Structure-guided design of 18F-FD4—a PET tracer of α-synuclein fibrils	Liu | Li | Wang | Zuo | Tan | Bian | Fan | Liang	**Qing, Liang**	3
62	Intersections of gender/sex and neighborhood deprivation on cognition: Are there mediation effects of Alzheimer's disease biomarkers?	Reese | Royse | Snitz | Crane | Mukherjee | Choi | Hengenius | Huppert | Roush | Cisneros | Lopresti | Rameriz Tirado | Willie-Permor | Felix | Cohen | Shaaban	**Reese, Alexandria**	2
106	The adjusted Centiloid: Improving reliability by correcting for white matter uptake variability	Reilhac | Irizarry | Reyderman | Charil	**Reilhac, Anthonin**	3
01	Longitudinal harmonization effects on tau-PET SUVRs trajectories in ADNI study	Ren | Luo | Laymon | Minhas | Cohen | Wu | Tudorascu	**Ren, Yuxin**	1
118	Digital maze test reveals features related to cortical tau in cognitively normal Aβ+ older adults	Robinson | Fu | Amariglio | Sperling | Johnson | Davis | Penney | Rentz	**Robinson, Talia**	3

Board #	Poster Title	Authors	Presenter	Day
103	Amyloid-PET and white matter hyperintensities but not military service duration nor combat exposure are associated with neurodegeneration and cognitive impairment in older veterans	Rocha | Pasternak | Lesman Segev | Schwartz | Blazhenets | Maiti | Rosen Lang | Hantke | Livny-Ezer | Yaffe | Shaw | Weiner | Hills | Kritikos | Soleimani-Meigooni | Silbert | La Joie | Gardner	**Rocha, Salma**	3
03	Amyloid-induced neuronal hyperactivity and metabolism are associated with faster tau accumulation in Alzheimer's Disease	Roemer-Cassiano | Zhang | Evangelista | Klonowski | Hirsch | Frontzkowski | Steward | Dewenter | Biel | Zhu | Gnoerich | Jaekel | Hoeglinger | Brendel | Yeo | Franzmeier	**Roemer-Cassiano, Sebastian**	1
111	Key quantitative benchmarks with CenTauR in cross-sectional and longitudinal large datasets	Dore | Bourgeat | Betthauser | Feizpour | Moscoso | Leuzy | Fripp | Johnson | Rowe | Villemagne	**Rowe, Christopher**	3
131	High-resolution NAV template using the Siemens Biograph Vision	Bourgeat | Rowe | Paranawithana | Feizpour | Huang | Villemagne | Fripp | Dore	**Rowe, Christopher**	3
132	Higher clinical throughput quantitative amyloid-β PET using abbreviated acquisition windows	Paranawithana | Gillman | Bourgeat | Fripp | Villemagne | O'Keefe | Huang | Benzinger | LaMontagne | Morris | Doré | Rowe	**Rowe, Christopher**	3
59	Regional white matter injury modifies the association between ß-amyloid and cognition	Royse | Reese | Snitz | Hengenius | Crane | Mukherjee | Choi | Willie-Permor | Felix | Huppert | Roush | Cisneros | Potopenko | Lopresti | Cohen | Shaaban	**Royse, Sarah**	2
55	High-resolution ex-vivo MRI reveals layer-specific atrophy of hippocampal subregions to earliest tau pathology	Salman | Tomé | Joudiou | Thal | Annettesdotter | Khandelwal | Yushkevich | Gallez | Wisse | Hanseeuw	**Salman, Yasmine**	2
09	Distinct mechanisms underlying APOE-ε4 and sex effects on medial temporal tau pathology: A neuropathology study	Salvadó | Groot | Wisse | Vogel | Beach | Serrano | Reiman | Schneider | Bennett | Ossenkoppele | Hansson	**Salvadó, Gemma**	1
74	Neuroimaging correlates of loneliness	Sanchez | Guzman | Smith | Houlihan | Stern | Bockting | Lao	**Sanchez, Thairi**	2
49	CSF oligodendrocyte biomarkers are associated with amyloid burden in Alzheimer's disease	Santos Machado | De Bastiani | Lebrun | Povala | Pola | Vizlin-Hodzic | Rosa-Neto | Zimmer | Blennow | Zetterberg | Benedet | Ashton	**Santos Machado, Luiza**	2
94	Free-water interacts with amyloid positivity to predict regional tau pathology in both early and late Braak stages	Sathe | Durant | Koran | Dumitrescu | Cody | Sokołowski | Kim | Mez | Saykin | Toga | Cuccaro | Tosun | Johnson | Barber | O'Bryant | Landman | Mormino | Hohman | Archer	**Sathe, Aditi**	2
37	The influence of β-amyloid on neuroinflammatory 11C-ER176 uptake in progressive apraxia of speech	Satoh | Utianski | Duffy | Clark | Botha | Lowe | Josephs | Whitwell	**Satoh, Ryota**	1
38	Subtracting first principal component may improve detectability of subtle 4R tau signals in 18F flortaucipir tau PET imaging	Satoh | Ali | Clark | Dickson | Lowe | Josephs | Whitwell	**Satoh, Ryota**	1

Board #	Poster Title	Authors	Presenter	Day
19	Amyloid-pet substantiates clinical decision-making in real-life clinical settings in Brazil	Schaffer Aguzzoli | Flach | Alves Da Silva | C.L Ferreira | Povala | Ferrari-Souza | Bieger | Teixeira Leffa | Bellaver | Guevara Werlang | Teribele Venturin | Wetters Portuguez | Possa Marroni | Irigoyen da Costa | Bernardi Soder | Sebastião Matushita | Juarez Amorim | Pasquotto Souza | Dario Ramos | Leite | Hygino | Amorim Nogueira | Sturzeneker Tres | Okada de Oliveira | Moriguchi Jeckel | Cortes Domingues | Mosci | Rosado de Castro | Buchpiguel | Paiva Proença Lobo Lopes | Carvalho Campos Neto | Figueiredo Balthazar | Tovar Moll | Martins Novaes Coutinho | Pascoal | Zimmer | Schilling | Costa da Costa	**Schaffer Aguzzoli, Cristiano**	1
17	Predicting tau PET burden using brain-derived plasma p-tau measures in the British 1946 birth cohort	Schott | Coath | Wiltshire | Brown | Cash | Whittington | Heslegrave | Zetterberg | Keshavan	**Schott, Jonathan**	1
78	Evaluating occipital-to-global amyloid PET as a predictor of CAA at autopsy in Mayo Clinic cohorts	Schwarz | Hu | Cogswell | Graff-Radford | Vemuri | Przybelski | Wiste | Nguyen | Reichard | Dickson | Lowe | Ramanan | Knopman | Petersen | Jack	**Schwarz, Christopher**	2
79	SCAN: Standardized Centralized Alzheimer's and related dementias Neuroimaging	Schwarz | Harrison | DeCarli | Kantarci | Baker | La Joie | Maillard | Rabinovici | Toga | Jack | Jagust	**Schwarz, Christopher**	2
97	Longitudinal trajectories of plasma p-tau217 across multiple assays in relation to amyloid and tau PET and cognition	Shekari | Tosun | Dage | Schindler | Shaw | Jagust | Landau	**Shekari, Mahnaz**	3
123	Early ventral temporal tau burden marks functional vulnerability in aging	Sheng | Trelle | Sai | Young | Romero | Park | Vossler | Younes | Davidzon | Wagner | Mormino	**Sheng, Jintao**	3
143	NULISAseq CNS proteomic signatures of astrocytic reactivity in Alzheimer's disease	Shi | Zeng | Balogun | Farinas | Lopresti | Gogola | Ikonomovic | Aizenstein | Villemagne | Cohen | Karikari	**Shi, Ruyu**	3
144	High p-tau217 levels nullify the slower cognitive progression in younger older adults	Shi | Choity | Brodman | Zeng | Deek | Gu | Farinas | Nafash | Bedison | Mercurio | Matan | Gogola | Kofler | Tudorascu | Nadkarni | Aizenstein | Shaaban | Lingler | Pascoal | Villemagne | Berman | Sweet | Snitz | Ikonomovic | Cohen | Kamboh | Lopez | Karikari	**Shi, Ruyu**	3
90	Differential sensitivity of T1-MRI and FDG-PET for tracking neurodegeneration across progressive stages of tau pathology in Alzheimer's disease	Vourkas | Karagianni | Moscoso | Zhang | Sanchez-Juan | Schöll | Grothe | Silva-Rodríguez	**Silva-Rodríguez, Jesús**	2
85	Early cortical thickness change in preclinical AD development	Sinclair | Chen	**Sinclair, Stephanie**	2

Board #	Poster Title	Authors	Presenter	Day
80	Differential contributions of amyloid spatial extent and tau burden to domain-specific cognitive decline in early Alzheimer's disease	Slade | Thibault | Thompson | Fanglu Fu | Price | Rentz | Sperling | Johnson | Farrell	**Slade, Elliott**	2
58	Associations between TSPO PET and CSF and blood-based biomarkers	Smith | Guzman | Houlihan | Sanchez | Kreisl | Talmasov | De Jager | Herman | Simoes | Small | Lao	**Smith, Anna**	2
63	Disentangling cognitive severity and phenotype across dementia syndromes	Smith | Coyle-Gilchrist | Murley | Rouse | Stockton | Naessens | Savulich | Wiggins | Malpetti | Bowns | Perquin | Lanskey | Karadag | Kocagoncu | Quinn | Pitt | Alcock | O'Brien | Rittman | Rowe | Lambon-Ralph	**Smith, Viktorija**	2
08	Quantitative relationship between Lumipulse G measures of pTau217 in plasma and in brain	Vandenberghe | Tomé | De Meyer | Goossens | Lambrechts | Poesen | Vanbrabant | Vanmechelen | Thal	**Thal, Dietmar**	1
82	Elevated medial temporal lobe tau predicts cross-sectional association between neocortical tau and global amyloid burden	Thibault | Reilhac-Laborde | Charil | Irizarry | Johnson	**Thibault, Emma**	2
126	Cluster-based MK-6240 PET detects early neocortical temporal tau spread	Thompson | Becker | Fanglu Fu | Farrell | Thibault | Slade | Sperling | Price | Johnson	**Thompson, Jackson**	3
117	Novel pet tracer [11C]-CS1P1 uptake reflects decreased sphingosine-1-phosphate receptor 1 activity in vivo in Alzheimer's disease and related dementias	Tiemann Powles | Friedrichsen | Flores | Rajamanickam | Keefe | Simmons | Doering | McKay | Hoagey | Sabaredzovic | Ibanez | Morris | An | Brier | Tu | Benzinger	**Tiemann Powles, Savannah**	3
52	Evaluation of [18F]MK6240 test-retest reproducibility for different processing pipelines	Tiss | Thibault | Fu | Becker | Price | Johnson	**Tiss, Amal**	2
133	Tracer-specific effects of hormone replacement therapy on age-related tau accumulation	Tissot | Shi | Tsai | Maboudian | Fonseca | Rahmouni | Lussier | Therriault | Trudel | Cassa Macedo | Stevenson | Bellaver | Ferreira | Povala | Gordon | Pascual | Lowe | Soleimani-Meigooni | Oh | Klunk | Rosa-Neto | Jagust | Buckley | Pascoal | Baker	**Tissot, Cécile**	3
134	Cognitive and age-related differences in low-tau individuals assessed with [18F]FTP and [18F]MK6240	Tissot | Shankar | Tsai | Rahmouni | Lussier | Therriault | Trudel | Cassa Macedo | Stevenson | Bellaver | Ferreira | Povala | Gordon | Pascual | Lowe | Soleimani-Meigooni | Oh | Klunk | Rosa-Neto | Jagust | Landau | Pascoal | Baker	**Tissot, Cécile**	3
10	Harmonizing amyloid PET tracers at the regional level: evaluation of regional centiloid equations	Silvestri | Chaggar | Gobbi | Aldea | Klein | Tonietto	**Tonietto, Matteo**	1
25	Amyloid PET quantitation using skewness: Autopsy validation and test-retest performance	Tunali | Iaccarino | Wang | Kennedy | Lu | Shcherbinin	**Tunali, Ilke**	1
120	Cluster-based metric of early tau-PET aggregation is associated with plasma	Varghese | Brock | Taylor | Thomas | Yassa | Adams	**Varghese, Leah**	3

Board #	Poster Title	Authors	Presenter	Day
	p-tau217 in cognitively unimpaired older adults with subthreshold amyloid-beta			
16	Associations between tau pathology and cortical microstructure are modulated by amyloid burden independent of cortical atrophy in cognitively unimpaired older adults	Vogt | Koops | Schultz | Properzi | Salat | Pascual-Leone | Huang | Buckley | Rentz | Johnson | Sperling | Jacobs	**Vogt, Nicholas**	1
91	SPARE-Tau, a machine-learning derived tau-PET index, correlates with Alzheimer's disease and related dementias biomarkers	Wang | Zeng | Toledo | Gonzales | Honnorat | Charisis | Dong | Ho | Rashid | Kutty | Salman | Vroman | Seshadri | Habes	**Wang, David**	2
61	Evaluation of the tau PET ligand [18F]florzolotau in frontotemporal dementia	Clarke | Whittington | Sholaja | Hield | Huiban | van den Berg | Margolin | Rowe | Rohrer | Salinas | Rabiner	**Whittington, Alex**	2
98	The relation of psychosocial coping mechanisms to ATN pathophysiology differ across demographics.	Schatz | Snitz | Roush | Lopresti | Villemagne | Lopez | Williams | Cohen	**Williams, Lilcelia**	3
71	Agreement between amyloid status prediction from visual read, SUVR thresholding, and AI-based interpretation of amyloid PET	Peraza | Joules | Mohs | Beauregard | Dwyer | Hughes | Wolz	**Wolz, Robin**	2
86	Immuno-vascular crosstalk drives tau pathology preferentially in women	Wood Alexander | Kang | Rusdi | Yin | Rahmouni | Wang | Benedet | Zetterberg | Blennow | Karikari | Ashton | Black | Goubran | Rabin | Ottoy	**Wood Alexander, Madeline**	2
87	Midlife physical activity attenuates the association of earlier menopause with tau pathology and cognitive decline	Wood Alexander | Cadwallader | Johnson | Casaletto | Rabin	**Wood Alexander, Madeline**	2
29	Network-based mechanistic modeling of Alzheimer's disease for evaluating diverse therapeutic mechanisms of action	Wooten | Stage | Mazer | Townsend | Comley | Guo	**Wooten, Dustin**	1
50	Associations between systolic blood pressure and amyloid burden on cross-sectional inferior temporal tau across mid- to late-life	Yau | Scott | Palmgren | Coughlan | Kirn | Properzi | Schultz | Ghosh | Buckley | Amariglio | Rentz | Johnson | Sperling | Beiser | Seshadri | Chhatwal	**Yau, Wai-Ying Wendy**	2
121	Sex differences in regional Aβ burden are associated with decreased cingulum integrity uniquely in older cognitively unimpaired women	Yi | Parker | Tang | Taylor | Tuteja | Meza | Avila | Chang | Simmons | Bamford | McMillan | Kim | Thomas | Adams | Yassa	**Yi, Emily**	3
88	Improved tau PET signal detection with total-body PET compared to conventional PET: A preliminary study	Young | Bayerlein | Bhattarai | DeCarli | Badawi | Fan	**Young, Christina**	2
89	Demographic associations with plasma biomarkers in the oldest-old: The LifeAfter90 Study	Young | Colbeth | Gilsanz | Corrada | Rizvi | Zhou | di Lucente | DeCarli | Jin | Whitmer	**Young, Christina**	2
33	Episodic memory decline and tau biomarkers progress earlier along the amyloid timeline in Down syndrome compared to neurotypical adults	Zammit | Bruzzone | Morse | Batchelar | Bettcher | McLachlan | McVea | Carey | Tudorascu | Hartley | Clark | Ances | Caldwell | Johnson | Handen | Head |	**Zammit, Matt**	1

Board #	Poster Title	Authors	Presenter	Day
		Mapstone | Christian | Investigators | Betthauser		
15	Trajectory of neurodegeneration and brain aging in relation to amyloid timing and duration	Zhang | Robb | Erus | Castellano | Cui | Cody | Harrison | Engelman | Albert | Resnick | Sperling | Bilgel | Vardarajan | Mayeux | Risacher | Arfanakis | Tosun | Habes | Wang | Toga | Thompson | Kukull | Biber | Landman | Bendlin | Johnson | Schneider | Barnes | Bennett | Saykin | De Jager | Menon | Harrison | Mormino | Cuccaro | Davatzikos | Betthauser | Archer | Hohman | Dumitrescu | Koran	**Zhang, Mengna**	1
44	Harmonization methods to mitigate batch effects in blood biomarker analysis	Zhang | Lukasewicz Ferreira | Minhas | Pascoal | Zeng | Karikari | Cohen | Tudorascu	**Zhang, Vivian**	1
99	Intermediate blood-based biomarker status clarified by PET and CSF in cognitively impaired individuals	Ziontz | Blazhenets | Lin | Landau | Shaw | Dage | Hammers | Eloyan | Koeppe | Carillo | Dickerson | Rabinovici | La Joie	**Ziontz, Jacob**	3

HAI 2026 PROGRAM

Monday, January 12, 2026		
08:00 am - 08:30 am	*Check-in and Breakfast*	
08:30 am - 08:45 am	**Welcome Notes**	**Keith Johnson**, Massachusetts General Hospital, Boston, MA, USA
08:45 am - 08:55 am	**Alzheimer's Association Note**	**Maria Carrillo**, Alzheimer's Association, Chicago, IL, USA
08:55 am - 10:25 am	**SESSION I: Amyloid-beta pathology: PET imaging**	**Chairs:** **Keith Johnson**, Massachusetts General Hospital, Boston, MA, USA **Christopher Rowe**, Austin Health, Melbourne, Vic, Australia
08:55 am - 09:00 am	Session Overview	Chairs
09:00 am – 09:15 am	Auto-rADiology: Toward automated and explainable amyloid-PET interpretation using deep learning	**Yu Xiao**, Lund University, Lund, Sweden
09:15 am – 09:30 am	Choroidal-ventricular remodeling is associated with amyloid aggregation in Alzheimer's disease	**Brandon Hall**, McGill University, Montréal, QC, Canada
09:30 am – 09:45 am	Updated evaluation of the baseline distribution of amyloid positivity and cognitive impairment among adults with Down syndrome in the ABC-DS project	**Max McLachlan**, University of Wisconsin-Madison, Madison, WI, USA
09:45 am – 10:00 am	Heterogeneous patterns of off target signal with [18F]flutafuranol PET in ADNI4	**Renaud La Joie**, University of California, San Francisco, San Francisco, CA, USA
10:00 am - 10:25 am	Discussion	
10:25 am - 10:30 am	**Blitz Session 1A: Short Poster Presentations**	
	Stronger amyloid–tau coupling explains faster tau progression in early-onset Alzheimer's disease	**Nicolai Franzmeier,** LMU University Hospital, Ludwig-Maximilians-University (LMU) Munich, Germany
	Amyloid-induced neuronal hyperactivity and metabolism are associated with faster tau accumulation in Alzheimer's Disease	**Roemer-Cassiano, Sebastian**, University Hospital, LMU Munich, Germany
	Episodic memory decline and tau biomarkers progress earlier along the amyloid timeline in Down syndrome compared to neurotypical adults	**Matt Zammit**, University of Wisconsin, Madison, WI, US
10:30 am - 11:30 am	**Poster Session 1A**	
11:30 am - 01:00 pm	**SESSION II: Tau pathology: In vivo and postmortem measurements**	**Chairs:** **Bradley Christian,** University of Wisconsin-Madison, Madison, WI, USA **Melissa Murray,** Mayo Clinic, Jacksonville, FL, USA
11:30 am - 11:35 am	Session Overview	Chairs
11:35 am – 11:50 am	The effects of 18F-MK-6240 PET extracerebellar off-target signal on the cerebellum and its substructures	**Charles Chen**, Athinoula A. Martinos Center for Biomedical Imaging, Charlestown, MA, USA

Monday, January 12, 2026		
11:50 am – 12:05 pm	Examining spatial relationships between ex-vivo flortaucipir retention and TMEM106b protein expression in a subset of neuropathologically confirmed frontotemporal lobar degeneration cases with TAR DNA-binding protein 43 pathology	**Rodolfo Gatto**, Mayo Clinic, Rochester, MN, USA
12:05 pm – 12:20 pm	Hypometabolism and atrophy patterns associated with advanced primary age-related tauopathy mimicking early-stage AD	**Jesús Silva-Rodríguez**, CIEN Foundation, Madrid, Spain
12:20 pm – 12:35 pm	Differential age- and Aβ-related tau-PET patterns between [18F]FTP and [18F]MK6240	**Cécile Tissot**, Lawrence Berkeley National Laboratory, Berkeley, CA, USA
12:35 pm - 01:00 pm	Discussion	
01:00 pm - 02:00 pm	Lunch break	
02:00 pm - 02:30 pm	Keynote: **The neuropathological basis of current AD biomarkers: Sensitivity and pathogenetic implications**	**Dietmar Thal**, KU Leuven, Leuven, Belgium
02:30 pm - 02:45 pm	Keynote Discussion	
02:45 pm - 04:15 pm	**SESSION III: Alzheimer's disease biological staging and applications**	**Chairs:** **Tobey Betthauser**, University of Wisconsin-Madison, Madison, WI, USA **Thomas Karikari**, University of Pittsburgh, Pittsburgh, PA, USA
02:45 pm - 02:50 pm	Session Overview	Chairs
02:50 pm – 03:05 pm	Combining quantitative and visual read approaches to tau-PET positivity and staging: The Tau-PET Working Group	**Gil Rabinovici**, University of California San Francisco, San Francisco, CA, USA
03:05 pm – 03:20 pm	Association between PET-based Alzheimer's disease biological stage and autopsy findings	**Derek Johnson**, Mayo Clinic, Rochester, MN, USA
03:20 pm – 03:35 pm	Associations among plasma p-tau217, amyloid PET, tau PET, and cognitive testing in the screening cohort for the AHEAD 3-45 Study	**Reisa Sperling**, Brigham and Women's Hospital, Massachusetts General Hospital, Harvard Medical School, Boston, MA, USA
03:35 pm – 03:50 pm	Genetic predictors of multimodal brain tau pathology in older adults	**Ting-Chen Wang**, Vanderbilt University Medical Center, Nashville, TN, USA
03:50 pm - 04:15 pm	Discussion	
04:15 pm - 04:20 pm	**Blitz Session 1B: Short Poster Presentations**	
	OMG: a proteomic determinant of neurodegenerative resiliency	**Michael Duggan,** NIH, Baltimore, MD, USA
	Lifetime and 10-year absolute risk of cognitive impairment associated with amyloid PET severity: a retrospective, longitudinal cohort study	**Mingzhao Hu,** Mayo Clinic, Rochester, MN, USA
	Stratifying preclinical Alzheimer's disease by hippocampal volume to detect concomitant LATE	**Nidhi Mundada,** University of Pennsylvania, Philadelphia, PA, USA
04:20 pm - 05:20 pm	**Poster Session 1B**	
05:20 pm – 05:25 pm	The PET-tle Royale (HAI's very own synaptic showdown quiz)	**Christopher Schwarz**, Mayo Clinic, Rochester, MN, USA
05:30 pm - 07:30 pm	Welcome Reception	

Tuesday, January 13, 2026		
08:00 am - 08:30 am	*Check-in and Breakfast*	
08:00 am - 08:30 am	Mentoring Session	
08:30 am - 09:45 am	**ISTAART Collaborations:** **Neuroimaging in clinical decision making: presentation and interactive discussion of real-world cases to identify evolving research needs** *Session Organizers: Tobey Betthauser, Alexa Pichet Binette, Yara Yakoub*	**Chairs:** **Alexa Pichet Binette**, University of Montreal, Montreal, QC, Canada **Tobey Betthauser**, University of Wisconsin-Madison, Madison, WI, USA **Kathleen Poston**, Stanford University, Stanford, CA, USA
08:30 am – 08:35 am	Session Introduction	
08:35 am – 08:50 am	Case 1	**Petrice Cogswell**, Mayo Clinic, Rochester, MN, US
08:50 am – 09:05 am	Case 2	**Christopher Rowe**, Austin Health, Melbourne, Vic, Australia
09:05 am – 09:20 am	Case 3	**Gil Rabinovici**, University of California San Francisco, San Francisco, CA, USA
09:20 am – 09:45 am	Discussion	
09:45 am - 09:50 am	**Blitz Session 2A: Short Poster Presentations**	
	Early concordance between Aβ PET spatial extent and plasma %ptau217	**Michelle Farrell,** Massachusetts General Hospital, Harvard Medical School, Boston, MA, USA
	Head-to-head comparison of tau PET tracers across the Alzheimer's disease spectrum: baseline results from the HEAD study	**Guilherme Povala,** University of Pittsburgh, Pittsburgh, PA, USA
	Evaluating occipital-to-global amyloid PET as a predictor of CAA at autopsy in Mayo Clinic cohorts	**Christopher Schwarz,** Mayo Clinic, Rochester, MN, USA
09:50 am - 10:50 am	**Poster Session 2A**	
10:50 am - 12:20 pm	**SESSION IV: Longitudinal biomarker measurements of tau pathology**	**Chairs:** **William Jagust,** University of California, Berkeley, Berkeley, CA, USA **Heidi Jacobs,** Massachusetts General Hospital, Boston, MA, USA
10:50 am - 10:55 am	Session Overview	Chairs
10:55 am – 11:10 am	Preliminary comparative longitudinal performance of Flortaucipir and MK6240: rates of change, effect sizes, and power estimates in the HEAD Study	**Guilherme Bauer-Negrini**, University of Pittsburgh, Department of Psychiatry, Pittsburgh, PA, USA
11:10 am – 11:25 am	Standardized expression of longitudinal tau accumulation using the CenTauR scale	**Brian Lopresti**, University of Pittsburgh, Pittsburgh, PA, USA
11:25 am – 11:40 am	TauPace as a novel, time-based metric to investigate accelerated tau and clinical progression in preclinical AD	**William Coath**, University of Wisconsin School of Medicine and Public Health, Madison, WI, USA

Tuesday, January 13, 2026		
11:40 am – 11:55 am	Proteomic signatures track tau spread in Alzheimer's disease	**Arthur Macedo**, McGill University, Montreal, QC, Canada
11:55 am - 12:20 pm	Discussion	
12:20 pm - 01:20 pm	Lunch break	
01:20 pm - 01:50 pm	Keynote: **The role of AI in neuroimaging for Alzheimer's disease diagnosis, staging, and prognosis**	**Joyita Dutta**, University of Massachusetts-Amherst, MA, USA
01:50 pm - 02:05 pm	Keynote Discussion	
02:05 pm - 03:35 pm	**SESSION V: Alpha-synuclein in PD and MSA: PET imaging**	**Chairs:** **Jamie Eberling**, Michael J. Fox Foundation for Parkinson's Research, New York, NY, USA **Robert Mach**, University of Pennsylvania, Philadelphia, PA, USA
02:05 pm - 02:10 pm	Session Overview	Chairs
02:10 pm – 02:25 pm	Preclinical and early clinical assessment of [11C]MODAG-005, a novel PET tracer for imaging alpha-synuclein aggregates	**Ann-Kathrin Grotegerd**, University Tuebingen, Tuebingen, Germany
02:25 pm – 02:40 pm	Clinical evaluation of [11C]MK-7337: insights into the distribution of a-synuclein pathology in Parkinson's disease	**Eric Hostetler**, Merck & Co., Inc., West Point, PA, USA
02:40 pm – 02:55 pm	[11C]M503-1619 alpha synuclein PET imaging in Parkinson's disease and multiple system atrophy	**Chia-Ju Hsieh**, University of Pennsylvania, Philadelphia, PA, USA
02:55 pm – 03:10 pm	Quantitative analysis of human ^{18}F-FD4 α-synuclein PET imaging data in Parkinson's Disease and Multiple System Atrophy subtypes	**Roger Gunn**, XingImaging, London, UK
03:10 pm - 03:35 pm	Discussion	
03:35 pm - 03:40 pm	**Blitz Session 2B: Short Poster Presentations**	
	MK6240 and Tauvid positivity, cognitive decline, and their relationship to Aβ PET deposition across the Alzheimer's spectrum	**Bruna Bellaver,** University of Pittsburgh, Pittsburgh, PA, USA
	Differential sensitivity of T1-MRI and FDG-PET for tracking neurodegeneration across progressive stages of tau pathology in Alzheimer's disease	**Jesús Silva-Rodríguez,** CIEN Foundation, Reina Sofia Alzheimer Center, ISCIII, Madrid, Spain
	Midlife physical activity attenuates the association of earlier menopause with tau pathology and cognitive decline	**Madeline Wood Alexander,** Sunnybrook Research Institute, Toronto, ON, Canada
03:40 pm - 04:40 pm	**Poster Session 2B**	
04:40 pm - 06:10 pm	**SESSION VI: Neuroinflammation**	**Chairs:** **Chuck Kreisl,** Eisai, Washington DC, USA **David Morgan,** Michigan State University, Grand Rapids, MI, USA

Tuesday, January 13, 2026		
04:40 pm - 04:45 pm	Session Overview	Chairs
04:45 pm – 05:00 pm	Deep mass spectrometry-based plasma proteomics reveals signatures of reactive astrocytes in Alzheimer's disease	**Ruyu Shi**, University of Pittsburgh, Pittsburgh, PA, USA
05:00 pm – 05:15 pm	Microglia-Astrocyte interplay modulates tau phosphorylation in Alzheimer's disease	**Tevy Chan**, McGill University, Montreal, QC, Canada
05:15 pm – 05:30 pm	Astrogliosis mediates the effects of amyloid, moderated by CVD, on tau and cognition in non-demented individuals	**Victor Villemagne**, University of Pittsburgh, Pittsburgh, PA, USA
05:30 pm – 05:45 pm	TSPO expression patterns in the postmortem brain: relevance to neuroinflammation imaging	**Christina Moloney,** Mayo Clinic, Rochester, MN, USA
05:45 pm - 06:10 pm	Discussion	
06:10 pm – 06:15 pm	The PET-tle Royale (HAI's Re-Myelination Showdown Quiz)	**Christopher Schwarz**, Mayo Clinic, Rochester, MN, USA

Wednesday, January 14, 2026		
08:00 am – 09:00 am	*Check-in and Breakfast*	
08:15 am - 08:45 am	Mentoring Session	
09:00 am - 10:20 am	**SESSION VII: Early and intermediate signals and prognostic value**	**Chairs:** **Sterling Johnson**, University of Wisconsin-Madison, Madison, WI, USA **Sylvia Villeneuve**, McGill University, Montreal, QC, Canada
09:00 am - 09:05 am	Session Overview	Chairs
09:05 am – 09:20 am	Discordance between amyloid PET visual read and quantitation: false positives or early pathology detection?	**Margo Heston**, University of California, San Francisco, San Francisco, CA, USA
09:20 am – 09:35 am	Considerations for repeat testing of amyloid PET-validated plasma pTau217 diagnostic assays in the screening cohort for the AHEAD 3-45 study	**Robert Rissman**, Keck School of Medicine of the University of Southern California, San Diego CA, USA
09:35 am – 09:50 am	The prognostic value of p-tau217 levels on progression to clinical impairment over 2, 5 and 10 years	**Rachel Buckley**, Massachusetts General Hospital, Boston, MA, USA
09:50 am – 10:05 am	Distribution of tau and amyloid pathology across cognitive states in a population-based, admixed autopsy cohort	**Lea Grinberg**, Mayo Clinic, Jacksonville, FL, USA
10:05 am - 10:30 am	Discussion	
10:30 am - 10:35 am	**Blitz Session 3A: Short Poster Presentations**	
	Amyloid does not discriminate: a meta-analysis of sex differences in Centiloids from 35,468 participants across 33 cohorts	**Ganna Blazhenets**, University of California, San Francisco, San Francisco, CA, USA
	Longitudinal tau PET progression follows language network spread in primary progressive aphasia	**Adam Martersteck**, University of Chicago, Chicago, IL, USA

Wednesday, January 14, 2026		
10:35 am - 11:35 am	**Poster Session 3A**	
11:35 am - 12:05 am	Keynote: **Integrated proteomics for target and biomarker discovery in Alzheimer's disease**	**Nick Seyfried**, Emory University, Atlanta, GA, USA
12:05 pm - 12:20 pm	Keynote Discussion	
12:20 pm - 01:10 pm	Lunch break	
01:10 pm - 02:40 pm	**SESSION VII: Moderators and co-pathologies**	**Chairs:** **Annie Cohen**, University of Pittsburgh, Pittsburgh, PA, USA **Trey Hedden**, Icahn School of Medicine at Mount Sinai, New York, NY, USA
01:10 pm - 01:15 pm	Session Overview	Chairs
01:15 pm – 01:30 pm	Investigating the role of socioeconomic status on AD biomarker relationships	**Nazanin Ovaici**, University of California, Berkeley, Berkeley, CA, USA
01:30 pm – 01:45 pm	Blood LDL cholesterol synergistically amplifies tau pathology and cognitive outcome in an APOE4-dependent manner	**Tina Wang**, Eli Lilly and Company, Indianapolis, IN, USA
01:45 pm – 02:00 pm	Mismatch between tau burden and cognitive domain performance identifies sub-groups with specific co-pathologies	**Christopher Brown**, University of Pennsylvania, Philadelphia, PA, USA
02:00 pm – 02:15 pm	Characterizing the brain-wide atrophy pattern of LATE-NC-associated hippocampal sclerosis: an imaging-pathologic association study	**Michel Grothe**, Reina Sofia Alzheimer Center, CIEN Foundation, Spain
02:15 pm - 02:40 pm	Discussion	
02:40 pm - 02:45 pm	**Blitz Session 3B: Short Poster Presentations**	
02:40 pm - 02:45 pm	**Blitz Session 3B: Short Poster Presentations**	
	Perivascular spaces: Predictors of longitudinal amyloid, tau, cerebrovascular biomarkers?	**Audrey Low,** Mayo Clinic, Rochester, MN, USA
	Preliminary associations of plasma phosphorylated tau217 with regional tau deposition and accumulation in medial temporal and neocortical regions	**Eva Pintucci,** Massachusetts General Hospital, Harvard Medical School, Boston, MA, USA
	Intermediate blood-based biomarker status clarified by PET and CSF in cognitively impaired individuals	**Jacob Ziontz,** University of California, San Francisco, San Francisco, CA, USA
02:45 pm - 03:45 pm	**Poster Session 3B**	
03:45 pm - 05:20 pm	**SESSION IX: Therapeutics: Anti-abeta and anti-tau effects**	**Chair:** **Christopher Van Dyck**, Yale School of Medicine, New Haven, CT, USA
03:45 pm - 03:50 pm	Session Overview	Chairs
03:50 pm – 04:05 pm	Tau pathology interferes with amyloid removal by gantenerumab	**Matteo Tonietto**, Hoffmann-La Roche, Basel, Switzerland
04:05 pm – 04:20 pm	Clinical and PET outcomes following Aβ-targeting therapies in sporadic early-onset Alzheimer's disease: Trial emulation using the LEADS cohort	**Konstantinos Chiotis**, University of California San Francisco, San Francisco, CA, USA
04:20 pm – 04:35 pm	Tau positron emission tomography data from the open-label extension study of TOGETHER: a double-blind,	**Joël Mercier**, UCB, Braine-l'Alleud, Belgium

Wednesday, January 14, 2026		
	placebo-controlled Phase II study of bepranemab in prodromal–mild Alzheimer's disease (AD)	
04:35 pm – 04:50 pm	Cortical laminar and Aβ species-specific correspondence between antemortem Aβ-PET and postmortem pathology in aducanumab-treated Alzheimer's disease	**Baayla Boon**, Mayo Clinic, Jacksonville, FL, USA
04:50 pm – 05:05 pm	In vivo and post-mortem evidence of downstream pathophysiologic effects of treatment-related amyloid clearance	**David Wolk**, University of Pennsylvania, Philadelphia, PA, USA
05:05 pm - 05:30 pm	Discussion	
05:30 pm - 05:40 pm	**Awards Ceremony**	HAI Executive Committee
05:40 pm – 05:45 pm	Concluding Remarks	**Keith Johnson**, Massachusetts General Hospital, Boston, MA, USA

HAI 2026 ABSTRACTS

Monday, January 12, 2026 - 08:55 am - 10:25 am

Podium Session

SESSION I: Amyloid-beta pathology: PET imaging

CHAIRS:

***Keith Johnson**, Massachusetts General Hospital, Boston, MA, USA*

***Christopher Rowe**, Austin Health, Melbourne, Australia*

Monday, January 12, 2026			
08:55 am – 10:25 am	**Podium Presentation**	**Authors**	**Presenters**
08:55 am – 09:00 am	**Auto-rADiology: Toward automated and explainable amyloid-PET interpretation using deep learning**	Xiao | La Joie | Rittmo | Zhao | Soleimani-Migooni | An | Ovaici | Blazhenets | Harrison | Landau | Rabinovici | Jagust | Vogel	**Yu Xiao**, Department of Clinical Sciences Malmö, SciLifeLab, Lund University, Lund, Sweden
09:00 am – 09:15 am	**Choroidal-ventricular remodeling is associated with amyloid aggregation in Alzheimer's disease**	Hosseini | Rahmouni | Macedo | Hall | Chan | Bezgin | Zheng | Woo | Pascoal | Rosa-Neto	**Brandon Hall**, McGill University, Montréal, QC, Canada
09:15 am – 09:30 am	**Updated evaluation of the baseline distribution of amyloid positivity and cognitive impairment among adults with Down syndrome in the ABC-DS project**	McLachlan | Bettcher | LeMerise | McVea | Zammit | Price | Tudorascu | Laymon | Lao | Handen | Cohen | Zaman | Ances | Johnson | Betthauser | Head | Mapstone | Hartley | Christian	**Max McLachlan**, University of Wisconsin-Madison, Madison, WI, US
09:30 am – 09:45 am	**Heterogeneous patterns of off target signal with [18F]flutafuranol PET in ADNI4**	La Joie | Ovaici | Lin | Koeppe | Weiner | Landau | Rabinovici | Jagust	**Renaud La Joie**, University of California, San Francisco, San Francisco, CA, US

Auto-rADiology: Toward automated and explainable amyloid-PET interpretation using deep learning

Yu Xiao[1], Renaud La Joie[2], Jonathan Rittmo[1], Ruoyi Zhao[1], David N. Soleimani-Migooni[2], Lijun An[1], Nazanin Ovaici[3], Ganna Blazhenets[2], Theresa M. Harrison[3], Susan Landau[3], Gil D. Rabinovici[2,4], William J. Jagust[3], Jacob W. Vogel[1]

[1]*Department of Clinical Sciences Malmö, SciLifeLab, Lund University, Lund, Sweden*
[2]*Department of Neurology, Alzheimer's Disease Research Center, Memory & Aging Center, University of California San Francisco, San Francisco, CA, US*
[3]*Department of Neuroscience, University of California Berkeley, Berkeley, CA, US*
[4]*Department of Radiology & Biomedical Imaging, University of California San Francisco, San Francisco, CA, US*

Objectives: We present *Auto-rADiology*, an interpretable deep-learning framework that automates visual reads and Centiloid (CL) quantification for Aβ-PET scans to enhance standardization, efficiency, and confidence in clinical implementation of Aβ-PET.

Methods: Aβ-PET (Florbetapir/florbetaben/flutametamol) scans were sourced from IDEAS (n=10,346, population-based) and ADNI (n=1,157, research-based). Visual reads (VR) were performed by local radiologists (IDEAS), or by expert consensus (ADNI). Image processing details are in **Fig.1A**. CL values were derived via MRI-free pipeline for IDEAS and MRI-coregistered processing for ADNI. 3D convolutional neural networks were trained on 80% of IDEAS to classify scans as Aβ-positive/negative or predict CL, respectively. Testing was performed on 20% unseen IDEAS and ADNI. Model attention was evaluated using Grad-CAM. Agreement among model-predicted reads (mV), human reads (V), and CL-based dichotomy (Q: CL≥24) was evaluated, along with demographics effects on agreement.

Results: The VR model achieved 89% agreement with human reads in IDEAS (AUC=0.94), and performance was similar in ADNI (accuracy=89%, AUC=0.96). The CL model reached a mean error of 3.7 CL (R^2=0.99) in IDEAS, but systematically underestimated CL in ADNI (MAE=18, R^2=0.78). For VR, model attention was focused on mediofrontal and posterior brain regions, and on lateral and ventromedial regions for CL (**Fig.1B-E**). In IDEAS, 84.1% scans showed agreement across V, mV, and Q. mV aligned with V and Q better than V and Q aligned with each other (**Fig.2A**). Agreement decreased near the CL threshold (CL=10-40), though greatest agreement within this window was between mV and V (**Fig.2B,C**). Disagreement did not relate to age, sex, tracer, race, ethnicity or diagnosis. A prototype interface was built for real-time processing, inference and explainability of new scans (**Fig.3**).

Conclusions: Auto-rADiology exceeded expert-level agreement with CL despite being trained only on VR. Out-of-sample generalization can be improved through fine-tuning. This framework demonstrates a scalable, interpretable approach to standardizing Aβ-PET evaluation.

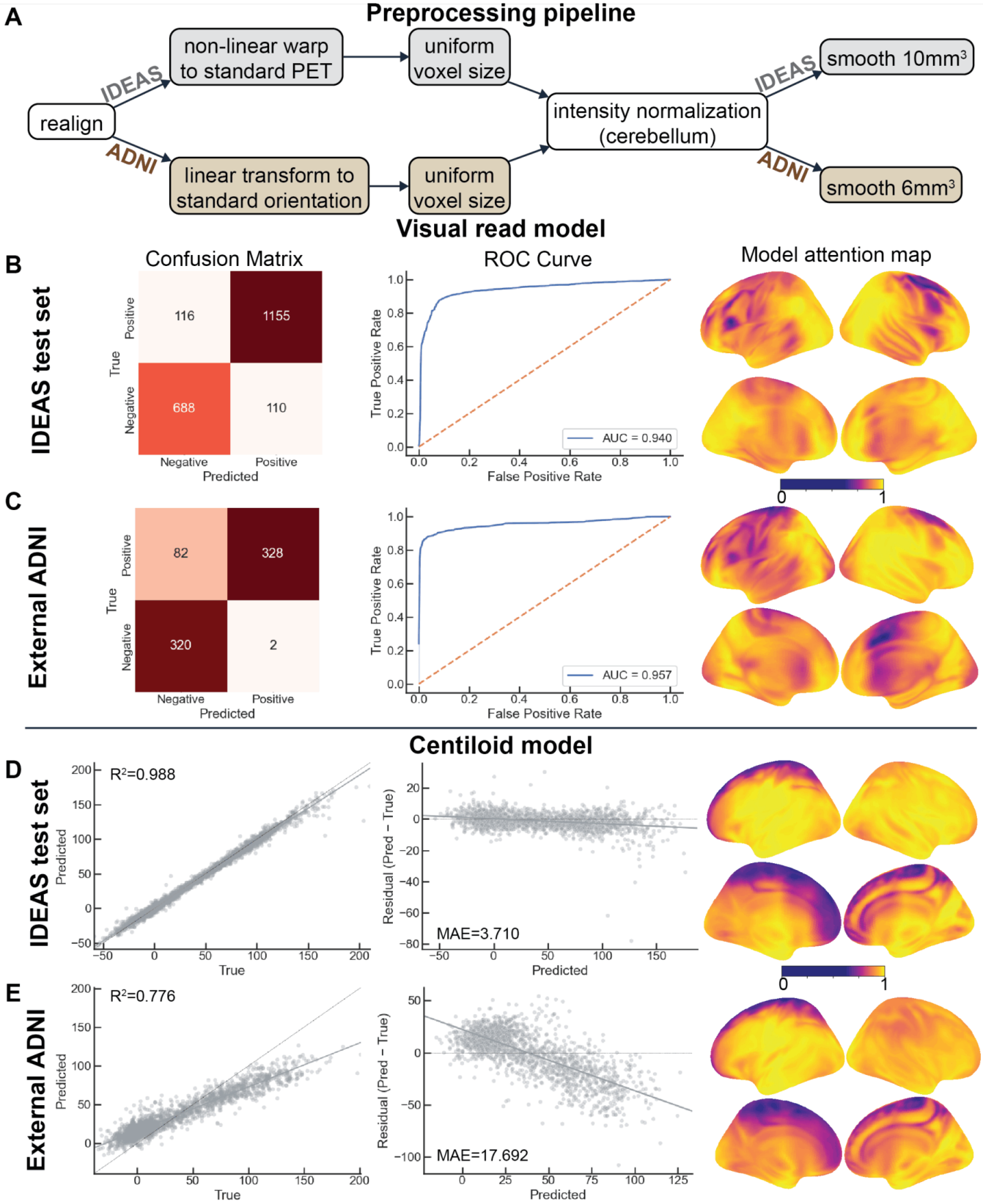


Figure 1. Performance of visual read and Centiloid prediction models on IDEAS and external ADNI datasets.
(A) Images were realigned and averaged, then warped to stereotaxic space (IDEAS) or transformed to standard orientation (ADNI), harmonized to uniform voxel size within each dataset, intensity normalized to cerebellum, and smoothed to 10mm³ (IDEAS) or 6mm³ (ADNI).
(B-C) Visual read classification results, including confusion matrices, ROC curves, and GradCAM-derived model attention map, for IDEAS testing **(B)** and ADNI external validation **(C)**. For Grad-CAM map, higher values indicate the model paid more attention to these parts of the brain in making inferences.
(D-E) Centiloid regression results showing predicted versus true values, residual distributions, and GradCAM-derived model attention maps for IDEAS testing **(D)** and ADNI external validation **(E)**. Each dot represents one PET scan.

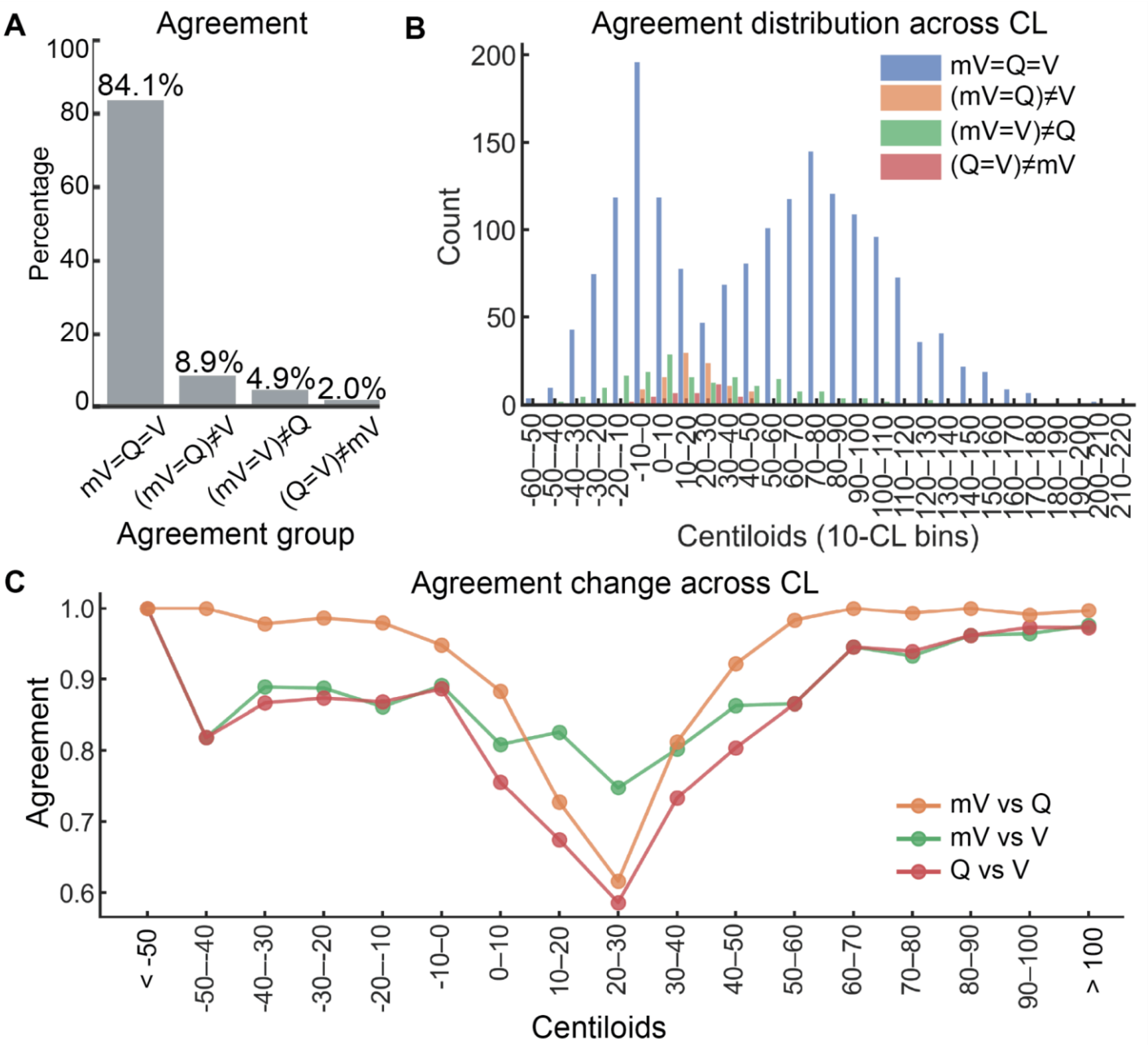


Figure 2. Demographics and agreement analyses of the IDEAS test set.
V=human Visual read; mV = model Visual read; Q = CL dichotomization
Note that, for this figure, CL always means "ground truth CL" and not model-derived CL.
(A) Percentage of subjects across four agreement groups:
* mV=Q=V: model visual reads, CL-based dichotomy, and human visual reads all agree with each other;
* (mV=Q)≠V: model visual reads agree with CL-based dichotomy but not with human visual reads;
* (mV=V)≠Q: model visual reads agree with human visual reads but not CL-based dichotomy;
* (Q=V)≠mV: human visual reads agree with CL-based dichotomy but not with model visual reads.
(B) Distribution of subjects across four agreement groups (mV=Q=V, (mV=Q)≠V, (mV=V)≠Q, (Q=V)≠mV) along CL. Agreement increases when moving away from the CL cutoff.
(C) Change in agreement across CL windows. Within each window, agreement was calculated between each pair of dichotomization approaches: (mV vs V, mV vs Q, V vs Q). Agreement was calculated the same way one would calculate accuracy, but we use agreement here because of the lack of a true ground truth. mV agreed more with Q than with V, except surrounding the centiloid cutoff (CL 10-40), where mV agreed more with V.

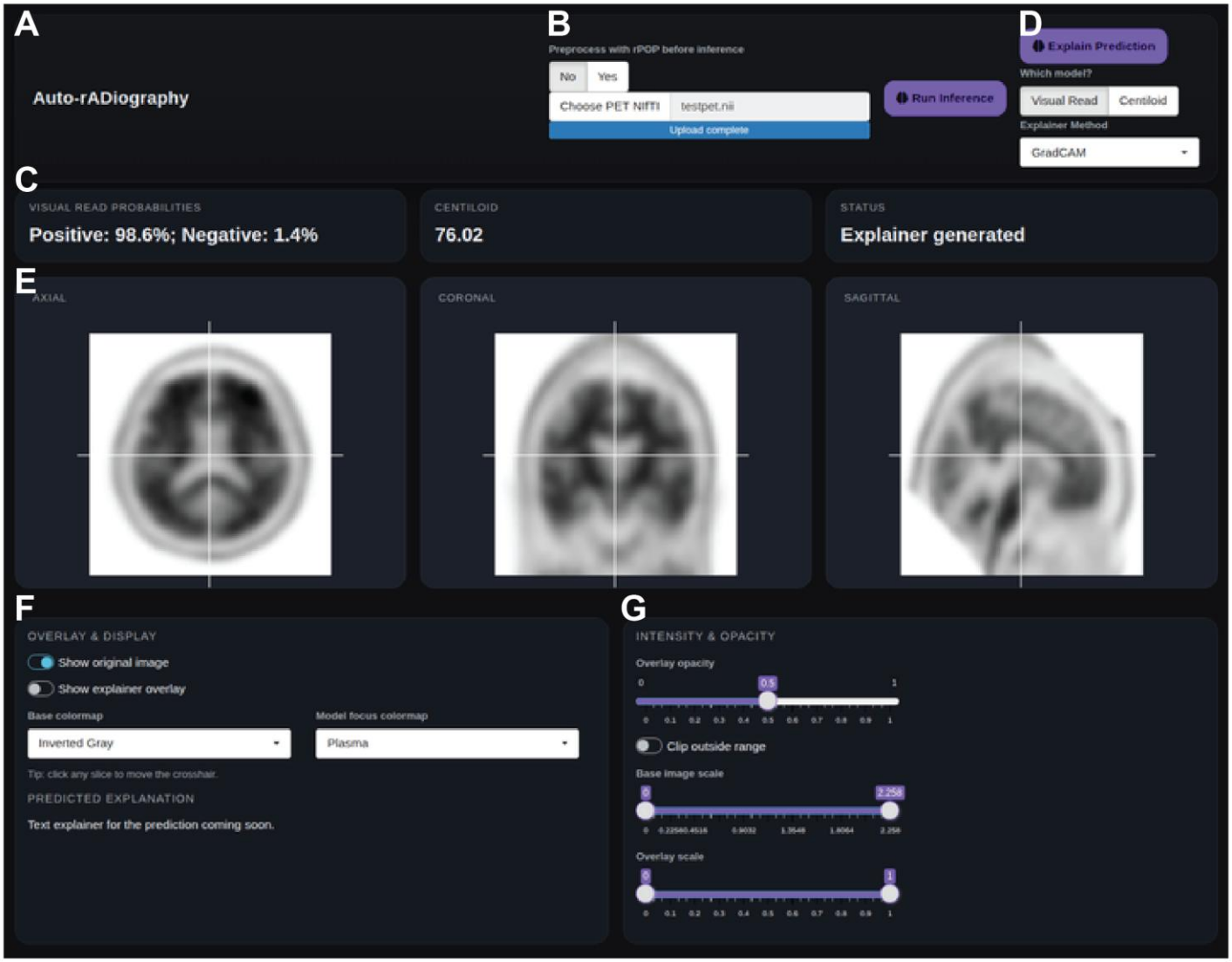


Figure 3. Prototype interface of the Auto-rADiography visualization app. We built an interactive application to facilitate seamless integration of automated VR and CL quantification into the patient management pipeline, complete with automated processing and visual explanation of model choice.
(A) The overall interface of the app.
(B) Scans can be dragged-and-dropped or selected, with the option to run rPOP processing pipeline before model inference.
(C) After running inference, app displays the probability of positive and negative read, as well as the predicted centiloid. Probabilities are generated directly from the model during inference as a measure of model confidence.
(D) Optionally, users can run one of several deep-learning explainability models to get a visual explanation of the model's choice (i.e. what parts of the image contribute most to the model's decision).
(E) 3D scrollable real-time display of image and overlays.
(F) Options to change colormaps and overlay.
(G) Options to control opacity and thresholding of overlay (i.e. explainer image).
(H) Future applications will implement model-generated text explaining model choice.

Keywords: Aβ-PET, AI, visual read, centiloid, translation

Choroidal-ventricular remodeling is associated with amyloid aggregation in Alzheimer's disease

Seyyed Ali Hosseini[1], Nesrine Rahmouni[1], Arthur C. Macedo[1], Brandon Hall[1], Tevy Chan[1], Gleb Bezgin[1], Yansheng Zheng[1], Marcel S. Woo[1], Tharick A. Pascoal[1], Pedro Rosa-Neto[1]

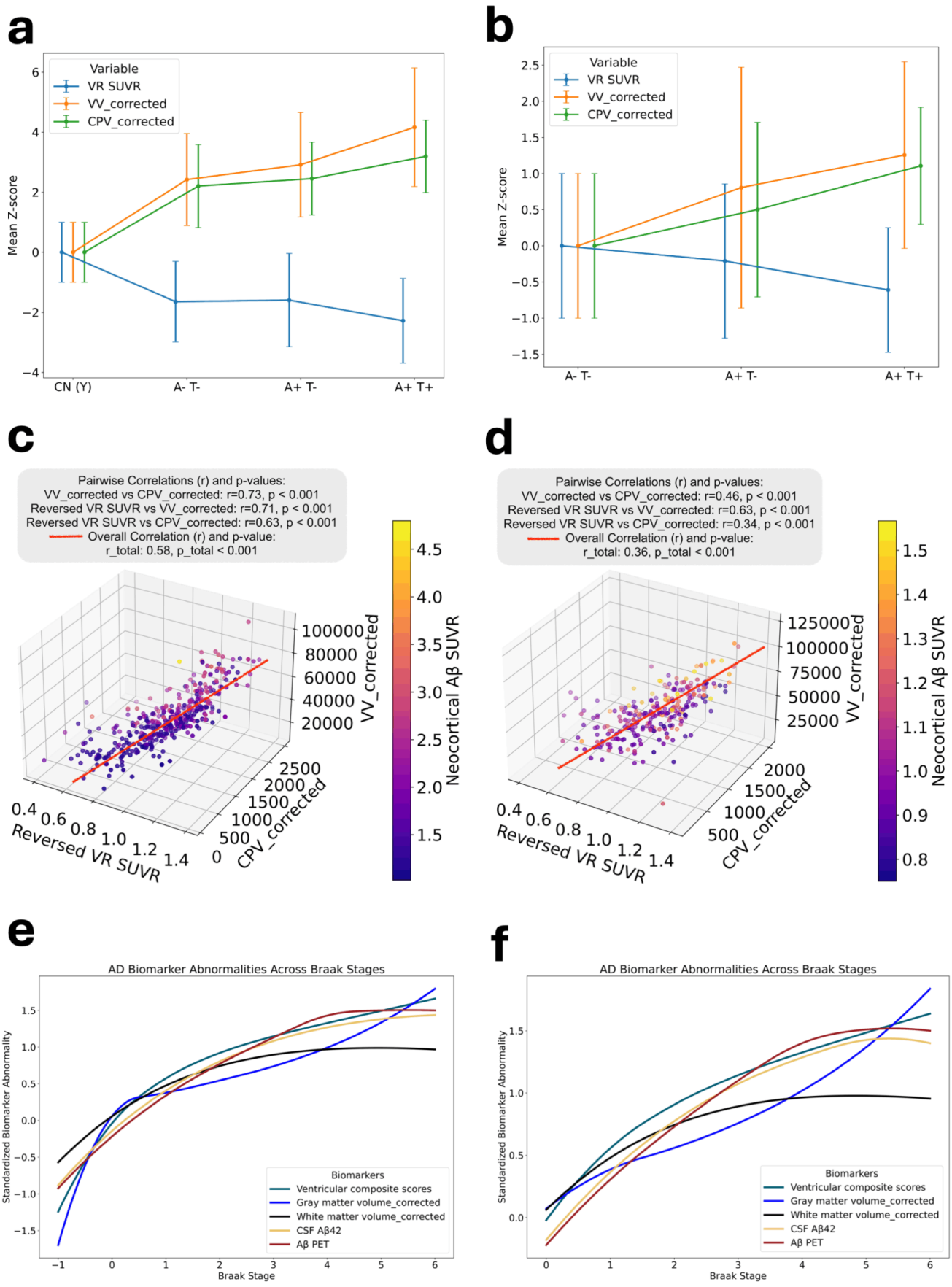
[1]*McGill University, Montréal, QC, Canada*

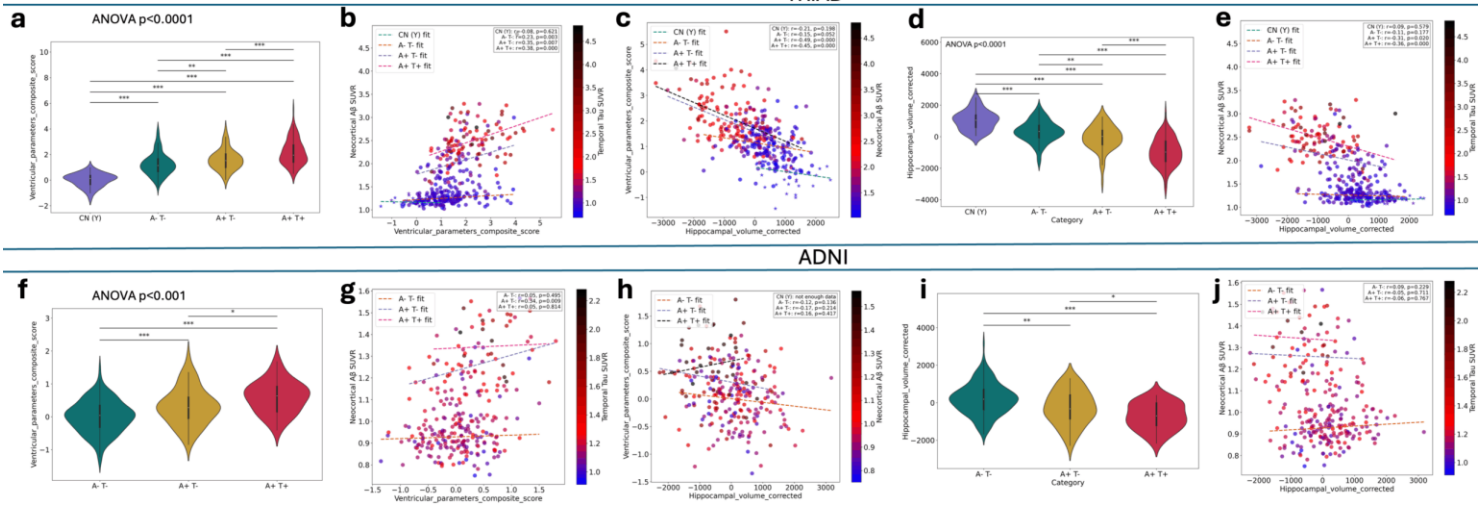
Background: While impaired cerebrospinal fluid (CSF) clearance has long been hypothesized to initiate Alzheimer's disease (AD), direct in-vivo evidence linking functional and structural CSF dysfunction to Aβ and tau pathology has been lacking. We introduce the first multimodal choroidal-ventricular composite biomarker integrating PET- and MRI-derived measures of CSF clearance and demonstrate its pivotal role in early AD-pathophysiology.

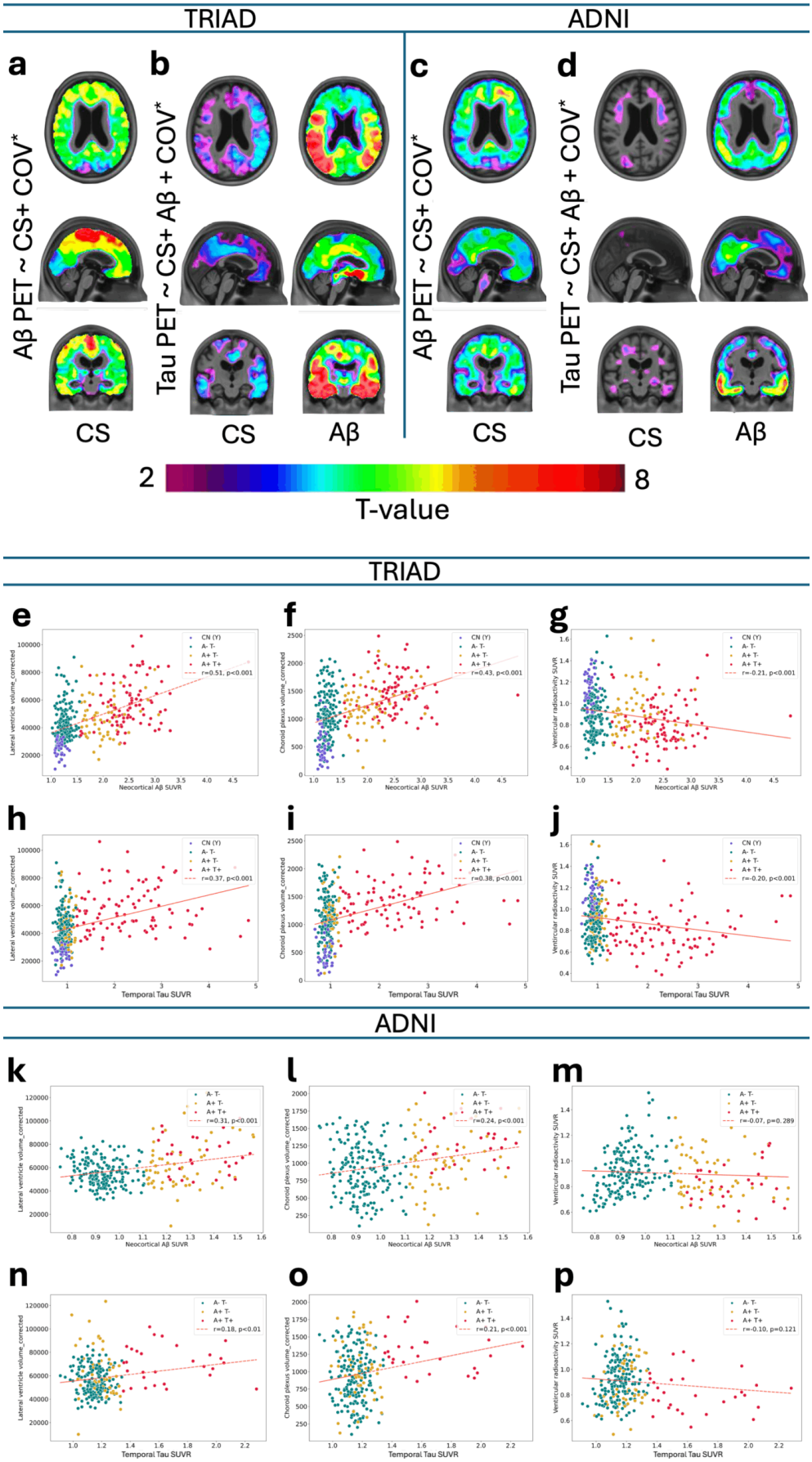
Methods: In 667 participants across TRIAD (n = 385) and ADNI (n = 282), we quantified three mechanistically related parameters, choroid plexus volume (CPV), ventricular volume (VV), and ventricular radioactivity (VR), a PET-based proxy of CSF flux, standardized to z-scores and combined into a composite clearance score. Group differences, partial correlations, and voxel-wise linear models were adjusted for age, sex, APOE4, and gray-matter volume.

Results: Across A/T stages, CPV and VV progressively enlarged while VR declined, reflecting concurrent structural expansion and functional slowdown of CSF circulation (Fig. 1). These metrics were strongly inter-correlated (r = 0.58 TRIAD; r = 0.36 ADNI), forming a unified clearance phenotype (Fig. 2). The composite score showed superior sensitivity to Aβ burden than any individual parameter and remained abnormal even in Aβ-negative older adults, identifying a preclinical phase of CSF-dysfunction (Fig. 3). Voxel-wise models confirmed widespread cortical Aβ-associations, with tau effects fully mediated by Aβ load. The composite further correlated with plasma and CSF p-tau (181/217/231), GFAP, and cognition, highlighting its biological- and clinical-relevance.

Conclusions: This study provides the first integrative in-vivo evidence that choroidal-ventricular remodeling represents an upstream, multimodal clearance failure preceding Aβ- and tau-aggregation. The proposed composite biomarker bridges structural and functional imaging domains, offering a novel mechanistic framework and translatable tool for early detection, disease staging, and therapeutic monitoring of CSF-targeted interventions in AD. Choroidal-ventricular alterations across AD. Composite clearance score reveals preclinical remodeling linked to Aβ. Choroidal-ventricular composite score associates with cortical Aβ load.


a
Variable
VR SUVR
VV_corrected
CPV_corrected
Mean Z-score
CN (Y)
A- T-
A+ T-
A+ T+
b
Variable
VR SUVR
VV_corrected
CPV_corrected
Mean Z-score
A- T-
A+ T-
A+ T+
c
Pairwise Correlations (r) and p-values:
VV_corrected vs CPV_corrected: r=0.73, p < 0.001
Reversed VR SUVR vs VV_corrected: r=0.71, p < 0.001
Reversed VR SUVR vs CPV_corrected: r=0.63, p < 0.001
Overall Correlation (r) and p-value:
r_total: 0.58, p_total < 0.001
Reversed VR SUVR
CPV_corrected
VV_corrected
Neocortical Aβ SUVR
d
Pairwise Correlations (r) and p-values:
VV_corrected vs CPV_corrected: r=0.46, p < 0.001
Reversed VR SUVR vs VV_corrected: r=0.63, p < 0.001
Reversed VR SUVR vs CPV_corrected: r=0.34, p < 0.001
Overall Correlation (r) and p-value:
r_total: 0.36, p_total < 0.001
Reversed VR SUVR
CPV_corrected
VV_corrected
Neocortical Aβ SUVR
e
AD Biomarker Abnormalities Across Braak Stages
Standardized Biomarker Abnormality
Braak Stage
Biomarkers
Ventricular composite scores
Gray matter volume_corrected
White matter volume_corrected
CSF Aβ42
Aβ PET
f
AD Biomarker Abnormalities Across Braak Stages
Standardized Biomarker Abnormality
Braak Stage
Biomarkers
Ventricular composite scores
Gray matter volume_corrected
White matter volume_corrected
CSF Aβ42
Aβ PET


TRIAD
a
ANOVA p<0.0001
Ventricular_parameters_composite_score
CN (Y)
A- T-
A+ T-
A+ T+
b
CN (Y) fit
A- T- fit
A+ T- fit
A+ T+ fit
Neocortical Aβ SUVR
Ventricular_parameters_composite_score
Temporal Tau SUVR
c
Ventricular_parameters_composite_score
Hippocampal_volume_corrected
Neocortical Aβ SUVR
d
ANOVA p<0.0001
Hippocampal_volume_corrected
Category
e
Neocortical Aβ SUVR
Hippocampal_volume_corrected
Temporal Tau SUVR
ADNI
f
ANOVA p<0.001
g
h
i
j



Keywords: Alzheimer's disease, CSF clearance, choroid plexus, amyloid-β, PET biomarkers, ventricular remodeling

Updated evaluation of the baseline distribution of amyloid positivity and cognitive impairment among adults with Down syndrome in the ABC-DS project

Max McLachlan[1], Brecca Bettcher[1], Lisette LeMerise[1], Andrew McVea[1], Matthew Zammit[1], Julie Price[2], Dana Tudorascu[3], Charles Laymon[3], Patrick Lao[4], Ben Handen[3], Annie Cohen[3], Shahid Zaman[5], Beau Ances[6], Sterling Johnson[1], Tobey Betthauser[1], Elizabeth Head[7], Mark Mapstone[7], Sigan Hartley[1], Bradley Christian[1]

[1]*University of Wisconsin-Madison, Madison, WI, US*
[2]*MGH Martinos Center, Harvard, Boston, MA, US*
[3]*University of Pittsburgh, Pittsburgh, PA, US*
[4]*Columbia University Irving Medical Center, New York, NY, US*
[5]*University of Cambridge, Cambridge, UK*
[6]*Washington University in St. Louis, St. Louis, MO, US*
[7]*University of California, Irvine, Irvine, CA, US*

Background: Since 2015, the Alzheimer's Biomarkers Consortium–Down Syndrome (ABC-DS) project has recruited over 500 participants with Down syndrome (DS) to understand the onset of Alzheimer's disease (AD) in this at-risk population. These participants are well-characterized for amyloid PET positivity and cognitive function (Krasny 2024). Recent work proposed updated processing for [^{18}F]florbetapir PET and supported using the striatum as an early amyloid marker for [^{11}C]PiB PET (McLachlan 2024). This work investigates the baseline distribution of regional amyloid positivity across age and cognitive status in the ABC-DS cohort.

Methods: Baseline amyloid PET and cognitive data were compiled for a subset of 354 adults with Down syndrome (42.7% female; 41.6 (SD=9.6) years). Amyloid PET was processed using a calibrated Centiloid (CL) pipeline with tracer-specific reference regions (PiB: whole cerebellum; florbetapir: eroded whole-brain white matter). Global Centiloid values were calculated for all scans, and striatum SUVR was calculated for PiB scans. Case consensus conference determined cognitive status. Participants were grouped by 5-year age increments. Each group was evaluated for amyloid positivity and cognitive impairment prevalence.

Results: The largest increases to global Centiloid positivity occurred between the 35-39 year and 45-49 year groupings. Striatum SUVR positivity was earlier and higher than that for global Centiloids (Figure 1). The amyloid positive group consisted of mostly cognitively stable (CS) participants, even in older age groups and particularly when measured using striatum SUVR (Figure 2). Both CS and impaired groups show elevated Centiloids and striatum SUVR by the 40-44 year grouping, although CS has a lower average (Figure 3).

Conclusions: The DS population demonstrates high prevalence of amyloid positivity across age groups and cognitive status, particularly when measured using striatum SUVR with PiB. The continued characterization of AD pathology in DS is critical for improving health outcomes in this population and developing a holistic understanding of AD.

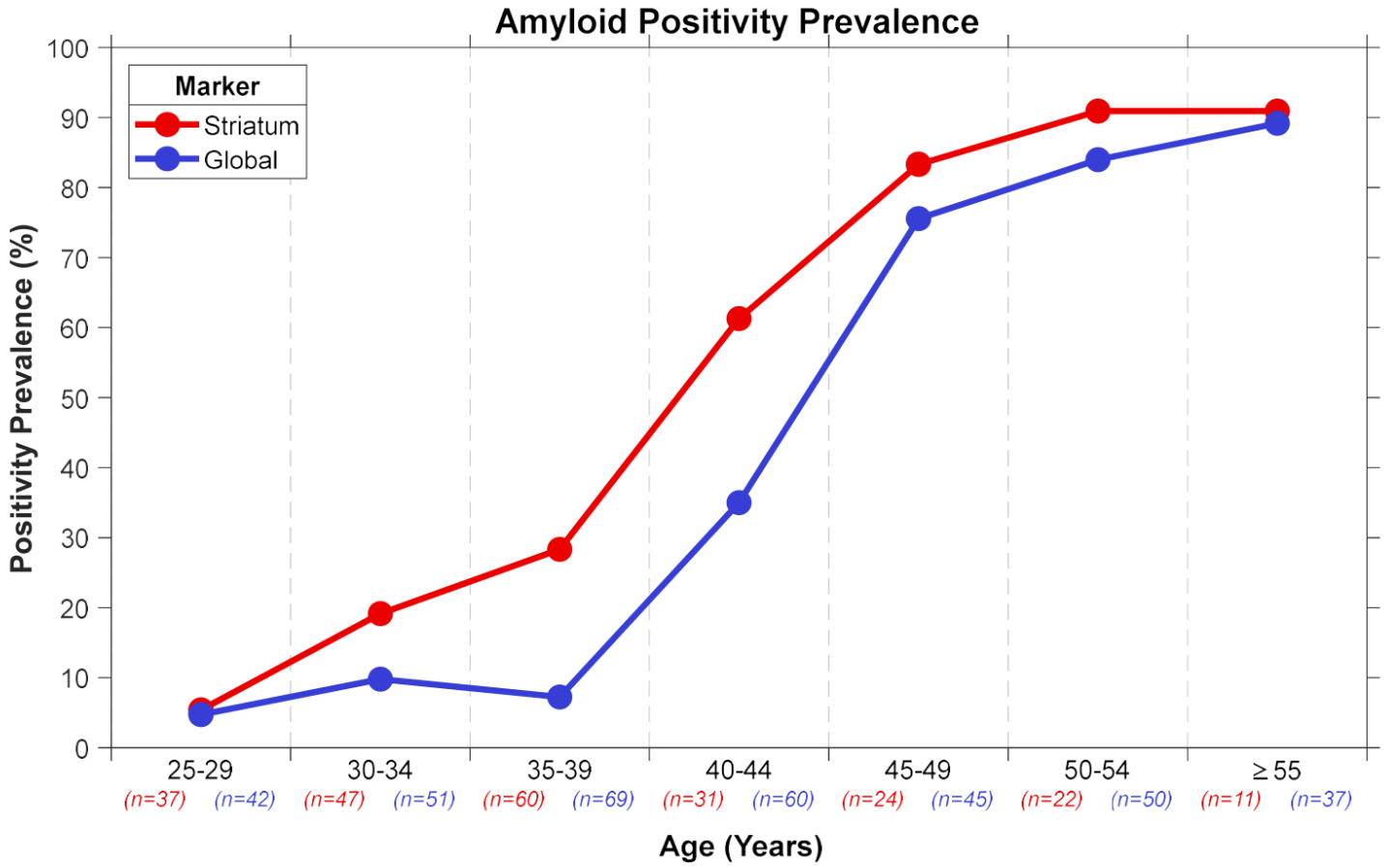


Figure 1 – Amyloid positivity prevalence for global Centiloids (18.1 CL threshold) and striatum SUVR (1.12 SUVR threshold). Prevalence is calculated in each group using *Prevalence = 100 x (Number of positive participants in group)/(Total group size)*. Both global and striatum positivity prevalence increase substantially between the 35-39 year and 45-49 year age groupings. Striatum positivity prevalence shows a gradual increase up to the 35-39 year grouping, followed by large increases similar to global positivity. Striatum positivity prevalence is greater across all age groups. Striatum data only includes PiB scans (n=232).

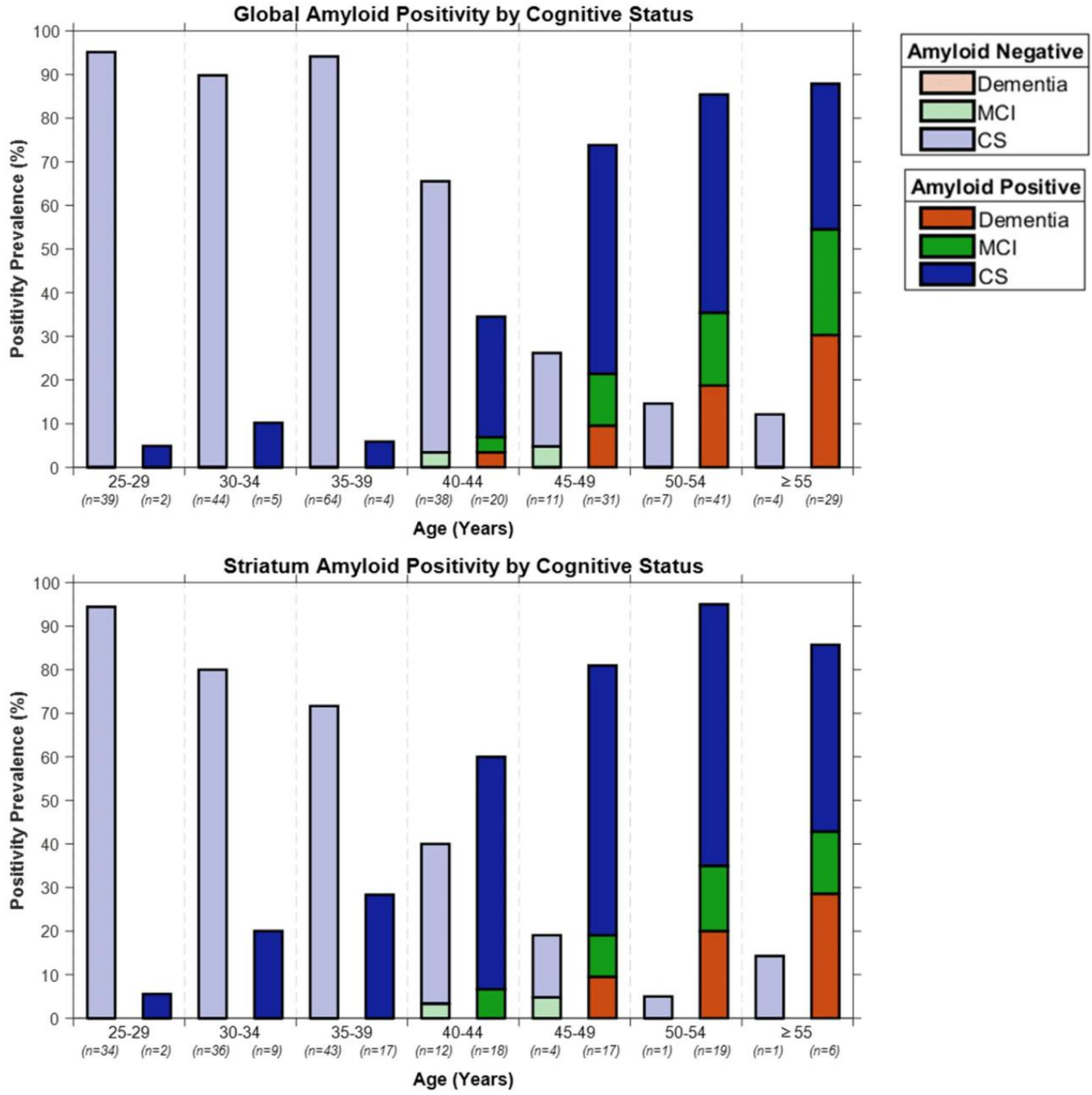


Figure 2 – Global Centiloid positivity prevalence (top) and striatum SUVR positivity prevalence (bottom), stratified by cognitive status. The amyloid negative group (light bar in each age group) shows a steady decline in prevalence, with nearly all participants in the cognitively stable group. The amyloid positive group shows a steady increase, with a greater proportion of participants with MCI and dementia in each subsequent age group. CS participants make up the majority of the amyloid positive group in all age groups, except the ≥55 year grouping. The amyloid positive group becomes the majority earlier for the striatum (40-44 year grouping) than the global marker (45-49 year grouping). Individuals with an "Undetermined" cognitive status are not displayed here.

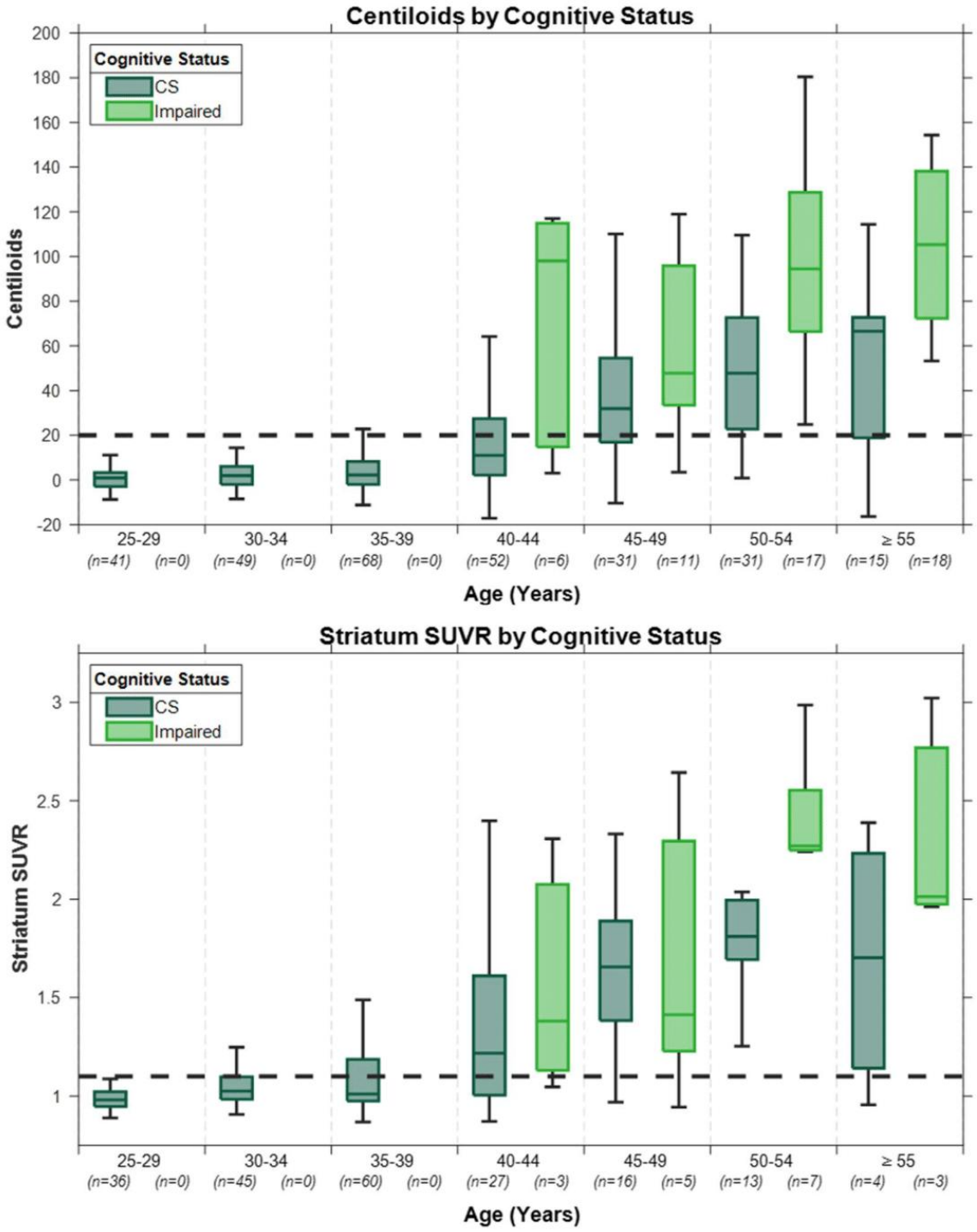


Figure 3 – Centiloids (top) and striatum SUVR (bottom), grouped by age and cognitive status. Impaired refers to participants with either MCI or dementia. Both Centiloids and striatum SUVR are significantly higher than the 25-29 year grouping by the 40-44 year grouping. Individuals with an "Undetermined" cognitive status are not displayed here.

Keywords: amyloid, Down syndrome, Alzheimer's disease, PiB, striatum

Heterogeneous patterns of off target signal with [18F]flutafuranol PET in ADNI4

Renaud La Joie[1], Nazanin Ovaici[2], Zoe Lin[1], Robert Koeppe[3], Michael Weiner[1], Susan Landau[2], Gil Rabinovici[1], William Jagust[2]

[1]*University of California, San Francisco, San Francisco, CA, US*
[2]*University of California, Berkeley, Berkeley, CA, US*
[3]*University of Michigan Medical School, Ann Harbor, MI, US*

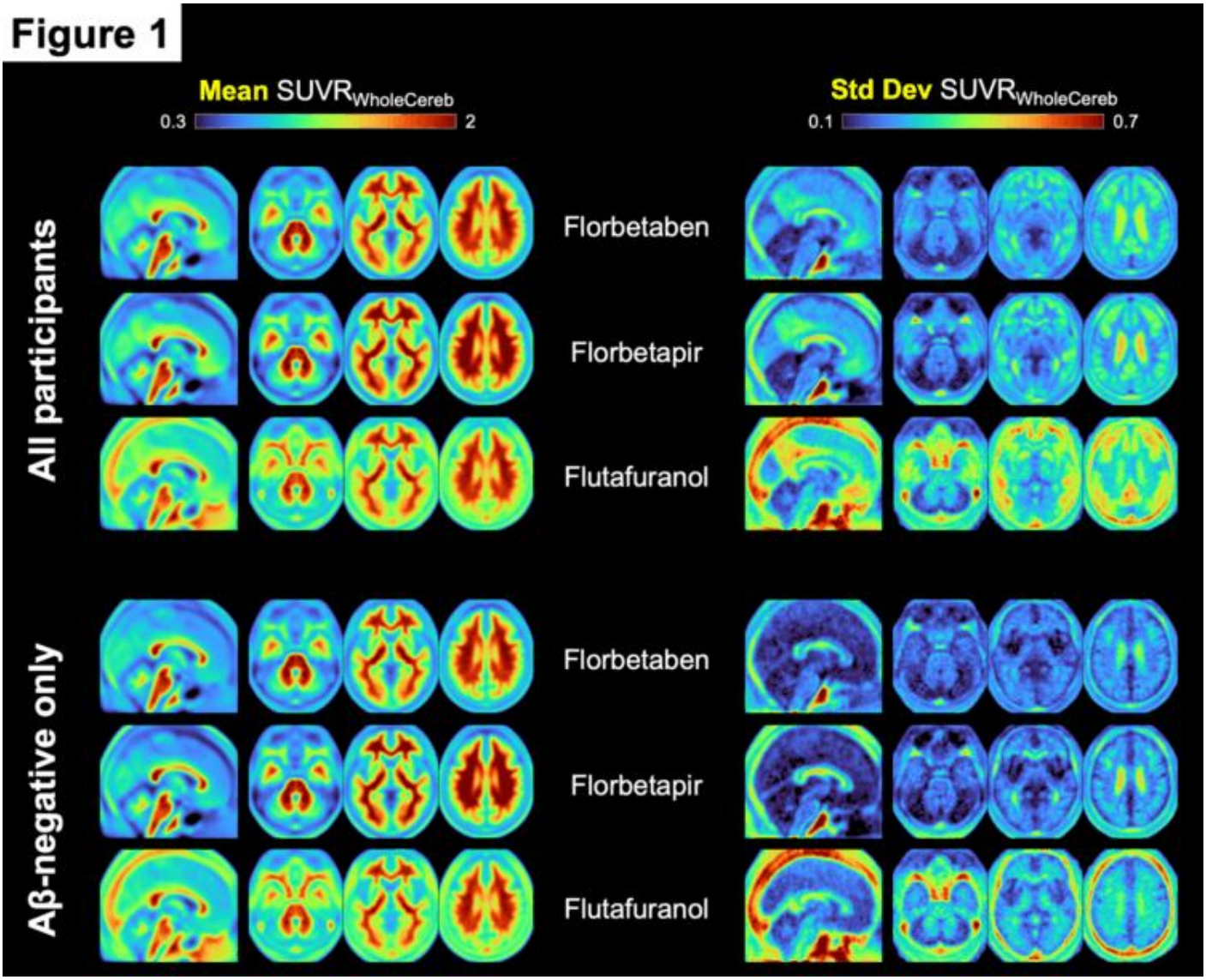
Objective: We aimed to characterize patterns of Off Target Signal (OTS) with Flutafuranol compared to Florbetapir and Florbetaben following its introduction into ADNI4.

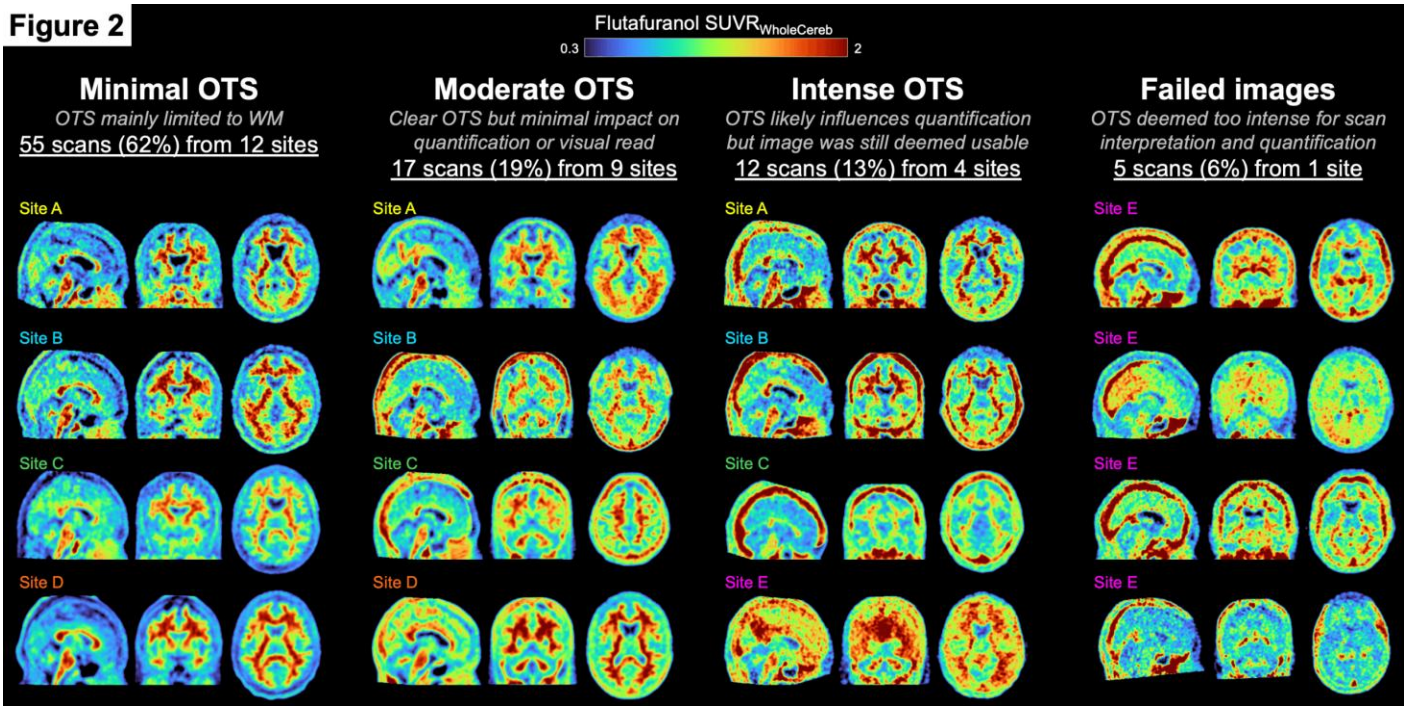
Methods: We selected ADNI4 participants who i) received an amyloid PET that passed quality control based on injection time and injected dose and ii) had a concurrent MRI. This search identified 409 Florbetapir (52 sites), 322 Florbetaben (32 sites), and 89 Flutafuranol scans (14 sites). To avoid differences due to sample size, we identified 89 Florbetapir and 89 Florbetaben scans that were age/sex/clinical diagnosis matched to the Flutafuranol sample using 1:1 nearest neighbor matching (MatchIt package, R). Scans were preprocessed using consistent procedures (defacing, frame realignment, smoothing to an effective 6mm FWHM resolution). Centiloids were calculated in native space (Freesurfer-based method, reference: whole cerebellum). SUVR images were warped to MNI space using MRI-defined parameters to create voxelwise maps of mean and standard deviation (SD) within each tracer.

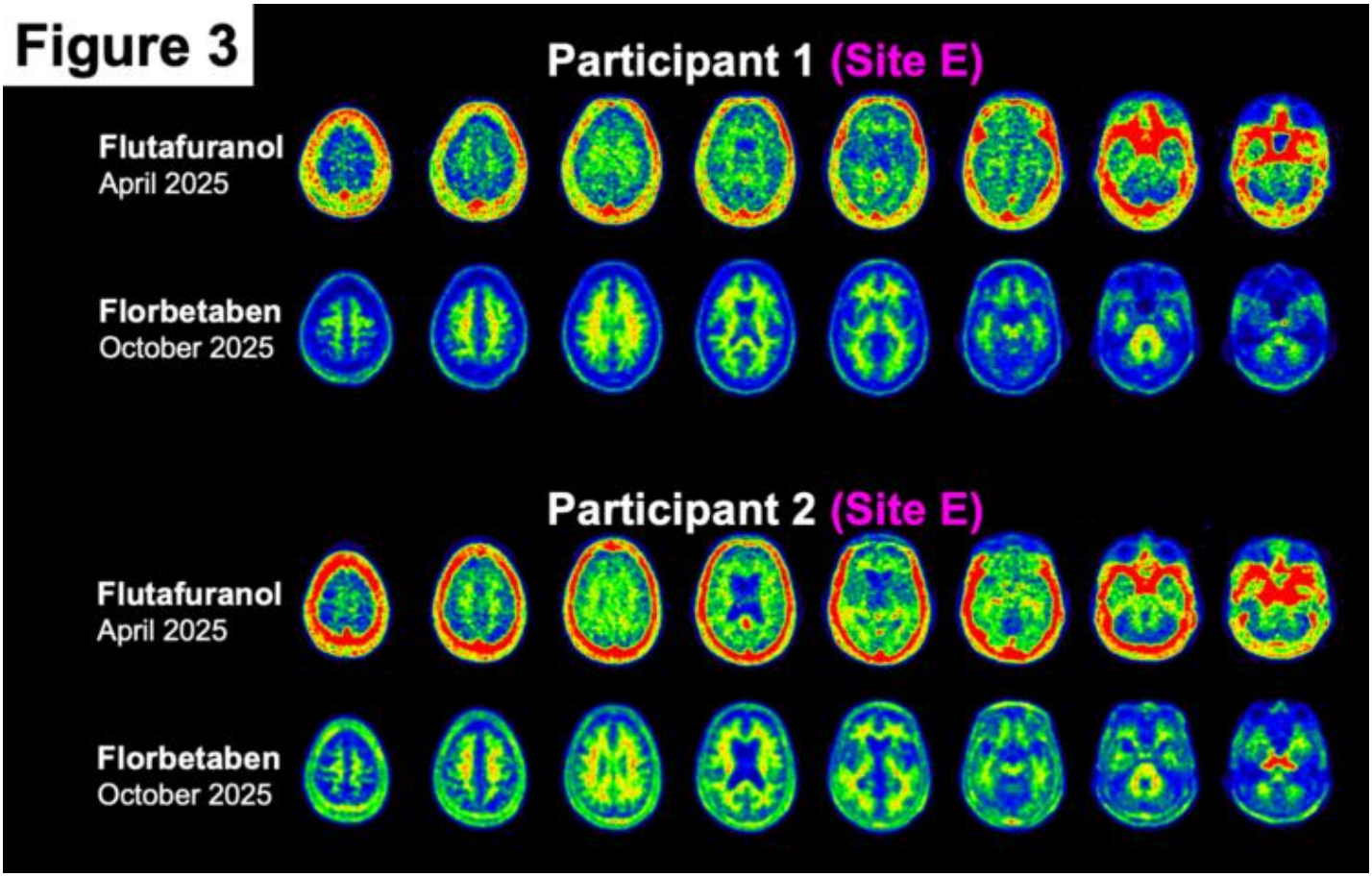
Results: The sample included 267 individuals (89 per tracer; age=68+/-7.5; 61% women; 52% unimpaired, 41% MCI, 7% dementia). **Figure 1** shows mean and SD maps for each tracer (in the whole group, and in the subsample with <18 centiloids) highlighting higher levels and variability of OTS in extra-axial areas (e.g. venous sinuses, meninges, skull) with Flutafuranol compared to other tracers. All 89 Flutafuranol scans were visually inspected by ADNI4 PET core investigators, showing a gradient of OTS severity across sites (**Figure 2**). Five Flutafuranol scans (out of 20) from site E could not be quantified or visually read due to intense OTS and low brain counts; 2 of them were scanned with Florbetaben 6 months later, showing minimal OTS (**Figure 3**).

Conclusions: ADNI4 Flutafuranol scans had higher OTS than Florbetapir or Florbetaben scans, which prevented image interpretation for the worst cases. Investigations on the sources of this OTS are ongoing.

Figure 1


Mean SUVR WholeCereb
0.3
2
Std Dev SUVR WholeCereb
0.1
0.7
All participants
Florbetaben
Florbetapir
Flutafuranol
Aβ-negative only
Florbetaben
Florbetapir
Flutafuranol





Keywords: Flutafuranol, NAV-4694, off target binding, artifacts

Monday, January 12, 2026 - 10:25 am - 10:30 am

Podium Session

B1 - A: Blitz Session

Monday, January 12, 2026			
10:25 am - 10:30 am	Title	Authors	Presenter
Board # 43	**Stronger amyloid–tau coupling explains faster tau progression in early-onset Alzheimer's disease**	Franzmeier	Frontzkowski	Steward	Klonowski	Dewenter	Hirsch	Biel	Zhu	Gnörich	Höglinger	Brendel	Roemer-Cassiano	**Nicolai Franzmeier,** LMU University Hospital, Ludwig-Maximilians-University (LMU) Munich, Germany
Board # 03	**Amyloid-induced neuronal hyperactivity and metabolism are associated with faster tau accumulation in Alzheimer's Disease**	Roemer-Cassiano	Zhang	Evangelista	Klonowski	Hirsch	Frontzkowski	Steward	Dewenter	Biel	Zhu	Gnoerich	Jaekel	Hoeglinger	Brendel	Yeo	Franzmeier	**Sebastian Roemer-Cassian**, University Hospital, LMU Munich, Germany
Board # 33	**Episodic memory decline and tau biomarkers progress earlier along the amyloid timeline in Down syndrome compared to neurotypical adults**	Zammit	Bruzzone	Morse	Batchelar	Bettcher	McLachlan	McVea	Carey	Tudorascu	Hartley	Clark	Ances	Caldwell	Johnson	Handen	Head	Mapstone	Christian	Investigators	Betthauser	**Matt Zammit,** University of Wisconsin, Madison, WI, USA

Monday, January 12, 2026 - 10:30 am - 11:30 am

Poster Session

Poster Session 1A

Monday, January 12, 2026			
10:30 am – 11:30 am	**Poster Presentation**	**Authors**	**Presenter**
Board 01	Longitudinal harmonization effects on tau-PET SUVRs trajectories in ADNI study	Ren | Luo | Laymon | Minhas | Cohen | Wu | Tudorascu	**Yuxin Ren**, Department of Biostatistics and Health Data Science, School of Public Health, University of Pittsburgh, Pittsburgh, PA, US
Board 02	Integrating digital cognitive metrics with PET biomarkers to identify individuals at imminent risk of tau accumulation	Fu | Robinson | Farrell | Jutten | Thibault | Thompson | Tiss | Chen | Becker | Healy | Penney | Davis | Sperling | Price | Rentz | Johnson	**Jessie Fang-Lu Fu**, Massachusetts General Brigham, Boston, MA, US
Board 03	Amyloid-induced neuronal hyperactivity and metabolism are associated with faster tau accumulation in Alzheimer's Disease	Roemer-Cassiano | Zhang | Evangelista | Klonowski | Hirsch | Frontzkowski | Steward | Dewenter | Biel | Zhu | Gnoerich | Jaekel | Hoeglinger | Brendel | Yeo | Franzmeier	**Sebastian Roemer-Cassiano**, Department of Neurology, University Hospital, LMU Munich, Germany, Munich, Germany
Board 04	Sex differences in white matter microstructure and associations with amyloid and tau pathology in autosomal dominant Alzheimer's disease	Giudicessi | Koops, PhD | Baena | Alvarez | Vidal | Martinez | Gonzalez | Tristão-Pereira | Malotaux | He | Aguillon | Jacobs | Cronin-Golomb | Quiroz	**Averi Giudicessi**, Department of Psychiatry, Massachusetts General Hospital, Harvard Medical School, Boston, MA, US
Board 05	Concordance between amyloid PET and biomarkers of Alzheimer's disease in plasma and cerebrospinal fluid in cognitively unimpaired individuals	Bermudez | Fought | Hofrenning | Lowe | Petersen | Vemuri | Jack, Jr. | Algeciral-Schimnich | Bornhorst | Graff-Radford	**Camilo Bermudez**, Department of Neurology, Mayo Clinic, Rochester, MN, US
Board 06	Comparing performance of different amyloid PET markers of spatial extent in their ability to predict future amyloid conversion	Honhar | Farrell | Properzi | Thibault | Schultz | Becker | Fu | Sperling | Price | Johnson	**Praveen Honhar**, Athinoula A. Martinos Center for Biomedical Imaging, Charlestown, MA, US
Board 07	Elevated ptau217 is more strongly associated with tau accumulation and cognitive decline in younger adults	Coughlan | Townsend | Li | Seto | Birkenbihl | Cody | Klinger | Healy | Farrell | Thibault | Rissman | Properzi | Schultz | Chhatwal | Yang | Donohue | Betthauser | Johnson | Johnson | Sperling | Buckley	**Madison Cuppels**, Massachusetts General Hospital, Harvard Medical School, Boston, MA, US

Board 08	Quantitative relationship between Lumipulse G measures of pTau217 in plasma and in brain	Vandenberghe | Tomé | De Meyer | Goossens | Lambrechts | Poesen | Vanbrabant | Vanmechelen | Thal	**Dietmar Thal**, KU-Leuven, Leuven, Belgium
Board 09	Distinct mechanisms underlying APOE-ε4 and sex effects on medial temporal tau pathology: A neuropathology study	Salvadó | Groot | Wisse | Vogel | Beach | Serrano | Reiman | Schneider | Bennett | Ossenkoppele | Hansson	**Gemma Salvadó**, Clinical Memory Research Unit, Department of Clinical Sciences, Malmö, Lund University, Lund, Sweden
Board 10	Harmonizing amyloid PET tracers at the regional level: evaluation of regional centiloid equations	Silvestri | Chaggar | Gobbi | Aldea | Klein | Tonietto	**Matteo Tonietto**, Research and Early Development (pRED), Hoffmann-La Roche, Basel, Switzerland
Board 11	A case series of lecanemab treatment response in patients across the clinical phenotypic spectrum of AD	Corriveau-Lecavalier | Machulda | Fields | Boots | Whitwell | Day | Aduen | Frank | Kremers | Ramanan | Graff-Radford | Lowe | Boeve | Knopman | Petersen | Jack | Stricker | Jones	**Nick Corriveau-Lecavalier**, Mayo Clinic, Rochester, MN, US
Board 12	Validation of a pseudo-reference region for [11C]-ER176 in healthy volunteers and Alzheimer's disease patients	Finn | Zanotti-Fregonara | Yu | Masdeu | Pascual	**Quentin Finn**, Nantz National Alzheimer Center, Stanley H. Appel Department of Neurology, Houston Methodist Research Institute, Houston, TX, US
Board 13	β-amyloid PET signal reduction is higher in regions with ARIA-E due to anti-amyloid therapy	Finn | Pascual | Toledo | Schulz | Masdeu	**Quentin Finn**, Nantz National Alzheimer Center, Houston Methodist Neurological and Research Institute, Houston, TX, US
Board 14	Lifetime and 10-year absolute risk of cognitive impairment associated with amyloid PET severity: a retrospective, longitudinal cohort study	Hu | Therneau | Wiste | Knopman | Vemuri | Graff-Radford | Lowe | Vassilaki | Cogswell | Schwarz | Algeciras-Schimnich | Petersen | Jack Jr.	**Mingzhao Hu**, Department of Quantitative Health Sciences, Mayo Clinic, Rochester, MN, US
Board 15	Trajectory of neurodegeneration and brain aging in relation to amyloid timing and duration	Zhang | Robb | Erus | Castellano | Cui | Cody | Harrison | Engelman | Albert | Resnick | Sperling | Bilgel | Vardarajan | Mayeux | Risacher | Arfanakis | Tosun | Habes | Wang | Toga | Thompson | Kukull | Biber | Landman | Bendlin | Johnson | Schneider | Barnes | Bennett | Saykin | De Jager | Menon | Harrison | Mormino | Cuccaro | Davatzikos | Betthauser | Archer | Hohman | Dumitrescu | Koran	**Mengna Zhang**, Vanderbilt Memory and Alzheimer's Center, Vanderbilt University School of Medicine, Nashville, TN, US

Board 16	Associations between tau pathology and cortical microstructure are modulated by amyloid burden independent of cortical atrophy in cognitively unimpaired older adults	Vogt | Koops | Schultz | Properzi | Salat | Pascual-Leone | Huang | Buckley | Rentz | Johnson | Sperling | Jacobs	**Nicholas Vogt**, Athinoula A. Martinos Center for Biomedical Imaging, Department of Radiology, Massachusetts General Hospital, Charlestown, MA, US
Board 17	Predicting tau PET burden using brain-derived plasma p-tau measures in the British 1946 birth cohort	Schott | Coath | Wiltshire | Brown | Cash | Whittington | Heslegrave | Zetterberg | Keshavan	**Jonathan Schott**, University College London, London, UK
Board 18	Association of combined cardiovascular risk factors and treatments with longitudinal amyloid and tau PET in cognitively normal older adults	Ourry | Thériault-Dubé | Breitner | Poirier | Villeneuve	**Valentin Ourry**, Department of Psychiatry, Faculty of Medicine, McGill University, Montréal, QC, Canada
Board 19	Amyloid-pet substantiates clinical decision-making in real-life clinical settings in Brazil	Schaffer Aguzzoli | Flach | Alves Da Silva | C.L Ferreira | Povala | Ferrari-Souza | Bieger | Teixeira Leffa | Bellaver | Guevara Werlang | Teribele Venturin | Wetters Portuguez | Possa Marroni | Irigoyen da Costa | Bernardi Soder | Sebastião Matushita | Juarez Amorim | Pasquotto Souza | Dario Ramos | Leite | Hygino | Amorim Nogueira | Sturzeneker Tres | Okada de Oliveira | Moriguchi Jeckel | Cortes Domingues | Mosci | Rosado de Castro | Buchpiguel | Paiva Proença Lobo Lopes | Carvalho Campos Neto | Figueiredo Balthazar | Tovar Moll | Martins Novaes Coutinho | Pascoal | Zimmer | Schilling | Costa da Costa	**Cristiano Schaffer Aguzzoli**, Brain Institute of Rio Grande do Sul (BraIns), Porto Alegre, Brazil
Board 20	Neuropathological validation of Tau-PET CenTauR units: Preliminary data from a multicenter study	Iaccarino | Chiotis | Grinberg | Kotari | La Joie | Leuzy | Lowe | Lu | Moscoso | Nguyen | Schwarz | Seeley | Jack | Rabinovici | Shcherbinin	**Renaud La Joie**, UCSF Memory and Aging Center, San Francisco, CA, US
Board 21	Molecular evaluation of a tau-PET analog and pathological TAR DNA-binding protein 43 docking in a cellular model of frontotemporal lobar degeneration	Gatto | Weissmann | Salinas Castellanos | Montes | Uruk | Youssef | Reichard | Josephs	**Rodolfo G. Gatto**, Department of Neurology, Mayo Clinic, Rochester, MN, US
Board 22	Anterior cingulate sulcal pattern is associated with successful cognitive aging	Maboudian | Kellerman | Willbrand | Pezzoli | Weiner | Jagust	**Samira Maboudian**, Department of Neuroscience, University of California, Berkeley, Berkeley, CA, US

Board 23	Microstructural white matter injury mediates the association between vascular risk and plasma biomarkers: Preliminary findings from the Diverse VCID study	Lee | Sapkota | Rajan | Jin | Hinman | Johnson | Harvey | Maillard | Fornage | DeCarli	**Seunghoon Lee**, Department of Neurology, University of California at Davis, Sacramento, CA, US
Board 24	VeraBIND Tau: a novel plasma assay reflecting tau aggregation increases over time in individuals with positive tau-PET signal	Hanseeuw | Quenon | Bayart | Salman | Pak | Shamsundar | Soldo | Iqbal	**Bernard Hanseeuw**, Cliniques Universitaires Saint-Luc, Brussels, Belgium
Board 25	Amyloid PET quantitation using skewness: Autopsy validation and test–retest performance	Tunali | Iaccarino | Wang | Kennedy | Lu | Shcherbinin	**Ilke Tunali**, Eli Lilly and Company, Indianapolis, IN, US
Board 26	Stratifying preclinical Alzheimer's disease by hippocampal volume to detect concomitant LATE	Mundada | Lyu | Sadeghpour | Brown | McGrew | Yushkevich | Das | Wolk	**Nidhi Mundada**, University of Pennsylvania, Philadelphia, PA, US
Board 27	Differential sensitivity of [^{18}F]MK6240 and [^{18}F]FTP to measure tau before and after anti-amyloid therapy	Deng | Finn | Pando | Matutue | Lussier | Fortea | Tudorascu | Soleimani-Meigooni | Lowe | Oh | Gordon | Rosa-Neto | Baker | Pascoal | Masdeu | Pascual	**Han Deng**, Stanley H. Appel Department of Neurology, Houston Methodist Research Institute, Houston, TX, US
Board 28	Development of a highly sensitive and automated immunoassay for Brain-Derived pTau-217: Analytical performance in human plasma samples	Ma | Wang | Danthanarayana | Kim | Ji | Jhaveri | Zhang | Qiu | Mudumba | Luo	**Xiao-Jun Ma**, Alamar Biosciences, Fremont, CA, US
Board 29	Network-based mechanistic modeling of Alzheimer's disease for evaluating diverse therapeutic mechanisms of action	Wooten | Stage | Mazer | Townsend | Comley | Guo	**Dustin Wooten**, AbbVie Inc., North Chicago, IL, US
Board 30	Neuroimaging compendium of microglia, amyloid, tau, and neurodegeneration across clinical variants of Alzheimer's disease	Houlihan | Guzman | Smith | Sanchez | Kreisl | Cosentino | Noble | Lao	**Hannah Houlihan**, Columbia University Medical Center, New York, NY, US
Board 31	Predictors of longitudinal atrophy across NIA-AA biological PET stages	Fonseca | Maboudian | Chao | Jagust | Harrison	**Corrina Fonseca**, Department of Neuroscience, University of California Berkeley, Berkeley, CA, US
Board 32	Effect of uptake time on [18F]-flutemetamol visual interpretation and Centiloid quantification	Bollack | Buckley | Schwarz | Battle | Smith | Stromrud | Hansson | Palmqvist | Matttsson-Carlgren | La Joie | Farrar	**Ariane Bollack**, GE HealthCare, Chalfont St Giles, UK
Board 33	Episodic memory decline and tau biomarkers progress earlier along the amyloid timeline in Down syndrome compared to neurotypical adults	Zammit | Bruzzone | Morse | Batchelar | Bettcher | McLachlan | McVea | Carey | Tudorascu | Hartley | Clark | Ances | Caldwell | Johnson |	**Matt Zammit**, University of Wisconsin, Madison, WI, US

		Handen | Head | Mapstone | Christian | Investigators | Betthauser	
Board 34	Relationship between p-tau217 and PET in preclinical AD: The moderating effect of white matter hyperintensity	Moon | Chen	**Hasom Moon**, Department of Psychology, Stony Brook University, Stony Brook, NY, US
Board 35	Systemic inflammation–tau interaction: Insights from CRP modulation of p-tau217 association with tau PET positivity	Monto | Boots | Zeng | Farinas | Sehrawat | Saeed | Cohen | Reis | Lopez | Snitz | Karikari	**Abdul Razak Monto**, Department of Psychiatry, School of Medicine, University of Pittsburgh, Pittsburgh, PA 15213, USA, Pittsburgh, PA, US
Board 36	Examining elevated choroid plexus binding of tau PET tracers in aging and Alzheimer's disease	Marin | Wales | Ruais | Richard | Hedden	**Anna Marin**, Department of Neurology, Icahn School of Medicine at Mount Sinai, New York, NY, US
Board 37	The influence of β-amyloid on neuroinflammatory 11C-ER176 uptake in progressive apraxia of speech	Satoh | Utianski | Duffy | Clark | Botha | Lowe | Josephs | Whitwell	**Ryota Satoh**, Mayo Clinic, Rochester, MN, US
Board 38	Subtracting first principal component may improve detectability of subtle 4R tau signals in 18F flortaucipir tau PET imaging	Satoh | Ali | Clark | Dickson | Lowe | Josephs | Whitwell	**Ryota Satoh**, Department of Radiology, Mayo Clinic, Rochester, MN, US
Board 39	OMG: a proteomic determinant of neurodegenerative resiliency	Duggan | Oh | Frank | Gomez | Zweibaum | Cui | Chen | Surapaneni | Blew | Dark | Joynes | Kandala | Bilgel | Farinas | Erus | Tian | Candia | Pucha | Landman | Dumitrescu | Hohman | Lewis | Moghekar | Siavoshi | Ali | Liu | Xu | Western | Kaneko | Kato | Furuichi | Shibayama | Katsuno | Nishita | Otsuka | Gottesman | Dammer | Seyfried | Levey | Johnson | Mormino | Wagner | Poston | Kapogiannis | Grams | Bhargava | Waga | Davatzikos | Resnick | Ferrucci | Bennett | Cruchaga | Wyss-Coray | Kivimäki | Coresh | Walker	**Michael Duggan**, National Institute on Aging, Baltimore, MD, US
Board 40	Frequency and consequences of extreme PET based pathological profiles in preclinical Alzheimer's disease	Medina Guerra | Cody | Young | Sheng | Sokolowski | Younes | Trelle | Tosun | Hohman | Mormino	**Lucah Medina Guerra**, Department of Neurology and Neurological Sciences, Stanford University, Palo Alto, CA, US
Board 41	Periventricular diffusivity moderates the relationship between astrocyte reactivity and amyloid deposition in non-demented older adults	Chen | Wu | Yang | Gogola | Luo | Villemagne | Laymon | Lopresti | Cohen | Ikonomovic | Snitz | Wilckens | Lopez |	**Chang-Le Chen**, Department of Bioengineering, University of Pittsburgh, Pittsburgh, PA, US

		Tudorascu | Aizenstein | Minhas	
Board 42	Disentangling the effects of age and Alzheimer's disease pathology on longitudinal atrophy in cognitively normal older adults	Haque | Fonseca | Maboudian | La Joie | Jagust	**Miraal Haque**, Department of Neuroscience, University of California, Berkeley, Berkeley, CA, US
Board 43	Stronger amyloid–tau coupling explains faster tau progression in early-onset Alzheimer's disease	Franzmeier | Frontzkowski | Steward | Klonowski | Dewenter | Hirsch | Biel | Zhu | Gnörich | Höglinger | Brendel | Roemer-Cassiano	**Nicolai Franzmeier**, 1. Institute for Stroke and Dementia Research (ISD), LMU University Hospital, Ludwig-Maximilians-University (LMU) Munich, Germany, Munich, Germany
Board 44	Harmonization methods to mitigate batch effects in blood biomarker analysis	Zhang | Lukasewicz Ferreira | Minhas | Pascoal | Zeng | Karikari | Cohen | Tudorascu	**Vivian Zhang**, Department of Biostatistics and Health Data Science, University of Pittsburgh School of Public Health, Pittsburgh, PA, US
Board 45	IGFR1, but not BDNF, acts as a suppressive neuroprotective factor between astrogliosis and visuospatial function among non-demented individuals	Ramirez Tirado | Cohen | Lopresti | Ikonomovic | Gogola | Matan | Zeng | Karikari | Lopez | Shaaban | Villemagne	**Ann D Cohen**, Department of Psychiatry, School of Medicine, University of Pittsburgh, Pittsburgh, PA, US
Board 46	The relation of psychosocial coping mechanisms to ATN pathophysiology differ across demographics	Schatz | Snitz | Roush | Lopresti | Villemagne | Lopez | Williams | Cohen	**Ann Cohen**, University of Pittsburgh Department of Psychiatry, Pittsburgh, PA, US
Board 47	Evaluation of the Clinical IMpact of Blood-Based Biomarker Assays on dementia specialists' decision-making (CIMBBBA): Preliminary report from a real-world dementia subspecialty clinic study	Eldaief | Krahn | Murdock | Rezaii | Chan | Arnold | Avetisyan | Ramirez Gomez | Gale | McGinnis | Dickerson	**Mark Eldaief**, Frontotemporal Disorders Unit, Department of Neurology, Massachusetts General Hospital and Harvard Medical School, Boston, MA, US
Board 48	Dynamic interplay of vascular injury and inflammation on Alzheimer's disease pathophysiology	Rusdi | Kang | Yin | Gibson | Rahmouni | Benedet | Zetterberg | Blennow | Karikari | Ashton | Black | Rosa-Neto | Goubran | Ottoy	**Julie Ottoy**, Centre for Brain Resilience & Recovery, Hurvitz Brain Sciences Program, Sunnybrook Research Institute, University of Toronto, Toronto, ON, Canada

1 Longitudinal harmonization effects on tau-PET SUVRs trajectories in ADNI study

Yuxin Ren[1], Weiquan Luo[2], Charles Laymon[2,3], Davneet Minhas[3], Ann Cohen[4], Qiong Wu[1], Dana Tudorascu[1,4]

[1]*Department of Biostatistics and Health Data Science, School of Public Health, University of Pittsburgh, Pittsburgh, PA, US*
[2]*Department of Bioengineering, Swanson School of Engineering, University of Pittsburgh, Pittsburgh, PA, US*
[3]*Department of Radiology, School of Medicine, University of Pittsburgh, Pittsburgh, PA, US*
[4]*Department of Psychiatry, School of Medicine, University of Pittsburgh, Pittsburgh, PA, US*

Introduction: Multisite neuroimaging studies of Alzheimer's disease (AD) enable large-scale analyses but are often affected by scanner- and site-related variability, which could introduce potential bias. In this study, we evaluated the impact of longitudinal ComBat (LComBat) harmonization on tau PET outcomes across Braak regions in the Alzheimer's Disease Neuroimaging Initiative (ADNI) cohort.

Methods: We analyzed longitudinal tau-PET SUVRs using the FTP tracer (6mm resolution) across Braak I-VI regions from 205 ADNI participants (mean age = 70.5 ± 6.9 yrs; 105 females) spanning five diagnostic groups: AD, Cognitively Normal (CN), Early/Late Mild Cognitive Impairment (EMCI/LMCI), and Subjective Memory Complaints (SMC). For each Braak region, SUVR trajectories were modeled using mixed-effect models before and after LComBat to assess site effects and covariate associations over time. To further control for potential confounding, we conducted a secondary analysis on an age- and sex-matched subset of 17 AD and 17 CN participants using the same modeling procedures.

Results: LComBat reduced site-related variability, as reflected by lower intraclass correlation coefficients (ICCs) across regions (Figure 1). Baseline AD diagnosis, APOE ε4 carrier status, and RAVLT cognitive measures were significantly associated with SUVRs across all Braaks ($p < 0.05$), and these associations remained robust after harmonization. The interactions between time and diagnosis were significant in Braaks I-II, while age and sex effects varied by region. In the matched subset, APOE ε4 effects persisted, whereas RAVLT cognitive associations decreased in early Braaks. Minor changes in age and education effects were observed after harmonization. For Braaks I, II, and VI, forest plots showed no statistically significant differences in model estimates with 95% confidence intervals (CIs) before and after LComBat (Figures 2 and 3).

Conclusion: LComBat effectively corrected site-related variability, but its practical impact may be limited when models account for key demographic and genetic covariates.

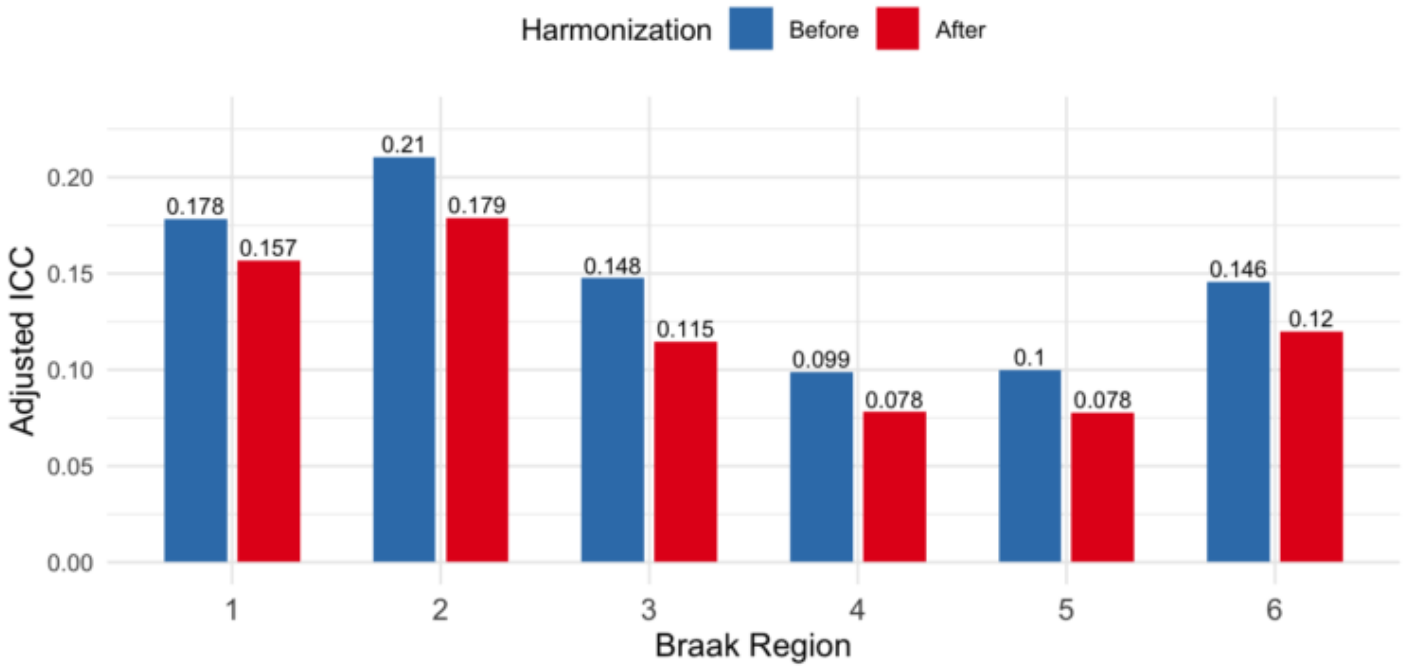


Figure 1. Impact of LComBat on site effects across Braak regions.

Bar plots show ICCs by Braak region before and after harmonization, estimated by mixed-effects models adjusting for demographic and clinical covariates. Higher ICCs indicate greater between-site variability. LComBat reduced site effects across all Braak regions.

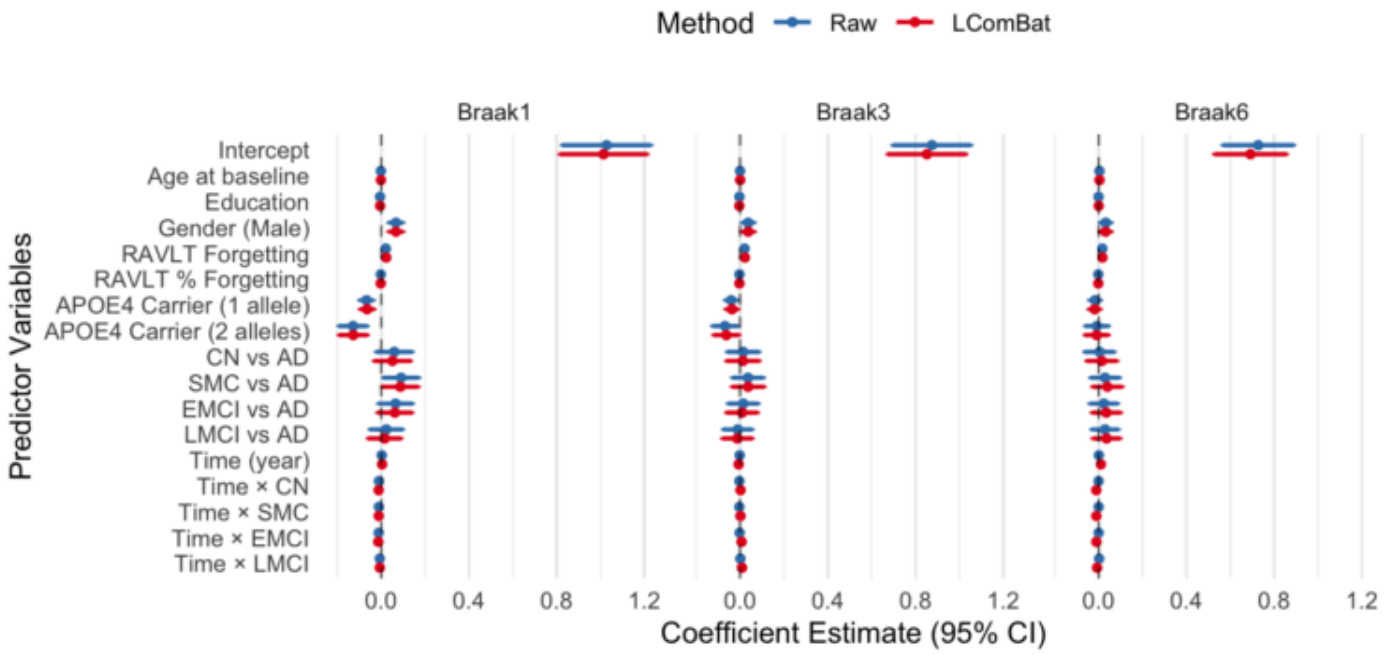


Figure 2. Comparison of model coefficients before and after LComBat in the full sample for Braaks I, III, VI.

Forest plots display fixed-effect coefficient estimates with 95% CIs from mixed-effects models fitted to raw and harmonized SUVR data. The overlapping CIs indicate that LComBat preserved key associations while reducing site effects.

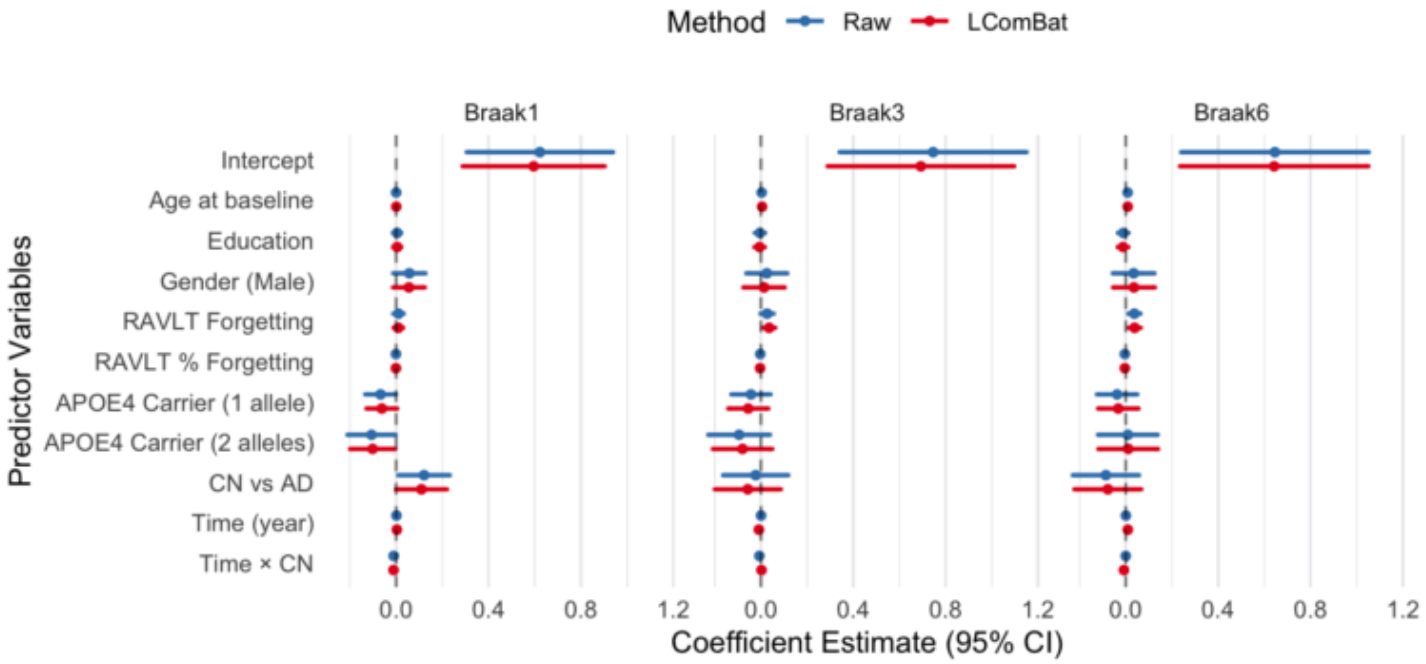


Figure 3. Comparison of model coefficients before and after LComBat in the matched group for Braaks I, III, VI.

Forest plots display fixed-effect coefficient estimates with 95% CIs from mixed-effects models fitted to raw and harmonized SUVR data. The overlapping CIs indicate that LComBat preserved key associations while reducing site effects.

Keywords: harmonization, long ComBat, trajectory, statistical analysis

2 Integrating digital cognitive metrics with PET biomarkers to identify individuals at imminent risk of tau accumulation

Jessie Fang-Lu Fu[1], Talia Robinson[1], Michelle Farrell[1], Roos Jutten[1], Emma Thibault[1], Jackson Thompson[1], Amal Tiss[1], Charles Chen[1], Alex Becker[1], Brian Healy[1], Dana Penney[2], Randall Davis[3], Reisa Sperling[1], Julie Price[1], Dorene Rentz[1], Keith Johnson[1]

[1]*Massachusetts General Brigham, Boston, MA, US*
[2]*Lahey Hospital and Medical Center, Burlington, MA, US*
[3]*Massachusetts Institute of Technology, Cambridge, MA, US*

Background: Anti-Aβ/tau therapies show greatest benefit in cognitively unimpaired (CU) and MCI individuals with low-to-moderate tau burden. However, rates of tau accumulation better predict near-term clinical progression than baseline burden. Targeting individuals with rapid tau accumulation could improve trial enrichment and reduce required sample size. While PET imaging remains the gold standard, it is impractical for large-scale screening. Digital cognitive tools, such as the digital Clock Drawing Test (dCDT), offer a scalable complement by dynamically capturing subtle impairments of cognitive processes sensitive to early AD-related changes. Building on prior work linking dCDT performance to tau accumulation, we aim to identify CU/MCI individuals with rapid tau accumulation and systematically evaluate multimodal predictors of tau accumulation.

Methods: Seventy-nine participants (74 CU, 5 MCI) underwent longitudinal ^{18}F-MK-6240 tau-PET (up to four years) and baseline ^{11}C-PiB Aβ-PET, dCDT and PACC5 assessments (**Table.1**). Global Aβ and regional tau burden were quantified. Linear mixed-effects models estimated within-subject tau slopes and were then classified individuals as "slow" vs. "rapid" accumulators using Gaussian Mixture Modeling (**Fig.1**). Elastic net models predicted entorhinal cluster membership and continuous slopes from baseline demographics, dCDT, PACC5 and neuroimaging features. Post-hoc regressions evaluated dCDT features selected in >80% of cross-validated iterations. ANOVA compared model performance across predictor sets.

Results: Models using demographics and neuroimaging measures showed moderate performance in classifying rapid accumulators (AUC=0.86). Including dCDT features enhanced prediction beyond demographics (Δchi^2=14.4, p=0.006) and neuroimaging (Δchi^2=10.0, p=0.039) alone, but not PACC5. In continuous-slopes models, dCDT explained additional variance beyond demographics and neuroimaging (Δadjusted R^2=0.10; F=8.56, p =0.005; **Fig.2**), but not PACC5. Key dCDT predictors included vertical spatial placement and component placement metrics.

Conclusion: Baseline dCDT performance provides complementary predictive value beyond PET for identifying rapid tau accumulators. Future work will develop novel digital metrics optimized for predicting tau accumulation and expand to larger MCI cohorts.

Table 1. Participants and data characteristics.				
	All	CU Aβ- (n = 51)	CU Aβ+ (n = 23)	MCI (n = 5)
Sex (M)	33 (46.5%)	23 (52.3%)	7 (31.8%)	3 (60.0%)
Age	68.46 (9.70)	65.01 (9.27)	74.41 (7.41)	72.06 (10.05)
Education (years)	17.11 (2.50)	16.80 (2.26)	18.14 (2.47)	15.40 (3.44)
PACC5	-0.39 (1.26)	-0.08 (0.98)	-0.39 (0.73)	-3.11 (2.10)
dCDT summary scores	70.51 (28.40)	76.34 (24.54)	67.50 (27.52)	32.45 (40.35)
Aβ PET imaging (^{11}C-PiB)				
PiB FLR DVR	1.23 (0.28)	1.05 (0.04)	1.53 (0.20)	1.50 (0.41)
Tau PET imaging (^{18}F-MK-6240)				
Entorhinal SUVR	1.16 (0.60)	0.92 (0.29)	1.42 (0.48)	2.11 (1.43)
Amygdala SUVR	0.78 (0.53)	0.59 (0.19)	0.96 (0.36)	1.67 (1.51)
Inferior Temporal SUVR	1.18 (0.71)	1.00 (0.13)	1.24 (0.47)	2.42 (2.29)
Precuneus SUVR	0.95 (0.72)	0.85 (0.09)	0.87 (0.11)	2.15 (2.63)
Tau PET imaging follow-up time points				
Baseline	79	51	23	5
6-month follow-up	44	27	13	4
1-year follow-up	45	28	14	3
>2-year follow-up	47	31	13	3
Values are expressed as mean (standard deviation) when appropriate.				

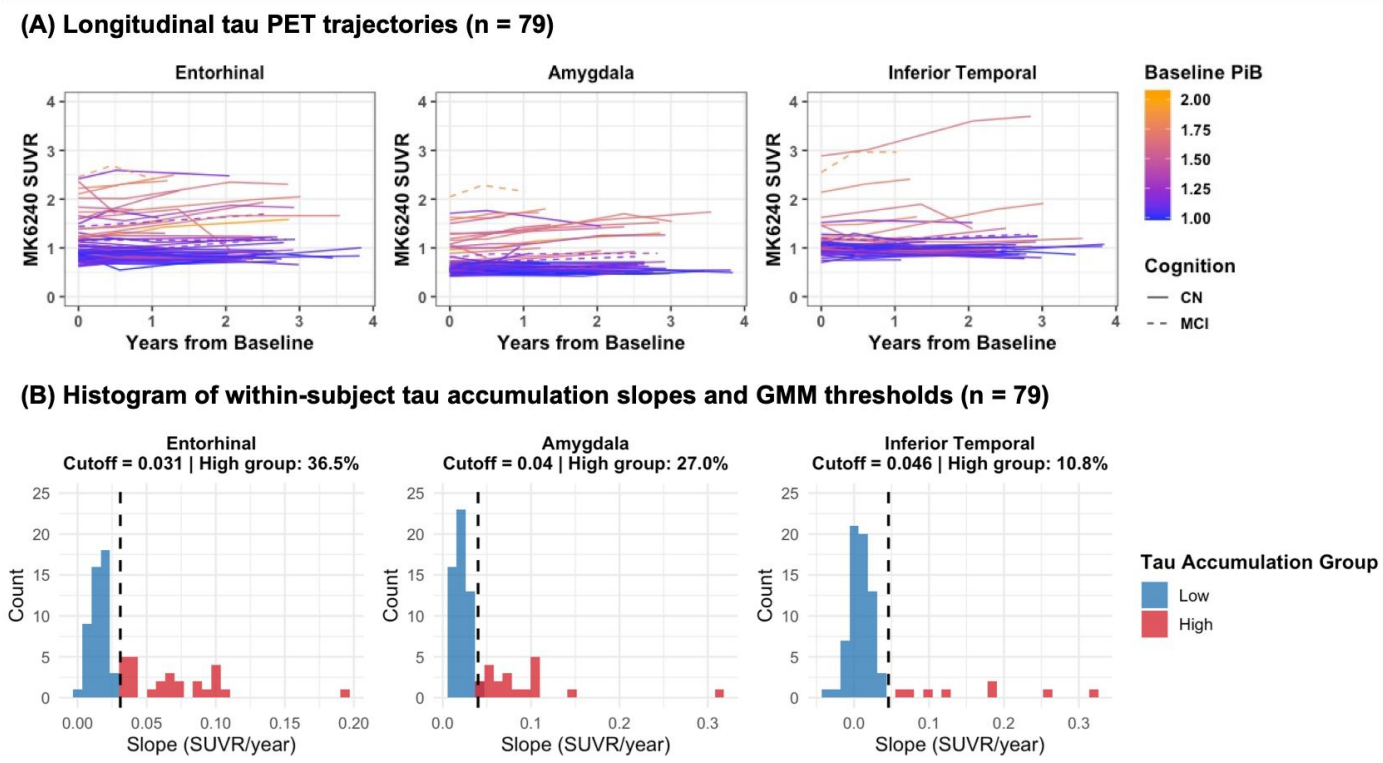


Figure 1. Longitudinal tau PET trajectories and identification of rapid tau accumulation subgroups.
(A) Longitudinal ^{18}F-MK-6240 SUVR trajectories are shown for entorhinal, amygdala, and inferior temporal regions over time (colored by baseline ^{11}C-PiB Aβ burden). **(B)** Histograms of within-subject tau accumulation slopes (SUVR/year) derived from LME models. GMM identified thresholds separating "low" and "high" (rapid) tau accumulation groups (vertical dashed lines). The proportion of participants in the high-accumulation group is indicated for each region. Early tau regions (entorhinal, amygdala) show higher proportions of rapid accumulators compared to mid-stage regions (inferior temporal).

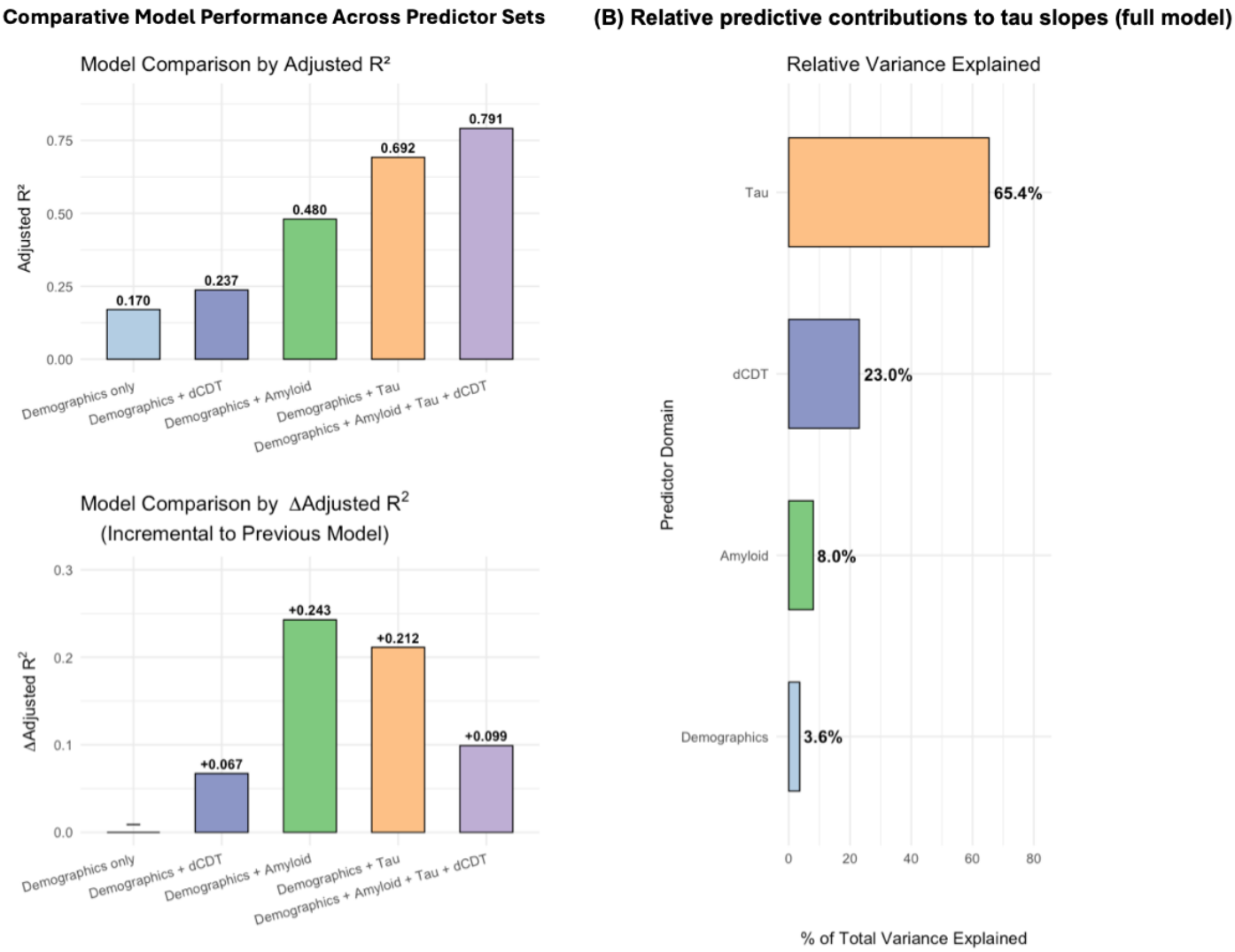


Figure 2. Post hoc model performance and relative contributions of multimodal predictors. (A) Stepwise model comparison showing improved prediction of tau accumulation slopes with the sequential addition of dCDT, Aβ PET, and tau PET measures (final model adjusted $R^2 = 0.79$). **(B)** In the full model, tau PET provided the largest explanatory power, while dCDT features contributed substantial additional variance beyond neuroimaging and demographic factors, underscoring their complementary value for predicting future tau accumulation.

Keywords: Positron emission tomography, tau, digital clock drawing test, longitudinal analysis, Alzheimer's disease

3 Amyloid-induced neuronal hyperactivity and metabolism are associated with faster tau accumulation in Alzheimer's Disease

Sebastian Roemer-Cassiano[1], Shaoshi Zhang[4], Lisa Evangelista[2], Madleen Klonowski[2], Fabian Hirsch[2], Lukas Frontzkowski[2], Anna Steward[2], Anna Dewenter[2], Davina Biel[2], Zeyu Zhu[2], Johannes Gnoerich[7], Sarah Jaekel[2], Guenter Hoeglinger[1], Matthias Brendel[2,7], Thomas Yeo[4], Nicolai Franzmeier[2,5,6]

[1]*Department of Neurology, University Hospital, LMU Munich, Germany, Munich, Germany*
[2]*Institute for Stroke and Dementia Research (ISD), University Hospital, LMU Munich, Germany, Munich, Germany*
[3]*Max Planck School of Cognition, 04103 Leipzig, Germany, Leipzig, Germany*
[4]*Centre for Sleep and Cognition and Centre for Translational Magnetic Resonance Research, Yong Loo Lin School of Medicine, National University of Singapore, Singapore 117594, Singapore, Singapore, Singapore*
[5]*Munich Cluster for Systems Neurology (SyNergy), Munich, Germany, Munich, Germany*
[6]*German Center for Neurodegenerative Diseases (DZNE) Munich, Munich, Germany, Munich, Germany*
[7]*Department of Nuclear Medicine, University Hospital, LMU Munich, Germany, Munich, Germany*

Background: The link between amyloid and tau accumulation in AD remains elusive, impeding the development of interventions targeting the Aβ–tau axis. Studies have shown that amyloid induces neuronal hyperexcitability, while tau spreads trans-synaptically in an activity-dependent manner. Congruently, we demonstrated that tau spreads across brain networks, where Aβ-associated increases in functional connectivity facilitate this process. However, it remains unclear whether Aβ-related hyperconnectivity indeed reflects neuronal hyperexcitability. To address this, we integrated resting-state fMRI, FDG-PET, and post-mortem data to test whether Aβ promotes neuronal hyperactivity, thereby facilitating tau spread.

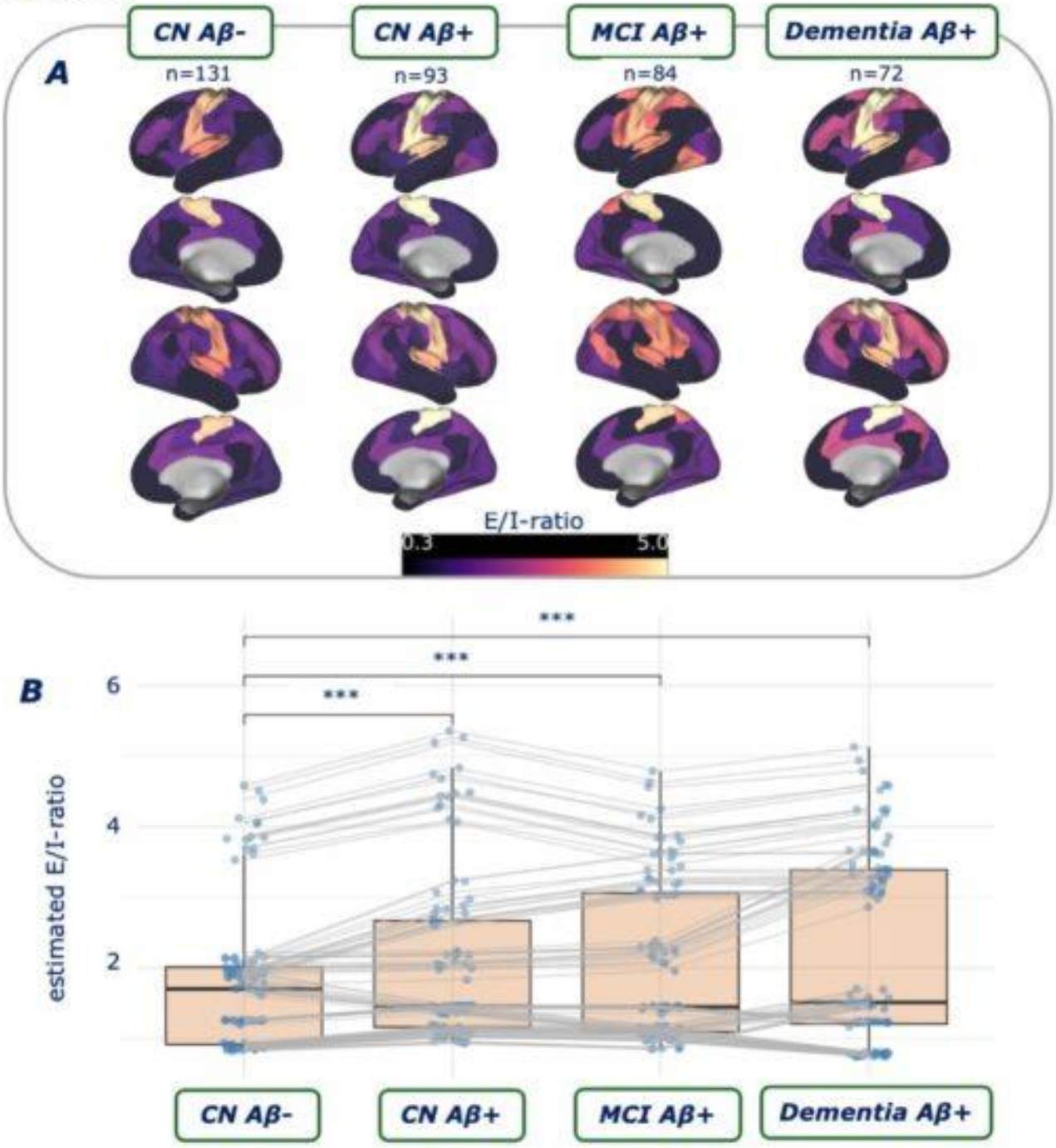
Methods: We assessed the effect Aβ on neuronal hyperactivity by estimating the excitatory to inhibitory (E/I) ratio from resting-state fMRI in 131 amyloid-PET-negative controls and 249 amyloid-PET-positive AD spectrum patients. Second, we used glucose metabolism (FDG-PET) as a marker of neuronal activity in 638 amyloid-PET-positive AD spectrum patients, with a subset (n=215) having tau-PET at a later timepoint. Lastly, we analysed post-mortem data of 5 AD patients and 4 controls stained for c-Fos as a marker of ante-mortem neuronal activity.

Results: fMRI-based E/I-ratio assessment in Aβ- controls showed biologically plausible stronger inhibition in association cortices (Fig.1A). Across the AD spectrum we found an E/I-ratio increase, indicating a hyperexitatory shift across the disease continuum (Fig.1B). Within individuals, higher amyloid-PET was linked to higher FDG-PET z-scores (correlation$_{\text{amyloid-PET vs. FDG-PET}}$: 95%CI[0.08,0.32] p<0.01), suggesting higher neuronal activity in Aβ-harbouring regions (Fig.2A). Similarly, we found post-mortem elevated neuronal c-Fos in AD patients vs. controls, indicating higher ante-mortem neuronal activity (Fig.3G). Finally, amyloid-PET-based prediction of future tau accumulation improved when including regional FDG-PET z-scores (Fig.2B) where FDG-PET-assessed hypermetabolism mediated Aβ-effects on subsequent tau accumulation in preclinical AD (Fig.2C).

Conclusions: Aβ promotes a hyperexcitatory neuronal activity shift manifesting in glucose hypermetabolism, promoting Ab-related tau accumulation. Thus, Aβ-associated neuronal hyperexcitability is a potential target for attenuating the Ab-tau axis.

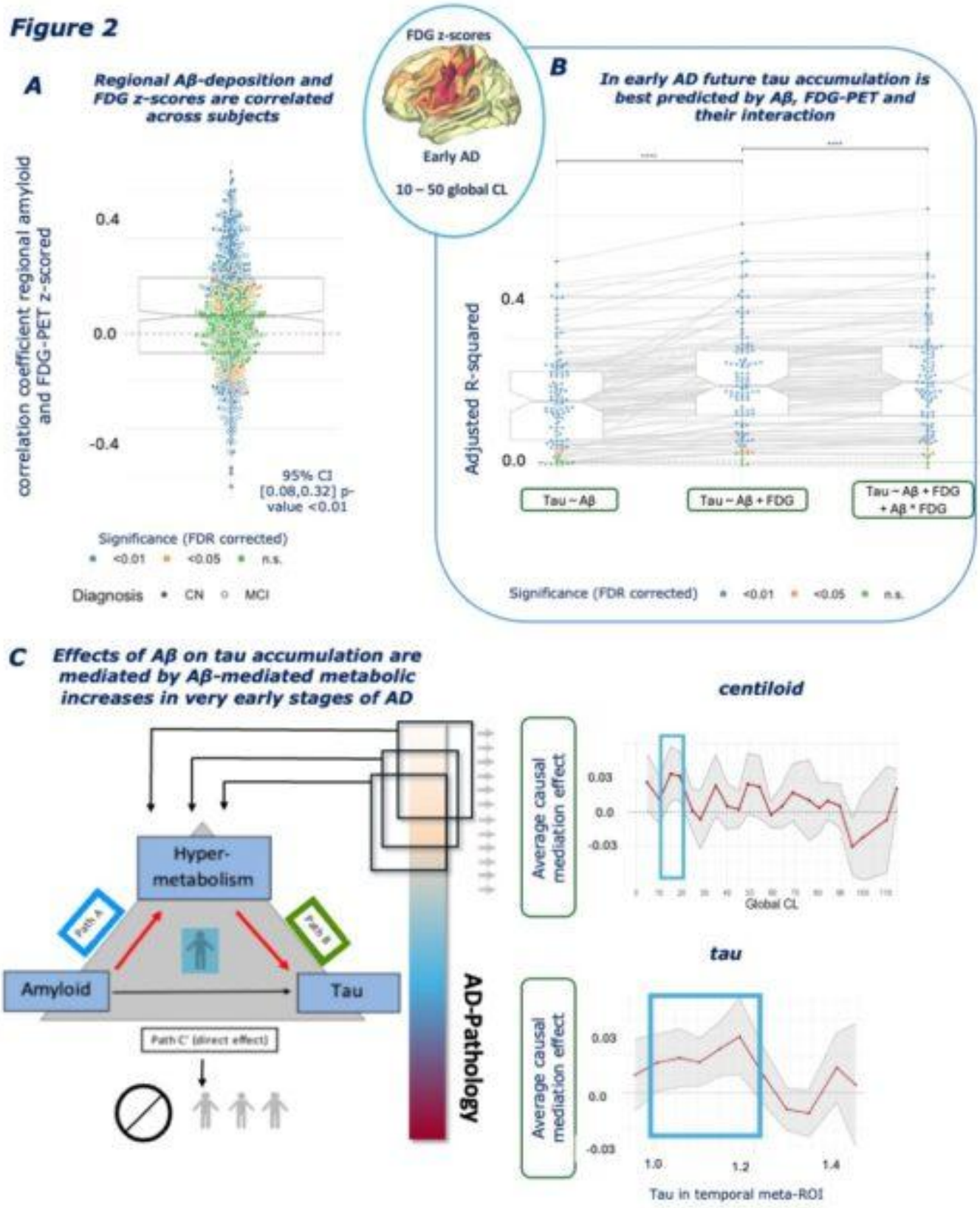
Figure 1

Estimated exitation/inhibition-ratio increases across the AD-spectrum



(A) *Surface rendering of the mean ROI-wise E/I-ratio estimation via the pFIC algorithm by Zhang et al., PNAS, 2024 across the AD spectrum; The distribution of the E/I-ratio in healthy controls matches biologically expected distributions (high in the motor cortex, low in the frontal lobes), indicating biologically plausible E/I-ratio estimation by the pFIC algorithm;* ***(B)*** *Paired t-tests of ROI-wise E/I-ratio across the AD spectrum. E/I-ratio estimates increase across the AD-spectrum. E/I-ratio estimation and amyloid-PET data was parcellated to the Schaefer 100 homotopic atlas by Yan et al 2023.*

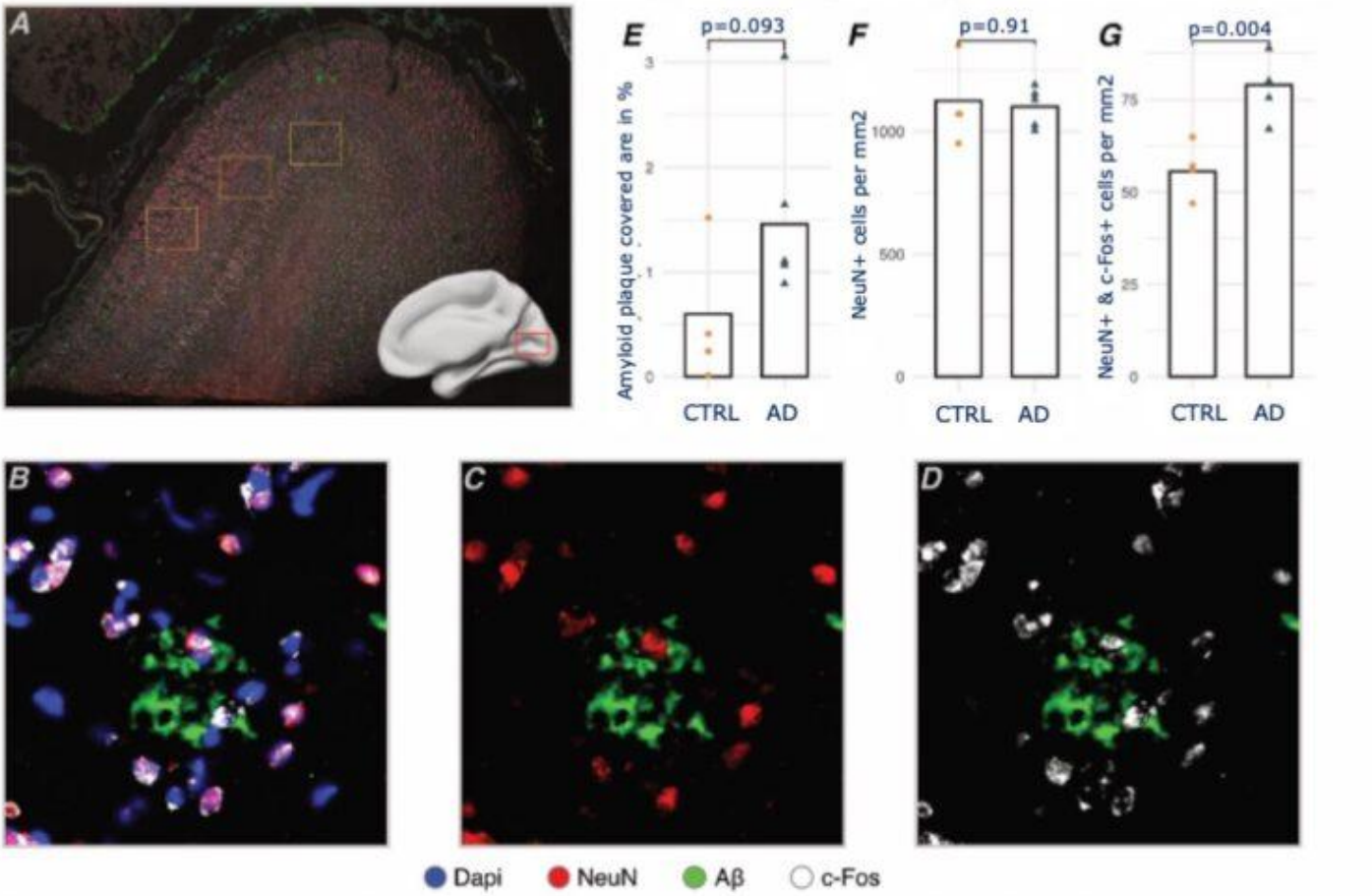
Figure 2



(A) Subject-wise correlation analysis of regional amyloid-PET signal in centiloid and regional FDG-PET signal (z-scored, n=648). Overall, the correlation coefficients are significantly greater than zero (95% CI [0.08,0.32], p<0.01), indicating an overall positive correlation between Aβ-deposition and metabolism assessed via FDG-PET. **(B)** R-squared values of the model predicting future tau-PET signal in early AD (global centiloid 10-50) based on centiloid, centiloid + FDG-PET and centiloid + FDG-PET + centiloid*FDG-PET, showing a significant better prediction for the last model. **(C)** Bootstrapped mediation analysis yielding the effect of Aβ on tau accumulation mediated by metabolism assessed via FDG-PET. The effect average causal mediated effect of amyloid on tau via hypermetabolism is small but significantly greater than zero (95% CI [0.001,0.03], p<0.01) in early AD stages with tau load in the temporal meta-ROI below 1.22 and global centiloid levels below 20, indicating that this mechanisms plays a role in very early stages of the AD disease cascade. Average Causal Mediated Effect = ACME; All PET data was parcellated to the Schaefer 200 atlas.

Figure 3

Post-mortem assessment of neuronal hyperactivity in AD patients vs. controls



Post-mortem analyses of the occipital lobe of AD vs. control (CTRL) brains. ***(A)*** *Overview of tissue stainings.* ***(B)*** *Merged image of Dapi (cell nuclei), NeuN (Neurons), Aβ and c-Fos (marker of ante-mortem neuronal activity),* ***(C)*** *merged image of NeuN and Aβ stainings and* ***(D)*** *merged image of Aβ and c-Fos staining. Group differences in* ***(E)*** *Aβ-Plaque area, indicating a greater amount of Aβ pathology in the AD probes,* ***(F)*** *neuron count (i.e. NeuN), demonstrating the absence of significant neurodegeneration in the occipital lobe, and* ***(G)*** *the proportion of neurons with c-Fos positive signal. AD patients showed a significantly greater number of c-Fos positive neurons, indicating a higher ante-mortem neuronal activity in AD patients in the occipital lobes, where Aβ is the dominant pathology.*

Keywords: hyperactivity, early AD, EI-ratio, amyloid-PET, tau-PET

4 Sex differences in white matter microstructure and associations with amyloid and tau pathology in autosomal dominant Alzheimer's disease

Averi Giudicessi[1,2], Elouise Koops, PhD[3], Ana Baena[4], Sergio Alvarez[5], Monica Vidal[5], Lusiana Martinez[1,2], Isabela Gonzalez[1,2], Catarina Tristão-Pereira[1,2], Vincent Malotaux[1,2], Bing He[1,2], David Aguillon[4], Heidi Jacobs[3], Alice Cronin-Golomb[2], Yakeel Quiroz[1,2]

[1]*Department of Psychiatry, Massachusetts General Hospital, Harvard Medical School, Boston, MA, US*
[2]*Boston University, Boston, MA, US*
[3]*Department of Radiology, Massachusetts General Hospital, Harvard Medical School, Boston, MA, US*
[4]*Grupo de Neurociencias de Antioquia, Universidad de Antioquia, Medellín, CO*
[5]*Hospital Pablo Tobon Uribe, Department of Radiology, Colombia, Medellín, CO*

Background: Women comprise two-thirds of Alzheimer's disease (AD) cases, yet sex-specific mechanisms of disease vulnerability remain understudied. White matter degeneration is increasingly recognized as a critical contributor to AD progression, but whether biological sex modulates white matter vulnerability to amyloid-β (Aβ) and tau pathology is unknown. We investigated sex-specific patterns of white matter microstructure and associations with PET-derived pathology in autosomal dominant AD (ADAD).

Methods: We investigated white matter integrity in the COLombia-Boston cohort with PSEN1-E280A mutation (n=30 carriers) and healthy controls (n=33 non-carriers) using fixel-based analyses. Multiple linear regressions examined fiber density (FD), fiber-bundle cross-section (FC), and combined metrics (FDC) across major white matter tracts in relation to sex, PET-derived amyloid and tau burden, and cognitive performance.

Results: Females exhibited higher fiber cross-section than males in the anterior thalamic radiation (β=0.057, p=0.004), forceps minor of the corpus callosum (β=0.047, p=0.012), and inferior fronto-occipital fasciculus (β=0.030, p=0.015), but lower values in the cingulum cingulate gyrus (β=-0.07, p=0.031). Sex significantly moderated the association between pathology and white matter. In the right temporal superior longitudinal fasciculus, females showed relatively preserved integrity compared to males as tau burden increased (β=0.23, p=0.016), while males exhibited greater Aβ-associated disruption than females in the uncinate fasciculus (β=-0.14, p=0.05). Sex also moderated relations between white matter integrity and cognition, with males showing stronger structure-function coupling than females in tracts such as the cingulum hippocampus, forceps major, and corticospinal tract (β: -12.8 to -34.6, all p≤0.001).

Conclusion: We observed complex, tract-specific sex differences in white matter vulnerability to AD pathology in ADAD. Sex influenced both baseline white matter structure and pathology-related degeneration, with females showing structural advantages in some tracts but greater vulnerability in others. These divergent patterns suggest distinct neurobiological mechanisms by which biological sex modulates white matter degeneration and its cognitive consequences, warranting further investigation.

Figures:

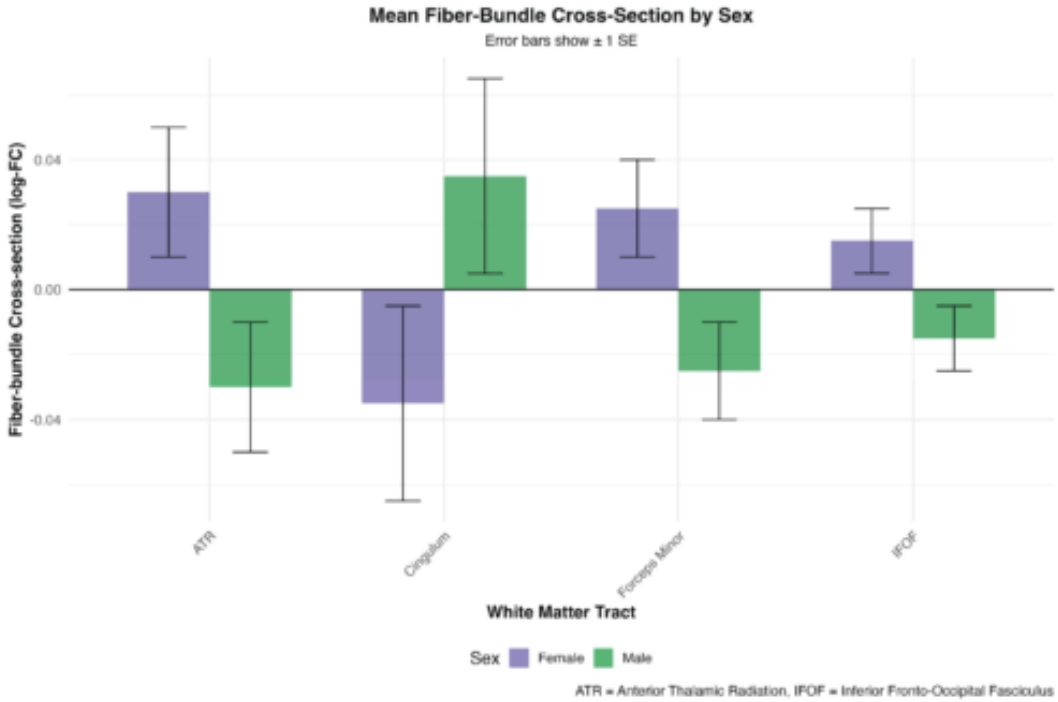


Figure 1. Sex differences in mean fiber-bundle cross-section across white matter tracts. Bar plot comparing log-transformed fiber cross-section (log-FC) between males and females across four major white matter tracts. Females show higher fiber cross-section in the anterior thalamic radiation (ATR), forceps minor, and inferior fronto-occipital fasciculus (IFOF). Males demonstrate higher values in the cingulum (cingulate gyrus portion)gyrus and Error bars represent ±1 standard error. ATR = anterior thalamic radiation; IFOF = inferior fronto-occipital fasciculus.

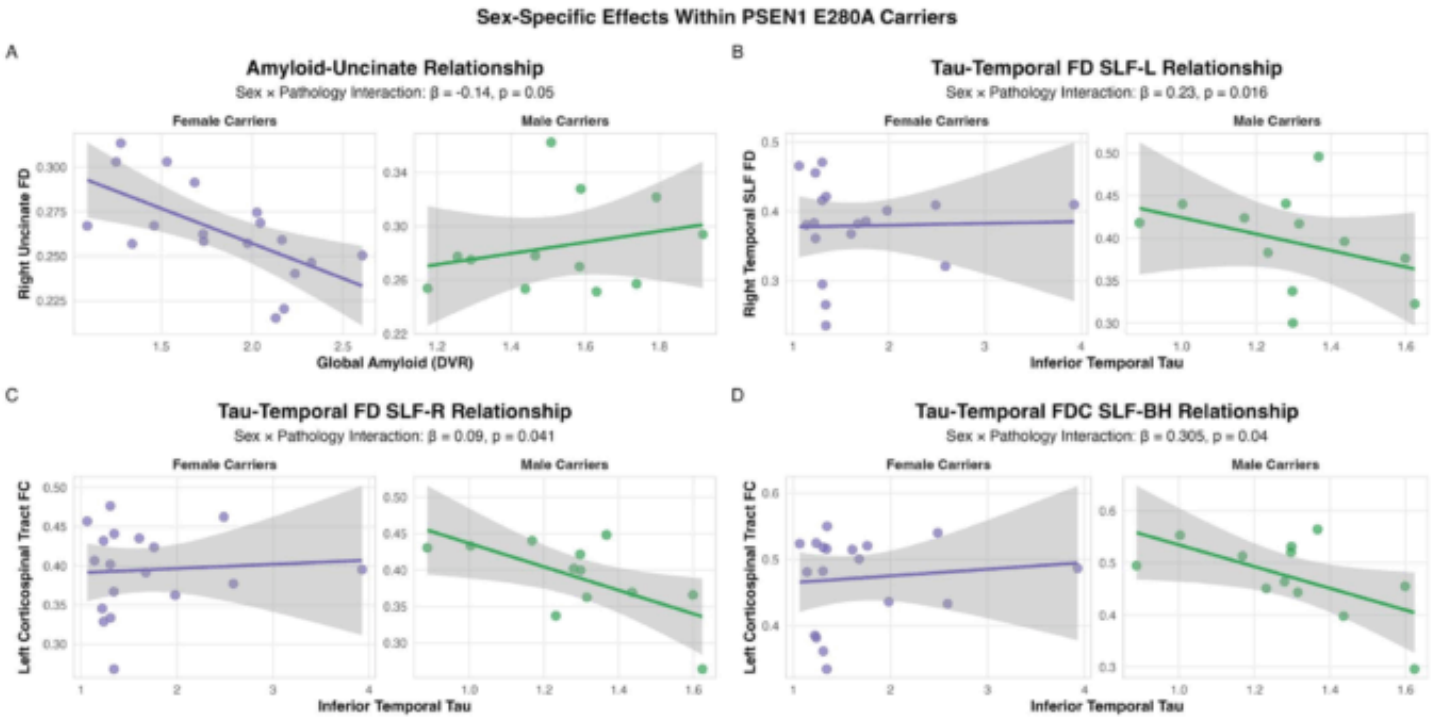


Figure 2. Sex-specific effects of pathological proteins on white matter integrity within PSEN1 E280A carriers. Sex-stratified relationships between pathological protein burden and white matter measures in mutation carriers show distinct patterns by sex. (A) Global amyloid-right uncinate fasciculus fiber density relationship demonstrates significant sex × pathology interaction (β = -0.14, p = 0.05), with females showing negative associations while males show positive associations. (B-D) Inferior temporal tau relationships with superior longitudinal fasciculus measures show consistent patterns where males exhibit stronger negative associations than females: (B) Right temporal SLF fiber density (β = 0.23, p = 0.016), (C) Left temporal SLF fiber cross-section (β = 0.09, p = 0.041), and (D) Right temporal SLF fiber density and cross-section (β = 0.305, p = 0.04). Points represent individual carriers; lines show sex-specific regression fits with 95% confidence intervals. FD = fiber density; FC = fiber cross-section; FDC = fiber density and cross-section; SLF = superior longitudinal fasciculus.

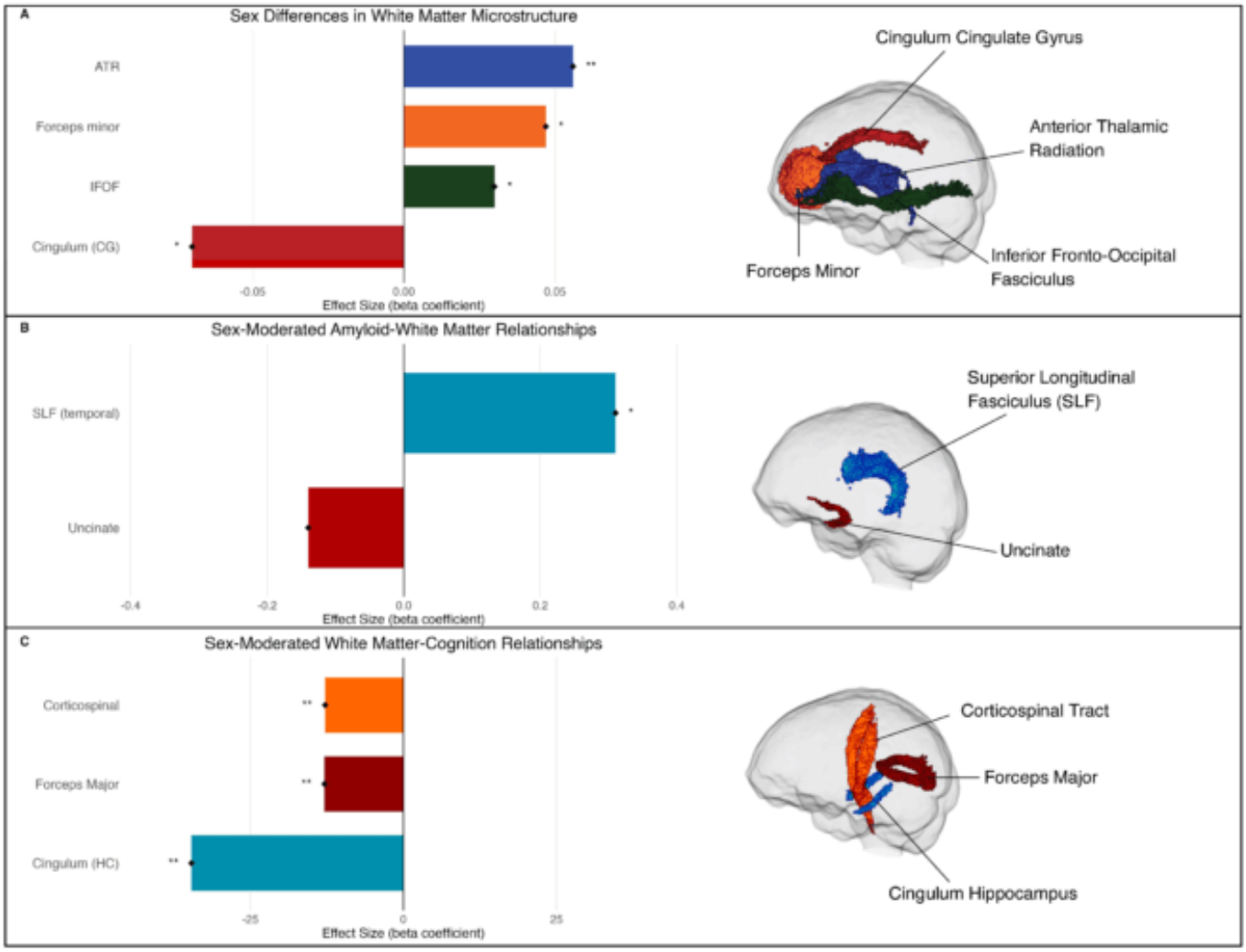


Figure 3. Sex differences and sex-moderated relationships in white matter microstructure among PSEN1 E280A mutation carriers and non-carriers. (A) Sex differences in fiber cross-section (log-FC). (B) Significant sex interactions were observed for amyloid and tau burden (C) Sex-moderated white matter-cognition relationships. Visualizations show anatomical locations of significant white matter tracts using the same color scheme as the bar plots. Significance levels: *p < 0.05, **p < 0.01.

Keywords: Sex differences, White matter microstructure, Autosomal dominant Alzheimer's disease, Cognitive function, biomarkers

5 Concordance between amyloid PET and biomarkers of Alzheimer's disease in plasma and cerebrospinal fluid in cognitively unimpaired individuals

Camilo Bermudez[1], Angela J. Fought[2], Ekaterina Hofrenning[3], Val Lowe[3], Ronald C. Petersen[1], Prashanthi Vemuri[3], Clifford R. Jack, Jr.[3], Alicia Algeciral-Schimnich[4], Joshua A. Bornhorst[4], Jonathan Graff-Radford[1]

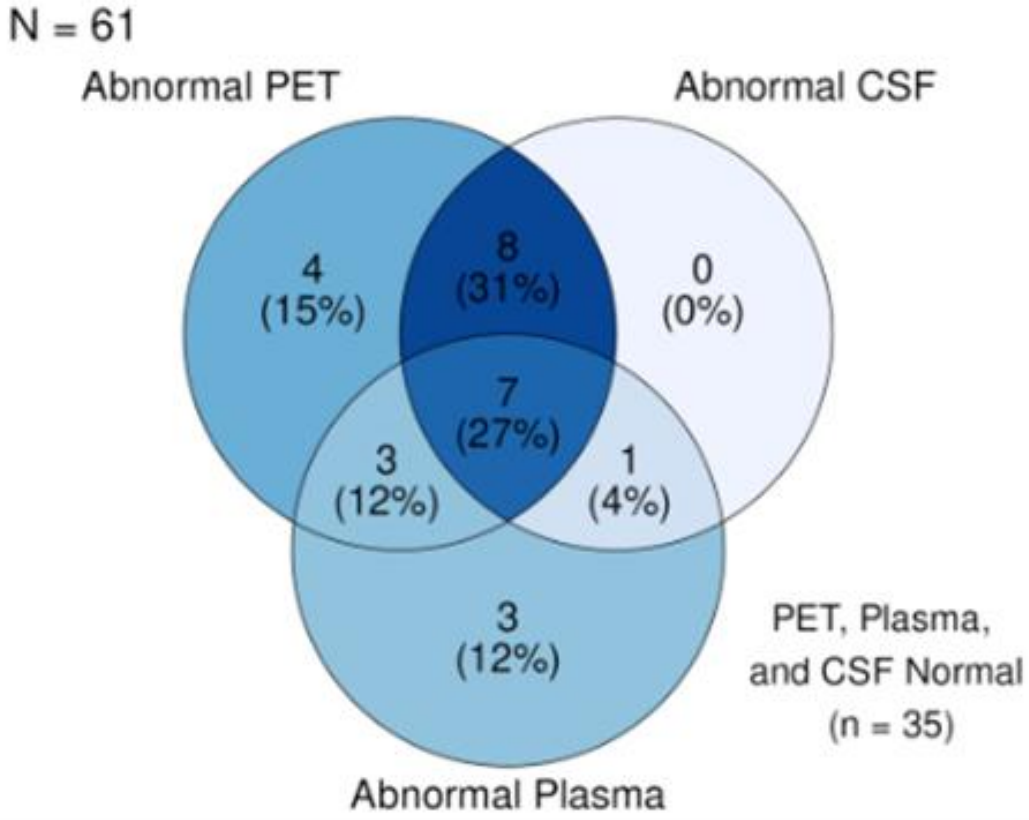
[1]*Department of Neurology, Mayo Clinic, Rochester, MN, US*
[2]*Department of Quantitative Health Sciences, Mayo Clinic, Rochester, MN, US*
[3]*Department of Radiology, Mayo Clinic, Rochester, MN, US*
[4]*Department of Laboratory Medicine and Pathology, Mayo Clinic, Rochester, MN, US*

With the development of anti-amyloid therapies, there is increasing reliance on biomarkers for detecting Alzheimer's Disease (AD) amyloid pathology, but practices differ on what biomarker is used to establish a diagnosis between plasma, cerebrospinal fluid (CSF), or amyloid PET. There is limited data about the three-way agreement between these tests, particularly in a cognitively unimpaired population. As interventions move towards the cognitively unimpaired, understanding differences is of key importance.

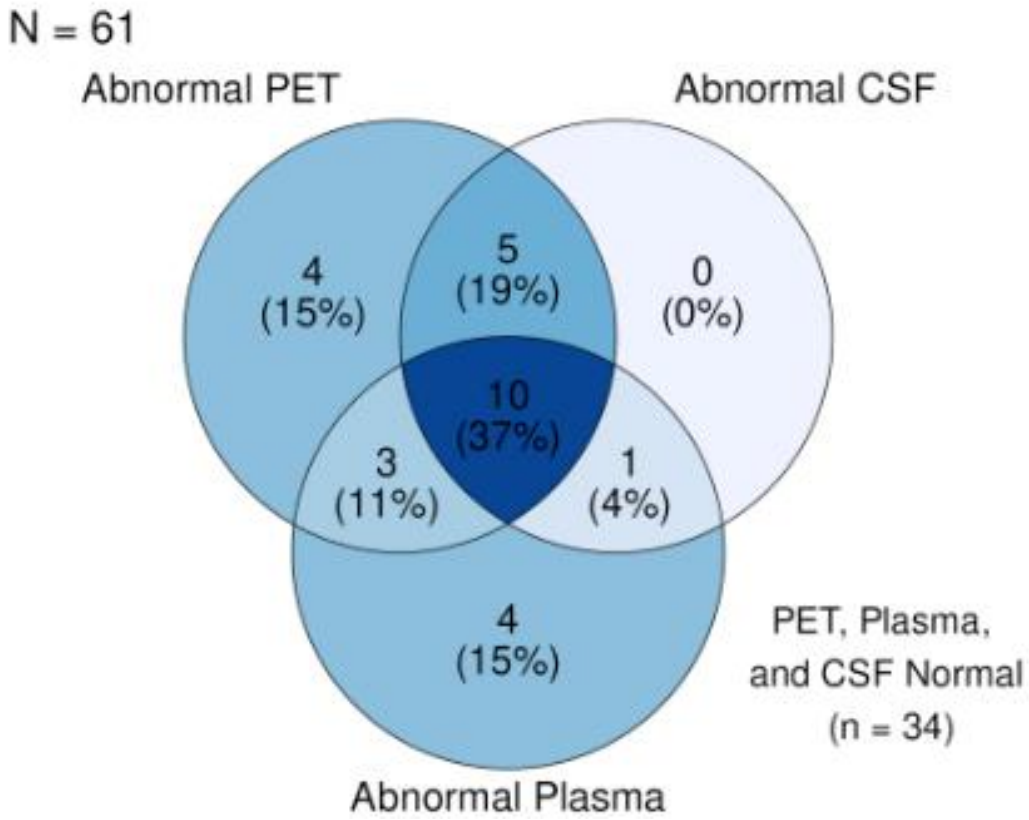
Here we examined a cohort of 61 cognitively unimpaired participants over age 50 with mass-spectroscopy plasma biomarkers including %ptau217 (positive > 1.55%) and APS2 (positive > 47), CSF biomarker p-tau/Aβ42 (positive > 0.028), and amyloid PET (positive >25 centiloid) obtained within two years of each other as part of the Mayo Clinic Study of Aging and Alzheimer's Disease Research Center to assess for agreement between measures for detection of AD. Overall, 28 (72.6%) of participants had at least one positive biomarker across plasma, CSF, or amyloid PET. For the 22 PET positive participants, 13 (59%) had a positive %ptau-217, 10 (45%) had a positive APS2, and 15 (68%) were CSF positive. For the 16 patients who were CSF positive, 15 (94%) had a positive amyloid PET, 8 (50%) has positive AP2 and 10 (63%) had positive %ptau217. Of the 14 participants with positive APS2, 10 (71%) has positive amyloid PET and 8 (57%) has positive CSF. Of the 18 participants with positive %ptau217, 13 (72%) has positive amyloid PET and 11 (61%) had positive CSF testing.

Overall, %ptau217 had higher 3-way positive agreement with 10 (37%) participantscompared APS2 with 7 (27%) participants.Understanding the agreement between biomarkers of AD will be increasingly important for scalability and resource management in early screening of asymptomatic individuals that may benefit from amyloid reducing therapies, although concordance may be less than in impaired individuals.

APS2 : Amyloid PET : CSF ratio (old APS2 cutoff)



%ptau217 : Amyloid PET : CSF ratio (old %ptau217 cutoff)



Keywords: biomarker concordance, Alzheimer's disease, plasma, CSF, PET

6 Comparing performance of different amyloid PET markers of spatial extent in their ability to predict future amyloid conversion

Praveen Honhar[1,2], Michelle Farrell[1,3], Michael Properzi[2], Emma Thibault[2], Aaron Schultz[1,3], Alex Becker[2], Jessie Fu[1,2], Reisa Sperling[3,4], Julie Price[1,2], Keith Johnson[2,3]

[1]*Athinoula A. Martinos Center for Biomedical Imaging, Charlestown, MA, US*
[2]*Department of Radiology, Massachusetts General Hospital, Harvard Medical School, Boston, MA, US*
[3]*Department of Neurology, Massachusetts General Hospital, Harvard Medical School, Boston, MA, US*
[4]*Department of Neurology, Center for Alzheimer's Research and Treatment, Brigham and Women's Hospital, Harvard Medical School, Boston, MA, US*

Background: Previously, an amyloid PET spatial-extent metric (EXT) based on region-of-interest distribution volume ratios (*DVR* ROI-EXT) was found to be more sensitive than neocortical-*DVR* for early detection of subthreshold amyloid leading to future global PIB(+) status. In this work, we compared regional and voxel-level EXT measures, computed from standardized uptake value ratios (*SUVR* ROI-EXT and *SUVR* Voxel-EXT) against *DVR* ROI-EXT.

Methods: Pittsburgh compound-B (PIB) *SUVR*(40–60 min) images were analyzed in 207 older adults from the Harvard Aging Brain Study, all PIB(–) at baseline (neocortical-*DVR*<1.19,<24CL), see Table1. ROI-EXT was defined as the percent volume classified as PIB+ within a published neocortical mask, computed by comparing PIB *DVR* or *SUVR* within 42 ROIs with each ROI's Gaussian mixture model-based (GMM) threshold. For Voxel-EXT, *SUVR* images were normalized and smoothed (Gaussian 6mm-FWHM) before GMM application within the mask. Percent *SUVR* Voxel-EXT was computed relative to voxels where GMM converged. Baseline *SUVR* ROI-EXT, *DVR* ROI-EXT, neocortical-*DVR*, neocortical-*SUVR*, and *SUVR* Voxel-EXT were compared for predicting future global neocortical PIB(+)(neocortical-*DVR*>1.19) within 5y using receiver-operating-characteristics (ROC). Thresholds for PET measures were selected at specificity>0.9 to minimize type-I errors.

Results: Baseline *SUVR* ROI-EXT's performance was nearly identical to *DVR* ROI-EXT (Youden sensitivity and specificity:0.86 and 0.97, Figure1A). Baseline *SUVR* ROI-EXT and *DVR* ROI-EXT values were highly correlated across individuals (Pearson's r=0.91,p<0.001,Figure1B). Voxel-level GMM converged for 90.1% voxels within the neocortical mask with reasonable thresholds (see Figure2), but *SUVR* Voxel-EXT was inferior (Youden sensitivity and specificity:0.71 and 0.96, Figure3) than its ROI-EXT variant in ROC analysis.

Conclusion: Our results indicate that simplified *SUVR*-based spatial EXT metrics retain the predictive power of *DVR*-based EXT. Weaker Voxel-EXT performance may reflect a fundamental constraint; binning to larger regions could improve sensitivity for future global amyloid prediction. Overall, EXT metrics can enhance studies of early AD pathogenesis and support earlier prevention-trial interventions.

Table 1. Cohort Demographics. Reported values are Mean ± SD.

	N		Sex		Baseline Age	Follow-up Period	Baseline PET Measures (Ref: Cerebellar Cortex)	
	BL	FU	F	M			Logan *DVR*	*SUVR*
HABS-Cohort	207	605	131	76	72 ± 8 y	4.4 ± 3.3 y	1.07 ± 0.05	1.33 ± 0.32

HABS – Harvard Aging Brain Study, Ref – Reference Region.

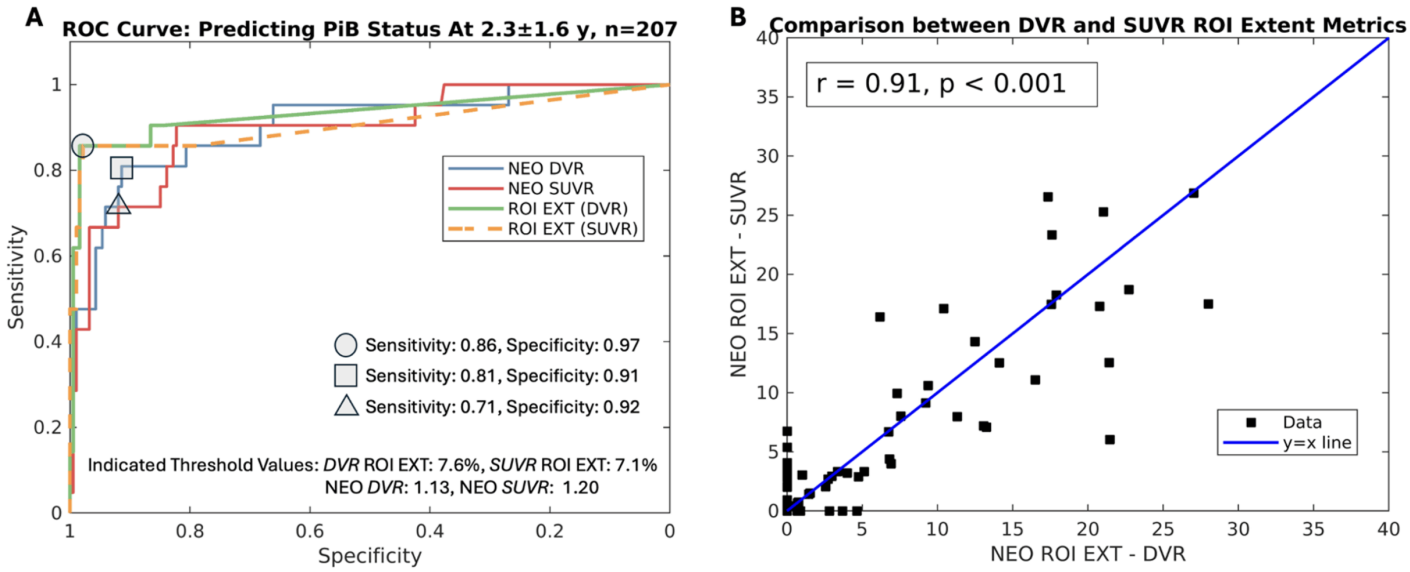


Figure 1: A: ROC analysis comparing *DVR* ROI-EXT, *SUVR* ROI-EXT, Neocortical-*DVR* and Neocortical- *SUVR* in the prediction of future (up to 5y) PIB(+) status in 207 subjects that were PIB(-) at baseline. 21/207 subjects converted to PIB(+) status during follow-up period. Indicated thresholds are based on Youden's J statistic, though an additional criterion to maintain specificity>0.9 due to predominance of type-I errors was important for Neocortical-*DVR* and Neocortical- *SUVR*. B: Scatter plot of *SUVR* ROI-EXT and *DVR* ROI-EXT across 207 baseline scans show a high correlation (Pearson's r = 0.91, p < 0.001).

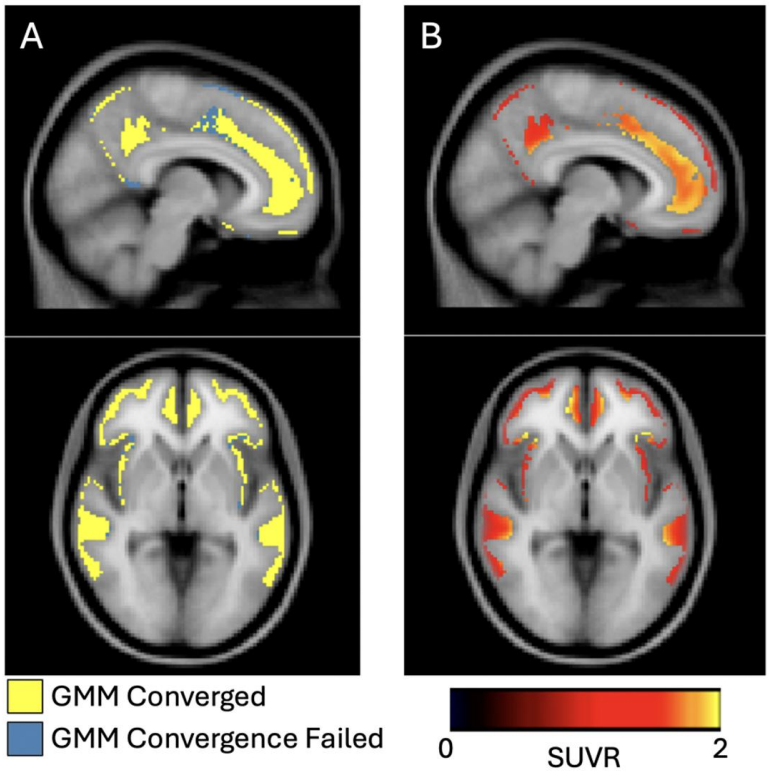


Figure 2: A: Overlay of neocortical mask voxels where the voxel-level GMM analyses on *SUVR* values converged (yellow) and did not converge (blue) on a T1 image in MNI space. Overall, GMM converged in >90% voxels with prominent exceptions being voxels close to white-matter (WM) in the anterior cingulate, insula and other regions. B: GMM (70^{th}-percentile) *SUVR* thresholds for EXT+ in the neocortical mask overlaid on T1 image. The thresholds become increasingly higher towards gray-white matter boundaries as expected due to higher PIB *SUVR* values within WM.

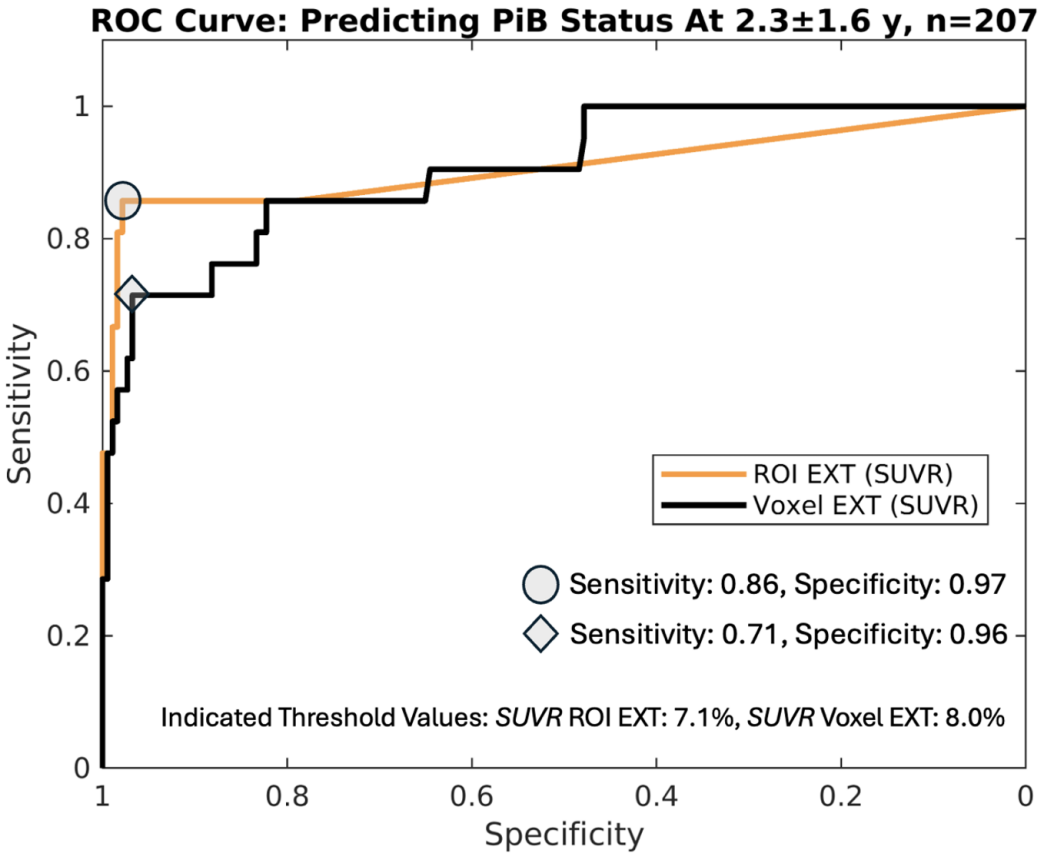


Figure 3: ROC analysis comparing *SUVR* ROI-EXT and *SUVR* Voxel-EXT in the prediction of future (up to 5y) PIB(+) status in 207 subjects that were PIB(-) at baseline. *SUVR* Voxel-EXT (EXT+ established using voxel-level GMM thresholds) compared unfavorably to *SUVR* ROI-EXT.

Keywords: PET Biomarkers, Amyloid, Early Detection, Spatial Extent, Simplified Quantification

7 Elevated ptau217 is more strongly associated with tau accumulation and cognitive decline in younger adults

Gillian Coughlan[1,5], Diana Townsend[1], Annie Li[1], Mabel Seto[1,5], Colin Birkenbihl[1], Karly Cody[2], Hannah Klinger[1], Brian Healy[1,3], Michelle Farrell[1], Emma Thibault[1], Robert Rissman[4], Michael Properzi[1], Aaron Schultz[1], Jasmeer Chhatwal[1,5], Hyun-Sik Yang[1,5], Michael Donohue[4], Tobey Betthauser[2], Sterling Johnson[2], Keith Johnson[6], Reisa Sperling[1,5], Rachel Buckley[1,5,7]

[1]*Department of Neurology, Massachusetts General Hospital, Harvard Medical School, Boston, MA, US*
[2]*Department of Medicine, University of Wisconsin-Madison School of Medicine and Public Health, Madison, WI, US*
[3]*Harvard T.H. Chan School of Public Health, Boston, MA, USA, Boston, MA, US*
[4]*Alzheimer's Therapeutic Research Institute, University of Southern California, San Diego, CA, US*
[5]*Brigham and Women's Hospital, Boston, MA, US*
[6]*Gordon Center for Medical Imaging, Department of Radiology, Boston, MA, US*
[7]*Melbourne School of Psychological Sciences, University of Melbourne, Melbourne, AU*

Background: PET neuroimaging studies consistently show that younger individuals with symptomatic Alzheimer's disease(AD) experience a more aggressive disease course. However, it remains unclear whether age influences disease trajectories in the preclinical stage. To address this, we examined whether younger age at the time of elevated plasma pTau217, a validated preclinical AD biomarker, predicts accelerated tau accumulation and cognitive decline.

Methods: We included 1208 clinically normal individuals(age 46-92; Aβ-centiloid=31; 499-*APOE*ε4-carriers; Table) from four longitudinal cohorts including the A4 and LEARN studies(A4LEARN), the Wisconsin Registry for Alzheimer's Prevention(WRAP), the Harvard Aging Brain Study(HABS) and the Alzheimer's Disease Neuroimaging Initiative(ADNI). Participants underwent baseline plasma pTau217 and repeated tau-PET imaging (mean follow-up=3.5 years, SD=1.6). Regional tau-PET composites were derived for medial-temporal and neocortical regions. Cognition was assessed using the Preclinical Alzheimer's Cognitive Composite(PACC). For each cohort, random-effects models(covarying sex*time) examined pTau217(continuous)×age(continuous)×time interactions on longitudinal tau and PACC. Meta-analyses estimated the global fixed effect(β) and between studies heterogeneity(I^2).

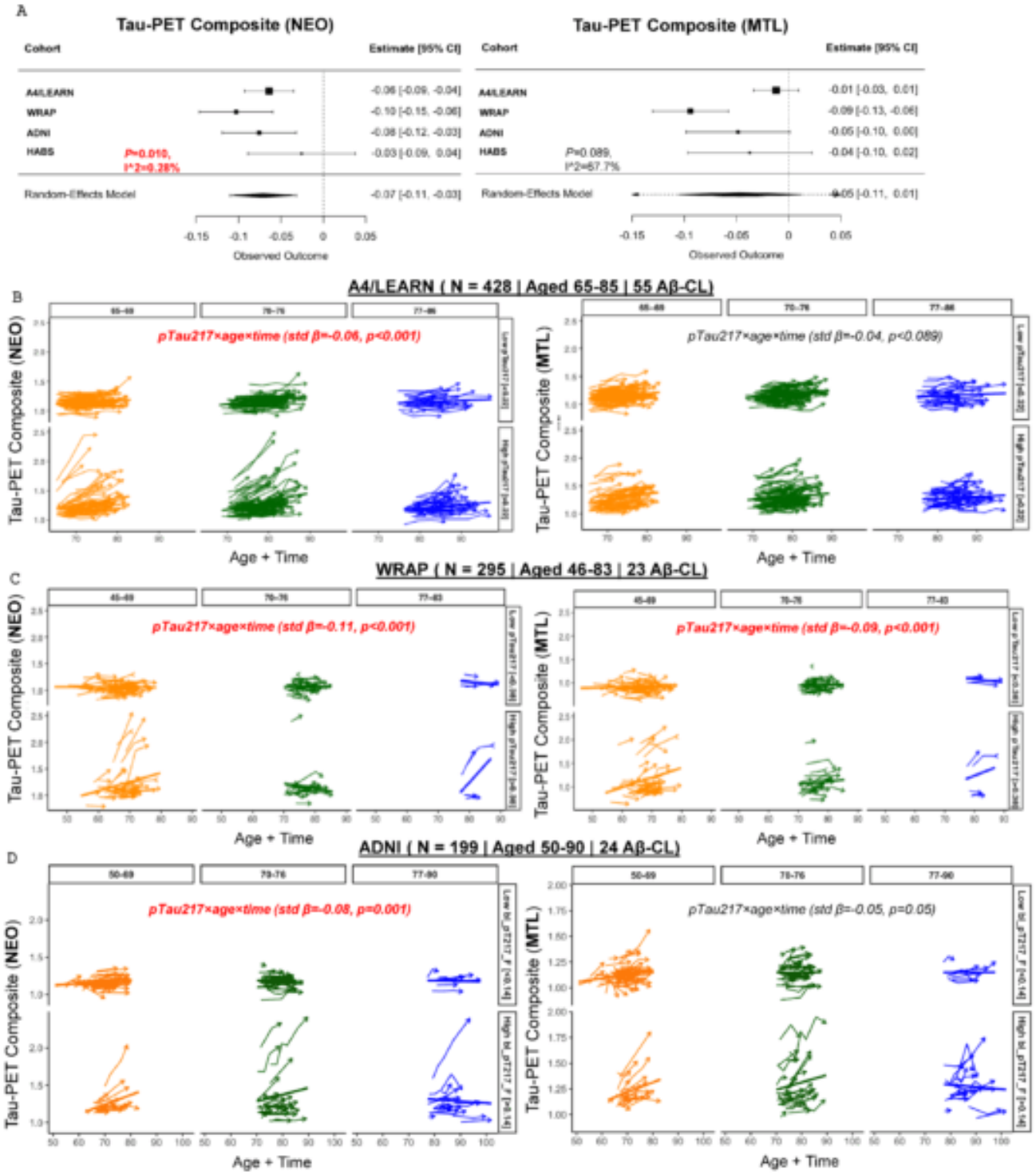
Results: At younger ages, individuals with high pTau217 show much steeper neocortical tau accumulation relative to older ages(global-β=-.07[95%CI=-.11,-.03], I^2=.28, *p*=.010). Meta-analysis yielded non-significant associations with medial temporal tau accumulation(*p*=.089; Figure1A). When analyzed by cohort, the pTau217×age×time interaction was significant for neocortical tau in A4LEARN(stdβ=-0.06,*p*<0.001; Figure1B), WRAP(stdβ=-0.11,*p*<0.001; Figure1C), and ADNI(stdβ=-0.08,*p*=0.001;Figure1D), and for medial temporal tau in WRAP(stdβ=-0.09,*p*<0.001, Figure1C) and marginally in ADNI(stdβ=-0.05,*p*=0.05;Figure1D). While the meta-analysis on longitudinal PACC was not significant(*p*=.149), individuals with high pTau217 exhibited faster PACC decline in A4/LEARN, particularly at younger ages(stdβ=0.06, p=.006;Figure 2A), supported by non-linear spline modeling(Figure 2B), including education and PACC-version as covariates. All effects remained significant adjusting for Aβ-centiloid.

Discussion: These findings suggest that in those with elevated high-pTau217, risk of tau accumulation and cognitive decline increases at younger ages; supporting the prioritization of clinical normal younger adults for detection and intervention in AD clinical trials.

Table: Baseline demographic and clinical characteristics

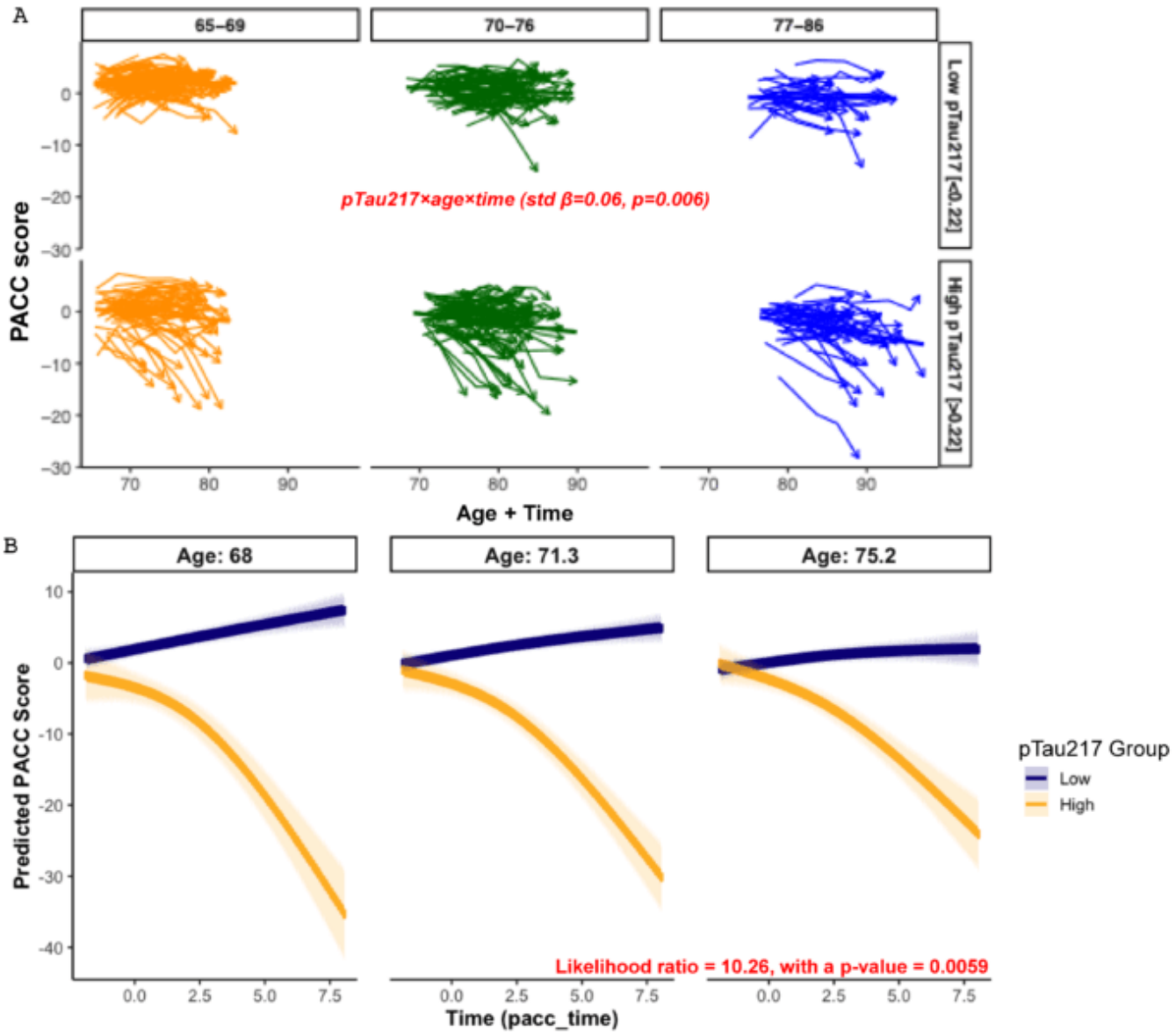
	A4/LEARN (N = 428 | Aged 65-86)				WRAP (N = 295 | Aged 46-83)				ADNI (N = 195 | Aged 51-90)				HABS (N = 286 | Aged 50-93)			
Characteristics	**65-69**	**70-76**	**77-86**	**p value**	**46-69**	**70-76**	**77-83**	**p value**	**51-69**	**70-76**	**77-90**	**p value**	**50-70**	**70-76**	**77-93**	**p value**
N	168	169	91		177	84	34		91	64	44		95	92	99	
Female sex %	119 (71)	86 (51)	46 (51)	<0.001	117 (66)	55 (65)	27 (71)	0.9	62 (68)	33 (52)	22 (50)	<0.001	62 (65)	54 (59)	54 (55)	0.3
Mean Age (SD)	67.5 (1.4)	72.8 (1.8)	79.1 (2.9)	<0.001	63.7 (4.6)	72.8 (1.7)	78.3 (1.6)	<0.001	65.8 (3.6)	72.8 (1.7)	80.4 (3.9)	<0.001	63.1 (5.2)	72.7 (2.1)	82.7 (3.9)	<0.001
Aβ Centiloid	49.5 (34)	56.2 (34)	67.4 (38)	<0.001	15.6 (30)	16.3 (30)	43 (49)	0.017	16.5 (30)	21.7 (40)	41.2 (50)	0.019	13.3 (18)	26.5 (30)	30.6 (35)	<0.001
APOE-ε4	79 (46)	22 (26)	14 (41)	0.14	79 (46)	22 (26)	14 (41)	0.008	40 (44)	24 (38)	17 (39)	0.7	25 (27)	27 (30)	24 (25)	0.8
Education	16.2 (3.0)	16.3 (2.7)	15.9 (2.8)	0.6	16.8 (3.0)	16.2 (2.7)	16.6 (2.4)	0.6	-	-	-	-	16.2 (2.7)	16.6 (2.7)	15.7 (3.4)	0.2
Baseline P-tau217*	0.23 (0.2)	0.26 (0.2)	0.31 (0.2)	0.001	0.47 (0.36)	0.51 (0.4)	0.71 (0.6)	0.001	0.0057 (0.0064)	0.0078 (0.0071)	0.0134 (0.0185)	<0.001	2.8 (2.5)	3.7 (2.8)	5.1 (3.6)	<0.001
MTL-PET SUVr	1.16 (0.13)	1.20 (0.15)	1.24 (0.14)	<0.001	0.99 (0.25)	1.00 (0.22)	1.14 (0.30)	<0.001	1.14 (0.10)	1.19 (0.15)	1.20 (0.12)	0.006	1.11 (0.08)	1.18 (0.10)	1.20 (0.11)	<0.001
NEO-PET SUVr	1.17 (0.11)	1.17 (0.11)	1.18 (0.10)	0.042	1.10 (0.21)	1.12 (0.28)	1.16 (0.24)	0.04	1.16 (0.06)	1.22 (0.16)	1.21 (0.11)	0.008	1.13 (0.07)	1.16 (0.08)	1.18 (0.09)	<0.001
Tau FU time	3.49 (1.62)	3.48 (1.64)	3.41 (1.63)	0.6	3.03 (1.21)	3.11 (1.35)	2.92 (1.11)	0.1	3.31 (1.91)	3.44 (1.85)	3.00 (1.86)	0.05	4.21 (1.97	4.04 (2.29)	3.71 (1.99)	0.04

Figure 1. In the context of elevated p-Tau217, younger adults exhibited accelerated tau accumulation relative to older adults.



A: Meta-analysis confirmed a significant age×pTau217×time effect on tau accumulation. Within cohort, significant interactions on neocortical accumulation were present in **B:** A4/LEARN, **C:** WRAP and **D:** ADNI. For context, within the high-pTau217 group in A4LEARN, younger (65–69) participants showed the steepest neo tau-PET slopes (~0.058 SUVR/year), followed by those aged 70–76 (~0.045 SUVR/year) and ≥77 (~0.027 SUVR/year). In WRAP, younger (45–69) participants exhibited the fastest neo tau-PET accumulation (~0.09 SUVR/year), while mid-older ages (70–76 and ≥77) showed more modest slopes (~0.03–0.04 SUVR/year). In ADNI, the estimated annual tau-PET slope was 0.045 SUVR/year for those aged 50–69, compared with 0.028SUVR/year for those aged 70–76, and 0.007SUVR/year for participants aged 77 or older. Significant interactions on medial temporal accumulation were present in **C:** WRAP (WRAP was the only cohort using the [^{18}F]MK-6240 tau-PET tracer) and were marginally significant in **D:** ADNI. Age and pTau217 were visualized as categorical but analyzed as continuous variables. Ptau217 assays included ECE immunoassay in A4LEARN, ALZPath in WRAP, Lumipulse in ADNI, and C^{2}N in HABS. NEO: Neocortical (Inferior temporal gyrus | Inferior parietal gyrus | Fusiform gyrus). MTL: Medial temporal lobe (Entorhinal cortex | Amygdala | Parahippocampus), CL=centiloid. I^2=heterogeneity in a meta-analysis due to differences across studies rather than chance.

Figure 2. In the context of elevated p-Tau217, younger adults exhibited accelerated cognitive decline relative to older adults in A4LEARN (*N*=428)



A: Linear mixed models show a significant pTau217×age×time interaction on cognitive decline **B:** Spline modeling using a natural cubic spline basis (2 degrees of freedom; boundary knots = [-1.88, 8.05]) significantly improved model fit compared to a reduced model. Age and pTau217 were visualized as categorical but analyzed as a continuous variable. pTau217 group was categorized at the 50th percentile for visualization.

Keywords: Longitudinal tau-PET, ptau217, cognition, age

8 Quantitative relationship between Lumipulse G measures of pTau217 in plasma and in brain

Rik Vandenberghe[1], Sandra Tomé[2], Steffi De Meyer[1,4], Julie Goossens[3], Charlotte Lambrechts[3], Koen Poesen[4], Jeroen Vanbrabant[3], Eugeen Vanmechelen[3], Dietmar R. Thal[2]

[1]*Laboratory for Cognitive Neurology, Leuven, Belgium*
[2]*Laboratory of Neuropathology, Leuven, Belgium*
[3]*ADx Neurosciences, Zwijnaarde, Belgium*
[4]*Laboratory for Molecular Neurobiomarker Research, Leuven, Belgium*

Objective: To determine the quantitative relationship between Lumipulse G pTau217 levels and pTau217/β amyloid 1-42 ratio in plasma, on the one hand, and pTau217 levels in brain, on the other hand.

Background: Recently, the Lumipulse G pTau217/$A\beta_{1-42}$ ratio in plasma has been FDA approved for early detection of amyloid plaques associated with Alzheimer's disease (AD) in patients aged above 55 years exhibiting symptoms of the disease.

Methods: The study cohort consisted of 32 academic memory clinic recruited dementia cases selected from the UZ/KU Leuven Brain bank based on the conjoint availability of in vivo plasma samples stored at -80° and postmortem brain tissue. Mean (SD) age at blood sampling was 66 (10) years, 12 (32%) were women. Mean (SD) time interval between blood sampling and autopsy was 5 (3) years. The neuropathological diagnoses were AD, FTLD-TDP (n=10) or FTLD-Tau (n=3).). The N-terminal pTau217 assay ($pTau217_{ADx}$) optimized for measuring in brain tissue and plasma was used to measure both matrices. The FDA approved mid-region pTau217 ($pTau217_{Fuji}$) assay and the $pTau217_{Fuji}/_{A\beta1-42}$ assay was used on all plasma samples.

Results: Plasma $pTau217_{ADx}$, $pTau217_{Fuji}$ and $pTau217_{Fuji}/A\beta_{1-42}$ assays strongly correlated with brain $pTau217_{ADx}$ levels ($0.73 \leq$ partial $\rho \leq 0.78$). Generalized additive models adjusted for ages at blood sampling, time interval between blood sampling and death, sex, and post-mortem interval showed a non-linear relationship between all plasma pTau217 assays and brain pTau217 levels ($P < 0.0005$). Numerically, the plasma $pTau217_{ADx}$ assay (adj. $R^2 = 0.59$) and the $pTau217_{Fuji}/A\beta_{1-42}$ ratio (adj. $R^2 = 0.58$) showed slightly higher predictive value for brain pTau217 levels compared to $pTau217_{Fuji}$ (adj. $R^2 = 0.56$). All Lumipulse assays showed excellent diagnostic performances in distinguishing AD patients from non-AD disease controls ($0.88 < AUC < 0.94$).

Conclusions: Plasma $pTau217_{ADx}$, $pTau217_{Fuji}$ and $pTau217_{Fuji}/A\beta_{1-42}$ assays accurately predict brain pTau217 levels.

Keywords: validation, Lumipulse, ptau217

9 Distinct mechanisms underlying APOE-ε4 and sex effects on medial temporal tau pathology: A neuropathology study

Gemma Salvadó[1], Colin Groot[3,4], Laura E Wisse[5], Jacob W Vogel[6], Thomas G Beach[7], Geidy E Serrano[7], Eric M Reiman[8], Julie A Schneider[9], David A Bennett[9,10], Rik Ossenkoppele[1,3,4], Oskar Hansson[1]

[1]*Clinical Memory Research Unit, Department of Clinical Sciences, Malmö, Lund University, Lund, Sweden*
[2]*Barcelonaβeta Brain Research Center (BBRC), Pasqual Maragall Foundation, Barcelona, Spain*
[3]*Alzheimer Center Amsterdam, Neurology, Amsterdam UMC; location VUmc, Amsterdam, The Netherlands*
[4]*Neurodegeneration, Amsterdam Neuroscience, Amsterdam, The Netherlands*
[5]*Department of Clinical Sciences Lund, Lund University, Lund, Sweden*
[6]*Department of Clinical Sciences Malmö, SciLifeLab, Lund University, Lund, Sweden*
[7]*Banner Sun Health Research Institute, Sun city, AZ, US*
[8]*Banner Alzheimer's Institute, Arizona State University and University of Arizona, Phoenix, AZ, US*
[9]*Rush Alzheimer's Disease Center, Rush University Medical Center, Chicago, IL, US*
[10]*Department of Neurological Sciences, Rush University Medical Center, Chicago, IL, US*

Introduction: The medial temporal lobe (MTL) is among the earliest regions affected by tau pathology in Alzheimer's disease (AD), and its deterioration relates to memory decline. Although female sex and *APOE*-ε4 carriership are well-established AD risk factors, their specific effects on tau accumulation within the MTL, and the extent to which these effects are mediated by amyloid-β, remain unclear. We examined the effects of *APOE*-e4 carriership and sex on MTL tau load, and explored its mediation by MTL and/or global amyloid-β.

Methods: Neuropathological data were obtained for 2,550 participants from ROS/MAP (n=1,587) and the Arizona Study of Aging and Neurodegenerative Disorders (AZSAND, n=963). Amyloid-β and tau were quantified across cortical regions as percentage of area occupied (ROS/MAP) or on a semiquantitative scale (AZSAND). MTL composites were derived from averaging entorhinal cortex and hippocampus, and global composites from all other cortical areas. Linear regression models were fitted with MTL tau as the dependent variable, sex and APOE-ε4 as predictors in the same model, adjusting for age and copathologies (cerebral amyloid angiopathy, Lewy bodies and, ROSMAP only, atherosclerosis). Mediation models tested whether MTL and/or global amyloid-β accounted for observed effects.

Results: APOE-e4 carriership (ROS/MAP: b[95%CI]=0.35[0.24,0.47], AZSAND: b[95%CI]=0.32[0.20,0.43], both p<0.001) and female sex (ROS/MAP: b[95%CI]=0.27[0.17,0.37], AZSAND: b[95%CI]=0.20[0.09,0.30], both p<0.001) were associated with higher MTL tau burden (Figure-1). Only when MTL and global Aβ were simultaneously entered into the model, the *APOE*-ε4 effect was fully mediated and became non-significant (ROS/MAP: b[95%CI]=0.07[-0.04,0.18], p=0.209; AZSAND: b[95%CI]=0.08[-0.04,0.19], p=0.185, row three Figure-2). whereas the sex effect persisted (ROS/MAP: b[95%CI]=0.14[0.04,0.23], AZSAND: b[95%CI]=0.16[0.07,0.26], both p<0.001, Figure-3). Similar results were observed after adjusting for global tau.

Conclusions: The association between APOE-ε4 carriership and MTL tau is largely amyloid-β–mediated. In contrast, the effect of sex on MTL tau is amyloid-β independent, suggesting distinct biological mechanisms underlying tau vulnerability in females.

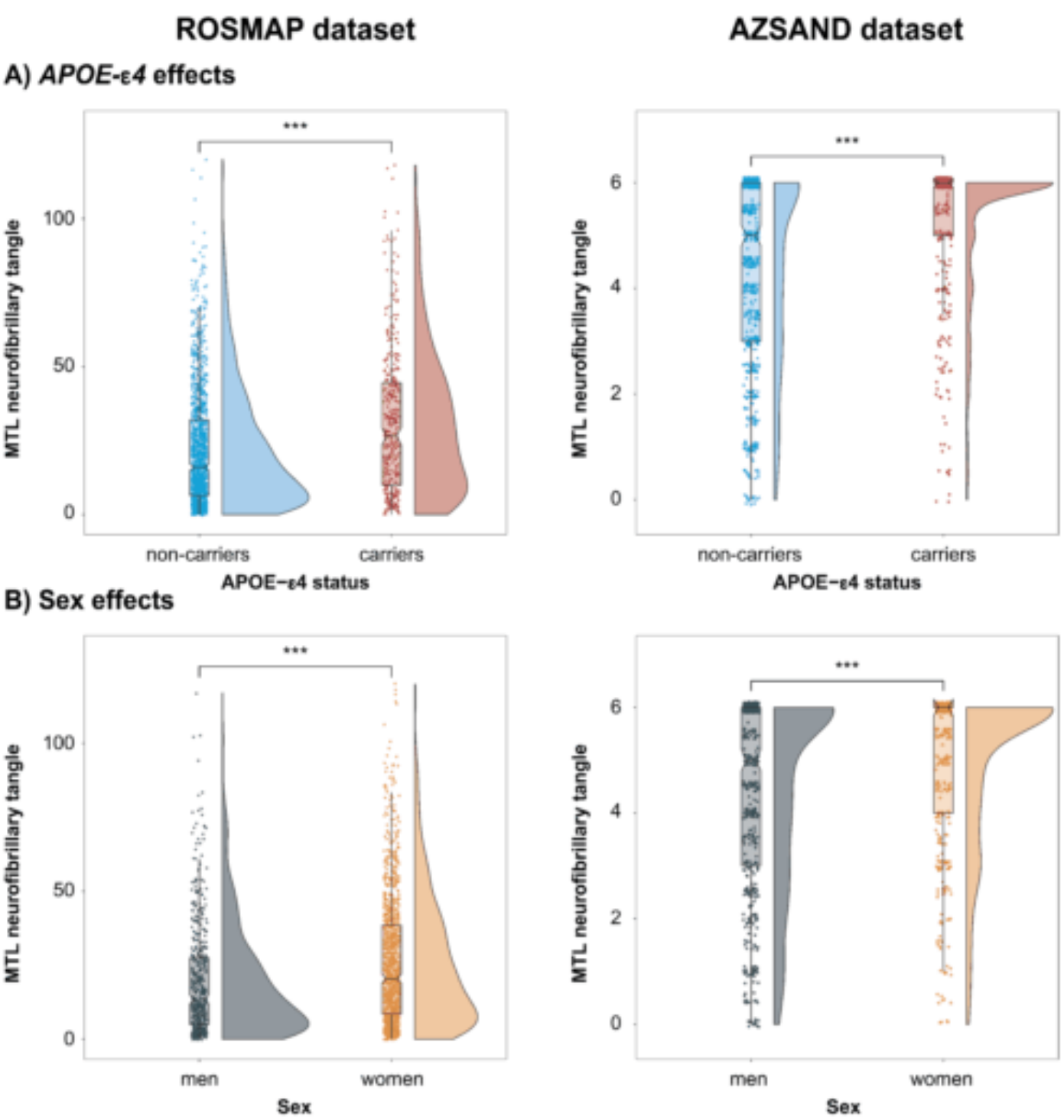


Figure 1 Total effects of APOE-ε4 carriership and female sex on MTL tau

APOE-ε4 carriership (A) and female sex (B) effects on MTL neurofibrillary tau tangles in ROS/MAP (first column) and AZSAND (second column) datasets. Both effects are calculated from the same model. P-values were calculated adjusting for age and presence of co-pathologies (ROS/MAP: CAA, LB and atherosclerosis and, AZSAND: CAA and LB). Differences in scale are due to fully quantitative (ROS/MAP) and semi-quantitative (AZSAND) methods of pathology measurement.

***p<0.001

Abbreviations: AZSAND, Arizona Study of Aging and Neurodegenerative Disorders; CAA, cerebral amyloid angiopathy; LB, Lewy-body pathology; MTL, medial temporal lobe; ROS/MAP, Religious Orders Study and Rush Memory and Aging Project.

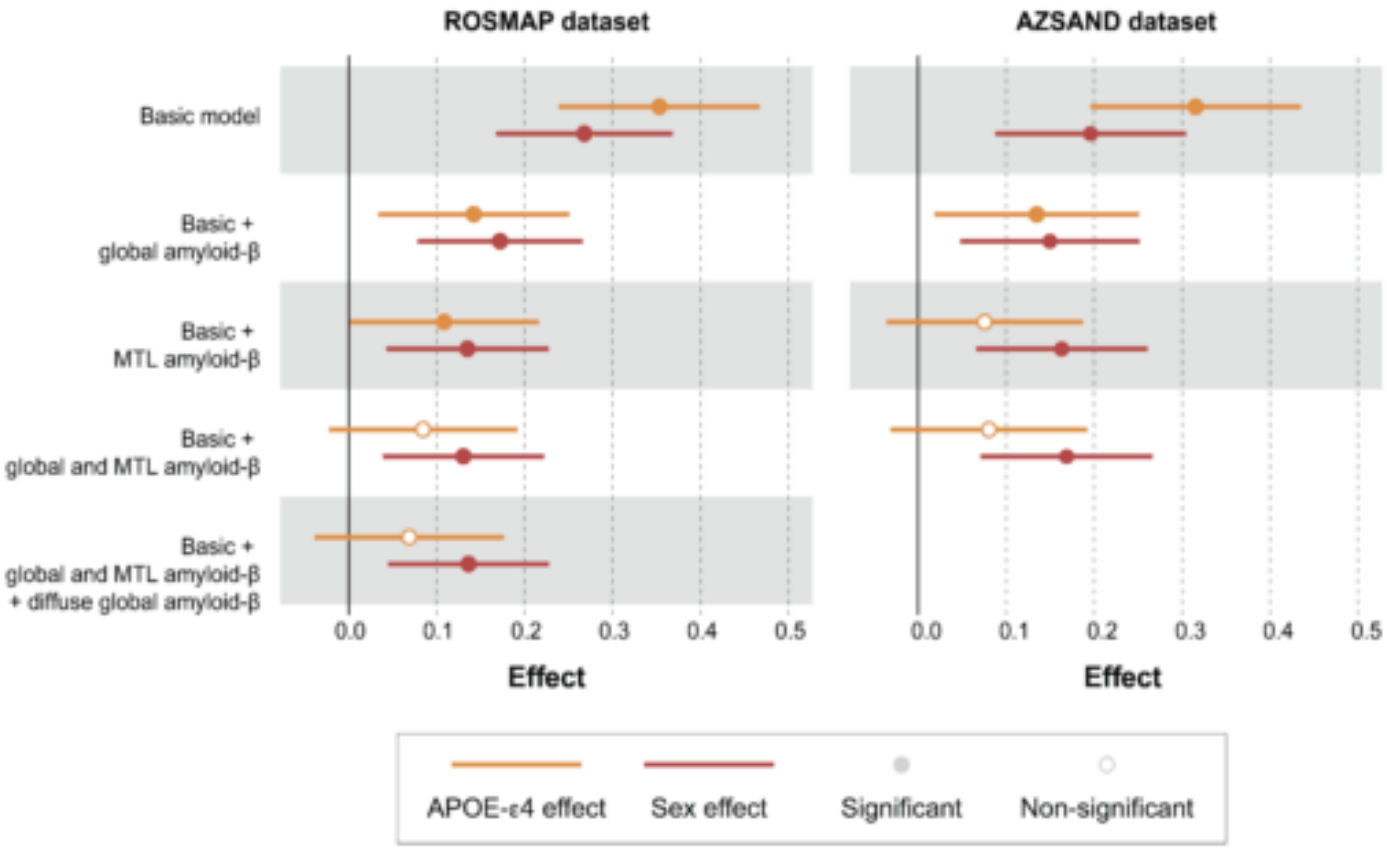


Figure 2 Independent effects of APOE-ε4 carriership and female sex on MTL

APOE-ε4 carriership (light brown) and female sex (red) effects on MTL neurofibrillary tau tangles in ROS/MAP (A) and AZSAND (B) datasets, in different statistical models. Both effects are calculated from a single model in each case. Model 1 shows the total APOE-ε4 carriership and female sex effects on MTL tau while Models 2-5 represent direct effects (independent of amyloid-β burden). Model 2 and Model 3 are adjusted for global (neocortical) and regional (MTL) amyloid-β burden, respectively and, Model 4 includes the two amyloid-β measures. Finally, in the ROS/MAP dataset we included a fifth model (Model 5) additionally adjusting for neocortical diffuse amyloid-β burden. Diffuse amyloid-β burden was not available in the AZSAND dataset. All models included age and presence of co-pathologies (ROS/MAP: CAA, LB and atherosclerosis and, AZSAND: CAA and LB) as covariates. Filled (empty) dots represent significant (non-significant) effects, and bar length corresponds to the 95%CI.

Abbreviations: AZSAND, Arizona Study of Aging and Neurodegenerative Disorders; CAA, cerebral amyloid angiopathy; CI, confidence intervals; LBS, Lewy-body pathology; MTL, medial temporal lobe; ROS/MAP, Religious Orders Study and Rush Memory and Aging Project.

Keywords: medial temporal lobe, tau pathology, neuropathology, APOE, sex

10 Harmonizing amyloid PET tracers at the regional level: evaluation of regional centiloid equations

Erica Silvestri[1,2], Pavan Chaggar[3], Susanna Gobbi[1], Roxana Aldea[1], Gregory Klein[1], Matteo Tonietto[1]

[1]*Research and Early Development (pRED), Hoffmann-La Roche, Basel, Switzerland*
[2]*A4P Consulting Ltd., Sandwich, UK*
[3]*BrainWaves Consulting Ltd, London, UK*

Introduction: The Centiloid (CL) framework harmonizes amyloid PET tracers by converting tracer-specific SUVR values from a global cortical target region into centiloid values using a linear equation. While this remains the standard for harmonizing amyloid-PET data, adopting regional CL assessments could enhance understanding of amyloid-targeting therapies' effects by revealing how regions respond to treatment, uncovering variability in amyloid clearance and rates, identifying interactions with other AD-related processes, and linking effects to cognitively critical regions. This work evaluates whether a global CL equation provides a sufficiently accurate model for harmonizing regional fluorinated SUVRs or if region-specific equations are necessary.

Methods: The study utilized GAAIN [^{11}C]PiB and head-to-head images for four fluorinated tracers ([^{18}F]Florbetaben, [^{18}F]Florbetapir, [^{18}F]Flutemetamol, and [^{18}F]NAV4694) segmented into five cortical (frontal, cingulate, parietal, temporal, occipital) and five subcortical (thalamus, caudate, putamen, pallidum, hippocampus) regions using FreeSurfer. The CL framework's first step (converting [^{11}C]PiB SUVR to CL) remained unchanged. For the second step (converting fluorinate to [^{11}C]PiB SUVR), we evaluated three models: Model1, a global equation for all regions (estimated from global cortical target region SUVRs); Model2, a global slope with region-specific intercepts, and Model3, both region-specific slopes and intercepts. Model performance was assessed using the Akaike (AIC), Bayesian Information Criteria (BIC), and the mean absolute error (MAE) between harmonized fluorinated tracer values and the [^{11}C]PiB reference.

Results: Model2 consistently demonstrated the best performance across tracers, achieving the lowest AIC and BIC values (Table1) and reducing errors compared to Model1, especially in subcortical regions. Model1 yielded comparable MAE to the global cortical target in cortical regions but performed poorly in subcortical regions likely due to off-target binding (Figure1).

Conclusion: While the global CL equation is adequate for cortical regions, a hybrid approach using a global slope with region-specific intercepts is necessary for accurate regional CL harmonization, especially in subcortical regions.

Tracer	Model	Slope	Intercept	Parameters	AIC	ΔAIC	BIC	ΔBIC
	Model1	Global	Global	2	1950.9	126.4	2951.8	91.7
[^{18}F]Florbetaben	***Model2***	***Global***	***Regional***	***11***	***1824.4***	***0.0***	***2860.1***	***0.0***
	Model3	Regional	Regional	20	1964.3	139.9	3034.7	174.6
	Model1	Global	Global	2	2856.1	124.3	4112.9	87.5
[^{18}F]Florbetapir	***Model2***	***Global***	***Regional***	***11***	***2731.8***	***0.0***	***4025.4***	***0.0***
	Model3	Regional	Regional	20	2860.0	128.2	4190.4	165.0
	Model1	Global	Global	2	4512.4	906.5	6621.7	865.1
[^{18}F]Flutemetamol	***Model2***	***Global***	***Regional***	***11***	***3605.9***	***0.0***	***5756.6***	***0.0***
	Model3	Regional	Regional	20	3667.5	61.6	5859.7	103.1
	Model1	Global	Global	2	2181.8	53.9	3751.3	15.1
[^{18}F]NAV4694	***Model2***	***Global***	***Regional***	***11***	***2128.0***	***0.0***	***3736.2***	***0.0***
	Model3	Regional	Regional	20	2190.8	62.8	3837.8	101.6

Table1 Models comparison. Model2, which uses a global slope and region-specific intercept, is the best performing as it achieved the lowest Akaike Information Criterion (AIC) and Bayesian Information Criterion (BIC) across all tracers. ΔAIC and ΔBIC represent per-tracer differences between each model and Model2.

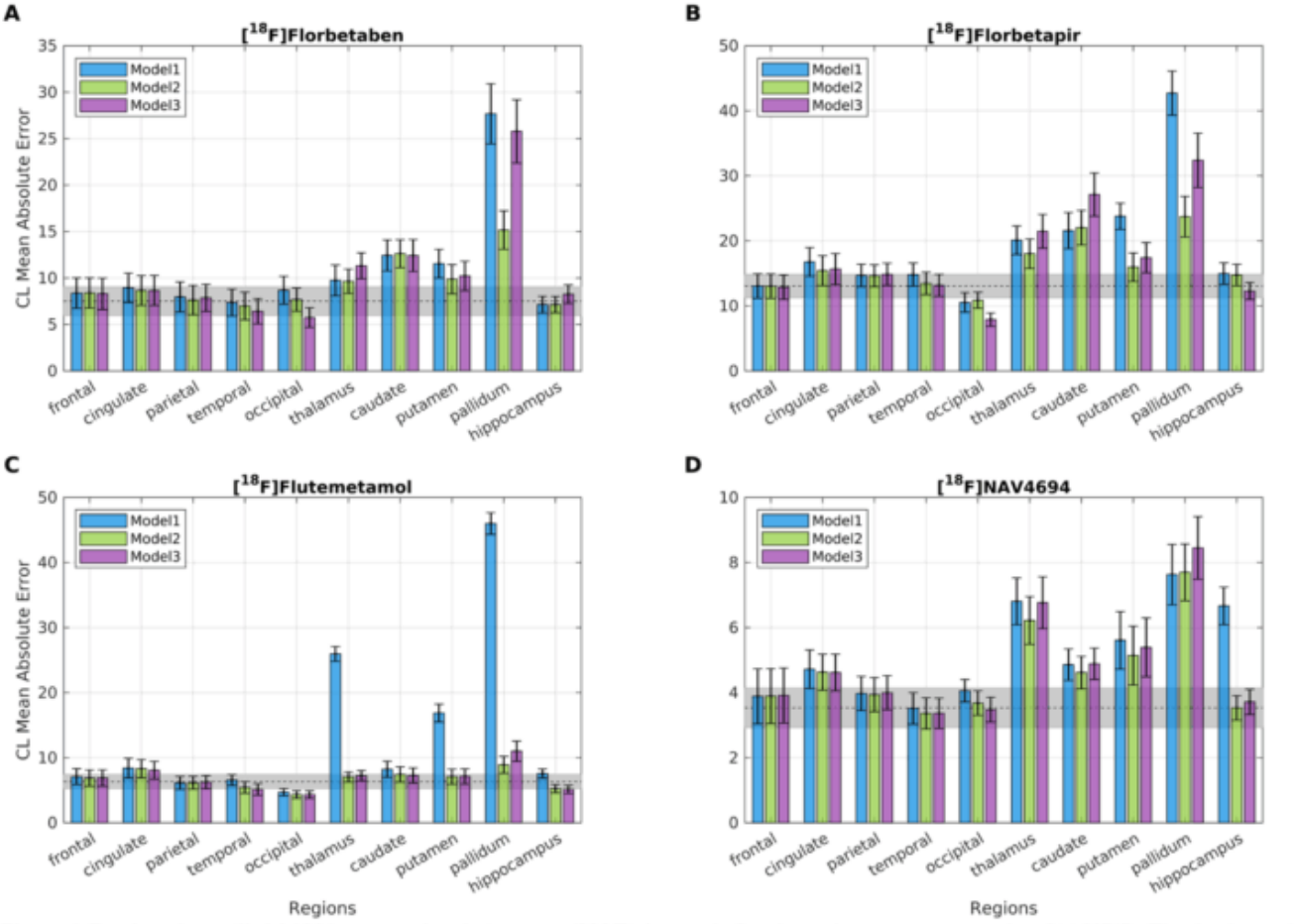


Figure1 Regional centiloid (CL) mean absolute error (MAE) for each fluorinated tracer compared to [11C]PiB. The horizontal grey bar represents the MAE of the global cortical target region (± standard error), serving as a comparator, while colored bars correspond to region-specific MAE (± region standard error). Model2 (green) generally reduces MAE across regions compared to Model1 (blue), particularly in subcortical regions, with Model3 (purple) providing limited further improvement.

Keywords: centiloid, amyloid PET, harmonization

11 A case series of lecanemab treatment response in patients across the clinical phenotypic spectrum of AD

Nick Corriveau-Lecavalier[1], Mary Machulda[1], Julie Fields[1], Elizabeth Boots[1], Jennifer Whitwell[1], Gregory Day[2], Paula Aduen[2], Ryan Frank[1], Walter Kremers[1], Vijay Ramanan[1], Jonathan Graff-Radford[1], Val Lowe[1], Bradley Boeve[1], David Knopman[1], Ronald Petersen[1], Clifford Jack[1], Nikki Stricker[1], David Jones[1]

[1]*Mayo Clinic, Rochester, MN, US*
[2]*Mayo Clinic, Jacksonville, FL, US*

Lecanemab is an FDA-approved monoclonal antibody that slows clinical progression in patients with early symptomatic Alzheimer's disease (AD). To date, clinical trials have largely focused on patients with the "typical" amnestic presentation, leaving treatment response in atypical variants and late-onset cases with suspected co-pathology unknown. We report longitudinal clinical, neuropsychological, and FDG-PET findings from five patients treated with lecanemab in our AD Treatment Clinic (ADTC): one with logopenic variant primary progressive aphasia (lvPPA), two with dysexecutive AD (dAD), one with late-onset amnestic AD with limbic degeneration and features suggestive of TDP-43 co-pathology, and one with typical amnestic AD. Treated cases were matched 1:1 to untreated historical controls based on phenotype, age, sex, education, and baseline cognitive impairment. Qualitative FDG-PET review suggested mild progression of hypometabolism across treated cases. Cognitive findings showed variable pre–post changes across phenotypes, with relative stabilization on measures of global cognition (lvPPA and amnestic AD) and executive functions (lvPPA, limbic, and amnestic AD), whereas dAD cases did not qualitatively differ from controls on these measures. We additionally describe outcomes from a novel self-administered digital cognitive battery (Mayo Test Drive, MTD) in six patients with typical amnestic AD who completed lecanemab treatment. This indicated stable or improved performance in treated AD patients compared to untreated historical AD controls. Evaluating treatment efficacy across the broader phenotypic spectrum of AD in real-world settings remains an important challenge. Although this series is underpowered and not randomized to determine efficacy in atypical AD, these findings inform control matching strategies for precision medicine approaches and future randomized studies.

Keywords: Lecanemab; Atypical Alzheimer's Disease; Cognition; Neuroimaging

12 Validation of a pseudo-reference region for [11C]-ER176 in healthy volunteers and Alzheimer's disease patients

Quentin Finn[1], Paolo Zanotti-Fregonara[3], Meixiang Yu[2], Joseph Masdeu[1], Belen Pascual[1]

[1]*Nantz National Alzheimer Center, Stanley H. Appel Department of Neurology, Houston Methodist Research Institute, Houston, TX, US*
[2]*Cyclotron and Radiopharmaceutical Core, Houston Methodist Research Institute, Houston, TX, US*
[3]*Xingimaging LLC, New Haven, CT, US*

Background: The 18-kDa translocator protein (TSPO) is expressed in activated microglia and serves as a key biomarker of neuroinflammation in positron emission tomography (PET) studies. Quantification of TSPO binding typically requires an arterial input function, but pseudo-reference region (PRR) approaches can simplify performance and analysis. The cerebellum has been validated as a PRR for the TSPO tracer 11C-PBR28 in patients with Alzheimer's disease (AD). However, it is unknown whether the cerebellum can serve as a valid PRR for the newer tracer 11C-ER176, which allows imaging across all TSPO genotypes (High-, Mixed-, and Low-Affinity Binders).

Methods: Twenty-nine healthy volunteers (age 64±5 years; 4 female; HAB/MAB/LAB=12/4/13) and 25 amyloid-positive patients with early onset AD (age 65±6 years; 12 female; HAB/MAB/LAB=12/8/5, Clinical Dementia Rating=0.5) underwent 90-minute 11C-ER176 PET scans. Regional distribution volume (*VT*) was estimated using a two-tissue compartment model (2TCM). Standardized Uptake Value Ratios (SUVRs) were calculated using the whole cerebellum (WC) and the cerebellar gray matter (CG) as PRRs across multiple thirty-minute time windows. PET outcomes were calculated for PET-Braak stages I/II, III, IV, V and VI. Correlations between *VT* and SUVR were used to identify optimal time-windows. Group differences and covariate effects were evaluated using linear mixed models (LMM).

Results: Correlations between *VT* and SUVR stabilized for time-windows starting 35 minutes post-injection. WC showed stronger correlations across Braak regions than the CG (Braak III/IV/V mean *r* for Braak III-V: CG=0.34, WC=0.4). In Braak III-V, SUVR exhibited larger group differences than *VT* (normalized β for WC SUVR=1.0/1.3/0.9; for 2TCM *VT*=0.8/0.9/0.8).

Conclusions: 11C-ER176 SUVR using the whole cerebellum as a pseudo-reference region effectively captures regional TSPO-related neuroinflammation in patients with AD and reduces dependence on genotype covariates, although it may underestimate global signal changes better detected by kinetic modelling.

Keywords: PET, TSPO, inflammation, Alzheimer's, cerebellum

13 β-amyloid PET signal reduction is higher in regions with ARIA-E due to anti-amyloid therapy

Quentin Finn[1], Belen Pascual[1], Jon Toledo[1], Paul Schulz[2], Joseph Masdeu[1]

[1]*Nantz National Alzheimer Center, Houston Methodist Neurological and Research Institute, Houston, TX, US*
[2]*Department of Neurology, McGovern Medical School, University of Texas Health Science Center at Houston, Houston, TX, US*

Objective: To determine the relationship between regional brain edema (ARIA-E) caused by anti-amyloid monoclonal antibody therapy and the degree of regional β-amyloid (Aβ) positron emission tomography (PET) signal reduction.

Background: Although ARIA has been considered to result from an exacerbation of amyloid angiopathy, the transient nature of ARIA-E suggests less severe vascular changes may also be at work. If these changes are related to the removal of Aβ, it could be postulated that greater Aβ removal occurs in areas with ARIA-E. To test this hypothesis, we used PET to measure the regional density of Aβ before ARIA-E occurred and after ARIA-E resolved

Design/Methods: In patients with moderate or severe ARIA-E after anti-amyloid therapy, we quantified the regional degree of ARIA-E on FLAIR MRI and the regional Aβ level with PET, both in baseline, pre-anti-amyloid therapy, and after ARIA-E resolved, as documented on FLAIR MRI. Aβ level was expressed as Standard Uptake Value Ratio (SUVR), using whole cerebellum as region of reference. The significance of SUVR change (Δ) within each subject across 40 brain regions was calculated using the Mann-Whitney U test.

Results: Six patients (age 71.5 ± 8.6 years, 4 women), had moderate or severe ARIA-E. In three cases there was coexisting ARIA-H in some of the regions exhibiting ARIA-E. Except in one patient with a small ARIA-E region and a marked global Aβ decrease in the follow up PET, all others had a statistically significant greater Aβ PET signal decrease in regions with ARIA-E.

Conclusion: Greater regional Aβ PET signal reduction in areas involved by ARIA-E may reflect enhanced local Aβ clearance, reduced tracer binding site availability, impaired glymphatic flow from immune complex deposition, or other mechanisms. Our finding refines the characterization of ARIA-E and raises the possibility that its occurrence may have beneficial as well as adverse implications.

Keywords: ARIA, amyloid, PET, treatment, anti-amyloid monoclonal antibodies

14 Lifetime and 10-year absolute risk of cognitive impairment associated with amyloid PET severity: a retrospective, longitudinal cohort study

Mingzhao Hu[1], Terry M. Therneau[1], Heather J. Wiste[1], David S. Knopman[2], Prashanthi Vemuri[3], Jonathan Graff-Radford[2], Val J. Lowe[4], Maria Vassilaki[1], Petrice M. Cogswell[3], Christopher G. Schwarz[3], Alicia Algeciras-Schimnich[5], Ronald C. Petersen[2], Clifford R. Jack Jr.[3]

[1]*Department of Quantitative Health Sciences, Mayo Clinic, Rochester, MN, US*
[2]*Department of Neurology, Mayo Clinic, Rochester, MN, US*
[3]*Department of Radiology, Mayo Clinic, Rochester, MN, US*
[4]*Department of Nuclear Medicine, Mayo Clinic, Rochester, MN, US*
[5]*Department of Laboratory Medicine, Mayo Clinic, Rochester, MN, US*

Background: Predicting risks of progression from cognitively unimpaired to impaired (either MCI or dementia) is of high interest. However, most of the literature on this topic has focused on relative risk and/or has not accounted for attrition bias. Relative risk ignores patients' top question which is their percent likelihood of experiencing impairment. Dropout rates often mirror or anticipate decline and bias risk estimates if informative censoring is neglected. Finally, current risk literature has mostly binarized AD biomarkers rather than employing continuous measures. Addressing this knowledge gap will be critical for optimizing clinical care of pre-clinical AD patients considered for disease modifying treatments.

Methods: We studied 5,858 Mayo Clinic Study of Aging participants (CU, age ≥ 50 at enrollment) with long-term follow-up. Dementia was ascertained in-person during study visits; out-of-study death and dementia were captured via the Rochester Epidemiology Project, addressing informative censoring. A multi-state hidden Markov model estimated 10-year and lifetime absolute risks with misclassification for diagnostic error, using age, sex, APOE ε4 status and amyloid PET as predictors for transitions among CU, MCI, dementia, and death (**Fig 1**).

Results: Amyloid PET Centiloid was the strongest predictor of 10-year and lifetime risk. For a female APOE ε4 carrier aged 65, lifetime risk of dementia was 45%/61%/68% across Centiloid 5/50/100 (**Fig 2**). 10-year absolute MCI risk for a female APOE ε4 carrier with Centiloid 50 was 9%/36%/69% when assessed at starting ages 65/75/85. Dementia cases from EHR reviews (out-of-study) doubled in-person (in-study) evaluations, confirming informative censoring (**Fig 3**). Analyses ignoring post-dropout information underestimated absolute risks by ~15%.

Conclusions: Biological AD severity using amyloid PET yields interpretable 10-year and lifetime absolute risks that are patient-specific and actionable for sample-size planning and bedside decisions. Considering competing death and informative dropout is essential for avoiding risk underestimation. This supports individualized counseling and trial enrichment.

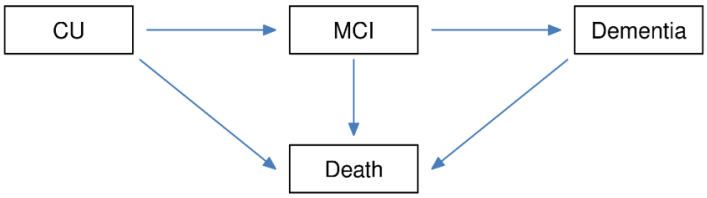


Figure 1. Multi-state Hidden Markov model transitions. The four latent states in this model are denoted by boxes: alive and cognitively unimpaired (CU), alive with mild cognitive impairment (MCI), alive with dementia, and deceased (death). The five possible transition paths are denoted by arrows: progression from CU to MCI, from MCI to dementia, and from CU, MCI or dementia to death. The Multi-state Hidden Markov model estimates are based on transition rates denoted by the arrows.

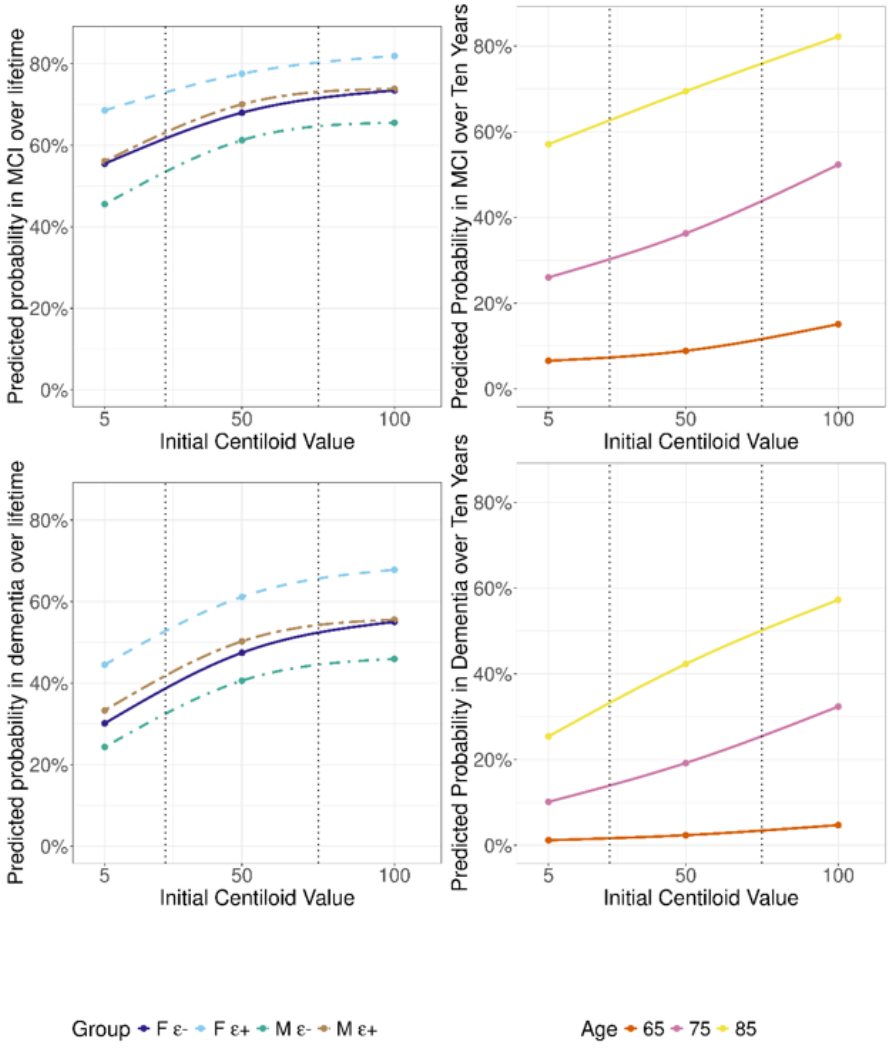


Figure 2. Lifetime and 10-year absolute risk of MCI and dementia as a function of continuous amyloid PET Centiloid value. Lifetime risk of MCI (top left) and dementia (bottom left). Both plots have 4 lifetime risk curves for the 4 sex and APOE ε4 status (carrier vs non carrier) groups given a selected starting age of 65. 10-year absolute risk of MCI (top right) and dementia (bottom right) for a female APOE ε4 carrier with Centiloid 50. Both plots have three 10-year absolute risk curves, one each for starting ages, 65, 75, and 85 years. Two vertical lines were added at Centiloid values 25 and 75 for reference. To fully explore all possible predictor permutations, we have created an online app for Calculating Absolute Cognitive Risk version 1.0 (https://rtools.mayo.edu/CACR/).

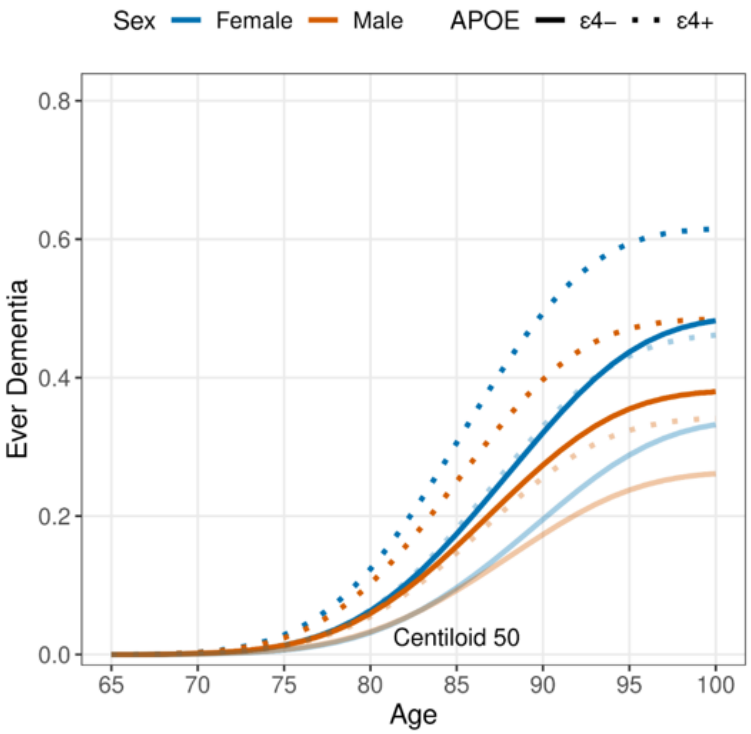


Figure 3. Cumulative absolute risk of dementia by age, sex, and APOE ε4 carrier status at PET Centiloid 50. Each curve represents the estimated cumulative absolute risk of developing dementia before death as a function of age. Results are shown separately for females and males with (F ε+, M ε+) and without (F ε-, M ε-) the APOE ε4 allele, assuming an initial amyloid PET Centiloid value of 50. Dashed lines denote APOE ε4 carriers, and solid lines denote APOE ε4 noncarriers. The model accounts for competing risks of death and provides age-specific cumulative probabilities of ever developing dementia. The corresponding lighter colored curves represent risk estimates if out-of-study events were not included in the model, which illustrates the 15% underestimation of risk if informative censoring due to dropouts is not addressed.

Keywords: Absolute risks, competing risks, multistate hidden Markov model, amyloid PET, informative censoring

15 Trajectory of neurodegeneration and brain aging in relation to amyloid timing and duration

Mengna Zhang[1], W. Hudson Robb[2,3], Guray Erus[4], Tonnar Castellano[1], Yuhan Cui[5], Karly Cody[6], Theresa Harrison[7], Corinne Engelman[8], Marilyn Albert[9], Susan Resnick[10], Reisa Sperling[11,12], Murat Bilgel[10], Badri Vardarajan[13,14,15,16], Richard Mayeux[13,14,15,16], Shannon Risacher[17,18,41], Konstantinos Arfanakis[19,20,21], Duygu Tosun[22], Mohamad Habes[23], Di Wang[24], Arthur Toga[25], Paul Thompson[26], Walter Kukull[27], Sarah Biber[27], Bennett Landman[2,28,29,30,31,32,33], Barbara Bendlin[34], Sterling Johnson[34,35], Julie Schneider[20], Lisa Barnes[20], David Bennett[20], Andrew Saykin[17,18], Philip De Jager[15,36], Vilas Menon[15], Tessa Harrison[7], Elizabeth Mormino[6], Michael Cuccaro[37,38], Christos Davatzikos[4], Tobey Betthauser[39], Derek Archer[1,28,31,40], Timothy Hohman[1,28,31,40], Logan Dumitrescu[1,28,31,40], Mary Ellen Koran[2,3]

[1]*Vanderbilt Memory and Alzheimer's Center, Vanderbilt University School of Medicine, Nashville, TN, US*
[2]*Department of Radiology & Radiological Sciences, Vanderbilt University Medical Center, Nashville, TN, US*
[3]*Mayo Clinic of Arizona, Department of Radiology, Scottsdale, AZ, US*
[4]*Department of Radiology, University of Pennsylvania, Philadelphia, PA, US*
[5]*Artificial Intelligence in Biomedical Imaging Laboratory, Center for and Data Science for Integrated Diagnostics, Perelman School of Medicine, University of Pennsylvania, Philadelphia, PA, US*
[6]*Stanford University, Department of Neurology and Neurological Sciences, Palo Alto, CA, US*
[7]*Helen Wills Neuroscience Institute, University of California, Berkeley, CA, US*
[8]*University of Wisconsin, Department of Population Health Sciences, University of Wisconsin School of Medicine and Public Health, Madison, WI, US*
[9]*Department of Neurology, Johns Hopkins University School of Medicine, Baltimore, MD, US*
[10]*Laboratory of Behavioral Neuroscience, National Institute on Aging, National Institutes of Health, Baltimore, MD, US*
[11]*Massachusetts General Hospital, Department of Neurology, Boston, MA, US*
[12]*Center for Alzheimer Research and Treatment, Department of Neurology, Brigham and Women's Hospital, Boston, MA, US*
[13]*Department of Neurology, Columbia University Medical Center, New York, NY, US*
[14]*Department of Neurology, The New York Presbyterian Hospital, New York, NY, US*
[15]*Taub Institute for Research on Alzheimer's Disease and The Aging Brain, Columbia University Medical Center, New York, NY, US*
[16]*The Institute for Genomic Medicine, Columbia University Medical Center, New York, NY, US*
[17]*Department of Radiology and Imaging Sciences, Indiana University School of Medicine, Indianapolis, IN, US*
[18]*Indiana Alzheimer's Disease Research Center, Indiana University School of Medicine, Indianapolis, IN, US*
[19]*Department of Biomedical Engineering, Illinois Institute of Technology, Chicago, IL, US*
[20]*Rush Alzheimer's Disease Center, Rush University Medical Center, Chicago, IL, US*
[21]*Department of Diagnostic Radiology, Rush University Medical Center, Chicago, IL, US*
[22]*Department of Radiology and Biomedical Imaging, University of California San Francisco, San Francisco, CA, US*
[23]*Glenn Biggs Institute for Alzheimer's and Neurodegenerative Diseases, University of Texas Health Science Center at San Antonio, San Antonio, TX, US*
[24]*University of Texas Health Science Center at San Antonio, San Antionio, TX, US*
[25]*Laboratory of Neuroimaging, USC Stevens Institute of Neuroimaging and Informatics, Keck School of Medicine, University of Southern California, Los Angeles, CA, US*
[26]*Imaging Genetics Center, Mark and Mary Stevens Institute for Neuroimaging and Informatics, Keck School of Medicine, University of Southern California, Marina del Rey, CA, US*
[27]*National Alzheimer's Coordinating Center, University of Washington, Seattle, WA, US*
[28]*Department of Neurology, Vanderbilt University Medical Center, Nashville, TN, US*

[29]*Department of Computer Science, Vanderbilt University, Nashville, TN, US*
[30]*Department of Electrical and Computer Engineering, Vanderbilt University, Nashville, TN, US*
[31]*Vanderbilt Brain Institute, Vanderbilt University Medical Center, Nashville, TN, US*
[32]*Vanderbilt University Institute of Imaging Science, Vanderbilt University Medical Center, Nashville, TN, US*
[33]*Department of Biomedical Engineering, Vanderbilt University, Nashville, TN, US*
[34]*Wisconsin Alzheimer's Disease Research Center, School of Medicine and Public Health, University of Wisconsin, Madison, WI, US*
[35]*Wisconsin Alzheimer's Institute, School of Medicine and Public Health, University of Wisconsin, Madison, WI, US*
[36]*Department of Neurology, Center for Translational and Computational Neuroimmunology, Columbia University Irving Medical Center, New York, NY, US*
[37]*The John P. Hussman Institute for Human Genomics, University of Miami, Miami, FL, US*
[38]*Dr. John T. MacDonald Foundation, Department of Human Genetics, University of Miami, Miami, FL, US*
[39]*Department of Medicine, University of Wisconsin School of Medicine and Public Health, Health Sciences Learning Center, Madison, WI, US*
[40]*Vanderbilt Genetics Institute, Vanderbilt University Medical Center, Nashville, TN, US*
[41]*Department of Internal Medicine - Section on Gerontology and Geriatric Medicine - Wake Forest University School of Medicine, Winston-Salem, NC, US*

Background: Estimated age of amyloid onset (EAOA) and amyloid chronicity provide a temporal "amyloid clock" framework that situates individuals along the disease timeline, expressed as years since amyloid positivity. These measures offer clinically interpretable markers for disease staging and prognosis. Using imaging-based biomarkers of AD-related atrophy (SPARE-AD) and brain aging (SPARE-BA), we examined how amyloid onset timing and duration relate to neurodegeneration and brain aging across the AD continuum.

Methods: This study included 1,647 participants (mean EAOA=63.6; mean baseline chronicity = 8.56; mean age=72.2; females = 851 (51.7%); AD cases = 245 (14.9%)) from four Alzheimer's and cognitive aging cohorts (ADNI, HABS-HD, NACC, WRAP). EAOA and amyloid chronicity were estimated using the Sampled Iterative Local Approximation method. Brain age delta (BA-Delta) was calculated by subtracting chronological age from the SPARE-BA estimate. Cross-sectional associations between amyloid timing variables and SPARE indices were assessed using Pearson correlations. Longitudinal trajectories were modeled with linear mixed-effects models to test three hypotheses: (1) earlier amyloid onset predicts faster progression of SPARE-AD and BA-Delta; (2) longer amyloid chronicity predicts greater longitudinal change in these indices; and (3) these effects follow a non-linear trajectory across baseline amyloid accumulation stages.

Results: At baseline, longer amyloid chronicity and younger EAOA were significantly associated with greater AD-like atrophy and more advanced brain aging (**Figure 1**). Longitudinally, both earlier amyloid onset and longer baseline chronicity predicted accelerated progression of SPARE-AD and BA-Delta (**Table 1**). Notably, these trajectories exhibited a non-linear pattern—progression rates accelerated during early amyloid positivity, peaked at approximately 15–20 years of chronicity, and then gradually declined but remained significantly elevated thereafter (**Figure 2**).

Conclusion: Earlier amyloid onset and longer amyloid exposure predict greater brain aging and AD-related atrophy, following non-linear trajectories that illustrates the temporal dynamics of amyloid-driven neurodegeneration and inform intervention strategies.

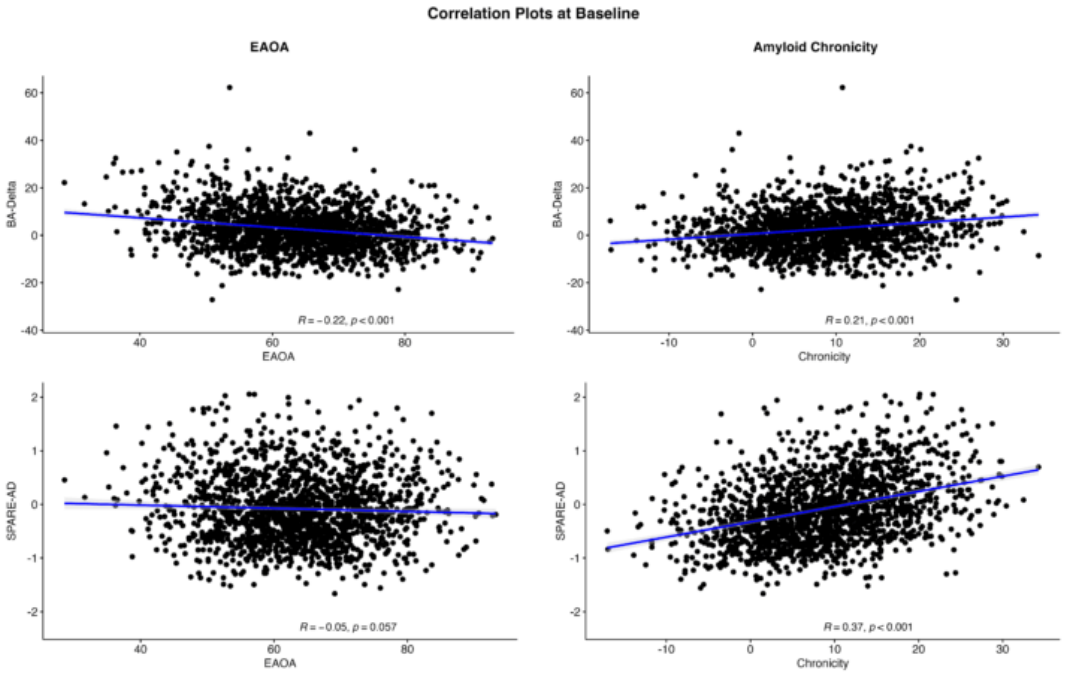
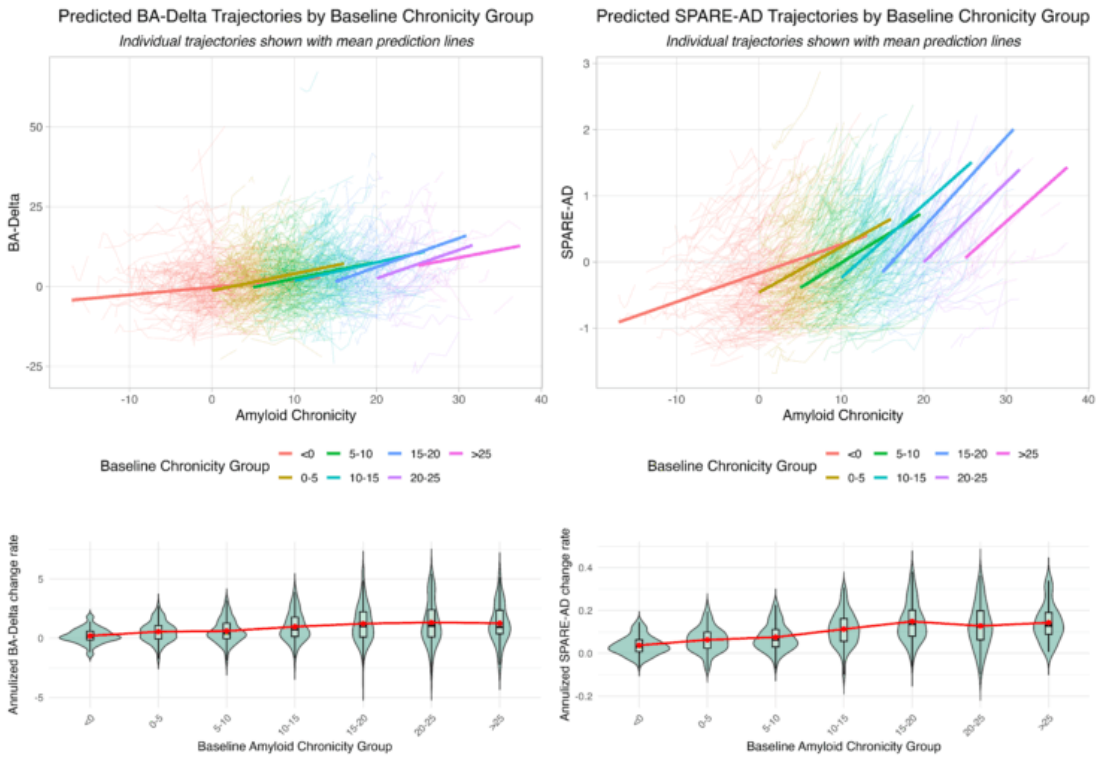


Figure 1.

Effects of Estimated Amyloid Onset Age on the Progression of BA-Delta and SPARE-AD								
	BA-Delta				**SPARE-AD**			
	Beta	95% CI		P-value	Beta	95% CI		P-value
(Intercept)	0.413	-5.163	5.989	0.88	-3.285	-3.672	-2.899	**5.1e-57**
Baseline Age	-0.362	-0.447	-0.276	**1.5e-16**	-0.031	-0.036	-0.025	**3.8e-24**
Female (vs Male)	-2.527	-3.424	-1.630	**4e-8**	-0.075	-0.138	-0.012	**0.02**
Education Level	0.025	-0.114	0.163	0.73	-0.00001	-0.010	0.009	0.94
APOE e4 Carrier (vs Non-Carrier)	0.669	-0.255	1.593	0.16	0.126	0.062	0.191	**1.4e-4**
Chronicity (in years)	1.422	1.157	1.687	**2.2e-24**	0.172	0.151	0.193	**3.3e-52**
EAOA	0.373	0.292	0.454	**5.4e-19**	0.071	0.065	0.076	**1.1e-125**
EAOA : Chronicity	-0.014	-0.018	-0.010	**5.6e-12**	-0.001	-0.002	-0.001	**1.1e-16**
Effects of Baseline Amyloid Chronicity on the Progression of BA-Delta and SPARE-AD								
(Intercept)	12.664	7.574	17.754	**1.2E-6**	-2.013	-2.334	-1.691	**3.6E-33**
Baseline Age	-0.155	-0.216	-0.094	**6.7E-7**	0.023	0.02	0.027	**1.6E-31**
Female (vs Male)	-2.981	-3.871	-2.09	**7.3E-11**	-0.12	-0.176	-0.064	**3E-5**
Education Level	0.045	-0.094	0.184	0.53	0.002	-0.007	0.01	0.72
APOE e4 Carrier (vs Non-Carrier)	0.13	-0.793	1.053	0.78	0.105	0.047	0.163	**4E-4**
Time (in years)	0.394	0.327	0.461	**8.6E-27**	0.061	0.055	0.066	**5.1E-85**
Baseline Chronicity	0.249	0.195	0.303	**4.1E-19**	0.023	0.02	0.027	**4.8E-37**
Baseline Chronicity : Time	0.02	0.014	0.027	**6.8E-9**	0.004	0.003	0.004	**3E-42**

Table 1.

Figure 2.



Keywords: Amyloid Chronicity, EAOA, SPARE-AD, Brain Aging, Amyloid PET

16 Associations between tau pathology and cortical microstructure are modulated by amyloid burden independent of cortical atrophy in cognitively unimpaired older adults

Nicholas Vogt[1,2], Elouise Koops[1], Aaron Schultz[3], Michael Properzi[3], David Salat[1], Alvaro Pascual-Leone[2,4], Susie Huang[1,5], Rachel Buckley[3], Dorene Rentz[3,6], Keith Johnson[5], Reisa Sperling[3,6], Heidi Jacobs[1,5]

[1]*Athinoula A. Martinos Center for Biomedical Imaging, Department of Radiology, Massachusetts General Hospital, Charlestown, MA, US*
[2]*Marcus Institute for Aging Research, Hebrew SeniorLife, Boston, MA, US*
[3]*Department of Neurology, Massachusetts General Hospital, Harvard Medical School, Boston, MA, US*
[4]*Department of Neurology, Harvard Medical School, Boston, MA, US*
[5]*Department of Radiology, Massachusetts General Hospital, Harvard Medical School, Boston, MA, US*
[6]*Department of Neurology, Center for Alzheimer Research and Treatment, Brigham and Women's Hospital, Harvard Medical School, Boston, MA, US*

Background: In Alzheimer's disease, conventional structural neuroimaging detects brain changes only after substantial pathology has accumulated. Diffusion MRI (dMRI) measures cortical microstructural alterations that precede atrophy, potentially revealing how amyloid and tau pathology affect brain tissue in preclinical stages. Here, we tested whether regional tau pathology was related to regional cortical diffusion metrics independent of atrophy, and whether amyloid burden modified these relationships.

Methods: 103 cognitively unimpaired participants (Table 1) from the Harvard Aging Brain Study underwent C-11 PIB PET (amyloid), F-18 flortaucipir PET (FTP, tau), T1w-MRI and multi-shell dMRI. PIB DVR, FTP SUVR, cortical thickness, and NODDI metrics (neurite density [NDI], orientation dispersion [ODI], free water [FWF]) were extracted from PET-defined Braak ROIs (I-II: entorhinal, III-IV: temporal-limbic, V-VI: neocortical; Figure 1A). Linear models tested tau-diffusion associations within each ROI, including tau × amyloid interactions. Models were adjusted for age, sex, APOE4, and cortical thickness.

Results: Tau-microstructure associations differed by Braak stage (Table 2, Figure 1B-E). In Braak I-II, higher tau burden was associated with greater FWF across all participants ($\beta = 0.218$, $p = 0.039$, Figure 1B), while PIB+ individuals also showed a steeper positive tau-NDI slope relative to PIB- (Figure 1C). In Braak III-IV, amyloid status significantly moderated tau-FWF relationships: PIB+ individuals exhibited stronger positive associations (Figure 1D), and a similar local moderating effect was seen when using Braak III-IV regional PIB burden (Figure 1E). No significant associations were detected for ODI or in Braak V-VI.

Discussion: Advanced diffusion MRI detected tau-related cortical microstructural changes in cognitively unimpaired individuals, independent of atrophy. Tau was associated with increased free water in entorhinal cortex regardless of amyloid, while tau and amyloid interacted in temporal-limbic regions, indicating amyloid confers regional vulnerability to tau-related microstructural disruption. These findings highlight dMRI as a sensitive marker of incipient neurodegenerative processes in preclinical AD.

Table 1. Participant demographics and neuroimaging values

Characteristic	Value
N	103
Age, years (mean ± SD)	74.90 ± 9.17
Sex, % female (n)	66% (68/103)
APOE ε4 allele, % positive (n)	26% (27/103)
Amyloid positive†, % (n)	30% (31/103)

Neuroimaging values	Braak I-II	Braak III-IV	Braak V-VI
C-11 Pittsburgh compound B (PIB), DVR (mean ± SD)	---	1.30 ± 0.35	1.43 ± 0.41
F-18 Flortaucipir (FTP), SUVR (mean ± SD)	1.38 ± 0.34	1.36 ± 0.18	1.30 ± 0.12
Neurite Density Index (mean ± SD)	0.34 ± 0.06	0.26 ± 0.01	0.24 ± 0.01
Orientation Dispersion Index (mean ± SD)	0.60 ± 0.04	0.51 ± 0.02	0.50 ± 0.02
Free Water Fraction (mean ± SD)	0.16 ± 0.06	0.08 ± 0.03	0.09 ± 0.03
Cortical thickness, mm (mean ± SD)	2.82 ± 0.29	2.48 ± 0.09	2.26 ± 0.08

†Amyloid positivity defined as PIB+ if frontal, lateral temporal, retrosplenial (FLR) DVR > 1.324.
PIB and FTP values are partial-volume corrected.

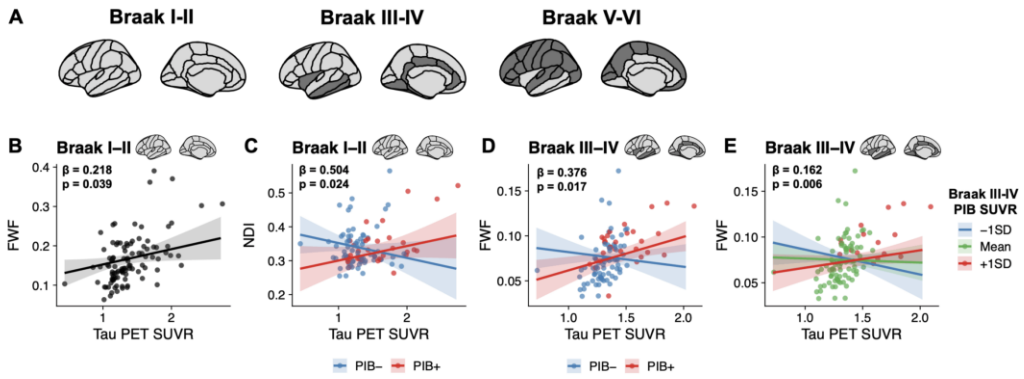
Table 1. Participant demographics and neuroimaging values

Characteristic	Value
N	103
Age, years (mean ± SD)	74.90 ± 9.17
Sex, % female (n)	66% (68/103)
APOE ε4 allele, % positive (n)	26% (27/103)
Amyloid positive†, % (n)	30% (31/103)

Neuroimaging values	Braak I-II	Braak III-IV	Braak V-VI
C-11 Pittsburgh compound B (PIB), DVR (mean ± SD)	---	1.30 ± 0.35	1.43 ± 0.41
F-18 Flortaucipir (FTP), SUVR (mean ± SD)	1.38 ± 0.34	1.36 ± 0.18	1.30 ± 0.12
Neurite Density Index (mean ± SD)	0.34 ± 0.06	0.26 ± 0.01	0.24 ± 0.01
Orientation Dispersion Index (mean ± SD)	0.60 ± 0.04	0.51 ± 0.02	0.50 ± 0.02
Free Water Fraction (mean ± SD)	0.16 ± 0.06	0.08 ± 0.03	0.09 ± 0.03
Cortical thickness, mm (mean ± SD)	2.82 ± 0.29	2.48 ± 0.09	2.26 ± 0.08

†Amyloid positivity defined as PIB+ if frontal, lateral temporal, retrosplenial (FLR) DVR > 1.324.
PIB and FTP values are partial-volume corrected.

Figure 1. Significant tau-amyloid effects on NODDI metrics by Braak stage.



A) Braak regions defined using Desikan atlas ROIs. **B)** Association between tau burden and free water fraction (FWF) in Braak I–II, showing a main effect of tau. **C)** Tau × PIB status interaction on neurite density index (NDI) in Braak I–II. **D)** Tau × PIB status interaction on FWF in Braak III–IV. **E)** Tau × regional PIB interaction on FWF in Braak III–IV.

Keywords: Diffusion, microstructure, NODDI, PET, MRI

17 Predicting tau PET burden using brain-derived plasma p-tau measures in the British 1946 birth cohort

Jonathan Schott[1], William Coath[1,2], Katherine Wiltshire[1], Thomas Brown[1], David Cash[1], Alex Whittington[1,4], Amanda Heslegrave[1], Henrik Zetterberg[1,2,3], Ashvini Keshavan[1]

[1]*University College London, London, UK*
[2]*University of Wisconsin, Madison, WI, US*
[3]*University of Gothenburg, Gothenburg, Sweden*
[4]*Perceptive, London, UK*

Brain-derived (BD) variants of plasma phosphorylated tau (p-tau) may allow determination of tau deposition and hence proximity to symptom onset in preclinical Alzheimer's disease. We investigated the ability of BD p-tau217 to predict in vivo tau pathology indexed by MK-6240 PET Braak staging in asymptomatic members of a population based birth cohort born in the UK in one week in 1946.

Methods: n=217 participants from the *Insight 46* study were included. All had previously undergone amyloid (18F-Florbetapir) PET at 69-71 and 70-73 years, and were 77–79 years at the time of contemporaneous tau PET and blood sampling. Plasma samples were analysed using the NULISA v2 CNS multiplex panel to quantify both standard and BD-enriched isoforms of p-tau181, 217, and 231. MK-6240 tau PET was performed on the same 3T PET/MRI from which Braak Stage and CenTauR scores were calculated. Associations between plasma measures and PET-defined tau pathology were examined using fold-change analyses and ROC analysis.

Results: 83.9%, 6.5% and 9.6% were Braak stage 0, 1-2, and 3+. BD p-tau181, BD p-tau217 and BD p-tau231 concentrations outperformed the respective standard versions for predicting Braak stage 3+ ($p<0.05$). Relative to Braak 0, BD p-tau217 and BD p-tau181 showed increasing fold change with increasing tau PET burden, being 1.88x and 1.71x higher in Braak 3-4, and 2.59x and 2.82x higher in Braak 5-6. The universal CenTauR score was more strongly associated with BD- than standard p-tau measures.

Conclusions: NULISA brain-derived plasma p-tau217 and p-tau181 demonstrate high accuracy for detecting and staging tau pathology in asymptomatic individuals, with an AUC~0.9 to detect Braak Stage 3+. BD-tau assays may have utility in identifying preclinical AD with potential as minimally invasive, scalable tools for early diagnosis and stratification of at-risk individuals who may be at imminent risk of developing clinical features of Alzheimer's disease.

Keywords: tau PET, Braak Stage, plasma ptau, brain derived, asymptomatic

18 Association of combined cardiovascular risk factors and treatments with longitudinal amyloid and tau PET in cognitively normal older adults

Valentin Ourry[1,2], Julien Thériault-Dubé[2], John Breitner[1,2], Judes Poirier[1,2], Sylvia Villeneuve[1,2,3]

[1]*Department of Psychiatry, Faculty of Medicine, McGill University, Montréal, QC, Canada*
[2]*Douglas Mental Health University Institute, Montréal, QC, Canada*
[3]*McConnell Brain Imaging Center, Montreal Neurological Institute, McGill University, Montréal, QC, Canada*

Background: Cardiovascular risk factors (CVRF) are associated with increased risk of Alzheimer's disease (AD) dementia. Previous studies have shown mixed interactions between vascular pathology, vascular treatments, and AD dementia. We evaluated whether combined CVRF and their treatments are associated longitudinally with amyloid and tau burden.

Methods: We performed [18F]-NAV4694 and [18F]-AV1451 positron emission tomography on 241 older adults (age 68.3 ± 5.1 years, 69.3% female) from the PREVENT-AD participants who were cognitively unimpaired at baseline. Longitudinal scans were available for 115 persons (4.4 ± 0.6 years follow-up). We assessed three CVRF: cholesterol, blood pressure, and body mass index (BMI). CVRF clinical norms were: HDL/LDL < 2.5; diastolic < 80 mmHg; systolic < 120 mmHg; BMI 25–30 kg/m^2. Each CVRF was scored (0 = normal / untreated; 1 = normal / treated; 2 = abnormal / treated; or 3 = abnormal / untreated), and scores were summed to create a combined CVRF score. We examined associations between the combined score or individual CVRF and global Aβ as well as temporal META-ROI tau burden, and their annual change. Analyses were adjusted for age, sex, and education.

Results: The combined CVRF score predicted annual change in amyloid (p=0.028), although its association with baseline amyloid was only at a trend level (p=0.069). No significant association was found with tau (**Figure 1**). Among individual CVRFs, we observed no association with amyloid or tau though a trend appeared between pulse pressure and tau change (p=0.083) (**Figure 2**). We found no interaction between individual CVRF and treatments on amyloid or tau.

Conclusions: Higher CVRF and their treatments, were associated with greater amyloid accumulation in cognitively normal older adults. Accounting for CVRF treatments is important in studies of AD pathology and, especially, in AD clinical trials.

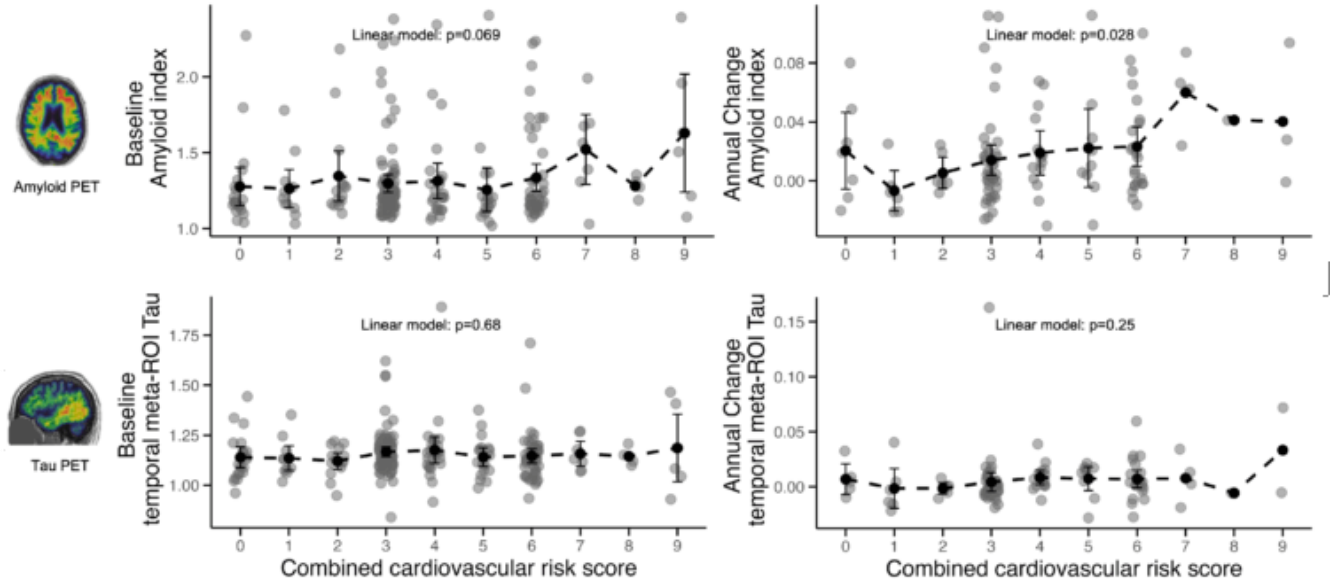


Figure 1.

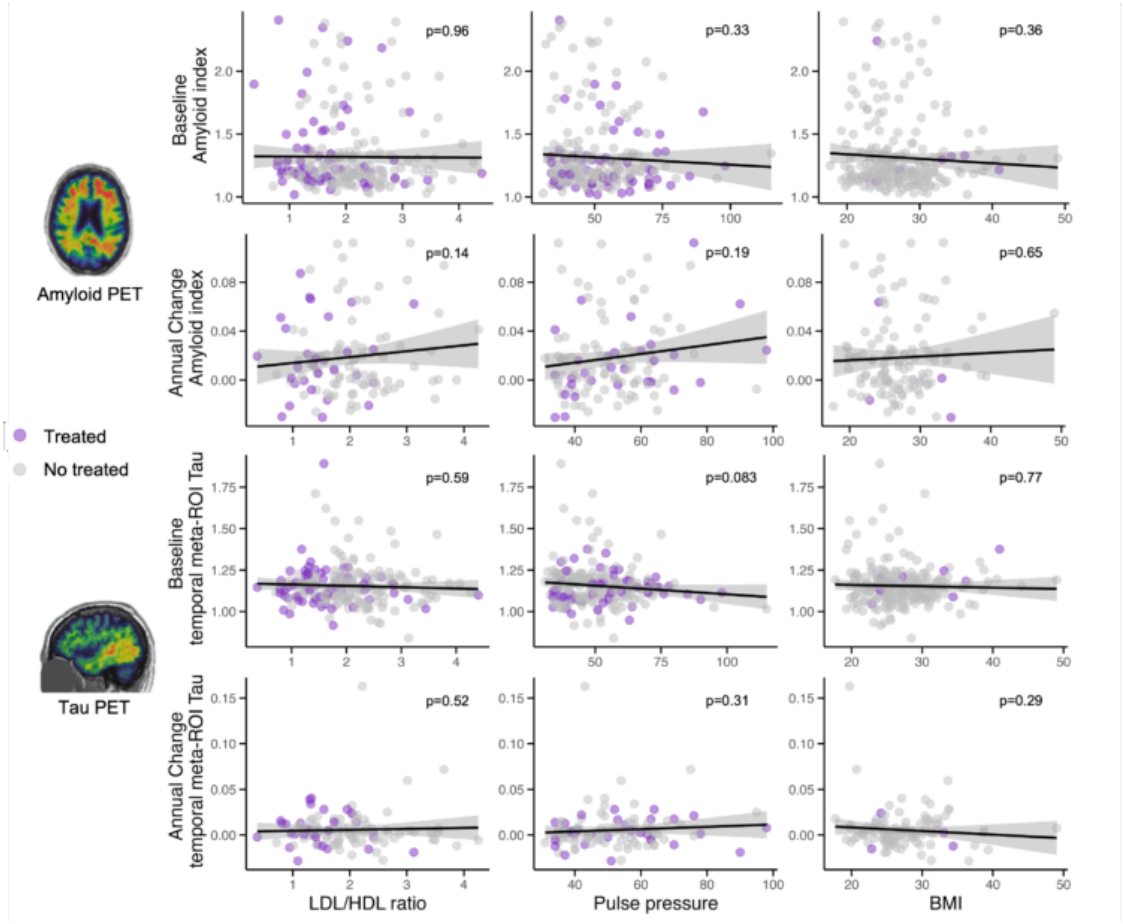


Figure 2

Keywords: cardiovascular risk factors, treatments, amyloid, tau, PET, Alzheimer's disease

19 Amyloid-pet substantiates clinical decision-making in real-life clinical settings in Brazil

Cristiano Schaffer Aguzzoli[1,2,3], Karoline Flach[1], Maria Rosa Alves Da Silva[1], Pamela C.L Ferreira[8], Guilherme Povala[8], João Pedro Ferrari-Souza[5], Andrei Bieger[2], Douglas Teixeira Leffa[8], Bruna Bellaver[8], Frederico Guevara Werlang[1], Gianina Teribele Venturin[1], Mirna Wetters Portuguez[1], Sabine Possa Marroni[1], Danielle Irigoyen da Costa[1], Ricardo Bernardi Soder[1], Cristina Sebastião Matushita[1], Bárbara Juarez Amorim[12], Juliana Pasquotto Souza[12], Celso Dario Ramos[12], José Leite[6], Celso Hygino[6], Solange Amorim Nogueira[9], Eduardo Sturzeneker Tres[7], Maira Okada de Oliveira[7], Cristina Maria Moriguchi Jeckel[1], Roberto Cortes Domingues[6], Camila Mosci[11], Paulo Henrique Rosado de Castro[11], Carlos Alberto Buchpiguel[7], Flávia Paiva Proença Lobo Lopes[6], Guilherme Carvalho Campos Neto[9], Márcio Luiz Figueiredo Balthazar[12], Fernanda Tovar Moll[10], Artur Martins Novaes Coutinho[7], Tharick A. Pascoal[8], Eduardo R. Zimmer[4,5], Lucas P. Schilling[1,2], Jaderson Costa da Costa[1,2]

[1]*Brain Institute of Rio Grande do Sul (BraIns), Porto Alegre, Brazil*
[2]*Department of Neurology, São Lucas Hospital from PUCRS, Porto Alegre, Brazil*
[3]*Global Brain Health Institute, University of California - San Francisco, San Francisco, CA, US*
[4]*Graduate Program in Biological Sciences: Biochemistry, Universidade Federal do Rio Grande do Sul, Porto Alegre, Brazil*
[5]*Department of Pharmacology, Graduate Program in Biological Sciences: Pharmacology and Therapeutics, Universidade Federal do Rio Grande do Sul, Porto Alegre, Brazil*
[6]*Dasa, Rio de Janeiro, Brazil*
[7]*Sírio-Libanês Institute of Research and Education, São Paulo, Brazil*
[8]*Department of Psychiatry, University of Pittsburgh, Pittsburgh, PA, US*
[9]*Sociedade Beneficente Israelita Brasileira Hospital Albert Einstein, São Paulo, Brazil*
[10]*Instituto D'Or de Pesquisa e Ensino (IDOR), Rio de Janeiro, Brazil*
[11]*Instituto D'Or de Pesquisa e Ensino (IDOR), São Paulo, Brazil*
[12]*Universidade Estadual de Campinas (UNICAMP), São Paulo, Brazil*

Background: Amyloid-PET (Aß-PET) is a well-established technique for identifying amyloid-beta plaques in the human brain. However, its impact on the diagnosis and treatment remains elusive in LMICs. Here, we investigate the clinical impact of Aß-PET in Brazil.

Methods: We assessed 49 individuals recruited from six memory clinics across three Brazilian states as part of a prospective multi-site study. Recruitment was based on a convenience sample meeting criteria for undergoing Aß-PET. We used [^{18}F]Florbetaben radiopharmaceutical for all individuals. All participants were cognitively impaired and underwent Aß-PET and clinical assessment before the scan. Participants with a previous diagnosis of Alzheimer's disease (AD) had a mild-to-moderate stage of dementia and met the 2018 NIA-AA criteria for Alzheimer's clinical syndrome. Data was re-accessed after the scans to check for changes in diagnosis and treatment. We estimated the global Aß-PET SUVR based on a mask outlined by Jack et al 2017.

Results: Mean age (SD) was 66 (8.8) years; 27 participants (55%) were women; 36 participants had a clinical diagnosis of probable AD at baseline (**Table 1**). Thirty-seven (76%) individuals had a positive Aß-PET, 81% of whom showed high Centiloid values (**Figure 1A, 1B**). Following Aß-PET, 5 individuals (13.8%) initially diagnosed with probable AD were reclassified as non-AD, while 7 (53.8%) initially diagnosed as probable non-AD were reclassified as AD biologically defined (**Figure 2A**). Aß-PET modified treatment for 21 (58.3%) individuals, who received pharmacological and/or non-pharmacological interventions. A change in cholinesterase inhibitor and memantine

was significant following an Aß-PET positive result (**Figure 2B**).

Conclusion: Our results highlight the substantial impact of amyloid-PET on diagnostic and treatment decision-making for individuals across the AD continuum in the real-life clinical setting in Brazil. These data provide an additional rationale for the potential utility of amyloid-PET as a diagnostic tool in clinical practice in public and private healthcare settings.

Table 1. Demographic characteristics of the study population.

	Probable AD (N=36)	Probable Non-AD (N=13)	Overall (N=49)
Sex, female	22 (61 %)	5 (38 %)	27 (55 %)
Age	66 (± 9.1)	67 (± 8.0)	66 (± 8.8)
Education, years	12 (± 5.5)	15 (± 7.0)	13 (± 6.0)
MEEM†	20 (± 7.3)	20 (± 7.1)	20 (± 7.2)
Taking AD drugs at enrollment	20 (56 %)	1 (8 %)*	21 (43 %)
Aß-PET positive	30 (83 %)	7 (54 %)	37 (76 %)
Aß-PET, SUVR	1.4 (± 0.24)	1.3 (± 0.25)	1.4 (± 0.25)
Aß-PET, Centiloid Unit	63 (± 38)	45 (± 39)	58 (± 39)

Abbreviations: MMSE = Mini-mental state examination; SUVR = standardized uptake value ratio. Values are shown as mean (± standard deviation) for continuous variables, and n (%) for categorical variables. Welch's T-test and contingency chi-square models tested differences in continuous and categorical variables, respectively. *P < 0.05. †Two missing values

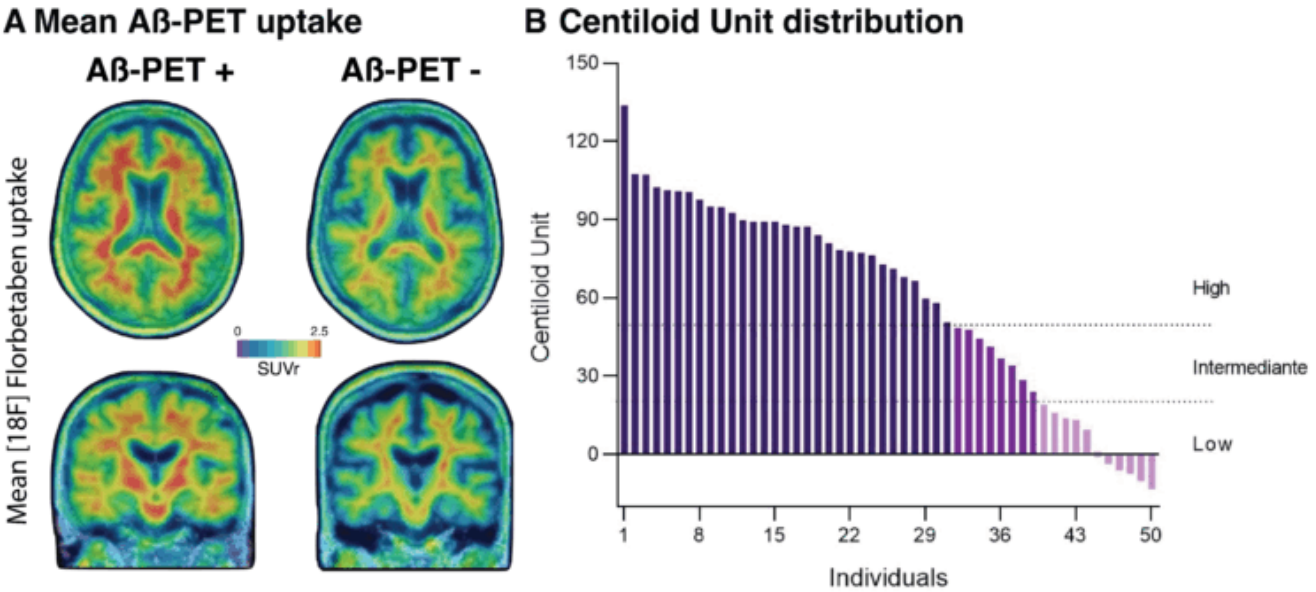


Figure 1. (A) Mean [18F] Florbetaben uptake in Aß-PET positive and negative groups. **(B)** Centiloid Unit distribution in the study population.

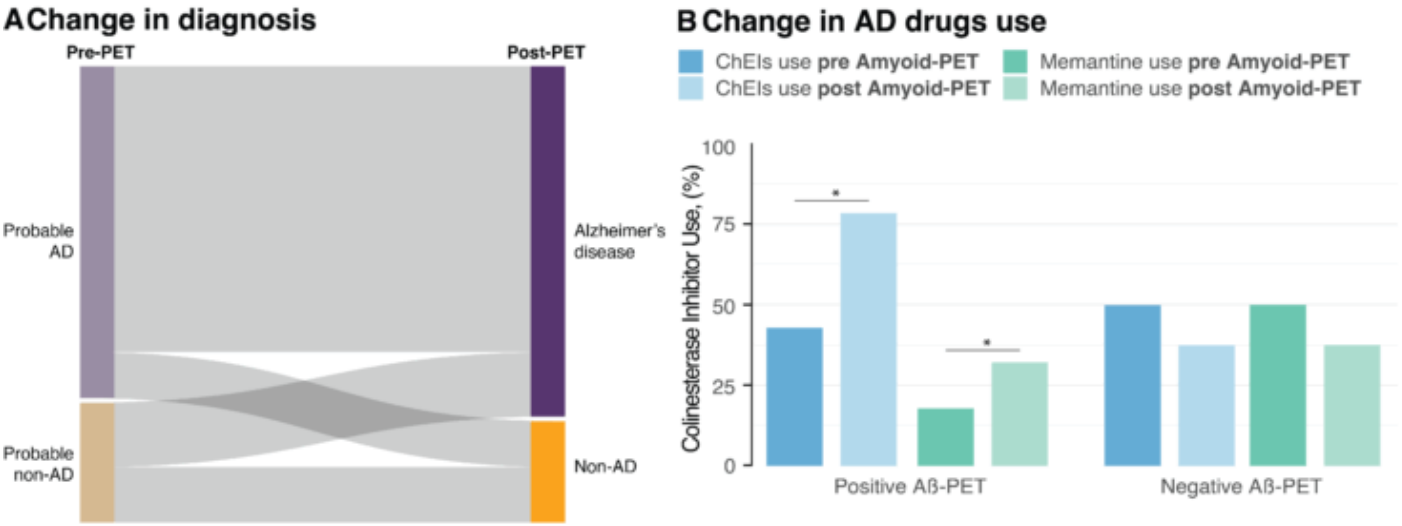


Figure 2. Aß-PET supports diagnostic and treatment decision-making in clinical settings. (A) Sankey plot depicts the proportion of individuals who changed diagnostic category after Aß-PET. In total, changes in diagnosis occurred in 12 individuals (24.4%) out of the study population. **(B)** bars show the change in cholinesterase inhibitor (ChEIs) and memantine use in Aß-PET positive and negative individuals. *P<0.05

Keywords: Alzheimer's disease; Aß-PET; diagnosis; treatment, biomarker

20 Neuropathological validation of Tau-PET CenTauR units: Preliminary data from a multicenter study

Leonardo Iaccarino[1], Konstantinos Chiotis[2,3], Lea Grinberg[2,4], Vikas Kotari[1], Renaud La Joie[2], Antoine Leuzy[5], Val Lowe[6], Ming Lu[1], Alexis Moscoso[5], Aivi Nguyen[6], Christopher Schwarz[6], William Seeley[2], Clifford Jack[6], Gil Rabinovici[2], Sergey Shcherbinin[1]

[2]*Eli Lilly and Company, Indianapolis, IN, US*
[2]*2UCSF Memory and Aging Center, San Francisco, CA, US*
[3]*Karolinska Institutet, Stockholm, Sweden*
[4]*Mayo Clinic Jacksonville, Jacksonville, FL, US*
[5]*Critical Path for Alzheimer's Disease (CPAD) Consortium, Tucson, AZ, US*
[6]*Mayo Clinic Rochester, Rochester, NY, US*

Introduction: The recently developed CenTauR initiative[1] holds promise to benefit research and clinical studies by enabling harmonization and integration across multiple tau-PET tracers (^{18}F-flortaucipir, ^{18}F-PI2620, ^{18}F-RO948, ^{18}F-MK6240, ^{18}F-GTP1). A multicenter study was launched to evaluate the diagnostic performance of CenTauR units converted from standardized uptake value ratios (SUVRs) against neuropathology data.

Methods: To date, the study includes cases with available antemortem ^{18}F-flortaucipir PET (FTP-PET) and neuropathology data from 3 US sites. FTP-PET scans, acquired 80–100 minutes post-injection, were processed using standard (or calibrated) CenTauR SPM12-based methodology and volumes of interest (VOIs).[1] Universal and regional SUVRs were estimated and converted to CenTauR units. Neuropathological assessments included Thal (A), Braak (B), and Consortium to Establish a Registry for Alzheimer's Disease (C) scores, Alzheimer's Disease neuropathological change classifications, and other information as available. Preliminary descriptive analyses evaluated the pooled cohort.

Results: As of September 2025, the database included 283 cases (Site 1: n=60, Site 2: n=150, Site 3: n=73). The mean age (standard deviation [SD]) at FTP-PET was 73 (11.8) years, with 40.6% female participants. The mean interval between PET and death was 2.5 (2.0) years. The amyloid positivity rate based on neuropathological assessments (C score ≥2) was 71.6%. Braak B0 (none), B1 (I/II), B2 (III/IV), and B3 (V/VI) scores were observed in 13 (4.7%), 50 (18.3%), 55 (20.1%), and 156 (56.9%) participants, respectively. Mean universal VOI CenTauRs (SD) were 2.5 (12.2), 6.4 (12.5), 6.5 (14.0), and 99.0 (73.1), for B0, B1, B2, and B3 groups, respectively. For the mesial temporal VOI, CenTauRs (SD) were 9.1 (20.0), 7.0 (14.2), 14.2 (23.7), and 78.2 (45.8), respectively (Table 1).

Conclusion: This dataset, constituting the largest tau-PET autopsy cohort to date, will support further diagnostic performance analyses, providing operational thresholds potentially applicable to various tau-PET tracers.

Reference

1. Leuzy A, et al. *Alzheimers Dement*. 2024;20:5833-5848.

Table 1. Mean Universal and Regional CenTauR Values (SD) According to B and C Scores

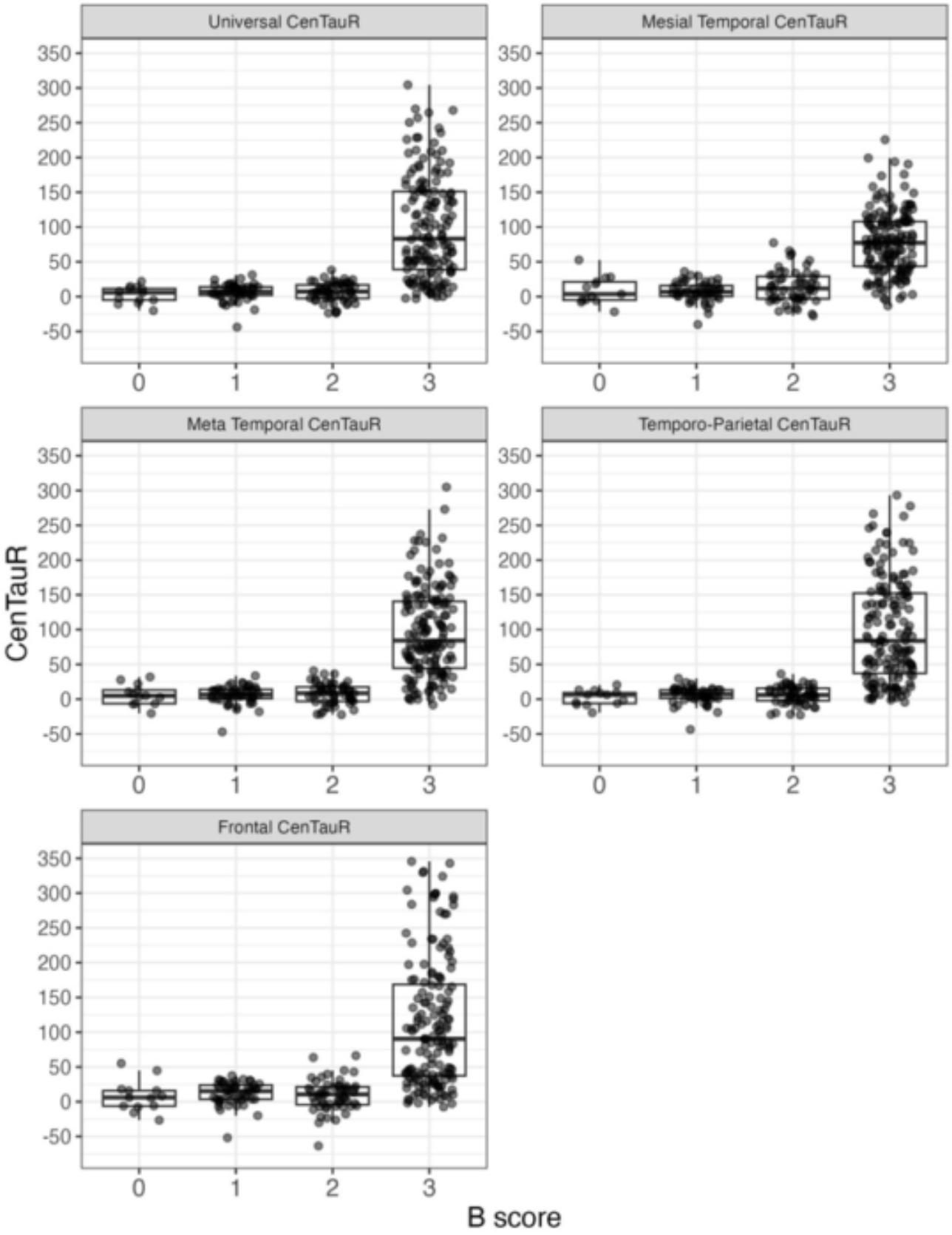
	All patients			
	B0 (none)	**B1 (I/II)**	**B2 (III/IV)**	**B3 (V/VI)**
Sample size	13	50	55	156
Universal	2.5 (12.2)	6.4 (12.5)	6.5 (14.0)	99.0 (73.1)
Mesial temporal	9.1 (20.0)	7.0 (14.2)	14.2 (23.7)	78.2 (45.8)
Meta temporal	6.4 (14.9)	6.0 (13.1)	7.7 (15.1)	96.5 (63.6)
Temporo-parietal	2.2 (11.2)	5.5 (12.1)	5.8 (13.1)	98.5 (73.2)
Frontal	8.3 (22.7)	12.3 (16.1)	9.2 (22.6)	112.0 (92.3)
	Amyloid negative (C score ≤1)			
Sample size	12	33	24	3
Universal	0.9 (11.2)	4.0 (13.1)	4.5 (13.4)	11.9 (6.5)
Mesial temporal	5.5 (15.8)	5.0 (14.9)	10.1 (18.5)	14.0 (20.0)
Meta temporal	4.6 (14.1)	3.9 (13.9)	6.4 (14.2)	18.5 (20.2)
Temporo-parietal	0.7 (10.1)	3.1 (12.6)	4.0 (12.7)	11.1 (6.6)
Frontal	5.2 (20.8)	10.8 (16.2)	3.6 (15.8)	35.6 (15.8)
	Amyloid positive (C score ≥2)			
Sample size	1	17	30	153
Universal	21.8 (NA)	10.9 (10.1)	8.0 (14.7)	101.0 (72.8)
Mesial temporal	52.7 (NA)	10.7 (12.4)	18.0 (27.3)	79.4 (45.3)
Meta temporal	27.8 (NA)	10.1 (10.4)	9.0 (16.1)	98.0 (63.3)
Temporo-parietal	20.5 (NA)	10.2 (9.71)	7.3 (13.7)	100.0 (72.9)
Frontal	44.8 (NA)	15.1 (16.0)	13.1 (26.5)	114.0 (92.6)

B=Braak; C=Consortium to Establish a Registry for Alzheimer's Disease; NA=not available; SD=standard deviation; I/II=Braak I/II; III/IV=Braak III/IV; V/VI=Braak V/VI.
Note: C score was missing for 1 subject; B scores were missing for 9 subjects.

***Table 2.The CenTauR-to-Pathology (CTR2PATH) Study Group**

Names	Affiliations
Leonardo Iaccarino	Eli Lilly and Company, Indianapolis, USA
Vikas Kotari	
Ming Lu	
Sergey Shcherbinin	
Michael Pontecorvo	
Konstantinos Chiotis	UCSF Memory and Aging Center, San Francisco, USA, Karolinska Institutet, Stockholm, Sweden
Lea T. Grinberg	UCSF Memory and Aging Center, San Francisco, USA Mayo Clinic Jacksonville, Jacksonville, USA
Renaud La Joie	UCSF Memory and Aging Center, San Francisco, USA
Gil D. Rabinovici	
William Seeley	
Ganna Blazhenets	
Salvatore Spina	
Antoine Leuzy	Critical Path for Alzheimer's Disease (CPAD) Consortium, Critical Path Institute, Tucson, USA
Alexis Moscoso	
Val J. Lowe	Mayo Clinic Rochester, Rochester, USA
Aivi T. Nguyen	
Christopher G. Schwarz	
Clifford R. Jack	
Ronald C. Petersen	
Jonathan Graff-Radford	
Hoon-Ki Min	
Matthew L. Senjem	
Mary M. Machulda	
Dennis W. Dickson	
Kejal Kantarci	
Bradley Boeve	
Prashanthi Vemuri	
David T. Jones	
David Knopman	
Salvatore Spina	
Melissa E. Murray	Mayo Clinic Jacksonville, Jacksonville, USA

Figure 1. Distribution of Universal and Regional CenTauRs According to B Score at Autopsy



B=Braak

Keywords: Tau-PET, CenTauR, Harmonization, Autopsy

21 Molecular evaluation of a tau-PET analog and pathological TAR DNA-binding protein 43 docking in a cellular model of frontotemporal lobar degeneration

Rodolfo G. Gatto[1], Carina Weissmann[2], Libia C. Salinas Castellanos[2], Mayra M. Montes[2], Gokhan Uruk[1], Hossam Youssef[1], R. Ross Reichard[3], Keith A. Josephs[1]

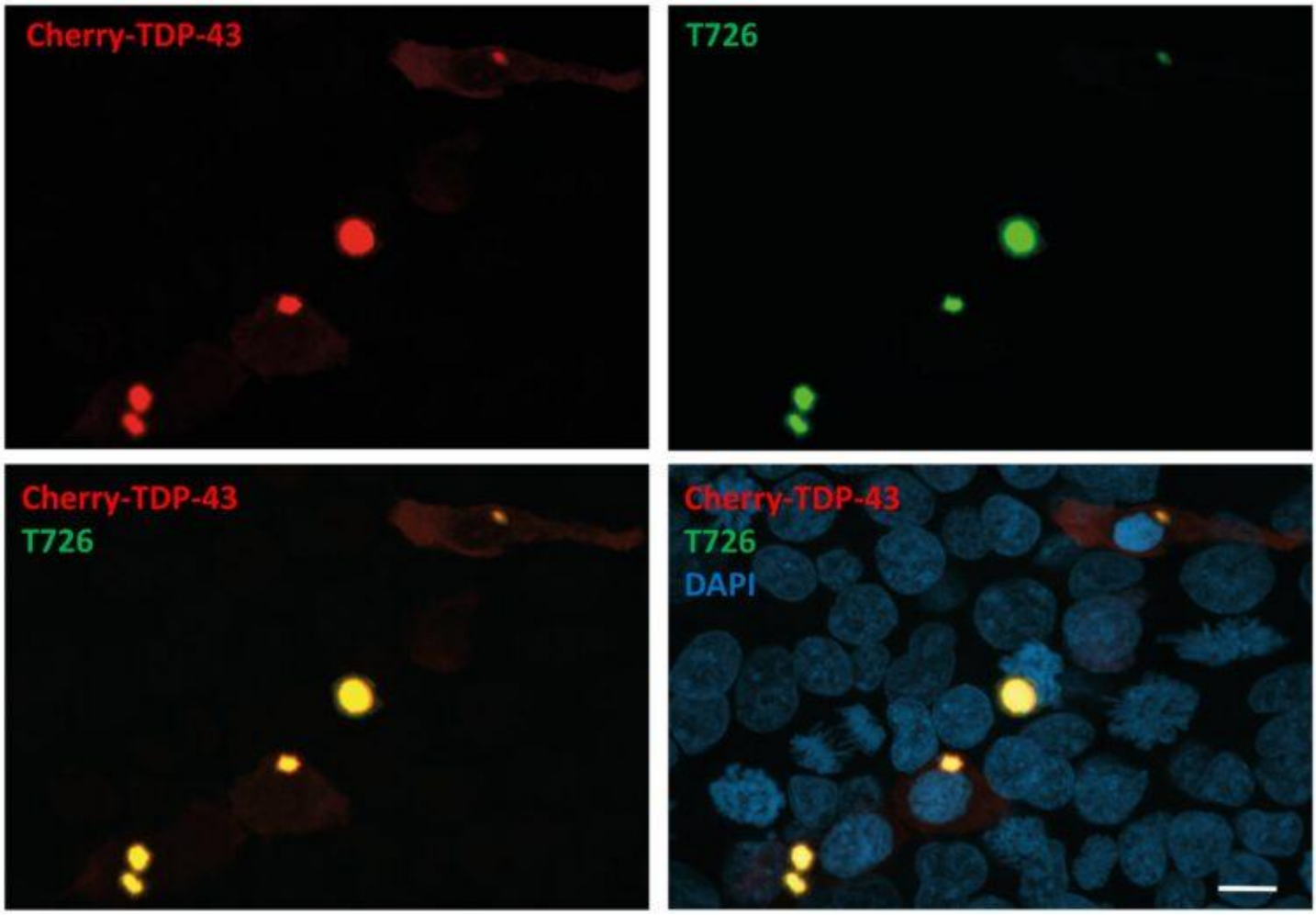
[1]*Department of Neurology, Mayo Clinic, Rochester, MN, US*
[2]*FIBYNE-UBA-CONICET, Buenos Aires, Argentina*
[3]*Department of Laboratory Medicine and Pathology, Mayo Clinic, Rochester, MN, US*

Introduction: We previously evaluated the [^{18}F]flortaucipir (FTP) analog T726 and demonstrated its colocalization with paired helical filament (PHF) tau, along with partial binding to both 3-repeat (3R) and 4-repeat (4R) tau isoforms in frontotemporal lobar degeneration (FTLD). These findings suggested that FTP may have broader binding capabilities, potentially extending to other proteinopathies. Given that FTP uptake has been identified in cases of frontotemporal lobar degeneration with phosphorylated TAR DNA-binding protein 43 (pTDP-43) (FTLD-TDP), we sought to investigate whether T726 is also capable of binding to pTDP-43 aggregates in vitro.

Materials and Methods: To assess this, HEK cells were transfected with a plasmid encoding mCherry-tagged TDP-43 under conditions that promote aggregation. Additionally, control experiments were performed to confirm the specificity of T726 binding. T726 immunofluorescence was evaluated in multiple experimental conditions: cells expressing mCherry-TDP-43 with and without aggregates, cells expressing mCherry alone, and cells containing aggregates of an unrelated protein (fluorescently tagged huntingtin). In parallel, representative human brain samples from Alzheimer's disease patients with TDP-43 pathology and FTLD-TDP cases (temporal and hippocampal regions) were examined using fluorescence immunohistochemistry with pTDP-43 antibodies and co-incubation with T726 to assess colocalization and regional distribution.

Results: T726 fluorescence was observed exclusively in cells exhibiting mCherry-TDP-43 aggregation, with no signal detected in control conditions. In human tissue samples, T726 colocalized with pTDP-43 pathology across limbic regions in both AD+pTDP-43 and FTLD-TDP cases.

Conclusions: These findings suggest that the flortaucipir (FTP) analog may bind to pTDP-43 aggregates in cases of FTLD-TDP, and potentially to pTDP-43 in AD+pTDP-43 cases as well. Future studies are planned to further characterize these molecular interactions and evaluate their representation in human samples.



HEK cells expressing mCherry–TDP-43, stained with T726 and DAPI. Aggregates are visible in both the red channel (mCherry signal) and the green channel (T726 fluorescence). Scale bar: 10 µm.

Keywords: Flortaucipir fluorescent analog, TAR DNA-binding protein 43, HEK cells, frontotemporal lobar degeneration, neuropathology

22 Anterior cingulate sulcal pattern is associated with successful cognitive aging

Samira Maboudian[1], Gabriella Kellerman[2], Ethan Willbrand[3], Stefania Pezzoli[4], Kevin Weiner[1,2], William Jagust[1]

[1]*Department of Neuroscience, University of California, Berkeley, Berkeley, CA, US*
[2]*Department of Psychology, University of California, Berkeley, Berkeley, CA, US*
[3]*School of Medicine and Public Health, University of Wisconsin–Madison, Madison, WI, US*
[4]*Edward and Pearl Fein Memory and Aging Center, Department of Neurology, UCSF, San Francisco, CA, US*

Background: Cognitive aging trajectories vary, but neurobiological factors underlying this heterogeneity remain unclear. Successful cognitive aging (better cognition than expected by age) is associated with preserved left anterior cingulate (ACC) thickness. The paracingulate sulcus (PCGS), a variably-present sulcus in ACC, is associated with cognition, psychiatric traits, and connectivity differences. Here, we investigated whether PCGS morphology is associated with cognitive aging.

Methods: Using MRIs from 180 older adults (OA) from the Berkeley Aging Cohort Study and 72 younger adults (YA) from the Human Connectome Project (Table 1), 3 raters labeled the PCGS in every hemisphere along established criteria in FreeSurfer, measuring asymmetry categorically as presence/absence pattern (Fig.1A) and continuously as right minus left hemisphere length.

Machine learning models estimated participants' "cognitive-age" from neuropsychological testing; cognitive-age gap (CAG=chronological-age – cognitive-age) scores reflect deviation from expected cognition (positive is better than expected for age).

We examined PCGS pattern associations with demographic factors, cognition (memory composite), and CAG. Correlation between vertex-wise cortical thickness and asymmetry was performed via FreeSurfer's GLM pipeline. We assessed whether PCGS asymmetry predicts CAG using nested multiple linear regression models predicting CAG from age, sex, education, hippocampal volume, amyloid (PIB) load, entorhinal tau (FTP), and ACC thickness, with and without PCGS asymmetry. We then examined whether the CAG-asymmetry relationship is mediated by left ACC thickness.

Results: Rightward PCGS asymmetry was associated with higher CAG (Fig.1B-C), better cognition (Fig.1D), and preserved ACC thickness in OA (Fig.2A). Left ACC thickness was associated with CAG in a regression model without PCGS asymmetry ($p<.01$; model $R^2=.22$); adding asymmetry improved fit ($R^2=.31$), with asymmetry significant ($p<.001$) but not ACC thickness. The association between rightward asymmetry and higher CAG was partially mediated by ACC thickness (Fig.2B).

Conclusions: PCGS asymmetry, a developmental morphological trait, is associated with better cognitive outcomes in aging, partially through preserved ACC thickness.

	All	Absent	Symmetric	Leftward	Rightward	p
BACS (OA)						
n	180	29	77	54	20	
Sex: % Female	57.8	75.9	48.1	59.3	65.0	>0.05
Age: μ (std)	75.75 (5.19)	75.24 (5.64)	75.31 (4.86)	76.43 (5.58)	76.35 (4.72)	>0.5
Edu: μ (std)	16.73 (2.07)	16.66 (2.68)	16.64 (1.95)	17.15 (1.81)	16.05 (2.09)	>0.2
APOE4: % Positive	25.6	17.2	24.7	29.6	30.0	>0.6
Handedness: % Right	83.3	75.9	83.1	83.3	95.0	>0.3
HCP (YA)						
n	72	14	28	20	10	
Sex: % Female	50.0	78.6	39.3	45.0	50.0	>0.1
Age: μ (std)	29.06 (3.59)	29.29 (4.51)	28.79 (2.73)	29.95 (3.87)	27.70 (3.77)	>0.4
Edu: μ (std)	15.07 (1.89)	14.29 (2.05)	15.29 (1.76)	15.60 (1.85)	14.50 (1.84)	>0.1
APOE4: % Positive	15.3	28.6	17.9	10.0	0.0	>0.2
Handedness: % Right	87.5	85.7	92.9	75.0	100.0	>0.2

Table 1. Participant characteristics.
Demographic variables for older adults (OA, 70-97 years old) from the Berkeley Aging Cohort Study (BACS) and younger adults (YA, 22-36 years old) from the Human Connectome Project (HCP) in the full sample ("All") and across the 4 paracingulate sulcus (PCGS) subtype categories (see Fig.1A). P-values represent the results of an ANOVA for continuous variables or a Chi-square test for categorical variables, across the 4 PCGS subtypes.

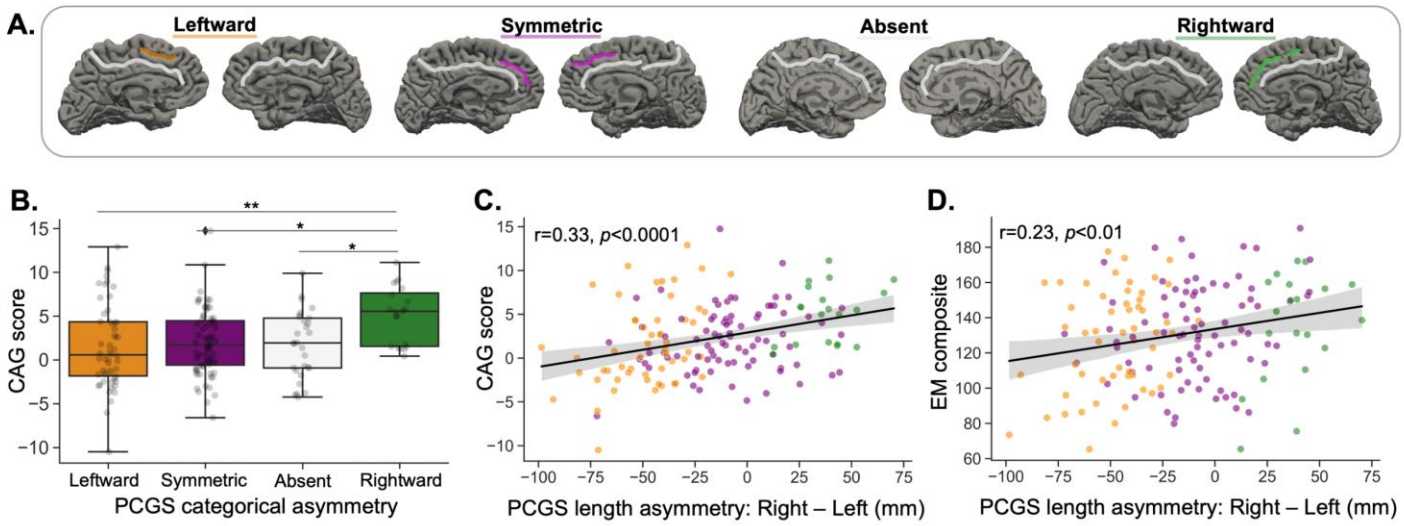


Fig. 1: Rightward PCGS asymmetry is associated with successful cognitive aging in OA cohort.
(**A**) Examples of categorical paracingulate sulcus (PCGS) presence patterns: absent (absent in both hemispheres), symmetric (present in both hemispheres), leftward (present in the left, absent in the right), and rightward (present in the right, absent in the left). Classification based on previous established criteria, e.g. Fornito et al., *Cerebral Cortex* 2004.
(**B**) Cognitive-age gap (CAG) scores (CAG=chronological-age – cognitive-age: positive values indicate better than expected cognition for age) by categorical PCGS asymmetry group. Significant difference in CAG scores across groups (ANOVA p<0.01); asterisks represent significance levels for post hoc pairwise comparisons using Tukey's HSD correction (*=p<0.05, **=p<0.01). Colors correspond to categorical asymmetry group.
(**C**) Association between continuous PCGS length asymmetry (right – left hemisphere length: positive values more rightward) and CAG scores. For C & D, point colors correspond to categorical asymmetry group assignment, as in 1A and 1B; a single regression line is fit across all data.
(**D**) Association between continuous PCGS length asymmetry and episodic memory (EM) composite scores.

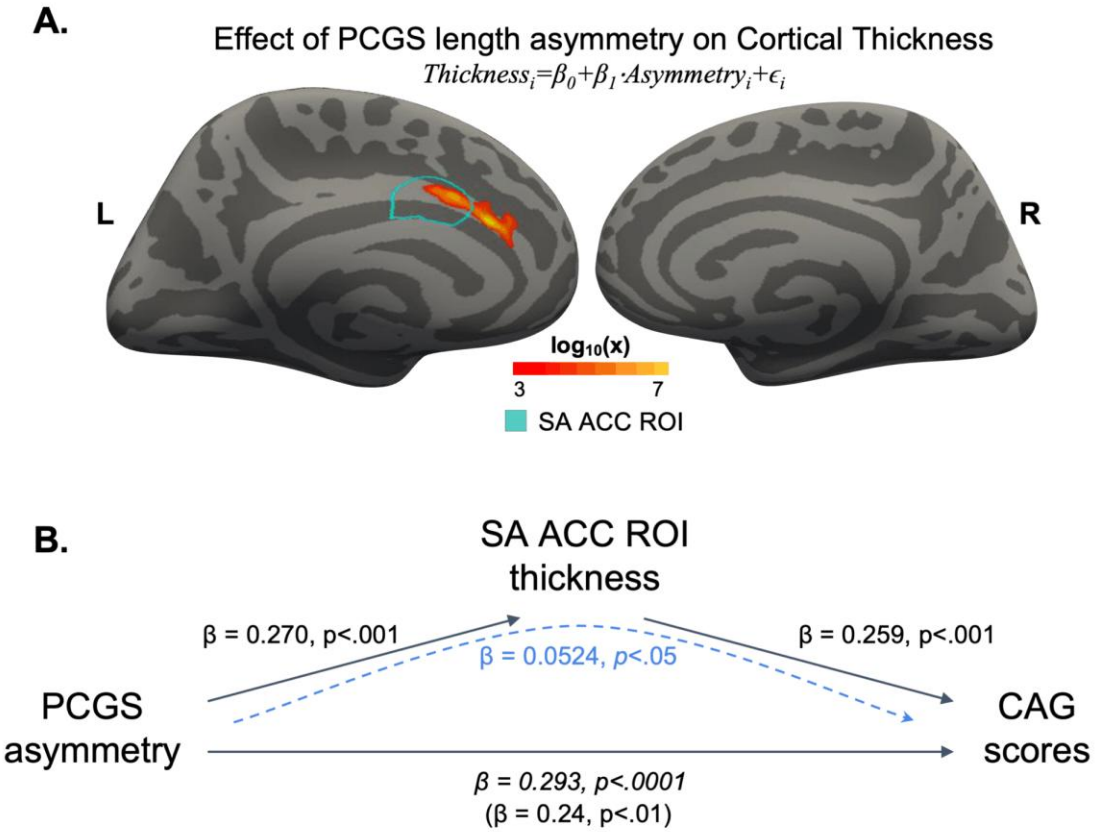


Fig. 2: Rightward PCGS asymmetry is associated with preserved ACC thickness and CAG scores. (**A**) Color bar: Clusters of significant vertex-wise cortical thickness and PCGS length asymmetry correlations in OA, with significance values (uncorrected) masked by clusters surviving multiple comparison correction (vertex-wise cluster threshold = 0.001, cluster-wise p-value threshold = 0.05). No significant clusters emerged when running the same model in YA. Teal line: outline of ACC ROI associated with successful aging (SA) in previous work (Pezzoli et al., *Alz Dem*, 2024).
(**B**) Mediation analysis testing whether left caudal ACC thickness (teal ROI in 2A) mediates the relationship between PCGS length asymmetry and CAG scores. All variables were z-scored. Total effect of asymmetry on CAG is in italics. Direct effect of asymmetry on CAG, controlling for SA ROI thickness, is in parentheses.

Keywords: MRI, sulci, neuroanatomy, cognition, development

23 Microstructural white matter injury mediates the association between vascular risk and plasma biomarkers: Preliminary findings from the Diverse VCID study

Seunghoon Lee[1], Shraddha Sapkota[1], Kumar B Rajan[2], Lee-Way Jin[3], Jason Hinman[4], David K Johnson[1], Danielle Harvey[5], Pauline Maillard[1], Myriam Fornage[6], Charles DeCarli[1]

[1]*Department of Neurology, University of California at Davis, Sacramento, CA, US*
[2]*Rush Institute for Healthy Aging, Rush University Medical Center, Chicago, IL, US*
[3]*Department of Pathology and Laboratory Medicine, University of California at Davis, Sacramento, CA, US*
[4]*Department of Neurology, University of California, Los Angeles, Los Angeles, CA, US*
[5]*Department of Public Health Sciences, University of California at Davis, Sacramento, CA, US*
[6]*Brown Foundation Institute of Molecular Medicine, McGovern Medical School, University of Texas Health Science Center at Houston, Houston, TX, US*

Background: Vascular risk factors (VRFs) contribute to cerebral small vessel disease (SVD) and neurodegeneration. Yet, the biological link between systemic vascular burden and neuroaxonal injury remains unclear. This study investigated whether diffusion-derived free-water (FW), an MRI marker of microstructural white matter injury, mediates the association between vascular risk score (VRS) and plasma biomarkers of Alzheimer's disease (AD) pathology and neurodegeneration.

Methods: We included 936 participants (mean age = 73.7 ± 5.8 years, 69.8% female, 34.4% MCI, and 38.5% White, 32.6% African-American, 29.0% Hispanic) from the Diverse Vascular Contributions to Cognitive Impairment and Dementia (VCID) cohort. VRS summed six cerebrovascular risk factors (hypertension, diabetes, hyperlipidemia, stroke, TIA, and coronary artery disease). Linear mediation analysis estimated the indirect effect of VRS on six plasma biomarkers (Ab42/40, t-tau, p-tau181, p-tau217, neurofilament light [NfL], glial fibrillary acidic protein [GFAP]) through FW, adjusting for age, sex, education, and ethnicity.

Results:
Higher VRS was associated with increased FW (β = 0.003, p = 0.008), elevated total tau (β= 0.052, p= 0.047), and plasma NfL (β= 0.015, p = 0.034). FW showed significant associations with p-tau181 (β = 41.186, p = 0.023), GFAP (β = 1.691, p < 0.001), and NfL (β = 1.006, p < 0.001). Mediation analysis indicated a significant indirect effect of VRS on NfL through FW (β = 0.003, p = 0.003), explaining ~ 21% of the total effect. By ethnic subgroup, VRS was associated with FW only in African Americans, and FW was associated with elevated NfL in Whites and Hispanics.

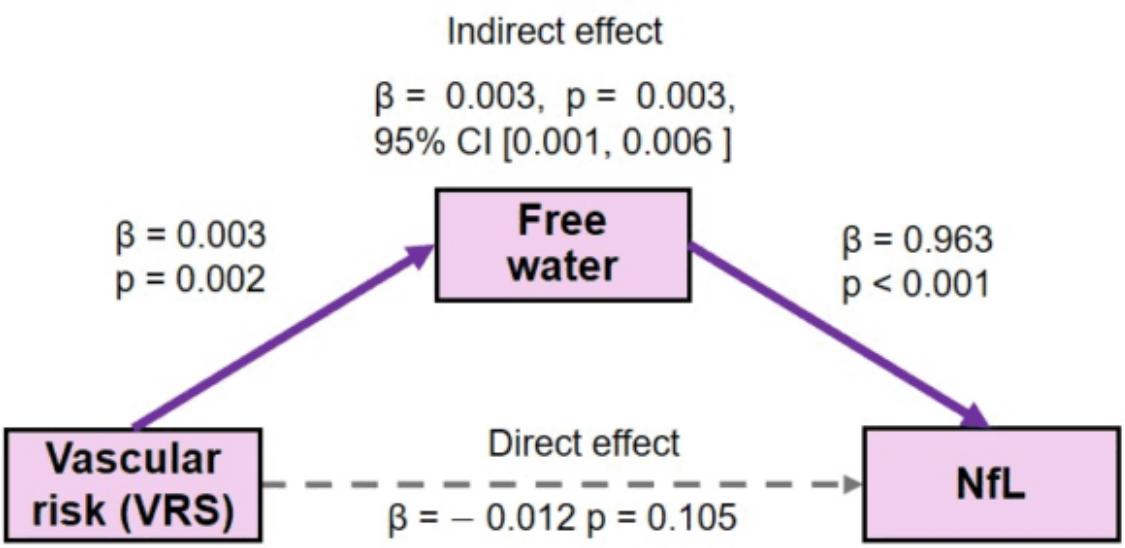


Figure. Mediation effects of free-water on the association between vascular risk score and plasma neurofilament light

Abbreviations; NfL, neurofilament light; VRS, vascular risk score.

The indirect pathway via FW was significant, accounting for ~21% of the total effect. The bold lines indicate p-values of < 0.05.

Conclusions: In the Diverse VCID cohort, elevated vascular risk increased plasma NfL primarily via FW, suggesting that microstructural white matter injury serve as an intermediate pathway linking vascular burden to axonal degeneration. These findings highlight FW as a potential imaging biomarker and therapeutic target for early vascular intervention to mitigate neurodegeneration.

Keywords: Vascular risk factors, free-water, Neurofilament light, small vessel disease, plasma biomarkers

24 VeraBIND Tau: a novel plasma assay reflecting tau aggregation increases over time in individuals with positive tau-PET signal

Bernard Hanseeuw[1,2,3], Lisa Quenon[1,3], Jean-Louis Bayart[1,3], Yasmine Salman[3], Winnie Pak[4], Kavya Shamsundar[4], Joshua Soldo[4], Khalid Iqbal[5]

[1]*Cliniques Universitaires Saint-Luc, Brussels, Belgium*
[2]*Mass General Brigham, Boston, MA, US*
[3]*Université Catholique de Louvain, Brussels, Belgium*
[4]*Veravas Inc, Oakdale, MN, US*
[5]*New York State Institute for Basic Research in Developmental Disabilities, Staten Island, NY, US*

Background: To track AD progression, Tau-PET imaging is the only clinically-validated biomarker (core2). However, it is not available for closely monitoring all patients. The plasma concentration of hyperphosphorylated tau species (pTau) rises with amyloid-β pathology (A+, core 1), and blood-based biomarkers reflecting tau aggregates are still in development, with few longitudinal data available. Here, we present longitudinal results of the VeraBIND Tau assay, a plasma biomarker designed to assess whether pTau can bind to and aggregate normal tau, thus indicating pathologically active tau species.

Methods: Two hundred sixty-eight plasma samples were collected from 145 participants in a prospective UCLouvain study (Table). Amyloid status was determined by CSF ($A\beta_{42}$≤544pg/mL) or amyloid-PET (Centiloid≥20); Tau status by visual assessment of ^{F18}MK6240-PET images (Braak≥1). Plasma pTau217 was quantified using Lumipulse.

Results: Using tau-PET as reference, VeraBIND Tau identified 58 of 60 A+T+ individuals (96% sensitivity) and excluded tauopathy in 59 of 63 A–T– (94% specificity). VeraBIND Tau more frequently detected A–T+ (7/9) than A+T– (4/13) cases, indicating stronger association with tau aggregation than amyloid burden. Sensitivity remained high across early (Braak 1–3, 88%) and advanced (Braak 4–6, 96%) tau-PET stages. In contrast, pTau217 sensitivity dropped markedly in early tau stages (24%, Fig.1).

Longitudinally, annual VeraBIND Tau increases were associated with higher Braak stages and higher tau-PET SUVR, lower episodic memory, and lower MMSE scores. Several participants initially negative on VeraBIND Tau became positive during follow-up, consistent with emerging tau pathology visible on PET (Fig.2). After retest, discordant results between VeraBIND Tau and tau-PET dropped from 12 (8.3%) to 4 (2.8%) cases with 98% sensitivity and 98% specificity for predicting Tau-PET positivity.

Conclusions: VeraBIND Tau demonstrated high reproducibility (>94%), strong sensitivity to early tau aggregation, and robust associations with tau-PET and cognition. VeraBIND Tau is a promising marker to track disease progression and drug efficacy.

Mean value *(SD)*	All N=145	CU N=79	CI N=66	Two-tail p-value
Age at Tau-PET (years)	70.5 *(8.5)*	69.4 *(7.6)*	71.9 *(9.3)*	0.07
Follow-up duration (years)	1.72 *(0.94)*	1.85 *(0.93)*	1.47 *(0.93)*	0.08
Male (%)	44.8%	39.2%	51.5%	0.14
Education (years)	16.3 *(3.5)*	16.9 *(2.9)*	15.5 *(4.0)*	**0.02**
E4 carriers (%)	54.6%	48.1%	62.5%	0.09
% High-Aβ individuals	50.3%	26.6%	78.8%	**<0.001**
MMSE (/30)	26.8 *(3.6)*	28.9 *(1.0)*	24.3 *(4.0)*	**<0.001**
Episodic memory z-score	-1.29 *(2.26)*	0.22 *(0.72)*	-3.29 *(2.02)*	**<0.001**
Entorhinal ^{F18}MK6240 Tau-SUVr	1.56 *(0.92)*	1.04 *(0.42)*	2.24 *(0.96)*	**<0.001**
Plasma $pTau_{217}$ (pg/ml)	0.37 *(0.41)*	0.19 *(0.22)*	0.59 *(0.48)*	**<0.001**
VeraBIND Tau Assay Score	1.02 *(0.21)*	0.94 *(0.17)*	1.11 *(0.21)*	**<0.001**

Fig.1 Sensitivity per Braak-like tau-PET stage

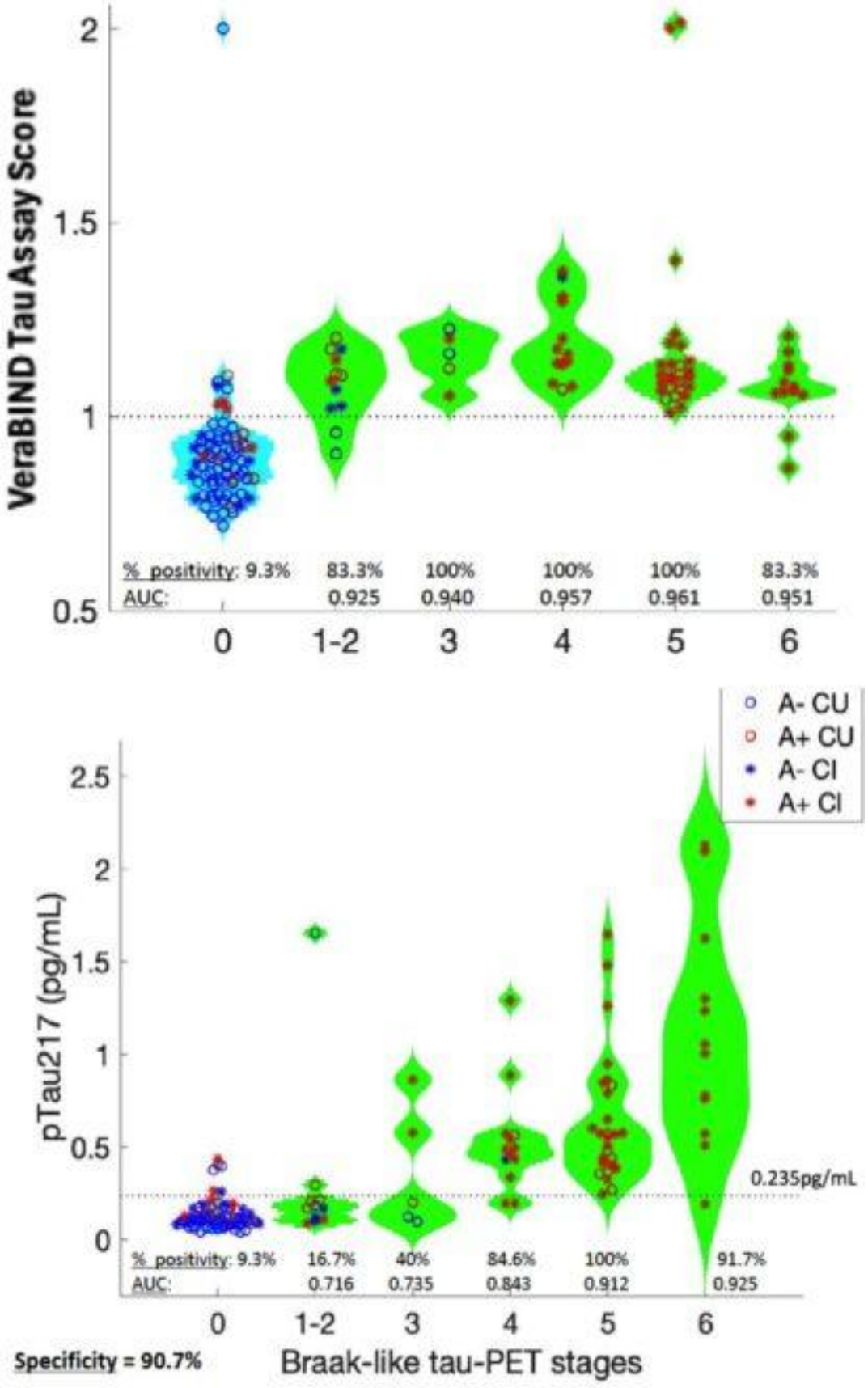
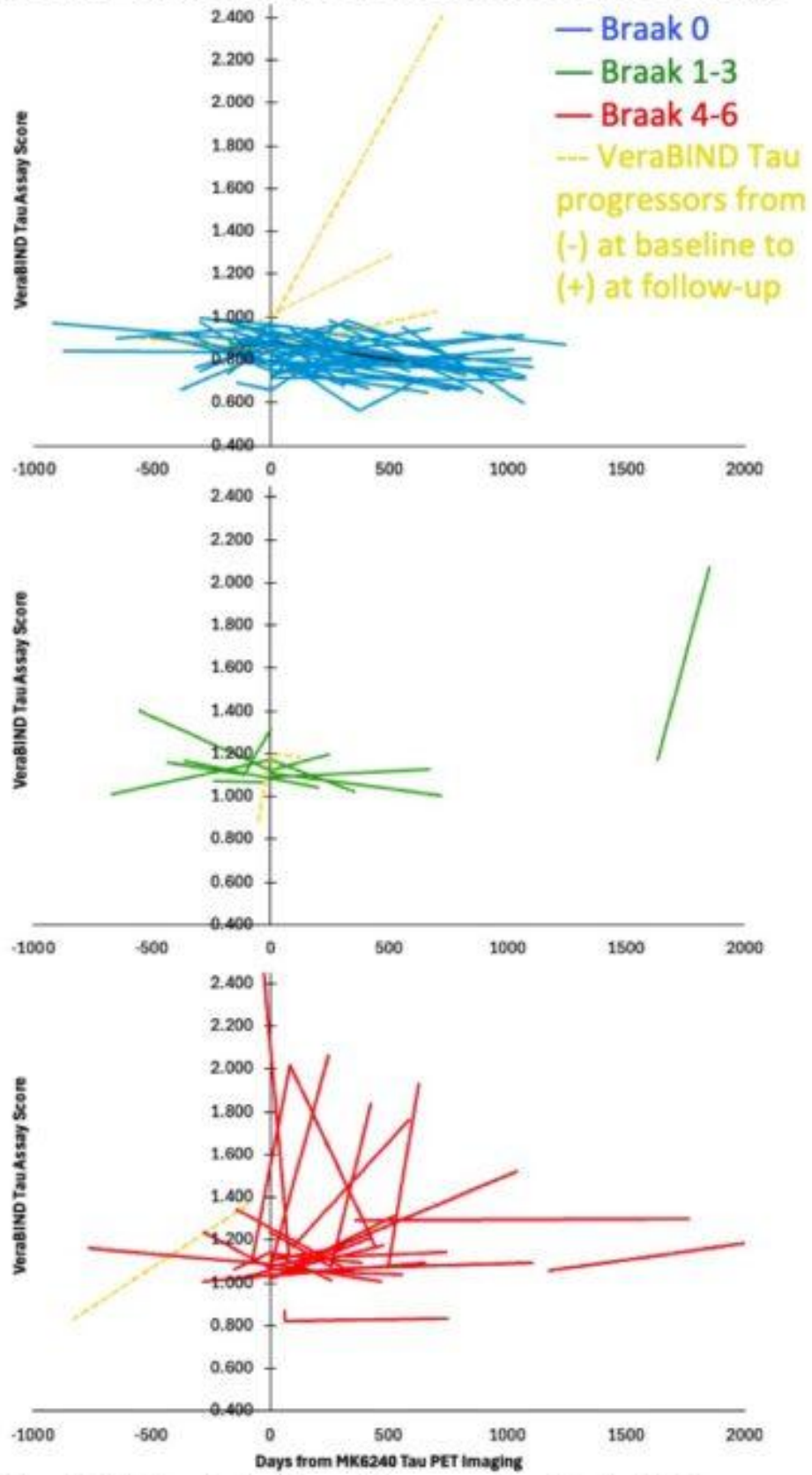


Fig.2 VeraBIND Tau Assay scores increase faster in individuals with advanced Braak-like Tau-PET stage



All VeraBIND Tau (+) at baseline remained (+) at follow-up

Keywords: longitudinal plasma, monitoring disease progression, core 2 biomarker, MK6240 , pTau217

25 Amyloid PET quantitation using skewness: Autopsy validation and test–retest performance

Ilke Tunali[1], Leonardo Iaccarino[1], Jian Wang[1], Ian Kennedy[1], Ming Lu[1], Sergey Shcherbinin[1]

[1]*Eli Lilly and Company, Indianapolis, IN, US*

Background: Amyloid-PET quantitation via Standardized Uptake Value ratio (SUVr) and Centiloid (CL) depends on target and reference region choice and may be impacted by factors including region misregistration. Radiomic features are increasingly recognized as valuable quantitative metrics for amyloid PET (e.g. Gao et al., 2025). We tested a radiomic feature, moment coefficient of skewness, captured from whole-brain as an additional metric to SUVr/CL and evaluated its (i) test–retest reliability and (ii) diagnostic accuracy vs autopsy.

Methods: A test-retest cohort (18F-AV-45-A04, NCT01565343) included 19 participants (10 Alzheimer's Disease (AD)-dementia, 9 cognitively normal (CN)) scanned ≤4-weeks apart. The autopsy cohort (18F-AV-45-A07, NCT01447719) included 59 participants (aged 47–103 years; CN-to-advanced AD-dementia) with PET and autopsy CERAD neuritic plaque score available. Processed florbetapir PET scans were masked using a T1-weighted MNI-template-derived brain mask including supra-tentorial grey and white matter (Figure 1A). Voxel intensities were used to calculate skewness, reflecting asymmetry of intensity distribution (Figure 1B), without reference region normalization. Intra-class correlation coefficient (ICC) and Bland-Altman plots were generated to assess test–retest reliability. Receiver operating characteristic (ROC) analysis was conducted to assess diagnostic performance compared to autopsy findings.

Results: Skewness was correlated with CL values (Figure 2A; R^2=0.77) and showed high test-retest reliability (Figure 2B; ICC=0.98 vs 0.99, respectively). Bland–Altman analysis indicated no evidence of systematic bias (Figure 2C). In the autopsy dataset, skewness discriminated autopsy-positive (CERAD moderate-to-frequent) from autopsy-negative (CERAD none-to-sparse) cases (Figure 3A; AUC=0.930 vs 0.996 for skewness and CL, respectively). Furthermore, skewness values significantly differed across participants' clinical diagnoses (Figure 3B; $p<0.0001$).

Conclusion: Whole-brain skewness may serve as an intensity normalization-free complement to CL/SUVr to assess amyloid burden. Given its independence from intensity scaling, skewness could simplify standardization across acquisitions. Future directions include testing regional and weighted applications, validating across radiotracers and acquisitions, and testing in patients receiving amyloid-targeting therapies.

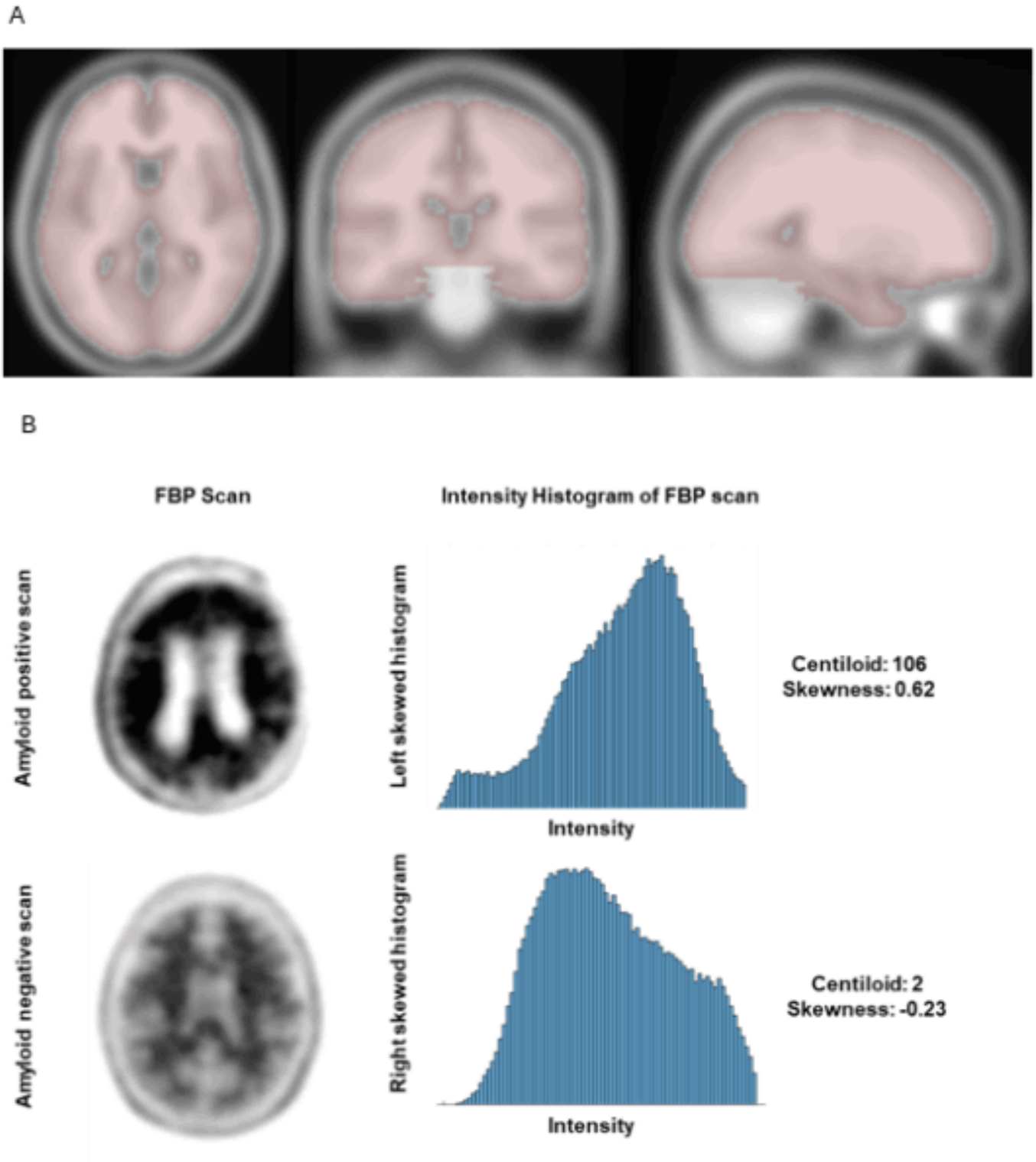


Figure 1. Amyloid PET skewness calculation and example cases of positive and negative scans. A) T1-weighted MNI template-derived brain mask including supra-tentorial grey and white matter, where skewness is calculated. B) Top row: Example of presentation of a high amyloid burden (106 CL; left-skewed intensity distribution). Bottom row: Example of presentation of no/very low amyloid burden (2 CL; slightly right-skewed intensity distribution). Skewness values were multiplied by -1 to make interpretation intuitive, such that positive values indicate higher amyloid levels.

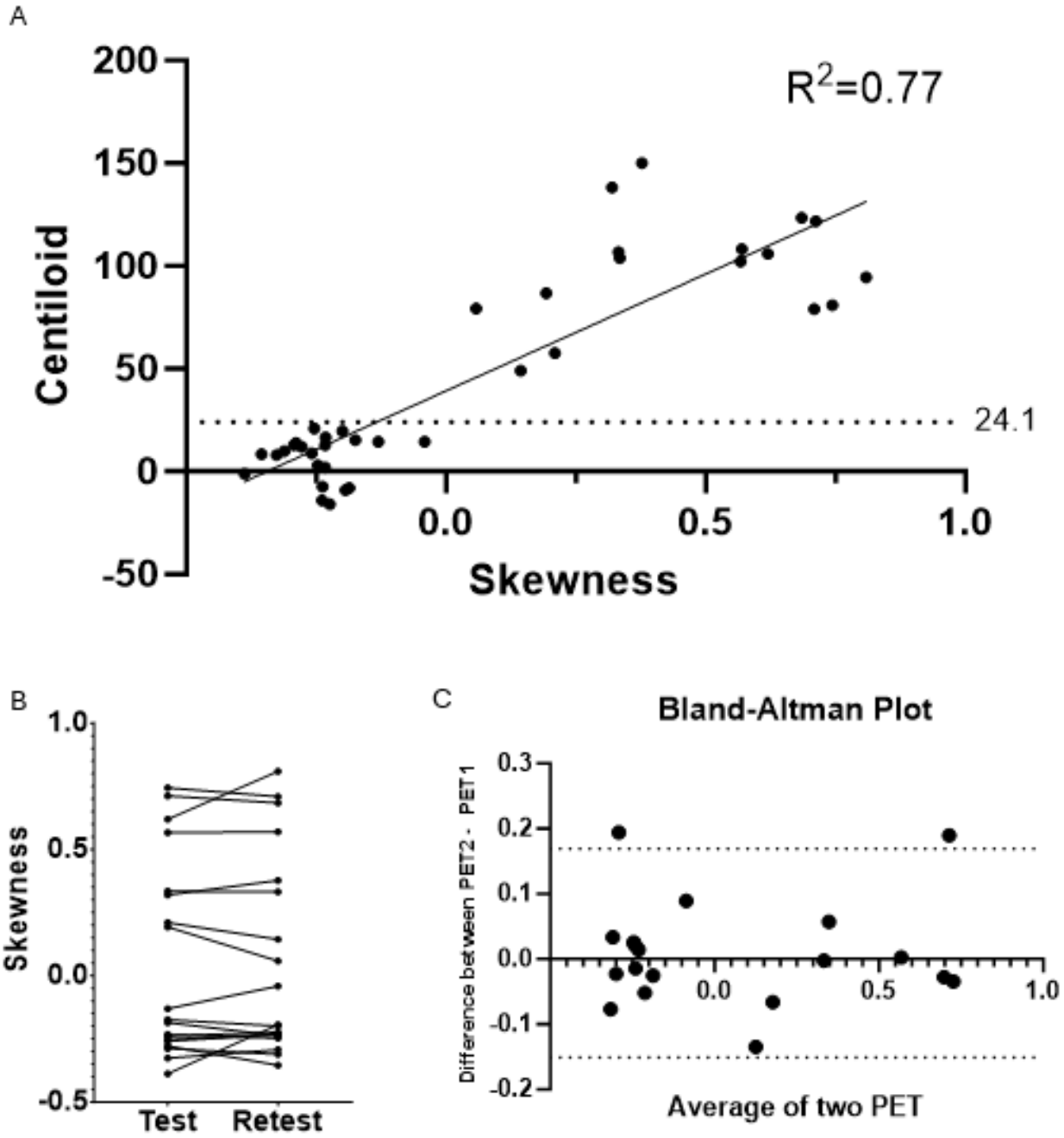


Figure 2. Assessment of skewness measure using test-retest cohort. Florbetapir PET test-retest reliability was confirmed using A) Scatter plot between skewness and Centiloid values utilizing all test-retest images showed high correlation between the two measures. B) Skewness measures acquired from test-retest scans that were <=4 weeks apart. ICC score = 0.98. C) The Bland-Altman plot shows no systematic bias across the dynamic range of skewness estimates. For Centiloid scores derived using standard Avid processing pipeline (Navitsky et al., 2018) the ICC score was 0.99. Dashed lines represent autopsy-based optimal thresholds for amyloid positivity.

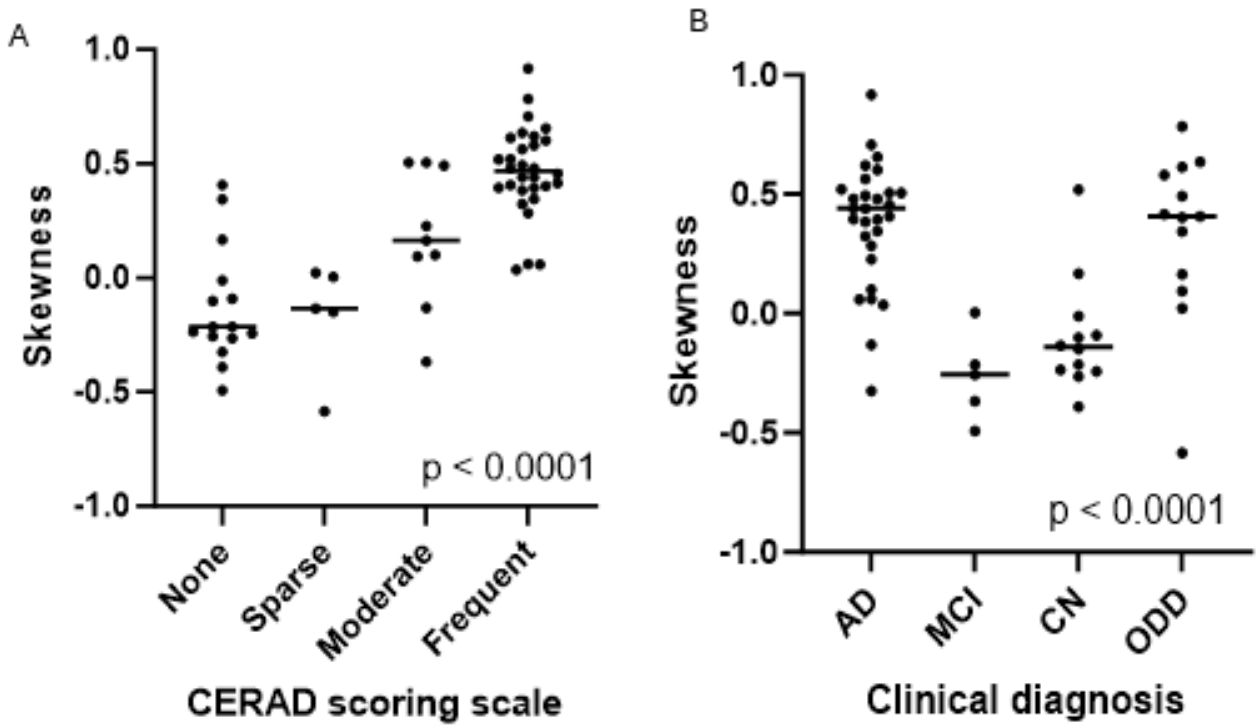


Figure 3. Skewness in the autopsy cohort on the basis of CERAD scoring and clinical diagnosis. Distribution of skewness values in N = 59 subjects classified by A) CERAD scoring scale and B) clinical diagnosis who underwent autopsy within 2 years of florbetapir imaging. AUC = 0.93. Utilizing the same cohort, SUVr score (whole cerebellum reference) was able to discriminate autopsy positive and negative (Joshi et al., 2015) with AUC = 0.99. The p-values were calculated using ANOVA testing (Amyloid-positive=CERAD moderate-frequent; Amyloid-negative=CERAD none-sparse)

ODD: Other dementia disease; MCI: mild cognitive impairment; CN: cognitively normal; CERAD: Consortium to Establish a Registry for AD

Keywords: Amyloid, Florbetapir PET, Skewness, Autopsy, Test-Retest

26 Stratifying preclinical Alzheimer's disease by hippocampal volume to detect concomitant LATE

Nidhi Mundada[1], Xueying Lyu[1], Niyousha Sadeghpour[1], Christopher Brown[1], Emily McGrew[1], Paul Yushkevich[1], Sandhitsu Das[1], David Wolk[1]

[1]*University of Pennsylvania, Philadelphia, PA, US*

Objective: We previously used a cutoff of the lowest quartile of hippocampal volume (HV) to identify a subgroup of patients with symptomatic AD likely enriched for concomitant limbic-predominant age-related TDP-43 encephalopathy (LATE). As copathology likely exists before symptom onset, we investigated whether similar low-HV profiles in preclinical AD capture early imaging and cognitive signatures of mixed disease.

Methods: 1709 cognitively unimpaired (CU) participants from A4/LEARN with T1-MRI were grouped based on HV distribution (adjusted for age/intracranial volume) and amyloid-status into *suspected-(s)* AD+sLATE- (HV>median, Ab+), AD+sLATE+ (HV<16th-percentile(~1SD), Ab+), and CU-Ab-sLATE- (Ab-). We used a surface-based pointwise regional thickness analysis framework to examine cross-sectional and longitudinal atrophy patterns in the medial temporal lobe (MTL). We also assessed cross-sectional and longitudinal cognitive trajectories using linear-mixed effects models controlling for entorhinal-tau-SUVR, when available, to mitigate the role of AD severity in differences between the AD groups.

Results: Within preclinical AD, AD+sLATE+ had higher, though overlapping, entorhinal-tau-SUVR than AD+sLATE- (Figure-1A). AD+sLATE+ showed imaging features suggestive of LATE: lower amygdala volumes, greater hippocampal asymmetry, and a trend toward lower ERC/PHC ratio relative to AD+sLATE- (Figure-1B). Cross-sectionally, AD+sLATE+ showed significantly thinner MTL cortex than AD+sLATE-, particularly in anterior regions when controlling for tau (Figure-2A). Longitudinally, AD+sLATE+ exhibited faster atrophy than AD+sLATE-, again including entorhinal-tau-SUVR as covariate (Figure-2B). Cognitively, AD+sLATE+ had lower baseline memory scores versus AD+sLATE- (Figure-3A). Over time, AD+sLATE+ showed steeper decline across memory and global composites (PACC), even after accounting for tau (Figure-3B), consistent with synergistic effects of coexisting AD and LATE pathology.

Conclusions: In preclinical AD, low-HV identifies a subgroup with distinct MTL atrophy patterns and early cognitive vulnerability, consistent with enrichment in concomitant LATE pathology. This simple approach may be helpful for stratification of preclinical AD populations in trials to determine whether there are differences in benefit based on the presence of co-pathologies.

A. Demographics & Cohort Description (A4/LEARN)

mean (SD)	Aβ-CU (n=366)	AD+sLATE- (n=366)	AD+sLATE+ (n=183)
Age	72.1 (4.5)	72.7 (4.8)	73.5 (5.6)
Sex (M/F)	142/224	146/220	78/105
Education	16.7 (2.7)	16.3 (2.7)	16.7 (2.6)
Adjusted Hippocampal Vol	3383 (312)	3626 (209)	2874 (174)
Plasma p-tau$_{217}$	0.2 (0.1)	0.3 (0.2)	0.3 (0.2)
Entorhinal Tau SUVR (n)	1.1 (0.1) (n=40)	1.2 (0.1) (n=123)	1.3 (0.2) (n=72)

B. Imaging Features

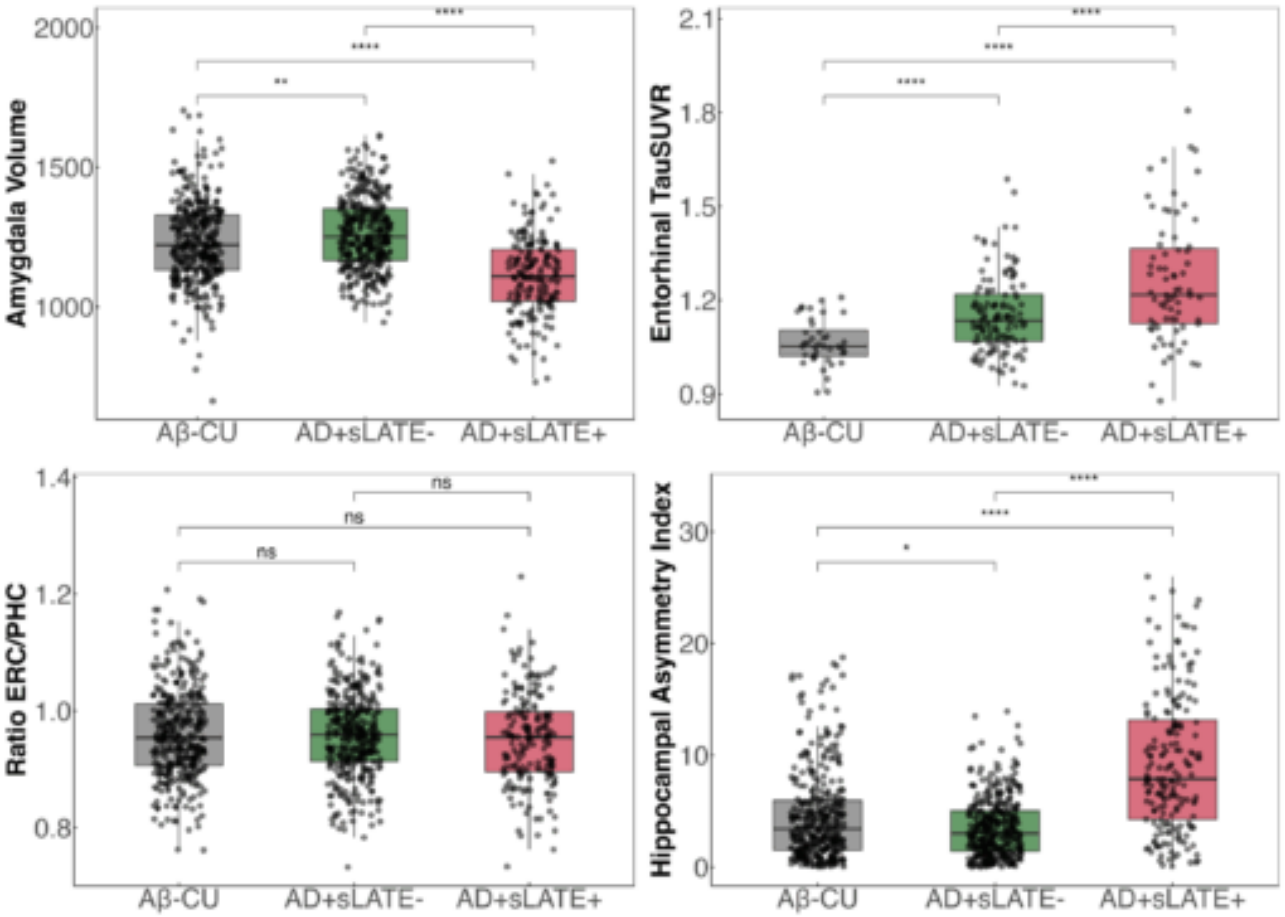


Figure 1: Cohort description and imaging features

A. *Summary statistics across groups. Note that only a subset of individuals available tau-PET data. Aβ-CU and AD+sLATE- groups were propensity matched (2:1) to AD+sLATE+ using age and sex to create balanced groups.* ***B.*** *Distribution of amygdala volume and tau burden as measured by entorhinal Tau-SUVR from tau-PET across groups. Distribution of imaging features suggestive of LATE, from prior work, ratio of ERC to PHC, and hippocampal asymmetry calculated as (|(L-R)| / (L+R))*200. Hypothesis for sLATE+: ↓ amygdala volume, ↓ ERC/PHC ratio, ↑ Hippocampal Asymmetry. Significance levels are indicated as follows: p ≤ 0.05 (*), p ≤ 0.01 (**), p ≤ 0.001 (***), and p ≤ 0.0001 (****). 'ns' indicates not significant (p > 0.05).*

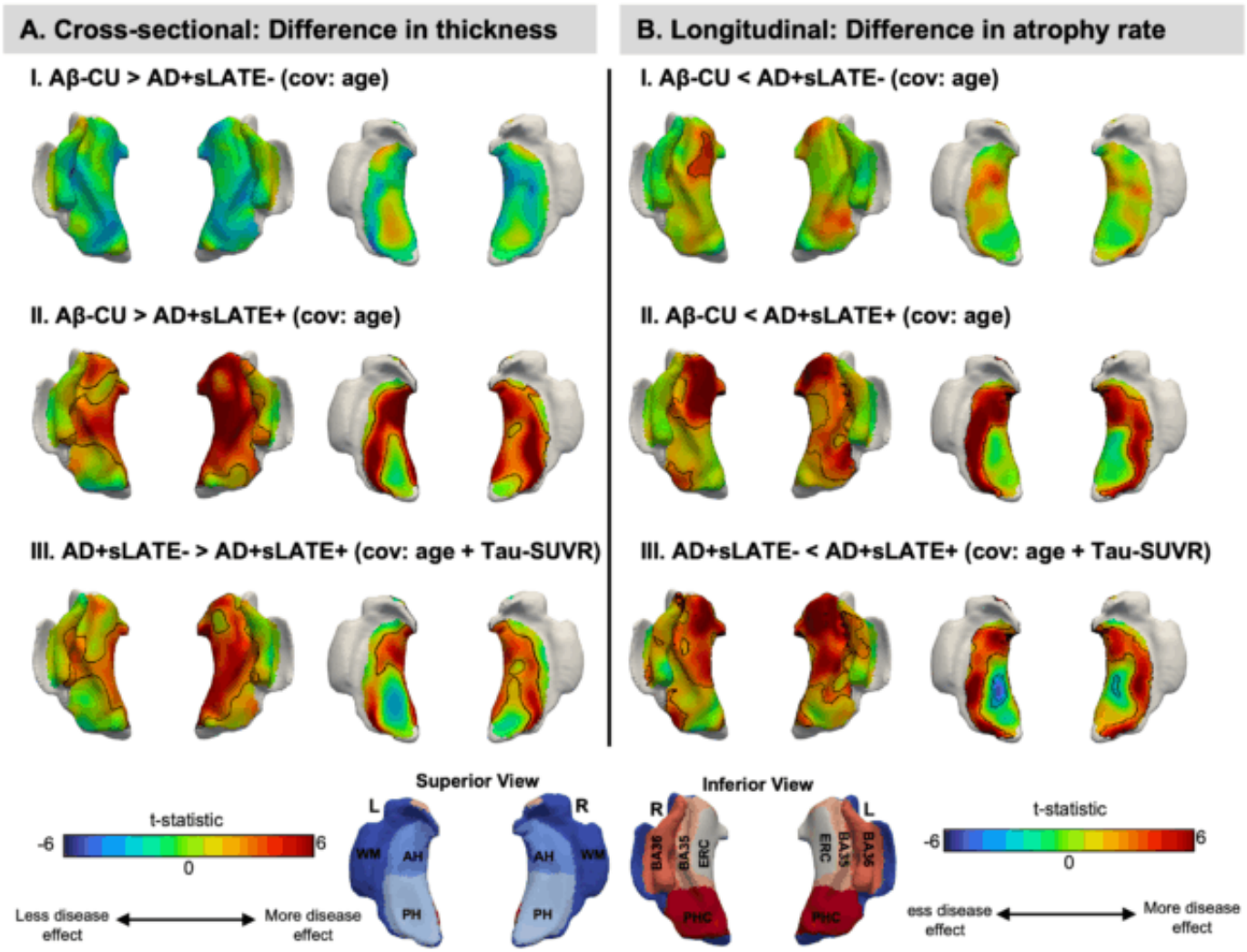


Figure 2: Pointwise structural cross-sectional and longitudinal group differences in the MTL. ***A.*** *Maps represent group differences in thickness obtained using a surface-based MTL analysis pipeline, CRASHS. Each 3D model represents the inflated representation of the mid-surface between the MTL gray matter and white matter, shown either from superior or inferior. Age (I-III) and entorhinal Tau-SUVR (III) were used as covariates. Black outlines represent clusters significant at p<0.05 FWER-corrected (using the threshold-free cluster enhancement (TFCE) method with 10,000 permutations).* ***B.*** *Linear mixed-effects models were run at every point in the MTL thickness maps. For comparisons with Aβ-CU (I-II), the following equation was used: Thickness ~ time + group + age at baseline scan + time*group + (1 | ID). For comparisons between AD groups (III), the following equation was used: Thickness ~ time + group + age at baseline scan + entorhinal TauSUVR + time*group + (1 | ID). Black outlines represent clusters significant at p<0.05 FDR-corrected (using false discovery rate). AH=anterior hippocampus, PH=posterior hippocampus, ERC=entorhinal cortex, BA35/36=Brodmann areas 35/36, PHC=parahippocampal cortex, WM=white matter. While effects for the cross-sectional analysis are as expected based on group definitions, there is also extension to cortical regions, particularly anterior. Further, longitudinal analyses show clear group differences.*

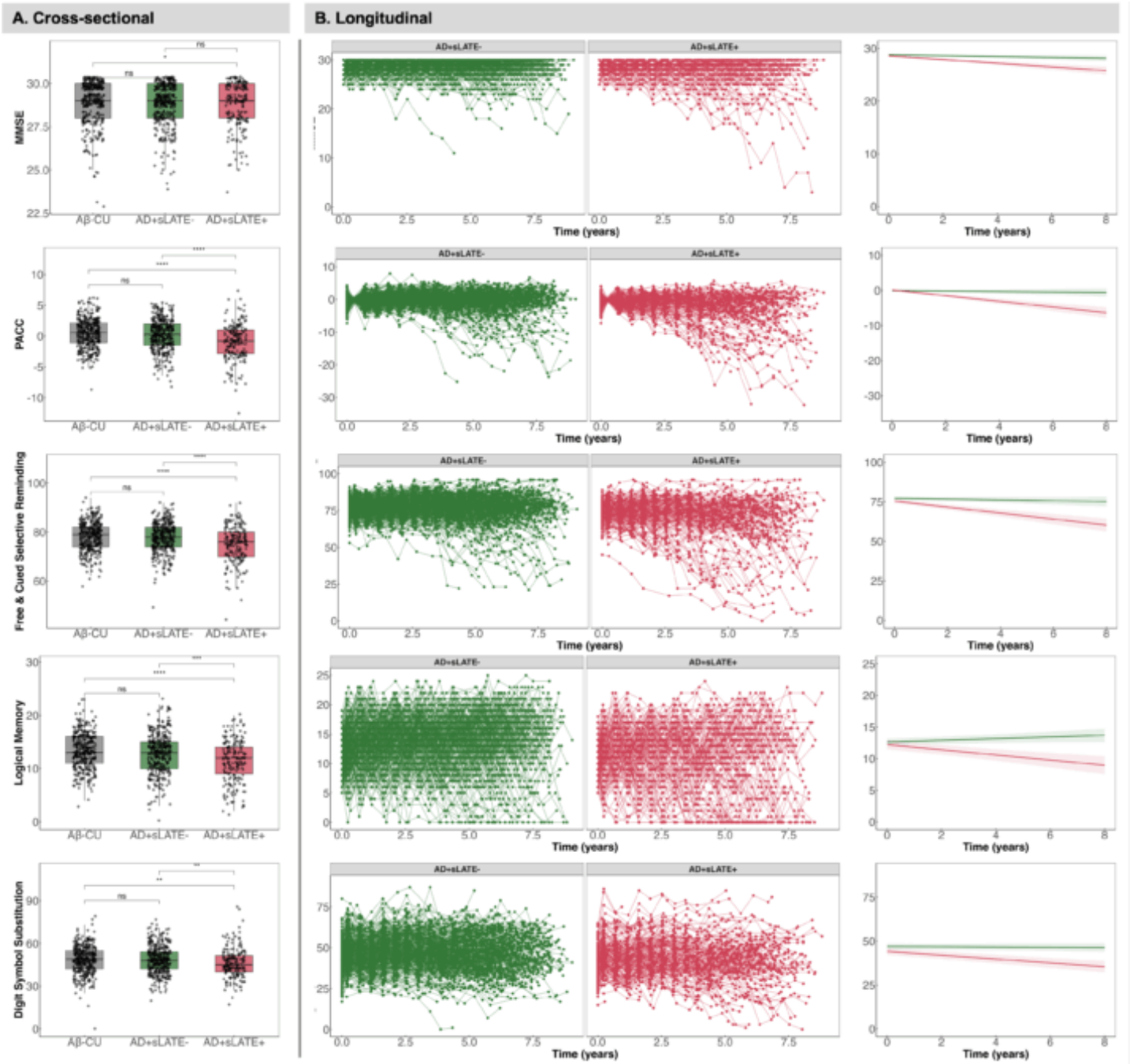


Figure 3. Cross-sectional and longitudinal differences in cognitive domains and trajectories.
A. *Pairwise group differences (*p<0.05, ***p<0.001, ****p<0.0001) at baseline. No significant differences when controlling for entorhinal tau-SUVR.*
B. *Linear mixed-effects model controlling for entorhinal tau-SUVR and time difference in years across cognitive tests. Score ~ time + group + age at baseline assessment + years of education + entorhinal Tau-SUVR + time*group + (1 + time | ID). Model allows for random slopes and intercepts. On the right most, slopes for AD+sLATE- and AD+sLATE+ are significantly different.*

Keywords: preclinical AD, LATE, TDP-43, copathology, hippocampal volume

27 Differential sensitivity of [^{18}F]MK6240 and [^{18}F]FTP to measure tau before and after anti-amyloid therapy

Han Deng[1], Quentin Finn[1], Andrea Pando[1], Nicole Matutue[1], Firoza Lussier[2], Juan Fortea[3], Dana Tudorascu[2], David Soleimani-Meigooni[4], Val Lowe[5], Hwamee Oh[6], Brian Gordon[7], Pedro Rosa-Neto[8], Suzanne Baker[9], Tharick Pascoal[2,10], Joseph Masdeu[1], Belen Pascual[1]

[1]*Stanley H. Appel Department of Neurology, Houston Methodist Research Institute, Houston, TX, US*
[2]*Department of Psychiatry, University of Pittsburgh, Pittsburgh, PA, US*
[3]*Sant Pau Memory Unit, Department of Neurology, Hospital de la Santa Creu i Sant Pau, Barcelona, Spain*
[4]*Memory and Aging Center, University of California San Francisco, San Francisco, CA, US*
[5]*Department of Radiology, Mayo Clinic, Rochester, MN, US*
[6]*Department of Psychiatry and Human Behavior, Brown University, Providence, RI, US*
[7]*Department of Radiology, Washington University in St. Louis, St. Louis, MO, US*
[8]*Translational Neuroimaging Laboratory, McGill University Research Centre for Studies in Aging, Douglas Research Institute, Montréal, QC, Canada*
[9]*Lawrence Berkeley National Laboratory, Berkeley, CA, US*
[10]*Department of Neurology, University of Pittsburgh, Pittsburgh, PA, US*

Background: Assessing how different tau PET tracers capture longitudinal changes following amyloid-targeting therapy is essential for understanding its downstream effects and improving imaging strategies in Alzheimer's disease research. This study compared [^{18}F]MK6240 and [^{18}F]FTP in detecting tau changes before and after administration of lecanemab, an anti-amyloid monoclonal antibody. Amyloid burden was concomitantly evaluated with [^{11}C]PIB to confirm treatment response, and exploratory analyses examined potential sex-related differences.

Methods: Eleven participants from the HEAD study (six males, 74.5 ± 9.3 years; five females, 71.6 ± 11.6 years) underwent baseline MRI, [^{11}C]PIB, [^{18}F]MK6240, and [^{18}F]FTP scans, followed by repeat imaging approximately 18 months later. Lecanemab therapy was initiated after baseline imaging. PET data were co-registered to the nearest-in-time MRI and corrected for partial volume effects. Regional standardized uptake value ratios (SUVRs) were calculated using cerebellar gray matter as the reference region across six PET-based Braak stages (Braak I–II combined). Longitudinal SUVR changes were analyzed for each tracer and compared across tracers and sexes.

Results: Lecanemab treatment produced significant [^{11}C]PIB SUVR reductions across all PET-based Braak stages ($p<0.01$), confirming effective amyloid clearance. Men had larger mean reductions than women, particularly in Braak III–V. Both tau tracers demonstrated significant longitudinal SUVR increases. [^{18}F]MK6240 showed significant tau accumulation in Braak III–VI ($p<0.05$), while [^{18}F]FTP increases were significant in Braak III–V ($p<0.05$). Female participants had greater mean SUVR increases. Across PET-based Braak stages, [^{18}F]MK6240 consistently detected larger SUVR changes than [^{18}F]FTP, suggesting higher sensitivity to tau progression.

Conclusion: Despite effective amyloid clearance with lecanemab, tau pathology continued to progress over time. [^{18}F]MK6240 demonstrated greater sensitivity than [^{18}F]FTP in detecting longitudinal tau changes, supporting its use for monitoring downstream effects of anti-amyloid therapies.

Keywords: Alzheimer's disease, [^{18}F]MK6240, [^{18}F]FTP, Lecanemab Therapy, sex differences

28 Development of a highly sensitive and automated immunoassay for Brain-Derived pTau-217: Analytical performance in human plasma samples

Xiao-Jun Ma[1], Li Wang[1], Adheesha Danthanarayana[1], Sean Kim[1], HaYeun Ji[1], Niyati Jhaveri[1], Bingqing Zhang[1], Xiaolei Qiu[1], Sasi Mudumba[1], Yuling Luo[1]

[1]*Alamar Biosciences, Fremont, CA, US*

Background: Blood-based biomarkers are increasingly recognized as valuable tools for early detection and longitudinal monitoring of Alzheimer's Disease (AD). Among these, plasma pTau-217 demonstrates high discriminative accuracy for amyloid-PET positivity. However, most circulating pTau-217 originates from peripheral sources, with only ~20% derived from the brain. This highlights the need for a highly sensitive and specific assay to detect brain-derived (BD) pTau-217, a brain-specific isoform that more accurately reflects AD neuropathology.

Methods: We previously developed a novel proximity ligation-based NULISA technology, which integrates background suppression steps to enable attomolar sensitivity and automated protein detection across diverse biofluids[1]. Building on our prior development of a 120-plex NULISAseq CNS Disease Panel that enables relative quantification of BD-phosphorylated Tau isoforms along with other markers related to neurodegeneration and inflammation, we have developed a singleplex NULISA assay for absolute quantification of BD-pTau217 with high specificity and sensitivity. The assay was rigorously evaluated for key analytical parameters including dilution linearity, spike recovery, parallelism, accuracy, precision, reproducibility, and specificity.

Results: Our novel BD-pTau217 singleplex assay demonstrated strong analytical performance, with inter-plate CVs consistently below 20% across multiple operators, ARGO HT instruments, and days. The assay features a broad dynamic range (0.4–14,655 pg/mL) and a limit of detection of 0.08 pg/mL. In plasma samples from both healthy individuals and AD patients, overall BD-pTau217 detectability was over 95%. Characterization studies such as dilutional linearity, parallelism, and spike recovery confirmed robust assay performance. Additionally, the BD-pTau217 antibody exhibited minimal cross-reactivity with other Tau species, including total Tau, pTau181, pTau205, and pTau212, confirming its high specificity.

Conclusions: The NULISA BD-pTau217 singleplex assay represents a significant advance in blood-based biomarkers for AD, providing brain specificity without the need for cerebrospinal fluid.

1Feng, W., Beer, J.C., Hao, Q. et al. Nat Commun 14, 7238 (2023).

Keywords: NULISA, BD pTau-217, Alzheimer's Disease, Blood-based biomarkers, early disease detection

29 Network-based mechanistic modeling of Alzheimer's disease for evaluating diverse therapeutic mechanisms of action

Dustin Wooten[1], Edwin Stage[1], Norman Mazer[2], Matthew Townsend[1], Robert Comley[1], Qi Guo[1]

[1]*AbbVie Inc., North Chicago, IL, US*
[2]*NAM Consulting, Baselland, Switzerland*

Introduction: To better understand the impact of tau interventions with drugs that act through various mechanisms (stopping production, halting spread, or active removal) in Alzheimer's disease (AD), we developed a novel mechanistic modeling approach inspired by the Q-ATN model (Mazer et al., 2023). Leveraging a structural brain network to simulate tau propagation, this approach facilitates future integration of various tau-directed therapies. Here, we present the natural history trajectory of AD as predicted by this model.

Methods: The network-based model used differential equations relating amyloid PET (Centiloid), tau (oligomers), and neurofibrillary tangles (NFT) to Clinical Dementia Rating-Sum of Boxes (CDR-SB) scores. Tau seeding, spreading, and accumulation were simulated within an MRI-based connectome, with replication at nodes and inter-node spread determined by connection strength (Putra et al., 2021). Increases in amyloid PET triggered tau seeding in the entorhinal nodes and increased the tau replication rate (Schäfer et al., 2021), with NFT formation occurring as a function of tau burden. Cognitive decline was modeled as a function of NFT and amyloid pathology. Model parameters were calibrated using available data from natural history studies and clinical trials.

Results: Increasing amyloid and associated tau seeding led to tau replication and propagation across the network (Figure 1). Simulated NFT trajectories reproduced the expected Braak staging, with sequential tau accumulation from Braak I to Braak VI regions. Pathological progression was reflected in the model by concurrent rises in amyloid and tau and their interaction, all of which were associated with increases in CDR-SB.

Summary: This work, inspired by the Q-ATN framework, introduces a mechanistic modeling approach to AD that captures the spatiotemporal complexity of tau pathology to support the evaluation of amyloid and tau-targeted therapies with diverse MoAs. Ongoing work will focus on further model validation and refinement as additional data and clinical trial results become available.

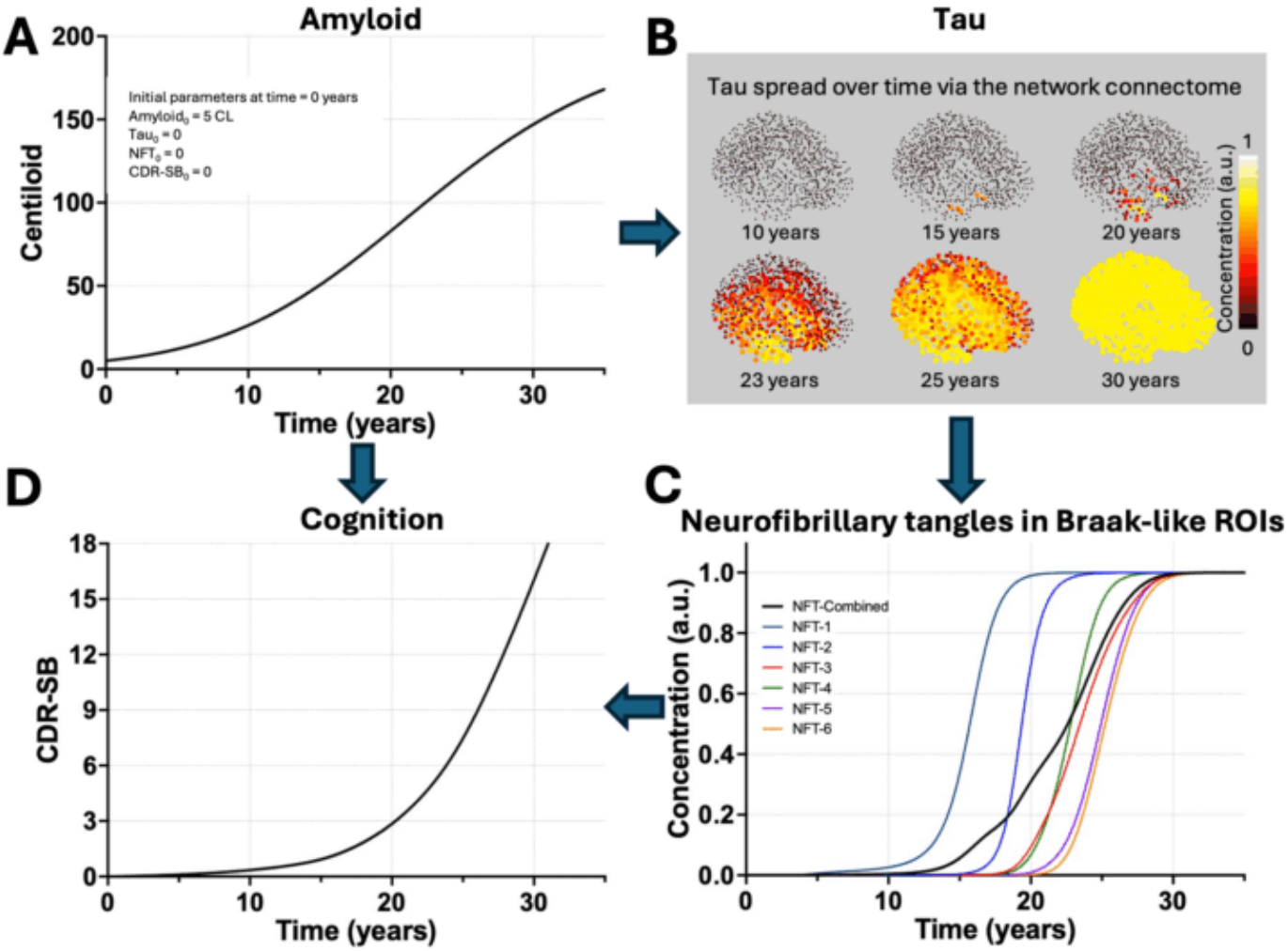


Figure 1. Model-simulated Alzheimer's disease progression: (A) initial amyloid Centiloid accumulation, (B) tau propagation across the brain network over time, (C) subsequent neurofibrillary tangle (NFT) buildup in Braak-like regions (arbitrary units), and (D) resulting cognitive decline in Clinical Dementia Rating-Sum of Boxes (CDR-SB). Arrows indicate the modeled sequential influence of pathology leading to cognitive impairment.

Keywords: mathematical model, amyloid, tau, cognition

30 Neuroimaging compendium of microglia, amyloid, tau, and neurodegeneration across clinical variants of Alzheimer's disease

Hannah Houlihan[1], Diana Guzman[1], Anna Smith[1], Thairi Sanchez[1], William Kreisl[1], Stephanie Cosentino[1], James Noble[1], Patrick Lao[1]

[1]*Columbia University Medical Center, New York, NY, US*

Introduction: Alzheimer's disease (AD) and its clinical variants have characteristic spatial and temporal progression patterns of amyloid and tau driving symptomatology, but the distribution of microglia density, as measured by 18kDa translocator protein (TSPO) PET, is unknown.

Methods: Baseline TSPO (ER176), amyloid (Florbetaben), and tau (MK6240) PET as well as T1 MRI from the Longitudinal Imaging of Microglial Activation in Different Clinical Variants of Alzheimer's Disease study were quantified for this analysis. Through our center's consensus conferences, participants were categorized as cognitively unimpaired (n=20) or as having symptomatic Alzheimer's disease or related dementias, including mild cognitive impairment (MCI, n=8), amnestic multidomain dementia (AD, n=7), posterior cortical atrophy (PCA, n=5), logopenic primary progressive aphasia (lvPPA, n=1), Limbic-predominant age-related TDP-43 encephalopathy (LATE-NC, n=1), and frontotemporal dementia (FTD, n=1). Imaging outcomes were standardized against cognitively unimpaired older adults, adjusting for age, sex, body mass index, APOE4 status, TSPO genotype, and intracranial total volume, across the brain and placed along a pseudo-longitudinal timeline using disease duration.

Results: Microglia density generally colocalized with tau in amyloid-positive individuals (Figure 1) and with neurodegeneration in amyloid-negative individuals (Figure 2). Visually, there were cases with elevated TSPO without neurodegeneration or elevated neurodegeneration without TSPO. An amyloid-positive individual with early onset AD (<65 years old) had aggressive tau and TSPO. Individuals with MCI for a duration of longer than 10 years had relatively low tau and TSPO, potentially informing their stable, non-progressive diagnosis.

Discussion: The magnitude, location, and timing of elevated microglia density relative to amyloid, tau, and neurodegeneration is specific to different clinical subtypes of AD. TSPO PET may serve similar clinical utility as FDG PET, but with the potential to inform therapeutic approaches that recruit inflammatory cells for the clearance of pathology.

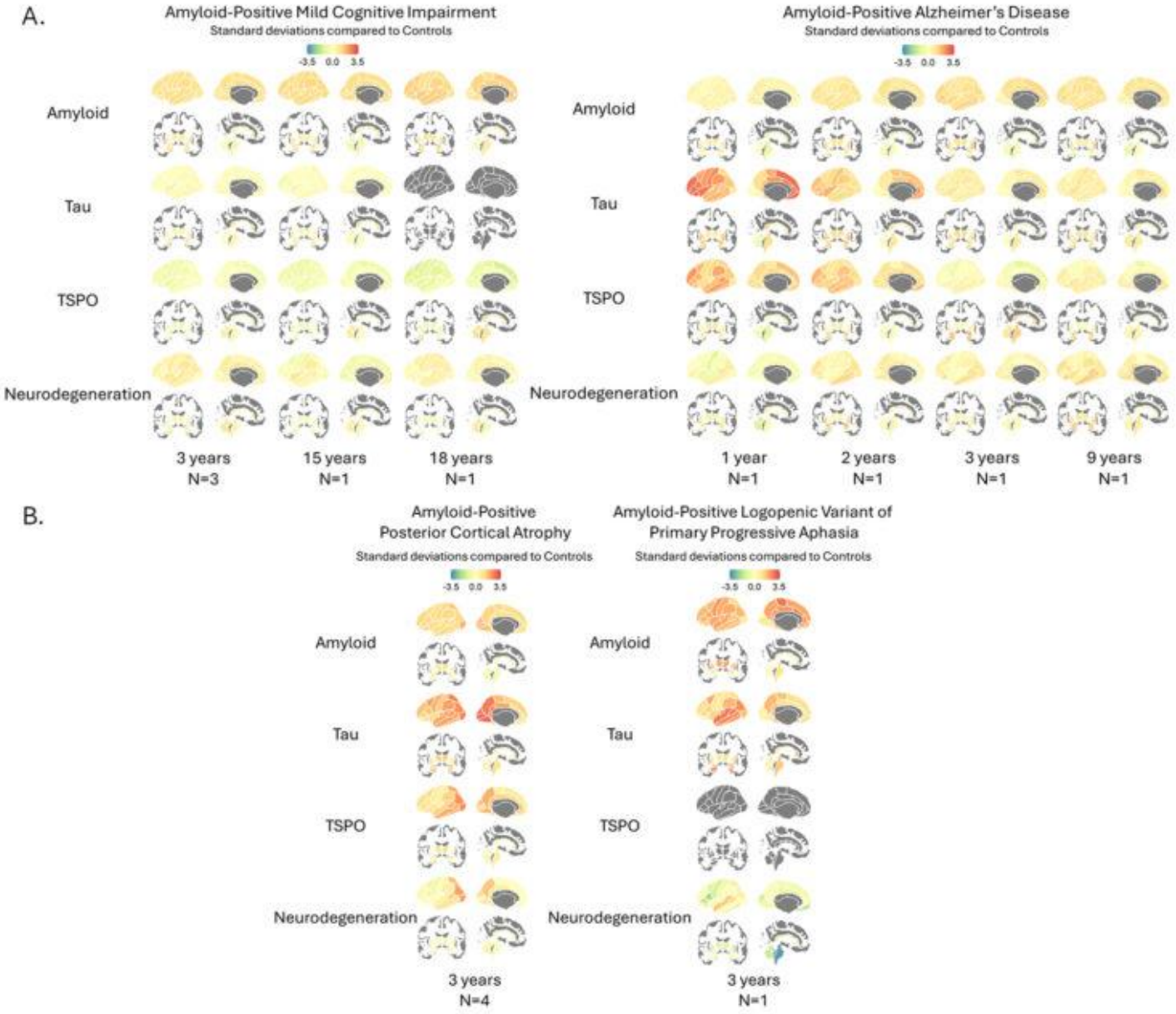


Figure 1. Regional amyloid, tau, TSPO, and Neurodegeneration for amyloid-positive individuals with (A) mild cognitive impairment or typical Alzheimer's disease or (B) clinical variants of AD. Note, volume was inverted so hotter colors represent more neurodegeneration and grayed out brains do not have available imaging data.

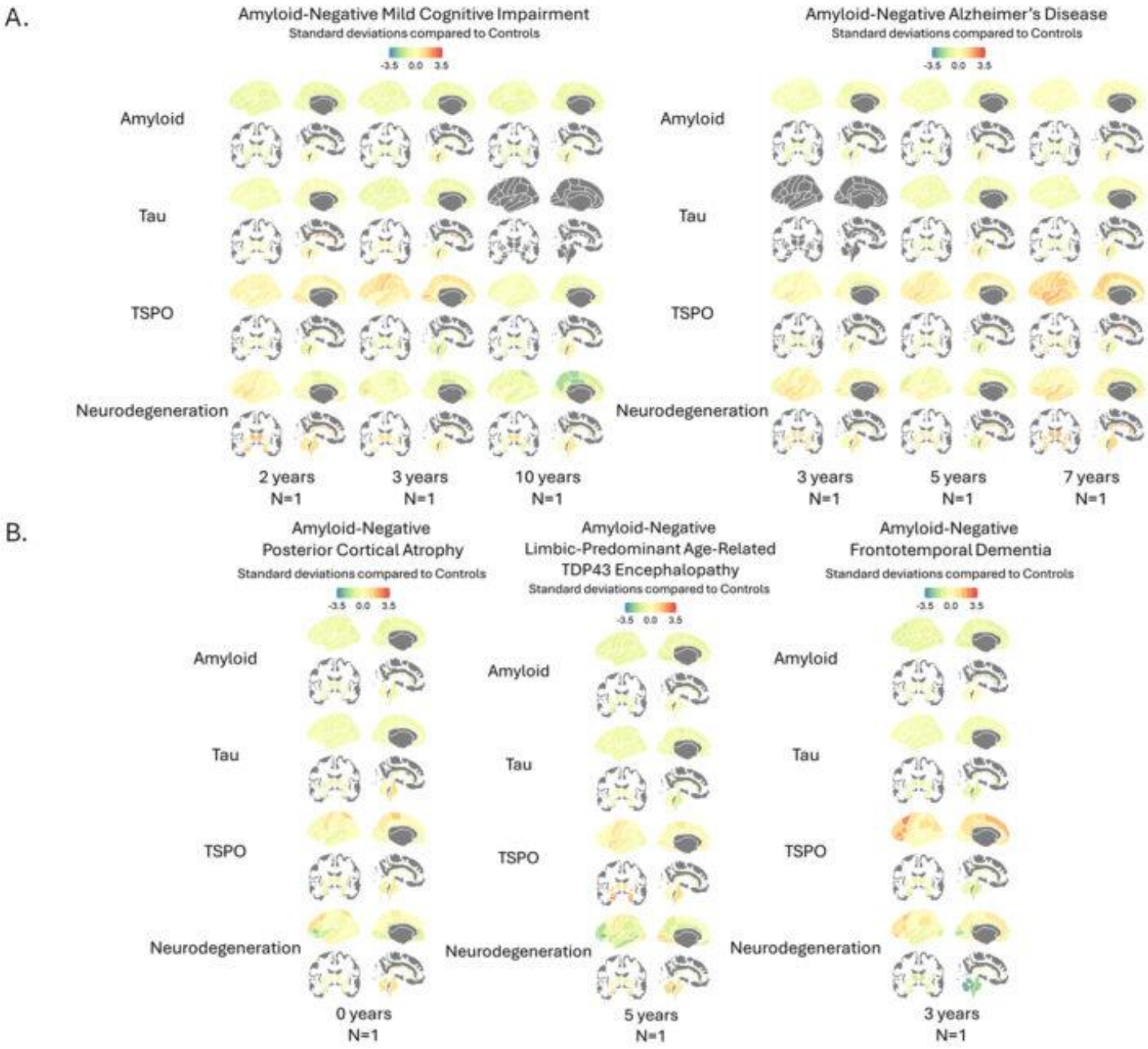


Figure 2. Regional amyloid, tau, TSPO, and Neurodegeneration for amyloid-negative individuals with (A) mild cognitive impairment (MCI) or typical Alzheimer's disease (AD) or (B) clinical variants of AD. Note, volume was inverted so hotter colors represent more neurodegeneration and grayed out brains do not have available imaging data.

Keywords: differential diagnosis, TSPO, amyloid, tau, neurodegeneration

31 Predictors of longitudinal atrophy across NIA-AA biological PET stages

Corrina Fonseca[1], Samira Maboudian[1], Yishu Chao[1], William Jagust[1], Theresa Harrison[1]

[1]*Department of Neuroscience, University of California Berkeley, Berkeley, CA, US*

Background: Previous studies suggest tau is a stronger predictor of atrophy than baseline age, Aβ, and structure in AD. It is unclear whether this extends across the NIA-AA biological PET stages in cognitively impaired (CI) and unimpaired (CU) adults.

Methods: 6,293 longitudinal MRI scans in 2,252 participants with baseline Aβ-PET (FBB, FBP, PIB) and tau-PET (FTP, MK6240, PI2620) were pooled from 7 studies (Table 1). Whole-brain Jacobian slope maps were generated to measure atrophy. A CU-vs-CI two-sample t-test was used to identify regions more vulnerable to degeneration. We then assessed bivariate relationships between atrophy in these regions and baseline age, Aβ, MTL and neocortical temporal (neoT) tau z-scores, and volume. Participants were grouped by clinical diagnosis and NIA-AA biological PET stages. Significant bivariate predictors of atrophy within each group were included in multiple regression models.

Results: CI showed faster temporoparietal and frontal atrophy than CU participants (Figure 1A). Rates of atrophy increased with stage in CI and CU (Figure 1B). In non-AD participants, faster atrophy was linked to older age and lower baseline volume in CI and CU and higher MTL tau in CI (Figure 2). In stage A, greater age and Aβ in CU and MTL tau in CI were associated with faster atrophy. Aβ was associated with faster atrophy in stage B CU participants. In stage C+D, faster atrophy correlated with younger age in CI but neoT tau was the strongest predictor in both CU and CI. Multiple regressions showed volume was the strongest predictor in non/early stages and neoT tau in later stages.

Conclusions: Our results suggest that while neocortical tau is the strongest predictor of atrophy at advanced biological stages (when tau is suprathreshold), age, Aβ, MTL tau, and baseline volume play important roles in predicting atrophy in CU and CI participants with subthreshold AD pathology.

Table 1. Participant characteristics

	CU	CI	Full Sample
N	1710	542	2252
Age mean (SD)	69.69 (6.95)	71.23 (8.80)	70.06 (7.46)
Education (SD)	15.89 (2.79)	15.95 (2.92)	15.9 (2.82)
% Female	61.5%	46.2%	57.8%
% APOEε4+	28.4%	42.9%	31.4%
% Aβ+	28.5%	56.3%	35.2%
Aβ CL mean (SD)	17.56 (28.57)	46.99 (51.67)	24.64 (37.68)
% Cognitively Unimpaired	100.0%	0.0%	75.9%
% CDR 0	87.1%	6.5%	67.8%
Baseline CDR global mean (SD)	0.07 (0.18)	0.59 (0.36)	0.19 (0.32)
Baseline MMSE mean (SD)	28.81 (1.46)	26.36 (3.56)	28.28 (2.33)
3T MRI baseline to follow-up years mean (SD)	2.64 (1.42)	2.41 (1.48)	2.58 (1.44)
Total 3T MRI time points mean (SD)	2.70 (0.72)	2.65 (0.98)	2.69 (0.79)
Total 2 MRI TP (n)	42% (715)	60% (323)	46% (1038)
Total 3+ MRI TP (n)	58% (995)	40% (219)	54% (1214)
% Non-AD Stage (n)	69% (1180)	41% (223)	62% (1403)
% Stage A (n)	22% (382)	18% (97)	21% (479)
% Stages B (n)	4% (60)	5% (29)	4% (89)
% Stages C + D (n)	2% (38)	30% (164)	9% (193)
% Others (A-T+ or A+Tmtl-Tneot+) (n)	3% (50)	5% (29)	4% (79)
% Included Studies (n)			
ADNI	20% (341)	51% (278)	27% (619)
BACS	4% (65)	--	3% (65)
HABS	7% (112)	--	5% (112)
HABS-HD	17% (288)	17% (91)	17% (379)
U.S. POINTER	48% (826)	--	37% (826)
SCAN	5% (78)	15% (82)	7% (160)
UCSF ADRC	--	17% (90)	4% (90)

Values represent mean with standard deviation (SD) in parentheses for continuous variables. Categorical variables are shown in percentage with count (n) in parentheses. *APOEε4: apolipoprotein ε4 allele; CL: centiloids; CDR: Clinical Dementia Rating; MMSE: Mini-Mental State Examination; ADNI: Alzheimer's Disease Neuroimaging Initiative; BACS: Berkeley Aging Cohort Study; HABS: Harvard Aging Brain Study; HABS-HD: The Health and Aging Brain Study-Health Disparities; U.S. POINTER: U.S. Study to Protect Brain Health Through Lifestyle Intervention to Reduce Risk; SCAN: Standardized Centralized Alzheimer's & Related Dementias Neuroimaging; UCSF ADRC: University of California San Francisco Alzheimer's Disease Research Center*

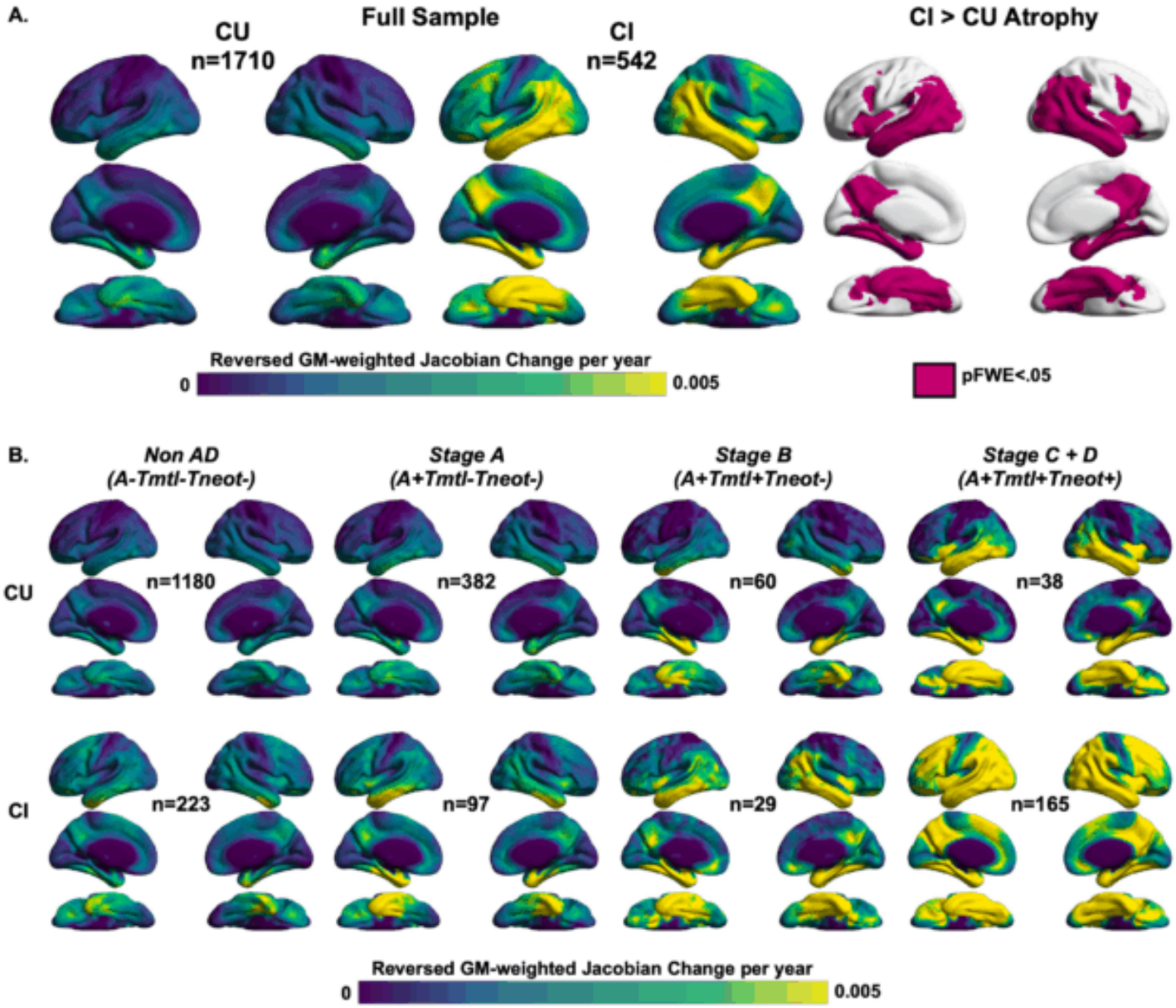


Figure 1 Average group-level voxel-wise atrophy slope maps by cognitive status and NIA-AA stage
(A) Voxel-wise maps show average rate of reversed GM-weighted Jacobian change per year in full sample by cognitive status. Results from a whole-brain slope two-sample t-test (CU-vs-CI) adjusted for TIV and cohort are shown in pink (CI>CU atrophy) which was thresholded at pFWE<.05, binarized, and used as an atrophy-vulnerable ROI in subsequent analyses. Sample sizes (n) within each cognitive status group are also shown. **(B)** Voxel-wise atrophy maps by cognitive status and NIA-AA Biological PET stage are shown. Aβ positivity was determined based on tracer-specific SUVR or DVR cutoffs (PIB DVR [BACS] >1.065; PIB DVR [HABS] >1.20; PIB SUVR >1.21; FBB SUVR >1.08; FBP SUVR >1.11). MTL and neoT positivity were determined using gaussian mixture modelling within region and tracer across a multi-cohort sample (FTP SUVR >1.37 & 1.38; MK6240 SUVR >1.14 & 1.32; PI2620 SUVR >1.39 & 1.29, respectively). *CU: cognitively unimpaired; CI: cognitively impaired; GM: gray matter; FWE: family-wise error; A-/+: Aβ negative/positive; Tmtl-/+: medial temporal lobe tau negative/positive; neoT-/+: neocortical temporal tau negative/positive; TIV: total intracranial volume; ROI: region of interest.*

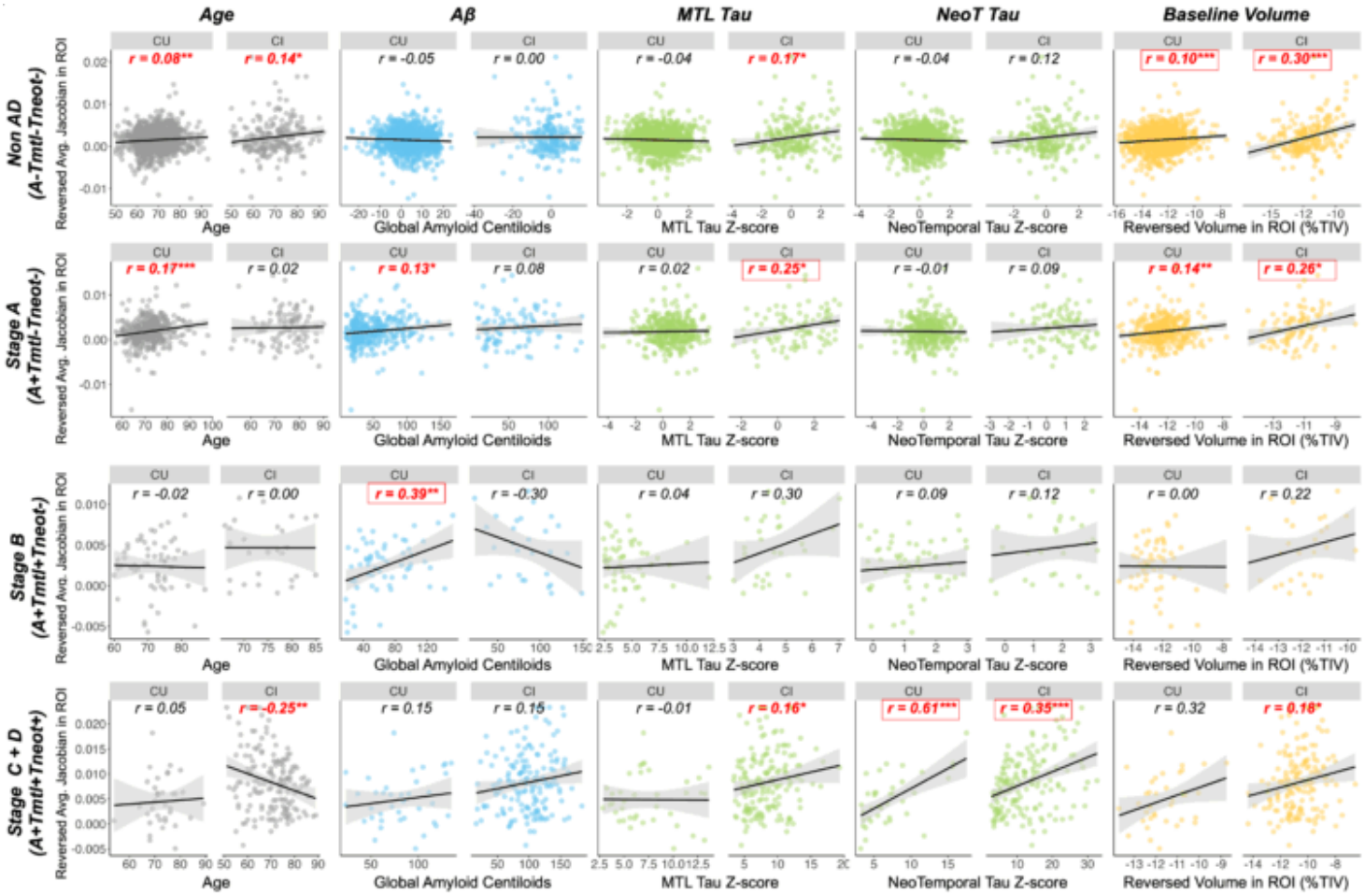


Figure 2 Relationships between atrophy and baseline measures of age, Aβ, tau and volume. Scatter plots show bivariate relationships between reversed GM-weighted Jacobian averaged within the atrophy-vulnerable ROI (Figure 1A) and baseline age, Aβ, MTL and neoT tau, and volume by cognitive status and NIA-AA Biological PET stage. Significant bivariate correlation coefficients (r) are shown in red and non-significant in black. Correlation coefficients for variables that remain significant in within group and stage multiple regression analyses including all significant predictors, sex, education, and APOEε4 status are indicated with a red box. *p<.05 **p<.01 ***p<.001. CU: cognitively unimpaired; CI: cognitively impaired; GM: gray matter; TIV: total intracranial volume; MTL: medial temporal lobe NeoT: neocortical temporal.

Keywords: longitudinal atrophy, NIA-AA PET stages, cognitively unimpaired, tau-PET, Aβ-PET

32 Effect of uptake time on [18F]-flutemetamol visual interpretation and Centiloid quantification

Ariane Bollack[1,2], Christopher Buckley[1], Adam J Schwarz[1], Mark Battle[1], Ruben Smith[3,4], Erik Stromrud[3,4], Oskar Hansson[3,5], Sebastian Palmqvist[3,4], Niklas Matttsson-Carlgren[3,4], Renaud La Joie[6], Gill Farrar[1]

[1]*GE HealthCare, Chalfont St Giles, UK*
[2]*Department of Medical Physics and Biomedical Engineering,University College London, London, UK*
[3]*Clinical Memory Research Unit, Department of Clinical Sciences Malmö, Faculty of Medicine, Lund University, Malmö, Sweden*
[4]*Memory Clinic, Skåne University Hospital, Malmö, Sweden*
[5]*Eli Lilly and Company, Indianapolis, IN, US*
[6]*Memory and Aging Center, Department of Neurology, University of California San Francisco, San Francisco, CA, US*

Quantification was recently added to the prescribing information of amyloid-PET tracers allowing its use to support visual read. Centiloid scaling is increasingly important for decision-making, but differences in scanning parameters could influence image interpretation. We examined the impact of radiotracer uptake time on the clinical interpretability of [^{18}F]flutemetamol scans, using visual read and quantification.

We analyzed two datasets: (1) real-world static scans from the IDEAS study (*N*=477) acquired during the recommended timeframe (start 60-120min p.i.), and (2) 'dynamic' data from BioFINDER-2 and [^{18}F]-flutemetamol phase-1 studies, reconstructed into pseudo-static 10/20min frames in the same individual at varying start times (60-135min p.i., *N*=35). IDEAS visual reads were performed by local and expert readers. Centiloids were calculated using rPOP and linear models were used to assess the impact of acquisition start time and duration on quantification. Measurement variability was compared to test-retest repeatability.

In IDEAS, local and expert read confidence was consistent across acquisition start times (<90min/90-110min/>110min). Lower grey-white matter contrast was exhibited in some images, mainly early acquisitions and amyloid-negative scans (70% acquired <80min p.i., 95% with CL<30), which could reduce reader confidence. In both IDEAS and the 'dynamic' data (Figures-1-2), Centiloid values increased with later acquisition times, especially in amyloid-positive scans (4CL/10min for CL>30, Figure-1C). In the intermediate range (10–30CL), differences between 60- and 90-min start times were <6CL, within test-retest repeatability. Group-level adjustment factors can partially mitigate timing effects, but substantial inter-individual variability remains. Scan duration did not significantly affect interpretation.

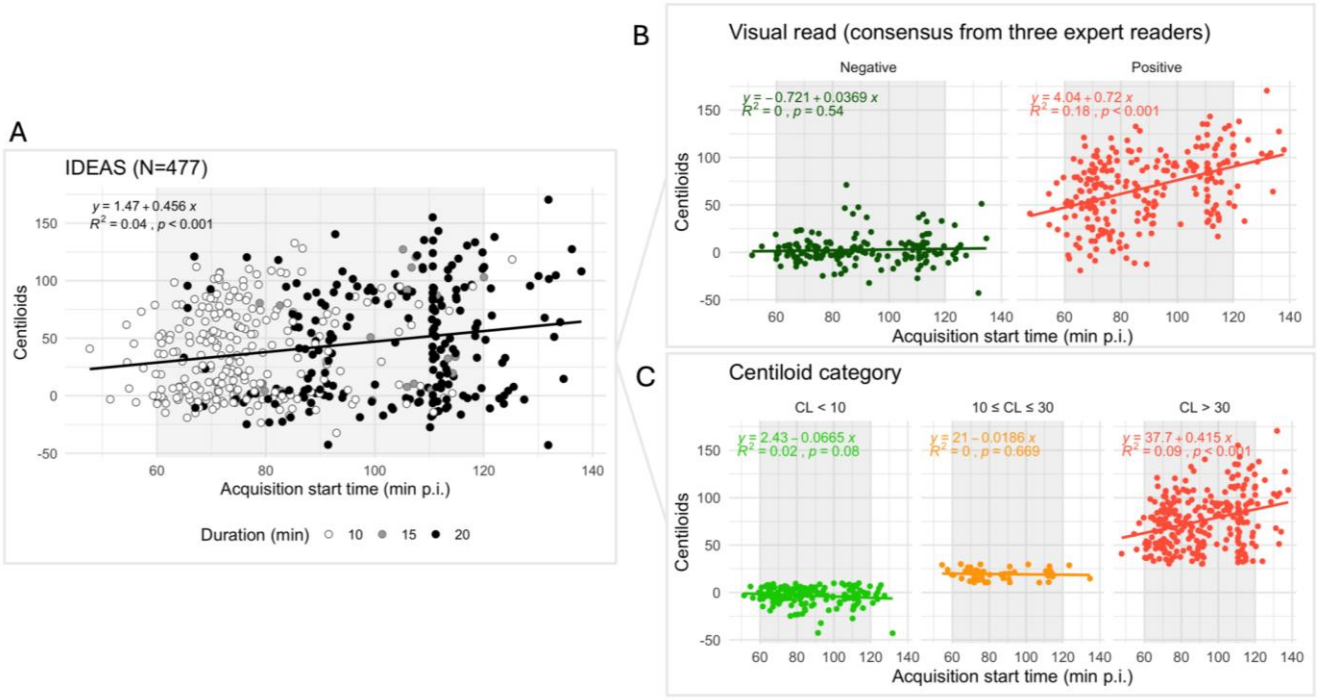


Figure-1 (**A**) Centiloid values in IDEAS across acquisition start time p.i., fitted with a linear model (**B**) Centiloid values split by visual read results from a consensus of three expert readers (**C**) Centiloid values across Centiloid categories <10, 10≤CL ≤ 30, CL>30. The grey area represents the start times recommended in the prescribing information (60 to 120 min p.i.). CL = Centiloid, p.i. = post injection

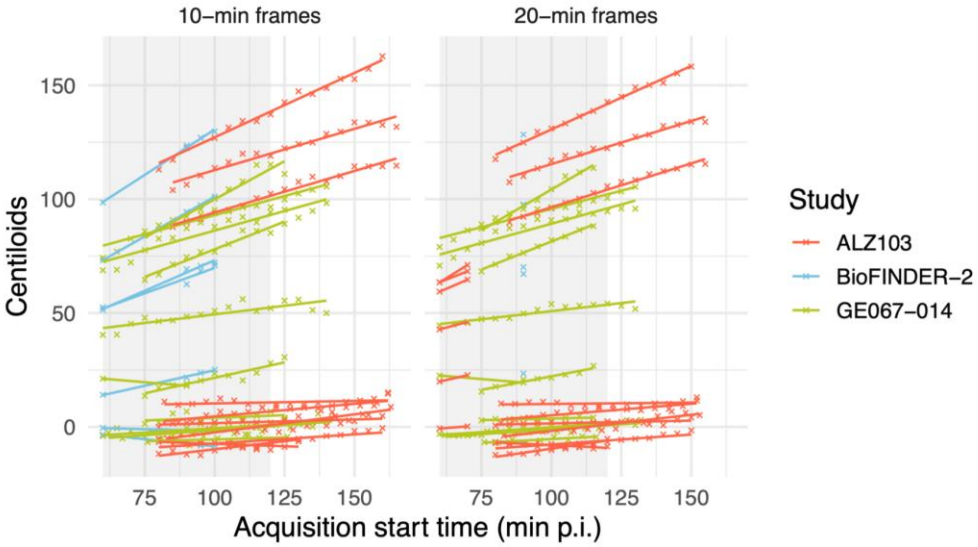


Figure-2 Centiloid values across acquisition start time calculated in the 'dynamic' data (scans from BioFINDER-2 and two [^{18}F]-Flutemetamol phase-1 studies). Centiloids values are modelled linearly for each individual, using 10- and 20-min frames (where available).

Combined visual and quantitative assessment of [^{18}F]-Flutemetamol PET scans across the recommended timeframe supports reliable clinical interpretation. While quantification is increasingly used, visual read remains essential. Uptake time affects Centiloid most in high amyloid burden cases, but a universal correction factor is not currently justified due to high inter-individual variability. Consistency in acquisition parameters is recommended for repeat scans.

Keywords: Centiloid, quantification, radiotracer uptake time, flutemetamol

33 Episodic memory decline and tau biomarkers progress earlier along the amyloid timeline in Down syndrome compared to neurotypical adults

Matt Zammit[1], Hailey Bruzzone[1], Jacob Morse[1], Elizabeth Batchelar[1], Brecca Bettcher[1], Max McLachlan[1], Andrew McVea[1], Finnuella Carey[1], Dana Tudorascu[2], Sigan Hartley[1], Lindsay Clark[1], Beau Ances[3], Jessica Caldwell[1], Sterling Johnson[1], Benjamin Handen[2], Elizabeth Head[4], Mark Mapstone[4], Bradley Christian[1], ABC-DS Investigators[1,2,3,4], Tobey Betthauser[1]

[1]*University of Wisconsin, Madison, WI, US*
[2]*University of Pittsburgh, Pittsburgh, PA, US*
[3]*Washington University in St Louis, St Louis, MO, US*
[4]*University of California - Irvine, Irvine, CA, US*

Background: Episodic memory is an early indicator of cognitive decline in Down syndrome (DS). Episodic memory decline relative to imaging biomarkers can be practical in the design of clinical interventions for DSAD. Here, we compare cognitive decline, pTau271, and amyloid and tau PET between DS (ABC-DS) and neurotypical (NT; WRAP) cohorts.

Methods: Episodic memory was assessed in 250 DS and 171 NT participants (DS:Modified Cued Recall Test; NT:RAVLT Long-Delay Free Recall) and Z-scored within-cohort (Table1). A+ time was estimated using a sampled iterative local approximation (SILA) with an A+ threshold of ≥18 Centiloids. Linear mixed-effects models tested differences in episodic memory trajectories over A+ time, adjusting for baseline age, sex, APOE-ε4 status, cohort, and number of cognitive evaluations, with participant-level random intercepts and slopes. Positivity rates were modeled for pTau217 and tau PET with respect to A+ time. In a DS subset (n = 244) with intellectual disability (ID) measures (mild/moderate/severe), an additional model evaluated the effect of ID on episodic memory with the other covariates (Fig1).

Results: Memory declined over A+ time and the DS group displayed earlier pTau217+ and tau PET+ onset (Fig2). The cohort×A+ interaction indicated slower decline in the NT group ($p < 0.001$). Older baseline age and male sex associated with lower memory scores at baseline across both groups ($p = 0.003$). More cognitive visits correlated with better performance ($p < 0.001$). ID did not significantly affect memory decline within DS but did indicate overall lower memory at baseline for both the moderate ($p = 0.04$) and severe ($p < 0.001$) ID groups.

Conclusion: With earlier onset of pTau217+ and tau PET+, episodic memory declined faster in DS following A+, independent of prior intellectual disability. This highlights that episodic memory decline can serve as an outcome measure in DSAD clinical trials aimed at early intervention.

Table 1. Participant demographics categorized by cohort.

	DS (N=250)	NT (N=171)
Baseline Age		
Mean (SD)	42.6 (9.55)	62.5 (6.19)
Median [Min, Max]	42.0 [25.0, 66.0]	62.6 [48.9, 74.7]
Sex		
Female	106 (42.4%)	110 (64.3%)
Male	144 (57.6%)	61 (35.7%)
APOE-e4+		
e4-	192 (76.8%)	90 (52.6%)
e4+	55 (22.0%)	81 (47.4%)
Missing	3 (1.2%)	0 (0%)
Premorbid ID		
1	134 (53.6%)	0 (0%)
2	87 (34.8%)	0 (0%)
3	26 (10.4%)	0 (0%)
# Cognitive Visits		
Mean (SD)	1.52 (0.539)	4.37 (1.22)
Median [Min, Max]	2.00 [1.00, 3.00]	4.00 [1.00, 7.00]
Amyloid PET Tracer		
FBP	80 (32.0%)	0 (0%)
PiB	170 (68.0%)	171 (100%)
CL at Baseline		
Mean (SD)	27.1 (36.2)	20.6 (31.4)
Median [Min, Max]	8.80 [-10.1, 180]	5.89 [-10.9, 129]
Estimated A+ Age		
Mean (SD)	45.0 (7.20)	55.4 (8.94)
Median [Min, Max]	44.8 [24.8, 82.8]	54.3 [36.8, 77.3]
pTau217 (pg/mL) at Baseline		
Mean (SD)	0.527 (0.350)	0.300 (0.165)
Median [Min, Max]	0.413 [0.109, 2.21]	0.250 [0.125, 1.45]
Tau PET Tracer		
FTP	250 (100%)	0 (0%)
MK-6240	0 (0%)	171 (100%)
Mesial Temporal Tau PET SUVR at Baseline		
Mean (SD)	1.34 (0.334)	1.11 (0.333)
Median [Min, Max]	1.23 [0.915, 2.54]	1.01 [0.715, 2.68]
Universal CenTauR Tau PET SUVR at Baseline		
Mean (SD)	1.33 (0.441)	1.12 (0.325)
Median [Min, Max]	1.17 [0.942, 3.71]	1.05 [0.759, 3.20]
Baseline Episodic Memory Score		
Mean (SD)	29.0 (9.50)	10.1 (3.16)
Median [Min, Max]	33.0 [0, 36.0]	10.0 [0, 15.0]

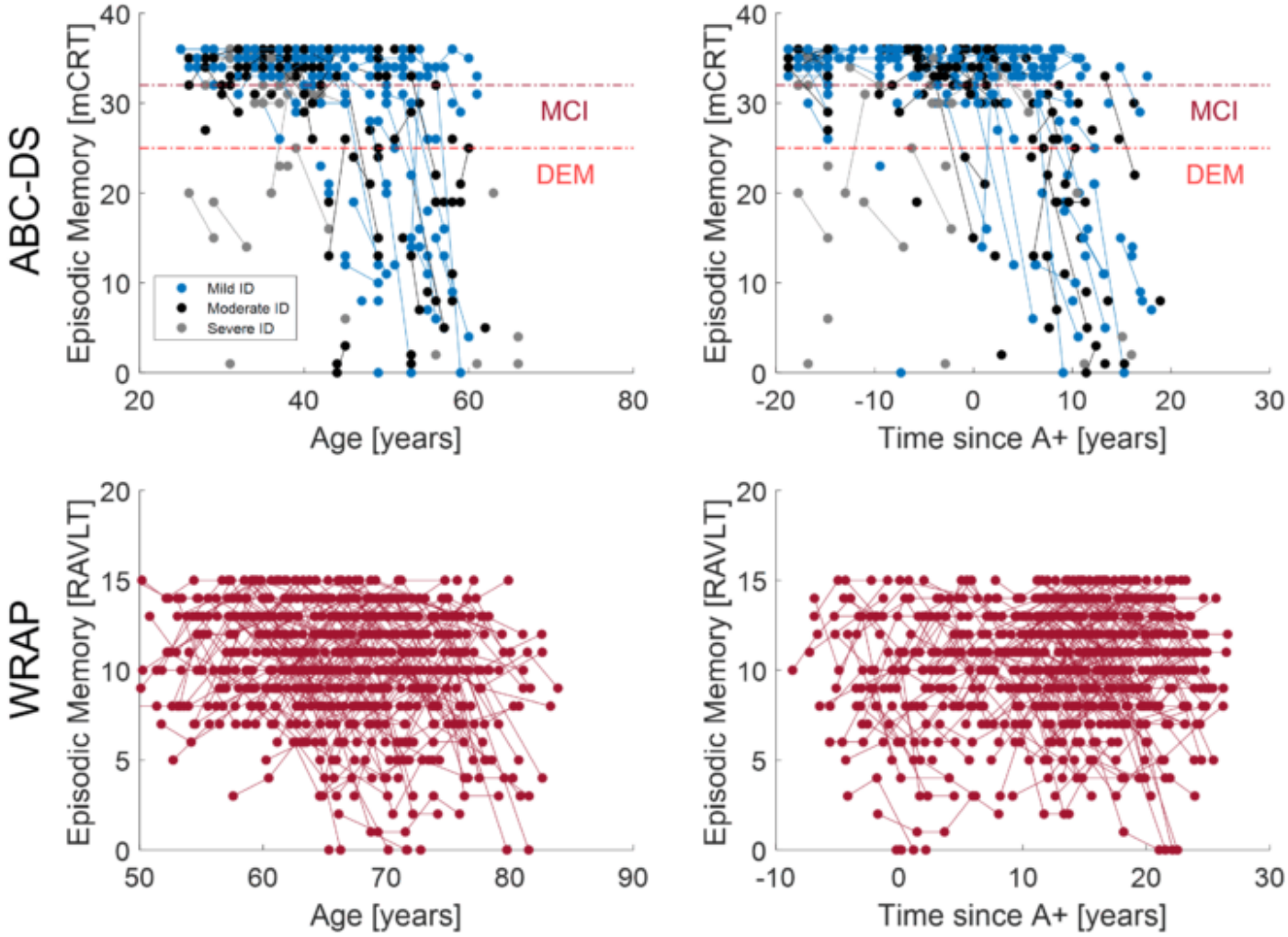


Figure 1. Episodic memory scores in ABC-DS and WRAP with respect to age (left) and A+ time (right). Participants with DS are categorized by intellectual disability level (ID). Dashed lines represent established cutoffs for MCI and dementia for the modified cued recall test for individuals with mild and moderate ID.

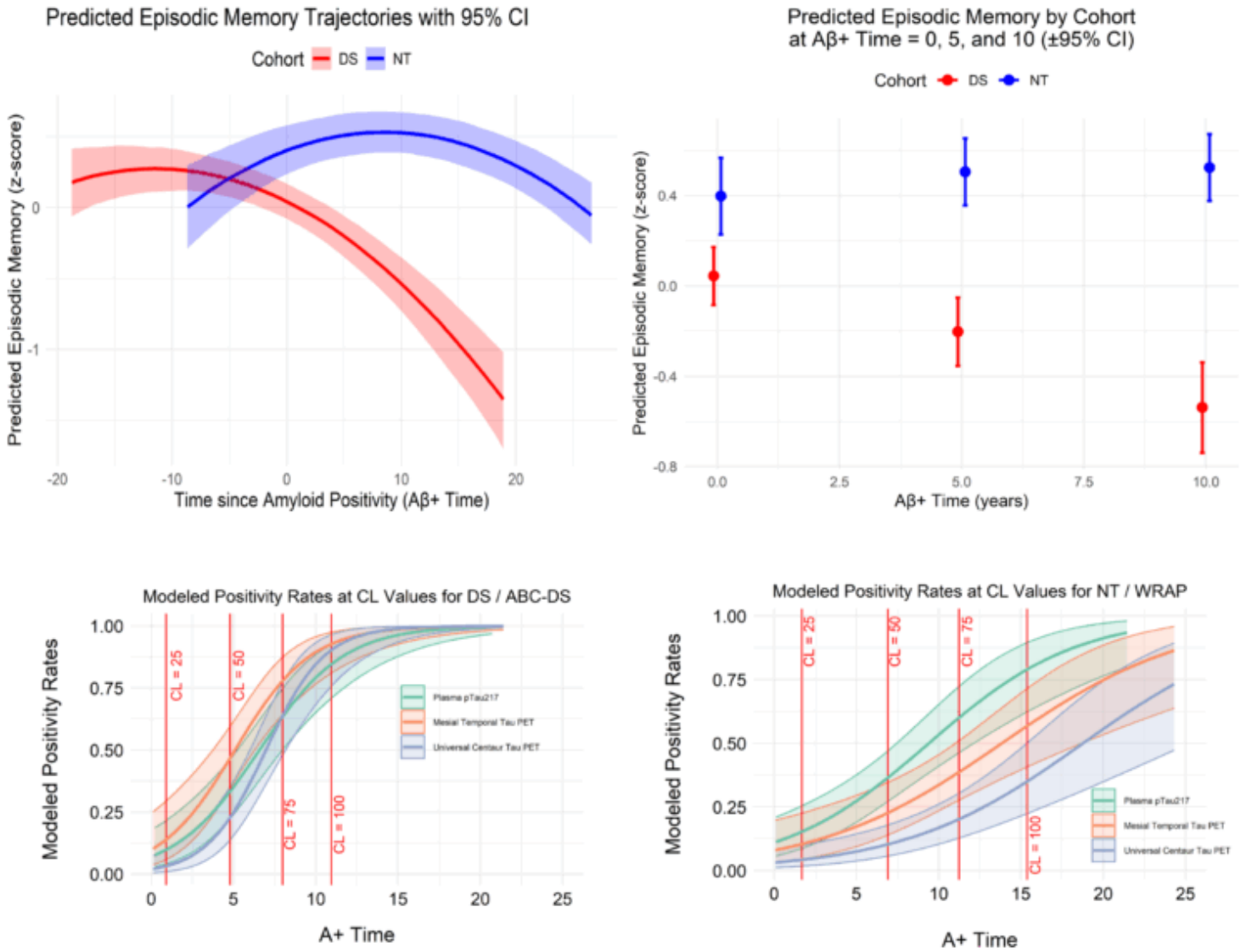


Figure 2. Predicted episodic memory trajectories with 95% CIs with respect to A+ time from LMEs (top left). Predicted episodic memory scores at 0, 5 and 10 years of A+ time with 95% CIs (top right). Modeled positivity rates for pTau217 and Tau PET with respect to A+ time in DS (bottom left) and WRAP (bottom right). Participants with Down syndrome show earlier and faster episodic memory decline as well as earlier tau biomarker presence as amyloid increases.

Keywords: PET, Cognition, Down syndrome, neurotypical

34 Relationship between p-tau217 and PET in preclinical AD: The moderating effect of white matter hyperintensity

Hasom Moon[1], Xi Chen[1]

[1]*Department of Psychology, Stony Brook University, Stony Brook, NY, US*

Backgrounds: Despite the promise of plasma p-tau217 for detecting Alzheimer's disease (AD) with its recent FDA clearance, discrepancies between plasma and PET biomarkers remain poorly understood. This study examined white matter hyperintensity (WMH) as a potential moderator in the association between plasma p-tau217 and PET-measured AD pathology, both cross-sectionally and longitudinally.

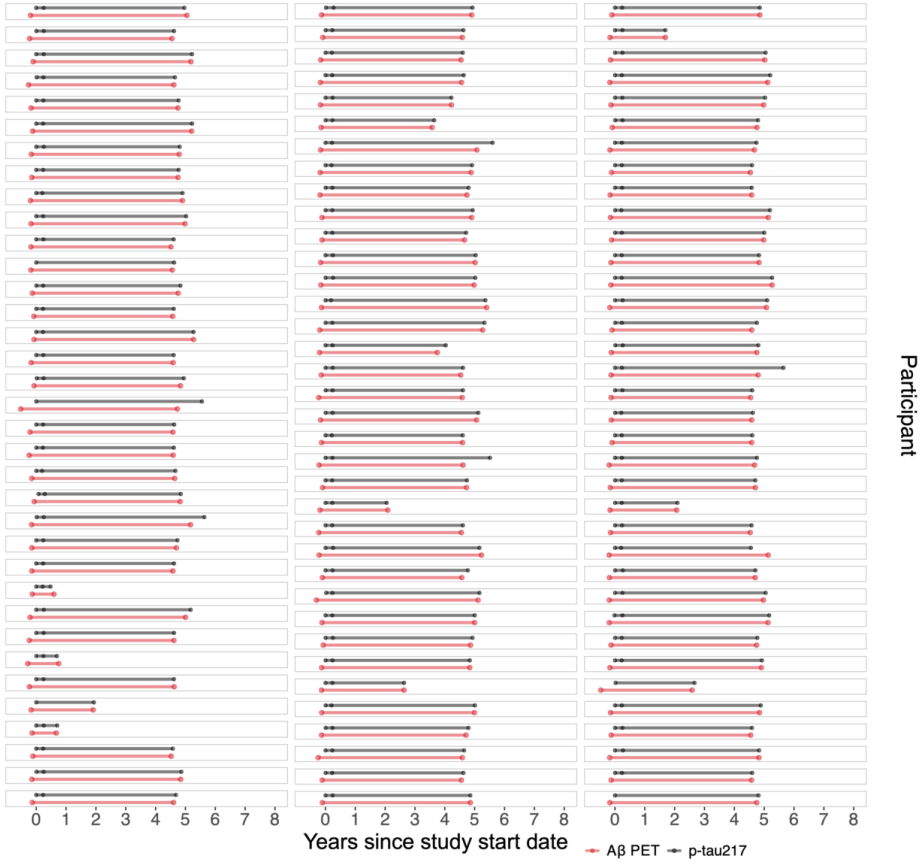
Methods: This study included 330 Aβ+ cognitively unimpaired older adults (age ≥ 65 years) from the Anti-Amyloid Treatment in Asymptomatic Alzheimer's disease (A4) study, who had baseline FLAIR MRI, plasma p-tau217$_{Lilly}$, $^{18\text{-}F}$Florbetapir Aβ PET, and $^{18\text{-}F}$Flortaucipir tau PET. For longitudinal analysis, we focused on the placebo group and removed p-tau217 measurements collected more than one year after the last PET for synchronized measurements (Figure 1). Linear mixed effects models were used to estimate longitudinal changes in p-tau217 and tau. Longitudinal Aβ changes were calculated based on the only two available scans. False discovery rate correction was used for multiple comparisons.

Results: Plasma p-tau217 was indicative of concurrent Aβ and temporo-parieto-occipital tau (Figure 2, top). However, this relationship was moderated by WMH: In individual with higher WMH, p-tau217 showed weak-to-nonsignificant associations with Aβ and tau (Figure 2, bottom). Longitudinally, p-tau217 slopes tracked tau progression in widespread regions, but not Aβ changes (Figure 3, top). Similar to cross-sectional results, the longitudinal associations between p-tau217 change and tau PET change were not present in high WMH individuals (Figure 3, bottom).

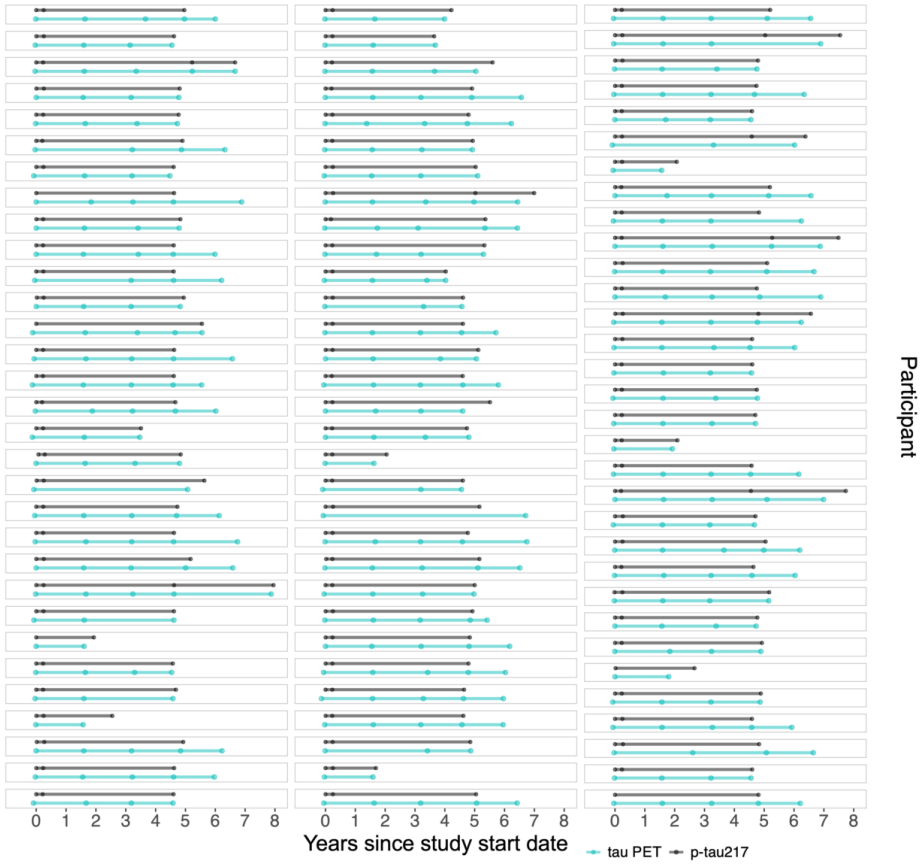
Conclusion: P-tau217 is useful for alerting elevated Aβ and early tau in cognitively normal older people. More importantly, repeated p-tau217 measurements can track longitudinal tau development, providing valuable information when frequent, repeated PET is infeasible. However, its use may be unwarranted in people with severe white matter lesion. Given the common comorbidity and heterogeneity in AD, caution should be taken when using p-tau217 in older individuals and those potentially having neurovascular diseases.

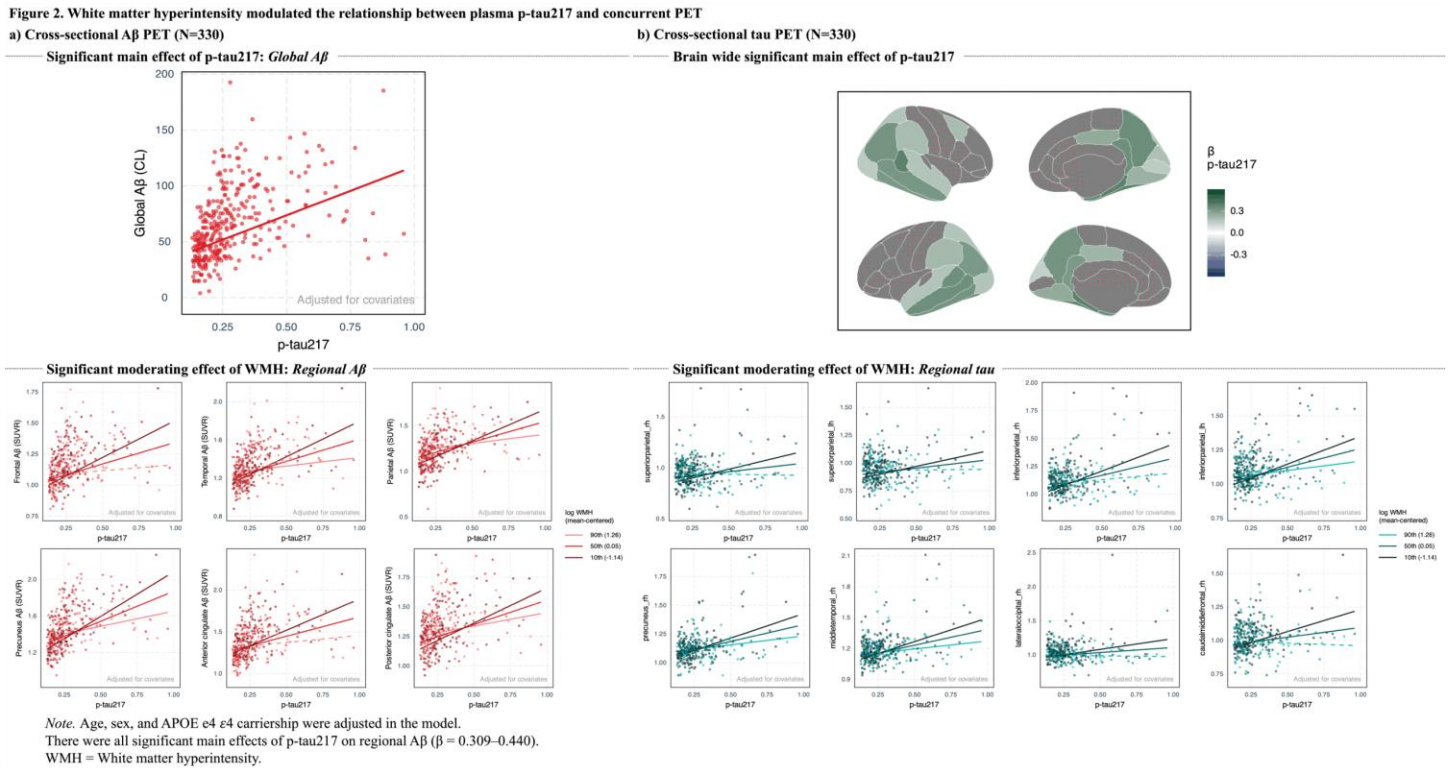
Figure 1. Synchronized longitudinal visits

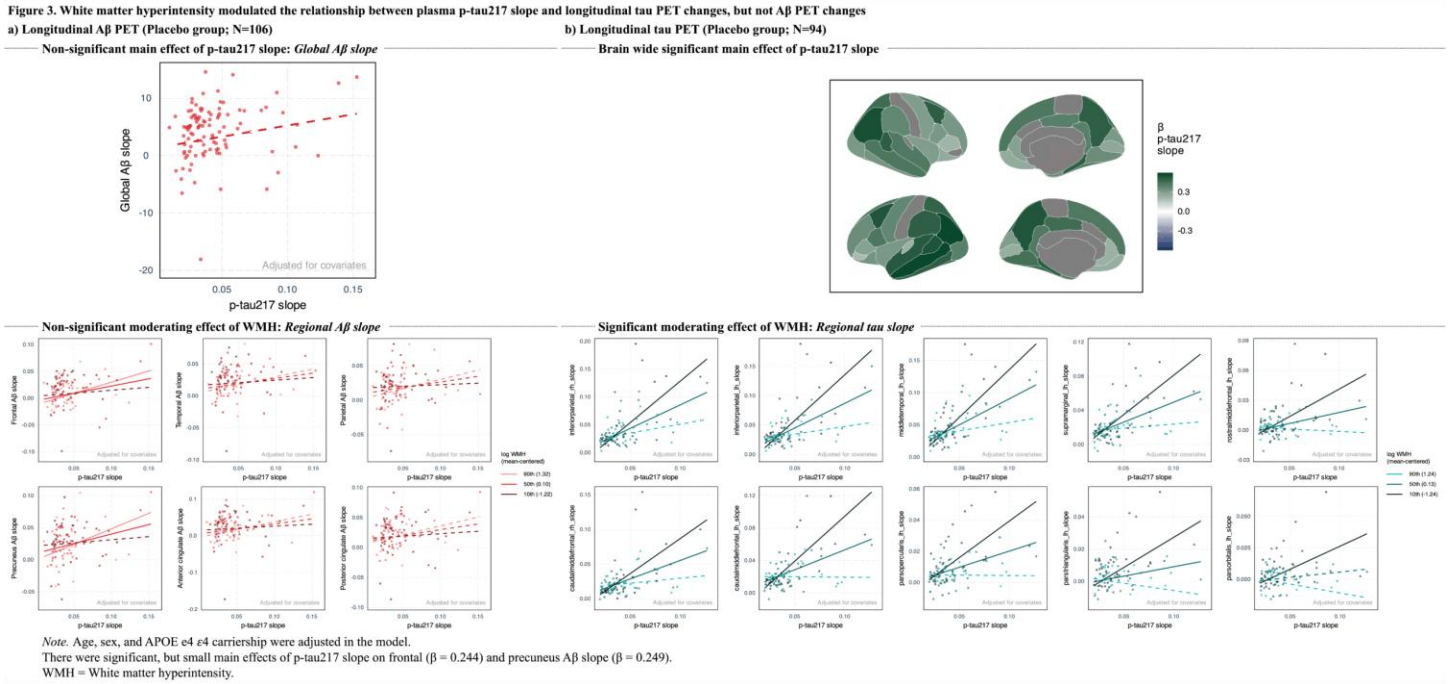
a) Longitudinal Aβ PET and p-tau217 (N=106)



b) Longitudinal tau PET and p-tau217 (N=94)







Keywords: p-tau217, Alzheimer's disease, PET, white matter hyperintensity

35 Systemic inflammation–tau interaction: Insights from CRP modulation of p-tau217 association with tau PET positivity

Abdul Razak Monto[1,2,3], Theresa Boots[1,2,3], Xuemei Zeng[1,2,3], Marissa F. Farinas[1,2,3], Anuradha Sehrawat[1,2,3], Anum Saeed[2], Ann D. Cohen[1], Steven E. Reis[1], Oscar L. Lopez[2,5], Beth Snitz[2,5], Thomas K. Karikari[1,2,3]

[1]*Department of Psychiatry, School of Medicine, University of Pittsburgh, Pittsburgh, PA 15213, USA, Pittsburgh, PA, US*
[2]*Alzheimer's Disease Research Center, University of Pittsburgh, Pittsburgh, PA USA, Pittsburgh, PA, US*
[3]*Biofluid Biomarker Laboratory, Western Psychiatric Hospital, University of Pittsburgh Medical Center, Pittsburgh, PA USA, Pittsburgh, PA, US*
[4]*School of Medicine, University of Pittsburgh, Pittsburgh, PA 15213, USA, Pittsburgh, PA, US*
[5]*Department of Neurology, School of Medicine, University of Pittsburgh, Pittsburgh, PA 15213, USA, Pittsburgh, PA, US*

Background: Plasma p-tau217, a promising biomarker for AD, and the p-tau217/Aβ42 ratio measured by the Lumipulse assays is FDA-cleared for detecting amyloid pathology. However, its association with tau pathology remains suboptimal. C-reactive protein (CRP), a marker of systemic inflammation, reflects biological processes central to AD pathogenesis. We hypothesize that inflammation may interact with disease mechanisms and modulate the relationship between plasma p-tau217 and tau pathology.

Methods: We evaluated the impact of CRP levels on p-tau217's association with tau pathology across MYHAT-NI (n=111), HeartSCORE (n=135), and Pitt-ADRC (n=107) cohorts. Plasma p-tau217 and CRP were measured using NULISAseq CNS panel, and tau pathology was assessed with [^{18}F]AV-1451 PET. Participants were grouped into high or low inflammation by age-adjusted CRP z-scores. Statistical analyses included Wilcoxon rank-sum tests, logistic regression, and Spearman correlations.

Results: P-tau217 correlated stronger with Tau-PET SUVR in individuals with high-inflammation, with Spearman's coefficients of 0.547 ($p<0.001$) in HeartSCORE, 0.364 ($p = 0.003$) in MYHAT-NI, and 0.763 ($p<0.001$) in Pitt-ADRC, compared to -0.021 ($p=0.883$), 0.190 ($p=0.204$), and 0.618 ($p<0.001$), respectively, in the low-inflammation individuals. P-tau217 also differentiated T+ from T- individuals better among those with high-inflammation, with AUCs of 0.866, 0.729, and 0.914 in HeartSCORE, MYHAT-NI, and Pitt-ADRC, respectively (adjusted for age, sex, race, and *APOE4* status). In the low-inflammation group, the AUCs were 0.774, 0.774, and 0.844. Fold change between T+ and T– were also greater in the high-inflammation group: 2.71 ($p<0.001$) in HeartSCORE, 1.18 ($p=0.034$) in MYHAT-NI, and 2.52 ($p<0.001$) in Pitt-ADRC. Corresponding fold changes in the low-inflammation group were 0.845 ($p=0.550$), 1.46 ($p=0.098$), and 2.43 ($p<0.001$).

Conclusion: Our results suggest that plasma p-tau217 correlates stronger with tau pathology in people with high systemic inflammation, indicating inflammation may increase tau tangle burden vulnerability. This association and its implications on AD progression need further evaluation in bigger and longitudinal populations.

Keywords: Plasma p-tau217, C-reactive protein, Systemic-inflammation, Tau-PET, NULISAseq CNS panel

36 Examining elevated choroid plexus binding of tau PET tracers in aging and Alzheimer's disease

Anna Marin[1,2,3], Ryan Wales[1,2,3], Cody Ruais[1,2,3], Jasmin Richard[1,2,3], Trey Hedden[1,2,3,4,5,6]

[1]*Department of Neurology, Icahn School of Medicine at Mount Sinai, New York, NY, US*
[2]*Mount Sinai Alzheimer's Disease Research Center, Icahn School of Medicine at Mount Sinai, New York, NY, US*
[3]*Sanford J. Grossman Interdisciplinary Center in Neural Circuitry and Immune Function, Icahn School of Medicine at Mount Sinai, New York, NY, US*
[4]*Department of Diagnostic, Molecular, and Interventional Radiology, Icahn School of Medicine at Mount Sinai, New York, NY, US*
[5]*BioMedical Engineering and Imaging Institute, Icahn School of Medicine at Mount Sinai, New York, NY, US*
[6]*Nash Family Department of Neuroscience, Icahn School of Medicine at Mount Sinai, New York, NY, US*

Background: A challenge for accurate quantification of tau pathology in Alzheimer's disease (AD) using PET is previously noted "off-target" binding localized to the choroid plexus (CP), adjacent to the hippocampus. Our study examines the prevalence of CP binding across PET tracers and evaluates the potential sources of such binding and their implications for AD pathophysiology.

Methods: Tau (PI-2620), amyloid (Florbetaben), and dopamine (Fallypride) PET data were collected at Mount Sinai from a sample of 168 older adults. PET data using other tracers (Flortaucipir and MK-6240 for tau; PiB, Florbetapir, NAV-4694 for amyloid; FDG for glucose) were examined using two publicly available datasets (SCAN and ADNI).

Results: Using PI-2620, nine cases had extremely high CP signal (> 1.8 SUVR, 7%), not explained by any notable clinical characteristics (Figure 1). The elevated uptake was confirmed after partial volume correction using the Geometric Transfer Matrix method. A quality assurance analysis did not show abnormalities in time activity curves, tracer uptake in the reference region, or in framewise displacement. A race effect was found such that Black/African American participants had relatively increased CP binding compared to White participants, for PI-2620, FTP, PiB and FBP (Figure 2). However, two-thirds of cases with extremely high uptake were White, suggesting other mechanisms are likely involved. Tau, amyloid, dopamine and glucose CP binding were positively associated with each other, after controlling for age, sex, race, diagnosis, CP and hippocampal volume.

Conclusion: High CP tau signal may be partially driven by binding to melanocytes in the CP epithelium, reflected by the race effect. Yet, the association between different tracers indicates that part of the signal is likely related to other properties. Further work should examine individual differences in sources of CP binding and test whether they are related to impaired clearance mechanisms linked to AD pathophysiology.

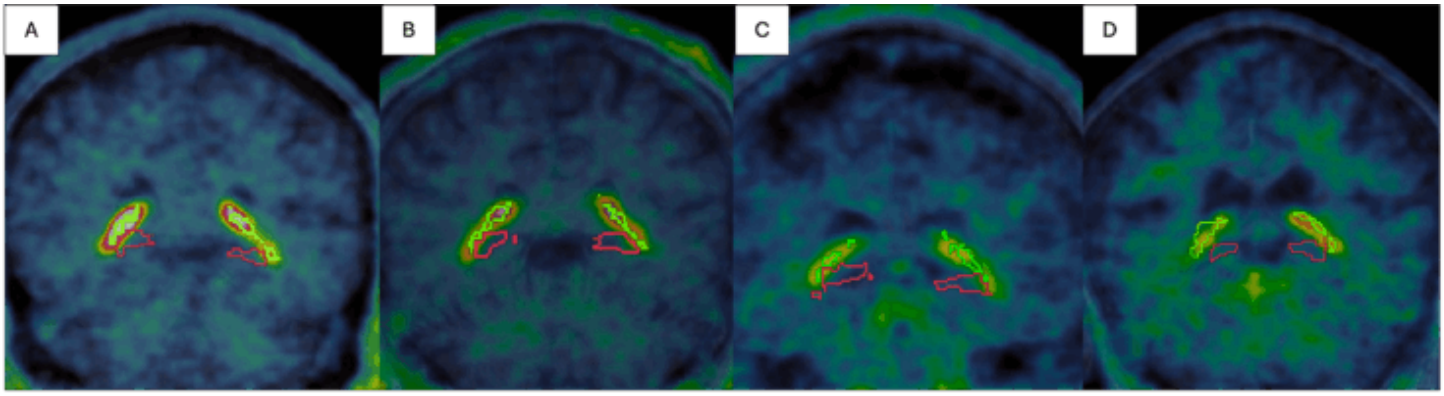


Figure 1. Tau (18F-PI-2620) PET SUVR images overlaid with the T1 structural images for four of the participants with elevated CP binding. Individual characteristics:(A) CP SUVR= 4.9, 78yo, CN, Male, White. (B) CP SUVR= 2.9, 73yo, CN, Female, White. (C) CP SUVR= 2.26, 60yo, CN, Female, B/AA. (D) CP SUVR= 1.97, 78yo, CN, Female, B/AA. Green and red labels represent the FreeSurfer CP and hippocampal masks, respectively.

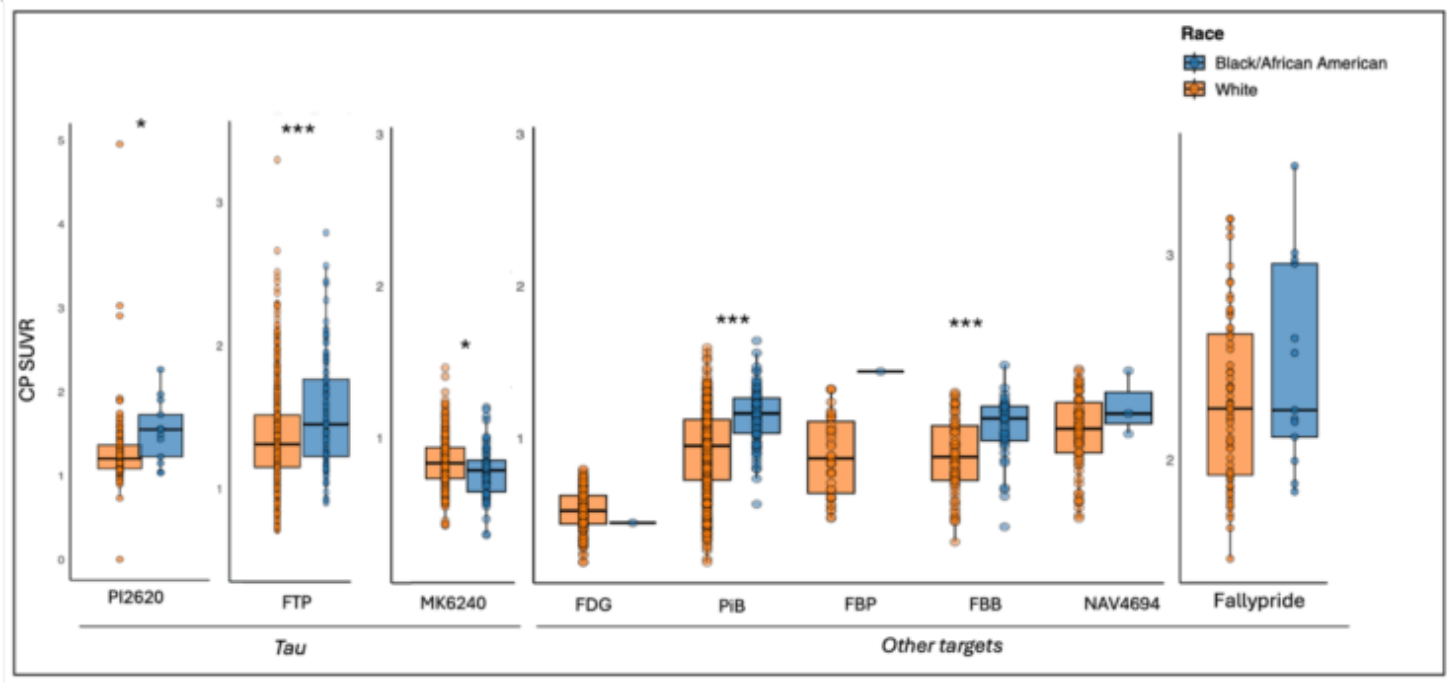


Figure 2. Boxplot of CP binding differences for each tracer between B/AA and White participants. *$p < .05$

Keywords: Tau PET, Choroid Plexus, PI-2620

37 The influence of β-amyloid on neuroinflammatory 11C-ER176 uptake in progressive apraxia of speech

Ryota Satoh[1], Rene Utianski[1], Joseph Duffy[1], Heather Clark[1], Hugo Botha[1], Val Lowe[1], Keith Josephs[1], Jennifer Whitwell[1]

[1]*Mayo Clinic, Rochester, MN, US*

Background: Progressive apraxia of speech (PAOS) is a neurodegenerative disorder that affects the planning or programming of speech. Most PAOS patients have four-repeat tau as their primary underlying pathology, but some can also have low levels of Alzheimer's disease (AD) co-pathology. Although a previous study has found that AD pathology, such as β-amyloid, does not affect clinical symptoms in PAOS, it remains unknown whether it could impact pathophysiological processes. This study aimed to clarify whether the presence of β-amyloid is associated with the pattern of neuroinflammation, tau deposition, and atrophy in PAOS.

Methods: Thirty-five prospectively recruited PAOS participants underwent ^{11}C-ER176, ^{18}F-flortaucipir, and Pittsburgh compound-B (PiB) PET, and 3T MRI scans. Of the 35 participants, 15 (43%) had β-amyloid positivity, as determined by global uptake on PiB PET. We compared regional neuroinflammation, flortaucipir uptake, and gray matter volumes in ten Braak associated cortical regions between β-amyloid-positive and β-amyloid-negative participants. A multiple linear regression analysis was performed in each region, with age, sex, and total intracranial volume (volumes only) as covariates, and a false discovery rate (FDR) correction was applied to adjust for multiple comparisons.

Results: β-amyloid-positive participants were older than β-amyloid-negative participants. There were no other differences in sex, education, or clinical scores between the two groups (**Table 1**). Regional analysis revealed greater neuroinflammation in β-amyloid-positive participants in the entorhinal cortex (Braak I/II) and inferior temporal cortex (Braak IV) (**Figure 1**, FDR-corrected $p<0.05$). There were no regions that survived FDR correction in flortaucipir uptake. Smaller gray matter volumes were observed in β-amyloid-positive participants in the fusiform (Braak III, FDR-corrected $p<0.05$).

Conclusions: The ^{11}C-ER176 PET analysis suggests the existence of neuroinflammation in temporal lobe regions in PAOS patients who have comorbid AD pathology.

Table 1 Demographics and clinical findings for β-amyloid-positive and β-amyloid-negative PAOS patients.

	β-amyloid positive (n=15)	β-amyloid negative (n=20)	*p*
Female, n	8 (53%)	7 (35%)	0.32
Education, y	16 (12, 18)	16 (14, 18)	0.87
Age, y	78 (72, 80)	71 (59, 73)	**<0.01**
Disease duration, y	3.9 (3.3, 6.2)	4.9 (3.6, 7.6)	0.68
MoCA (/30)	23 (16, 24)	23 (20, 24)	0.88
FAB (/18)	14 (12, 17)	15 (11, 16)	0.92
WAB praxis (/60)	55 (52, 59)	55 (53, 59)	0.88
UPDRS III (/132)	13 (9, 23)	18 (6, 34)	0.79
PSP rating scale (/100)	12 (7, 19)	19 (6, 28)	0.29
WAB-AQ (/100)	92 (90, 97)	95 (93, 97)	0.32
ASRS-3 (/52)	26 (20, 29)	24 (16, 27)	0.53
BNT (/15)	14 (12, 14)	14 (12, 15)	0.68
NVOA (/32)	23 (14, 30)	29 (8, 31)	0.92

Results are shown as median (first and third quartiles) for all continuous values. Abbreviations: MoCA = Montreal Cognitive Assessment; FAB = Frontal Assessment Battery; MDS-UPDRS III = Movement Disorders Society-sponsored revision of the Unified Parkinson's Disease Rating Scale Part III; PSP = Progressive supranuclear palsy; AOS = Apraxia of speech; WAB AQ = Western Aphasia Battery Aphasia Quotient; ASRS = Apraxia of Speech Rating Scale; BNT = Boston Naming Test Short Form; NVOA = nonverbal oral apraxia scale.

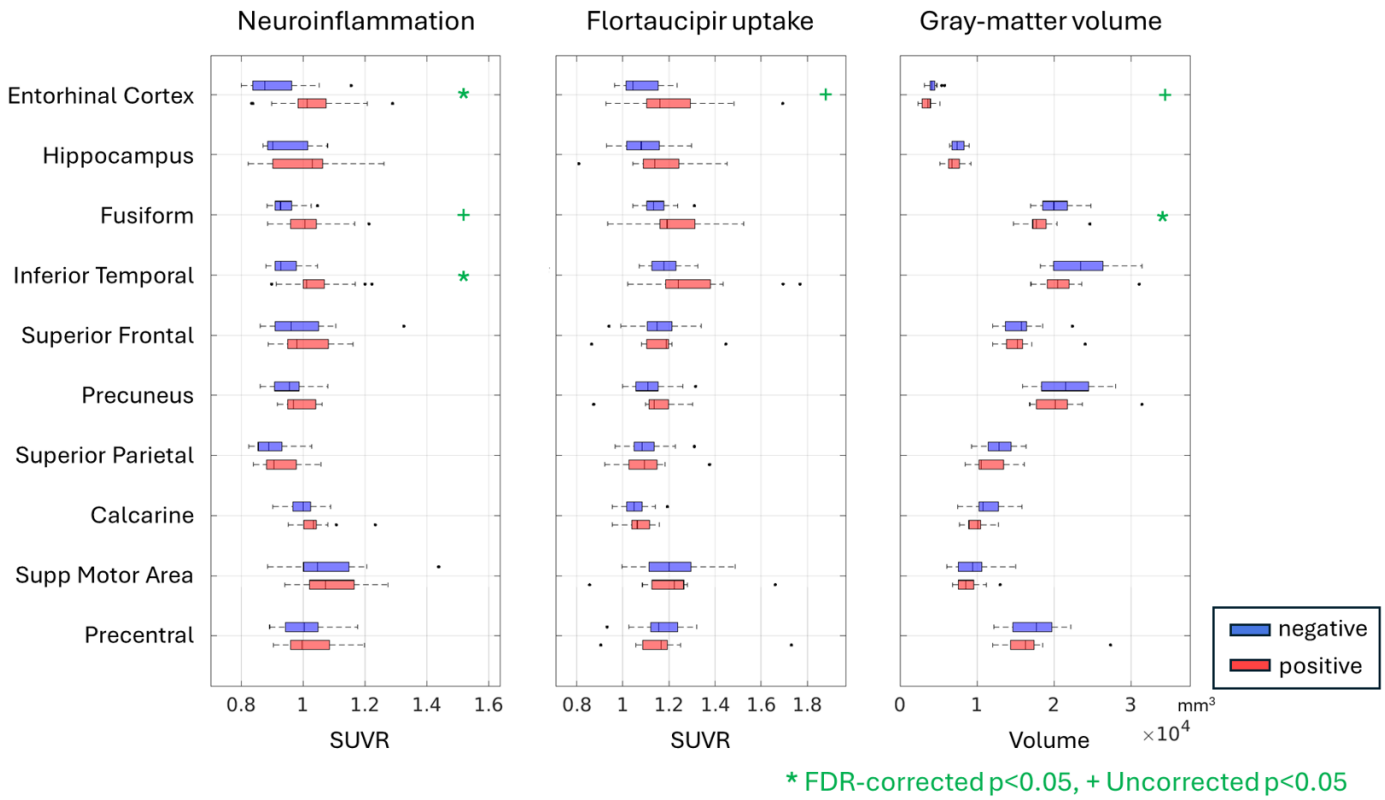


Figure 1 Regional ER176 uptake, flortaucipir uptake, and gray-matter volumes in β-amyloid-positive and β-amyloid-negative PAOS patients.

Keywords: neuroinflammation, 11C-ER176, β-amyloid, apraxia of speech, flortaucipir

38 Subtracting first principal component may improve detectability of subtle 4R tau signals in 18F flortaucipir tau PET imaging

Ryota Satoh[1], Farwa Ali[2], Heather Clark[2], Dennis Dickson[3], Val Lowe[1], Keith Josephs[2], Jennifer Whitwell[1]

[1]*Department of Radiology, Mayo Clinic, Rochester, MN, US*
[2]*Department of Neurology, Mayo Clinic, Rochester, MN, US*
[3]*Department of Neuroscience, Mayo Clinic, Jacksonville, FL, US*

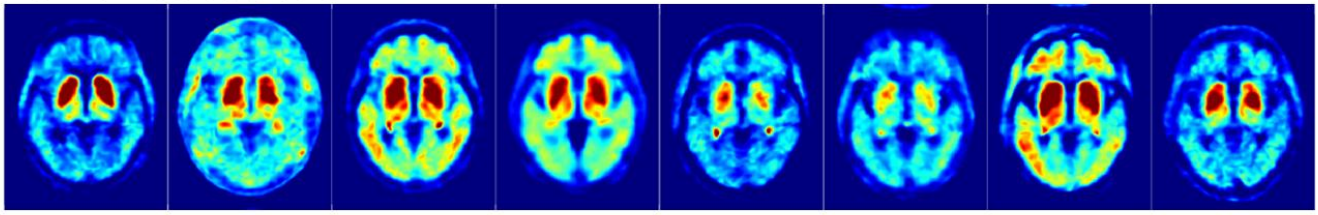
Background: ^{18}F-Flortaucipir tau PET images have shown less sensitivity to 4R tau in progressive supranuclear palsy (PSP) compared to 3R/4R tau in Alzheimer's disease (AD). Several studies using principal component analysis have shown that the first principal component (PC1) generally exhibits non-specific, global uptake patterns unrelated to diagnosis or disease progression in non-AD tauopathies. This study tested the hypothesis that subtracting PC1 would increase sensitivity to subtle 4R tau signals in PSP.

Methods: One hundred forty-one prospectively recruited PSP participants (80 with Richardson syndrome, 44 with subcortical, and 17 with cortical variants) and 40 age-matched healthy controls underwent 18F-flortaucipir PET scans. Of these PSP participants, 38 had died and underwent an autopsy. A proposed post-processing algorithm estimated and subtracted each participant's PC1 from the unseen standardized uptake value ratio (SUVR) image by projecting the image onto a pre-calculated PC1 subspace. Regional and voxel-based analyses compared two SUVRs (before and after PC1-subtraction) between PSP and controls, across PSP clinical variants, and across pathological diagnoses.

Results: Variability (standard deviation) of frontal SUVR across PSP participants was reduced by 46% (gray-matter) and 55% (white-matter) by PC1-subtraction (**Figure 1**). SUVR before PC1-subtraction showed higher uptake only in subcortical regions in PSP compared to controls. In contrast, SUVR after PC1-subtraction showed higher uptake in both frontal and subcortical regions (**Figure 2**). PC1-subtraction also improved differentiation across PSP clinical variants, where PSP-cortical showed the greatest uptake in frontal white-matter regions, and PSP-Richardson syndrome showed the greatest uptake in subcortical regions (**Figure 3a**). Only after PC1-subtraction, PSP pathology exhibited higher uptake than corticobasal degeneration (CBD) in the red nucleus and higher uptake than multiple system atrophy (MSA) pathology in multiple regions (**Figure 3b**).

Conclusions: The results suggest that PC1-subtraction reduced non-specific global components in flortaucipir images, thereby increasing sensitivity to subtle, localized 4R tau signals in PSP.

Before PC1 Subtraction



After PC1 Subtraction

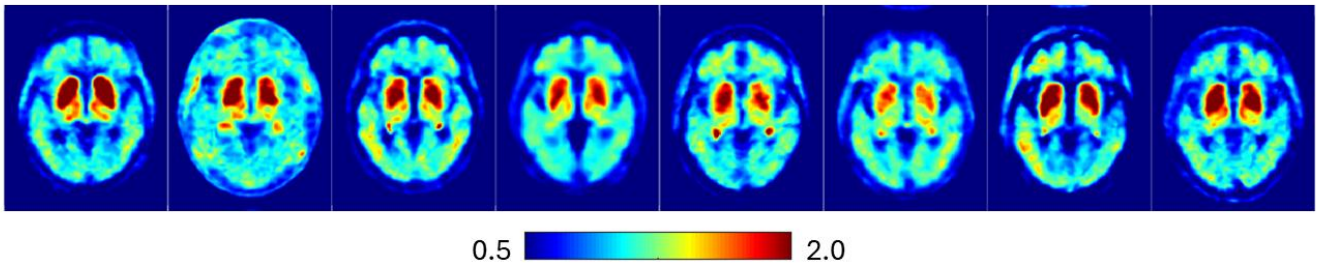


Figure 1 Representative SUVR images in the template space in randomly selected eight PSP participants. Cortical uptake was more homogeneous among patients after PC1-subtraction.

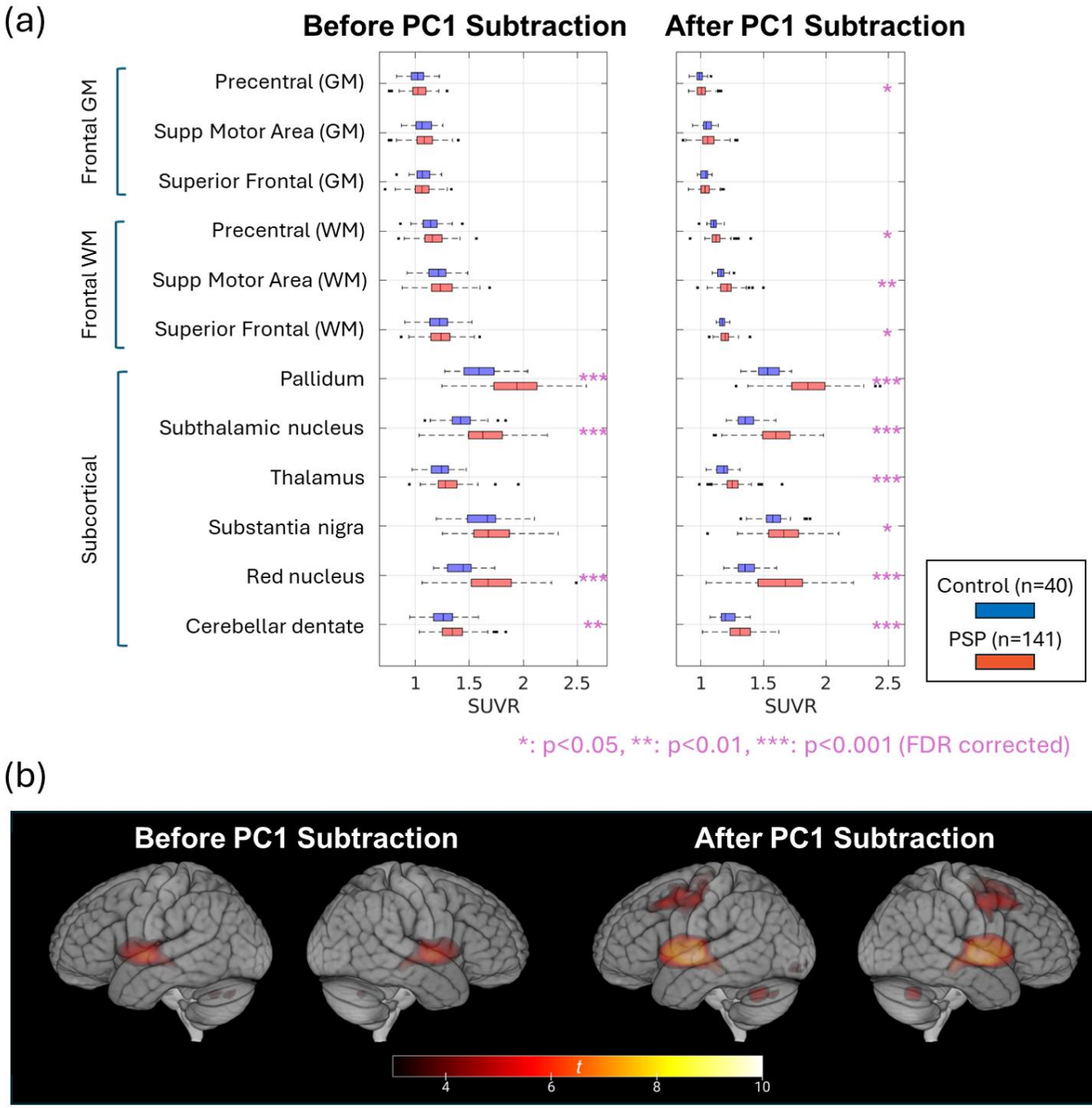


Figure 2 SUVR comparison between PSP and controls. (a) Boxplots for 12 affected regions in PSP, including three frontal gray-matter (GM), three frontal white-matter (WM), and six subcortical regions. Asterisks indicate significant differences, as determined by multiple linear regression adjusted for age and sex, with a false discovery rate (FDR) correction applied. (b) The regions showing PSP had greater flortaucipir uptake than controls (uncorrected p<0.001). The colors indicate the T-values. Age and sex were included as covariates in the model.

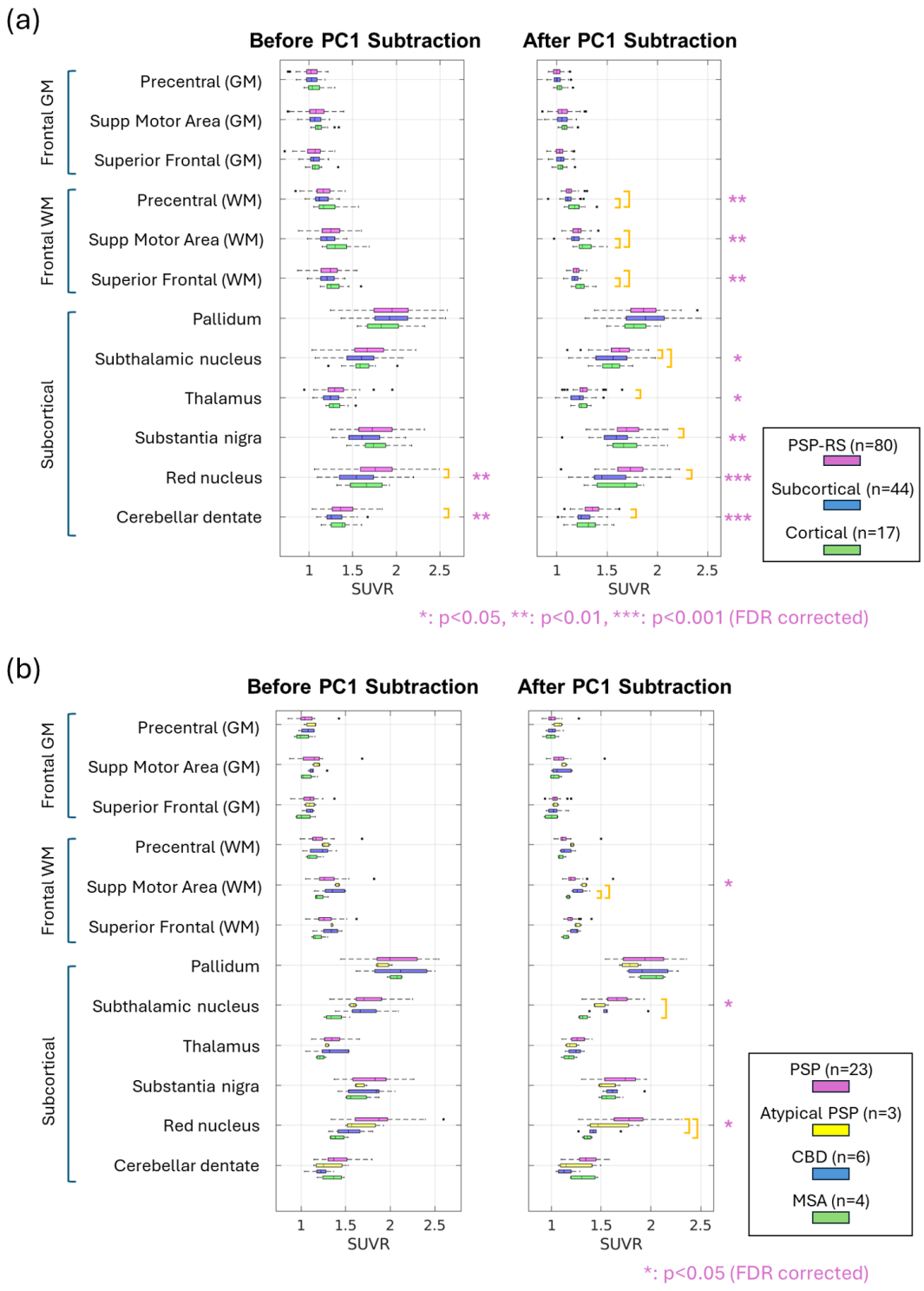


Figure 3. SUVR comparisons across PSP subgroups. (a) Comparison across PSP clinical variants. (b) Comparison across pathological diagnoses. Asterisks indicate significant differences, as determined by a Kruskal–Wallis test and a false discovery rate (FDR) correction. The yellow lines indicate the significant differences found in the post-hoc pairwise comparisons, as determined by Dunn's test. Atypical PSP indicates a pathological type of PSP with a greater cortical tau burden. Abbreviations: PSP-RS, PSP-Richardson syndrome; CBD, corticobasal degeneration; MSA, multiple system atrophy.

Keywords: flortaucipir, 4R tau, principal component analysis, progressive supranuclear palsy

39 OMG: a proteomic determinant of neurodegenerative resiliency

Michael Duggan[1], Hamilton Oh[2], Philipp Frank[3], Gabriela Gomez[4], David Zweibaum[1], Yuhan Cui[5], Jingsha Chen[6], Aditya Surapaneni[7], Cassandra Blew[1], Heather Dark[1], Cassandra Joynes[1], Sridhar Kandala[1], Murat Bilgel[1], Amelia Farinas[2], Guray Erus[5], Qu Tian[1], Julián Candia[1], Krishna Pucha[1], Bennett Landman[8], Logan Dumitrescu[8], Timothy Hohman[8], Alexandria Lewis[6], Abhay Moghekar[6], Fatemeh Siavoshi[6], Muhammad Ali[9], Menghan Liu[9], Ying Xu[9], Daniel Western[9], Naoto Kaneko[10], Shintaro Kato[10], Makio Furuichi[10], Masaki Shibayama[10], Masahisa Katsuno[11], Yukiko Nishita[12], Rei Otsuka[12], Rebecca Gottesman[13], Eric Dammer[14], Nicholas Seyfried[14], Allan Levey[14], Erik Johnson[14], Elizabeth Mormino[2], Anthony Wagner[2], Kathleen Poston[2], Dimitrios Kapogiannis[1], Morgan Grams[7], Pavan Bhargava[6], Iwao Waga[10], Christos Davatzikos[5], Susan Resnick[1], Luigi Ferrucci[1], David Bennett[15], Carlos Cruchaga[9], Tony Wyss-Coray[2], Mika Kivimäki[3], Josef Coresh[7], Keenan Walker[1]

[1]*National Institute on Aging, Baltimore, MD, US*
[2]*Stanford University, Stanford, CA, US*
[3]*University College London, London, UK*
[4]*Brigham and Women's Hospital, Boston, MA, US*
[5]*University of Pennsylvania, Philadelphia, PA, US*
[6]*Johns Hopkins University, Baltimore, MD, US*
[7]*New York University, New York City, NY, US*
[8]*Vanderbilt University, Nashville, TN, US*
[9]*Washington University, St. Louis, MO, US*
[10]*NEC Solution Innovators Limited, Tokyo, Japan*
[11]*Nagoya University Graduate School of Medicine, Nagoya, Japan*
[12]*National Center for Geriatrics and Gerontology, Obu, Japan*
[13]*National Institute of Neurological Disorders and Stroke, Bethesda, MD, US*
[14]*Emory University, Atlanta, GA, US*
[15]*Rush University, Chicago, IL, US*

Biofluid proteomics can enhance our understanding of the neurodegenerative mechanisms underlying Alzheimer's disease and related dementias (ADRDs). Oligodendrocyte myelin glycoprotein (OMG) is a brain-specific protein implicated in myelination, but its potential mechanistic, biomarker, and therapeutic roles in ADRDs requires further elucidation. After detecting an inverse association between its abundance in peripheral circulation and cortical amyloid deposition in two community-based cohorts, the current study characterized OMG's role in ADRDs with high-throughput proteomics from ***sixteen*** independent cohorts (**Figure 1**). Data included a variety of cross-sectional and longitudinal community-based and clinical samples from North America, Europe, and Asia, and incorporated complementary biofluids, biospecimens, and proteomic platforms. OMG's CSF and brain proteomic signatures reflected broader neuroprotective mechanisms, especially axonal structural integrity, and two-sample Mendelian randomization causally implicated OMG as protective against multiple neurodegenerative diseases (**Figure 2**). We detected lower plasma OMG in individuals with cortical amyloid deposition, compromised brain structure, dementia, and multiple sclerosis, as well as in individuals who developed dementia over 7- to 20-year follow-up periods (**Figure 3**). Our findings implicate OMG as a mechanistic determinant of neurodegenerative resiliency among older adults, which is reliably captured by its abundance in peripheral circulation.

Figure 1

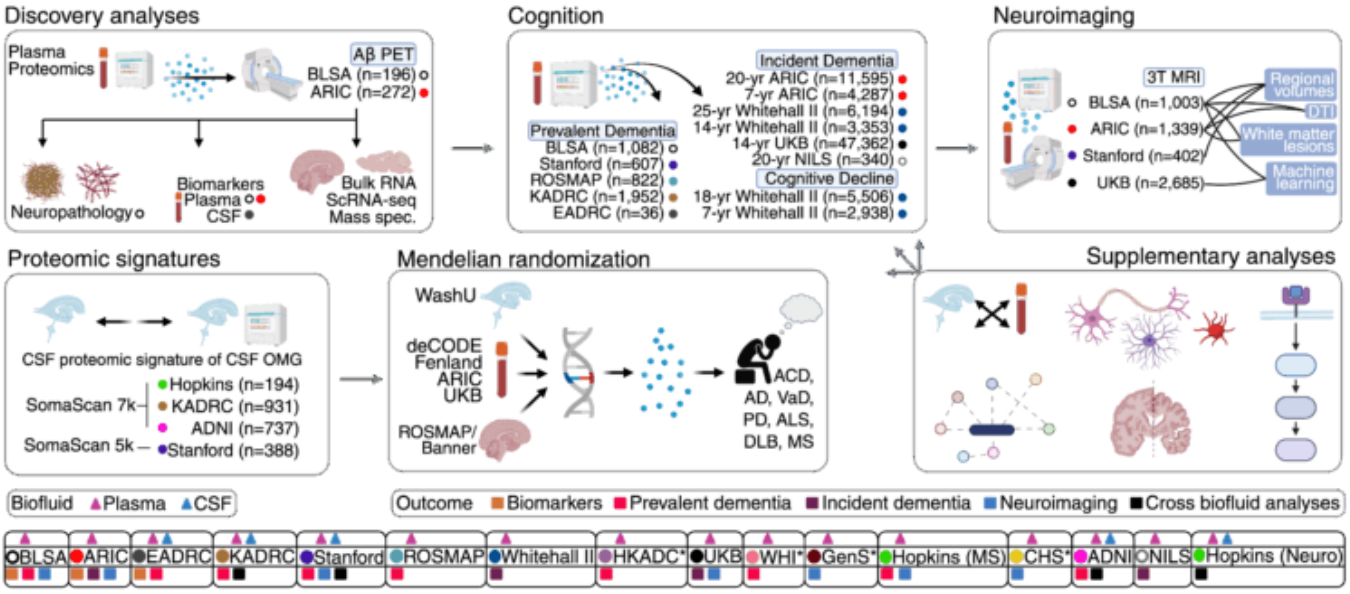


Figure 2

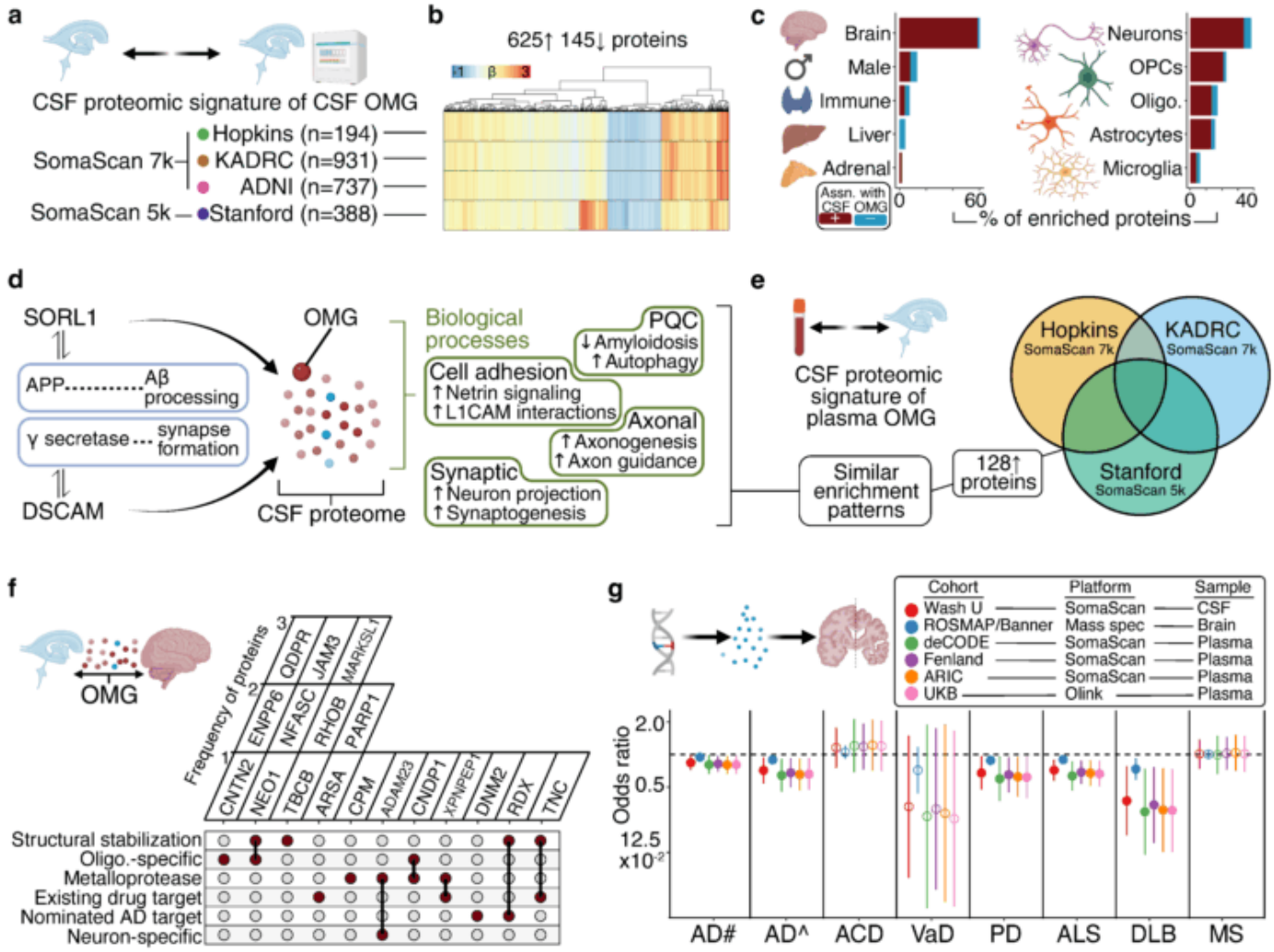
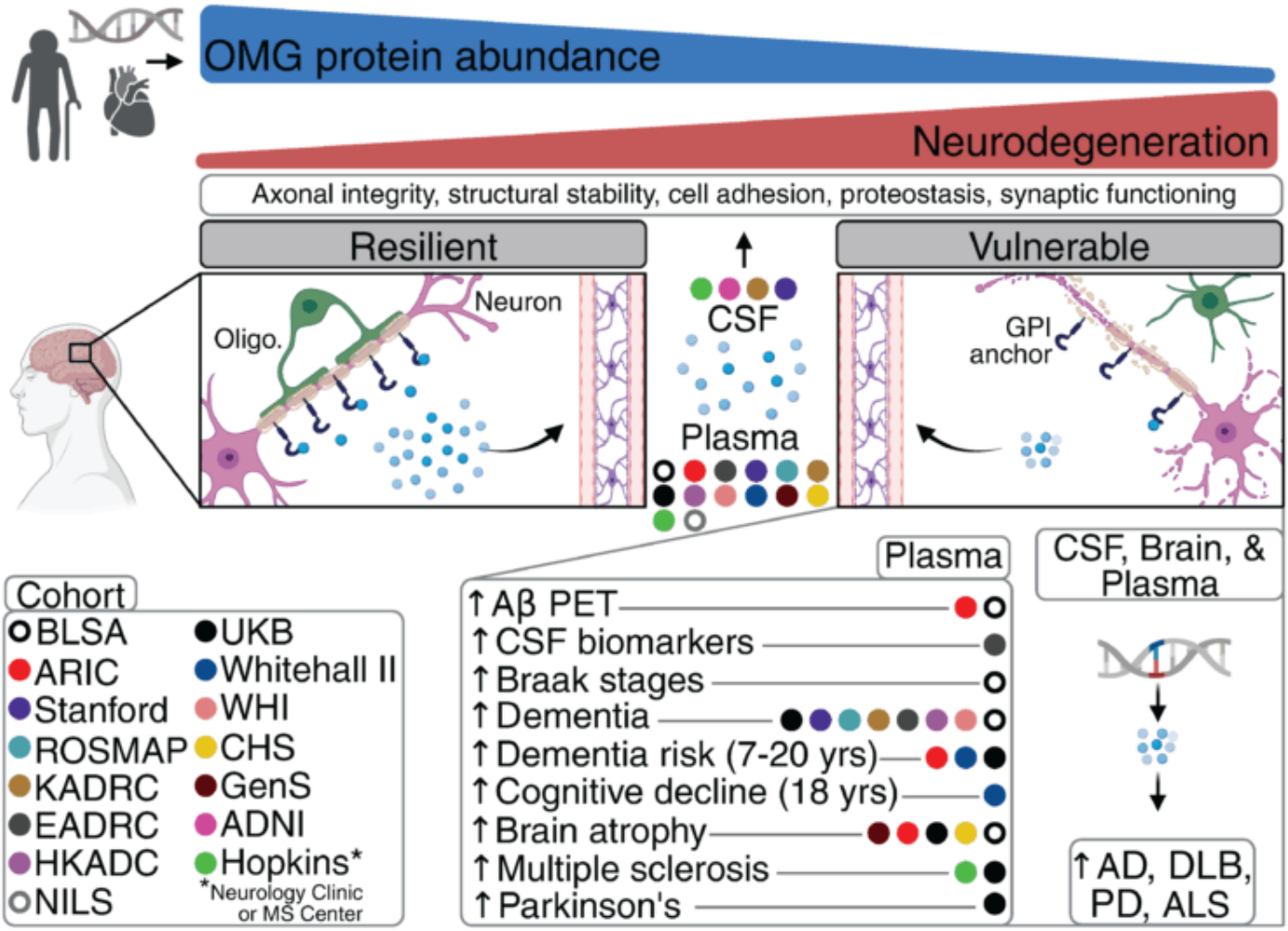


Figure 3



Keywords: proteomics, amyloid PET, incident dementia, genetics

40 Frequency and consequences of extreme PET based pathological profiles in preclinical Alzheimer's disease

Lucah Medina Guerra[1], Karly Cody[1], Christina Young[7,8], Jintao Sheng[1,3,4], Andrzej Sokolowski[1], Kyan Younes[1], Alexandra Trelle[1], Duygu Tosun[5], Timothy Hohman[6], Elizabeth Mormino[1,2]

[1]*Department of Neurology and Neurological Sciences, Stanford University, Palo Alto, CA, US*
[2]*Division of Molecular Imaging Program at Stanford, Stanford University, Palo Alto, CA, US*
[3]*Department of Psychology, Stanford University, Palo Alto, CA, US*
[4]*Wu Tsai Neurosciences Institute, Stanford University, Palo Alto, CA, US*
[5]*Department of Radiology, University of California-San Francisco, San Francisco, CA, US*
[6]*Vanderbilt Memory and Alzheimer's Center, Vanderbilt Genetics Institute, Department of Neurology, Vanderbilt University Medical Center, Nashville, TN, US*
[7]*Department of Neurology, University of California Davis, Davis, CA, US*
[8]*Department of Radiology, University of California Davis, Davis, CA, US*

Objective: Preclinical Alzheimer's disease (AD) is normally characterized by moderate amyloid and medial temporal tau. We investigated the frequency and longitudinal trajectories of cognitively unimpaired (CU) individuals with abnormally high amyloid and/or widespread tau PET pathology.

Methods: We characterized amyloid and tau PET data from CU individuals in ADNI, A4, WRAP, and NACC. All PET data were processed locally with an MRI-Free pipeline. Centiloids (CL) were used to quantify amyloid PET. A Braak-based hierarchical schema was applied to assess regional tau PET. We identified two abnormal preclinical biomarker groups, both with very high amyloid (A++; ≥100CL), and either (1) with widespread neocortical tau (Braak 5/6+; A++/T++; N=9) or (2) without tau elevation (A++/T−; N=40). Visual review confirmed widespread tau in 8/9 A++/T++ (one excluded) and low tau in 37/40 A++/T− (three excluded for focal uptake). Selected preclinical comparison groups had 25-99CL and no tau (A+/T−; N=470) or moderate tau (Braak3/4+; A+/T+; N=164). Longitudinal cognitive performance was characterized across groups. In A4, tau PET trajectories were similarly examined (Table 2).

Results: In this preclinical sample (N=2149) abnormally high amyloid with or without widespread tau were uncommon (e.g., A++/T++, n=8, 0.37%; A++/T-, n=37, 1.72%). A++/T- were generally older and more frequently male (Table1). Cognitive decline was observed in 5/8 (62%) A++/T++, which was higher than the A+/T+ comparison group (N=31/154 , 20%). Conversely, only 4/34 (12%) of A++/T- progressed, similarly to rates of progression in A+/T- comparison group (N=67/463, 14.5%). Within A4, rates of meta-temporal tau accumulation were slower in A++/T- and A+/T- compared to A+/T+ (Figure1).

Summary: We identified two abnormal PET-based groups within preclinical AD, one represents high clinical risk (A++/T++) and another that may be resilient to amyloid-mediated tau accumulation and future clinical progression (A++/T−). Further examination of A++/T- is warranted to identify underlying mechanisms.

Variable	A++/T– CU N = 37[1]	A++/T++ CU N = 8[1]	A+/T+ CU N = 164[1]	A+/T- CU N = 470[1]	N = 679 Overall[1]
Age (years)	75.8 ± 5.1	73.4 ± 9.5	74.1 ± 6.9	72.8 ± 6.2	73.3 ± 6.4
Education (years)	16.4 ± 2.8	15.9 ± 3.6	16.7 ± 2.4	16.3 ± 2.7	16.4 ± 2.7
Sex					
Female	15 (41%)	6 (75%)	101 (62%)	270 (57%)	392 (58%)
Male	22 (59%)	2 (25%)	63 (38%)	200 (43%)	287 (42%)
Race/Ethnicity					
American Indian or Alaska Native	0 (0%)	1 (13%)	0 (0%)	1 (0.2%)	2 (0.3%)
Asian	1 (2.7%)	0 (0%)	1 (0.6%)	16 (3.4%)	18 (2.7%)
Black or African American	2 (5.4%)	0 (0%)	10 (6.1%)	13 (2.8%)	25 (3.7%)
Hispanic/Latino	0 (0%)	1 (13%)	8 (4.9%)	13 (2.8%)	22 (3.2%)
Multiple, Other, Unknown	0 (0%)	0 (0%)	4 (2.4%)	3 (0.6%)	7 (1.0%)
Native Hawaiian or Other Pacific Islander	0 (0%)	0 (0%)	2 (1.2%)	11 (2.3%)	13 (1.9%)
White	34 (92%)	6 (75%)	139 (85%)	413 (88%)	592 (87%)
APOE status					
APOE4–	12 (32%)	3 (38%)	39 (24%)	191 (41%)	245 (36%)
APOE4+	20 (54%)	4 (50%)	86 (52%)	228 (49%)	338 (50%)
Unknown	5 (14%)	1 (13%)	39 (24%)	51 (11%)	96 (14%)
Cohort					
A4	18 (49%)	1 (13%)	43 (26%)	254 (54%)	316 (47%)
ADNI	8 (22%)	2 (25%)	37 (23%)	87 (19%)	134 (20%)
NACC	6 (16%)	4 (50%)	47 (29%)	87 (19%)	144 (21%)
WRAP	5 (14%)	1 (13%)	37 (23%)	42 (8.9%)	85 (13%)

[1] Mean ± SD; n (%)

Table 1. Demographics Table of CU PET Defined Groups of all leveraged cohorts (ADNI, WRAP, A4 and NACC). The A++/T- and A+/T+ groups were slightly older that the A++/T++ and A+/T- groups, A++/T- was the only group with a larger number of males than females. A4 had the largest number of cases with cognitive and imaging data available for further analysis.

Characteristic	A++/T– CU N = 18[1]	A+/T+ CU N = 43[1]	A+/T– CU N = 254[1]	N = 315 Overall[1]
Age (years)	74.8 ± 4.6	72.6 ± 4.4	71.9 ± 4.8	72.2 ± 4.8
Education (years)	16.8 ± 3.3	16.7 ± 2.6	16.0 ± 2.9	16.2 ± 2.9
Sex				
Female	6 (33%)	22 (51%)	143 (56%)	171 (54%)
Male	12 (67%)	21 (49%)	111 (44%)	144 (46%)
Race/Ethnicity				
Asian	1 (5.6%)	0 (0%)	15 (5.9%)	16 (5.1%)
Black or African American	1 (5.6%)	2 (4.7%)	5 (2.0%)	8 (2.5%)
Hispanic/Latino	0 (0%)	0 (0%)	4 (1.6%)	4 (1.3%)
Multiple, Other, Unknown	0 (0%)	2 (4.7%)	2 (0.8%)	4 (1.3%)
White	16 (89%)	39 (91%)	228 (90%)	283 (90%)
APOE genotype				
e2/e2	0 (0%)	0 (0%)	1 (0.4%)	1 (0.3%)
e2/e3	1 (5.6%)	1 (2.3%)	11 (4.3%)	13 (4.1%)
e2/e4	0 (0%)	1 (2.3%)	10 (3.9%)	11 (3.5%)
e3/e3	3 (17%)	11 (26%)	102 (40%)	116 (37%)
e3/e4	12 (67%)	25 (58%)	118 (46%)	155 (49%)
e4/e4	2 (11%)	5 (12%)	12 (4.7%)	19 (6.0%)
Median and IQR # of scans	4 [2, 4]	4 [3, 4]	4 [3, 5]	4 [3, 4]
Tau PET Follow-up time (years)	3.72 ± 2.63	4.05 ± 2.02	4.29 ± 2.07	4.22 ± 2.09

[1] Mean ± SD; n (%)

Table 2. Demographics Table of A4 CU PET Defined Groups. The A++/T- group was slightly older that the other A+ groups, this group also had a larger number of males than females.

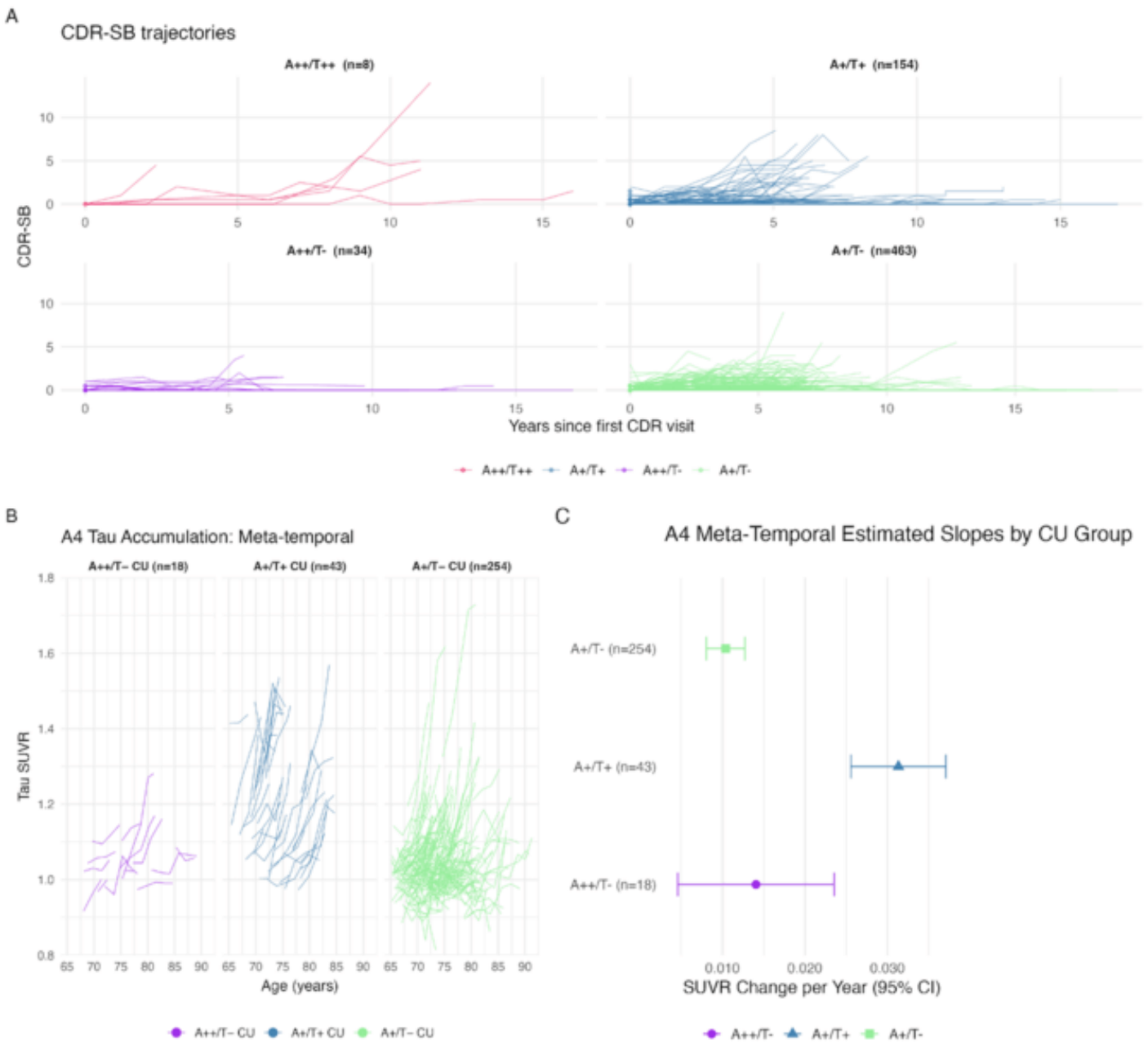


Figure 1. (A) CDR-SB longitudinal trajectories of very high amyloid burden CU individuals from ADNI, WRAP, A4 and NACC cohorts. Among those with longitudinal CDR follow up (n= 659), cognitive decline was defined as an increase of ≥1.5 in CDR-SB or ≥1.0 in the memory domain from baseline to any follow-up visit. Cognitive decline was observed in 5/8 (62 %) of A++/T++; 31/154 (20%) A+T+; 4/34 (12%) of A++/T-; 67/463 (14.5%) of A+T-. **(B)** Longitudinal Trajectories of A4 Tau PET SUVR in the Meta-temporal region of A++/T- (n=18), A+/T+ (n=43) and A+/T- (n=254) CU groups. **(C)** A4 Slope Estimates of Tau Accumulation in the Meta-temporal region of A++/T (n=18), A+/T+ (n=43) and A+/T- (n=254) CU groups. The A++/T- group in the A4 cohort showed similar tau accumulation to the A+/T- group, and both groups were slower than the A+/T+ group.

Keywords: preclinical, pet, resilience

41 Periventricular diffusivity moderates the relationship between astrocyte reactivity and amyloid deposition in non-demented older adults

Chang-Le Chen[1], Minjie Wu[1,2], Shaolin Yang[1,2], Alexandra Gogola[1,3], Weiquan Luo[1], Victor Villemagne[2], Charles Laymon[1,3], Brian Lopresti[3], Ann Cohen[2], Milos Ikonomovic[4], Beth Snitz[4], Kristine Wilckens[2], Oscar Lopez[4], Dana Tudorascu[2,5], Howard Aizenstein[1,2], Davneet Minhas[3]

[1]*Department of Bioengineering, University of Pittsburgh, Pittsburgh, PA, US*
[2]*Department of Psychiatry, University of Pittsburgh, Pittsburgh, PA, US*
[3]*Department of Radiology, University of Pittsburgh, Pittsburgh, PA, US*
[4]*Department of Neurology, University of Pittsburgh, Pittsburgh, PA, US*
[5]*Department of Biostatistics, University of Pittsburgh, Pittsburgh, PA, US*

Introduction: Evidence from animal studies indicates that reactive astrogliosis may affect amyloid clearance through altered brain fluid dynamics. However, such mechanisms remain uncharacterized *in vivo* in humans. Utilizing ^{18}F-SMBT-1, a surrogate PET marker of reactive astrogliosis, we hypothesized that the relationship between astrocyte reactivity and amyloid burden is modulated by periventricular diffusivity (PVeD), a diffusion marker of cerebral fluid dynamics (Chen et al., Alzheimer's & Dementia, 2025).

Methods: We analyzed neuroimaging data from 104 non-demented older adults (age = 67.1 ± 6.9 yrs; 52 females; MoCA = 26.1 ± 2.6). Participants underwent PET imaging with MAO-B tracer ^{18}F-SMBT-1 to characterize astrocyte reactivity, and ^{11}C-PiB for β-amyloid deposition. Regional standardized uptake value ratio (SUVR) values were calculated for both tracers. PVeD was estimated using diffusion MRI to reflect fluid clearance dynamics. We first assessed the association between regional ^{18}F-SMBT-1 SUVR and ^{11}C-PiB SUVR, controlling for age, sex, education, and cortical thickness composite values. For significant associations, we then tested for interaction between ^{18}F-SMBT-1 SUVR and PVeD on ^{11}C-PiB SUVR while controlling for the same covariates and local mean diffusivity.

Results: We observed significant positive associations between ^{18}F-SMBT-1 SUVR in the precuneus and ^{11}C-PiB SUVR in the superior frontal, precuneus, posterior cingulate, and parietal regions (all *P*'s < 0.001) after multiple comparison correction (Figure 1). Furthermore, the interaction terms of ^{18}F-SMBT-1 SUVR in the precuneus with PVeD were significant across all identified regions (all *P*'s < 0.006), which indicates that participants with lower PVeD exhibited a stronger positive correlation between astrocyte reactivity and amyloid burden compared to those with higher diffusivity.

Prior regression analysis	Dependent variables	Independent variables	Coefficients	SE	*p*-value
	PiB SUVR in the superior frontal	SMBT-1 SUVR in the precuneus	0.465	0.111	6.1×10^{-5}
	PiB SUVR in the precuneus	SMBT-1 SUVR in the precuneus	0.567	0.137	7.4×10^{-5}
	PiB SUVR in the posterior cingulate	SMBT-1 SUVR in the precuneus	0.543	0.130	6.6×10^{-5}
	PiB SUVR in the parietal	SMBT-1 SUVR in the precuneus	0.442	0.109	9.4×10^{-5}
Interaction analysis	Dependent variables	Independent variables	Coefficients	SE	*p*-value
	PiB SUVR in the superior frontal	SMBT-1 SUVR in the precuneus	3.983	1.184	0.0011
		Interaction with PVeD	-8.108	2.759	0.0041
	PiB SUVR in the precuneus	SMBT-1 SUVR in the precuneus	4.864	1.423	0.0009
		Interaction with PVeD	-10.066	3.317	0.0031
	PiB SUVR in the posterior cingulate	SMBT-1 SUVR in the precuneus	3.960	1.241	0.0019
		Interaction with PVeD	-8.142	2.892	0.0059
	PiB SUVR in the parietal	SMBT-1 SUVR in the precuneus	3.353	1.064	0.0022
		Interaction with PVeD	-6.960	2.480	0.0060

Note: robust linear regression was used to fit the models

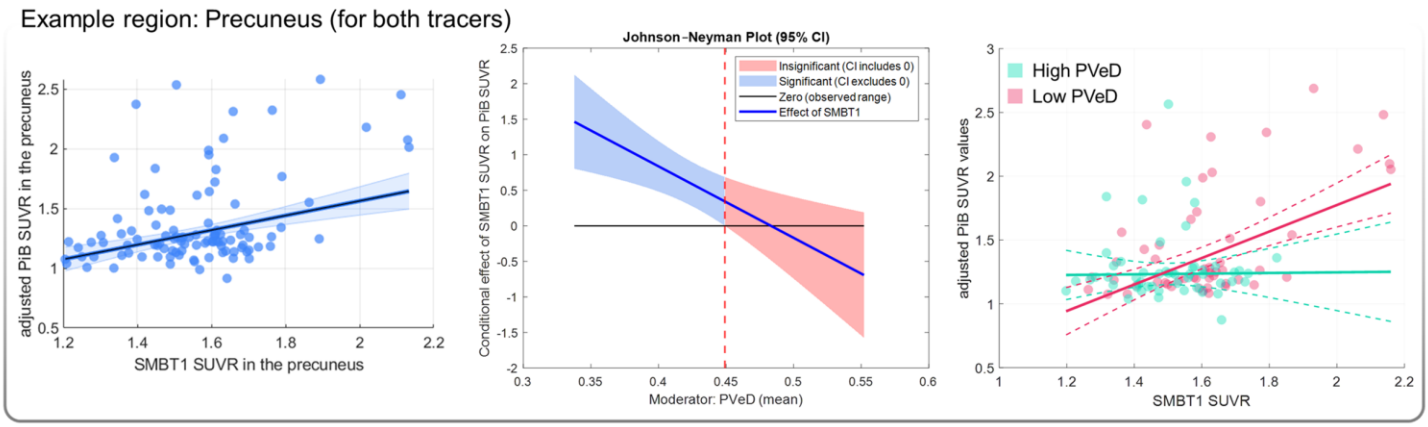


Figure 1. Regression and interaction analyses of reactive astrogliosis, amyloid burden, and periventricular diffusivity (PVeD). Visualization presents statistical plots (i.e., regression plot, Johnson–Neyman plot, and interaction plot for SMBT-1 SUVR in the precuneus and PiB SUVR in the precuneus) illustrating the linear relationship between astrogliosis and amyloid burden as moderated by PVeD.

Conclusion: Our findings suggest that altered fluid dynamics represented by PVeD might moderate the link between astrogliosis and amyloid deposition. This modulation indicates fluid-related clearance mechanisms as a possible path between astrocyte reactivity and amyloid accumulation in preclinical Alzheimer's disease.

Keywords: periventricular diffusivity, astrocyte reactivity, amyloid deposition, PET, diffusion MRI

42 Disentangling the effects of age and Alzheimer's disease pathology on longitudinal atrophy in cognitively normal older adults

Miraal Haque[1,2], Corrina Fonseca[1], Samira Maboudian[1], Renaud La Joie[2], William Jagust[1]

[1]*Department of Neuroscience, University of California, Berkeley, Berkeley, CA, US*
[2]*Edward and Pearl Fein Memory and Aging Center, Department of Neurology, Weill Institute for Neuroscience, University of California, San Francisco, San Francisco, CA, US*

Background: Age and Alzheimer's disease (AD) pathology have complex relationships with longitudinal atrophy that are poorly understood. Here, we investigated effects of age, beta-amyloid (Aβ), and tau on prospective gray matter atrophy in cognitively normal older adults.

Methods: 417 participants from 3 observational studies underwent Aβ-PET (PiB, FBB, FBP), tau-PET (FTP), and ≥ 2 MRI scans anchored to baseline tau-PET. Using voxel-wise multiple regression analyses, we examined relationships between the following baseline predictors and atrophy: (1) age unadjusted and adjusted for Aβ and entorhinal [ERC] tau; (2) Global Aβ unadjusted and adjusted for age and tau; and (3) ERC tau before and after adjusting for age and Aβ. All analyses included TIV, sex and cohort as covariates.

Results: Older age was associated with faster atrophy in the parahippocampal cortex ($p < 0.001$, $k \geq 100$; Figure 1). After adjusting for Aβ and ERC tau, only clusters in the right precentral gyrus were significant. Higher global Aβ was associated with faster atrophy in the parahippocampal, fusiform and inferior temporal gyri (Figure 2). However, controlling for age and ERC tau removed the effect of Aβ on atrophy almost entirely. Finally, greater baseline ERC tau was correlated with faster atrophy in the medial and lateral temporal lobes (Figure 3). Peak voxels were observed in the ERC. These effects were only slightly attenuated after adjusting for age and Aβ.

Conclusions: These findings suggest that tau is the main driver of prospective atrophy even among cognitively normal older individuals, with ERC tau effects predominating in the medial temporal lobes. In contrast, the effect of both older age and Aβ on atrophy is small and largely reflects the influence of tau.

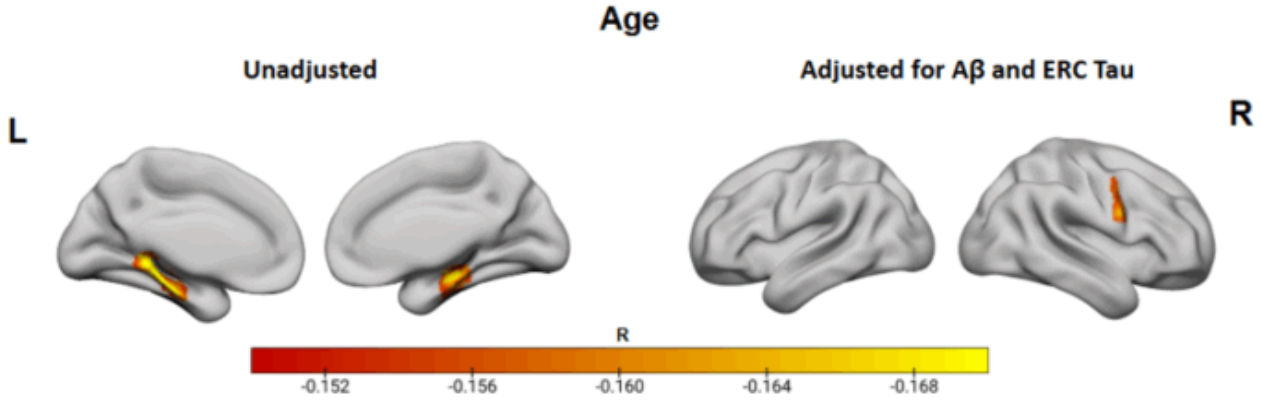


Figure 1 Effects of age on atrophy with and without adjusting for Aβ and ERC tau: Statistical voxel-wise r-maps of whole brain GM atrophy from multiple regression analyses of age, unadjusted and adjusted for Aβ and ERC tau. Clusters indicate regions where older age is associated with faster atrophy, i.e. the parahippocampal and right precentral cortices. All maps are thresholded at p voxel < 0.001, cluster k =100. *GM: Gray Matter. Aβ: Beta-Amyloid. ERC Tau: Entorhinal Tau.*

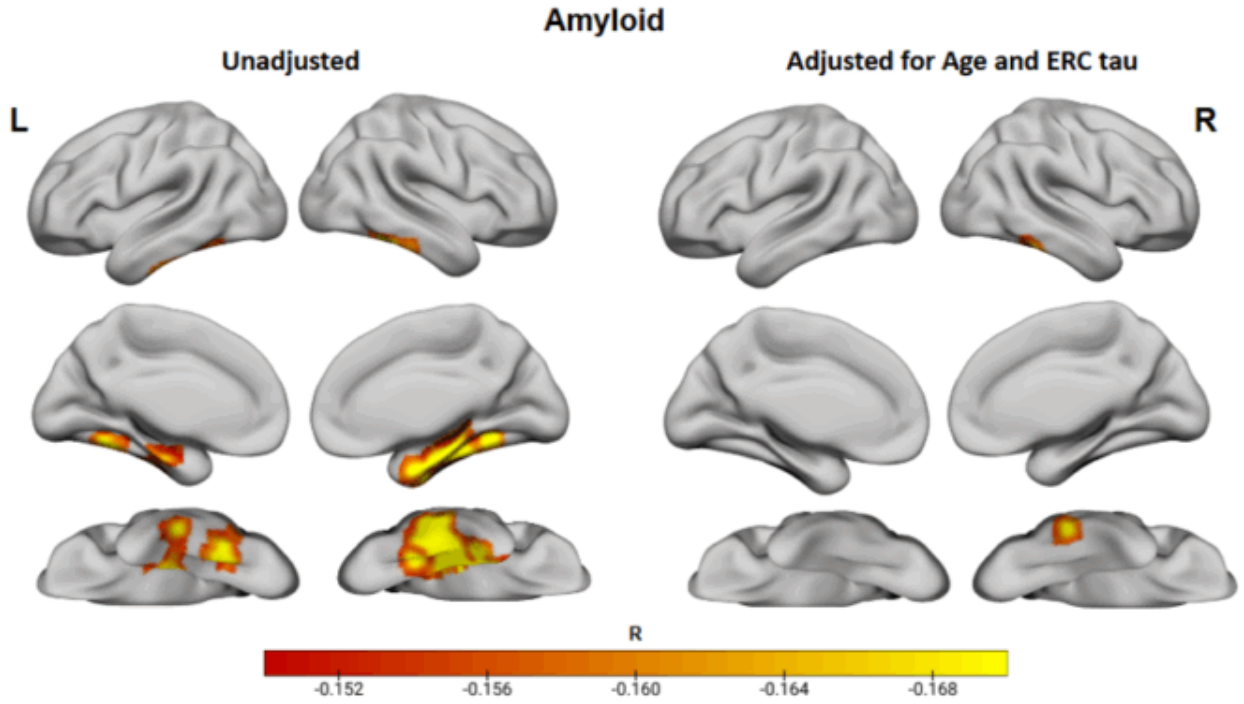


Figure 2 Effects of Aβ on atrophy with and without adjusting for age and ERC tau: Statistical voxel-wise r-maps of whole brain GM atrophy from multiple regression analyses of Aβ, unadjusted and adjusted for age and ERC tau. Clusters indicate regions where higher Aβ is correlated with faster atrophy, i.e. the parahippocampal, fusiform and inferior temporal gyri. All maps are thresholded at p voxel < 0.001, cluster k = 100. *GM: Gray Matter. Aβ: Beta-Amyloid. ERC Tau: Entorhinal Tau.*

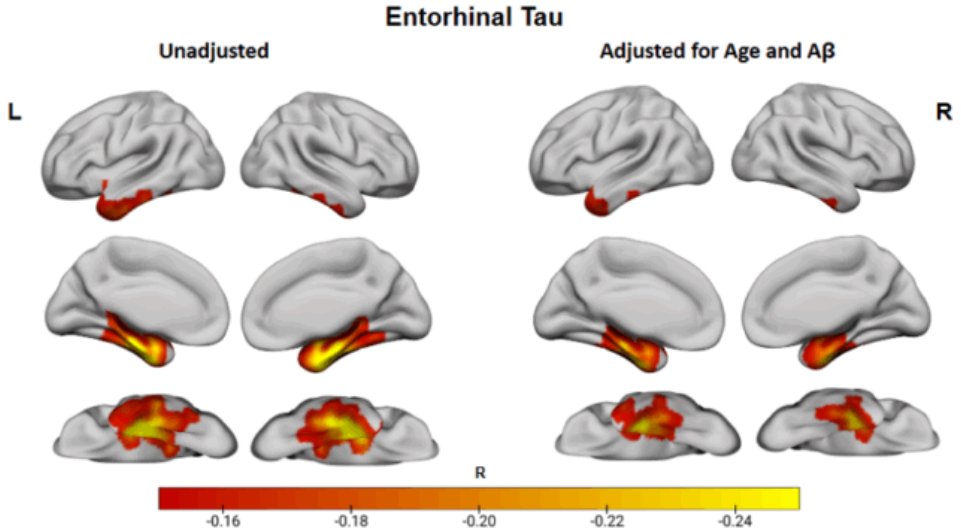


Figure 3 Effects of ERC tau on atrophy with and without adjusting for age and Aβ: Statistical voxel-wise r-maps of whole brain GM atrophy from multiple regression analyses of ERC tau, unadjusted and adjusted for age and Aβ. Clusters indicate regions higher ERC tau is associated with GM atrophy i.e. medial and lateral temporal lobes. All maps are thresholded at p voxel < 0.001, cluster k = 100. *GM: Gray Matter. Aβ: Beta-Amyloid. ERC Tau: Entorhinal Tau.*

Keywords: age, Aβ, tau

43 Stronger amyloid–tau coupling explains faster tau progression in early-onset Alzheimer's disease

Nicolai Franzmeier[1,2,3], Lukas Frontzkowski[1,4], Anna Steward[1], Madleen Klonowski[1], Anna Dewenter[1], Fabian Hirsch[1], Davina Biel[1], Zeyu Zhu[1], Johannes Gnörich[4], Günter Höglinger[2,5,6], Matthias Brendel[2,4], Sebastian N. Roemer-Cassiano[1,5]

[1]*1. Institute for Stroke and Dementia Research (ISD), LMU University Hospital, Ludwig-Maximilians-University (LMU) Munich, Germany, Munich, Germany*
[2]*2. Munich Cluster for Systems Neurology (SyNergy), Munich, Germany, Munich, Germany*
[3]*3. University of Gothenburg, The Sahlgrenska Academy, Institute of Neuroscience and Physiology, Department of Psychiatry and Neurochemistry, Mölndal and Gothenburg, Sweden, Gothenburg, Sweden*
[4]*4. Department of Nuclear Medicine, University Hospital, LMU Munich, Germany, Munich, Germany*
[5]*5. Department of Neurology, LMU University Hospital, Ludwig-Maximilians-University (LMU) Munich, Germany, Munich, Germany*
[6]*6. German Center for Neurodegenerative Diseases (DZNE), Munich, Germany, Munich, Germany*

Objectives: Early-onset Alzheimer's disease (EOAD), defined by symptom onset before age 65, shows more rapid tau accumulation and faster clinical progression than late-onset Alzheimer's disease (LOAD), yet the mechanisms remain unclear. Given that tau spreads along connected brain regions influenced by amyloid deposition, we hypothesized that stronger spatial and network-level amyloid–tau coupling drives faster tau propagation in EOAD.

Methods: We included 53 EOAD and 169 LOAD patients from ADNI with amyloid- and Flortaucipir tau-PET data, including 19 EOAD and 52 LOAD subjects with longitudinal tau-PET (mean follow-up=3.2±1.7 years). Amyloid and tau epicenters were defined as the top 20% and 5% of regions with highest baseline SUVRs, respectively. A normative resting-state fMRI-based connectome from 66 amyloid/tau negative controls was used to assess network-level amyloid–tau coupling.

Results: Global amyloid-PET did not differ between EOAD and LOAD (87.4±36.1 vs. 88.1±33.6 centiloids, p=0.92), whereas global tau-PET SUVRs were higher in EOAD vs. LOAD (1.46±0.42 vs. 1.24±0.23, p<0.001). Amyloid–tau coupling was stronger in EOAD, with higher amyloid associated with greater and faster tau accumulation globally and regionally (Fig.1). Earlier symptom onset related to shorter connectivity-based distances between amyloid and tau epicenters, indicating that tau emerges in regions more tightly connected to amyloid-affected areas, where a closer connectomic proximity of amyloid and tau epicenters predicted faster subsequent tau accumulation (Fig.2). Moreover, tau epicenters in EOAD showed higher local amyloid burden than those in LOAD, further promoting accelerated tau propagation (Fig.3). This suggests that increased co-localization of Aβ and tau may facilitate network-level tau dissemination

Conclusion: Stronger amyloid-tau coupling and shorter network distance between their epicenters are linked to faster tau propagation and earlier symptom onset, revealing that a closer amyloid-tau interplay may propel the more aggressive course of EOAD vs. LOAD.

Figure 1: Early onset AD is linked to stronger/faster amyloid-related tau aggregation

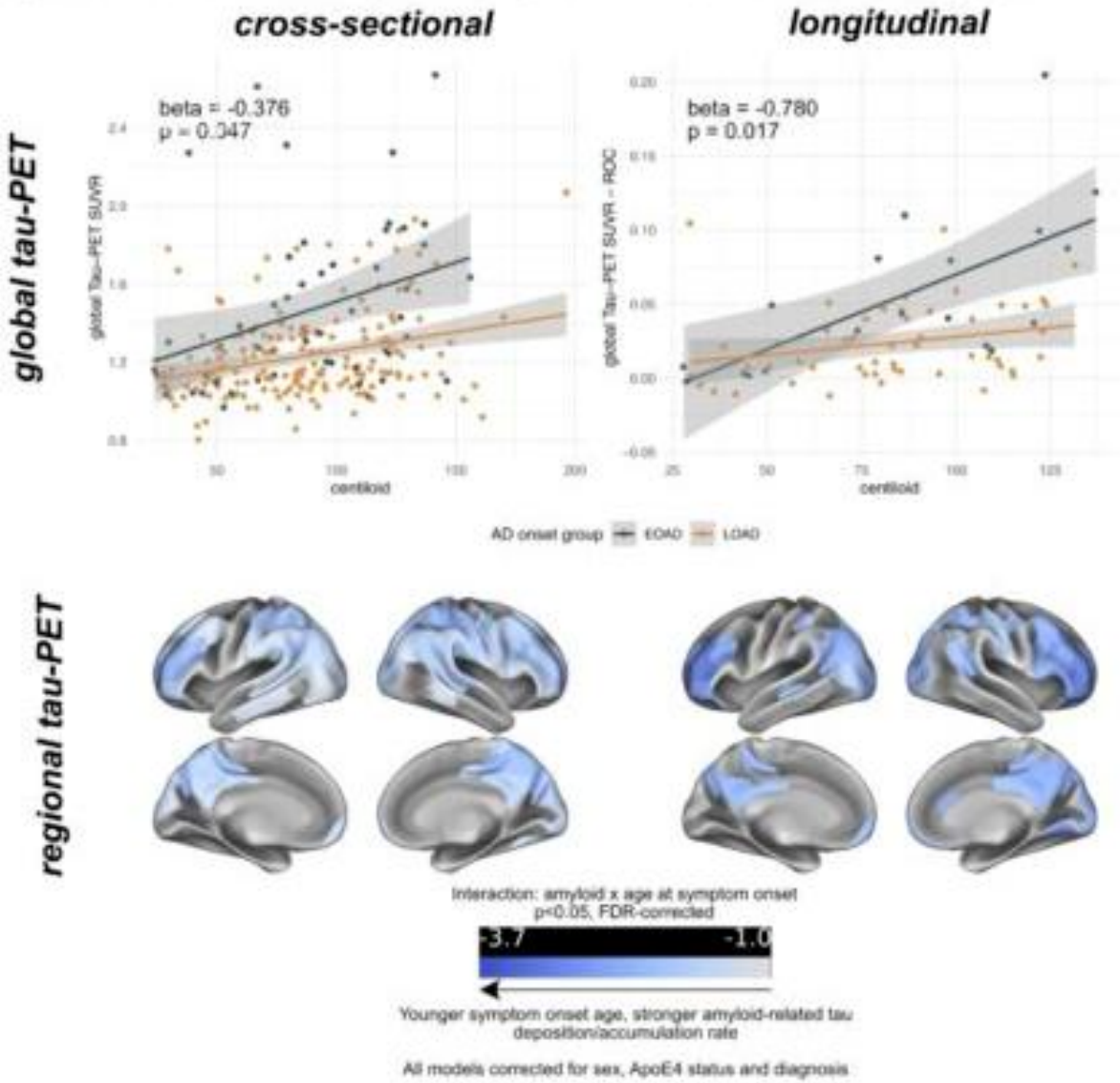


Figure 2: Younger age of symptom onset is linked to a closer connectivity-based proximity of amyloid and tau epicenters, leading to faster tau accumulation

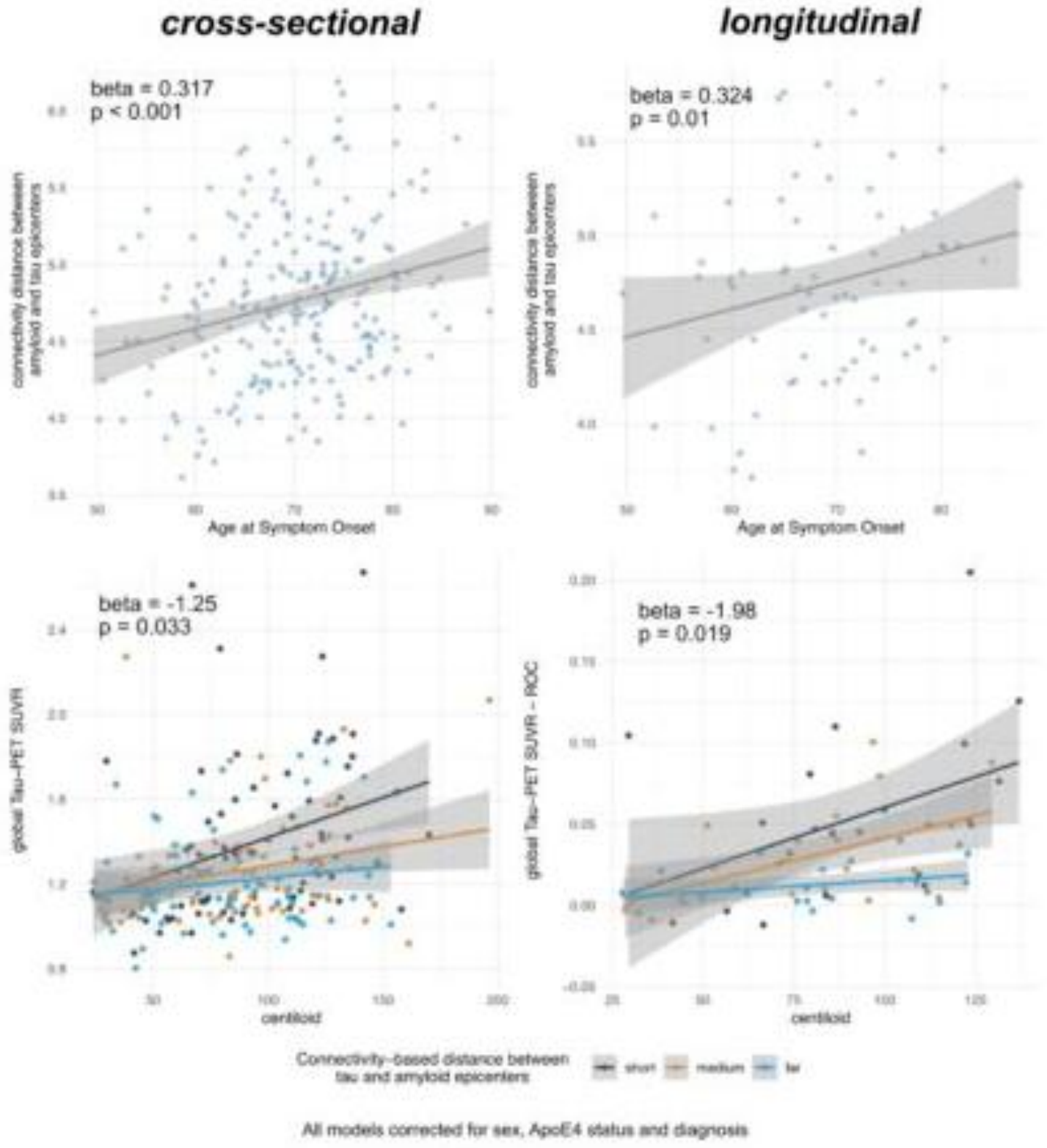
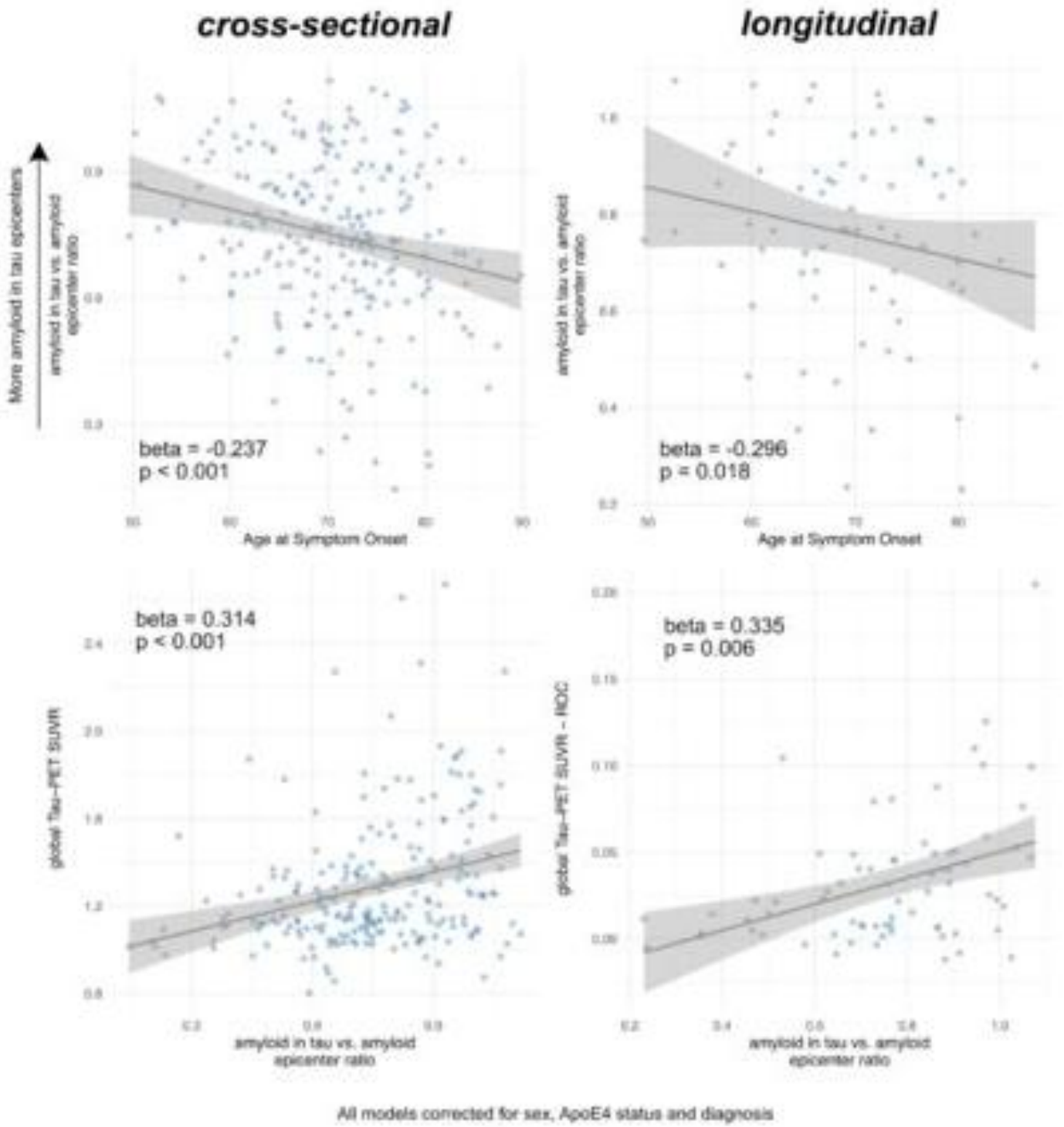


Figure 3: Younger age of symptom onset is linked to higher amyloid levels in tau epicenters, leading to faster tau aggregation



Keywords: Tau, Early Onset Alzheimer's disease, Late Onset Alzheimer's Disease, Amyloid, Brain Networks

44 Harmonization methods to mitigate batch effects in blood biomarker analysis

Vivian Zhang[1], Pamela Lukasewicz Ferreira[2], Davneet Minhas[3], Tharick Pascoal[2,4], Xuemei Zeng[2], Thomas Karikari[2], Ann Cohen[2], Dana Tudorascu[1,2]

[1]*Department of Biostatistics and Health Data Science, University of Pittsburgh School of Public Health, Pittsburgh, PA, US*
[2]*Department of Psychiatry, University of Pittsburgh School of Medicine, Pittsburgh, PA, US*
[3]*Department of Radiology, University of Pittsburgh School of Medicine, Pittsburgh, PA, US*
[4]*Department of Neurology, University of Pittsburgh School of Medicine, Pittsburgh, PA, US*

Introduction: The reproducibility of blood-based Alzheimer's disease biomarker measurements remains a challenge for translating them into clinical use. While efforts have been made to standardize data collection, guidelines to select harmonization methods to handle batch effects remain needed. In this study, we assessed the performance of several harmonization approaches for plasma p-tau217 measurements.

Methods: We evaluated six harmonization methods to account for technical variability due to different blood assays, including simple mean adjustment, marginal standardization, inverse-probability weighting, quantile regression, quantile normalization, and Z-score standardization. We implemented these methods in data from Alzheimer's Disease Neuroimaging Initiative (ADNI, n = 219) and the Human Connectome Project (HCP, n =77), an ancillary ADRC study. All participants from the ADNI cohort had p-tau217 levels from four different assays (ALZpath, Janssen, Fujirebio, and C2N), and all HCP participants had ALZpath, Janssen, Fujirebio, NULISA, and an In-house assay. We used linear mixed models (LMM) to test p-tau217 differences between the cognitively impaired and cognitively unimpaired groups before and after harmonization, controlling for assay and demographic variables.

Results: In the ADNI data (Table 1), the mean and standard deviation (SD) p-tau217 values ranged from 0.083 (0.055) using Janssen to 3.54 (2.66) using C2N assay before harmonization. The HCP data had similar evidence of batch effects (Table 2). Implementing each batch correction method resulted in more consistent means across assays. In the HCP data, LMM showed no significant difference between diagnostic groups (p=0.06) in the raw data but became significant after applying quantile regression (p=0.02), quantile normalization (p=0.02), or Z-score standardization (p=0.04) (Table 3). In both ADNI and HCP data, the estimate variability decreased using the quantile normalization method.

Conclusion: Our results show that quantile normalization outperformed all other methods. However, caution should be used in interpretation, given that quantile normalization uses ranking and may underestimate the variability.

Table 1: ADNI data

Harmonization Method	P-tau217 Levels (mean (SD))			
	ALZpath (n = 219)	Janssen (n = 219)	Fujirebio (n = 219)	C2N (n = 219)
Raw Data	0.579 (0.356)	0.0834 (0.0548)	0.284 (0.307)	3.54 (2.66)
Simple Means	1.12 (0.356)	1.12 (0.0548)	1.12 (0.307)	1.12 (2.66)
Marginal Standardization	1.13 (0.356)	1.13 (0.0548)	1.13 (0.307)	1.11 (2.66)
Inverse-Probability Weighting	1.13 (0.356)	1.13 (0.0548)	1.13 (0.307)	1.11 (2.66)
Quantile Regression	0.856 (0.937)	0.661 (0.811)	1.05 (1.68)	0.949 (1.26)
Quantile Normalization	1.12 (0.840)	1.12 (0.840)	1.12 (0.840)	1.12 (0.840)
Z-Score Standardization	2.57 (3.18)	1.83 (2.54)	3.96 (6.63)	2.37 (3.99)

Table 2: HCP data

Harmonization Method	P-tau217 Levels (mean (SD))				
	ALZpath (n = 77)	Janssen (n = 77)	Fujirebio (n = 77)	NULISA (n = 77)	In-House (n = 77)
Raw	0.421 (0.434)	0.0528 (0.0327)	0.257 (1.13)	12.6 (0.724)	29.4 (58.3)
Simple Means	8.53 (0.434)	8.53 (0.0327)	8.53 (1.13)	8.53 (0.724)	8.53 (58.3)
Marginal Standardization	8.53 (0.434)	8.53 (0.0327)	8.53 (1.13)	8.53 (0.724)	8.53 (58.3)
Inverse-Probability Weighting	8.53 (0.434)	8.53 (0.0327)	8.53 (1.13)	8.53 (0.724)	8.53 (58.3)
Quantile Regression	9.43 (20.3)	3.11 (4.20)	16.1 (86.5)	6.28 (9.94)	10.3 (28.4)
Quantile Normalization	8.54 (12.1)	8.54 (12.1)	8.55 (12.1)	8.54 (12.1)	8.54 (12.1)
Z-Score Standardization	0.289 (1.80)	0.0430 (0.843)	1.71 (11.7)	-0.0484 (0.931)	0.485 (2.67)

Table 3: Linear mixed model results

Method	Pre-Harmonization		Post-Harmonization	
	Estimate (SD)	p-value	Estimate (SD)	p-value
ADNI Data				
Simple	0.29 (0.12)	0.01	0.29 (0.12)	0.01
Marginal Standardization			0.29 (0.12)	0.01
Inverse-Probability Weighting			0.29 (0.12)	0.01
Quantile Regression			0.37 (0.15)	0.01
Quantile Normalization			0.30 (0.11)	0.01
Z-Score Standardization			1.26 (0.53)	0.02
HCP Data				
Simple	5.47 (2.89)	0.06	5.47 (2.89)	0.06
Marginal Standardization			5.47 (2.89)	0.06
Inverse-Probability Weighting			5.47 (2.89)	0.06
Quantile Regression			11.16 (4.62)	0.02
Quantile Normalization			4.35 (1.81)	0.02
Z-Score Standardization			1.28 (0.60)	0.04

Keywords: Blood biomarker, harmonization, batch effects, methodology

45 IGFR1, but not BDNF, acts as a suppressive neuroprotective factor between astrogliosis and visuospatial function among non-demented individuals

Laura Alejandra Ramirez Tirado[1], Ann D Cohen[2,3], Brian J Lopresti[4], Milos D Ikonomovic[3,5], Alexandra Gogola[4], Cristy Matan[4], Xuemei Zeng[2], Thomas K Karikari[2,3], Oscar L Lopez[3,5], C Elizabeth Shaaban[1,3], Victor L Villemagne[2,3]

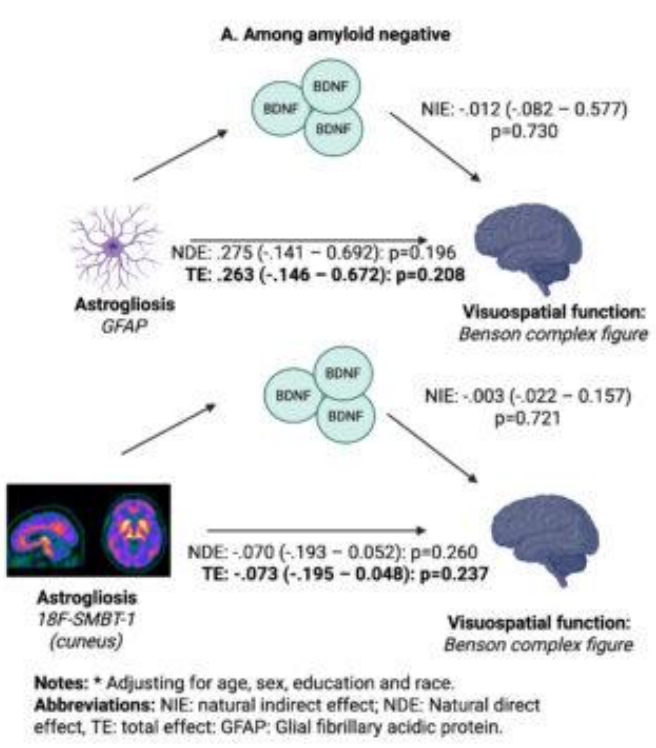
[1]*Department of Epidemiology, University of Pittsburgh, Pittsburgh, PA, US*
[2]*Department of Psychiatry, School of Medicine, University of Pittsburgh, Pittsburgh, PA, US*
[3]*Alzheimer's Disease Research Center, University of Pittsburgh, Pittsburgh, PA, US*
[4]*Department of Radiology, University of Pittsburgh, Pittsburgh, PA, US*
[5]*Department of Neurology, University of Pittsburgh, Pittsburgh, PA, US*

Background: Astrogliosis, as assessed by plasma levels of glial fibrillary acidic protein (GFAP), associates with worse cognition in the population of non-demented individuals. Compared to ubiquitous expression of GFAP, reactive astrocytes surrounding classic Ab plaques upregulate monoamine oxidase B. Thus, the novel MAO-B selective PET radiotracer ^{18}F-SMBT-1 could be a more specific biomarker of Alzheimer's disease (AD) pathology-relevant astrogliosis. Whether neuroprotective growth factors could modify the effects of AD neuropathology, including astrogliosis, on cognitive impairment is not known. Our study explored whether the association between astrogliosis and cognition was mediated either by BDNF or IGFR1.

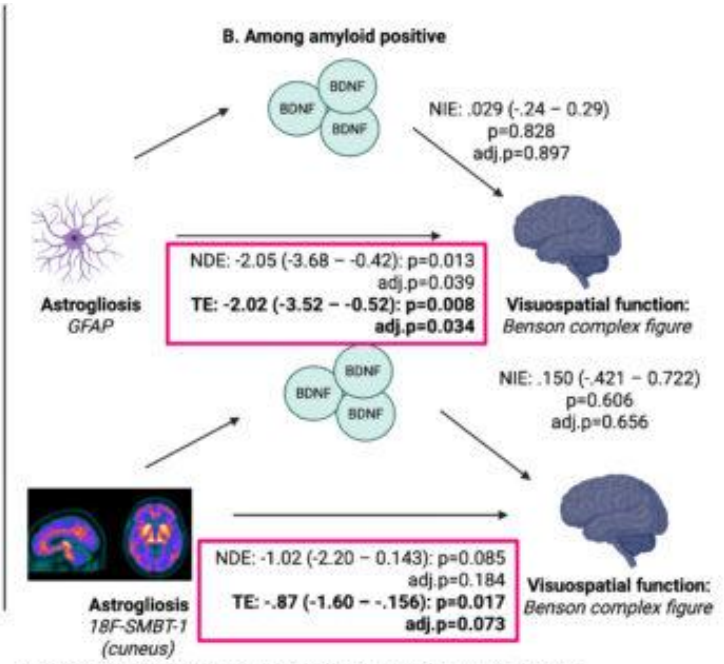
Methods: We evaluated the relationship between astrogliosis (via plasma GFAP and ^{18}F-SMBT-1 PET) as to overall cognition and domain-specific cognitive performance among non-demented participants. ^{11}C-PiB and ^{18}F-SMBT-1 were used for PET imaging of Ab load and astrogliosis, respectively. NULISAseq CNS disease panel measured plasma levels of BDNF and IGFR1. We used multivariable robust linear regression models to examine the relationship between astrogliosis and cognition. To address the effects of BDNF and IGFR1 on this relationship we ran causal mediation analyses stratified by PET Ab status (A-/A+).

Results: Ninety-four non-demented participants (age: 68±7yrs., 52%women) included 76 A- and 18 A+ individuals. Groups did not differ by demographic characteristics. Of the 22 brain regions assessed for ^{18}F-SMBT-1, only precuneus showed a higher SUVR among non-demented A+. Both plasma GFAP and ^{18}F-SMBT-1 PET were associated with worse visuospatial function but only in A+ individuals. Lastly, IGFR1 but not BDNF had a suppressive effect on the association of ^{18}F-SMBT-1 astrogliosis with worse visuospatial function, but only among A+ individuals.

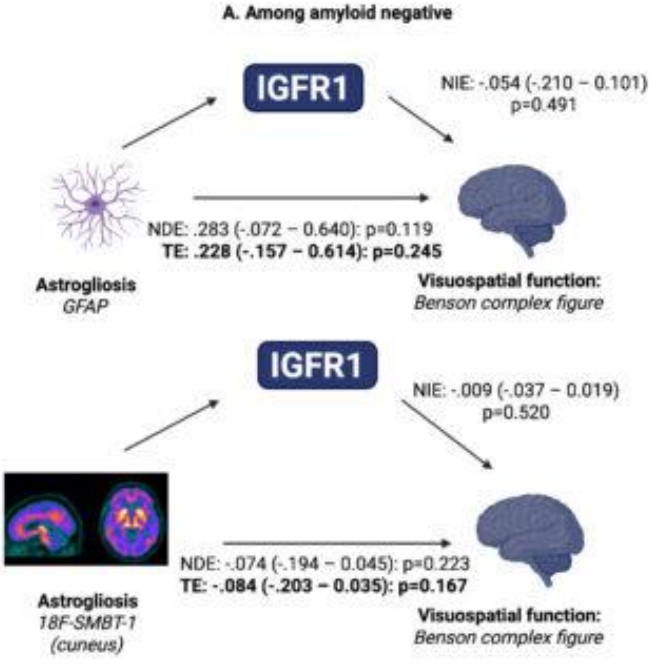
Conclusion: This biomarker study suggests that astrogliosis is related to worse visuospatial function in nondemented A+ individuals. IGFR1 may play a neuroprotective role by suppressing the effects of Aβ-related astrogliosis on visuospatial function.



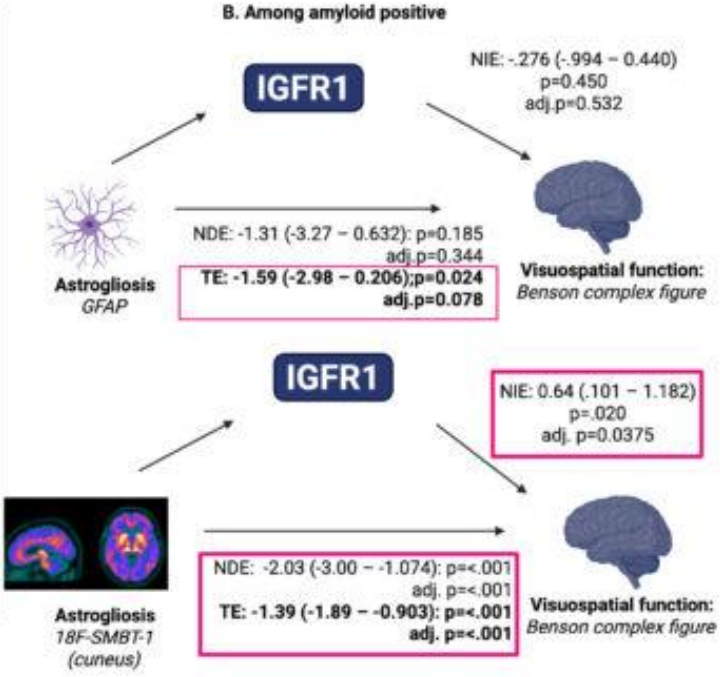
Notes: * Adjusting for age, sex, education and race.
Abbreviations: NIE: natural indirect effect; NDE: Natural direct effect, TE: total effect: GFAP: Glial fibrillary acidic protein.



Notes: * Adjusting for age and education. **Abbreviations:** NIE: natural indirect effect; NDE: Natural direct effect, TE: total effect: GFAP: Glial fibrillary acidic protein. Adjusted p-values for multiple comparisons w/ Benjamini-Hochberg method.



Notes: * Adjusting for age, sex, education and race.
Abbreviations: NIE: natural indirect effect; NDE: Natural direct effect, TE: total effect: GFAP: Glial fibrillary acidic protein.



Notes: * Adjusting for age and education. **Abbreviations:** NIE: natural indirect effect; NDE: Natural direct effect, TE: total effect: GFAP: Glial fibrillary acidic protein. Adjusted p-values for multiple comparisons w/ Benjamini-Hochberg method.

Keywords: BDNF, IGFR1, biomarker, astrogliosis, 18F-SMBT-1

46 The relation of psychosocial coping mechanisms to ATN pathophysiology differ across demographics

Brooke Schatz[1], Beth Snitz[2,4], Rebecca Roush[1], Brian Lopresti[3], Victor Villemagne[1,2], Oscar Lopez[2,4], Lilcelia Williams[1,2], Ann Cohen[1,2]

[1]*University of Pittsburgh Department of Psychiatry, Pittsburgh, PA, US*
[2]*University of Pittsburgh Alzheimer's Disease Research Center, Pittsburgh, PA, US*
[3]*University of Pittsburgh Department of Neurology, Pittsburgh, PA, US*
[4]*University of Pittsburgh Department of Radiology, Pittsburgh, PA, US*

Background: Existing data indicate that demographic, social, and environmental factors influence imaging pathology differences, and exploration of how these factors vary across racialized older adults is vital to uncover the mechanism of differences.

Methods: 130 participants (50-86 years of age, 73.8% female, 23.8% African American (AA), 76.2% non-Hispanic white (NHW) from the CoBRA study underwent ATN neuroimaging and a battery of standardized cognitive and psychosocial assessments. Participants received [11C]PiB for A, [18F]MK6240 for T, 3T MRI for N. FreeSurfer v5.3 was used to define regions-of-interest.

Results: AA and NHW participants did not differ significantly in age with a mean age of 67 and 66 years respectively, or education. Consistent with previous findings, the frequency of amyloid positivity was higher in the non-Hispanic white population (41/99, 41.4%) than the African American population (5/31, 16.1%). The full group displays a correlation trend between higher COPE and global PiB SUVR (r^2 = 0.0282, p = 0.056). Further dissection revealed this trend is driven by the AA group (r^2 = 0.188, p = 0.015), while the NHW group displays no correlation (r^2 = 0.0073, p = 0.3997). Additionally, the mean COPE score for the amyloid positive group (n = 36, mean = 25.7) is higher than the mean score of the amyloid negative group (n = 94, mean = 22.8). No relations were observed with T or N measures and COPE.

Conclusions: These data support the conclusion that amyloid staging differs across racialized groups and that a complex series of psychosocial factors, including coping strategies are involved. Further, these data suggest a potential compounding effect of psychosocial stress and pathology that warrants further interrogation, particularly to understand differences in the types of specific coping responses used by a diverse array of individuals.

Keywords: Social factors, racial differences, cognitive resilience

47 Evaluation of the Clinical IMpact of Blood-Based Biomarker Assays on dementia specialists' decision-making (CIMBBBA): Preliminary report from a real-world dementia subspecialty clinic study

Mark Eldaief[1,2,3,4,5,6], Erin Krahn[1], Sam Murdock[1], Neguine Rezaii[1,2], Diane Chan[1,2], Steven Arnold[2,4], Marina Avetisyan[2], Liliana Ramirez Gomez[2,4], Seth Gale[7], Scott McGinnis[1,7], Bradford Dickerson[1,2,3,4,5]

[1]*Frontotemporal Disorders Unit, Department of Neurology, Massachusetts General Hospital and Harvard Medical School, Boston, MA, US*
[2]*Memory Disorders Unit, Department of Neurology, Massachusetts General Hospital and Harvard Medical School, Boston, MA, US*
[3]*Athinoula A. Martinos Center for Biomedical Imaging, Massachusetts General Hospital, Charlestown, MA, US*
[4]*4Alzheimer's Disease Research Center, Massachusetts General Hospital, Charlestown, MA, US*
[5]*5Department of Psychiatry, Massachusetts General Hospital and Harvard Medical School, Charlestown, MA, US*
[6]*Center for Brain Science, Harvard University, Cambridge, MA, US*
[7]*Center for Brain Mind Medicine, Department of Neurology, Brigham & Women's Hospital and Harvard Medical School, Boston, MA, US*

Blood-based biomarkers (BBBs) for the diagnosis of Alzheimer's disease are increasingly being used in clinical contexts. Here, we evaluated two commercially available BBBs in our diagnostic workflow to determine their role in clinicians' decision-making and with validation against gold standard testing.

Clinicians were offered the opportunity to order the Lucent ptau217 assay and/or the LucentAD Complete panel as standard sendout labs for their clinic patients. Clinicians served as research subjects. Prior to and after learning the results of the test(s), clinicians completed forms detailing their differential diagnoses and their plans for testing and treatment.

131 patients (70 with MCI and 61 with dementia) were tested. Lucent ptau 217 was obtained on 123 cases and LucentAD Complete on 47 cases; 39 cases had both. Compared against gold-standard biomarkers, plasma ptau217 demonstrated a true positive rate of 70/73 (96%) and a true negative rate of 18/23 (78%). Results were intermediate for 27 cases (21%). Plasma LucentAD Complete demonstrated a true positive rate of 24/26 (92%) and a true negative rate of 11/13 (85%). Results were intermediate for 8 cases (17%). For 24 cases in which both biomarkers were obtained, and neither was intermediate, results were 100% convergent. For 15 cases in which p tau217 was intermediate, LucentAD Complete resolved 66%, producing a true negative or true positive result in 9, a false positive in 1, and an intermediate result in 5. For 4 cases in which LucentAD Complete produced an intermediate result, ptau217 resolved 25%, producing a true negative in 1 and an intermediate result in 3. Clinician decision-making data are currently being analyzed.

Consistent with published reports, we found that both the Lucent ptau217 assay and the LucentAD Complete panel were highly sensitive and specific for detecting likely AD pathologic changes when measured against widely accepted gold standard AD biomarkers.

Keywords: Blood based biomarkers, Alzheimer's disease, ptau217, clinician decision making

48 Dynamic interplay of vascular injury and inflammation on Alzheimer's disease pathophysiology

Naila Rusdi[1], Min Su Kang[1], Eric Yin[1], Erin Gibson[1], Nesrine Rahmouni[2], Andrea Benedet[5], Henrik Zetterberg[5], Kaj Blennow[5], Thomas Karikari[6], Nicholas Ashton[7], Sandra Black[1,4], Pedro Rosa-Neto[2], Maged Goubran[1,3], Julie Ottoy[1,4]

[1]*Centre for Brain Resilience & Recovery, Hurvitz Brain Sciences Program, Sunnybrook Research Institute, University of Toronto, Toronto, ON, Canada*
[2]*Translational Neuroimaging laboratory, McGill Centre for Studies in Aging, McGill University, Montreal, QC, Canada*
[3]*Department of Medical Biophysics, University of Toronto, Toronto, ON, Canada*
[4]*Department of Medicine (Neurology), University of Toronto, Toronto, ON, Canada*
[5]*Department of Psychiatry and Neurochemistry, The Sahlgrenska Academy at the University of Gothenburg, Gothenburg, Sweden*
[6]*Department of Psychiatry, University of Pittsburgh School of Medicine, Pittsburgh, PA, US*
[7]*Banner Alzheimer's Institute, Phoenix, AZ, US*

Introduction: Cerebrovascular injury and neuroinflammation are critical contributors to Alzheimer's disease (AD) progression. However, their joint effects on amyloid and tau pathology remain unclear. We investigated whether central and peripheral inflammatory markers interact with vascular injury markers to predict amyloid and tau burden.

Methods: We included 206 participants from the TRIAD cohort: 99 cognitively normal amyloid-negative (CN Aβ–), 30 CN Aβ+, 19 MCI/AD Aβ–, and 58 MCI/AD Aβ+. Amyloid and tau were quantified using 18F-NAV4694 and 18F-MK6240 PET SUVR. Vascular injury was measured as white matter hyperintensity (WMH) and MRI-visible perivascular space (PVS) volumes. Inflammation was measured using white matter imaging (11C-PBR28 PET and free-water diffusion-MRI) or fluid (CSF YKL-40, CSF sTREM2, and plasma GFAP). Linear regressions tested interaction effects between vascular and inflammatory markers on lobar amyloid and tau SUVR (summarized in **Figure 1**), adjusting for age, sex, and APOE-ε4 status.

Results: We observed a positive interaction effect between brain vascular injury and inflammation on tau but a negative interaction effect on amyloid. Specifically, fronto-parieto-temporal tau SUVR was associated with higher PVS, only in individuals with high inflammation (**Figure 2A**). Similarly, occipital tau SUVR was associated with higher posterior WMH, only in individuals with high inflammation. Conversely, amyloid SUVR was associated with high PVS or WMH, only in individuals with low (but not high) inflammation (**Figure 2B**). APOE-ε4 further modified these effects: three-way interactions between APOE-ε4 status, PVS, and free-water on tau suggested stronger vascular–tau associations among APOE-ε4 carriers with greater inflammation.

Conclusions: Brain vascular injury and inflammation interact differently on amyloid vs tau pathology. The interaction effects on tau pathology were found in APOE-ε4 carriers but not in non-carriers. These findings suggest an (APOE4-dependent) immuno–vascular interplay that shapes AD pathophysiology, and highlight the critical need for stratified intervention strategies.

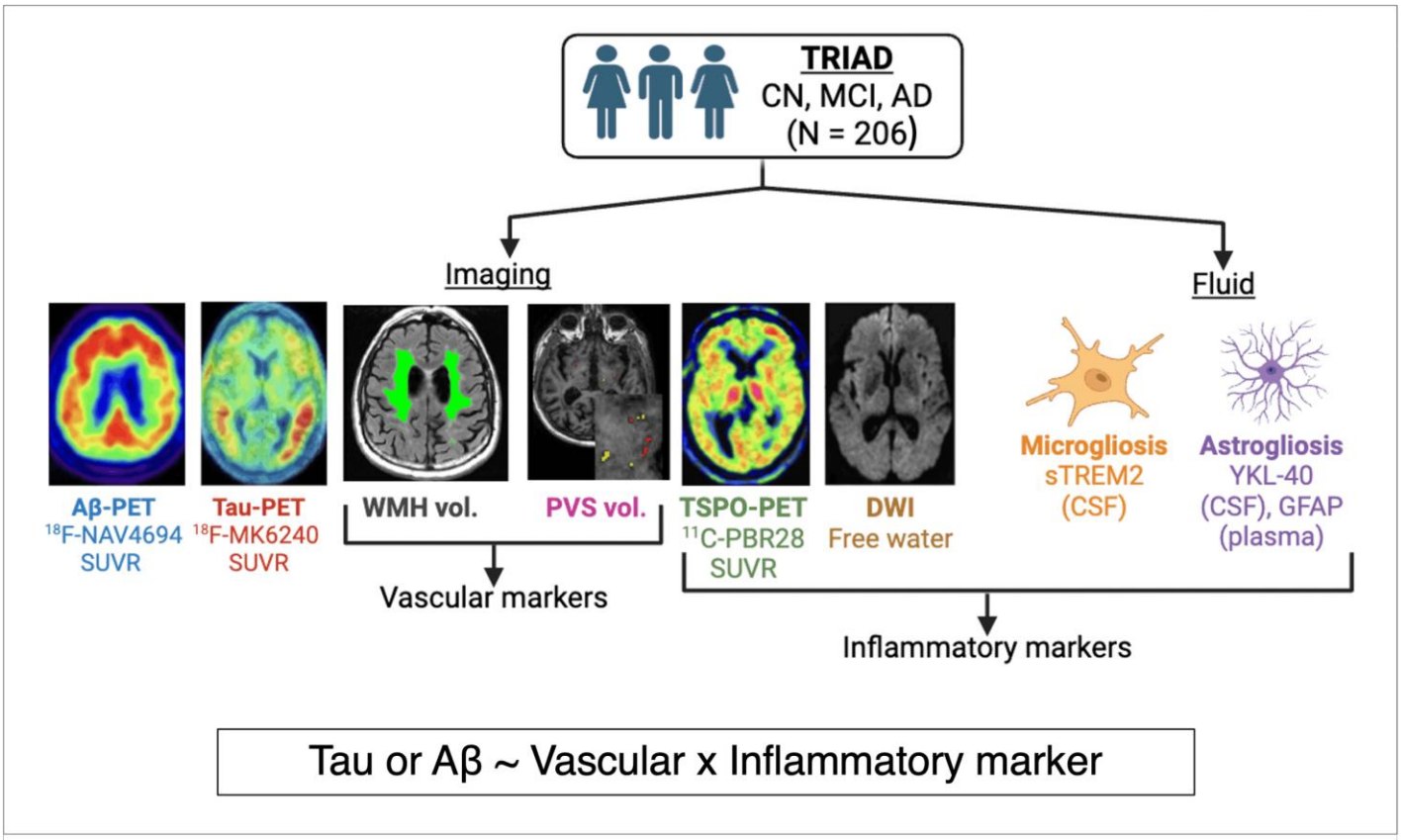


Figure 1. Overview of included imaging and fluid markers

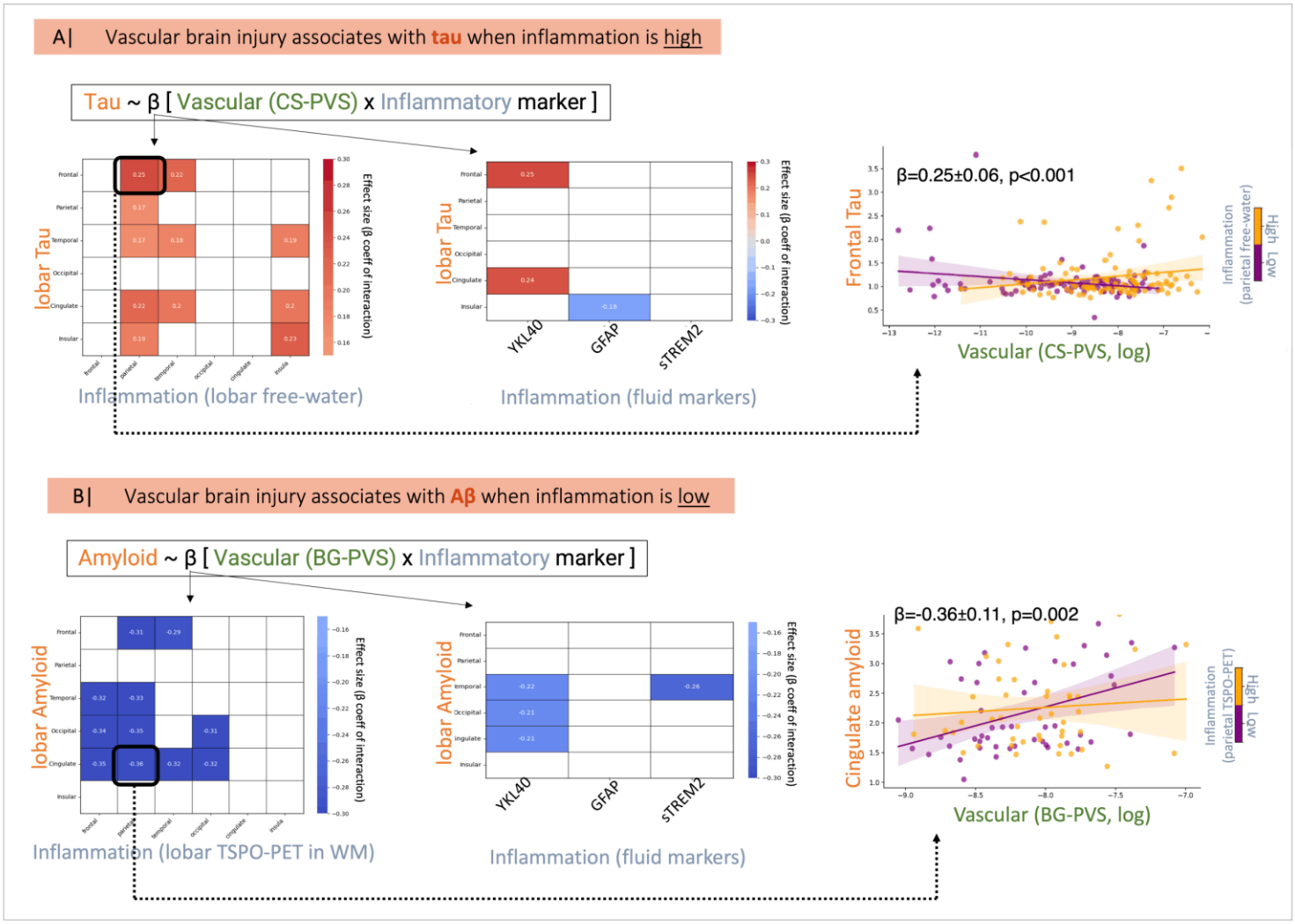


Figure 2. Interaction effects between vascular and inflammatory markers on tau (panel A) and amyloid (panel B).
The heatmaps represent the effect size (standardized beta coefficient) of the interaction effect between a vascular marker (PVS) and an inflammatory imaging (left panel) or fluid (middle panel) marker on lobar tau (panel A) or amyloid (panel B). Red and blue indicate positive and negative interaction effects, respectively. White cells in the heatmaps reflect models that did not survive FDR correction (Bonferroni P<0.008 across 6 ROIs).The left figure of both panels displays the interaction effect by classifying individuals into high (yellow) versus low (purple) inflammation groups for a given model.
Abbreviations: BG-PVS, basal ganglia MR-visible perivascular space volume; CS-PVS, centrum semiovale MR-visible perivascular space volume

Keywords: Alzheimer's disease, Vascular disease, Neuroimaging, Inflammation, Tau

Monday, January 12, 2026 - 11:30 am - 01:00 pm

Podium Session

SESSION II: Tau pathology: In vivo and postmortem measurements

CHAIRS:

***Bradley Christian**, University of Wisconsin-Madison, Madison, WI, USA*

***Melissa Murray**, Mayo Clinic, Jacksonville, FL, USA*

Monday, January 12, 2026			
11:30 am – 01:00 pm	**Podium Presentation**	**Authors**	**Presenters**
11:35 am – 11:50 am	The effects of 18F-MK-6240 PET extracerebellar off-target signal on the cerebellum and its substructures	Chen | Fu | Tiss | Slade | Thibault | Johnson | Price	**Charles Chen**, Athinoula A. Martinos Center for Biomedical Imaging, Charlestown, MA, US
11:50 am – 12:05 pm	Examining spatial relationships between ex-vivo flortaucipir retention and TMEM106b protein expression in a subset of neuropathologically confirmed frontotemporal lobar degeneration cases with TAR DNA-binding protein 43 pathology	Gatto | Uruk | Youssef | Hossain | Reichard | Lowe | Whitwell | Josephs	**Rodolfo Gatto**, Department of Neurology, Mayo Clinic, Rochester, MN, US
12:05 pm – 12:20 pm	Hypometabolism and atrophy patterns associated with advanced primary age-related tauopathy mimicking early-stage AD	Silva-Rodríguez | Moscoso | Karagianni | Vourkas | Labrador-Espinosa | Sanchez-Juan | Schöll | Grothe	**Jesús Silva-Rodríguez**, CIEN Foundation, Madrid, Spain
12:20 pm – 12:35 pm	Differential age- and Aβ-related tau-PET patterns between [18F]FTP and [18F]MK6240	Tissot | Tsai | Maboudian | Fonseca | Rahmouni | Lussier | Therriault | Trudel | Cassa Macedo | Stevenson | Bellaver | Ferreira | Povala | Gordon | Pascual | Lowe | Soleimani-Meigooni | Oh | Klunk | Rosa-Neto | Jagust | Pascoal | Baker	**Cécile Tissot**, Lawrence Berkeley National Laboratory, Berkeley, CA, US

The effects of 18F-MK-6240 PET extracerebellar off-target signal on the cerebellum and its substructures

Charles Chen[1], Jessie Fanglu Fu[1], Amal Tiss[2], Elliott Slade[2], Emma Thibault[2], Keith Johnson[2], Julie Price[1]

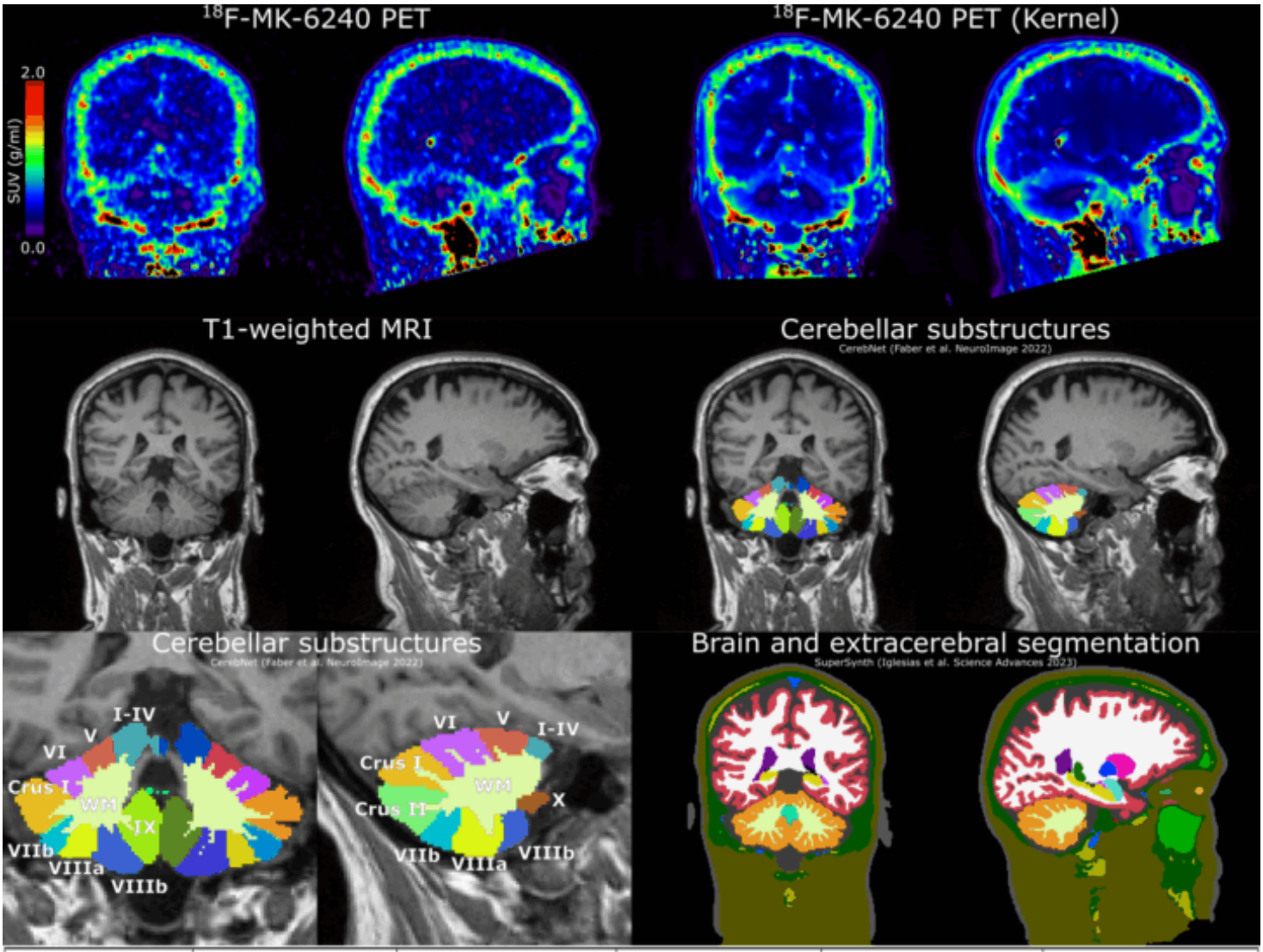
[1]*Athinoula A. Martinos Center for Biomedical Imaging, Charlestown, MA, US*
[2]*Gordon Center for Medical Imaging, Boston, MA, US*

Background: ^{18}F-MK-6240 PET is a second-generation tau PET radioligand that promises improved quantification of Alzheimer's disease (AD) tauopathy. However, ^{18}F-MK-6240 off-target signal (OTS) can confound tau quantification by spilling into cerebellar reference regions. Herein, we apply a novel evaluation of which cerebellar substructures are least affected by extracerebellar OTS.

Methods: We applied CerebNet (Faber et al. NeuroImage 2022) to segment 27 cerebellar substructures from T1-weighted MRIs in 118 participants and used these to extract SUVRs (standardized uptake value ratios, cerebellar cortex reference region) from ^{18}F-MK-6240 PET images (Figure 1). Extracerebellar tissues were segmented by dilating substructures by a 2-mm cube and excluding the original cerebellum, and labeled using SuperSynth (Iglesias et al. Science Advances 2023). We compared results from ^{18}F-MK-6240 PET images reconstructed by traditional ordered subset expectation maximization (OSEM) and by kernel-based reconstruction (Gong et al. IEEE Trans Med Imaging 2018).

Results: ^{18}F-MK-6240 signal differs across cerebellar substructures (linear mixed-effects model: $F(26,3042)=277.94$, $p<2.2\times10^{-16}$, partial-$\eta^2=0.66$), with lobule IX having the lowest signal in cerebellar cortex, but higher signal than cerebellar white matter; these differences are also present in kernel-reconstructed images ($F(26,3042)=204.27$, $p=2.2\times10^{-16}$, partial-$\eta^2=0.64$), suggesting that kernel reconstruction does not reduce extracerebellar OTS spill-in (Figure 2). More superior substructures have higher ^{18}F-MK-6240 signal than adjacent extracerebellar tissues, which include meninges and CSF (relatively low OTS), and more inferior substructures have lower signal than adjacent tissues, which include meninges, CSF and bone (relatively high OTS); the exception is lobule IX and adjacent tissues, which show no appreciable difference in signal (Figure 3).

Conclusion: Lobule IX is the cerebellar cortex substructure with the lowest ^{18}F-MK-6240 signal and is not adjacent to high-OTS tissues; thus, it may be least affected by OTS spill-in. Future work will investigate whether a lobule IX reference region will improve ^{18}F-MK-6240 PET quantification of tau burden.



	CN (n=98)	CN/SCC (n=2)	MCI (n=15)	AD (n=3)	Total (n=118)
Age	67.40 ± 9.89	59.25 ± 6.72	72.50 ± 8.73	69.67 ± 12.29	67.97 ± 9.87
Female Sex	59 (60%)	1 (50%)	4 (27%)	1 (33%)	65 (55%)
MMSE	28.48 ± 1.42	27.50 ± 2.12	24.53 ± 4.22	20.00 ± 6.24	27.75 ± 2.80
Aβ positive	27 (28%)	0 (0%)	11 (73%)	2 (67%)	40 (34%)

Figure 1: Exemplar ^{18}F-MK-6240 PET images and cerebellar segmentation. Top row: Coronal and sagittal views of an OSEM-reconstructed ^{18}F-MK-6240 PET SUV image (left) and its corresponding kernel-reconstructed ^{18}F-MK-6240 PET SUV image (right) from a 54-year-old male participant with low cerebellar but high extracerebellar ^{18}F-MK-6240 uptake and no cognitive impairment. Second row: Coronal and sagittal views of a T1-weighted MR image (left) and its corresponding cerebellar substructure segmentation (right) using CerebNet (Faber et al. NeuroImage 2022) from the same participant. Third row: Coronal and sagittal views of the cerebellar substructure segmentation in detail (labels correspond to right hemisphere cerebellar substructures) and a brain and extracerebral segmentation using SuperSynth (right, Iglesias et al. Science Advances 2023). Bottom row: Participant demographics. Notes: Participants are enrolled in the Harvard Aging Brain Study 2 (HABS-2). Aβ positivity is classified as having a ^{11}C-PiB PET FLR DVR greater than 1.15 (or Centiloid greater than 19.1). Three CN participants have unknown Aβ positivity. Abbreviations: Aβ=amyloid-β, AD=Alzheimer disease, CN=cognitively normal, DVR=distribution volume ratio, FLR=frontal, lateral temporal, parietal, and retrosplenial cortices, MCI=mild cognitive impairment, MMSE=Mini-Mental State Examination, SCC=subjective cognitive complaints.

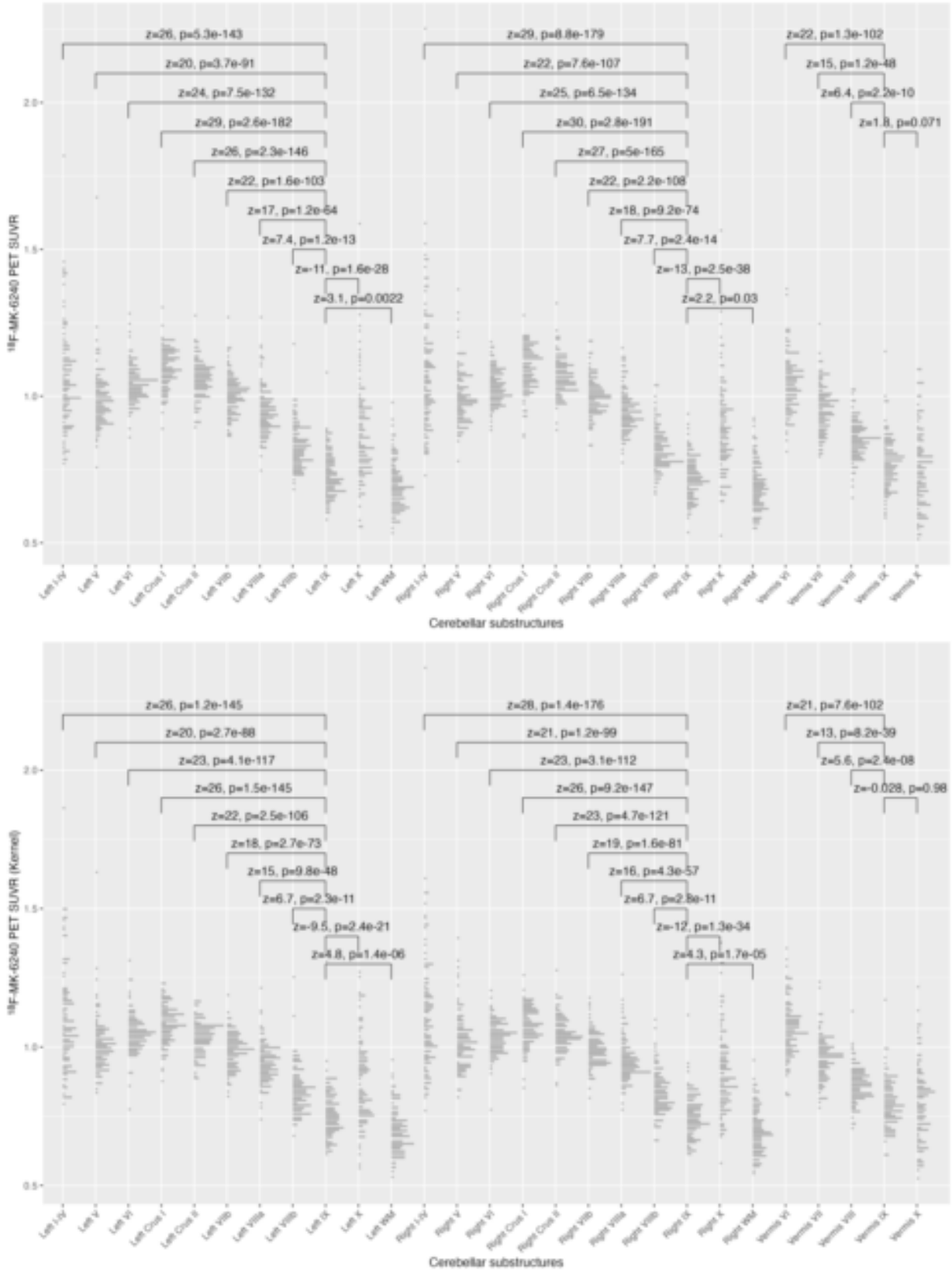


Figure 2: ^{18}F-MK-6240 PET signal across cerebellar substructures. Top: ^{18}F-MK-6240 PET SUVR across cerebellar substructures. Bottom: Kernel-reconstructed ^{18}F-MK-6240 PET SUVRs across cerebellar substructures. Notes: Cerebellar substructures are listed from left to right starting with left hemisphere substructures, then right hemisphere substructures, then vermis substructures. Within each hemisphere or vermis, substructures are listed roughly from the superior to the inferior aspect of the cerebellum. The estimated marginal means of cerebellar substructures in each hemisphere or vermis are compared to their corresponding lobule IX substructure in a pairwise manner after the initial fit to a linear mixed-effects model; z-ratios and p-values (FDR-controlled) are reported.

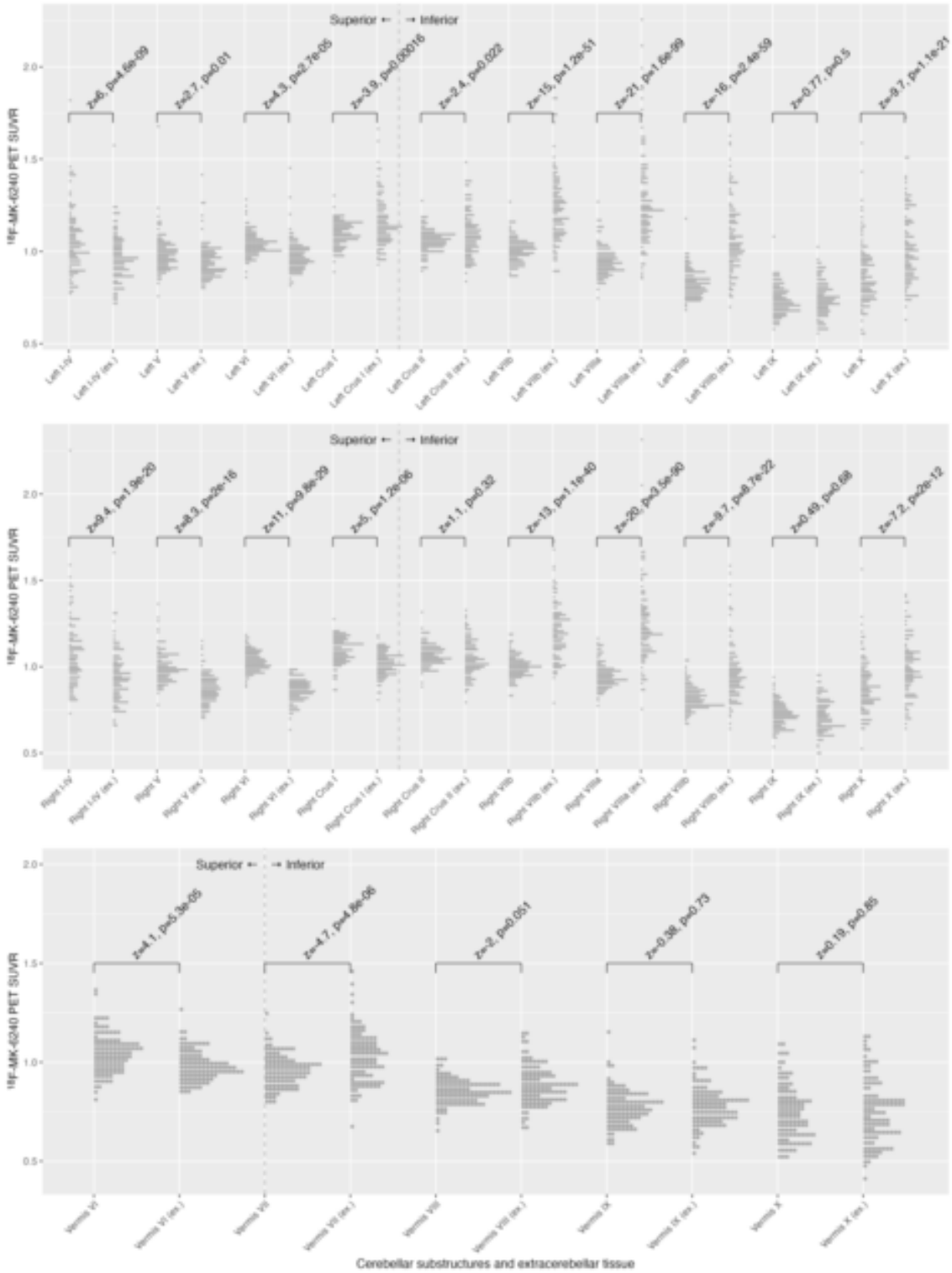


Figure 3: ^{18}F-MK-6240 PET signal across cerebellar substructures and their adjacent extracerebellar tissues. Top: ^{18}F-MK-6240 PET SUVRs across left hemisphere cerebellar substructures and adjacent extracerebellar tissues. Middle: ^{18}F-MK-6240 PET SUVRs across right hemisphere cerebellar substructures and adjacent extracerebellar tissues. Bottom: ^{18}F-MK-6240 PET SUVRs across vermis cerebellar substructures and adjacent extracerebellar tissues. Notes: Within each hemisphere or vermis, substructures are listed roughly from the superior to the inferior aspect of the cerebellum. The horizontal fissure separates superior from inferior cerebellar substructures, and its location is represented as a dashed vertical line. The estimated marginal means of cerebellar substructures and adjacent extracerebellar tissues are compared in a pairwise manner after the initial fit to a linear mixed-effects model; z-ratios and p-values (FDR-controlled) are reported. Abbreviations: ex.=extracerebellar tissue.

Keywords: 18F-MK-6240 PET, extracerebellar off-target signal, cerebellar substructures, kernel-based reconstruction, deep-learning tissue segmentation

Examining spatial relationships between ex-vivo flortaucipir retention and TMEM106b protein expression in a subset of neuropathologically confirmed frontotemporal lobar degeneration cases with TAR DNA-binding protein 43 pathology

Rodolfo G. Gatto[1], Gokhan Uruk[1], Hossam Youssef[1], Nadia Hossain[1], R. Ross Reichard[3], Val J. Lowe[2], Jennifer W. Whitwell[2], Keith A. Josephs[1]

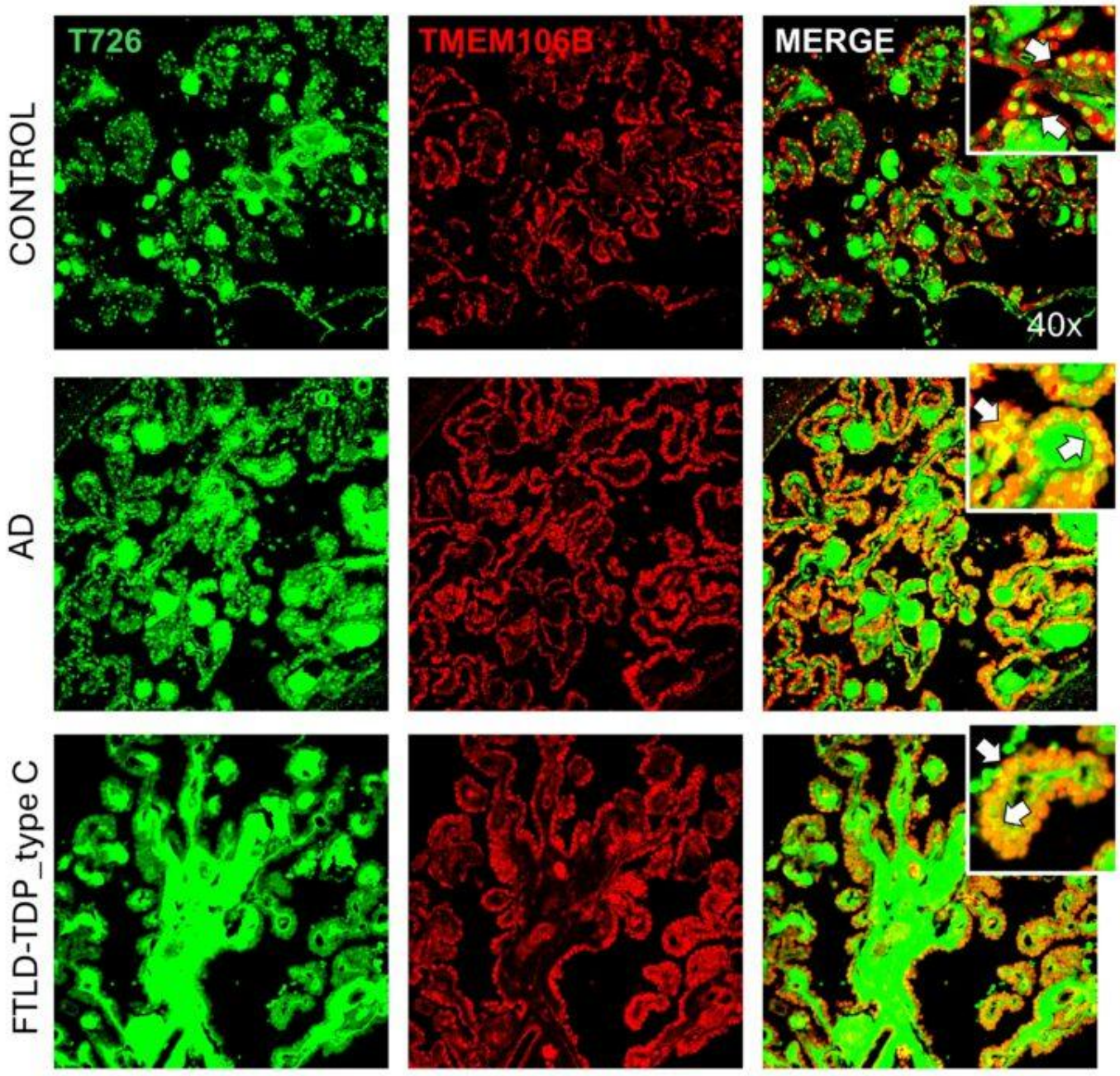
[1]*Department of Neurology, Mayo Clinic, Rochester, MN, US*
[2]*Department of Radiology, Mayo Clinic, Rochester, MN, US*
[3]*Department of Laboratory Medicine and Pathology, Mayo Clinic, Rochester, MN, US*

Introduction: Flortaucipir (FTP) is a tau-PET tracer used to detect tau pathology in neurodegenerative diseases. However, FTP exhibits off-target binding in frontotemporal lobar degeneration (FTLD), particularly in cases with phosphorylated TAR DNA-binding protein 43 (pTDP-43), raising concerns about its regional specificity. Transmembrane protein 106B (TMEM106B), a lysosomal protein, is genetically and pathologically linked to FTLD.. We hypothesize that the TMEM106B protein contributes to FTP off-target binding in FTLD-TDP, especially in regions affected by TDP-43 pathology. This study investigates the spatial relationship between FTP retention and TMEM106B expression in FTLD-TDP patients.

Materials and Methods: Tissue samples were obtained from one cognitively normal control, one Alzheimer's disease (AD) patient, and ten FTLD-TDP patients (five type A, five type C). Formalin-fixed, paraffin-embedded sections from hippocampal and limbic subregions, including the dentate gyrus, CA1–CA4, subiculum, entorhinal cortex, and choroid plexus, were analyzed. A fluorescent FTP analog (T726) was used to assess tracer binding, and fluorescence immunohistochemistry was employed to detect TMEM106B and pTDP-43. Confocal microscopy enabled colocalization analysis.

Results: Increased TMEM106B protein was observed in both AD and FTLD-TDP cases across all examined subregions. In the AD patient, there were distinct TMEM106B staining patterns compared to those with FTLD-TDP.. Colocalization between T726 and TMEM106B was most prominent in the choroid plexus (a common hotspot for off-target binding) in controls, AD, and FTLD patients. Additional colocalization was observed in the entorhinal cortex, subiculum, and CA1 regions, particularly in FTLD-TDP type C cases.

Conclusions: These results suggest that FTP off-target binding in FTLD-TDP may be partially attributable to the TMEM106B protein, particularly in the choroid plexus. Further investigations may enhance our understanding of disease mechanisms and refine flortaucipir imaging interpretation in the context of FTLD-TDP.



Fluorescent immunohistochemistry microscopy illustrating the overlap between the flortaucipir (FTP) analog T726 and TMEM106B protein in the choroid plexus (arrows).

Keywords: Frontotemporal lobar degeneration, flortaucipir fluorescent analog, TAR DNA-binding protein 43, TMEM106B

Hypometabolism and atrophy patterns associated with advanced primary age-related tauopathy mimicking early-stage AD

Jesús Silva-Rodríguez[1], Alexis Moscoso[2], Stamatia Karagianni[2], Orfeas Vourkas[1], Miguel Ángel Labrador-Espinosa[2], Pascual Sanchez-Juan[1], Michael Schöll[2], Michel J. Grothe[1]

[1]*CIEN Foundation, Madrid, Spain*
[2]*University of Gothenburg, Gothenburg, Sweden*

Background: Primary age-related tauopathy (PART) is typically confined to the medial temporal lobe (MTL), but in rare instances it can extend to the neocortex and mimic Alzheimer's disease (AD), a condition historically termed as tangle-predominant dementia. In a recent large-scale prevalence study (Moscoso et al. JAMA 2025), we found that approximately 11% of Aβ-negative ('A-'; <24.4 Centiloids) amnestic individuals were neocortical tau-positive ('T+', Flortaucipir visual read), representing a potential in-vivo analogue of this rare neuro-pathological condition.

Methods: We first examined longitudinal ante-mortem hypometabolism (FDG-PET) and atrophy (T1-MRI) patterns in an autopsy-confirmed case of tangle-predominant disease (aMCI diagnosis, Braak V, Thal 0, CERAD 0). We then studied hypometabolism and atrophy patterns in a PET-based A-T+ sample (N=24) compared to A+T+ (N=168) and an A-T- cognitively unimpaired control group (N=327).

Results: In ante-mortem Aβ- and tau-PET, the autopsy-confirmed case was consistently Aβ-negative but neocortical tau-positive 2 years before death (Fig-1). Hypometabolism spreaded from the MTL towards posterior temporo-parietal regions, but progressive atrophy remained largely confined to the MTL. PET-based A-T+ individuals had similarly low Centiloids as controls (p=0.84), but a hypometabolic pattern spatially resembling that of A+T+ cases (spatial correlation, ρ=0.88, Fig-2A). In quantitative ROI-based analyses, both groups showed comparable hypometabolism in regions typically affected in early AD (posterior cingulate, p=0.88, Fig-2B) and had similarly low inferior temporal-to-MTL ratios (p=0.41), indicating good discriminability against the hypometabolic signature of LATE. By contrast, atrophy in A–T+ was largely restricted to the MTL, unlike the more widespread temporo-parietal involvement observed in A+T+ (Fig-3).

Conclusion: The neuroimaging patterns of PET-defined A–T+ resemble that of an autopsy-confirmed case of tangle-predominant disease, characterized by atrophy confined to the MTL and a more widespread pattern of temporo-parietal hypometabolism resembling early AD. Delineating the FDG-PET/MRI imaging signature of advanced PART has important implications for the differential diagnosis of Aβ-negative individuals.

Keywords: Tau-PET, FDG-PET, MRI, PART

Differential age- and Aβ-related tau-PET patterns between [18F]FTP and [18F]MK6240

Cécile Tissot[1], Hsin-Yeh Tsai[1], Samira Maboudian[2], Corrina Fonseca[2], Nesrine Rahmouni[3], Firoza Lussier[4], Joseph Therriault[3], Lydia Trudel[3], Arthur Cassa Macedo[3], Jenna Stevenson[3], Bruna Bellaver[4], Pamela Ferreira[4], Guilherme Povala[4], Brian Gordon[5], Belen Pascual[6], Val Lowe[7], David Soleimani-Meigooni[8], Hwamee Oh[9], William Klunk[4], Pedro Rosa-Neto[3,10], William Jagust[1,2], Tharick Pascoal[4], Suzanne Baker[1]

[1]*Lawrence Berkeley National Laboratory, Berkeley, CA, US*
[2]*University of California Berkeley, Berkeley, CA, US*
[3]*McGill University, Montreal, QC, Canada*
[4]*University of Pittsburgh, Pittsburgh, PA, US*
[5]*Washington University in Saint-Louis, Saint Louis, MO, US*
[6]*Houston Methodist, Houston, TX, US*
[7]*Mayo Clinic, Rochester, MN, US*
[8]*University of California San Francisco, San Francisco, CA, US*
[9]*Brown University, Providence, RI, US*
[10]*University of Texas Southwestern, Dallas, TX, US*

Background: Tau-PET tracers are necessary to visualize Alzheimer's disease (AD) pathology *in vivo*, and early detection is critical for tracking disease progression. Here we compare [^{18}F]FTP and [^{18}F]MK6240 binding patterns over different age ranges.

Methods: 414 cognitively unimpaired (CU) HEAD participants (38 CU young (CUY), 288 CU old (CUO) Aβ- and 88 CUO Aβ+) underwent [^{18}F]FTP and [^{18}F]MK6240 tau-PET scans. They were processed using identical pipelines with inferior cerebellar gray as reference region. Participants were categorized by age (<65, 65–75, >75 years) and tau level (meta-temporal ROI SUVR < or ≥1.5 in both tracers). We generated mean images per group and computed voxel-wise z-scores using different reference groups.

Results: In low-tau, [^{18}F]FTP showed widespread age-related temporal retention independent of Aβ status, [^{18}F]MK6240 showed elevated entorhinal cortical (EC) in Aβ+ individuals (Figure1). Quantitatively, [^{18}F]FTP showed higher SUVRs than [^{18}F]MK6240 in low-tau groups, whereas [^{18}F]MK6240 exhibited greater variability in CUO Aβ+ (Figure2). In Z-score maps referenced against CUY, (a) CUO Aβ- revealed age-related increase in temporal signal (stronger in [^{18}F]FTP), and (b) CUO Aβ+ low-tau showed higher and more widespread retention (especially in EC for [^{18}F]MK6240). In Z-score maps of CUO Aβ+ low-tau referenced against age-matched CUO Aβ-, [^{18}F]MK6240 displayed strong EC signal particularly in individuals <65, which persisted, though reduced, at older ages. CUO Aβ+ high tau individuals presented widespread uptake compared to low tau groups (Figure3).

Discussion: These findings reveal distinct age- and Aβ-related tau-PET patterns across tracers. [^{18}F]FTP exhibited diffuse temporal retention across the lifespan, even among Aβ- individuals, suggesting sensitivity to age-related binding. [^{18}F]MK6240 demonstrated regionally specific, Aβ-driven EC signal, with subtle spread into adjacent temporal regions. Tracer-dependent differences were most evident before 75 years, converging later in life. These results emphasize the need to account for tracer characteristics when interpreting early tau-PET signal.

Figure1: mean images based on diagnostic groups and age

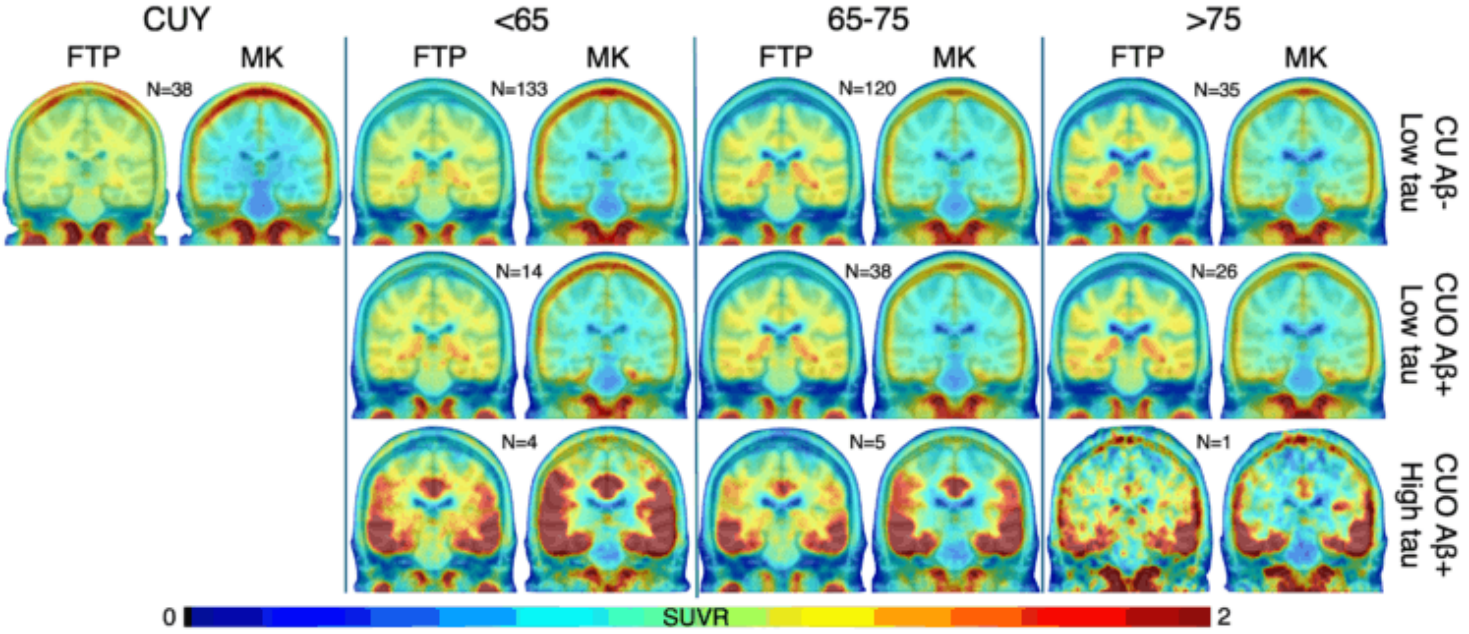


Figure 2: Boxplots of meta-temporal ROI SUVR by diagnosis

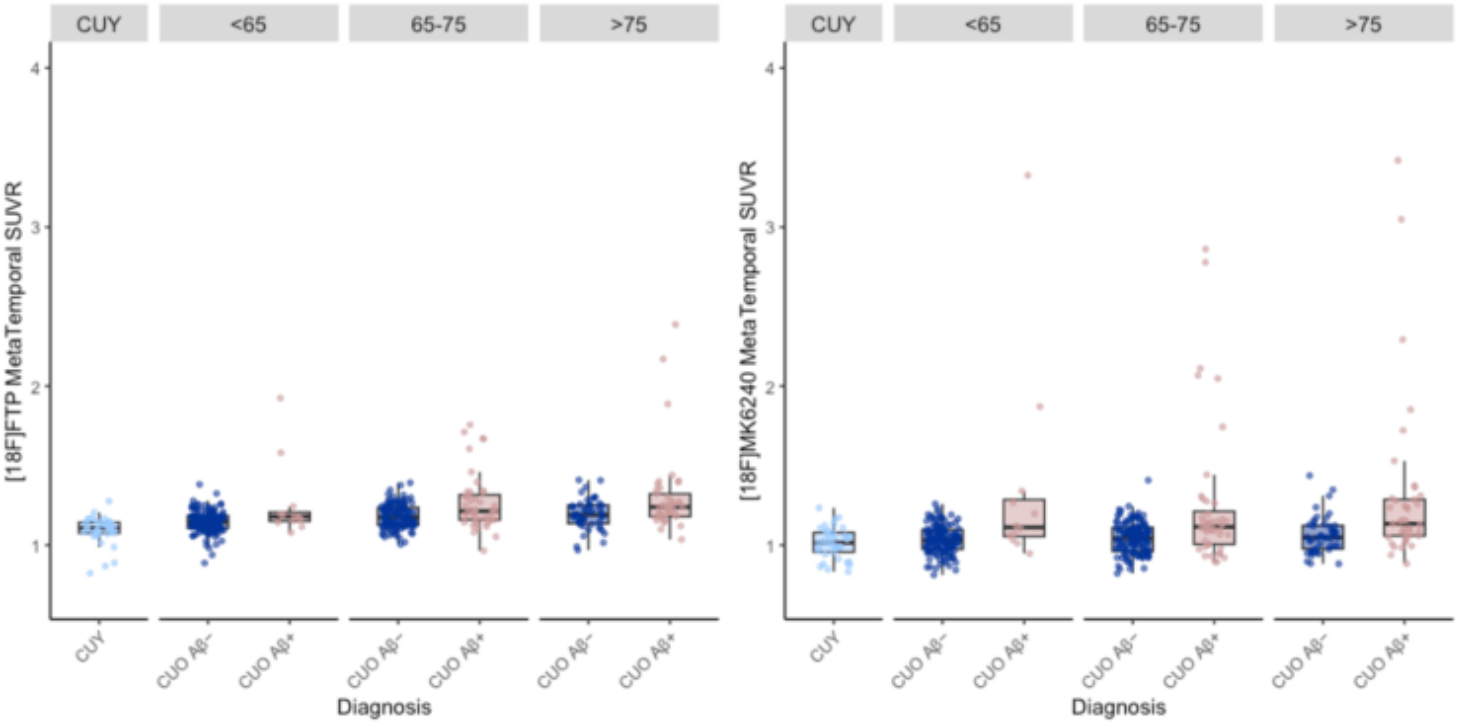
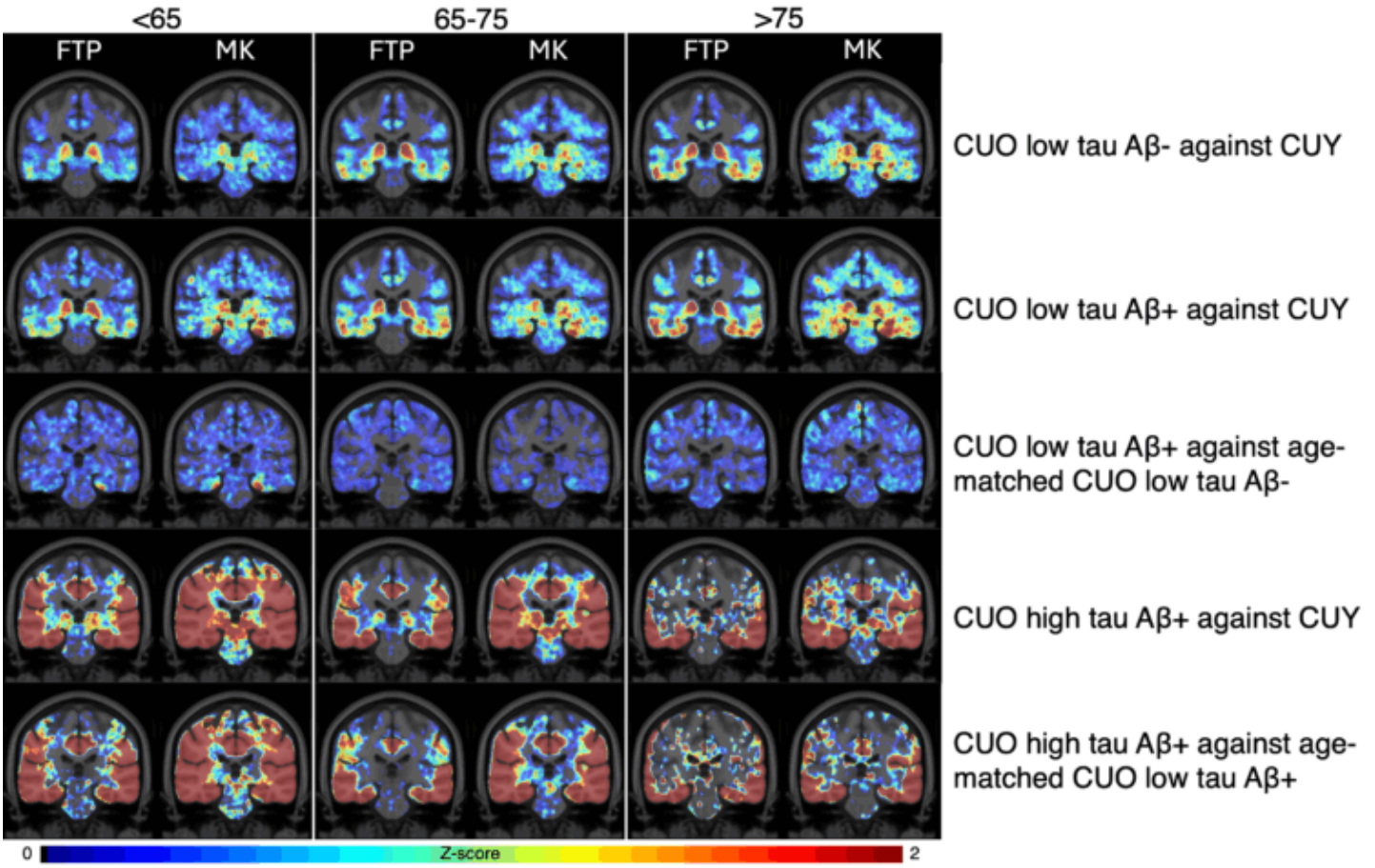


Figure 3: Z-score based on different diagnostic groups



Keywords: early tau, tracer comparison, zscore, age-related binding

Monday, January 12, 2026 - 02:45 pm - 04:15 pm

Podium Session

KEYNOTE: The neuropathological basis of current AD biomarkers: Sensitivity and pathogenetic implications

Monday, January 12, 2026		
02:00 pm - 02:30 pm	Keynote: **The neuropathological basis of current AD biomarkers: Sensitivity and pathogenetic implications**	**Dietmar Thal**, KU Leuven, Leuven, Belgium

The neuropathological basis of current AD biomarkers: Sensitivity and pathogenetic implications

Dietmar R. Thal

Laboratory of Neuropathology, Department of Imaging and Leuven Brain Institute, KU-Leuven, Belgium
Department of Pathology, University Hospital Leuven, Leuven Belgium

Imaging and liquid biomarkers for Alzheimer's disease (AD) pathology have been recently established. Amyloid positron emission tomography (PET), cerebrospinal fluid (CSF) and blood Aβ40 and Aβ42 are established to detect Aβ-related pathology in patients. Tau PET, CSF and blood phosphorylated tau (p-tau) markers provide estimates for abnormal phosphorylated tau pathology in the brain. Despite the fact that Aβ and tau biomarkers also identify asymptomatic stages of Aβ and p-tau pathology, end of life studies have shown that initial stages of Aβ plaque deposition in the brain and of p-tau pathology cannot be distinguished from non-affected controls with the respective biomarkers. Moreover, biomarkers differ in their sensitivity. In this context, Aβ-related markers appear to be more sensitive for cerebral Aβ pathology than tau biomarkers for tau pathology in the brain. Accordingly, knowledge about biomarker sensitivity is essential when interpreting biomarker-based studies. Neuropathologically p-tau pathology appears to precede Aβ deposition in most of the cases whereas Aβ biomarkers show abnormalities earlier than p-tau biomarkers. This phenomenon is a good example of how sensitivity of biomarkers influences our interpretation of the respective results.

Given the current lack of sensitive biomarkers for α-synuclein and TDP-43 co-pathologies, these co-pathologies are currently clinically underdiagnosed in AD cases. However, neuropathological studies showed the presence of these co-pathologies in more than 30 % of the AD cases. Biochemical studies indicated that TDP-43 and α-synuclein can physically interact with p-tau. The interaction of TDP-43 and p-tau increased p-tau seeding and neuron loss. Thus, sensitive biomarkers for co-pathologies such as TDP-43/limbic predominant age-related TDP-43 encephalopathy neuropathological changes (LATE-NC) and α-synuclein are needed to properly subclassify potentially biologically different forms of AD. Taken together, current imaging and liquid biomarkers are excellent for detecting Aβ and p-tau pathology whereas sensitive markers for TDP-43 and α-synuclein pathology are still needed for proper subclassification of AD cases. When comparing different biomarkers related to the biological disease process it is important to take differences in the sensitivity of these markers into account.

Funding: FWO, KU-Leuven internal funding, Alzheimer's Association

Monday, January 12, 2026 - 02:45 pm - 04:15 pm

Podium Session

SESSION III: Alzheimer's disease biological staging and applications

CHAIRS:

***Tobey Betthauser**, University of Wisconsin-Madison, Madison, WI, USA*

***Thomas Karikari**, University of Pittsburgh, Pittsburgh, PA, USA*

Monday, January 12, 2026			
02:45 pm – 04:15 pm	**Podium Presentation**	**Authors**	**Presenter**
02:50 pm – 03:05 pm	Combining quantitative and visual read approaches to tau-PET positivity and staging: The Tau-PET Working Group	Harrison | Chao | Soleimani-Meigooni | Baker | Benzinger | Blazhenets | Burkett | Chiotis | Dickerson | Franceschi | Jack | Johnson | Koran | Landau | Lowe | Pascoal | Ruppert | Schwarz | Tanner | Villemagne | Zeineh | La Joie | Johnson | Mormino | Jagust | Rabinovici	**Gil Rabinovici**, University of California San Francisco, San Francisco, CA, US
03:05 pm – 03:20 pm	Association between PET-based Alzheimer's disease biological stage and autopsy findings	Johnson | Wiste | Lowe | Schwarz | Knopman | Vemuri | Kantarci | Boeve | Graff-Radford | Cogswell | Burkett | Senjem | Therneau | Weigand | Griswold | Mingzhao | Petersen | Jack	**Derek Johnson**, Department of Radiology, Mayo Clinic, Rochester, MN, US
03:20 pm – 03:35 pm	Associations among plasma p-tau217, amyloid PET, tau PET, and cognitive testing in the screening cohort for the AHEAD 3-45 Study	Sperling | Langford | Rissman | Donohue | Molina-Henry | Jimenez-Maggiora | Raman | Schultz | Grill | Dhadda | Irizarry | Zhou | Braunstein | Aisen | Johnson | AHEAD 3-45 Study Team	**Reisa Sperling**, Center for Alzheimer Research and Treatment, Brigham and Women's Hospital, Massachusetts General Hospital, Harvard Medical School, Boston, MA, US
03:35 pm – 03:50 pm	Genetic predictors of multimodal brain tau pathology in older adults	Wang | Walters | Archer | Crane | Keene | Larson | Mukherjee | Saykin | Schneider | Bennett | Barnes | De Jager | Sperling | Mormino | Beecham | Mena | Montine | Wang | Vardarajan | Mayeux | Kunkle | Bush | Schellenberg | Pericak-Vance | Haines | Biber | Kukull | Cuccaro | Toga | Johnson | Engelman | Cody | Sokolowski | Buckley | (A4) | (ADNI) | (ADSP) | Hohman | Koran | Dumitrescu	**Ting-Chen Wang**, Vanderbilt Memory and Alzheimer's Center, Department of Neurology, Vanderbilt University Medical Center, Nashville, TN, US

Combining quantitative and visual read approaches to tau-PET positivity and staging: The Tau-PET Working Group

Theresa Harrison[1], Yishu Chao[1], David Soleimani-Meigooni[2], Suzanne Baker[3], Tammie Benzinger[4], Ganna Blazhenets[2], Brian Burkett[5], Konstantinos Chiotis[6], Bradford Dickerson[7], Ana Franceschi[8], Clifford Jack[5], Derek Johnson[5], Mary Ellen Koran[9], Susan Landau[1], Val Lowe[5], Tharick Pascoal[10], Emma Ruppert[10], Christopher Schwarz[5], Jeremy Tanner[11], Victor Villemagne[10], Michael Zeineh[12], Renaud La Joie[2], Sterling Johnson[13], Elizabeth Mormino[12], William Jagust[1,3], Gil Rabinovici[2]

[1]*University of California Berkeley, Berkeley, CA, US*
[2]*University of California San Francisco, San Francisco, CA, US*
[3]*Lawrence Berkeley National Laboratory, Berkeley, CA, US*
[4]*Washington University School of Medicine, St Louis, MO, US*
[5]*Mayo Clinic, Rochester, MN, US*
[6]*Karolinska Institutet, Stockholm, Sweden*
[7]*Massachusetts General Hospital, Boston, MA, US*
[8]*Donald and Barbara Zucker School of Medicine at Hofstra/Northwell, Hempstead, NY, US*
[9]*Mayo Clinic, Scottsdale, AZ, US*
[10]*University of Pittsburgh, Pittsburgh, PA, US*
[11]*University of Texas Health San Antonio, San Antonio, TX, US*
[12]*Stanford University School of Medicine, Palo Alto, CA, US*
[13]*University of Wisconsin School of Medicine and Public Health, Madison, WI, US*

Background: Tau-PET is a critical tool for Alzheimer's disease (AD) staging, but quantitative and visual read implementation of PET-based biological staging (2024 AD Research Criteria) are not standardized.

Methods: We formed a Tau-PET Working Group with two goals: defining tracer-specific quantitative thresholds in key ROIs (Quantitative Group) and creating a reliable tau-PET visual read workflow integrating quantitative data (Visual Reads Group). The Quantitative Group used a large, generalizable multicohort dataset (Table) and several statistical approaches (mean+2SDs of reference group, Gaussian mixture models [GMM] and receiver operating characteristic [ROC] curves) to generate 1) positivity thresholds for medial temporal lobe (MTL) and neocortical ROIs and 2) thresholds for moderate (Stage C: T_{2MOD}+) vs. high (Stage D: T_{2HIGH}+) neocortical tau for flortaucipir (FTP), MK6240 and PI2620. Longitudinal change in Clinical Dementia Rating scale Sum-of-Boxes was compared across baseline PET-based biological stage groups. The Visual Reads Group conducted a comprehensive literature review to evaluate methods and tools for standardizing the visual assessment of MTL and neocortical regions.

Results: We showed that three statistical methods resulted in ROI-specific thresholds with relatively low variability within-tracer (Figure1A). Positivity rates were higher for amyloid+ CI compared to CU but varied by region and tracer (Figure1B). Three methods to distinguish moderate-vs-high neocortical tau burden allowed for tau-PET-based biological staging (Figure2A). Quantitative tau-PET biological stages (based on GMM positivity thresholds and MCI-vs-AD ROC Stage C-vs-D thresholds) were clinically relevant, tracking as expected with future clinical decline (Figure2B). The Visual Reads Group created a pilot workflow incorporating sequential ROI visual assessments, comparison with quantitative data and consensus procedures.

Conclusions: The Tau-PET Working Group will establish standardized approaches for visual reads and quantification. Our clinically relevant MTL and neocortical positivity thresholds, as well as thresholds to distinguish moderate-vs-high neocortical tau, will be used to determine AD biological stage as a complement to visual reads.

Table. Multicohort PET Dataset Characteristics by Tracer

	FTP (n=2,009)	MK6240 (n=1,521)	PI2620 (n=1,684)
Diagnosis			
Cognitive Normal	1,256 (63%)	1,162 (77%)	1,218 (73%)
MCI	557 (28%)	283 (19%)	367 (22%)
Dementia	180 (9%)	66 (4%)	81 (5%)
Sex (%F)	1,124 (56%)	927 (61%)	993 (59%)
Age (yrs)	73 (±8)	70 (±6)	68 (±8)
Amyloid Status (% Positive)	651 (43%)	480 (36%)	364 (22%)
Study			
BACS	174 (9%)	-	-
ADNI	1,022 (51%)	43 (3%)	25 (1%)
POINTER	--	881 (58%)	-
SCAN	813 (40%)	384 (25%)	81 (5%)
HEAD	-	213 (14%)	-
HABS-HD	-	-	1,578 (94%)

FTP=flortaucipir; MCI=mild cognitive impairment; F=female; yrs=years; BACS=Berkeley Aging Cohort Study; ADNI=Alzheimer's Disease Neuroimaging Initiative; POINTER= US Study to Protect Brain Health Through Lifestyle Intervention to Reduce Risk Imaging ancillary study; SCAN=Standardized Centralized Alzheimer's & Related Dementias Neuroimaging study; HEAD=Longitudinal multicenter head-to-head harmonization of tau PET tracers study; HABS-HD=Health and Aging Brain Study - Health Disparities

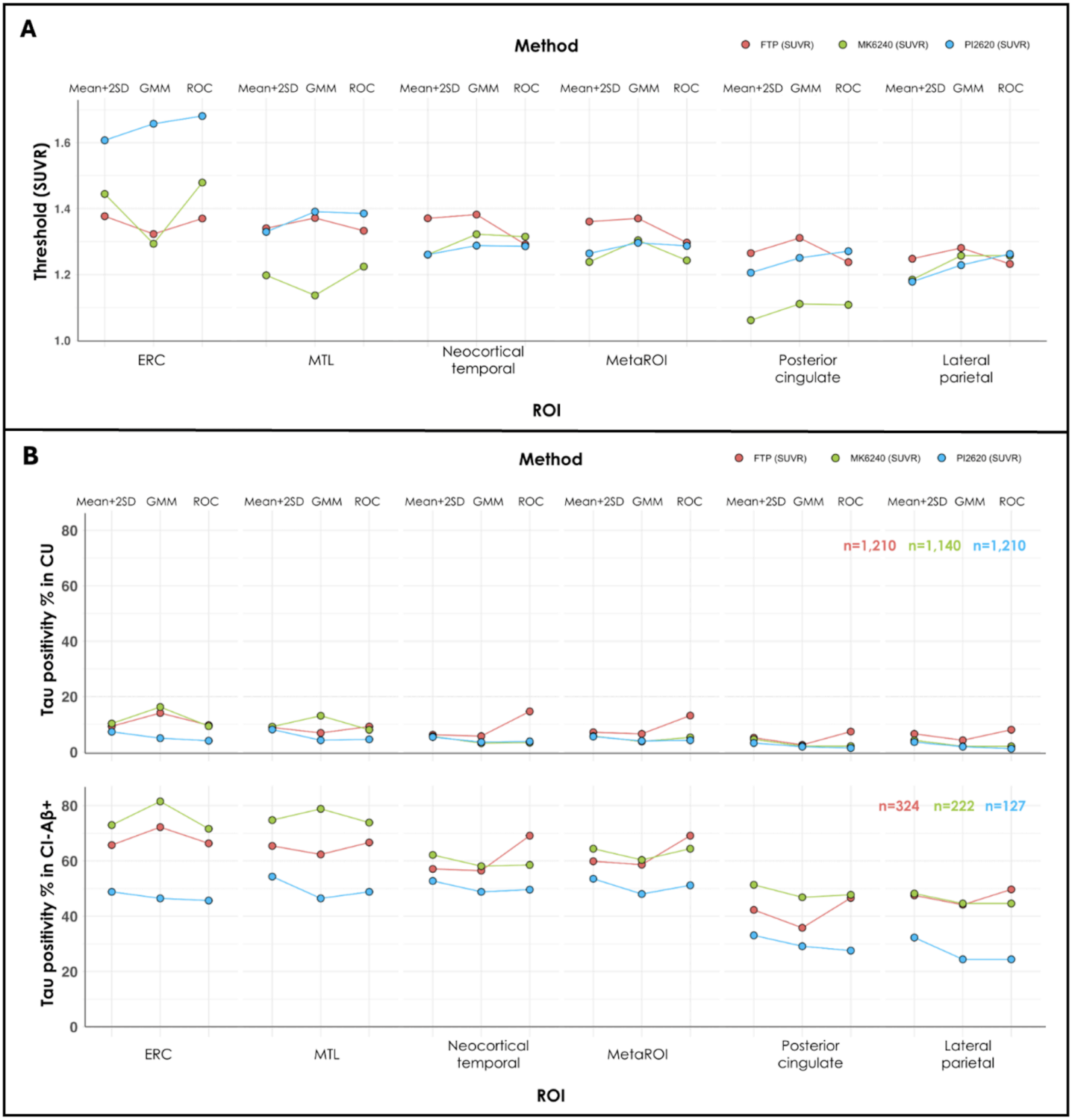


Figure 1: Tau-PET positivity SUVR thresholds and positivity rates by statistical method, ROI and tracer. Bilateral tau-PET positivity thresholds were determined by calculating the Mean+2SD of unimpaired Aβ- (Mean+2SD), mean+2.5SD of lowest peak in Gaussian mixture model (GMM) or accuracy from a receiver operating characteristic (ROC) curve to distinguish unimpaired Aβ- from impaired Aβ+. Thresholds (A) or positivity rates (B) for 3 tracers are plotted in 6 ROIs: entorhinal cortex (ERC), medial temporal lobe (MTL; ERC, amygdala and parahippocampal gyrus), neocortical temporal (fusiform, inferior temporal gyrus and middle temporal gyrus), MetaROI (all ROIs from MTL composite and neocortical temporal composite combined), posterior cingulate (posterior and isthmus cingulate) and lateral parietal (supramarginal gyrus, superior parietal, inferior parietal).

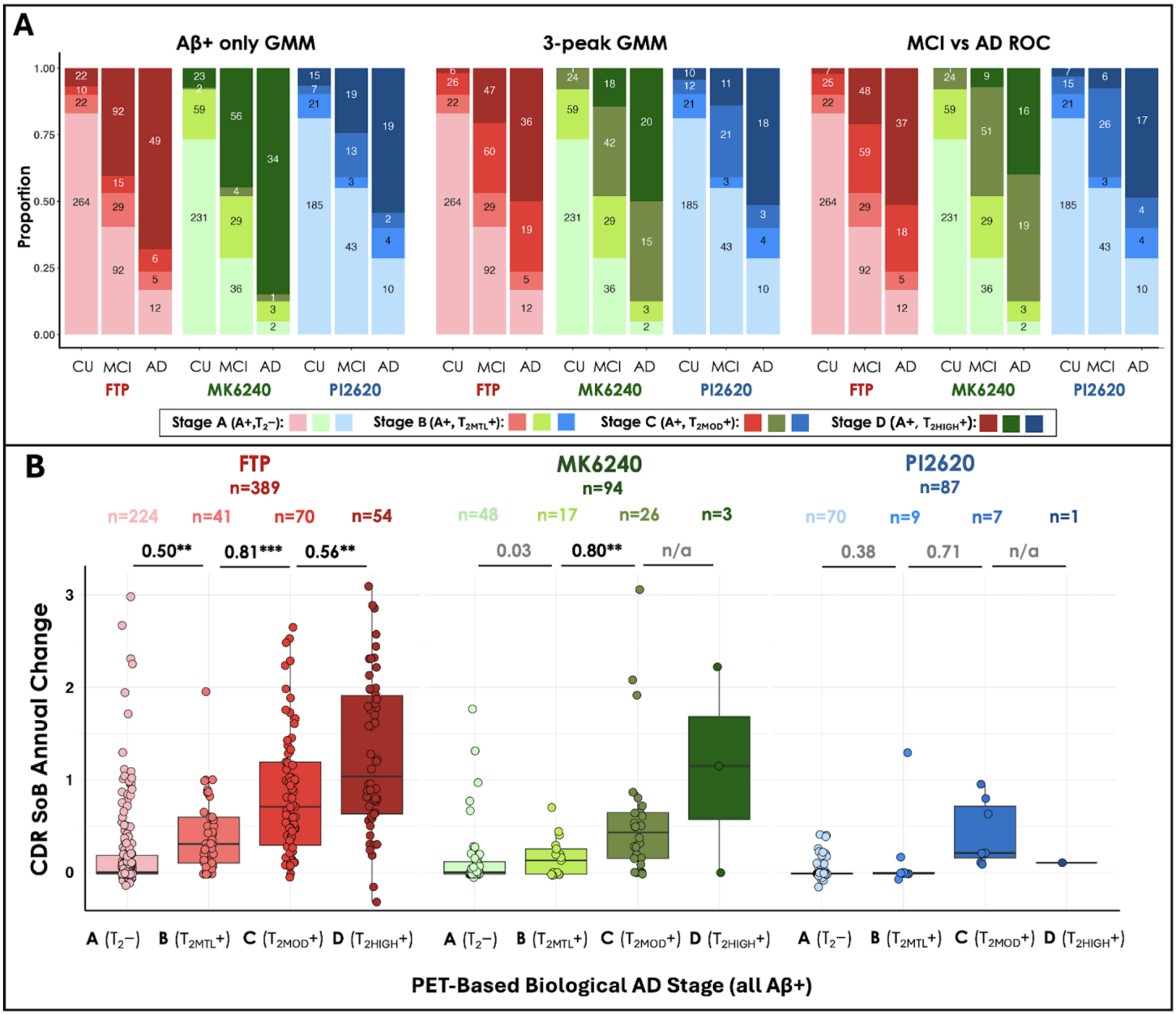


Figure 2: PET-based biological staging of Alzheimer's disease (AD) using quantitative thresholds. **A)** Thresholds to distinguish moderate (Stage C:T_{2MOD}+) vs. high (Stage D:T_{2HIGH}+) neocortical tau were determined by calculating the mean+2.5SD of lowest Gaussian in Gaussian mixture model (GMM) including only Aβ+ participants, mean+2.5SD of middle peak in a forced 3-peak GMM including all participants or accuracy from a receiver operating characteristic (ROC) curve to distinguish Aβ+ MCI from Aβ+ AD dementia. Only Aβ-PET+ participants were included in plots and GMM-based positivity thresholds for MTL and neocortical temporal composites (**Figure1**) were used to determine MTL or neocortical positivity, respectively. **B)** Clinical Dementia Rating scale Sum of Boxes (CDR SoB) change over time was related to baseline PET-based biological AD stage. Stage C-vs-D thresholds based on MCI-vs-AD ROC were used. Cohen's d for comparisons between increasing severity stages are shown. **=t-test p<0.01, ***=t-test p<0.001

Keywords: positivity thresholds, biological staging, research criteria, return of results, harmonization

Association between PET-based Alzheimer's disease biological stage and autopsy findings

Derek Johnson[1], Heather Wiste[2], Val Lowe[1], Christopher Schwarz[1], David Knopman[3], Prashanthi Vemuri[1], Kejal Kantarci[1], Bradley Boeve[3], Jonathan Graff-Radford[3], Petrice Cogswell[1], Brian Burkett[1], Matthew Senjem[1,4], Terry Therneau[2], Stephen Weigand[2], Michael Griswold[5], Hu Mingzhao[2], Ronald Petersen[3], Clifford Jack[1]

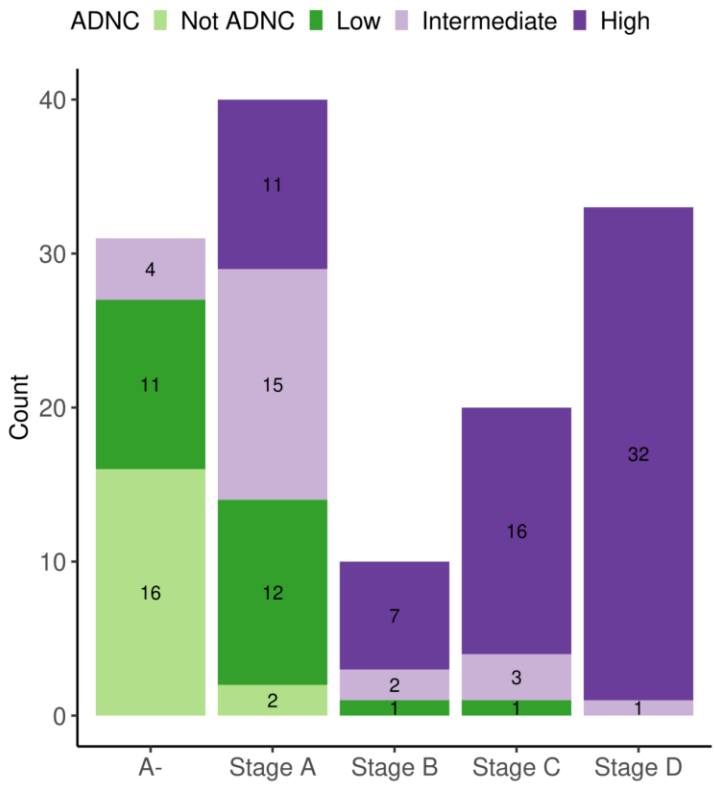
[1]*Department of Radiology, Mayo Clinic, Rochester, MN, US*
[2]*Department of Quantitative Health Sciences, Mayo Clinic, Rochester, MN, US*
[3]*Department of Neurology, Mayo Clinic, Rochester, MN, US*
[4]*Department of Information Technology, Mayo Clinic, Rochester, MN, US*
[5]*Department of Data Science, University of Mississippi Medical Center, Jackson, MS, US*

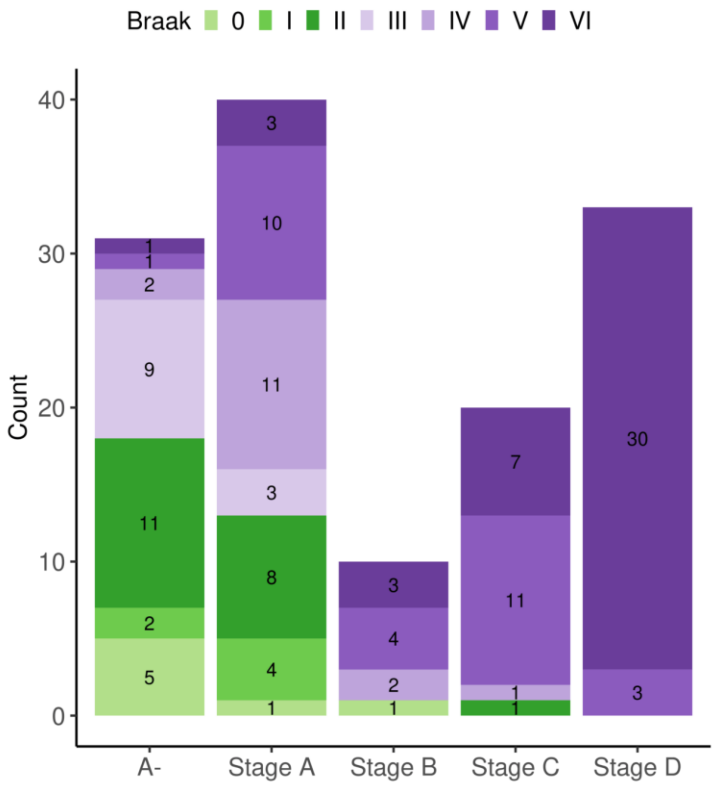
Background: The recently updated Alzheimer's Association Diagnosis and Staging Criteria for Alzheimer's Disease (AD) introduced the concept of biological AD staging with PET, and subsequent publications have shown that biological stage both correlates with degree of cognitive impairment and predicts future cognitive trajectory. Associations between PET-based AD biological stage and subsequent findings at autopsy are not well described.

Methods: We identified 134 individuals who underwent autopsy within four years of amyloid (C-11 PiB) and tau (AV-1451) PET imaging from within the Mayo Clinic Study of Aging (MCSA) and Mayo ADRC. Amyloid PET positivity (A+) and tau-PET based AD biological stages were defined via published methods. Alzheimer's Disease neuropathologic change (ADNC) levels and Braak stages were evaluated within each group.

Results: Median (IQR) age at death was 80 (72, 88), with time from PET imaging to death of 2.1 (1.3, 3.0) years. Amyloid PET was negative in 31 individuals (23%). Amongst A+ individuals, tau PET based AD biological stages were A in 40 (30%), B in 10 (7%), C in 20 (15%), and D in 33 (25%). The distribution of ADNC level and Braak stage by AD biological stage are displayed in accompanying figures. The proportion of intermediate/high level ADNC increased from 13% in A-, to 65% in AD biological stage A to 90-100% in stages B-D. The proportion of subjects in Braak stage V/VI increased from 6% in A- to 33% in biological stage A to 70% in stage B and to 90-100% in stages C-D.

Conclusions: High levels of ADNC and high Braak stages are commonly found in A+ individuals with any degree of tau PET abnormality (i.e. AD biological stages B-D). PET-based AD biological staging may provide information regarding distribution and severity of AD pathology beyond that which can be ascertained by standard neuropathological evaluations.





Keywords: Alzheimer's, stage, staging, tau, amyloid

Associations among plasma p-tau217, amyloid PET, tau PET, and cognitive testing in the screening cohort for the AHEAD 3-45 Study

Reisa Sperling[1], Oliver Langford[2], Robert Rissman[2], Michael Donohue[2], Doris Molina-Henry[2], Gustavo Jimenez-Maggiora[2], Rema Raman[2], Aaron Schultz[1], Joshua Grill[3], Shobha Dhadda[4], Michael Irizarry[4], Jin Zhou[4], Joel Braunstein[5], Paul Aisen[2], Keith Johnson[1], The AHEAD 3-45 Study Team[6]

[1]*Center for Alzheimer Research and Treatment, Brigham and Women's Hospital, Massachusetts General Hospital, Harvard Medical School, Boston, MA, US*
[2]*Alzheimer's Therapeutic Research Institute, University of Southern California, San Diego, CA, US*
[3]*University of California Irvine, Irvine, CA, US*
[4]*Eisai, Inc., Nutley, NJ, US*
[5]*C2N Diagnostics, St. Louis, MO, US*
[6]*Alzheimer's Clinical Trial Consortium, San Diego, CA, US*

Background: The AHEAD 3-45 Study used a plasma biomarker informed algorithm to enroll cognitively unimpaired individuals into two sister trials (A3 and A45) testing lecanemab in preclinical Alzheimer's disease (AD). We assessed the cross-sectional relationships of plasma markers, amyloid and tau PET imaging, and cognitive testing acquired during screening.

Methods: An algorithm including age, APOE, Ab42/40 ratio and plasma phosphorylated-tau217/non-phosphorylated tau (%p-tau217 from C_2N Diagnostics) was iteratively optimized to predict amyloid PET (18-F-NAV4694) eligibility (A3: 20-40 Centiloid; A45: >40CL). Screening cognition was assessed with the Preclinical Alzheimer's Cognitive Composite (PACC5). Tau PET (18-F-MK6240) imaging was acquired on amyloid-eligible participants. Individualized anatomic regions defined with FreeSurfer MRI were utilized to measure tau PET in medial temporal lobe (MTL) and early neocortical (NEO) composite regions.

Results: Plasma %p-tau217 was measured in 15,612 individuals (Table 1). The prevalence of %p-tau217 abnormalities (predicting >20CL) increased with age and with APOE ε4 allele (Figure 1A). Plasma %p-tau217 correlated strongly with Amyloid PET CL (N=3811; Spearman ρ=.743); and moderately associated with MTL (N=1514;ρ=.381) and NEO (N=1514;ρ=.385) Tau PET SUVr among amyloid eligible participants (Figure 1B). Lower PACC5 performance, controlling for age, sex, and education, was associated with higher %p-tau217 (N=4707; partial Spearman ρ=-0.187;p<0.001); amyloid CL: (N=4478;partialρ=-0.079;p<0.001); MTL Tau (N=1717;partialρ=-0.095; p<0.001); NEO (N=1717;partialρ=-0.096;p<0.001). In multivariate analyses among amyloid eligible, MTL and NEO tau PET explained greater variance in cross-sectional PACC5 performance than amyloid CL and p-tau217 (Figure 2).

Conclusion: Abnormal plasma %p-tau217 is increasingly prevalent with age among cognitively unimpaired individuals and demonstrates a stronger relationship with amyloid than tau deposition in preclinical AD. Among participants with elevated amyloid, tau PET demonstrated the strongest relationship with cross-sectional cognition. Tau PET may serve as a key endpoint in preclinical AD trials, serving as a potential bridging outcome between amyloid and cognition at these very early stages of AD.

Table 1. Screening Participant Demographics by Biomarker/Imaging Modality Groups

	%p-tau217 (N=15612)	PACC (N=6423)	Amyloid PET (N=4497)	Tau PET (N=1721)
Age				
Mean (SD)	68.4 (6.2)	69.3 (6.0)	68.8 (6.0)	70.0 (5.5)
Range	55.0 - 82.0	55.0 - 84.0	55.0 - 80.0	55.0 - 80.0
Sex				
Female	9941 (63.7%)	3848 (60.0%)	2789 (62.0%)	1111 (64.6%)
Male	5667 (36.3%)	2569 (40.0%)	1707 (38.0%)	610 (35.4%)
Race				
American Indian or Alaska Native	51 (0.3%)	12 (0.2%)	8 (0.2%)	2 (0.1%)
Asian	1424 (9.1%)	638 (9.9%)	387 (8.6%)	99 (5.8%)
Black or African American	1334 (8.5%)	254 (4.0%)	132 (2.9%)	36 (2.1%)
Multiple	222 (1.4%)	65 (1.0%)	41 (0.9%)	9 (0.5%)
Native Hawaiian or Other Pacific Islander	18 (0.1%)	6 (0.1%)	4 (0.1%)	2 (0.1%)
Other	175 (1.1%)	48 (0.7%)	31 (0.7%)	13 (0.8%)
Unknown or Not Reported	79 (0.5%)	21 (0.3%)	5 (0.1%)	1 (0.1%)
White	12308 (78.8%)	5376 (83.7%)	3889 (86.5%)	1559 (90.6%)
Ethnicity				
Hispanic or Latino	2431 (15.6%)	632 (9.9%)	450 (10.0%)	127 (7.4%)
Not Hispanic or Latino	13180 (84.4%)	5784 (90.1%)	4047 (90.0%)	1594 (92.6%)
APOE Genotyple				
ε2/ε2	66 (0.4%)	7 (0.1%)	6 (0.1%)	4 (0.2%)
ε2/ε3	1428 (9.2%)	302 (5.0%)	228 (5.1%)	44 (2.6%)
ε2/ε4	392 (2.5%)	222 (3.7%)	160 (3.6%)	74 (4.3%)
ε3/ε3	8354 (53.5%)	2137 (35.4%)	1630 (36.3%)	423 (24.6%)
ε3/ε4	4624 (29.6%)	2745 (45.5%)	2007 (44.7%)	950 (55.2%)
ε4/ε4	742 (4.8%)	616 (10.2%)	459 (10.2%)	226 (13.1%)
MMSE				
Mean (SD)	28.7 (1.5)	28.6 (1.6)	29.0 (1.0)	28.9 (1.0)
Range	10.0 - 30.0	10.0 - 30.0	25.0 - 30.0	25.0 - 30.0

Figure 1. Plasma %p-tau217 by demographic categories and imaging modalities

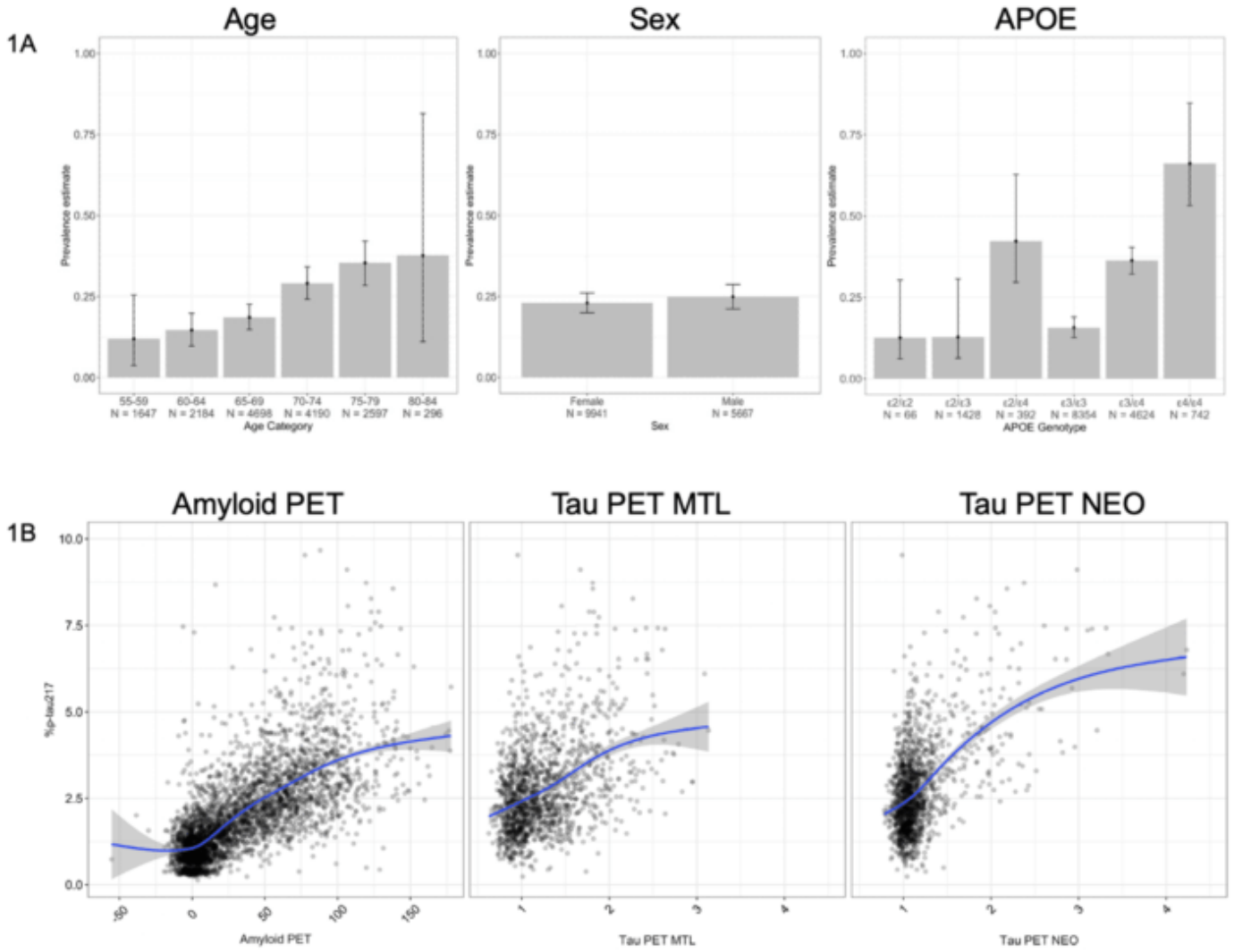


Figure 1. Figure 1A (Top row) Prevalence of plasma %p-tau217 (corresponding to optimal threshold to predict >20CL based on Youden index reported in Rissman R et al *Alz & Dem* 2024) by Age (left), Sex (middle), and APOE genotypes (right). Figure 1B (Bottom row) LOESS plots demonstrating relationship of plasma %p-tau217 with Amyloid PET centiloids (left), MTL Tau PET SUVr (middle), and Neocortical Tau PET SUVR (right).

Figure 2. Explained variance in screening PACC5 performance

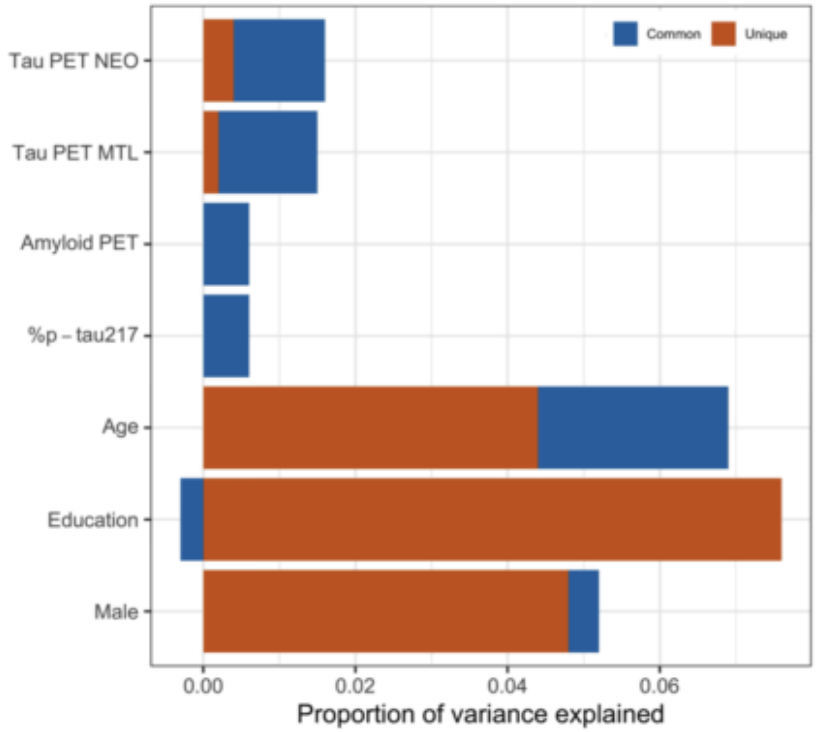


Figure 2. Cross-sectional PACC variance explained (R^2) in the amyloid eligible (>20CL) screening cohort with data available for all variables (N=1510), partitioned into common (blue) and unique (red) R^2. Demographic variables (age, education, sex) explained the greatest proportion of variance in screening cognitive performance. Among the biomarkers/imaging, tau PET explained higher proportion of variances, with both medial temporal lobe (MTL) and necortical (NEO) tau SUVr contributing unique variance to PACC5 performance.

Keywords: preclinical AD, cognitive testing, plasma biomarkers, amyloid PET, tau PET

Genetic predictors of multimodal brain tau pathology in older adults

Ting-Chen Wang[1,2], Skylar Walters[1], Derek Archer[1,2], Paul Crane[3], C. Dirk Keene[4], Eric B. Larson[3], Shubhabrata Mukherjee[3], Andrew J. Saykin[5,6], Julie A. Schneider[7], David A. Bennett[7], Lisa L. Barnes[7], Philip L. De Jager[8,9,10,11], Reisa A. Sperling[12,13], Elizabeth Mormino[14], Gary Beecham[15], Pedro Mena[16], Thomas J. Montine[17], Li-San Wang[20], Badri Vardarajan[8,9,10,18], Richard Mayeux[8,9,10,18], Brian W. Kunkle[16], William S. Bush[19], Gerard D. Schellenberg[20], Margaret A. Pericak-Vance[16], Jonathan L. Haines[19], Sarah Biber[21], Walter A. Kukull[21], Michael L. Cuccaro[16], Arthur W. Toga[22], Sterling C. Johnson[23], Corinne D. Engelman[24], Karly Cody[25], Andrzej Sokolowski[25], Rachel F. Buckley[12], A4 (A4)[28], Alzheimer's Disease Neuroimaging Initiative (ADNI)[29], Alzheimer's Disease Sequencing Project (ADSP)[30], Timothy Hohman[1,2], Mary Ellen Koran[26,27], Logan Dumitrescu[1,2]

[1]*Vanderbilt Memory and Alzheimer's Center, Department of Neurology, Vanderbilt University Medical Center, Nashville, TN, US*
[2]*Vanderbilt Genetics Institute, Vanderbilt University Medical Center, Nashville, TN, US*
[3]*School of Medicine, University of Washington, Seattle, WA, US*
[4]*Department of Laboratory Medicine and Pathology, University of Washington, Seattle, WA, US*
[5]*Department of Radiology and Imaging Sciences, Center for Neuroimaging, School of Medicine, Indiana University, Bloomington, IN, US*
[6]*Department of Medical and Molecular Genetics, School of Medicine, Indiana University, Bloomington, IN, US*
[7]*Rush Alzheimer's Disease Center, Rush University Medical Center, Chicago, IL, US*
[8]*Department of Neurology, Columbia University Medical Center, New York, NY, US*
[9]*Department of Neurology, The New York Presbyterian Hospital, New York, NY, US*
[10]*Taub Institute for Research on Alzheimer's Disease and The Aging Brain, Columbia University Medical Center, New York, NY, US*
[11]*Center for Translational and Computational Neuroimmunology, Department of Neurology, Columbia University Medical Center, New York, NY, US*
[12]*Department of Neurology, Harvard Medical School, Boston, MA, US*
[13]*Brigham and Women's Hospital and Department of Neurology, Massachusetts General Hospital, Harvard Medical School, Boston, MA, US*
[14]*Department of Neurology and Neurological Sciences, Stanford University, Stanford, CA, US*
[15]*Department of Biostatistics and Data Science, Wake Forest University School of Medicine, Winston-Salem, NC, US*
[16]*John P. Hussman Institute for Human Genomics, University of Miami School of Medicine, Miami, FL, US*
[17]*Department of Pathology, Stanford University, Palo Alto, CA, US*
[18]*The Institute for Genomic Medicine, Columbia University Medical Center, New York, NY, US*
[19]*Department of Population and Quantitative Health Sciences, Institute for Computational Biology, Case Western Reserve University, Cleveland, OH, US*
[20]*Department of Pathology and Laboratory Medicine, Perelman School of Medicine, University of Pennsylvania, Philadelphia, PA, US*
[21]*Department of Epidemiology, School of Public Health, University of Washington, Seattle, WA, US*
[22]*Laboratory of Neuroimaging, USC Stevens Neuroimaging and Informatics Institute, Keck School of Medicine, University of Southern California, Los Angeles, CA, US*
[23]*Alzheimer's Disease Research Center, University of Wisconsin School of Public Health, Madison, WI, US*
[24]*Department of Population Health Sciences, University of Wisconsin-Madison, School of Medicine and Public Health, Madison, WI, US*
[25]*Department of Neurology and Neurological Sciences, Stanford University, Palo Alto, CA, US*
[26]*Department of Radiology and Radiological Sciences, Vanderbilt University Medical Center, Nashville, TN, US*
[27]*Department of Radiology, Mayo Clinic of Arizona, Scottsdale, AZ, US*

[28]*A4, , US*
[29]*Alzheimer's Disease Neuroimaging Initiative (ADNI), , US*
[30]*Alzheimer's Disease Sequencing Project (ADSP), , US*

Objectives: Tau proteinopathy is a hallmark of Alzheimer's disease (AD) pathology, yet its genetic drivers remain understudied. While autopsy and biomarker studies have begun to characterize genetic architecture of tau pathology, limited sample sizes often restrict genomic discovery. Recent studies linking neuropathology measured *in vivo* by positron emission tomography (PET) and quantified at autopsy offer an exciting roadmap to combine tau definitions across modalities and increase sample sizes. This study combines autopsy and PET measures of tau neuropathology, enhancing sample size and better characterizing genetic architecture of tau.

Methods: Across 7 aging and AD cohorts, tau status (positive/negative) was determined for participants of European ancestry based on either medial temporal lobe composite of *in vivo* tau PET imaging (N=1,352, 16.35% tau positive, 56.07% female, mean age=71.98 years) or on BRAAK Stage ≥III at autopsy (N=5,466, 75.32% tau positive, 48.98% female, mean age at death=81.97 years). GWAS was performed within each modality and meta-analyzed. Covariates included age, sex, and the first five genetic principal components.

Results: We identified two genome-wide significant known AD loci (*BIN1* and *APOE*) and one suggestive significant chromosome 17 locus (index SNP: rs148990267, MAF=0.038, OR=0.578, P=2.61x10-7) (**Figure 1A-D**). Expression levels of proximal genes *PCTP* (lipid metabolism) and *TMEM100* (vasculature) of this locus show inverse associations with BRAAK staging, suggesting a protective link with reduced tau pathology (AGORA).

Conclusions: By combining imaging biomarker and postmortem measures of tau pathology, we replicate known AD loci and observe a potential novel chromosome 17 locus associated with tau proteinopathy. This proof-of-concept study demonstrates the potential of cross-modality approaches to increase sample size while retaining molecular specificity. Given challenges that binarized tau PET burden often does not align with neuropathological BRAAK staging, future work will explore refined strategies defining modality-specific tau positivity, expanding this project to incorporate additional datasets and tau biomarkers.

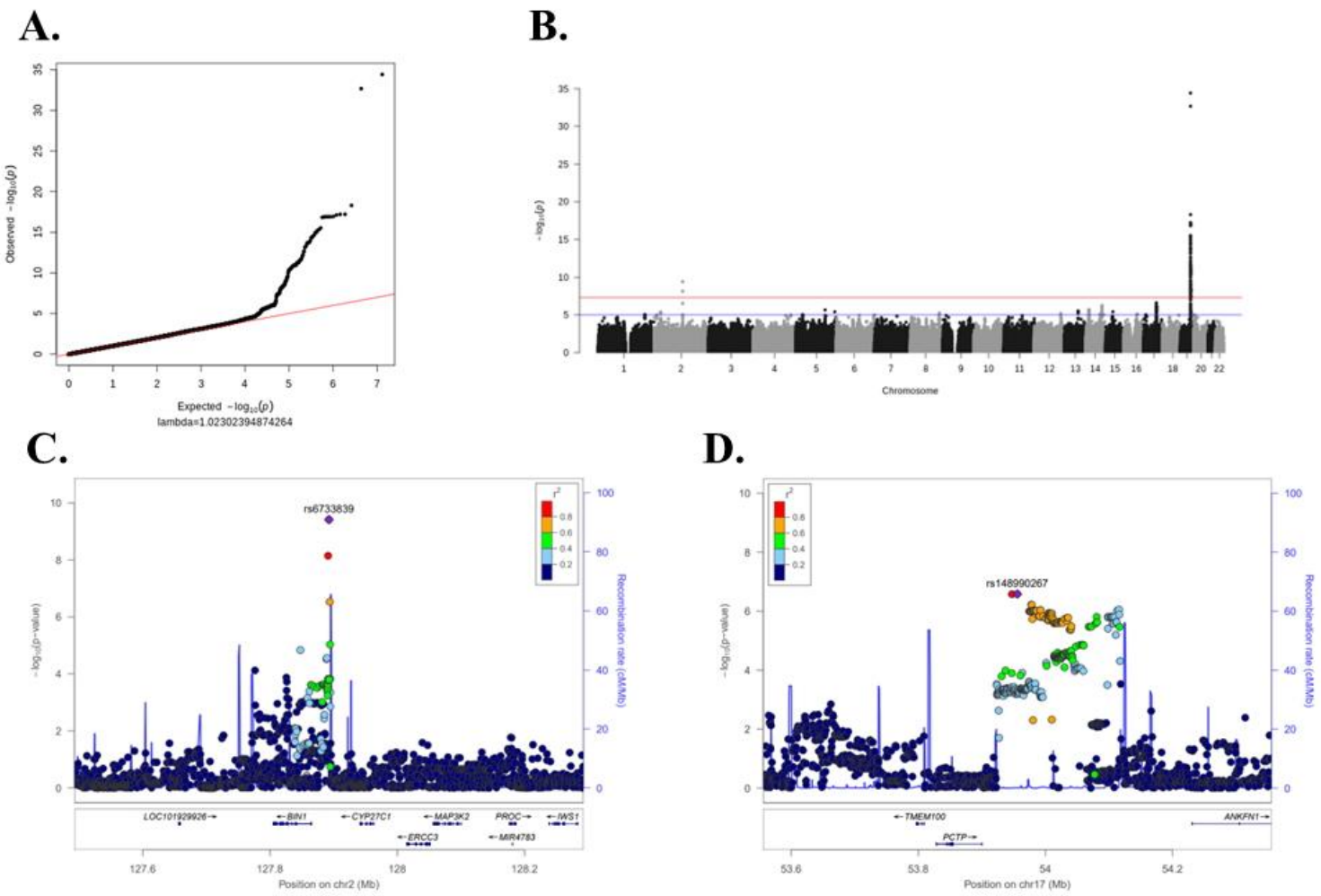
Table 1. Participant Demographics for Tau PET Imaging (By Tracer)

	FTP Tracer	MK Tracer	Total
Total, N	998	354	1,352
Sex, N (%)			
Males	477 (47.80)	117 (33.05)	594 (43.93)
Females	521 (52.20)	237 (66.95)	758 (56.07)
Age (At Tau PET Scan), Mean±SD	72.86±8.74	69.50±7.22	71.98±8.50
Tau Positivity, N (%)			
No	803 (80.46)	328 (92.66)	1131 (83.65)
Yes	195 (19.54)	26 (7.34)	221 (16.35)

Table 2. Participant Demographics for Neuropath Autopsy (By Cohort)

	ACT	NACC	NIA-AD FBS	ROS/MAP/MARS	Total
Total, N	458	4,320	64	624	5,466
Sex, N (%)					
Males	202 (44.10)	2,339 (54.14)	30 (46.88)	218 (34.94)	2,789 (51.02)
Females	256 (55.90)	1,981 (45.86)	34 (53.12)	406 (65.06)	2,677 (48.98)
Age (At Death), Mean±SD	87.40±4.26	80.44±11.29	83.31±8.67	88.39±6.76	81.97±10.83
Tau Positivity, N (%)					
No	139 (30.35)	1,092 (25.28)	8 (12.50)	110 (17.63)	1,349 (24.68)
Yes	319 (69.65)	3,228 (74.72)	56 (87.50)	514 (82.37)	4,117 (75.32)

Figure 1.



Keywords: tau pathology, PET imaging, postmortem, GWAS, multimodal

Monday, January 12, 2026 - 04:15 pm - 04:20 pm

Podium Session

B1 - B: Blitz Session

CHAIRS:

Monday, January 12, 2026			
04:15 pm – 04:20 pm	Title	Authors	Presenter
Board # 39	**OMG: a proteomic determinant of neurodegenerative resiliency**	Duggan | Oh | Frank | Gomez | Zweibaum | Cui | Chen | Surapaneni | Blew | Dark | Joynes | Kandala | Bilgel | Farinas | Erus | Tian | Candia | Pucha | Landman | Dumitrescu | Hohman | Lewis | Moghekar | Siavoshi | Ali | Liu | Xu | Western | Kaneko | Kato | Furuichi | Shibayama | Katsuno | Nishita | Otsuka | Gottesman | Dammer | Seyfried | Levey | Johnson | Mormino | Wagner | Poston | Kapogiannis | Grams | Bhargava | Waga | Davatzikos | Resnick | Ferrucci | Bennett | Cruchaga | Wyss-Coray | Kivimäki | Coresh | Walker	**Michael Duggan,** NIH, Baltimore, MD, USA
Board # 14	**Lifetime and 10-year absolute risk of cognitive impairment associated with amyloid PET severity: a retrospective, longitudinal cohort study**	Hu | Therneau | Wiste | Knopman | Vemuri | Graff-Radford | Lowe | Vassilaki | Cogswell | Schwarz | Algeciras-Schimnich | Petersen | Jack Jr.	**Mingzhao Hu,** Mayo Clinic, Rochester, MN, USA
Board # 26	**Stratifying preclinical Alzheimer's disease by hippocampal volume to detect concomitant LATE**	Mundada | Lyu | Sadeghpour | Brown | McGrew | Yushkevich | Das | Wolk	**Nidhi Mundada,** University of Pennsylvania, Philadelphia, PA, USA

Monday, January 12, 2026 - 04:15 pm - 04:20 pm

[Special] Podium Session

The PET-tle Royale (HAI's very own synaptic showdown quiz)

Christopher Schwarz, Mayo Clinic, Rochester, MN, USA

Step aside, battle royale gamers--this one's for the biomarker buffs. For the first time ever, HAI attendees will face off in a rapid-fire quiz showdown that tests not just your reflexes, but your PET prowess.

Armed only with your phone or laptop, you'll dive into *Slido* and tackle a cascade of multiple-choice questions spanning the full HAI universe: Amyloid PET, Tau PET, plasma biomarkers, ADRD at large, plus a dash of HAI lore and culture for good measure.

But wait, there's more. We'll flash scans for you to rate: positive vs. negative, signal vs. artifact, real vs. off-target binding. And because we like to keep you on your toes, some questions will pull straight from the day's presentations. Translation: pay attention, or prepare to be outpaced.

The spoils? Eternal glory, peer admiration, and the coveted title of HAI Quiz Champion, complete with certificate suitable for framing (or humble-bragging).

Tuesday, January 13, 2026 - 08:30 am - 09:45 am

Podium Session

ISTAART Collaborations: Neuroimaging in clinical decision making: presentation and interactive discussion of real-world cases to identify evolving research needs

SESSION ORGANIZERS:

***Tobey Betthauser**, University of Wisconsin-Madison, Madison, WI, USA*

***Alexa Pichet Binette**, University of Montreal, Montreal, QC, Canada*

***Yara Yakoub**, McGill university, Montreal, QC, Canada*

CHAIRS:

***Tobey Betthauser**, University of Wisconsin-Madison, Madison, WI, USA*

Kathleen Poston, *Stanford University, Stanford, CA, USA*

Tuesday, January 13, 2026		
08:30 am - 09:45 am	ISTAART Collaborations	
08:30 am – 08:35 am	Session Introduction and Overview	**Alexa Pichet Binette**, University of Montreal, Montreal, QC, Canada **Tobey Betthauser**, University of Wisconsin-Madison, Madison, WI, USA **Kathleen Poston**, Stanford University, Stanford, CA, USA
08:35 am – 08:50 am	Case 1	**Petrice Cogswell**, Mayo Clinic, Rochester, MN, US
08:50 am – 09:05 am	Case 2	**Christopher Rowe**, Austin Health, Melbourne, Vic, Australia
09:05 am – 09:20 am	Case 3	**Gil Rabinovici**, University of California San Francisco, San Francisco, CA, USA
09:20 am – 09:45 am	Discussion	

Changes in regulatory policy and appropriate use recommendations coupled with approved anti-amyloid therapies have led to neuroimaging increasingly being used in clinical decision making including for differential diagnosis, patient management, treatment qualification, and treatment monitoring for anti-amyloid therapies. Information and experiences from real-world clinical scenarios utilizing neuroimaging to inform clinical decisions provides a valuable resource to identify challenges in implementing qualitative and quantitative neuroimaging in clinical practice and areas of needed research that will address current clinical demands. The goal of this session is to identify neuroimaging research priorities that address current and future clinical needs based on current clinical experiences. This session will feature interactive presentations of real-world clinical cases from expert clinicians with interactive audience polling and discussion at key clinical decision points.

Tuesday, January 13, 2026 - 09:45 am - 09:50 am

Podium Session

B2 - A: Blitz Session

Tuesday, January 13, 2026			
09:45 am – 09:50 am	Title	Authors	Presenter
Board # 96	**Early concordance between Aβ PET spatial extent and plasma %ptau217**	Farrell | Thibault | Yang | Price | Chhatwal | Coughlan | Buckley | Sperling | Johnson	**Michelle Farrell**, Massachusetts General Hospital, Harvard Medical School, Boston, MA, USA
Board # 69	**Head-to-head comparison of tau PET tracers across the Alzheimer's disease spectrum: baseline results from the HEAD study**	Povala | Bellaver | Lussier | Amaral | Bauer-Negrini | Ferreira | Jagust | Masdeu | Fortea | Tudorascu | Soleimani-Meigooni | Lowe | Oh | Pascual | Gordon | Rosa-Neto | Baker | Pascoal	**Guilherme Povala**, University of Pittsburgh, Pittsburgh, PA, USA
Board # 78	**Evaluating occipital-to-global amyloid PET as a predictor of CAA at autopsy in Mayo Clinic cohorts**	Schwarz | Hu | Cogswell | Graff-Radford | Vemuri | Przybelski | Wiste | Nguyen | Reichard | Dickson | Lowe | Ramanan | Knopman | Petersen | Jack	**Christopher Schwarz**, Mayo Clinic, Rochester, MN, USA

Tuesday, January 13, 2026 - 09:50 am - 10:50 am

Poster Session

Poster Session 2A

Tuesday, January 13, 2026			
09:50 am – 10:50 am	**Poster Presentation**	**Authors**	**Presenter**
Board 49	CSF oligodendrocyte biomarkers are associated with amyloid burden in Alzheimer's disease	Santos Machado | De Bastiani | Lebrun | Povala | Pola | Vizlin-Hodzic | Rosa-Neto | Zimmer | Blennow | Zetterberg | Benedet | Ashton	**Luiza Santos Machado**, University of Gothenburg, Gothenburg, Sweden
Board 50	Associations between systolic blood pressure and amyloid burden on cross-sectional inferior temporal tau across mid- to late-life	Yau | Scott | Palmgren | Coughlan | Kirn | Properzi | Schultz | Ghosh | Buckley | Amariglio | Rentz | Johnson | Sperling | Beiser | Seshadri | Chhatwal	**Wai-Ying Wendy Yau**, Department of Neurology, Mass General Brigham, Boston, MA, US
Board 51	Associations of ER176 TSPO PET with blood-based AD and neuroinflammation biomarkers	Cogswell | Lundt | Ou | Algeciras-Schimnich | Zekeridou | Lim | Graff-Radford | Schwarz | Vemuri | Petersen | Jack Jr | Lowe	**Petrice Cogswell**, Mayo Clinic, Rochester, MN, US
Board 52	Evaluation of [18F]MK6240 test-retest reproducibility for different processing pipelines	Tiss | Thibault | Fu | Becker | Price | Johnson	**Amal Tiss**, Gordon Center for Medical Imaging, Massachusetts General Hospital, Boston, MA, US
Board 53	Temporal dynamics of tau PET subtypes and its association with heterogeneous neurodegeneration in Alzheimer's disease	Kwon | Song | Lee | Seong	**Taw Youn Kwon**, Department of Artificial Intelligence, Korea University, Seoul, South Korea
Board 54	A-T-N-C generative model for predicting and simulating patient-tailored cognitive decline trajectories in Alzheimer's disease	Lee | Song | Kwon | Lee | Seong	**Tae Youn Kwon**, Department of Artificial Intelligence, Korea University, Seoul, South Korea
Board 55	High-resolution ex-vivo MRI reveals layer-specific atrophy of hippocampal subregions to earliest tau pathology	Salman | Tomé | Joudiou | Thal | Annettesdotter | Khandelwal | Yushkevich | Gallez | Wisse | Hanseeuw	**Yasmine Salman**, Institute of Neuroscience, Université Catholique de Louvain, Brussels, Belgium
Board 56	Blood volume influences the association between baseline plasma biomarker values and amyloid PET outcomes over time	Burns | Gogola | Zeng | Karikari | Jacobs | Lopresti | Osorio	**Kelsey Burns**, Department of Radiology, University of Pittsburgh School of Medicine, Pittsburgh, PA, US
Board 57	Visual interpretation methods for tau-PET imaging with Flortaucipir and MK-6240: Insights from the HEAD study	Ruppert | Vermeiren | Scop Medeiros | Povala | Rocha | Soares | Ferreira | Amaral | Bauer-Negrini | Lussier | Scarpatto Rodrigues | Oliveira Jr. | Mroue | Bellaver |	**Tharick Pascoal**, University of Pittsburgh, Pittsburgh, PA, US

		Moscoso | Ossenkoppele | van de Giessen | Masdeu | Tudorascu | Soleimani-Meigooni | Fortea | Lowe | Oh | Pascual | Gordon | Rosa-Neto | Baker | Pascoal	
Board 58	Associations between TSPO PET and CSF and blood-based biomarkers	Smith | Guzman | Houlihan | Sanchez | Kreisl | Talmasov | De Jager | Herman | Simoes | Small | Lao	**Anna Smith**, Columbia University Medical Center, New York, NY, US
Board 59	Regional white matter injury modifies the association between ß-amyloid and cognition	Royse | Reese | Snitz | Hengenius | Crane | Mukherjee | Choi | Willie-Permor | Felix | Huppert | Roush | Cisneros | Potopenko | Lopresti | Cohen | Shaaban	**Sarah Royse**, Department of Radiology, University of Pittsburgh, Pittsburgh, PA, US
Board 60	Sex differences in neuroinflammation, amyloid, tau, and neurodegeneration	Guzman | Smith | Houlihan | Sanchez | Akinci | Luchsinger | Lao	**Diana Guzman**, Columbia University Irving Medical Center, New York, NY, US
Board 61	Evaluation of the tau PET ligand [18F]florzolotau in frontotemporal dementia	Clarke | Whittington | Sholaja | Hield | Huiban | van den Berg | Margolin | Rowe | Rohrer | Salinas | Rabiner	**Alex Whittington**, Perceptive, London, UK
Board 62	Intersections of gender/sex and neighborhood deprivation on cognition: Are there mediation effects of Alzheimer's disease biomarkers?	Reese | Royse | Snitz | Crane | Mukherjee | Choi | Hengenius | Huppert | Roush | Cisneros | Lopresti | Rameriz Tirado | Willie-Permor | Felix | Cohen | Shaaban	**Alexandria Reese**, Department of Radiology, University of Pittsburgh, Pittsburgh, PA, US
Board 63	Disentangling cognitive severity and phenotype across dementia syndromes	Smith | Coyle-Gilchrist | Murley | Rouse | Stockton | Naessens | Savulich | Wiggins | Malpetti | Bowns | Perquin | Lanskey | Karadag | Kocagoncu | Quinn | Pitt | Alcock | O'Brien | Rittman | Rowe | Lambon-Ralph	**Viktorija Smith**, MRC Cognition and Brain Sciences Unit, University of Cambridge, Cambridge, UK
Board 64	Standardized indices of tau burden using the CenTauR universal scale predict distinct cognitive trajectories across Alzheimer's disease biological stages	Lopresti | DelBene | Leuzy | Gogola | Harrison | Landau | Jagust | Villemagne	**Brian Lopresti**, Department of Radiology, University of Pittsburgh School of Medicine, Pittsburgh, PA, US
Board 65	SPARE-SVD: An integrated machine-learning metric for cerebral small vessel disease within the ATN(V) framework	Dong | Zhang | Zeng | Wang | Wang | Toledo | Gonzales | Charisis | Rashid | Seshadri | Crane | Archer | Jefferson | Hohman | Habes	**Mengjin Dong**, Neuroimage Analytics Laboratory (NAL) and the Biggs Institute Neuroimaging Core (BINC), Glenn Biggs Institute for Alzheimer's and Neurodegenerative Diseases, University of Texas Health Science Center San Antonio, San Antonio, TX, US
Board 66	Risk factors and AD prevention: a multivariate and multimodal study	Fajardo Valdez | Qiu | Ourry | Yakoub | Villeneuve | Research Group	**Alfonso Fajardo Valdez**, Department of Psychiatry, Faculty of

			Medicine, McGill University., Montreal, QC, Canada
Board 67	MK6240 and Tauvid positivity, cognitive decline, and their relationship to Aβ PET deposition across the Alzheimer's spectrum	Bellaver | Povala | Lussier | Amaral | Bauer-Negrini | Ferreira | Jagust | Masdeu | Fortea | Tudorascu | Soleimani-Meigooni | Lowe | Oh | Pascual | Gordon | Rosa-Neto | Baker | Pascoal	**Bruna Bellaver**, University of Pittsburgh, Department of Psychiatry, Pittsburgh, PA, US
Board 68	Differential tau-PET load predominance along shared progression trajectories determines clinical variability in Alzheimer's disease	Mroué | Povala | Bellaver | Lukasewicz Ferreira | Bauer-Negrini | Lussier | Amaral | Scop Medeiros | Ruppert | Silva da Rocha | Scarpatto Rodrigues | Silva Oliveira | Soares Katz | Teixeira Leffa | Saha | Masdeu | Soleimani-Meigooni | Fortea | Lowe | Oh | Pascual | Gordon | Rosa-Neto | Baker | Pascoal	**Guilherme Povala**, University of Pittsburgh, Department of Psychiatry, Pittsburgh, PA, US
Board 69	Head-to-head comparison of tau PET tracers across the Alzheimer's disease spectrum: baseline results from the HEAD study	Povala | Bellaver | Lussier | Amaral | Bauer-Negrini | Ferreira | Jagust | Masdeu | Fortea | Tudorascu | Soleimani-Meigooni | Lowe | Oh | Pascual | Gordon | Rosa-Neto | Baker | Pascoal	**Guilherme Povala**, University of Pittsburgh, Department of Psychiatry, Pittsburgh, PA, US
Board 70	Comparison of Sampled Iterative Local Approximation (SILA) implemented in R and MATLAB	Bruzzone | Coath | Navaratna | Carey | Morse | Bilgel | Betthauser	**Hailey Bruzzone**, Department of Medicine, University of Wisconsin-Madison School of Medicine and Public Health, Madison, WI, US
Board 71	Agreement between amyloid status prediction from visual read, SUVR thresholding, and AI-based interpretation of amyloid PET	Peraza | Joules | Mohs | Beauregard | Dwyer | Hughes | Wolz	**Robin Wolz**, IXICO, London, UK
Board 72	CenTauR thresholds generated using Gaussian Mixture Models for biological staging of amyloid positive ADNI participants	DelBene | Villemagne | Gogola | Leuzy | Harrison | Landau | Jagust | Lopresti	**Alexander DelBene**, Department of Radiology, University of Pittsburgh School of Medicine, Pittsburgh, PA, US
Board 73	Progression to tau-PET positivity by plasma P-tau217 levels and its association with clinical decline in preclinical Alzheimer's disease: data from A4 study	Kim | Kotari | Morris | Shcherbinin | Yaari | Holdridge | Sims | Ossenkoppele | Collins | Hansson | Lu	**Min Jung Kim**, Eli Lilly and Company, Indianapolis, IN, US
Board 74	Neuroimaging correlates of loneliness	Sanchez | Guzman | Smith | Houlihan | Stern | Bockting | Lao	**Thairi Sanchez**, Columbia University Irving Medical Center, New York, NY, US
Board 75	Age-dependent associations between salivary inflammatory cytokines and amyloid-beta in cognitively unimpaired older adults	Parker | Tang | Taylor | Bock | Meza | Tuteja | Avila | Chang | Simmons | Bamford | Yi | Mcmillan | Kim | Thomas | Adams | Yassa	**Dana Parker**, Department of Neurobiology and Behavior, University of California Irvine, Irvine, CA, US

Board 76	Tau accumulation drives worsening depressive symptoms in cognitively normal older adults	Markova | Berry	**Teodora Markova**, Brandeis University, Volen Center for Complex Systems, Waltham, MA, US
Board 77	Dorsal raphe nucleus and locus coeruleus differentially relate to depressive symptoms in cognitively normal older adults	Markova | Chen | Carlson | Cao | Ciampa | Marcus | Adornato | Matulonis | Morin | Hooker | Berry	**Teodora Markova**, Brandeis University, Volen Center for Complex Systems, Waltham, MA, US
Board 78	Evaluating occipital-to-global amyloid PET as a predictor of CAA at autopsy in Mayo Clinic cohorts	Schwarz | Hu | Cogswell | Graff-Radford | Vemuri | Przybelski | Wiste | Nguyen | Reichard | Dickson | Lowe | Ramanan | Knopman | Petersen | Jack	**Christopher Schwarz**, Mayo Clinic, Rochester, MN, US
Board 79	SCAN: Standardized Centralized Alzheimer's and related dementias Neuroimaging	Schwarz | Harrison | DeCarli | Kantarci | Baker | La Joie | Maillard | Rabinovici | Toga | Jack | Jagust	**Christopher Schwarz**, Mayo Clinic, Rochester, MN, US
Board 80	Differential contributions of amyloid spatial extent and tau burden to domain-specific cognitive decline in early Alzheimer's disease	Slade | Thibault | Thompson | Fanglu Fu | Price | Rentz | Sperling | Johnson | Farrell	**Elliott Slade**, Massachusetts General Hospital, Harvard Medical School, Boston, MA, US
Board 81	PET-measured amyloid accumulation rate modulates tau accumulation rate in individuals with Down syndrome	Bettcher | McLachlan | Zammit | McVea | Betthauser | Laymon | Tudorascu | Cohen | Price | Head | Mapstone | Lao | Johnson | Ances | Handen | Christian	**Brecca Bettcher**, University of Wisconsin-Madison School of Medicine and Public Health and Waisman Center, Madison, WI, US
Board 82	Elevated medial temporal lobe tau predicts cross-sectional association between neocortical tau and global amyloid burden	Thibault | Reilhac-Laborde | Charil | Irizarry | Johnson	**Emma Thibault**, Massachusetts General Hospital, Boston, MA, US
Board 83	Assessing the effect of amyloid status on the relationship between glucose metabolism and synaptic density in the aging population	McLachlan | Bettcher | DiFilippo | LeMerise | McVea | Zammit | Langhough | Johnson | Bendlin | Christian	**Max McLachlan**, University of Wisconsin-Madison, Madison, WI, US
Board 84	Associations between p-tau217 and brain atrophy are amplified by Aβ burden and APOEε4	Brown | Properzi | Cuppels | Birkenbihl | Coughlin | Seto | Townsend | Betthauser | Schultz | Chhatwal | Yang | Jacobs | Farrell | Johnson | Johnson | Li | Sperling | Hohman | Donohue | Buckley	**Jane Brown**, Massachusetts General Brigham, Boston, MA, US
Board 85	Early cortical thickness change in preclinical AD development	Sinclair | Chen	**Stephanie Sinclair**, Stony Brook University, Stony Brook, NY, US
Board 86	Immuno-vascular crosstalk drives tau pathology preferentially in women	Wood Alexander | Kang | Rusdi | Yin | Rahmouni | Wang | Benedet | Zetterberg | Blennow | Karikari | Ashton | Black | Goubran | Rabin | Ottoy	**Madeline Wood Alexander**, Centre for Brain Resilience & Recovery, Hurvitz Brain Sciences Program, Sunnybrook Research

			Institute, University of Toronto, Toronto, ON, Canada
Board 87	Midlife physical activity attenuates the association of earlier menopause with tau pathology and cognitive decline	Wood Alexander | Cadwallader | Johnson | Casaletto | Rabin	**Madeline Wood Alexander**, Sunnybrook Research Institute, Toronto, ON, Canada
Board 88	Improved tau PET signal detection with total-body PET compared to conventional PET: A preliminary study	Young | Bayerlein | Bhattarai | DeCarli | Badawi | Fan	**Christina Young**, University of California Davis, Davis, CA, US
Board 89	Demographic associations with plasma biomarkers in the oldest-old: The LifeAfter90 Study	Young | Colbeth | Gilsanz | Corrada | Rizvi | Zhou | di Lucente | DeCarli | Jin | Whitmer	**Christina Young**, University of California Davis, Davis, CA, US
Board 90	Differential sensitivity of T1-MRI and FDG-PET for tracking neurodegeneration across progressive stages of tau pathology in Alzheimer's disease	Vourkas | Karagianni | Moscoso | Zhang | Sanchez-Juan | Schöll | Grothe | Silva-Rodríguez	**Jesús Silva-Rodríguez**, CIEN Foundation, Reina Sofia Alzheimer Center, ISCIII, Madrid, Spain
Board 91	SPARE-Tau, a machine-learning derived tau-PET index, correlates with Alzheimer's disease and related dementias biomarkers	Wang | Zeng | Toledo | Gonzales | Honnorat | Charisis | Dong | Ho | Rashid | Kutty | Salman | Vroman | Seshadri | Habes	**David Wang**, Neuroimage Analytics Laboratory (NAL) and the Biggs Institute Neuroimaging Core (BINC), Glenn Biggs Institute for Alzheimer's and Neurodegenerative Diseases, University of Texas Health Science Center San Antonio, San Antonio, TX, US
Board 92	Assessing the generalizability of plasma p-tau217 cutpoints for amyloid-β detection across clinical and preclinical cohorts	Liu | Zeng | Nafash | Sehrawat | Choity | Gu | Farinas | Bedison | Matan | Gogola | Huang | Sewell | McAuley | Hillman | Kramer | Burns | Kang | Vidoni | Nadkarni | Aizenstein | Kofler | Tudorascu | Shaaban | Lingler | Pascoal | Villemagne | Berman | Sweet | Snitz | Ikonomovic | Kamboh | Erickson | Cohen | Lopez | Deek | Karikari	**Tianshu Liu**, Department of Biostatistics and Health Data Science, School of Public Health, University of Pittsburgh, Pittsburgh, PA, US
Board 93	Evaluating the transferability of dual cutpoints for plasma p-tau217 in detecting brain amyloid-β across diverse cohorts	Liu | Zeng | Nafash | Sehrawat | Choity | Gu | Farinas | Bedison | Matan | Gogola | Huang | Sewell | McAuley | Hillman | Kramer | Burns | Kang | Vidoni | Nadkarni | Aizenstein | Kofler | Tudorascu | Shaaban | Lingler | Pascoal | Villemagne | Berman | Sweet | Snitz | Ikonomovic | Kamboh | Erickson | Cohen | Lopez | Deek | Karikari	**Tianshu Liu**, Department of Biostatistics and Health Data Science, School of Public Health, University of Pittsburgh, Pittsburgh, PA, US
Board 94	Free-water interacts with amyloid positivity to predict regional tau	Sathe | Durant | Koran | Dumitrescu | Cody | Sokołowski |	**Aditi Sathe**, Vanderbilt Memory and Alzheimer's

	pathology in both early and late Braak stages	Kim | Mez | Saykin | Toga | Cuccaro | Tosun | Johnson | Barber | O'Bryant | Landman | Mormino | Hohman | Archer	Center, Vanderbilt University Medical Center, Nashville, TN, US
Board 95	Integration of data-driven biomarker discovery with established Alzheimer's disease biomarkers in an African American cohort	Kuchenbecker | Heckman | Nguyen | Casellas | Sotelo | Schwarz | Senjem | Jain | Lucas | Willis | Ertekin-Taner | Graff-Radford | Kantarci | Lowe | Lachner | Day | Carrasquillo	**Lindsey Kuchenbecker**, Department of Neuroscience, Mayo Clinic Florida, Jacksonville, FL, US
Board 96	Early concordance between Aβ PET spatial extent and plasma %ptau217	Farrell | Thibault | Yang | Price | Chhatwal | Coughlan | Buckley | Sperling | Johnson	**Michelle Farrell**, Massachusetts General Hospital, Harvard Medical School, Boston, MA, US

49 CSF oligodendrocyte biomarkers are associated with amyloid burden in Alzheimer's disease

Luiza Santos Machado[1], Marco De Bastiani[2], Aurélie Lebrun[3], Guilherme Povala[4], Ilaria Pola[1], Dzeneta Vizlin-Hodzic[1], Pedro Rosa-Neto[3], Eduardo Zimmer[2], Kaj Blennow[1], Henrik Zetterberg[1], Andrea Benedet[1], Nicholas Ashton[1,5]

[1]*University of Gothenburg, Gothenburg, Sweden*
[2]*Federal University of Rio Grande do Sul, Porto Alegre, Brazil*
[3]*McGill University, Montreal, QC, Canada*
[4]*University of Pittsburgh, Pittsburgh, PE, US*
[5]*Banner Alzheimer's Institute, Phoenix, AZ, US*

Background: Oligodendrocytes are glial cells implicated in amyloid ß (Aß) pathology and Alzheimer's disease (AD) pathophysiology. Despite growing evidence for their involvement, biomarkers assessing oligodendrocyte changes in AD are under-investigated. We aimed to identify novel oligodendrocyte biomarkers in CSF and evaluate their association with AD amyloid pathology.

Methods: Oligodendrocyte- and oligodendrocyte precursor cell (OPC)-enriched genes were identified using single-cell and single-nucleus transcriptomic datasets from the Allen Brain Atlas and SEA-AD consortia. CSF proteomic data (SomaLogic) from 663 ADNI participants were analyzed, focusing on proteins encoded by these genes. Group comparisons were performed in cognitively unimpaired (CU) versus cognitively impaired (CI) individuals and in Aß+ versus Aß– groups (ptau181/Aß42 cut-off=0.028) using linear regression. The differentially expressed proteins (DEPs) had their trajectories across centiloid-defined stages examined with regression models. Voxelwise association analyses were then conducted between DEPs and regional [18F]Florbetapir-PET uptake. Models were adjusted for age and sex, with random field theory correction applied to imaging results and false discovery rate correction for linear regressions.

Results: We identified 1081 oligodendrocyte- and/or OPC-enriched genes, of which 267 were found to be present in CSF. In CI versus CU individuals, 37 DEPs were identified (Fig.1A), whereas 68 proteins differed between Aß+ and Aß- individuals (Fig.1B). Across centiloid stages, 16 proteins showed positive and 8 negative associations with Aß burden (Fig.2). Voxelwise analyses confirmed regional associations between these proteins and Aβ burden, particularly in the cortex (Fig.3).

Conclusion: This study identifies 86 oligodendrocyte-enriched CSF proteins altered in AD, including 24 associated to cortical Aß burden. These findings provide candidate biomarkers for oligodendrocyte-related pathology in AD and will be further validated in an independent cohort.

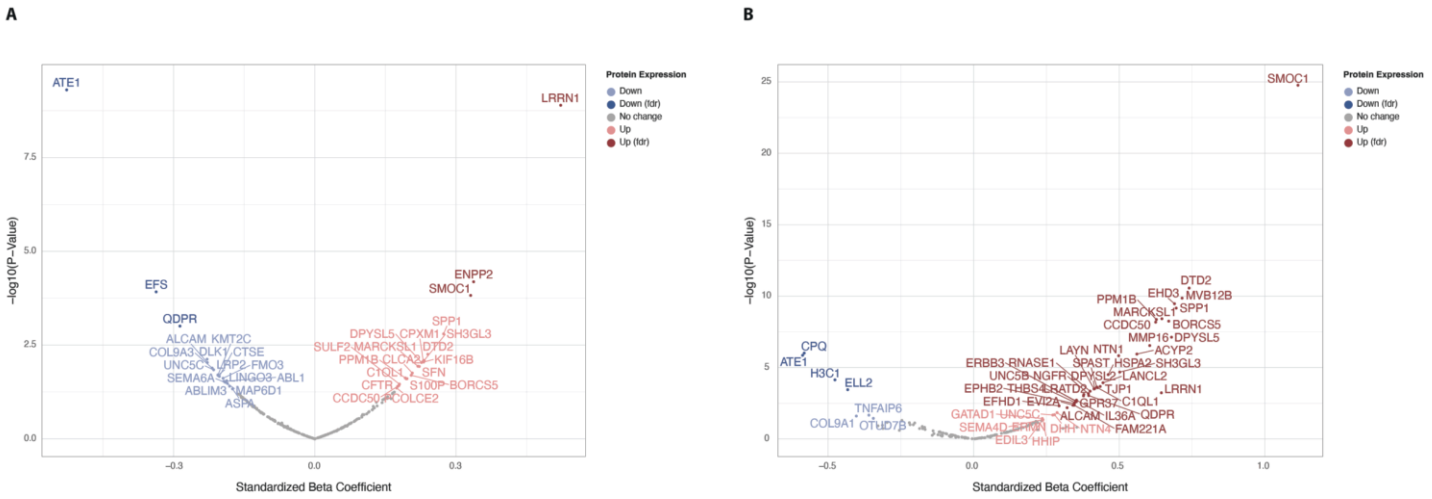


Figure 1. Volcano plots of differentially expressed CSF proteins in ADNI participants.

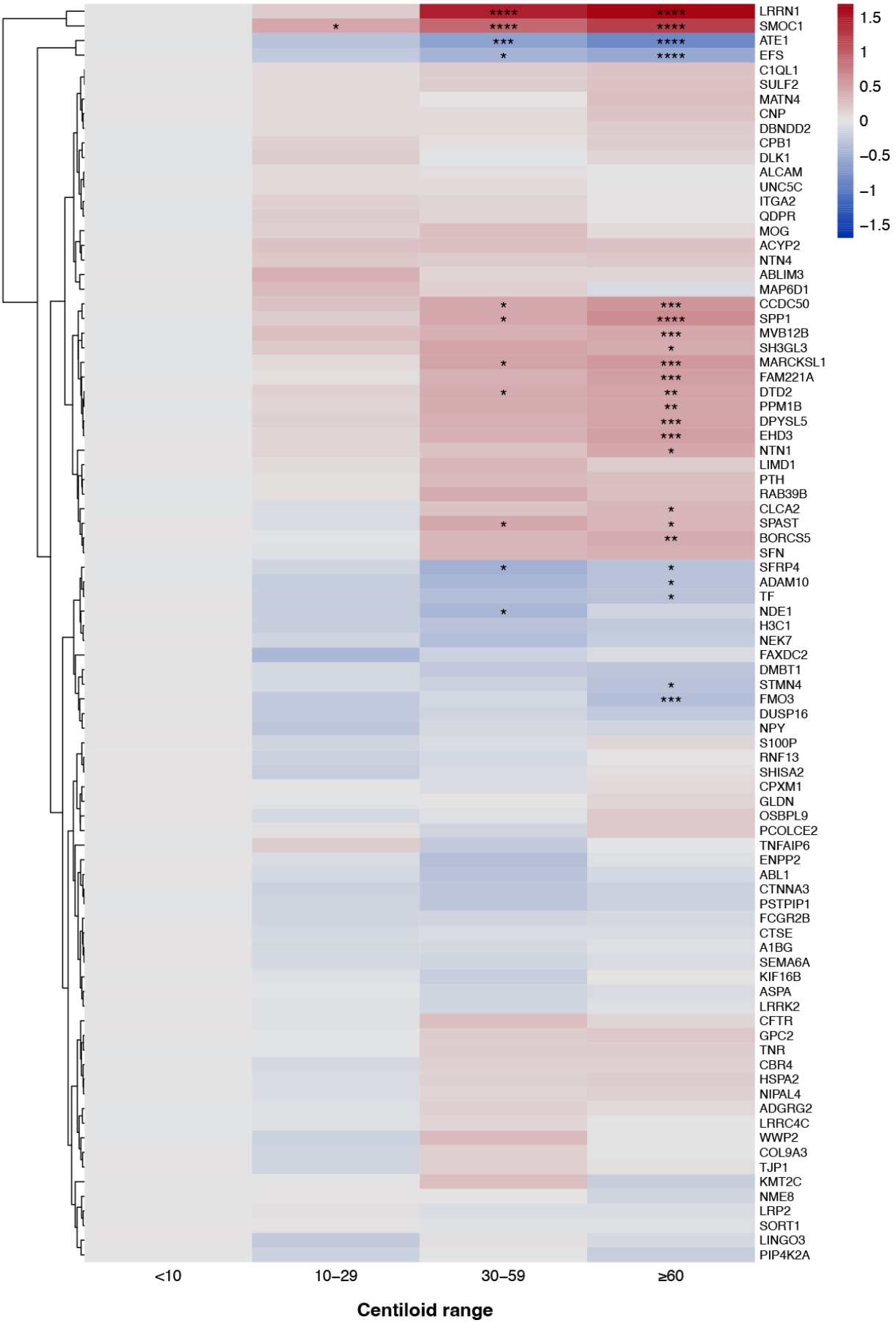


Figure 2. Heatmap of CSF protein levels across centiloid ranges.



Figure 3. Voxelwise associations between CSF proteins and [18F]Florbetapir-PET.

Keywords: Amyloid, PET, Oligodendrocytes, CSF

50 Associations between systolic blood pressure and amyloid burden on cross-sectional inferior temporal tau across mid- to late-life

Wai-Ying Wendy Yau[1,2], Matthew Scott[3,4], Kailee Palmgren[1], Gillian Coughlan[1,2], Dylan Kirn[1], Michael Properzi[1], Aaron Schultz[1,2], Saptaparni Ghosh[4,5], Rachel Buckley[1,2], Rebecca Amariglio[1,2], Dorene Rentz[1,2], Keith Johnson[1,2,6], Reisa Sperling[1,2], Alexa Beiser[3,4,5], Sudha Seshadri[4,7], Jasmeer Chhatwal[1,2]

[1]*Department of Neurology, Mass General Brigham, Boston, MA, US*
[2]*Harvard Medical School, Boston, MA, US*
[3]*Department of Biostatistics, School of Public Health, Boston University, Boston, MA, US*
[4]*The Framingham Heart Study, Framingham, MA, US*
[5]*Department of Neurology, Chobanian and Avedisian School of Medicine, Boston University School of Medicine, Boston, MA, US*
[6]*Department of Radiology, Mass General Brigham, Boston, MA, US*
[7]*Glen Biggs Institute for Alzheimer's & Neurodegenerative Diseases, University of Texas Health San Antonio, San Antonio, TX, US*

Background: Hypertension is the most prevalent modifiable risk factor for Alzheimer's disease (AD) and related dementias. The evidence is strongest for midlife hypertension, with mixed findings in late-life. Prior work from Harvard Aging Brain Study (HABS) identified a synergistic association between higher systolic blood pressure (SBP) and amyloid burden with greater inferior temporal (IT) tau accumulation in cognitively unimpaired individuals. However, whether this SBP–amyloid interaction varies across mid- to late-life remains unknown.

Method: We examined cross-sectional data from 230 cognitively unimpaired adults aged 50-90 from HABS and 184 younger participants aged 40-75 from Framingham Heart Study (FHS) (Table 1). Amyloid (Pittsburgh Compound-B) and tau (Flortaucipir) PET from both cohorts were acquired and processed identically, except some FHS scans were performed on GE Discovery scanner and smoothed with 6mm Gaussian filter. We examined the interactive association between SBP and global amyloid (both modeled continuously) on IT tau burden within each cohort across mid- to late-life, using overlapping 20-year sliding age-windows (Table 2). Linear regression models adjusted for age, sex, APOE, time between SBP exam and PET, and (in FHS) PET camera.

Result: Across both HABS and FHS, there was a significant SBP*amyloid interaction where higher SBP and amyloid burden were associated with greater IT tau in the 50-70 (HABS: β=0.008, SE=0.002, p=0.002; FHS: β=0.01, SE=0.004, p=0.007) and 55-75 (HABS: β=0.005, SE=0.002, p=0.003; FHS: β=0.01, SE=0.005, p=0.01) age-windows, but not in younger or older age ranges. Figure 1 illustrates the SBP*amyloid interaction by plotting estimated SBP–tau associations at increasing levels of amyloid burden.

Conclusion: Our findings suggest the synergy between hypertension and amyloid on tau pathology may be most prominent from late midlife to early late-life, highlighting this period as a potential critical window to target hypertension in future AD prevention trials. Future studies should examine additional cohorts and longitudinal tau data.

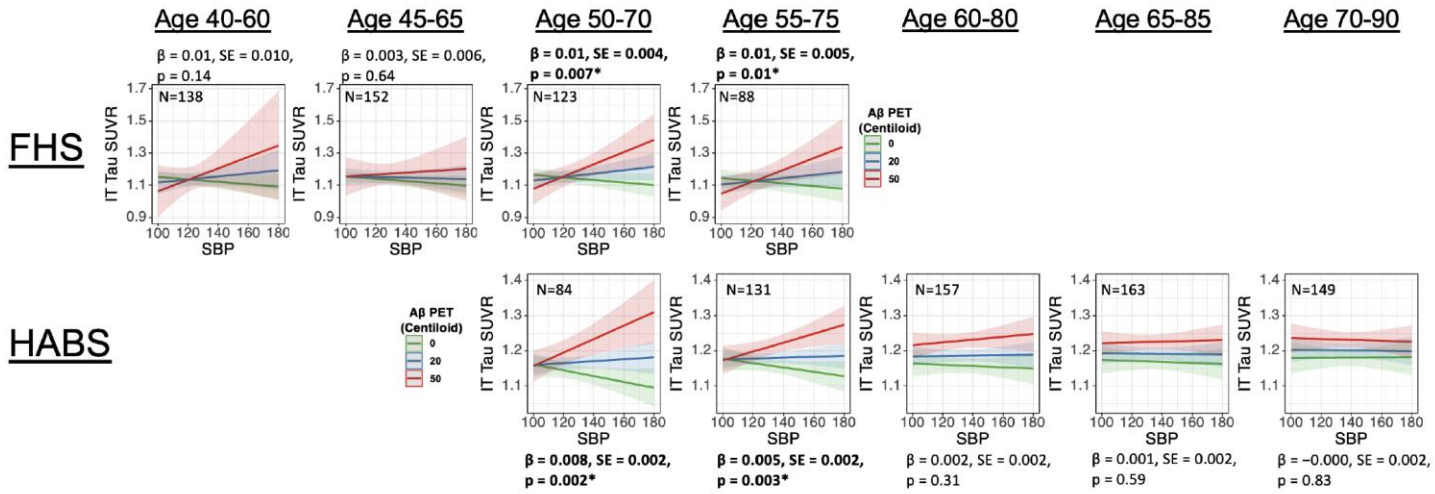
Table 1. Participant characteristics
DVR = distribution volume ratio; FLR = frontal, lateral temporal and parietal, and retrosplenial regional uptake; PET = positron emission tomography; PiB = Pittsburgh compound-B; SD = standard deviation; SUVR = standardized uptake value ratio

	HABS N=230	**FHS N=184**
Age, yr, mean (SD), range	72.5 (9.0) 50-89.8	54.8 (7.8) 40-74
Females, n (%)	140 (60.9)	99 (53.8)
APOE ε4 carriers, n (%)	64 (27.8)	43 (23.4)
Systolic blood pressure, mmHg, mean (SD)	135 (19.4)	120.1 (13.9)
PiB PET FLR DVR, mean (SD)	1.18 (0.2)	1.07 (0.1)
Inferior temporal tau SUVR, mean (SD)	1.18 (0.1)	1.13 (0.1)
Time between blood pressure exam and PET, yr, mean (SD)	-0.32 (0.3)	-0.70 (0.7)

Table 2. Number of participants in overlapping 20-year sliding age-windows across mid- to late-life in HABS and FHS.

		Number of Participants in Overlapping 20-year Sliding Age-Windows						
	Overall N	**40-60**	**45-65**	**50-70**	**55-75**	**60-80**	**65-85**	**70-90**
HABS	**230**	-	-	84	131	157	163	149
FHS	**184**	138	152	123	88	-	-	-

Figure 1. Systolic blood pressure (SBP) by amyloid interaction on cross-sectional inferior temporal tau burden across overlapping 20-year sliding age-windows from mid- to late-life in HABS and FHS. Both SBP and amyloid were modeled as continuous variables. To illustrate the SBP*Amyloid interaction, estimated SBP–IT tau associations were plotted across increasing levels of amyloid burden (at 0, 20 and 50 Centiloids). Aβ = Amyloid; FHS = Framingham Heart Study; HABS = Harvard Aging Brain Study; IT = inferior temporal cortex; SUVR = standardized uptake value ratio.



Keywords: Hypertension, SBP, amyloid, tau, preclinical Alzheimer's disease

51 Associations of ER176 TSPO PET with blood-based AD and neuroinflammation biomarkers

Petrice Cogswell[1], Emily Lundt[1], Fang-Shu Ou[1], Alicia Algeciras-Schimnich[1], Anastasia Zekeridou[1], Seokbeen Lim[1], Jonathan Graff-Radford[1], Christopher Schwarz[1], Prashanthi Vemuri[1], Ronald Petersen[1], Clifford Jack Jr[1], Val Lowe[1]

[1]*Mayo Clinic, Rochester, MN, US*

Objective: Neuroinflammation is a co-occurring process with Alzheimer's disease (AD) and a potential therapeutic target. In vivo biomarkers of neuroinflammation are needed to understand relationships of these processes, identify individuals in whom targeting inflammation would be most beneficial, and monitor therapy effects. ^{11}C-ER176 TSPO PET is a robust measure of neuroinflammation, sensitive across TSPO genotypes, feasible via delayed-uptake imaging, and modestly associated with amyloid and tau PET uptake. In this study we evaluate the association of blood-based AD and inflammatory biomarkers with TSPO PET.

Methods: ^{11}C-ER176 TSPO PET has been performed in 96 Mayo Clinic Study of Aging and Mayo Alzheimer's Disease Research Center participants with diagnoses of cognitively unimpaired (CU), mild cognitive impairment MCI, and AD dementia (**Table**). A subset of 37 individuals had plasma analyzed for p-tau217, and a subset of 36 individuals had serum analyzed for inflammation biomarkers, including sTREM2, GFAP, YKL-40, and a cytokine/chemokine panel on the ELLA multiplexed automated immunoassay system. Blood samples were collected within 7 months of TSPO PET. TSPO PET SUVR was summarized in the amyloid PET meta-ROI. Pearson's correlations were used to evaluate associations between each blood-based biomarker concentration and TSPO PET SUVR.

Results: Plasma p-tau217 concentration showed a modest association with TSPO PET SUVR (R=0.42) (**Figure 1**). Weak correlations of blood neuroinflammation markers with TSPO PET were observed with R=0.26 for sTREM2 (**Figure 2**), 0.18 for GFAP and 0.11 for YKL-40. CXCL9 showed the greatest association of the targets in the cytokine/chemokine panel (R=0.42).

Conclusions: Plasma p-tau217 showed a modest association with TSPO PET SUVR, supporting an association between AD pathology and neuroinflammation. Associations of blood-based inflammation markers with TSPO PET were variable and suggest utility of specific markers as indicators of neuroinflammation. Future work will evaluate these associations within each diagnostic group and after adjusting for relevant covariates.

Table 1: Demographics for the full TSPO PET cohort and for the plasma p-tau217 and serum inflammatory biomarker subgroups.

	Plasma p-tau217 cohort (N=37)	Serum inflammation cohort (N=36)	Full TSPO PET cohort (N=96)
Age at visit, years			
Mean (SD)	75 (7)	76 (9)	77 (8)
Range	62 - 91	61 - 91	61 - 92
Sex, n(%)			
Female	16 (43%)	18 (50%)	47 (49%)
Male	21 (57%)	18 (50%)	49 (51%)
Education, years			
Mean (SD)	15 (3)	16 (3)	15 (3)
Range	12 - 20	12 - 20	12 - 20
Affinity with ER176*, n(%)			
HAB	20 (54%)	16 (44%)	48 (50%)
MAB	10 (27%)	12 (33%)	35 (36%)
LAB	7 (19%)	8 (22%)	13 (14%)
APOE ε4 genotype, n(%)			
N-Miss	1	1	3
Carrier	16 (44%)	16 (46%)	43 (46%)
Non-carrier	20 (56%)	19 (54%)	50 (54%)
Diagnostic group**			
CU A-	14 (38%)	12 (33%)	25 (26%)
CU A+	13 (35%)	12 (33%)	25 (26%)
MCI/AD dem A+	10 (27%)	12 (33%)	46 (48%)
Pearson correlation with TSPO			
p-tau217	0.42	---	---
CXCL9	---	0.42	---
IL-6	---	0.41	---
CXCL13	---	0.39	---
IL-10	---	0.39	---
NFL	---	0.35	---
IL-12	---	0.31	---
TNFα	---	0.27	---
sTREM2	---	0.26	---
CXCL-10	---	0.23	---
IL-2	---	0.22	---
GFAP	---	0.18	---
IL-8	---	0.17	---
YKL-40	---	0.11	---
INFg	---	0.10	---
UCHL1	---	0.05	---

*HAB = high affinity binder, MAX = mixed affinity binder, LAB = low affinity binder
**CU = cognitively unimpaired, MCI = mild cognitive impairment,

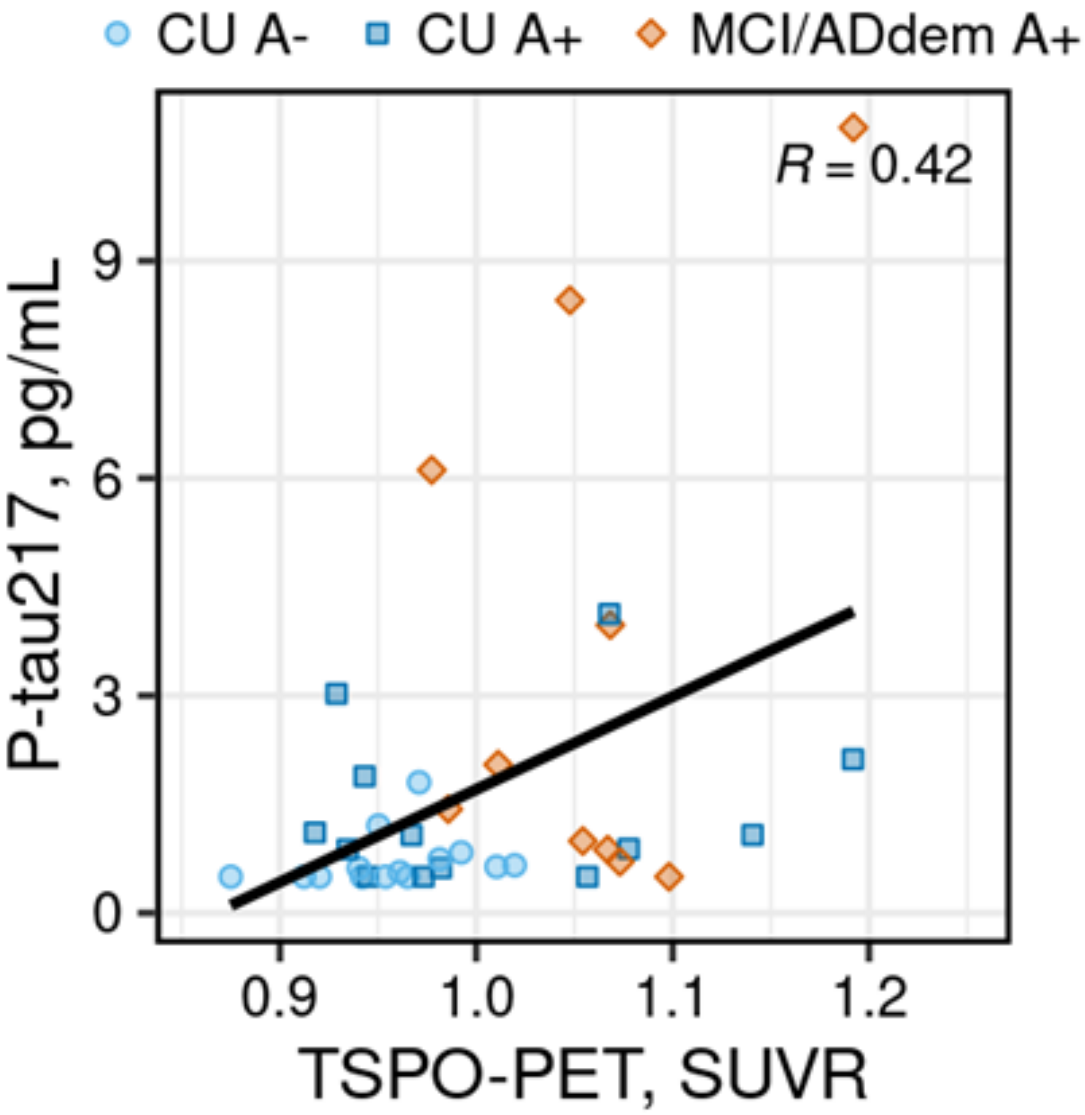


Figure 1: Scatter plot of plasma p-tau217 concentration (C2N) with TSPO PET SUVR in the amyloid PET meta-ROI, an existing atlas that contains regions of highest ER176 uptake in preliminary work. Each dot represents a participant and is colored based on the diagnostic group: cognitively unimpaired (CU) amyloid negative (A-), CU amyloid positive (A+, defined based on an amyloid PET SUVR > 1.42), and mild cognitive impairment (MCI) or Alzheimer's dementia (AD dem) A+.

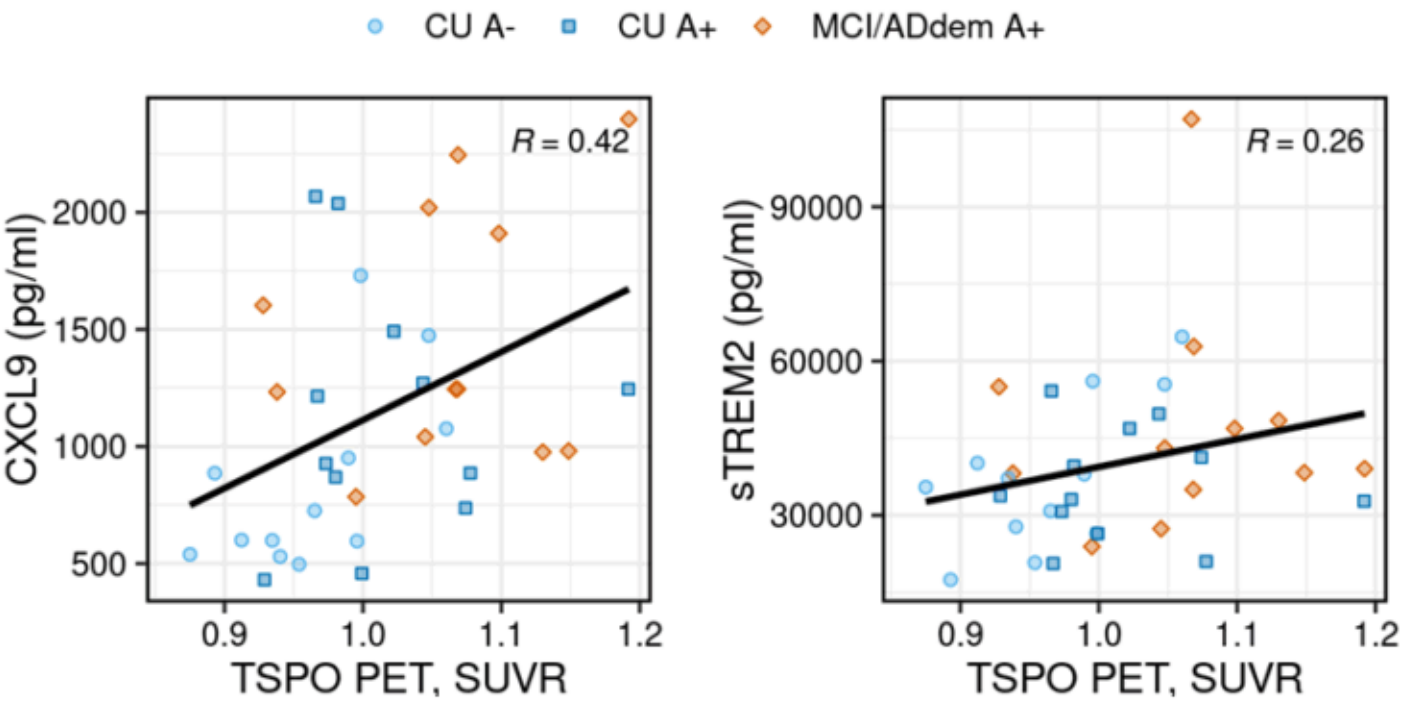


Figure 2: Scatter plots of serum CXCL9 and sTREM2 concentration vs TSPO PET SUVR in the amyloid PET meta-ROI. Pearson's correlations among all participants was 0.42 for CXCL9 and 0.26 for sTREM2.

Keywords: Alzheimer's disease, neuroinflammation, TSPO PET, blood-based biomarkers, sTREM2, cytokines

52 Evaluation of [18F]MK6240 test-retest reproducibility for different processing pipelines

Amal Tiss[1], Emma Thibault[1], Jessie Fang-Lu Fu[2], Alex Becker[1], Julie Price[2], Keith Johnson[1]

[1]*Gordon Center for Medical Imaging, Massachusetts General Hospital, Boston, MA, US*
[2]*Athinoula A. Martinos Center for Biomedical Imaging, Massachusetts General Hospital, Boston, MA, US*

Background. Test-retest data provides a robust framework for validating image processing methods by assessing reproducibility across repeated scans: the most reliable approach is the one that yields minimal variation between the test and retest outcomes. In this context, we compare test-retest absolute percentage differences (T-RT) obtained for [^{18}F]MK6240 PET outcomes across four pipelines.

Methods. Thirteen cognitively normal (CN) Harvard Aging Brain Study 2 (HABS-2) participants underwent two dynamic [^{18}F]MK6240 scans within three weeks (Table 1) on a GE Discovery MI PET system. Data processing involved three pipelines for generating standardized uptake values (SUV) and their ratio to the cerebellar cortex (SUVR): [1] conventional (Conv) with inter-frame motion correction, [2] list-mode reconstruction with intra-frame motion correction (MoCo), and [3] partial volume correction (PVC) using MR-based kernel reconstruction. Additionally, we applied conventional processing to the dynamic data to generate distribution volume ratios (DVR). Target regions included mesial-temporal and neocortical areas. Analysis outcomes were generated as described (Lois et al. Imaging Neuroscience 2024 - a prior test-retest study of Siemens Biograph mMR PET data).

Results. Our results were consistent with previously published values, despite outliers (T-RT of 30%). Figure 1 shows violin plots reporting reference-region SUV, and target region SUVR values for Conv, MoCo, and PVC methods, as well as their corresponding T-RT. No significant difference was found after application of intra-frame MoCo or PVC (Wilcoxon signed-rank test). Comparing conventional DVR to SUVR (Table 2) yielded four regions with significant differences in baseline outcome. Only the T-RT in the lingual region was significantly higher with DVR as compared to SUVR.

Conclusions. Surprisingly, sophisticated processing methods did not yield significantly lower T-RT percentages. Nonetheless, we confirmed that [^{18}F]MK6240 test-retest variability is acceptable for SUVR computed by conventional processing in CN individuals, consistent with previous reports.

Table 1: Participants characteristics

Sex (F/M)	9 / 4
Age (years)	67 ± 9 [46 — 78]
Diagnosis (CN/MCI/AD)	13 / 0 / 0
Race	
White	10
Black / African American	3
Ethnicity	
Non-Hispanic	11
Hispanic	1
PiB FLR DVR	1.05 ± 0.09 [0.96 — 1.30]
Number of days between [^{18}F]MK6240 test-retest	13 ± 6 [7 — 26]

Participants are enrolled in the Harvard Aging Brain Study 2 (HABS-2). Abbreviations: CN: cognitively normal; MCI: mild cognitive impairment; AD: Alzheimer's disease; FLR: frontal, lateral-temporal, and retrosplenial cortices; DVR: distribution volume ratio.

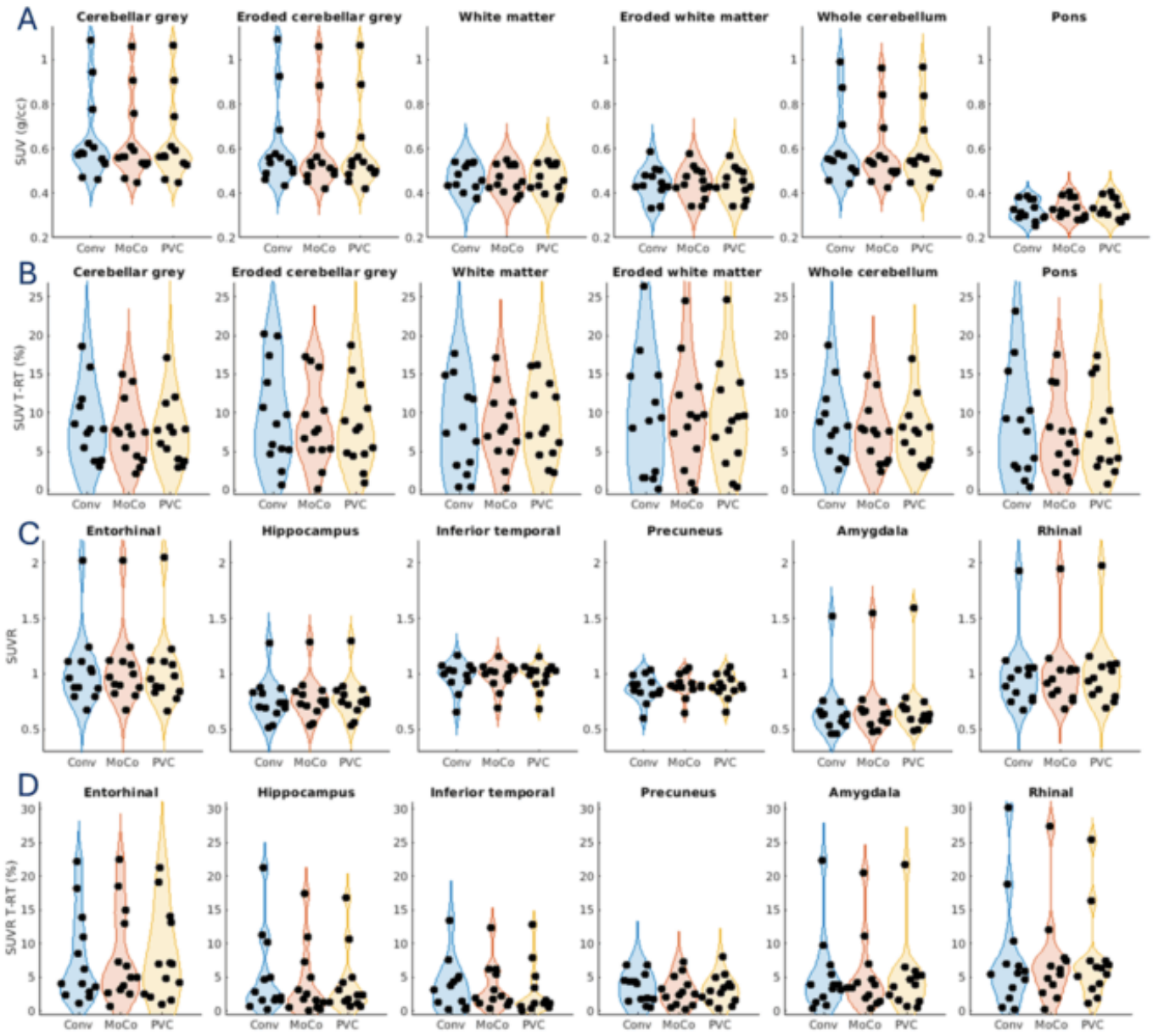


Figure 1: Violin plots showing [^{18}F]MK6240 results: (A) the baseline SUV in candidate reference regions, (B) their corresponding T-RT (%), (C) the baseline SUVR in selected target regions, and (D) their corresponding T-RT (%). Three methods are reported: "Conv" for conventional processing including inter-frame motion correction, "MoCo" for intra-frame motion correction, and "PVC" for partial volume correction using MR-based kernel reconstruction.

Table 2: Comparison of conventional [^{18}F]MK6240 SUVR and DVR baseline measures and their corresponding T-RT (%) [GE Discovery MI PET]

Target regions	Baseline SUVR	Baseline DVR	SUVR T-RT (%)	DVR T-RT (%)
Entorhinal	1.03 ± 0.34	1.10 ± 0.31	7.7 ± 6.7	14.0 ± 8.1
Hippocampus	0.77 ± 0.19	0.76 ± 0.14	5.0 ± 6.0	6.7 ± 7.9
Fusiform	0.95 ± 0.12	1.05 ± 0.06 *	3.8 ± 3.5	5.9 ± 5.4
Inferior temporal	0.98 ± 0.13	1.09 ± 0.11 *	3.5 ± 3.8	5.7 ± 4.6
Parahippocampal	0.89 ± 0.15	0.94 ± 0.13	5.0 ± 5.9	5.8 ± 3.9
Lateral occipital	1.12 ± 0.16	1.25 ± 0.20 *	2.6 ± 1.8	9.4 ± 8.6
Inferior parietal	1.03 ± 0.14	1.04 ± 0.11	2.8 ± 2.1	3.9 ± 4.2
Cuneus	1.02 ± 0.11	0.99 ± 0.10	3.3 ± 2.4	4.4 ± 3.6
Lingual	0.98 ± 0.10	1.06 ± 0.08	2.3 ± 1.6	6.2 ± 3.2 *
Precuneus	0.87 ± 0.12	0.90 ± 0.09	3.4 ± 2.2	3.4 ± 4.1
Rostral middle frontal	0.84 ± 0.13	0.87 ± 0.10	3.6 ± 4.6	4.3 ± 5.1
Precentral	0.82 ± 0.15	0.84 ± 0.11	4.4 ± 4.5	5.0 ± 5.8
Pericalcarine	0.92 ± 0.11	0.97 ± 0.10 *	2.2 ± 2.0	4.3 ± 5.2
Insula	0.75 ± 0.11	0.77 ± 0.09	3.2 ± 4.2	3.9 ± 5.1
Amygdala	0.68 ± 0.27	0.73 ± 0.22	5.1 ± 5.8	6.1 ± 7.5

Ratios were calculated with the cerebellar cortex as the reference. Asterisk indicates that the DVR measure (baseline or T-RT) is significantly different from the SUVR measure in that region (p-value < 0.05/30 for paired Wilcoxon signed-rank tests). Abbreviations: SUVR: standardized uptake value ratio; DVR: distribution volume ratio; T-RT (%): test-retest absolute differences.

Keywords: Test-retest, MRTM2 DVR, motion correction, [18F]MK6240

53 Temporal dynamics of tau PET subtypes and its association with heterogeneous neurodegeneration in Alzheimer's disease

Tae Youn Kwon[1], Jeong-Yeon Song[3], Wha Jin Lee[3], Joon-Kyung Seong[1,2,3]

[1]*Department of Artificial Intelligence, Korea University, Seoul, South Korea*
[2]*Department of Bioengineering, Korea University, Seoul, South Korea*
[3]*NeuroXT, Seoul, South Korea*

Background: Heterogeneity of tau accumulation patterns becomes critical to better understand individual variability of long-term changes for clinical profiles in patients with Alzheimer's disease. Among AD, atypical cases such as hippocampal sparing and limbic-predominant subtypes account for about 25% of cases. In this study, we developed an automated method to determine an individual tau subtypes and show its association with heterogeneous neurodegeneration in AD.

Methods: A three-tier severity grading system automatically classified tau burden in each meta-ROI using z-transformed regional tau uptake values. To distinguish limbic-predominant from cortical-predominant patterns, we computed a cortical-to-entorhinal(C/EC) ratio, and participants were classified into five subtypes via hierarchical decision tree: S0(tau-negative), S1(limbic-predominant), S2(cortical-predominant typical AD), S3(occipital-predominant atypical AD), and S4(asymmetric atypical AD). Longitudinal MRI-derived cortical thickness underwent identical processing for structural-functional correlation analysis.

Results: Cross-sectional analysis of amyloid-positive AD patients revealed highly consistent subtype distributions across independent cohorts, validating the reproducibility of our classification system(Figure 1). Temporal changes of tau subtypes show highly stable after tau onset: approximately 72.6% are maintained across disease progression. Longitudinal MRI-based structural subtyping was compared against baseline tau subtypes to assess inter-modality concordance. In ADNI, baseline matching rates between tau and neurodegeneration subtypes progressively declined from S0(88.1%) to S1(38.8%) to S2(10.9%), indicating that structural changes lag behind tau deposition(Figure 2). S1 and S2 showed substantial proportions of not-yet-progressed cases at 49.0% and 49.1%, respectively, suggesting considerable temporal delays before structural manifestation. Final follow-up matching rates were 94.9% for S0, 45.9% for S1, and 16.4% for S2.

Conclusions: Automated classification of an individual tau PET and structural MRI subtypes reliably idendified 4 different patterns, that show lagged representation of structural change after tau accumulation. Both tau and neurodegeneration subtypes are very stable along longitudinal follow-ups and inter-modality concordance rate between pathological and structural subtypes show considerable temporal delays while largely maintained.

Table 1. Baseline Characteristics of Aβ-positive Participants in ADNI and NACC Cohorts

Cohort	ADNI			NACC		
Baseline Diagnosis	**CN**	**MCI**	**Dementia**	**CN**	**MCI**	**Dementia**
Aβ-positive, *n*	115	108	60	130	89	92
Age	74.8±7.4	75.1±7.2	77.8±7.9	73.3±7.9	73.7±6.1	70.9±9.1
Male sex, *n* (%)	38 (33.9)	57 (52.8)	34 (56.7)	47 (36.2)	55 (61.8)	39 (42.4)
Education	16.6±2.3	16.1±2.5	15.8±2.5	16.4±2.4	16.2±2.7	16.2±2.4
Total Follow-up	133	165	59	41	59	55
# of APOE ε4						
0	54	31	18	64	21	21
1	47	42	26	46	30	36
2	6	15	10	12	18	11

Abbreviations: CN = Cognitively Normal individuals; MCI = Mild Cognitive Impairment

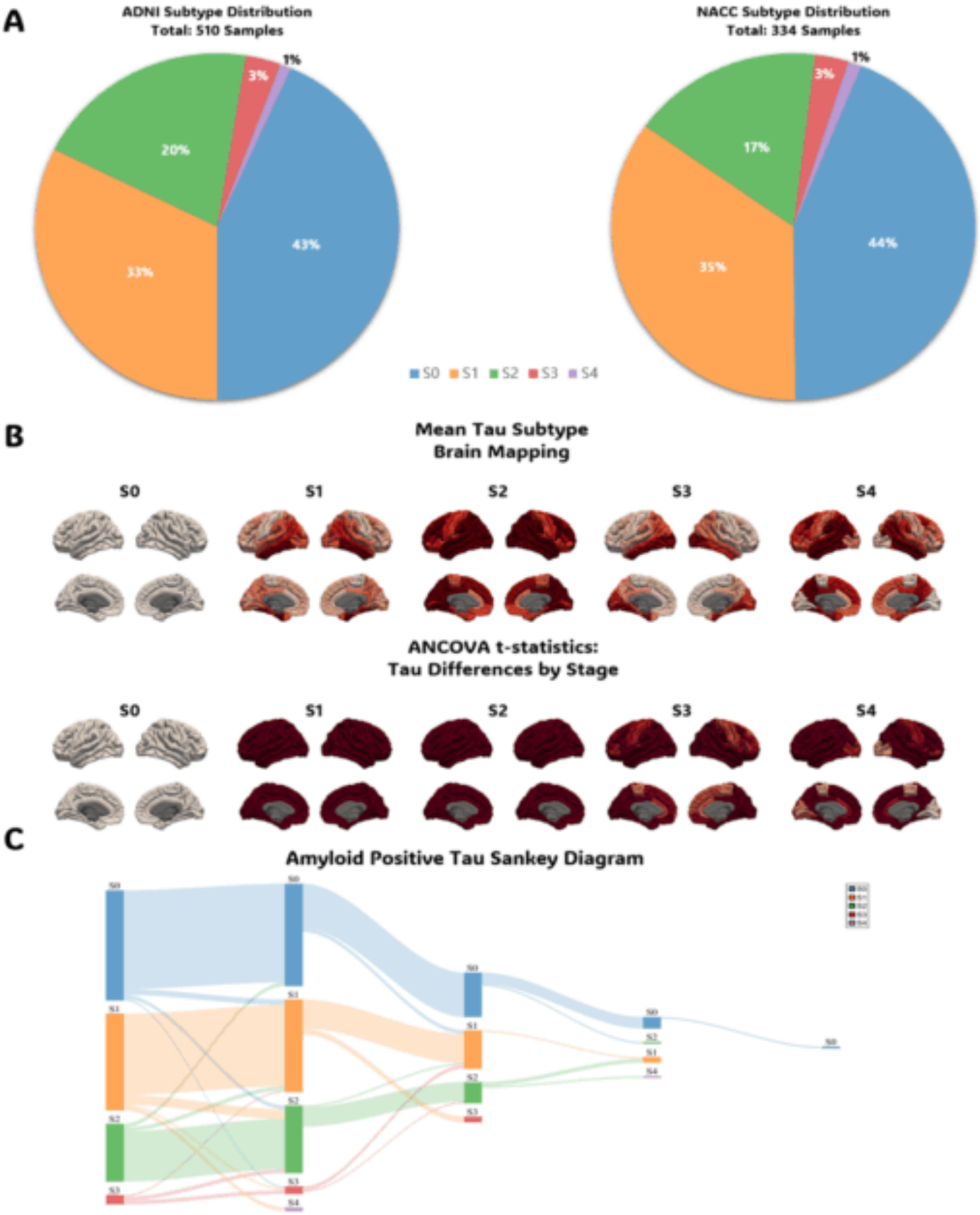


Figure 1. Cross-sectional tau PET subtype distribution and spatial patterns in amyloid-positive patients. (A) Subtype prevalence in ADNI (n=510, left) and NACC (n=334, right) cohorts showing reproducible distributions across independent datasets. (B) Cortical tau mapping by subtype. Upper: mean tau SUVR z-score maps displaying characteristic regional patterns. Lower: ANCOVA t-statistics comparing each pathological subtype (S1-S4) against S0, revealing statistically significant regional differences. (C) Sankey diagram illustrating longitudinal subtype transitions from baseline to follow-up in amyloid-positive patients, demonstrating temporal progression trajectories.



Figure 2. Figure 2. Baseline tau-matched neurodegeneration (ND) subtype distributions (left) and longitudinal transitions via Sankey diagram (right). (B) Delayed presentation of structural atrophy relative to tau deposition in ADNI (upper) and NACC (lower) cohorts. Pie charts show baseline match(Green), Follow-up Additional Match(Blue), Final mismatch(Red), and Not-Yet-Progressed (cases remaining at ND S0 despite tau positivity, Yellow) proportions for each tau subtype, demonstrating temporal lag between tau accumulation and structural neurodegeneration..

Keywords: Alzheimer's disease, amyloid-beta, tau, MRI, imaging

54 A-T-N-C generative model for predicting and simulating patient-tailored cognitive decline trajectories in Alzheimer's disease

Ji-Hyeon Lee[1], Yeong-Hun Song[1,3], Tae-Youn Kwon[1,3], Wha Jin Lee[3], Joon-Kyung Seong[1,2,3]

[1]*Department of Artificial Intelligence, Korea University, Seoul, South Korea*
[2]*Department of Bioengineering, Korea University, Seoul, South Korea*
[3]*NeuroXT, Seoul, South Korea*

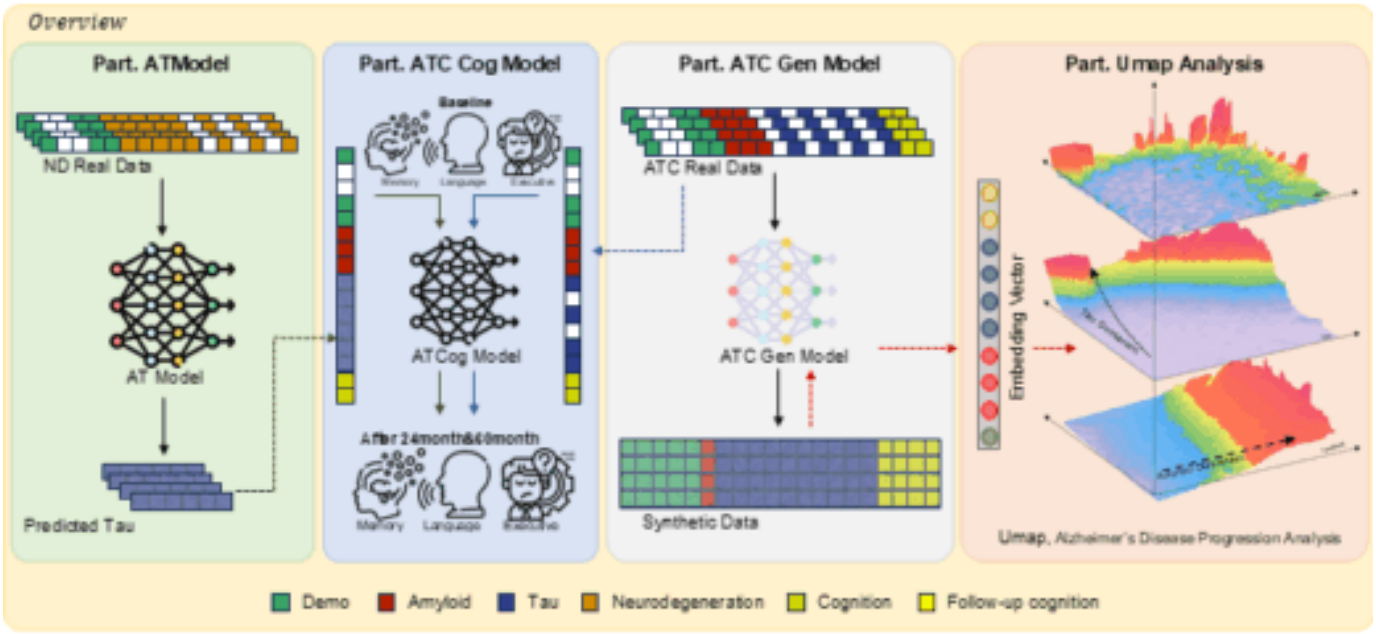
Background: Relating amyloid, tau, neurodegeneration, and domain-specific cognition in an interpretable way is difficult. Tau PET patterns are high dimensional and spatially correlated. Amyloid and tau PET are inconsistently available and use different scales. We integrated regional amyloid, tau, and neurodegeneration with cognition data (ATNC) to learn associations across normal aging and Alzheimer's disease (AD), and applied this foundation model to predict 2-year and 5-year domain-specific decline.

Methods: We pooled records from the Alzheimer's Disease Neuroimaging Initiative (ADNI) and the National Alzheimer's Coordinating Center (NACC) (total n=5,296). Amyloid PET was available in 89.8% and tau PET in 37.5%. We learned co-occurrence patterns among Desikan–Killiany 68 regions of interest for amyloid, tau, cortical atrophy, and domain-specific cognitive scores. Each record was encoded into a low-dimensional representation and mapped to a two-dimensional ATNC space using UMAP. Longitudinal cognitive slopes were estimated with linear mixed-effects models. The learned ATNC model predicted 2-year and 5-year trajectories for memory, language, and executive function.

Results: The model generates separate maps for amyloid, tau, and cognition. Amyloid-beta aligned with global centiloids, whereas tau burden increased along a diagonal axis. Domain-specific cognition was not linearly aligned but reflected interaction between amyloid and tau. Longitudinally, cognitive change was largely associated with tau burden rather than amyloid. The model displays joint distributions across ATNC features. Prediction performance: 2-year R^2=0.86 (memory), 0.72 (language), 0.72 (executive); 5-year R^2=0.70 (memory), 0.59 (language), 0.57 (executive).

Conclusion: We developed a novel ATNC generative and foundation model integrating regional amyloid and tau PET, MRI-based neurodegeneration, and domain-specific cognition scores. The generated ATC cascade maps provide an interpretable and usable view of pathology–cognition coupling in Alzheimer's disease, and the foundation model forecast short- and long-tem cognitive decline trajectories with best-in-class precision at an individual-level.

A.



B.

Characteristic	ADNI(n=3,748)	NACC(n=1,548)	Total(n=5,296)
N (visit-level)	3,748	1,548	5,296
Age, years	74.8 ± 7.8	71.9 ± 8.6	73.9 ± 8.1
Female sex, n(%)	1,856 (49.5)	920 (59.4)	2,776 (52.4)
Education, years	16.4 ± 2.6	16.4 ± 2.4	16.4 ± 2.5
MMSE score	27.5 ± 3.3	29.3 ± 1.0	27.5 ± 3.3
CDR-SB score	1.40 ± 2.24	1.06 ± 2.12	1.29 ± 2.21
Cognitive Normal	1,713 (45.7)	1,052 (68.0)	2,765 (52.2)
Mild Cognitive Impairment	1,369 (36.5)	265 (17.1)	1,634 (30.9)
Dementia	533 (14.2)	231 (14.9)	764 (14.4)
APOE4 carrier status	1407/3540 (39.7)	569/1359 (41.9)	1976/4899 (40.3)
Amyloid PET available	3,435 (91.6)	1,321 (85.3)	4,756 (89.8)
Tau PET available	1,173 (31.3)	813 (52.5)	1,986 (37.5)
Amyloid-Positive	1486/3165 (47.0)	648/1321 (49.1)	2134/4486 (47.6)

Figure 1. Overview of the A-T-N-C generative model architecture and cohort characteristics

A. Schematic workflow of the four-part ATNC model pipeline

The AT Model predicts regional tau PET from neurodegeneration. The ATC Cog Model forecasts domain-specific cognitive trajectories at 24-month and 60-month follow-up. The ATC Gen Model learns joint distributions of ATNC features and generates complete synthetic ATNC data. Umap Analysis projects high-dimensional embeddings into three-dimensional space along Centiloid(amyloid burden), Tau(tau burden), and MMSE(cognitive status)axes.

B. Demographic and clinical characteristics of the ADNI and NACC cohorts.

Abbreviations : ATNC, amyloid-tau-neurodegeneration-cognition; AT Model, amyloid-tau model; ATC Cog Model, amyloid-tau-cognition cognitive model; ATC Gen Model, amyloid-tau-cognition generative model; UMAP, Uniform Manifold Approximation and Projection; PET, positron emission tomography; MRI, magnetic resonance imaging; MMSE, Mini-Mental State Examination; ADNI, Alzheimer's Disease Neuroimaging Initiative; NACC, National Alzheimer's Coordinating Center; APOE4, apolipoprotein E ε4 allele; EDU, education; CN, cognitively normal; MCI, mild cognitive impairment

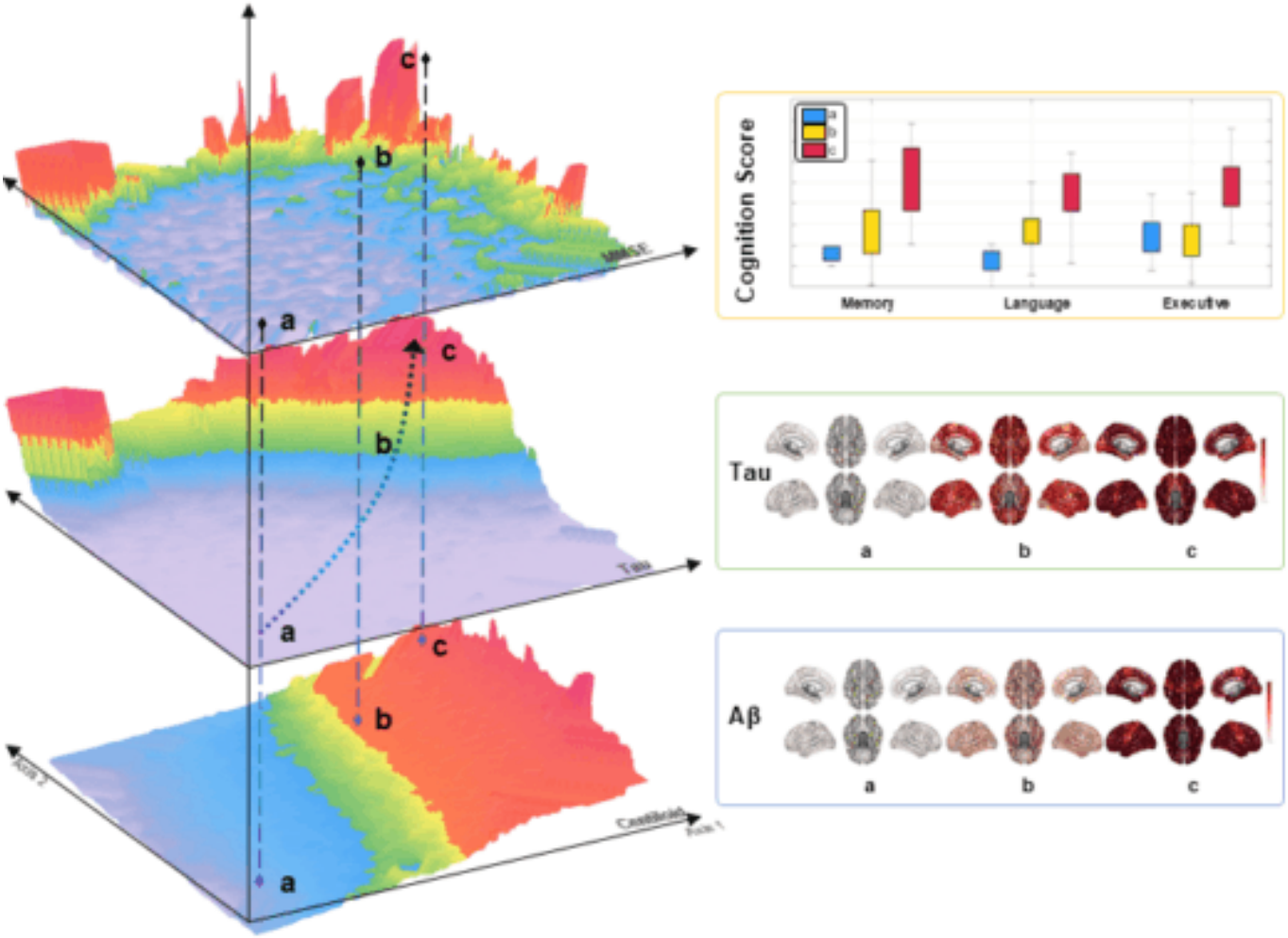


Figure 2. UMAP visualization reveals distinct pathology partterns across Alzheimer's Disease progression

A. Separate UMAP landscapes for Amyloid pathology(Aβ), Tau pathology and Cognition scores

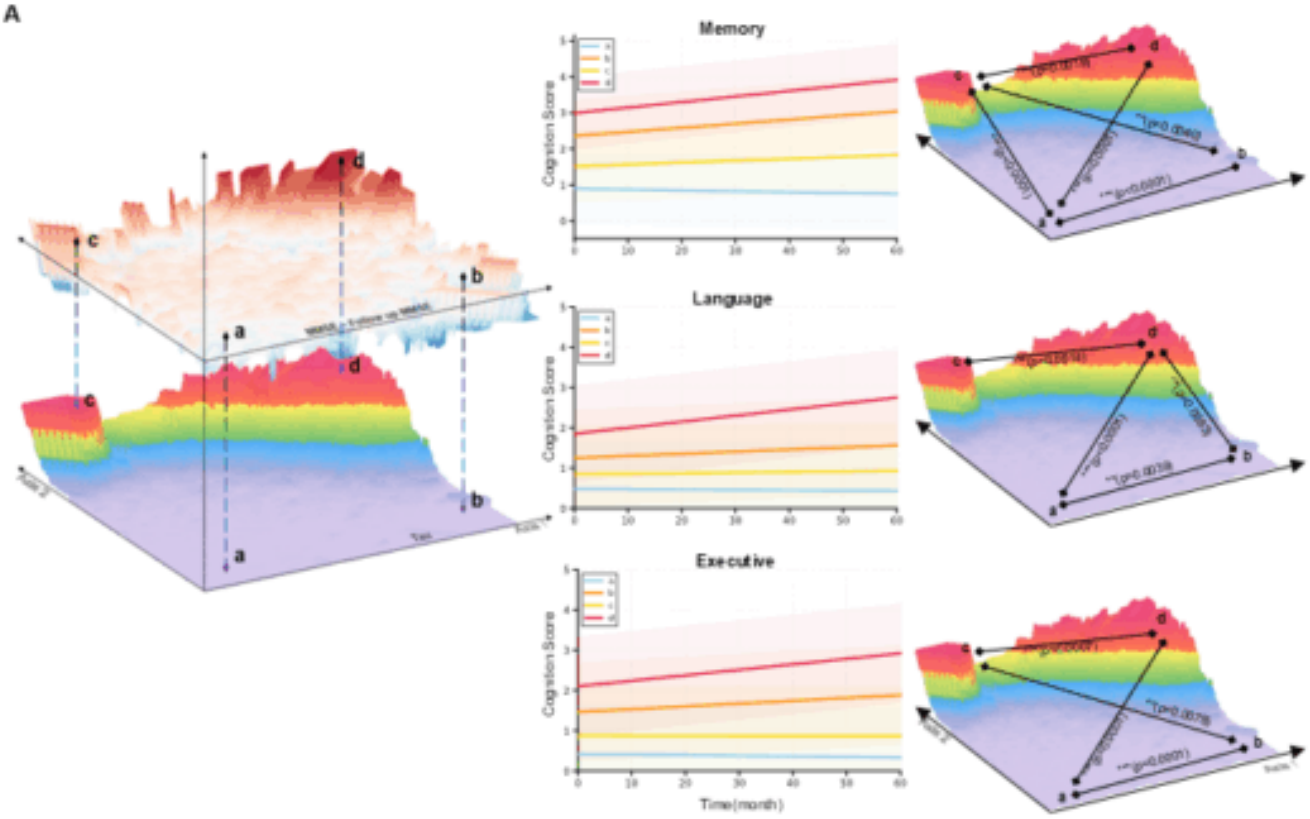
Amyloid burden increases primarily along axis 1, while tau burden increases along axis 2 and diagonally, both color-coded by severity: blue (low), green (intermediate), and red (high). The cognition map displays MMSE scores stratified by cognitive status: blue (27–30, cognitively normal), green (22–27, mild cognitive impairment), and red (<22, Alzheimer's disease).

B. Tau-stratified brain profiles illustrating regional distribution patterns of amyloid, tau, cognition pathology at three representative positions(a, b, c) on the UMAP space

Cognitive score progressively decline across memory, language, and executive domain form position a to c. Regional tau accumulation maps clearly demonstrate this diagonal progression pattern, with tau burden transitioning from minimal (gray, position a) to moderate (orange/red, position b) to severe and widespread (deep red, position c). In contrast, amyloid distribution shows a preferential increase along axis 1, accumulating relatively uniformly across cortical regions as burden increases from position a to c.

Abbreviations: UMAP, Uniform Manifold Approximation and Projection; Aβ, amyloid-beta; MMSE, Mini-Mental State Examination

A



B

ATC Cog Model	24 Month Follow-Up Prediction(N=3,231)			60 Month Follow-Up Prediction(N=984)		
Cognition Score	Memory	Language	Executive	Memory	Language	Executive
MAE	0.537	0.608	**0.660**	0.768	0.722	**0.792**
RMSE	0.706	0.788	**0.842**	**1.050**	0.961	1.030
R^2	**0.857**	0.722	0.715	**0.694**	0.581	0.567
Pearson	**0.926**	0.851	0.846	**0.834**	0.763	0.753

Figure 3. Longitudinal cognitive decline trajectories and prediction performance of the ATCog Model

A. Domain-specific cognitive trajectories projected from the UMAP embedding space over 60 months

Left panel shows four representative positions(a, b, c, d) on two-layered UMAP visualization : the lower layer displays tau burden, and the upper layer shows predicted MMSE decline at follow-up(red indicated substantial decline; blue indicateds minimal decline). Middle panels display linear mixed-effects model-fitted trajectories for memory, language, and executive function. Steeper increase in slopes, indicating greater cognitive deterioration, is observed at positions with higher tau burden(position d) compared to lower burden positions(position a) Group comparisons across positions revealed statistically significant slope differences in most cases($p<0.001$), with memory exhibiting the steepest gradient.

B. Quantitative prediction performance metrics for 24-month and 60-month cognitive scores prediction

For 24-month follow-up (N=3,231), the ATCog model achieved R^2 values of 0.857 (memory), 0.722 (language), and 0.715 (executive function). For 60-month predictions (N=984), R^2 values were 0.694 (memory), 0.581 (language), and 0.567 (executive function). Memory consistently demonstrated the highest predictability, suggesting stronger coupling between ATN pathology and memory decline compared to other cognitive domains.

Abbreviations: UMAP, Uniform Manifold Approximation and Projection; MMSE, Mini-Mental State Examination; ATCog Model, amyloid-tau-cognition cognitive model; MAE, mean absolute error; RMSE, root mean squared error; R^2, coefficient of determination.

Keywords: Cognition decline trajectory, Generative Model, Alzheimer's Disease, Amyloid, Tau

55 High-resolution ex-vivo MRI reveals layer-specific atrophy of hippocampal subregions to earliest tau pathology

Yasmine Salman[1], Sandra Tomé[2], Nicolas Joudiou[3], Dietmar Thal[2,4], Amanda Annettesdotter[5], Pulkit Khandelwal[6], Paul Yushkevich[6], Bernard Gallez[7], Laura Wisse[5], Bernard Hanseeuw[1,8]

[1]*Institute of Neuroscience, Université Catholique de Louvain, Brussels, Belgium*
[2]*Laboratory of Neuropathology - Department of Imaging and Pathology and Leuven Brain Institute, Katholieke Universiteit Leuven, Leuven, Belgium*
[3]*Louvain Nuclear and Electron Spin Technologies Platform, Louvain Drug Research Institute, Université Catholique de Louvain, Brussels, Belgium*
[4]*Department of Pathology, University Hospitals Leuven, Leuven, Belgium*
[5]*Department of Clinical Sciences, Lund University, Lund, Sweden*
[6]*Department of Radiology, University of Pennsylvania., Philadelphia, PA, US*
[7]*Biomedical Magnetic Resonance Research Group, Louvain Drug Research Institute, Université Catholique de Louvain, Brussels, Belgium*
[8]*Department of Radiology, Massachusetts General Hospital, Harvard Medical School, Boston, MA, US*

Background: Tau deposition primarily targets the medial temporal lobe (MTL), making this region critical for understanding preclinical Alzheimer's disease (AD). While in-vivo MRI detects MTL atrophy, the relationship between structural MRI and underlying tau pathology at the earliest stages remains poorly understood. We aimed to identify MTL subregions affected by early tau pathology (Braak stage I-II) using high-resolution ex-vivo MRI combined with histopathology.

Methods: High-resolution (50µm in-plane) ex-vivo MRI scans of the human MTL from 15 donors were acquired using an 11.7 T Bruker scanner. The anterior MTL was manually segmented into 12 subfields (Fig.1). Region-of-interest landmarks were placed within each subfield to calculate the cortical thickness, which was computed as the diameter of the largest sphere centered on each landmark location fully inscribed within cortical gray matter segmentation. Specimens were then paraffin-embedded for immunohistochemistry to obtain ipsilateral neuropathological assessment: quantifications of (pre)tangles density per mm^2 in the anterior MTL were done. We performed contrast analyses to compare cortical thickness between Braak stage I and II, and Spearman partial correlations between cortical thickness and (pre)tangles. All analyses were adjusted for age, sex, and co-pathologies (TDP-43/α-syn).

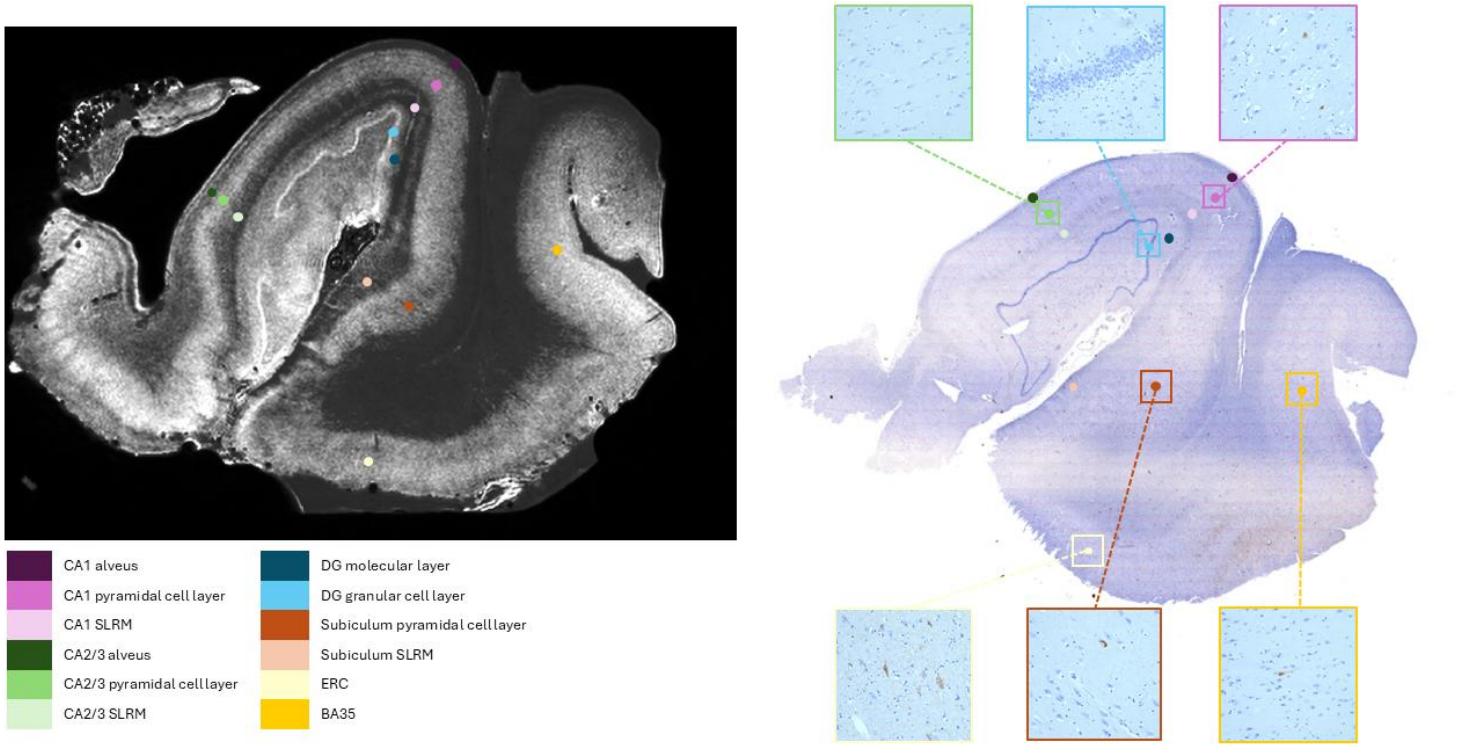


Figure 1 : MTL scans were acquired on an 11.7 T Bruker MRI scanner using a T1-weighted FLASH 3D sequence (TE = 4.425 ms, TR = 70 ms, flip angle = 20°, resolution = 50 × 150 × 100 μm^3). Thickness measurements were performed in the entorhinal cortex (ERC), Brodmann area 35 (BA35), Cornu Ammonis (CA) 1 and 2/3 in the alveus, pyramidal cell layer, and stratum radiatum moleculare (SRLM), subiculum (SUB), including the pyramidal cell layer and SRLM, and the dentate gyrus (DG), including the granule cell layer (GCL) and molecular layer (ML) (all marked with a dot). Subsequently, MTLs were neuropathologically analyzed to quantify tangles and pretangles per mm^2 in CA1, CA2/3, SUB pyramidal cell layer, DG GCL, ERC layer 4, and BA35 layer 4.

Results: Braak stage II individuals exhibited a significantly thinner anterior CA1 pyramidal layer than Braak stage I donors (β=-0.22 mm; $p<0.01$, Fig.2).

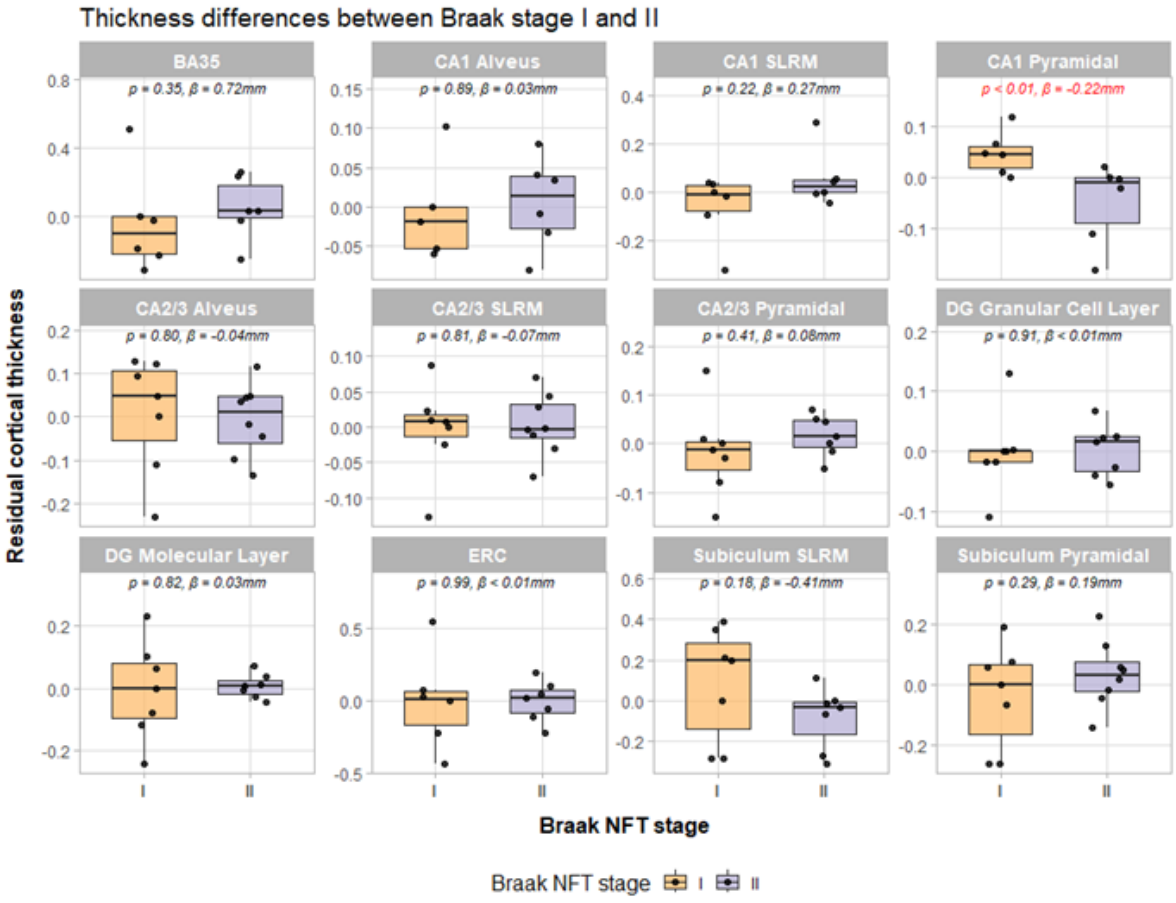


Figure 2: Differences in cortical thickness between Braak stage I and Braak stage II. Analyses were adjusted for co-pathologies (TDP-43 and α-synuclein), age, and sex. Adjusted thickness measurements are displayed.

Additionally, tangle density in BA35 significantly correlated negatively with anterior CA1 pyramidal layer thickness (R=-0.97; p<0.01, Fig.3), and the subiculum neuropil layer 'SRLM' (R=-0.91; p<0.01, Fig.3).

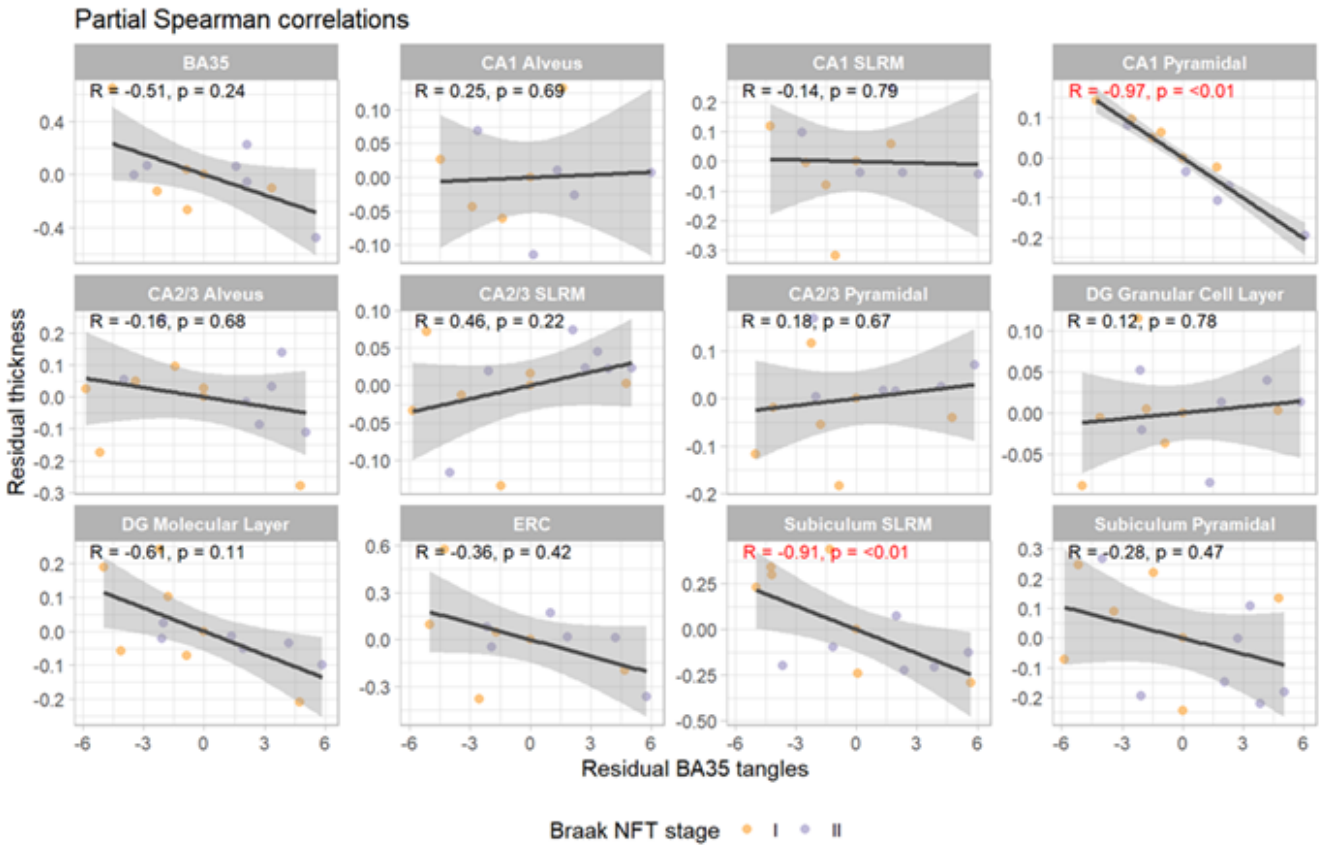


Figure 3: Partial correlations between cortical thickness and tangle counts for each ROI. Analyses were adjusted for co-pathologies (TDP-43 and α-synuclein), age, and sex. Adjusted thickness measurements and tangles counts are displayed.

Discussion: By combining ultra-high-field ex-vivo MRI with tau histopathology, we demonstrate that early tau pathology in AD is associated with atrophy of the CA1 pyramidal layer. These findings highlight the CA1 subfield as a priority target for in-vivo studies aimed at detecting preclinical AD. Future work will include more specimens, investigate posterior MTL subfield thickness, and examine the relationship between MRI intensity measurements and tau pathology.

Keywords: Ex-vivo MRI, hippocampal subfields, atrophy, Tau, Braak staging

56 Blood volume influences the association between baseline plasma biomarker values and amyloid PET outcomes over time

Kelsey Burns[1], Alexandra Gogola[1], Xuemei Zeng[2], Thomas Karikari[2], Tovia Jacobs[3], Brian Lopresti[1], Ricardo Osorio[3]

[1]*Department of Radiology, University of Pittsburgh School of Medicine, Pittsburgh, PA, US*
[2]*Department of Psychiatry, University of Pittsburgh School of Medicine, Pittsburgh, PA, US*
[3]*Department of Psychiatry, New York University Grossman School of Medicine, New York, NY, US*

Background: Increased plasma biomarker utilization for detecting Alzheimer's Disease pathology requires investigation into how blood volume (BV) influences their associations with amyloid PET accumulation over time.

Methods: We evaluated plasma samples from 140 subjects (age 73.65.9y) who underwent 3T MR and [^{11}C]Pittsburgh Compound-B (PiB) PET imaging at two separate time points (3.51.4y between visits) and were PET A(-) at baseline. Centiloid (CL) values were calculated from Global PiB standardized uptake value ratios. BV was calculated using the Nadler equations and was stratified based on cohort median. Blood samples were processed and sampled to obtain baseline measures of plasma amyloid-β(Aβ)42, Aβ40, p-tau181, p-tau217, p-tau231, glial fibrillary acidic protein (GFAP) and neurofilament light (NfL). Plasma Aβ was expressed as Aβ42/Aβ40 ratio while p-tau181, p-tau217 p-tau231 and NfL were log-transformed to normalize distributions. Linear mixed-effects models (LMM) assessed whether BV had an effect when added to models associating each plasma biomarker and Centiloids over time.

Results: For Aβ42/40, p-tau217, and p-tau181 LMMs demonstrated time to have an independent effect on CL outcomes as well as significant interactions with the plasma biomarkers (Table 1). BV had a significant effect within the models for all plasma biomarkers except GFAP. Figure 2 illustrates a divergence in the predicted CL accumulation rate between BV strata within the Aβ42/40 LMM.

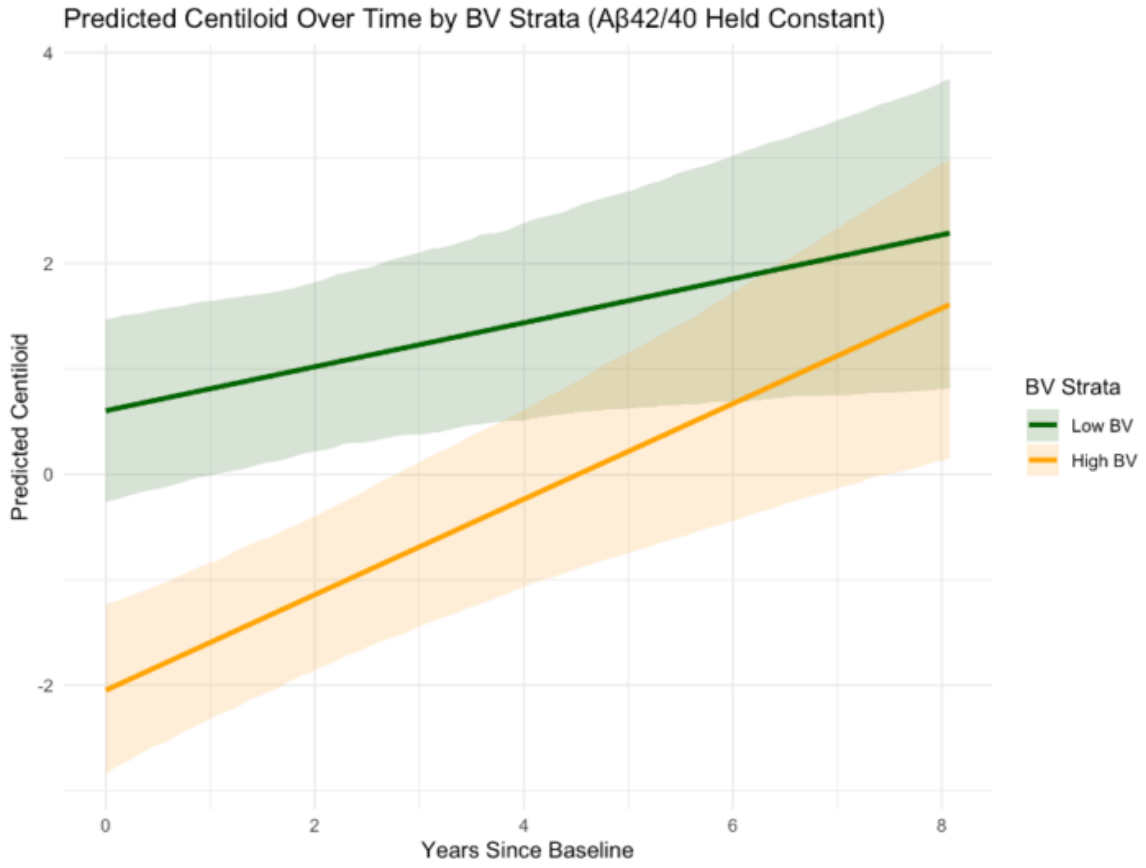
Conclusions: These findings highlight the dynamic interplay between plasma biomarkers, BV, and time in the prediction of longitudinal Aβ accumulation. The significant interaction of Aβ42/40, p-tau217, and p-tau181 with time suggests that individuals with lower baseline levels of plasma biomarkers accumulate insoluble Aβ faster. Importantly, BV emerged as an independent predictor, with higher BV associated with lower baseline CL alongside steeper increases over time. These results support the presence of dilution effects and underscore the importance of considering BV when studying plasma biomarkers in relation to PET amyloid accumulation.

Table 1. β ± SE and p-values for linear mixed effect models between BBM and Centiloid with Time*BBM Interaction and BV added as a covariate

BBM (Exposure)	Exposure β ± SE	Exposure p-Value	Time β ± SE	Time p-Value	BV β ± SE	BV p-Value	Time*BBM β ± SE	Time*BBM p-Value
Aβ42/40	29 ± 29	0.332	1.6 ± 0.55	**0.003****	-1.1 ± 0.57	**0.055***	-18 ± 6.9	**0.011****
GFAP	2.7 ± 2.5	0.281	-1.4 ± 1.2	0.254	-0.8 ± 0.59	0.166	0.88 ± 0.64	0.172
NfL	-0.57 ± 2.9	0.846	-0.29 ± 0.91	0.755	-1.1 ± 0.6	**0.063***	0.46 ± 0.74	0.538
p-Tau$_{181}$	2.6 ± 2.6	0.315	-1.2 ± 0.75	**0.100***	-1.3 ± 0.57	**0.027****	1.3 ± 0.63	**0.043****
p-Tau$_{231}$	1.4 ± 2.2	0.512	-0.29 ± 0.52	0.578	-1.2 ± 0.58	**0.036****	0.59 ± 0.53	0.266
p-Tau$_{217}$	-0.4 ± 3.1	0.898	2.6 ± 1.3	**0.047****	-0.95 ± 0.58	**0.099***	1.8 ± 0.89	**0.052****

*p < 0.10
** p < 0.05

Figure 1. Predicted Centiloid over time by blood volume stratified at the cohort median, with Aβ42/Aβ40 ratios held constant.



Keywords: Dilution, Blood Volume, Biomarker Biofluids, Plasma, Centiloid

57 Visual interpretation methods for tau-PET imaging with Flortaucipir and MK-6240: Insights from the HEAD study

Emma Ruppert[1], Marie Vermeiren[2], Marina Scop Medeiros[1], Guilherme Povala[1], Andreia Rocha[1], Carolina Soares[1], Pamela Ferreira[1], Livia Amaral[1], Guilherme Bauer-Negrini[1], Firoza Lussier[1], Matheus Scarpatto Rodrigues[1], Markley Oliveira Jr.[1], Rayan Mroue[1], Bruna Bellaver[1], Alexis Moscoso[3], Rik Ossenkoppele[2], Elsmarieke van de Giessen[2], Joseph Masdeu[4], Dana Tudorascu[1], David Soleimani-Meigooni[5], Juan Fortea[6], Val Lowe[7], Hwamee Oh[8], Belen Pascual[4], Brian Gordon[9], Pedro Rosa-Neto[10], Suzanne Baker[11], Tharick Pascoal[1,11]

[1]*University of Pittsburgh, Pittsburgh, PA, US*
[2]*Amsterdam UMC, Amsterdam, The Netherlands*
[3]*University of Gothenburg, Gothenburg, Sweden*
[4]*Houston Methodist Research Institute, Houston, TX, US*
[5]*University of California San Francisco, Memory and Aging Center, San Francisco, CA, US*
[6]*Hospital de la Santa Creu i Sant Pau, Sant Pau Memory Unit, Barcelona, Spain*
[7]*Mayo Clinic, Rochester, MN, US*
[8]*Brown University, Providence, RI, US*
[9]*Washington University in St. Louis, St. Louis, MO, US*
[10]*McGill University, Montréal, QC, Canada*
[11]*Lawrence Berkeley National Laboratory, Berkeley, CA, US*

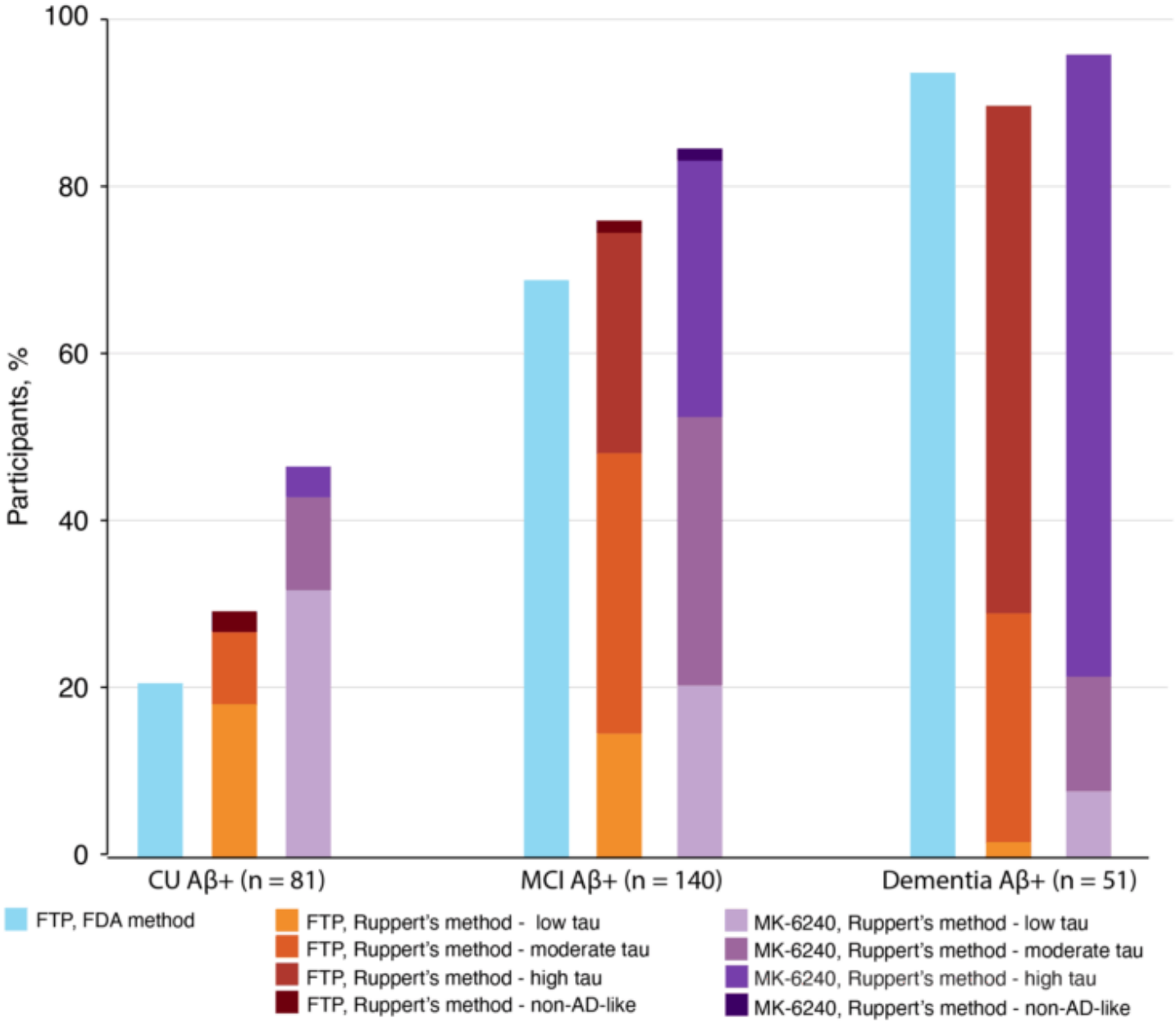
Background: Tau-PET provides critical topographic information on tau deposition in the living brain. Integrating research-based practices into clinical settings through qualitative methods, such as visual reads, is becoming increasingly important. We compared the performance of the FDA-approved visual reading method for Flortaucipir (FTP) with a newly developed harmonized method (Ruppert's method) applicable to both FTP and MK-6240 tracers, enabling cross-tracer comparisons.

Methods: We analyzed 623 participants from the multi-site HEAD cohort spanning the Alzheimer's disease continuum. Each participant underwent MRI and tau-PET imaging with both tracers. Expert rater, blinded to demographics and diagnosis, classified scans using the FDA-approved FTP method and Ruppert's harmonized method. Generalized additive models adjusted for site were used to estimate tau-PET positivity across age.

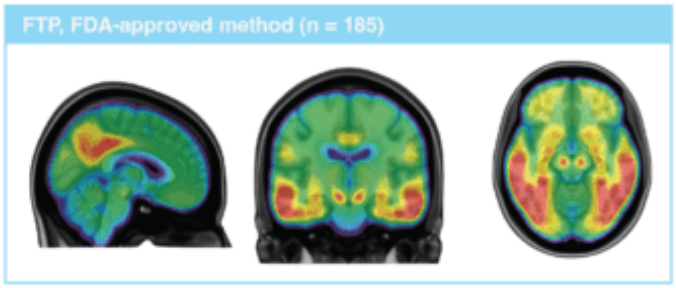
Results: Ruppert's harmonized method identified higher tau-PET positivity among CU Aβ+ and MCI Aβ+ participants compared to the FDA-approved method, with comparable rates in dementia Aβ+ (Fig. 1). The inclusion of tau burden categories (low, moderate and high) allowed for a finer characterization of disease stages, which is the greatest advantage of tau imaging. Group SUVR averages demonstrated distinct spatial patterns consistent with increasing tau burden (Fig 2), while Centiloid and MoCA distributions differed significantly across categories, reflecting underlying biological and clinical heterogeneity (Fig. 3)

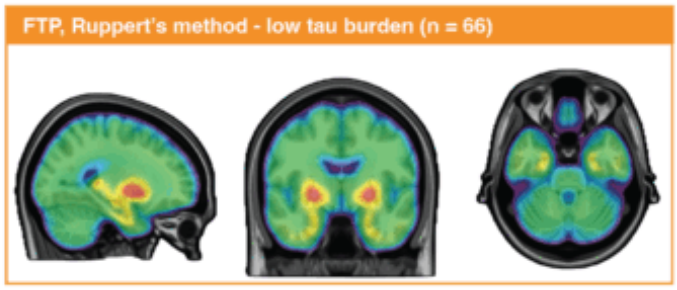
Conclusion: The novel harmonized method provides a tracer-independent framework for visual interpretation of tau-PET, improving disease staging and clinical interpretability across tracers.

1. Tau-PET positivity rates using FDA-approved visual reading method and using Ruppert's harmonized visual reading method

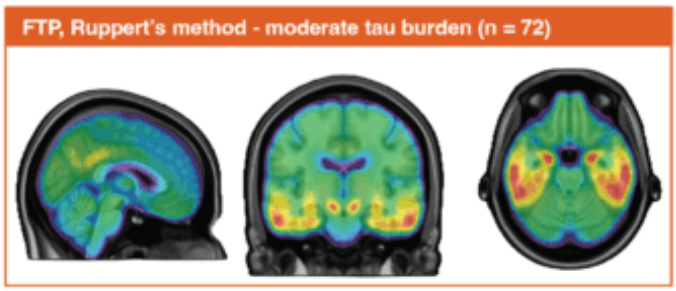


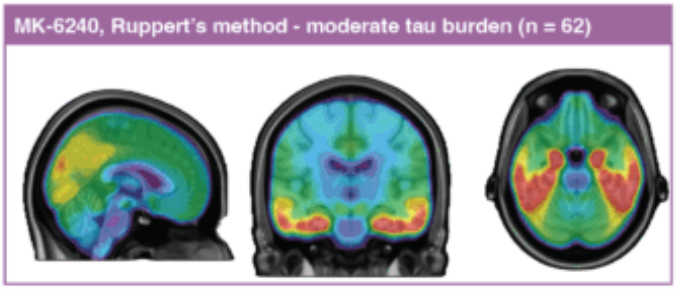
2. SUVR image averages according to each visual reads method classification group

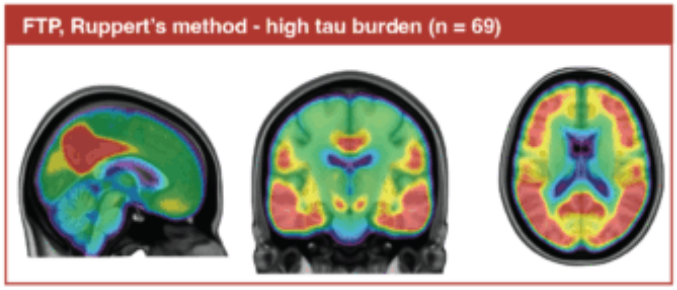


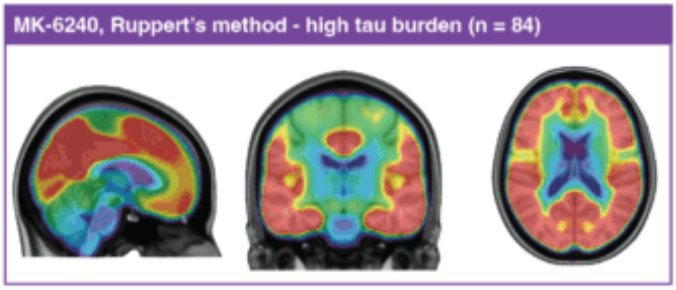


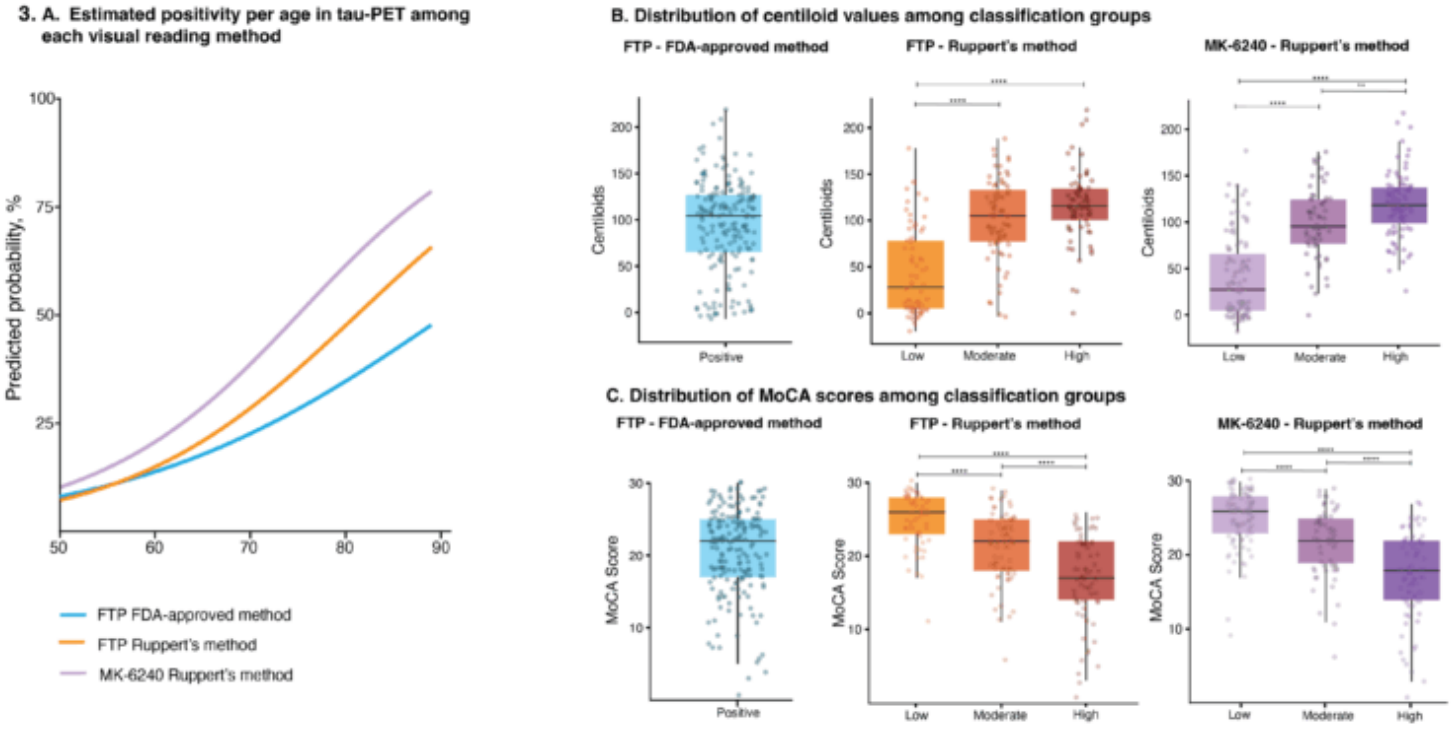












Keywords: visual reads, tau-PET, head-to-head, Flortaucipir, MK6240

58 Associations between TSPO PET and CSF and blood-based biomarkers

Anna Smith[1], Diana Guzman[1], Hannah Houlihan[1], Thairi Sanchez[1], William Kreisl[1], Daniel Talmasov[1], Philip De Jager[1], Mathieu Herman[1], Sabrina Simoes[1], Scott Small[1], Patrick Lao[1]

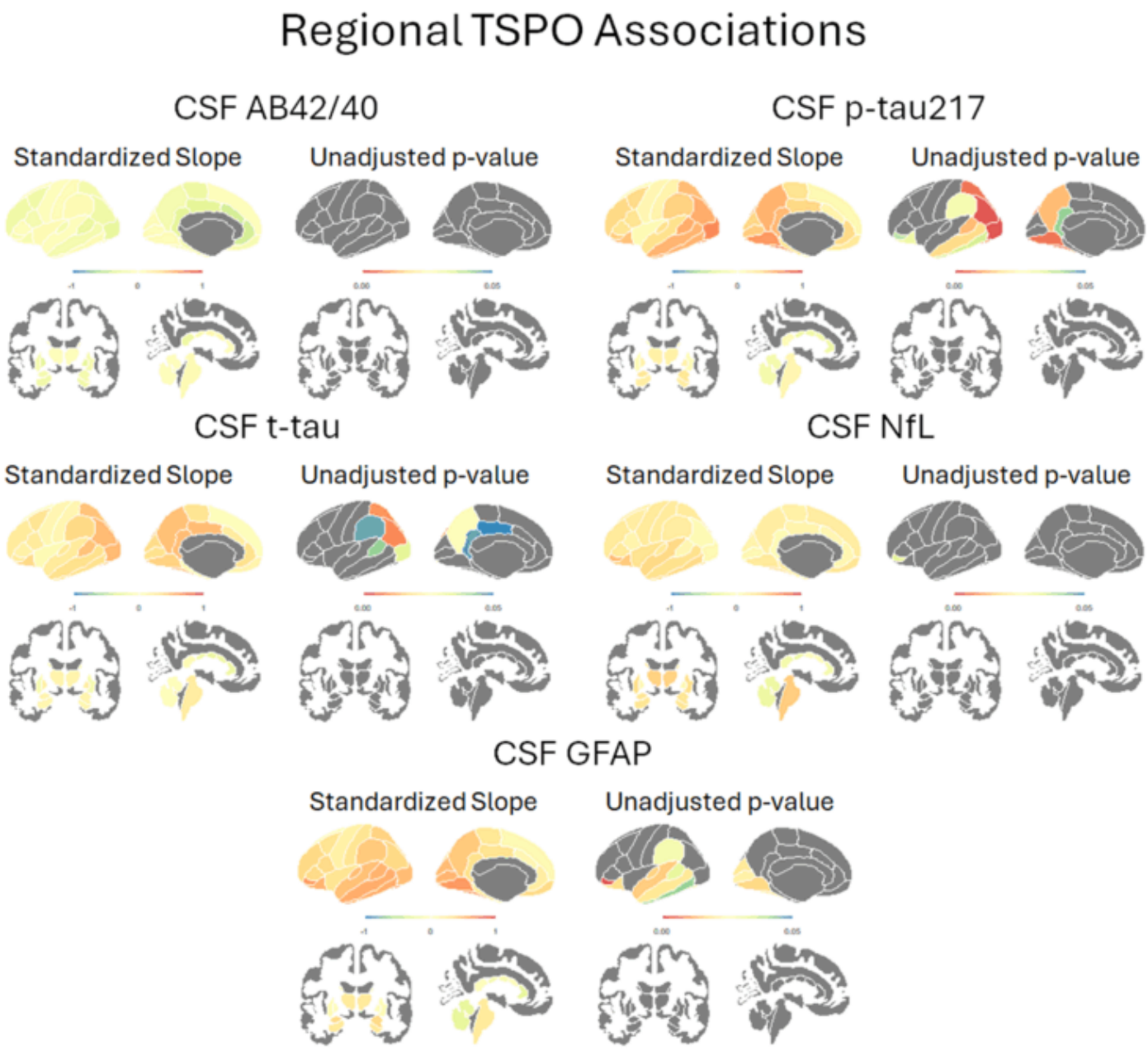
[1]*Columbia University Medical Center, New York, NY, US*

Introduction: TSPO PET can serve as a general marker that captures the location and timing of microglia density, recruitment to stimuli, and cross-talk with other cell types. Our objective was to further characterize TSPO PET relative to biofluidic biomarkers.

Methods: Participants underwent TSPO PET (ER176 SUVR), amyloid PET (Florbetaben SUVR), tau PET (MK6240 SUVR), and structural MRI (gray matter volume). At the Columbia Alzheimer's Disease Research Center, participants were clinically determined to be cognitively unimpaired or having Alzheimer's disease or related dementias. Due to inclusion in ancillary studies, a subset of individuals (n=23; 70±6 yrs, 48% women; 17 control, 2 MCI, 2 AD, 1 PCA, 1 lvPPA) underwent lumbar puncture from which we derived AB42/40, p-tau217, t-tau, NfL, and GFAP (Quanterix SIMOA HD-X system), while a different subset (n=10; 73±6 yrs, 40% women; 6 control, 2 MCI, 1 AD, 1 PCA) with banked serum samples had similar measures derived (Alamar NULISA). We tested for brain-wide regional SUVR associations with biofluidic biomarkers, adjusting for age, sex, BMI, TSPO affinity, and APOE genotype.

Results: Greater TSPO was associated with greater CSF p-tau217, t-tau, NfL, and GFAP. However, after multiple comparisons correction, associations were only trend-level significant for p-tau217 in some occipital, parietal, and temporal regions and GFAP in one frontal region. Expected associations were observed with CSF AB42/40, p-tau217, and t-tau and amyloid and tau PET, while structural MRI results were mixed as CSF markers were associated with lower volume in some regions and greater volume in others. In blood, no significant associations were observed with TSPO PET in this smaller subset, but there were expected associations with amyloid and tau PET and mixed results with structural MRI.

Conclusion: Biofluidic biomarkers, particularly those in CSF, may offer additional insight into TSPO PET as it relates to tau phosphorylation, astrocytosis, and neurodegeneration.



Keywords: Biofluidic biomarkers, TSPO, amyloid, tau, neurodegeneration

59 Regional white matter injury modifies the association between ß-amyloid and cognition

Sarah Royse[1], Alexandria Reese[1], Beth Snitz[2], James Hengenius[3], Paul Crane[4], Shubhabrata Mukherjee[4], Seo-Eun Choi[4], Daniel Willie-Permor[5], Cynthia Felix[6], Theodore Huppert[7], Rebecca Roush[2], Geraldine Cisneros[8], Katey Potopenko[8], Brian Lopresti[1], Ann Cohen[6], C. Elizabeth Shaaban[5,9]

[1]*Department of Radiology, University of Pittsburgh, Pittsburgh, PA, US*
[2]*Department of Neurology, University of Pittsburgh, Pittsburgh, PA, US*
[3]*Centre de Recherche Azrieli, Centre Hospitalier Universitaire Sainte-Justine, Montreal, QC, Canada*
[4]*Department of Medicine, University of Washington, Seattle, WA, US*
[5]*Department of Epidemiology, University of Pittsburgh, Pittsburgh, PA, US*
[6]*Department of Psychiatry, University of Pittsburgh, Pittsburgh, PA, US*
[7]*Department of Electrical Engineering, University of Pittsburgh, Pittsburgh, PA, US*
[8]*Department of Psychology, University of Pittsburgh, Pittsburgh, PA, US*
[9]*Department of Health Promotion and Development, University of Pittsburgh, Pittsburgh, PA, US*

Introduction: White matter injury (WMI) is common in Alzheimer's disease (AD), but its synergistic influence with AD pathology on cognition remains unclear. We tested whether regional WMI, quantified using our novel spatially precise measure, unhealthy white matter connectivity (UWMC), interacts with co-localized ß-amyloid (Aß) in relation to cognition.

Methods: We collected the following data in 207 participants (63.6±8.5 years; 136 (65.7%) female; 153 (73.9%) cognitively unimpaired): (1) T1, T2, and diffusion tensor-weighted (DTI) magnetic resonance imaging (MRI) scans, (2) [^{11}C]Pittsburgh Compound-B (PiB) positron emission tomography (PET) scans, and (3) a neuropsychological battery assessment. We used T1, T2, and DTI scans to define regions-of-interest (ROIs), white matter hyperintensities (WMH), and full-brain connectomes, respectively. We combined these outcomes to calculate UWMC as the proportion of white matter connections passing though WMH within nine Aß-affected ROIs. In these same ROIs, we calculated [^{11}C]PiB standardized uptake value ratios (SUVRs). We created memory, executive function, and language domain scores using item response theory. We used individual robust regression models to test interactions between each corresponding pair of regional UWMC and [^{11}C]PiB SUVR outcomes with each cognitive domain score.

Results: Greater parietal UWMC was more strongly associated with worse memory (P=0.0003; Figure 1A), executive function (P=0.01), and language (P=0.01) performance in those with higher, versus lower, parietal [^{11}C]PiB SUVR (Table 1). Conversely, in those with higher, versus lower anterior cingulate [^{11}C]PiB SUVR, more anterior cingulate UWMC was associated with better memory performance (P=0.03; Figure 1B). No other interactions were significant (P≥0.07; Table 1).

Conclusions: The combined influence of co-localized WMI and Aß on cognition varies by brain region. These results suggest that (1) targeting parietal WMI may curb cognitive decline in AD, whereas (2) anterior cingulate integrity may support compensatory function despite greater pathological burden in AD.

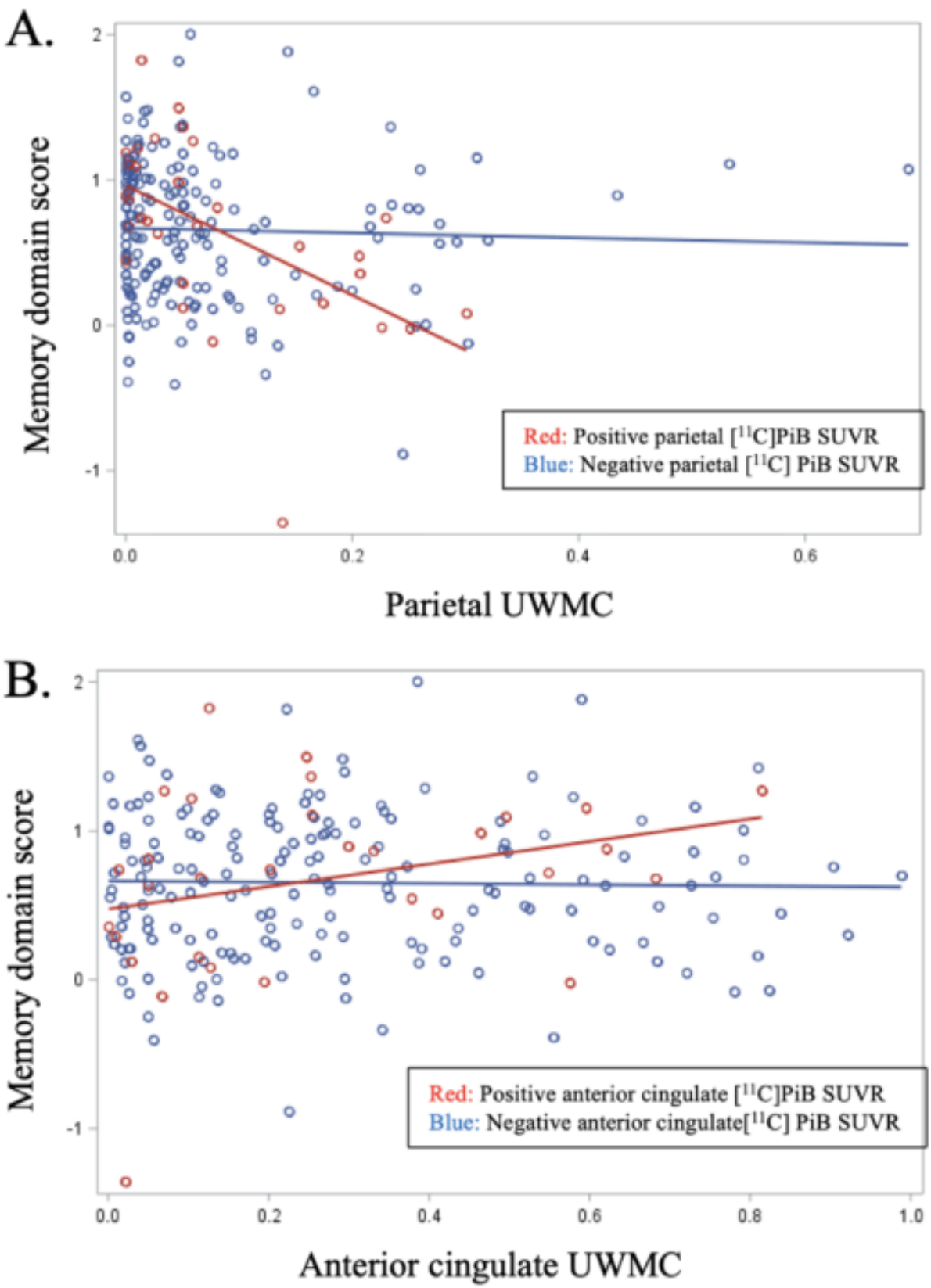
Table 1. Results from linear models

	Standardized β (*P* value)		
	UWMC	**[^{11}C]PiB SUVR**	**Interaction**
Region	*Memory*		
Anterior Cingulate	0.003 (0.93)	-0.02 (0.70)	0.08 (0.03)*
Anterior Ventral Striatum	0.02 (0.64)	-0.05 (0.21)	0.02 (0.65)
Superior Frontal	-0.04 (0.29)	-0.02 (0.63)	0.05 (0.35)
Orbitofrontal	-0.01 (0.84)	-0.01 (0.88)	0.07 (0.07)
Insula	0.03 (0.38)	-0.01 (0.74)	0.07 (0.18)
Lateral Temporal	-0.03 (0.43)	-0.04 (0.30)	-0.04 (0.28)
Parietal	-0.06 (0.08)	-0.03 (0.37)	-0.14 (0.0003)*
Posterior Cingulate	0.01 (0.77)	-0.04 (0.36)	-0.002 (0.96)
Precuneus	-0.08 (0.049)*	-0.08 (0.049)*	-0.06 (0.30)
	Executive function		
Anterior Cingulate	-0.04 (0.36)	0.04 (0.42)	0.07 (0.12)
Anterior Ventral Striatum	0.06 (0.18)	-0.02 (0.67)	-0.04 (0.43)
Superior Frontal	-0.11 (0.01)*	-0.03 (0.57)	-0.03 (0.71)
Orbitofrontal	-0.08 (0.08)	-0.01 (0.81)	-0.05 (0.32)
Insula	-0.05 (0.32)	-0.0004 (0.99)	0.05 (0.44)
Lateral Temporal	-0.13 (0.001)*	-0.06 (0.20)	-0.06 (0.11)
Parietal	-0.01 (0.01)*	-0.04 (0.41)	-0.12 (0.01)*
Posterior Cingulate	-0.01 (0.82)	-0.01 (0.78)	0.02 (0.60)
Precuneus	-0.09 (0.04)*	-0.08 (0.11)	-0.10 (0.16)
	Language		
Anterior Cingulate	-0.03 (0.38)	-0.04 (0.31)	-0.03 (0.65)
Anterior Ventral Striatum	-0.07 (0.36)	-0.12 (0.45)	-0.07 (0.83)
Superior Frontal	-0.05 (0.21)	-0.03 (0.47)	0.04 (0.51)
Orbitofrontal	-0.07 (0.06)	-0.07 (0.09)	-0.05 (0.15)
Insula	0.03 (0.50)	-0.04 (0.39)	0.07 (0.19)
Lateral Temporal	-0.01 (0.76)	-0.05 (0.22)	-0.03 (0.40)
Parietal	-0.03 (0.32)	-0.01 (0.72)	-0.12 (0.04)*
Posterior Cingulate	0.003 (0.94)	-0.03 (0.41)	0.03 (0.40)
Precuneus	-0.01 (0.83)	-0.04 (0.28)	-0.01 (0.98)

*Significant at $P<0.05$

*Note: all models adjusted for age, sex, racialized group, education, APOE*4, hypertension, diabetes, high cholesterol|*

Figure 1. Scatter plots showing the relationships between regional UWMC and composite memory score by regional [^{11}C]PiB positivity



Keywords: white matter injury, amyloid, cognition, compensation

60 Sex differences in neuroinflammation, amyloid, tau, and neurodegeneration

Diana Guzman[1], Anna Smith[1], Hannah Houlihan[1], Thairi Sanchez[1], Muge Akinci[1], Jose Luchsinger[1], Patrick Lao[1]

[1]*Columbia University Irving Medical Center, New York, NY, US*

Introduction: PET imaging of the 18kDa translocator protein (TSPO) can provide critical information about microglia-related processes, which may differ between women and men and contribute to sex differences in Alzheimer's disease (AD) pathogenesis and progression. Our objective was to characterize TSPO, amyloid, tau, and neurodegeneration with respect to sex.

Methods: Participants (71±7 years old, 49% women) underwent TSPO PET (ER176 SUVR), amyloid PET (Florbetaben SUVR), tau PET (MK6240 SUVR), and T1 MRI (gray matter volume). Participants were determined to be cognitively unimpaired (Control, n=20) or as having Alzheimer's disease or related dementias (ADRD, n=23) at the Columbia Alzheimer's Disease Research Center. We tested for TSPO, amyloid, and tau SUVR and volume associations with sex, adjusted for age, BMI, TSPO affinity, and *APOE*-ε4 genotype across FreeSurfer-defined regions with False Detection Rate (FDR) correction for multiple comparisons. We further stratified analyses by control and ADRD groups to understand disease stage dependence.

Results: Men had trend-level greater TSPO in frontal regions ($0.06<p<0.08$) compared to women. When restricted to controls, men had greater TSPO in transverse temporal cortex ($\beta=1.8$, $p=0.02$), superior parietal cortex ($\beta=1.5$, $p=0.046$), postcentral gyrus ($\beta=1.5$, $p=0.046$), and frontal pole ($\beta=1.4$, $p=0.046$). With ADRD, men had greater TSPO in similar but fewer regions that did not survive FDR correction. While these did not survive FDR correction, men in the control group had similar amyloid, lower tau, and greater volume, whereas men in the ADRD group had lower volume (Figure 1).

Conclusion: Men had greater TSPO despite similar amyloid, lower tau, and greater volume compared to women, particularly in controls. While sex differences in TSPO were not apparent in the ADRD group, men may have lower volume, suggesting that TSPO may play a role in neurodegeneration beyond amyloid and tau.

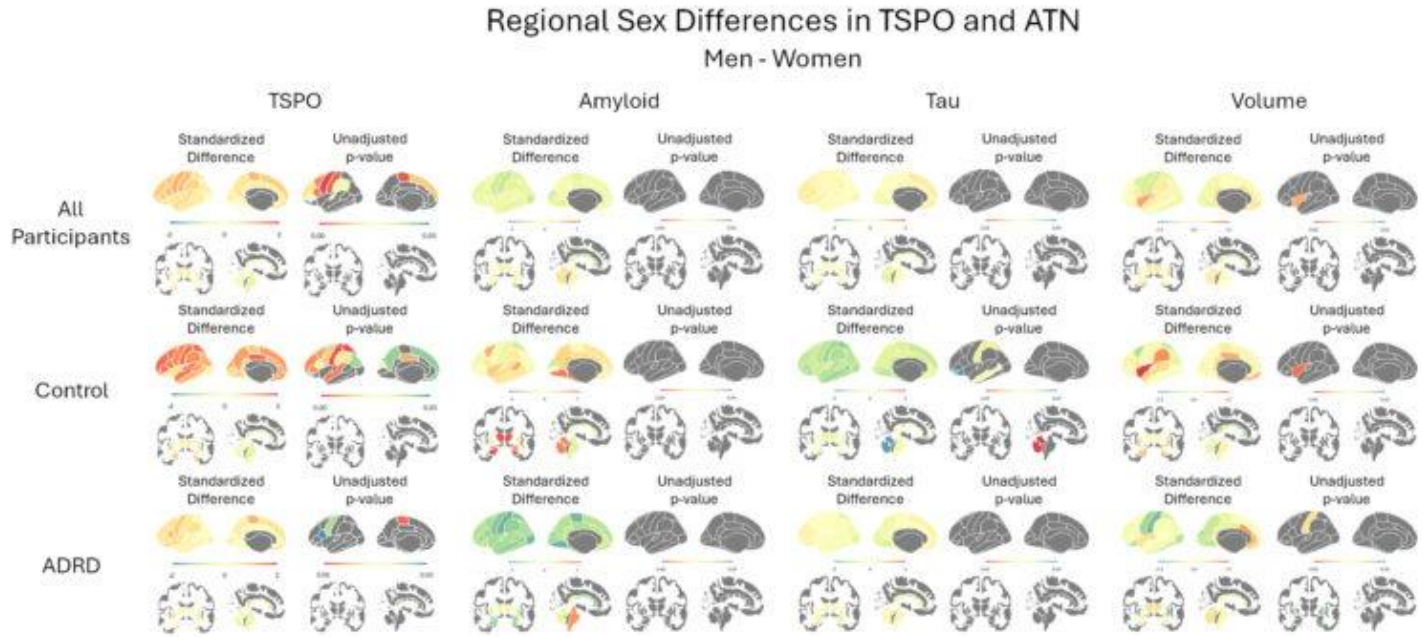


Figure 1. Regional sex differences in TSPO and ATN neuroimaging. Reference group: women.

Keywords: TSPO PET, microglia, tau, neurodegeneration, sex

61 Evaluation of the tau PET ligand [18F]florzolotau in frontotemporal dementia

Mica Clarke[1], Alex Whittington[1], Olayinka Sholaja[1], Emma Hield[1], Mickael Huiban[1], Frans van den Berg[1], Richard Margolin[2], James Rowe[3], Jonathan Rohrer[4], Cristian Salinas[5], Eugenii A Rabiner[1]

[1]*Perceptive, London, UK*
[2]*Aprinoia, Boston, MA, US*
[3]*University of Cambridge, Cambridge, UK*
[4]*University College London, London, UK*
[5]*Takeda, Cambridge, MA, US*

[^{18}F]florzolotau (previously [^{18}F]APN-1607) has been used successfully to detect 3R/4R tau deposition in patients with regional distribution profiles consistent with Alzheimer's disease (AD), as well as 4R tau deposits in non-AD tauopathies such as progressive supranuclear palsy (PSP). Preliminary evidence suggests that [^{18}F]florzolotau also binds to cortical 4R and 3R tau deposits in frontotemporal dementia (FTD) syndromes (Tagai et al. 2021, Zhou et al. 2022). This study aimed to evaluate differences in [^{18}F]florzolotau binding in FTD caused by a *MAPT* mutation (*MAPT*-FTD) compared to non-*MAPT*-FTD and healthy controls. Six subjects, two with *MAPT*-FTD, two with non-*MAPT*-FTD and two controls, each underwent a 120-minute dynamic PET acquisition following intravenous bolus injection of [^{18}F]florzolotau with arterial blood sampling, as well as a T1-weighted structural MRI scan. Injected radioactivity ranged from 96 to 107MBq (mean 103; SD 3.41MBq), with injected mass ranging from 0.02 to 0.43µg (mean 0.19; SD 0.13µg). PET images were registered to MR images which were used to define regions of interest (ROIs). The PET images displayed a heterogeneous signal (see Figure 1 for representative SUV images). Regional time activity curve (TAC) data were fitted using a two-tissue compartment (2TC) model with volume of distribution (V_T) as the outcome parameter of interest. TACs were characterised by a peak by ~5 minutes post-injection, followed by washout. The 2TC model produced acceptable fits to TACs in all subjects (see Figure 2 for representative TACs). V_T values (Table 1) were greatest in non-*MAPT*-FTD across ROIs including cortical regions affected in FTD, but scans did not reveal clear differences in binding between *MAPT*-FTD and controls. *MAPT*-FTD subjects were selected under the assumption tau pathology will be present whilst other pathologies are not, however it is very hypothetical at a subject level. This highlights the difficulty of evaluating and developing tracers for tau in FTD.

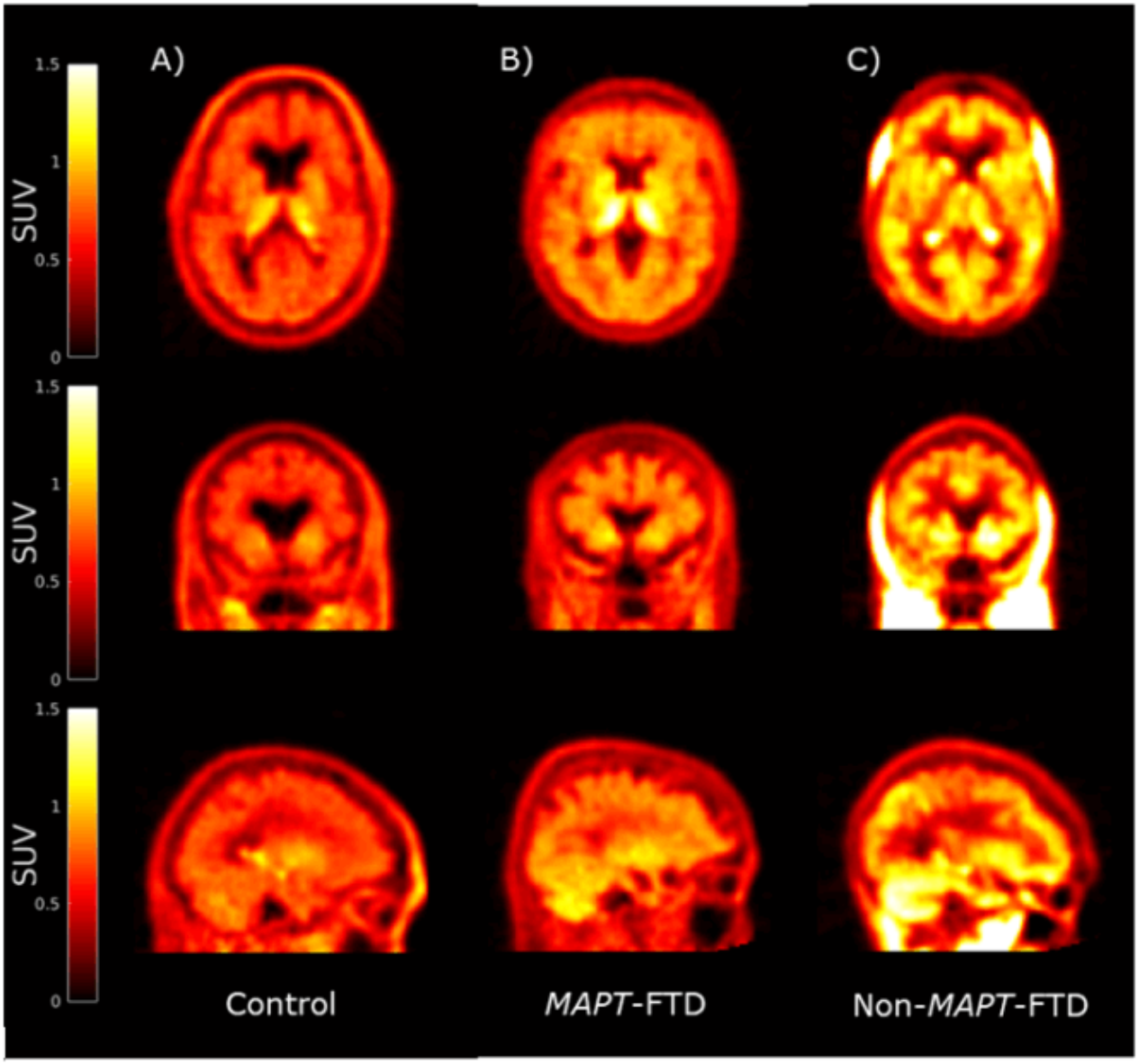


Figure 1. Representative integral (10-120 minute) SUV images from A) one healthy control subject (1), B) one subject with *MAPT*-FTD (1) and C) one subject with non-*MAPT*-FTD (2).

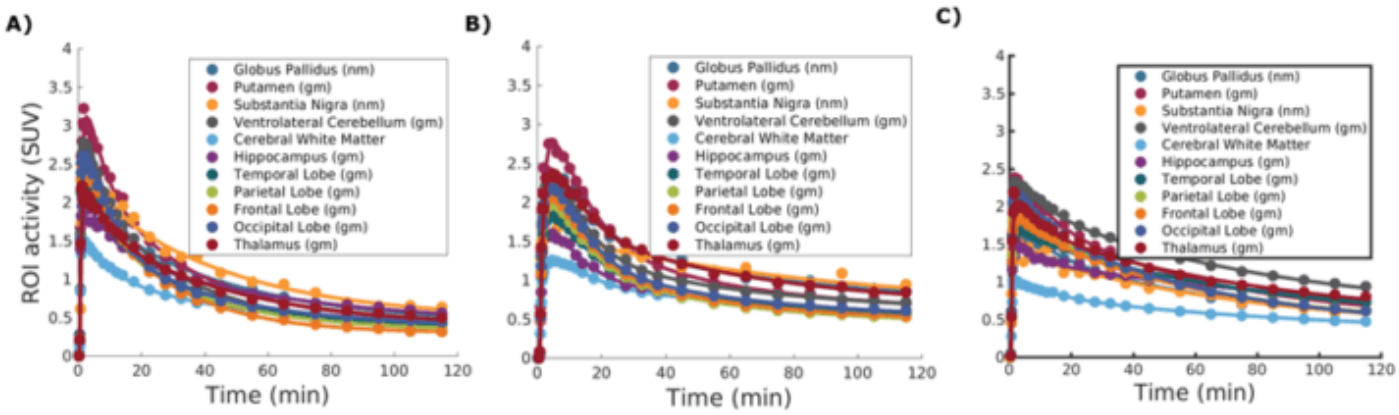


Figure 2. Representative time activity curves with 2TC model fits from A) one healthy control subject (1), B) one subject with *MAPT*-FTD (1) and C) one subject with non-*MAPT*-FTD (2).

Table 1. Volume of distribution (V_T) values for all subjects

Subject	FL	TL	PL	OL	Hi	Th	VLCe	CWM
Healthy control 1	2.42	2.75	2.63	2.95	3.49	3.19	2.96	2.48
Healthy control 2	3.22	3.63	3.18	3.65	3.89	4.04	3.70	3.88
MAPT-FTD 1	3.49	3.55	3.34	3.85	3.52	5.20	4.47	3.66
MAPT-FTD 2	1.85	2.23	2.03	2.23	3.40	3.35	2.35	2.19
Non-*MAPT*-FTD 1	4.61	5.41	4.71	4.63	7.13	8.09	4.73	3.76
Non-*MAPT*-FTD 2	5.22	6.11	5.31	5.32	6.65	6.57	7.81	3.96

Note. *FL = frontal lobe; TL = temporal lobe; PL = parietal lobe; OL = occipital lobe; Hi = hippocampus; Th = thalamus; VLCe = ventrolateral cerebellum; CWM = cerebral white matter.*

Keywords: frontotemporal dementia, FTD, tau, florzolotau

62 Intersections of gender/sex and neighborhood deprivation on cognition: Are there mediation effects of Alzheimer's disease biomarkers?

Alexandria Reese[1], Sarah Royse[1,2], Beth Snitz[2,3], Paul Crane[4], Shubhabrata Mukherjee[4], Seo-Eun Choi[4], James Hengenius[5], Theodore Huppert[6], Rebecca Roush[7], Geraldine Cisneros[7], Brian Lopresti[1], Laura Alejandra Rameriz Tirado[8], Daniel Willie-Permor[8], Cynthia Felix[7], Ann Cohen[2,7], C. Elizabeth Shaaban[2,8,9]

[1]*Department of Radiology, University of Pittsburgh, Pittsburgh, PA, US*
[2]*Alzheimer's Disease Research Center, University of Pittsburgh, Pittsburgh, PA, US*
[3]*Department of Neurology, University of Pittsburgh, Pittsburgh, PA, US*
[4]*Department of Medicine, University of Washington, Seattle, WA, US*
[5]*Centre de Recherche Azrieli, Centre Hospitalier Universitaire Sainte-Justine, Montreal, QC, Canada*
[6]*Department of Electrical Engineering, University of Pittsburgh, Pittsburgh, PA, US*
[7]*Department of Psychiatry, University of Pittsburgh, Pittsburgh, PA, US*
[8]*Department of Epidemiology, University of Pittsburgh, Pittsburgh, PA, US*
[9]*Department of Health Promotion and Development, University of Pittsburgh, Pittsburgh, PA, US*

Background: We have previously found differences in AD biomarkers by neighborhood deprivation (ND)/gender/sex strata. We therefore assessed intersectional patterns in cognition and tested whether intersectional patterns in AD biomarkers explain cognitive differences.

Methods: Among participants of the Connectomics in Brain Aging study, ND was assessed using the national area deprivation index (higher = greater disadvantage). We measured AD-related biomarkers, including: β-amyloid (Aβ) via global ^{11}C-PiB SUVR; vascular disease burden via lobar unhealthy white matter connectivity (UWMC), the proportion of white matter (WM) connections intersecting WM hyperintensities; and neurodegeneration via cortical thickness in an AD-meta region of interest. We calculated memory, executive function (EF), and language domain scores using item response theory. ND/gender/sex strata differences in cognition and biomarkers were tested via Kruskal Wallis tests. When intersectional differences of cognition or biomarkers were found, the mediating effects of biomarkers on cognition were tested via causal mediation analyses. All models were adjusted for age, racialization, *APOE4+*, and education.

Results: The sample included N=196 participants (Table 1). Intersectional differences in cognition were found in memory and language (high ND men had the worst scores, p=0.004 and p=0.002, respectively) but not EF. Additionally, low ND men had the greatest burden of Aβ positivity (p=0.007), and high ND women had the greatest burden of frontal (p=<0.0001) and temporal (p=0.01) UWMC. Total effects (TE) were found such that, compared to low ND women, high ND men had significantly lower memory scores (TE in Frontal UWMC Models: β=-0.285, SE=0.110, p=0.009, Figure 1). No biomarkers mediated the relationship between intersectional strata and memory or language.

Conclusions: High ND combined with male gender/sex was associated with lower memory performance, independent of Aβ or UWMC burden. These findings highlight the importance of examining intersectional social determinants in understanding pathways to cognitive aging and AD risk.

Table 1: Connectomics of Brain Aging Study Participant Characteristics

	Overall N=196	Low Neighborhood Deprivation (N=59)		High Neighborhood Deprivation (N=137)		p-value
		Male N=21 (35.59%)	Female N=38 (64.41%)	Male N=44 (32.12%)	Female N=93 (67.88%)	
ADI, National Rank	76.00 (45.00, 93.00)	38.00 (27.00, 43.00)	36.00 (29.00, 41.00)	82.00 (72.00, 96.50)	87.00 (76.00, 97.00)	<0.0001*
Racialization, Black American	97 (49.49%)	5 (23.81%)	7 (18.42%)	24 (54.55%)	61 (65.59%)	<0.0001*
Age, years	62.00 (57.00, 70.00)	67.00 (63.00, 73.00)	66.00 (57.00, 72.00)	61.50 (56.00, 71.00)	61.00 (56.00, 68.00)	0.06
Education, years	14.00 (12.00, 16.00)	16.00 (14.00, 18.00)	14.00 (12.00, 18.00)	14.00 (12.00, 16.00)	14.00 (12.00, 16.00)	0.01*
APOE4+	62 (31.63%)	8 (38.10%)	5 (13.16%)	17 (38.64%)	32 (34.41%)	0.05
Hypertension	75 (38.27%)	9 (42.86%)	11 (28.95%)	19 (43.18%)	36 (38.71%)	0.56
MoCA score	25.00 (23.00, 27.00)	26.00 (24.00, 27.00)	27.00 (23.00, 28.00)	24.00 (22.00, 25.50)	25.00 (23.00, 27.00)	0.003*
Memory Domain	0.66 (0.28, 0.98)	0.68 (0.30, 0.95)	0.79 (0.62, 1.11)	0.47 (0.16, 0.74)	0.69 (0.27, 0.99)	0.004*
EF Domain	0.88 (0.49, 1.29)	1.04 (0.72, 1.24)	0.89 (0.64, 1.45)	0.53 (0.08, 1.09)	0.94 (0.54, 1.32)	0.05
Language Domain	0.47 (0.15, 0.85)	0.79 (0.50, 1.03)	0.66 (0.26, 1.04)	0.32 (0.11, 0.62)	0.34 (0.12, 0.69)	0.002*
Cognitively impaired	53 (27.04%)	6 (28.57%)	11 (28.95%)	13 (29.55%)	23 (24.73%)	0.92
AD	3 (1.53%)	2 (9.52%)	0 (0.00%)	0 (0.00%)	1 (1.08%)	0.300
Amyloid PET+***	29 (16.48%)	7 (36.84%)	6 (20.00%)	9 (22.50%)	7 (8.05%)	0.007*
Amyloid PET SUVR**	1.11 (1.06, 1.19)	1.18 (1.07, 1.57)	1.11 (1.07, 1.20)	1.06 (1.03, 1.20)	1.11 (1.06, 1.18)	0.05
Cortical thickness, mm**	2.74 (2.66, 2.80)	2.72 (2.65, 2.80)	2.75 (2.68, 2.79)	2.75 (2.66, 2.81)	2.73 (2.65, 2.79)	0.83
UWMC						
Frontal	0.14 (0.09, 0.26)	0.09 (0.04, 0.12)	0.12 (0.09, 0.24)	0.13 (0.08, 0.16)	0.20 (0.11, 0.35)	<0.0001*
Parietal	0.05 (0.01, 0.15)	0.08 (0.01, 0.14)	0.05 (0.02, 0.10)	0.08 (0.03, 0.15)	0.05 (0.01, 0.17)	0.39
Temporal	0.19 (0.10, 0.26)	0.15 (0.08, 0.24)	0.14 (0.08, 0.21)	0.16 (0.09, 0.23)	0.21 (0.13, 0.29)	0.01*
Occipital	0.06 (0.02, 0.20)	0.08 (0.04, 0.25)	0.05 (0.02, 0.20)	0.10 (0.04, 0.23)	0.05 (0.01, 0.16)	0.03*

N (%) or median (IQR)

*p<0.05

**N=176 for Amyloid SUVR and Cortical Thickness

***cut-off for amyloid PET positivity ≥ 1.346

Abbreviations: Alzheimer's disease (AD), area deprivation index (ADI), Apolipoprotein E (APOE), millimeter (mm), executive function (EF), Montreal Cognitive Assessment (MoCA), positron emission tomography (PET), standardized uptake value ratio (SUVR), unhealthy white matter connectivity (UWMC)

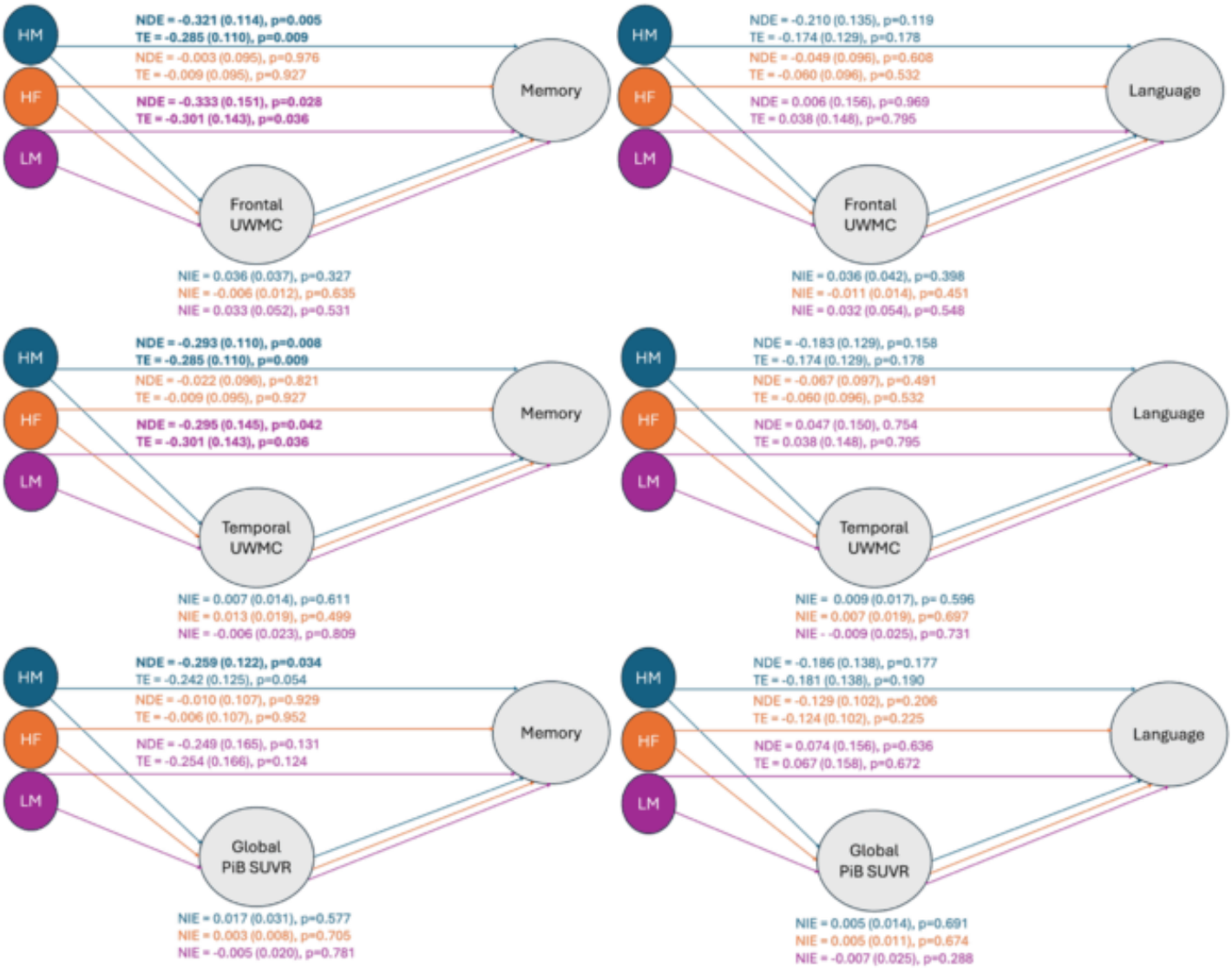


Figure 1: The mediation effects of frontal UWMC, temporal UWMC, and global PiB SUVR on the relationship between intersectional neighborhood deprivation/sex strata and memory/language. All estimates are adjusted for age, education, racialization, and *APOE*4+. Bolded results indicate significance.

Abbreviations: HF = female in high deprivation neighborhood, HM = male in high deprivation neighborhood, LM = male in low deprivation neighborhood, NDE = natural direct effect, NIE = natural indirect effect, PiB = Pittsburgh Compound B, SUVR = standardized uptake value ratio, TE = total effect, UWMC = unhealthy white matter connectivity.

Keywords: intersectionality, diffusion weighted imaging, item response theory

63 Disentangling cognitive severity and phenotype across dementia syndromes

Viktorija Smith[1], Ian Coyle-Gilchrist[2], Alexander G Murley[3], Matthew A Rouse[1], Katherine Stockton[3], Michelle Naessens[3], George Savulich[3], Julie Wiggins[3], Maura Malpetti[3], Lucy Bowns[3], Marlou N Perquin[1], Juliette H Lanskey[1], Melek Karadag[3], Ece Kocagoncu[3], Andrew Quinn[4,5], Jemma Pitt[4], Cara Alcock[4], John T O'Brien[3], Timothy Rittman[3], James B Rowe[1,2], Matthew A Lambon-Ralph[1]

[1]*MRC Cognition and Brain Sciences Unit, University of Cambridge, Cambridge, UK*
[2]*Norfolk and Norwich University Hospital NHS Foundation Trust, Norfolk, UK*
[3]*Department of Clinical Neurosciences and Cambridge University Hospitals NHS Trust, University of Cambridge, Cambridge, UK*
[4]*Oxford Centre for Human Brain Activity, Wellcome Centre for Integrative Neuroimaging, Department of Psychiatry, University of Oxford, Oxford, UK*
[5]*Centre for Human Brain Health, School of Psychology, University of Birmingham, Birmingham, UK*

Introduction: Dementia syndromes are characterised by substantial clinical heterogeneity that arises due to distinct clinical subtypes and varying stages of disease progression. Traditional categorical models fail to capture the phenotypic heterogeneity, whilst existing temporal proxies for disease severity have significant limitations. This study applies a data-driven, transdiagnostic approach to identify the cognitive dimensions underlying clinical groups and to disentangle the effects of phenotype and severity.

Methods: We analysed data from 286 individuals (age mean=71.5 +- 7.9 years) across several local cohort studies. Participants were included if they met at least one of the following Alzheimer 's disease (AD) biomarker criteria: amyloid PET CL>19, plasma p-tau217>=0.63), CSF tau/Aβ ratio>1, CSF ptau>57 or confirmed post-mortem AD pathology. Across 1389 visits, all Addenbrooke's Cognitive Examination-Revised (ACE-R) subscores were entered into an unrotated principal component analysis (PCA) to derive a transdiagnostic phenotype-severity model.

Results: Individuals with AD pathology spanned multiple diagnostic groups: AD (n=93), behavioral frontotemporal dementia (n=20), primary progressive aphasia (PPA, n=38: logopenic PPA =6, semantic PPA=18, non-fluent PPA=12, mixed=2), progressive supranuclear palsy (n=43), corticobasal syndrome (n=28), Parkinson's disease (n=31), other (n=11) and asymptomatic controls (n=22). PCA yielded a first component (KMO=0.94), explaining 42.3% of variance, with all ACE-R subscores loading strongly (0.526-0.821), reflecting overall global severity (Figure 1). The second component, explaining 10% of variance captured phenotypic differentiation across cognitive domains. Association analyses showed that phenotypic differentiation became only apparent as severity increased, but diminished with advanced global impairment (Figure 2).

Conclusions: This highlights the dynamic relationship between disease severity and phenotypic expression across dementia syndromes. Research and clinical trials emphasize early detection of at-risk people, however our results highlight the challenge of distinguishing clinical phenotype early on. Our approach enables the identification of maximal behavioral differentiation and comparison to baseline imaging to assess whether phenotypic divergence may be predicted earlier.

Figure 1: ACE-R subscore loadings on the first (A) and second (B) principal components. ACE-R subscores presented in assessment order.

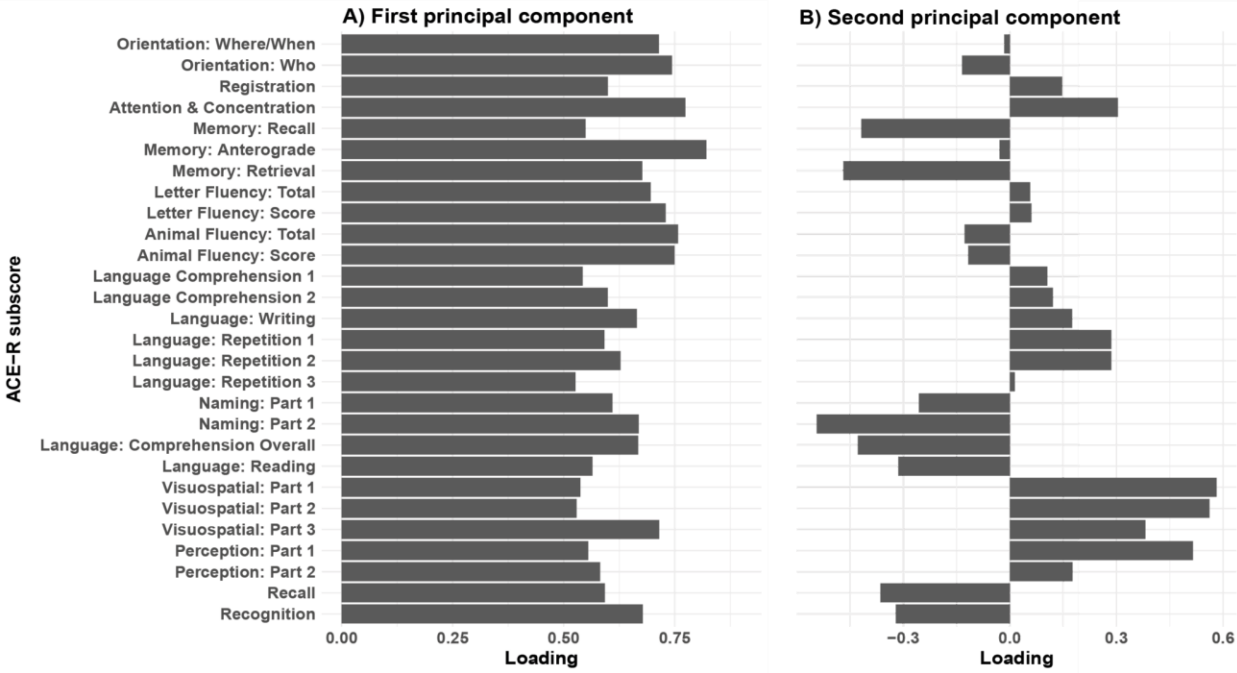
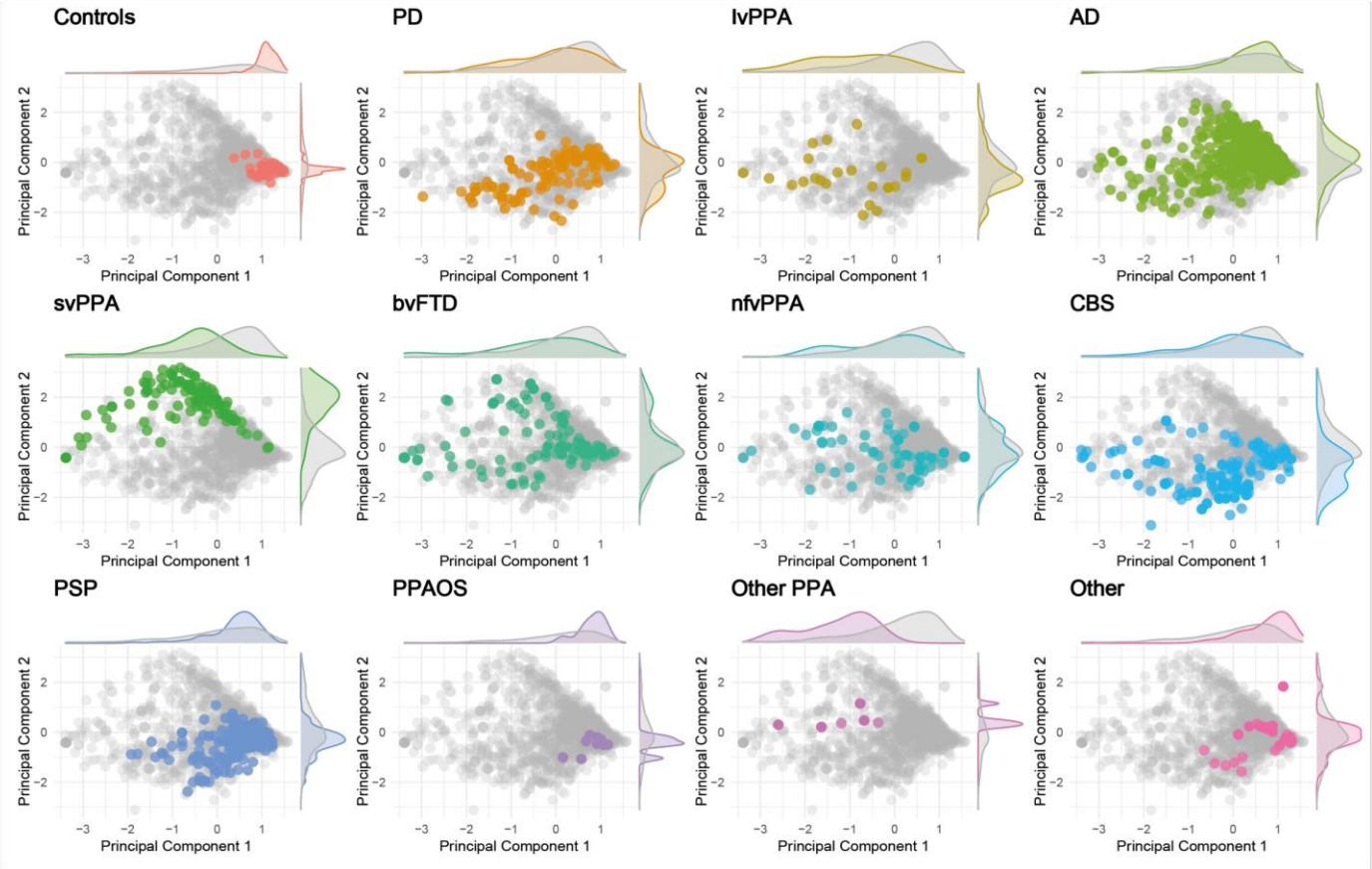


Figure 2: Associations between principal component one (global severity) and two (phenotype) across diagnostic groups with cohort and group density plots. Whole cohort in grey, unique diagnostic group highlighted in colour in each plot. PD – Parkinson's diease, lvPPA – logopenic primary progressive aphasia, AD – Alzheimer's Diseases, svPPA – semantic primary progressive aphasia, bvFTD - behavioural variant frontotemporal dementia, nfvPPA – non-fluent primary progressive aphasia, CBS – corticobasal syndrome, PSP – progressive supranuclear palsy, PPAOS – primary progressive apraxia of speech, Other PPA – mixed primary progressive aphasia.



Keywords: transdiagnostic, phenotypic heterogeneity, disease severity, cognitive profiling, biomarkers

64 Standardized indices of tau burden using the CenTauR universal scale predict distinct cognitive trajectories across Alzheimer's disease biological stages

Brian Lopresti[1], Alex DelBene[1], Antoine Leuzy[2,3], Alexandra Gogola[1], Tessa Harrison[4], Susan Landau[4], William Jagust[4], Victor Villemagne[5]

[1]*Department of Radiology, University of Pittsburgh School of Medicine, Pittsburgh, PA, US*
[2]*Critical Path for Alzheimer's Disease (CPAD) Consortium, Critical Path Institute, Tucson, AZ, US*
[3]*Enigma Biomedical Group, Knoxville, TN, US*
[4]*Department of Neuroscience, University of California, Berkeley, Berkeley, CA, US*
[5]*Department of Psychiatry, University of Pittsburgh School of Medicine, Pittsburgh, PA, US*

Background: The CenTauR (CTR) method implements a standard scale expressing results from different tau radiotracers in universal units. An Alzheimer's Association Workgroup (AAW) recently proposed a framework for biological staging of Alzheimer's disease (AD) based on Aβ and tau biomarker presentations. This work tested whether biologic staging of participants at baseline using standardized indices of Aβ (CL) and tau (CTR) burden predicts distinct trajectories of subsequent cognitive decline.

Methods: 480 participants were selected from the Alzheimer's Disease Neuroimaging Initiative (ADNI) cohort with available [^{18}F]flortaucipir (FTP) and Aβ PET images and serial cognitive assessments (MMSE). FTP images were processed using the SPM-12 based CTR pipeline. Gaussian mixture model-defined thresholds were applied to FTP CTR outcomes to determine mesial temporal (MTL) tau status (+/-), temporoparietal (TP) tau status (+/-), and stage (moderate, high). Aβ+ (≥20 CL) participants were classified by AD biological stages (A-D): A) MTL-, TP- ; B) MTL+, TP-; C) TP+(moderate); D: TP+ (high). Subjects who were Aβ-, MTL-, and TP- were considered pathology negative (N) and used as a reference group. Linear mixed models predicted MMSE trajectories for each biological stage. The final model incorporated time and its interaction with biological stage with sex, baseline age, and baseline CL as covariates.

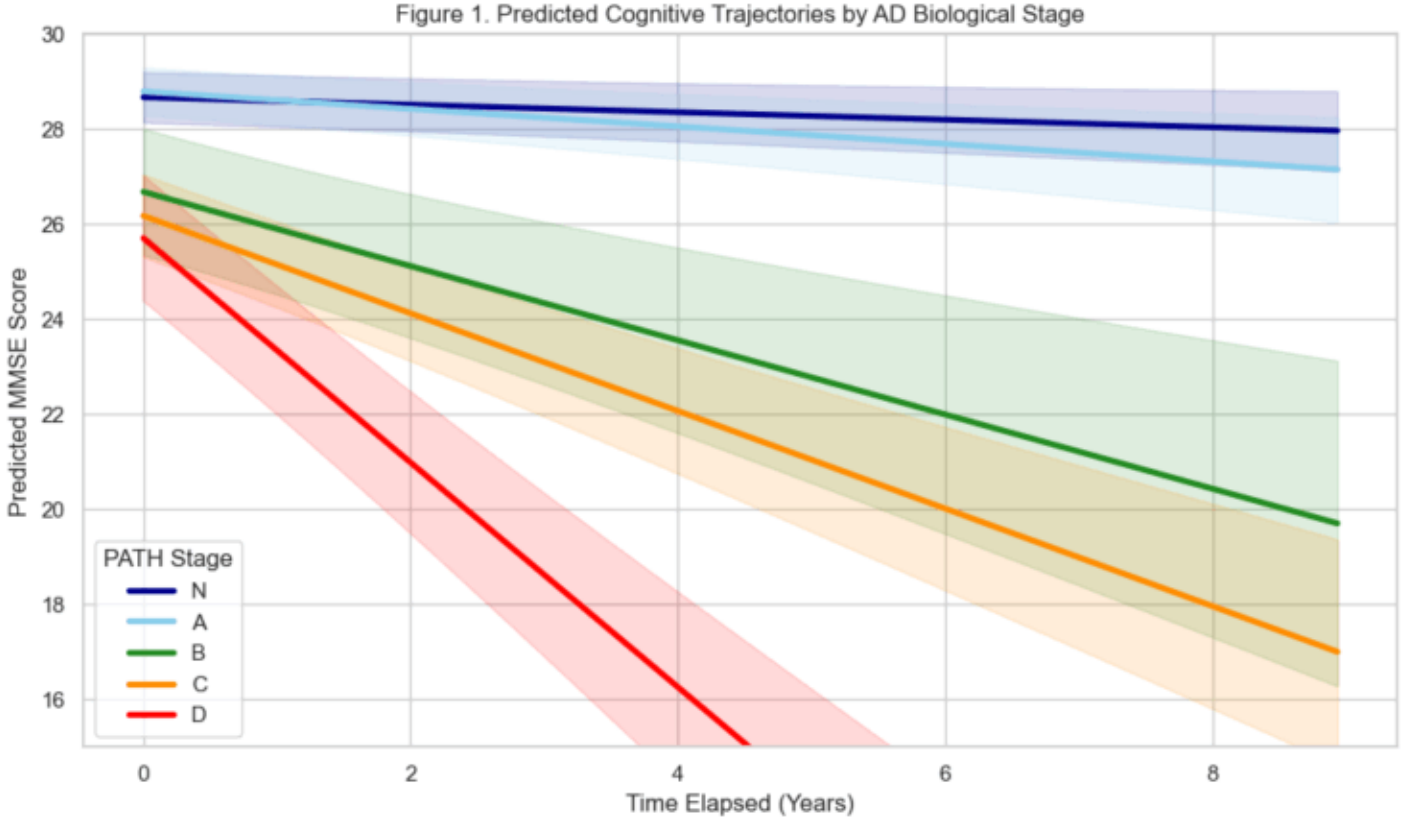
Results: Participants' AD biologic stage is shown in Table 1. The reference group showed a small but significant cognitive decline (-0.08 MMSE points/yr, p=0.023). Compared to the N reference group, significantly lower baseline MMSE was found for stages B (-2.0 points, p=0.011), C (-2.5 pts, p<0.001), and D (-3.0 points, p<0.001), whereas significantly faster rates of cognitive decline were observed for stages B (-0.7 points/yr, p<0.001) C (-1.0 points/yr, p<0.001) and D (-2.3 points/yr, p<0.001) (Figure 1).

Conclusions: The CenTauR method can be used for biologic staging of tau pathology.

Table 1. Classification of Participants by AD Biological Stage

Stage	N	Sex	% CI	Baseline Age (SD)	Baseline MMSE (SD)	# Obs (SD)	F/U, y (SD)	Centiloids (SD)	MTL CTR (SD)	TP CTR (SD)
A	143	53.8% F	30%	76.5 (7.1)	28.5 (2.4)	2.9 (0.9)	4.0 (2.2)	61 (30)	20 (18)	5 (9)
B	16	68.8% F	88%	75.8 (7.1)	25.9 (2.7)	3.1 (1.1)	3.4 (1.7)	96 (38)	73 (8)	17 (8)
C	56	50.0% F	75%	77.3 (6.8)	25.6 (3.8)	2.7 (0.9)	2.8 (1.8)	95 (31)	83 (29)	55 (19)
D	19	36.9% F	95%	71.1 (8.5)	24.9 (3.6)	2.6 (0.6)	2.5 (1.4)	104 (35)	114 (33)	139 (55)
N	243	50.7% F	33%	73.7 (7.6)	28.8 (1.6)	2.6 (0.9)	4.3 (2.0)	0 (10)	9 (14)	2 (9)
A-T+	3	33.0% F	67%	78.7(6.1)	26.3 (2.5)	2.7 (0.6)	3.5 (1.2)	4 (10)	76 (25)	53 (29)

Figure 1. Predicted Cognitive Trajectories by AD Biological Stage



Keywords: Tau, cognitive decline, CenTauR, standardization

65 SPARE-SVD: An integrated machine-learning metric for cerebral small vessel disease within the ATN(V) framework

Mengjin Dong[1], Mengna Zhang[2], Yuheng Zeng[1], David Wang[1], Di Wang[1], Jon Toledo[3], Mitzi Gonzales[4], Sokratis Charisis[5,6], Tanweer Rashid[1], Sudha Seshadri[1], Paul Crane[7], Derek Archer[2], Angela Jefferson[2], Timothy Hohman[2], Mohamad Habes[1]

[1]*Neuroimage Analytics Laboratory (NAL) and the Biggs Institute Neuroimaging Core (BINC), Glenn Biggs Institute for Alzheimer's and Neurodegenerative Diseases, University of Texas Health Science Center San Antonio, San Antonio, TX, US*
[2]*Vanderbilt Memory and Alzheimer's Center, Vanderbilt University Medical Center, Nashville, TN, US*
[3]*Nantz National Alzheimer Center, Stanley Appel Department of Neurology, Houston Methodist Hospital, Houston, TX, US*
[4]*Department of Neurology, Cedars-Sinai Medical Center, Los Angeles, CA, US*
[5]*Department of Neurology, Massachusetts General Hospital, Boston, MA, US*
[6]*Harvard Medical School, Boston, MA, US*
[7]*Department of Medicine, University of Washington, Seattle, WA, US*

Introduction: Cerebral small vessel disease (SVD) contributes to cognitive impairment in Alzheimer's disease (AD). Although the revised AD framework recognizes **vascular (V)** pathology as an copathology alongside β-amyloid, tau, and neurodegeneration (ATN), prior research has focused on individual SVD markers. To address this gap, we developed the Spatial Pattern of Abnormality for Recognition of SVD **(SPARE-SVD)** score, a machine-learning–based "V" biomarker that integrates multiple SVD features to provide a comprehensive measure of vascular burden, complementing ATN(V) framework.

Methods: SPARE-SVD was trained using a leave-one-out cross-validation on DTI features (fractional anisotropy and mean diffusivity) and white matter lesion (WML) burden from 362 ADNI participants (Figure 1) using a Support Vector Machine to differentiate participants with AD dementia (ADD) from CN. Its effectiveness was compared with individual SVD biomarkers. Associations between SPARE-SVD and cognitive scores were examined using linear regression models, adjusting for age, sex, education, SPARE-AD score, CSF β-amyloid, and CSF ptau positivity.

Results: SPARE-SVD achieved a balanced accuracy of 0.82 and ROC AUC of 0.85 for predicting CN/ADD, outperforming total WML or free-water-corrected FA alone. SPARE-SVD was significantly associated with poorer cognitive performance in memory, executive function, and language performances (Figure 2). After stratifying by β-amyloid and tau positivity, these associations remain significant only in the SPARE-SVD positive (V+, SPARE-SVD>0) group, but not in the V- group (Figure 3).

Discussion: The SPARE-SVD score captures the global SVD impact on AD, offering a robust imaging biomarker for the 'V' dimension of the ATN(V) framework. By integrating various MRI features into a single interpretable index, SPARE-SVD provides a scalable approach to quantify vascular burden and its interaction with neurodegenerative processes for cognitive decline. SPARE-SVD holds strong potential to enhance early risk stratification, monitor disease progression, and serves as a sensitive clinical trial outcome measure targeting vascular contributions to AD.

Figure 1. Characteristics of participants and biomarkers included from the ADNI cohort. (A) Demographic and clinical characteristics of study participants. (B) Correlation matrix illustrating relationships among β-amyloid (A positivity), CSF ptau (T positivity), neurodegeneration (N; SPARE-AD positivity), vascular (V; SPARE-SVD positivity), and individual vascular markers. (C) Scatter plots showing the associations between SPARE-SVD and individual vascular markers.

Abbreviations: CN, cognitively normal; MCI, mild cognitive impairment; ADD, Alzheimer's disease dementia; SVD, small vessel disease; FA, fractional anisotropy; WML, white matter lesion; *ρ* (rho), Spearman correlation coefficient; *p*, p-value.

A

	CN	MCI	ADD	Total/Average
Number of Subjects	154	155	53	362
Age (years)	76.02 (6.96)	75.39 (7.43)	77.25 (8.69)	75.93 (7.44)
Sex (Male/Female)	71/83	86/69	32/21	189/173
Education (<=12/13-17/>=18 years)	68/14/72	78/26/51	28/10/15	174/138/50
CSF β-amyloid (A+/A-)	59/95	97/58	48/5	204/158
CSF ptau (T+/T-)	54/100	76/79	39/14	169/193
Neurodegeneration (N+/N-)	24/130	68/87	46/7	138/224
Vascular (V+/V-)	55/99	85/70	44/9	184/178
Total Free-Water-Corrected FA	0.125 (0.030)	0.128 (0.027)	0.127 (0.032)	0.116 (0.030)
Total White Matter Lesion (mm³)	7004 (10001)	5155 (7791)	8246 (12127)	8747 (7898)
SPARE-SVD	-0.380 (0.929)	0.005 (0.926)	0.971 (0.906)	-0.017 (1.024)

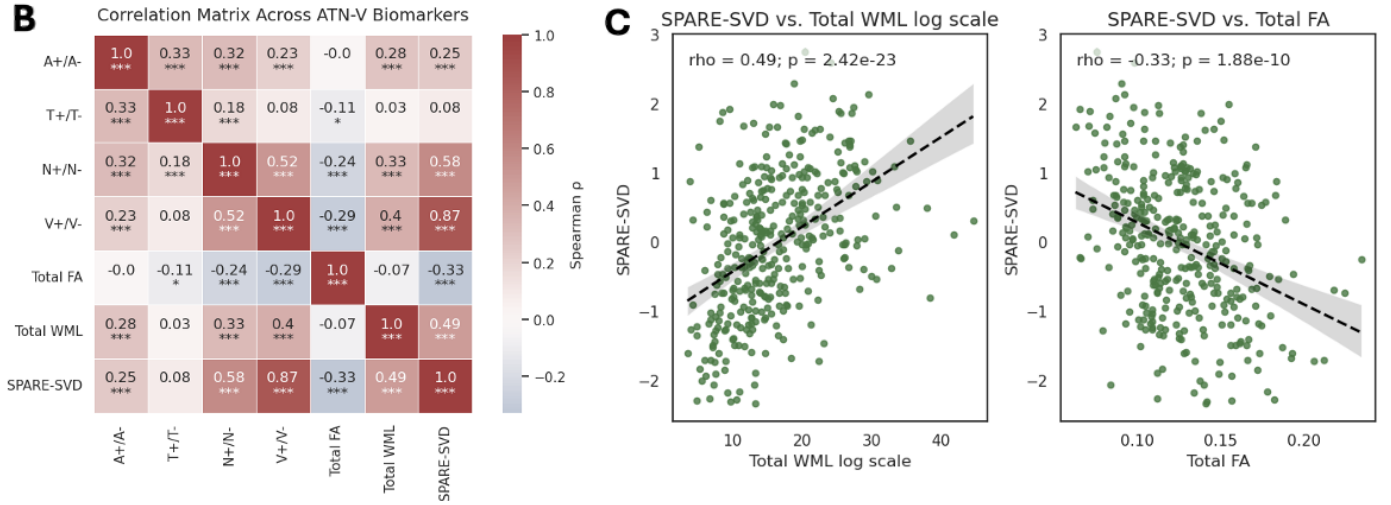


Figure 2. Evaluation of SPARE-SVD performance. (A) Receiver operating characteristic (ROC) curves of SVD biomarkers for distinguishing cognitively normal (CN) and Alzheimer's disease dementia (ADD) participants. (B) Association between SPARE-SVD and age at scan. (C) Association between SPARE-SVD and cognitive scores. Linear regression models were adjusted for SPARE-AD score, age, sex, years of education, β-amyloid positivity, and tau positivity.

Abbreviations: *b*, linear regression slope; *p*, p-value; *ρ* (rho), Spearman correlation coefficient; SVD, small vessel disease; FA, fractional anisotropy; WML, white matter lesion; CN, cognitively normal; MCI, mild cognitive impairment; ADD, Alzheimer's disease dementia.

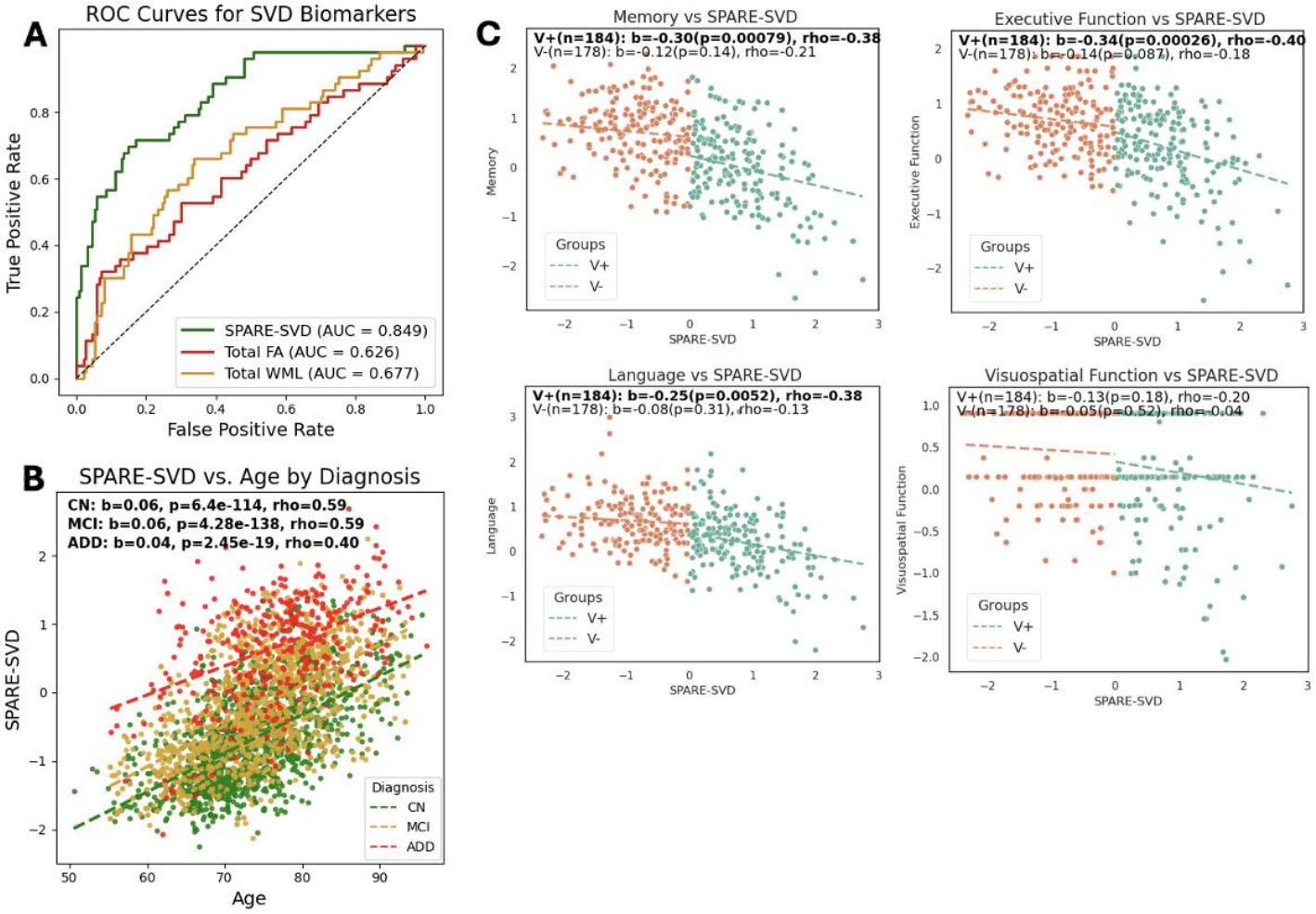
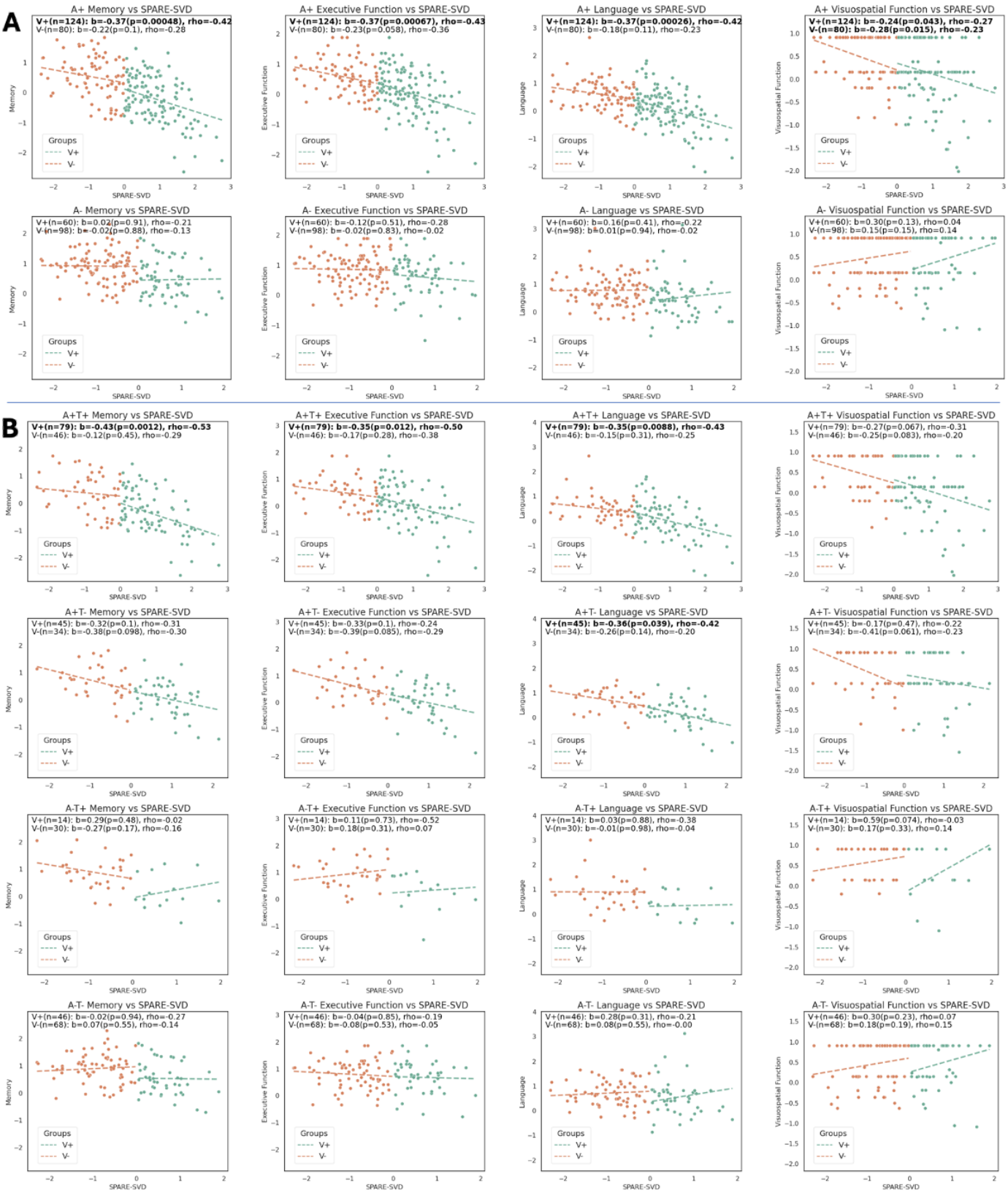


Figure 3. SPARE-SVD as a vascular ("V") biomarker and its association with worse cognition. Linear regression models were adjusted for SPARE-AD score, age, sex, and years of education. (A). Association stratified with CSF β-amyloid positivity. (B). Association stratified by both CSF β-amyloid and tau positivity.



Keywords: Small vessel disease, Vascular Contributions to Cognitive Impairment and Dementia, revised diagnostic criteria, DTI, white matter hyperintensity

66 Risk factors and AD prevention: a multivariate and multimodal study

Alfonso Fajardo Valdez[1,2], Ting Qiu[1,2], Valentin Ourry[1,2], Yara Yakoub[1,2], Sylvia Villeneuve[1,2,3], for the Prevent-AD Research Group[1,2]

[1]*Department of Psychiatry, Faculty of Medicine, McGill University., Montreal, QC, Canada*
[2]*Douglas Mental Health University Institute., Montreal, QC, Canada*
[3]*McConnell Brain Imaging Center, Montreal Neurological Institute, McGill University., Montreal, QC, Canada*

Modifiable risk factors, highlighted by the Lancet Commission in 2024, account for about 45% of dementia cases, including Alzheimer's disease (AD). We conducted a multivariate approach to examine the association between modifiable risk factors – identified by the Lancet commission – related to amyloid, tau PET burden, and cortical thickness in cognitively unimpaired older adults. Additional modifiable factors that could influence AD risk were also examined. We included 254 older adults (average age = 66.5, 69.2% Females) from the PREVENT-AD cohort. Most participants were cognitively unimpaired when they underwent amyloid (18F-NAV4694) and tau (18F-AV1451) PET scans, from which we extracted SUVR based on Desikan-Killiany atlas. Cortical thickness was derived from T1-weigted MRI. Modifiable risk factors were assessed using self-reported questionnaire based on the Lancet commission, as well as other factors such as sleep disturbance, mindfulness, optimism, stress, apathy and perseverative negative thinking (PNT). Six partial least squares (PLS) analyses were performed to investigate multivariate associations between (1) Lancet risk factors, and (2) Lancet + additional factors, with amyloid PET, tau PET burden, and cortical thickness. Across analyses, the first latent variable explained 60-90% of covariance between modifiable and neuroimaging variables. Lower education, physical inactivity, social isolation, alcohol and smoking consumption were associated to higher amyloid burden. Hearing loss and physical inactivity were associated with higher tau levels, while social isolation, alcohol use, smoking, obesity and lower education were related to reduced cortical thickness (**Figure 1**). Psychological factors such as higher stress, PNT, apathy, and anxiety, and lower mindfulness, purpose in life and optimism were associated with higher amyloid and/or tau; lower purpose in life also related to reduced cortical thickness (**Figure 2**).These findings reveal multifactorial associations between modifiable factors with early AD biomarkers. Beyond Lancet risk factors, mindfulness and purpose in life emerged as potential protective traits.

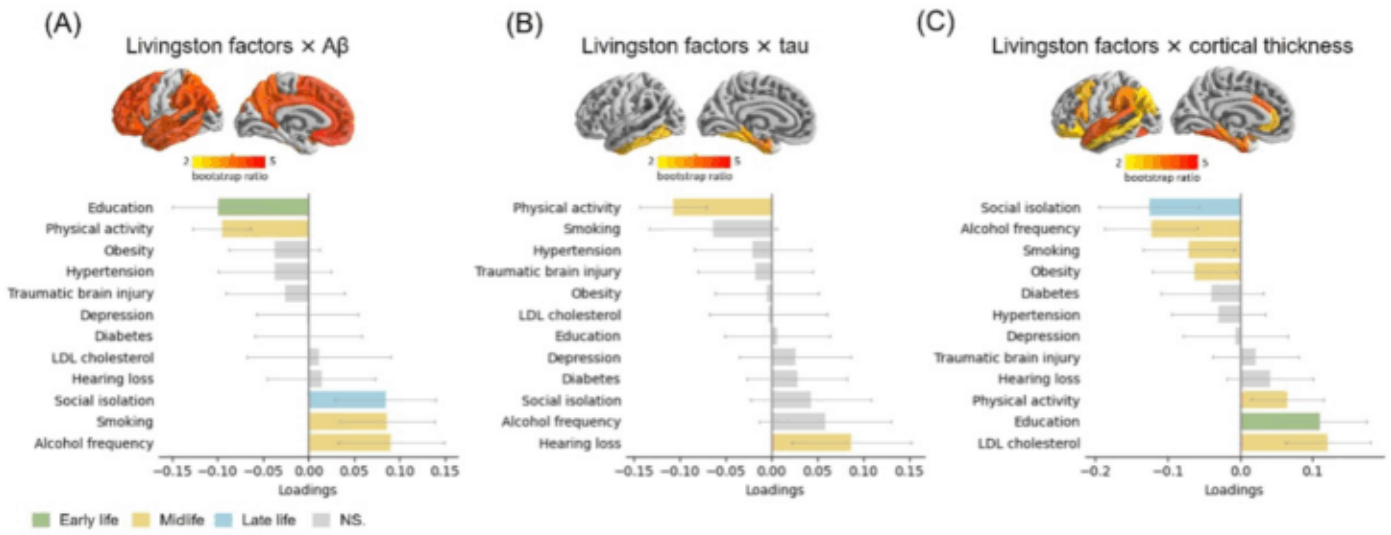


Figure 1. Latent variables from partial least squares analyses relating Livingston factors to Alzheimer's disease pathology in the PREVENT-AD cohort. Partial least squares (PLS) analyses were conducted to identify multivariate relationships between behavioral and lifestyle factors proposed by Livingston et al. (2024) and Alzheimer's pathology in the PREVENT-AD cohort. Separate models examined associations with (A) amyloid-β (Aβ) and (B) tau pathology, as well as (C) cortical thickness. Bar plots show factor loadings, representing the correlations between individual Livingston factors and the PLS-derived pathology scores. Confidence intervals were estimated using bootstrap resampling. Brain maps display regions with bootstrap ratios exceeding ±2, indicating areas that contributed most strongly to the identified multivariate relationships. Significance of latent variables (LVs) was considered significant at a value < 0.05 via 1000 permutation test, and additionally, we bootstrapped obtained loadings to find significant factor contributions on LVs.

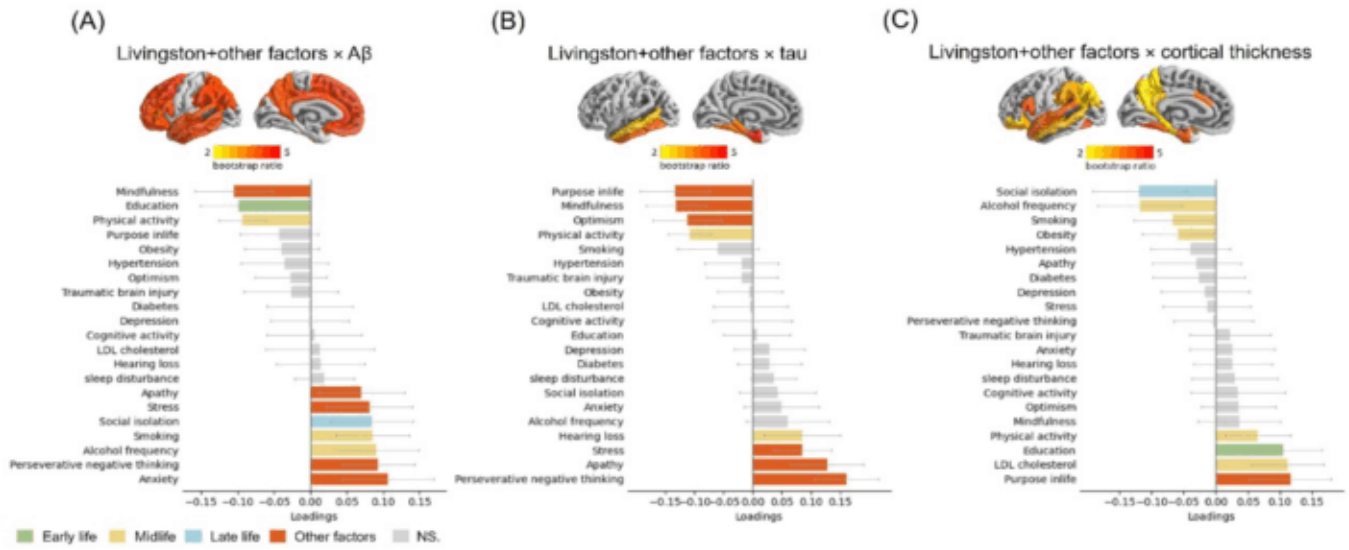


Figure 2. Latent variables from partial least squares analyses relating Livingston and additional factors to Alzheimer's disease pathology in the PREVENT-AD cohort. Partial least squares (PLS) analyses were conducted to identify multivariate relationships between modifiable factors from Livingston et al. (2024), combined with additional psychological and neuropsychiatric variables, and Alzheimer's pathology in the PREVENT-AD cohort. Separate models examined associations with (A) amyloid-β (Aβ) and (B) tau pathology, as well as (C) cortical thickness. Bar plots show factor loadings, representing the correlations between individual features and the PLS-derived pathology scores. Confidence intervals were estimated using bootstrap resampling. Brain maps display regions with bootstrap ratios greater than ±2, indicating areas that contributed most strongly to the identified multivariate relationships. Significance of latent variables (LVs) was considered significant at a value < 0.05 via 1000 permutation test, and additionally, we bootstrapped obtained loadings to find significant factor contributions on LVs.

Keywords: Modifiable risk factors, neuropathology, amyloid, tau, cortical thickness

67 MK6240 and Tauvid positivity, cognitive decline, and their relationship to Aβ PET deposition across the Alzheimer's spectrum

Bruna Bellaver[1], Guilherme Povala[1], Firoza Lussier[1], Livia Amaral[1], Guilherme Bauer-Negrini[1], Pamela Ferreira[1], William Jagust[2], Joseph Masdeu[3], Juan Fortea[4], Dana Tudorascu[1], David Soleimani-Meigooni[5], Val Lowe[6], Hwamee Oh[7], Belen Pascual[3], Brian Gordon[8], Pedro Rosa-Neto[9,10], Suzanne Baker[2], Tharick Pascoal[1,11]

[1]*University of Pittsburgh, Department of Psychiatry, Pittsburgh, PA, US*
[2]*Lawrence Berkeley National Laboratory, Berkeley, CA, US*
[3]*Houston Methodist Research Institute, Department of Neurology, Houston, TX, US*
[4]*Sant Pau Memory Unit, IR SANT PAU, Hospital de la Santa Creu i Sant Pau, Barcelona, Spain*
[5]*University of California San Francisco, Memory and Aging Center, San Francisco, CA, US*
[6]*Mayo Clinic, Department of Radiology, Rochester, MN, US*
[7]*Brown University, Department of Psychiatry and Human Behavior, Providence, Providence, RI, US*
[8]*Washington University in St. Louis, Department of Radiology, St. Louis, MO, US*
[9]*Translational Neuroimaging Laboratory, McGill University Research Centre for Studies in Aging, Douglas Research Institute, Montreal, QC, Canada*
[10]*Peter O'Donnell Jr. Brain Institute (OBI), University of Texas Southwestern Medical Centre (UTSW), Dallas, TX, US*
[11]*University of Pittsburgh, Department of Neurology, Pittsburgh, PA, US*

Background: Tau PET tracers differ in binding characteristics, dynamic range, and off-target signal, which may influence tau detection. In a head-to-head study, we investigated the relationship between the emergence of MK6240 and Tauvid positivity as a function of Aβ PET deposition.

Methods: We enrolled 822 individuals, 682 had complete Tauvid and MK6240, including 38 young adults (aged 18-28), 362 cognitively unimpaired elderly (CU) and 282 cognitively impaired. Tau positivity in the medial temporal lobe (MTL) and neocortex was defined as uptake exceeding the mean + 2.5 SD of young adults. Logistic regressions estimated the probability of tau and cognitive-domain positivity as a function of Centiloid values.

Results: MTL tau positivity increased stepwise with Centiloid for both tracers (**Fig.1A**). Visually, MK6240 showed clear abnormal uptake between 20–50 Centiloids, whereas Tauvid remained similar to individuals with lower Centiloid levels. (**Fig.1B**). The gap between tracers became smaller above 100 Centiloids, and by >150 Centiloids almost everyone was positive with both tracers. The 50% probability threshold for MTL positivity occurred at 50 Centiloids (95% CI 44–56) for MK6240 and 75 Centiloids (68–82) for Tauvid (**Fig.2A**). At the MK6240 MTL 50% probability threshold, Tauvid positivity probability was 28%, when Tauvid reached 50%, MK6240 was 74% (**Fig.2B**). Both tracers reached MTL tau positivity before memory impairment (120 Centiloids [108–133]). For neocortical, thresholds were 129 Centiloids (118–140) for MK6240 and 171 (149–192) for Tauvid. MK6240 neocortical positivity occurred shortly after memory decline but before other domains. Tauvid neocortical positivity occurred after both memory and executive function (171 Centiloids [149-192]; **Fig.2C**).

Conclusions: Our results demonstrated that both tau PET tracers present a stepwise increase in uptake with Centiloid levels, however, MK6240 identified tau deposition at lower levels of Aβ burden than Tauvid.

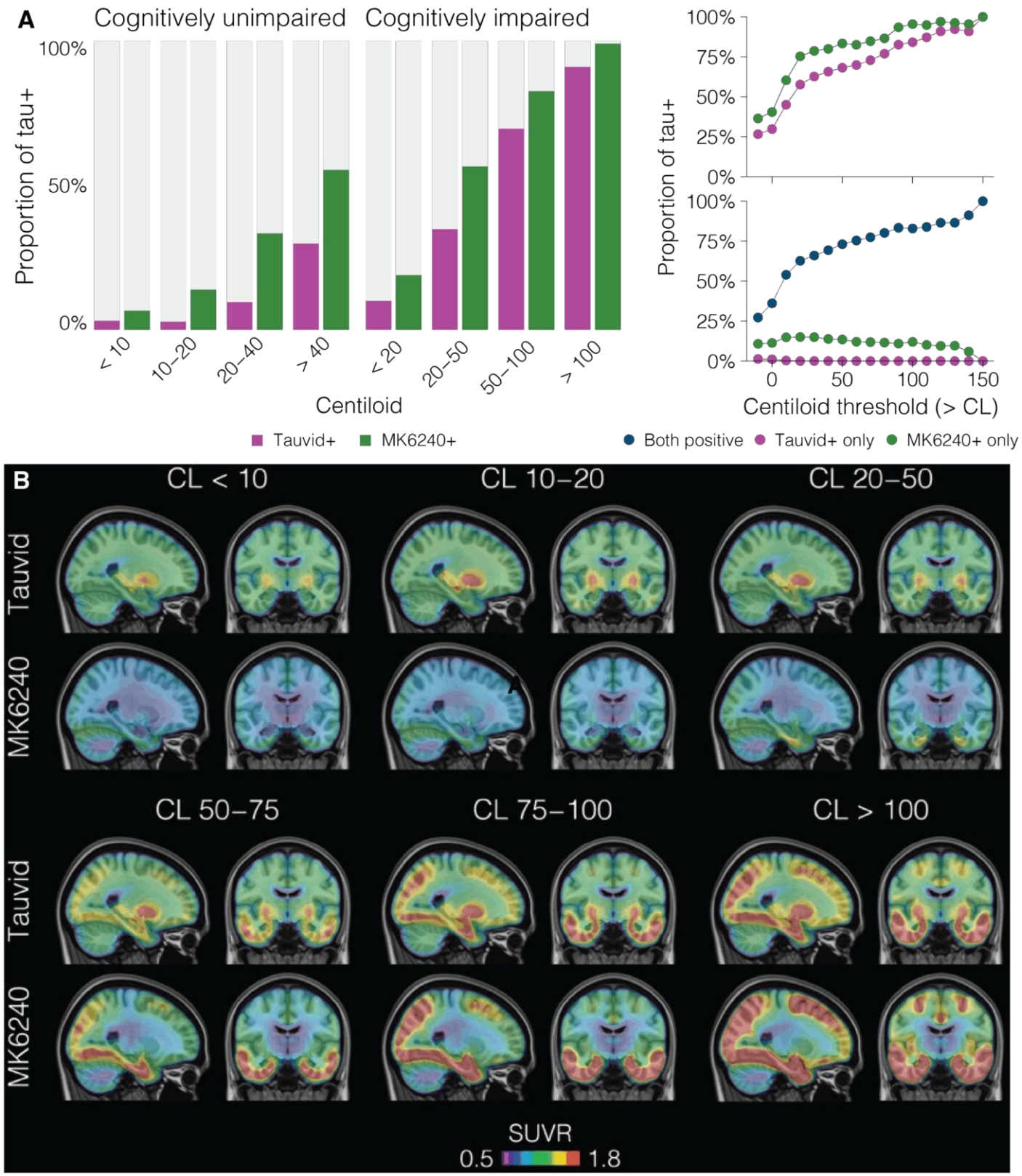


Fig.1. (A) Tau tracer MTL positivity stratified by Centiloid and clinical status. (B) Average SUVR images for Tauvid and MK6240 across Centiloid (CL) ranges.

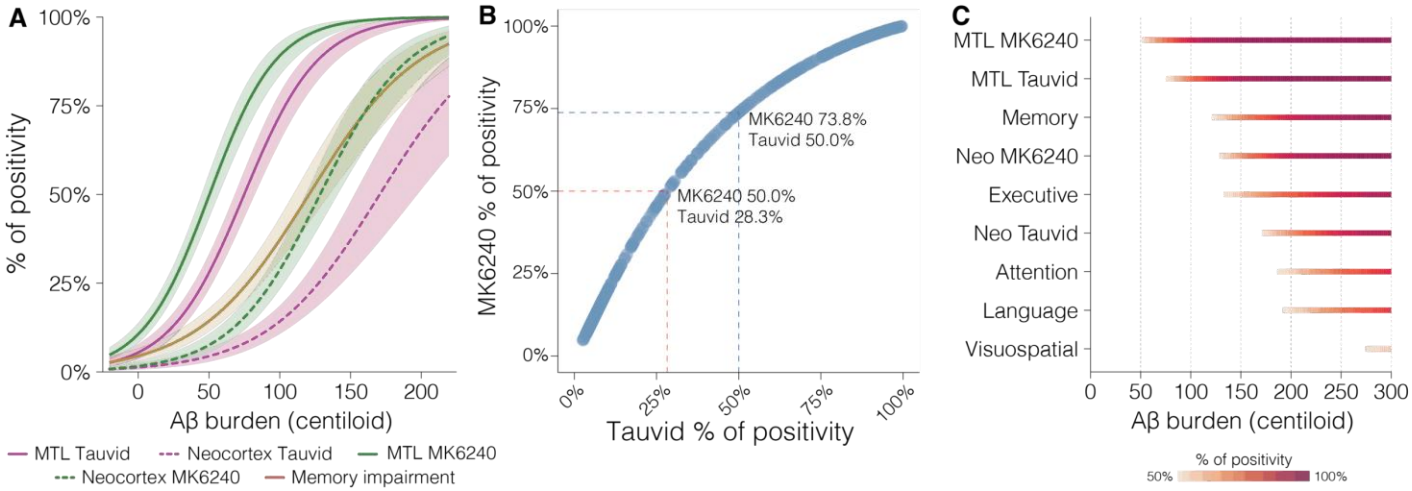


Fig.2. (A) Probability of positivity for Tauvid (purple) and MK6240 (green) in the medial temporal lobe (MTL; solid lines) and neocortex (dashed lines), shown as a function of amyloid-β (Aβ) burden (Centiloids). The probability of memory impairment is depicted in orange for comparison. (B) Direct comparison of positivity probabilities between MK6240 and Tauvid. (C) Aβ Centiloid thresholds corresponding to a 50% probability of tau positivity for each tracer and for a 50% probability of decline in memory, executive function, attention, language, and visuospatial domains. Shaded areas indicate 95% confidence intervals.

Keywords: tau PET, head-to-head comparison, amyloid-β

68 Differential tau-PET load predominance along shared progression trajectories determines clinical variability in Alzheimer's disease

Rayan Mroué[1], Guilherme Povala[1], Bruna Bellaver[1], Pamela Lukasewicz Ferreira[1], Guilherme Bauer-Negrini[1], Firoza Lussier[1], Livia Amaral[1], Marina Scop Medeiros[1], Emma Ruppert[1], Andreia Silva da Rocha[1], Matheus Scarpatto Rodrigues[1], Markley Silva Oliveira[1], Carolina Soares Katz[1], Douglas Teixeira Leffa[1], Pampa Saha[1], Joseph Masdeu[2], David Soleimani-Meigooni[3], Juan Fortea[4], Val Lowe[5], Hwamee Oh[6], Belen Pascual[2], Brian Gordon[7], Pedro Rosa-Neto[8], Suzanne Baker[9], Tharick Pascoal[1]

[1]*University of Pittsburgh, Department of Psychiatry, Pittsburgh, PA, US*
[2]*Houston Methodist Research Institute, Department of Neurology, Houston, TX, US*
[3]*University of California San Francisco, Memory and Aging Center, San Francisco, CA, US*
[4]*Hospital de la Santa Creu i Sant Pau, Department of Neurology, Barcelona, Spain*
[5]*Mayo Clinic, Department of Radiology, Rochester, MN, US*
[6]*Brown University, Department of Psychiatry and Human Behavior, Providence, RI, US*
[7]*Washington University in St. Louis, Department of Radiology, St. Louis, MO, US*
[8]*McGill University, Translational Neuroimaging Laboratory, Douglas Research Institute, Montréal, QC, Canada*
[9]*Lawrence Berkeley National Laboratory, Berkeley, CA, US*

One of the hallmarks of Alzheimer's disease is the progressive spread of tau pathology. However, heterogeneity in spatial patterns of tau deposition may contribute to distinct clinical presentations. Here, we investigated tau deposition patterns across disease progression and their cognitive correlates.

We studied 644 individuals (56% cognitively unimpaired, 44% amnestic cognitively impaired) from the HEAD study who underwent head-to-head Flortaucipir and MK6240 tau-PET. For each tracer, we extracted median SUVRs from the Entorhinal Cortex and seven brain network regions: Limbic, Visual (Vis), Default Mode (Default), Dorsal Attention (DorsAttn), Frontoparietal, Somatomotor (SomMot), and Salience Ventral Attention (SalVentAttn). Event-Based Modeling (EBM) was fit per tracer to estimate a canonical sequence using a reference group. Within each participant, EBM-positive regions were ranked by SUVR to identify different deposition peaks. Stage-standardized tau-PET subtype images and voxel-wise contrasts were generated per pattern and tracer. Cognition was assessed using linear regressions for MoCA and domain-specific composites (Memory, Attention, Executive, Visuospatial).

EBM revealed a hierarchical sequence across tracers: tau emerged in the Entorhinal Cortex, spread to the Limbic network then involved the remaining network regions. Positional variance diagrams showed diagonal dominance, indicating consistent ordering (**Figure 1**). After positivity, accumulation was non-uniform. Within-participant rankings identified three dominant peak patterns: Vis, Default, and DorsAttn. Voxel-wise contrasts across these patterns showed clear differences in tau-PET uptake for both tracers (**Figure 2**). Across tracers, MoCA did not differ between groups, individuals assigned to the Vis and DorsAttn patterns showed lower Visuospatial scores compared to the Default; the Vis pattern also showed lower Attention relative to the Default. With MK6240 only, the Default group showed lower Memory but higher Executive scores compared to the DorsAttn (**Figure 3**).

Our results indicate a model in which, although tau progresses hierarchically, its deposition peaks along specific network regions, driving clinical phenotyping in Alzheimer's disease.

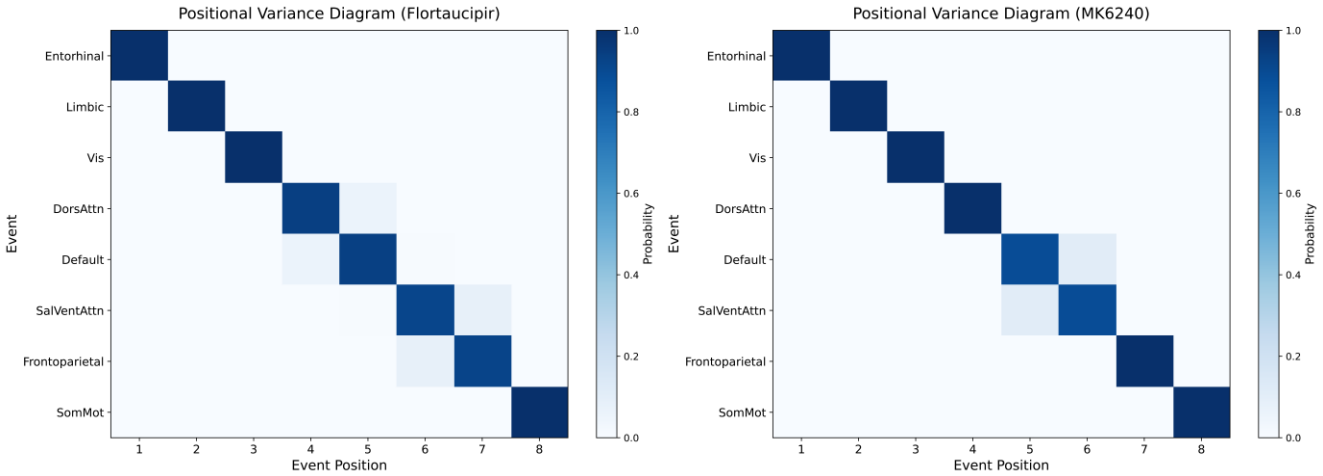


Figure 1. Event-Based Model Positional Variance Diagrams (PVDs) for tau-PET Network Region Involvement. Each heatmap shows the probability that an EBM event (i.e. region becoming tau-positive) occurs at each position in the sequence.

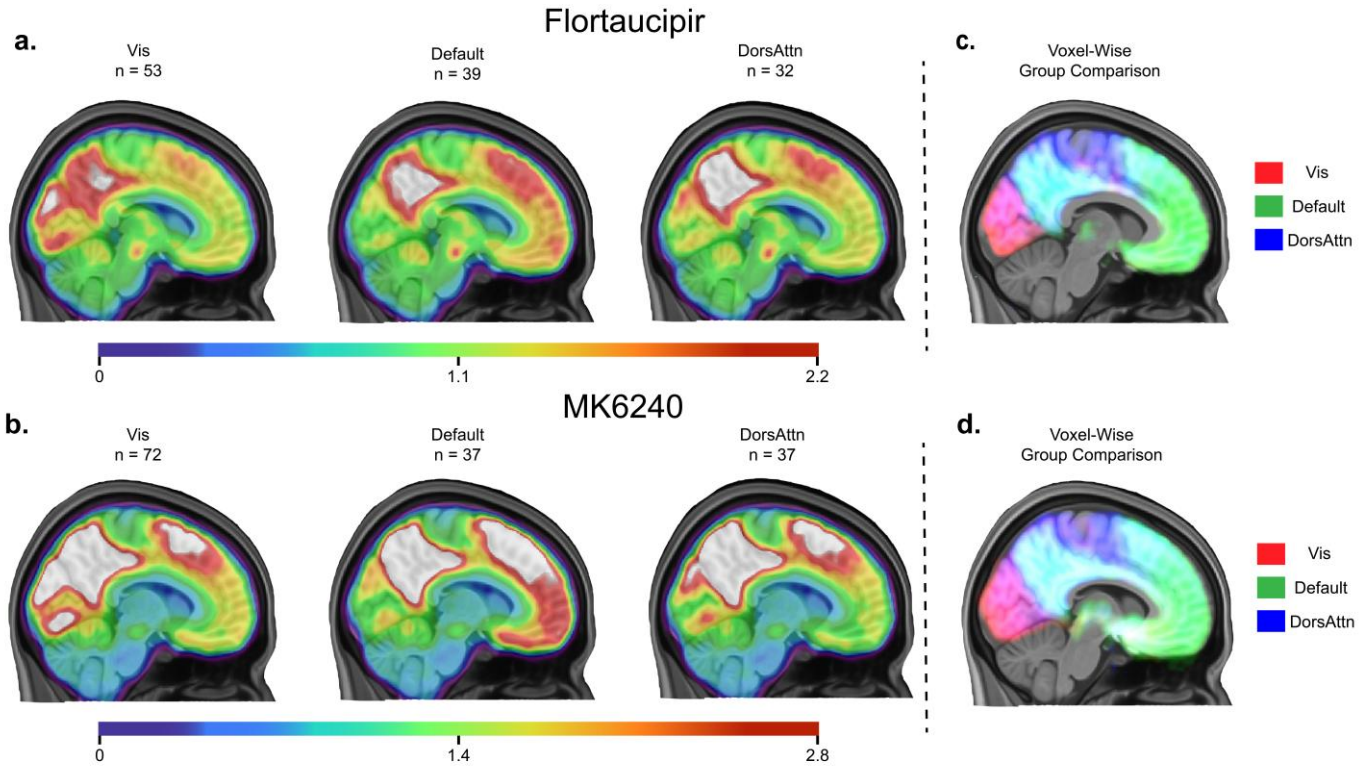


Figure 2. Stage-standardized tau-PET subtype images (a,b) and voxelwise group comparisons (c,d). Panels a–b show predicted SUVR images for the Visual, Default Mode, and Dorsal Attention groups, adjusted for EBM stage (Flortaucipir; MK6240). Panels c–d show voxelwise contrasts of late-stage individuals in each group vs low tau individuals, (red=Visual, green=Default Mode, blue=Dorsal Attention); blended colors indicate overlap. All models adjust for age, sex, and scanner.

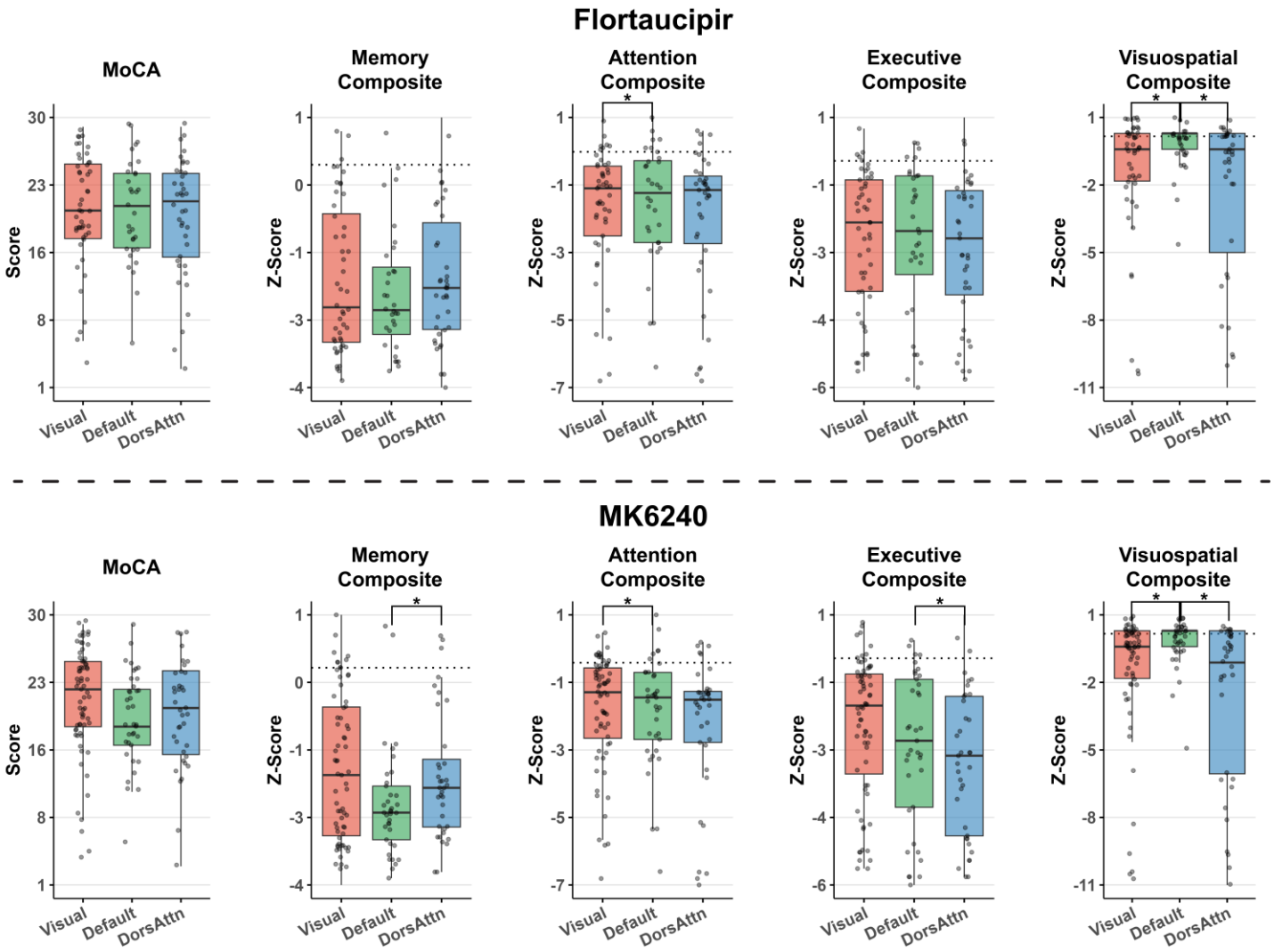


Figure 3: MoCA and Memory, Attention, Executive and Visuospatial Composite Scores by Tau Deposition Patterns. Linear regressions are corrected for age, sex, years of education, site, EBM assigned stage and clinical diagnosis. Lower scores indicate greater impairment in the respective cognitive domain. *: p-value < 0.05

Keywords: tau-PET, Alzheimer, Cognition, Event-Based Modeling

69 Head-to-head comparison of tau PET tracers across the Alzheimer's disease spectrum: baseline results from the HEAD study

Guilherme Povala[1], Bruna Bellaver[1], Firoza Z. Lussier[1], Livia Amaral[1], Guilherme Bauer-Negrini[1], Pamela C. L. Ferreira[1], William J. Jagust[2], Joseph Masdeu[3], Juan Fortea[4], Dana L. Tudorascu[1], David N. Soleimani-Meigooni[5], Val Lowe[6], Hwamee Oh[7], Belen Pascual[3], Brian A. Gordon[8], Pedro Rosa-Neto[9], Suzanne Baker[2], Tharick A. Pascoal[1]

[1]*University of Pittsburgh, Department of Psychiatry, Pittsburgh, PA, US*
[2]*Lawrence Berkeley National Laboratory, Berkeley, CA, US*
[3]*Houston Methodist Research Institute, Department of Neurology, Houston, TX, US*
[4]*Sant Pau Memory Unit, IR SANT PAU, Hospital de la Santa Creu i Sant Pau, Barcelona, Spain*
[5]*University of California San Francisco, Memory and Aging Center, San Francisco, CA, US*
[6]*Mayo Clinic, Department of Radiology, Rochester, MN, US*
[7]*Brown University, Department of Psychiatry and Human Behavior, Providence, RI, US*
[8]*Washington University in St. Louis, Department of Radiology, St. Louis, MO, US*
[9]*Translational Neuroimaging Laboratory, McGill University Research Centre for Studies in Aging, Douglas Research Institute, Montréal, QC, Canada*

Background: Tau PET imaging is an important tool for AD clinical trials, diagnosis, and biomarker research. Here, we present for the first time the final analysis of the primary cross-sectional outcomes from the HEAD study comparing Tauvid and MK6240 uptake.

Methods: We enrolled 822 individuals, 682 had complete Tauvid and MK6240, including 38 young adults (aged 18-28), 362 cognitively unimpaired elderly (CU) and 282 cognitively impaired. Tau positivity in the medial temporal lobe (MTL) and neocortex was defined as uptake exceeding the mean + 2.5 SD of young adults. Prevalence ratios (PR) were estimated with Poisson regression with robust variance adjusting for Centiloid. The number of participants needed to identify one tau-positive was defined as the inverse of the observed positivity rate (1/prevalence).

Results: In CU, MTL positivity was detected in 6.9% with Tauvid and 15.2% with MK6240, corresponding to a twofold higher prevalence for MK6240, (PR=2.19, p=0.0013; **Fig.1A**). Among cognitively impaired, MTL positivity was 55% versus 66% (PR=1.15; p=0.002), and neocortical positivity 16% versus 28% (PR=1.74; p=0.0002), driven by Aβ+ cases (**Fig.1B**). To identify one MTL-positive case, 5.5 CU Aβ+ individuals would need to be scanned with Tauvid and 2.5 with MK6240. For neocortical positivity, 10.8 and 4.2 MCI Aβ+, and 2.5 and 1.6 AD dementia participants would need to be scanned with Tauvid and MK6240, respectively (**Fig.1C**). Among discordant cases, 10.6% were positive only with MK6240 and 1.2% only with Tauvid (**Fig.2A**). MK6240-only individuals showed higher Aβ burden, APOEε4 carriership, and worse memory scores than dual-negative participants (**Fig.2B-E**). Representative discordant cases are shown in **Fig.3**.

Conclusions: Our results highlight that quantitative detection of tau pathology differs between tracers, with MK6240 detecting substantially more MTL and neocortical tau pathology than Tauvid. MK6240-only participants had higher Centiloid and worse cognitive scores, supporting the pathological relevance of MK6240-only uptake.

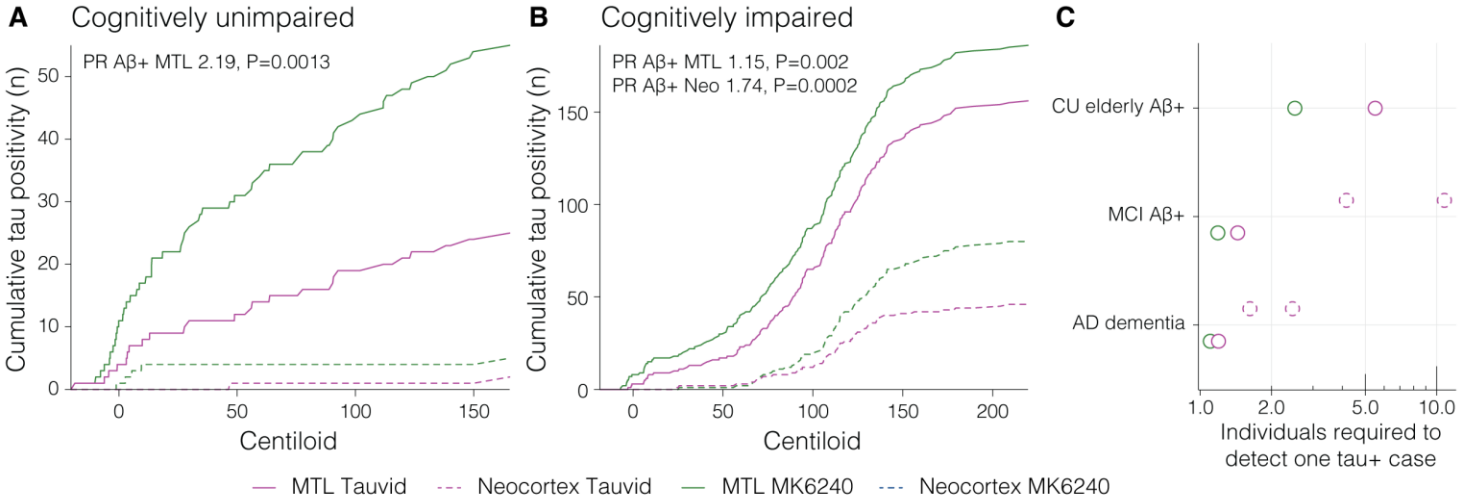


Figure 1. Cumulative proportion of tau-positive individuals in the medial temporal lobe (MTL; solid lines) and neocortex (dashed lines) for Tauvid (purple) and MK6240 (green), plotted as a function of Centiloids in (A) cognitively unimpaired (CU) and (B) cognitively impaired groups. (C) shows the estimated number of participants needed to identify one tau-positive case stratified by diagnosis and Aβ status. Aβ = amyloid-β; AD = Alzheimer's disease; MCI = mild cognitive impairment; PR = prevalence ratio.

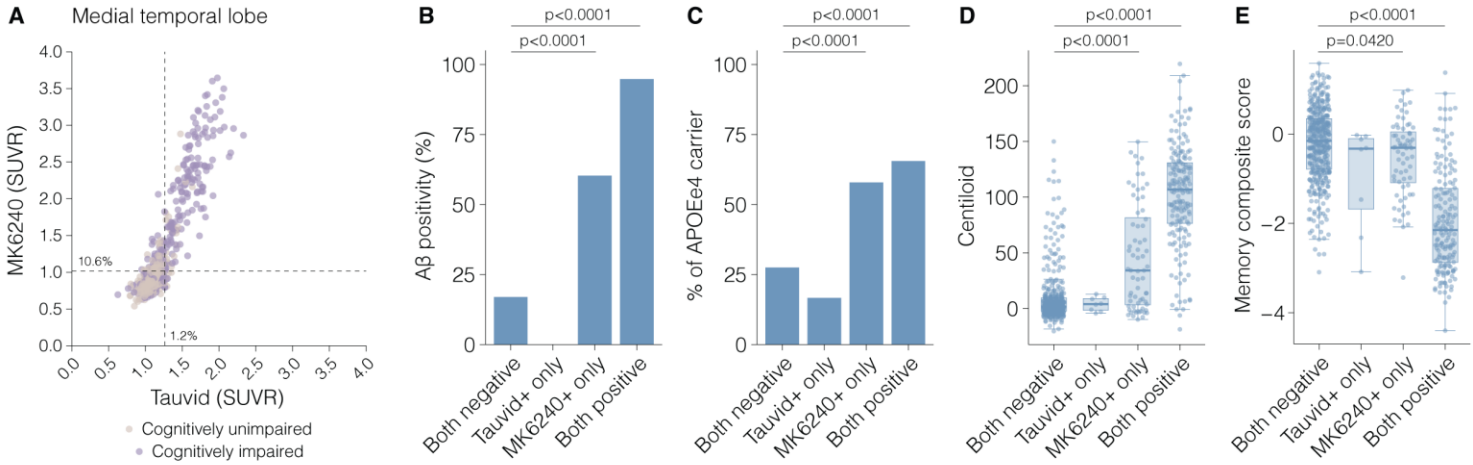


Figure 2. Scatterplot of SUVR values for Tauvid versus MK6240 in the medial temporal lobe stratified by cognitive status. Panels B–E display the corresponding distributions of (B) Aβ positivity, (C) APOE ε4 genotype, (D) Centiloid values, and (E) memory composite scores across Tauvid and MK6240 groups. Values are presented as median ± interquartile range. Aβ = amyloid-β; SUVR = standardized uptake value ratio.

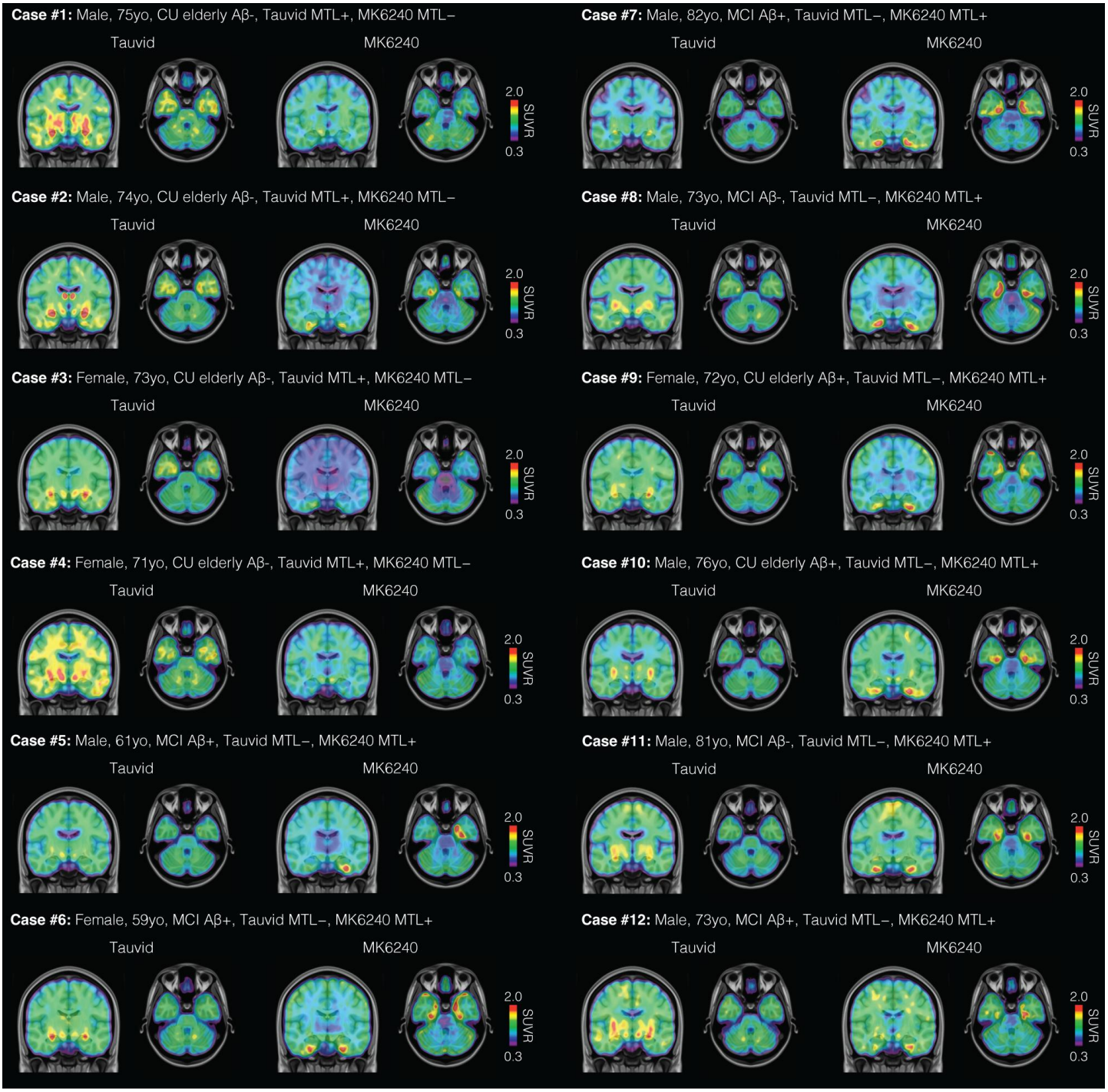


Figure 3. Patterns of tau PET uptake in representative cases scanned with both Tauvid and MK6240. These cases highlight instances of tracer-specific differences in medial temporal lobe (MTL) binding in the same individuals. SUVR: standardized uptake value ratio. Aβ: amyloid-β; CU: cognitively unimpaired; MCI: mild cognitive impairment.

Keywords: Head-to-head comparison, tau PET, MK6240, Tauvid

70 Comparison of Sampled Iterative Local Approximation (SILA) implemented in R and MATLAB

Hailey Bruzzone[1], William Coath[1], Ruvini Navaratna[1], Finnuella Carey[1], Jacob Morse[1], Murat Bilgel[2], Tobey Betthauser[1]

[1]*Department of Medicine, University of Wisconsin-Madison School of Medicine and Public Health, Madison, WI, US*
[2]*Laboratory of Behavioral Neuroscience, National Institute on Aging, National Institutes of Health, Baltimore, MD, US*

Background: The Sampled Iterative Local Approximation (SILA) algorithm models longitudinal amyloid PET accumulation to estimate person-level amyloid onset age (EAOA), a key clinical biomarker of Alzheimer's disease progression. Originally developed in MATLAB, SILA outputs are often analyzed in R. We developed silaR (https://github.com/Betthauser-Neuro-Lab/silaR), an R implementation of SILA, and evaluated its performance using simulated data and three observational cohorts.

Methods: SILA was applied to amyloid PET centiloid (CL) values for simulated data provided in the silaR package (n=200) and three observational cohorts (ADNI; n=880, OASIS; n=422, WISC; n=736). MATLAB and R implementations were compared by visualizing SILA curves, assessing sampling rates (A+ defined as CL ≥ 21 for time = 0), and evaluating model fit (RMSE). Backward-prediction residuals were compared using Kruskal-Wallis tests. EAOAs were compared with Friedman and paired Wilcoxon Signed-Rank tests and evaluated against midpoint EAOA (midpoint between last A- and first A+ scan) in observed converters.

Results: MATLAB showed lower RMSE on simulated data (5.6 CL vs 7.4 CL), while silaR performed better on observed data (mean RMSE across cohorts 5.4 CL vs. 7.6 CL). EAOA estimates were generally earlier in MATLAB (Figure 3). The largest EAOA difference occurred in ADNI (median = -0.31 years; 95% CI = [-0.44, -0.22]) and the smallest in simulated data (difference in medians -0.00004 years; 95% CI = [-0.002, 0.00002]). In converters, EAOA distributions from both versions did not differ from midpoint EAOA in OASIS or simulated data ($p_{sim} = 0.24$, $p_{OASIS} = 0.64$) but differed in ADNI and WISC ($p_{ADNI} = 0.05$, $p_{WISC} < 0.001$).

Conclusion: silaR provides an accurate R-based implementation of SILA, yielding comparable results to MATLAB in both group-level trends and individual EAOA estimates. Its integration into R enhances accessibility in biomarker research and statistical testing. Future work will focus on model performance optimization and error estimation.

Table 1: Cohort Demographic Comparisons

Variable	ADNI (N=880)	OASIS (N=422)	WISC (N=736)	Simulated Data (N=600)
Sex				
Female	454 (51.6%)	243 (57.6%)	496 (67.4%)	-
Male	426 (48.4%)	179 (42.4%)	240 (32.6%)	-
APOE-e4+				
e4+	333 (37.8%)	163 (38.6%)	282 (38.3%)	-
Missing	8 (0.9%)	3 (0.7%)	32 (4.3%)	-
Years Education				
Mean (SD)	16.4 (2.45)	16.3 (2.36)	16.0 (2.33)	-
Missing	0 (0%)	0 (0%)	1 (0.1%)	-
CDR Global				
0	471 (53.5%)	357 (84.6%)	576 (78.3%)	-
0.5	278 (31.6%)	31 (7.3%)	128 (17.4%)	-
1	73 (8.3%)	19 (4.5%)	13 (1.8%)	-
2	49 (5.6%)	15 (3.6%)	5 (0.7%)	-
3	8 (0.9%)	0 (0%)	2 (0.3%)	-
Missing	1 (0.1%)	0 (0%)	12 (1.6%)	-
Baseline Amyloid Age				
Mean (SD)	71.6 (7.41)	68.2 (8.50)	66.0 (7.89)	72.8 (4.38)
No. Amyloid Scans				
Mean (SD)	2.53 (1.50)	1.57 (0.806)	2.01 (1.24)	3.00 (0.00)
Median [Min, Max]	2.00 [1.00, 7.00]	1.00 [1.00, 5.00]	2.00 [1.00, 7.00]	3.00 [3.00, 3.00]
Amyloid Follow-up (Years)				
Mean (SD)	3.59 (3.40)	1.91 (2.72)	3.12 (4.09)	3.98 (0.31)
Median [Min, Max]	2.89 [0, 13.2]	0 [0, 13.8]	2.02 [0, 13.3]	4.00 [3.51, 4.49]
A+ Cases				
N (%)	413 (46.9%)	126 (29.9%)	222 (30.2%)	69 (34.5%)
A- To A+ Convertors				
N (%)	85 (9.7%)	9 (2.1%)	55 (7.5%)	9 (4.5%)

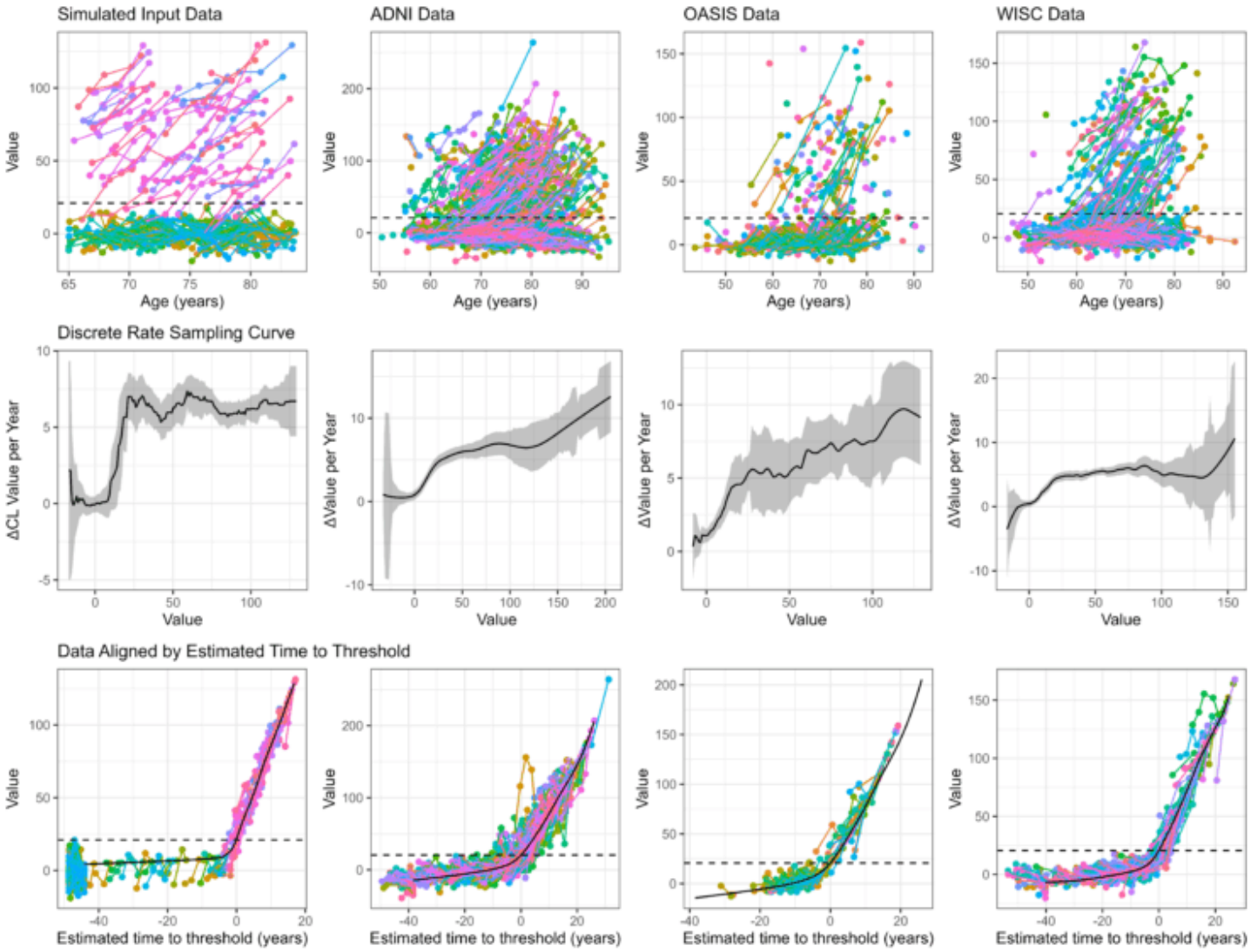
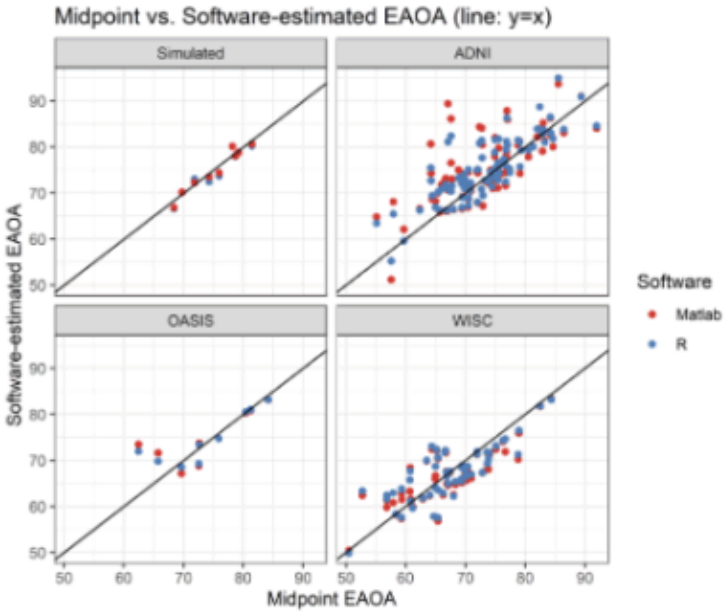


Figure 2:
Row 1: Observed cohort data with CL ≥ 21 threshold shown by dotted line.
Row 2: Discrete rate sampling curve fit for each cohort in silaR.
Row 3: Individual observations aligned to each cohort's value-vs-time curve fit in silaR.



Median EAOA (Q1, Q3)	silaR	SILA Matlab	Median Difference (Matlab – R; [95% CI])	Wilcoxon p
Simulated Data	113.3 (72.1, 121.89)	115.8 (71.4, 122.5)	-0.00 [-0.00, 0.00]	0.51
ADNI	75.0 (66.8, 85.0)	75.3 (67.1, 86.4)	-0.31 [-0.43, -0.22]	< 0.001
OASIS	71.7 (65.8, 78.0)	72.3 (65.9, 78.6)	-0.02 [-0.05, -0.02]	< 0.001
WISC	73.5 (66.2, 83.4)	73.6 (66.3, 84.2)	-0.002 [-0.00, -0.00]	0.001

Median EAOA in A+ (Q1, Q3)	silaR	SILA Matlab	Median Difference (Matlab – R; [95% CI])	Wilcoxon p
Simulated Data	67.4 (63.4, 72.2)	67.6 (63.2, 71.8)	0.20 [0.01, 0.40]	0.04
ADNI	67.0 (60.7, 73.1)	67.4 (60.8, 74.2)	-0.16 [-0.29, -0.04]	< 0.001
OASIS	66.3 (60.6, 71.2)	66.4 (60.9, 71.3)	0.02 [-0.03, -0.01]	< 0.001
WISC	63.0 (56.8, 68.5)	62.8 (56.8, 68.1)	0.09 [-0.03, 0.22]	0.14

Figure 3: Differences between midpoint estimated amyloid onset age (EAOA) and software-predicted EAOA in observed A- to A+ converters (left). Median EAOA by software and median difference with 95% Hodges-Lehmann CIs shown from paired Wilcoxon signed rank test results both in full cohorts and restricted to those only A+ (right; rounded to the nearest hundredths).

Keywords: Amyloid PET, Alzheimer's Disease, Amyloid Onset Age (EAOA), SILA, Temporal Modeling

71 Agreement between amyloid status prediction from visual read, SUVR thresholding, and AI-based interpretation of amyloid PET

Luis Peraza[1], Richard Joules[1], Richard Mohs[2], Douglas Beauregard[2], John Dwyer[2], Lynne Hughes[2], Robin Wolz[1]

[1]*IXICO, London, UK*
[2]*The Global Alzheimer's Platform, Washington, DC, US*

Visual read remains the gold standard for assessing amyloid status in positron emission tomography (PET) imaging. However, variability in reader interpretation, particularly in scans near the boundary between amyloid-negative and -positive states, can introduce uncertainty. Quantitative approaches such as the standardized uptake value ratio (SUVR) have been proposed to complement visual interpretation, and recent regulatory guidance has encouraged the integration of quantitative metrics to support reader confidence. The centiloid framework has additionally been used as a banded rather than single-value thresholds to better capture ambiguous levels of tracer uptake (Collij;Alzh&Dem;2024). SUVR-based quantification, typically derived from large cortical regions, may overlook subtle, spatially heterogeneous uptake patterns that human readers intuitively recognize.

Here, we evaluated the agreement between visual reads, SUVR thresholding, and an artificial intelligence (AI)–based classifier trained to predict amyloid status from PET scans using the BioHermes (Mohs;Alzh&Dem;2024) dataset (n=833; Florbetapir tracer). A deep learning Siamese network was trained, in a cross-validated manner, using contrastive loss on amyloid-positive and -negative image pairs to learn a latent representation sensitive to amyloid burden. Within each fold, latent vectors were then used as input features to a CatBoost classifier trained to predict visual read labels on the held-out test data. Amyloid SUVRs were computed using MIM Software, with positivity defined as SUVR > 1.12.

Both SUVR (Accuracy:0.92, F1:0.89, Sensitivity:0.93, Specificity:0.92) and the AI-based approach (Accuracy:0.92, F1:0.90, Sensitivity:0.89, Specificity:0.95) demonstrated strong agreement with visual reads. Notably, the methods misclassified different subsets of cases (Fig 1), suggesting that SUVR and AI may capture complementary aspects of amyloid uptake patterns.

Limitations include the use of a single dataset and tracer; on-going work will assess generalizability across independent cohorts and additional tracers and investigate integration of AI-derived metrics with quantitative SUVR as support to visual interpretation.

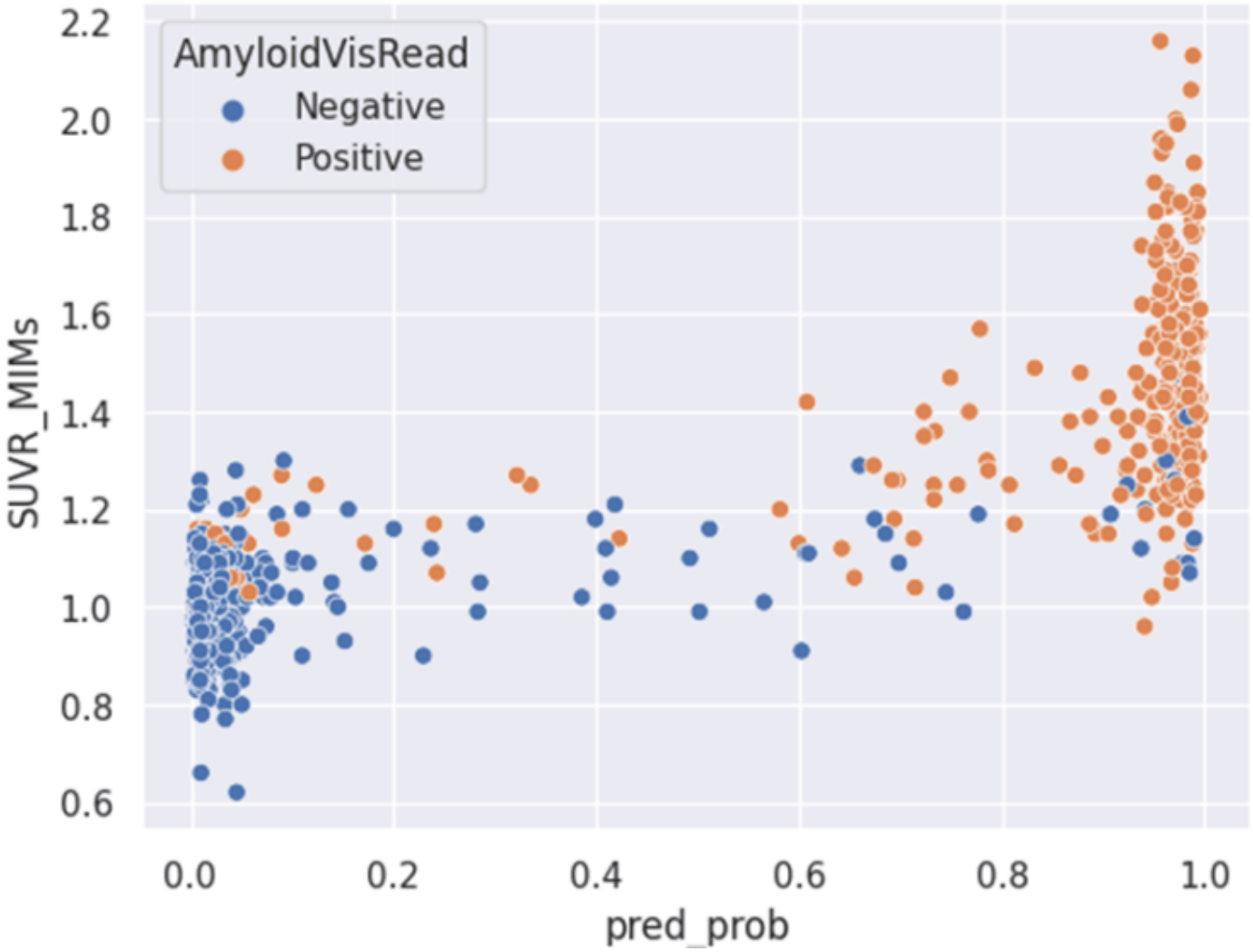


Figure 1 - SUVR compared to predictive probabilities of Amyloid abnormality

Keywords: Amyloid PET; visual read; AI; SUVR

72 CenTauR thresholds generated using Gaussian Mixture Models for biological staging of amyloid positive ADNI participants

Alexander DelBene[1], Victor Villemagne[2], Alexandra Gogola[1], Antoine Leuzy[3,4], Tessa Harrison[5], Susan Landau[5], William Jagust[5], Brian Lopresti[1]

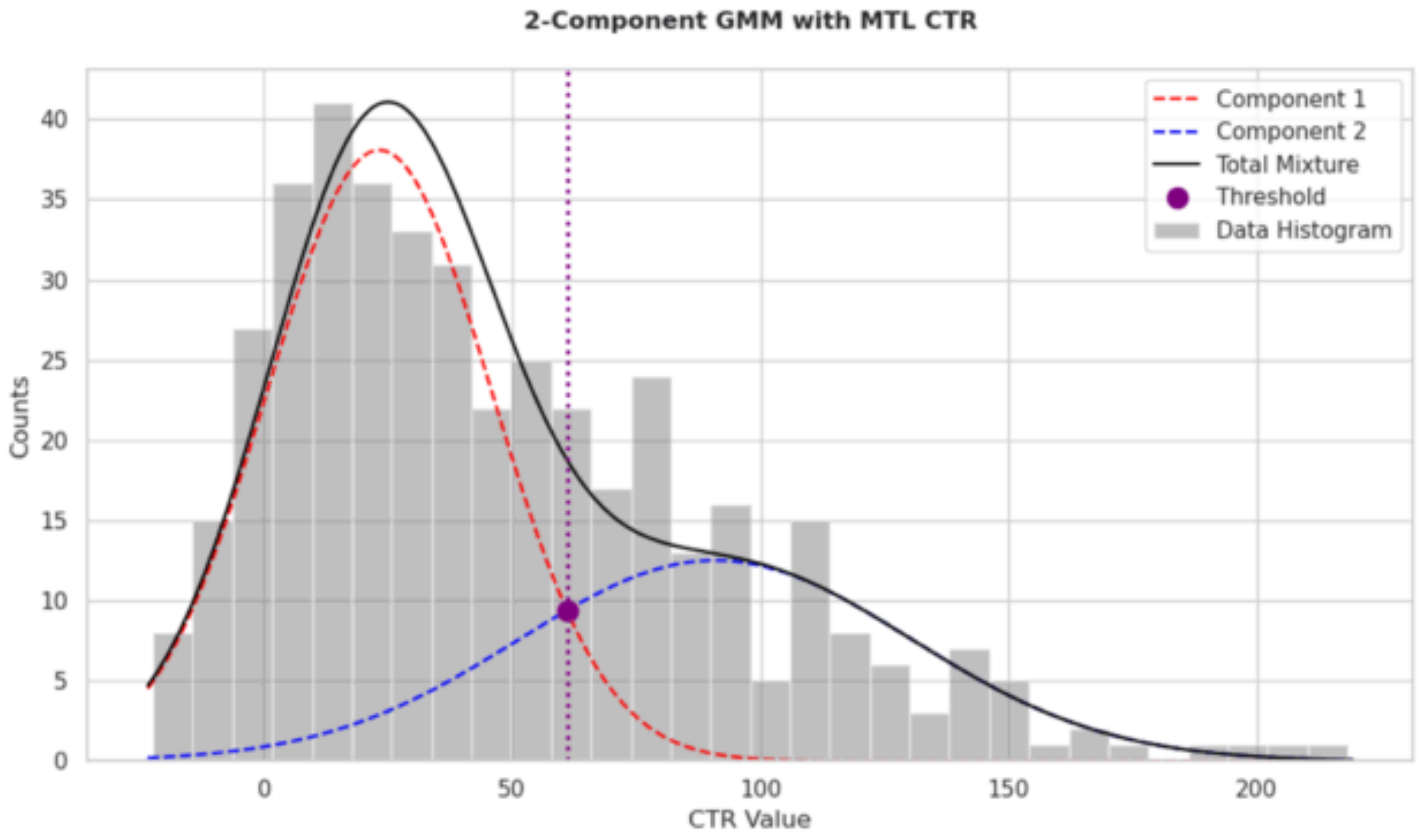
[1]*Department of Radiology, University of Pittsburgh School of Medicine, Pittsburgh, PA, US*
[2]*Department of Psychiatry, University of Pittsburgh School of Medicine, Pittsburgh, PA, US*
[3]*Critical Path for Alzheimer's Disease (CPAD) Consortium, Critical Path Institute, Tucson, AZ, US*
[4]*Enigma Biomedical Group, Knoxville, TN, US*
[5]*Department of Neuroscience, University of California, Berkeley, Berkeley, CA, US*

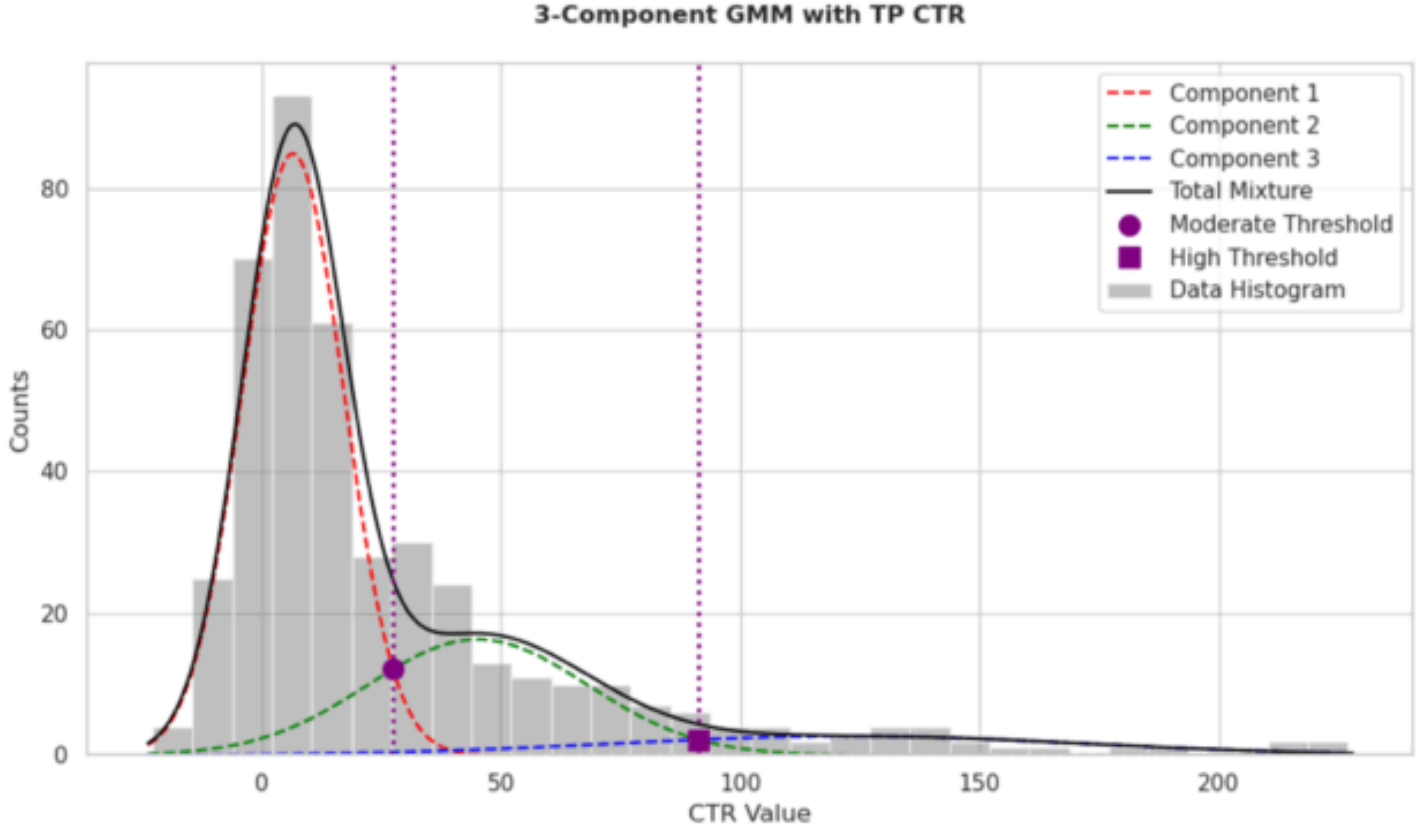
Background: The Alzheimer's Association Workgroup recently proposed a framework for the biomarker-based staging of Alzheimer's disease (AD) using Aβ (A) and tau (T) positron emission tomography (PET). Stage-specific thresholds have been recently defined using CenTauRz (CTRz) but not using the newly available CenTauR (CTR) units. Gaussian mixture models (GMM) were run on a cohort of Alzheimer's Disease Neuroimaging Initiative (ADNI) participants with available Aβ and [18F] flortaucipir (FTP) tau PET to establish stage specific thresholds using CTR.

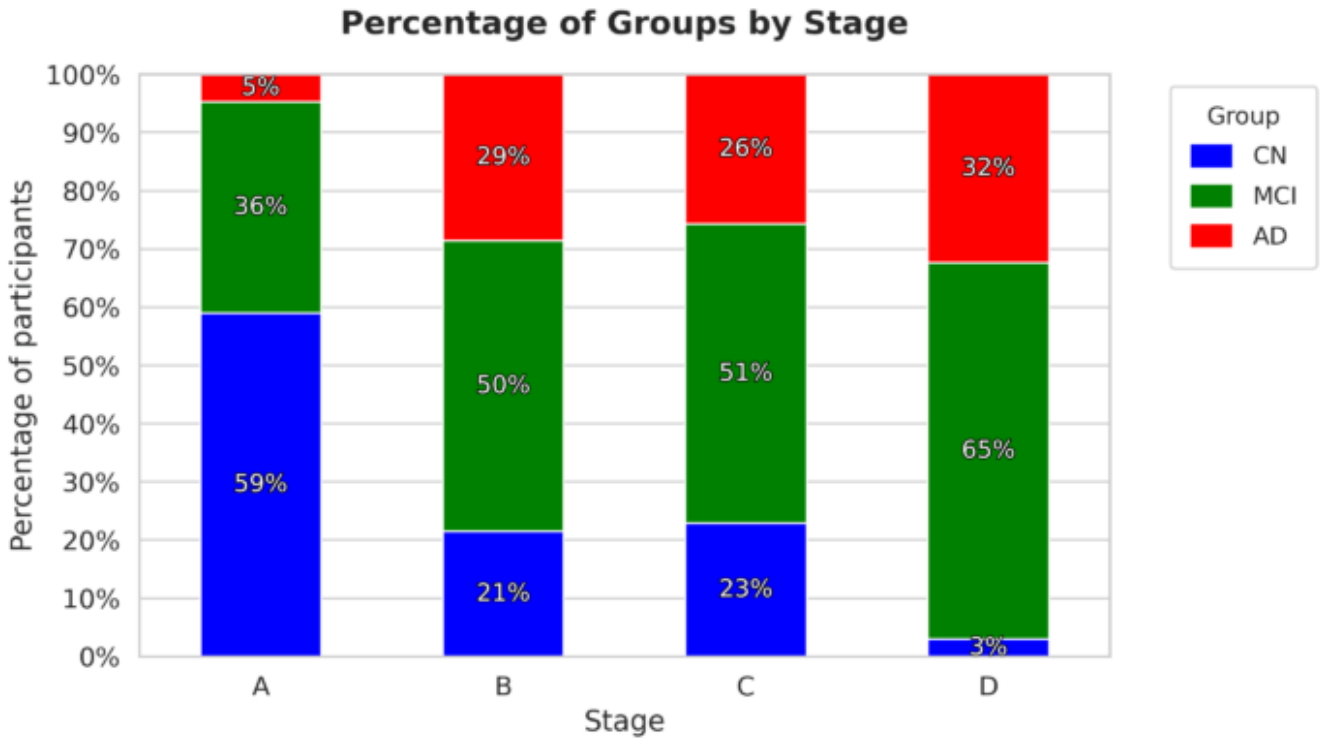
Methods: 423 ADNI participants (75.3±7.9 years, 54% female) with A+ PET and FTP PET imaging were analyzed using the SPM12-based CTR pipeline. SUVR outcomes were converted to CTR using Joint Propagation Model-derived conversion equations. Two and three component GMMs were run on Mesial temporal (MTL) and Temporoparietal (TP) CTR to generate thresholds separating tau pathology into 4 stages (A-D). The number of components included in the models were based on the minimum Bayesian information criterion (BIC). The intersections of Gaussians were used as the threshold between stages and compared to CTRz.

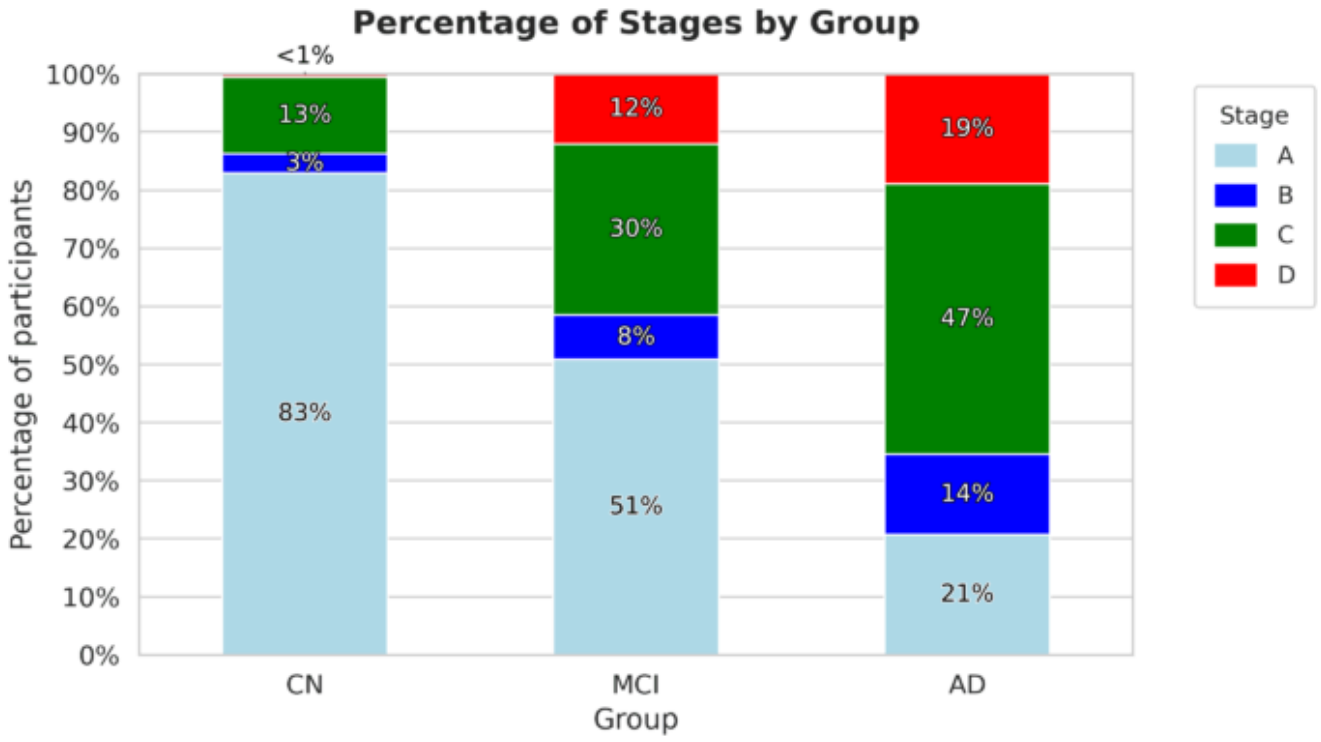
Results: The derived thresholds were as follows: Mesial temporal (61CTR/3.9CTRz/1.65SUVR), moderate TP (28CTR/2.8CTRz/1.47SUVR), high TP (91CTR/9.4CTRz/2.10SUVR). Gaussians with the points of intersection used to determine the thresholds can be found in Figure 1. A total of 83% of CU participants were classified as stage A (A+/MTL-/TP-) and 66% of AD participants were classified as stage C/D (A+/moderate-TP+; A+/high-TP+, respectively). Findings were similar to previously reported distributions of diagnoses across stages. Figures 2 and 3 show stacked bar charts that illustrate the distribution of diagnoses across stages and stages within diagnoses.

Conclusion: Thresholds identified in this work provide a potential framework for CTR-based tau staging and align with previous reports. Future work will refine CTR thresholds using multiple cohorts and multiple tau tracers to determine the generalizability of these findings.


2-Component GMM with MTL CTR
Component 1
Component 2
Total Mixture
Threshold
Data Histogram
Counts
CTR Value
0
5
10
15
20
25
30
35
40
0
50
100
150
200


3-Component GMM with TP CTR
Component 1
Component 2
Component 3
Total Mixture
Moderate Threshold
High Threshold
Data Histogram
Counts
CTR Value
0
20
40
60
80
0
50
100
150
200





Keywords: CenTauR, thresholds, PET

73 Progression to tau-PET positivity by plasma P-tau217 levels and its association with clinical decline in preclinical Alzheimer's disease: data from A4 study

Min Jung Kim[1], Vikas Kotari[1], Amanda Morris[1], Sergey Shcherbinin[1], Roy Yaari[1], Karen Holdridge[1], John Sims[1], Rik Ossenkoppele[1], Emily Collins[1], Oskar Hansson[1], Ming Lu[1]

[1]*Eli Lilly and Company, Indianapolis, IN, US*

Background: Plasma P-tau217 correlates with beta-amyloid and other tau pathologies and may mediate the association between beta-amyloid plaques and tau tangles. Elevated plasma P-tau217 is associated with a high risk of cognitive decline among cognitively unimpaired individuals. This study evaluated how plasma P-tau217 levels influence the risk of progression to tau-PET positivity and subsequent cognitive worsening in a cognitively unimpaired amyloid-PET positive/tau-PET negative population.

Methods: Tau-PET (flortaucipir F 18) positivity was defined as SUVR greater than 2.5 SD above mean values, from a young-cognitively-normal cohort. Participants were stratified as having "high" and "low" P-tau217 levels based on median baseline values measured by a Lilly-developed P-tau217 assay. Kaplan-Meier and Cox-proportional-hazards analyses were applied to estimate time, and hazard for converting to tau-PET positivity. Natural cubic spline model was used to assess longitudinal changes in Preclinical Alzheimer Cognitive Composite score in participants who converted to tau-PET positivity, with the conversion time set as zero.

Results: Of the amyloid-PET positive participants enrolled in the A4 tau-PET substudy (NCT02008357), 238 (70.0%) and 251 (73.8%) were tau-PET negative in the medial temporal lobe (MTL) and inferior temporal gyrus (ITG), respectively. Restricted mean time to MTL and ITG positivity in the low P-tau217 group were 4.7 and 4.8 years, and in the high P-tau217 group 4.0 and 4.3 years, respectively. The hazard ratios were 2.1 and 1.6 for MTL and ITG conversion respectively when comparing P-tau217 high vs. low levels. High P-tau217 showed a greater risk of clinical worsening when compared to low group (LS means at 3.5 years: -2.16 vs. 0.16 for MTL converters, -8.30 vs. -3.79 for ITG converters, $p<0.035$).

Conclusion: Amyloid-PET positive cognitively unimpaired participants are found to convert to MTL/ITG tau-PET positivity within 5 years and demonstrate faster cognitive decline after the conversion, particularly among those with higher baseline P-tau217 levels.

Table 1.

	MTL Tau PET status		ITG Tau PET status	
	Converted to T+ (N=70)	**Not Converted (N=168)**	**Converted to T+ (N=81)**	**Not Converted (N=170)**
Age (yr)				
Mean (SD)	72.1 (5.0)	71.5 (4.6)	72.8 (4.7)	71.5 (4.6)
Median [Min, Max]	70.9 [65.3, 84.7]	70.8 [65.0, 85.3]	72.4 [65.0, 84.7]	70.9 [65.0, 85.3]
Sex				
F	41 (58.6%)	93 (55.4%)	50 (61.7%)	95 (55.9%)
M	29 (41.4%)	75 (44.6%)	31 (38.3%)	75 (44.1%)
Race				
Black	1 (1.4%)	3 (1.8%)	0 (0%)	4 (2.4%)
White	65 (92.9%)	155 (92.3%)	74 (91.4%)	151 (88.8%)
Asian	3 (4.3%)	9 (5.4%)	5 (6.2%)	13 (7.6%)
Other	1 (1.4%)	1 (0.6%)	2 (2.5%)	2 (1.2%)
Ethnicity				
Hispanic or Latino	2 (2.9%)	3 (1.8%)	2 (2.5%)	3 (1.8%)
Not Hispanic or Latino	68 (97.1%)	161 (95.8%)	78 (96.3%)	163 (95.9%)
Missing	0 (0%)	4 (2.4%)	1 (1.2%)	4 (2.4%)
ApoE4 Status				
Carrier	46 (65.7%)	80 (47.6%)	50 (61.7%)	83 (48.8%)
Non-carrier	24 (34.3%)	88 (52.4%)	31 (38.3%)	87 (51.2%)
MMSE Score				
Mean (SD)	28.6 (1.2)	28.8 (1.2)	28.4 (1.4)	28.8 (1.2)
Median [Min, Max]	29.0 [24.0, 30.0]	29.0 [25.0, 30.0]	29.0 [24.0, 30.0]	29.0 [25.0, 30.0]
Centiloid				
Mean (SD)	65.2 (29.9)	54.2 (26.1)	74.5 (32.4)	52.1 (23.2)
Median [Min, Max]	62.6 [0.3, 134.0]	51.6 [0.3, 130.3]	71.7 [5.8, 159.6]	47.9 [0.3, 124.8]
Plasma P-tau217				
Mean (SD)	0.28 (0.14)	0.22 (0.10)	0.30 (0.16)	0.23 (0.11)
Median [Min, Max]	0.24 [0.11, 0.77]	0.20 [0.09, 0.72]	0.25 [0.13, 0.82]	0.20 [0.09, 0.81]
Missing	4	14	2	11

Participants from A4 study with amyloid positivity confirmed by PET, following the study enrollment criteria

Figure 1.

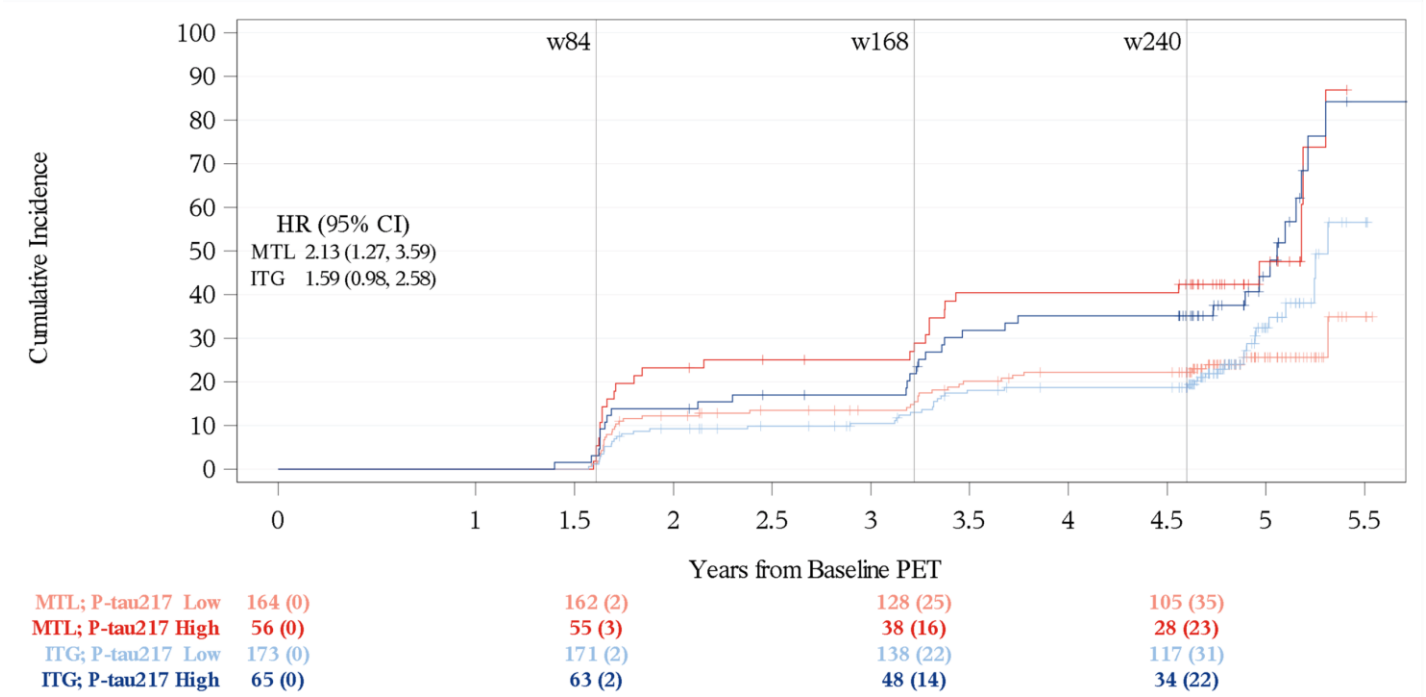
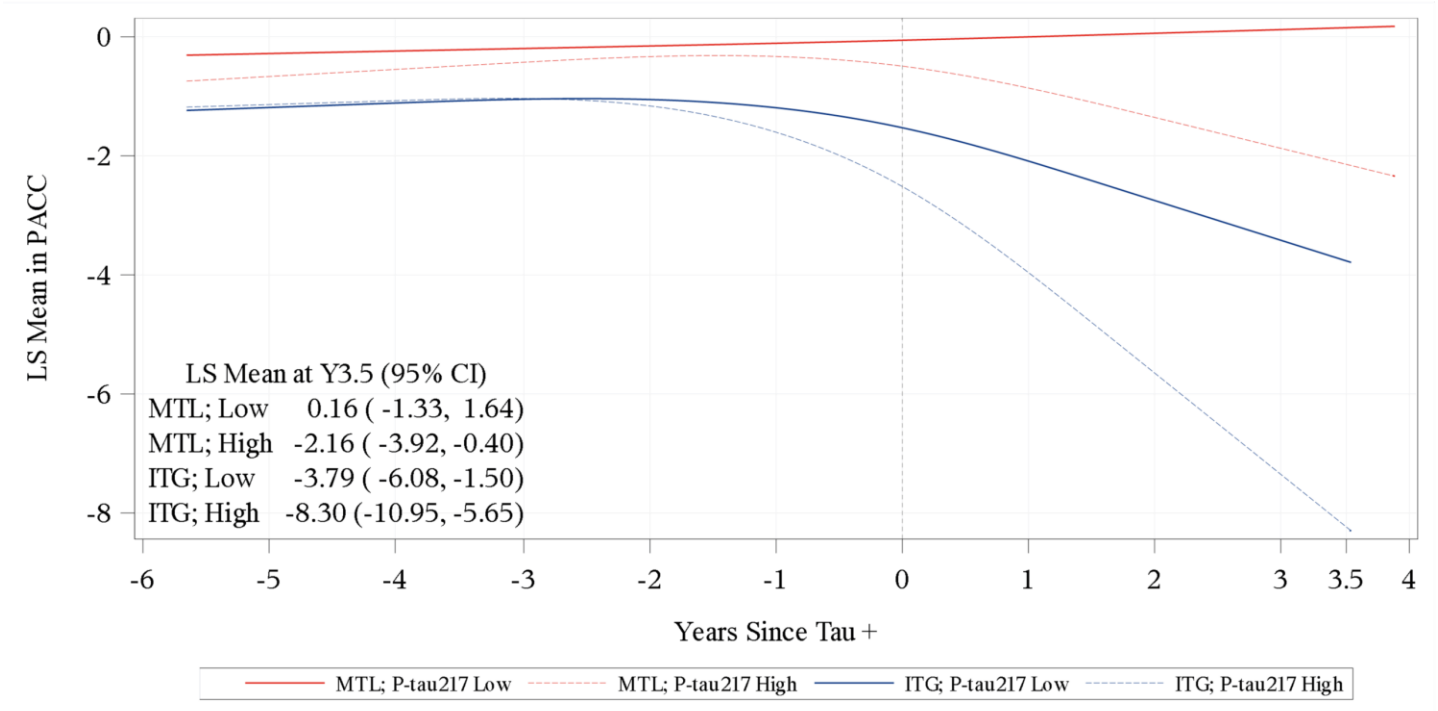


Figure 2.



Keywords: tau-PET, plasma P-tau217, time to tau-PET positivity, cognitive decline

74 Neuroimaging correlates of loneliness

Thairi Sanchez[1], Diana Guzman[1], Anna Smith[1], Hannah Houlihan[1], Yakov Stern[1], Walter Bockting[1], Patrick Lao[1]

[1]*Columbia University Irving Medical Center, New York, NY, US*

Introduction: Loneliness is an increasingly prevalent psychosocial risk factor for dementia that may become biological through chronic stress, inflammation, and vascular disease. We sought to take a biopsychosocial approach to characterize the neuroimaging correlates of loneliness.

Methods: At Columbia Alzheimer's Disease Center case consensus, participants were categorized as cognitively unimpaired (n=14) or as having Alzheimer's disease or related dementias (n=28). Participants (71±7 years old, 67% women) underwent TSPO (ER176), amyloid (Florbetaben), and tau (MK6240) PET as well as volumetric T1 MRI neuroimaging. Loneliness was assessed using the modified DeJong-Gierveld (i.e., emotional loneliness, not social isolation), while depressive symptoms measured by the modified CESD-9 (i.e., removing the "I feel lonely" question). We tested for regional biomarker associations with loneliness, adjusting for depressive symptoms, age, sex, body mass index, diagnosis, and TSPO affinity.

Results: Loneliness was not associated with amyloid, but greater loneliness was associated with lower tau in the brainstem (β=-0.35, p=0.046). Greater loneliness was associated with greater TSPO SUVR in the posterior corpus callosum (β=0.35, p=0.020), rostral middle frontal gyrus (β=0.54, p=0.020), insula (β=0.57, p=0.021), cerebellum (β=0.41, p=0.022), superior frontal gyrus (β=0.50, p=0.022), lateral orbitofrontal gyrus (β=0.56, p=0.038), medial orbitofrontal gyrus (β=0.51, p=0.045), pars opercularis (β=0.47, p=0.047), and middle temporal gyrus (β=0.50, p=0.047). Greater loneliness was also associated with lower volume in posterior corpus callosum (β=-0.44, p=0.012), anterior corpus callosum (β=-0.37, p=0.041), and medial orbitofrontal gyrus (β=-0.23, p=0.045).

Discussion: Loneliness, one component of social connectedness, was not associated directly with AD pathology, but was associated with neuroinflammatory and neurodegenerative measures in key regions. The insula, prefrontal cortex, and cerebellum have been implicated in social, cognitive, and affective processes. Future longitudinal work with additional measures of social connectedness (e.g., social support) can provide additional insight into the mechanisms by which loneliness is associated with greater risk for dementia.

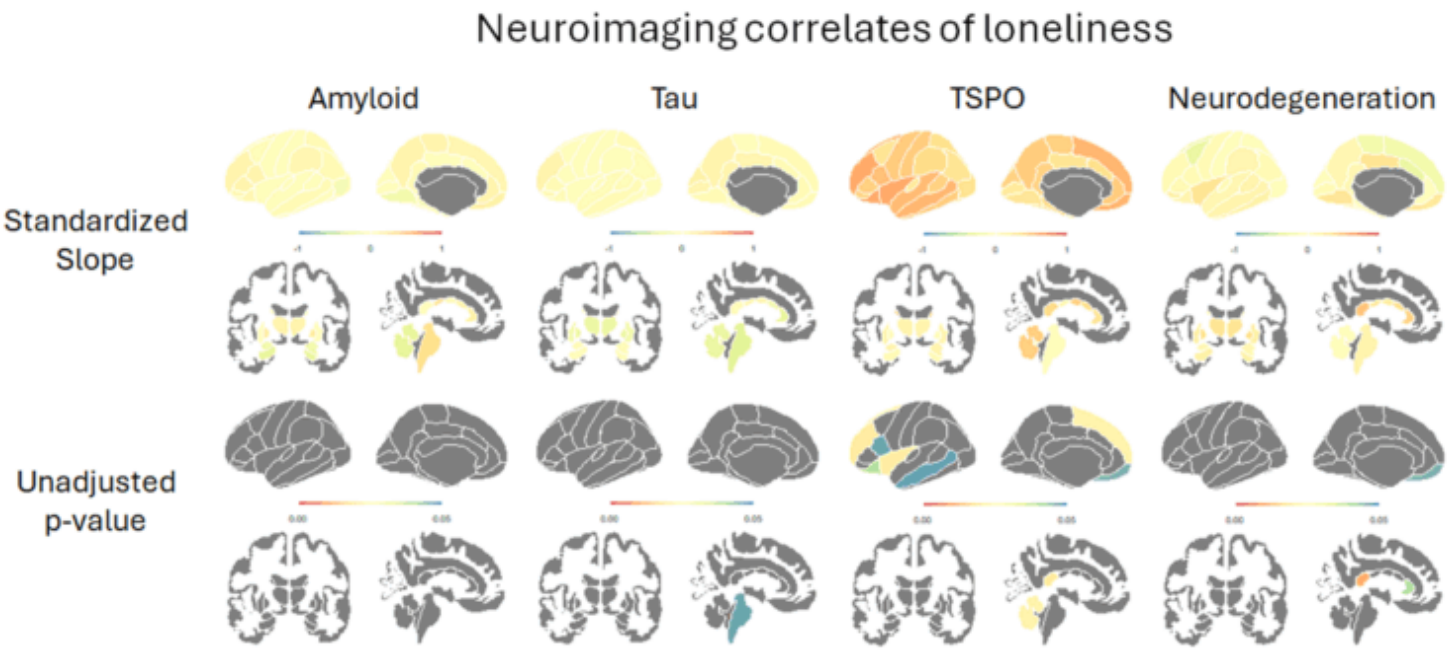


Figure 1. Neuroimaging correlates of loneliness. Note, volume was inverted so hotter colors represent greater loneliness was associated with greater neurodegeneration.

Keywords: loneliness, TSPO, amyloid, tau, neurodegeneration

75 Age-dependent associations between salivary inflammatory cytokines and amyloid-beta in cognitively unimpaired older adults

Dana Parker[1], Whitney Tang[1], Lisa Taylor[1], Jason Bock[1], Novelle Meza[1], Nandita Tuteja[1], Brenda Avila[1], Evelyn Chang[1], Scotty Simmons[1], Alison Bamford[2], Emily Yi[1], Liv Mcmillan[1], Soyun Kim[1], Elizabeth Thomas[2], Jenna Adams[1], Michael Yassa[1]

[1]*Department of Neurobiology and Behavior, University of California Irvine, Irvine, CA, US*
[2]*Institute for Interdisciplinary Salivary Bioscience Research, University of California Irvine, Irvine, CA, US*

Introduction: Alzheimer's disease (AD) is characterized by amyloid-beta (Aβ) accumulation and neuroinflammation, both of which have been linked to cognitive decline. While CSF and plasma studies link Aβ burden to inflammation in healthy agers, little is known about salivary cytokines and their relationship to regional amyloid deposition. Saliva provides a non-invasive window into systemic immune responses, examining its association with Aβ may reveal mechanisms linking amyloid pathology, immune activity, and aging, as well as identify accessible biomarkers for early detection.

Methods: We analyzed 80 cognitively unimpaired (CU) adults (mean age 69, std 8.6, 65% female) from the BEACoN study. We quantified Aβ using 18F-florbetapir-PET (FBP) and calculated global Aβ SUVR, and regional Aβ SUVR in early, intermediate and late accumulating regions **(fig 1A)**. Salivary inflammatory markers were quantified using saliva-optimized immunoassays and log-transformed before analysis. FDR-adjusted linear regression models were fit for each cytokine, with sex and age included.

Results: We observed significant associations between FBP SUVR and multiple saliva inflammatory markers across early, intermediate, and late accumulating regions, as well as global FBP SUVR. For early FBP regions, the main effects of IFN-**γ**, IL-13, IL-1β, IL-8, and TNF- were all significant after FDR correction ($pFDR < 0.05$), with significant marker × age interactions indicating that these relationships changed with age **(fig 1B-E)**. Similar patterns were observed in intermediate and late FBP regions as well as the overall composite SUVR, with IFN-**γ**, IL-13, IL-1β, and IL-8 consistently showing significant main effects and interactions with age.

Discussion: Salivary inflammatory markers were significantly associated with regional and composite Aβ burden in cognitively unimpaired older adults, with these relationships changing in older age. These findings demonstrate that peripheral inflammation is associated with brain amyloid pathology, highlighting the role of salivary assays as potential non-invasive biomarkers for monitoring Alzheimer's pathology during the preclinical stage.

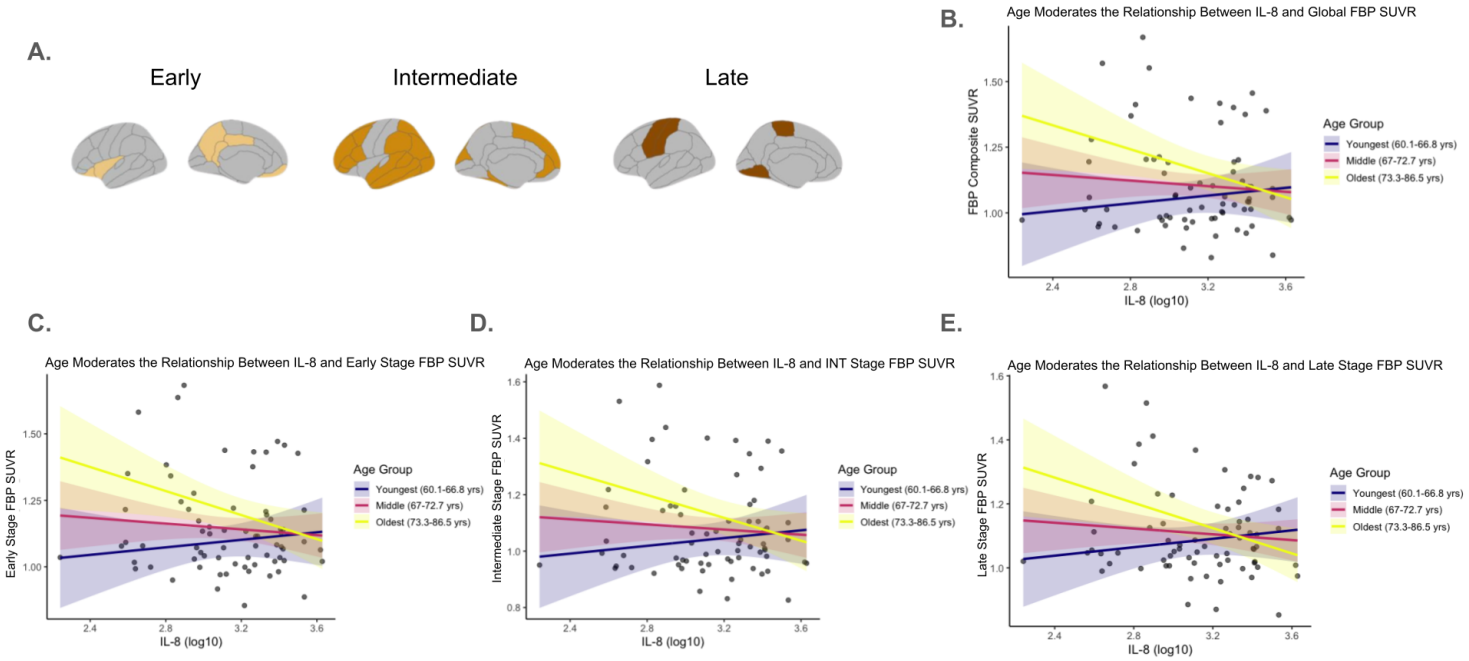


Figure 1. Composites of regions showing early, intermediate, and late Aβ accumulation are presented from left to right **(A)**. Linear regression analyses demonstrate that inflammatory IL-8 is positively associated with FBP SUVR across age. Specifically, global FBP SUVR shows a significant relationship with IL-8 (β = 2.06, p = 0.0097*) **(B)**, with similarly strong associations observed in early (β = 2.08, p = 0.0054*) **(C)**, intermediate (β = 2.08, p = 0.0111*) **(D)**, and late (β = 1.39, p = 0.0054*) **(E)** Aβ regions. All p-values were corrected for multiple comparisons using FDR. Abbreviations: Aβ = Amyloid Beta; FBP = 18F-florbetapir-PET; SUVR = Standardized Uptake Value Ratio; IL = Interleukin.

Keywords: Inflammation, PET, Amyloid-Beta

76 Tau accumulation drives worsening depressive symptoms in cognitively normal older adults

Teodora Markova[1], Anne Berry[2]

[1]*Brandeis University, Volen Center for Complex Systems, Waltham, MA, US*
[2]*Brandeis University, Department of Psychology, Waltham, MA, US*

Tau accumulation is related to subclinical depressive symptoms in aging and Alzheimer's disease (AD). Emerging late-life depressive symptoms are among the first AD-related changes to appear. There is a need to clarify the temporal relationships between affective and tau pathological changes in aging and AD to understand early disease pathophysiology. We leveraged longitudinal tau PET ([18F]Flortaucipir, subject-specific regions of interest) and Geriatric Depression Scale (GDS) data from the Alzheimer's Disease Neuroimaging Initiative. To establish probable causality between tau accumulation and depressive symptom trajectories, we applied three complementary analysis approaches.

First, in the cognitively normal sample, rates of tau accumulation moderated how quickly depressive symptoms increased over time (beta=0.08, p=.034), while GDS slopes did not moderate tau accumulation (beta=0.02, p=.102), suggesting that faster tau accumulation may contribute to accelerated worsening of depressive symptoms, but not vice-versa (**Figure 1**).

Next, we used continuous time structural equation modeling (*ctsem*, R) to test directionality and found that, in cognitively normal older adults, elevated tau predicted higher subsequent GDS (drift matrix fixed effects=1.012, 95% CI (0.020, 2.341) while variability in GDS did not predict later tau (drift matrix fixed effects=-0.101, 95% CI (-0.364, 0.133), **Figure 2**).

Finally, we tested the hypothesis that, if tau drives increasing depressive symptoms, the onset of tau positivity would be accompanied by a worsening of depressive trajectories. We found that, in cognitively normal older adults, GDS scores increased more rapidly after the onset of tau positivity relative to before (SILA-estimated time of tau positivity onset; beta=0.18, p=.035, **Figure 3**). No significant findings were observed in the MCI/AD sample. These findings support a model in which early tau-related disruptions in cognitively unimpaired older adults are a key driver of emerging depressive symptoms, while depressive symptoms exert little influence on tau at this stage.

Figure 1:

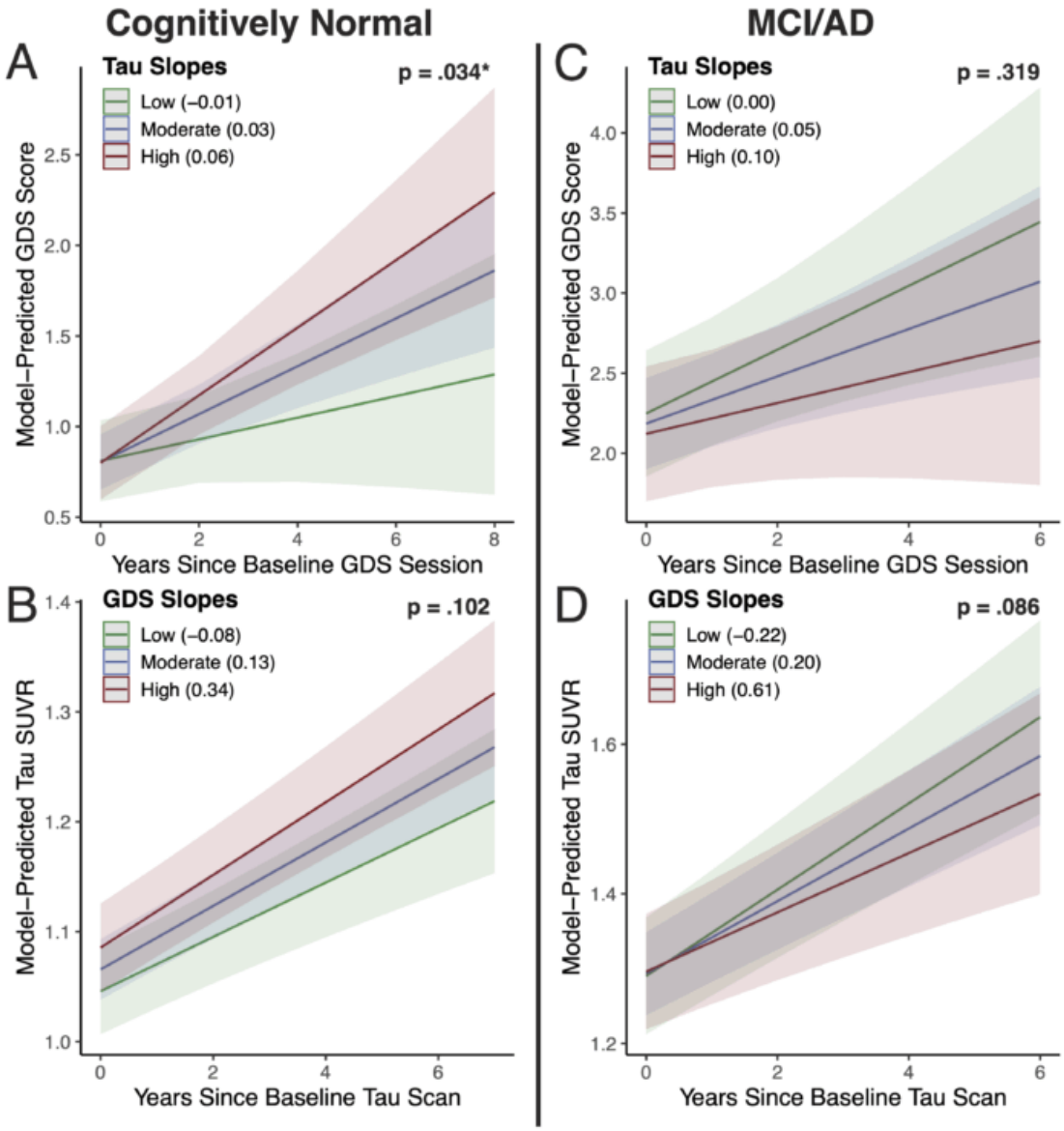


Figure 2:

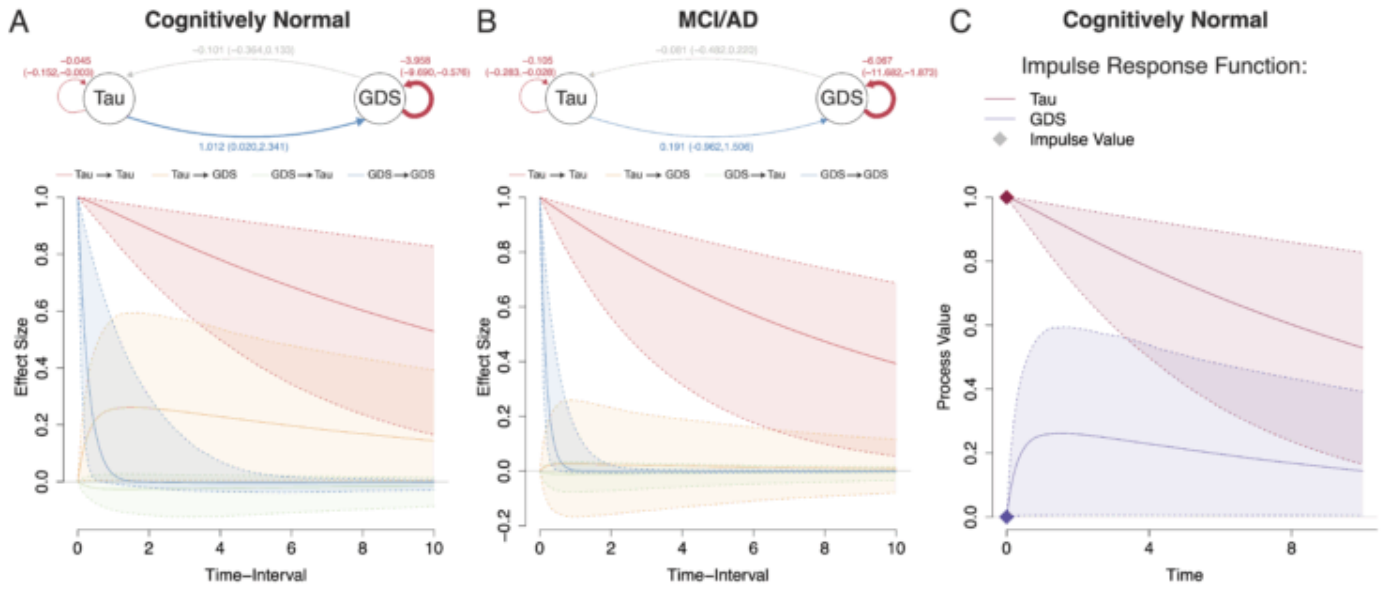
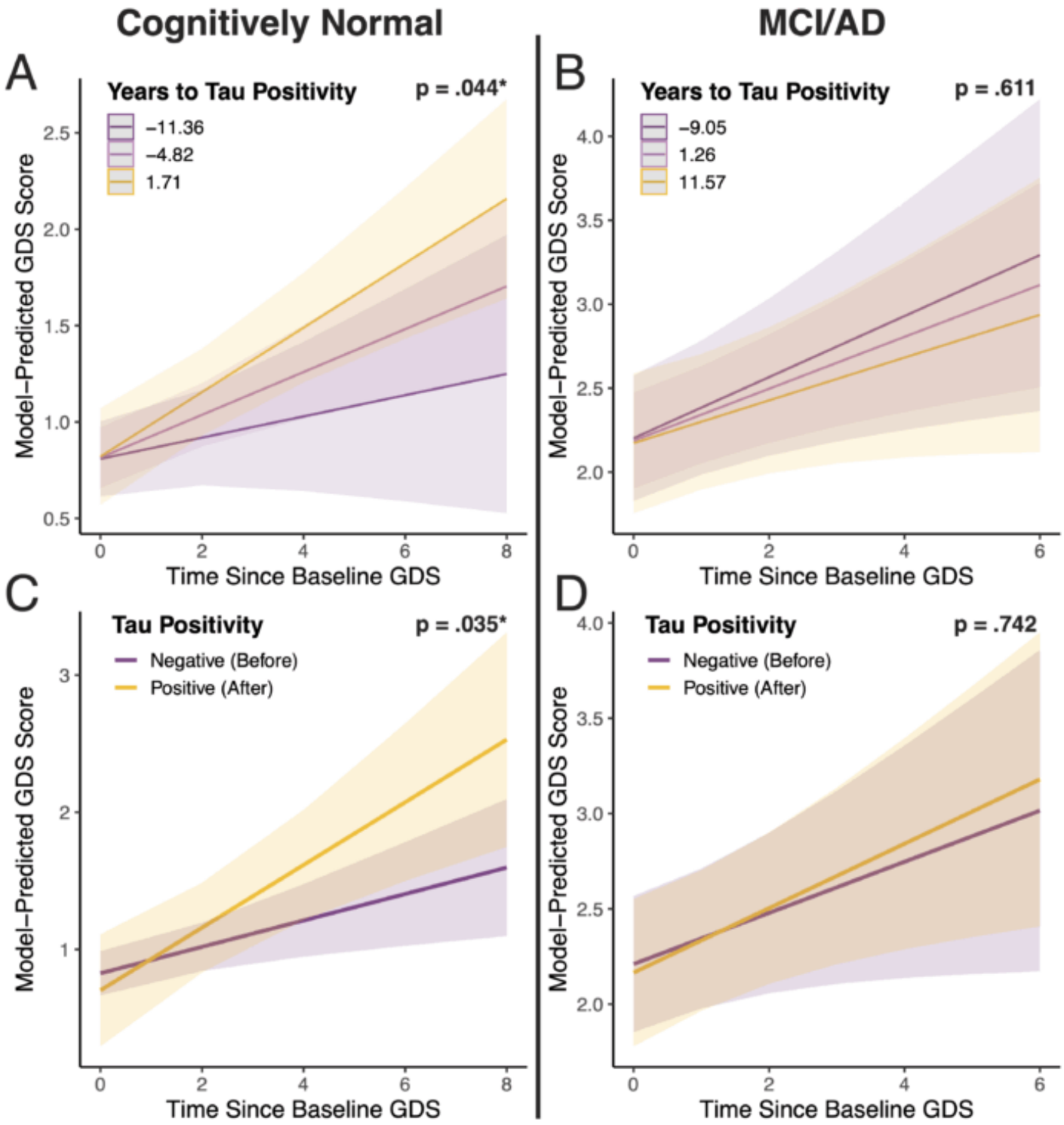


Figure 3:



Keywords: tau PET, depressive symptoms, temporal dynamics

77 Dorsal raphe nucleus and locus coeruleus differentially relate to depressive symptoms in cognitively normal older adults

Teodora Markova[1], Hsiang-Yu Chen[2], Emma Carlson[2], Patrick Cao[2,3], Claire Ciampa[1], Rachel Marcus[2], Alex Adornato[2], Johanna Matulonis[2], Thomas Morin[2,3], Jacob Hooker[3], Anne Berry[2]

[1]*Brandeis University, Volen Center for Complex Systems, Waltham, MA, US*
[2]*Brandeis University, Department of Psychology, Waltham, MA, US*
[3]*Massachusetts General Hospital, Martinos Center for Biomedical Imaging, Charlestown, MA, US*

The dorsal raphe nucleus (DRN) and locus coeruleus (LC) produce serotonin and norepinephrine, and are among the first regions to develop abnormal tau. Tau-related impacts on these two nuclei likely contribute to the early neuropsychiatric changes observed in pathological aging, though their distinct contributions remain unclear. Using [18F]Fluoro-meta-tyrosine (FMT) PET in a sample of cognitively normal older adults, we quantified monoamine synthesis capacity in both the DRN and LC. A partial least squares correlation analysis showed a marginal latent association (r=.32, p=.087, **Figure 1A**) between [18F]FMT net tracer influx (Ki) and a battery of affective assessments including the Geriatric Depression Scale (GDS), Mood and Anxiety Symptom Questionnaire, and Penn State Worry Questionnaire. Of the affective assessments, only GDS reliably contributed to the latent variable (bootstrap ratio=2.96, **Figure 1B**). Neither of the [18F]FMT indicators were significantly correlated with the affective assessments (LC r=-.17, p=.232; DRN r=.19, p=.175), though post-hoc simple linear regression focusing only on GDS (GDS ~ [18F]FMT * region) showed significant diverging relationships (t(107)=-2.24, p=.027). Higher LC [18F]FMT Ki was associated with lower depressive symptoms, while higher DRN [18F]FMT Ki was associated with higher depressive symptoms (**Figure 2**). Secondary sex-differences analyses found that these effects were present in females (t(60)=-2.09, p=.041) but not in males (t(43)=0.46, p=.647). These results mirror previous observations that higher LC structural and functional integrity predicts better affective outcomes. Our DRN results complement our prior work which established that DRN-monoamine synthesis capacity appears to be upregulated in aging, but that this age or disease-related elevation of DRN-monoamine synthesis capacity does not confer a behavioral benefit. Instead, elevated DRN [18F]FMT Ki may signal early affective dysfunction. By directly contrasting DRN and LC neuromodulator function within the same sample, we highlight system-specific individual differences that may differentially shape the emergence of depressive symptoms.

Figure 1:

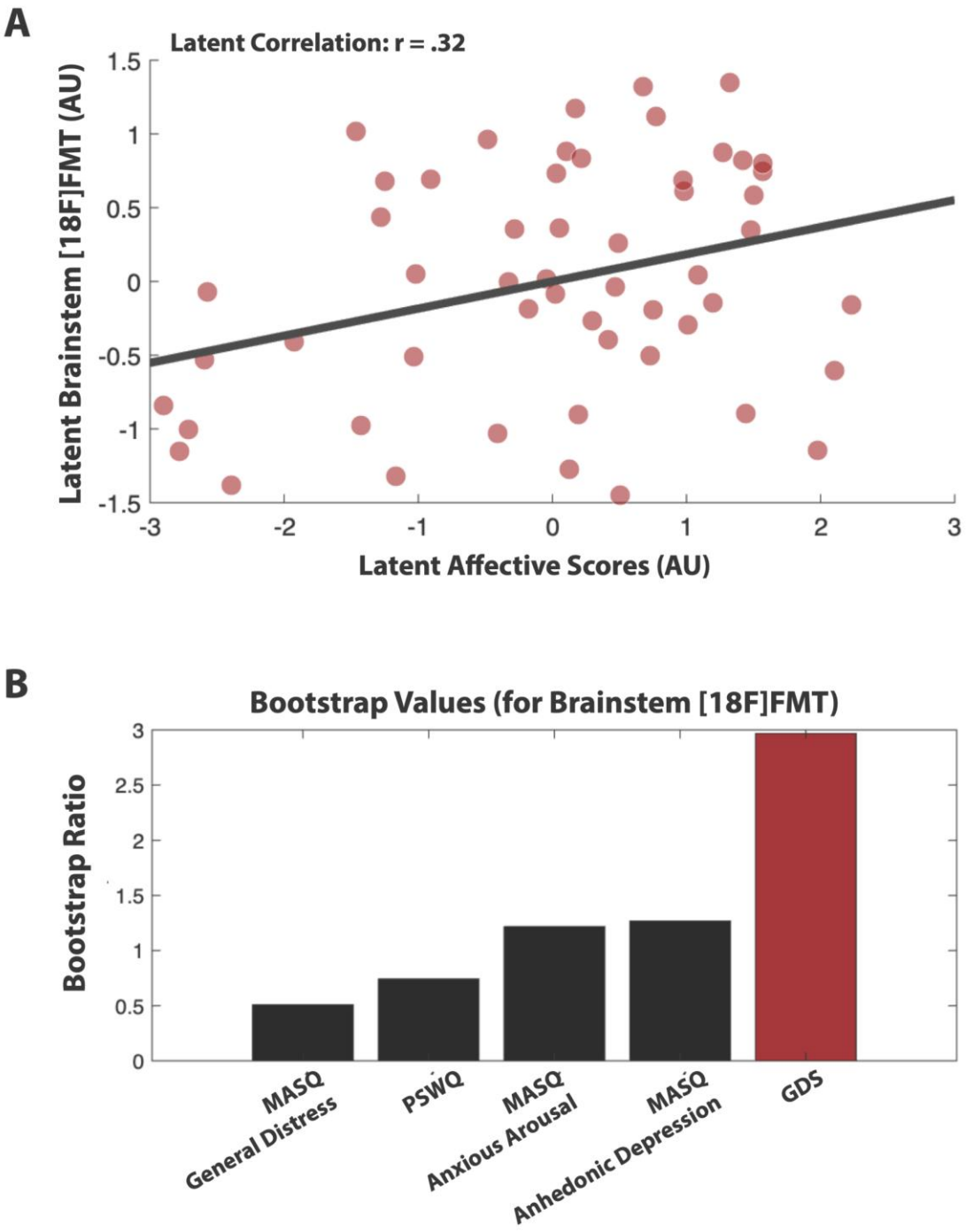
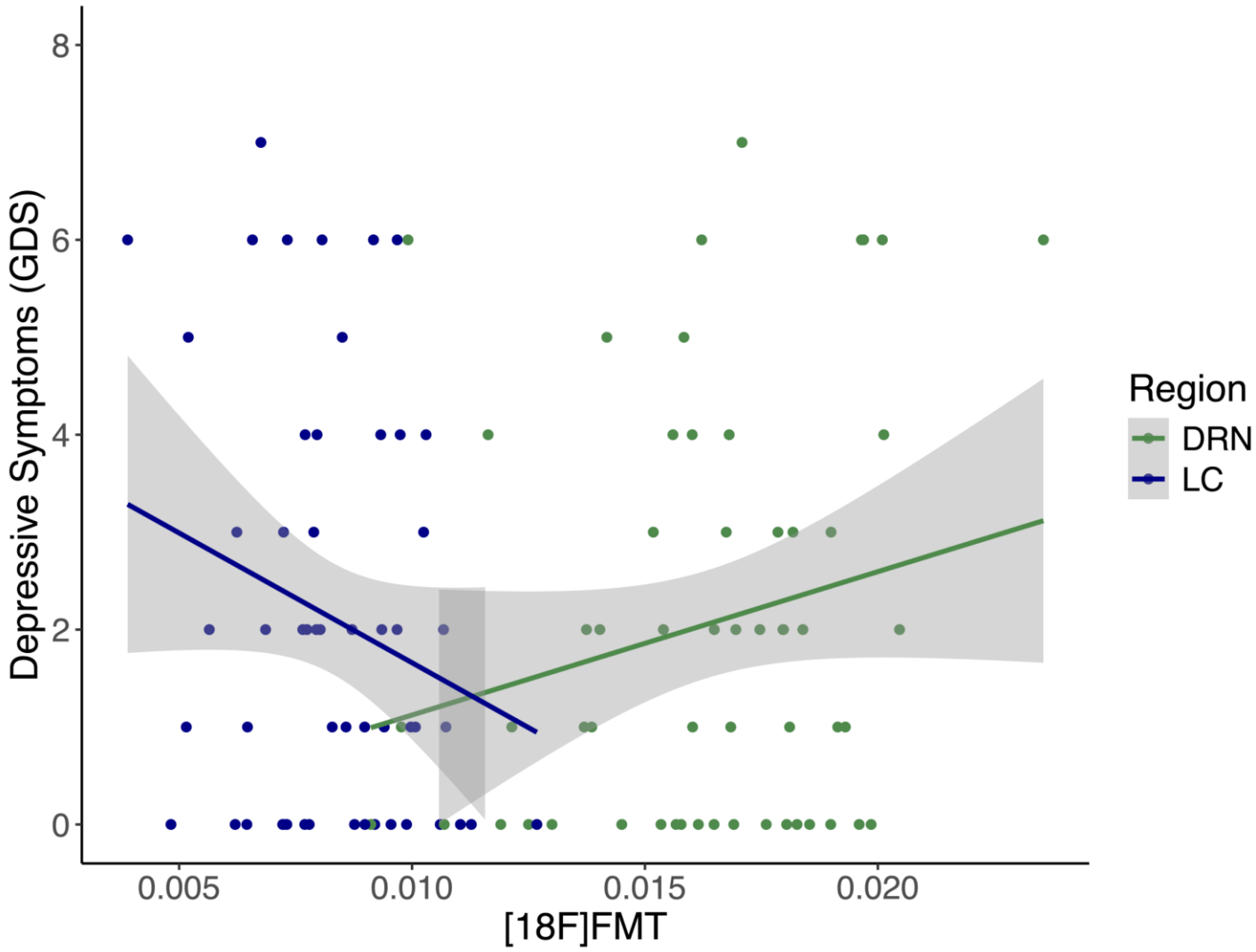

A
Latent Correlation: r = .32
Latent Brainstem [18F]FMT (AU)
Latent Affective Scores (AU)
1.5
1
0.5
0
-0.5
-1
-1.5
-3
-2
-1
0
1
2
3
B
Bootstrap Values (for Brainstem [18F]FMT)
Bootstrap Ratio
3
2.5
2
1.5
1
0.5
0
MASQ General Distress
PSWQ
MASQ Anxious Arousal
MASQ Anhedonic Depression
GDS

Figure 2:



Keywords: brainstem, neuromodulator systems, depressive symptoms

78 Evaluating occipital-to-global amyloid PET as a predictor of CAA at autopsy in Mayo Clinic cohorts

Christopher Schwarz[1], Mingzhao Hu[1], Petrice Cogswell[1], Jonathan Graff-Radford[1], Prashanthi Vemuri[1], Scott Przybelski[1], Heather Wiste[1], Aivi Nguyen[1], Ross Reichard[1], Dennis Dickson[2], Val Lowe[1], Vijay Ramanan[1], David Knopman[1], Ronald Petersen[1], Clifford Jack[1]

[1]*Mayo Clinic, Rochester, MN, US*
[2]*Mayo Clinic, Jacksonville, FL, US*

Aims: Previous works have proposed that individuals with a high ratio of occipital/global amyloid PET signal are more likely to have cerebral amyloid angiopathy (CAA) than AD at later autopsy. Higher relative occipital binding has also been recently proposed as a risk factor for ARIA-E from anti-amyloid therapeutics. We tested whether this PET ratio was associated with CAA in a large autopsy cohort from the Mayo Clinic Study of Aging (MCSA) and Mayo ADRC.

Methods: Participants (Table 1) were selected retrospectively by antemortem PIB PET and CAA measurements at later autopsy. CAA in both cortical and parenchymal areas was graded using H&E-stained sections from the frontal, parietal, temporal, occipital, and hippocampal regions using the Love criteria, later thresholded (>0) into CAA presence/absence. We measured PIB PET SUVR with our standard automated pipeline in L/R occipital lobar regions, and the standard "global" meta-region. We defined occipital ratio=max(occipital_left,occipital_right)/global, and a "high" ratio as >1.05. We performed likelihood ratio tests with logistic regression models for predicting CAA presence, controlling for age, sex, post-mortem interval (PMI), and APOE ε4 positivity, and weighting all observations by 1/PMI.

Results: Occipital ratio was associated with lower odds of CAA presence (Figure 1, p<.001), but this relationship (odds ratio=0.52) was attenuated (p=0.13) when controlling for listed covariates (Figure 2).

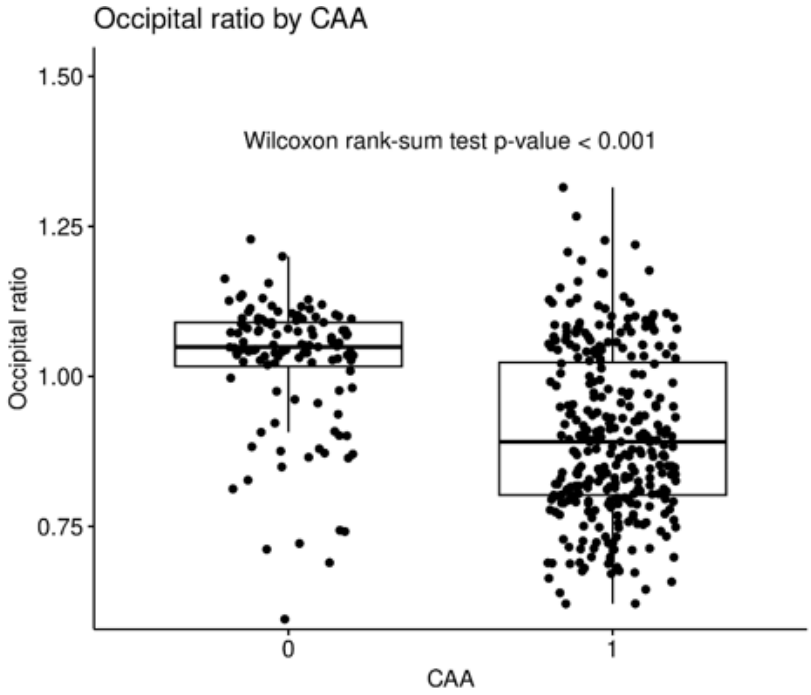
Conclusions: A higher predominance of occipital PIB signal was significantly associated with lower odds of CAA at autopsy, i.e. the opposite direction from that previously proposed, but only without covariates. CAA and global amyloid SUVR were highly associated in our sample (p<0.001), which may explain our different findings from other cohorts that considered CAA and AD as separate groups (even though CAA is present in most AD brains). Our findings do not support using this measure as a predictor of CAA without further research to understand these discrepancies.

Table 1: Demographics

Number of participants	n=435
Age at imaging, years	
Mean (SD) [Min,Max]	78 (10.59) [34, 98]
Sex	
M	n=254 (60.9%)
F	n=170 (39.1%)
Post-mortem interval, years	
Mean (SD) [Min,Max]	4.55 (3.21) [0.00, 15.30]
APOE ε4 carriers	n=185 (42%)
Amyloid PET (CL from PIB PET)	
Mean (SD) [Min,Max]	65.05 (52.46) [-15.00, 231.00]
>25 (A+)	n=276 (63.4%)
CAA burden (Love consensus criteria), n (%)	
0=absent	n=116 (26.7%)
1=scant	n=105 (24.1%)
2=moderate	n=145 (33.3%)
3=widespread	n=69 (15.9%)
Occipital ratio	
Mean (SD) [Min,Max]	0.93 (0.14) [0.60, 1.31]
>1.05	119 (27.3%)

CAA vs Occipital high
Fisher's exact test p-value < 0.001

	Occipital–	Occipital+
CAA–	60	58
CAA+	259	63



CAA vs Global amyloid (PIB+)
Fisher's exact test p-value < 0.001

	PIB–	PIB+
CAA–	86	30
CAA+	73	246

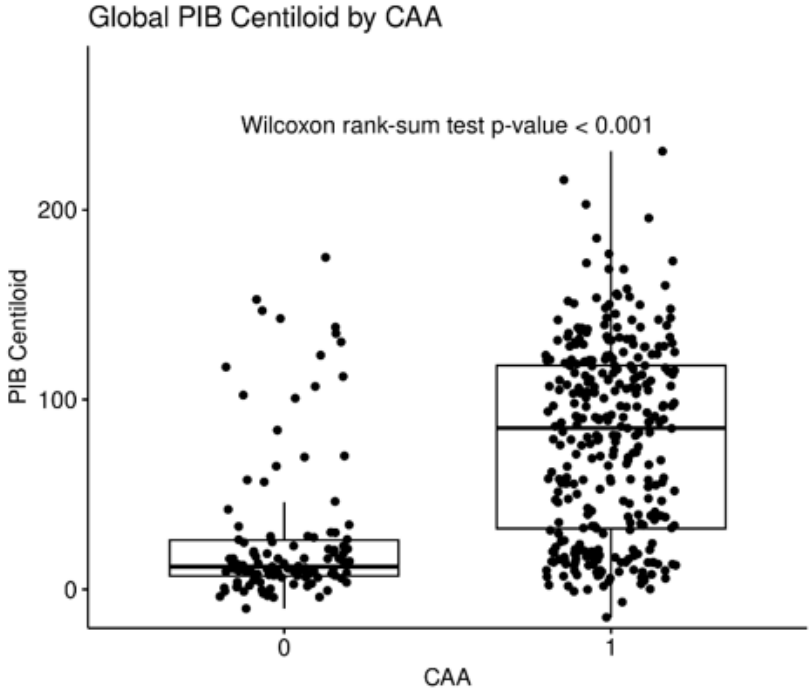


Figure 1: **Top left:** There was a significant (p<0.001) relationship between the groupings of occipital ratio > 1.05 and CAA+/-. **Top right:** There was a significant (p<0.001) relationship between (continuous) occipital ratio and CAA+/-, in the direction where a larger ratio was associated with less chance of CAA. **Bottom left:** There was a significant (p<0.001) relationship between the groupings of A+/- and CAA+/-, indicating that CAA and AD are not separable in this sample. **Bottom right:** There was a significant (p<0.001) relationship between PIB CL and CAA, with more amyloid associated with a larger chance of CAA, as expected.



Figure 2: We compared participants with occipital ratio >1.05 vs. ≤ 1.05 using a logistic regression model that included sex, APOE ε4 positivity, age, and postmortem interval (PMI), weighting each observation by 1/PMI. Occipital ratio > 1.05 had an estimated odds ratio of 0.52 (52% lower odds of CAA than ratio ≤ 1.05 cases), but this finding was not significant (p=0.13).

Keywords: PIB,CAA, cerebral amyloid angiopathy, amyloid

79 SCAN: Standardized Centralized Alzheimer's and related dementias Neuroimaging

Christopher Schwarz[1], Tessa Harrison[2], Charles DeCarli[3], Kejal Kantarci[1], Suzanne Baker[4], Renaud La Joie[5], Pauline Maillard[3], Gil Rabinovici[5], Arthur Toga[6], Clifford Jack[1], William Jagust[2]

[1]*Mayo Clinic, Rochester, MN, US*
[2]*University of California, Berkeley, Berkeley, CA, US*
[3]*University of California, Davis, Davis, CA, US*
[4]*Lawrence Berkeley National Lab, Berkeley, CA, US*
[5]*University of California, San Francisco, San Francisco, CA, US*
[6]*University of Southern California, Los Angeles, CA, US*

Aims: The Alzheimer's Disease Research Center (ADRC) program includes over 30 centers across the USA. The SCAN project (Standardized Centralized Alzheimer's and related dementias Neuroimaging) began in 2020 and standardizes methods for acquisition, quality control, and analysis of MRI and PET across the ADRC network. Collected images and analyses are shared via the National Alzheimer's Coordinating Center (NACC) and LONI, and they are linked with richly characterized, harmonized clinical, psychometric, fluid biomarker, genetic, and neuropathology data available at NACC.

Methods: SCAN includes an unusually high proportion of participants with atypical AD phenotypes (e.g. PCA, PPA, dysexecutive) and non-AD etiologies including FTLD, DLB, CBD, and vascular brain injury, and those with multiple etiologies. SCAN imaging methods are also identical to those in ADNI, CLARiTI, HEAD, US POINTER, MCSA, and others, facilitating meta-analyses across major public datasets.

Results: SCAN currently (September 2025) includes de-identified and de-faced imaging data from 6645 participants, including 7499 MRI exams from 5691 participants and 6249 PET exams (amyloid, tau, and FDG) from 3474 participants. Roughly 60% of SCAN participants are cognitively unimpaired, 20% have MCI, and 16% have dementia. 29% of the cognitively impaired individuals had a predominantly non-amnestic initial presentation, and 16% have suspected primarily vascular etiology. 74% of participants have longitudinal data from more than one visit. The median age is 72 years old, and 59% are female. Nearly 30% identify as ethnoracial groups typically underrepresented in the USA.

Conclusions: SCAN imaging data are available to all qualified researchers, providing images and standardized ATN imaging biomarkers for a richly characterized, highly heterogeneous group of cognitively unimpaired individuals, and those with AD, non-AD, and multiple dementia etiologies.

Keywords: dataset, open science, data sharing, ADRC, SCAN

80 Differential contributions of amyloid spatial extent and tau burden to domain-specific cognitive decline in early Alzheimer's disease

Elliott Slade[1], Emma Thibault[1], Jackson Thompson[1], Jessie Fanglu Fu[1,2], Julie Price[1,2], Dorene Rentz[1,3], Reisa Sperling[1,3], Keith Johnson[1,3], Michelle Farrell[1]

[1]*Massachusetts General Hospital, Harvard Medical School, Boston, MA, US*
[2]*Athinoula A. Martinos Center for Biomedical Imaging, Charlestown, MA, US*
[3]*Brigham and Women's Hospital, Harvard Medical School, Boston, MA, US*

Background: Amyloid-β (Aβ) accumulation and tau pathology jointly contribute to cognitive decline in Alzheimer's disease (AD), but their relative impact on different cognitive domains may shift across the course of preclinical AD. While tau is typically associated with memory decline later in amyloidosis, we hypothesized that executive decline may emerge earlier in amyloidosis in association with spreading Aβ.

Methods: We examined 248 cognitively-unimpaired older adults (Table1) from the Harvard Aging Brain Study (HABS) with at least one [^{11}C]Pittsburgh-Compound-B (PiB) and [^{18}F]Flortaucipir (FTP) PET scan and a median annual cognitive follow-up of 7.9±3.2 years. Aβ spatial extent (EXT%) was quantified as the proportion of the neocortex that is regionally PiB+. Linear mixed-effects models assessed longitudinal change in cognition on three domains (executive function, immediate memory, delayed memory; tests detailed in Table1) as a function of time, baseline EXT%, and baseline temporal tau burden. Additional analyses focused on participants with EXT<80% (n=200) to assess Aβ and tau effects in earlier stages of Aβ spread. Further analysis was performed on participants with 2+ Aβ and tau PET scans to examine the effect of concurrent changes in Aβ EXT and tau slope on cognition.

Results: The Time*EXT*Tau interaction was significant across domains (Figure1A), with maximum decline when both Aβ and tau are high (Figure2). Within the EXT<80%, greater temporal tau in the presence of high Aβ EXT predicted steeper decline in immediate memory ($p<0.01$) and a trend toward delayed memory ($p=0.079$) despite limited tau in this early cohort. Executive function decline was not related to tau but was significantly associated with greater Aβ EXT slope ($p<0.001$, Figure1C).

Conclusions: These results suggest a progressive shift in the mechanisms underlying cognitive decline across the course of amyloid spread in preclinical AD, with tau predominating in memory decline while spreading Aβ has early effects on executive function.

	EXT < 80% (n = 200)	EXT ≥ 80% (n = 48)	Overall (n = 248)
Age*, years, mean ± SD	72.07 ± 9.21	77.65 ± 6.22	73.15 ± 8.97
Sex, n female (%)	117 (58.5%)	28 (58.3%)	145 (58.5%)
Education, years, mean ± SD	16.02 ± 2.89	16.73 ± 2.59	16.16 ± 2.85
MMSE*, mean ± SD	29.22 ± 1.10	28.79 ± 1.24	29.14 ± 1.14
Executive function[1]**,** mean ± SD	0.02 ± 0.87	-0.10 ± 0.66	-0.00 ± 0.83
Immediate memory*[2]**,** mean ± SD	0.04 ± 0.38	-0.15 ± 0.45	0.00 ± 0.40
Delayed memory*[3]**,** mean ± SD	0.04 ± 0.42	-0.16 ± 0.48	0.00 ± 0.44
APOE*[4]**,** n e4+ (%)	40 (20.0%)	30 (62.5%)	70 (28.2%)
PiB FLR DVR*, mean ± SD	1.10 ± 0.07	1.57 ± 0.16	1.19 ± 0.21
Centiloids*, mean ± SD	11.74 ± 9.57	78.33 ± 22.96	24.62 ± 29.48
FTP temporal SUVR*, mean ± SD	1.15 ± 0.07	1.26 ± 0.13	1.17 ± 0.09
Cognitive follow-up length*, years, mean ± SD	7.64 ± 3.10	6.14 ± 3.52	7.35 ± 3.23
PiB-Tau Interval, days, mean ± SD	26.84 ± 91.63	24.04 ± 85.12	26.30 ± 90.25

Table 1. Baseline participant characteristics. Asterisks (*) indicate significant differences between EXT < 80% and EXT ≥ 80% groups, assessed using *t*-tests for continuous measures and χ^2 for categorical variables. The temporal SUVR aggregate includes the following regions: entorhinal cortex, parahippocampal gyrus, amygdala, inferior temporal lobe, middle temporal lobe, and fusiform. Cognitive domains were composited from standardized z-scores: Executive function (Digit Symbol Substitution Test, Trail Making Test B – A), Immediate memory (Free and Cued Selective Reminding Test–Free Recall, Selective Reminding Test–Total Recall, Logical Memory–Immediate), and Delayed memory (Free and Cued Selective Reminding Test–Total Recall, Selective Reminding Test–Delayed, Logical Memory–Delayed). Superscript numbers indicate variables with missing data: [1] Executive function missing for 2 participants (1 EXT < 80%, 1 EXT ≥ 80%); [2] Immediate memory missing for 3 participants (2 EXT < 80%, 1 EXT ≥ 80%); [3] Delayed memory missing for 3 participants (2 EXT < 80%, 1 EXT ≥ 80%); [4] APOE ε4 status missing for 2 participants (1 EXT < 80%, 1 EXT ≥ 80%).

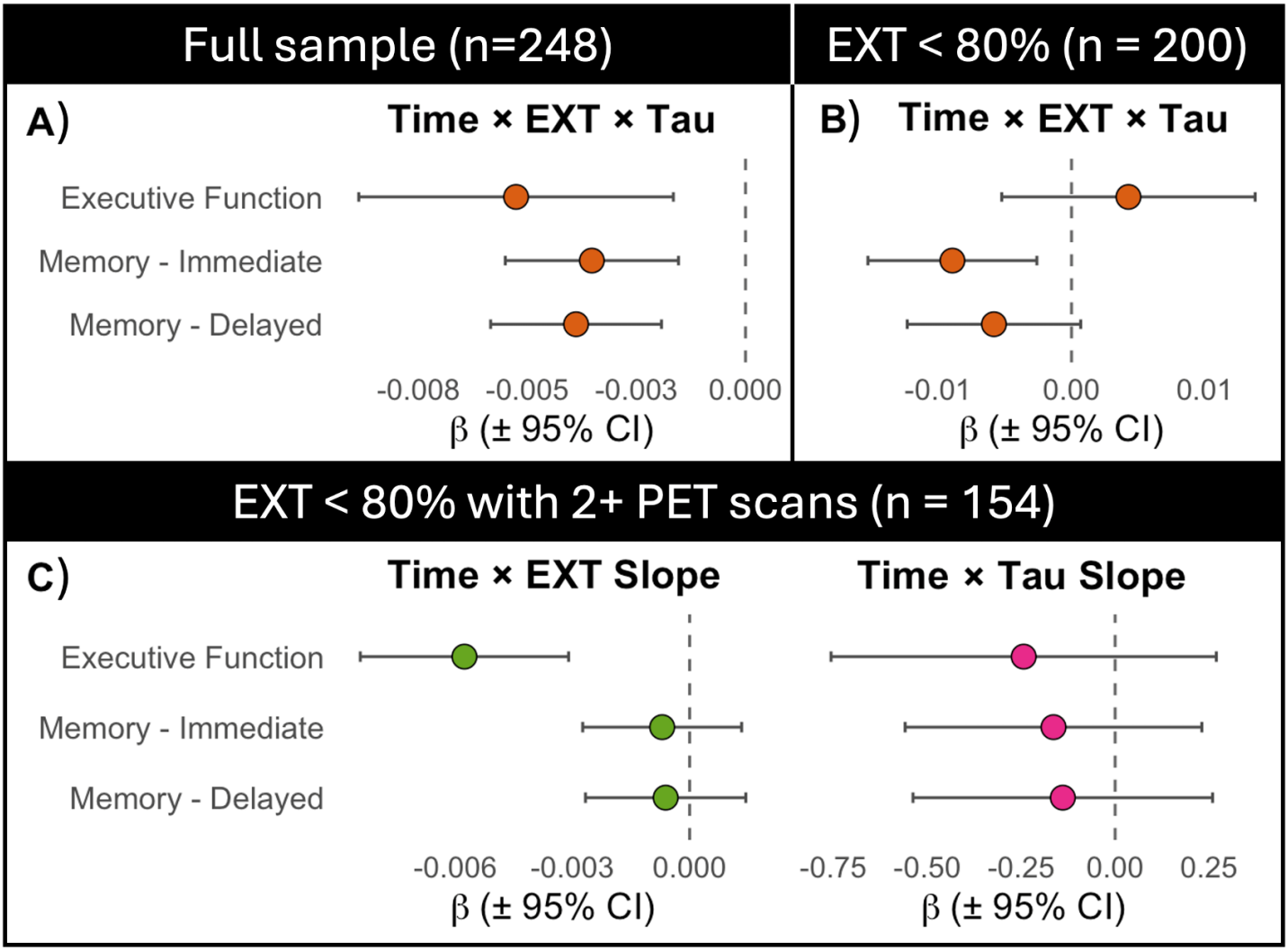


Figure 1. Differential contributions of amyloid extent and tau burden to cognitive decline across domains. A) Linear mixed-effects models revealed significant *Time* × *EXT* × *Tau* interactions across all cognitive domains in the full sample (n = 248), indicating faster decline among individuals with both greater amyloid extent and higher temporal tau. B) When analyses were restricted to earlier stages of amyloidosis (EXT < 80%; n = 200), the *Time* × *EXT* × *Tau* interaction predicted decline in immediate memory and showed a trend for delayed memory. *Time* × *EXT* and *Time* × *Tau* effects were also nonsignificant for executive function. C) Executive function decline was associated with concurrent change in EXT (*Time* × *EXT Slope*) but not change in tau (*Time* × *Tau Slope)*. All models were adjusted for age, sex, education, APOE-ε4 status, and their interactions with time, and included random intercepts and slopes (except for the Figure 1C model, which included only a random intercept due to non-convergence).

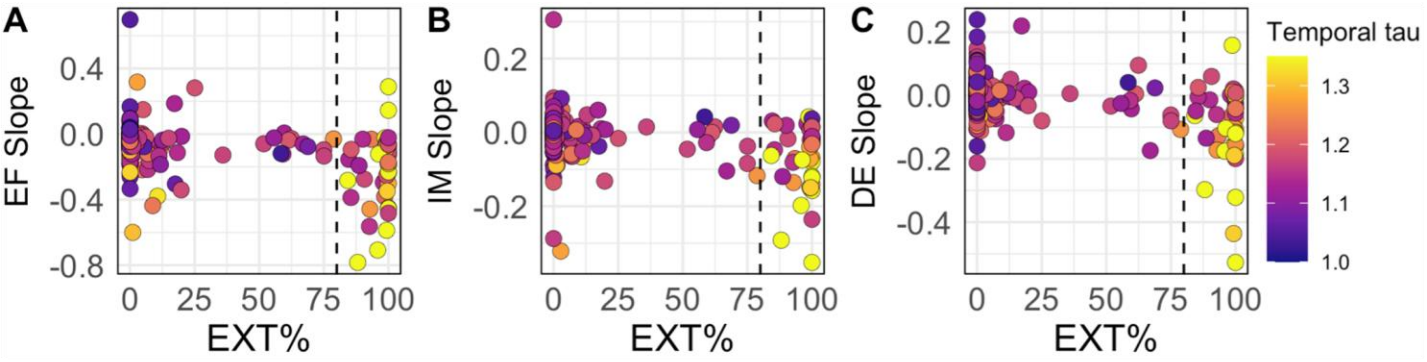


Figure 2. Continuous associations between amyloid extent and domain-specific decline. Scatterplots show participant-level extracted slopes for A) executive function (EF Slope), B) immediate memory (IM Slope), and C) delayed memory (DE Slope), as a function of baseline EXT%, color-coded by baseline FTP temporal tau SUVR. High decline on each domain was primarily observed above EXT 80% (dashed line) in association with high temporal tau. Cognitive decline associations with EXT and temporal tau were nevertheless observed below EXT 80% (Figure1).

Keywords: Amyloid PET, tau PET, executive function, memory, longitudinal analysis

81 PET-measured amyloid accumulation rate modulates tau accumulation rate in individuals with Down syndrome

Brecca Bettcher[1], Max McLachlan[1], Matt Zammit[1], Andrew McVea[1], Tobey Betthauser[1], Charles Laymon[2], Dana Tudorascu[2], Annie Cohen[2], Julie Price[3], Elizabeth Head[4], Mark Mapstone[4], Patrick Lao[5], Sterling Johnson[1], Beau Ances[6], Benjamin Handen[2], Bradley Christian[1]

[1]*University of Wisconsin-Madison School of Medicine and Public Health and Waisman Center, Madison, WI, US*
[2]*University of Pittsburgh, Pittsburgh, PA, US*
[3]*Massachusetts General Hospital, Harvard, Boston, MA, US*
[4]*University of California, Irvine, Irvine, CA, US*
[5]*Columbia University, New York, NY, US*
[6]*Washington University, St. Louis, MO, US*

Background: This work examines the association between the rate of amyloid (Aβ) accumulation measured with longitudinal [^{11}C]PiB imaging and tau accumulation with longitudinal [^{18}F]AV1451 imaging in adults with DS.

Methods: 23 DS participants with ≥3 [^{11}C]PiB scans with ≥1 Aβ+ scan (spanning >6yrs) and >1 [^{18}F]AV1451 scan were recruited from the ABC-DS study. An amyloid accumulation rate, r, was estimated by fitting a logistic growth model ($f(t)=K/(1+exp[-r(t-t_{50})])$, to each participant's set of centiloid values. Here, *t* is the subject's age and *r* and *t50* are fit parameters. The carrying capacity, *K*, was set to 142, the highest CL value in this cohort. For each subject, amyloid age is measured from the point at which the subject's growth curve reaches Aβ+ positivity (18CL). Tau burden was measured in the CentauR mesial temporal, meta temporal, temporo parietal, universal, and entorhinal cortex (ERC) regions normalized by the inferior grey cerebellum. The rate for each sequential pair of tau observations was calculated as the annualized change in SUVR. The Aβ accumulation rate was examined in relation to the tau accumulation rate and classified as slow or fast based on comparison to the median. A Wilcoxon rank-sum test assessed whether fast Aβ accumulators had a higher median tau rate than slow Aβ accumulators. APOE-ε2 and APOE-ε4 carriage was observed in both Aβ accumulation groups and APOE status was not included in the model.

Results: The average Aβ growth rate was 0.26 ±0.07 yr^{-1} (figure 1). Positive associations between the accumulation rate of amyloid and tau were observed in all tau associated regions (figure 2). Fast Aβ accumulators had significantly higher rates of tau accumulation than the slow Aβ accumulators in all regions (figure 2).

Conclusion: The rate of Aβ accumulation may vary among individuals with DS and associate with an individual's rate of tau accumulation.

Participants (n)	**23**
Age, years (At last observation)	48±7
Sex (Female/Male)	13/10
Average inter-scan interval (years)	3±1
Average cumulative follow-up time (years)	9±3
Total [^{11}C]PiB Scans	**92**
Participants with 3 PiB Scan	7
Participants with 4 PiB Scans	10
Participants with 5 PiB Scans	5
Participants with 6 PiB Scans	1
Total [^{11}F]AV1451 Scans	**60**
Participants with 2 AV1451 Scans	9
Participants with 3 AV1451 Scans	14
APOE Status	
APOE ε4 Carrier (%)	5(22%)
APOE ε2 Carrier (%)	6(26%)
Fast Aβ accumulators (ε4/ε2)	2/4
Slow Aβ accumulators (ε4/ε2)	3/2

Table 1: Participant demographics.

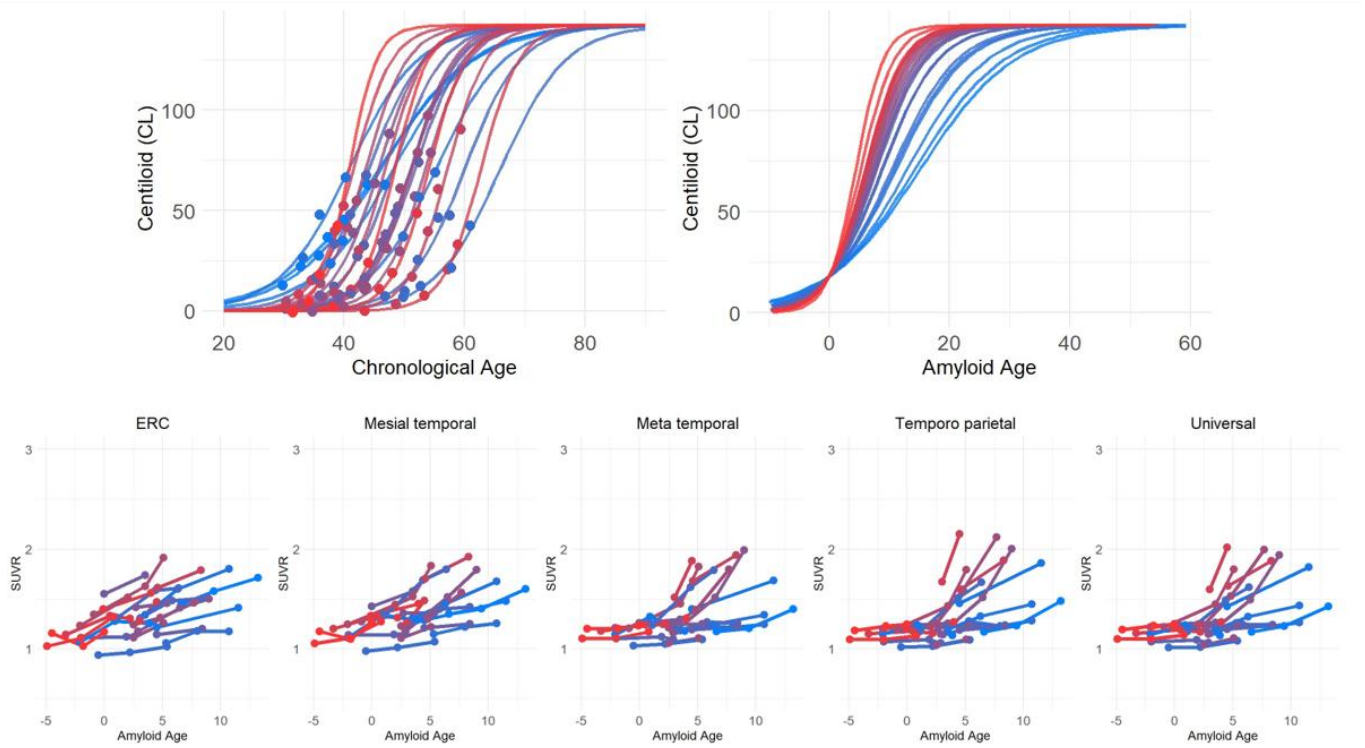


Figure 2: Individuals [^{11}C]PiB data were fit to the follow logistic growth curve $(f(t))=K/(1+e-r(t-t50))$, with a carrying capacity (K) set to 142, the highest observed CL value in this cohort of DS individuals. The growth rate is represented by a color gradient ranging from red (faster) to blue (slower). Color was assigned based on amyloid rate rank. Top: Modeled amyloid trajectories by chronological age and aligned by amyloid age. Bottom: Amyloid age against tau SUVr in associated CentauR regions.

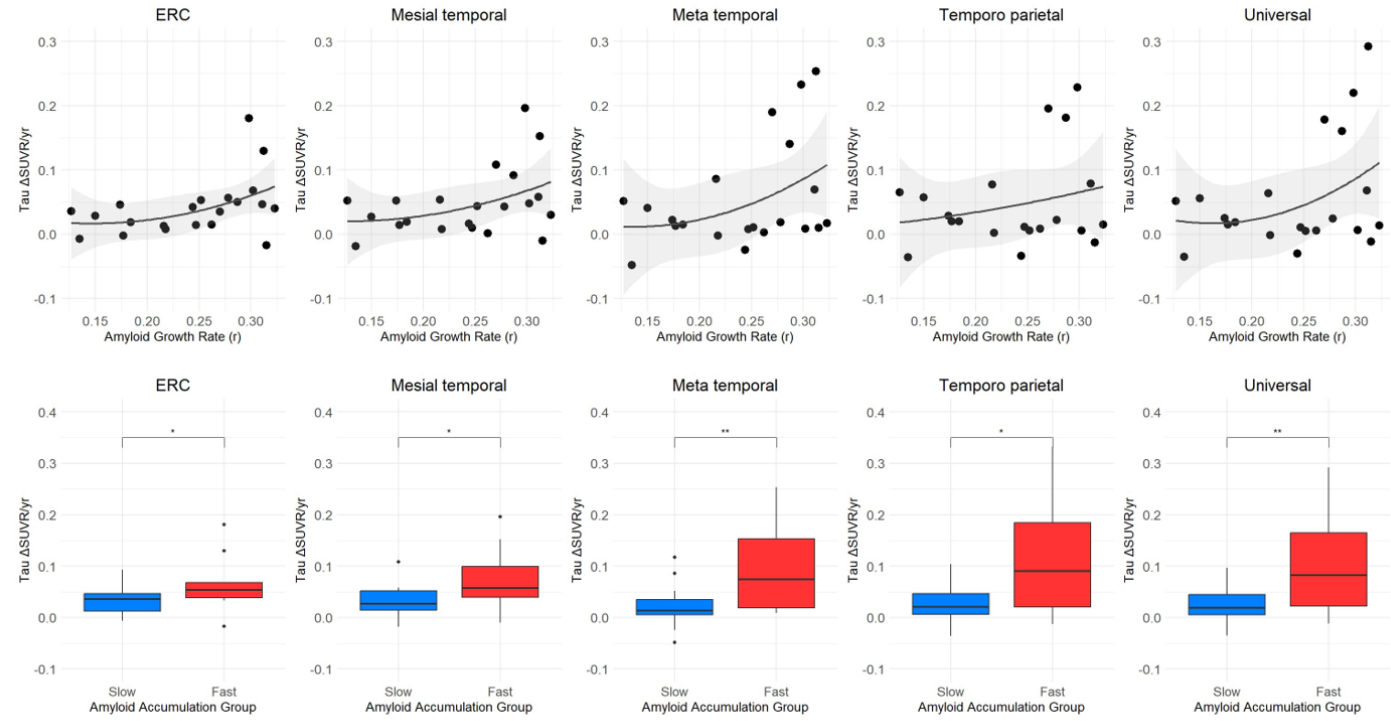


Figure 3: Top: Amyloid growth factor (r) against tau rate as measured in annualized SUVR change. Data were restricted to include only individuals whose amyloid value at the time of the terminal tau observation was >25 CL. Participants under this criterion are represented once by their last pair of sequential tau observations. Data were fit with a linear quadratic model. Positive associations between amyloid growth factor and annualized tau change were observed. Bottom: Annualized tau accumulation by amyloid accumulation group. Participants who have three tau observations are represented twice. Significance codes: **p < 0.01, *p < 0.05.

Keywords: amyloid rate, tau rate, [11C]PiB, [18F]AV1451, longitudinal

82 Elevated medial temporal lobe tau predicts cross-sectional association between neocortical tau and global amyloid burden

Emma G. Thibault[1], Anthonin Reilhac-Laborde[2], Arnaud Charil[2], Michael C. Irizarry[2], Keith A. Johnson[1]

[1]*Massachusetts General Hospital, Boston, MA, US*
[2]*Eisai Inc., Nutley, NJ, US*

Background: Recent clinical trials have shown that monoclonal anti-amyloid (Aβ) therapies are most effective when global tau burden is low. However, regional patterns of tau deposition and their relationships with Aβ remain poorly characterized. We aim to better understand cross-sectional relationships of global Aβ and individually sampled anatomic regions for baseline tau in CLARITY-AD to inform trial screening algorithms and interpretation of longitudinal analyses evaluating treatment effects. We hypothesize that at low levels of medial temporal lobe (MTL) tau, neocortical tau is low regardless of Aβ burden, Age, or Sex, and cognitive performance is better than those with high MTL tau.

Methods: We analyzed 314 participants with mild cognitive impairment or mild dementia from CLARITY-AD who underwent [^{18}F]MK6240-tau- and Aβ-PET imaging (Table 1). MRIs were processed using FreeSurfer v7.4 and coregistered to tau-PET. Tau SUVRs were computed using cerebellar cortex as reference; Aβ burden was expressed in Centiloids (CL). Gaussian mixture modeling defined high/low tau thresholds for entorhinal (SUVR=1.366) and amygdala (SUVR=0.888). Welch's t-tests compared cognitive and imaging measures between groups. Hierarchical linear models evaluated associations between neocortical tau SUVR and CL, including terms for CL tertiles, amygdala/entorhinal tau group, age, and sex. Model fit was ass essed using AIC, BIC, and adjusted-R^2.

Results: Model fit indices indicate CL*Entorhinal group as best fitting (Table 2). Participants with low MTL tau showed better cognition, lower neocortical tau, and no significant Aβ–tau association. Those with high MTL tau had poorer cognition, higher neocortical tau (Table 1), and strong positive Aβ–tau associations (Figure 2). Age was significant, and sex was nonsignificant for all models.

Conclusions: Combined assessment of Aβ and MTL tau level may better define disease stage and treatment responsiveness. Ongoing longitudinal analyses will test whether Aβ reduction differentially modifies tau propagation in participants with low vs. high baseline MTL tau.

	Overall N=314	ERC- N=121	ERC+ N=193	P-Value
Age	71.7 ± 7.9 (51-88)	71 ± 8.4 (53-86)	72 ± 7.5 (51-88)	0.157
Sex, n Female (%)	160 (51%)	61 (50.4%%)	99 (51.3%)	0.971
Centiloid	70.6 ± 44.5 (-17 – 170)	33.4 ± 32.7 (-17 – 145)	94.0 ± 33.6 (-0.4 – 170)	**<.001**
CDR-Global	0.62 ± 0.21 (0.5-1)	0.6 ± 0.3 (0.5-2)	0.7 ± 0.4 (0-2)	**0.022**
CDR-SB	3.4 ± 1.3 (0.5-8)	3.4 ± 1.4 (0.5-7)	3.3 ± 1.3 (0.5-8)	0.488
ADAS-Cog	22.6 ± 6.7 (4.7-54)	20.9 ± 6.7 (5-35)	23.7 ± 6.6 (5-54)	**<.001**
MMSE	25.6 ± 2.14 (22-30)	25.6 ± 2.1 (22-30)	25.6 ± 2.2 (22-30)	0.745
Entorhinal SUVR	1.80 ± 0.73 (0.74-4)	1.08 ± 0.16 (0.74-1.36)	2.25 ± 0.56 (1.37-3.98)	**<.001**
Parahippocampal SUVR	1.49 ± 0.60 (0.56-3.3)	0.95 ± 0.15 (0.56-1.35)	1.82 ± 0.53 (0.95-3.34)	**<.001**
Amygdala SUVR	1.55 ± 0.84 (0.47-4)	0.76 ± 0.19 (0.47-1.74)	2.04 ± 0.70 (0.77-3.98)	**<.001**
Fusiform SUVR	1.57 ± 0.74 (0.81-4.3)	1.03 ± 0.12 (0.81-1.66)	1.91 ± 0.76 (0.88-4.31)	**<.001**
Inferior Temporal SUVR	1.75 ± 0.93 (0.74-5.6)	1.09 ± 0.12 (0.74-1.47)	2.17 ± 0.97 (0.90-5.62)	**<.001**
Middle Temporal SUVR	1.66 ± 0.90 (0.61-5.5)	1.05 ± 0.13 (0.61-1.60)	2.04 ± 0.97 (0.87-5.52)	**<.001**

Table 1. Demographics table grouped by entorhinal tau SUVR group. Group differences were evaluated using Welch's t-tests for continuous variables and chi-square analysis for categorical variables. Groups did not differ in Age, Sex, CDR-SB, or MMSE.
Abbreviations: CDR-Global = Clinical Dementia Rating Global; CDR-SB = Clinical Dementia Rating – Sum of Boxes; ADAS-Cog = Alzheimer's Disease Assessment Scale – Cognitive Subscale; MMSE = Mini Mental State Evaluation; SUVR = Standardized Uptake Volume Ratio, measurement of tau-PET signal.

	Model	Term	Estimate	SE	P-value	Adjusted R^2	AIC	BIC
FF	Model 1	Age	-0.083	0.058	**0.044**	0.008	702.39	717.39
	Model 2	CL	0.405	0.035	**<.0001**	0.311	588.99	607.74
	Model 3	$CL*Tertile_2$	0.645	0.262	**0.015**	0.316	590.78	624.52
		$CL*Tertile_3$	0.218	0.205	0.289			
	Model 4	$CL*ERC_{high}$	0.201	0.090	**0.027**	**0.408**	**543.43**	**569.68**
	Model 5	$CL*AM_{high}$	0.251	0.088	**0.005**	0.397	549.41	575.66
IT	Model 1	Age	-0.151	0.051	**0.004**	0.012	843.05	858.05
	Model 2	CL	0.520	0.043	**<.0001**	0.336	722.24	740.99
	Model 3	$CL*Tertile_2$	0.844	0.324	**0.010**	0.342	723.27	757.02
		$CL*Tertile_3$	0.282	0.253	0.265			
	Model 4	$CL*ERC_{high}$	0.316	0.112	**0.005**	**0.428**	**677.38**	**703.62**
	Model 5	$CL*AM_{high}$	0.352	0.109	**0.001**	0.413	685.44	711.69
MT	Model 1	Age	-0.205	0.0490	**<.0001**	0.047	816.56	831.56
	Model 2	CL	0.495	0.041	**<.0001**	0.349	697.65	716.40
	Model 3	$CL*Tertile_2$	0.749	0.312	**0.017**	0.354	699.46	733.2
		$CL*Tertile_3$	0.335	0.243	0.170			
	Model 4	$CL*ERC_{high}$	0.288	0.109	**0.009**	**0.425**	**660.89**	**687.14**
	Model 5	$CL*AM_{high}$	0.315	0.106	**0.003**	0.412	668.04	694.29

Table 2. Hierarchical linear models examining regional tau SUVR as a function of age, amyloid burden, and medial temporal lobe tau group interactions. Each row presents model parameter estimates, standard error, *P*-values, adjusted R^2, and model fit indices (AIC, BIC) for five nested models predicting tau SUVR in the fusiform (FF), inferior temporal (IT), and middle temporal (MT) cortices. Model 1 includes age + sex alone; Model 2 adds global amyloid (Centiloid, CL); Model 3 to 5 test interactions between CL and group level factors: Aβ tertile (CL × $Tertile_2/_3$), entorhinal tau status (CL × entorhinal (ERC) high/low group), and amygdala tau status (CL × amygdala (AM) high/low group) with reference group listed in the Term column. Bolded models indicate best fit (lowest AIC/BIC). All numerical predictors were standardized. Across regions, inclusion of CL × regional ERC tau terms substantially improved model fit and increased adjusted-R^2, suggesting that Aβ-related tau accumulation in the neocortex varies by local accumulation within the medial temporal lobe.

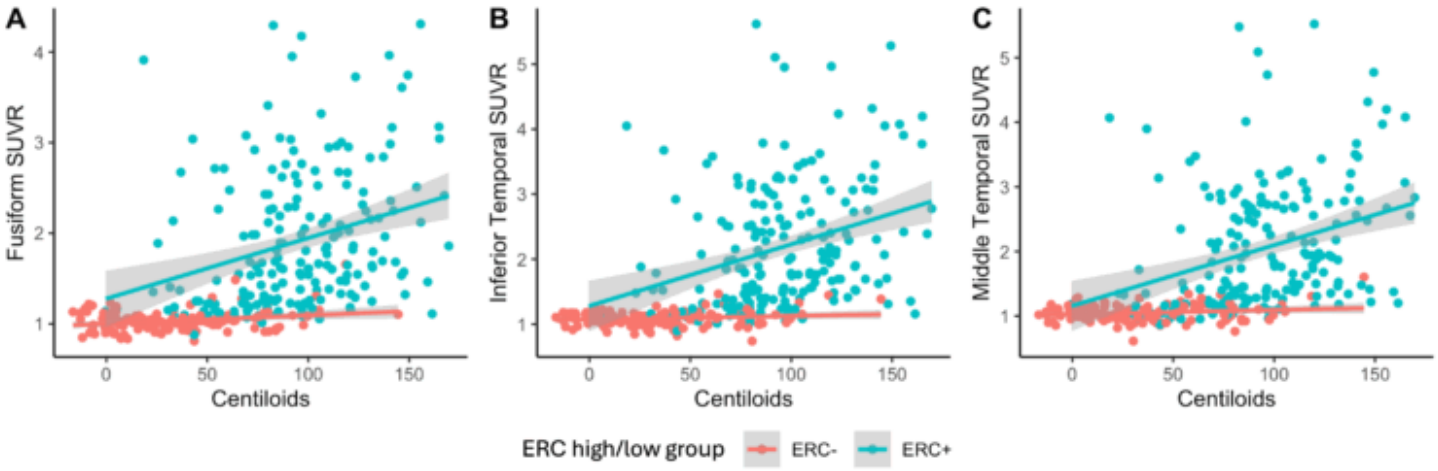


Figure 1. Association between global amyloid (Aβ) burden and neocortical tau by entorhinal tau group. Scatterplots show relationships between Centiloids and tau SUVR in the (A) fusiform, (B) inferior temporal, and (C) middle temporal cortices, stratified by entorhinal tau group (ERC_{low} = red; ERC_{high} = blue). Shaded areas represent 95% confidence intervals from linear fits. Among participants with high ERC tau, higher Aβ burden was strongly associated with greater neocortical tau, whereas no significant relationship was observed in the low ERC tau group. These findings indicate that amyloid–tau coupling in temporal neocortex depends on the presence of elevated medial temporal tau.

Keywords: MK-6240, tau-PET, CLARITY-AD, medial temporal lobe

83 Assessing the effect of amyloid status on the relationship between glucose metabolism and synaptic density in the aging population

Max McLachlan[1], Brecca Bettcher[1], Alexandra DiFilippo[2], Lisette LeMerise[1], Andrew McVea[1], Matthew Zammit[1], Rebecca Langhough[1], Sterling Johnson[1], Barbara Bendlin[1], Bradley Christian[1]

[1]*University of Wisconsin-Madison, Madison, WI, US*
[2]*Yale School of Medicine, New Haven, CT, US*

Background: Synaptic density loss has been proposed as a primary mechanism through which cognition degrades over the course of Alzheimer's disease (AD). Glucose metabolism ([^{18}F]FDG), amyloid ([^{11}C]PiB), and tau PET have historically been used to assess the severity of AD pathology. Recent work characterized the relationship between [^{18}F]MK-6240 tau and [^{11}C]UCB-J synaptic density, where the entorhinal cortex and hippocampus showed the strongest associations (DiFilippo 2025). This study examines the effect of amyloid status on the relationship between metabolism and synaptic density as measured with UCB-J PET.

Methods: 50 participants completed T1-weighted MRIs and PET imaging with UCB-J, FDG, and PiB (Table 1). PiB scans were processed using a calibrated Centiloid pipeline; participants were grouped by amyloid status. MRIs underwent FreeSurfer grey matter parcellation. FDG and UCB-J scans underwent frame realignment and were warped into MRI space. UCB-J DVR (cerebellar white matter reference) and FDG SUVR (pontine reference) parametric images were created; average signal was calculated for each region of the parcellation. Inter-regional Pearson correlation coefficients (PCC) were calculated between UCB-J and FDG for each pair of regions. The parametric images were then warped into MNI space and smoothed to 12mm isotropic resolution. Voxel-based analysis was performed by calculating the PCC between tracers for each voxel in MNI space.

Results: Inter-regional analysis revealed moderate-to-strong correlations throughout the medial cortex, lateral sulci, and mesial temporal regions for the full cohort and the amyloid positive group (Figure 1). The strongest correlation was found in the entorhinal cortex for the amyloid positive group, with PCC=0.77. The amyloid negative group showed weaker correlations than the positive group, with a smaller spatial extent of significance (Figure 2).

Conclusions: Synaptic density showed moderate-to-strong correlations with glucose metabolism throughout the brain for amyloid positive individuals, suggesting there exists a complex relationship between AD pathology and synaptic density.

	Full Cohort	Amyloid Negative	Amyloid Positive
Cohort size [n]	50	23	27
Average age [years]	70.3 (SD = 6.7)	67.5 (SD = 6.7)	72.6 (SD = 6.0)
Female [n (%)]	28 (56.0)	18 (78.3)	10 (37.0)
Average Centiloid [CL]	39.7 (SD = 41.2)	2.9 (SD = 7.0)	71.0 (SD = 30.7)
Cognitively impaired [n (%)]	12 (24.0)	1 (4.4)	11 (40.7)
Intra-regional UCB-J/FDG correlations [PCC [95% C.I.]]			
Entorhinal	**0.52 [0.28, 0.70]**	0.03 [-0.39, 0.43]	**0.77 [0.55, 0.89]**
Hippocampus	**0.49 [0.24, 0.68]**	0.06 [-0.36, 0.46]	**0.65 [0.36, 0.83]**
Parahippocampal	**0.45 [0.19, 0.65]**	0.23 [-0.20, 0.58]	**0.56 [0.23, 0.78]**
Precuneus	**0.47 [0.22, 0.66]**	0.44 [0.04, 0.72]	0.46 [0.10, 0.72]
Cuneus	**0.56 [0.33, 0.72]**	0.52 [0.14, 0.77]	**0.58 [0.25, 0.79]**
Cingulate isthmus	**0.56 [0.34, 0.73]**	0.44 [0.04, 0.72]	**0.55 [0.21, 0.77]**
Posterior cingulate	0.40 [0.13, 0.61]	0.30 [-0.13, 0.64]	0.45 [0.08, 0.71]
Fusiform	0.32 [0.05, 0.55]	0.05 [-0.37, 0.45]	0.49 [0.13, 0.73]
Paracentral	**0.56 [0.34, 0.73]**	0.53 [0.15, 0.77]	**0.62 [0.31, 0.81]**
Inferior parietal	0.36 [0.09, 0.58]	0.42 [0.00, 0.71]	0.32 [-0.07, 0.63]
Superior parietal	0.40 [0.14, 0.61]	0.28 [-0.15, 0.62]	0.48 [0.13, 0.73]
Inferior temporal	0.20 [-0.09, 0.45]	0.03 [-0.39, 0.43]	0.37 [-0.02, 0.66]
Middle temporal	0.27 [-0.01, 0.51]	0.22 [-0.21, 0.58]	0.37 [-0.01, 0.66]
Transverse temporal	**0.60 [0.38, 0.75]**	0.47 [0.07, 0.74]	**0.64 [0.34, 0.82]**
Superior temporal	0.37 [0.10, 0.59]	0.18 [-0.25, 0.55]	0.50 [0.14, 0.74]
Insula	**0.44 [0.19, 0.64]**	0.15 [-0.28, 0.53]	**0.56 [0.22, 0.77]**

Table 1 – Participant demographics. Amyloid positivity was determined using a threshold of 21.6 Centiloids (Betthauser 2022). FDG scans were completed within 3 months of the UCB-J scan, and PiB scans were completed within 1 year of the UCB-J scan. Intra-regional PCCs are bolded if they are significant following multiple comparison correction.

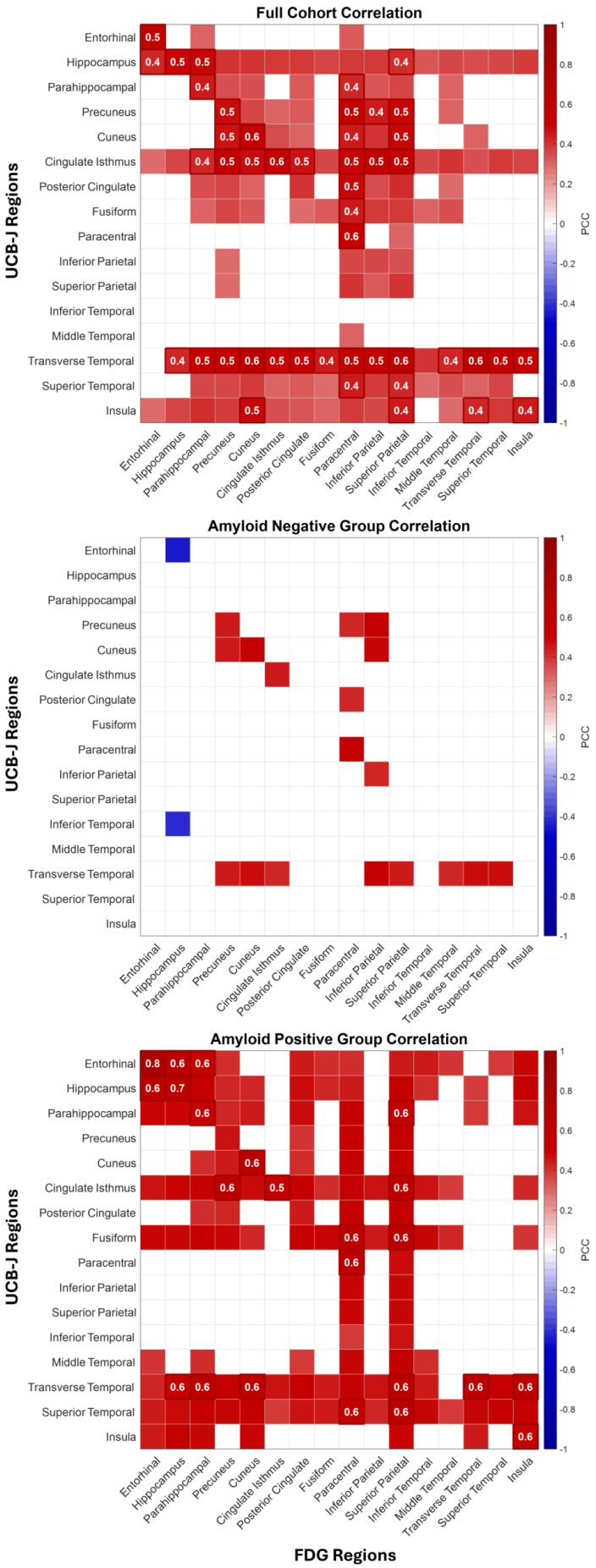


Figure 1 – Inter-regional correlation analysis for the full cohort (top), amyloid negative group (middle), and amyloid positive group (bottom). FDG regions are listed on the x-axis, and UCB-J regions are listed on the y-axis. Each cell represents the PCC for the relevant pair of regions. Cells with color reflect PCC with $p < 0.05$, and bolded cells with the PCC value overlaid survive multiple comparison correction. The full cohort and amyloid positive group show moderate-to-strong correlations across inter-regional pairs; in particular, FDG SUVR in the paracentral gyrus and parietal lobe appears to broadly correlate with UCB-J DVR, while UCB-J DVR in the transverse temporal gyrus appears to broadly correlate with FDG SUVR. No correlation survives multiple comparison correction in the amyloid negative group.

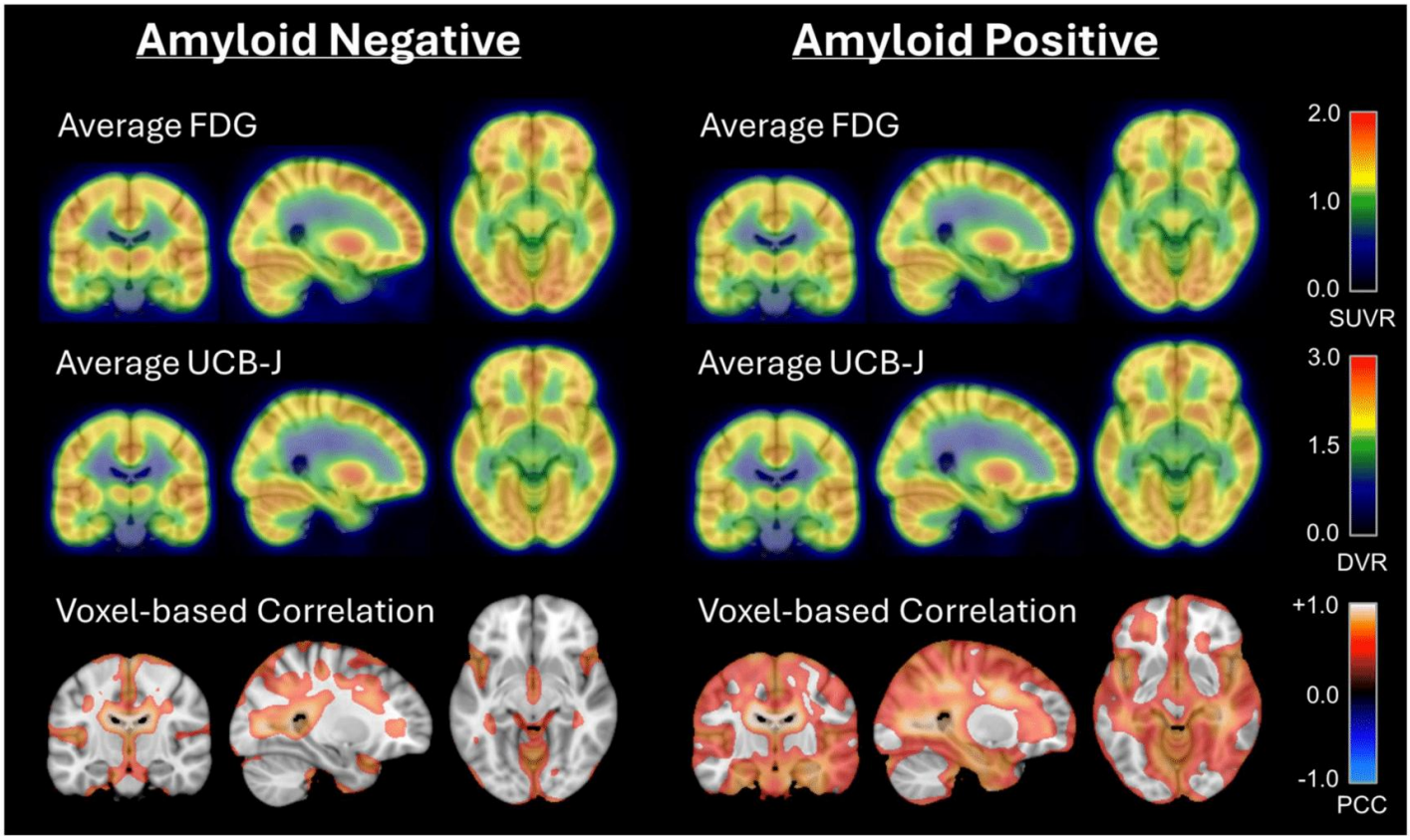


Figure 2 – Cohort-averaged FDG PET (top), UCB-J PET (middle), and voxel-based correlations between the tracers (bottom). The averaged scans show similar signal distribution across grey matter regions of the brain. FDG shows relatively lower uptake in inferior and anterior parts of the temporal lobe than UCB-J. The amyloid positive group shows generally lower PET signal than the amyloid negative group across both tracers. The voxel-based correlation analysis displays PCCs for voxels after correcting for false detection rate. The amyloid positive group shows stronger and more wide-spread correlations than the amyloid negative group.

Keywords: amyloid, synaptic density, glucose metabolism, PET, Alzheimer's disease

84 Associations between p-tau217 and brain atrophy are amplified by Aβ burden and APOEε4

Jane Brown[1], Michael Properzi[1], Madison Cuppels[1], Colin Birkenbihl[1], Gillian Coughlin[1], Mabel Seto[1], Diana Townsend[1], Tobey Betthauser[2,4], Aaron Schultz[1], Jasmeer Chhatwal[1], Hyun-Sik Yang[1], Heidi Jacobs[1], Michelle Farrell[1], Keith Johnson[1], Sterling Johnson[2], Annie Li[1], Reisa Sperling[1], Timothy Hohman[3], Michael Donohue[4], Rachel Buckley[1]

[1]*Massachusetts General Brigham, Boston, MA, US*
[2]*University of Wisconsin-Madison, Madison, WI, US*
[3]*Vanderbilt Medical Center, Nashville, TN, US*
[4]*University of Southern California, San Diego, CA, US*

Objective: Blood-based biomarkers of p-tau$_{217}$ demonstrate strong sensitivity for abnormal Aβ burden, tau accumulation, and Aβ-related cognitive decline. Recent evidence also suggests robust associations with brain atrophy. Here, we sought to examine synergistic associations between p-tau$_{217,}$ Aβ burden, and *APOE*ε4 that influence subsequent brain atrophy in a harmonized, pooled sample of clinically unimpaired and impaired older adults.

Methods: We used data from 1,547 participants (n=75 MCI/Dementia) across four cohorts (A4, N=954; ADNI, N=162; HABS, N=215; WRAP, N=216). All participants had at least two MRI time points ($N_{Observations}$=6,953, follow-up=3.0 ±2.1 years; min-max=0.02-12.83) and one p-tau$_{217}$ measure within 12 months of the first MRI scan. Data were harmonized across cohorts, then pooled. We ran a series of linear mixed effects models with cross-sectional p-tau$_{217}$ as a predictor of longitudinal cortical thickness (entorhinal, inferior/middle temporal, and fusiform composite) and baseline ICV-adjusted bilateral hippocampal volume and gray matter volume, as well as interactions with Aβ status and *APOE*ε4 status. We adjusted for age, sex, and cohort, as well as random intercept and slopes.

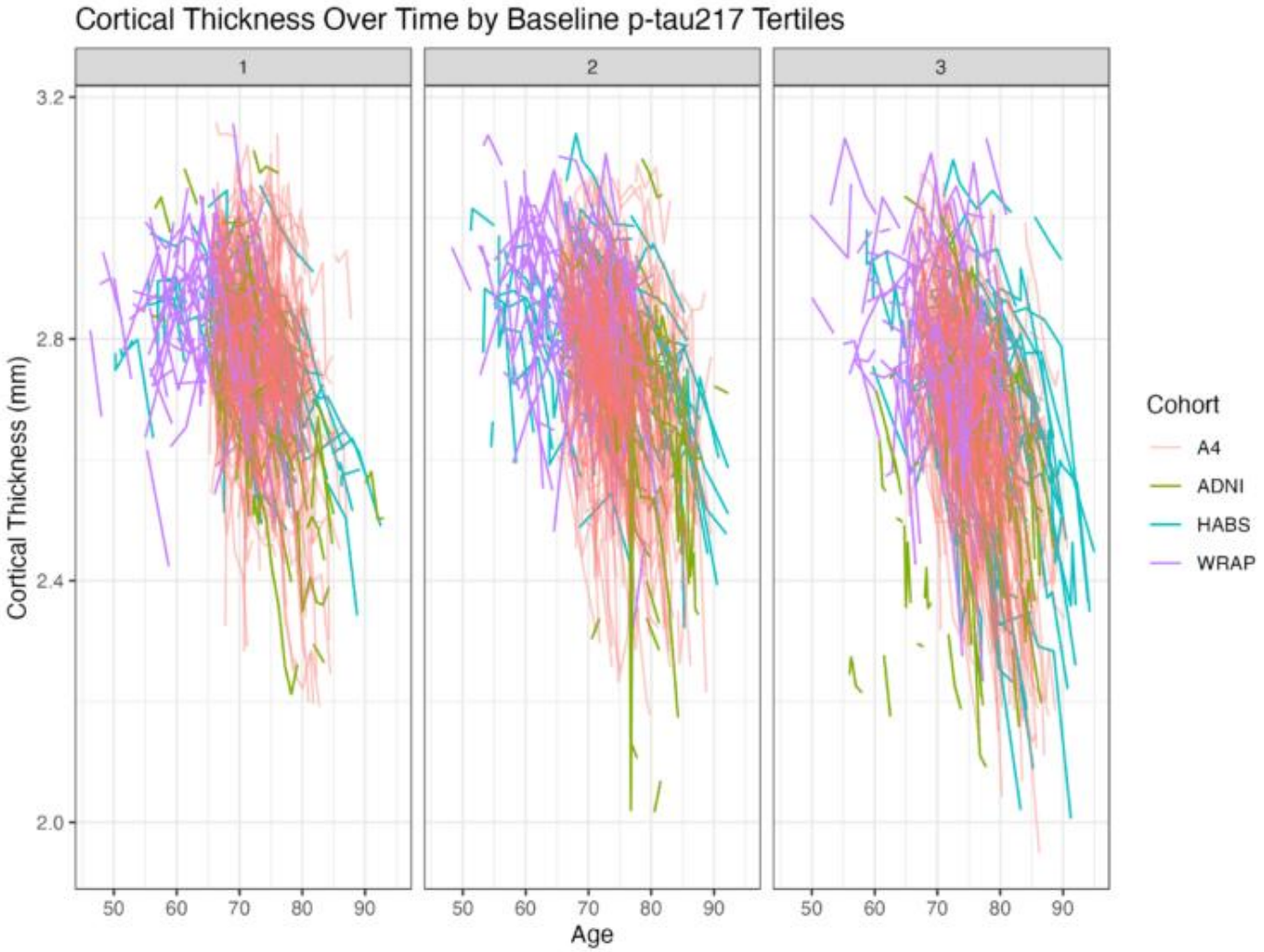
Results: Plasma p-tau$_{217}$ was associated with cortical thinning (β=-0.10(0.01), p<0.001), hippocampal atrophy (β=-0.06(0.01), p<0.001), and gray matter atrophy (β=-0.08(0.01), p<0.001). Associations remained significant (p<0.001) after adjusting for Aβ status. We found significant interactions between p-tau$_{217}$ and Aβ status on cortical thinning (β=-0.01(0.01) p=0.005) and hippocampal atrophy (β=-18.53(8.52), p=0.030), with p-tau$_{217}$ associations stronger in Aβ+ individuals. Additionally, an interaction between *APOE*ε4 status and p-tau$_{217}$ was evident on cortical thinning (β=-0.01(0.00), p=0.029). We found no interaction between p-tau$_{217}$, Aβ, and *APOE*ε4 (p>0.15).

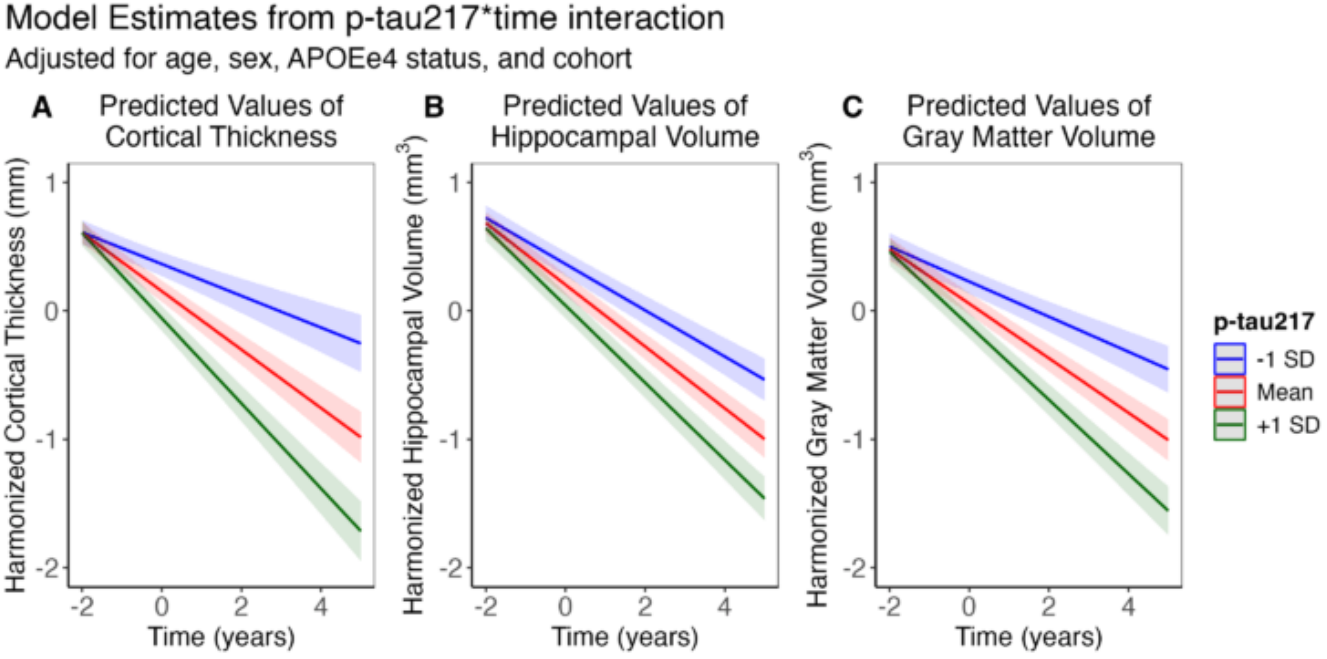
Conclusion: Brain atrophy was significantly associated with p-tau$_{217}$ and was exacerbated by Aβ positivity and *APOE*ε4. Our findings support the moderating roles of Aβ and *APOE*ε4 in signaling future risk of brain atrophy and emphasize the importance of integrating plasma biomarkers into multimodal models of disease progression.

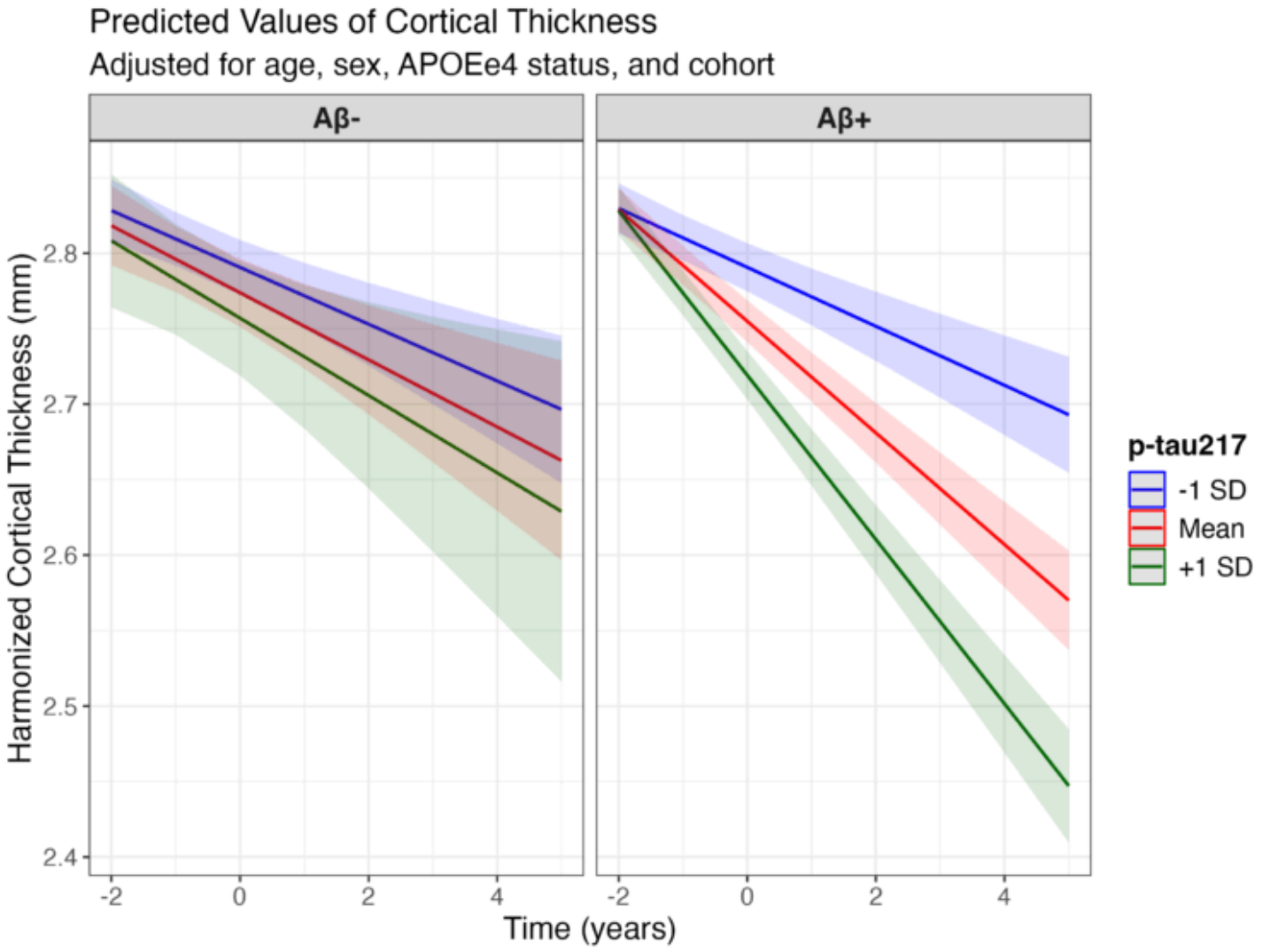
Table 1. Sample Demographics at Baseline

Characteristic	**Overall**, N = 1,547[†]	**A4**, N = 954[†]	**ADNI**, N = 162[†]	**HABS**, N = 215[†]	**WRAP**, N = 216[†]
Sex					
Female	1,009 (65%)	576 (60%)	77 (48%)	215 (100%)	141 (65%)
Male	538 (35%)	378 (40%)	85 (52%)	0 (0%)	75 (35%)
Years of Education					
Mean (SD)	16.5 (2.8)	16.6 (2.8)	16.5 (2.4)	16.0 (2.9)	16.6 (2.9)
Median	16.0	16.0	16.0	16.0	17.0
Age					
Mean (SD)	71.1 (6.5)	72.2 (4.8)	73.7 (6.7)	71.1 (8.0)	64.5 (6.9)
Median	70.8	71.5	73.8	70.3	65.4
p-tau217 (Harmonized)					
Mean (SD)	1.8 (2.3)	2.3 (2.4)	2.2 (2.2)	0.9 (1.5)	0.5 (1.3)
Median	1.4	2.0	2.3	0.6	0.3
APOEε4 Status					
ε4-	738 (48%)	376 (39%)	85 (52%)	150 (70%)	127 (59%)
ε4+	809 (52%)	578 (61%)	77 (48%)	65 (30%)	89 (41%)
Aβ Status					
Aβ-	471 (30%)	65 (6.8%)	73 (45%)	161 (75%)	172 (80%)
Aβ+	1,076 (70%)	889 (93%)	89 (55%)	54 (25%)	44 (20%)
Race					
American Indian or Alaskan Native	3 (0.2%)	1 (0.1%)	0 (0%)	2 (0.9%)	0 (0%)
Asian	26 (1.7%)	19 (2.0%)	2 (1.2%)	5 (2.3%)	0 (0%)
Black or African American	69 (4.5%)	19 (2.0%)	10 (6.2%)	31 (14%)	9 (4.2%)
More than one race	12 (0.8%)	8 (0.8%)	2 (1.2%)	2 (0.9%)	0 (0%)
Unknown	7 (0.5%)	6 (0.6%)	0 (0%)	0 (0%)	1 (0.5%)
White	1,430 (92%)	901 (94%)	148 (91%)	175 (81%)	206 (95%)
Baseline Diagnosis					
CN	1,472 (95%)	954 (100%)	89 (55%)	214 (100%)	215 (100%)
Dementia	26 (1.7%)	0 (0%)	26 (16%)	0 (0%)	0 (0%)
MCI	49 (3.2%)	0 (0%)	47 (29%)	1 (0.5%)	1 (0.5%)

[†] n (%)


Cortical Thickness Over Time by Baseline p-tau217 Tertiles
1
2
3
Cortical Thickness (mm)
3.2
2.8
2.4
2.0
50
60
70
80
90
Age
Cohort
A4
ADNI
HABS
WRAP


Model Estimates from p-tau217*time interaction
Adjusted for age, sex, APOEe4 status, and cohort
A
Predicted Values of Cortical Thickness
Harmonized Cortical Thickness (mm)
B
Predicted Values of Hippocampal Volume
Harmonized Hippocampal Volume (mm3)
C
Predicted Values of Gray Matter Volume
Harmonized Gray Matter Volume (mm3)
1
0
-1
-2
-2
0
2
4
Time (years)
p-tau217
-1 SD
Mean
+1 SD



Keywords: amyloid-beta, p-tau217, atrophy

85 Early cortical thickness change in preclinical AD development

Stephanie Sinclair[1], Xi Chen[1]

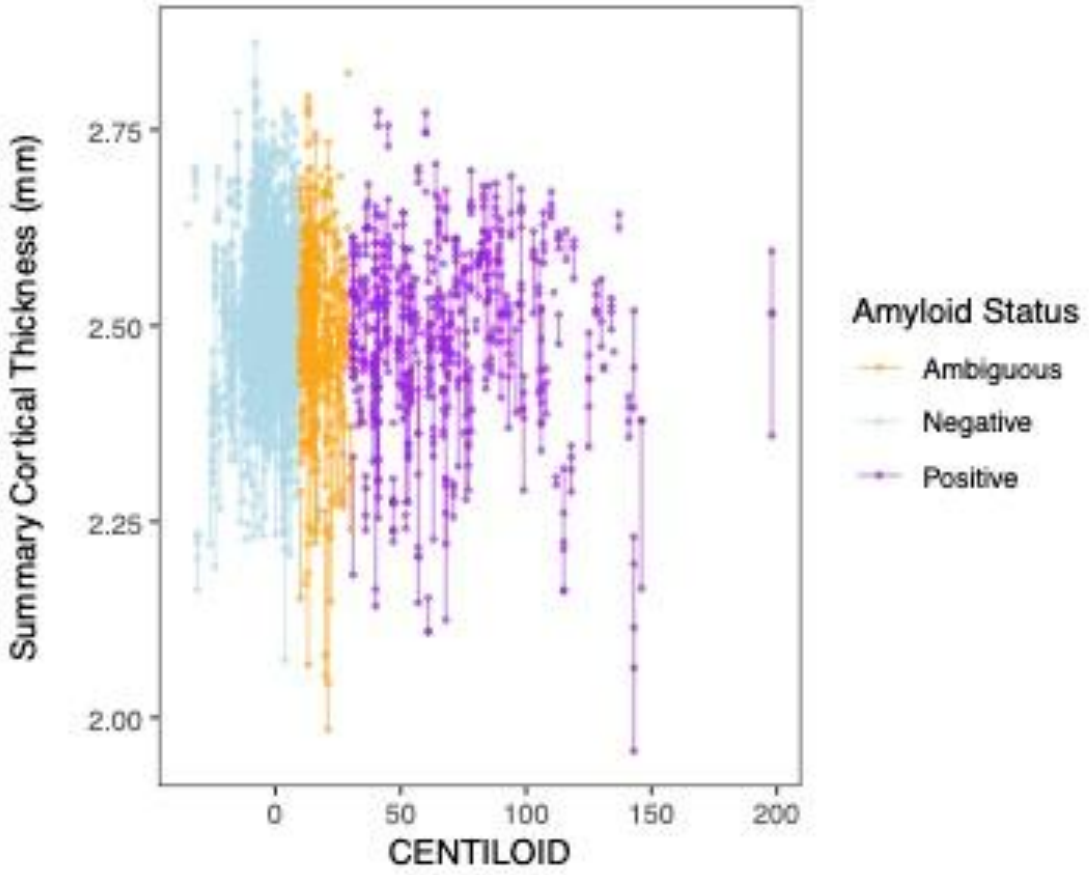
[1]*Stony Brook University, Stony Brook, NY, US*

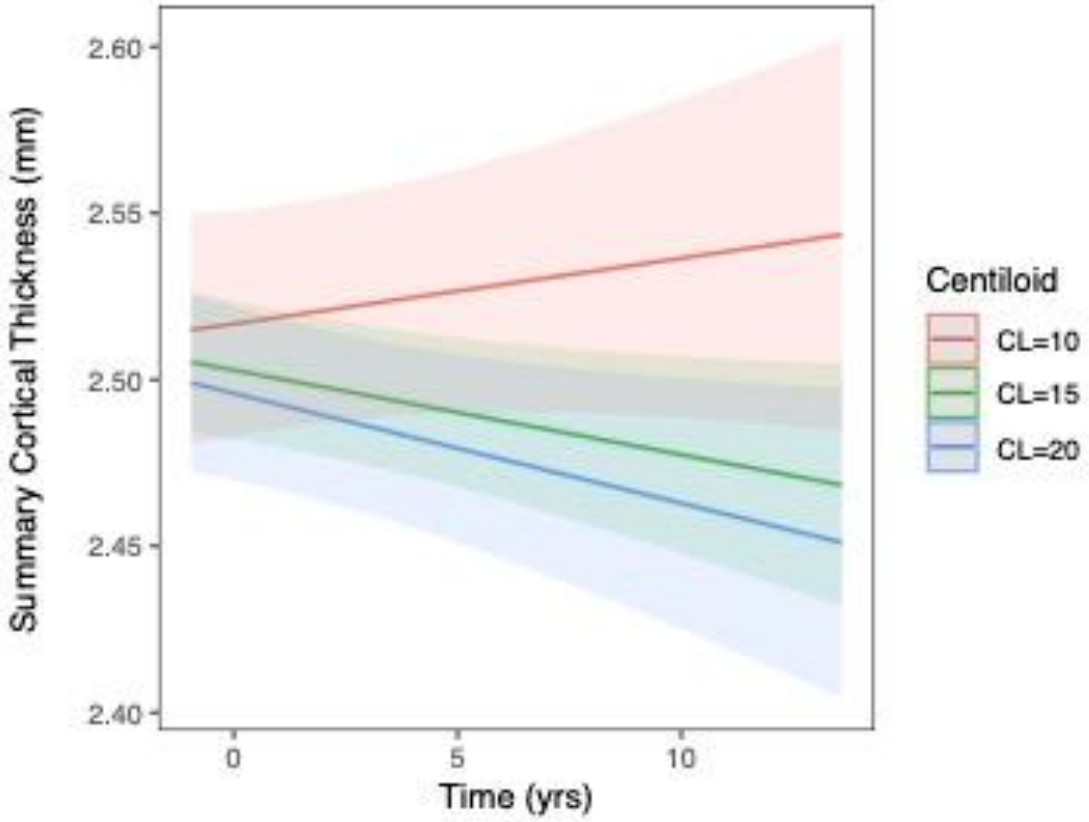
Background: A growing body of research supports a biphasic trajectory of cortical thickness over neurodegenerative disease progression. Early, preclinical stages in Alzheimer's disease (AD) marked by slightly elevated beta-amyloid (Aβ) burden may be associated with transient cortical thickening, which precedes later atrophy. Our study aims to identify early, non-linear structural changes related to initial Aβ in preclinical AD.

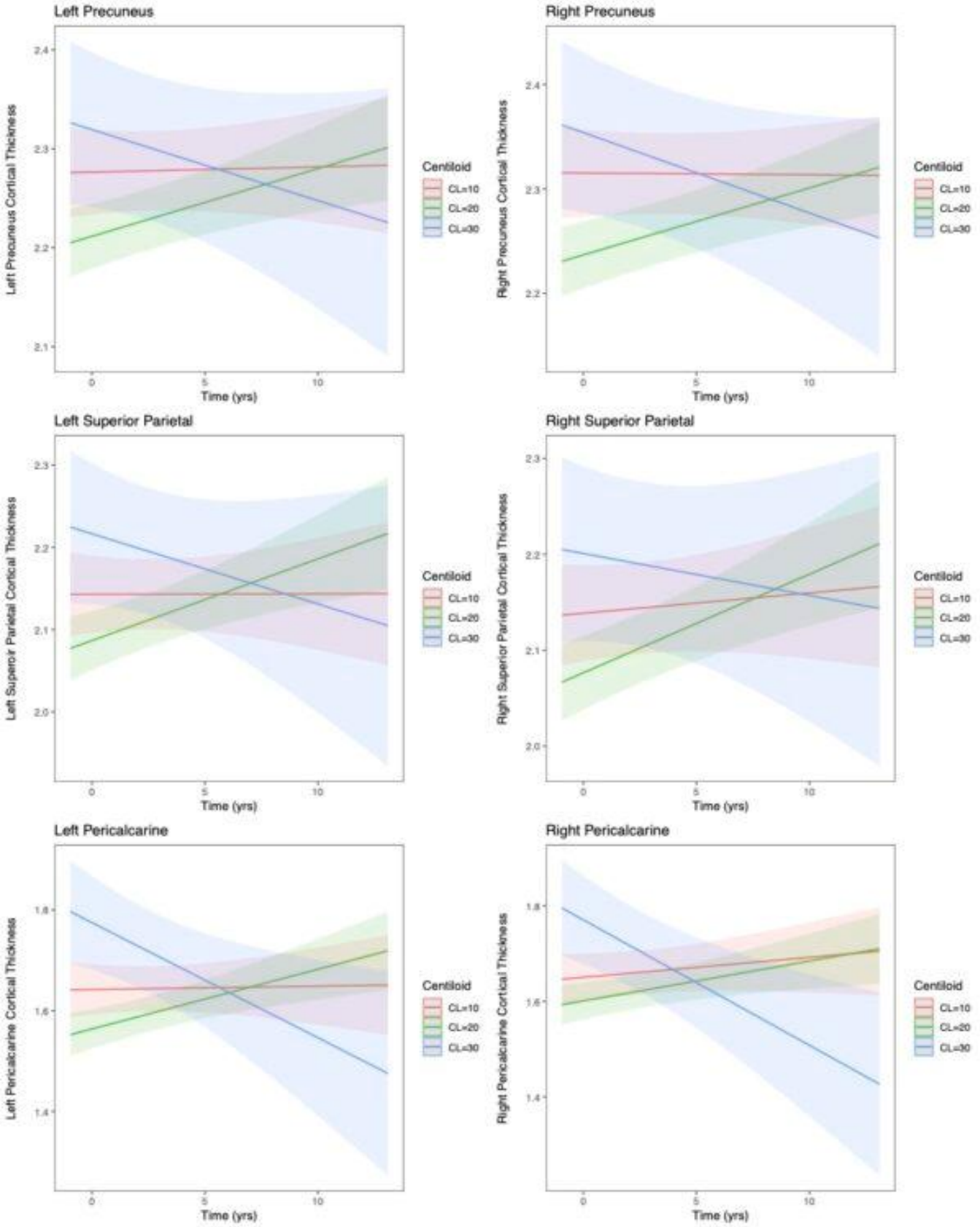
Methods: Utilizing data from the Alzheimer's Disease Neuroimaging Initiative (ADNI), we examined the relationship between Aβ quantified by global centiloids (CL) and longitudinal change in cortical thickness. We particularly focused on the early, emerging group of cognitively normal individuals with slightly elevated Aβ between 10-30 CL, who are often considered the ambiguous group in Aβ status (Figure 1). A total of 164 individuals were included with a mean age of 71.3 and a mean centiloid of 17.1. Linear mixed effects models assessed the effect of baseline Aβ on global and regional trajectories of cortical thickness prospectively measured over time.

Results: We found a significant quadratic effect of Aβ on global cortical thickness (p=.029; Figure 2), suggesting that early increase in global Aβ was associated with higher global cortical thickness, followed by progressive cortical thinning associated with moderate centiloid levels and the steepest shrinkage associated with relatively high centiloid levels. This pattern was evident in multiple cortical areas often accumulating Aβ early, including frontal, parietal, and medial regions (Figure 3).

Conclusions: These findings suggest a non-linear relationship between Aβ and cortical thickness consistent with a biphasic trajectory: early amyloid burden may coincide with hypertrophy or transient thickening as a compensatory or inflammatory response, followed by accelerated thinning as Aβ further increases. Clinical trials targeting the early stages using cortical shrinkage as a neurodegenerative marker should take into account this variability when monitoring disease progression and treatment response.


Summary Cortical Thickness (mm)
2.75
2.50
2.25
2.00
0
50
100
150
200
CENTILOID
Amyloid Status
Ambiguous
Negative
Positive


Summary Cortical Thickness (mm)
2.60
2.55
2.50
2.45
2.40
0
5
10
Time (yrs)
Centiloid
CL=10
CL=15
CL=20



Keywords: Amyloid, Cortical thickness, PET, MRI, Preclinical AD

86 Immuno-vascular crosstalk drives tau pathology preferentially in women

Madeline Wood Alexander[1,2], Min Su Kang[1], Naila Rusdi[1], Eric Yin[1], Nesrine Rahmouni[4], Yi-Ting Wang[4], Andrea L. Benedet[5], Henrik Zetterberg[5], Kaj Blennow[5], Thomas K. Karikari[6], Nicholas J. Ashton[7], Sandra E. Black[1,2,3], Maged Goubran[1,8], Jennifer S. Rabin[1,2,3], Julie Ottoy[1,3]

[1]*Centre for Brain Resilience & Recovery, Hurvitz Brain Sciences Program, Sunnybrook Research Institute, University of Toronto, Toronto, ON, Canada*
[2]*Rehabilitation Sciences Institute, Faculty of Medicine, University of Toronto, Toronto, ON, Canada*
[3]*Temerty Faculty of Medicine, Department of Medicine (Neurology), University of Toronto, Toronto, ON, Canada*
[4]*Translational Neuroimaging laboratory, McGill Centre for Studies in Aging, Montreal, ON, Canada*
[5]*Department of Psychiatry and Neurochemistry, The Sahlgrenska Academy at the University of Gothenburg, Gothenburg, Sweden*
[6]*Department of Psychiatry, University of Pittsburgh School of Medicine, Pittsburgh, PA, US*
[7]*Banner Alzheimer's Institute, Phoenix, AZ, US*
[8]*Department of Medical Biophysics, University of Toronto, Toronto, ON, Canada*

Introduction. Women's elevated risk for Alzheimer's disease (AD) may stem from sex differences in neuroimmune and cerebrovascular function. We investigated sex-specific associations between neuroinflammation and tau, and whether these effects were moderated by vascular contributions.

Methods. We included *N*=120 women (age=72.0±5.66, 31.6%MCI/dementia) and *N*=75 men (age=72.2±5.62, 42.7%MCI/dementia) from TRIAD. Tau was quantified with 18F-MK6240-PET SUVR, and Aβ with 18F-AZD4694-PET SUVR. Neuroinflammation was quantified with cingulate 11C-PBR28 TSPO-PET SUVR (*N*=94) and parietal/occipital diffusion MRI-derived free-water (FW), regions previously identified in our work as robustly associated with AD pathology. AD-related vascular burden was quantified with parietal/occipital white matter hyperintensity (WMH) volume. Linear models tested interactions between sex and inflammatory and vascular imaging markers on tau-PET, adjusting for sex*Aβ-PET, age, and *APOE4*.

Results. Inflammation was associated with greater tau-PET in women, but not men (Sex*TSPO: β=0.46±0.20, p=.02; Sex*FW: β=0.36±0.12, p=.005). Post-hoc analyses showed that these effects were strongest in Braak I/II (i.e., earliest) tau regions for TSPO-PET, and Braak III-VI (i.e., later) regions for FW (**Fig.1A-C**). FW correlated with plasma GFAP (but not TSPO), particularly in women (FW: β=0.25±0.07, p<.001; Sex*FW: β=0.31±0.14, p=.02). These results suggest that the female-specific link between neuroinflammation and tau may be driven by microglial activity (proxied via TSPO-PET) in earlier Braak stages, and astroglia-driven responses (proxied via FW) in later Braak stages. To probe the role of vascular contributions, we next tested whether the interactive effects of sex and inflammation were further moderated by WMH. There was a three-way interaction between sex, TSPO-PET, and WMH on Braak I/II tau (**Fig.1D**), such that the sex-specific association of microglial inflammation with elevated tau was strongest in women with greater vascular burden.

Significance. Neuroinflammation and its interplay with vascular processes may drive tau pathogenesis disproportionately in women. These findings highlight the critical need for sex-informed approaches to prevent and treat AD.

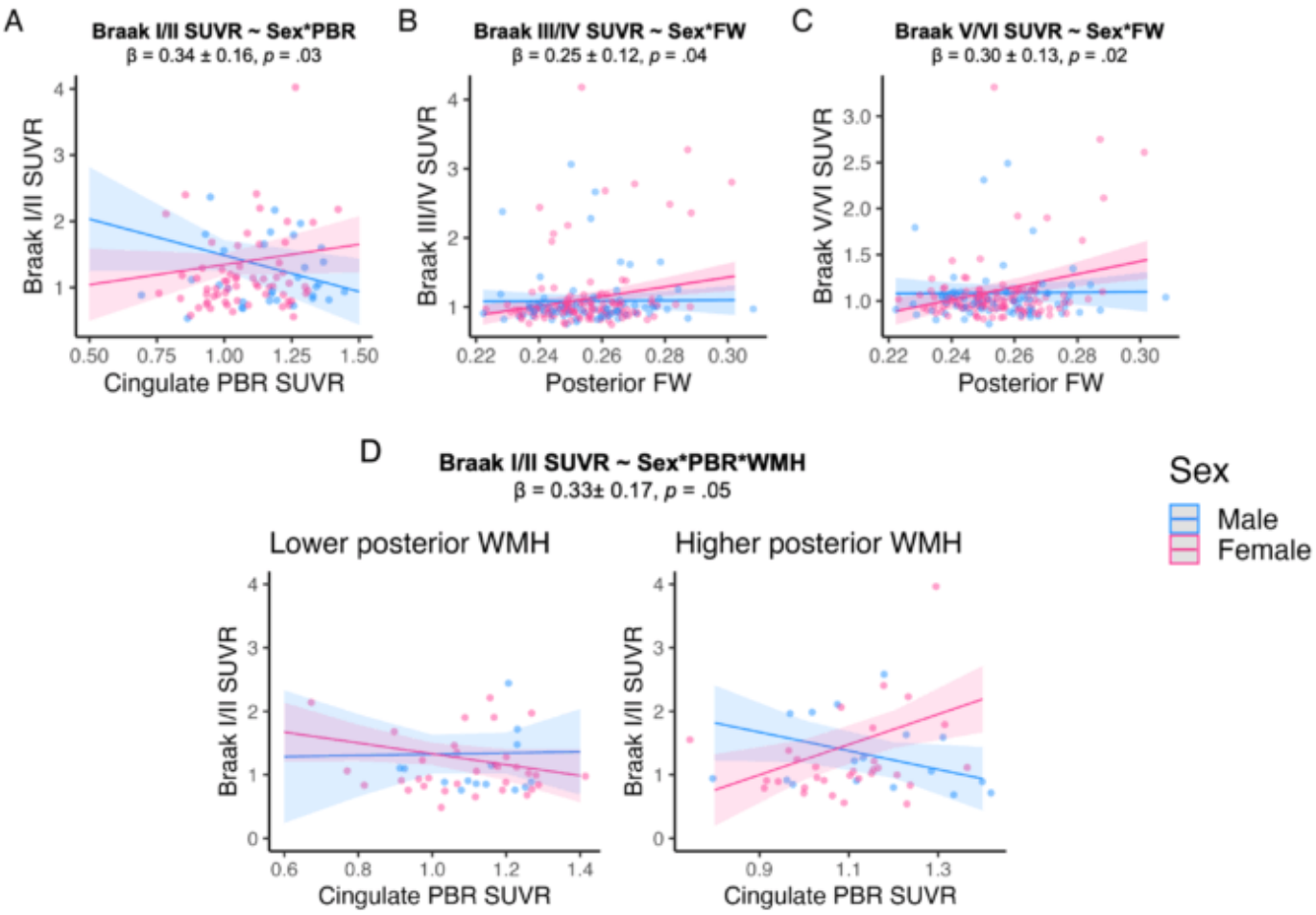


Figure 1. Synergistic associations of sex, inflammatory and vascular markers on tau-PET signal in Braak meta-regions. Panels A-C plots depict regional post-hoc analyses testing the interactions between (A) sex and cingulate PBR-SUVR on Braak I/II MK-SUVR, (B) posterior FW on Braak III/IV MK-SUVR, and (C) posterior FW on Braak V/VI MK-SUVR. Only regions showing sex-specific associations with inflammatory markers are shown. Panel D depicts the three-way interaction between sex, cingulate PBR-SUVR, and posterior WMH on Braak I/II MK-SUVR. For visualization purposes, sex differences in associations of cingulate PBR-SUVR with tau-SUVR are shown at lower (i.e., <50th percentile) and higher (i.e., ≥50th percentile) levels of WMH burden. The models are adjusted sex*Aβ-PET, age, and *APOE4*. Shaded regions depict 95% confidence intervals. Abbreviations: SUVR: standardized uptake value ratio, PBR: peripheral benzodiazepine receptor, FW: free-water, WMH: white matter hyperintensities.

Keywords: tau-PET, TSPO-PET, inflammation, sex differences, vascular contributions

87 Midlife physical activity attenuates the association of earlier menopause with tau pathology and cognitive decline

Madeline Wood Alexander[1], Claire J. Cadwallader[3], Sterling C. Johnson[4], Kaitlin B. Casaletto[3], Jennifer S. Rabin[1,2]

[1]*Sunnybrook Research Institute, Toronto, ON, Canada*
[2]*University of Toronto, Toronto, ON, Canada*
[3]*University of California San Francisco, San Francisco, CA, US*
[4]*University of Wisconsin-Madison, Madison, WI, US*

Background. Earlier menopause is associated with increased risk for Alzheimer's disease (AD) dementia. Physical activity (PA) promotes brain health and may help protect against the effects of earlier menopause, but this has not been studied.

Methods. We used data from postmenopausal women (*N*=322, baseline age=57.5±4.87 years, age at menopause=49.2±6.34) in the Wisconsin Registry for Alzheimer's Prevention (WRAP). Baseline PA was self-reported and quantified in metabolic-equivalent hours/week. Longitudinal cognition was quantified with the Preclinical Alzheimer Cognitive Composite (PACC). In a subset of participants (*N*=148), longitudinal measures of plasma p-tau217 and Aβ42 were quantified using Simoa assays. Another subset (*N*=172) underwent ^{11}C-PiB or ^{18}F-NAV4694 and ^{18}F-MK6240 PET, at an average of 12 years post-baseline. Global cortical Aβ burden was quantified in centiloids, and tau-PET signal was measured as SUVR in a temporal cortex meta-ROI comprising the entorhinal cortex, amygdala, parahippocampal gyrus, fusiform gyrus, inferior and middle temporal gyri. Linear mixed-effects models tested the interactions of age at menopause, PA, and time on PACC scores and p-tau217/Aβ42 ratio. A linear regression model tested the interaction of age at menopause and PA on tau-PET signal. Models adjusted for age, years of education, and global Aβ (for the tau-PET analysis).

Results. There were three-way interactions between age at menopause, PA, and time on both cognitive decline (β=-0.12, p<.001, **Fig.1**), and p-tau217/Aβ42 (β=0.09 p<.001, **Fig.2**). In both cases, higher PA attenuated the association between earlier menopause and these adverse outcomes. PA also diminished the association of earlier menopause with greater tau-PET signal in the temporal cortex (β=0.14, p=.02; **Fig.3**).

Conclusion. PA may protect against the negative effects of earlier menopause on AD risk. Interventions to increase PA may be especially effective in preserving brain health in women with earlier menopause.

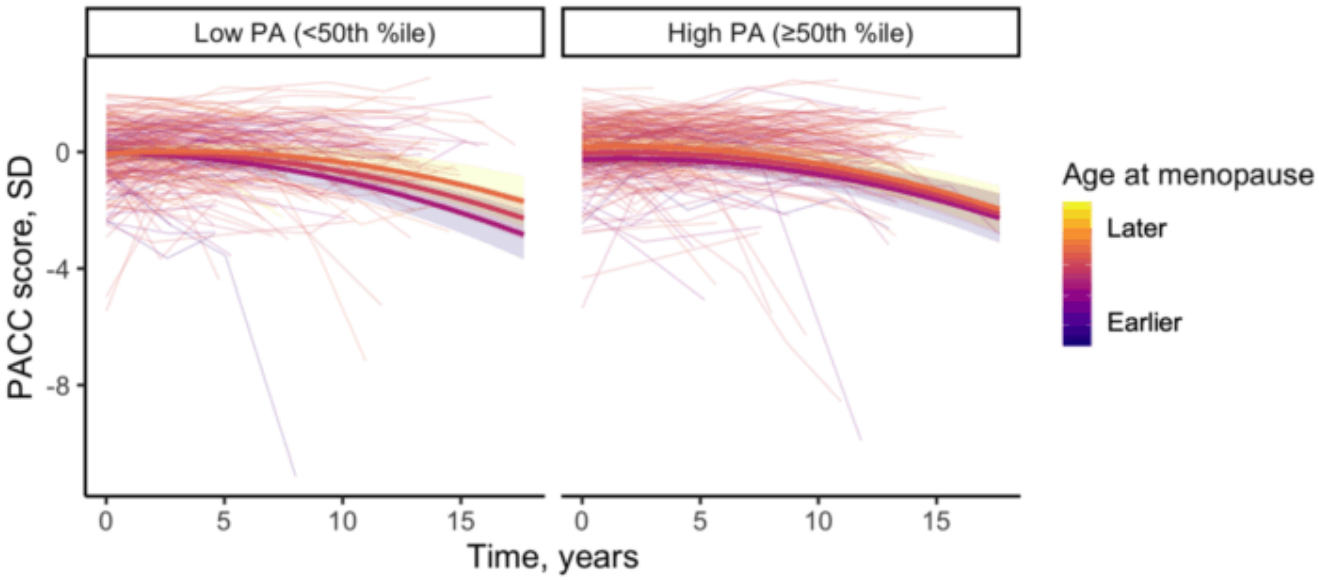


Figure 1. Interactive association of age at menopause and physical activity (PA) with longitudinal cognitive decline. The plot depicts the three-way interaction between age at menopause, midlife physical activity level, and time on PACC scores, adjusted for baseline age and years of education plus their interactions with time. Shaded regions depict 95% confidence intervals.

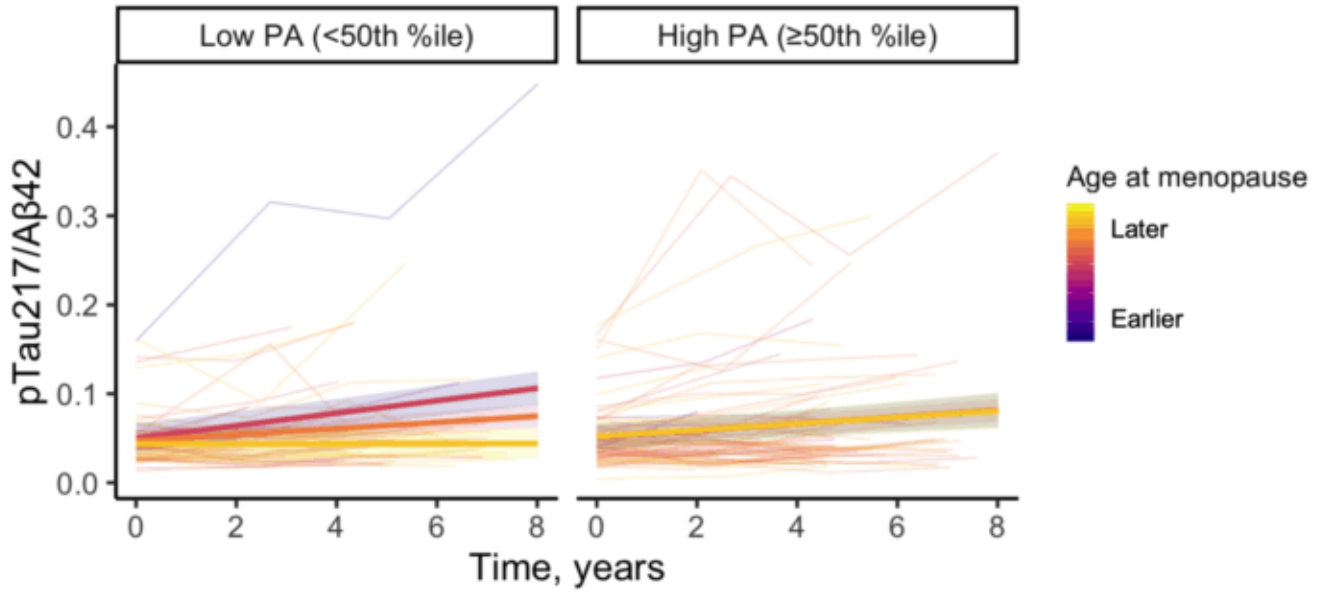


Figure 2. Interactive association of age at menopause and physical activity (PA) with longitudinal change in p-tau217/Aβ42. The plot depicts the three-way interaction between age at menopause, midlife physical activity level, and time on plasma p-tau217/Aβ42 ratio, adjusted for baseline age and years of education plus their interactions with time. Shaded regions depict 95% confidence intervals.

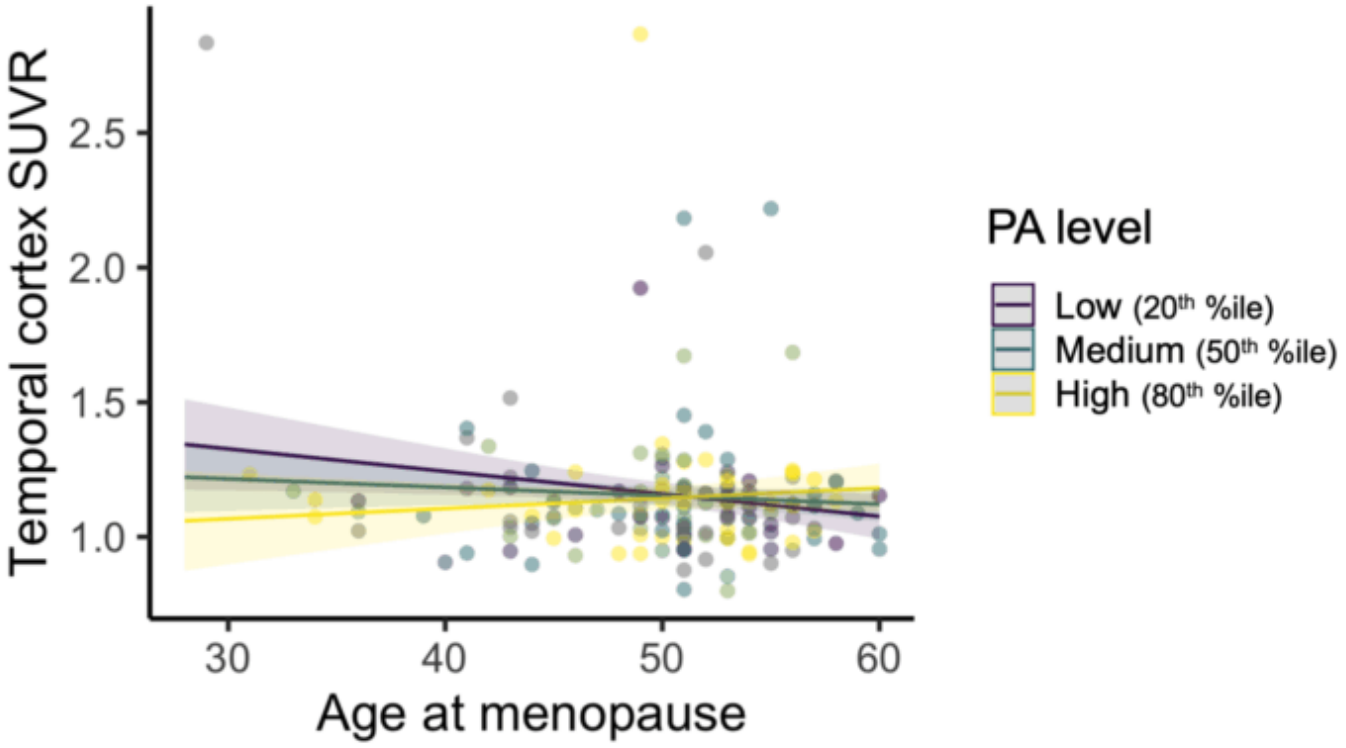


Figure 3. Interactive association of age at menopause and physical activity (PA) with temporal cortex tau-PET SUVR. The plot depicts the interaction between age at menopause and midlife physical activity level on SUVR in a temporal cortex meta-ROI, adjusted for global Aβ-PET, age and years of education. Shaded regions depict 95% confidence intervals.

Keywords: tau-PET, menopause, physical activity, plasma biomarkers, cognitive decline

88 Improved tau PET signal detection with total-body PET compared to conventional PET: A preliminary study

Christina Young[1], Reimund Bayerlein[1], Anjan Bhattarai[1], Charles DeCarli[1], Ramsey Badawi[1], Audrey Fan[1]

[1]*University of California Davis, Davis, CA, US*

Background: In addition to efforts to develop new PET tracers and processing pipelines to improve early detection of amyloid and tau, there has also been substantial innovation in PET scanners themselves. One notable example of this is the uEXPLORER PET/CT scanner, which is the first total-body PET/CT scanner with a sensitivity that is higher than a conventional high-performance PET scanner for single organ imaging. Currently, how the improved sensitivity on new PET scanners impacts tau quantification, and thus its potential for improving early detection, is unknown.

Objective: To compare tau PET signal obtained on the uEXPLORER to a conventional high-performance PET scanner.

Methods: 18F-PI-2620 tau PET data were collected on the uEXPLORER from 16 older adults (**Table 1**). Data collected 45-75 min post-injection were reconstructed in two ways: (1) using all counts from the uEXPLORER and (2) a spatially downsampled dataset to mimic the event collection on a conventional high-performance PET scanner. More specifically, the uMI 550 was emulated and the Thalamus was centered in the 30-cm long field-of-view. PET data were co-registered with each participant's MRI data and SUVRs were calculated using an inferior cerebellum reference regions.

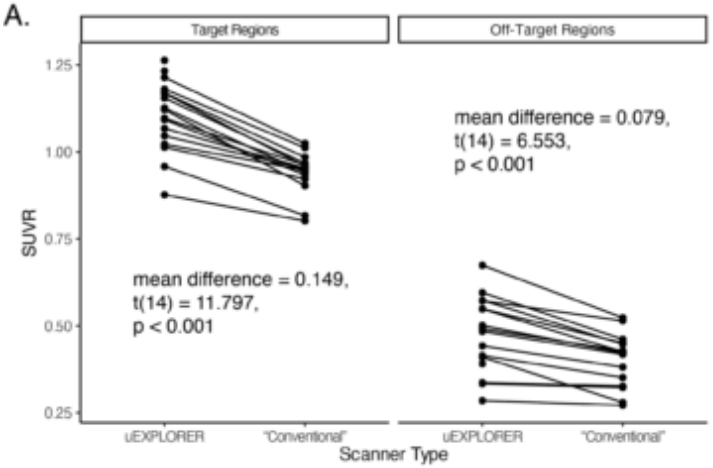
Results: In our sample of participants with low tau burden, the uEXPLORER provided images with higher SUVRs in both target and off-target regions (**Figure 1**). Across participants, regions with greater tau signal also showed the greatest increase in signal with the uEXPLORER (**Figure 2**). Qualitatively, hotspots of tau burden were easier to visualize on uEXPLORER images compared to conventional PET scanner images, though increased signal in off-target regions including cerebral white matter are important to consider (**Figure 2**).

Conclusions: The total-body PET scanner has the potential to improve early detection of tau, though further evaluation with more participants with a range of tau burden is needed.

Table 1. Participant demographics.

	Diagnosis		
	Cognitively Unimpaired (n=12)	Mild Cognitive Impairment (n=2)	Dementia (n=2)
Age, mean (SD) years	76 (6.6)	79 (6.6)	77 (5.7)
Sex, n (%)			
Male	8 (67%)	1 (50%)	1 (50%)
Female	4 (33%)	1 (50%)	1 (50%)

Figure 1. SUVR differences between uEXPLORER and “conventional” PET data shown as a (A) spaghetti plot averaged over all target and off-target regions and as a (B) heatmap with each individual FreeSurfer region.



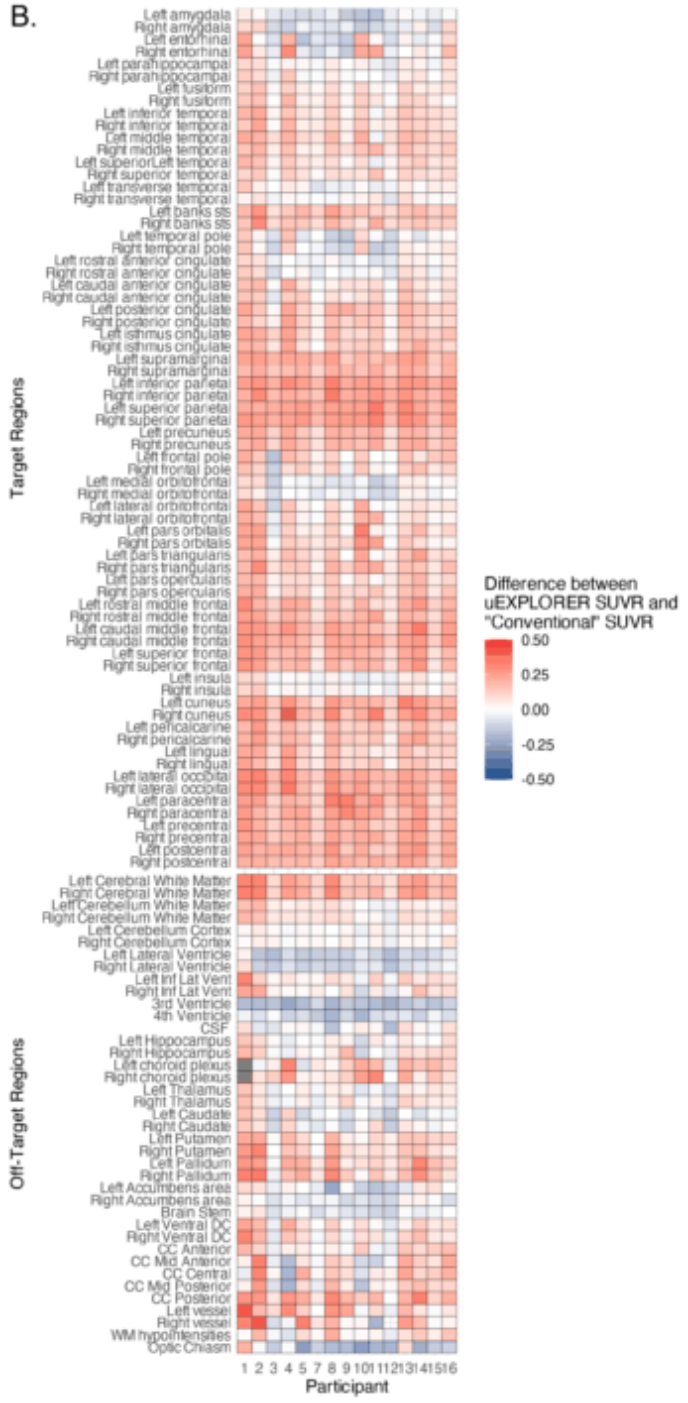
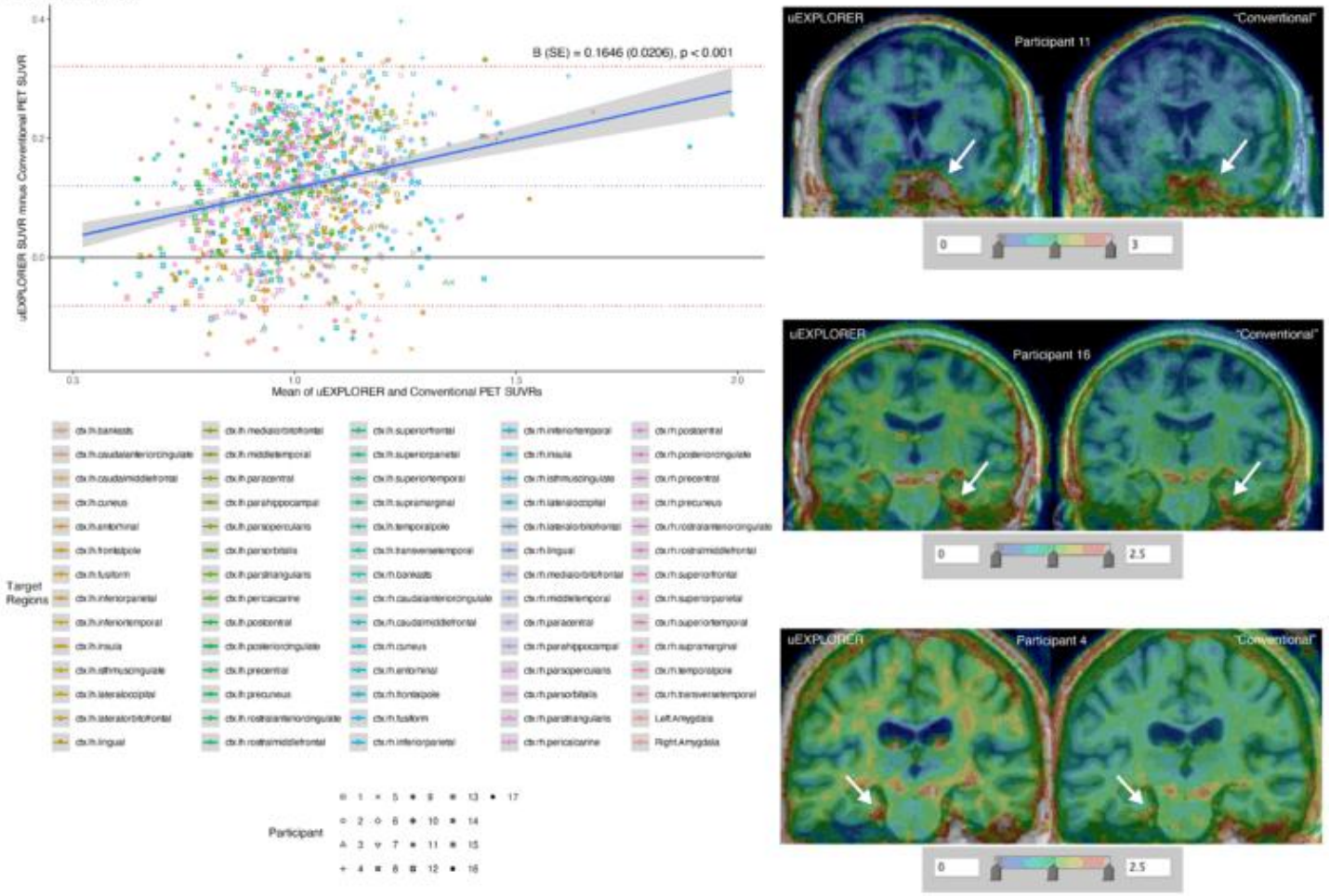


Figure 2. Increased SUVR with the uEXPLORER compared to "conventional" PET data in regions with more tau burden shown both (A) quantitatively and (B) qualitatively.



Keywords: tau PET, total-body PET, 18F-PI-2620, PET scanners, uEXPLORER

89 Demographic associations with plasma biomarkers in the oldest-old: The LifeAfter90 Study

Christina Young[1], Hilary Colbeth[1], Paola Gilsanz[2], Maria Corrada[3], Batool Rizvi[1], Sitong Zhou[1], Jacopo di Lucente[1], Charles DeCarli[1], Lee-Way Jin[1], Rachel Whitmer[1]

[1]*University of California Davis, Davis, CA, US*
[2]*Kaiser Permanente Northern California, Pleasanton, CA, US*
[3]*University of California Irvine, Irvine, CA, US*

Background: Although plasma biomarkers are increasingly used for the diagnosis of Alzheimer's disease, our understanding of these biomarkers in the oldest-old is limited. This study examines the association of plasma biomarkers with age, sex, and ethnoracial group in the LifeAfter90 cohort, a population-based sample of those over 90 years old.

Methods: Plasma biomarkers from 435 participants without dementia in the *LifeAfter90* Study (**Table 1**) were measured on the Quanterix Simoa platform. Participants had a mean (SD) age of 94 years (SD: 2.3, range = 90-103), were majority female (62%, n=270), and were from diverse ethnoracial backgrounds [30% Asian (n=131), 23% Black (n=100), 18% LatinX (n=79), 6% Multiple/Other (n=28), 22% White (n=96)]. Blood samples were analyzed for AB42/AB40, pTau-181, pTau-217, GFAP, and NfL. A series of linear models were used to examine the effects of age, sex, and ethnoracial effects on each plasma biomarker.

Results: Even in this restricted age range, older age was significantly associated with higher pTau-217, GFAP, and NfL levels (**Figure 1A**). Males had higher pTau-181 values than females, whereas females had higher GFAP values than males (**Figure 1B**). Significant differences between White, Asian, and Multiple ethnoracial groups were found with pTau-217 and GFAP with the White group having the lowest values (**Figure 1C**). All results adjusted for other demographic variables.

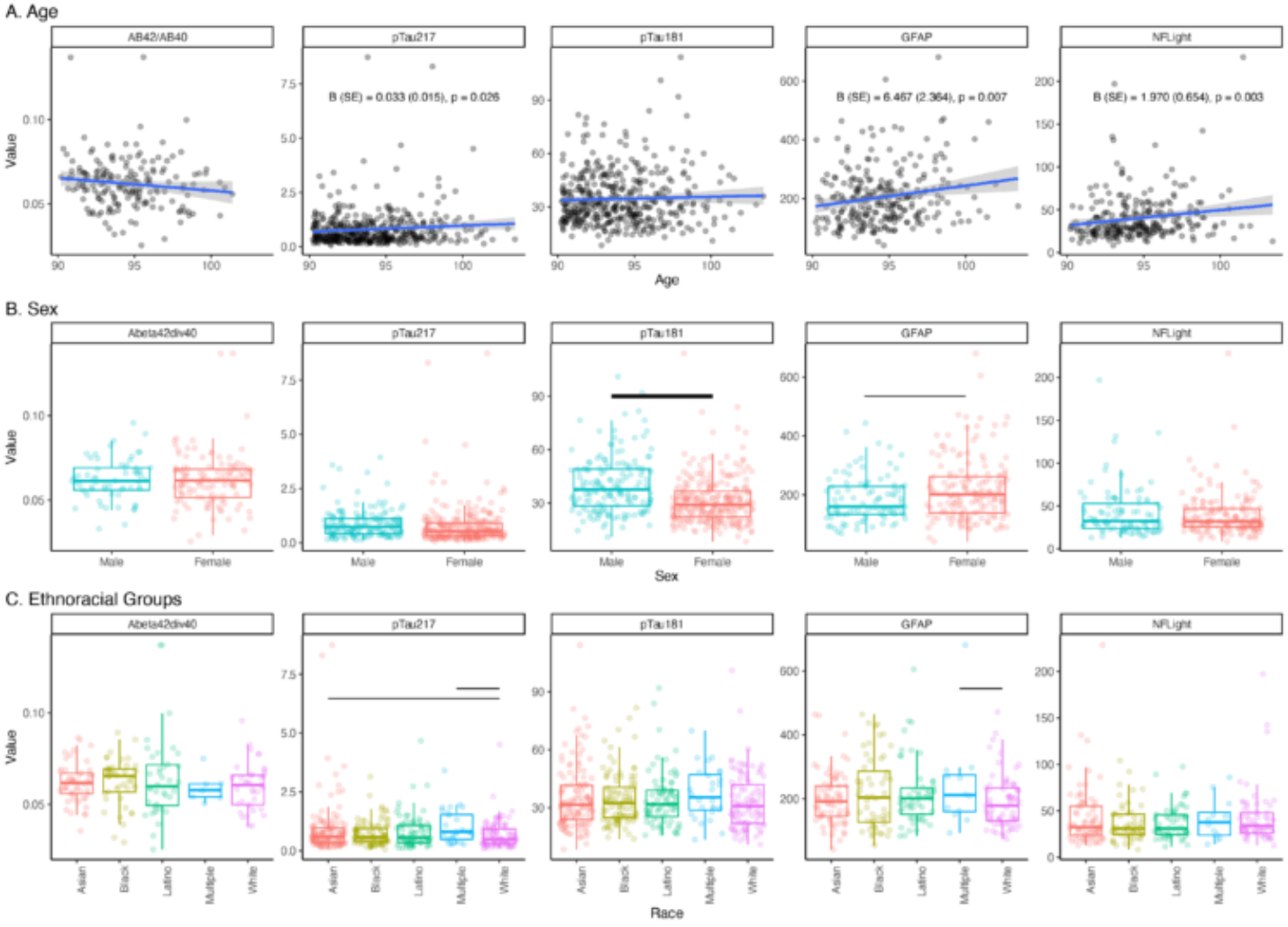
Conclusions: Plasma biomarkers are associated with key demographic variables including age, sex, and race/ethnicity in the oldest-old. Future work will further investigate these differences including examining plasma biomarker associations cognition and amyloid PET.

Table 1. Participant demographics.

	Asian N = 131[1]	Black N = 100[1]	LatinX N = 79[1]	Multiple N = 28[1]	White N = 96[1]	Overall N = 434[1]
Age	93.80 (2.75)	93.62 (2.74)	94.51 (2.71)	93.32 (2.58)	94.61 (2.58)	94.04 (2.72)
Sex						
Male	51 (39%)	38 (38%)	28 (35%)	12 (43%)	36 (38%)	165 (38%)
Female	80 (61%)	62 (62%)	51 (65%)	16 (57%)	60 (63%)	269 (62%)
AB42/40	0.06 (0.01)	0.06 (0.01)	0.06 (0.02)	0.06 (0.01)	0.06 (0.01)	0.06 (0.01)
Unknown	81	56	41	20	59	257
pTau-217	0.90 (1.18)	0.72 (0.50)	0.81 (0.71)	1.01 (0.73)	0.68 (0.58)	0.80 (0.83)
Unknown	1	2	1	0	0	4
pTau-181	35.06 (16.25)	34.40 (13.26)	34.55 (13.91)	37.31 (13.26)	33.29 (14.77)	34.57 (14.62)
Unknown	2	0	0	0	0	2
GFAP	198.72 (81.19)	217.32 (111.52)	216.04 (100.59)	244.90 (152.18)	191.25 (82.29)	206.33 (96.66)
Unknown	57	44	25	16	27	169
NfL	43.04 (32.94)	36.58 (19.75)	37.55 (17.83)	40.93 (22.66)	42.23 (29.38)	40.25 (26.39)
Unknown	57	44	25	16	27	169

[1] Mean (SD); n (%)

Figure 1. Demographic associations with (A) age, (B) sex, (C) ethnoracial group for AB42/AB40, pTau-217, pTau-181, GFAP, and NfL plasma biomarkers. Linear models were conducted for each plasma biomarker and included age, sex, and ethnoracial group. Note: horizontal black lines denote significant differences at $p < 0.05$ whereas the thick black line denotes significant differences at $p < 0.001$.



Keywords: plasma biomarkers, oldest-old, Quanterix Simoa

90 Differential sensitivity of T1-MRI and FDG-PET for tracking neurodegeneration across progressive stages of tau pathology in Alzheimer's disease

Orfeas Vourkas[1], Stamatia Karagianni[2], Alexis Moscoso[2], Linda Zhang[1], Pascual Sanchez-Juan[1], Michael Schöll[2], Michel. J Grothe[1], Jesús Silva-Rodríguez[1]

[1]*CIEN Foundation, Reina Sofia Alzheimer Center, ISCIII, Madrid, Spain*
[2]*University of Gothenburg, Gothenburg, Sweden*

Introduction: Structural MRI and FDG-PET are typically considered interchangeable modalities for assessing Alzheimer's disease (AD)-related neurodegeneration. However, their relative sensitivity and complementarity across advancing stages of tau pathology remain unclear. Here, we directly compared MRI and FDG-PET patterns across progressively increasing stages of tau-PET burden.

Methods: The study involved 544 ADNI participants who underwent FDG-PET, T1-MRI and tau-PET using [^{18}F]Flortaucipir. Tau-PET burden was classified using two different staging schemes. First, stages 0–3 were defined based on the sequential regional involvement of the medial temporal lobe (MTL), temporoparietal, and frontal cortices, paralleling neuropathological Braak staging. Second, *Tau-SPEX* was applied, a novel approach categorizing individuals based solely on the spatial extent of suprathreshold tau-PET signal (Stage 0: 0-0.5%, 1: 0.5-5%. 2: 5-15%, 3: >15%). MRI-derived gray matter volumes and FDG-PET SUVRs were compared across tau-PET stages via ANCOVA, correcting for age and inter-scan interval. Cognitively unimpaired individuals at stage 0 served as a reference group.

Results: Using pseudo-Braak staging (Fig.1), MRI detected pronounced MTL atrophy at stages 1–2 (hippocampus, $d = 1.29$), whereas FDG-PET showed smaller but notable temporo-parietal hypometabolism at stage 2 ($d < 0.63$). At stage 3, MRI effects remained strongest in the hippocampus ($d = 1.57$), while FDG-PET revealed a broader temporo-parietal pattern. Using *Tau-SPEX* (Fig. 2), neither modality showed significant effects at stage 1. At stage 2, MRI changes were confined to the temporal lobe (hippocampus, $d = 1.2$), whereas FDG-PET already exhibited extensive temporoparietal hypometabolism, which intensified at stage 3, when MRI effects also became more pronounced ($d = 1.6$).

Discussion: MRI appeared more sensitive to localized tau-PET burden restricted to the MTL, while FDG-PET hypometabolism was more correlated with progressive cortical tau-PET accumulation. The stage- and region-specific differences between the two modalities highlight their synergistic roles in detecting and tracking AD-related neurodegeneration in vivo.

Fig.1

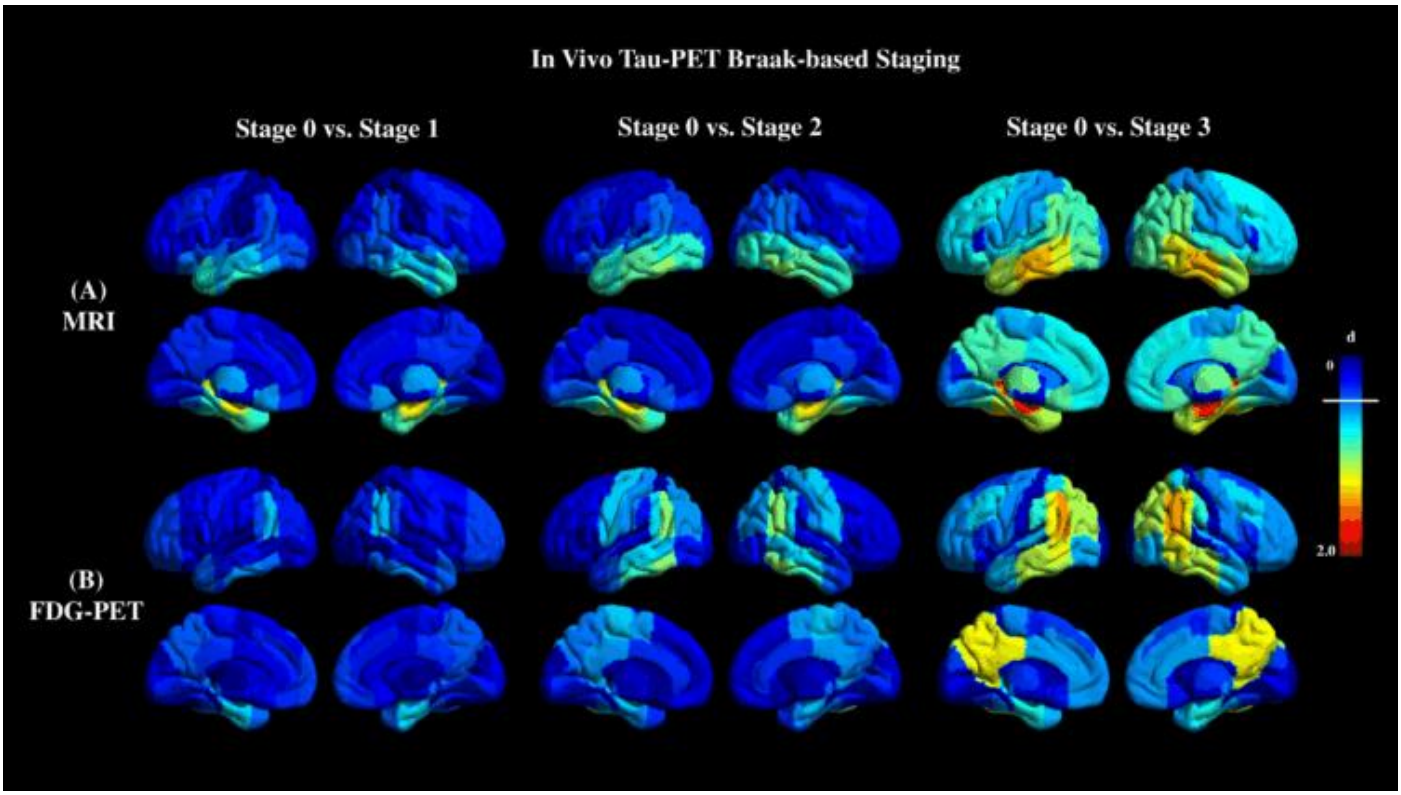
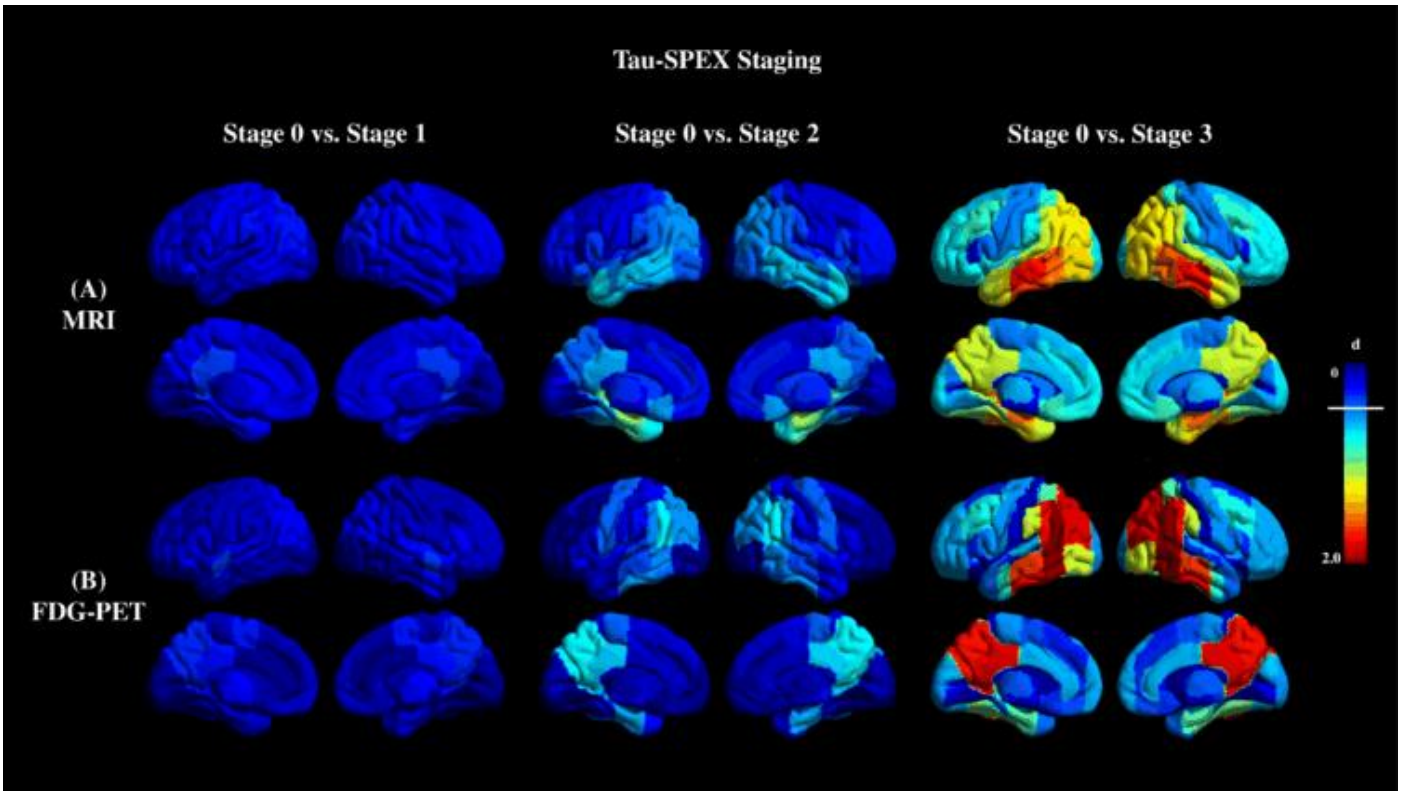


Fig.2



Keywords: Alzheimer's disease, Tau pathology, FDG-PET, MRI, Neurodegeneration

91 SPARE-Tau, a machine-learning derived tau-PET index, correlates with Alzheimer's disease and related dementias biomarkers

David Wang[1], Yuheng Zeng[1], Jon Toledo[2], Mitzi Gonzales[3], Nicolas Honnorat[1], Sokratis Charisis[1,4,5], Mengjin Dong[1], Ngoc Huynh Ho[1], Tanweer Rashid[1], Niyas Shamsudin Kutty[1], Umber Salman[6], Penny Vroman[6], Sudha Seshadri[1], Mohammad Habes[1]

[1]*Neuroimage Analytics Laboratory (NAL) and the Biggs Institute Neuroimaging Core (BINC), Glenn Biggs Institute for Alzheimer's and Neurodegenerative Diseases, University of Texas Health Science Center San Antonio, San Antonio, TX, US*
[2]*Nantz National Alzheimer Center, Stanley Appel Department of Neurology, Houston Methodist Hospital, Houston, TX, US*
[3]*Department of Neurology, Cedars-Sinai Medical Center, Los Angeles, CA, US*
[4]*Department of Neurology, Massachusetts General Hospital, Boston, MA, US*
[5]*Harvard Medical School, Boston, TX, US*
[6]*Department of Radiology, University of Texas Health Science Center San Antonio, San Antonio, TX, US*

Importance: Tau pathology drives Alzheimer's disease (AD) clinical progression, but current global tau-PET measures such as standardized uptake value ratios (SUVR) treat all brain regions equally, obscuring clinically meaningful patterns of tau deposition. We developed SPARE-Tau (Spatial Pattern of Abnormality for Recognition of Tau), a machine-learning index, to summarize weighted regional tau deposition, enhancing sensitivity and precision. We then validated SPARE-Tau with established AD CSF markers, and investigated SPARE-Tau's association with established AD plasma markers.

Methods: Using 1,034 ADNI participants with 18F-Flortaucipir tau-PET, SPARE-Tau was trained on 625 control and pathological participants (269 Aβ+ MCI/dementia, 356 Aβ- CN) via support vector machines and validated through leave-one-out cross-validation. Linear regression models examined SPARE-Tau associations with CSF and plasma AD biomarkers, adjusting for age, sex, and education. Analyses were stratified by β-amyloid status with interaction terms testing differential associations. Spearman's rank correlation compared biomarker associations. We controlled for multiple comparisons using the Benjamini-Hochberg procedure with a false discovery rate (FDR) threshold of 5%.

Results: SPARE-Tau achieved AUC=0.912 [0.895,0.942] (sensitivity=0.781 [0.730,0.829], specificity=0.946 [0.922,0.969]) in classifying Aβ+ MCI/dementia. Top regions contributing to SPARE-Tau followed the Braak staging, including medial temporal lobes and limbic structures. In β-amyloid-positive participants, SPARE-Tau showed strong associations with AD biomarkers, particularly tau-related markers: CSF pTau181/Aβ42 (β=0.513 [0.414,0.612]; ρ=0.577 [0.487,0.650]) and plasma pTau217/Aβ42 (β=0.766 [0.686,0.847]; ρ=0.752 [0.697,0.800]). CSF pTau181/Aβ42 showed stronger associations than CSF pTau181 (β=0.261 [0.191,0.331]; ρ=0.439 [0.327,0.543]), but plasma pTau217/Aβ42 and pTau217 (β=0.729 [0.647,0.811]; ρ=0.735 [0.677,0.784]) were comparable to each other. Associations were consistently stronger in β-amyloid-positive participants. SPARE-Tau associated more strongly with GFAP (β=0.184 [0.115,0.252]; ρ=0.320 [0.205,0.427]) than NfL (β=0.086 [0.037,0.134]; ρ=0.221 [0.111,0.324]), p<0.001.

Conclusion: SPARE-Tau demonstrates robust alignment with CSF tau while enabling plasma tau evaluation relative to PET, advancing noninvasive tau pathology monitoring.

	Total (N=1034)	β-Amyloid Positive (N=451)	β-Amyloid Negative (N=537)
Age at PET	74.7(8.6)	76.9(8.1)	72.9(8.5)
Male	476/1034(46.0%)	205/451(45.5%)	250/537(46.6%)
Female	558/1034(54.0%)	246/451(54.5%)	287/537 (53.4%)
Education Years	16.4(2.4)	16.3(2.5)	16.6(2.4)
White	832/1034(80.5%)	390/451(86.5%)	411/537(76.5%)
Black	126/1034(12.2%)	42/451(9.3%)	74/537(13.8%)
Other	76/1034(7.4%)	19/451(4.2%)	52/537 (9.7%)
Hispanic	72/1034(7.0%)	24/451(5.3%)	45/537(8.4%)
Non-Hispanic	959/1034(92.7%)	425/451(94.2%)	491/537(91.4%)
Cognitively Normal	550/1017(54.1%)	174/443(39.3%)	356/530(67.2%)
Mildly Cognitively Impaired	321/1017(31.6%)	152/443(34.3%)	153/530(28.9%)
Dementia	146/1017(14.4%)	117/443(26.4%)	21/530(4.0%)
SPARE-Tau	0.132(2.202)	1.329(2.630)	-0.917(0.801)

Table 1. Baseline Characteristics of Study Participants by Amyloid Status

Continuous variables presented as mean (SD); categorical variables as No./total No. (%). Clinical diagnoses determined using standardized ADNI criteria. Totals may vary due to missing data. Abbreviations: ADNI, Alzheimer's Disease Neuroimaging Initiative; SPARE-Tau, Spatial Pattern of Abnormality for Recognition of Tau.

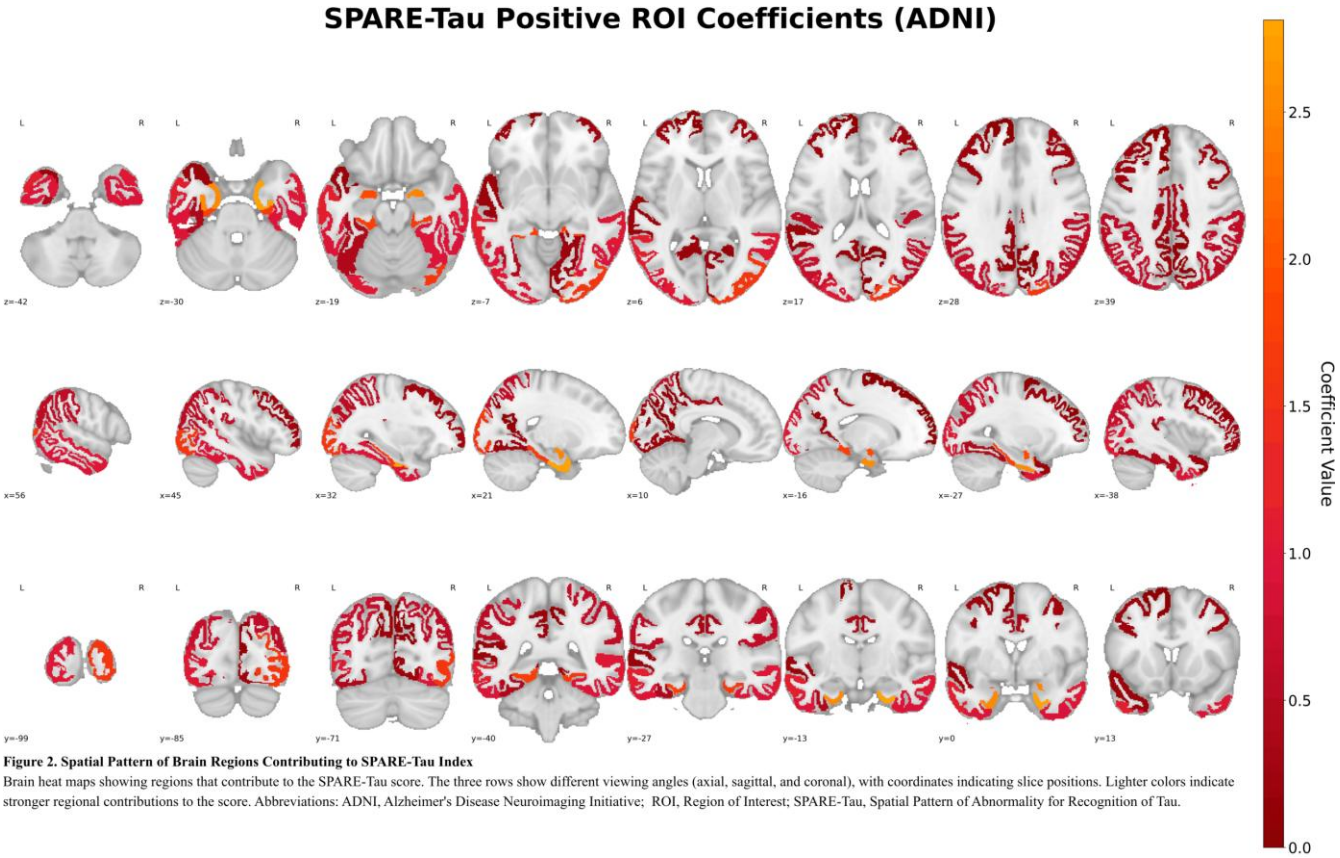


Figure 2. Spatial Pattern of Brain Regions Contributing to SPARE-Tau Index

Brain heat maps showing regions that contribute to the SPARE-Tau score. The three rows show different viewing angles (axial, sagittal, and coronal), with coordinates indicating slice positions. Lighter colors indicate stronger regional contributions to the score. Abbreviations: ADNI, Alzheimer's Disease Neuroimaging Initiative; ROI, Region of Interest; SPARE-Tau, Spatial Pattern of Abnormality for Recognition of Tau.

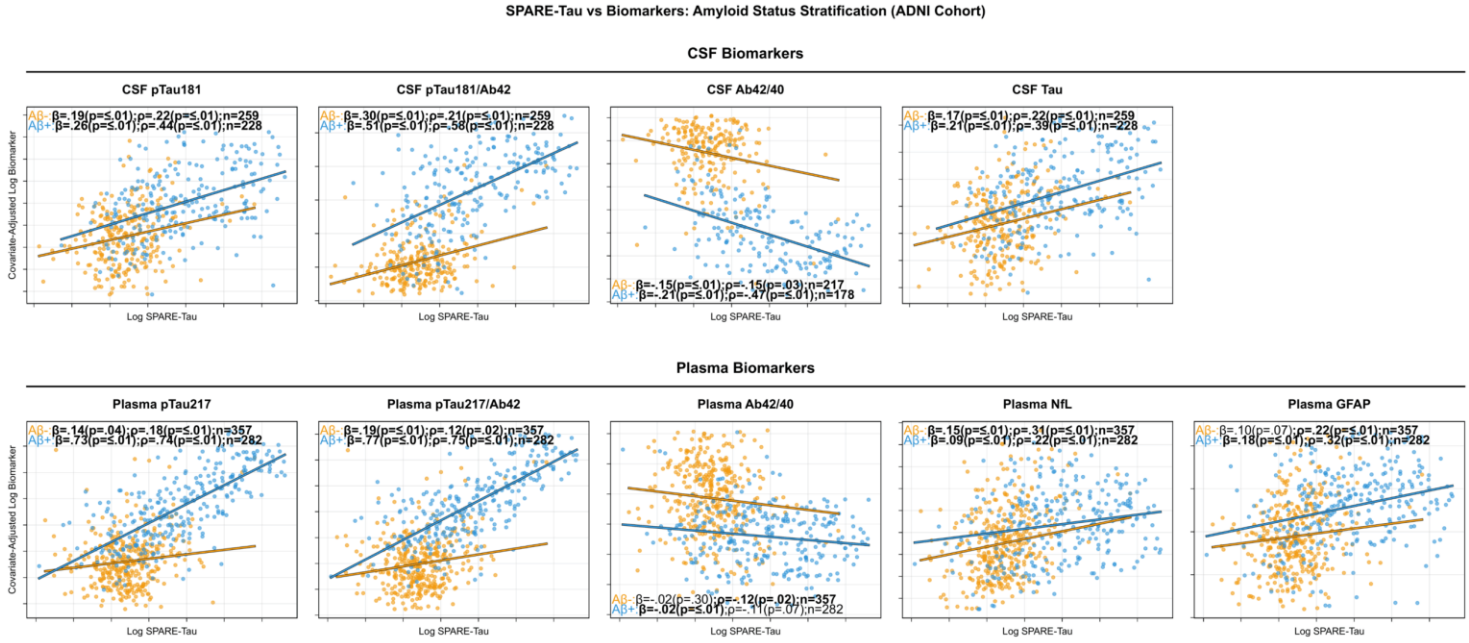


Figure 3. Association Between CSF and Plasma Biomarkers and SPARE-Tau Scores in Amyloid-Positive Participants from the ADNI Cohort

Scatter plots showing associations between log-transformed biomarker concentrations and log-transformed SPARE-Tau scores in β-amyloid-positive participants. Biomarkers and tau PET scans were collected within 180 days. Each point represents one participant. Solid lines show linear regression fits. Standardized regression coefficients (β) and Spearman correlation coefficients (ρ) are displayed with FDR-corrected P values. Regressions were adjusted for age at PET, sex, and education. Abbreviations: Aβ, amyloid-β; ADNI, Alzheimer's Disease Neuroimaging Initiative; CSF, cerebrospinal fluid; GFAP, glial fibrillary acidic protein; NfL, neurofilament light chain; pTau, phosphorylated tau; SPARE-Tau, Spatial Pattern of Abnormality for Recognition of Tau.

Keywords: Alzheimer's disease, Tau pathology, Tau-PET, Biofliud Biomakers, Machine Learning

92 Assessing the generalizability of plasma p-tau217 cutpoints for amyloid-β detection across clinical and preclinical cohorts

Tianshu Liu[1], Xuemei Zeng[2], Michel Nafash[2], Anuradha Sehrawat[2], Lamia Choity[2], Jeremy Gu[2], Marissa Farinas[2], Annie Bedison[3], Cristy Matan[4], Alexandra Gogola[4], Haiqing Huang[5], Kelsey Sewell[5], Eddie McAuley[6], Chuck Hillman[7], Art Kramer[7], Jeff Burns[8], Chaeryon Kang[2], Eric Vidoni[8], Neelesh Nadkarni[9], Howard Aizenstein[2], Julia Kofler[10], Dana Tudorascu[2], C. Elizabeth Shaaban[11], Jennifer Lingler[12], Tharick Pascoal[2], Victor Villemagne[2], Sarah Berman[9], Robert Sweet[2], Beth Snitz[9], Milos Ikonomovic[2], M. Ilyas Kamboh[3], Kirk Erickson[5], Ann Cohen[2], Oscar Lopez[9], Rebecca Deek[1], Thomas Karikari[2]

[1]*Department of Biostatistics and Health Data Science, School of Public Health, University of Pittsburgh, Pittsburgh, PA, US*
[2]*Department of Psychiatry, School of Medicine, University of Pittsburgh, Pittsburgh, PA, US*
[3]*Department of Human Genetics, School of Public Health, University of Pittsburgh, Pittsburgh, PA, US*
[4]*Department of Radiology, School of Medicine, University of Pittsburgh, Pittsburgh, PA, US*
[5]*AdventHealth Research Institute, Orlando, FL, US*
[6]*Department of Health and Kinesiology, University of Illinois at Urbana Champaign, Champaign, IL, US*
[7]*Department of Psychology, College of Science, Northeastern University, Boston, MA, US*
[8]*Department of Neurology, University of Kansas Medical Center, Kansas City, KS, US*
[9]*Department of Neurology, School of Medicine, University of Pittsburgh, Pittsburgh, PA, US*
[10]*Department of Pathology, School of Medicine, University of Pittsburgh, Pittsburgh, PA, US*
[11]*Department of Health Promotion and Development, School of Nursing, University of Pittsburgh, Pittsburgh, PA, US*
[12]*Department of Health and Community Systems, School of Nursing, University of Pittsburgh, Pittsburgh, PA, US*

Background: Plasma p-tau217 is a promising blood biomarker in tracking abnormal AD pathology. Although various cutpoints have been proposed across studies, it remains unclear how transferable these thresholds are when derived from diverse cohorts.

Methods: We evaluated the transferability of plasma p-tau217 cutpoints across an academic memory clinic cohort (ADRC [n=243]) and two preclinical cohorts (HCP [n=224] and IGNITE [n=348]). Plasma p-tau217 was measured using the Quanterix ALZpath assay, and amyloid pathology was determined via PiB PET (ADRC, 55% A+; HCP, 15% A+) or Florbetaben PET (IGNITE, 17% A+). Cutpoints were derived using logistic regression within each cohort as the training set by maximizing F1 score. We then transferred these cutpoints to the other cohorts to assess their generalizability.

Results: ADRC had highest plasma p-tau217 levels (median 0.68pg/mL), followed by IGNITE (0.34pg/mL) and HCP (0.25pg/mL). Logistic regression identified the optimal cutpoints to be highest in ADRC (0.69pg/mL), followed by IGNITE (0.52pg/mL) and HCP (0.39pg/mL). Transferring the cutpoint from the clinical cohort (ADRC) to the preclinical cohorts (HCP and IGNTE) substantially reduced positive predictive values (PPV) from 90.9% in ADRC to 70.6% in HCP and 68.9% in IGNITE, while increasing negative predictive values (NPV) to 89.9% in HCP and 90.8% in IGNITE (from 74.4% in ADRC). More comparable performance was observed when transferring cutpoints between preclinical cohorts. Applying the HCP-derived cutpoint to IGNITE yielded a PPV of 41.4% and NPV of 97.3%, compared to 47.1% PPV and 98.0% NPV in HCP. In the reverse direction, transferring the IGNITE cutpoint to HCP resulted in 54.5% PPV and 93.8% NPV, compared to 64.0% PPV and 91.5% NPV in IGNITE.

Conclusion: Our results underscore the variability in transferring plasma p-tau217 cutpoints across cohorts with differing characteristics. Effective clinical implementation of p-tau217 requires careful consideration of the demographic and clinical context of the intended population.

Keywords: Blood biomarkers, p-tau217 assay, cognition, cutpoints

93 Evaluating the transferability of dual cutpoints for plasma p-tau217 in detecting brain amyloid-β across diverse cohorts

Tianshu Liu[1], Xuemei Zeng[2], Michel Nafash[2], Anuradha Sehrawat[2], Lamia Choity[2], Jeremy Gu[2], Marissa Farinas[2], Annie Bedison[3], Cristy Matan[4], Alexandra Gogola[4], Haiqing Huang[5], Kelsey Sewell[5], Eddie McAuley[6], Chuck Hillman[7], Art Kramer[7], Jeff Burns[8], Chaeryon Kang[2], Eric Vidoni[8], Neelesh Nadkarni[9], Howard Aizenstein[2], Julia Kofler[10], Dana Tudorascu[2], C. Elizabeth Shaaban[11], Jennifer Lingler[12], Tharick Pascoal[2], Victor Villemagne[2], Sarah Berman[9], Robert Sweet[2], Beth Snitz[9], Milos Ikonomovic[2], M. Ilyas Kamboh[3], Kirk Erickson[5], Ann Cohen[2], Oscar Lopez[9], Rebecca Deek[1], Thomas Karikari[2]

[1]*Department of Biostatistics and Health Data Science, School of Public Health, University of Pittsburgh, Pittsburgh, PA, US*
[2]*Department of Psychiatry, School of Medicine, University of Pittsburgh, Pittsburgh, PA, US*
[3]*Department of Human Genetics, School of Public Health, University of Pittsburgh, Pittsburgh, PA, US*
[4]*Department of Radiology, School of Medicine, University of Pittsburgh, Pittsburgh, PA, US*
[5]*AdventHealth Research Institute, Orlando, FL, US*
[6]*Department of Health and Kinesiology, University of Illinois at Urbana Champaign, Champaign, IL, US*
[7]*Department of Psychology, College of Science, Northeastern University, Boston, MA, US*
[8]*Department of Neurology, University of Kansas Medical Center, Kansas City, KS, US*
[9]*Department of Neurology, School of Medicine, University of Pittsburgh, Pittsburgh, PA, US*
[10]*Department of Pathology, School of Medicine, University of Pittsburgh, Pittsburgh, PA, US*
[11]*Department of Health Promotion and Development, School of Nursing, University of Pittsburgh, Pittsburgh, PA, US*
[12]*Department of Health and Community Systems, School of Nursing, University of Pittsburgh, Pittsburgh, PA, US*

Background: Plasma p-tau217 is robust for detecting amyloid pathology, but ideal classification thresholds are not yet established. A dual cutpoint approach with an intermediate zone is increasingly used to reduce misclassification. This study evaluates the transferability of dual cutpoints across diverse cohorts.

Methods: We included three cohorts: one clinical (ADRC, n=3484; 243 with PET [ADRC-PET]) and two preclinical (HCP, n=224; IGNITE, n=348). Plasma p-tau217 was measured using the ALZpath assay, and amyloid status in ADRC-PET (55% A+) and HCP (15% A+) was determined by PiB PET and IGNITE (17% A+) by Florbetaben PET. Dementia status was defined by a Clinical Dementia Rating, with global score≥1 as demented. Dual cutpoints (90% sensitivity and 90%specificity) were derived via logistic regression on 70% of each cohort and tested on the remaining 30% and across cohorts.

Results: Plasma p-tau217 levels were highest in ADRC (median 0.68pg/mL), followed by IGNITE (0.34pg/mL) and HCP (0.25pg/mL). Dual cutpoints from ADRC-PET performed well within the same cohort, achieving 75% accuracy for A+, 84.4% for A− cases, with 11.1% unclassified. In the full ADRC cohort, both A+ and intermediate-zone individuals had higher odds of baseline dementia (OR = 4.99 and 2.23, respectively), with the intermediate group showing the fastest progression. Transferring ADRC cutpoints to IGNITE and HCP reduced A+ accuracy (52.5% and 36.4%) but maintained high A− accuracy (90.7% and 96.3%) and low unclassified rates (6.6% and 1.8%). Transfers between preclinical cohorts improved A+ detection but lowered A− accuracy: HCP-to-IGNITE yielded 89.8% A+, 26.6% A−, and 41.1% unclassified; IGNITE-to-HCP yielded 42.4% A+, 91.1% A−, and 8.5% unclassified.

Conclusion: Our results show that cutpoints from clinical cohorts worked well for identifying A- individuals in preclinical cohorts but were less accurate for A+. This highlights the importance of considering population characteristics when applying plasma p-tau217 in the clinic.

Keywords: Blood biomarkers, p-tau217 assay, cognition, cutpoints

94 Free-water interacts with amyloid positivity to predict regional tau pathology in both early and late Braak stages

Aditi Sathe[1], Alaina Durant[1], Mary Ellen Koran[2,3], Logan Dumitrescu[1,4,5], Karly Cody[6], Andrzej Sokołowski[6], Michael Kim[7], Jesse Mez[8], Andrew Saykin[9], Arthur Toga[10], Michael Cuccaro[11], Duygu Tosun[12], Sterling Johnson[13], Robert Barber[14], Sid O'Bryant[14], Bennett Landman[2,15], Elizabeth Mormino[16,17], Timothy Hohman[1,4,5], Derek Archer[1,4,5]

[1]*Vanderbilt Memory and Alzheimer's Center, Vanderbilt University Medical Center, Nashville, TN, US*
[2]*Department of Radiology and Radiological Sciences, Vanderbilt University Medical Center, Nashville, TN, US*
[3]*Department of Radiology, Mayo Clinic of Arizona, Scottsdale, AZ, US*
[4]*Department of Neurology, Vanderbilt University Medical Center, Nashville, TN, US*
[5]*Vanderbilt Genetics Institute, Vanderbilt University Medical Center, Nashville, TN, US*
[6]*Department of Neurology and Neurological Sciences, Stanford University, Stanford, CA, US*
[7]*Department of Computer Science, Vanderbilt University, Nashville, TN, US*
[8]*Department of Neurology, Boston University Chobanian & Avedisian School of Medicine, Boston, MA, US*
[9]*Indiana Alzheimer's Disease Research Center, Department of Radiology and Imaging Sciences and Department of Medical and Molecular Genetics, Indiana University School of Medicine, Indianapolis, IN, US*
[10]*Alzheimer's Disease Research Center, Keck School of Medicine, University of Southern California, Los Angeles, CA, US*
[11]*Department of Human Genetics, University of Miami, Miami, FL, US*
[12]*Department of Radiology and Biomedical Imaging, University of California San Francisco, San Francisco, CA, US*
[13]*Alzheimer's Disease Research Center, Department of Medicine, University of Wisconsin, Madison, WI, US*
[14]*Texas College of Osteopathic Medicine, UNT Health, Fort Worth, TX, US*
[15]*Vanderbilt University Institute of Imaging Science, Vanderbilt University Medical Center, Nashville, TN, US*
[16]*Department of Neurology and Neurological Sciences, Stanford University, Stanford, CA, US*
[17]*Wu Tsai Neuroscience Institute, Stanford University, Stanford, CA, US*

Diffusion MRI (dMRI)-derived bi-tensor free-water (FW) is sensitive to microstructural alterations in extracellular space, a key feature of neuroinflammation and neurodegeneration in Alzheimer's disease (AD). We hypothesized that higher regional white matter FW would be linked to greater tau accumulation in both early and late Braak stage regions, in an amyloid-dependent manner. Using harmonized, multi-site imaging data from the ADSP Phenotype Harmonization Consortium (N=1246; 69.35 ± 8.92 years; 56% female; 59% Non-Hispanic White; 34% APOE-ε4 positive; 66% cognitively unimpaired), we analyzed cross-sectional interactions between FW from 43 JHU atlas white matter regions and global amyloid positivity status on tau-PET SUVRs in Braak 1–2 (early) and Braak 6 (late) regions. Separate analyses were conducted for 18F-flortaucipir and 18F-PI-2620 tau tracers and meta-analyzed across the two. All models included age, sex, education, race/ethnicity, and APOE-ε4 positivity as covariates, with false discovery rate correction for multiple comparisons.

Significant FW × amyloid interactions were observed in 27 of 43 WM regions for Braak 6 and in 21 regions for Braak 1/2 after FDR correction. The strongest effects for late-stage tau (Braak 6) involved the precuneus WM, splenium of the corpus callosum, and fornix column and body, while early-stage tau (Braak 1/2) effects were most prominent in the genu of the corpus callosum, superior temporal gyrus WM, and the inferior fronto-occipital fasciculus. When stratified by amyloid status, no FDR-significant associations remained in the amyloid-negative group, whereas the amyloid-positive group retained all major effects and showed additional WM regions with significant FW–tau SUVR associations.

These findings indicate that amyloid positivity amplifies the relationship between white matter microstructural changes and both early and late tau deposition, with the most robust effects observed in callosal and limbic tracts

central to AD. FW in these tracts may serve as a sensitive marker of amyloid-associated network vulnerability.

Table 1: Participant characteristics

Number of participants		1246
Age (years)		69.35 ± 8.92
Sex	Male	544 (44%)
	Female	702 (56%)
Education (years)		15.13 ± 3.36
Race	Non-Hispanic White	737 (59%)
	Non-Hispanic Black	261 (21%)
	Other	248 (20%)
APOE-ε4 positivity		422 (34%)
Tracer	^{18}F-flortaucipir	621 (50%)
	^{18}F-PI-2620	625 (50%)
Diagnostic status	Cognitively unimpaired	802 (66%)
	Mild cognitive impairment	349 (29%)
	Alzheimer's disease	62 (5.1%)
	Unknown	33

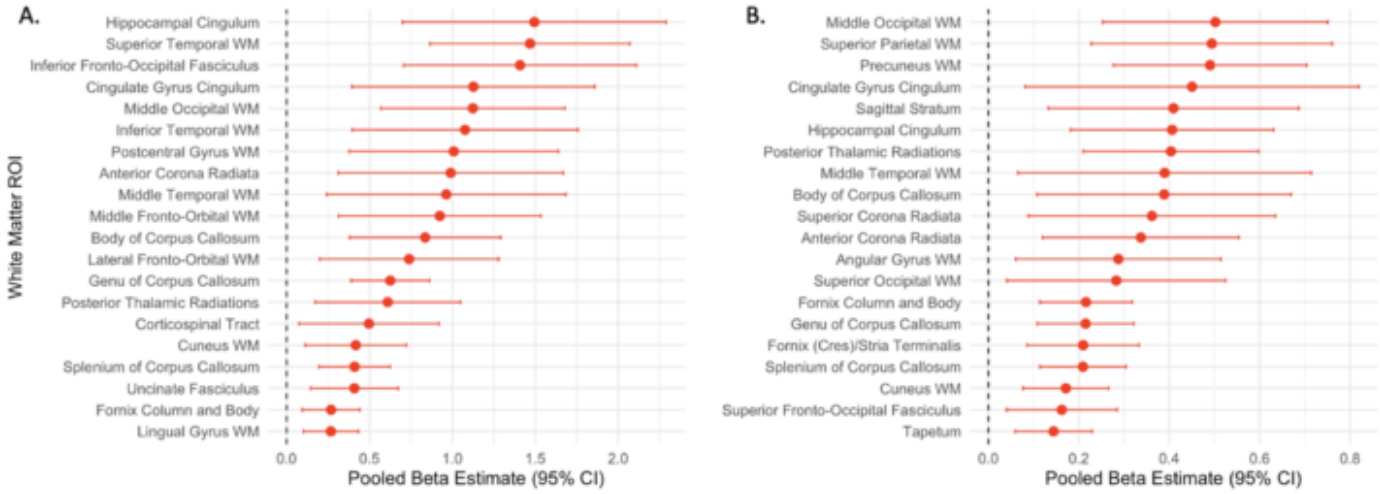


Figure 1: FDR-significant effects for FW × amyloid positivity on Tau SUVR in (A) Braak 1/2 regions (B) Braak 6 regions

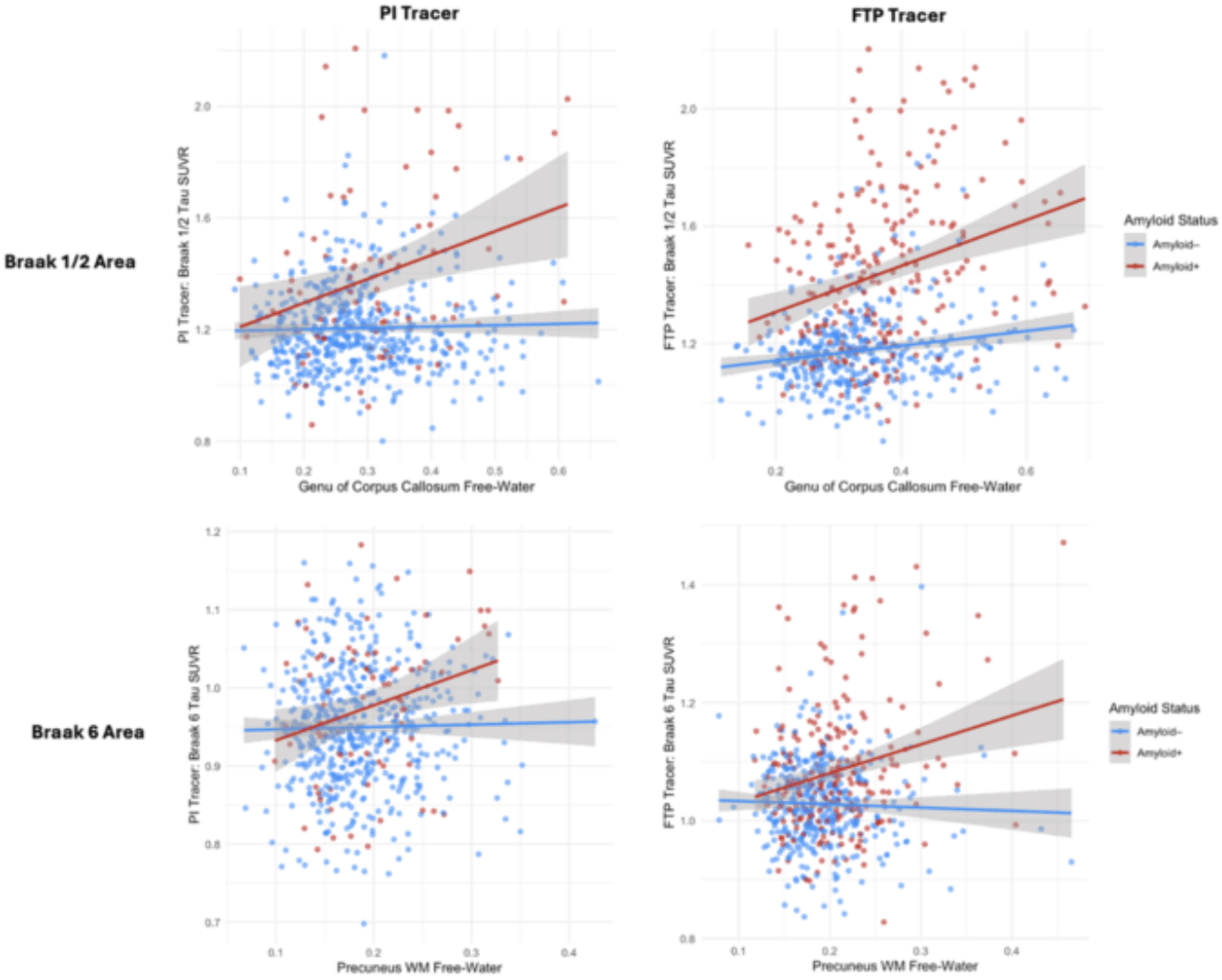


Figure 2: Interaction plots illustrating the relationship between regional FW and tau SUVR in white matter ROIs showing the strongest FW × amyloid status effects. Columns correspond to tau tracers (PI, left; FTP, right), and rows correspond to outcome regions (Braak 1/2, top; Braak 6, bottom).

Keywords: Tau-PET, Amyloid, Diffusion MRI, Free-water, Alzheimer's Disease

95 Integration of data-driven biomarker discovery with established Alzheimer's disease biomarkers in an African American cohort

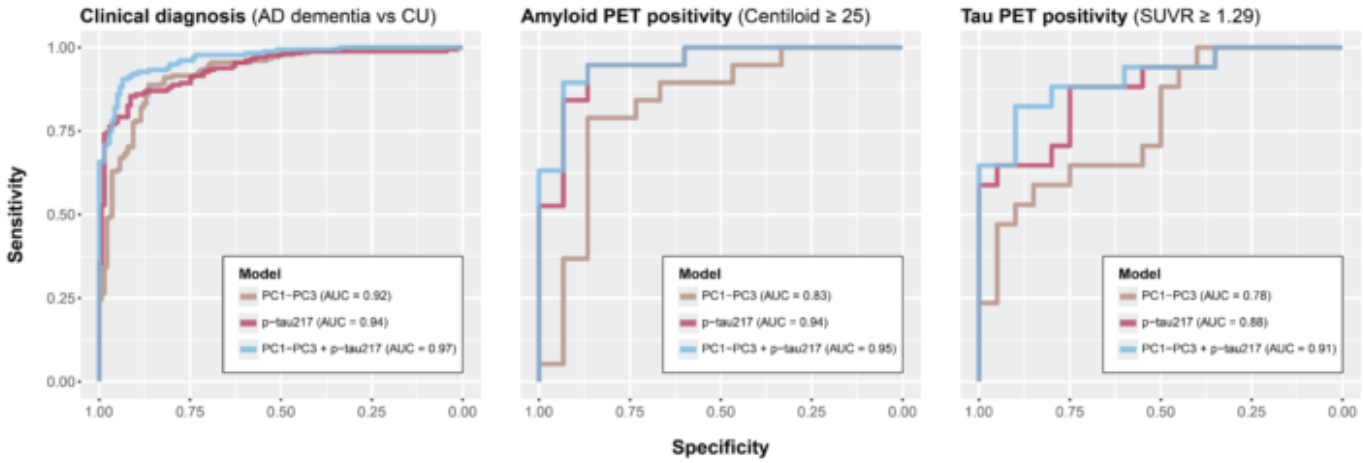
Lindsey Kuchenbecker[1], Michael Heckman[2], Thuy Nguyen[1], Heidi Casellas[1], Katie Sotelo[1], Christopher Schwarz[3], Matthew Senjem[3,4], Manoj Jain[5], John Lucas[6], Floyd Willis[7], Nilufer Ertekin-Taner[1,8], Neill Graff-Radford[8], Kejal Kantarci[3], Val Lowe[3], Christian Lachner[8], Gregory Day[8], Minerva Carrasquillo[1]

[1]*Department of Neuroscience, Mayo Clinic Florida, Jacksonville, FL, US*
[2]*Department of Quantitative Health Sciences, Mayo Clinic Florida, Jacksonville, FL, US*
[3]*Department of Radiology, Mayo Clinic, Rochester, MN, US*
[4]*Department of Information Technology, Mayo Clinic, Rochester, MN, US*
[5]*Department of Radiology, Mayo Clinic Florida, Jacksonville, FL, US*
[6]*Department of Psychiatry, Mayo Clinic Florida, Jacksonville, FL, US*
[7]*Department of Family Medicine, Mayo Clinic Florida, Jacksonville, FL, US*
[8]*Department of Neurology, Mayo Clinic Florida, Jacksonville, FL, US*

Background: Plasma biomarkers offer a more accessible alternative to established diagnostic tools for Alzheimer's disease (AD), yet current candidates capture only a subset of disease-related pathways and lack validation across broad populations. Previously, through untargeted proteomics and machine learning, we identified 36 plasma proteins that classified AD dementia versus cognitively unimpaired (CU) with an area under the curve (AUC) of 0.94 in an African American cohort. These results were consistent across external plasma and brain cohorts. Here, we evaluate the added value of these proteins alongside p-tau217.

Methods: Plasma proteome and p-tau217 measurements were obtained using SomaScan 7k and Simoa assays in participants clinically diagnosed with AD dementia (n=181) or CU (n=142). Given limited sample size, the top three principal components (PC1-PC3) of the 36 proteins, rather than individual proteins, were used as predictors in logistic regression models to classify AD dementia, amyloid PET positivity (PiB Centiloid ≥25), and tau PET positivity (flortaucipir temporal meta-ROI SUVR ≥1.29) in participants with amyloid (n=34) and tau (n=37) PET scans within one year of blood collection.

Results: The previously nominated 36 proteins consistently improved classification accuracy for clinical diagnoses and amyloid and tau PET positivity. To classify AD dementia diagnosis, AUCs were 0.92 (PC1-PC3), 0.94 (p-tau217), and 0.97 combined. To classify amyloid PET positivity, 0.83 (PC1-PC3), 0.94 (p-tau217), and 0.95 combined. To classify tau PET positivity, AUCs were 0.78 (PC1-PC3), 0.88 (p-tau217), and 0.91 combined. Notably, of the 36 proteins associated with diagnosis, 11 were not associated with p-tau217, suggesting that they capture diverse processes beyond endpoint AD pathology, including lipid trafficking, synaptic function, and matrisome biology.



Conclusion: This pilot study highlights the complementary value of data-driven biomarker discovery to enhance established AD biomarkers and promote precision medicine approaches. Future work aims to characterize the 36 proteins in larger, more diverse, longitudinal cohorts.

Keywords: plasma, proteome, health equity, precision medicine, neuroimaging

96 Early concordance between Aβ PET spatial extent and plasma %ptau217

Michelle Farrell[1], Emma Thibault[1], Hyun-sik Yang[1,2], Julie Price[1,3], Jasmeer Chhatwal[1,2], Gillain Coughlan[1], Rachel Buckley[1,2], Reisa Sperling[1,2], Keith Johnson[1,2]

[1]*Massachusetts General Hospital, Harvard Medical School, Boston, MA, US*
[2]*Brigham & Women's Hospital, Harvard Medical School, Boston, MA, US*
[3]*Athinoula A. Martinos Center for Biomedical Imaging, Charlestown, MA, US*

Background: Plasma %ptau217 is a sensitive predictor of global Aβ-PET positivity (>20CL), yet many individuals are ptau+/PET− (<20CL) and ptau-/PET+ in the 20-30CL range. We tested whether a more sensitive PET metric of early Aβ (spatial extent) reduces plasma-PET discordance at low global Aβ levels and used longitudinal follow-up to assess whether discordance reflects measurement error or temporal precedence in Aβ detection.

Methods: Analyses included 250 low Aβ (<30CL) cognitively-unimpaired older adults (Table 1) from the Harvard Aging Brain Study, followed for up to 10 years. Aβ spatial extent (EXT; %PIB+) was dichotomized as EXT+>7.3% PIB+, as previously determined. C2N mass spectrometry-derived plasma %ptau217 (ptau217/nptau217*100) was classified as ptau+>4.2%. Baseline analyses assessed plasma-PET concordance under 30CL using conventional PET criteria (PET− <20CL, PET+ 20–30CL) versus EXT+/−. Longitudinal analyses tracked participants from the first visit showing positivity on either biomarker (EXT+ or ptau+) to examine subsequent global Aβ accumulation (DVR slope) and to determine whether discordance reflected false positives (reversion to EXT-/ptau-) or temporal precedence (progression to EXT+/ptau+).

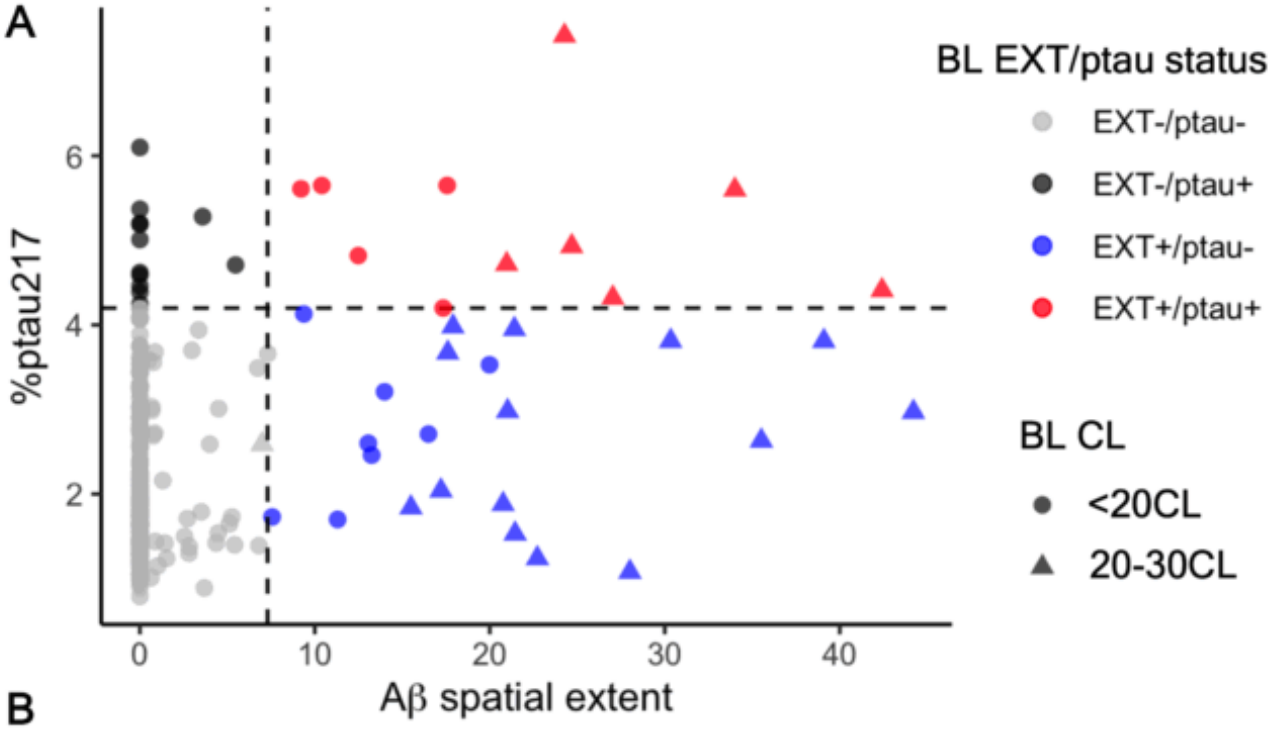
Results: Using EXT (Figure 1) modestly increased PET+/ptau+ concordance, reduced PET−/ptau+ discordant cases but increased PET+/ptau- cases. Longitudinally, EXT+/ptau+ participants showed the fastest Aβ accumulation, followed by EXT+/ptau- and EXT-/ptau+ groups (Figure 2). Among discordant cases, reversion was rare for EXT+/ptau- (1/16, 6%) but more common for EXT-/ptau+ (9/15, 60%; OR=20.0, p=.002). Progression to EXT+/ptau+ was more frequent in EXT+/ptau- (8/16, 50%) than in EXT-/ptau+ (3/15, 20%) but not significantly different.

Conclusion: Amyloid EXT reduced PET-/ptau+ discordance at low Aβ levels. Most EXT+/ptau- cases were longitudinally confirmed to continue accumulating Aβ, whereas EXT-/ptau+ cases often reflected false ptau positivity, though some were confirmed cases of ptau217 elevation preceding PET. EXT+/ptau+ individuals showed the fastest Aβ accumulation, suggesting that plasma %ptau217 may help identify those most likely to rapidly accumulate Aβ.

	EXT-/ptau-	EXT-/ptau+	EXT+/ptau-	EXT+/ptau+
n	205	12	22	11
n (%) 20-30CL	1 (0.4%)	0	14 (64%)	6 (55%)
Age, years	69.7 (0.54)	76.7 (2.25)	72.2 (1.66)	76.3 (2.35)
SEX, n (%) female	122 (60%)	6 (50%)	20 (91%)	7 (64%)
Education, years	15.8 (0.21)	16.3 (0.86)	14.9 (0.64)	15.1 (0.90)
APOE, n (%) e4	25/156 (16%)	1/10 (10%)	6/18 (33%)	5/11 (45%)
PIB follow-up length	4.67 (0.22)	3.51 (0.89)	3.53 (0.66)	2.26 (0.93)
Race				
White	161	9	16	7
Black	35	2	7	3
Asian/Native	7	1	0	0
%non-white	20%	25%	32%	27%

Table 1. Sample Demographics by baseline EXT/ptau status.

A



B

PET criteria	Visit	PET-/ptau-	PET-/ptau+	PET+/ptau-	PET+/ptau+	SE	SP	PPV	NPV
EXT>7.3%	BL	205	12	22	11	33%	94%	48%	90%
	First	164	29	37	18	33%	85%	38%	82%
CL>20	BL	212	17	15	6	28%	93%	26%	93%
	First	189	33	17	9	35%	85%	21%	92%

Figure 1. Correspondence of plasma %ptau217 and Aβ spatial extent below 30CL. A) A scatterplot depicts the baseline association between %ptau217 and Aβ EXT, colored by baseline EXT/ptau status based on the EXT>7.3% threshold (dashed vertical line) and %ptau217> 4.2% (dashed horizontal line). Additionally, global Aβ PET positivity is indicated by shape (PET- <20CL: circles, PET+ >20CL: triangles). B) Counts for PET/ptau status is reported using the EXT PET criteria and conventional CL>20 criteria both at baseline (BL) and expanded (First) to include individuals who were EXT-/ptau- at baseline but became either PET+ or ptau+ at any follow-up (whichever came first). Sensitivity (SE), specificity (SP), positive predictive value (PPV), and negative predictive value (NPV) of ptau+ for PET+ (EXT+ or CL+) are also shown.

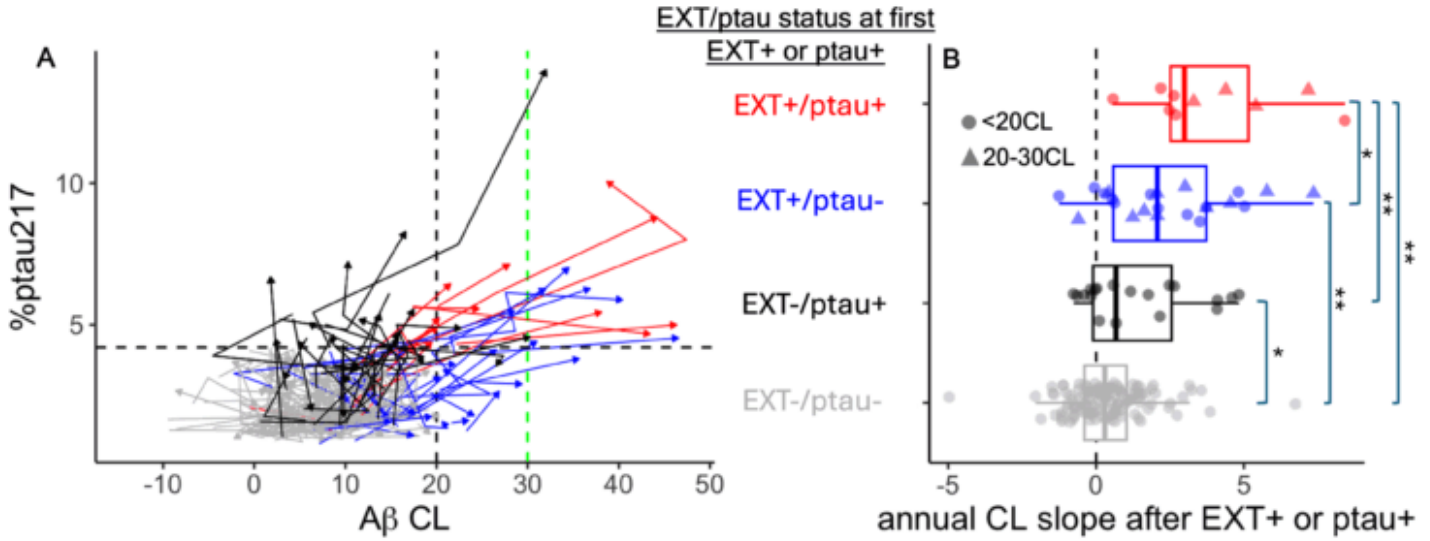


Figure 2. Longitudinal follow-up after first instance of EXT or %ptau217 positivity. For both panels, EXT/ptau status at the first instance of EXT+ or ptau+ is depicted by color. A) A spaghetti plot shows individual trajectories of global Aβ CL and %ptau217 over up to 4 visits over 10 years. All (10/10) EXT+/ptau+ individuals (red) with at least one follow-up PET scan after becoming EXT+/ptau+ remained EXT+, though 1/10 reverted to ptau-. Of 16 discordant EXT+/ptau- (blue) cases with available follow-up, 15/16 remained EXT+ and 8/16 progressed from ptau- to ptau+, supporting that EXT+/ptau- represent individuals for whom Aβ detection with PET preceded detection with plasma ptau217. Of 15 discordant EXT+/ptau- (blue) cases with available follow-up (EXT+/ptau-, black), 9/15 reverted to ptau- at follow-up and 3/15 remain ptau+ and progressed to EXT+. This suggests that while %ptau217 may sometimes reflect early Aβ detection before detectability with PET, EXT-/ptau+ cases are frequently false positives that revert to ptau-. However, replication in a larger sample is a critical next step. B) Slopes of global Aβ accumulation (CL slope) from first EXT or ptau positivity onwards were computed within each individual using ordinary least squares regression. A boxplot depicts differences in CL slope by EXT/ptau group, with global Aβ PET positivity indicated by shape (PET- <20CL: circles, PET+ >20CL: triangles). All pairwise comparisons for differences in CL slope were significant after correction for multiple comparisons (*<.05, **<.001) except between EXT+/ptau- and EXT-/ptau+. The rate of accumulation rate was greatest (and consistently positive) for the EXT+/ptau+ group.

Keywords: plasma, ptau217, early detection, spatial extent, preclinical

Tuesday, January 13, 2026 - 10:50 am - 12:20 pm

Podium Session

SESSION IV: Longitudinal biomarker measurements of tau pathology

CHAIRS:

***William Jagust**, University of California, Berkeley, Berkeley, CA, USA*

***Heidi Jacobs**, Massachusetts General Hospital, Boston, MA, USA*

Tuesday, January 13, 2026			
10:50 am – 12:20 pm	**Podium Presentation**	**Authors**	**Presenters**
10:55 am – 11:10 am	Preliminary comparative longitudinal performance of Flortaucipir and MK6240: rates of change, effect sizes, and power estimates in the HEAD Study	Bauer-Negrini | Ferreira | Povala | Bellaver | Lussier | Amaral | Tudorascu | Finn | Masdeu | Fortea | Soleimani-Meigooni | Lowe | Oh | Pascual | Gordon | Rosa-Neto | Baker | Pascoal	**Guilherme Bauer-Negrini**, University of Pittsburgh, Department of Psychiatry, Pittsburgh, PA, US
11:10 am – 11:25 am	Standardized expression of longitudinal tau accumulation using the CenTauR scale	Moscoso Rial | Leuzy | Lau Raket | Klein | Kolb | Iaccarino | Rowe | Saad | Jack Jr | Schwarz | Tonietto | Karten | Tatton | DelBene | Gogola | Villemagne | Doré | Lopresti	**Brian J Lopresti**, Department of Radiology, School of Medicine, University of Pittsburgh, Pittsburgh, PA, US
11:25 am – 11:40 am	TauPace as a novel, time-based metric to investigate accelerated tau and clinical progression in preclinical AD	Coath | Bruzzone | Morse | Navaratna | Carey | Christian | Asthana | Johnson | Betthauser	**William Coath**, Wisconsin Alzheimer's Disease Research Center, University of Wisconsin School of Medicine and Public Health, Madison, WI, US
11:40 am – 11:55 am	Proteomic signatures track tau spread in Alzheimer's disease	Macedo | Pola | Woo | Hosseini | Rahmouni | Trudel | Therriault | Bezgin | Beker | Machado | Chan | Aumont | Zheng | Hall | Lebrun | Tissot | Servaes | Gonçalves | Mitchel | Bellaver | Ashton | Zetterberg | Blennow | Pascoal | Zimmer | Benedet | Rosa-Neto	**Arthur C. Macedo**, McGill University, Montreal, QC, Canada

Preliminary comparative longitudinal performance of Flortaucipir and MK6240: rates of change, effect sizes, and power estimates in the HEAD Study

Guilherme Bauer-Negrini[1], Pamela C.L Ferreira[1], Guilherme Povala[1], Bruna Bellaver[1], Firoza Z. Lussier[1], Livia Amaral[1], Dana L. Tudorascu[1], Quentin Finn[2], Joseph Masdeu[2], Juan Fortea[3], David N. Soleimani-Meigooni[4,9], Val Lowe[5], Hwamee Oh[6], Belen Pascual[2], Brian A. Gordon[7], Pedro Rosa-Neto[8], Suzanne Baker[9], Tharick A. Pascoal[1]

[1]*University of Pittsburgh, Department of Psychiatry, Pittsburgh, PA, US*
[2]*Houston Methodist Research Institute, Department of Neurology, Houston, TX, US*
[3]*Hospital de la Santa Creu i Sant Pau, Sant Pau Memory Unit, Department of Neurology, Barcelona, Spain*
[4]*University of California San Francisco, Memory and Aging Center, San Francisco, CA, US*
[5]*Mayo Clinic, Department of Radiology, Rochester, MN, US*
[6]*Brown University, Department of Psychiatry and Human Behavior, Providence, RI, US*
[7]*Washington University in St. Louis, Department of Radiology, St. Louis, MO, US*
[8]*Translational Neuroimaging Laboratory, McGill University Research Centre for Studies in Aging, Douglas Research Institute, Montréal, Canada*
[9]*Lawrence Berkeley National Laboratory, Berkeley, CA, US*

Background: Tau-PET tracers identify and monitor tau pathology progression in Alzheimer's disease (AD). However, different tracers present distinct binding patterns throughout the brain. We provide a preliminary head-to-head comparison of the longitudinal performance of Flortaucipir and MK6240 by leveraging the HEAD Study.

Methods: We longitudinally assessed 129 individuals [8 young, 75 cognitively unimpaired (CU), 46 cognitively impaired (CI)] with head-to-head Flortaucipir and MK6240 (18-month follow-up). Individuals receiving anti-Aβ therapies between time points were excluded. SUVRs calculation used inferior cerebellar gray matter as reference. Effect size was defined as mean annual change divided by its standard deviation. SUVRs were harmonized using the Uni$\boldsymbol{\tau}$ Ecosystem (uni-tau.com).

Results: No statistically significant tau accumulation was observed in young or CI Aβ-. In CU Aβ-, small tau accumulation in Braak I-II ROI was observed only with MK6240 (Fig.1-2). In CU Aβ+, voxel-wise analyses revealed tau accumulation in temporal regions with both tracers (Fig.1B); however, only MK6240 detected statistically significant accumulation within Braak ROIs (Fig.2). In CI Aβ+, both tracers demonstrated widespread cortical tau accumulation (Fig.1D) with significant increases in Braak III-IV and V-VI ROIs (Fig.2). Overall, MK6240 showed higher rates of accumulation. We investigated how differing progression rates would impact a hypothetical clinical trial (25% drug effect, 80% power, and 0.05 significance) (Fig.3). MK6240 displayed larger effect sizes in both early and late regions of tau accumulation across clinical groups, leading to smaller sample sizes (Fig.3A). Unit harmonization did not fundamentally alter these findings (Fig.3B).

Conclusions: Our preliminary data demonstrate that both tracers can detect annual changes in ROIs for tau accumulation in CI Aβ+. MK6240 significantly detected tau accumulation in CU across Braak ROIs. MK6240's larger effect sizes translate to fewer participants needed for clinical trial recruitment. Additionally, Uni$\boldsymbol{\tau}$ harmonized tau-PET measurements maintain the longitudinal characteristics of each tracer for use in clinical trials.

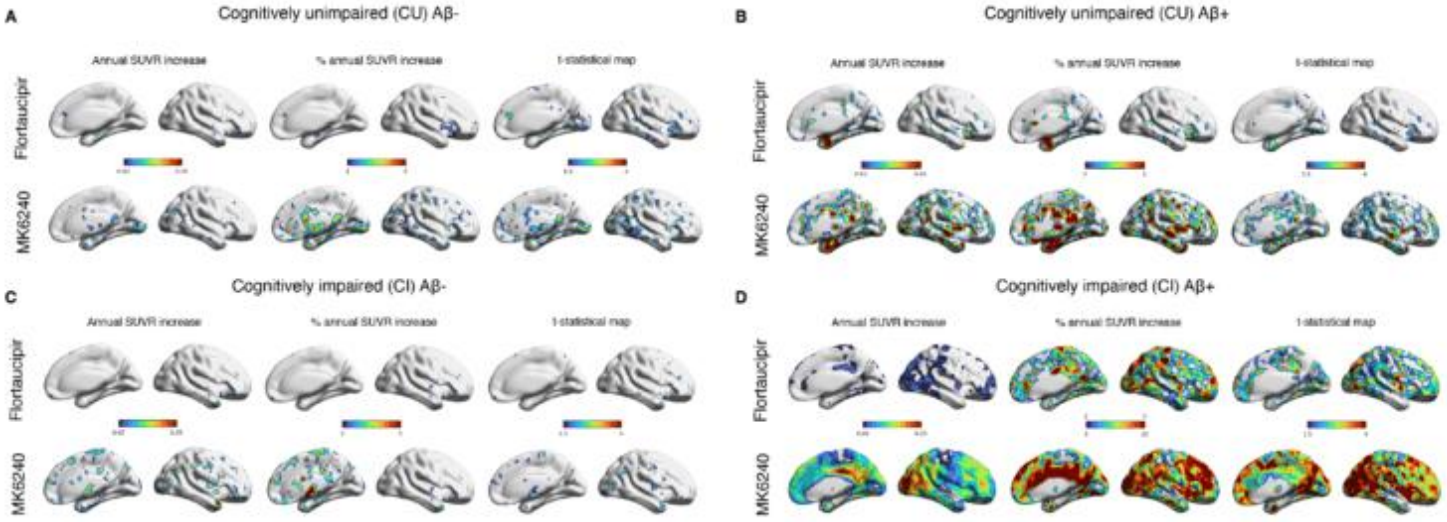


Figure 1 - The area and magnitude of Flortaucipir and MK6240 accumulation in clinical groups. The brain images show the mean annual rate (Δ) of change, percentage of annual change and t-statistical map of tracer uptake overlaid on a structural MRI template.

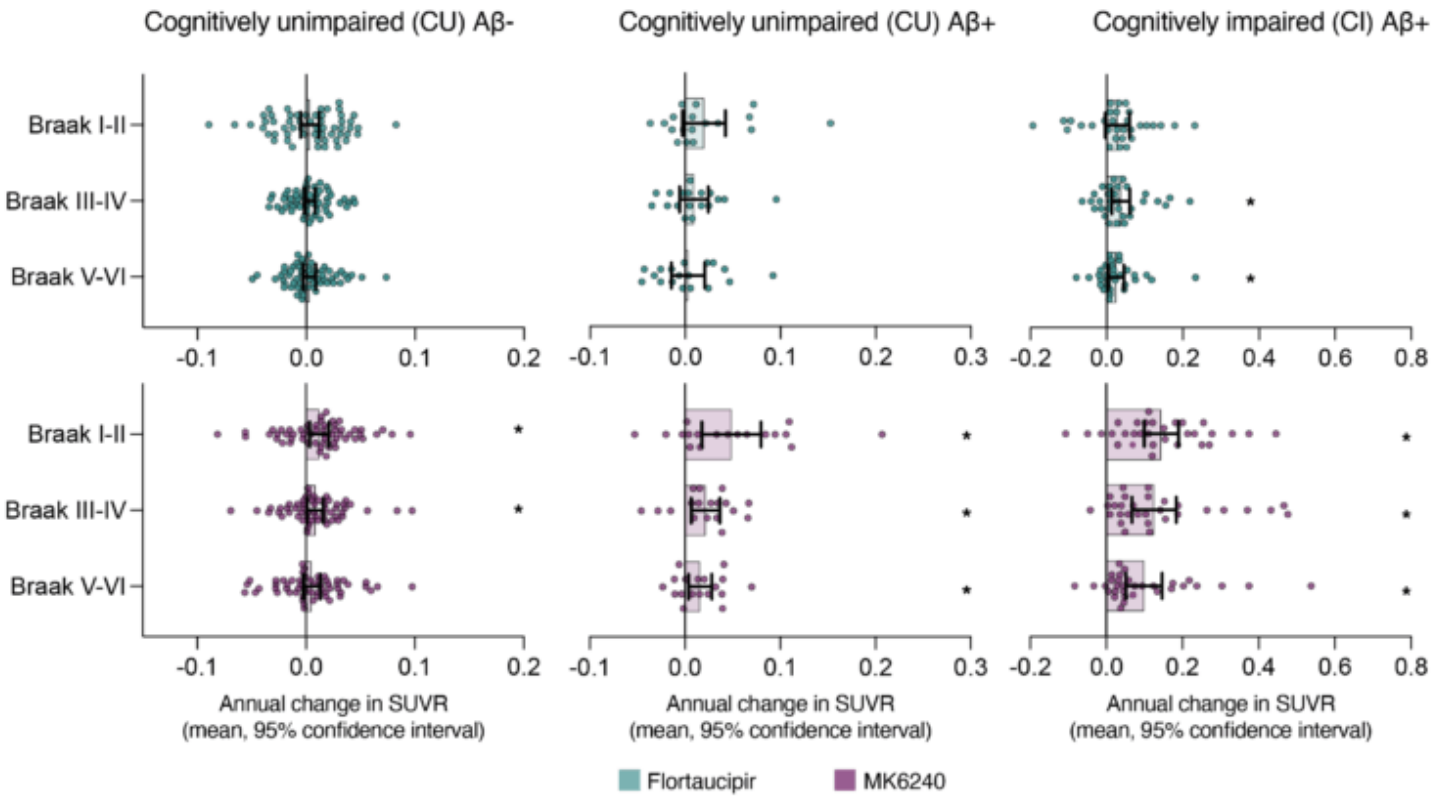


Figure 2 – Annual change in SUVR across Braak regions in clinical groups. Bars show the mean annual rate of change, and confidence intervals that do not cross the zero line indicate a statistically significant tau accumulation (*).

A

ROIs	CU Aβ- (n = 57)				CU Aβ+ (n = 18)				CI Aβ+ (n = 31)			
	Flortaucipir		MK6240		Flortaucipir		MK6240		Flortaucipir		MK6240	
	Effect size	Sample size	Effect size	Sample size	Effect size	Sample size	Effect size	Sample size	Effect size	Sample size	Effect size	Sample size
MTL	0.14	*NS*	0.33	2351	0.40	*NS*	0.75	452	0.34	*NS*	1.08	215
Braak V-VI	0.13	*NS*	0.18	*NS*	0.09	*NS*	0.65	589	0.45	1237	0.77	429

B

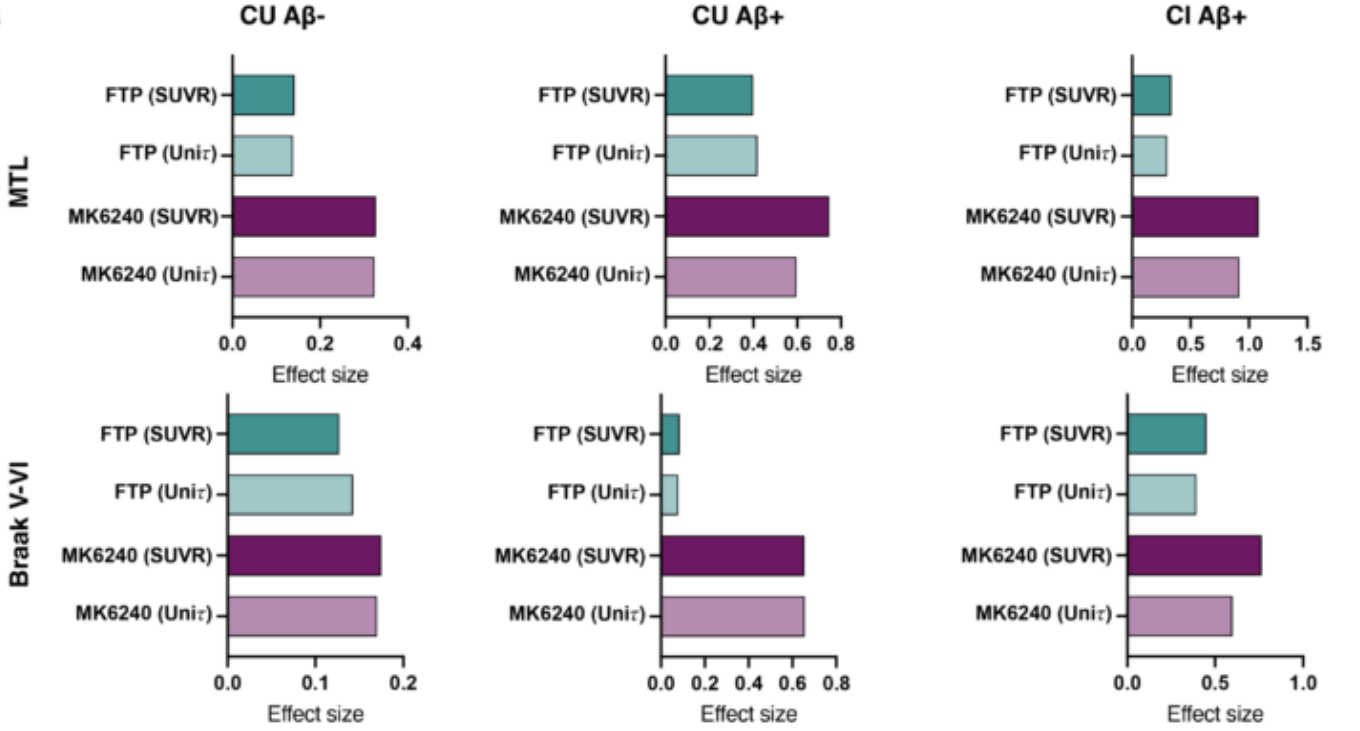


Figure 3 – (A) Effect size and sample size calculation (per arm) for a hypothetical clinical trial using Flortaucipir or MK6240. (B) Effect sizes for Flortaucipir and MK6240 calculated for SUVR and Unit in the medial-temporal lobe (top row) and Braak V-VI regions (bottom row). MTL: medial temporal lobe. NS: mean annual change was not significant.

Keywords: tau PET, longitudinal, Unitau, head-to-head

Standardized expression of longitudinal tau accumulation using the CenTauR scale

Alexis Moscoso Rial[1,2], Antoine Leuzy[1,3], Lars Lau Raket[4], Gregory Klein[5], Hartmuth C Kolb[3], Leonardo Iaccarino[4], Christopher C Rowe[6,7,8], Ziad S Saad[9], Clifford R Jack Jr[10], Christopher G Schwarz[10], Matteo Tonietto[5], Yashmin Karten[1], Nadine Tatton[1], Alex DelBene[11], Alexandra Gogola[11], Victor L Villemagne[12], Vincent Doré[7,13], Brian J Lopresti[11]

[1]*Critical Path for Alzheimer's Disease (CPAD) Consortium, Critical Path Institute, Tucson, AR, US*
[2]*Nuclear Medicine Department and Molecular Imaging Group, Instituto de Investigación Sanitaria de Santiago de Compostela, Santiago de Compostela, Spain*
[3]*Enigma Biomedical Group, Knoxville, TN, US*
[4]*Eli Lilly and Company, Indianapolis, IN, US*
[5]*F. Hoffmann-La Roche Ltd, Basel, Switzerland*
[6]*Department of Molecular Imaging & Therapy, Austin Health, Victoria, AU*
[7]*Florey Department of Neuroscience, University of Melbourne, Victoria, AU*
[8]*The Australian Dementia Network (ADNeT), The University of Melbourne, Victoria, AU*
[9]*Johnson & Johnson, San Diego, CA, US*
[10]*Department of Radiology, Mayo Clinic, Rochester, MN, US*
[11]*Department of Radiology, School of Medicine, University of Pittsburgh, Pittsburgh, PA, US*
[12]*Department of Psychiatry, School of Medicine, University of Pittsburgh, Pittsburgh, PA, US*
[13]*Health and Biosecurity Flagship, The Australian eHealth Research Centre, CSIRO, Victoria, AU*

Introduction: The CenTauR framework has proven effective for harmonizing tau-PET quantitative metrics across radiotracers and quantification pipelines. However, its longitudinal consistency has not yet been evaluated. This study assessed rates of tau accumulation expressed in the CenTauR scale across clinical trials and observational studies to determine the consistency of longitudinal tau-PET changes across populations scanned with different radiotracers.

Methods: Participants were included from the placebo and treatment arms of three clinical trials—A4 (n = 344; [^{18}F]flortaucipir), TANGO (n = 296; [^{18}F]MK-6240), and Tilavonemab (n = 106; [^{18}F]MK-6240)—as well as from the observational ADNI study (n = 219; [^{18}F]flortaucipir). All clinical trials showed nonsignificant treatment effects on tau-PET. Participants were amyloid-β–positive and had a baseline and at least one follow-up tau-PET scan. CenTauR values within the Meta-Temporal region of interest were computed using a standardized SPM12-based SUVR quantification pipeline and Joint Propagation Model–derived conversion equations (Moscoso et al., Alzheimer's Imaging Consortium, 2025). Longitudinal change in CenTauR values was estimated using linear mixed-effects models including baseline CenTauR and trial/cohort as covariates. Models were fitted separately for cognitively unimpaired (CU) and cognitively impaired (CI) groups.

Results: Among CI participants, the mean annual change in CenTauRs was consistent across the clinical trials using [^{18}F]MK-6240 (TANGO: 3.9 CenTauRs, 95% CI [3.0–4.9]; Tilavonemab: 4.4 CenTauRs, 95% CI [1.3–7.4]) and the ADNI study, which used [^{18}F]flortaucipir (3.7 CenTauRs, 95% CI [1.7–5.6])(Figure 1A). Similarly consistent results were observed among CU participants scanned with [^{18}F]flortaucipir in A4 (mean 4-year change: 6.1 CenTauRs, 95% CI [5.5–6.8]) and ADNI (8.4 CenTauRs, 95% CI [5.6–11.2])(Figure 1B).

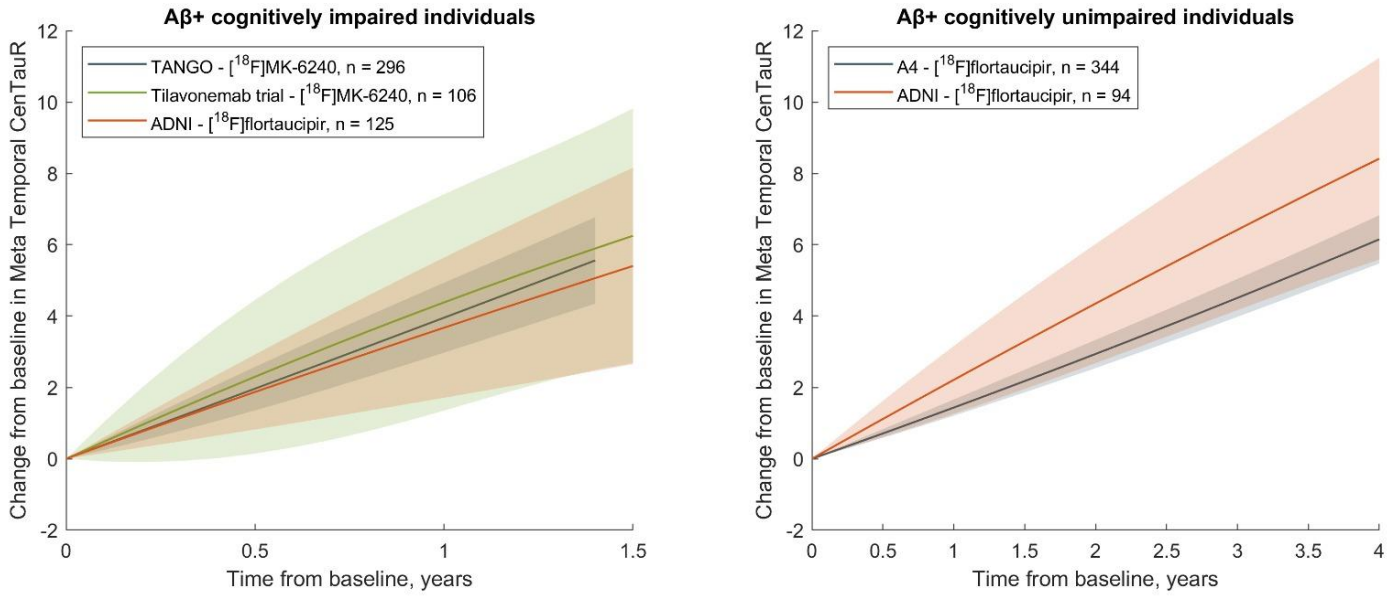


Figure 1. Estimated average change from baseline trajectories in the Meta Temporal CenTauR values for A) cognitively impaired individuals, and B) cognitively unimpaired individuals from different trials and studies using different tau-PET radiotracers. Estimations on A) and B) were conditional on the average baseline CenTauR values of cognitively impaired (65 CenTauRs) or cognitively unimpaired individuals (9 CenTauRs), respectively.

Conclusions: These findings suggest that the CenTauR harmonization approach yields consistent longitudinal estimates across populations scanned with different tau-PET tracers. Future work will extend this evaluation to additional trials, tau-PET tracers, and brain regions.

Keywords: Tau-PET, harmonization, CenTauR, longitudinal, trials

TauPace as a novel, time-based metric to investigate accelerated tau and clinical progression in preclinical AD

William Coath[1,2], Hailey Bruzzone[1,2], Jacob Morse[1,2], Ruvini Navaratna[1,2,4], Finnuella Carey[1,2], Bradley Christian[1,3], Sanjay Asthana[1,2], Sterling Johnson[1,2], Tobey Betthauser[1,2]

[1]*Wisconsin Alzheimer's Disease Research Center, University of Wisconsin School of Medicine and Public Health, Madison, WI, US*
[2]*Department of Medicine, University of Wisconsin-Madison School of Medicine and Public Health, Madison, WI, US*
[3]*Waisman Center, University of Wisconsin-Madison, Madison, WI, US*
[4]*Center for Health Disparities Research, University of Wisconsin School of Medicine and Public Health, Madison, WI, US*

Background: Tau-PET spatial deposition patterns have prognostic value in AD, but current staging systems do not capture tau progression rate. We extended the SILA algorithm to jointly model longitudinal tau trajectories in early and later regions, deriving a subject-specific "TauPace" metric reflecting the temporal offset between regional T+. We applied this metric to determine whether TauPace is associated with time from A+ to T+ and clinical decline.

Methods: Participants (n=762) with [^{18}F]MK-6240 tau and [^{11}C]PiB amyloid-PET from the Wisconsin Registry for Alzheimer's Prevention (WRAP) and Wisconsin ADRC were included. [^{18}F]MK-6240 SUVR in entorhinal and inferior temporal (IT) cortices were analyzed (70-90 min, inferior cerebellum reference). Regional SUVRs were z-scored using Gaussian mixture modeling; positivity was defined as >2SD above the lower distribution mean. SILA estimated regional trajectories were aligned on a unified timeline via nested optimization with basis functions. TauPace was computed as the time shift required to align each participant's IT SUVR to the entorhinal-predicted curve, with positive values indicating faster-than-average tau progression. The association between TauPace and amyloid-to-tau interval was examined. LOESS fits described clinical trajectories (CDR-SB) grouped by TauPace (Fast:>0)

Results: Demographics are summarized in Table 1. The joint model estimated a 3-year population-level delay between entorhinal and IT positivity. 76 individuals were T+ in both regions, all A+ at final scan. Among T+ individuals, TauPace ranged from -5.0 to 7.3 years (Figure 1). Faster TauPace was associated with longer time intervals between amyloid and entorhinal T+ (beta=0.18, *p*=.003, Figure 2A), even when adjusting for entorhinal (beta=0.14, *p*=.009) and IT (beta=0.14, *p*=.006) level. Figure 2B indicates some divergence in longitudinal CDR-SB by TauPace.

Conclusion: The TauPace metric captures individual differences in the temporal spread of tau pathology and relates to the amyloid-to-tau interval. Ongoing work will investigate the association between TauPace and dementia risk in larger samples.

Table 1. Participant demographics.

Total n		762
Female sex, n (%)		518 (68.0)
Mean age at baseline (SD)		67.7 (7.4)
Median (range) longitudinal tau scans (n = 376)		2 (2-6)
Amyloid positive (CL>=15)		254 (34.4)*
Entorhinal T+ (SUVR>=1.29)		166 (21.8)
Inferior Temporal T+ (SUVR>=1.40)		86 (11.8)
Global CDR, n (%)	0	591 (77.6)
	0.5	136 (17.8)
	1	12 (1.6)
	2	7 (0.9)
	3	2 (0.3)
	Unknown	14 (1.8)
APOE Genotype, n (%)	e2e2	2 (0.3)
	e2e3	66 (8.7)
	e2e4	18 (2.4)
	e3e3	362 (47.5)
	e3e4	221 (29.0)
	e4e4	51 (6.7)
	Unknown	42 (5.5)
Years of Education, median (range)**		16 (8-21)
Primary race, n (%)	White	649 (85.2)
	Black	70 (9.2)
	More than one	24 (3.1)
	Am Indian/Alaskan	12 (1.6)
	Unknown	3 (0.4)
	Other	1 (0.1)
Ethnicity, n (%)	Non-Hispanic	743 (97.5)
	Hispanic	12 (1.6)
	Unknown	5 (0.7)

*25 participants had unknown amyloid status; **four participants had unknown education.

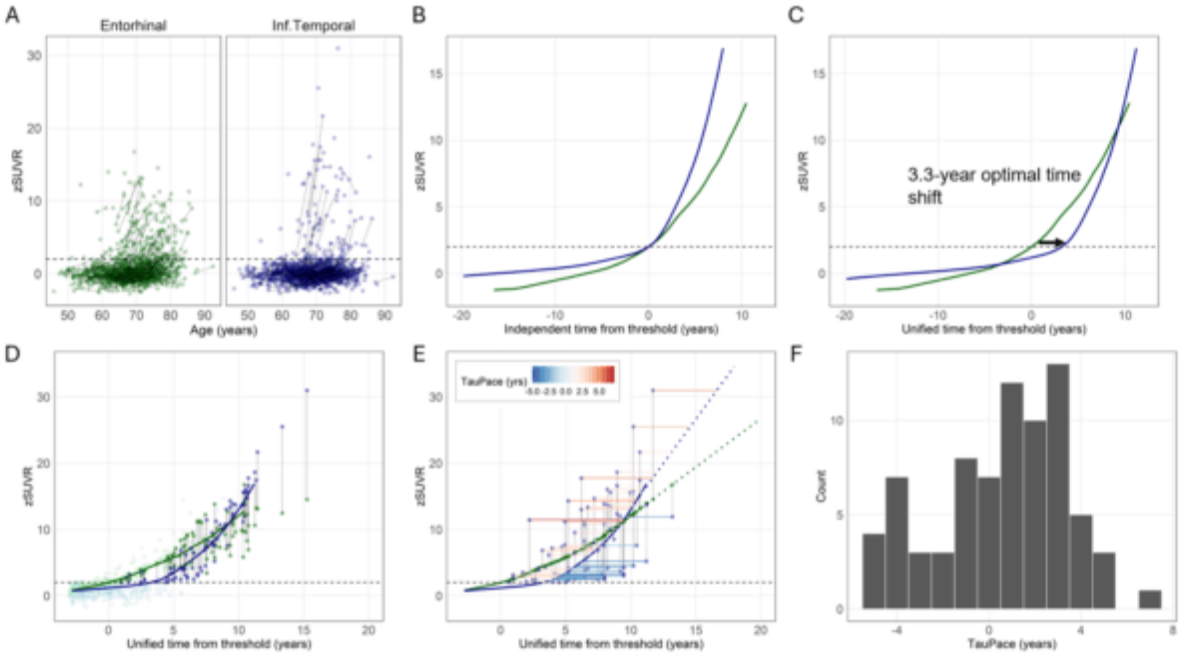


Figure 1. Joint modeling and TauPace calculation. **A**: Spaghetti plots showing entorhinal (green) and inferior temporal (purple) z-scored [18F]MK-6240 SUVR by age. **B**: Separately modeled trajectories aligned to time from tau positivity threshold (zSUVR=2). **C**: Trajectories were aligned on a unified timeline by calculating the optimal time shift that minimized the within subject residuals. **D**: Zoomed in plot showing each individual whose final scan is above the threshold in both regions. Points from the same individual are connected with vertical lines. Other datapoints are overlaid faintly. **E**: The curves are linearly extrapolated. Individuals are aligned to the entorhinal (green) curve and TauPace is shown as horizontal lines (red = faster, blue = slower). **F**: Histogram showing distribution of TauPace with bin widths equal to 1 year.

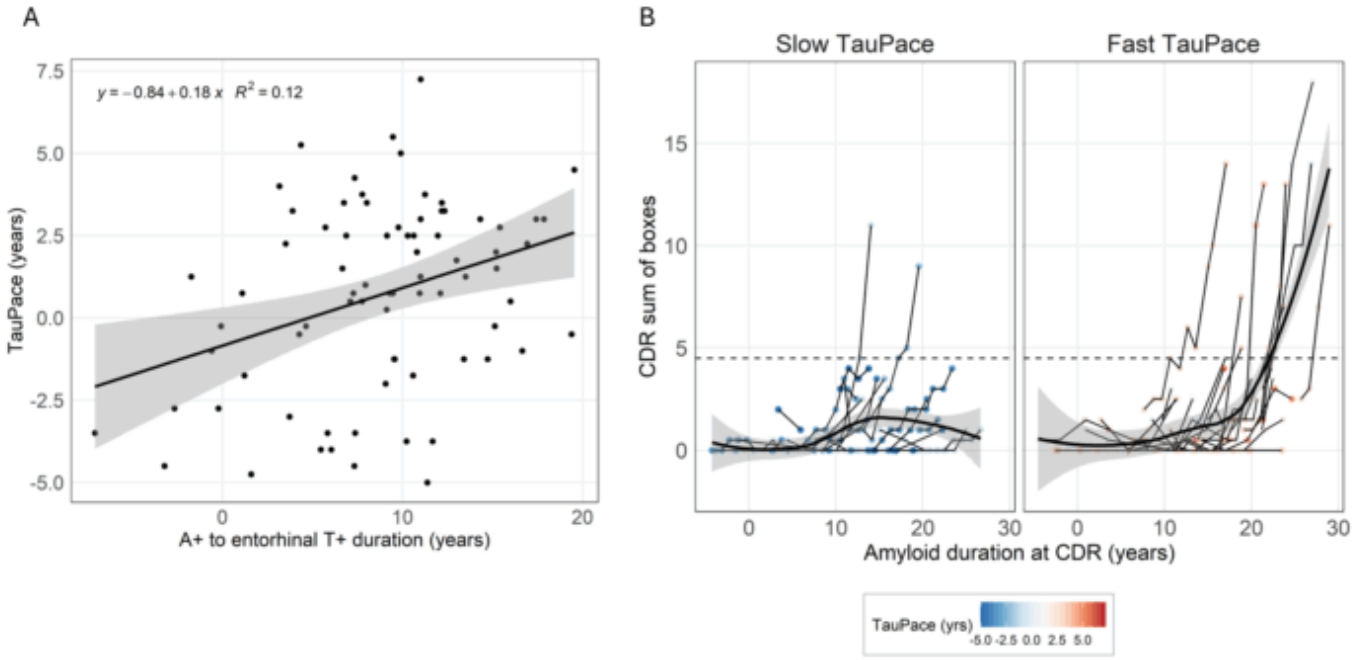


Figure 2. A: Faster TauPace is associated with longer intervals between amyloid and entorhinal tau positivity. B: Longitudinal CDR-SB trajectories (n = 76) for the subset of individuals that were tau positive in both entorhinal cortex and inferior temporal regions categorized by TauPace (Fast >0 years, n = 48; Slow n = 28). Dashed line represents CDR-SB = 4.5 indicating mild dementia and a LOESS fit is shown with 95% CI.

Keywords: tau, PET, disease progression, temporal modeling

Proteomic signatures track tau spread in Alzheimer's disease

Arthur C. Macedo[1], Ilaria Pola[2], Marcel S. Woo[3], Seyyed Ali Hosseini[1], Nesrine Rahmouni[1], Lydia Trudel[1], Joseph Therriault[1], Gleb Bezgin[1], Juliana Beker[1], Luiza S. Machado[2], Tevy Chan[1], Étienne Aumont[1], Yansheng Zheng[1], Brandon Hall[1], Aurelie Lebrun[1], Cécile Tissot[4], Stijn Servaes[1], Marina Pereira Gonçalves[1], Stuart Mitchel[1,7], Bruna Bellaver[5], Nicholas J Ashton[2], Henrik Zetterberg[2], Kaj Blennow[2], Tharick A Pascoal[5], Eduardo R Zimmer[2], Andréa L Benedet[2], Pedro Rosa-Neto[1,7]

[1]*McGill University, Montreal, QC, Canada*
[2]*University of Gothenburg, Gothenburg, Sweden*
[3]*University Medical Center Hamburg-Eppendorf, Hamburg, Germany*
[4]*Lawrence Berkeley National Laboratory, Berkeley, CA, US*
[5]*University of Pittsburgh, Pittsburgh, PA, US*
[6]*Universidade Federal do Rio Grande do Sul, Porto Alegre, Brazil*
[7]*University of Texas Southwestern Medical Centre, Dallas, TX, US*

Background: Proteomic alterations have been associated with Alzheimer's disease (AD) pathologies such as amyloid-β (Aβ) and tau. However, whether tau pathology stages correspond to distinct proteomic profiles remains unclear. Here, we aimed to characterize proteomic patterns and altered biological processes across tau stages.

Methods: We included 540 Aβ-positive participants from TRIAD and ROS-MAP cohorts (57% cognitively impaired; mean age 82 [SD=10] years). Tau staging was based on tau-PET (TRIAD) or postmortem histopathology (ROS-MAP), categorizing individuals as T_2^- (negative), T_2MTL$^+$ (entorhinal), T_2MOD$^+$ (limbic), or T_2HIGH$^+$ (neocortical) through Braak staging. Proteomic profiling was conducted using NULISA (TRIAD) or SomaScan (ROS-MAP) in plasma and/or CSF. Linear regressions contrasted protein levels across T_2^+ groups relative to T_2^-, adjusting for age and sex. Biological pathways (BPs) were derived from significantly differentially expressed proteins using GO-BP, then grouped into biological themes (BTs). Spearman correlations tested associations between pathway activity and tau-PET signal.

Results: Proteomic signatures evolved with tau progression (Fig.1). T_2MTL$^+$ showed an early heterogeneous immune disturbance, involving altered immune signaling and angiogenesis (Fig.2). T_2MOD$^+$ reflected a transitional phase marked by emerging abnormalities in tau phosphorylation and amyloid precursor protein (APP) processing, consistent with active tau propagation. T_2HIGH$^+$ demonstrated persistent immune disruption together with progressive metabolic and synaptic dysfunction, consistent with neurodegeneration. Although some overlap existed in dysregulated BTs across stages, each stage also showed unique alterations (Fig.3). Pathway activity correlated with tau-PET signal across Braak regions, supporting a dose-response relationship between proteomic dysregulation and tau burden.

Conclusions: Tau imprints a distinct and dynamic proteomic signature across T_2 stages, beyond the effects of Aβ-positivity. Our findings support a phased biological shift accompanying tau spread, from early immune-vascular imbalance to heightened tau/APP pathway involvement, ultimately culminating in metabolic-synaptic failure. This stage-specific proteomic landscape highlights candidate biomarkers for tracking and therapeutically targeting the immune-to-degenerative transition in AD.

Figure 1. Tau pathology stages map onto unique biological proteomic signatures.

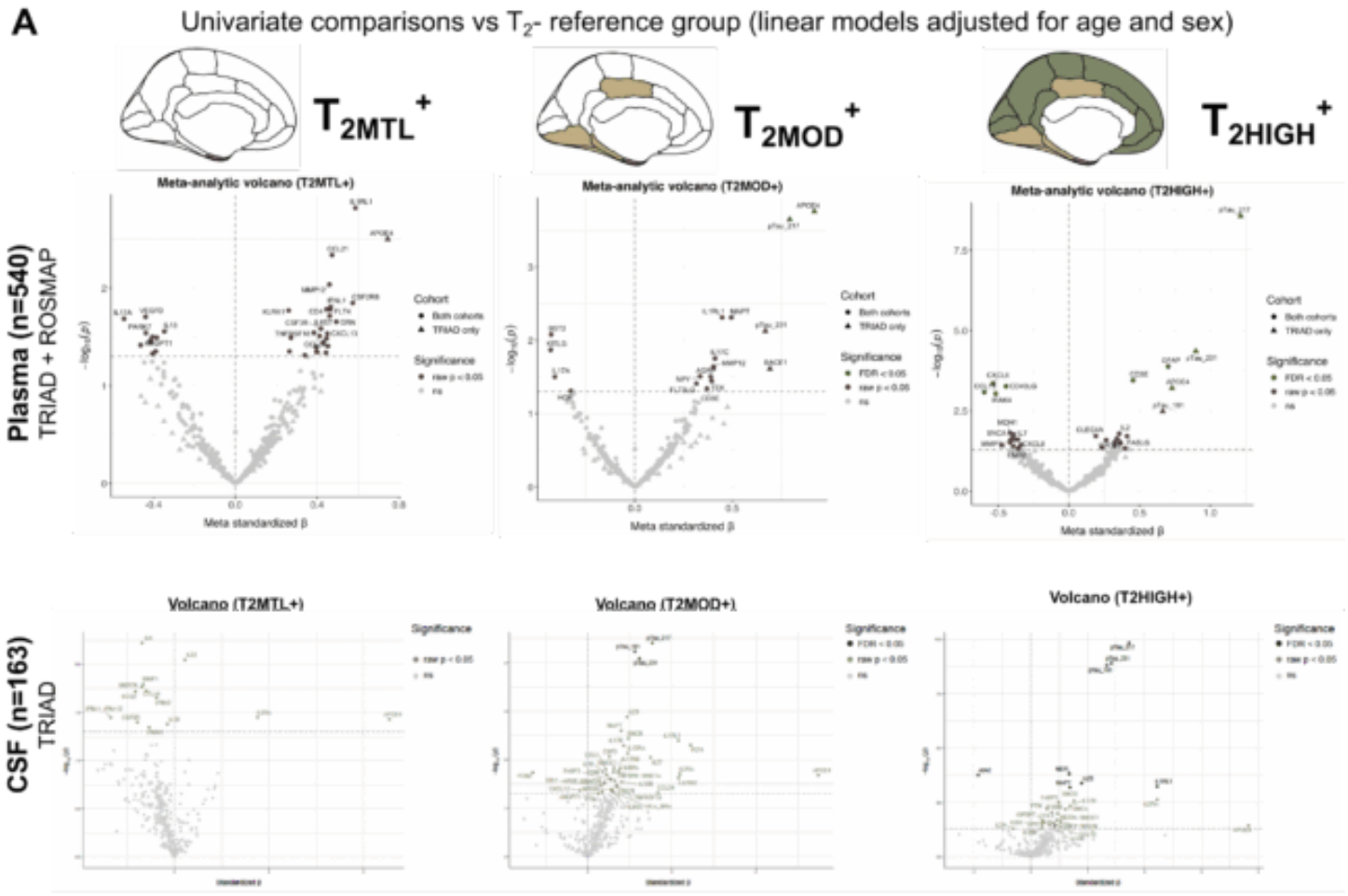
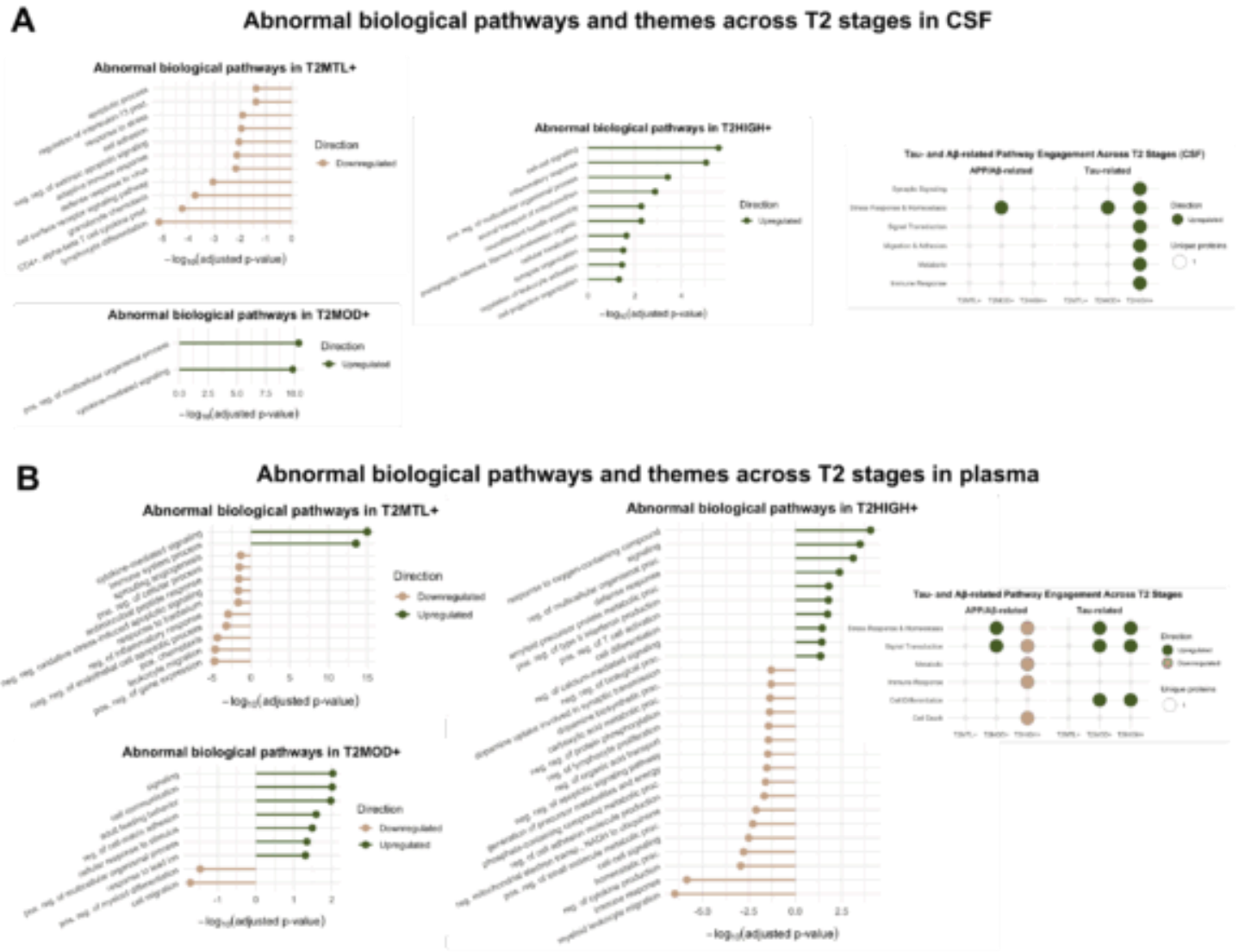


Figure A shows univariate comparisons between participants at early to advanced tau stages. Comparisons were established with linear regressions adjusted for age and sex

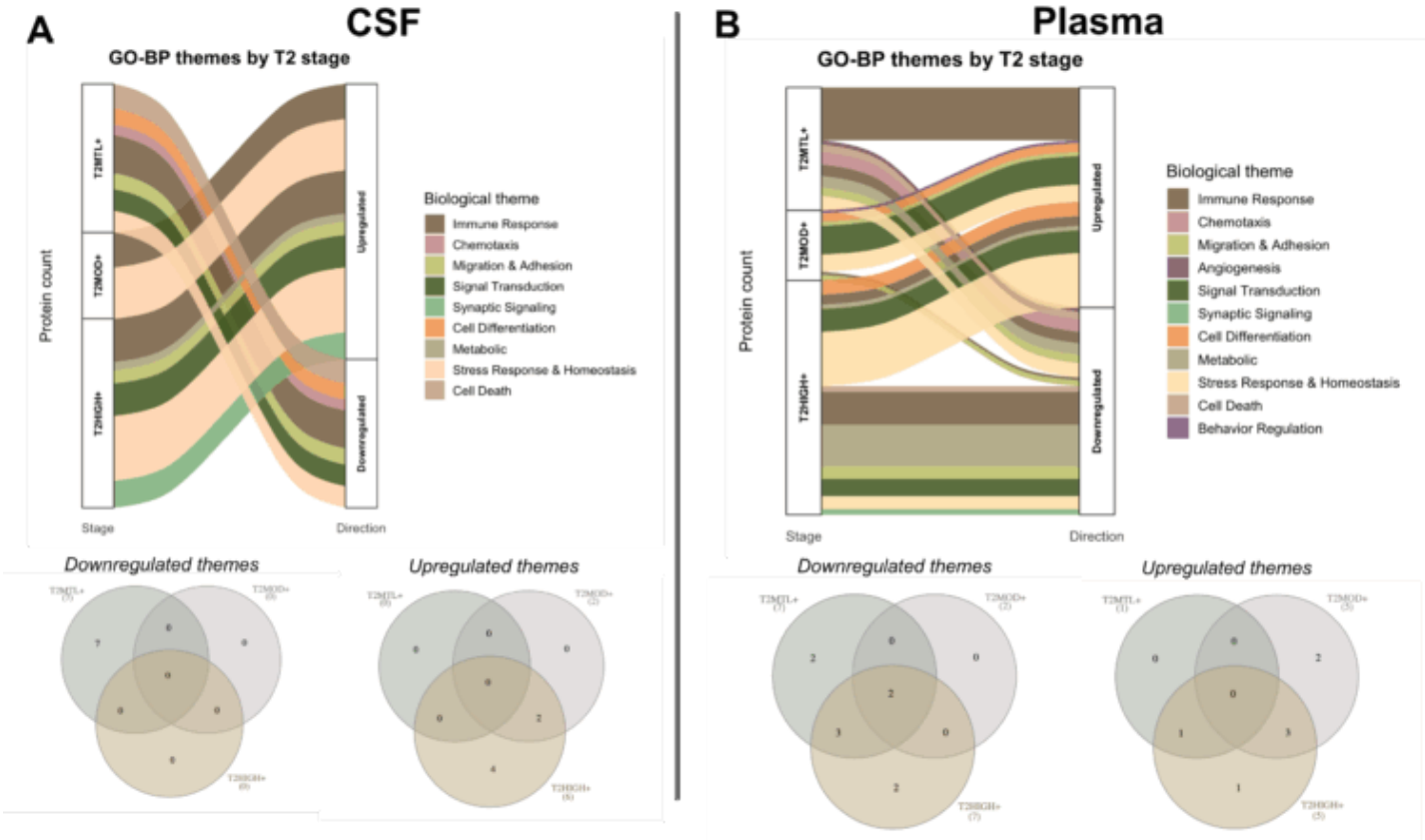
Figure B illustrates LOESS curves of the progression of the level of proteins found to be abnormal in at least two T2 stages.

Figure 2. Enrichment of Gene Ontology biological processes varies across T2 stages



Panels A and B show Gene Ontology biological pathways up- or downregulated at each T2+ stage relative to T2–. Pathways linked to core pathological features of AD are highlighted to pinpoint the stages at which abnormalities emerge. Panel C displays correlations between pathway activity scores and tau-PET signal in Braak regions.

Figure 3. Tau stages are associated to distinct abnormal biological themes



Panels A (CSF) and B (plasma) display alluvial plots illustrating how abnormal biological processes are distributed across T2 stages alongside Venn diagrams highlighting the overlap of dysregulated biological themes between stages.

Keywords: positron emission tomography; neurofibrillary tangles; proteomics; fluid biomarkers; staging

Podium Session

KEYNOTE: The role of AI in neuroimaging for Alzheimer's disease diagnosis and staging

Tuesday, January 13, 2026		
01:20 pm - 01:50 pm	Keynote: **The role of AI in neuroimaging for Alzheimer's disease diagnosis and staging**	**Joyita Dutta**, University of Massachusetts-Amherst, MA, USA

The role of AI in neuroimaging for Alzheimer's disease diagnosis and staging

Joyita Dutta

Department of Biomedical Engineering, University of Massachusetts Amherst

Recent advances in artificial intelligence (AI) have great promise and potential in medical image generation and interpretation. This talk will discuss novel AI approaches that have value in Alzheimer's disease (AD) diagnosis and staging. The first part of the talk will focus on AI-based enhancement of positron emission tomography (PET) images. The primary factors compromising PET image quality are low spatial resolution and high noise. The talk will present novel deep learning approaches for PET image super-resolution and denoising, demonstrating their applications to AD neuroimaging datasets. The second part of the talk will focus on an AI model for staging of AD based on contrastive learning. Unlike traditional Braak staging which was originally defined using postmortem histopathological data, our method is based on clinical tau PET imaging and is entirely data-driven. Compared with Braak staging, our staging scheme shows stronger correlations with cognitive endpoints. Our model, trained on one cohort, was validated on two independent cohorts without any fine-tuning, illustrating the robustness of the approach.

Tuesday, January 13, 2026 - 02:05 pm - 03:35 pm

Podium Session

SESSION V: Alpha-synuclein in PD and MSA: PET imaging

CHAIRS:

***Jamie Eberling**, Michael J. Fox Foundation for Parkinson's Research, New York, NY, USA*

***Robert Mach,** University of Pennsylvania, Philadelphia, PA, USA*

Tuesday, January 13, 2026			
02:05 pm – 03:35 pm	Podium Presentation	Authors	Presenter
02:10 pm – 02:25 pm	Preclinical and early clinical assessment of [11C]MODAG-005, a novel PET tracer for imaging alpha-synuclein aggregates	Grotegerd | Saw | Haas | Schmidt | Ryazanov | Leonov | Bleher | Kuebler | Kim | Roeben | Bonanno | Ruf | Sandiego | Henry | Levin | La Fougère | Pichler | Maurer | Griesinger | Giese | Herfert	**Ann-Kathrin Grotegerd**, Werner Siemens Imaging Center, Department of Preclinical Imaging and Radiopharmacy, Eberhard Karls University Tuebingen, Tuebingen, Germany
02:25 pm – 02:40 pm	Clinical evaluation of [11C]MK-7337: insights into the distribution of a-synuclein pathology in Parkinson's disease	Wang | Rabiner | van den Berg | Kassim | Huiban | Guibbal | Hield | Moz | Tai | Foster | Pavese | Bennacef | Boyce | Cislak | Fawaz | Gajdosik | Hou | Kuras | Lee | Liao | Mitchell | Morrow | Parisi | Pecoraro | Tafesse | Walraven | Drolet | Hostetler	**Eric Hostetler**, Merck & Co., Inc., West Point, PA, US
02:40 pm – 02:55 pm	[11C]M503-1619 alpha synuclein PET imaging in Parkinson's disease and multiple system atrophy	Hsieh | Young | Khattar | Siderowf | Nasrallah | Schmitz | Garcia | Schubert | Lee | Ebrahimian Sadabad | Huang | Carson | Matuskey | Perlmutter | Mach	**Chia-Ju Hsieh**, Department of Radiology, Perelman School of Medicine, University of Pennsylvania, Philadelphia, PA, US
02:55 pm – 03:10 pm	Quantitative analysis of human ^{18}F-FD4 α-synuclein PET imaging data in Parkinson's Disease and Multiple System Atrophy subtypes	Gunn | Rizzo | Searle | Fan | Albani | Prakash | Liu | Li | Fan | Wang | Zuo | Bian | Liang | Seibyl | Eberling | Marek | Tamagnan	**Roger Gunn**, XingImaging, London, UK

Preclinical and early clinical assessment of [11C]MODAG-005, a novel PET tracer for imaging alpha-synuclein aggregates

Ann-Kathrin Grotegerd[1], Ran Sing Saw[1], Sabrina Haas[1], Felix Schmidt[2], Sergey Ryazanov[2,3], Andrei Leonov[2,3], Daniel Bleher[1], Laura Kuebler[1], Myeongkyu Kim[3], Benjamin Roeben[4,5], Federica Bonanno[1], Viktoria C. Ruf[9], Christine M. Sandiego[6], Kelly E. Henry[6], Johannes Levin[2], Christian La Fougère[5], Bernd J. Pichler[1,7], Andreas Maurer[1,7], Christian Griesinger[3,8], Armin Giese[2], Kristina Herfert[1]

[1]*Werner Siemens Imaging Center, Department of Preclinical Imaging and Radiopharmacy, Eberhard Karls University Tuebingen, Tuebingen, Germany*
[2]*MODAG GmbH, Wendelsheim, Germany*
[3]*Department of NMR-based Structural Biology, Max Planck Institute for Multidisciplinary Sciences, Goettingen, Germany*
[4]*Hertie Institute for Clinical Brain Research, Department of Neurodegenerative Diseases, Eberhard Karls University Tuebingen, Tuebingen, Germany*
[5]*German Center for Neurodegenerative Diseases, Tuebingen, Germany*
[6]*Invicro, LLC, Needham, MA, US*
[7]*Cluster of Excellence iFIT (EXC 2180) "Image-Guided and Functionally Instructed Tumor Therapies", Eberhard Karls University Tuebingen, Tuebingen, Germany*
[8]*Cluster of Excellence "Multiscale Bioimaging: From Molecular Machines to Networks of Excitable Cells" (MBExC), University of Goettingen, Goettingen, Germany*
[9]*Ludwig Maximilians University, Center for Neuropathology and Prion Research, Munich, Germany*

Background: Currently, no clinically established PET tracer exists for imaging alpha-synuclein (aSYN), the central pathogenic protein in synucleinopathies such as Parkinson's disease (PD) and multiple system atrophy (MSA).

Aim: We aimed to develop a PET tracer capable of imaging aSYN pathology, enabling differential diagnosis of synucleinopathies and assessment of therapeutic efficacy in future clinical trials.

Method: MODAG-005 underwent extensive preclinical *in vitro* and *in vivo* evaluation and two first-in-human (FIH) scans in MSA and PD patients.

Results: Radioligand binding assays on pre-formed fibrils (PFFs) revealed high specificity for aSYN and good selectivity over other amyloid fibrils. NMR and cryo-EM confirmed specific binding to lipidic aSYN fibrils. Autoradiography on human tissue shows high affinity for MSA pathology, and micro-autoradiography verified specific binding to aSYN in MSA and PD tissue, as well as displacement by Emrusolmin. *In vivo*, MODAG-005 showed an excellent brain uptake (SUV ~ 2), rapid wash-out, and low brain penetrating metabolites. In PFF-inoculated rats, tracer retention was increased and significantly reduced upon Emrusolmin blocking (fig. 1). Elevated [^{11}C]MODAG-005 binding was also observed in pathology-rich regions of transgenic A30P mice. In non-human primates, tracer uptake was high (peak SUV 3.7) with homogeneous distribution and rapid clearance. FIH scans revealed rapid brain uptake (peak SUV of 2), a clearance half-life of 20 min, and elevated retention in brain regions expected to exhibit aSYN pathology in both MSA and PD (fig.2). Correlation of tracer binding with the clinical phenotype indicate that tracer signal corresponds to the expected relative distribution of aSYN pathology.

Conclusions: This study demonstrates *in vivo* PET imaging of intracellular aSYN pathology in animal models and humans, supporting MODAG-005 as a promising tracer for differential diagnosis of synucleinopathies and the potential for monitoring therapeutic efficacy in future clinical trials.

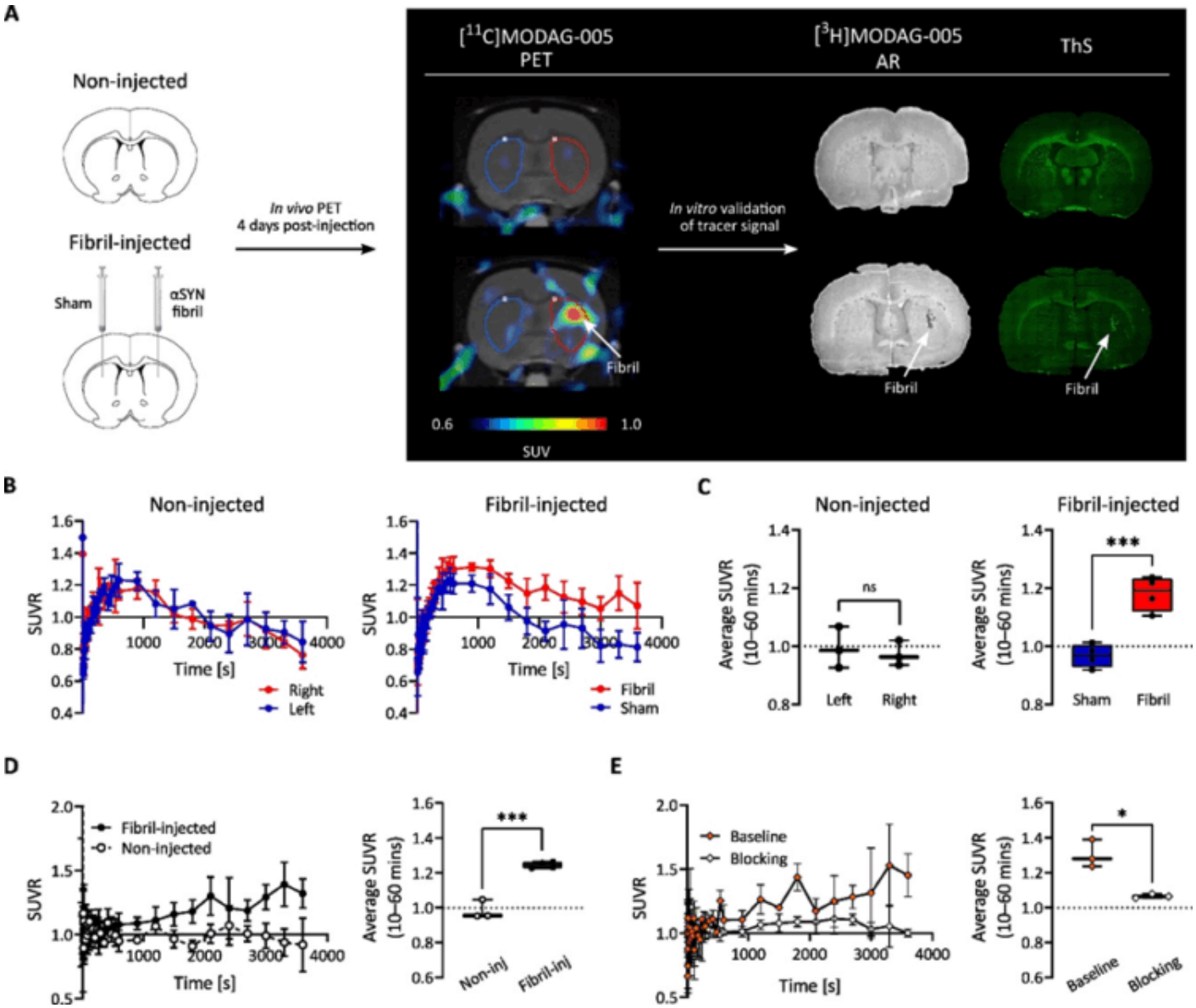


Figure 1: [11C]MODAG-005 in fibril-injected rats.

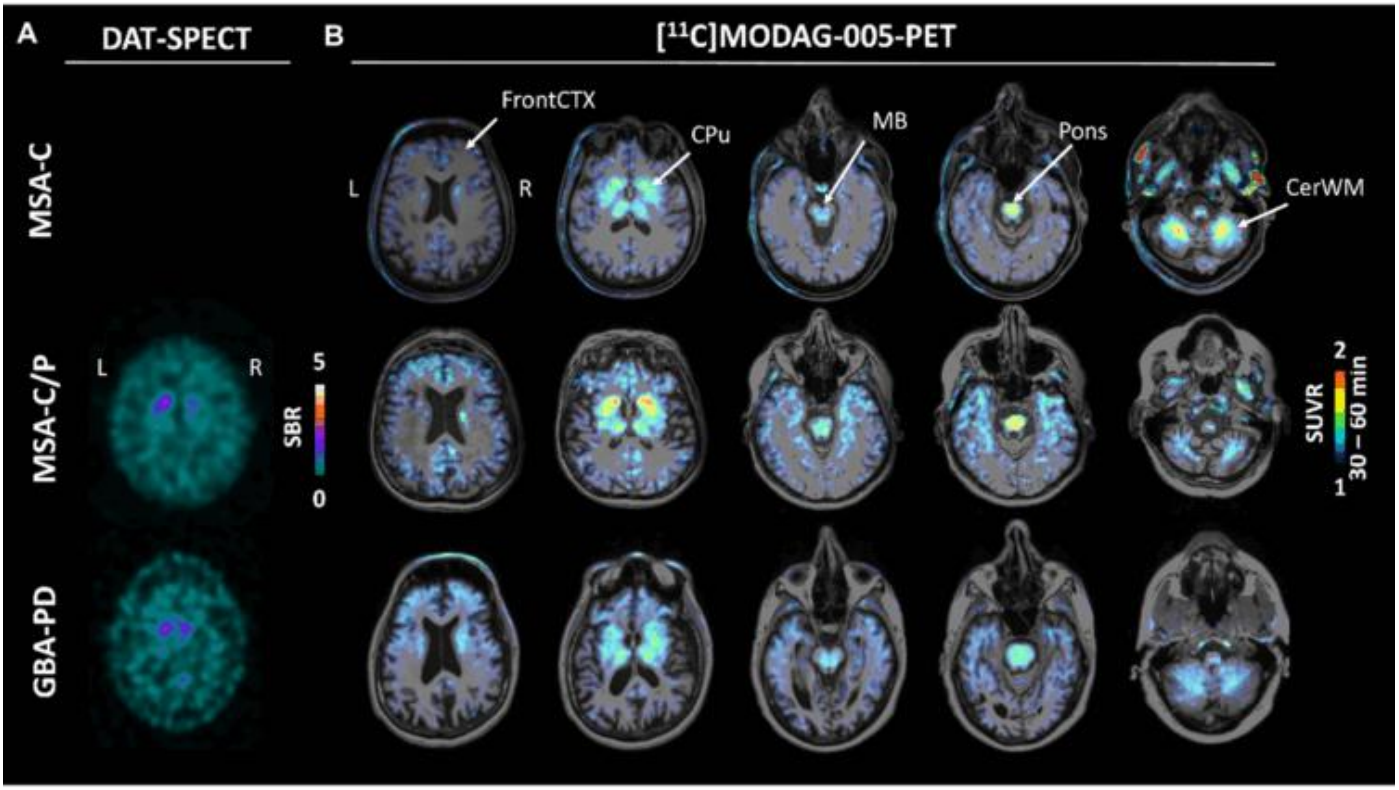


Figure 2: [11C]MODAG-005 first-in-human PET.

Keywords: alpha-synuclein, PET, MSA, PD,

Clinical evaluation of [11C]MK-7337: insights into the distribution of a-synuclein pathology in Parkinson's disease

Yuchuan Wang[1], Eugenii Rabiner[2], Frans van den Berg[2], Hashim Kassim[2], Mickael Huiban[2], Florian Guibbal[2], Emma Hield[2], Sara Moz[2], Yen Tai[4], Victoria Foster[3], Nicola Pavese[3], Idriss Bennacef[1], Chris Boyce[1], Dawn Cislak[1], Maria Fawaz[1], David Gajdosik[1], Jingyao Hou[1], Yuliya Kuras[1], Susi Lee[1], Jennie Liao[1], Helen Mitchell[1], Tom Morrow[1], Michael Parisi[1], Dianne Pecoraro[1], Laykea Tafesse[1], Jason Walraven[1], Rob Drolet[1], Eric Hostetler[1]

[1]*Merck & Co., Inc., West Point, PA, US*
[2]*Perceptive Discovery, London, UK*
[3]*Newcastle University, Newcastle, UK*
[4]*Imperial College, London, UK*

Abstract: Lewy bodies and Lewy neurites comprised of aggregated α-synuclein comprise the hallmark pathology of Parkinson's disease (PD). To date, no PET tracer has shown the ability to quantify α-synuclein pathology in PD patients. This abstract describes insights learned from the first-in-human evaluation of [^{11}C]MK-7337 in PD and healthy elderly (HE) participants.

Methods: Dynamic PET scans with [^{11}C]MK-7337, a sub-nM affinity ligand for α-synuclein pathology, were conducted on 8 PD (SAA+, DAT scan+, H&Y 2-3) and 4 HE participants. Decreased ability to detect odors (hyposmia), an early symptom of PD, was evaluated for all PD participants. [^{11}C]MK-7337 SUVR was determined for select regions using cortical white matter as the reference region.

Results: [^{11}C]MK-7337 demonstrated good delivery across the blood-brain barrier (peak SUV > 1) which was heterogeneous and cleared slowly, indicative of off-target binding throughout the brain. Regional distribution was similar in PD and HE, but higher SUVR was seen in PD in brainstem/pons and substantia nigra, regions expected to contain α-synuclein pathology. Of note, some PD participants showed elevated retention of [^{11}C]MK-7337 in the olfactory epithelium, which is outside of the BBB, but is known to contain α-synuclein pathology in PD. Furthermore, the SUVR in the olfactory epithelium was associated with the hyposmic status of the participants, with five of the six hyposmic PD participants showing elevated SUVR in the olfactory epithelium compared to HE. The two non-hyposmic PD participants showed low SUVR in the olfactory epithelium, similar to HE.

Conclusion: [^{11}C]MK-7337 demonstrated proof-of-concept for imaging α-synuclein in PD. A more selective PET tracer is needed to better understand the patterns of how α-synuclein deposition throughout the brain relate to disease-associated factors such as hyposmia.

Keywords: alpha-synuclein, MK-7337, Parkinson's disease, hyposmia

[11C]M503-1619 alpha synuclein PET imaging in Parkinson's disease and multiple system atrophy

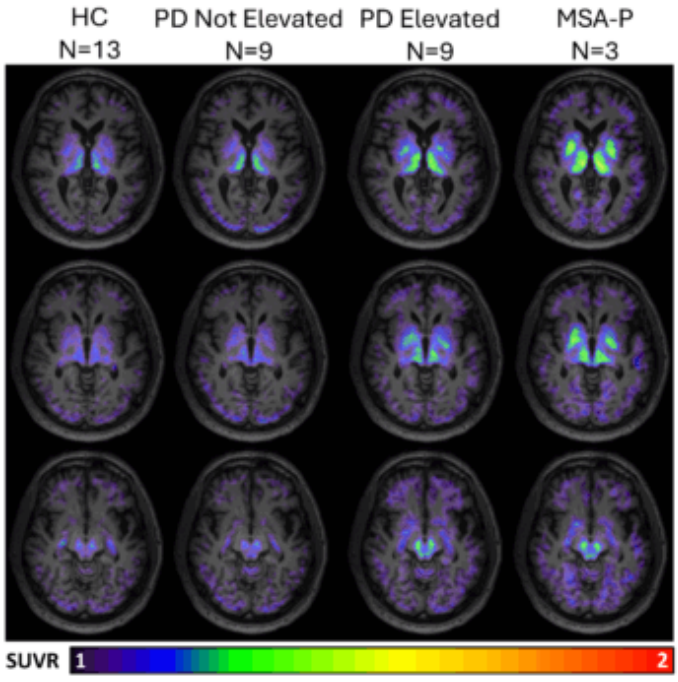
Chia-Ju Hsieh[1], Anthony Young[1], Nikkita Khattar[2], Andrew Siderowf[3], Ilya Nasrallah[1], Alexander Schmitz[1], Carol Garcia[1], Erin Schubert[1], Hsiaoju Lee[1], Faranak Ebrahimian Sadabad[2], Yiyun Huang[2], Richard Carson[2], David Matuskey[2], Joel Perlmutter[4], Robert Mach[1]

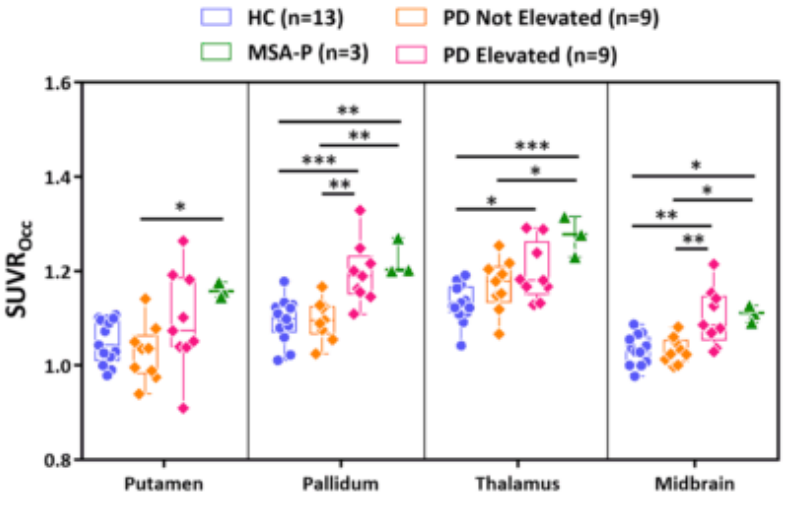
[1]*Department of Radiology, Perelman School of Medicine, University of Pennsylvania, Philadelphia, PA, US*
[2]*Department of Radiology and Biomedical Imaging, Yale University, New Haven, CT, US*
[3]*Department of Neurology, Perelman School of Medicine, University of Pennsylvania, Philadelphia, PA, US*
[4]*Department of Neurology, Washington University School of Medicine, Saint Louis, MO, US*

Aims: This study aims to assess [^{11}C]M503-1619[1], a novel alpha-synuclein (aSyn) positron emission tomography radioligand in synucleinopathies.

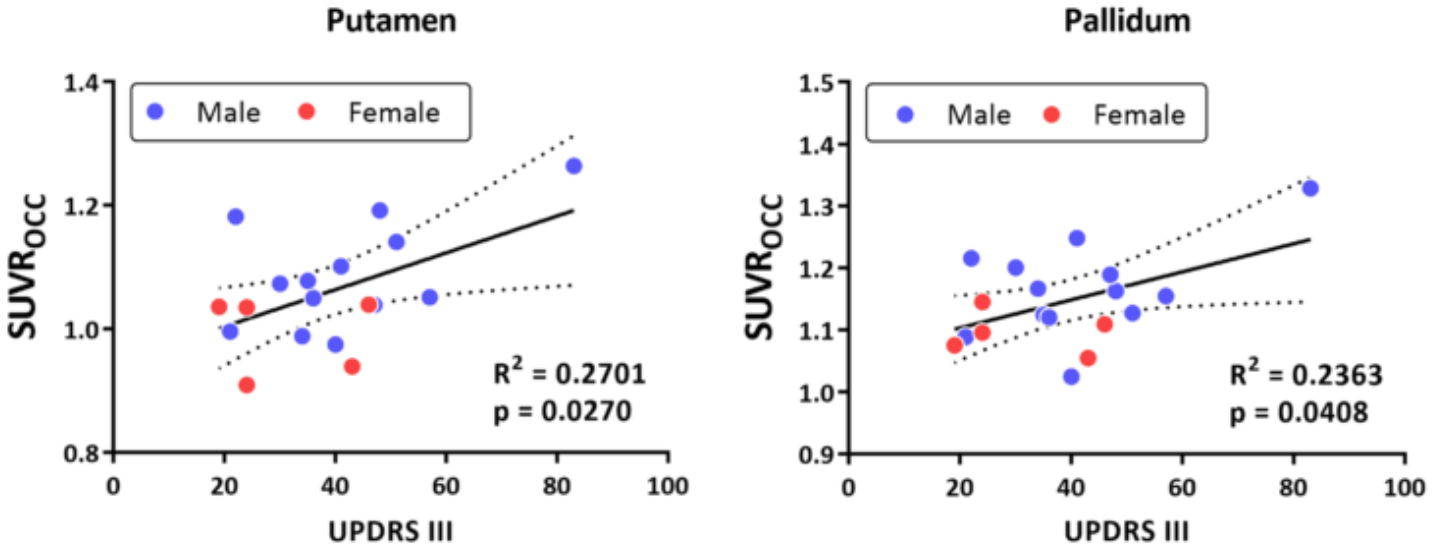
Methods: Thirteen healthy controls (HCs), 18 Parkinson's disease (PD) and 3 Parkinsonian type multiple system atrophy (MSA-P) patients underwent dynamic brain imaging with [^{11}C]M503-1619 across multiple sites. Arterial blood samples were collected for radiometabolite analyses. Images were analyzed by using 20-30 min post injection to minimize potential confounding effects of brain uptake of radiolabeled metabolites. Standardized uptake value ratios (SUVRs) were calculated by using occipital cortex as reference region for volumes of interest analyses. Voxel-wise comparison of individual PD versus HCs was performed to evaluate the heterogeneous uptake in PD.

Results: [^{11}C]M503-1619 was rapidly metabolized with a parent fraction of 33% and 17% at 15- and 30-min post injection. One-way ANOVA multiple comparisons revealed the SUVRs in PD were significantly higher than HC in the thalamus (p=0.0212) and elevated in the pallidum (p=0.0811). In MSA-P, SUVRs were significantly higher than HC in the pallidum (p=0.0080), thalamus (p=0.0004), and midbrain (p=0.0479) and elevated in the putamen (p=0.0641). Voxel-wise analysis comparing individual PD subjects to the HCs revealed a subset of 9 PD subjects with elevated SUVR in the thalamus and midbrain, and 9 PD subjects with similar uptake to HCs (Figure 1).





Female PD (n=5) showed lower SUVR in the putamen, pallidum and midbrain compared to male PD (n=13) with comparable UPDRS III scores. The UPDRS III scores of PD were significantly correlated with SUVRs in the putamen and pallidum (Figure 2).



Conclusions:

[^{11}C]M503-1619 has the potential to image aSyn aggregation in patients with PD and MSA-P. Heterogeneous uptake across the PD participants suggest possible subtypes of PD, which may be related to variability in aSyn burden or binding site accessibility, including a potential sex difference.

[1]*RSC Med Chem* 2025, **16**, 2743-2753

Keywords: Alpha-synuclein; Parkinson's disease; Multiple System Atrophy; PET

Quantitative analysis of human ^{18}F-FD4 α-synuclein PET imaging data in Parkinson's Disease and Multiple System Atrophy subtypes

Roger Gunn[1,2], Gaia Rizzo[1], Graham Searle[1], Zhen Fan[1], Justin Albani[3], Neha Prakash[3], Cong Liu[4], Dan Li[5], Mengqi Fan[6], Jian Wang[7], ChuanTao Zuo[8], Jiang Bian[5], Qing Liang[6,9], John Seibyl[10], Jamie Eberling[11], Ken Marek[10], Gilles Tamagnan[3]

[1]*XingImaging, London, UK*
[2]*Imperial College London, London, UK*
[3]*XingImaging, New Haven, CT, US*
[4]*Interdisciplinary Research Center of Biology and Chemistry, Shanghai Institute of Organic Chemistry, Chinese Academy of Sciences, Shanghai, CN*
[5]*Shanghai Jiao Tong University, Shanghai, CN*
[6]*Synusight Biotech (Shanghai) Co., Ltd., Shanghai, CN*
[7]*Department of Neurology, Huashan Hospital, Shanghai, CN*
[8]*Department of Nuclear Medicine, Huashan Hospital, Shanghai, CN*
[9]*Irad Bio LLC, Merion Station, MD, US*
[10]*Institute for Neurodegenerative Disorders, New Haven, CT, US*
[11]*Michael J. Fox Foundation, Research Resources, New York, NY, US*

Introduction: ^{18}F-FD4 is a novel alpha-synuclein PET tracer for Parkinson's disease (PD) and multiple system atrophy (MSA). Initial human imaging data and their quantitative analysis are presented to assess its potential as a differential biomarker of alpha-synuclein pathology.

Methods: Eighteen participants underwent MRI and static PET imaging acquired 60–80 minutes following injection of ^{18}F-FD4. Diagnostic groups included healthy controls (HC; n=4), Parkinson's disease (PD; n=6), and multiple system atrophy (MSA; n=8; comprising MSA-P, MSA-C, and mixed subtypes). Clinical and demographic characteristics are summarized in Table 1. All image analyses were performed using MIAKAT 5.0. Regions of interest (ROIs) were defined in MNI space and applied to the PET data after spatial normalization of each participant's T1-weighted MRI. Target ROIs included the substantia nigra, putamen, globus pallidus, pons, and middle cerebellar peduncles. Standardized uptake value ratios (SUVRs) were calculated using cerebellar grey matter as the reference region. Specific binding ratios (SBRs), defined as $SBR = SUVR - 1$, were used as the primary quantitative outcome measure.

Case	Diagnosis	Sex	Age		H-Y stage	Duration (mths)	MDS-UPDRS	MMSE
1	HC	F	53	55.5 +/- 5.4	-	-	-	30
2	HC	M	49		-	-	-	26
3	HC	M	60		-	-	-	29
4	HC	M	60		-	-	-	28
5	PD	F	54	58.5 +/- 5.7	2	51	39	27
6	PD	M	54		2	10	27	24
7	PD	M	67		1	20	5	30
8	PD	F	58		3	19	28	29
9	PD	M	54		1	3	13	28
10	PD	M	64		1	10	4	24
11	MSA-P	F	61	60.6 +/- 7.1	3	29	-	25
12	MSA-P	M	54		2	6	-	29
13	MSA-P	F	75		5	12	-	19
14	MSA-mixed	F	57		5	48	-	28
15	MSA-mixed	F	57		3	18	-	24
16	MSA-C	M	61		2	10	-	27
17	MSA-C	M	66		1	29	-	28
18	MSA-C	M	54		3	33	-	28

Table 1. Clinical demographics of 18 human subjects imaged with ^{18}F-FD4.

Results: SBR analysis revealed elevated ^{18}F-FD4 binding in the substantia nigra, globus pallidus and putamen of PD subjects compared to HC, consistent with localized alpha-synuclein accumulation (Figure 1). MSA subjects showed broader increases in SBR across the putamen, globus pallidus, pons, and middle cerebellar peduncles, with subtype-specific patterns (Figure 1). Parametric images supported these findings, highlighting distinct regional binding profiles between PD and MSA (Figure 2).

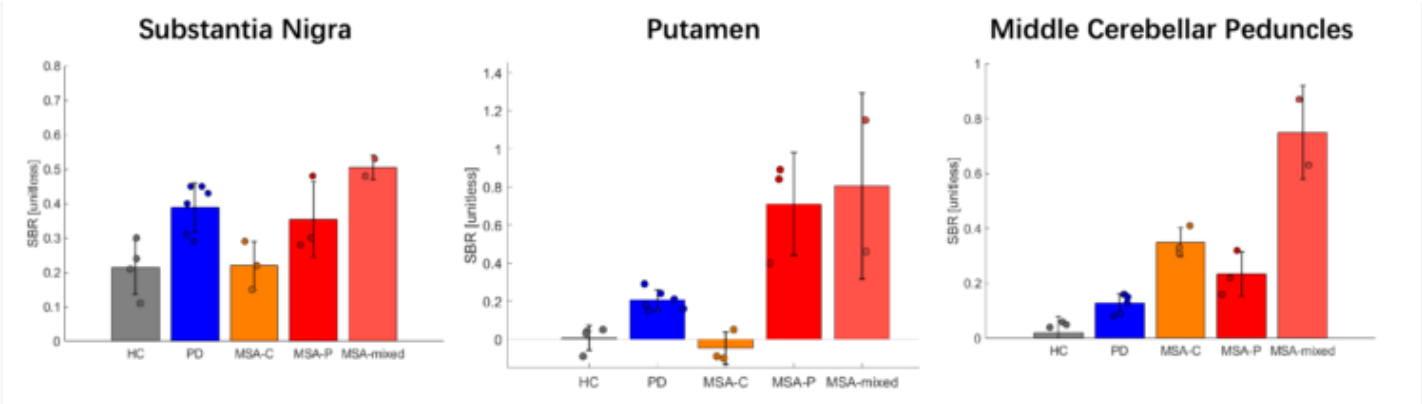


Figure 1. Regional ^{18}F-FD4 SBR values in Substantia Nigra, Putamen and Middle Cerebellar Peduncles.

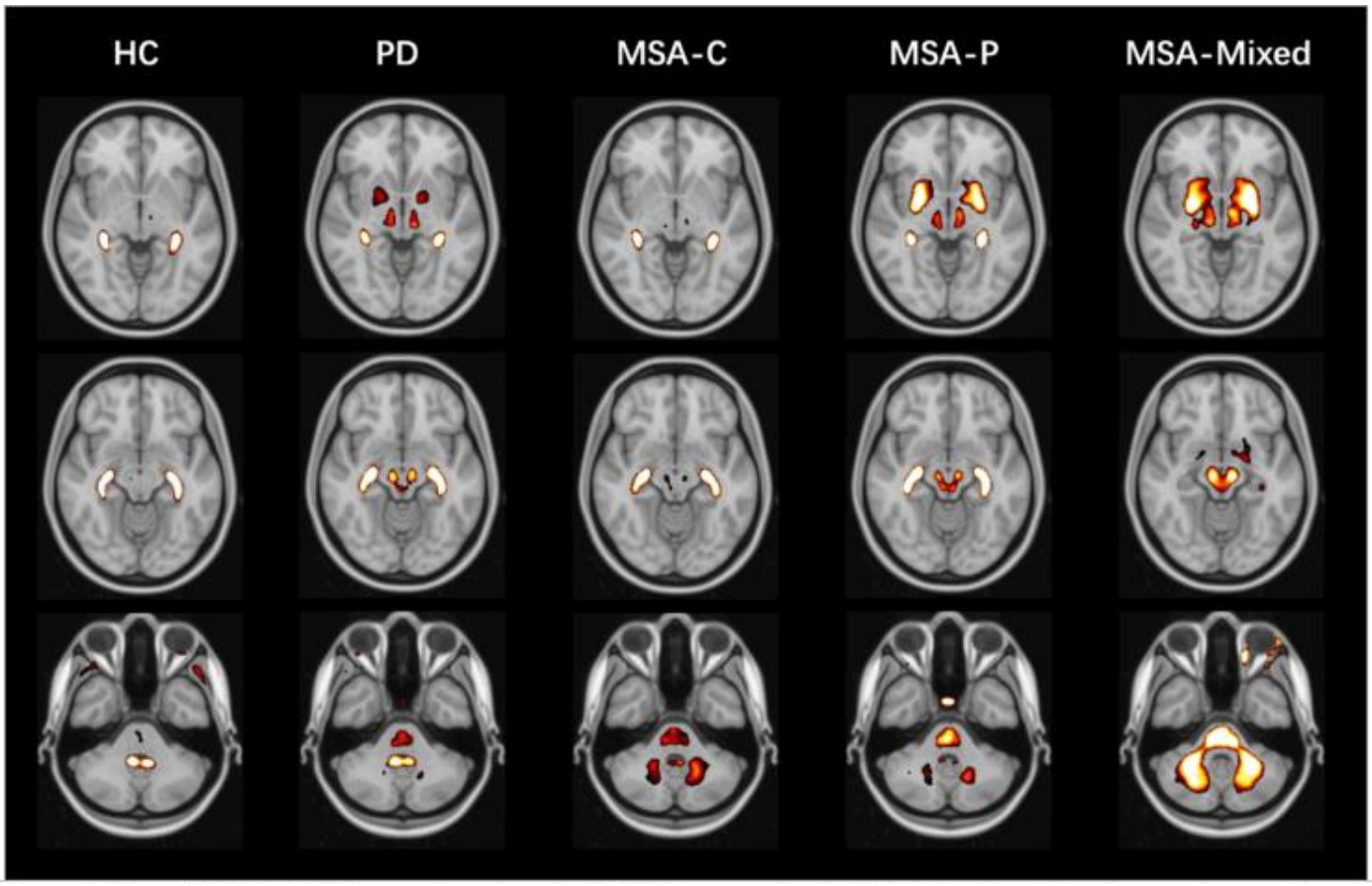


Figure 2. Mean ^{18}F-FD4 SBR images by cohort in MNI152 space thresholded at SBR > 0.3 and superimposed on structural T1 template. Increased signal, compared to healthy controls, observed in (Top Row) Globus Pallidus, Subthalamic Nucleus and Putamen, (Middle Row) Substantia Nigra, (Bottom Row) Pons and Middle Cerebellar Peduncles.

Conclusions: ^{18}F-FD4 PET imaging reveals disease-specific patterns of alpha-synuclein accumulation in PD and MSA. The tracer shows promise for in vivo differentiation of PD and MSA subtypes, and for early detection in at-risk individuals, supporting its potential as a biomarker for synucleinopathies.

Keywords: Imaging, PET, alpha-synuclein, Parkinson's disease, multiple system atrophy

Tuesday, January 13, 2026 - 03:35 pm - 03:40 pm

Podium Session

B2 - B: Blitz Session

Tuesday, January 13, 2026			
03:35 pm – 03:40 pm	Title	Authors	Presenter
Board # 67	**MK6240 and Tauvid positivity, cognitive decline, and their relationship to Aβ PET deposition across the Alzheimer's spectrum**	Bellaver | Povala | Lussier | Amaral | Bauer-Negrini | Ferreira | Jagust | Masdeu | Fortea | Tudorascu | Soleimani-Meigooni | Lowe | Oh | Pascual | Gordon | Rosa-Neto | Baker | Pascoal	**Bruna Bellaver**, University of Pittsburgh, Pittsburgh, PA, USA
Board # 90	**Differential sensitivity of T1-MRI and FDG-PET for tracking neurodegeneration across progressive stages of tau pathology in Alzheimer's disease**	Vourkas | Karagianni | Moscoso | Zhang | Sanchez-Juan | Schöll | Grothe | Silva-Rodríguez	**Jesús Silva-Rodríguez**, CIEN Foundation, Reina Sofia Alzheimer Center, ISCIII, Madrid, Spain
Board # 87	**Midlife physical activity attenuates the association of earlier menopause with tau pathology and cognitive decline**	Wood Alexander | Cadwallader | Johnson | Casaletto | Rabin	**Madeline Wood Alexander**, Sunnybrook Research Institute, Toronto, ON, Canada

Tuesday, January 13, 2026 - 04:40 pm - 06:10 pm

Podium Session

SESSION VI: Neuroinflammation

CHAIRS:

***Chuck Kreisl**, Eisai, Washington DC, USA*

***David Morgan**, Michigan State University, Grand Rapids, MI, USA*

Tuesday, January 13, 2026			
04:40 pm – 06:10 pm	**Podium Presentation**	**Authors**	**Presenters**
04:45 pm – 05:00 pm	Deep mass spectrometry-based plasma proteomics reveals signatures of reactive astrocytes in Alzheimer's disease	Shi | Zeng | Balogun | Farinas | Lopresti | Gogola | Ikonomovic | Aizenstein | Villemagne | Cohen | Karikari	**Ruyu Shi**, Department of Psychiatry, University of Pittburgh, Pittsburgh, PA, US
05:00 pm 05:15 pm	Microglia-Astrocyte interplay modulates tau phosphorylation in Alzheimer's disease	Rahmouni | Hosseini | Chan | Trudel | Aumont | Macedo | Bezgin | Hall | Therriault | Harada | Okamura | Benedet | Zimmer | Pascoal | Rosa-Neto	**Tevy Chan**, Department of Neurology and Neurosurgery, McGill University, Douglas Research Centre, Le Centre intégré universitaire de santé et de services sociaux (CIUSSS) de l'Ouest-de-l'Île-de-Montréal, Montreal, QC, Canada
05:15 pm – 05:30 pm	Astrogliosis mediates the effects of amyloid, moderated by CVD, on tau and cognition in non-demented individuals	Gogola | Lopresti | Cohen | Ikonomovic | Minhas | Snitz | Reese | Matan | Wu | Aizenstein | Lopez | Villemagne	**Victor Villemagne**, University of Pittsburgh, Pittsburgh, PA, US
05:30 pm – 05:45 pm	TSPO expression patterns in the postmortem brain: relevance to neuroinflammation imaging	Moloney | Lee | Emery | Kandimalla | Botha | Graff-Radford | Jones | Reichard | Knopman | Jack | Petersen | Nguyen | Lowe	**Christina Moloney**, Department of Radiology, Mayo Clinic, Rochester, MN, US

Deep mass spectrometry-based plasma proteomics reveals signatures of reactive astrocytes in Alzheimer's disease

Ruyu Shi[1,3], Xuemei Zeng[1,2,3], Wasiu G Balogun[1,2,3], Marissa F. Farinas[1,2,3], Brian J. Lopresti[1,3], Alexandra Gogola[6], Milos Ikonomovic[3,7,8], Howard J. Aizenstein[1,3], Victor L. Villemagne[1,3], Ann D. Cohen[1,3], Thomas K. Karikari[1,2,3]

[1]*Department of Psychiatry, University of Pittburgh, Pittsburgh, PA, US*
[2]*Biofluid Biomarker Laboratory, Western Psychiatric Hospital, University of Pittsburgh Medical Center, Pittsburgh, PA, US*
[3]*Alzheimer's Disease Research Center, University of Pittsburgh, Pittsburgh, PA, US*
[4]*Department of Radiology, University of Pittsburgh, Pittsburgh, PA, US*
[5]*Department of Neurology, University of Pittsburgh, Pittsburgh, PA, US*
[6]*Geriatric Research Education and Clinical Center, VA Pittsburgh HS, Pittsburgh, PA, US*

Objectives: Monitoring individuals across the Alzheimer's disease (AD) spectrum is essential to understanding how reactive astrocytes contribute to disease progression. PET imaging with the [18F]SMBT-1 tracer, targeting monoamine oxidase-B (MAO-B) overexpressed in reactive astrocytes, allows in vivo investigation of these processes. However, due to its high cost and limited availability, PET is not suitable for widespread use. In this study, we leveraged recent advances in sample preparation and mass spectrometry for deep plasma proteomic profiling, conducting a "PET-to-blood" analysis aimed at identifying blood-based biomarkers of reactive astrocytes.

Methods: Participants in the INflammation ROles in Aging and Alzheimer's disease Study (INROAADS) underwent blood collection, neuropsychiatric evaluations, consensus clinical diagnoses, [11C]PiB PET and [18F]SMBT-1 PET. We included 85 participants (51.8% female; 89.4% self-identified as non-Hispanic White), aged 68.1±7.4 years, 16.5% Aβ-positive (59.4±35.8 Centiloids). Low abundant plasma proteins were enriched using Proteograph XT, trypsinized, and analyzed on an Orbitrap Astral coupled to a Vanquish Neo UHPLC.

Results: A total of 94,712 peptides and 7,742 protein groups were identified, with 5,548 proteins reliably quantified by a minimum of two peptides. In a preliminary analysis, plasma proteomic profiles were correlated with [18F]SMBT-1 retention in the precuneus, a region characterized by early Aβ deposition. This analysis revealed 56 proteins significantly associated with [18F]SMBT-1 retention (Spearman $p < 0.001$; 9% FDR), with 50 showing a positive correlation. Top significant proteins include MFN1, NDUFA2, and MMUT. Notably, functional enrichment analysis highlighted significant involvement of mitochondrial proteins (n = 35) and the 2-oxocarboxylic acid metabolism pathway (n = 7), supporting the role of energy metabolism and mitochondrial dysfunction in AD pathogenesis.

Conclusions: This study highlights the potential of deep mass spectrometry-based proteomics for uncovering plasma proteomic signatures of reactive astrogliosis in AD.

Keywords: Proteomics, SMBT1, reactive astrogliosis, Alzheimer's disease

Microglia-Astrocyte interplay modulates tau phosphorylation in Alzheimer's disease

Nesrine Rahmouni[1], Seyyed Ali Hosseini[1], Tevy Chan[1], Lydia Trudel[1], Etienne Aumont[1], Arthur C Macedo[1], Gleb Bezgin[1], Brandon J Hall[1], Joseph Therriault[1], Ryuichi Harada[2], Nobuyuki Okamura[2], Andrea L. Benedet[3], Eduardo R. Zimmer[4], Tharick A. Pascoal[5], Pedro Rosa-Neto[1]

[1]*Department of Neurology and Neurosurgery, McGill University , Douglas Research Centre, Le Centre intégré universitaire de santé et de services sociaux (CIUSSS) de l'Ouest-de-l'Île-de-Montréal, Montreal, QC, Canada*
[2]*Division of Pharmacology, Faculty of Medicine, Tohoku Medical and Pharmaceutical University, Sendai, Japan*
[3]*Department of Psychiatry and Neurochemistry, Institute of Neuroscience and Physiology, The Sahlgrenska Academy, University of Gothenburg, Molndal, Sweden*
[4]*Graduate Program in Biological Sciences: Biochemistry, Universidade Federal do Rio Grande do Sul, Porto Alegre, Brazil*
[5]*Department of Psychiatry, School of Medicine, University of Pittsburgh, Pittsburgh, PA, US*

Aims: The interplay between microglia and astrocytes is crucial for innate inflammatory responses. However, the impact of this interplay in tau phosphorylation haven't been demonstrated in living individuals. Here, we investigated the associations between astroglia and microglia across the AD spectrum using PET with plasma phosphorylated tau.

Methods: We included 168 individuals from the TRIAD cohort. Aβ deposition, tau tangles, microglial activation (TSPO) were assessed via [^{18}F]AZD4694-PET, [^{18}F]MK6240-PET, [^{11}C]PBR28- PET. A subset of 34 individuals had an additional PET session assessing astrocyte reactivity (MAO-B) with [^{18}F]SMBT-1-PET. Voxel-based regression models evaluated the association of TSPO-PET and MAO-B-PET with plasma ptau217. We also evaluated the effect of TSPO-PET positivity on the association between MAO-B-PET and plasma ptau217.

Results: First, plasma pTau217 shows significant associations with both TSPO and MAO-B-PET in the same AD related regions, with the highest uptake in the precuneus and posterior cingulate **(Figure 1).** In addition, we noted that the association between MAO-B-PET and plasma pTau217 was only present in TSPO-positive individuals **(Figure 2A).**Moreover, the interaction between TSPO positivity and plasma pTau217 predicted higher MAOB uptake **(Figure 2B).**

Conclusion: This is the first PET study addressing the interaction between microglia, astrocyte and tau phosphorylation in living individuals. Our study highlights the overlapping associations in AD related regions of microglial activation, astrocytes reactivity and plasma pTau217. Our results support the framework in which microglia-dependant astrocyte activation plays a role in tau phosphorylation in AD pathophysiology.

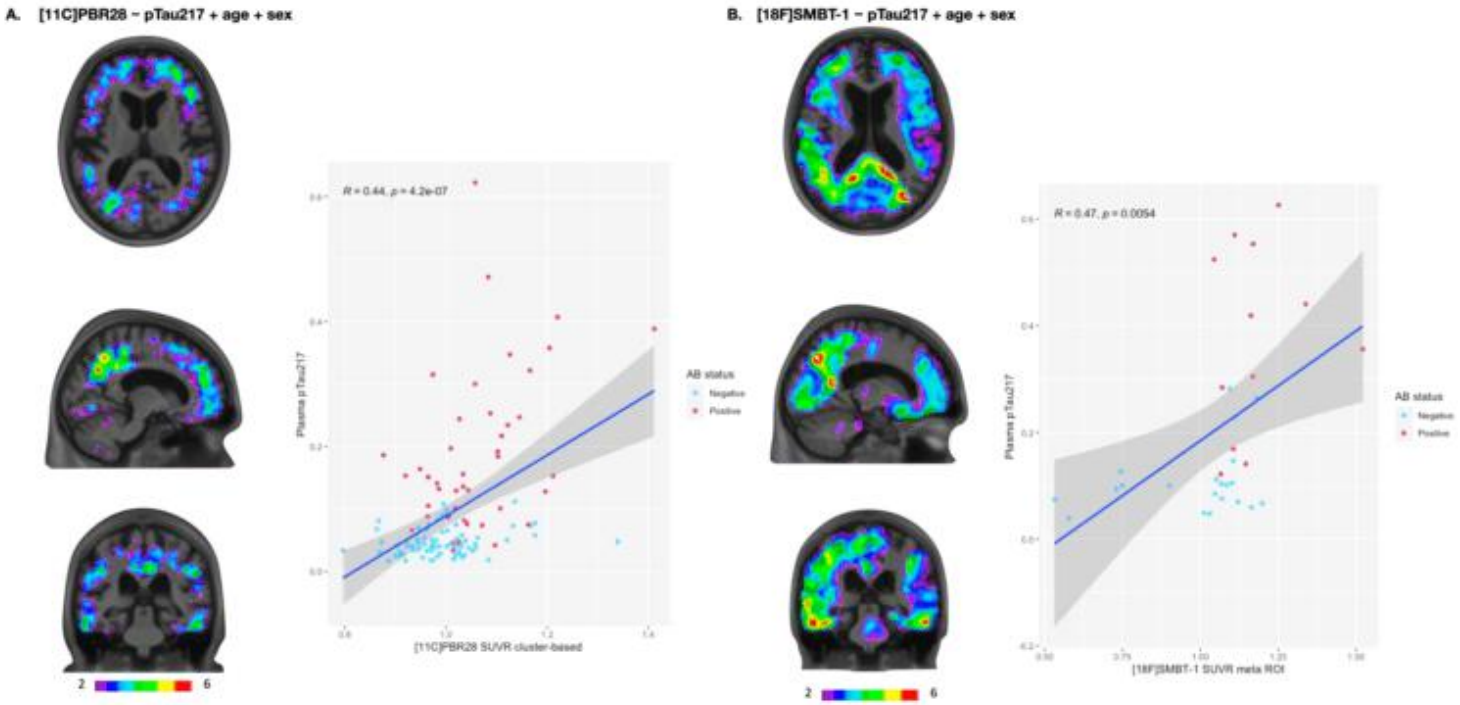


Figure 1: Associations between glial-PET and plasma pTau217
A. Voxel-based and linear regression models using Spearman evaluated the relationship between [11C]PBR28 plasma pTau217
B. Voxel-based and linear regression models using Spearman evaluated the relationship between [18F]SMBT-1 plasma pTau217

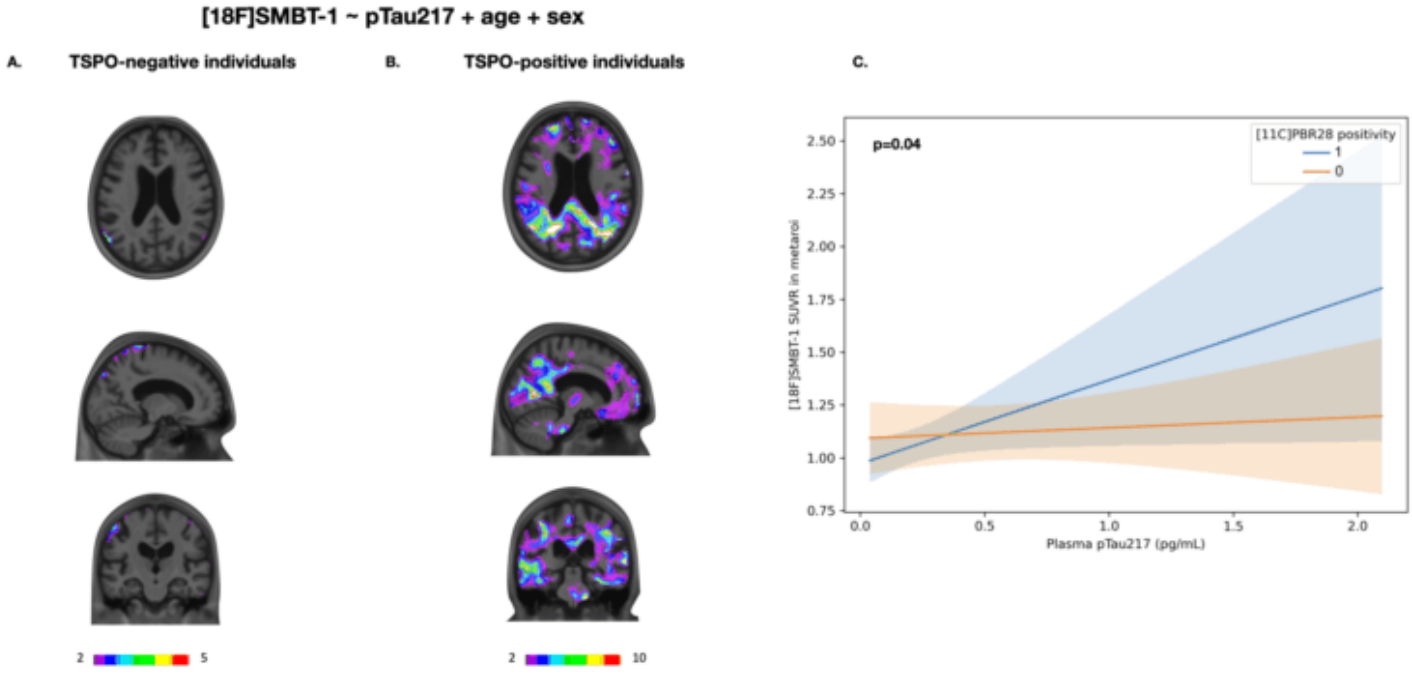


Figure 2: Effect of microglial positivity on the association between astroglia and plasma pTau217
A. Voxel-based regression models evaluated the relationship between [18F]SMBT-1 and plasma pTau217 in [11C]PBR28 negative individuals
B. Voxel-based regression models evaluated the relationship between [18F]SMBT-1 and plasma pTau217 in [11C]PBR28 positive individuals
C. Interaction plot showing the relationship between [18F]SMBT-1 and plasma pTau217 based on [11C]PBR28 positivity

Keywords: Inflammation, Microglia, Astroglia, PET, plasma ptau217

Astrogliosis mediates the effects of amyloid, moderated by CVD, on tau and cognition in non-demented individuals

Alexandra Gogola[1], Brian Lopresti[1], Ann Cohen[1], Milos Ikonomovic[1], Davneet Minhas[1], Beth Snitz[1], Alexandria Reese[1], Cristy Matan[1], Minjie Wu[1], Howard Aizenstein[1], Oscar Lopez[1], Victor Villemagne[1]

[1]*University of Pittsburgh, Pittsburgh, PA, US*

Objectives: We evaluated (I) the pairwise effects of ^{18}F-SMBT-1, a surrogate marker of reactive astrogliosis, measures of Alzheimer's disease (AD) pathology (b-amyloid -Ab-, and tau), cerebrovascular disease (CVD), and neurodegeneration, on cognition, and (II) potential moderating and mediating associations between each metric.

Methods: Data from 163 non-demented participants (Table 1) with available Clinical Dementia Rating Sum of Boxes (CDR SoB) data were processed and sampled to obtain measures of reactive astrogliosis (SMBT-1 standardized uptake value ratio -SUVR-), Ab (Centiloids, CL), CVD (white matter hyperintensities -WMH- relative to intracranial volume -ICV-), and neurodegeneration (hippocampal volume -HV- adjusted for ICV). A subset of 96 participants additionally had measures of tau (meta temporal CenTauRz -CTRz-). Pairwise associations were evaluated with linear regressions, moderating associations were evaluated by including interaction terms in the linear regressions, and mediating associations were evaluated with causal mediation analysis. All associations were adjusted for age.

Results: Significant associations were found between lateral temporal astrogliosis and Ab (p=0.02), meta temporal tau (p=0.0005) and CDR SoB (p=0.004). Posterior cingulate astrogliosis was associated at trend-level with WMH (p=0.098). Additional pairwise association are shown in Figure 1. All significant moderating associations involved WMH or HV (Figure 2). Mediation analyses revealed that lateral temporal astrogliosis partially mediates the associations between Ab and CDR SoB (p<2.6e-16) and between Ab and meta temporal tau (p<2.6e-16)(Figure 3). Furthermore, meta temporal tau partially mediates the association between lateral temporal astrogliosis and CDR SoB (p<2.6e-16) and between Ab and CDR SoB (p<2.6e-16)(Figure 3).

Conclusions: In non-demented participants we found that reactive astrogliosis was directly associated with hallmark metrics of AD pathology, while interacting with WMH and HV, and mediating the association between Ab with other metrics affecting cognition. This suggests that reactive astrogliosis is an early and relevant player in the AD development pathway.

Table 1. Participant demographics.

	CU	MCI
	Full Set	
N	144	19
Age (years)	70.1 ± 7.6	75.3 ± 7.8*
Sex	81 F, 66 M	10 F, 9 M
Race	130 NHW, 17 AA	16 NHW, 3 AA
Education (years)	15.9 ± 2.4	16.5 ± 2.7
CDR SoB	0.1 ±0.2	0.5 ± 0.6*
WMH (%ICV)	0.3 ± 0.4	0.4 ± 0.5
HV	0.5 ± 0.6	0.4 ± 0.7
CL	11.0 ± 24.9	33.1 ± 42.8*
CL+ (%)	32 (22%)	8 (42%)*
SMBT-1 SUVR	1.6 ± 0.2	1.6 ± 0.2
	Tau Subset	
N	85	11
CenTauRz	0.2 ± 1.9	3.2 ±7.4*
CTRz+ (%)	7 (8.2%)	3 (27.3%)*

*significantly different from CU participants

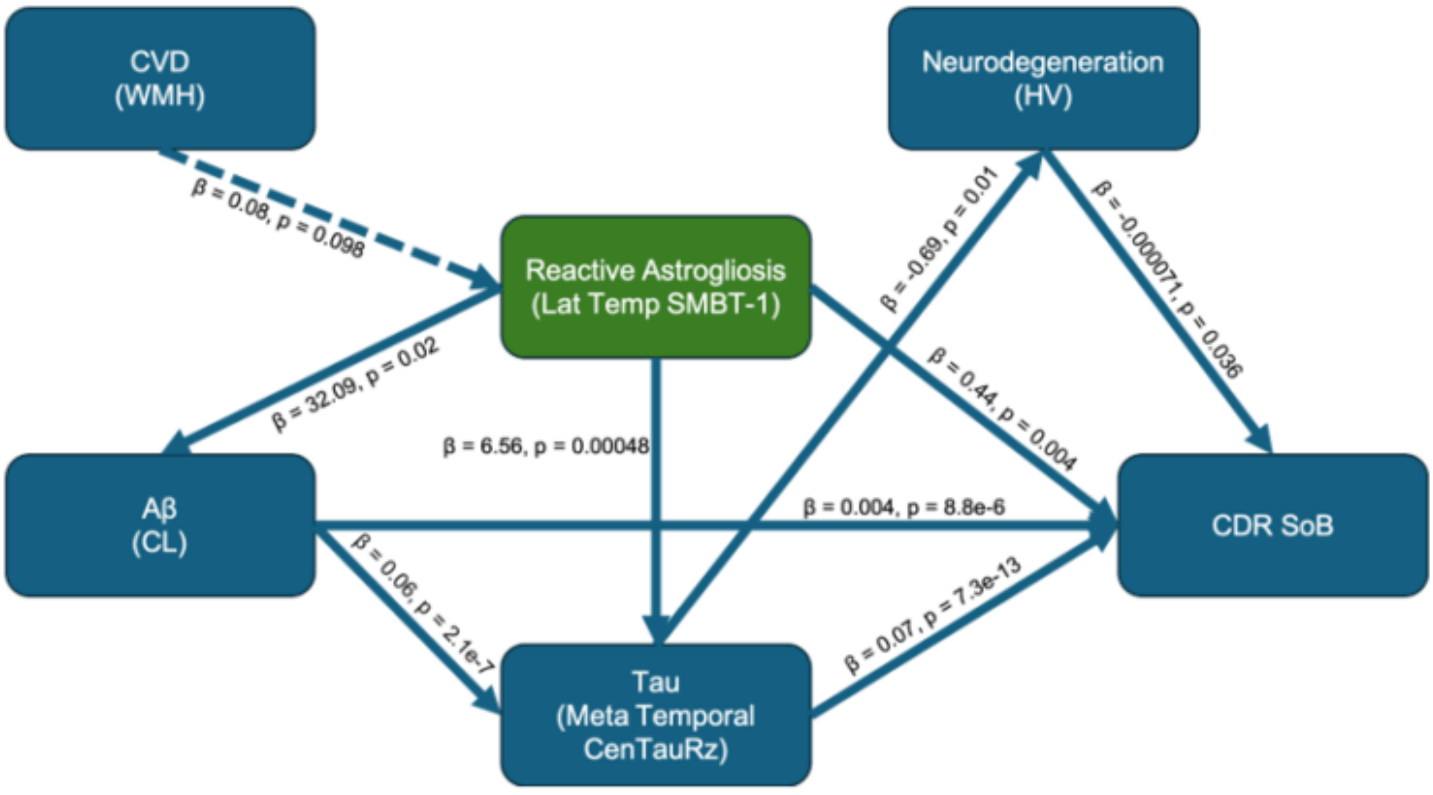


Figure 1. Significant pairwise associations.

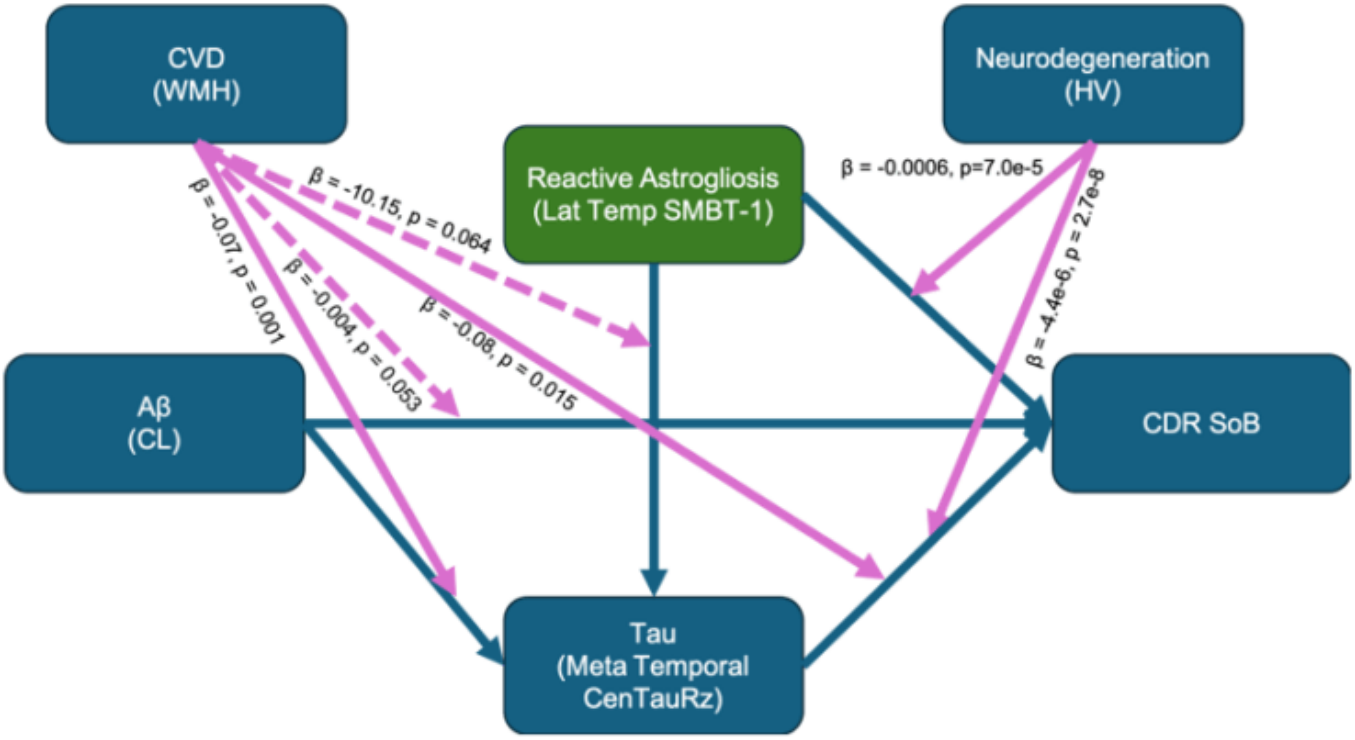
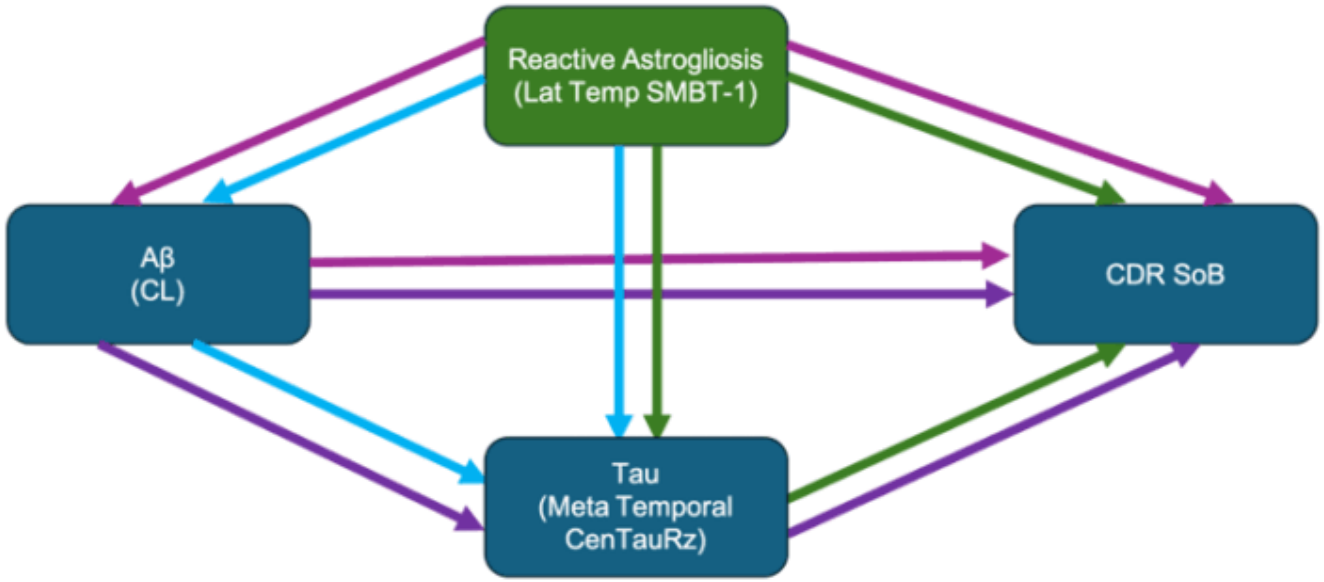


Figure 2. Significant moderating associations.



Mediation	Prop. Mediated	p-value
Tau on Aβ → CDR SoB	0.73	< 2.0e-16
Tau on Reactive Astrogliosis → CDR SoB	0.78	< 2.0e-16
Aβ on Reactive Astrogliosis → CDR SoB	0.38	< 2.0e-16
Aβ on Reactive Astrogliosis → Tau	0.39	< 2.0e-16

Figure 3. Significant mediating associations.

Keywords: astrogliosis, amyloid, mediation, cognition, CVD

TSPO expression patterns in the postmortem brain: relevance to neuroinflammation imaging

Christina Moloney[1], SeungBaek Lee[1], Josie Emery[2], Mahathi Kandimalla[1], Hugo Botha[3], Jonathan Graff-Radford[3], David Jones[3], R. Ross Reichard[2], David Knopman[3], Clifford Jack[1], Ronald Petersen[3], Aivi Nguyen[2], Val Lowe[1]

[1]*Department of Radiology, Mayo Clinic, Rochester, MN, US*
[2]*Department of Laboratory Medicine and Pathology, Mayo Clinic, Rochester, MN, US*
[3]*Department of Neurology, Mayo Clinic, Rochester, MN, US*

Background: ER176 is a positron emission tomography (PET) tracer used to image neuroinflammation by binding to the translocator protein (TSPO). While TSPO is known to be elevated in microglia, its expression across different cognitive states in the human brain remains poorly characterized. Our goal was to characterize the cellular expression of TSPO in the postmortem brain.

Methods: We performed multiplex immunofluorescence on amygdala and hippocampal sections from three postmortem cases with antemortem [C11] ER176 PET imaging: cognitively unimpaired (CU, n=1) and mild cognitive impairment (MCI, n=2). Sections were stained for TSPO, microglial marker IBA1, and nuclear marker DAPI. Subjects were genotyped for *TSPO* rs6971 polymorphism and classified as high-affinity binders (G/G), mixed-affinity binders (A/G), or low-affinity binders (A/A). Two cases (CU and one MCI) were mixed-affinity binders, while the other MCI case was a high-affinity binder.

Results: TSPO expression was detected in microglia, endothelial cells (including blood vessels and choroid plexus), astrocytes, and neurons (**Figure 1**). In microglia, TSPO did not fully overlap with IBA1-positive areas. In the CU case, neuronal TSPO staining was faint or absent, whereas MCI cases showed more intense and frequent neuronal TSPO staining (**Figure 2**). Interestingly, the case with a high-affinity binding genotype (G/G) had fewer microglia overall, as identified by IBA1 staining, compared to mixed-affinity binding cases (A/G). Given that ER176 is used to image neuroinflammation via TSPO, this observation may reflect a paradox between binding affinity and microglial abundance, warranting further investigation.

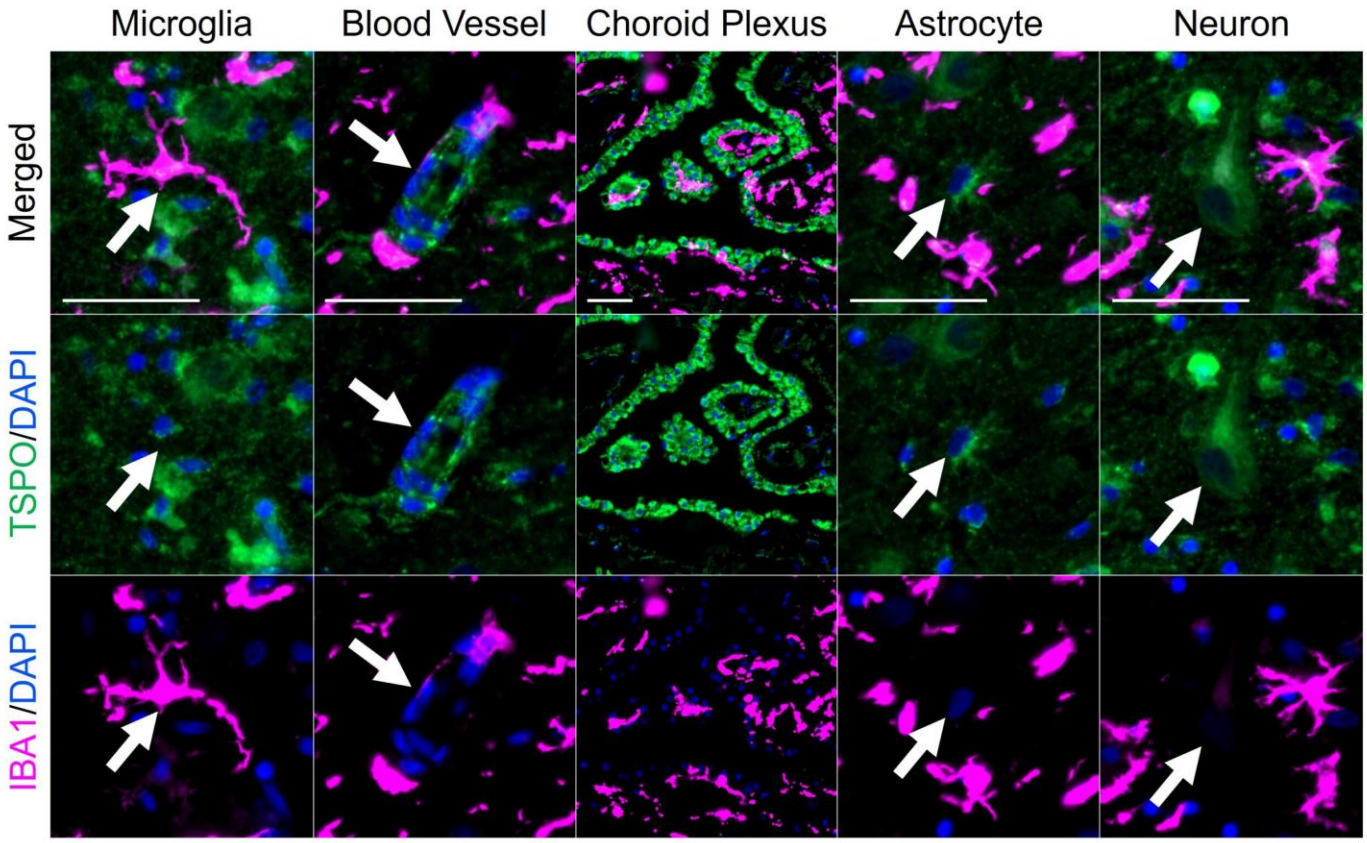


Figure 1. Cellular expression of TSPO. TSPO positivity (green) was observed in microglia (IBA1 positive, pink), blood vessel endothelia, choroid plexus endothelia, astrocytes, and neurons. Scale bar measures 50 µm. Microglia, blood vessel, astrocyte, and neuron images were from the MCI A/G case, and the choroid plexus image was from the CU A/G case.

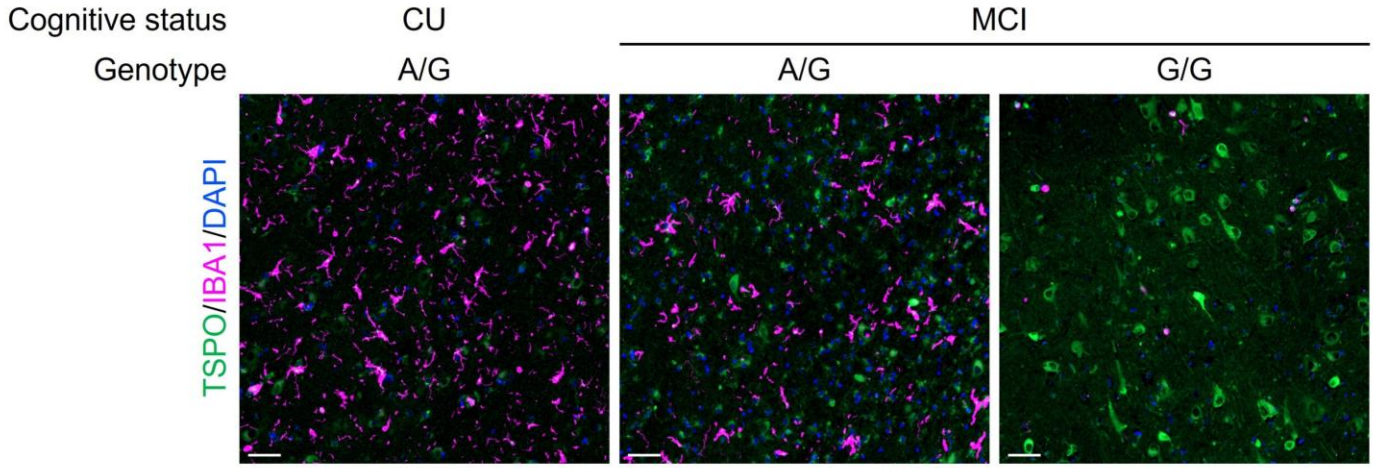


Figure 2. TSPO expression in the subiculum of the hippocampus. Images from multiplex immunofluorescence showing translocator protein (TSPO, green), microglia (IBA1, pink), and nuclei (DAPI, blue). TSPO is more strongly stained in the neurons from mild cognitive impairment (MCI) cases compared to the cognitively unimpaired case (CU). IBA1 expression is reduced in the TSPO G/G genotype compared to A/G. Scale bar measure 50 µm.

Conclusions: This preliminary study demonstrates that TSPO is expressed across multiple cell types in both CU and MCI brains, with variability in expression levels. These findings underscore the importance of further

characterizing TSPO distribution in healthy and neurodegenerative conditions. Future work will expand multiplex immunofluorescence to additional cell markers and cases and explore correlations between TSPO staining and ER176 PET signal.

Keywords: Neuropathology, TSPO, neuroinflammation

Tuesday, January 14, 2026 - 06:10 pm - 06:15 pm

[Special] Podium Session

The PET-tle Royale ((HAI's Re-Myelination Showdown Quiz))

This will be the grand finale – not to be missed!

Wednesday, January 14, 2026 - 09:00 am - 10:30 am

Podium Session

SESSION VII: Early and intermediate signals and prognostic value

CHAIRS:

Sterling Johnson, *University of Wisconsin-Madison, Madison, WI, USA*

Sylvia Villeneuve*, McGill University, Montreal, QC, Canada*

Wednesday, January 14, 2026			
09:00 am – 10:30 am	**Podium Presentation**	**Authors**	**Presenter**
09:05 am – 09:20 am	Discordance between amyloid PET visual read and quantitation: false positives or early pathology detection?	Heston | Maiti | Blazhenets | Soleimani-Meigooni | Lin | Hills | Windon | Tammewar | Dage | Eloyan | Jagust | Landau | Koeppe | Carrillo | Dickerson | Apostolova | Rabinovici | La Joie	**Margo Heston**, Edward and Pearl Fein Memory & Aging Center, Department of Neurology, University of California, San Francisco, San Francisco, CA, US
09:20 am – 09:35 am	Considerations for repeat testing of amyloid PET-validated plasma pTau217 diagnostic assays in the screening cohort for the AHEAD 3-45 study	Rissman | Langford | Ngolab | Sukreet | Raman | Donohue | Abdel-Latif | Jimenez-Maggiora | Rafii | Sachdev | Irizarry | Braunstein | Aisen | Johnson | Sperling	**Robert Rissman**, Alzheimer's Therapeutic Research Institute, Keck School of Medicine of the University of Southern California, SAN DIEGO, CA, US
09:35 am – 09:50 am	The prognostic value of p-tau217 levels on progression to clinical impairment over 2, 5 and 10 years	Buckley | Townsend | Coughlan | Birkenbihl | Seto | Brown | Cuppels | Properzi | Hönig | Li | Schultz | Chhatwal | Yang | Caldwell | Betthauser | Oomens | Carrigan | Healy | Garcia Condado | Johnson | Yau | Langford | Farrell | Amariglio | Rentz | Papp | Hohman | Donohue | Johnson | Sperling	**Rachel Buckley**, Department of Neurology, Mass General Brigham, Boston, MA, US
09:50 am – 10:05 am	Distribution of tau and amyloid pathology across cognitive states in a population-based, admixed autopsy cohort	Grinberg | Pereira | Paraizo Leite | Ribeiro Paes | Matos Silva | dos Reis Ururahy | Cunha de Moraes | Liguori Padrão | Pasqualucci | Diehl Rodriguez | Naslavsky | Ferretti-Rebustini | Nitrini | Ferriolli | Suemoto	**Lea Grinberg**, Departments of Laboratory Medicine and Pathology and Neurosciences, Mayo Clinic, Jacksonville, FL, US

Discordance between amyloid PET visual read and quantitation: false positives or early pathology detection?

Margo Heston[1], Piyush Maiti[1], Ganna Blazhenets[1], David Soleimani-Meigooni[1], Zoe Lin[1], Aidyn Rose Hills[1], Charles Windon[1], Gautam Tammewar[1], Jeffrey Dage[2,3], Ani Eloyan[4], William Jagust[5], Susan Landau[5], Robert Koeppe[6], Maria Carrillo[7], Bradford Dickerson[8], Liana Apostolova[2,9], Gil Rabinovici[1,10], Renaud La Joie[1]

[1]*Edward and Pearl Fein Memory & Aging Center, Department of Neurology, University of California, San Francisco, San Francisco, CA, US*
[2]*Department of Neurology, Indiana University School of Medicine, Indianapolis, IN, US*
[3]*Stark Neurosciences Research Institute, Indiana University School of Medicine, Indianapolis, IN, US*
[4]*Department of Biostatistics, Center for Statistical Sciences, Brown University, Providence, RI, US*
[5]*Department of Neuroscience, University of California, Berkeley, Berkeley, CA, US*
[6]*Department of Radiology, University of Michigan, Ann Arbor, MI, US*
[7]*Alzheimer's Association, Chicago, IL, US*
[8]*Department of Neurology, Massachusetts General Hospital, Harvard Medical School, Boston, MA, US*
[9]*Department of Radiology, Indiana University School of Medicine, Indianapolis, IN, US*
[10]*Department of Radiology and Biomedical Imaging, University of California, San Francisco, San Francisco, CA, US*

Background: Evaluating amyloid PET positivity has revealed some images show visual read and quantitation (V/Q) discordance. We investigated imaging, demographic, and plasma biomarker features associated with V/Q discordance.

Methods: Analyses included a cross-sectional ADNI and LEADS sample of ^{18}F-Florbetaben, ^{18}F-Florbetapir, and ^{18}F-Flutafuranol (n=997, 733, 78). Dichotomous visual interpretations were completed by expert raters, and a FreeSurfer 7-generated threshold of 18 CL defined quantitative amyloid positivity. We used logistic models with sex and *APOE* ε4 carriage and linear models with regional amyloid uptake and plasma biomarkers, regressing each outcome on V/Q status.

Results: Six percent of scans were V/Q discordant, evenly split between V-Q+ and V+Q- (Figure 1A); these comprised 8% of cognitively unimpaired and mild cognitive impairment groups vs. 2% of dementia cases (Figure 1B). V-Q+ were twice as likely as V+Q- to be female or *APOE* ε4 carriers (Figures 1C, 1D). By definition, both Q- subgroups were <18 CL, however the V+Q- subgroup had significantly higher CL values (median=6.5 CL) than V-Q- (0 CL) (Figure 2A). Additionally, while both Q+ subgroups were >18 CL by definition, V-Q+ showed only mild to moderate amyloid burden (<45 CL). Compared to the V-Q- group, V-Q+ had higher subcortical white matter (WM) tracer uptake, while V+Q- showed lower binding (Figure 2B). Renormalizing neocortical SUVR by subcortical WM eliminated SUVR differences between the discordant groups, both of which had higher amyloid than V-Q- (Figure 2C). Across several assays, plasma ptau217 markers were higher in V-Q+ and V+Q- compared to V-Q- (Figures 3A, 3B).

Conclusions: V/Q discordance may indicate early amyloid pathology undetected by either visual read or quantitation. Females and *APOE* ε4 carriers may be particularly affected by visual reads without accompanying quantitation. WM partial volume effects may also explain discordant patterns. This underscores the complementarity of visual read and quantitation in clinical contexts.

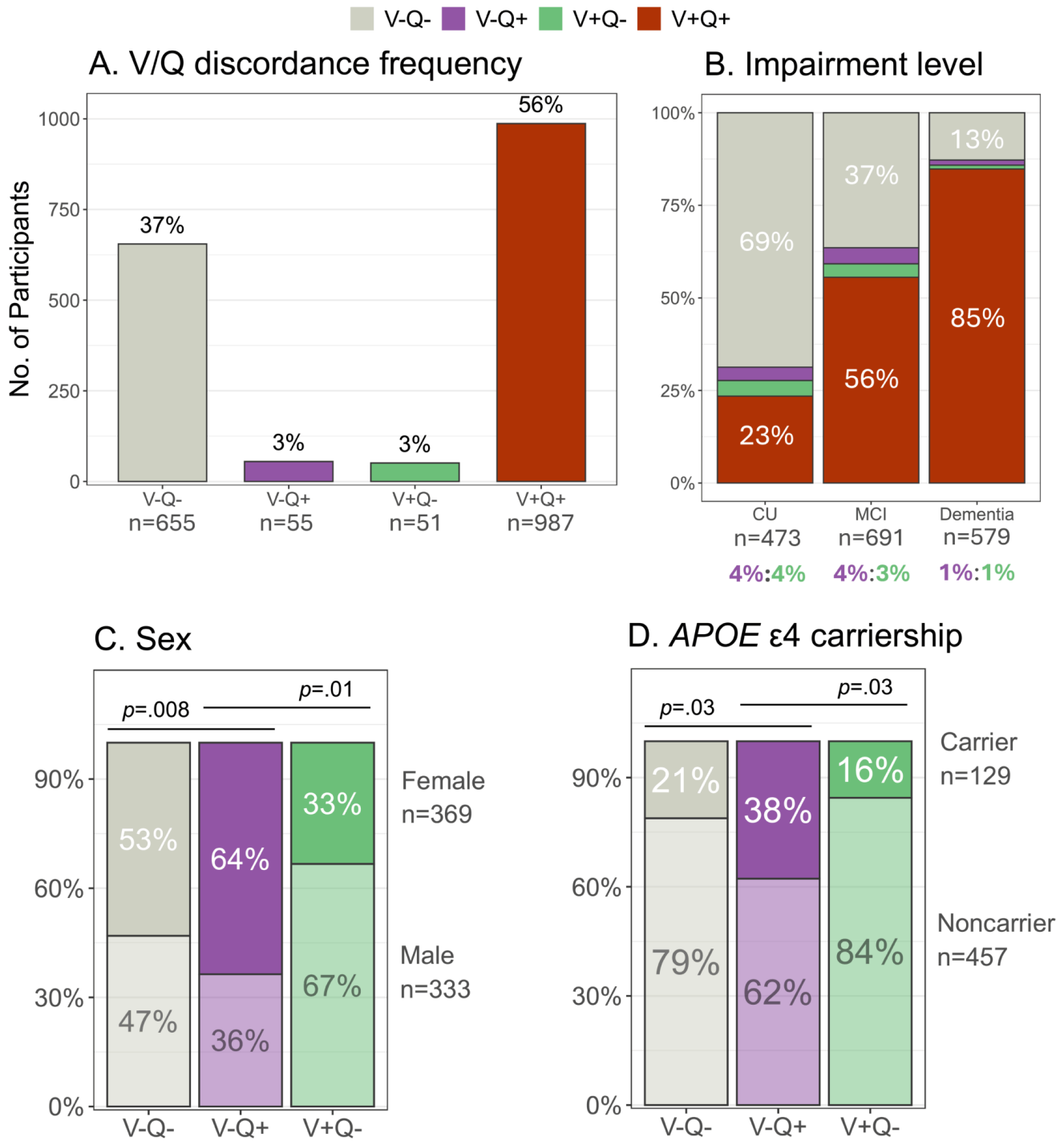


Figure 1. Demographics across V/Q groups. **(A)** Frequency of V/Q classifications across ADNI and LEADS **(B)** Proportion of V/Q classifications within cognitive status groups. Distribution of sex **(C)** and *APOE* ε4 carriership **(D)** across V/Q classifications. Statistical analyses were conducted referencing V-Q- because the discordant scans were hypothesized to be borderline cases (confirmed in Figure 2A). Per outcome in panels C and D, Benjamini-Hochberg adjustments corrected for inflated Type I error due to pairwise comparisons. Abbreviations: *APOE*, apolipoprotein E; CL, Centiloids; CU, cognitively unimpaired; MCI, mild cognitive impairment; Q, quantitation positive (+) or negative (-) status; V, visual read positive (+) or negative (-) status.

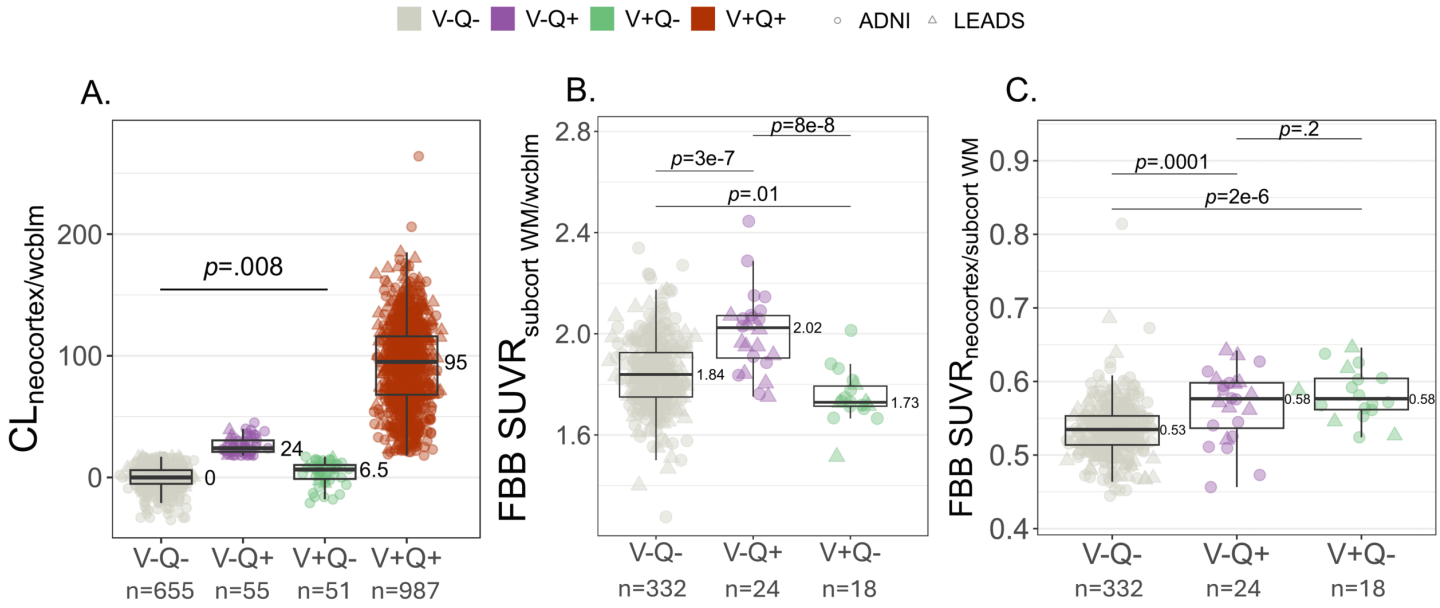


Figure 2. Amyloid tracer uptake across V/Q classifications. **(A)** Neocortical amyloid levels normalized by whole cerebellar uptake. **(B)** Eroded subcortical white matter FBB uptake normalized by whole cerebellum. **(C)** Neocortical FBB uptake renormalized by eroded subcortical white matter. Median values are highlighted per V/Q subgroup. Statistical analyses were conducted referencing V-Q- because the discordant scans were hypothesized to be borderline cases (confirmed in Figure 2A). All analyses showing results with FBB were replicated with FBP; statistical analyses were not performed with NAV scans separately due to small cell size. Per outcome, Benjamini-Hochberg adjustments corrected for inflated Type I error due to pairwise comparisons. Abbreviations: CL, Centiloids; FBB, ^{18}F-Florbetaben; FBP, ^{18}F-Florbetapir; NAV, ^{18}F-Flutafuranol; subcort WM, eroded subcortical white matter; SUVR, standardized uptake value ratio; Q, quantitation positive (+) or negative (-) status; V, visual read positive (+) or negative (-) status; wcblm, whole cerebellum.

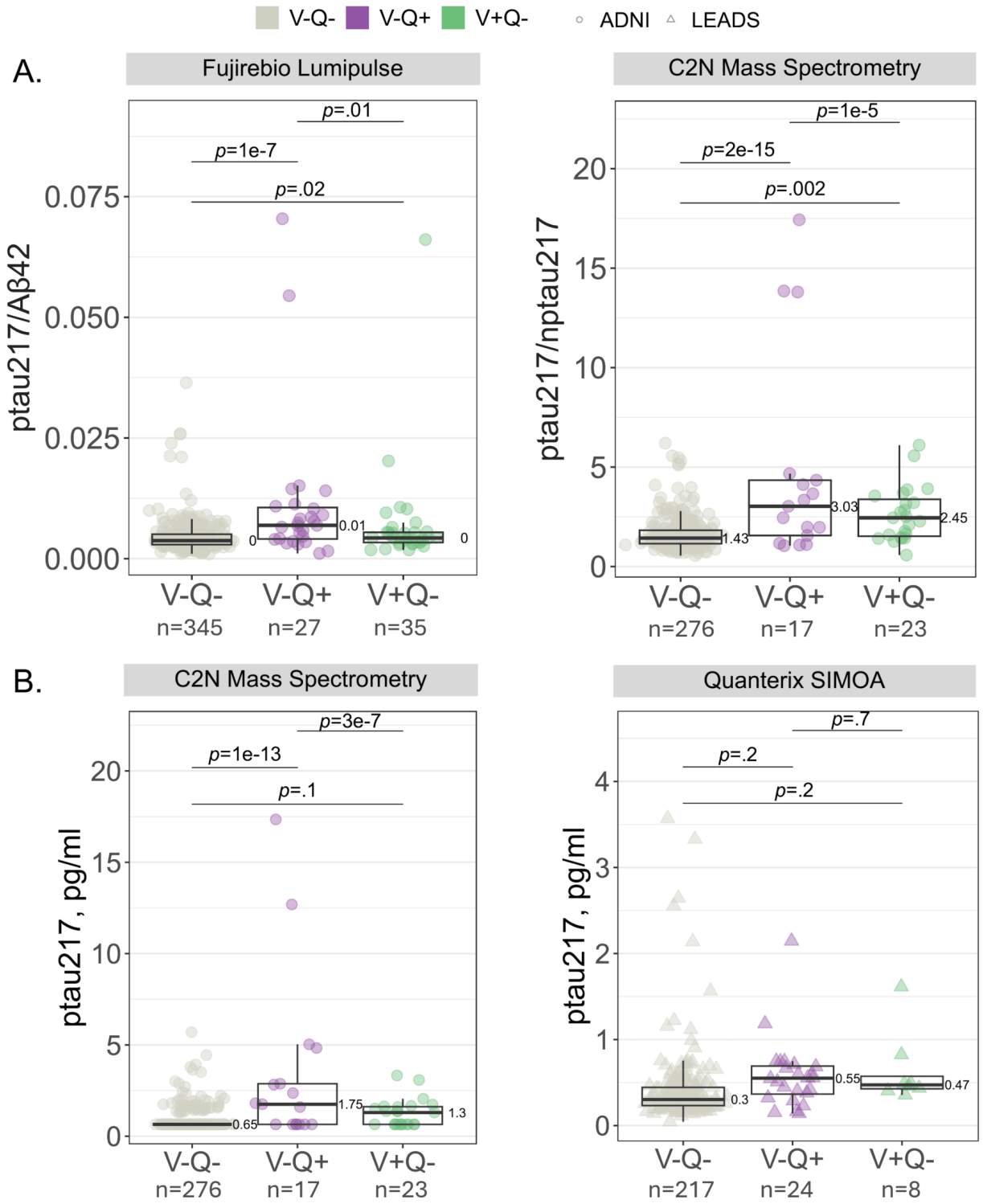


Figure 3. Plasma biomarkers across V/Q classifications. **(A)** ptau217/Aβ42 (left) and ptau217/nptau217 (right) measured in ADNI participants. **(B)** ptau217 measured with the C2N platform in ADNI (left) and with Quanterix SIMOA in LEADS (right). Median values are highlighted per V/Q subgroup. Per biomarker, Benjamini-Hochberg adjustments corrected for inflated Type I error due to pairwise comparisons. Abbreviations: Aβ, amyloid-beta; GFAP, glial fibrillary activation protein; (n)ptau, (non)phosphorylated tau; Q, quantitation positive (+) or negative (-) status; V, visual read positive (+) or negative (-) status.

Keywords: visual read, PET quantitation, amyloid PET, discordance, plasma ptau217

Considerations for repeat testing of amyloid PET-validated plasma pTau217 diagnostic assays in the screening cohort for the AHEAD 3-45 study

Robert Rissman[1], Oliver Langford[1], Jennifer Ngolab[1], Sonal Sukreet[1], Rema Raman[1], Michael Donohue[1], Sara Abdel-Latif[1], Gustavo Jimenez-Maggiora[1], Michael Rafii[1], Pallavi Sachdev[2], Michael Irizarry[2], Joel Braunstein[3], Paul Aisen[1], Keith Johnson[4], Reisa Sperling[4]

[1]*Alzheimer's Therapeutic Research Institute, Keck School of Medicine of the University of Southern California, SAN DIEGO, CA, US*
[2]*Eisai, Nutley, NJ, US*
[3]*C2N Diagnostics, St. Louis, MO, US*
[4]*Brigham and Women's Hospital, Massachusetts General Hospital, Harvard Medical School, Boston, MA, US*

Background: The AHEAD 3-45 clinical trial used plasma biomarkers to enroll cognitively unimpaired individuals to test Lecanemab in preclinical AD. To examine biomarker variability and repeat testing stability for predicting amyloid PET status in asymptomatic individuals, we conducted a cross-sectional analysis using samples from the AHEAD 3-45 screening period.

Methods: Plasma samples from 193 AHEAD participants were randomly selected. Biomarker measures in plasma collected from the first (Visit 1) and third screening visit (Visit 2), were evaluated using mass spectrometry (C2N) for Aβ42, Aβ40, p-tau217, np-tau217, %p-tau217; and immunoassay (Fujirebio Lumipulse) for p-tau217.

Results: Sample demographics are shown in Table 1. Assessment of Aβ biomarker concentrations had a strong positive relationship between visits, with Aβ40 exhibiting a higher relationship (r=0.78) than Aβ42 (r=0.71). Comparing Aβ42/40 between visits showed a moderate positive relationship (r=0.50) (Figure 1,2). C2N biomarker measures demonstrated a strong relationship of p-tau217 (r=0.83) and a moderate-strong relationship in np-tau217 (r=0.68) between visits. A moderate-strong positive relationship between %p-tau217 measures from different visits was also observed (r=0.69). The strongest relationship between biomarker measures from different visits was observed with Lumipulse p-tau217 (r=0.91). Loess regression revealed a similar relationship from linear regression amongst different visits, except for a subtle sinusoidal relationship for Aβ42/40 and a concave relationship in %p-tau217 (Figure 1). Repeat testing both of samples from the same visit and from a later visit resulted in approximately 20% of participants' amyloid PET status being classified inconsistently compared to the initial visit.

Conclusion: We find that both assays have excellent cross-sectional ability to predict amyloid PET status in asymptomatic individuals despite between-visit and between-run variations. We found C2N's APS2 and ATRI model 2 to have lowest reclassification rates. In the case of the C2N assays, levels of np-tau217 may be a contributing factor to repeat testing inconsistency in asymptomatic populations.

Table 1: Demographic characteristics by assay source and test-retest timepoint

	C2N		LUMIPULSE	
	Different Visit (Visit 1 vs Visit 2) (N=193)	Same Visit (Visit 2 vs Visit 2) (N=190)	Different Visit (Visit 1 vs Visit 2) (N=193)	Same Visit (Visit 2 vs Visit 2) (N=193)
Age (in Years)				
Mean (SD)	68.5 (6.2)	68.5 (6.2)	68.5 (6.2)	68.5 (6.2)
Median (Range)	69.0 (55.0, 80.0)	69.0 (55.0, 80.0)	69.0 (55.0, 80.0)	69.0 (55.0, 80.0)
Sex				
Female	134 (69.4%)	134 (70.5%)	134 (69.4%)	134 (69.4%)
Male	59 (30.6%)	56 (29.5%)	59 (30.6%)	59 (30.6%)
Race				
Asian	1 (0.5%)	1 (0.5%)	1 (0.5%)	1 (0.5%)
Black or African American	8 (4.1%)	7 (3.7%)	8 (4.1%)	8 (4.1%)
More than one race	2 (1.0%)	2 (1.1%)	2 (1.0%)	2 (1.0%)
White	182 (94.3%)	180 (94.7%)	182 (94.3%)	182 (94.3%)
Ethincity				
Hispanic or Latino	17 (8.8%)	17 (8.9%)	17 (8.8%)	17 (8.8%)
Not Hispanic or Latino	176 (91.2%)	173 (91.1%)	176 (91.2%)	176 (91.2%)
Education (in Years)				
Mean (SD)	16.4 (3.2)	16.4 (3.2)	16.4 (3.2)	16.4 (3.2)
Median (Range)	16.0 (8.0, 28.0)	16.0 (8.0, 28.0)	16.0 (8.0, 28.0)	16.0 (8.0, 28.0)
PET Amyloid Centiloid				
Mean (SD)	38.1 (34.9)	38.8 (34.8)	38.1 (34.9)	38.1 (34.9)
Median (Range)	34.7 (-14.9, 148.0)	34.9 (-14.9, 148.0)	34.7 (-14.9, 148.0)	34.7 (-14.9, 148.0)
Amyloid Status $>= 20$ PET Centiloid				
Negative	68 (35.2%)	65 (34.2%)	68 (35.2%)	68 (35.2%)
Positive	125 (64.8%)	125 (65.8%)	125 (64.8%)	125 (64.8%)
APOE *				
$\epsilon 2/\epsilon 3$	12 (6.2%)	12 (6.3%)	12 (6.2%)	12 (6.2%)
$\epsilon 2/\epsilon 4$	8 (4.1%)	8 (4.2%)	8 (4.1%)	8 (4.1%)
$\epsilon 3/\epsilon 3$	62 (32.1%)	61 (32.1%)	62 (32.1%)	62 (32.1%)
$\epsilon 3/\epsilon 4$	87 (45.1%)	85 (44.7%)	87 (45.1%)	87 (45.1%)
$\epsilon 4/\epsilon 4$	24 (12.4%)	24 (12.6%)	24 (12.4%)	24 (12.4%)
Has plasma Aβ?				
Yes	187 (100.0%)	0	0	0
Missing	6	190	193	193
Has plasma APOE?				
Yes	193 (100.0%)	0	0	0
Missing	0	190	193	193
Has plasma APS?				
Yes	187 (100.0%)	0	0	0
Missing	6	190	193	193
Has plasma APS2?				
Yes	180 (100.0%)	189 (100.0%)	0	0
Missing	13	1	193	193
Has plasma p-tau217?				
Yes	186 (100.0%)	190 (100.0%)	193 (100.0%)	193 (100.0%)
Missing	7	0	0	0

* Visit 1 and visit 2 represent screening visit 1 and screening visit 3 in the AHEAD study, respectively.

† APOE result that collected at visit 1 was used.

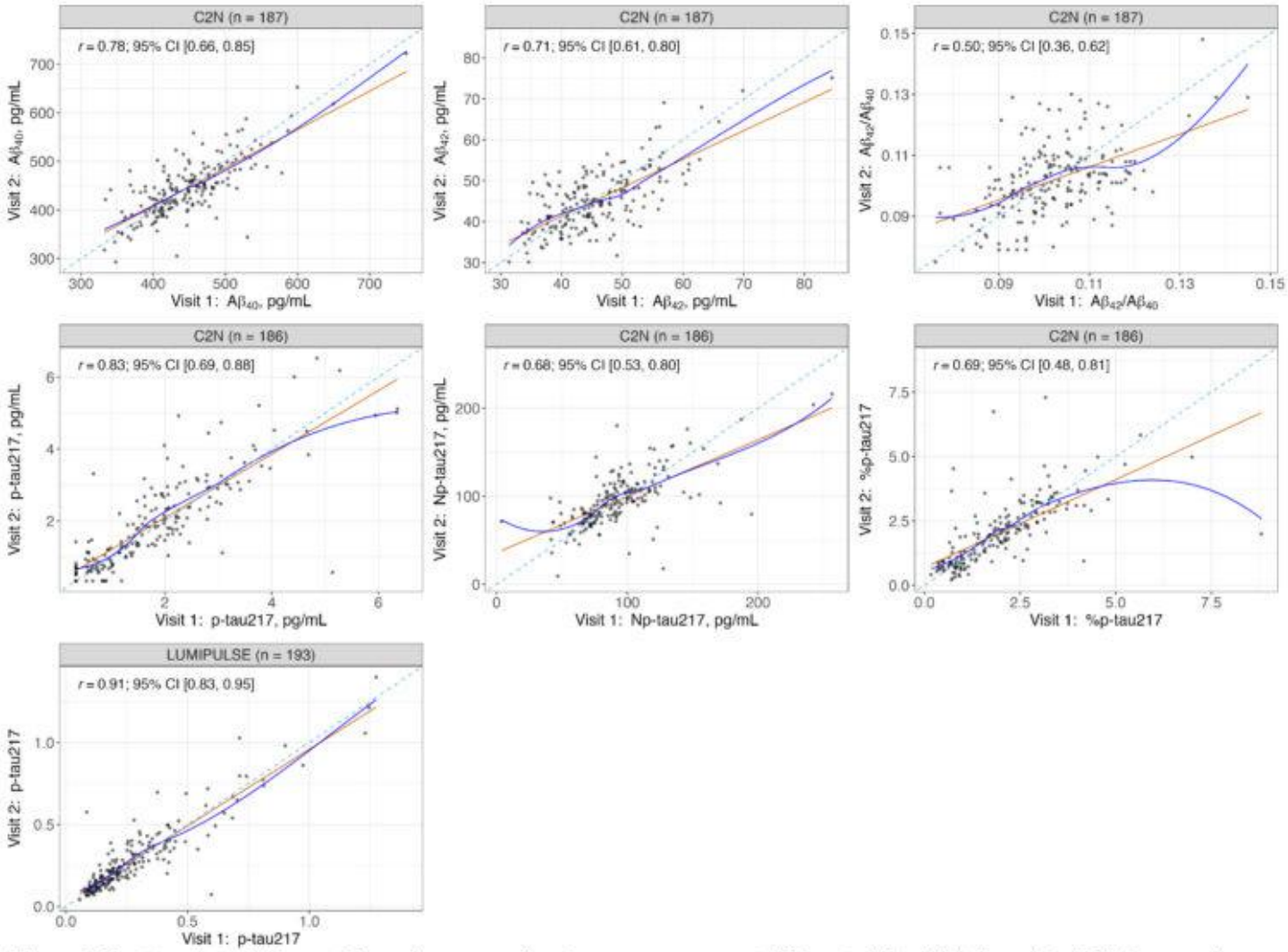


Figure 1 Scatter plot of plasma biomarkers samples by assay source at different visits (visit 1 and visit 2). Pearson's correlation coefficient with corresponding 95% confidence interval (CI) obtained through bootstrapping. Solid blue line represents a Loess line, solid red line represents linear regression fit line and dashed line represents identity line. All C2N plasma biomarkers with assay version 2 were mapped to C2N assay version 1 scale for combined analysis.

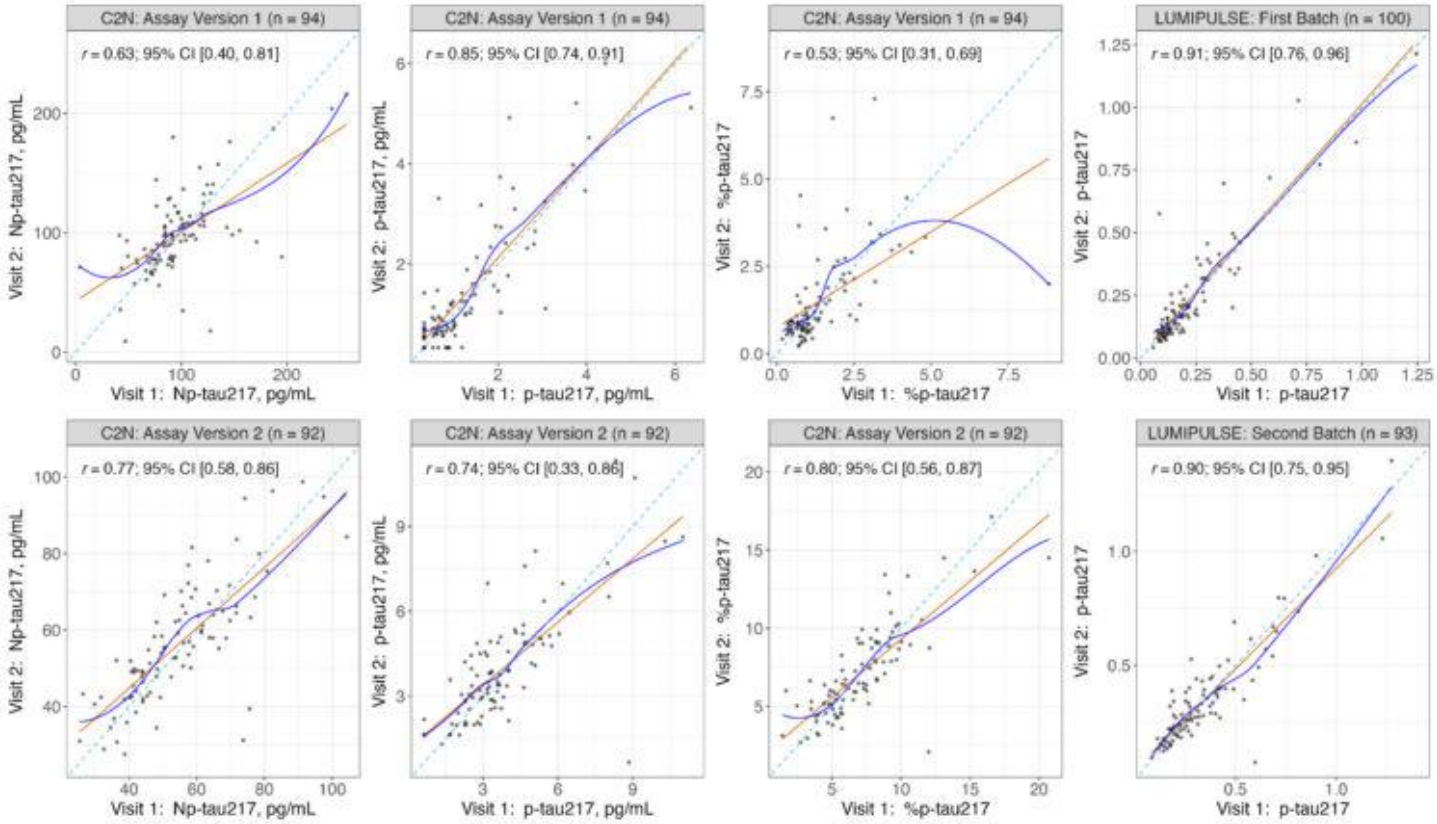


Figure 2. Summary of different visits repeat testing comparing visit 1 to visit 2. Estimated Pearson's correlation coefficient (r) with corresponding 95% confidence interval (CI) was calculated through bootstrapping. All C2N plasma biomarker concentrations derived from the C2N version 2 model were mapped to the C2N assay version 1 model to scale for combined analysis.

Keywords: Amyloid PET, pTau217, biomarker, asymptomatic, clinical trial

The prognostic value of p-tau217 levels on progression to clinical impairment over 2, 5 and 10 years

Rachel Buckley[1], Diana Townsend[1], Gillian Coughlan[1], Colin Birkenbihl[1], Mabel Seto[1], Jane Brown[1], Madison Cuppels[1], Michael Properzi[1], Merle Hönig[1], Annie Li[1], Aaron Schultz[1], Jasmeer Chhatwal[1], Hyun-Sik Yang[1], Jessica Caldwell[2], Tobey Betthauser[2], Julie Oomens[2], Maria Carrigan[3], Brian Healy[1], Jorge Garcia Condado[1], Sterling Johnson[2], Wai-Ying (Wendy) Yau[1], Oliver Langford[4], Michelle Farrell[1], Rebecca Amariglio[1], Dorene Rentz[1], Kathryn Papp[1], Timothy Hohman[5], Michael Donohue[4], Keith Johnson[1], Reisa Sperling[1]

[1]*Department of Neurology, Mass General Brigham, Boston, MA, US*
[2]*University of Wisconsin-Madison, Madison, WI, US*
[3]*Amsterdam UMC, Amsterdam, The Netherlands*
[4]*University of Southern California, Los Angeles, CA, US*
[5]*Vanderbilt University, Nashville, TN, US*

Background: Plasma p-Tau$_{217}$ shows strong correspondence with amyloid-β (Aβ)-PET, tau-PET and cognitive decline. The prognostic value of p-Tau$_{217}$ on long-term clinical progression among initially cognitively unimpaired (CU) adults remains unclear. Here, we provide prognostic estimates of clinical progression in a pooled, harmonized sample across multiple longitudinal cohorts.

Method: We used harmonized data from 2,537 CU participants (Age$_{mean}$ = 70±7.3 years; 62% female) across A4/LEARN, HABS, ADNI, WRAP. Participants were selected based on their first plasma p-Tau$_{217}$ measurement and ≥2 years of diagnostic and cognitive (harmonized PACC) follow-up (mean=6.3±2.8yrs, range=0.1–17.2yrs). Linear mixed-effects models examined associations with PACC change. Cox proportional-hazards models examined associations between standardized continuous p-Tau$_{217}$, and *APOE*ε4 status with time-to-event (MCI/Dementia/two-consecutive-visits of CDR≥0.5), adjusting for age, sex, *APOE*ε4 and education. Additional models included Aβ-PET status (using published cut-offs). Absolute 2-, 5-, and 10-year risk was estimated from model-derived survival functions.

Results: Higher p-Tau$_{217}$ predicted faster cognitive decline (p<0.01), with the strongest effects in Aβ+ (p<0.001). There were 526 events of progression to clinical impairment. Each +1SD of p-Tau$_{217}$ was associated with a 37% increased hazard ratio (95%CI:30%-43%), independent of covariates. Model discrimination was high (C-index=0.77; AUC$_{10}$=0.80; Brier$_{10}$=0.13). Predicted 2-, 5-, and 10-year risk in +1SD p-Tau$_{217}$ was associated with 5%, 25% and 54% risk, respectively. Covarying for Aβ-PET (n=2,537), p-Tau$_{217}$ remained associated with 30% increased risk (95%CI:23%-37%,p<0.001); Aβ-positivity was associated with 71% (95%CI:35%-117%,p<0.001). In Aβ+ individuals, corresponding risk was 6%$_{2\text{-year}}$, 27%$_{5\text{-year}}$ and 58%$_{10\text{-year}}$. In an Aβ- only model (n=1,365; 150 events), p-Tau$_{217}$ remained a significant predictor (HR=1.26,95%CI:1.11–1.42,p<0.001). Risk was 3%$_{2\text{-year}}$, 12%$_{5\text{-year}}$ and 25%$_{10\text{-year}}$, respectively.

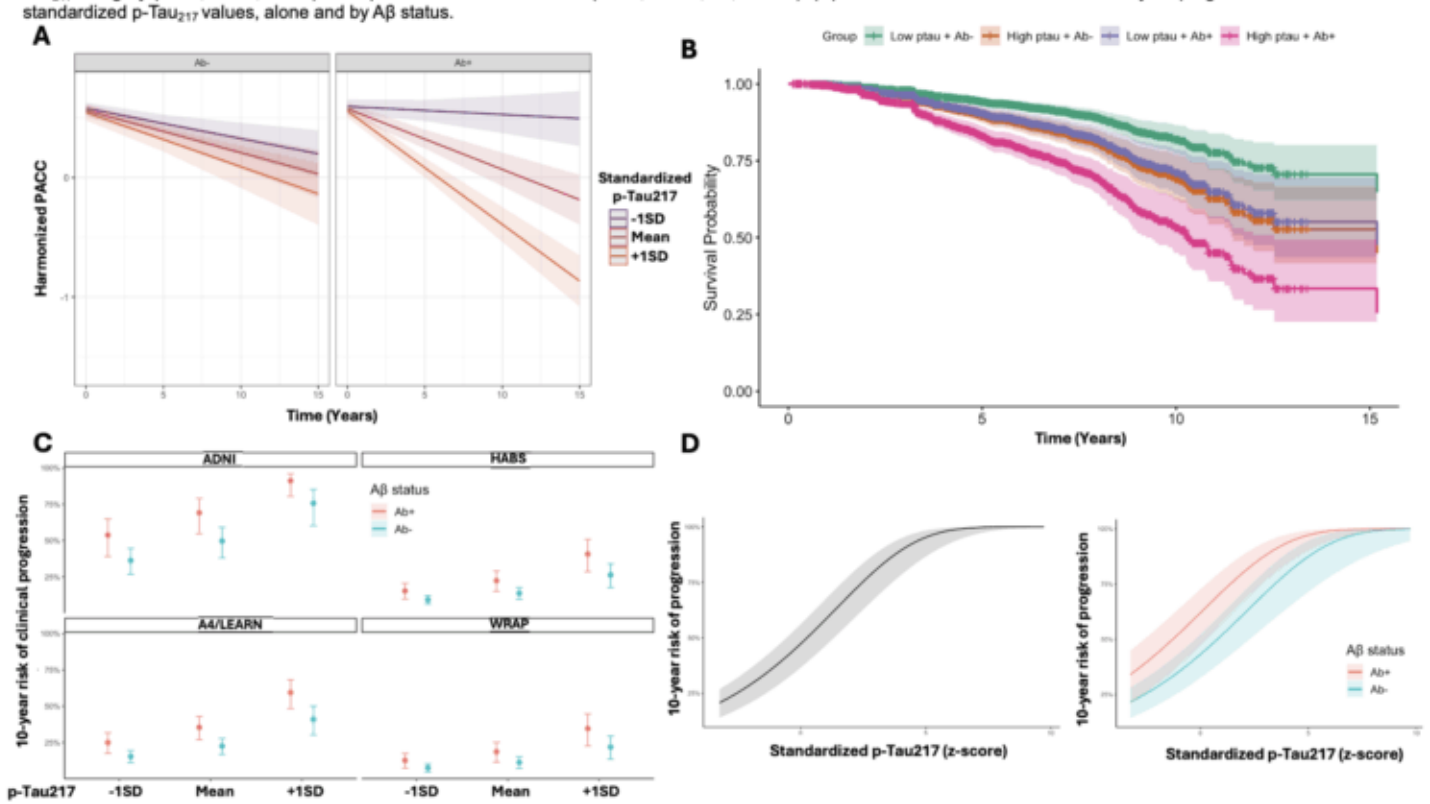
Conclusion: This study provides some of the first 10-year prognostic outcomes for progression to clinical impairment based on p-Tau$_{217}$. Defining clinically actionable thresholds will be essential to translate these findings into individualized prognostic guidance, enabling more informed monitoring and prevention strategies in preclinical AD.

Table 1. Participant Characteristics by Cohort

Characteristic	**Overall**, N = 2,537[†]	**adni**, N = 302[†]	**habs**, N = 294[†]	**a4**, N = 1,466[†]	**wrap**, N = 475[†]
Age	69.70 (7.34) [39.00, 98.22]	73.20 (6.90) [55.10, 98.22]	71.51 (7.70) [50.00, 89.00]	71.59 (4.71) [65.00, 86.66]	60.52 (6.93) [39.00, 77.93]
Sex					
Male	974 (38%)	137 (45%)	115 (39%)	577 (39%)	145 (31%)
Female	1,563 (62%)	165 (55%)	179 (61%)	889 (61%)	330 (69%)
Years of Education	16.52 (2.74) [7.00, 30.00]	16.64 (2.45) [8.00, 20.00]	15.95 (2.90) [8.00, 20.00]	16.61 (2.71) [7.00, 30.00]	16.54 (2.85) [12.00, 29.00]
APOE ε4 Carrier					
e4-	1,491 (59%)	194 (64%)	210 (71%)	795 (54%)	292 (61%)
e4+	1,046 (41%)	108 (36%)	84 (29%)	671 (46%)	183 (39%)
Race					
American Indian or Alaskan Native	8 (0.3%)	1 (0.3%)	2 (0.7%)	5 (0.3%)	0 (0%)
Asian	45 (1.8%)	8 (2.6%)	7 (2.4%)	29 (2.0%)	1 (0.2%)
Black or African American	106 (4.2%)	20 (6.6%)	43 (15%)	28 (1.9%)	15 (3.2%)
More than one race	23 (0.9%)	8 (2.6%)	2 (0.7%)	13 (0.9%)	0 (0%)
Unknown	10 (0.4%)	0 (0%)	0 (0%)	7 (0.5%)	3 (0.6%)
White	2,345 (92%)	265 (88%)	240 (82%)	1,384 (94%)	456 (96%)
Ethnicity					
Hispanic/Latino	65 (2.6%)	16 (5.3%)	4 (1.4%)	42 (2.9%)	3 (0.6%)
Not Hispanic/Latino	2,457 (97%)	286 (95%)	290 (99%)	1,410 (97%)	471 (99%)
Amyloid Status					
Ab-	1,365 (54%)	183 (61%)	218 (74%)	592 (40%)	372 (78%)
Ab+	1,172 (46%)	119 (39%)	76 (26%)	874 (60%)	103 (22%)
p-tau217	1.09 (1.78) [-3.25, 9.72]	1.01 (1.59) [-3.25, 6.41]	0.78 (1.44) [-2.08, 5.22]	1.40 (1.94) [-2.54, 9.72]	0.39 (1.29) [-2.74, 5.26]
Years of Follow-up	6.28 (2.80) [0.13, 17.15]	4.69 (3.38) [0.45, 17.15]	8.00 (3.55) [0.86, 13.50]	5.63 (2.15) [0.13, 9.04]	8.19 (2.03) [1.83, 11.76]
Number of MCI/Dem/2 consecutive 0.5 CDR events					
MCI/Dem/2 consecutive 0.5 CDR	526 (21%)	112 (37%)	63 (21%)	314 (21%)	37 (7.8%)
No decline	2,011 (79%)	190 (63%)	231 (79%)	1,152 (79%)	438 (92%)

[†] Mean (SD) [Range]; n (%)

Figure 1. Prognostic associations of plasma p-Tau$_{217}$ with longitudinal cognition and clinical progression in cognitively unimpaired older adults. (A) Predicted trajectories of the harmonized Preclinical Alzheimer Cognitive Composite (PACC) over 15 years, showing faster decline with higher baseline p-Tau$_{217}$ among Aβ+ individuals. (B) Survival curves for clinical progression to [MCI/dementia/2 consecutive visits with ≥0.5 CDR] by p-Tau$_{217}$ and Aβ status. (C) Model-based 10-year absolute risk by p-Tau$_{217}$ category (-1SD, mean, +1SD) and Aβ status within each cohort (ADNI, HABS, A4, WRAP). (D) Continuous function of estimated 10-year progression risk across standardized p-Tau$_{217}$ values, alone and by Aβ status.



Keywords: p-tau217, clinical progression, amyloid-PET, cognitive decline

Distribution of tau and amyloid pathology across cognitive states in a population-based, admixed autopsy cohort

Lea Grinberg[1,2], Felipe Pereira[3], Renata Paraizo Leite[2,4], Vitor Ribeiro Paes[2], Caroline Matos Silva[2], Raul dos Reis Ururahy[2], Filipe Cunha de Moraes[2], Ines Liguori Padrão[2], Carlos Pasqualucci[2], Roberta Diehl Rodriguez[5], Michel Naslavsky[6], Renata Ferretti-Rebustini[7], Ricardo Nitrini[4], Eduardo Ferriolli[4], Claudia Suemoto[4]

[1]*Departments of Laboratory Medicine and Pathology and Neurosciences, Mayo Clinic, Jacksonville, FL, US*
[2]*Physiopathology in Aging Laboratory (LIM-22), Department of Pathology, University of Sao Paulo Medical School, Sao Paulo, Brazil*
[3]*Quantitative Health Sciences, Mayo Clinic, Jacksonville, FL, US*
[4]*Division of Geriatrics, Department of Internal Medicine, University of São Paulo Medical School, Sao Paulo, Brazil*
[5]*Department of Neurology, University of São Paulo Medical School, Sao Paulo, Brazil*
[6]*Department of Genetics and Evolutionary Biology, Institute of Biosciences, University of São Paulo,, Sao Paulo, Brazil*
[7]*Nursing School, University of São Paulo,, Sao Paulo, Brazil*

Background: Imaging and biofluid biomarkers are reshaping Alzheimer's disease (AD) care; clinical use requires knowing population pathology frequency and how biomarker positivity relates to amyloid/tau burden and cognition. Positive predictive value depends on pathology prevalence, and biomarker sensitivity drops at low/moderate burden, thus population-based gold-standard autopsy data across the lifespan are essential to calibrate thresholds, explain why some biomarker-positive individuals remain cognitively normal, and refine counseling for early-stage detection and monitoring**.**

Methods: We analyzed 2,331 decedents from the Biobank for Aging Studies (Brazil), a general-population, admixed cohort (mean age 73.1 ± 14.3; 32.9% with cognitive impairment, defined as CDR > 0 near death. Neuropathology assigned Thal phase (0–5, amyloid) and Braak stage (0–VI, tau). A Braak×Thal matrix quantified: cell-wise prevalence and percent with CDR > 0. Sub-analyses stratified by sex and age at death; exploratory analyses assessed co-pathology and APOE genotype.

Results: The distribution was skewed to low/no pathology: Thal 0–1 = 61.9% (1,444/2,331); Braak 0–III=73.0% (1,701/2,331) (fig1/Tab1). High amyloid (Thal 4–5) occurred in 17.2%. Among these, 18.7%—3.2% of the cohort—had limited tau (Braak ≤III; A+T-low). The A+T-high subgroup (Thal 4–5 & Braak V–VI) comprised 10.4%; 18.6% were CDR = 0. Tau-high with lower amyloid (Braak V–VI & Thal ≤3) represented 3.0% (71/2,331). With increasing age, matrices shift right and upward, i.e., more individuals occupy Thal 4–5 & Braak V–VI. Impairment within A+T-high remains high but not universal: 61–70: 86%, 71–80: 79%, 81–90: 83.4%, ≥90: 81.1%.

Discussion: High amyloid did not guarantee advanced tau, and high amyloid + high tau was not synonymous with clinical impairment (≈1 in 5, cognitively unimpaired). Population frequency maps support age-calibrated priors for interpreting amyloid/ tau biomarkers, yielding more realistic PPVs for T-positivity and near-term decline, providing actionable, gold-standard baselines for biomarker-guided diagnosis, prognosis, and trial design in diverse populations.

Fig 1 - Distribution of cases per Thal Amyloid Phases and Braak Stages and corresponding Clinical Dementia Rating (CDR) . N =2,331

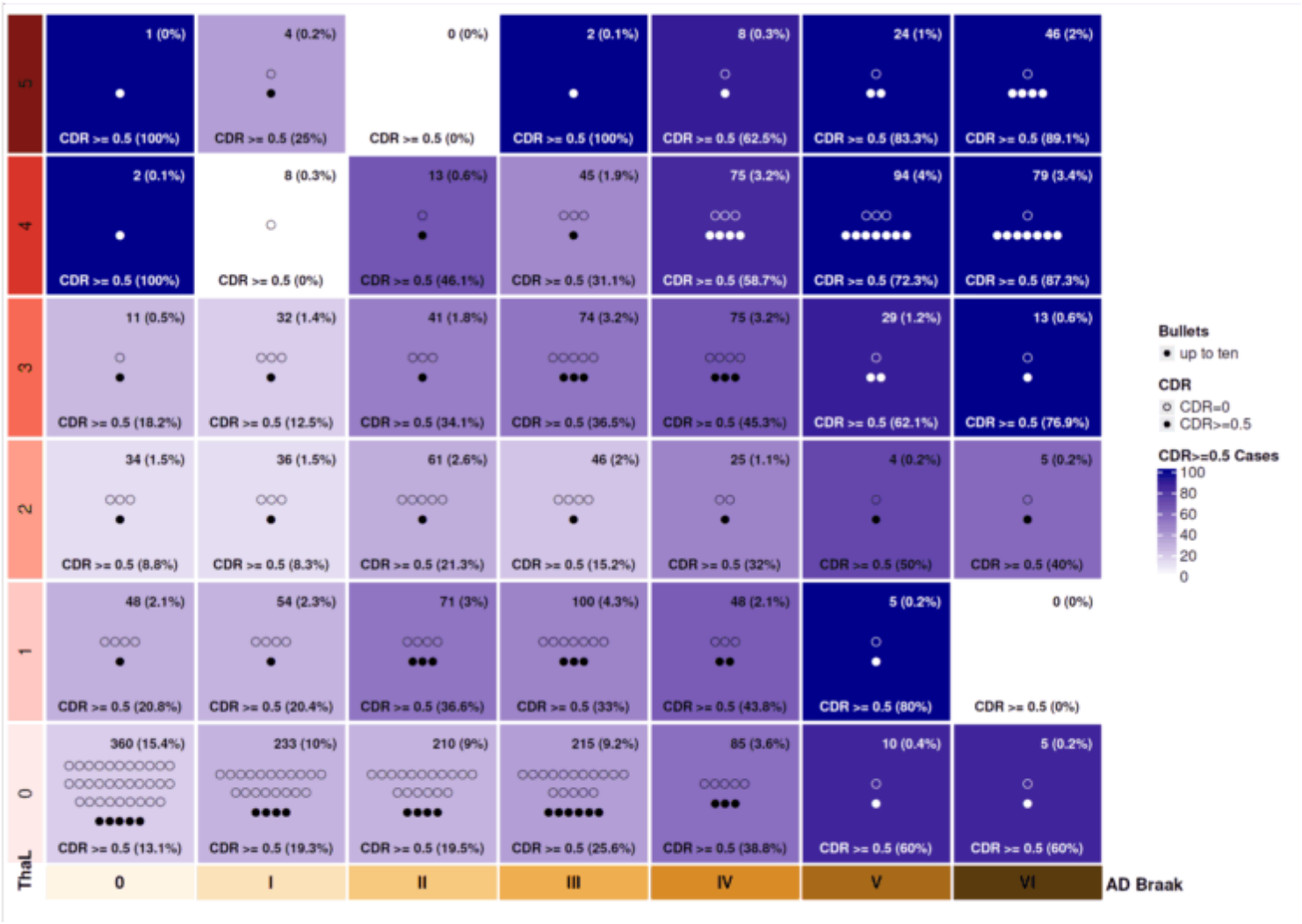


Table 1. Relationship Between Thal Amyloid Phases and Braak Stages: Distribution of Demographic, Clinical, and Pathological Variable

Table 1.									
		Braak stages							
Variable	Total	Braak 0	Braak I	Braak II	Braak III	Braak IV	Braak V	Braak VI	P-value
N (% on ThaL Stage)									
ThaL 5	85 (3 6)	1 (1 2)	4 (4 7)		2 (2 4)	8 (9 4)	24 (28 2)	46 (54 1)	< 001
ThaL 4	316 (' 3 6)	2 (0 6)	8 (2 5)	'3 (4 1)	45 (14 2)	75 (23 7)	94 (29 7)	79 (25)	< 001
ThaL 3	275 (' 1.8)	11 (4)	32 (' 1.6)	41 (' 4.9)	74 (26 9)	75 (27 3)	29 (10 5)	'3 (4.7)	< 001
ThaL 2	211 (9 1)	34 (16 1)	36 (' 7 1)	61 (28 9)	46 (2' 8)	25 (11 8)	4 (1 9)	5 (2 4)	< 001
ThaL 1	326 (' 4)	48 (14 7)	54 (' 6 6)	71 (21 8)	100 (30 7)	48 (14 7)	5 (1 5)		< 001
ThaL 0	1118 (48)	360 (32 2)	233 (20 8)	210 (18 8)	2' 5 (' 9 2)	85 (7 6)	10 (0 9)	5 (0 4)	< 001
Sex Female, N (%)									
ThaL 5	63 (74.1)		1 (25)		2 (' 00)	5 (62 5)	18 (75)	37 (80 4)	.095
ThaL 4	201 (63 6)	1 (50)	3 (37.5)	5 (38.5)	2' (46.7)	46 (6' 3)	70 (74 5)	55 (69 6)	< 05
ThaL 3	146 (53 1)	5 (45 5)	11 (34 4)	24 (58 5)	36 (48 6)	44 (58 7)	14 (48 3)	' 2 (92 3)	< 05
ThaL 2	106 (50 2)	18 (52 9)	15 (41 7)	37 (60 7)	22 (47 8)	10 (40)	2 (50)	2 (40)	' 32
ThaL 1	151 (46 3)	19 (39 6)	24 (44 4)	24 (33.8)	62 (52)	20 (4' 7)	2 (40)		< 01
ThaL 0	477 (42 7)	152 (42.2)	78 (33 5)	93 (44.3)	102 (47 4)	45 (52 9)	4 (40)	3 (60)	< 01
Age at Death, Mean (SD)									
ThaL 5	82 9 ±9 72	87 8	61 6 ±18 05		84 8 ±4 81	86 4 ±6 98	84 4 ±9 18	83 1 ±7 68	> 99
ThaL 4	83 3 ±8 84	90 5 ±1 27	74 2 ±8 29	77 ' ±11 13	8' 3 ±9 06	83 9 ±7 91	84 8 ±8 81	84 ±8 35	> 99
ThaL 3	78 6 ±' 1.45	64.7 ±1' 74	69 ±1' 02	75 9 ±11 58	8' 3 ±' 0 71	8' 5 ±9 19	81 6 ±8 3	85 2 ±11 08	> 99
ThaL 2	73 2 ±' 1.48	63.2 ±1' 63	66 2 ±8 37	75 3 ±9 21	76.7 ±8.66	79.8 ±10 71	83.7 ±11 04	74 3 ±14.36	> 99
ThaL 1	75 3 ±' 2 19	63 8 ±12 22	70 6 ±11 24	75 ' ±9 74	79 ±10 38	83 5 ±9 12	89 6 ±6 61		> 99
ThaL 0	67 4 ±' 4 82	56 8 ±14 33	64 4 ±10 31	73 ±10 53	76 9 ±' 1 48	80 5 ±9 71	83 2 ±11 24	80 4 ±10 35	> 99
ApoE4 carrier, N (%)									
ThaL 5	28 (32 9)		2 (50)			2 (25)	7 (29 2)	' 7 (37)	668
ThaL 4	107 (33 9)			5 (38.5)	14 (3' 1)	25 (33 3)	34 (36 2)	29 (36 7)	.099
ThaL 3	82 (29.8)	1 (9.1)	10 (31 2)	' 2 (29.3)	18 (24.3)	26 (34 7)	9 (31)	6 (46.2)	.241
ThaL 2	46 (2' 8)	10 (29 4)	10 (27 8)	' 4 (22)	6 (' 3)	5 (20)	1 (25)		208
ThaL 1	64 (19 6)	10 (20 8)	11 (20 4)	' 5 (21 ')	22 (22)	6 (' 2 5)			29
ThaL 0	125 (' 1.2)	46 (12 8)	33 (' 4 2)	' 6 (7.6)	2' (9 8)	7 (8 2)	1 (10)	' (20)	.' 25
CDR>=0.5, N (%)									
ThaL 5	70 (82.4)	1 (100)	1 (25)		2 (' 00)	5 (62 5)	20 (83 3)	41 (89 1)	< 05
ThaL 4	203 (64 2)	2 (100)		6 (46 2)	14 (3' 1)	44 (58 7)	68 (72 3)	69 (87 3)	< 001
ThaL 3	109 (39 6)	2 (18 2)	4 (12 5)	' 4 (34 ')	27 (36 5)	34 (45 3)	18 (62 1)	' 0 (76 9)	< 01
ThaL 2	38 (18)	3 (6.8)	3 (8 3)	' 3 (21.3)	7 (' 5 2)	8 (32)	2 (50)	2 (40)	.' 18
ThaL 1	105 (32 2)	10 (20 8)	11 (20.4)	26 (36.6)	33 (33)	2' (43 8)	4 (80)		.07
ThaL 0	230 (20 6)	47 (13 1)	45 (' 9 3)	41 (' 9 5)	55 (25 6)	33 (38 8)	6 (60)	3 (60)	< 001
CDR>=1, N (%)									
ThaL 5	67 (78 8)	1 (100)	1 (25)		2 (' 00)	5 (62 5)	19 (79 2)	39 (84 8)	< 05
ThaL 4	173 (54 7)	2 (100)		5 (36.5)	11 (24 4)	32 (42 7)	58 (61 7)	65 (82 3)	< 001
ThaL 3	86 (3' 3)	2 (18.2)	1 (3 1)	6 (14.6)	24 (32 4)	27 (36)	15 (55 2)	' 0 (76 9)	< 01
ThaL 2	21 (10)	2 (5 9)	2 (5 6)	8 (13 1)	4 (8 7)	3 (' 2)		2 (40)	' 36
ThaL 1	66 (20 2)	8 (16 7)	5 (9 3)	' 5 (21 ')	19 (19)	15 (2' 2)	4 (80)		< 01
ThaL 0	151 (' 3 5)	26 (7 2)	25 (' 0 7)	28 (' 3 3)	36 (16 7)	29 (34 1)	5 (50)	2 (40)	< 001
Co-pathology, N (%)									
ThaL 5	59 (69.4)	1 (100)	1 (25)		1 (50)	5 (62 5)	15 (62 5)	36 (78 3)	.' 66
ThaL 4	189 (59 8)	2 (100)	3 (37.5)	5 (38.5)	23 (5' 1)	43 (57 3)	54 (57 4)	59 (74 7)	< 01
ThaL 3	127 (46 2)	1 (9 1)	9 (28 1)	' 6 (39)	3' (4' 9)	48 (64)	13 (44 8)	9 (69 2)	< 01
ThaL 2	64 (30 3)	5 (14 7)	11 (30 6)	' 4 (22)	20 (43 5)	13 (52)		' (20)	< 05
ThaL 1	137 (42)	11 (22 9)	19 (35 2)	26 (36.6)	47 (47)	30 (62 5)	4 (80)		< 01
ThaL 0	337 (30 1)	72 (20)	62 (26 6)	62 (29 5)	77 (35 8)	55 (64 7)	7 (70)	2 (40)	< 001

Keywords: postmortem, amyloid, tau, cognitive decline, biomarker neuropathology

Wednesday, January 14, 2026 - 10:30 am - 10:35 am

Podium Session

B3 - A: Blitz Session

Wednesday, January 14, 2026			
10:30 am – 10:35 am	Title	Authors	Presenter
Board # 114	**Amyloid does not discriminate: a meta-analysis of sex differences in Centiloids from 35,468 participants across 33 cohorts**	Blazhenets	Pezzoli	Casaletto	Soleimani-Meigooni	Chiotis	Allen	Rabinovici	La Joie	Study Group	**Ganna Blazhenets**, University of California, San Francisco, San Francisco, CA, USA
Board # 105	**Longitudinal tau PET progression follows language network spread in primary progressive aphasia**	Martersteck	Rogalski	**Adam Martersteck**, University of Chicago, Chicago, IL, USA

Wednesday, January 14, 2026 - 10:35 am - 11:35 am

PosterSession

Poster Session 3A

Wednesday, January 14, 2026			
10:35 am – 11:35 am	**Poster Presentation**	**Authors**	**Presenter**
Board 97	Longitudinal trajectories of plasma p-tau217 across multiple assays in relation to amyloid and tau PET and cognition	Shekari | Tosun | Dage | Schindler | Shaw | Jagust | Landau	**Mahnaz Shekari**, Department of Neuroscience, University of California, Berkeley, California, USA, Berkeley, CA, US
Board 98	The relation of psychosocial coping mechanisms to ATN pathophysiology differ across demographics.	Schatz | Snitz | Roush | Lopresti | Villemagne | Lopez | Williams | Cohen	**Lilcelia Williams**, Department of Psychiatry, University of Pittsburgh School of Medicine, Pittsburgh, PA, US
Board 99	Intermediate blood-based biomarker status clarified by PET and CSF in cognitively impaired individuals	Ziontz | Blazhenets | Lin | Landau | Shaw | Dage | Hammers | Eloyan | Koeppe | Carillo | Dickerson | Rabinovici | La Joie	**Jacob Ziontz**, Edward and Pearl Fein Memory and Aging Center, Department of Neurology, University of California, San Francisco, San Francisco, CA, US
Board 100	Operationalizing clinical criteria for LATE using cognitive, MRI, and AD biomarker (biofluid or PET) data	Cuppels | Birkenbihl | Schneider | Bennett | Brown | Seto | Coughlan | Li | Townsend | Properzi | James | Arfanakis | Sperling | Yang | Chhatwal | Amariglio | Hohman | Donohue | Buckley	**Madison Cuppels**, Massachusetts General Brigham, Boston, MA, US
Board 101	CT-based processing is equivalent to MR-based processing for tau PET regional quantification	Povala | Bellaver | Amaral | Lussier | Ferreira | Bauer-Negrini | Tudorascu | Masdeu | Fortea | Soleimani-Meigooni | Lowe | Oh | Pascual | Gordon | Rosa-Neto | Baker | Pascoal	**Guilherme Povala**, University of Pittsburgh, Department of Psychiatry, Pittsburgh, PA, US
Board 102	A pilot study on the association of plasma proteins with neuroimaging biomarkers of Alzheimer's disease in African Americans	Arowolo | Kuchenbecker | Heckman | Nguyen | Casellas | Sotelo | Schwarz | Senjem | Jain | Lucas | Willis | Ertekin-Taner | Graff-Radford | Kantarci | Lowe | Lachner | Day | Carrasquillo	**Olatunbosun Arowolo**, Department of Neuroscience, Mayo Clinic Florida, Jacksonville, FL, US

Wednesday, January 14, 2026			
10:35 am – 11:35 am	**Poster Presentation**	**Authors**	**Presenter**
Board 103	Amyloid-PET and white matter hyperintensities but not military service duration nor combat exposure are associated with neurodegeneration and cognitive impairment in older veterans	Rocha | Pasternak | Lesman Segev | Schwartz | Blazhenets | Maiti | Rosen Lang | Hantke | Livny-Ezer | Yaffe | Shaw | Weiner | Hills | Kritikos | Soleimani-Meigooni | Silbert | La Joie | Gardner	**Salma Rocha**, University of California, San Francisco, San Francisco, CA, US
Board 104	The influence of cardiovascular risk on white matter integrity along the Alzheimer's disease trajectory: Early impact in preclinical stages	Edison | Arnold	**Paul Edison**, Imperial College London, London, UK
Board 105	Longitudinal tau PET progression follows language network spread in primary progressive aphasia	Martersteck | Rogalski	**Adam Martersteck**, Healthy Aging & Alzheimer's Research Care Center, Department of Neurology, University of Chicago, Chicago, IL, US
Board 106	The adjusted Centiloid: Improving reliability by correcting for white matter uptake variability	Reilhac | Irizarry | Reyderman | Charil	**Anthonin Reilhac**, Eisai Inc., Nutley, NY, US
Board 107	Perivascular spaces: Predictors of longitudinal amyloid, tau, cerebrovascular biomarkers?	Low | Gunter | Hu | Raghavan | Przybelski | Schwarz | Kantarci | Lowe | Graff-Radford | Petersen | Jack | Vemuri	**Audrey Low**, Department of Radiology, Mayo Clinic, Rochester, MN, 55905, USA, Rochester, MN, US
Board 108	Longitudinal evaluation of neuroinflammation using 11C-ER176 TSPO PET	Lim | Cogswell | Min | Lee | Brunn | Kandimalla | Jacobson | Nycklemoe | Lee | Lundt | Botha | Graff-Radford | Jones | Vemuri | Kantarci | Jack | Petersen | Lowe	**Seokbeen Lim**, Department of Radiology, Mayo Clinic, Rochester, MN, US
Board 109	Comparison of meningeal signal between [^{18}F]AV-1451 and [^{18}F]MK-6240 tau PET using a distance-based meningeal mask	Lim | Gunter | Baker | Tissot | Brunn | Soleimani-Meigooni | Oh | Fortea | Pascual | Gordon | Rosa-Neto | Pascoal | Klunk | Jagust | Senjem | Botha | Knopman | McCarter | Ramanan | Graff-Radford | Schwarz | Kantarci | Boeve | Vemuri | Jones | Jack | Petersen | Lowe	**Seokbeen Lim**, Department of Radiology, Mayo Clinic, Rochester, MN, US

Wednesday, January 14, 2026			
10:35 am – 11:35 am	**Poster Presentation**	**Authors**	**Presenter**
Board 110	Effects of regional tau accumulation on visual discrimination of novel objects in clinically unimpaired older adults	Kapadia | Medina Guerra | Sai | Bonnen | Wagner | Mormino | Trelle	**Dhruv Kapadia**, Stanford University, Stanford, CA, US
Board 111	Key quantitative benchmarks with CenTauR in cross-sectional and longitudinal large datasets	Dore | Bourgeat | Betthauser | Feizpour | Moscoso | Leuzy | Fripp | Johnson | Rowe | Villemagne	**Vincent Dore**, CSIRO, Melbourne, Australia
Board 112	Astrocytic reactivity is related to synchronization of regional amyloid-beta deposition	Adams | Parker | Taylor | Tang | Meza | Tuteja | Avila | Chang | Simmons | Malhas | Kim | McMillan | Mapstone | Yassa	**Jenna Adams**, Department of Neurobiology and Behavior, University of California, Irvine, Irvine, CA, US
Board 113	Synergistic effects of amyloid-beta and hyperexcitability on tau pathology and cognitive decline	Vanderlip | Adams	**Jenna Adams**, Department of Neurobiology and Behavior, University of California, Irvine, Irvine, CA, US
Board 114	Amyloid does not discriminate: a meta-analysis of sex differences in Centiloids from 35,468 participants across 33 cohorts	Blazhenets | Pezzoli | Casaletto | Soleimani-Meigooni | Chiotis | Allen | Rabinovici | La Joie | Study Group	**Ganna Blazhenets**, Edward and Pearl Fein Memory & Aging Center, Department of Neurology, University of California, San Francisco, San Francisco, CA, US
Board 115	Preliminary associations of plasma phosphorylated tau217 with regional tau deposition and accumulation in medial temporal and neocortical regions	Pintucci | Thibault | Farrell | Yang | Chhatwal | Properzi | Becker | Price | Sperling | Johnson	**Eva Pintucci**, Massachusetts General Hospital, Department of Neurology, Harvard Medical School, Boston, MA, US
Board 116	Contrasting neuropathology- and tau PET-based Braak stage associations with dementia severity to clarify differences between radiologic and pathologic findings	Evelhoch | Bruzzone | Rocha | Asthana | Nirschl | Johnson | Schneider | Hyman | Pascoal | Betthauser	**Jeffrey Evelhoch**, JLEvelhoch Consulting, Wayne, PA, US
Board 117	Novel pet tracer [11C]-CS1P1 uptake reflects decreased sphingosine-1-phosphate receptor 1 activity in vivo in Alzheimer's disease and related dementias	Tiemann Powles | Friedrichsen | Flores | Rajamanickam | Keefe | Simmons | Doering | McKay | Hoagey | Sabaredzovic | Ibanez | Morris | An | Brier | Tu | Benzinger	**Savannah Tiemann Powles**, Washington University in St. Louis School of Medicine, St. Louis, MO, US
Board 118	Digital maze test reveals features related to cortical tau in cognitively normal Aβ+ older adults	Robinson | Fu | Amariglio | Sperling | Johnson | Davis | Penney | Rentz	**Talia Robinson**, Brigham and Women's Hospital, Boston, MA, US
Board 119	Associations of regional neuroinflammation by ER176 PET SUVR with cognitive scores	Jacobson | Lim | Lundt | Nycklemoe | Min | Botha | Graff-Radford |	**David Jacobson**, Department of Radiology, Mayo Clinic, Rochester, MN, US

Wednesday, January 14, 2026			
10:35 am – 11:35 am	**Poster Presentation**	**Authors**	**Presenter**
		Jones | Vemuri | Kantarci | Knopman | Jack | Petersen | Lowe	
Board 120	Cluster-based metric of early tau-PET aggregation is associated with plasma p-tau217 in cognitively unimpaired older adults with subthreshold amyloid-beta	Varghese | Brock | Taylor | Thomas | Yassa | Adams	**Leah Varghese**, University of California, Irvine, Irvine, CA, US
Board 121	Sex differences in regional Aβ burden are associated with decreased cingulum integrity uniquely in older cognitively unimpaired women	Yi | Parker | Tang | Taylor | Tuteja | Meza | Avila | Chang | Simmons | Bamford | McMillan | Kim | Thomas | Adams | Yassa	**Emily Yi**, University of California, Irvine, Irvine, CA, US
Board 122	Cerebral vessel morphology is associated with white matter lesions burden	Huang | Li | Rocha | Stetten | Yang | Ibrahim | Wu | Aizenstein	**Yuanzhe Huang**, University of Pittsburgh, Pittsburgh, PA, US
Board 123	Early ventral temporal tau burden marks functional vulnerability in aging	Sheng | Trelle | Sai | Young | Romero | Park | Vossler | Younes | Davidzon | Wagner | Mormino	**Jintao Sheng**, Department of Psychology, Stanford University, Stanford, CA, US
Board 124	Alignment of antemortem images to postmortem fixed hemibrains using standard neuroimaging tools	Coath | Staruck | Carey | de Chavez | Karas | Abrahamson | Asthana | Johnson | Ikonomovic | Nirschl | Betthauser	**William Coath**, Wisconsin Alzheimer's Disease Research Center, University of Wisconsin School of Medicine and Public Health, Madison, WI, US
Board 125	Towards a harmonized amyloid clock: centralized image processing and temporal modeling with multiple cohorts and tracers	Coath | Bruzzone | Morse | Navaratna | Hammond | Staruck | Nowinski | Palmer | Kelley | Schwartz | Carey | Betthauser	**William Coath**, Wisconsin Alzheimer's Disease Research Center, University of Wisconsin School of Medicine and Public Health, Madison, WI, US
Board 126	Cluster-based MK-6240 PET detects early neocortical temporal tau spread	Thompson | Becker | Fanglu Fu | Farrell | Thibault | Slade | Sperling | Price | Johnson	**Jackson Thompson**, Massachusetts General Hospital, Harvard Medical School, Boston, MA, US
Board 127	Gaussian smoothing and partial volume correction modify relationships of tau burden with biological variables in longitudinal multi-site studies of 18F-Flortaucipir PET	Luo | Laymon | Baker | Cohen | Villemagne | Lopresti | Aizenstein | Tudorascu | Minhas	**Weiquan Luo**, University of Pittsburgh, Pittsburgh, PA, US
Board 128	No detectable association between BDNF Val66Met and hippocampal volume or regional tau PET in ADNI after propensity score matching and ComBat harmonization	Han | Minhas | Laymon | Villemagne | Tudorascu	**Yushui Han**, Intelligent Systems Program, University of Pittsburgh, Pittsburgh, PA, US

Wednesday, January 14, 2026			
10:35 am – 11:35 am	**Poster Presentation**	**Authors**	**Presenter**
Board 129	Centiloid and SUVR amyloid harmonization techniques comparisons for head-to-head unequally spaced data	Han | Lopresti | Bourgea | Laymon | Villemagne | Tafti | Minhas | Tudorascu	**Yushui Han**, Intelligent Systems Program, University of Pittsburgh, Pittsburgh, PA, US
Board 130	Plasma amyloid beta 42/40 modifies the associations between MRI biomarkers and subsequent cognitive impairment: a neuroimaging-wide longitudinal study in the BLSA	Duran | Bilgel | An | Kandala | Davatzikos | Landman | Erus | Ferrucci | Moghekar | Walker | Resnick	**Tugce Duran**, National Institute on Aging, Baltimore, MD, US
Board 131	High-resolution NAV template using the Siemens Biograph Vision	Bourgeat | Rowe | Paranawithana | Feizpour | Huang | Villemagne | Fripp | Dore	**Christopher Rowe**, Austin Health, Heidelberg, Australia
Board 132	Higher clinical throughput quantitative amyloid-β PET using abbreviated acquisition windows	Paranawithana | Gillman | Bourgeat | Fripp | Villemagne | O'Keefe | Huang | Benzinger | LaMontagne | Morris | Doré | Rowe	**Christopher Rowe**, Department of Molecular Imaging & Therapy, Austin Health, Melbourne, Australia
Board 133	Tracer-specific effects of hormone replacement therapy on age-related tau accumulation	Tissot | Shi | Tsai | Maboudian | Fonseca | Rahmouni | Lussier | Therriault | Trudel | Cassa Macedo | Stevenson | Bellaver | Ferreira | Povala | Gordon | Pascual | Lowe | Soleimani-Meigooni | Oh | Klunk | Rosa-Neto | Jagust | Buckley | Pascoal | Baker	**Cécile Tissot**, Lawrence Berkeley National Laboratory, Berkeley, CA, US
Board 134	Cognitive and age-related differences in low-tau individuals assessed with [18F]FTP and [18F]MK6240	Tissot | Shankar | Tsai | Rahmouni | Lussier | Therriault | Trudel | Cassa Macedo | Stevenson | Bellaver | Ferreira | Povala | Gordon | Pascual | Lowe | Soleimani-Meigooni | Oh | Klunk | Rosa-Neto | Jagust | Landau | Pascoal | Baker	**Cécile Tissot**, Lawrence Berkeley National Laboratory, Berkeley, CA, US
Board 135	Integration of network analysis of the plasma proteome with Alzheimer's disease neuroimaging	Hurst | Kuchenbecker | Heckman | Nguyen | Casellas | Sotelo |	**Cheyenne Hurst**, Mayo Clinic, Jacksonville, FL, US

Wednesday, January 14, 2026			
10:35 am – 11:35 am	**Poster Presentation**	**Authors**	**Presenter**
	outcomes in an African American cohort	Shwarz | Senjem | Jain | Lucas | Willis | Ertekin-Taner | Graff-Radford | Kantarci | Lowe | Lachner | Day | Carrasquillo	
Board 137	MK6240 and Flortaucipir Braak staging agreement in a head-to-head cohort	Rocha | Soares | Ruppert | Medeiros | Bellaver | Povala | Ferreira | Bauer-Negrini | Lussier | Tudorascu | Masdeu | Soleimani-Meigooni | Fortea | Lowe | Oh | Pascual | Gordon | Rosa-Neto | Baker | Pascoal	**Tharick Pascoal**, University of Pittsburgh, Pittsburgh, PA 15206-3561, PA, US
Board 138	Comparing neuropathologic and tau-PET Braak staging across clinical progression using MK6240 and flortaucipir	Rocha | Bruzzone | Ruppert | Medeiros | Soares | Bellaver | Povala | Ferreira | Lussier | Masdeu | Soleimani-Meigooni | Fortea | Lowe | Oh | Pascual | Gordon | Rosa-Neto | Baker | Johnson | Evelhoch | Betthauser | Pascoal	**Tharick Pascoal**, University of Pittsburgh, Pittsburgh, PA 15206-3561, PA, US
Board 139	Predictors of data exclusion in MR-dependent imaging analyses of Alzheimer's disease	Flores | Scott | Lu | Su | Keefe | Smith | Hornbeck | McKay | Strain | Simmons | Dombrowski | Rizzo | Shimony | Bateman | Babulal | Landau | Jagust | Wolk | Lah | Gleason | Johnson | Roberson | Sperling | Johnson | Morris | Xiong | Gordon | Benzinger	**Shaney Flores**, Washington University School of Medicine, St. Louis, MO, US
Board 140	Brain network architecture shapes the pattern of tau-induced neuronal dysfunction in Alzheimer's disease, while tau load drives local damage	Frontzkowski | Roemer-Cassiano | Gnörich | Dewenter | Steward | Zhu | Klonowski | Hirsch | Biel | Palleis | Höglinger | Brendel | Franzmeier	**Lukas Frontzkowski**, Institute for Stroke and Dementia Research (ISD), LMU University Hospital, Ludwig-Maximilians-University (LMU), Munich, Germany

Wednesday, January 14, 2026			
10:35 am – 11:35 am	**Poster Presentation**	**Authors**	**Presenter**
Board 141	Cortical thickness and female sex confer resilience to tau-related cognitive decline: A large multi-cohort study	Mitchell	**Stuart Mitchell**, McGill University, Translational Neuroimaging Lab, Montreal, QC, Canada
Board 142	Structure-guided design of 18F-FD4—a PET tracer of α-synuclein fibrils	Liu | Li | Wang | Zuo | Tan | Bian | Fan | Liang	**Liang Qing**, Interdisciplinary Research Center of Biology and Chemistry, Shanghai Institute of Organic Chemistry, Chinese Academy of Sciences, CN
Board 143	NULISAseq CNS proteomic signatures of astrocytic reactivity in Alzheimer's disease	Shi | Zeng | Balogun | Farinas | Lopresti | Gogola | Ikonomovic | Aizenstein | Villemagne | Cohen | Karikari	**Ruyu Shi**, Department of Psychiatry, School of Medicine, University of Pittsburgh, Pittsburgh, PA, US
Board 144	High p-tau217 levels nullify the slower cognitive progression in younger older adults	Shi | Choity | Brodman | Zeng | Deek | Gu | Farinas | Nafash | Bedison | Mercurio | Matan | Gogola | Kofler | Tudorascu | Nadkarni | Aizenstein | Shaaban | Lingler | Pascoal | Villemagne | Berman | Sweet | Snitz | Ikonomovic | Cohen | Kamboh | Lopez | Karikari	**Ruyu Shi**, Department of Psychiatry, School of Medicine, University of Pittsburgh, Pittsburgh, PA, US

97 Longitudinal trajectories of plasma p-tau217 across multiple assays in relation to amyloid and tau PET and cognition

Mahnaz Shekari[1], Duygu Tosun[2], Jeff Dage[4,5], Suzanne Schindler[3], Leslie Shaw[6], William J Jagust[1], Susan M Landau[1]

[1]*Department of Neuroscience, University of California, Berkeley, California, USA, Berkeley, CA, US*
[2]*Department of Radiology and Biomedical Imaging, University of California, San Francisco, San Francisco, CA, US*
[3]*Washington University School of Medicine, St Louis, MO, USA, St Louis, MO, US*
[4]*Indiana Alzheimer's Disease Research Center, Indianapolis, IN, USA, Indianapolis, IN, US*
[5]*Department of Neurology, Indiana University School of Medicine, Indianapolis, IN, USA, Indianapolis, IN, US*
[6]*Center for Neurodegenerative Research, Perelman School of Medicine, Department of Pathology and Laboratory Medicine and the PENN Alzheimer's Disease Research Center, University of Pennsylvania, Philadelphia, PA, USA, Philadelphia, PA, US*

Background: There is little concurrent longitudinal plasma p-tau217, amyloid and tau PET, and cognition. Here, we examined these longitudinal trajectories across stages of early Alzheimer's disease.

Methods: We included 385 cognitively normal and impaired ADNI participants from the FNIH Biomarker Consortium with three concurrent longitudinal plasma %p-tau217 measures, amyloid PET (in CL), and PACC assessments over 5.52±1.72 years. A subset of 116 participants also had two [^{18}F]flortaucipir tau PET scans (2.67±1.25 years follow-up). Participants were classified into four baseline Plasma/PET groups (Plasma-/PET-, Plasma+/PET-, Plasma-/PET+, Plasma+/PET+; **Table1**) for both amyloid and tau PET (assessed with meta-temporal tau SUVr +/- status) using published cutoffs. Annualized changes in biomarkers and PACC were estimated using linear models, and their associations evaluated with Spearman correlations adjusted for age, sex, APOE-ε4, and education.

Results: Primary analyses focus on plasma %p-tau217 measured with C2N-PrecivityAD2 assay. Plasma %p-tau217 slopes correlated moderately with CL slopes (ρ=0.31, 95%CI:0.22-0.40, p<0.0001), and this was driven by the Plasma-/AmyloidPET- group (ρ=0.34, p<0.001)(**Figure1**). In contrast, only plasma %p-tau217 C2N-PrecivityAD2 slopes showed strongest correlations with tau-PET slopes (ρ=0.4, 95%CI:0.23-0.54, p<0.001), and this was driven by the Plasma+/TauPET+ group (ρ=0.59, 95%CI:0.27-0.79, p<0.01). While associations between CL and p-tau217 slopes were consistent across assays (C2N-PrecivityAD2, Fujirebio-Lumipulse, ALZpath-Quanterix, Janssen LucentAD-Quanterix), tau-PET slopes correlated strongly with %p-tau217 only for the C2N PrecivityAD2 assay (**Figure2**). Both tau-PET and %p-tau217 slopes (but not CL slopes) were moderately associated with PACC decline (ρ=-0.20 [-0.37 to -0.01], p<0.05; ρ=-0.15 [-025 to -0.05], p<0.005).

Conclusions: Changes in plasma %p-tau217 over 5.5 years were moderately associated with amyloid PET and, over a shorter time interval of 2.7 years, with tau-PET slopes, but these correlations were inconsistent across disease stages, suggesting that change over time are influenced by different processes during AD progression and cannot be used interchangeably in clinical settings.

Demographics by Plasma/PET Group – C2N_plasma_ptau217_ratio_Precivity

Characteristic	Plasma- PET- N = 217[1]	Plasma+ PET- N = 24[1]	Plasma- PET+ N = 26[1]	Plasma+ PET+ N = 122[1]	p-value[2]
Age	71.15 (6.87)	77.74 (6.43)	73.16 (6.15)	74.82 (7.33)	<0.001
Sex					0.5
1	110 (51%)	9 (38%)	15 (58%)	62 (51%)	
2	107 (49%)	15 (63%)	11 (42%)	60 (49%)	
APOE4_BIN					<0.001
0	170 (78%)	18 (75%)	16 (62%)	53 (43%)	
1	47 (22%)	6 (25%)	10 (38%)	69 (57%)	
Diag					<0.001
AD	0 (0%)	0 (0%)	3 (12%)	7 (5.7%)	
MCI	93 (43%)	6 (25%)	9 (35%)	65 (53%)	
N	124 (57%)	18 (75%)	14 (54%)	50 (41%)	
Centiloid	-1.71 (10.40)	4.58 (11.45)	32.54 (13.09)	74.03 (33.72)	<0.001
MMSE	28.95 (1.29)	29.08 (1.25)	27.81 (2.83)	27.67 (2.23)	<0.001
plasma_ptau217	1.89 (0.79)	5.61 (2.57)	2.48 (0.86)	8.24 (3.68)	<0.001
CDR_GLOBAL					0.002
0	123 (57%)	16 (67%)	14 (54%)	50 (41%)	
0.5	94 (43%)	8 (33%)	10 (38%)	69 (57%)	
1	0 (0%)	0 (0%)	2 (7.7%)	3 (2.5%)	
PACC	-0.44 (3.34)	0.24 (3.54)	-3.19 (6.52)	-4.04 (5.37)	<0.001

[1] Mean (SD); n (%)

[2] Kruskal-Wallis rank sum test; Fisher's exact test

Table1. Demographic information of the participants at the baseline visit based on their plasma/AmyloidPET status. It should be noted that for the simplicity, the %p-tau217 measured by C2N-PrecivityAD2 is used for defining plasma status in this table.

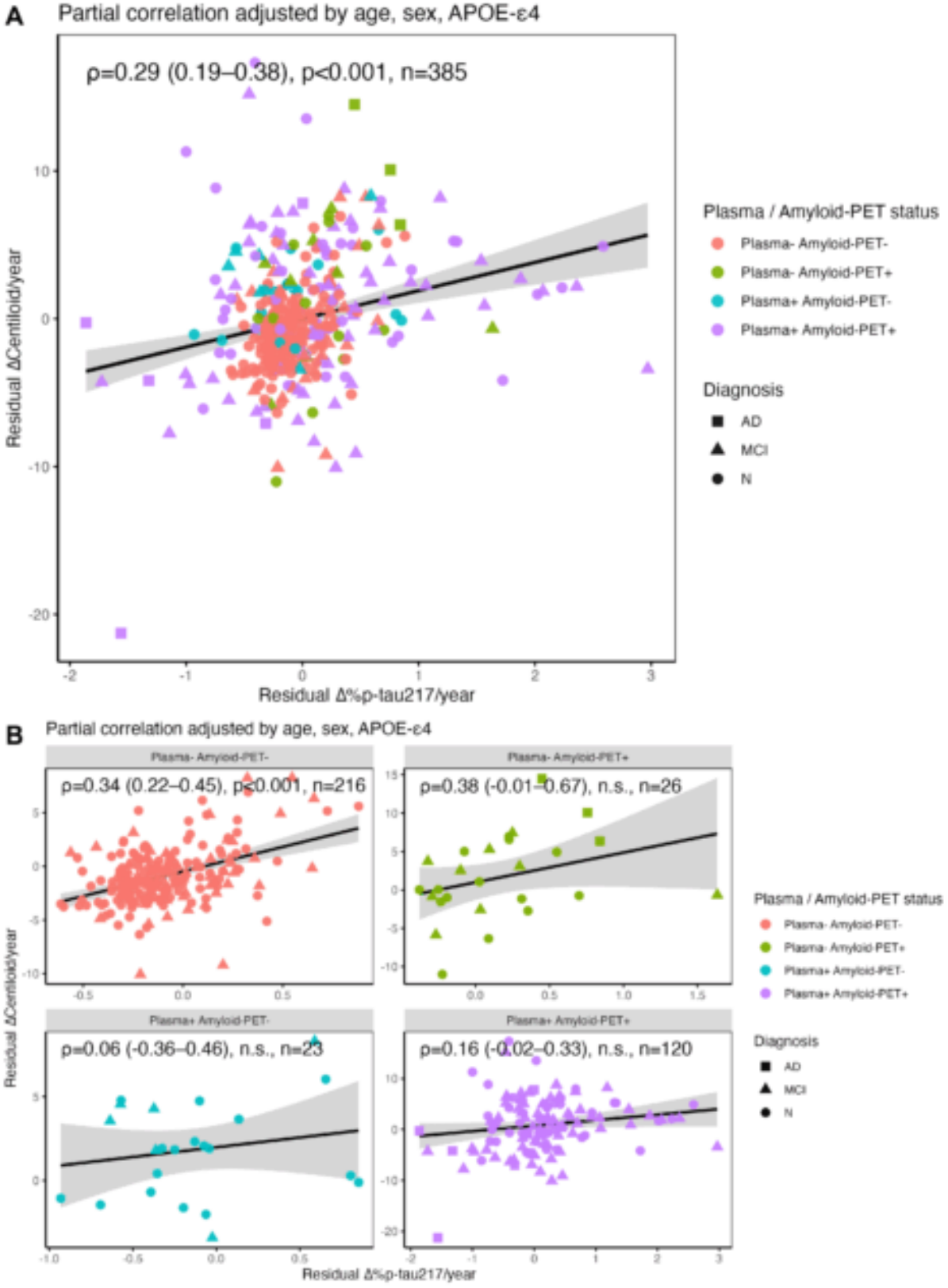


Figure1. Scatter plots showing annual rate of changes in %p-tau217 measured by C2N-PrecivityAD2 and Centiloid (A) for all all participants (B) startified by Plasma/AmyloidPET status. Annotations on the figures show partial correlations, 95% CI, p-values, and the number of individuals in each group. All correlations are adjusted for age, sex, and APOE-ε4 carriership.

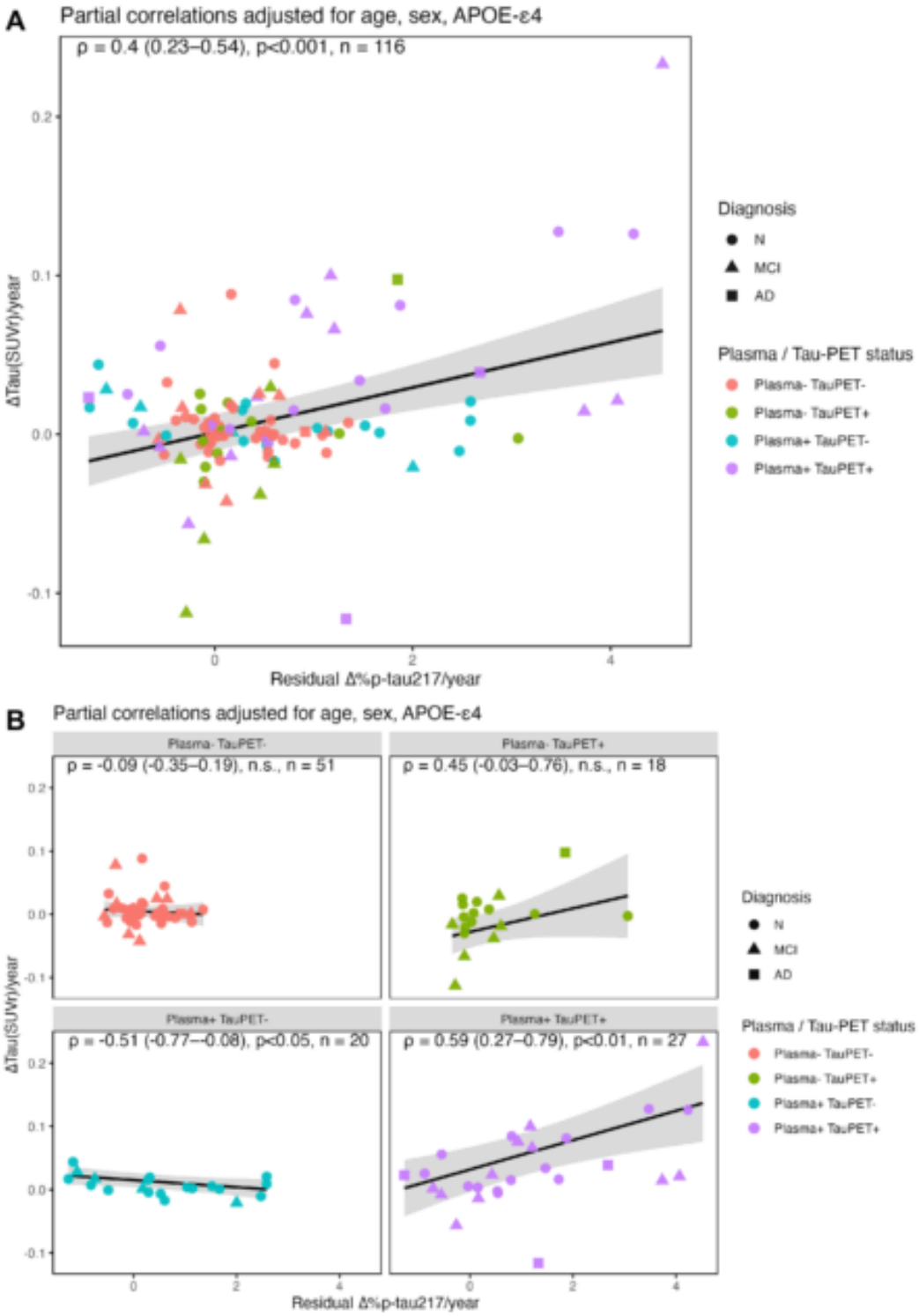


Figure 2. Scatter plots showing annual rates of change in %p-tau217 (C2N-PrecivityAD2) and tau-PET SUVR in the meta-temporal ROI: (A) all participants; (B) stratified by Plasma/tau-PET status. Annotations show partial correlations, 95% CIs, p-values, and the number of individuals per group. All correlations are adjusted for age, sex, and APOE-ε4 carriership.

Keywords: Alzheimer's disease, plasma p-tau217, amyloid PET, tau PET, PACC

98 The relation of psychosocial coping mechanisms to ATN pathophysiology differ across demographics.

Brooke Schatz[1,2], Beth Snitz[3,4], Rebecca Roush[1], Brian J. Lopresti[5], Victor Villemagne[1,3], Oscar L. Lopez[3,4], Lilcelia A. Williams[1,3], Ann Cohen[1,2,3]

[1]*Department of Psychiatry, University of Pittsburgh School of Medicine, Pittsburgh, PA, US*
[2]*Center for Neuroscience, University of Pittsburgh, Pittsburgh, PA, US*
[3]*Alzheimer's disease Research Center, University of Pittsburgh, Pittsburgh, PA, US*
[4]*Department of Neurology, University of Pittsburgh School of Medicine, Pittsburgh, PA, US*
[5]*Department of Radiology, University of Pittsburgh School of Medicine, Pittsburgh, PA, US*

Background – Existing data indicate that demographic, social, and environmental factors are associated with differences in AD pathologic burden assessed using imaging biomarkers. An exploration of how these factors vary across racialized older adults is vital to uncover the mechanism of these differences.

Methods –130 participants (50-86 yrs, 73.8% female, 23.8% African American (AA), 76.2% non-Hispanic white (NHW)) from the CoBRA study underwent ATN neuroimaging and a battery of standardized cognitive and psychosocial assessments, including the brief COPE, a measure to assess the different ways in which people respond to stress. Participants underwent [^{11}C]PiB PET for Ab, [^{18}F]MK6240 for tau, and 3T MRI for N.

Results – AA and NHW participants did not differ significantly in age or education. Consistent with previous findings, the frequency of Ab positivity was higher in the NHW population (41/99) than the African American population (5/31). The full group displays a correlation trend between higher COPE and global PiB SUVR (r^2 = 0.0282, p = 0.056). Further dissection revealed this trend is driven by the AA group (r^2 = 0.188, p = 0.015), while the NHW group displays no correlation (r^2 = 0.0073, p = 0.3997). Additionally, the mean COPE score for the Ab positive group (n = 36, mean = 25.7) is significantly higher than the mean score of the Ab negative group (n = 94, mean = 22.8). No relations were observed between T or N measures and COPE.

Conclusions – These data support the conclusion that Ab staging differs across racialized groups and that a complex series of psychosocial factors, including coping strategies are involved. Further, these data suggest a potential compounding effect of psychosocial stress and pathology that warrants further interrogation, particularly to understand differences in the types of specific coping mechanisms used by a diverse array of individuals.

Keywords: stress, amyloid PET, racialization

99 Intermediate blood-based biomarker status clarified by PET and CSF in cognitively impaired individuals

Jacob Ziontz[1], Ganna Blazhenets[1], Zoe Lin[1], Susan Landau[2], Leslie Shaw[3], Jeffrey Dage[4], Dustin Hammers[4], Ani Eloyan[5], Robert Koeppe[6], Maria Carillo[7], Bradford Dickerson[8], Gil Rabinovici[1], Renaud La Joie[1]

[1]*Edward and Pearl Fein Memory and Aging Center, Department of Neurology, University of California, San Francisco, San Francisco, CA, US*
[2]*Department of Neuroscience, University of California, Berkeley, Berkeley, CA, US*
[3]*Department of Pathology and Laboratory Medicine, Perelman School of Medicine, University of Pennsylvania, Philadelphia, PA, US*
[4]*Department of Neurology, Indiana University School of Medicine, Indianapolis, IN, US*
[5]*Department of Biostatistics, Brown University School of Public Health, Providence, RI, US*
[6]*Department of Radiology, University of Michigan, Ann Arbor, MI, US*
[7]*Medical & Scientific Relations Division, Alzheimer's Association, Chicago, IL, US*
[8]*Department of Neurology, Massachusetts General Hospital and Harvard Medical School, Boston, MA, US*

Background: A two-threshold approach for blood-based biomarkers distinguishes clearly negative/positive ranges from uncertain intermediate values. Here, we examine the frequency of intermediate results derived using a data-driven approach independently from plasma, PET, and CSF biomarkers, and whether an intermediate plasma result tends to be resolved by a second biomarker.

Methods: To maximize relevance to clinical settings, we included data from 3,688 individuals with MCI or mild dementia with either Aβ PET Centiloid, CSF Aβ42/40 ratio, or plasma pTau217 measures across 3 cohorts from the UCSF Memory and Aging Center (UCSF MAC), LEADS, and ADNI (Table 1). For each cohort, we used gaussian mixture modeling (GMM) to fit a two-component model to cross-sectional PET, CSF, and plasma data (Figure 1). We then computed 90% posterior probability thresholds to determine cutoffs for clearly-negative and clearly-positive ranges, with values in between representing intermediate status. Finally, we applied these cutoffs to individuals with concurrent data across modalities (within 6 months) to compare biomarker status between PET, CSF, and plasma.

Results: In individuals with concurrent PET and plasma pTau217, biomarker status from plasma was more often intermediate than from Centiloids (UCSF: 15.5% vs. 4.4%, $p = 0.002$; LEADS: 7.5% vs. 1.0%, $p < 0.001$; ADNI: 21.5% vs. 13.9%, $p = 0.02$). Similarly, plasma pTau217 status was more often intermediate than concurrent CSF Aβ42/40 status (UCSF: 10.1% vs. 3.7%, $p = 0.10$; LEADS: 8.7% vs. 1.3%, $p = 0.01$; ADNI: 25.2% vs. 11.7%, $p = 0.01$). Across all cohorts (Figure 2), plasma pTau217 resulted in the highest rate of intermediate status (7-22%), but 77-100% of these individuals had clearly positive/negative status from concurrent PET or CSF.

Conclusion: Intermediate plasma biomarker status is not uncommon among cognitively impaired individuals, but follow-up measures of PET or CSF frequently yield a clearly positive or negative result.

UCSF MAC (n=1519)			
	PET (n=1011)	*CSF (n=460)*	*Plasma (n=397)*
age: M (SD)	66.5 (9.3)	63.2 (8.7)	65.6 (10.0)
sex (female)	44.5%	49.8%	45.7%
APOE4+	31.8%	27.1%	41.4%
MMSE: M (SD)	24.7 (5.9)	23.7 (5.9)	24.6 (5.6)
PET tracer/Assay	PiB, FBB, FBP	Roche Elecsys	Electrochemiluminescence
LEADS (n=559)			
	PET (n=555)	*CSF (n=151)*	*Plasma (n=486)*
age: M (SD)	58.9 (4.7)	59.0 (4.8)	58.9 (4.7)
sex (female)	50.3%	48.3%	50.4%
APOE4+	46.5%	51.7%	50.2%
MMSE: M (SD)	22.4 (5.4)	22.6 (4.9)	22.3 (5.5)
PET tracer/Assay	FBB	Lumipulse	Simoa
ADNI (n=1610)			
	PET (n=1213)	*CSF (n=201)*	*Plasma (n=565)*
age: M (SD)	72.4 (7.8)	70.8 (7.9)	73.0 (7.8)
sex (female)	43.3%	42.3%	40.0%
APOE4+	46.9%	40.7%	43.8%
MMSE: M (SD)	26.54 (3.4)	26.6 (3.4)	25.8 (3.7)
PET tracer/Assay	FBB, FBP, NAV	Roche Elecsys	Fujiremio Lumipulse

Table 1. Demographics and assay details for PET Centiloid, CSF Aβ42/40, and plasma pTau217 data in cognitively impaired individuals from the University of California, San Francisco Memory and Aging Center (UCSF MAC; *top),* the Longitudinal Early Onset Alzheimer's Disease Study (LEADS; *middle*), and the Alzheimer's Disease Neuroimaging Initiative (ADNI; *bottom*).

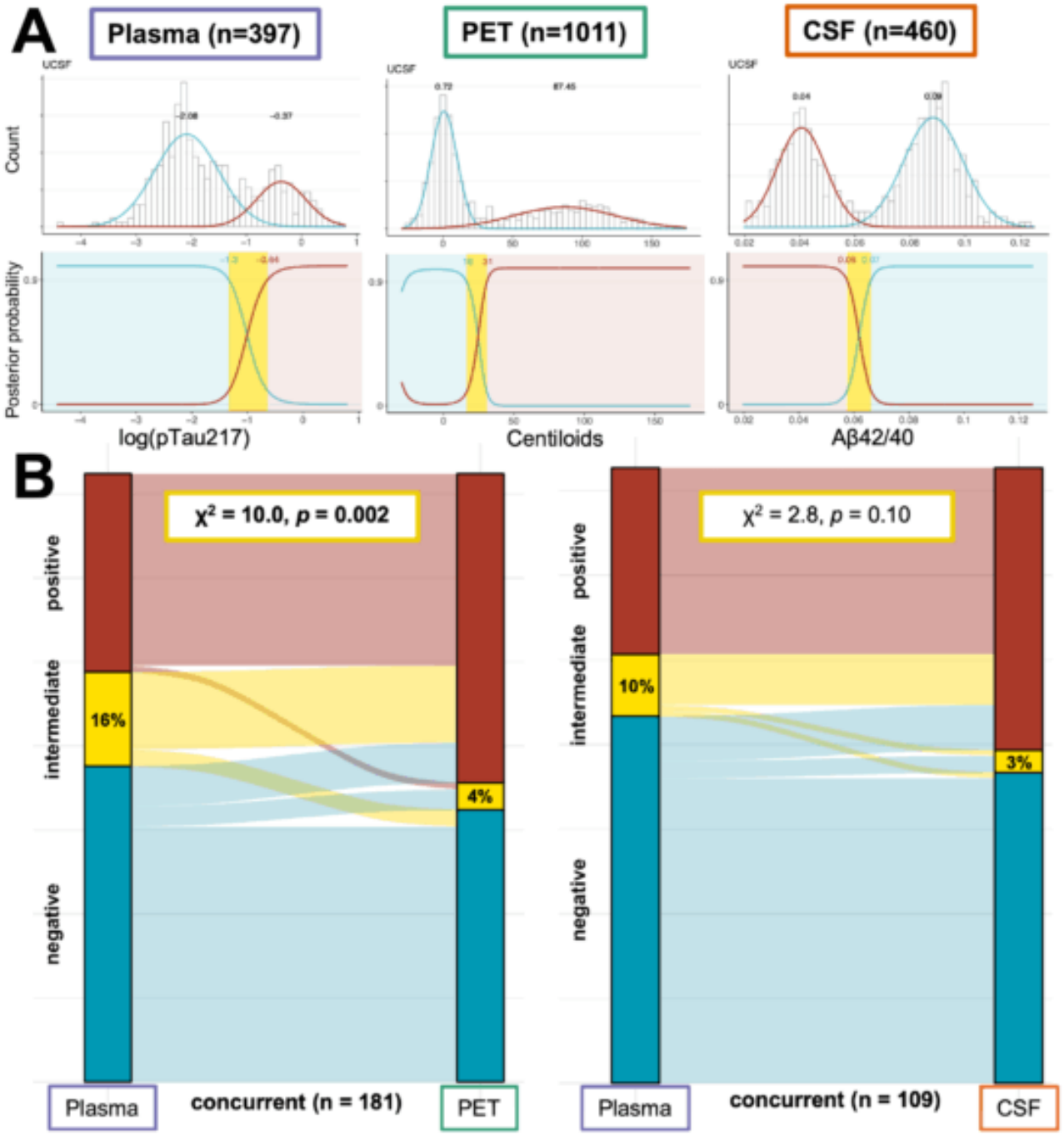


Figure 1. Example gaussian mixture modeling (GMM) procedure in the UCSF MAC cohort to determine negative, intermediate, or positive biomarker status from PET, CSF, and plasma data. **(A)** GMM fit of 2 components to the distribution of data from each modality. Central values for each component printed above each peak (*top*). A posterior probability threshold of 90% is applied to identify values as clearly negative, clearly positive, or intermediate for each modality. Cutoff values printed at each identified threshold *(bottom)*. **(B)** Alluvial plots showing biomarker status in individuals with concurrent measurements (within 6 months) between plasma and PET *(left)* and between plasma and CSF *(right)*. McNemar's χ^2 used to test the difference in proportion of intermediate cases between plasma and PET/CSF.

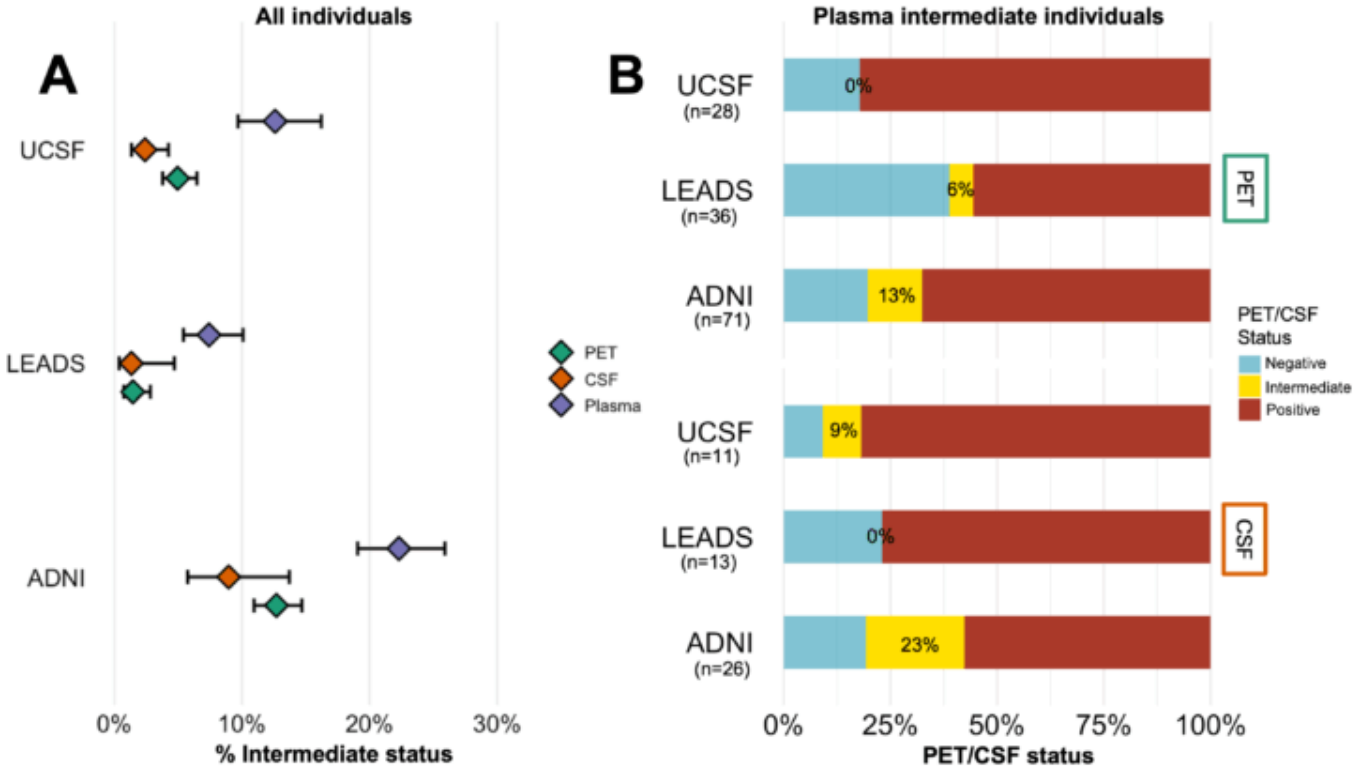


Figure 2. Intermediate biomarker status from Gaussian mixture modeling in PET, CSF, and plasma across cohorts. **(A)** Proportion of individuals with intermediate biomarker status across cohorts and modalities, Wilson's binomial proportion 95% confidence intervals. **(B)** Individuals with intermediate plasma biomarkers status and concurrent PET/CSF data. Proportion with negative, intermediate, or positive biomarker status from PET (*top*) and CSF (*lower*).

Keywords: Biomarker, PET, CSF, plasma, intermediate

100 Operationalizing clinical criteria for LATE using cognitive, MRI, and AD biomarker (biofluid or PET) data

Madison Cuppels[1], Colin Birkenbihl[1], Julie Schneider[2], David Bennett[2], Jane Brown[1], Mabel Seto[1], Gillian Coughlan[1], Annie Li[1], Diana Townsend[1], Michael Properzi[1], Bryan James[2], Konstantinos Arfanakis[2], Reisa Sperling[1], Hyun-Sik Yang[1], Jasmeer Chhatwal[1], Rebecca Amariglio[1], Timothy Hohman[3], Michael Donohue[4], Rachel Buckley[1]

[1]*Massachusetts General Brigham, Boston, MA, US*
[2]*Rush Alzheimer's Disease Center, Rush University Medical Center, Chicago, IL, US*
[3]*Vanderbilt Memory & Alzheimer's Center, Vanderbilt University Medical Center, Nashville, TN, US*
[4]*Alzheimer's Therapeutic Research Institute, University of Southern California, San Diego, CA, US*

Objective: Limbic-predominant age-related TDP-43 encephalopathy (LATE) is a disease primarily defined by post-mortem evidence of TDP-43 proteinopathy. Using a recently published clinical framework, we applied both theory-based and data-driven methods to identify individuals in whom LATE was likely the primary driver of clinical symptoms.

Method: We developed an operationalization of the LATE criteria based on Wolk et. al (2025). To define cognitive impairment, we thresholded composites across different cognitive domains at <= -1.5 SD relative to a cognitively unimpaired reference sample. To classify severe hippocampal atrophy, we identified the bottom tertile of a z-scored ratio of hippocampal volume against gray matter volume (antemortem MRI). Amyloid and tau positivity were determined from neuropathological data (ROSMAP) or established thresholds in PET/CSF for other datasets. Theory-based criteria were applied to the ROSMAP dataset (n=231) where LATE neuropathologic change (LATE-NC) was classified post-mortem (TDP-43o >= Stage 2). We compared the theory-based operationalization of the LATE criteria with a data-driven decision tree that was built using ROSMAP data, allowing the model to decide order and thresholding of the variables. Finally, we applied our theory-based approach to a larger, pooled non-postmortem dataset: A4/LEARN, HABS-HD, ADNI, EPAD, WRAP, BIOCARD, HABS (n=2,834).

Results: In ROSMAP, the sensitivity of the data-driven method outperformed that of the theory-based by an order of magnitude, however, both were poor (Figure 1). Both approaches demonstrated a strong specificity, indicating a robust prediction of negative LATE cases. Applying the theory-based approach across the seven cohorts resulted in a low estimated frequency of clinical cases of LATE.

Conclusion: Data-driven and theory-based approaches for operationalization of LATE struggle to classify positive cases, although there is an improvement with the data-driven model. While model performance may improve with further optimization, these results underscore the urgent need for a reliable *in vivo* TDP-43 biomarker.

Table 1: Demographics in ROSMAP

Characteristic	No LATE-NC N = 155[1]	LATE-NC N = 76[1]
Baseline Age	80.57 (6.75) [64, 100]	82.17 (5.49) [66, 93]
Sex		
Female	113 (72.90%)	63 (82.89%)
Male	42 (27.10%)	13 (17.11%)
Education	15.73 (3.07) [5, 24]	15.92 (3.24) [8, 30]
APOE4 Status		
E4-	107 (79.26%)	51 (77.27%)
E4+	28 (20.74%)	15 (22.73%)
Race		
White	152 (98.06%)	76 (100.00%)
Black or African American	2 (1.29%)	0 (0.00%)
Asian	1 (0.65%)	0 (0.00%)
Ethnicity		
Hispanic/Latino	3 (1.94%)	0 (0.00%)
Not Hispanic/Latino	152 (98.06%)	76 (100.00%)
Amyloid Status		
Aβ-	14 (9.03%)	6 (7.89%)
Aβ+	141 (90.97%)	70 (92.11%)

[1]Mean (SD) [Min, Max]; n (%)

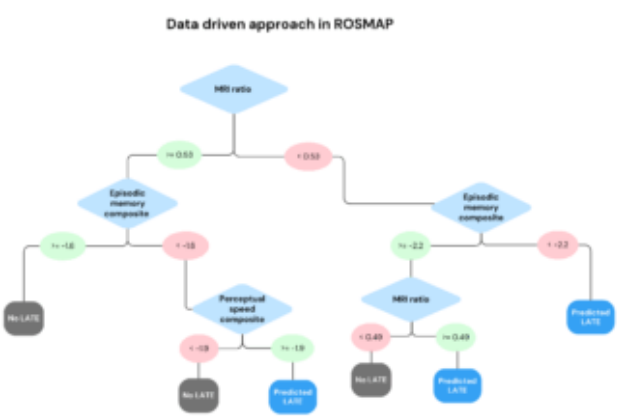
Table 2: Demographics in other cohorts

Characteristic	Overall N = 2,834[1]	A4/LEARN N = 386[1]	ADNI N = 716[1]	BIOCARD N = 157[1]	EPAD N = 214[1]	HABS N = 227[1]	HABS-HD N = 926[1]	WRAP N = 208[1]
Baseline Age	66.34 (9.31) [20, 90]	72.10 (4.85) [65, 86]	71.25 (7.08) [51, 90]	54.77 (8.35) [20, 73]	66.02 (7.13) [50, 88]	71.07 (8.28) [50, 89]	63.79 (8.11) [50, 88]	53.93 (6.24) [36, 65]
Sex								
Female	1,672 (59.00%)	224 (58.03%)	383 (53.49%)	101 (64.33%)	129 (60.28%)	135 (59.47%)	566 (61.12%)	134 (64.42%)
Male	1,162 (41.00%)	162 (41.97%)	333 (46.51%)	56 (35.67%)	85 (39.72%)	92 (40.53%)	360 (38.88%)	74 (35.58%)
Education	15.40 (3.37) [0, 30]	16.18 (2.86) [8, 30]	16.43 (2.44) [8, 20]	17.25 (2.36) [12, 20]	13.87 (3.69) [6, 25]	16.04 (2.95) [6, 20]	13.87 (3.76) [0, 20]	16.64 (2.60) [12, 25]
APOE4 Status								
E4-	1,766 (63.87%)	165 (42.75%)	451 (63.43%)	105 (66.88%)	132 (63.46%)	163 (72.44%)	614 (70.49%)	136 (65.70%)
E4+	999 (36.13%)	221 (57.25%)	260 (36.57%)	52 (33.12%)	76 (36.54%)	62 (27.56%)	257 (29.51%)	71 (34.30%)
Race								
White	2,303 (82.66%)	352 (91.19%)	603 (84.22%)	153 (97.45%)	164 (98.80%)	187 (82.38%)	643 (69.44%)	201 (96.63%)
Black or African American	393 (14.11%)	9 (2.33%)	71 (9.92%)	2 (1.27%)	1 (0.60%)	33 (14.54%)	272 (29.37%)	5 (2.40%)
Asian	48 (1.72%)	19 (4.92%)	21 (2.93%)	2 (1.27%)	1 (0.60%)	4 (1.76%)	0 (0.00%)	1 (0.48%)
More than one race	28 (1.01%)	4 (1.04%)	13 (1.82%)	0 (0.00%)	0 (0.00%)	2 (0.88%)	9 (0.97%)	0 (0.00%)
Unknown	11 (0.39%)	2 (0.52%)	7 (0.98%)	0 (0.00%)	0 (0.00%)	0 (0.00%)	1 (0.11%)	1 (0.48%)
American Indian or Alaskan Native	3 (0.11%)	0 (0.00%)	1 (0.14%)	0 (0.00%)	0 (0.00%)	1 (0.44%)	1 (0.11%)	0 (0.00%)
Ethnicity								
Hispanic/Latino	371 (13.36%)	9 (2.37%)	50 (7.00%)	3 (1.94%)	1 (0.60%)	2 (0.88%)	305 (32.94%)	1 (0.48%)
Not Hispanic/Latino	2,405 (86.64%)	371 (97.63%)	664 (93.00%)	152 (98.06%)	165 (99.40%)	225 (99.12%)	621 (67.06%)	207 (99.52%)
Amyloid Status								
Aβ-	1,846 (65.14%)	41 (10.62%)	436 (60.89%)	124 (78.98%)	157 (73.36%)	173 (76.21%)	747 (80.67%)	168 (80.77%)
Aβ+	988 (34.86%)	345 (89.38%)	280 (39.11%)	33 (21.02%)	57 (26.64%)	54 (23.79%)	179 (19.33%)	40 (19.23%)

[1]Mean (SD) [Min, Max]; n (%)

Table 3: Clinical criteria adapted from Wolk et al., 2025

Clinical Criteria for LATE as primary diagnosis	Probable LATE	Possible LATE
I. Core Clinical Syndrome (1 and 2 required)		
1. Primary amnestic syndrome with tempero-limbic memory loss 2. Other cognitive domains largely spared until much later in the course 3. May have mild semantic memory impairment 4. Indolent course with predominant amnestic syndrome present for at least 2 years 5. Age generally > 75 years old		
II. Required Imaging		
Significant hippocampal atrophy (out of proportion to global atrophy)		
III. Required Supportive Features for Probable LATE		
A negative test of one of the following to rule out β-amyloid: 1. Amyloid PET 2. CSF $A\beta_{42/40}$ 3. CSF $ptau_{181}$/ $A\beta_{42/40}$ or t-tau/ $A\beta_{42}$		
IV. Required Additional Measures if Amyloid-Positive		**Possible LATE**
If amyloid-positive based on III, a negative measure of one of the following Tau biomarkers in required: 1. MTL Tau PET (preferred measure) 2. CSF $ptau_{181}$		







Performance Metrics in ROSMAP

Model	Positive predictive value	Negative predictive value	Sensitivity	Specificity	False positive rate	False negative rate
Data driven	0.526	0.706	0.4	0.8	0.2	0.6
Theory based	0.75	0.678	0.0395	0.994	0.00645	0.961

Figure 1: Performance metrics and decision trees for theory-based and data-driven models. TP = true positive, TN = true negative, FP = false positive, FN = false negative. Positive predicted value = TP / (TP + FP). Negative predicted value = TN / (TN + FN). Sensitivity = TP / (TP + FN). Specificity = TN / (TN + FP). False positive rate = FP / (FP + TN). False negative rate = FN / (TP + FN).

Keywords: LATE, neuropathology, cognition, biomarker

101 CT-based processing is equivalent to MR-based processing for tau PET regional quantification

Guilherme Povala[1], Bruna Bellaver[1], Livia Amaral[1], Firoza Z. Lussier[1], Pamela C. L. Ferreira[1], Guilherme Bauer-Negrini[1], Dana L. Tudorascu[1], Joseph Masdeu[3], Juan Fortea[4], David N. Soleimani-Meigooni[5], Val Lowe[6], Hwamee Oh[7], Belen Pascual[3], Brian A. Gordon[8], Pedro Rosa-Neto[9], Suzanne Baker[2], Tharick A. Pascoal[1]

[1]*University of Pittsburgh, Department of Psychiatry, Pittsburgh, PA, US*
[2]*Lawrence Berkeley National Laboratory, Berkeley, CA, US*
[3]*Houston Methodist Research Institute, Department of Neurology, Houston, TX, US*
[4]*Sant Pau Memory Unit, IR SANT PAU, Hospital de la Santa Creu i Sant Pau, Barcelona, Spain*
[5]*University of California San Francisco, Memory and Aging Center, San Francisco, CA, US*
[6]*Mayo Clinic, Department of Radiology, Rochester, MN, US*
[7]*Brown University, Department of Psychiatry and Human Behavior, Providence, RI, US*
[8]*Washington University in St. Louis, Department of Radiology, St. Louis, MO, US*
[9]*Translational Neuroimaging Laboratory, McGill University Research Centre for Studies in Aging, Douglas Research Institute, Montréal, QC, Canada*

Background: Accurate quantification of tau PET is essential for diagnosis, prognosis, and treatment eligibility in Alzheimer's disease (AD). Conventional pipelines require PET-to-MR registration, a process that is time-consuming, error-prone, and often impractical in clinical settings where MRI is unavailable. We developed and validated a PET-CT–based quantification pipeline that repurposes the CT acquired with PET for anatomical reference, eliminating the need for PET-to-MR registration while maintaining quantitative accuracy.

Methods: We analyzed 235 HEAD study participants scanned with MK6240 using PET-CT and PET-MR pipelines. PET-to-MR alignment employed linear registration followed by nonlinear warping to ICBM152 space. PET-CT processing required only the nonlinear step because PET and CT are intrinsically co-registered. SUVRs were extracted for the medial temporal lobe (MTL) and neotemporal cortex. Positivity thresholds were derived from cognitively unimpaired adults (mean + 2SD). Concordance between PET-CT and PET-MR SUVRs and positivity classifications was assessed using correlation coefficients and confusion matrices.

Results: PET-CT SUVRs showed near-perfect correspondence with PET-MR values across all regions (R^2 = 0.94–0.97; **Fig. 1**). The MTL and neotemporal cortex showed R^2 values of 0.974, and 0.965, respectively, each with > 97% classification accuracy. Cutoffs for tau positivity were nearly identical between modalities (CT vs. MR: 1.10 vs. 1.09 in MTL; 1.17 vs. 1.19 in neotemporal). Disagreements were minimal, 6 participants in the MTL, and 5 in the neotemporal, and all occurred close to the positivity thresholds, consistent with expected gray-zone variability.

Conclusions: PET-CT provides quantitative results equivalent to PET-MR, supporting its use as a reliable and scalable alternative when MRI is unavailable or impractical. We are developing a dedicated PET-CT quantification tool to streamline implementation in clinical and research settings. Validation with additional tracers (Flortaucipir, PI2620, RO948, PiB, NAV4694, Florbetaben) and cohorts is ongoing, with results from all tracers and the tool expected to be available by HAI 2026.

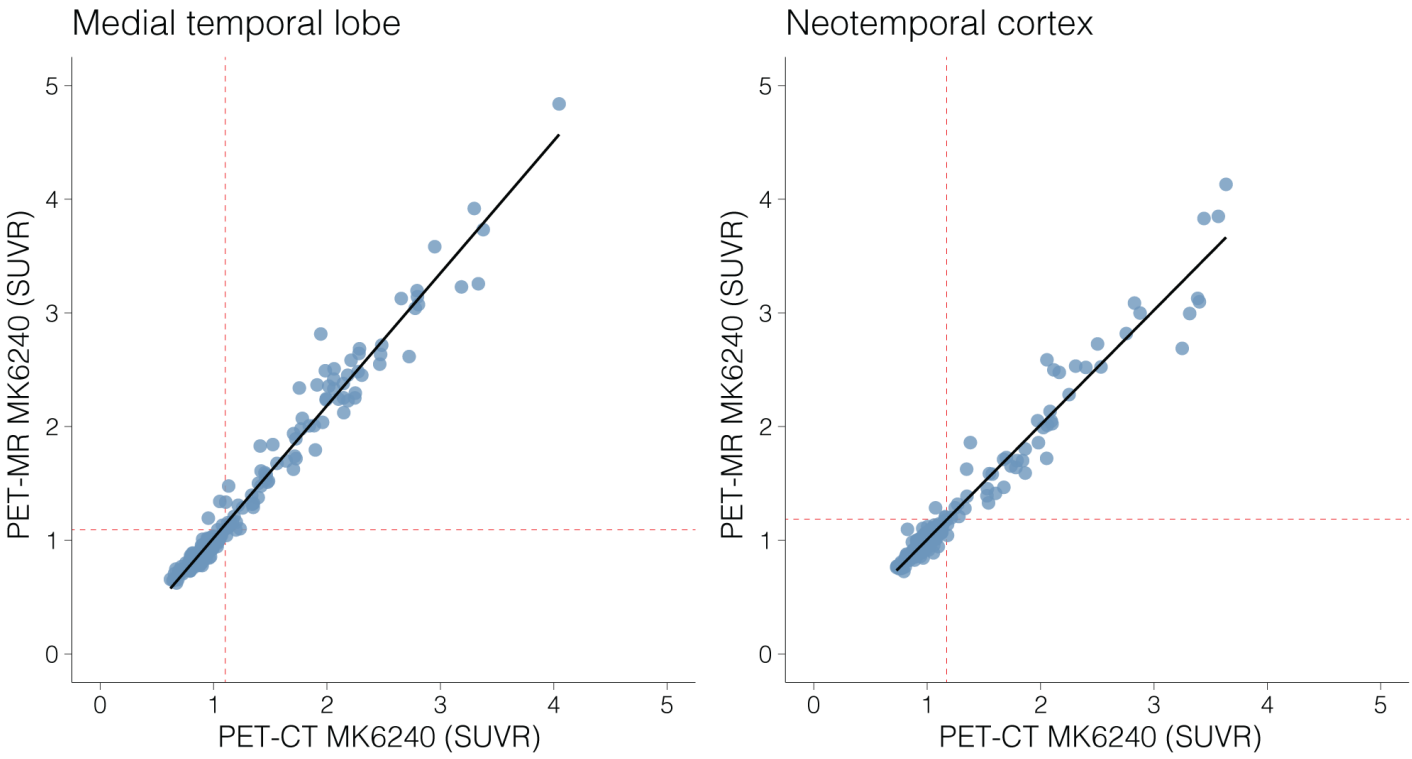


Figure 1. Scatter plots showing the correspondence between MK6240 SUVRs obtained with PET-CT and PET-MR in the medial temporal lobe and neotemporal cortex. Solid black lines indicate linear fits, and dashed red lines mark positivity thresholds derived from cognitively unimpaired adults (mean + 2 SD). The strong linear relationships (R^2 = 0.94–0.97) and near-identical cutoffs highlight the equivalence between PET-CT and PET-MR quantification.

Keywords: PET-CT quantification, PET-MR comparison, Neuroimaging harmonization, Clinical implementation

102 A pilot study on the association of plasma proteins with neuroimaging biomarkers of Alzheimer's disease in African Americans

Olatunbosun Arowolo[1], Lindsey Kuchenbecker[1], Michael Heckman[2], Thuy Nguyen[1], Heidi Casellas[1], Katie Sotelo[1], Christopher Schwarz[3], Matthew Senjem[4], Manoj Jain[5], John Lucas[6], Floyd Willis[7], Nilufer Ertekin-Taner[1,8], Neill Graff-Radford[8], Kejal Kantarci[3], Val Lowe[3], Christian Lachner[8], Gregory Day[8], Minerva Carrasquillo[1]

[1]*Department of Neuroscience, Mayo Clinic Florida, Jacksonville, FL, US*
[2]*Department of Quantitative Health Sciences, Mayo Clinic Florida, Jacksonville, FL, US*
[3]*Department of Radiology, Mayo Clinic Rochester, Rochester, MN, US*
[4]*Department of Information Technology, Mayo Clinic Rochester, Rochester, MN, US*
[5]*Department of Radiology, Mayo Clinic Florida, Jacksonville, FL, US*
[6]*Department of Psychiatry and Psychology, Mayo Clinic Florida, Jacksonville, FL, US*
[7]*Department of Family Medicine, Mayo Clinic Florida, Jacksonville, FL, US*
[8]*Department of Neurology, Mayo Clinic Florida, Jacksonville, FL, US*

Background: Alzheimer's disease (AD) is a neurodegenerative disease influenced by genetics and lifetime exposures (exposome). Despite African Americans (AA) being at greater risk of developing dementia, there are limited studies evaluating the relationship of plasma and neuroimaging biomarkers of AD in AA. Hence, we investigated the association between plasma protein levels and amyloid and tau burden in AA based on positron emission tomography (PET) imaging, exploring the interaction with exposome factors.

Methods: This study included Mayo Clinic Alzheimer's Disease Research Center AA participants for whom SomaScan7k plasma proteome, amyloid-PET (n=35) and tau-PET (n= 38) were obtained within one year. Key exposome factors were analyzed: presence/absence of hypertension, diabetes, hypercholesterolemia and high educational attainment (>12 years). Association of plasma proteins with amyloid-PET (PiB Centiloids) and tau-PET (flortaucipir temporal meta-ROI SUVR) was tested using linear regression adjusting for age, sex, *APOE*. Interaction of exposome factors with proteins associated with amyloid-PET or tau-PET was also assessed.

Results: After FDR correction, the association of tau-PET with ganglioside GM3 synthase (ST3GAL5, involved in signal transduction in white matter) remained significant (FDR q=0.04). Presence/absence of diabetes showed nominal interaction (p=0.018) with ST3GAL5 in the association with tau-PET. Associations of ST3GAL5 with tau-PET were evident in both diabetic and non-diabetic groups, though weaker in magnitude in non-diabetic (N=31, β=0.90, CI:0.54-1.27, $p=3.08\times10^{-5}$) compared to diabetic participants (N=7, β=2.52, CI:-0.55-5.58, p=0.07), despite only being significant in the larger non-diabetic group.

Conclusion: Despite the small sample size, we identified for the first time ST3GAL5 as a potential plasma biomarker for AD. ST3GAL5 was strongly associated with tau burden and appears to interact with the presence of diabetes in this AA cohort. This pilot study will be expanded to larger, multiethnic cohorts to validate these findings and to elucidate the potential role of ST3GAL5 in pathways underlying the risk of AD.

Keywords: Blood-based biomarkers, African Americans, Alzheimer's disease, Positron Emission Tomography, Exposome

103 Amyloid-PET and white matter hyperintensities but not military service duration nor combat exposure are associated with neurodegeneration and cognitive impairment in older veterans

Salma Rocha[1], Shlomit Pasternak[3], Orit Lesman Segev[3], Daniel Schwartz[2], Ganna Blazhenets[1], Piyush Maiti[1], Yael Rosen Lang[3], Nathan Hantke[2], Abigail Livny-Ezer[3], Kristine Yaffe[1], Leslie Shaw[4], Michael Weiner[1], Aidyn Rose Hills[1], Lisa Kritikos[1], David Soleimani-Meigooni[1], Lisa Silbert[2], Renaud La Joie[1], Raquel Gardner[3]

[1]*University of California, San Francisco, San Francisco, CA, US*
[2]*Oregon Health & Science University, Portland, OR, US*
[3]*Sheba Medical Center, Ramat Gan, IL*
[4]*University of Pennsylvania, Philadelphia, PA, US*

Objective: Older veterans have high prevalence of cardiovascular and environmental/occupational risk factors for dementia because of unique exposures that may occur throughout military service and combat exposure. We aimed to examine associations between amyloid PET, cerebral atrophy, white matter hyperintensities, cognitive function, military service years, and combat exposure in a cohort of older military veterans with MCI and dementia.

Participants and Methods: The Department of Defense Alzheimer's Disease Blood-testing Initiative (DOD-ADBI) bi-national study launched enrollment in 6/2024 of a planned 100 older veterans with MCI or dementia at 3 sites (San Francisco, Portland, Ramat Gan). All participants underwent 3T-MRI (T1 and FLAIR) to derive cortical parcellation using Freesurfer 7 and White Matter Hyperintensity (WMH) volume using the LST-AI toolbox. Amyloid-PET (Florbetapir or Flutemetamol) was visually interpreted by expert readers and quantified in Centiloids using an MRI-based pipeline. Linear models were used to assess relationships between amyloid-PET (positive/negative, Centiloids), MRI (cortical atrophy, WMH), MMSE, and military variables (service years, combat exposure score).

Results: As of 10/2025, 57 veterans have been enrolled (age=75.9±6.9, 75% male, 58% CDR=0.5). Amyloid positivity rate by visual read was 56%, with no significant difference across site, sex, and clinical stage (Figure 1a). Amyloid PET outcomes were not associated with WMH (p=0.70 & 0.81, Figure 1b), but both measures were independently associated with neurodegeneration (mean cortical thickness, Figure 2a) and cognitive impairment (MMSE, Figure 2b). Military variables were not significantly associated with amyloid PET, MRI metrics, or MMSE (Figure 3).

Conclusions: Preliminary analyses near the midpoint of data collection suggest that amyloid burden and cerebrovascular disease are independently associated with cognitive decline in veterans with MCI/dementia, while military service duration and combat exposure burden are not. This finding deserves confirmation in larger cohorts with additional investigation of the independent role of traumatic brain injury and post-traumatic stress disorder.

Figure 1

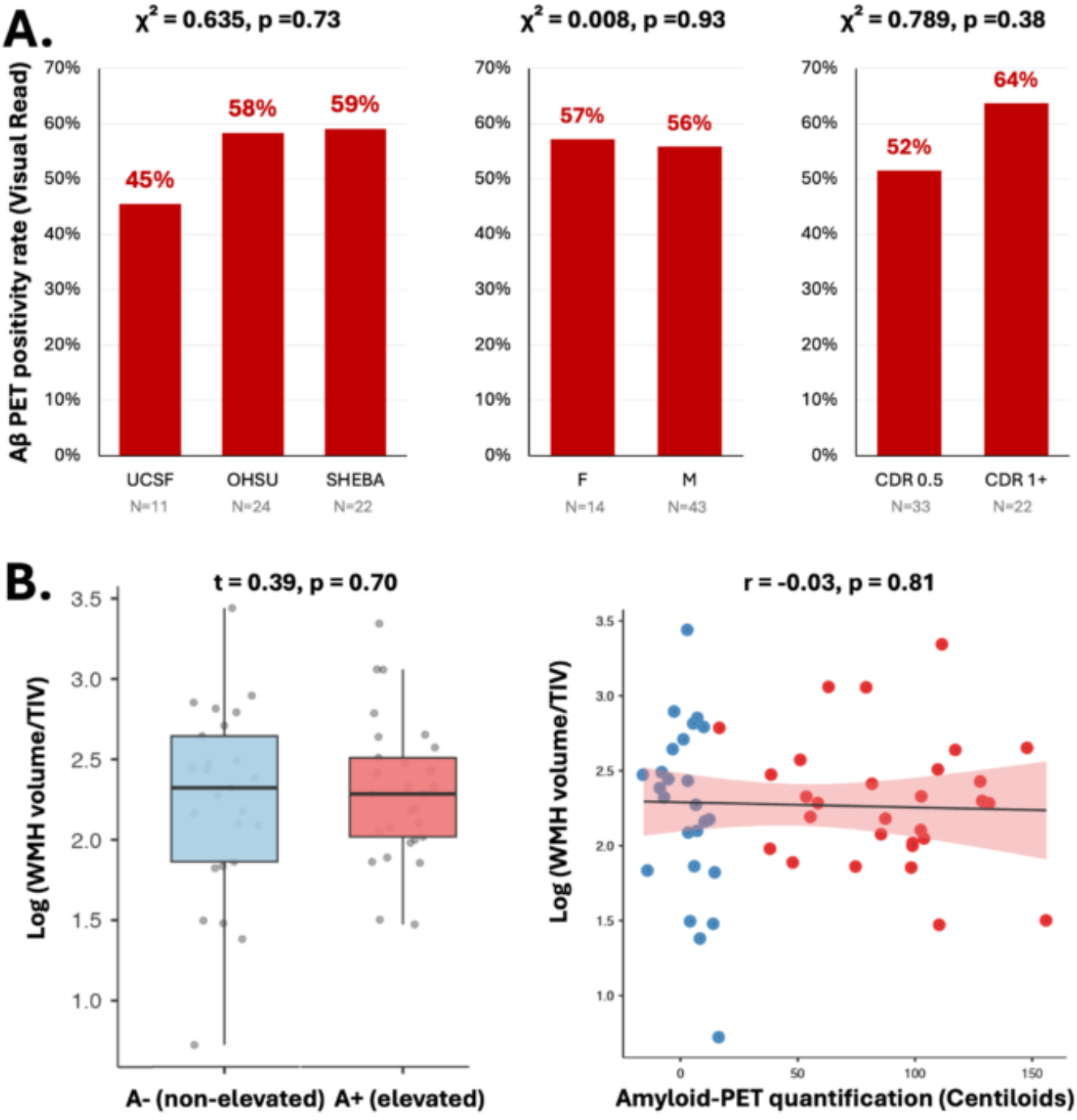
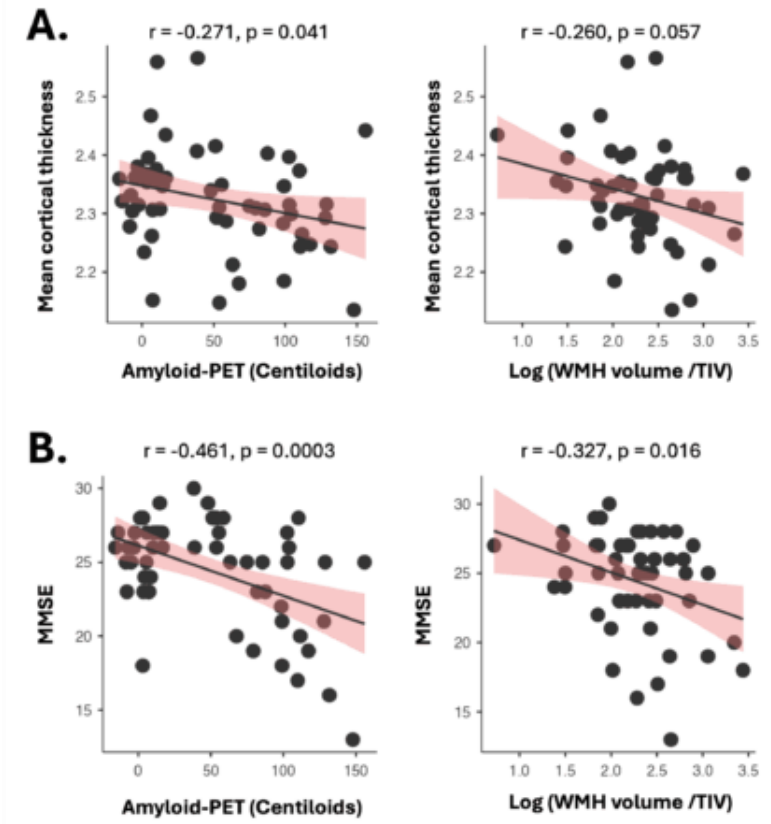

A.
χ² = 0.635, p =0.73
χ² = 0.008, p =0.93
χ² = 0.789, p =0.38
Aβ PET positivity rate (Visual Read)
70%
60%
50%
40%
30%
20%
10%
0%
45%
58%
59%
57%
56%
52%
64%
UCSF
N=11
OHSU
N=24
SHEBA
N=22
F
N=14
M
N=43
CDR 0.5
N=33
CDR 1+
N=22
B.
t = 0.39, p = 0.70
r = -0.03, p = 0.81
Log (WMH volume/TIV)
3.5
3.0
2.5
2.0
1.5
1.0
A- (non-elevated)
A+ (elevated)
0
50
100
150
Amyloid-PET quantification (Centiloids)

Figure 2



Multiple regression: $R^2 = 0.149$

	Std estimate [95% CI]	P value
Amyloid-PET, Centiloids	-0.285 [-0.530 to -0.010]	0.04
Log(WMH volume/TIV)	-0.270 [-0.544 to -0.025]	0.03

Multiple regression: $R^2 = 0.337$

	Std estimate [95% CI]	P value
Amyloid-PET, Centiloids	-0.481 [-0.710 to -0.252]	<0.001
Log(WMH volume/TIV)	-0.343 [-0.572 to -0.114]	0.004

Figure 3

	Military years	Combat exposure scale
Amyloid-PET, Centiloids	r=0.074 ,p=0.89	r=0.004 ,p=0.98
Log(WMH volume/TIV)	r=-0.088 ,p=0.53	r=-0.121 ,p=0.39
Mean cortical thickness	r=0.036 ,p=0.79	r=-0.128 ,p=0.35
MMSE	r=0.012 ,p=0.93	r=-0.157 ,p=0.25

Keywords: Military veterans, Neuroimaging, Combat exposure, White matter hyperintensities, Cognitive decline

104 The influence of cardiovascular risk on white matter integrity along the Alzheimer's disease trajectory: Early impact in preclinical stages

Paul Edison[1], Abby Arnold[1]

[1]*Imperial College London, London, UK*

Introduction: Cardiovascular risk plays a significant role in Alzheimer's disease. It remains imperative to establish how cardiovascular risk (CVR) influences neurodegeneration over the AD trajectory and how this is affected by other risk factors. Here, we investigate the influence of CVR on white matter (WM) integrity in older adults across different cognitive stages. Modulation of this relationship by sex and APOE genotype was also assessed.

Methods: 1224 participants from the Health and Ageing Brain Study – Health Disparities (HABS-HD) cohort had APOE genotyping, cardiovascular and cerebrovascular evaluations, along with diffusion-weighted MRI (DTI) scans. Data were analysed from 874 individuals with normal cognition (CN; mean age = 64.7 years, 62.8% female), 260 individuals with mild cognitive impairment (MCI; mean age = 65.7 years, 53.1% female), and 90 individuals with dementia (mean age = 68.1 years, 46.7% female). DTI scans were processed using tract-based spatial statistics to extract fractional anisotropy (FA) and mean diffusivity (MD) values. The relationship between Framingham Risk Score (FRS; cardiovascular risk) and diffusion metrics was assessed using tract-level and voxelwise general linear models, including interactions with sex and APOE.

Results: In the CN group, FRS was associated with MD and FA in multiple commissural, limbic, associative, and projection WM tracts. In MCI subjects, tract associations were limited; however, this group uniquely exhibited widespread voxelwise correlations with MD. In dementia, associations were also limited and in the opposite direction to those seen in the CN and MCI groups. Several tracts exhibited sex-specific vulnerability, whereas the APOE genotype exerted only a limited modulatory effect.

Conclusions: CVR has the most significant influence on WM disruption in the preclinical stages of AD, with particular susceptibility in frontal and medial tracts, as well as sex-specific anatomical vulnerabilities. These findings highlight the importance of early intervention in vascular health and support precision medicine strategies.

Keywords: Framingham Risk Score, DTI, FA, MD, ApoE4

105 Longitudinal tau PET progression follows language network spread in primary progressive aphasia

Adam Martersteck[1], Emily Rogalski[1]

[1]*Healthy Aging & Alzheimer's Research Care Center, Department of Neurology, University of Chicago, Chicago, IL, US*

Background: Primary progressive aphasia (PPA) is a clinical dementia syndrome characterized by selective vulnerability of the (usually) left-lateralized language network and is often caused by underlying Alzheimer's disease (AD) neuropathologic change. PPA is less frequently diagnosed compared to 'typical' amnestic sporadic late-onset AD, and fewer studies have examined the change in AD tau over time with PET imaging.

Methods: 27 PPA participants with positive AD biomarkers (PPA-AD) underwent 18F-flortaucipir (FTP; Tauvid) PET and MR imaging at baseline and repeated 1-3 years later. Analyses used 80–100-minute post-injection frames, motion corrected and registered to FreeSurfer's unbiased within-subject native space. Partial volume correction was not used. Region-wise multiple comparisons were controlled by false discovery rate (FDR; 68 Desikan-Killiany regions, q=0.05).

Results: PPA participants (mean age 66.7) had mild-to-moderate language impairment (average WAB-AQ=80.0%). 17 were subtyped logopenic, 3 agrammatic/nonfluent, and 7 mixed/unclassifiable. Baseline FTP was elevated in left perisylvian temporal cortex (PSTC) and left precuneus (Figure 1A). Over a median follow-up of 1.8 years, frontal regions and right-hemisphere PSTC homologues showed the largest increase in FTP standard uptake value ratio (SUVR; Figure 1B). Younger age related to higher baseline SUVR in inferior parietal and inferior frontal regions and to greater SUVR increase across cortical regions (Figure 2A). Baseline FTP showed no sex or APOE effects, but SUVR increases were higher in parietal cortex in females (Figure 2B) and near the temporoparietal junction in non-ε4 carriers, although the APOE association did not survive FDR.

Conclusions: Longitudinal FTP in PPA-AD indicates spread from left perisylvian/precuneus toward frontal and contralateral language regions, consistent with network-based progression and supporting tau PET for staging and prognosis. Younger age, and a possible female effect, tracked with faster tau accumulation, while APOE associations require follow-up. These patterns may inform trial stratification and outcome selection in atypical AD.

Figure 1

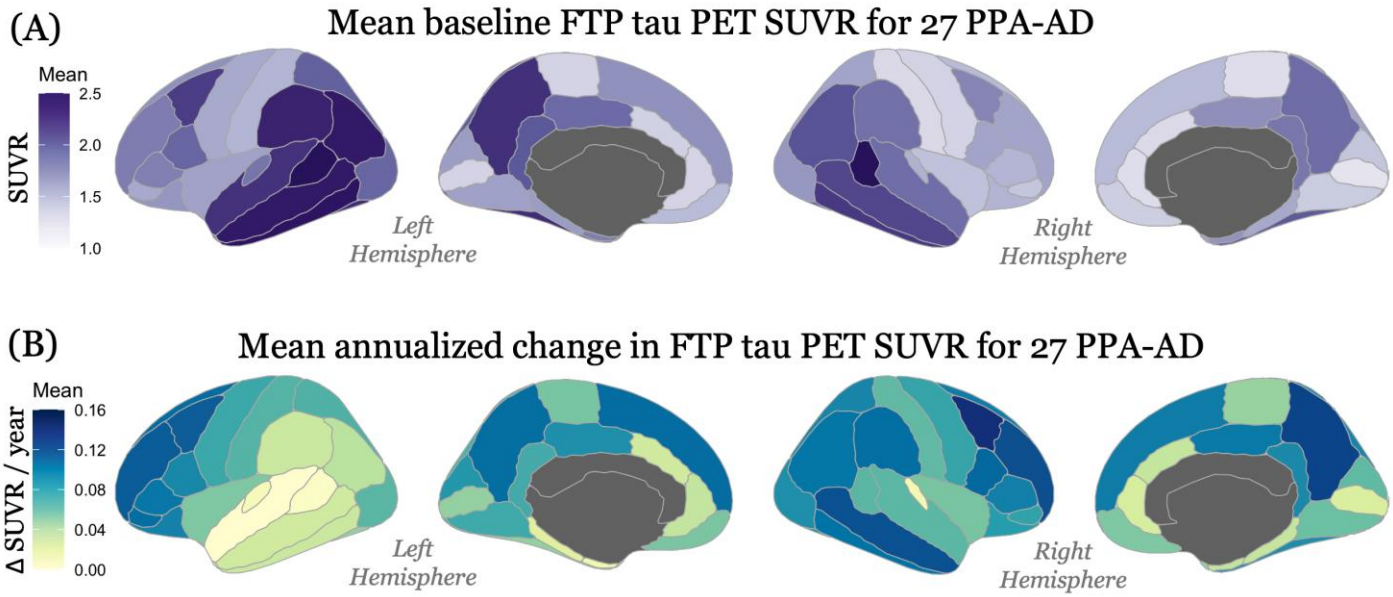


Figure 1. (A) The baseline flortaucipir (FTP) tau PET standard uptake value ratio (SUVR) for the group of 27 PPA-AD by the 68 region Desikan-Killiany parcellation (darker purple indicating higher SUVR); (B) the average annualized longitudinal change in FTP across the 27 PPA-AD group (darker, more blue colors indicating regions with higher rates of change).

Figure 2

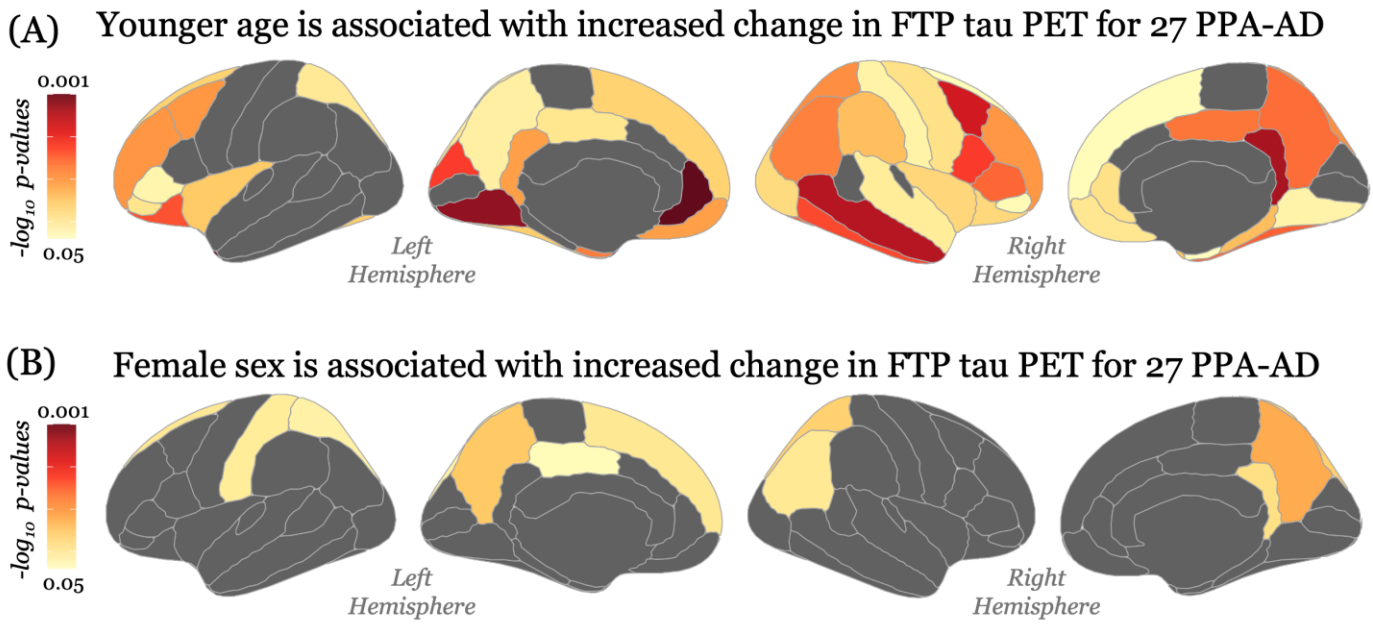


Figure 2. Statistical p-value maps, flamescaled with a -log10(p) scale, with warmer colors indicating lower p-values, displaying the significant regional relationship for the 27 PPA-AD group between (A) younger age and increased change in annualized flortaucipir (FTP) tau PET; (B) the significant regions associated with female sex and increased FTP PET burden (no significant male sex associations).

Keywords: tau PET, longitudinal, PPA, age, sex

106 The adjusted Centiloid: Improving reliability by correcting for white matter uptake variability

Anthonin Reilhac[1], Michael C. Irizarry[1], Larisa Reyderman[1], Arnaud Charil[1]

[1]*Eisai Inc., Nutley, NY, US*

Background: Amyloid tracer uptake in the cerebral White Matter (WM) is variable between and within subjects contributing significantly to noise in the computed Centiloid. We propose a novel data-driven and easy-to-implement Centiloid computational approach that corrects for WM contamination.

Methods: The proposed correction requires a mean WM contamination factor that is determined once using scans with low cortical SUVr values but exhibiting a wide range of WM uptakes (Fig. 1). For each scan, the correction is calculated by subtracting the product of the contamination factor and the subject's WM SUVr from the measured cortical SUVr.

The method was applied to an ADNI dataset consisting of 3376 Florbetapir scans (1466 subjects) that were processed using an in-house pipeline (motion correction, resolution harmonization at $8mm^3$, spatial normalization in MNI space). Amyloid burden was measured using the Standard Centiloid VOI (Klunk et al., 2015). WM SUVr values were obtained using an eroded cerebral WM mask. SUVr to Centiloid conversion equations were established for the uncorrected and corrected SUVr values, resulting in a 'Standard' and 'Adjusted' Centiloid, respectively.

Performance comparison between Standard and Adjusted Centiloid included their associations with plasma biomarkers of amyloid as well as longitudinal rates of change.

Results: Compared to the Standard Centiloid, the Adjusted Centiloid was better explained by Aβ42/Aβ40 and pTau217/npTau217, with increases in t-values by 13% and 20%, respectively. ROC analysis showed that pTau217 better discriminated amyloid status when expressed as Adjusted Centiloid rather than the Standard Centiloid (Fig. 2). Finally, longitudinal rates of change measured with the Adjusted Centiloid exhibited more robust and significant increases compared to those measured with the Standard Centiloid (Fig. 3).

Conclusion: The Adjusted Centiloid method provides an efficient solution to reduce white matter contamination, a major source of noise, thereby enhancing the consistency and reliability of Centiloid measurements.

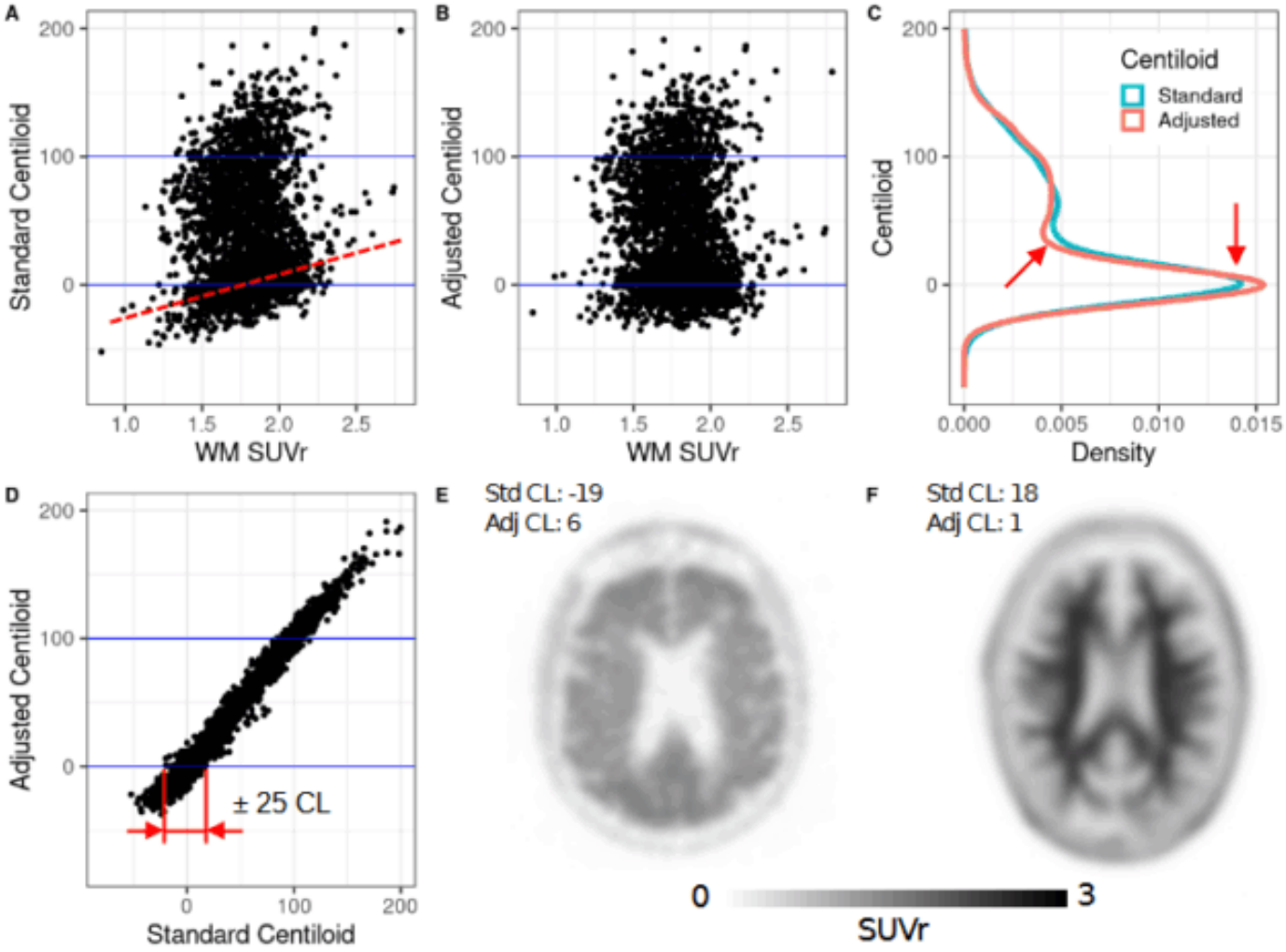


Figure 1. Centiloid values are impacted by inter- and intra-subject variabilities of the non-specific tracer uptake in the WM which directly contaminates the target cortical ROI. The variability of the WM uptake and its impact on the Centiloid is visible in **Fig. 1A.** The generic principle of the proposed correction uses a mean contamination factor, estimated once from the low Centiloid values (red line – that can be defined using quantile regression). It then corrects the measured Centiloid of every single scan based on its measured WM uptake and the estimated contamination factor, leading to the Adjusted Centiloid values that are independent of the WM uptake (**Fig. 1B**). The distribution of the Adjusted Centiloid shows a slightly improved discrimination (increased peak-to-valley ratio) (**Fig 1.C**). WM variability can cause variations of up to 25 Centiloid as shown on the Adjusted/Standard Centiloid plot in **Fig. 1D**. **Fig. 1E** shows a scan with an extremely low WM uptake and a standard Centiloid of -19, while the adjusted Centiloid value is 6. **Fig. 1F** shows a scan with a high WM uptake and a standard Centiloid value of 18, while the adjusted Centiloid value is 1.

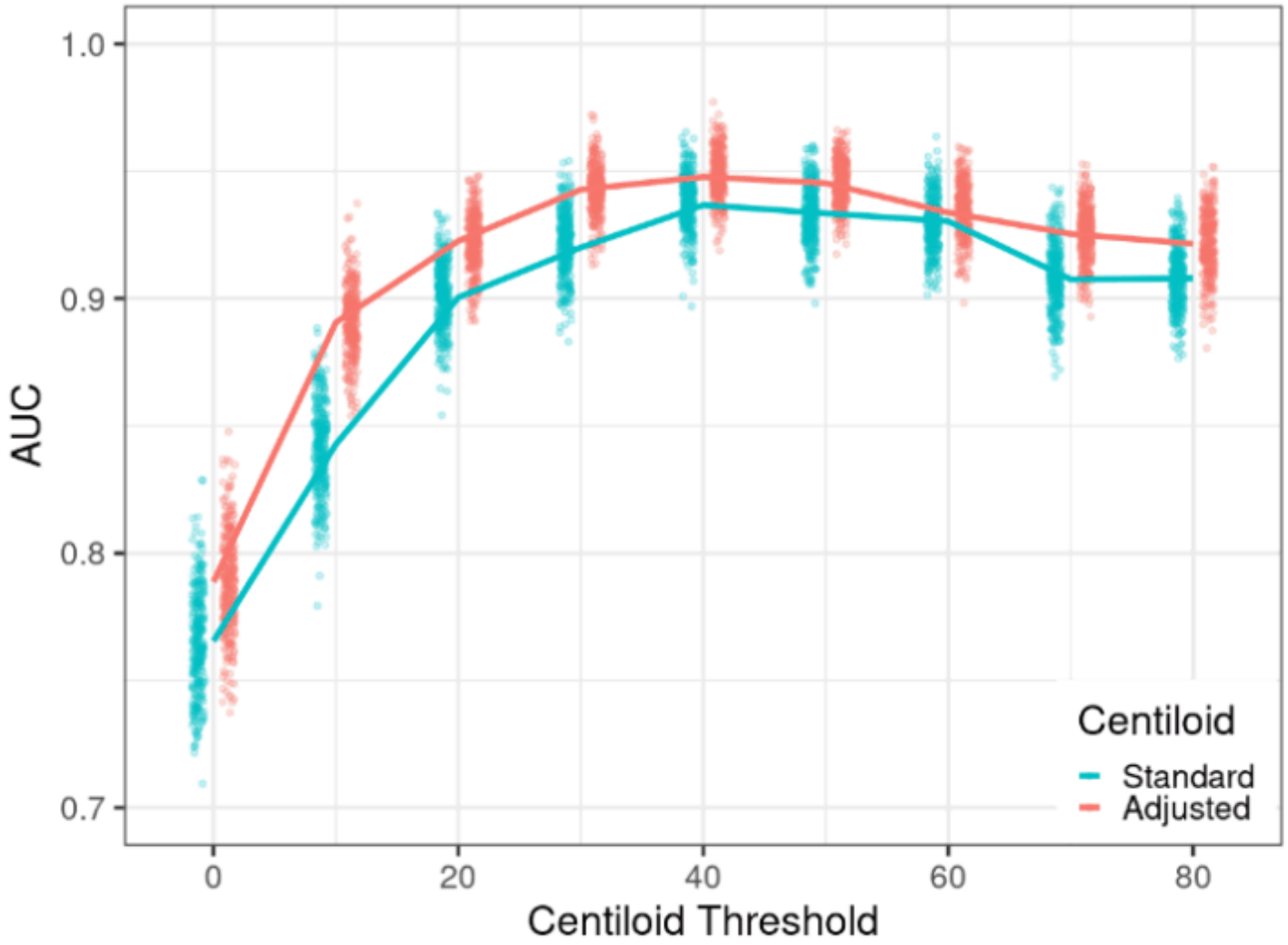


Figure 2. AUC obtained with pTau217 for the discremination of the Amyloid status as defined by the Standard and the Adjusted Centiloid and for increasing Centiloid positivity thresholds (0 CL to 80 CL). Solid lines show AUC obtained using all the observations in the ROC analysis (n = 544). Individual data points are AUC obtained in a 70%/30% training/testing framework repeated 500 times for each Centiloid threshold. Results indicate that pTau217 better discriminates amyloid status when expressed as Adjusted Centiloid vs Standard Centiloid across a wide range of Centiloid thresholds, but in particular for lower Centiloid thresholds (e.g., CL=10).

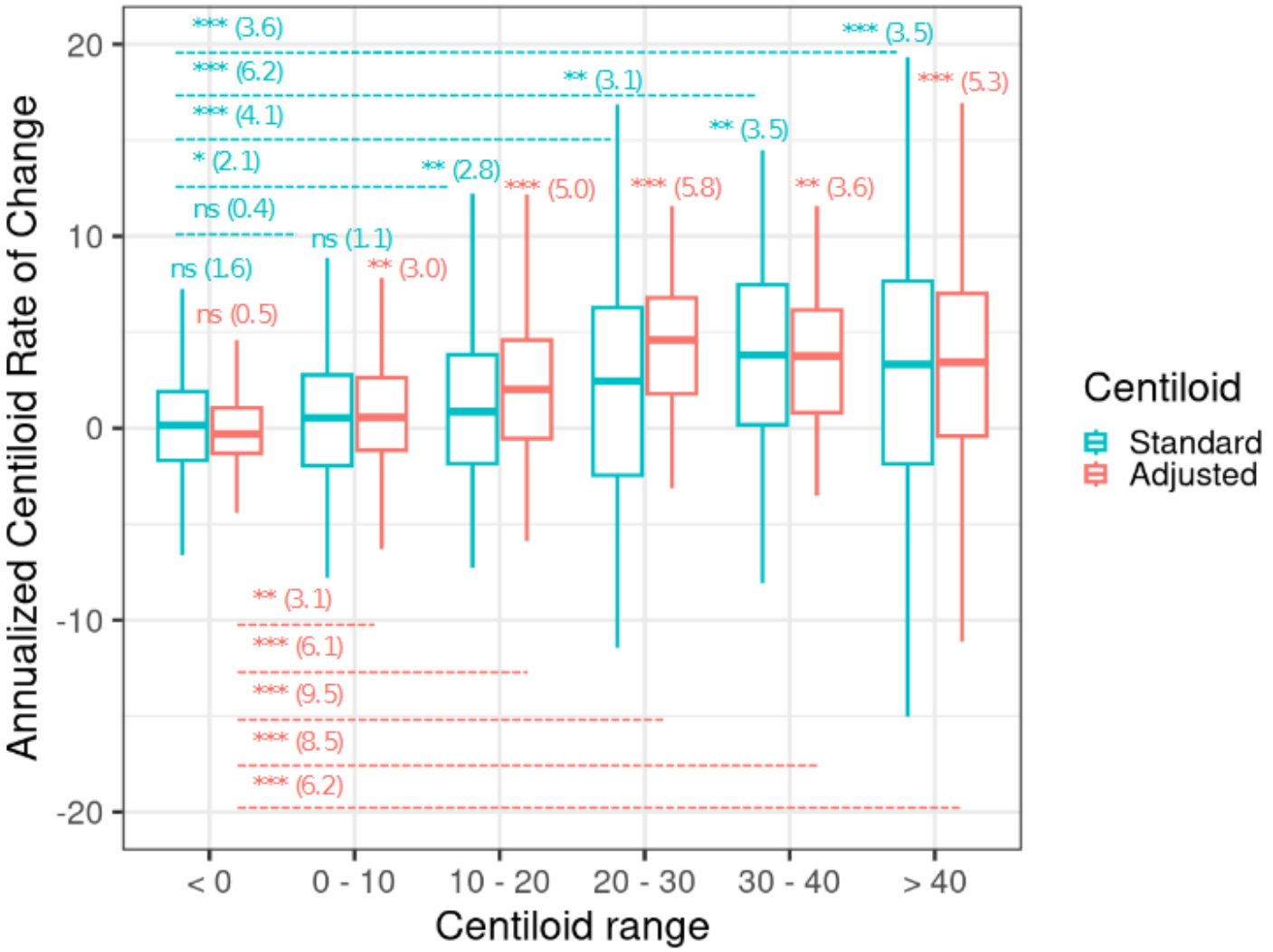


Figure 3. Annualized Centiloid rate of change, stratified by baseline Centiloid, and measured using the Standard and Adjusted Centiloid methods. Annualized rate of change, measured with the Adjusted Centiloid, shows overall more robust and significant increases than when measured with the Standard Centiloids, allowing the detection of significant increases at lower baseline Centiloid values.

Keywords: Centiloid, Amyloid PET, tracer quantification, white matter uptake

107 Perivascular spaces: Predictors of longitudinal amyloid, tau, cerebrovascular biomarkers?

Audrey Low[1], Jeffrey Gunter[1], Mingzhao Hu[2], Sheelakumari Raghavan[1], Scott Przybelski[2], Christopher Schwarz[1], Kejal Kantarci[1], Val Lowe[3], Jonathan Graff-Radford[3], Ronald Petersen[3], Clifford Jack[1], Prashanthi Vemuri[1]

[1]*Department of Radiology, Mayo Clinic, Rochester, MN, 55905, USA, Rochester, MN, US*
[2]*Department of Quantitative Health Sciences, Mayo Clinic, Rochester, MN, 55905, USA, Rochester, MN, US*
[3]*Department of Neurology, Mayo Clinic Rochester, MN, 55905, USA, Rochester, MN, US*

Background: Perivascular spaces (PVS) are increasingly recognized as markers of glymphatic and cerebrovascular dysfunction in Alzheimer's disease (AD), and are now included in the updated Boston Criteria 2.0 for cerebral amyloid angiopathy (CAA). However, no longitudinal PET studies have investigated PVS as a mechanism of longitudinal AD pathophysiological change. Our overall objective was to investigate the association of baseline PVS burden with white matter hyperintensity (WMH) volume, amyloid-PET, and tau-PET, both cross-sectionally and longitudinally.

Methods: 2265 participants from the Mayo Clinic Study of Aging (MCSA) and the Mayo Alzheimer's Disease Research Center (ADRC) were analyzed (mean age 68.5±12.6, 48.6% females). PVS and WMH were quantified using a novel in-house algorithm, and analyzed as percentages of total intracranial volume (**Figure 1**). Amyloid on PiB-PET and tau on AV1451-PET were measured. Regional and global cross-sectional associations were examined using canonical correlation analysis (**Figure 2**). Longitudinal associations with global measures were examined using age- and sex-adjusted linear mixed-effects models with natural splines and subject-wise 10-fold cross-validation (**Table 1**).

Results: PVS volume increased with age in both the basal ganglia (BG) and centrum semiovale (CSO), with distinct non-linear trajectories (**Figure 1**). Three distinct mechanistic associations were observed: (1) PVS-BG was associated with greater WMH volume both cross-sectionally and longitudinally (**Table 1, Figure 1, Figure 2**); (2) PVS-BG was also linked to PiB SUVR cross-sectionally but not longitudinally, and weakly related to off-target AV1451 BG binding (**Figure 2**); (3) PVS-CSO was not associated with amyloid or tau but related to occipital WMH.

Discussion: Findings lend support for PVS-BG as an early indicator of WMH progression, but less so for AD-specific biomarker progression. PVS-CSO's occipital-specific associations with WMH may position it as an early marker of CAA and predictor of amyloid-related imaging abnormalities (ARIA) associated with amyloid targeting therapies, although further investigations are needed and underway.

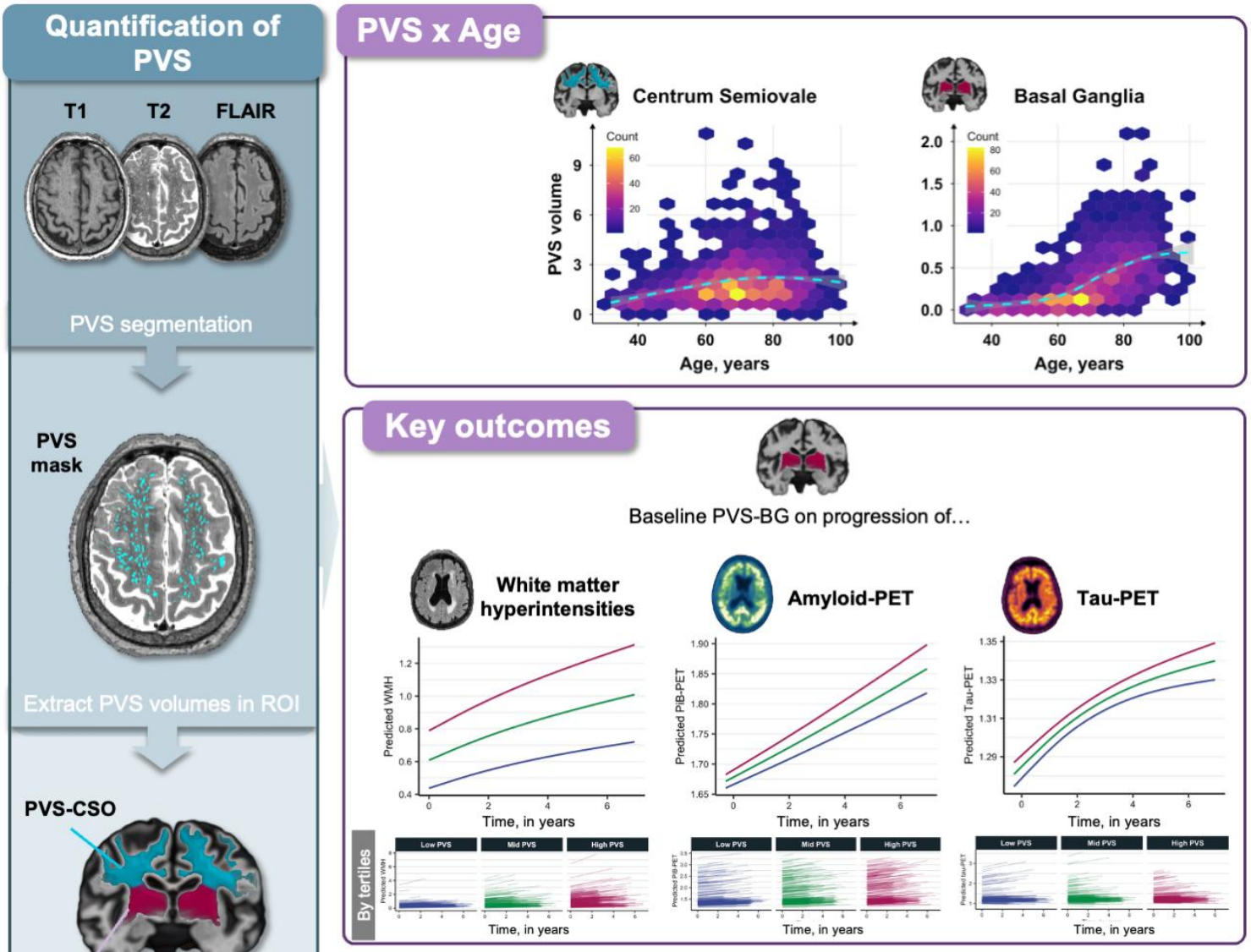


Fig 1. Study overview. Perivascular spaces (PVS) were quantified on structural imaging, and regional data PVS volume (% TIV) was extracted in the centrum semiovale (CSO) and basal ganglia (BG)

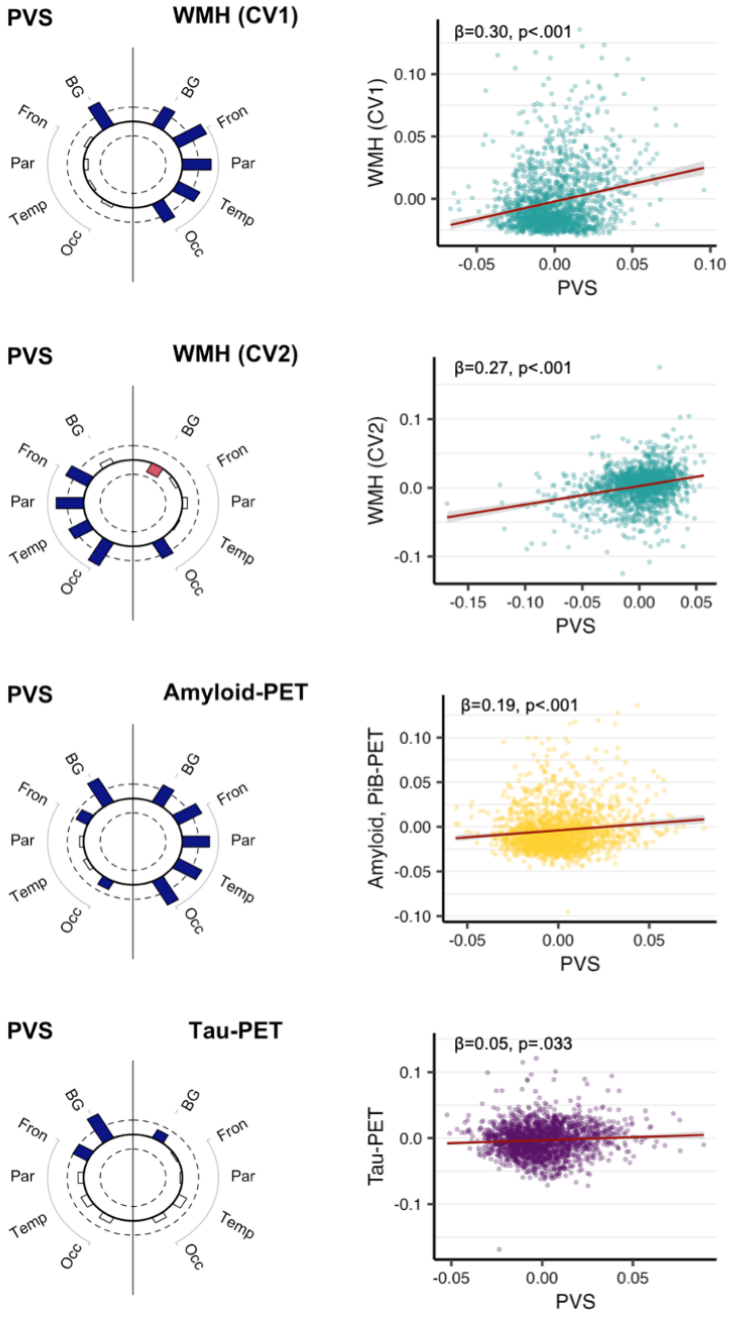


Fig 2. Canonical correlation analysis of cross-sectional PVS associations.

Each row represents a significant canonical variate; PVS-WMH analysis revealed two significant canonical variates, while PVS-amyloid and PVS-tau produced one significant canonical variate each.

Left: Heliographs of canonical variate loadings. Blue bars extending outwards represent positive weights (i.e., greater pathology); red bars extending inwards represent negative weights (i.e., lower pathology); uncolored bars indicate |r| < 0.3; length indicates strength of structural correlations (loadings). Half-maximum strength of correlation is indicated by the innermost (r = -0.5) and outermost (r = 0.5) circles.

Right: Bivariate correlation plots of canonical correlations (residuals adjusted for sex and age).

Abbreviations: CV = canonical variate, BG = basal ganglia, Fron = frontal lobe, Par = parietal lobe, Temp = temporal lobe, Occ = occipital lobe.

Table 1. Longitudinal analysis of PVS-BG on the progression of WMH, amyloid, and tau

	Full sample		10-fold cross-validation	
Outcome	**LRT $\chi^2(2)$**	**P**	**RMSE mean**	**RMSE SD**
WMH, Global	**43.04**	**<.001**	0.614	0.174
Amyloid PET	3.27	.195	0.383	0.061
Tau PET	0.53	.769	0.110	0.023

*Estimates represent the time*PVS-BG interaction effects, adjusted for the fixed effects of covariates sex and age, accounting for random intercepts and slopes. Abbreviations: WMH, white matter hyperintensities; PVS, perivascular spaces; LRT, likelihood ratio test.*

Keywords: cerebrovascular disease, perivascular spaces, amyloid, tau, longitudinal

108 Longitudinal evaluation of neuroinflammation using 11C-ER176 TSPO PET

Seokbeen Lim[1], Petrice Cogswell[1], Hoon-Ki Min[1], Jeyeon Lee[2], Jessica Brunn[1], Mahathi Kandimalla[3], David Jacobson[1], Marin Nycklemoe[1], Seung Baek Lee[1,4], Emily Lundt[5], Hugo Botha[6], Jonathan Graff-Radford[6], David Jones[6], Prashanthi Vemuri[1], Kejal Kantarci[1], Clifford Jack[1], Ronald Petersen[6], Val Lowe[1]

[1]*Department of Radiology, Mayo Clinic, Rochester, MN, US*
[2]*Department of Biomedical Engineering, Hanyang University, Seoul, South Korea*
[3]*Bloomberg School of Public Health, Johns Hopkins, Baltimore, MD, US*
[4]*Department of Pharmacology, Mayo Clinic, Rochester, MN, US*
[5]*Department of Quantitative Health Sciences, Mayo Clinic, Rochester, MN, US*
[6]*Department of Neurology, Mayo Clinic, Rochester, MN, US*

Background: Positron emission tomography (PET) of neuroinflammation provides important insights into the pathophysiological progression of Alzheimer's disease (AD) [1]. The translocator protein (TSPO), expressed on activated microglia, serves as a biomarker for neuroinflammation [2]. The third-generation TSPO radiotracer, ^{11}C-ER176, offers higher affinity than earlier tracers and enables sensitive detection of neuroinflammatory signals in AD [1]. This study aimed to characterize longitudinal changes in neuroinflammation across cognitive diagnostic groups, including cognitively unimpaired (CU), mild cognitive impairment (MCI), and AD dementia (ADD).

Methods: Twenty-nine participants from the Mayo Clinic Study of Aging and the Mayo Alzheimer's Disease Research Center underwent two serial ^{11}C-ER176 TSPO PET and 3T MRI scans, as well as serial ^{11}C-PiB and ^{18}F-AV1451 PET scans. PET SUVr images were normalized using the cerebellar crus, co-registered to individual mean MRIs, and analyzed with the MCALT-122 atlas [3]. Regional and meta-ROI SUVr values were visualized using boxplots to compare longitudinal changes across diagnostic groups and brain regions. Annualized SUVr changes, adjusted for baseline age, were calculated for all PET modalities and compared to assess associations among neuroinflammation, amyloid, and tau.

Results: Longitudinal ^{11}C-ER176 TSPO PET increased across frontal, temporal, parietal, occipital, and sensorimotor cortices in CU participants (n=20) as shown in Figure 1A. In MCI participants (n=6), the temporal cortex showed mainly longitudinal increases, while ADD participants demonstrated the largest overall increases, though interpretation was limited by small sample size (n=3). Annualized ^{11}C-ER176 SUVr changes were associated with corresponding alterations in both ^{11}C-PiB and ^{18}F-AV1451 PET measures (Figure 1B).

Conclusion: Progressive increases in neuroinflammation were observed even among CU individuals, with greater involvement of the temporal cortex in MCI and widespread increases in ADD. Correlation findings suggest that neuroinflammation progresses in parallel with amyloid and tau accumulation, reflecting close interactions between microglial density and protein aggregation during AD progression.

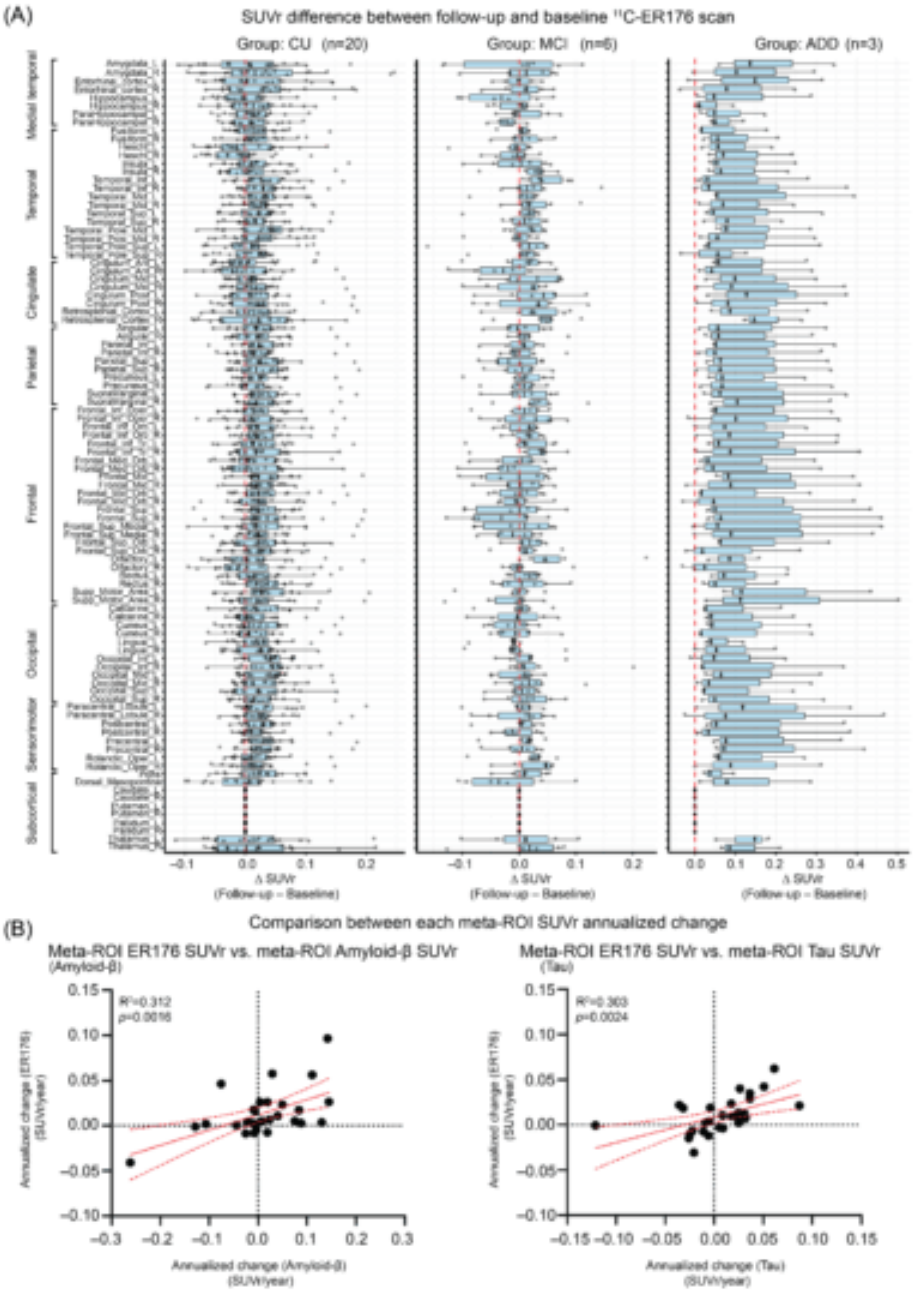


Figure 1. Analysis of longitudinal SUVr differences in 11C-ER176 TSPO PET. (A) Boxplot illustrating longitudinal SUVr differences in 11C-ER176 TSPO PET across cognitive diagnostic groups (CU, MCI, and ADD). The y-axis represents brain regions labeled according to the MCALT-122 atlas, with L and R denoting the left and right hemispheres, respectively. The x-axis represents SUVr differences calculated as follow-up minus baseline values, with the red dotted line indicating zero change. (B) Scatter plot showing annualized SUVr changes (SUVr/year) in 11C-ER176 TSPO PET within amyloid and tau META-ROIs, compared with 11C-PiB PET and 18F-AV1451 PET. The x-axis represents annualized amyloid (left) and tau (right) SUVr changes, and the y-axis represents annualized 11C-ER176 SUVr changes. Associations were evaluated after adjusting for baseline age. The amyloid-β meta-ROI included the prefrontal, orbitofrontal, parietal, temporal, anterior, and posterior cingulate, and precuneus regions, while the tau meta-ROI encompassed the amygdala, entorhinal cortex, fusiform gyrus, parahippocampal gyrus, inferior temporal gyrus, and middle temporal gyrus.

Reference
[1] J. Appleton et al., "Brain inflammation co-localizes highly with tau in mild cognitive impairment due to early-onset Alzheimer's disease," Brain, p. awae234, 2024, doi: 10.1093/brain/awae234.
[2] M. Cosenza-Nashat et al., "Expression of the translocator protein of 18kDa by microglia, macrophages and astrocytes based on immunohistochemical localization in abnormal human brain," Neuropathology and Applied Neurobiology, vol. 35, no. 3, pp. 306-328, 2009/06/01 2009, doi: https://doi.org/10.1111/j.1365-2990.2008.01006.x.
[3] C. G. Schwarz et al., "[P2–415]: THE MAYO CLINIC ADULT LIFESPAN TEMPLATE: BETTER QUANTIFICATION ACROSS THE LIFESPAN," Alzheimer's & Dementia, vol. 13, no. 7S_Part_16, pp. P792-P792, 2017/07/01 2017, doi: https://doi.org/10.1016/j.jalz.2017.06.1071.

Keywords: TSPO PET; 11C-ER176; Longitudinal study; Alzheimer's disease dementia

109 Comparison of meningeal signal between [^{18}F]AV-1451 and [^{18}F]MK-6240 tau PET using a distance-based meningeal mask

Seokbeen Lim[1], Jeffrey Gunter[1], Suzanne Baker[2], Cécile Tissot[2], Jessica Brunn[1], David Soleimani-Meigooni[3], Hwamee Oh[4], Juan Fortea[5], Belen Pascual[6], Brian Gordon[7], Pedro Rosa-Neto[8], Tharick Pascoal[9], Bill Klunk[9], William Jagust[10], Matthew Senjem[11], Hugo Botha[12], David Knopman[12], Stuart McCarter[12], Vijay Ramanan[12], Jonathan Graff-Radford[12], Christopher Schwarz[1], Kejal Kantarci[1], Bradley Boeve[12], Prashanthi Vemuri[1], David Jones[12], Clifford Jack[1], Ronald Petersen[12], Val Lowe[1]

[1]*Department of Radiology, Mayo Clinic, Rochester, MN, US*
[2]*Lawrence Berkeley National Laboratory, Berkeley, CA, US*
[3]*University of California San Francisco, Memory and Aging Center, San Francisco, CA, US*
[4]*Brown University, Department of Psychiatry and Human Behavior, Providence, RI, US*
[5]*Hospital de la Santa Creu i Sant Pau, Sant Pau Memory Unit, Department of Neurology, Barcelona, Spain*
[6]*Houston Methodist Research Institute, Department of Neurology, Houston, TX, US*
[7]*Washington University in St. Louis, Department of Radiology, St. Louis, MO, US*
[8]*Translational Neuroimaging Laboratory, McGill University Research Centre for Studies in Aging, Douglas Research Institute, Montréal, QC, Canada*
[9]*University of Pittsburgh, Department of Psychiatry, Pittsburgh, PA, US*
[10]*Department of Neuroscience, University of California, Berkeley, Berkeley, CA, US*
[11]*Information Technology, Mayo Clinic, Rochester, MN, US*
[12]*Department of Neurology, Mayo Clinic, Rochester, MN, US*

Background: Off-target signal characteristics in the meningeal region for the tau PET tracers [^{18}F]AV-1451 and [^{18}F]MK-6240 have been examined [1-2]. Quantitative segmentation of the meninges remains a significant challenge. Given a high-quality TIV mask, this study aimed to accurately segment the meningeal region and compare signal patterns between [^{18}F]AV-1451 and [^{18}F]MK-6240 PET images.

Methods: Thirty participants from the Mayo Clinic Study of Aging and the Mayo Alzheimer's Disease Research Center also participating in the HEAD study with available T1-weighted, FLAIR, and T2-weighted MR images, as well as [^{18}F]AV-1451 and [^{18}F]MK-6240 PET scans, were included. A voxel-wise distance map was generated from the TIV surface determined from multi-spectral segmentation. Voxels within –1 mm to 1 mm of the surface were defined as the meningeal mask (Figure 1A). Extra-cortical voxels were identified with the nearest brain region in the MCALT ADIR122 atlas (Figure 1B). 34 regions comprising a "skull cap" were chosen. PET images co-registered to each participant's MR image space. Mean SUVr values were extracted from the intersection of the meningeal atlas regions and the distance-based mask (Figure 1C and 1D). Linear mixed effects models were used to estimate the functional map between [^{18}F]AV-1451 and [^{18}F]MK-6240 meningeal signal.

Results: [^{18}F]MK-6240 showed greater meningeal signal than [^{18}F]AV-1451 across all regions (Figure 2A). Paired analyses revealed significantly higher [^{18}F]MK-6240 signal in the superior medial frontal regions (Figure 2B). Mixed-effects modeling demonstrated that [^{18}F]MK-6240 signal is proportional to [^{18}F]AV-1451, showing a strong positive association (Figure 2C). Lobe-wise region aggregation indicated tracer-specific differences (Figure 3).

Conclusion: These findings demonstrate that [^{18}F]MK-6240 exhibits consistently higher meningeal signal intensity than [^{18}F]AV-1451 across all examined regions. Off-target binding is subject specific (rank-order permutation test: mean rho = 0.8; n=29/30, $p_{FDR} < 0.01$). The lobe-wise ratios differed, suggesting spatial dependence of off-target binding properties between the two tracers.

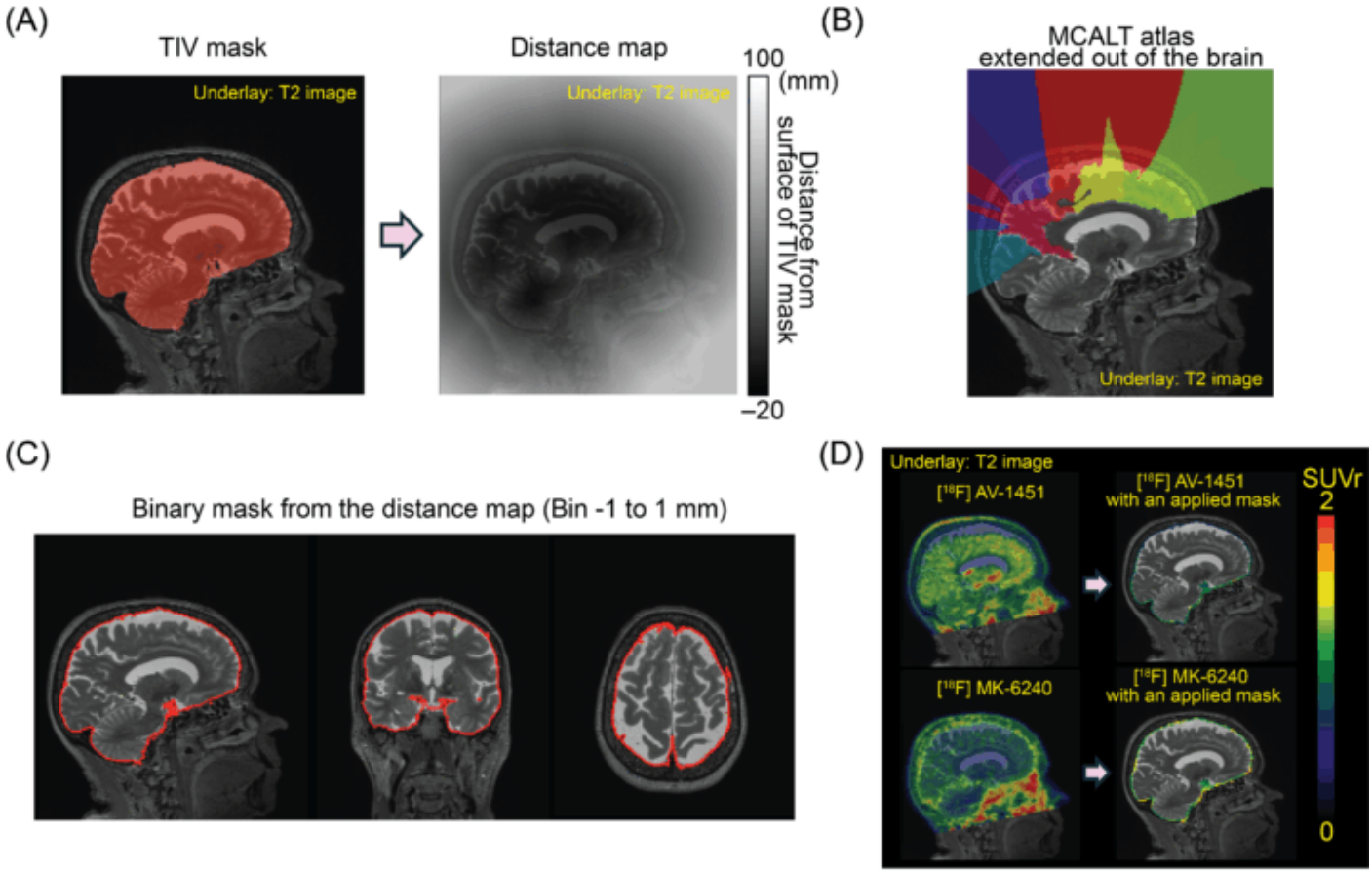


Figure 1. Construction of the meningeal mask and extraction of [^{18}F]AV-1451 and [^{18}F]MK-6240 PET signal within the corresponding mask area. (A) The total intracranial volume (TIV) mask was obtained from the T2-weighted image, and a distance map was computed based on the surface of this mask. (B) Using the distance-based map, the brain surface was extended beyond the brain boundary to include 34 regions (Precentral, Superior Frontal, Middle Frontal, Inferior Frontal Opercular, Inferior Frontal Triangular, Supplementary Motor Area, Superior Medial Frontal, Postcentral, Superior Parietal, Inferior Parietal, Supramarginal, Angular, Precuneus, Paracentral Lobule, Cuneus, Superior Occipital, and Middle Occipital; left and right hemispheres) defined by the MCALT ADIR122 atlas. (C) A binary meningeal mask was constructed to include voxels within the distance range of –1 mm to +1 mm. (D) PET signal intensity within the meningeal region was extracted by applying the binary mask to the co-registered [^{18}F]AV-1451 and [^{18}F]MK-6240 PET images.

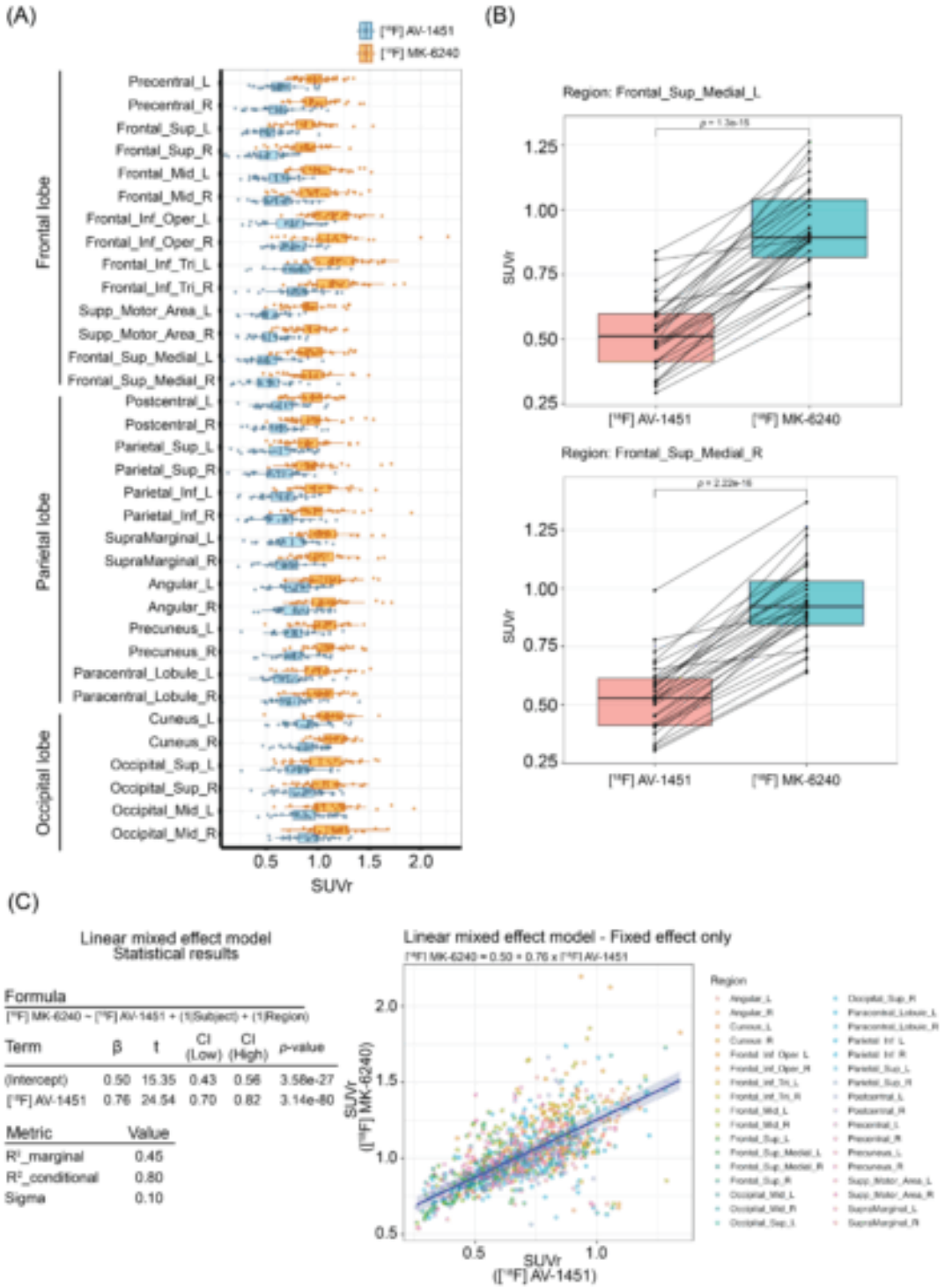


Figure 2. Comparison of regional mean SUVr patterns extracted from the MCALT ADIR122-based meningeal mask. The brain regions shown in the figures correspond to meningeal areas adjacent to the 34 cortical regions delineated in the MCALT ADIR122 atlas. (A) Boxplots showing the distributions of [^{18}F]AV-1451 and [^{18}F]MK-6240 SUVr values across 34 meningeal regions based on the MCALT ADIR122. Each PET SUVr was normalized to the cerebellar crus and co-registered to each participant's T1-weighted image. Blue boxes and data points represent [^{18}F]AV-1451, and orange boxes and data points represent [^{18}F]MK-6240. L and R indicate the left and right hemispheres, respectively. (B) Paired analysis results demonstrating significantly higher [^{18}F]MK-6240 signal compared with [^{18}F]AV-1451 in the superior medial frontal region and in both hemispheres ($p = 1.3 \times 10^{-15}$ and $p = 2.22 \times 10^{-16}$, respectively). L and R indicate the left and right hemispheres, respectively. (C) Results of the linear mixed-effects model examining the relationship between [^{18}F]AV-1451 (independent variable) and [^{18}F]MK-6240 (dependent variable), accounting for random effects of subjects and brain regions. Statistical results of the linear mixed-effect model are summarized on the left. Statistical parameters from the linear mixed-effects model were reported, including the β coefficient (representing the direction and magnitude of the predictor's effect), t value (test statistic for the fixed effect), 95% confidence interval (CI_low–CI_high, reflecting the uncertainty of the estimated effect), and p-value indicating statistical significance. Model performance metrics included R^2_marginal (variance explained by fixed effects), R^2_conditional (variance explained by both fixed and random effects), and σ (residual standard deviation reflecting unexplained variability). The right panel visualizes the model fit using a linear trend line representing the fixed effects. The blue line indicates the fitted linear trend from the mixed model, with the 95% confidence interval shown as a thin shaded blue area around the line. Dot colors correspond to individual brain regions as shown in the legend.

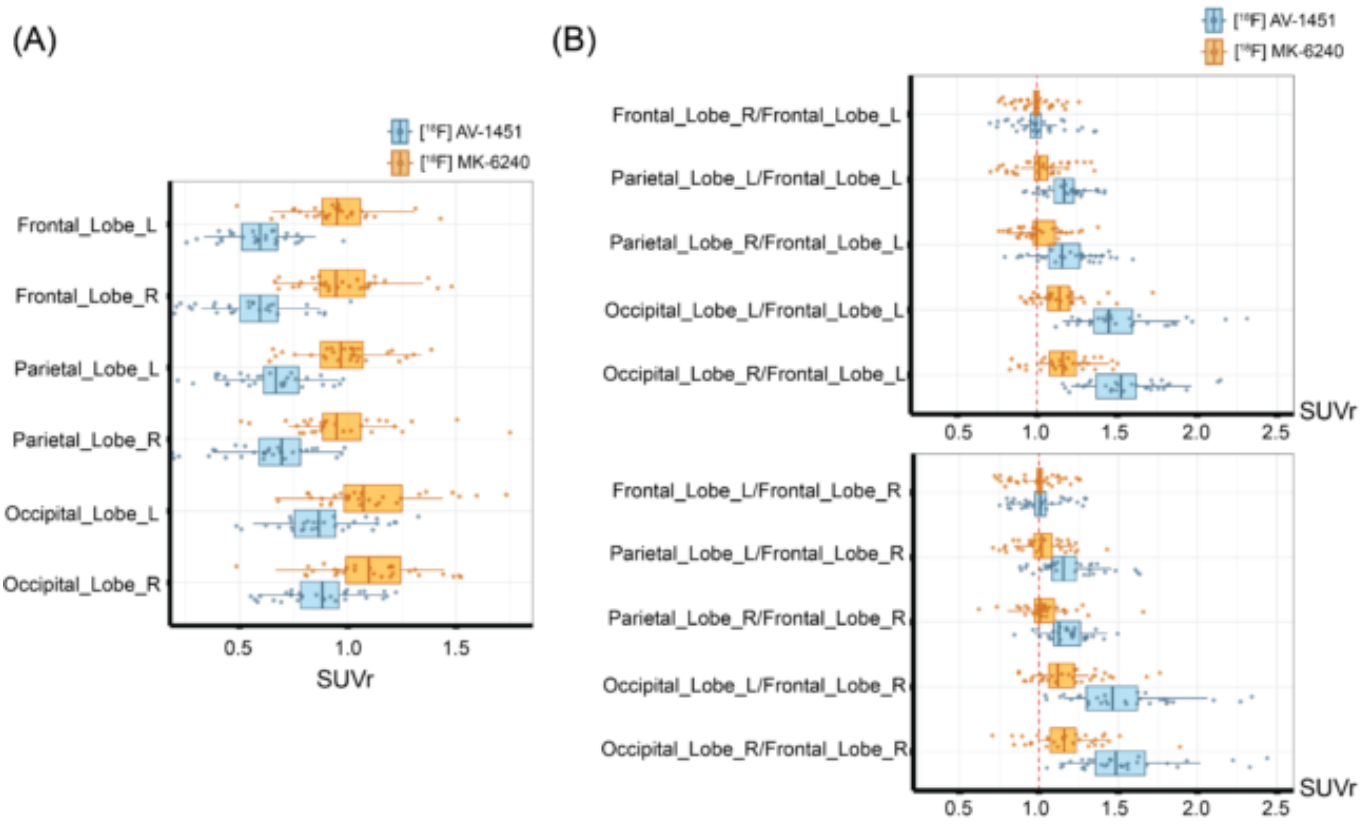


Figure 3. Comparison of weighted-average SUVr patterns by lobe and analysis of lobe-to-lobe ratio patterns extracted from the MCALT ADIR122-based meningeal mask. The brain regions shown in the figures correspond to meningeal areas adjacent to the 34 cortical regions delineated in the MCALT ADIR122 atlas. Each PET SUVr was normalized to the cerebellar crus and co-registered to each participant's T1-weighted image. (A) The distribution of weighted-average SUVr values for the frontal, parietal, and occipital lobes. Weighted averages were calculated using voxel size and SUVr values for each region. L and R indicate the left and right hemispheres, respectively. Blue boxes and data points represent [^{18}F]AV-1451, and orange boxes and data points represent [^{18}F]MK-6240. (B) Boxplots showing the distribution of lobe-to-lobe SUVr ratios based on the frontal lobe (L, R) as a reference. The red dotted line indicates a ratio of 1, representing equal SUVr between lobes. L and R denote the left and right hemispheres, respectively. Blue boxes and data points represent [^{18}F]AV-1451, and orange boxes and data points represent [^{18}F]MK-6240.

Reference

[1] A. Gogola et al., "Direct Comparison of the Tau PET Tracers 18F-Flortaucipir and 18F-MK-6240 in Human Subjects," J ournal of Nuclear Medicine, vol. 63, no. 1, p. 108, 2022, doi: 10.2967/jnumed.120.254961.
[2] C. Tissot et al., "The Association of Age-Related and Off-Target Retention with Longitudinal Quantification of [18F] MK6240 Tau PET in Target Regions," Journal of Nuclear Medicine, vol. 64, no. 3, p. 452, 2023, doi: 10.2967/jnumed.122. 264434.
[3] C. G. Schwarz et al., "[P2–415]: THE MAYO CLINIC ADULT LIFESPAN TEMPLATE: BETTER QUANTIFICATION ACROSS THE LIFESPAN," Alzheimer's & Dementia, vol. 13, no. 7S_Part_16, pp. P792-P792, 2017/07/01 2017, doi: https://doi.org/10.1016/j.jalz.2017.06.1071.

Keywords: Tau PET, Off-target binding, Meninges, Distance-based meninges mask

110 Effects of regional tau accumulation on visual discrimination of novel objects in clinically unimpaired older adults

Dhruv Kapadia[1], Lucah Medina Guerra[1], Isha Sai[1], Tyler Bonnen[2], Anthony Wagner[1], Elizabeth Mormino[1], Alexandra Trelle[1]

[1]*Stanford University, Stanford, CA, US*
[2]*University of California, Berkeley, Berkeley, CA, US*

Objective: Visual discrimination of complex objects with overlapping features relies on hierarchical neural representations supported by the ventral temporal cortex (VTC) that culminate in the medial temporal lobe. These regions are among the earliest neocortical sites to exhibit tau accumulation in aging. However, the impact of regional tau on visual discrimination behaviors in clinically unimpaired (CU) older adults remains unknown.

Methods: Sixty-one CU older adults (mean (SD) age=75.9 (6.13) years) enrolled in the Stanford Aging and Memory Study (SAMS) completed [^{18}F]PI2620 Tau PET imaging and a perceptual 'match-to-sample' task concurrent with eye-tracking. Participants were presented with a 'sample' image, followed by two images and asked to select the 'match' image (Figure 1). In this 2x2 design, stimuli were familiar objects or novel objects ('greebles') and shared either low or high feature overlap (i.e., 'ambiguity') with the match screen foil. Tau SUVRs were extracted from entorhinal cortex (ERC) and a portion of VTC, inferior temporal cortex (IT). Linear mixed-effect models estimated associations between regional tau, accuracy, and number of match screen fixations on correct trials, as a function of condition (novel-high, familiar-high, novel-low, familiar-low), controlling for age and sex.

Results: Discrimination accuracy was lower for high compared to low ambiguity discriminations and for discriminations involving novel compared to familiar objects (Figure 2A). Accurate high ambiguity discriminations garnered more fixations compared to low ambiguity discriminations, as did those for novel compared to familiar objects (Figure 2B). ERC tau was not significantly associated with accuracy or fixations (Figure 3AC), whereas IT tau was negatively associated with accuracy for high ambiguity discriminations of novel objects (Figure 3B) and linked to a greater number of fixations for accurate discriminations across conditions (Figure 3D).

Conclusions: Tau accumulation in VTC may impact visual discrimination behaviors in CU older adults, particularly when involving novel stimuli with overlapping features.

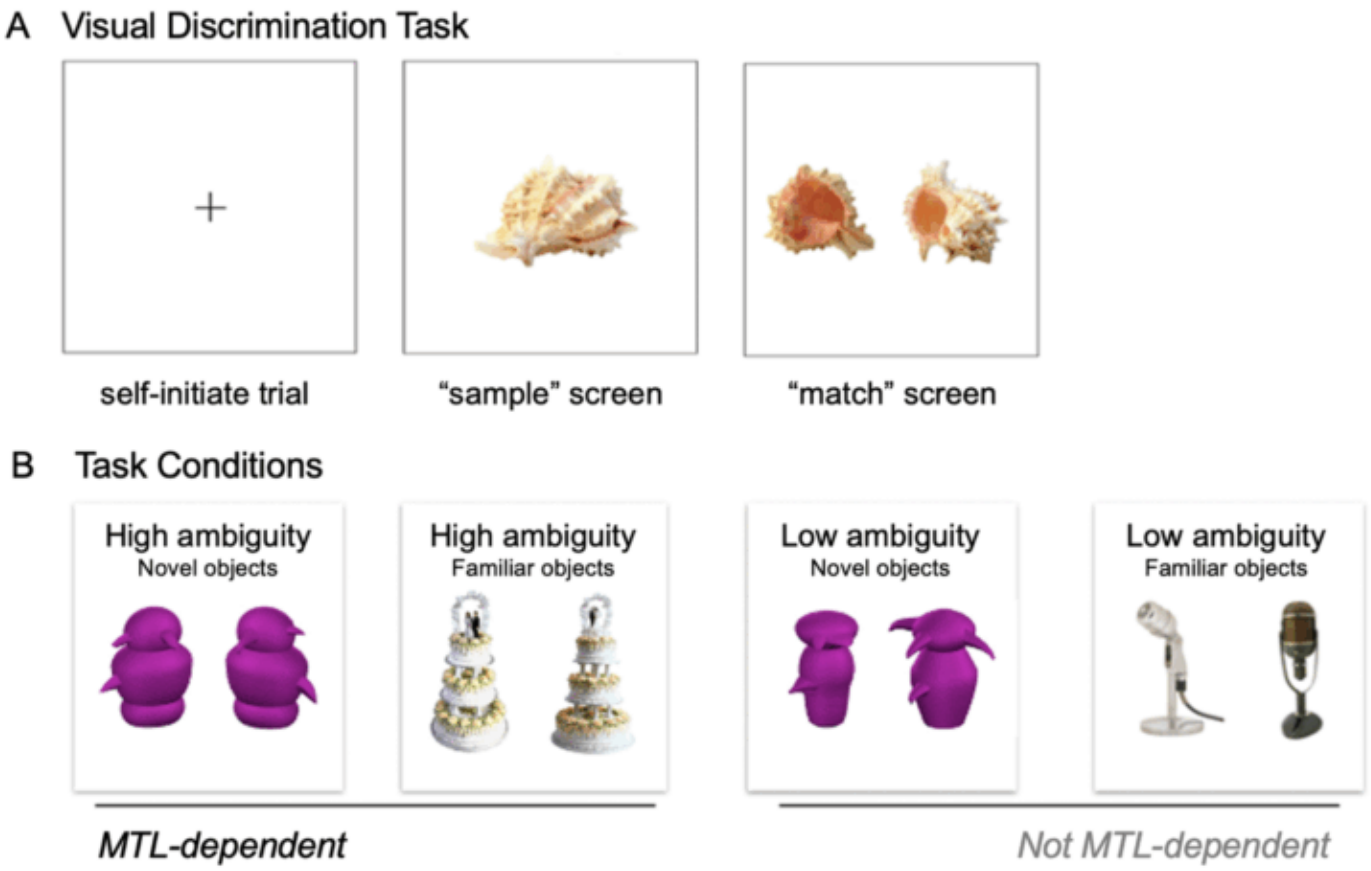


Figure 1. Experimental paradigm and task conditions. A. Match-to-sample task trial structure. Following initiation of the trial by participants, a single object was centrally presented. After studying the object, participants advanced to the match screen, where they were asked to select the 'match' image, and not the lure. Stimuli were always presented from a different viewpoint on the sample and match screens, and the task was self-paced. **B.** Example stimuli across the four task conditions. Stimuli were either familiar everyday objects or novel ("greeble") objects and shared either low or high feature overlap ("ambiguity") with the corresponding lure. Low ambiguity discriminations can be solved with single feature, whereas high ambiguity discriminations require representations of feature conjunctions to disambiguate the match from the lure. MTL, medial temporal lobe.

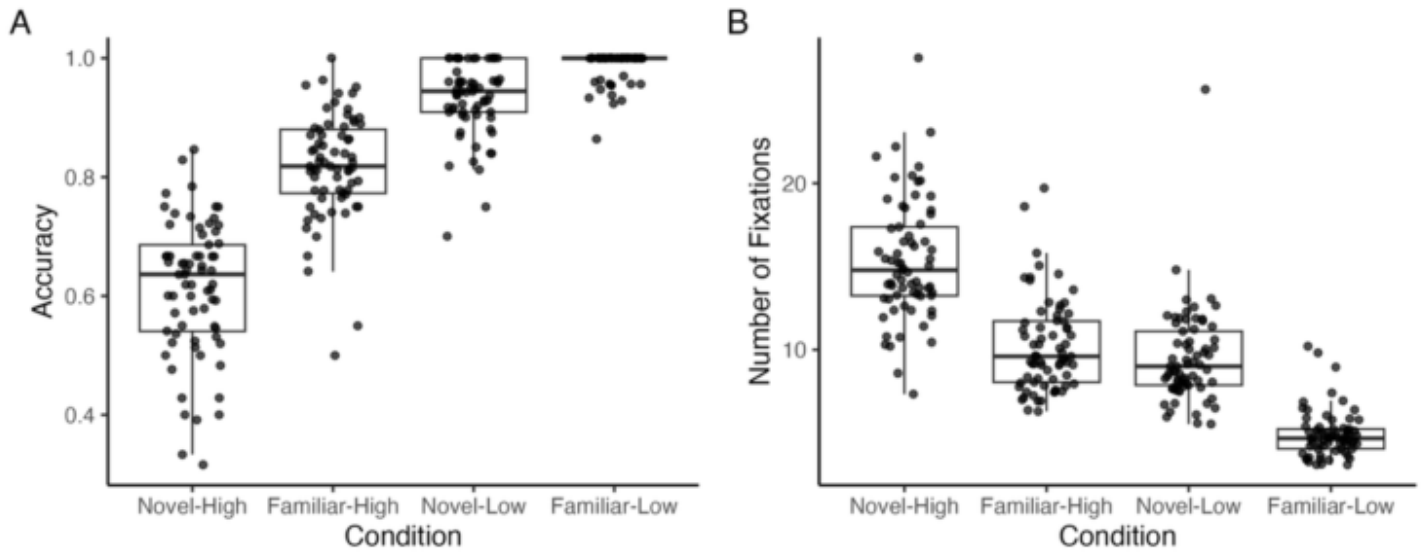


Figure 2. Accuracy and match screen fixations by condition. A. Discrimination accuracy was lower for high compared to low ambiguity trials ($F(1,268)=128.16$, $p<0.001$) and for novel objects compared to familiar objects ($F(1,268)=20.86$, $p<0.001$). The effect of novelty was greater for high ambiguity ($t(268)=4.856$, $p<0.001$) compared to low ambiguity ($t(268)=1.6$, $p=0.109$) discriminations. **B.** A greater number of match screen fixations were required for accurate high ambiguity compared to low ambiguity discriminations ($F(1,268)=52.59$, $p<0.001$) and for discriminations of novel compared to familiar objects ($F(1,268)=80.55$, $p<0.001$).

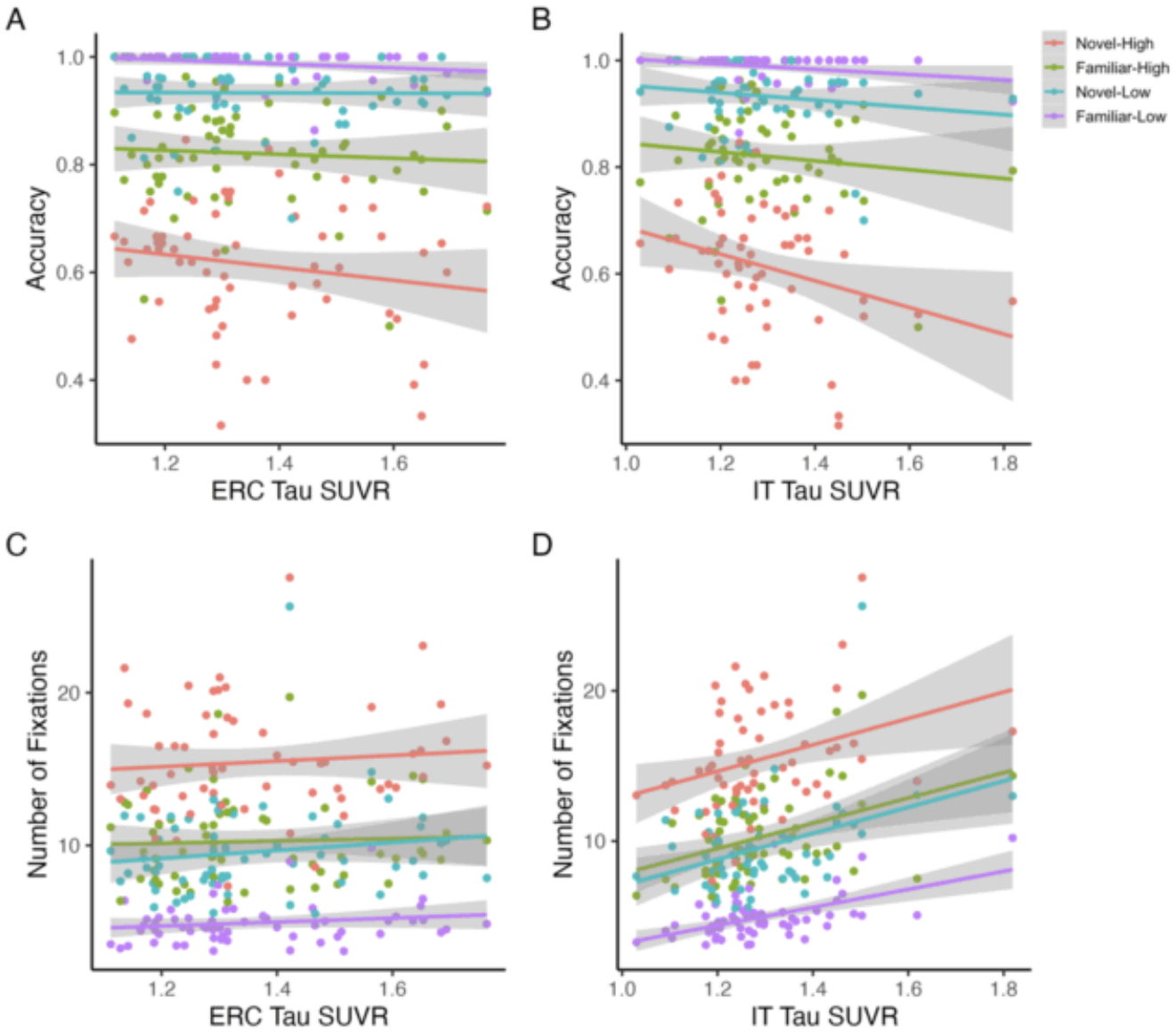


Figure 3. Associations of tau with discrimination accuracy and match screen fixations. **A.** ERC tau did not exhibit significant associations with accuracy across conditions (all $p >$ 0.145). **B.** IT tau was negatively associated with accuracy for high ambiguity discriminations of novel objects (β=-0.027, p=0.02), controlling for age and sex. **C.** ERC tau was not significantly associated with the number of match screen fixations made on correct trials (all $p > 0.479$). **D.** IT tau was associated with a greater number of match screen fixations during accurate discriminations, controlling for age, sex, and number of correct trials, and this relationship was observed across high ambiguity discriminations of novel (β=1.04, p=0.004) and familiar (β=0.994, p=0.006) objects and low ambiguity discriminations of novel (β=1.03, p=0.005) and familiar (β=0.678, p=0.06) objects.

Keywords: Tau PET, ventral temporal cortex, medial temporal lobe, visual discrimination, clinically unimpaired

111 Key quantitative benchmarks with CenTauR in cross-sectional and longitudinal large datasets

Vincent Dore[1,2], Pierrick Bourgeat[1], Tobey Betthauser[3,4], Azadeh Feizpour[2,6], Alexis Moscoso[7,8], Antoine Leuzy[7,9,10], Jurgen Fripp[1], Sterling Johnson[3,5], Christopher Rowe[2,6], Victor Villemagne[11]

[1]*CSIRO, Melbourne, Australia*
[2]*Austin Health, Melbourne, Australia*
[3]*Department of Medicine, University of Wisconsin-Madison School of Medicine and Public Health, Madison, WI, US*
[4]*Department of Medical Physics, University of Wisconsin-Madison School of Medicine and Public Health, Madison, WI, US*
[5]*School of Medicine and Public Health, Wisconsin Alzheimer's Institute, University of Wisconsin-Madison, Madison, WI, US*
[6]*The Florey Institute of Neuroscience and Mental Health, Melbourne, Australia*
[7]*Wallenberg Centre for Molecular and Translational Medicine, University of Gothenburg, Gothenburg, Sweden*
[8]*The Sahlgrenska Academy, Institute of Neuroscience and Physiology, Department of Psychiatry and Neurochemistry, University of Gothenburg, Gothenburg, Sweden*
[9]*Clinical Memory Research Unit, Department of Clinical Sciences, Lund University, Lund, Sweden*
[10]*Department of Neuropsychiatry, Sahlgrenska University Hospital, Gothenburg, Sweden*
[11]*University of Pittsburgh School of Medicine, Pittsburgh, PA, US*

Introduction: The new CenTauR equations have recently been released. Similar to Centiloid, we aimed to report key metrics for CenTauR across the Alzheimer's disease spectrum.

Methods: Participants (n=1112 with MK6240, n=1115 with FTP) from ADNI, AIBL, WRAP, and A4 placebo-arm were included. All PET scans were processed with CapAIBL, calibrated to SPM12 using the universal CTR equation, and tau was quantified in the five CTR-defined regions of interest. Aβ-PET scans were quantified with DeepSUVR, with A+ defined at 25CL.

Results – Cross-sectional:

- In A-CU, 2SD above the mean corresponded to **17 CTR** in the temporo-parietal (TP) ROI. Using this threshold: 10% of A+CU, 46% of A+MCI, and 75% of A+AD were deemed tau-positive (T+)
- Prevalence of individuals with cortical tau abnormality increased with increasing Ab burden: 25% at 75CL, 50% at 100CL, 75% at 110CL.
- Cognitive decline was associated with CTR_{TP}:
    - MMSE began declining around 15–30 CTR_{TP}; each 7.75CTR increase was associated with 1-point MMSE drop, 75% of the population had a MMSE below 28 at 56CTR_{TP}.
    - CDR-SB started rising around 25–49 CTR_{TP}; at 50CTR_{TP}, 75% had CDR>0, and then each 18CTR_{TP} increase corresponded to a 1-point CDR-SB increase.

Results – Longitudinal:

- A-CU and A-CI individuals showed no tau accumulation except a marginal increase over time in the MTL (0.7 CTR/year).
- A+CU and A+MCI subgroups accumulated fastest in the MTL (2.6–2.9 CTR/year).
- A+CU also accumulated tau in MTL and TP regions at a slower rate (1.3 CTR/year) but not in the frontal lobe, while A+MCI also accumulated in the frontal (1.5 CTR/year).
- A+AD showed rapid accumulation across MTL, TP, and frontal regions (6.0, 4.4, and 4.7 CTR/year, respectively).

Conclusion: CenTauR provides a robust framework for quantifying tau across the Alzheimer's spectrum. Key thresholds correlate with Aβ burden and cognitive decline, while longitudinal tracking highlights region-specific accumulation patterns across disease stages.

Keywords: CenTauR, Tau, CTR, longitudinal

112 Astrocytic reactivity is related to synchronization of regional amyloid-beta deposition

Jenna Adams[1,2], Dana Parker[1,2], Lisa Taylor[1,2], Whitney Tang[1,2], Novelle Meza[1,2], Nandita Tuteja[1,2], Brenda Avila[1,2], Evelyn Chang[1,2], Scotty Simmons[1,2], Rond Malhas[3], Soyun Kim[1,2], Liv McMillan[1,2], Mark Mapstone[1,2], Michael Yassa[1,2]

[1]*Department of Neurobiology and Behavior, University of California, Irvine, Irvine, CA, US*
[2]*Center for the Neurobiology of Learning and Memory, University of California, Irvine, Irvine, CA, US*
[3]*Department of Neurology, University of California, Irvine, Irvine, CA, US*

Background: Reactive astrocytes may promote synchronized Aβ accumulation by coupling neuronal activity and metabolic-vascular signaling across connected regions, such as the early-affected posteromedial cortical (PMC) and later-affected medial temporal lobe (MTL). We hypothesized that increased levels of plasma glial fibrillary acidic protein (GFAP), indexing astrocytic reactivity, would predict increased covariance of Aβ between PMC and MTL, reflecting astrocytic-mediated facilitation of network-level Aβ propagation.

Methods: Cognitively unimpaired older adults from the BEACoN study (N=59, 70.0±6.8 years, 54% female) received 18F-florbetapir-PET (FBP) to measure Aβ and plasma samples to quantify GFAP (Quanterix assay). FBP SUVRs were calculated for PMC (retrosplenial cortex, posterior cingulate cortex, precuneus) and MTL (entorhinal cortex, hippocampus, parahippocampal gyrus, fusiform gyrus) regions. Linear models tested whether plasma GFAP moderated the inter-regional covariance of FBP SUVRs between within-hemisphere PMC and MTL regions, controlling for age, sex, and education. Secondary models tested the moderation of GFAP on within-PMC and within-MTL covariance. Permutation testing was performed to assess significance.

Results: Higher plasma GFAP was associated with stronger covariance of FBP SUVRs between PMC and MTL regions (GFAP x FBP SUVR interactions ps<0.05; permutation p<0.05; Fig1A/C). Higher GFAP also moderated covariance within-PMC (interaction ps<0.01, permutation p<0.01; Fig1B/D), but not within-MTL (permutation p>0.05).

Conclusion: Elevated astrocytic reactivity was associated with a more tightly mirrored pattern of Aβ between PMC and MTL regions, suggesting an astrocyte-related enhancement of cortical-limbic Aβ synchronization. GFAP-related increases in Aβ covariance within PMC, but not MTL, suggests that astrocyte-mediated processes may first amplify local synchrony in high-vulnerability hubs before propagating toward connected MTL structures. Together, these findings support a model in which early astrocytic reactivity contributes not only to local PMC Aβ

deposition but also to the interregional synchronization of Aβ pathology along cortical pathways.

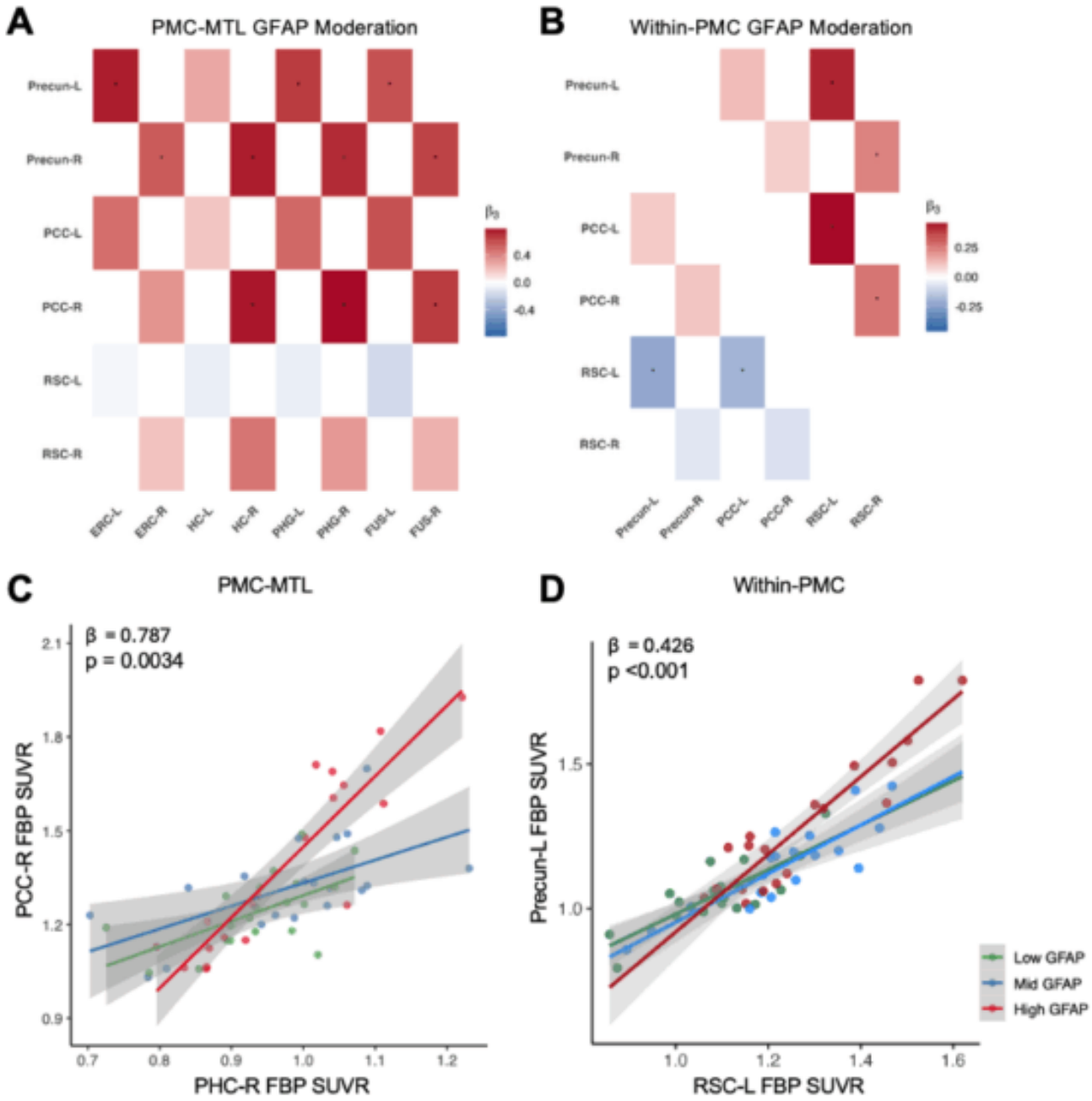


Figure 1. Moderation of Aβ covariance by GFAP. A-B, Posteromedial cortex (PMC)-medial temporal lobe (MTL) Aβ covariance (**A**) and within-PMC Aβ covariance (**B**) was significantly moderated by increased GFAP (* indicates region pairs in which GFAP x FBP SUVR interaction p<0.05). Hot colors (beta values) indicate that higher GFAP was associated with increased FBP SUVR covariance between region pairs. **C-D**, A representative example of PMC-MTL GFAP moderation (PHC-R and PCC-R FBP SUVR) and within-PMC GFAP moderation (RSC-L and Precun-L). GFAP tertiles indicate low (green), mid (blue), and high (red) GFAP levels on the covariance between regions. All models controlled for age, sex, and education, and were verified by network-level permutation analyses. MTL Regions: ERC, entorhinal cortex; HC, hippocampus; PHG, parahippocampal gyrus; FUS, fusiform gyrus. PMC Regions: RSC, retrosplenial cortex; PCC, posterior cingulate cortex; Precun, precuneus.

Keywords: amyloid-beta; astrocytes; GFAP; medial temporal lobe; cognitively unimpaired older adults

113 Synergistic effects of amyloid-beta and hyperexcitability on tau pathology and cognitive decline

Casey Vanderlip[1], Jenna Adams[1,2]

[1]*Department of Neurobiology and Behavior, University of California, Irvine, Irvine, CA, US*
[2]*Center for the Neurobiology of Learning and Memory, University of California, Irvine, Irvine, CA, US*

Background: Neurophysiological factors that interact with Aβ to facilitate tau progression and cognitive decline are not well understood. Hippocampal hyperexcitability, a key pathophysiological feature of the prodromal stages of Alzheimer's disease (AD), may potentiate these processes. We tested whether Aβ and hippocampal hyperexcitability have synergistic effects on tau and cognitive decline.

Methods: Data from ADNI (n=186 cognitively unimpaired [CU], n=83 mild cognitive impairment [MCI], n=22 dementia) and the Harvard Aging Brain Study (n=224 CU) were analyzed. Hippocampal hyperexcitability was indexed by resting-state fMRI amplitude of low-frequency fluctuations (ALFF; H-/H+, median split). Aβ-PET (Centiloids) and 18F-flortaucipir-PET quantified AD pathology. Cognition was assessed with the PACC and MMSE. Models tested main and interactive effects of Aβ and ALFF on tau and longitudinal cognition, adjusting for age, sex, and education.

Results: Participants with MCI showed elevated hippocampal ALFF relative to CU and dementia groups (ps<0.05), consistent with transient hyperexcitability early in AD. Hippocampal ALFF was not correlated with Aβ or hippocampal volume (Fig1A-B), indicating independence from these biomarkers. Within A+ individuals, higher hippocampal ALFF correlated with greater entorhinal tau (Fig 1C), and A+H+ participants showed higher entorhinal tau than those classified as A+H- (Fig 1D), supporting an additive effect of hyperexcitability on tau beyond Aβ. Further, CU individuals classified as A+H+ at baseline had steeper cognitive decline than the A+H- group (Fig2A). This effect was amplified in those positive for all three biomarkers (A+T+H+) compared to those positive for Aβ and tau alone (A+T+H-; Fig2B).

Conclusions: Aβ and hippocampal hyperexcitability demonstrate a synergistic effect on tau pathology and cognitive decline. Incorporating hyperexcitability as a biomarker identified CU individuals at risk for rapid cognitive decline, underscoring its potential value for early detection and therapeutic monitoring within the ATN framework.

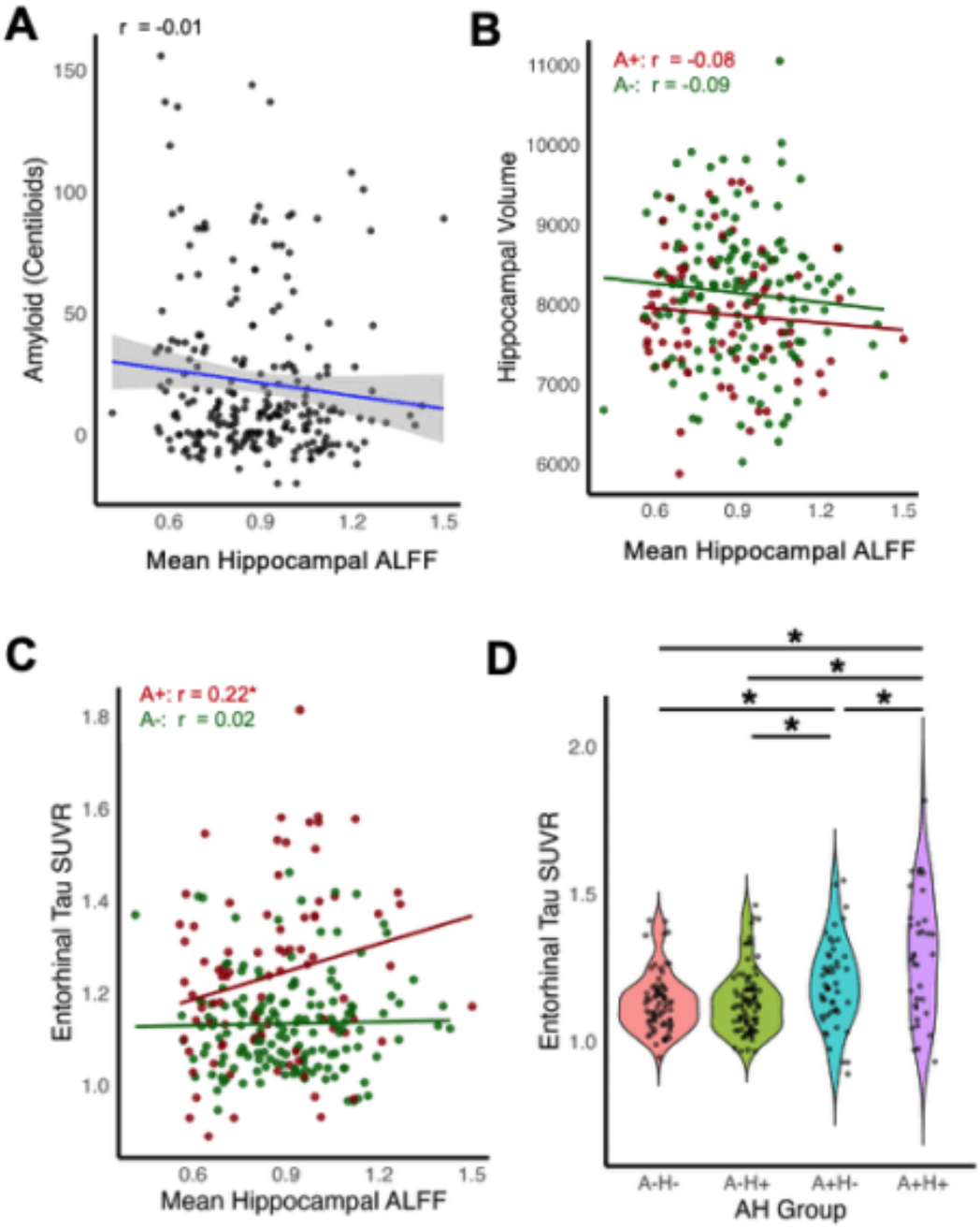


Figure 1. Relationships between hippocampal hyperexcitability and ATN biomarkers. Hippocampal hyperexcitability (mean amplitude of low frequency fluctuations, ALFF) was associated with standard A (Centiloids)/T (entorhinal FTP SUVR)/N (hippocampal volume) biomarkers. **A**, Hippocampal ALFF was not correlated with Centiloids. **B**, Hippocampal ALFF was not correlated with hippocampal volume in either A+ or A- groups, suggesting it is distinct from structural markers. **C**, Hippocampal ALFF was significantly associated with increased entorhinal tau (FTP SUVR) in A+, but not A-, individuals. **D**, Participants classified as A+H+ had significantly more entorhinal tau than all other groups, including compared to A+H- participants.

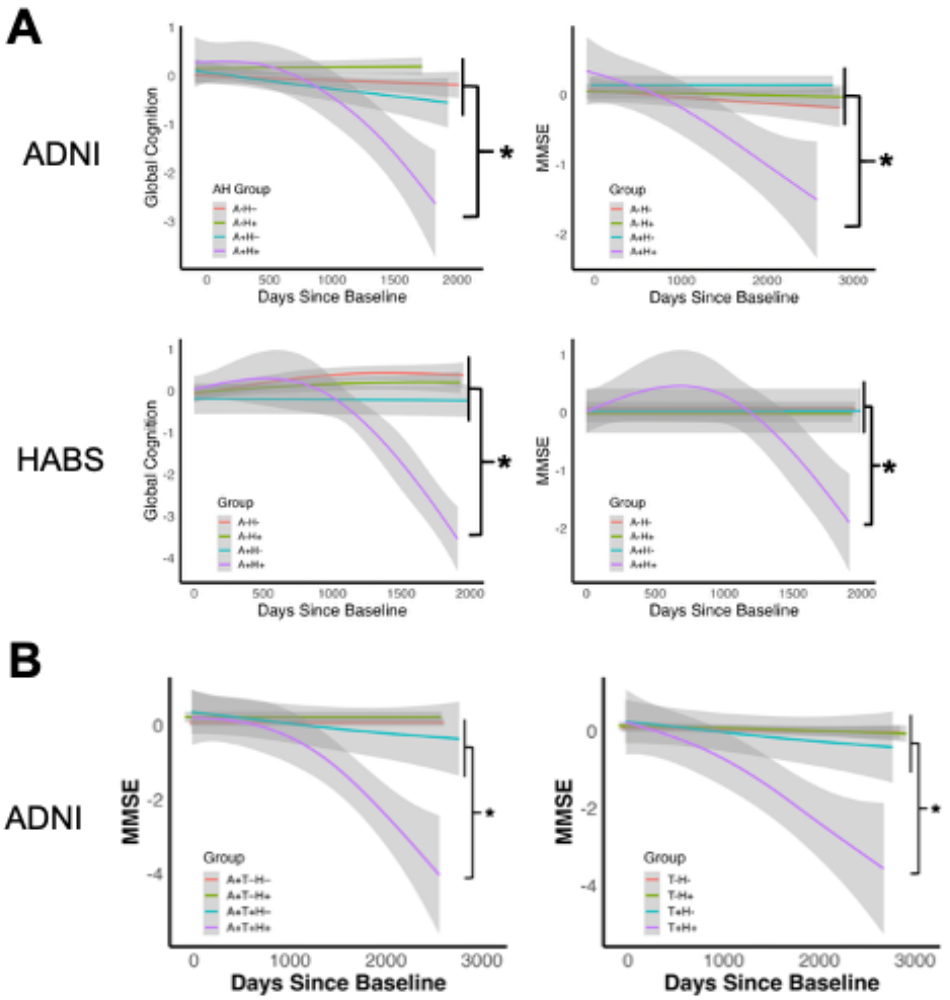


Figure 2. Associations between hyperexcitability ("H") biomarker status and longitudinal cognitive decline. Analyses were performed on older adults who were cognitively unimpaired at baseline in both the ADNI and Harvard Aging Brain Study (HABS) samples in **A**, and in ADNI in **B.** All models controlled for age, sex, education, and hippocampal volume. **A**, Participants classified as A+H+ at baseline had steeper cognitive decline on both PACC and MMSE across both samples compared to all other biomarker groups, including the A+H- group. **B,** Participants classified as A+H+T+ (left) or T+H+ (right) had steeper cognitive decline compared to all other biomarker groups.

Keywords: hyperexcitability, hippocampus, tau, amyloid-beta, cognition

114 Amyloid does not discriminate: a meta-analysis of sex differences in Centiloids from 35,468 participants across 33 cohorts

Ganna Blazhenets[1], Stefania Pezzoli[1], Kaitlin Casaletto[1], David N. Soleimani-Meigooni[1,2], Konstantinos Chiotis[1,3], Isabel E. Allen[4], Gil D. Rabinovici[1,5], Renaud La Joie[1], The Meta-Centiloid Study Group[1]

[1]*Edward and Pearl Fein Memory & Aging Center, Department of Neurology, University of California, San Francisco, San Francisco, CA, US*
[2]*Molecular Biophysics and Integrated Bioimaging, Lawrence Berkeley National Laboratory, Berkeley, CA, US*
[3]*Center of Alzheimer Research, Division of Clinical Geriatrics, Department of Neurobiology, Karolinska Institutet, Care Sciences and Society, Stockholm, Sweden*
[4]*Department of Epidemiology and Biostatistics, University of California, San Francisco, San Francisco, CA, US*
[5]*Department of Radiology and Biomedical Imaging, University of California, San Francisco, San Francisco, CA, US*

Background: Sex-associated differences in amyloid burden remain a matter of controversy in AD research. Leveraging the data from 33 independent studies, we examined the effect of sex on Centiloids (CL) in a large individual participant data meta-analysis.

Method: We gathered data from publicly available cohorts and reached out to investigators across the world to collect cross-sectional Centiloids, demographic, clinical, and genetic data. For each study, the mean Centiloids difference between sexes was calculated in the full cohort and split by clinical status (based on clinical diagnosis or CDR>0.5). In the cognitively impaired group, the moderating effect of age, the level of impairment (MCI/dementia), and *APOE* E4 status (carrier/non-carrier) was examined through sex-by-predictor interactions. Study-level estimates were combined using random-effects meta-analyses to estimate the pooled effects; between-study heterogeneity was assessed using the I^2 statistic (I^2>75% suggests non-random differences across studies).

Result: Meta-analysis included 35,468 participants (Table-1; 56% Females overall, with rates varying from 33 to 88% across studies). No sex difference was observed in the whole sample (Mean Difference [MD, Females>Males]=1.57 CL, 95%CI=[-0.64; 3.78]; I^2=72%), nor in the cognitively unimpaired subgroup (MD=1.24 CL [-0.13; 2.62]; I^2=33%). However, cognitively impaired females had slightly but statistically significantly higher Centiloids than males (MD=5.02 CL [1.42; 8.62]; I^2=60%; Figure-1). In the impaired group, sex differences were not modulated by age nor *APOE* E4 status, but a significant sex*level of impairment (MCI/dementia) interaction was observed, with greater sex differences in the dementia subgroup (p=0.004; I^2=29%, Figure-2A). This sex difference in Centiloids correlated with a sex difference in clinical impairment level: studies with greater Centiloids in females than males also showed lower MMSE in females (Figure-2B/C).

Conclusion: This meta-analysis suggests minimal sex differences in amyloid burden, particularly in early disease stages, though females show mild amyloid increases compared to males at later disease stages.

Table-1. Demographic and clinical characteristics of the included cohort.

	Full cohort		Cognitively Unimpaired		Cognitively Impaired	
Sex	Male	Female	Male	Female	Male	Female
N	16,255	19,213	6,732	9,698	8,844	9,169
Age (y, SD)	70.1 (4.9)	69.2 (5.0)	68.9 (6.2)	68.3 (5.9)	71.6 (4.8)	70.3 (5.2)
MMSE (mean, SD)	27.1 (1.8)	27.1 (2.2)	28.8 (0.4)	28.9 (0.5)	25.2 (1.8)	24.8 (2.4)
***APOE* E4 carrier (N, %)**	2,363 (40%)	2,917 (38%)	1,138 (34%)	1,683 (33%)	1,193 (47%)	1,183 (49%)

Reported mean values are a straight average of the mean values extracted from individual cohorts. MMSE and *APOE* E4 results are only available in a subsample of participants (MMSE: n = 32,126 [91% of full cohort]; *APOE* E4: n = 13,623 [39% of full cohort]).

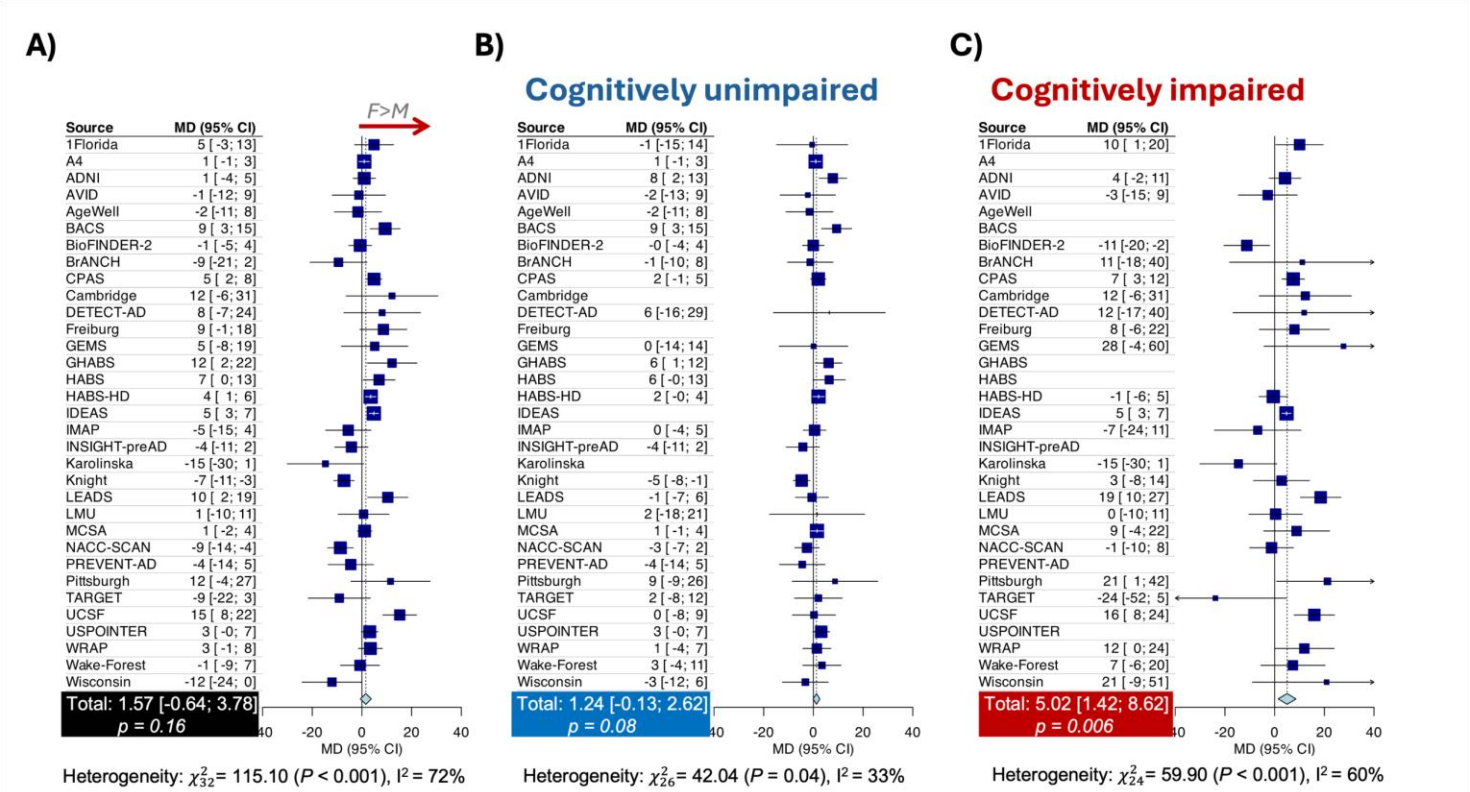
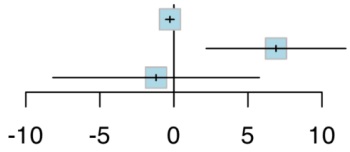


Figure-1. Results of the random-effects meta-analyses comparing mean difference (MD) in centiloids between males and females (reference group: male sex) in (A) full cohort and (B,C) by splitting by cognitive status. For meta-analyses, squares reflect study weights and whiskers are 95% confidence intervals for the estimates.

Cognitively impaired

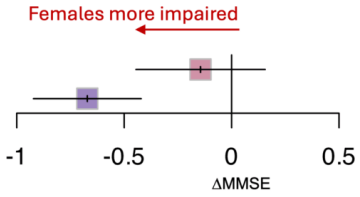
A)

Interaction	N Study	N	Pooled estimate	95% CI	P-value
Sex-by-Age	26	18013	-0.27	[-0.55; 0.01]	0.06
Sex-by-Diagnosis	19	16446	6.89	[2.18; 11.61]	< 0.01
Sex-by-APOE	19	4967	-1.20	[-8.17; 5.77]	0.74

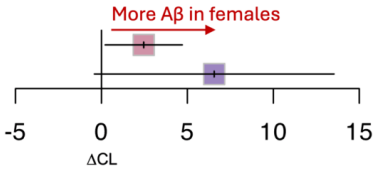


B)

Measure	N Study	N	ΔMMSE	95% CI	P-value
MCI	18	9468	-0.14	[-0.45; 0.16]	0.35
Dementia	16	6092	-0.67	[-0.92; -0.42]	< 0.01



Measure	N Study	N	ΔCL	95% CI	P-value
MCI	18	9965	2.46	[0.22; 4.70]	0.03
Dementia	16	6481	6.56	[-0.41; 13.53]	0.07



C)

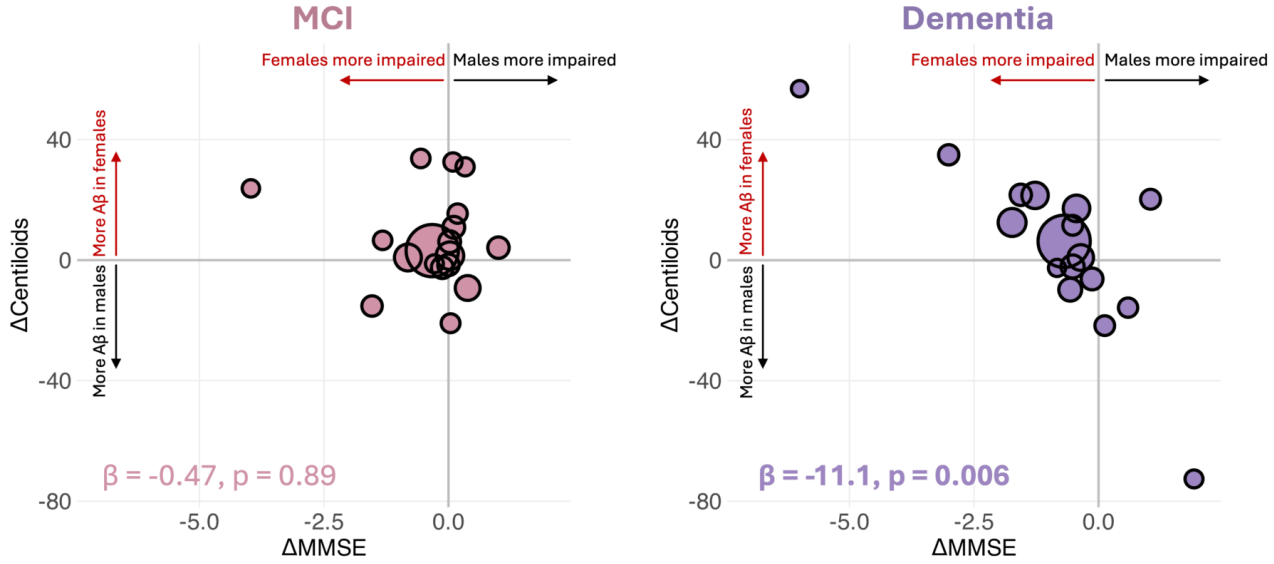


Figure-2. Results of the meta-analyses in the cognitively impaired subgroup. (A) Combined results of the individual meta-analysis on the estimates of the linear regression models assessing the interaction of sex-by-predictor (age, diagnosis, or *APOE* E4 carriership) on Centiloids. (B) A meta-analysis of sex differences in subgroups reveals that higher differences in Centiloids are accompanied by greater differences in cognitive impairment, suggesting that females show higher amyloid levels when they also show greater cognitive impairment. (C) Associations between MMSE and Centiloids differences are more pronounced in the dementia group, suggesting the level of cognitive impairment may relate to the differences in Centiloids between sexes across studies. Each point represents an individual study, with the circle size proportional to the number of participants.

Keywords: centiloids, sex, meta-analysis, PET, amyloid

115 Preliminary associations of plasma phosphorylated tau217 with regional tau deposition and accumulation in medial temporal and neocortical regions

Eva Pintucci[1], Emma Thibault[1], Michelle Farrell[1], Hyun-Sik Yang[1,2], Jasmeer Chhatwal[1,2], Michael Properzi[1,3], J. Alex Becker[1], Julie Price[1,3], Reisa Sperling[1,2], Keith Johnson[1,2]

[1]*Massachusetts General Hospital, Department of Neurology, Harvard Medical School, Boston, MA, US*
[2]*Brigham & Women's Hospital, Neurology Department, Boston, MA, US*
[3]*Athinoula A. Martinos Center for Biomedical Imaging, Charlestown, MA, US*

Introduction: Traditional methods for detecting Alzheimer's disease (AD) pathology *in vivo* are costly and burdensome. Plasma pTau217 is a leading blood-based biomarker candidate, showing predictive associations with fibrillar amyloid (Aß) burden. However, the Aß-independent associations of pTau217 with regional tau pathology are less certain. We therefore tested whether baseline pTau217 associates with regional tau deposition and accumulation, and assessed the impact of Aß in these relationships.

Methods: 108 individuals from the Harvard Aging Brain Study 2 (HABS-2) (CN=92,MCI/AD=16) underwent baseline pTau217 quantification by Mesoscale Discovery (MSD) assay, [^{11}C]-Pittsburgh Compound-B(PiB)-PET, and up to four [^{18}F]-MK-6240 PET scans over 1.44±1.1 years (**Tab.1**). We used linear regression to test whether pTau217 related to tau burden in medial temporal (entorhinal,EC; amygdala,AM; parahippocampal,PH) and neocortical (inferior temporal,IT; fusiform,FF; middle temporal,MT) regions of interest (ROIs). Linear mixed-effects models were used to evaluate tau change in the same ROIs. The contribution of Aß (pTau217* PiB-PET interaction term) was evaluated in all linear models, and the unique contribution of each model term was assessed using variance decomposition.

Results: Elevated pTau217 predicted greater tau deposition at baseline and longitudinal accumulation across all ROIs ($p<0.001$). Associations were strongest in neocortical ROIs, both cross-sectionally ($ß_{IT} = 0.621$, $ß_{FF} = 0.496$, $ß_{MT} = 0.566$) and longitudinally ($ß_{IT} = 0.132$, $ß_{FF} = 0.119$, $ß_{MT} = 0.121$; **Fig.1A,B)**. Cross-sectionally, the pTau217* PiB-PET interaction was universally significant ($p<0.001$). Longitudinally, only the neocortical ROIs showed significance **(Fig.1D,E).** Independently, pTau217 explained the most unique variance, compared to age and sex. However, when accounting for PiB-PET, the pTau217*PiB-PET interaction contributed most to variance in ROI outcomes, with additional unique variance explained by both pTau217 and PiB-PET **(Fig.1C)**.

Conclusion: Our preliminary results suggest that pTau217 may serve as an effective clinical trial screening tool for both Aß and tau deposition, particularly when targeting later-stage neocortical tauopathy.

Figures:

Characteristic	N = 108[1]
Age	67.98 (9.88), [36.75-86.75]
Sex	
F	60 (56%)
M	48 (44%)
Years of Ed.	16.83 (2.56), [11.00-20.00]
e4 Status	
e4-	51 (47%)
e4+	28 (26%)
Pending	29 (27%)
MK PET Time Points	2.67 (0.92), [1.00-4.00]
Total MK Scanning Window (yrs)	1.44 (1.07), [0.00-4.29]
pTau217 (pg/ml)	7.89 (7.20), [1.04-37.41]
PiB FLR DVR	1.23 (0.32), [0.96-2.12]
Diagnosis	
CN	92 (85%)
MCI/AD	16 (15%)

[1] Mean (SD), [Min-Max]; n (%)

Table 1. HABS-2 sample demographics. Participant characteristics at study baseline are summarized. PiB-PET is quantified as the distribution volume ratio (DVR) in the frontal–lateral–retrosplenial (FLR) composite region.

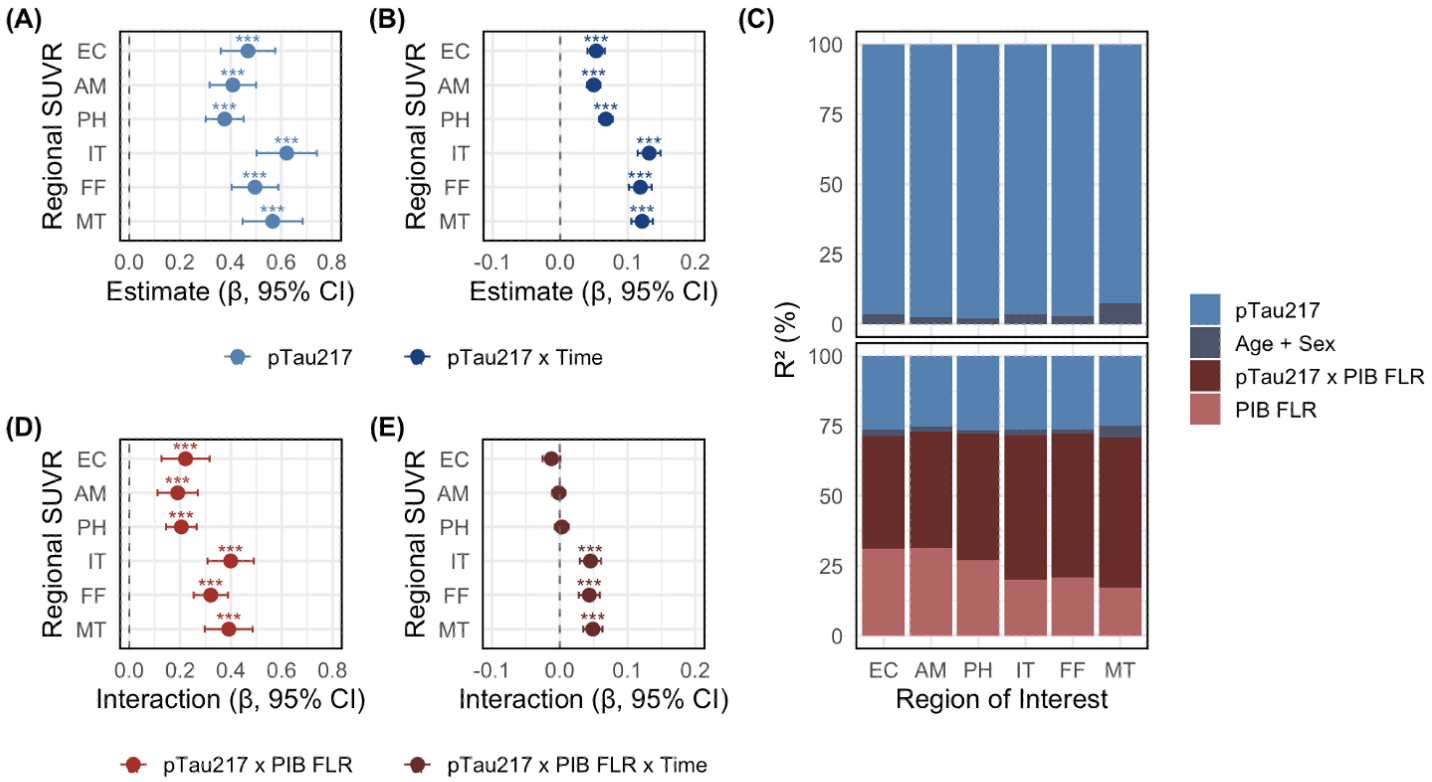


Figure 1. Increased tau deposition and accumulation in medial temporal lobe and neocortical ROIs are associated with elevated plasma pTau217 and moderated by PiB-PET. A,B) Across all ROIs, higher baseline pTau217 is associated to greater tau deposition and accumulation over time (*p < 0.05,**p < 0.01,***p < 0.001). C) pTau217 accounts for the largest unique variance ($R^2 > 0.4$) compared to age and sex. pTau217*PiB-PET explains the most regional tau SUVR variance ($R^2 > 0.246$), though pTau217 and PiB- PET alone still contribute substantially ($R^2 > 0.122$). D,E) pTau217 shows stronger cross-sectional associations with tau SUVRs at higher amyloid levels across all ROI. Longitudinally, these effects are seen in the neocortex, but not present in MTL ROIs.

Keywords: Plasma pTau217, [18F]-MK-6240 PET, Amyloid-ß, Clinical trial screening

116 Contrasting neuropathology- and tau PET-based Braak stage associations with dementia severity to clarify differences between radiologic and pathologic findings

Jeffrey Evelhoch[1], Hailey Bruzzone[2], Andréia Rocha[3], Sanjay Asthana[2], Jeffrey Nirschl[2], Sterling Johnson[2], Julie Schneider[4], Bradley Hyman[5], Tharick Pascoal[3], Tobey Betthauser[2]

[1]*JLEvelhoch Consulting, Wayne, PA, US*
[2]*University of Wisconsin-Madison, Madison, WI, US*
[3]*University of Pittsburgh, Pittsburgh, PA, US*
[4]*Rush University Medical Center, Chicago, IL, US*
[5]*Massachusetts General Hospital, Boston, MA, US*

Background: Braak NFT staging uses ROIs corresponding to the neuropathology-defined areas associated with the hierarchical spread of neurofibrillary tangles (NFT) recognized by Braak and Braak (1991). Neuropathology and PET likely provide different information since they measure NFTs differently in dissimilar contexts. Introduction of revised criteria for neuropathology of AD (Hyman et al. 2012) used Clinical Dementia Rating Sum-of-Boxes (CDR-SB) scores to provide a guide to clinical correlations with various levels of AD neuropathologic change. This study uses that CDR-SB approach to compare PET-based tau staging data from the Wisconsin Registry for Alzheimer's Prevention and Wisconsin ADRC (WISC collectively) with those 2012 results.

Methods: Data from 562 subjects (Table 1 in Hyman et al. 2012) were used to represent neuropathology. CERAD scores of moderate or frequent were considered amyloid positive (A+). WISC participants with CDR-SB, amyloid and tau PET data available (N=741, excluding 13 tau discordant subjects) represent PET. A+ was established as >24 Centiloids. Differences between the proportion of tau positive (T+) subjects assessed by neuropathology and PET in each amyloid/NFT stage/CDR-SB group were tested using the appropriate test of proportionality.

Results: Both measures show increasing %T+ for B2 and B3 with CDR-SB, but only 2% of subjects are negative for B1 by neuropathology whereas B1 %T+ generally increases with CDR-SB for PET in A+ individuals (Figures 1 and 2). B1 and B2 %T+ was significantly higher for neuropathology than PET in groups with enough subjects and/or large differences. Percent T+ for B3 did not differ in any group (Table 1).

Discussion: High neuropathology B1 %T+ in all subjects is consistent with the 2012 guidelines using B2 or B3 to determine if AD was a sufficient explanation for dementia. Higher proportion of neuropathologic B1 and B2 T+ in early AD are consistent with the greater sensitivity of neuropathology.

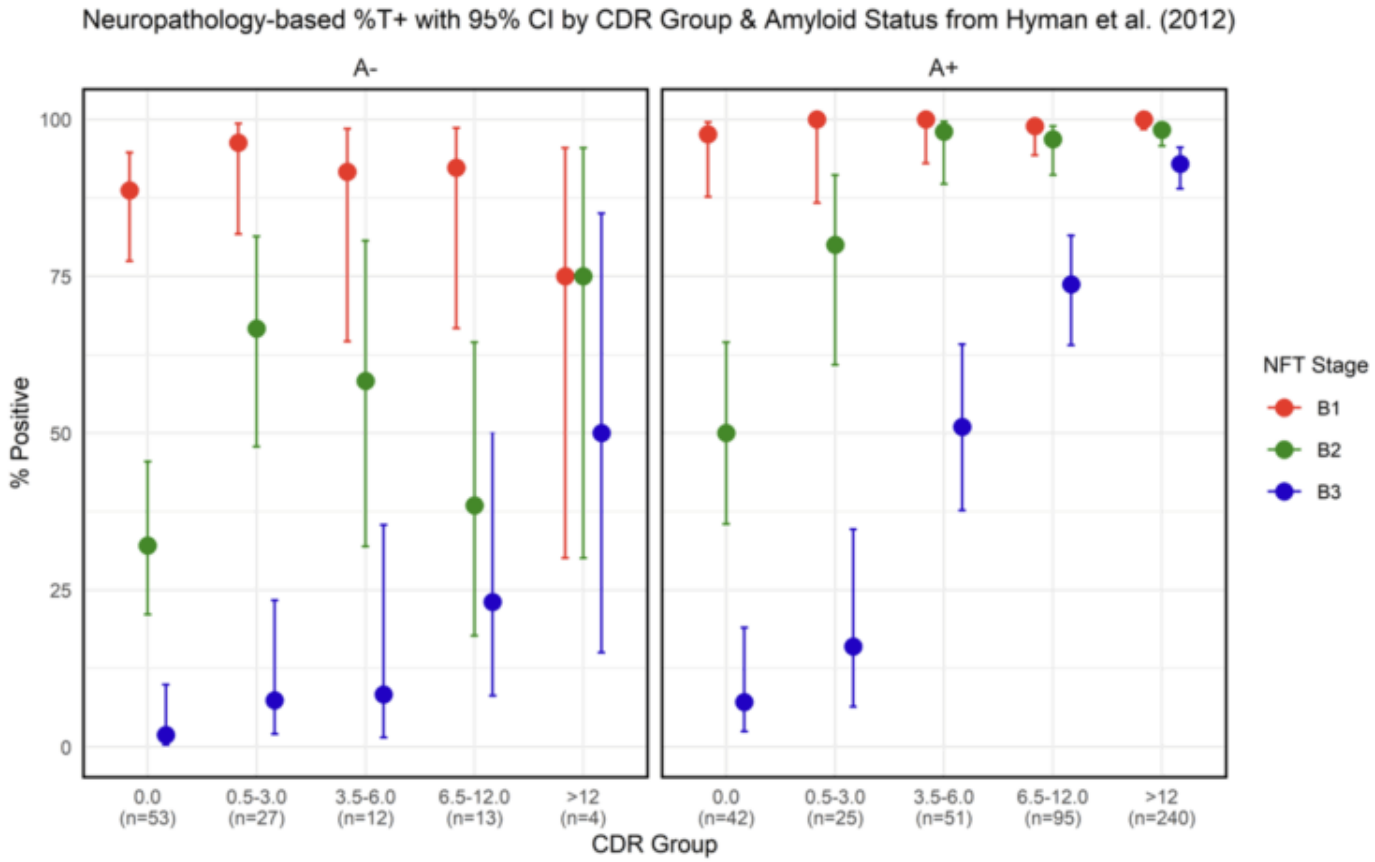


Figure 1. The percent of subjects considered positive by neuropathology in each NFT stage comprised of two Braak stage regions (B1, Braak I and II regions; B2, Braak III and IV regions; and B3, Braak V and VI regions) within each range of scores for the CDR-SB. Amyloid negative subjects on left, amyloid positive subjects on right.

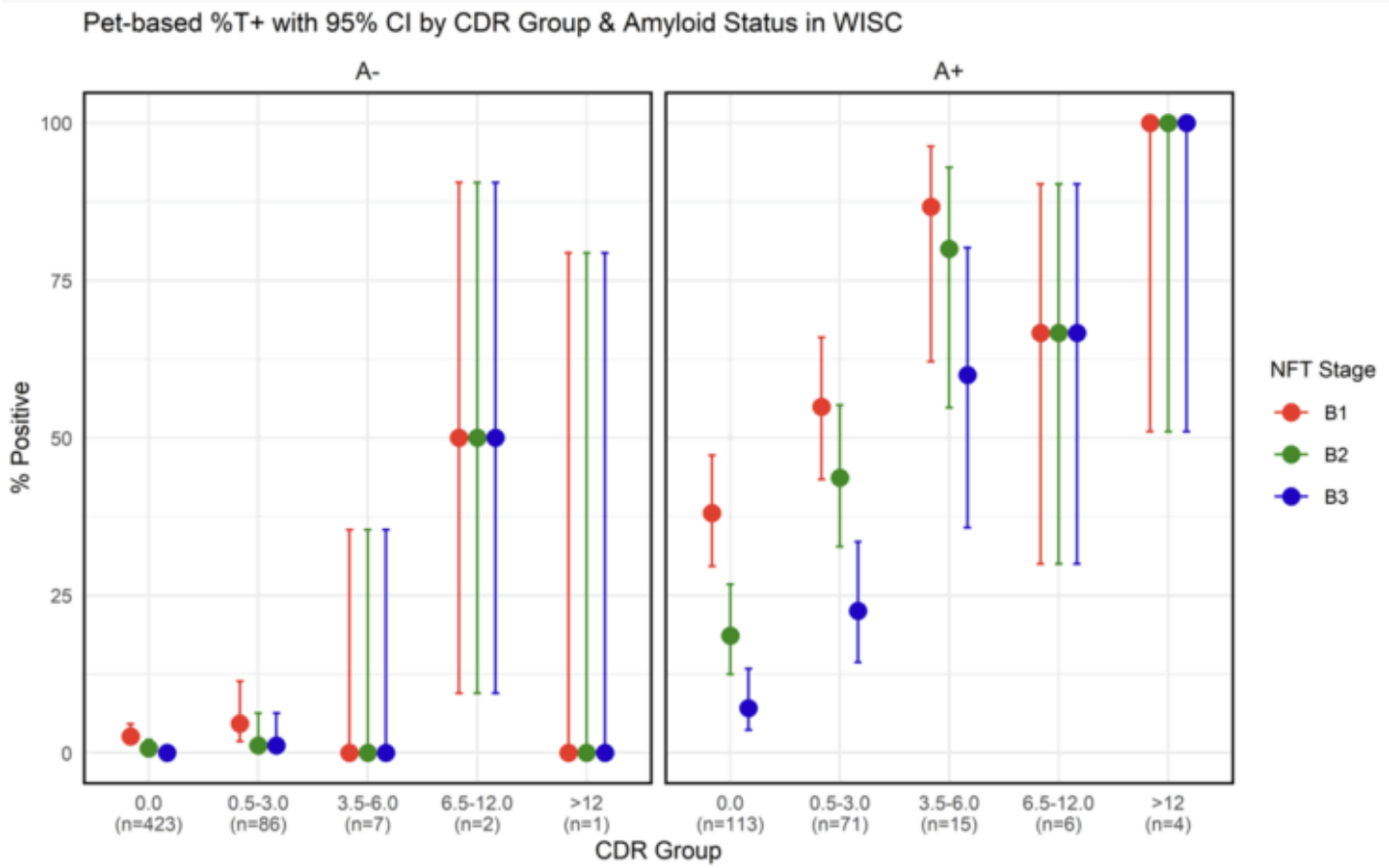


Figure 2. The percent of subjects considered positive by PET assessment in each NFT stage (B1, Braak I and II regions; B2, Braak III and IV regions; and B3, Braak V and VI regions) within each range of scores for the CDR-SB. Amyloid negative subjects on left, amyloid positive subjects on right. PET cut-off for positivity is 2 SD above the median of amyloid negative subjects less than 60 years old.

Positivity by Cohort and Amyloid Status within CDR Group

CDR-SB	Amyloid Status	NFT Stage	Test Type	Odds Ratio	Higher Odds Group	p value	p adj	sig
0.0	A-	B1	Chi-squared Test	NA	Neuropath	<0.001	<0.001	*
0.0	A-	B2	Fisher's Exact Test	0.02	Neuropath	<0.001	<0.001	*
0.0	A-	B3	Fisher's Exact Test	0.00	Neuropath	0.111	0.111	
0.5-3.0	A-	B1	Fisher's Exact Test	0.00	Neuropath	<0.001	<0.001	*
0.5-3.0	A-	B2	Fisher's Exact Test	0.01	Neuropath	<0.001	<0.001	*
0.5-3.0	A-	B3	Fisher's Exact Test	0.15	Neuropath	0.141	0.141	
3.5-6.0	A-	B1	Fisher's Exact Test	0.00	Neuropath	<0.001	<0.001	*
3.5-6.0	A-	B2	Fisher's Exact Test	0.00	Neuropath	0.017	0.026	*
3.5-6.0	A-	B3	Fisher's Exact Test	0.00	Neuropath	1.000	1.000	
6.5-12.0	A-	B1	Fisher's Exact Test	0.11	Neuropath	0.257	0.714	
6.5-12.0	A-	B2	Fisher's Exact Test	0.65	PET	1.000	1.000	
6.5-12.0	A-	B3	Fisher's Exact Test	0.33	PET	0.476	0.714	
>12	A-	B1	Fisher's Exact Test	0.00	Neuropath	0.400	0.600	
>12	A-	B2	Fisher's Exact Test	0.00	Neuropath	0.400	0.600	
>12	A-	B3	Fisher's Exact Test	0.00	Neuropath	1.000	1.000	
0.0	A+	B1	Fisher's Exact Test	0.02	Neuropath	<0.001	<0.001	*
0.0	A+	B2	Chi-squared Test	NA	Neuropath	<0.001	<0.001	*
0.0	A+	B3	Fisher's Exact Test	0.99	Neuropath	1.000	1.000	
0.5-3.0	A+	B1	Fisher's Exact Test	0.00	Neuropath	<0.001	<0.001	*
0.5-3.0	A+	B2	Chi-squared Test	NA	Neuropath	0.004	0.006	*
0.5-3.0	A+	B3	Fisher's Exact Test	0.66	PET	0.578	0.578	
3.5-6.0	A+	B1	Fisher's Exact Test	0.00	Neuropath	0.049	0.073	
3.5-6.0	A+	B2	Fisher's Exact Test	0.08	Neuropath	0.034	0.073	
3.5-6.0	A+	B3	Chi-squared Test	NA	PET	0.748	0.748	
6.5-12.0	A+	B1	Fisher's Exact Test	0.02	Neuropath	0.009	0.026	*
6.5-12.0	A+	B2	Fisher's Exact Test	0.07	Neuropath	0.027	0.041	*
6.5-12.0	A+	B3	Fisher's Exact Test	0.72	Neuropath	0.657	0.657	
>12	A+	B1	NA	NA	NA	NA	NA	NA
>12	A+	B2	Fisher's Exact Test	0.00	PET	1.000	1.000	
>12	A+	B3	Fisher's Exact Test	0.00	PET	1.000	1.000	

Table 1. Differences between the proportion of tau positive (T+) subjects assessed by neuropathology and PET by cohort and amyloid status within CDR Group. Adjusted p-value correction used the Benjamini-Hochberg procedure to account for multiple comparisons.

Keywords: Neuropathology, Tau PET, Dementia

117 Novel pet tracer [11C]-CS1P1 uptake reflects decreased sphingosine-1-phosphate receptor 1 activity in vivo in Alzheimer's disease and related dementias

Savannah Tiemann Powles[1], Karl Friedrichsen[1], Shaney Flores[1], Jayashree Rajamanickam[1], Sarah Keefe[1], Ashlee Simmons[1], Stephanie Doering[1], Nicole McKay[1], David Hoagey[1], Edita Sabaredzovic[1], Laura Ibanez[1], John Morris[1], Hongyu An[1], Matthew Brier[1], Zhude Tu[1], Tammie Benzinger[1]

[1]*Washington University in St. Louis School of Medicine, St. Louis, MO, US*

Background: Neuroinflammation plays a significant role in Alzheimer's Disease (AD) as both a driver and a consequence of disease pathology. [11C]-CS1P1 (CS1P1) is a novel PET tracer targeting sphingosine-1-phosphate receptor 1 (S1PR1), a receptor expressed on all immune cells. Human autopsy studies indicate S1PR1 is altered in AD progression (Martínez-Gardeazabal et al., 2024). There are FDA-approved drugs for MS modulating this pathway, thus, understanding how CNS S1PR1 relates to AD is a critical unmet need.

Objectives: To address this gap, we utilized CS1P1-PET, Aβ (PiB)-PET, MRI, and proteomics to examine whether CS1P1 uptake is associated with AD, white matter disease (WMD), and peripheral inflammation. We hypothesize that S1PR1 signaling, visualized with CS1P1-PET, can identify changes in neuroinflammation during disease progression.

Methods: Analyses included 18 healthy older controls (Aβ-, CDR=0), 5 preclinical AD (Aβ+, CDR=0), and 3 symptomatic AD (Aβ+, CDR>0). Cortical standard uptake values (SUVs) were normalized to young healthy controls to make a CS1P1 Z-score (Figure 1, Friedrichsen et al., 2025). PiB-PET determined Aβ status. TrUE-Net calculated white matter hyperintensity (WMH) volume; volumes greater than 3000mm^3 indicate WMH positivity. Plasma proteins were quantified using NULISAseq's CNS 120 panel. Group differences were evaluated using ANOVA and associations with linear regressions and Spearman's correlations.

Results: CS1P1 Z-score decreased across AD stages (F=2.15, p=0.14; Figure 2). Among Aβ+ individuals, CS1P1 Z-score was positively associated with Centiloid (R=0.40). WMD participants have elevated CS1P1, while participants with WMD and cognitive impairments (VCID) have lower CS1P1 Z-scores. CS1P1 was positively associated with body mass index, TNFα, and IL6 (R=0.70, R=0.19, R=0.25, respectively; Figure 3).

Conclusions: As the first in-human study confirming the autopsy results, we found decreased CS1P1 uptake with AD progression and positive associations between CS1P1 and Aβ-PET, suggesting impaired S1PR1 signaling in the CNS as AD advances. CS1P1 uptake reflects peripheral immune activation.

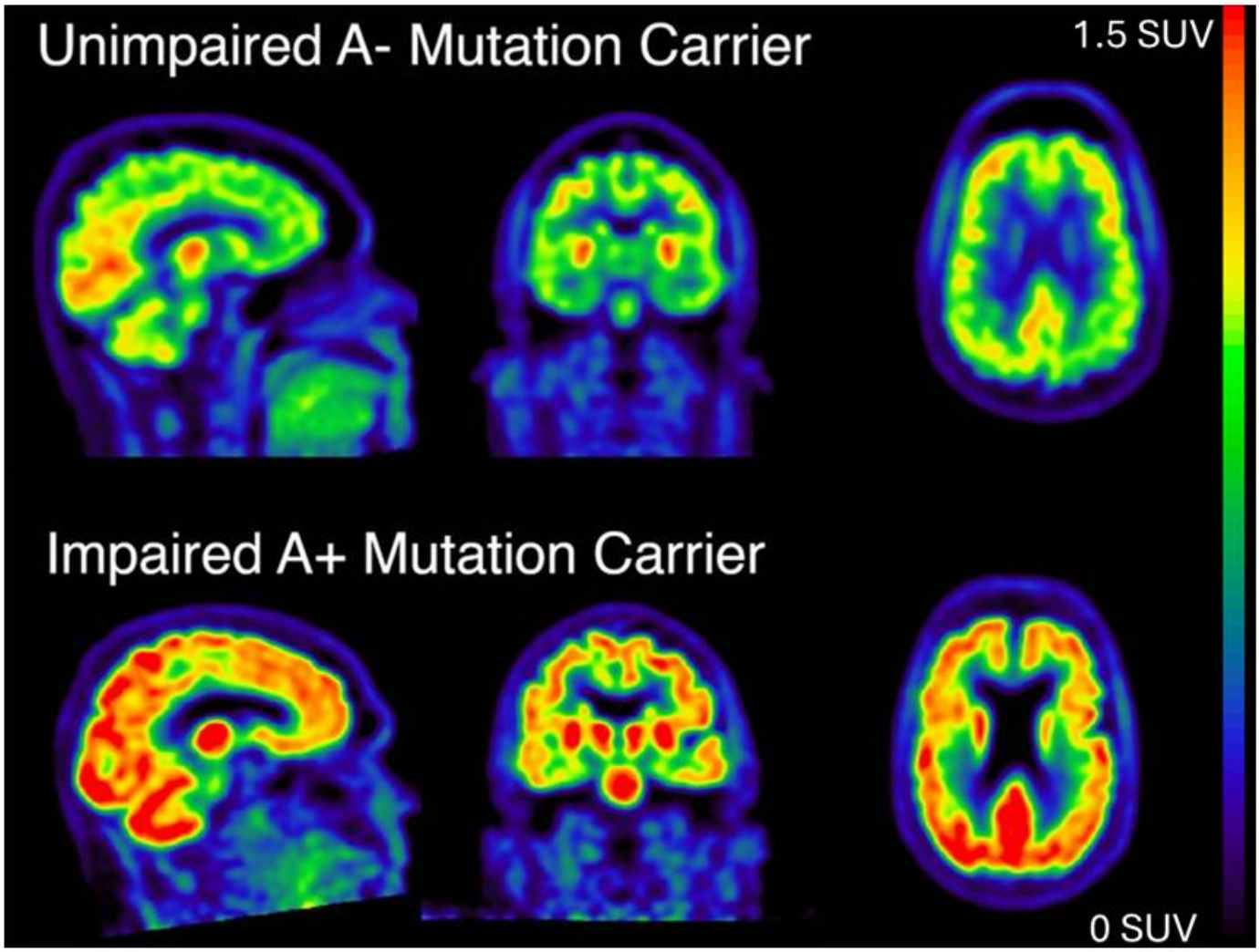


Figure 1: Standard uptake value (SUV) images to demonstrate [11C]-CS1P1 positron emission tomography (PET) uptake in participants from the Dominantly Inherited Alzheimer's Network (DIAN) cohort, with an Aβ- mutation carrier showing less CS1P1 uptake compared to an Aβ+ mutation carrier. Cortical standard uptake values (SUVs) between 30-60 minutes post-injection were extracted using FreeSurfer ROIs and normalized to a separate cohort of healthy young reference group to create a CS1P1 Z-score.

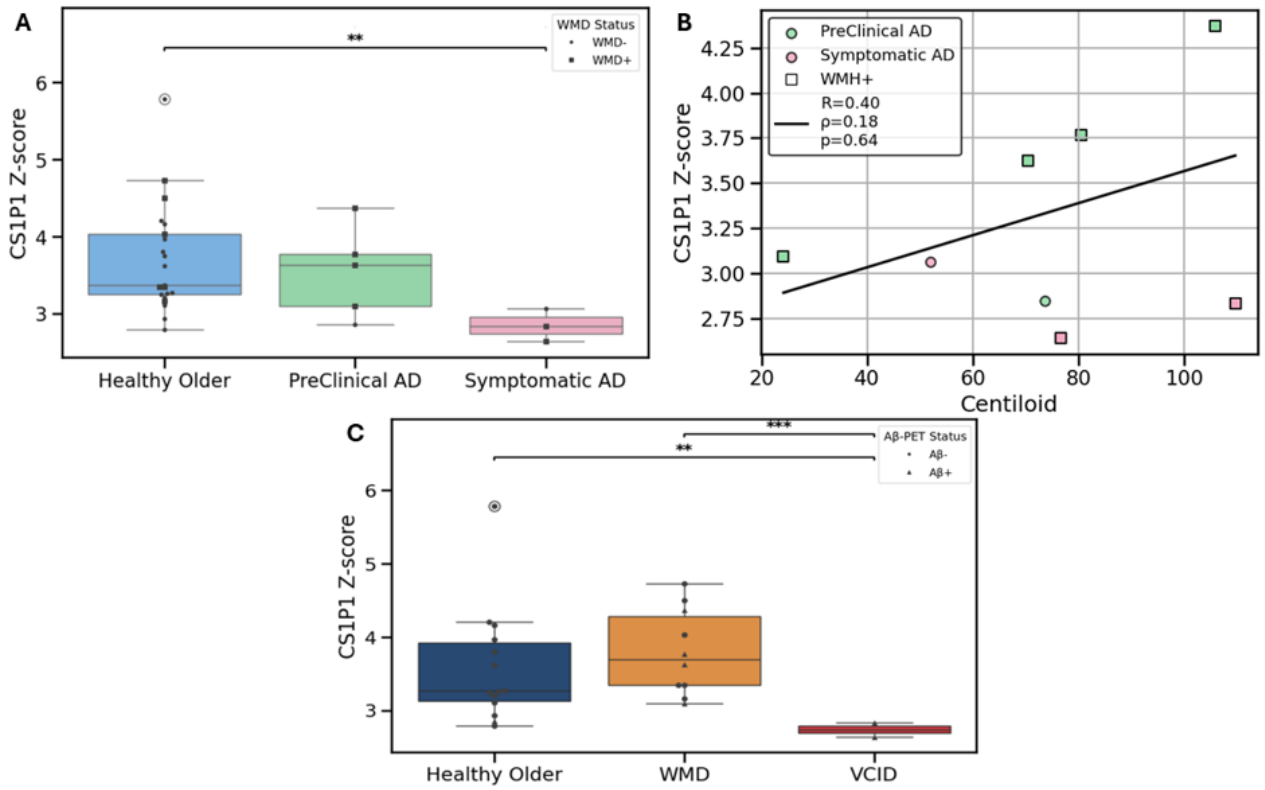


*Figure 2: [11C]-CS1P1 uptake decreases with AD pathology. A) CS1P1 uptake is significantly decreased in the symptomatic AD cohort compared to healthy controls (ANOVA: F = 2.1516, p = 1.3655e-01; **p = 0.0013). Squares denote participants who also have elevated white matter hyperintensity volumes (WMH>3000mm^3). B) CS1P1 Z-score increases with increasing amyloid-β burden, as determined with [11C]-Pittsburgh-Compound-B (PiB) in individuals that have a positive centiloid (R=0.40, Spearman rho: 0.18, p-value: 0.64). C) White matter hyperintensity volume affects CS1P1 uptake. WMD is WMH+, CDR=0, and Vascular contributions to cognitive impairment (VCID) is WMH+, CDR>0. VCID has lower CS1P1 uptake than white matter disease (WMD) and healthy older participants (ANOVA: F = 1.9425, p = 1.6615e-01; **p = 0.003, ***p<0.001).*

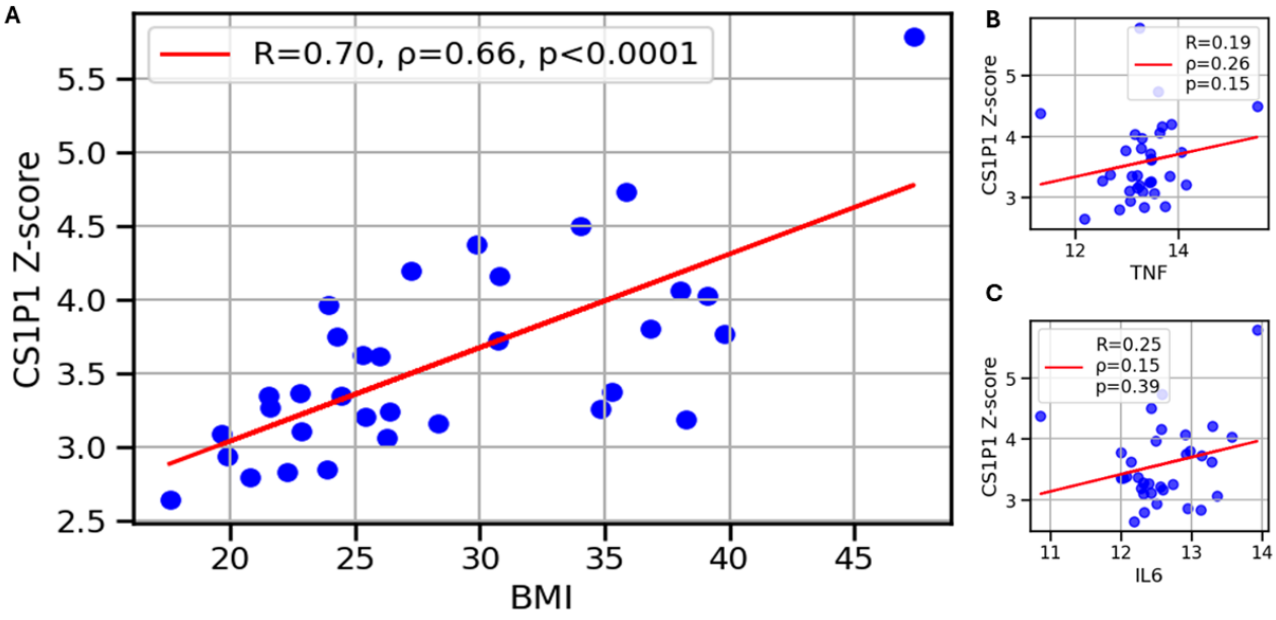


Figure 3: CS1P1 Z-scores in the CNS are positively associated with (A) body mass index (BMI) and indicators of peripheral inflammation (B) TNF and (C)IL6 in the periphery (R=0.70, R=0.19, R=0.25, respectively).

Keywords: Neuroinflammation, Aβ-PET, white matter hyperintensities, peripheral inflammation

118 Digital maze test reveals features related to cortical tau in cognitively normal Aβ+ older adults

Talia Robinson[1], Jessie Fu[2], Rebecca Amariglio[1,2], Reisa Sperling[1,2], Keith Johnson[2], Randall Davis[3], Dana Penney[4], Dorene Rentz[1]

[1]*Brigham and Women's Hospital, Boston, MA, US*
[2]*Massachusetts General Hospital, Boston, MA, US*
[3]*Massachusetts Insitute of Technology, Cambridge, MA, US*
[4]*Lahey Hospital and Medical Center, Burlington, MA, US*

Background: Digital cognitive tools may capture subtle aspects of cognitive performance that are not detectable using traditional measures, particularly among individuals in the preclinical stage of Alzheimer's disease (AD), who display strong cognitive performance despite elevated amyloid (Aβ+). Here, we aim to explore if a digital maze test (dMaze) can capture unique performance weaknesses associated with tau accumulation in cognitively unimpaired (CU) Aβ+ individuals.

Methods: Participants included 195 CU individuals (140 Aβ-, 55 Aβ+) from the Harvard Aging Brain Study who completed the dMaze with "choice" and "no-choice" conditions, and amyloid PET imaging visualized with ^{18}F-Pittsburgh Compound B (PiB). A subset (38 Aβ+, 108 Aβ-) also underwent tau PET visualized with ^{18}F-Flortaucipir (FTP). Multiple regression models tested the interaction of dMaze performance and PiB group on EC tau, to examine whether dMaze-EC tau associations differ by group.

Results: In interaction models, PiB group moderated the associations between no-choice Time in Start cells ($p < .05$), and Total Number of Strokes in the choice condition ($p < .05$)**,** with EC tau**,** indicating stronger tau-related associations between these maze features in Aβ+ relative to Aβ– individuals.

Conclusions: Results indicate specific digitally captured features of the dMaze test are uniquely related to EC tau among CU older adults with elevated Aβ. This suggests that the dMaze has some value in identifying subtle, biomarker-related cognitive performance differences in preclinical AD. These features could potentially be used to predict disease progression among CN Aβ+ individuals, and future work using longitudinal models should be used to validate their utility in predicting cognitive decline.

Keywords: digital tools, cognition, amyloid, tau, preclinical AD

119 Associations of regional neuroinflammation by ER176 PET SUVR with cognitive scores

David Jacobson[1], Seokbeen Lim[1], Emily Lundt[2], Marin Nycklemoe[1], Paul Min[1], Hugo Botha[3], Jonathan Graff-Radford[3], David Jones[3], Prashanthi Vemuri[1], Kejal Kantarci[1], David Knopman[3], Clifford Jack[1], Ronald Petersen[3], Val Lowe[1]

[1]*Department of Radiology, Mayo Clinic, Rochester, MN, US*
[2]*Department of Quantitative Health Sciences, Mayo Clinic, Rochester, MN, US*
[3]*Department of Neurology, Mayo Clinic, Rochester, MN, US*

Background: ER176 is a new generation of radioligand developed for imaging the 18-kDa translocator protein (TSPO). Unlike older generations sensitive to genotype limitations, ER176 addresses those limitations. Neuroinflammation plays a role in synaptic dysfunction and neuronal damage, assisting in Alzheimer's Disease. This study aims to understand the relationship between neuroinflammation and cognition.

Methods: Participants were recruited from the MCSA (n=76) and the ADRC (n=20). Cognition was measured by the MMSE. Neuroinflammation as measured by TSPO-PET SUVR. The study included 96 participants, who were categorized on the cognitive spectrum: cognitively unimpaired with normal amyloid (CU A-, n=25), cognitively unimpaired with abnormal amyloid (CU A+, n=25), mild cognitive impairment with increased amyloid (MCI A+, n=28), and AD dementia (AD, n=18). The SUVR values were calculated as grey+white matter sharpened target referenced to GM sharpened cerebellum crus and without partial volume correction. Meta-ROI regions with the MCALT atlas [1] were used to conduct a correlation analysis, not adjusted for other covariates. Pearson's correlation captured the strength of linear relationship while Spearman's assessed non-linear associations.

Results: MMSE was negatively associated with TSPO SUVR in meta-ROI regions (Figure 1) with Spearman and Pearson correlations indicating a slight non-linear relationship. For example, the temporal TSPO SUVR follows a modest negative trend vs MMSE vs. the postcentral gyrus which is less likely involved by AD pathology (Figure 2).

Conclusions: Correlations between cognition and neuroinflammation can be seen in participants in the AD pathway. These findings will likely be associated with other pathologic entities in this population [2]. Further statistical analysis of the cognitive spectrum (CU A-, CU A+, MCI A+, and AD+) could elaborate individual variation. Adjustment for important confounders would benefit from larger sample size.

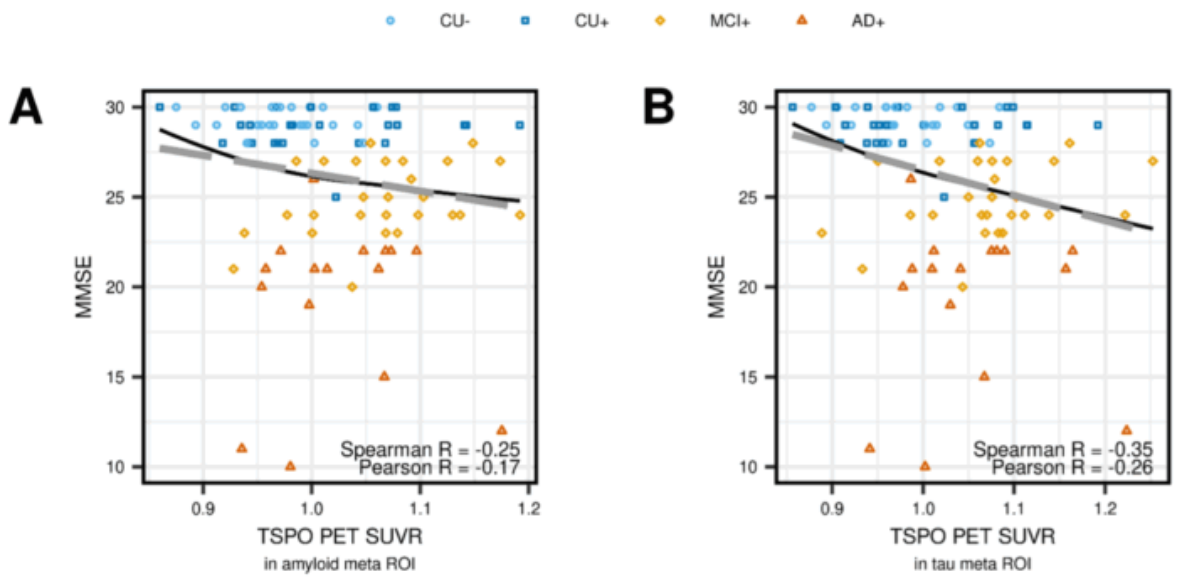


Figure 1.
Scatterplots between TSPO PET SUVR and MMSE score with linear (gray dashed) and local (black) regression curves in established meta-ROI biomarker regions. Local regression allows for curvilinear relationships. MCALT ADIR 42 atlas was selected for these analyses, with left and right combined. TSPO PET SUVR meta-ROI (A) in amyloid meta-ROI regions (include the prefrontal, orbitofrontal, parietal, temporal, anterior and posterior cingulate, and precuneus regions) had a negative trend (Spearman's R =. -0.25 and a Pearson's R = -0.17); (B) and in tau meta-ROI (regions include the amygdala, entorhinal cortex, fusiform, parahippocampal gyrus, inferior temporal gyrus, and middle temporal gyrus regions) had a negative trend (Spearman's R = -0.35 and Pearson R = -0.26).

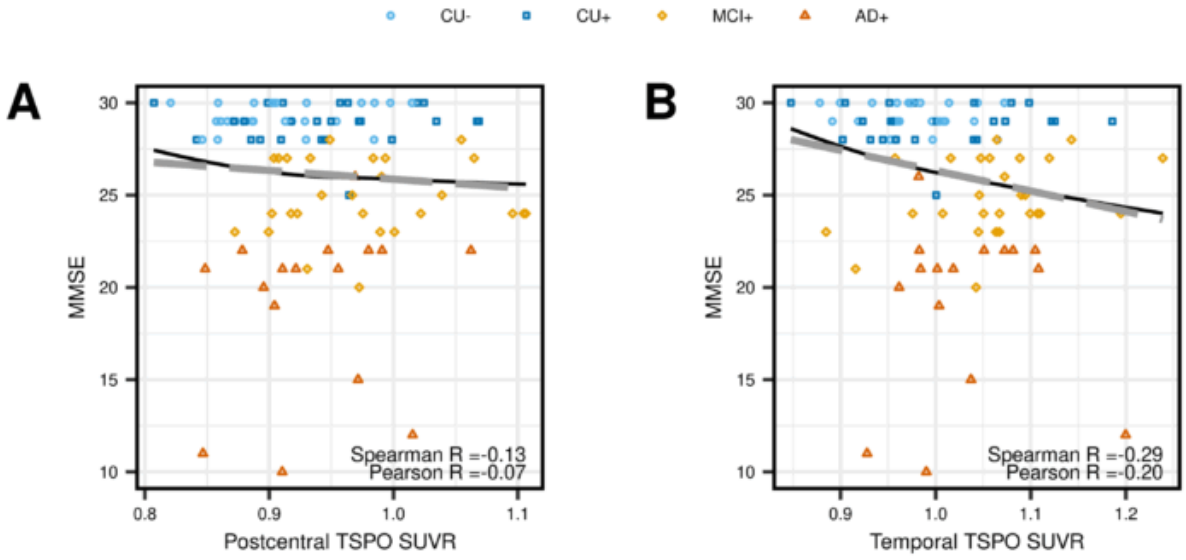


Figure 2.
Scatterplots between postcentral gyrus TSPO SUVR and MMSE (A) and temporal TSPO SUVR and MMSE (B) with linear (gray dashed) and local (black) regression curves. (A) The postcentral TSPO SUVR was weakly associated (Spearman's R = -0.13 and a Pearson's R = -0.17) while (B) temporal TSPO SUVR had a modest negative trend (Spearman's R = -0.29 and a Pearson's R = -0.20) with cognition.

Keywords: TSPO-PET, Alzheimer's Disease, Longitudinal study

120 Cluster-based metric of early tau-PET aggregation is associated with plasma p-tau217 in cognitively unimpaired older adults with subthreshold amyloid-beta

Leah Varghese[1], Jason Brock[1], Lisa Taylor[1], Elizabeth Thomas[1], Michael Yassa[1], Jenna Adams[1]

[1]*University of California, Irvine, Irvine, CA, US*

Background: Previous studies show weak or absent correlations between plasma p-tau217 and tau-PET in cognitively unimpaired (CU) individuals, limiting its utility in clinical trials. Although tau initially aggregates in focal clusters driven by local seeding and cell-specific vulnerability, traditional methods average tau-PET signal within a region, potentially overlooking this early deposition. We tested whether a cluster-based tau-PET approach could better detect focal tau deposition in the entorhinal cortex (EC), revealing stronger relationships with p-tau217.

Methods: We analyzed 142 CU older adults (95 Aβ-/47 Aβ+;1-3 sessions, 214 observations) from ADNI with paired plasma p-tau217 (Janssen) and 18F-Flortaucipir-PET. SUVR maps were thresholded at 1.3, and clusters identified using MATLAB's bwconncomp (Fig1). EC tau cluster volume (total cluster volume/number of clusters, normalized by EC volume) and mean SUVR were calculated. Spearman correlations and linear mixed effects models controlled for age, sex, and education.

Results: EC tau cluster volume correlated with plasma p-tau217 in both Aβ+ and Aβ- subgroups, whereas EC mean SUVR was significant only in Aβ+ (Fig2). In Aβ- participants, p-tau217 was more strongly correlated with EC tau cluster volume than with mean SUVR ($t[92]=2.34$, $p=0.002$). In Aβ- participants, a significant interaction between EC tau cluster volume and Centiloids indicates that subthreshold Aβ (<20 Centiloids) amplifies the EC tau–p-tau217 association ($\beta=0.0068$, $p=0.004$; Fig3A). In Aβ+ participants, this interaction was negative ($\beta=-0.0031$, $p=0.005$; Fig3B), suggesting that the moderating effect of Aβ weakens at high Aβ levels.

Conclusions: Our findings suggest plasma p-tau217 tracks Aβ-modulated entorhinal tau detectable by cluster-based tau-PET in CU adults with subthreshold Aβ. P-tau217 was not related to tau-PET clusters in Aβ- individuals with little to no measurable Aβ, where clusters likely reflect primary-age-related tauopathy or measurement noise. These findings highlight the potential utility of cluster-based tau-PET metrics for detecting and monitoring tau responses in anti-tau therapeutic trials in subthreshold-Aβ participants.

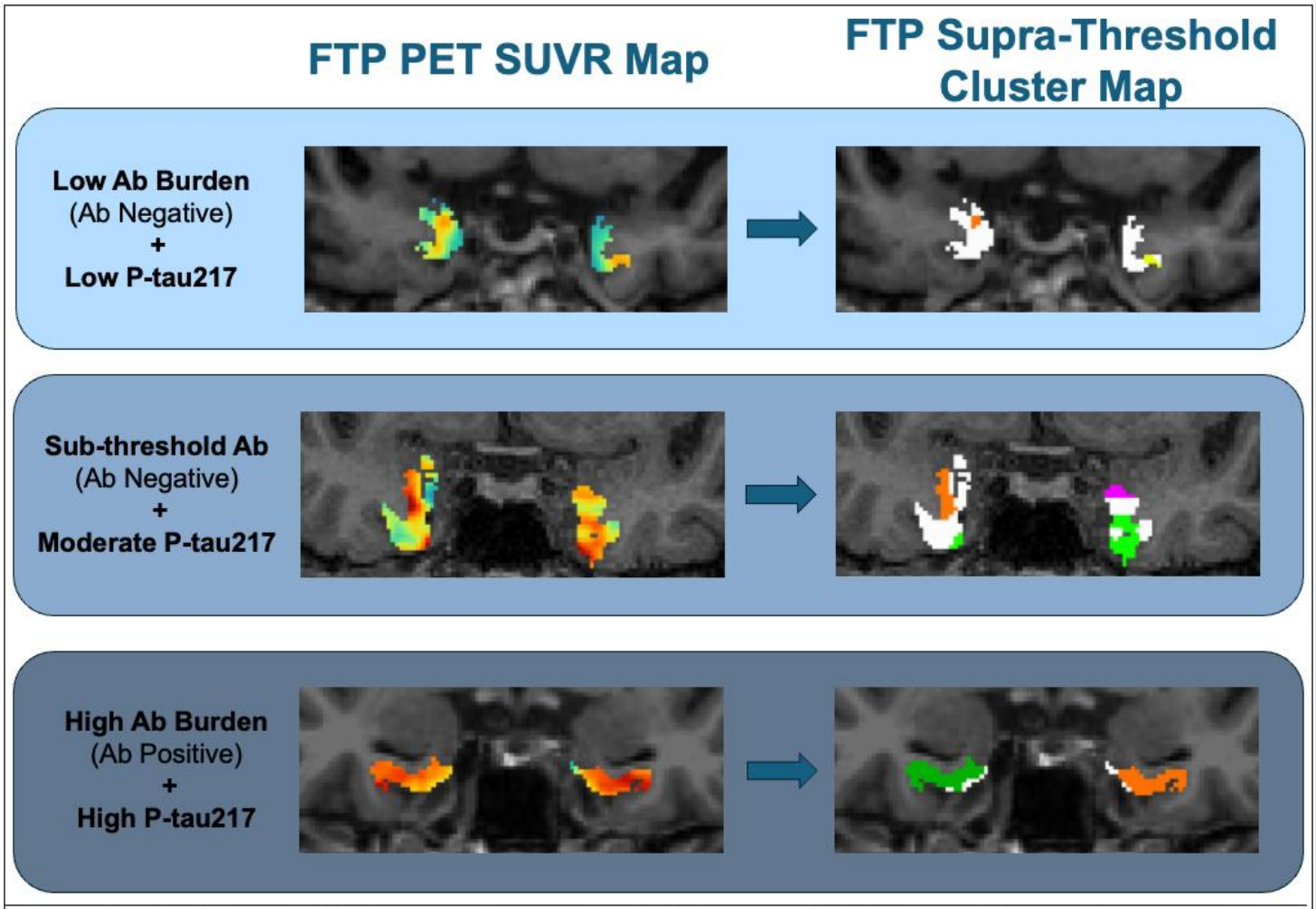


Figure 1: FTP PET SUVR maps (left) and corresponding supra-threshold cluster maps (right) are shown for three participants spanning the Alzheimer's disease biomarker continuum. Each participant was categorized based on Aβ burden and plasma p-tau217 levels. Voxelwise FTP SUVR maps were thresholded at SUVR > 1.3, and spatial clusters were identified using MATLAB's bwconncomp function. Voxels were considered connected if their faces, edges, or corners touched.

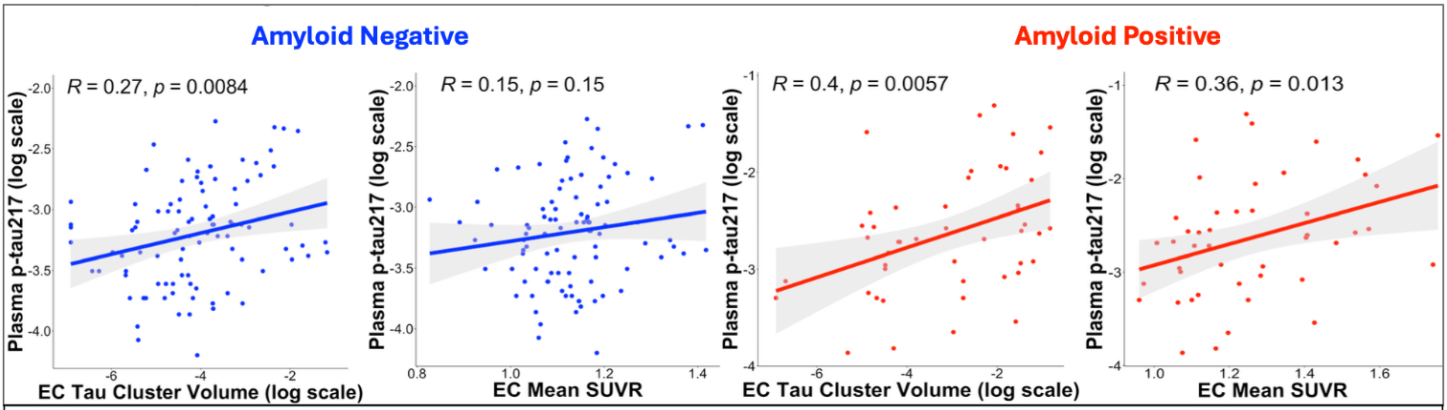


Figure 2. Scatter plots showing associations between plasma p-tau217 (log-transformed) and EC tau cluster volume (log-transformed) or mean SUVR, stratified by Aβ status. Spearman's rho (R) and corresponding p-values are shown for each association.

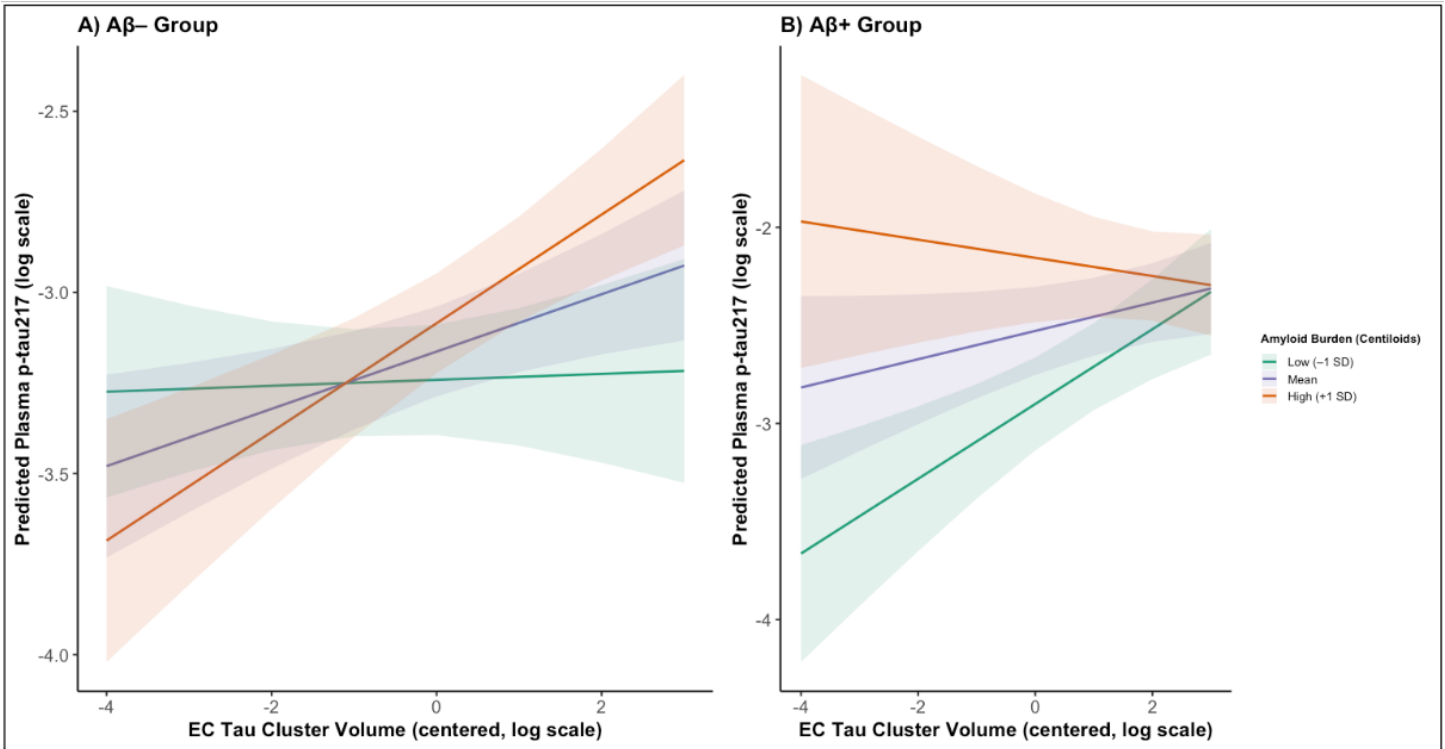


Figure 3. Predicted plasma p-tau217 (log scale) as a function of EC tau cluster volume (centered, log scale) and Aβ burden (Centiloids) at low, mean, and high levels, shown separately for (A) Aβ− and (B) Aβ+ participants. Shaded areas represent 95% confidence intervals.

Keywords: plasma p-tau217, tau-PET, subthreshold amyloid-beta, clustering-based analysis, early detection

121 Sex differences in regional Aβ burden are associated with decreased cingulum integrity uniquely in older cognitively unimpaired women

Emily Yi[1], Dana Parker[1], Whitney Tang[1], Lisa Taylor[1], Nandita Tuteja[1], Novelle Meza[1], Brenda Avila[1], Evelyn Chang[1], Scotty Simmons[1], Alison Bamford[1], Liv McMillan[1], Soyun Kim[1], Elizabeth Thomas[1], Jenna Adams[1], Michael Yassa[1]

[1]*University of California, Irvine, Irvine, CA, US*

Introduction: While men and women show similar global Aβ levels, sex differences in regional Aβ and their impact on neighboring white matter (WM) remain understudied, particularly in AD-vulnerable, estrogen receptor-dense regions including the medial temporal lobe (MTL) and posteromedial cortex (PMC). We hypothesized that, compared to men, postmenopausal women would have greater Aβ in MTL and PMC, which would be associated with worse hippocampal cingulum integrity, the WM tract connecting these regions. We tested whether lower estrone, the primary estrogen in postmenopausal women, exacerbated these effects.

Methods: We analyzed 162 cognitively unimpaired participants (Mean age=70.2 (6.6); 67% female) from the BEACoN study. 18F-florbetapir-PET was used to derive Aβ status, global Aβ, and regional Aβ in the MTL (hippocampus, amygdala, entorhinal cortex (EC), fusiform gyrus (FG)) and PMC (retrosplenial cortex (RSC), posterior cingulate cortex (PCC)). We assessed hippocampal cingulum and uncinate fasciculus (control region) integrity with multishell diffusion MRI-derived neurite density index. In 44 women, we measured estrone using saliva-optimized immunoassay. Holm-Bonferroni-adjusted Mann-Whitney U tests and linear regressions assessed hypothesized relationships.

Results: Global Aβ and Aβ status did not differ by sex. Compared to men, women had higher Aβ in the EC and FG, but not PMC regions (**Fig1**). While women had lower WM integrity than men in both the cingulum and uncinate, this effect was exacerbated in Aβ+ women in the cingulum (**Fig2**). Higher right EC, RSC, and PCC Aβ predicted reduced right cingulum integrity only in women (**Fig3A-C**). There was a trend-level interaction between estrone and RSC Aβ suggesting women with lower estrone showed worse right cingulum integrity related to RSC Aβ (**Fig3D**).

Discussion: Localized Aβ in the MTL and PMC may disproportionately disrupt hippocampal cingulum integrity in women, potentially weakening connection of these regions. Loss of estrone's protective effects may amplify this, contributing to early Alzheimer's-related WM changes.

Figure 1.

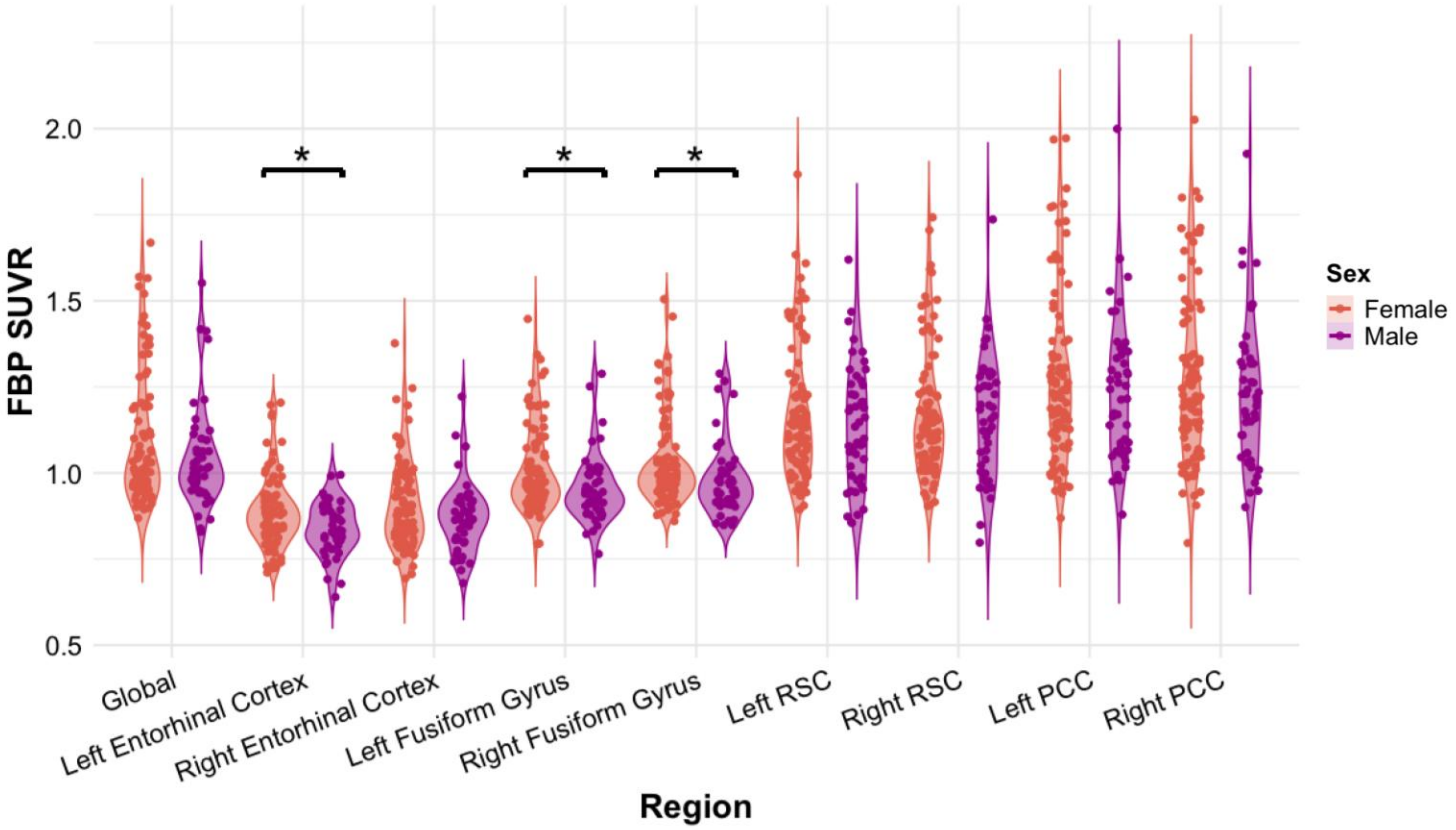


Figure 1. Women showed significantly higher levels of Aβ in the left entorhinal cortex (p = .02), left fusiform gyrus (p = .02), and right fusiform gyrus (p = .02) compared to men. All p-values were adjusted for multiple comparisons using the Holm-Bonferroni method. Significant differences are indicated by *p < .05.

Figure 2.

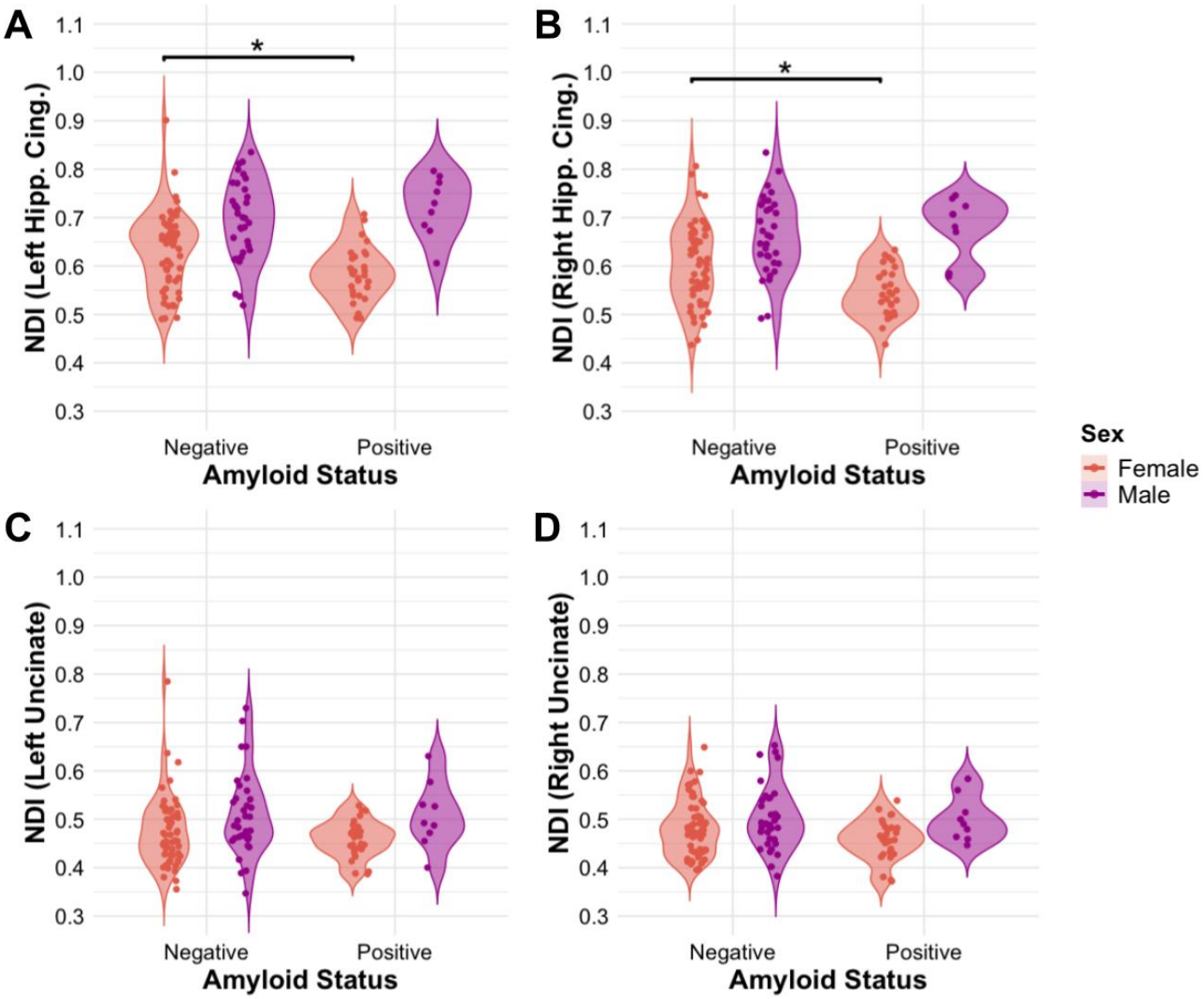


Figure 2. Aβ+ women, but not Aβ+ men, show significantly lower neurite density (NDI) in the hippocampal cingulum (L&R: $p = .03$) **(A–B)**, but not in the uncinate fasciculus (L&R: $p = .84$) **(C–D)**, compared to their Aβ− counterparts. All p-values were adjusted for multiple comparisons using the Holm-Bonferroni method. Significant differences are indicated by $*p < .05$.

Figure 3.

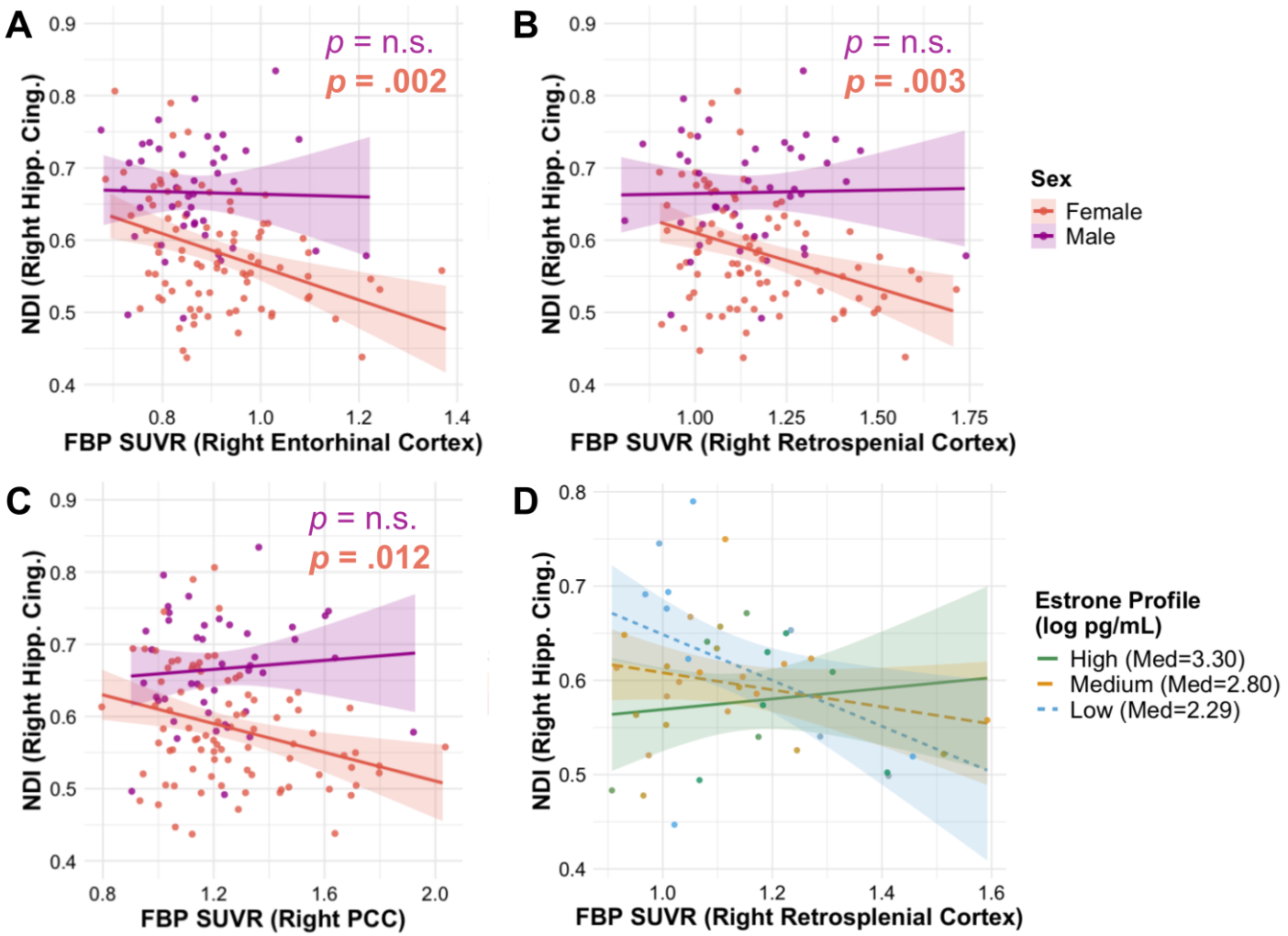


Figure 3. In women only, higher regional Aβ burden in the right entorhinal cortex (p = .002) **(A)**, right retrosplenial cortex (p = .003) **(B)**, and right posterior cingulate cortex (p = .012) **(C)** is associated with reduced neurite density (NDI) in the right hippocampal cingulum (adjusted for multiple comparisons using the Holm-Bonferroni method). There is a trend-level interaction between salivary estrone levels (log pg/mL) and retrosplenial cortex Aβ, indicating women with lower estrone and higher retrosplenial cortex Aβ have significantly lower neurite density in the right hippocampal cingulum (p = .050) **(D)**.

Keywords: sex differences, regional amyloid beta, white matter integrity, estrogen, preclinical Alzheimer's disease

122 Cerebral vessel morphology is associated with white matter lesions burden

Yuanzhe Huang[1], Jinghang Li[1], Marcelo Rocha[2], George Stetten[1], Shaolin Yang[1], Tamer Ibrahim[1], Minjie Wu[1], Howard Aizenstein[2]

[1]*University of Pittsburgh, Pittsburgh, PA, US*
[2]*School of Medicine, University of Pittsburgh, Pittsburgh, PA, US*

Background: Vessel diameter and tortuosity has been linked to cerebrovascular disease and to WMH burden, motivating morphology-based analyses within the brain's arterial tree. In this study, we quantify bilateral ACA/MCA/PCA diameter and tortuosity on TOF-MRA and test their associations with WMH burden.

Methods: This study included 49 older adults who underwent MRI on a 7T Siemens scanner at the University of Pittsburgh (N=49, 33F/16M, age 54–96 years). Time-of-flight MRA (TOF-MRA) used 0.38 × 0.38 × 0.38 mm^3 voxels (354 slices; ~12 min), and same-session 3D T2-FLAIR provided input for WMH segmentation. WMH masks were generated fully automatically with wmh_seg, a Transformer-based U-Net developed by our lab; total WMH volume was computed from the final masks, normalized by intracranial volume (ICV), and log-transformed to yield nWMH. The whole-brain arterial tree was segmented from TOF-MRA using VesselMapper, yielding a centerline graph with per-point diameter . eICAB provided Circle-of-Willis (CoW) labels (L/R MCA, L/R PCA, ACA). To capture proximal–distal structure, we designated the first n Breadth first search hops from each CoW seed as large vessels (Figure 1) and the remainder as small vessels (Figure 2). For each branch, tortuosity was computed using the distance metric (path length / Euclidean distance); within-subject features were then formed as the mean diameter and mean tortuosity for each category (L/R MCA large/small, L/R PCA large/small, ACA large/small).

Results: Higher L-MCA small-vessel tortuosity was associated with greater nWMH ($\beta = 1.40$, $p = 0.0032$), and higher ACA big-vessel tortuosity also related to increased nWMH ($\beta = 0.498$, $p = 0.0249$). (Figure 3)

Conclusion: Our findings highlight that vessel tortuosity is associated with greater White Matter Lesions.

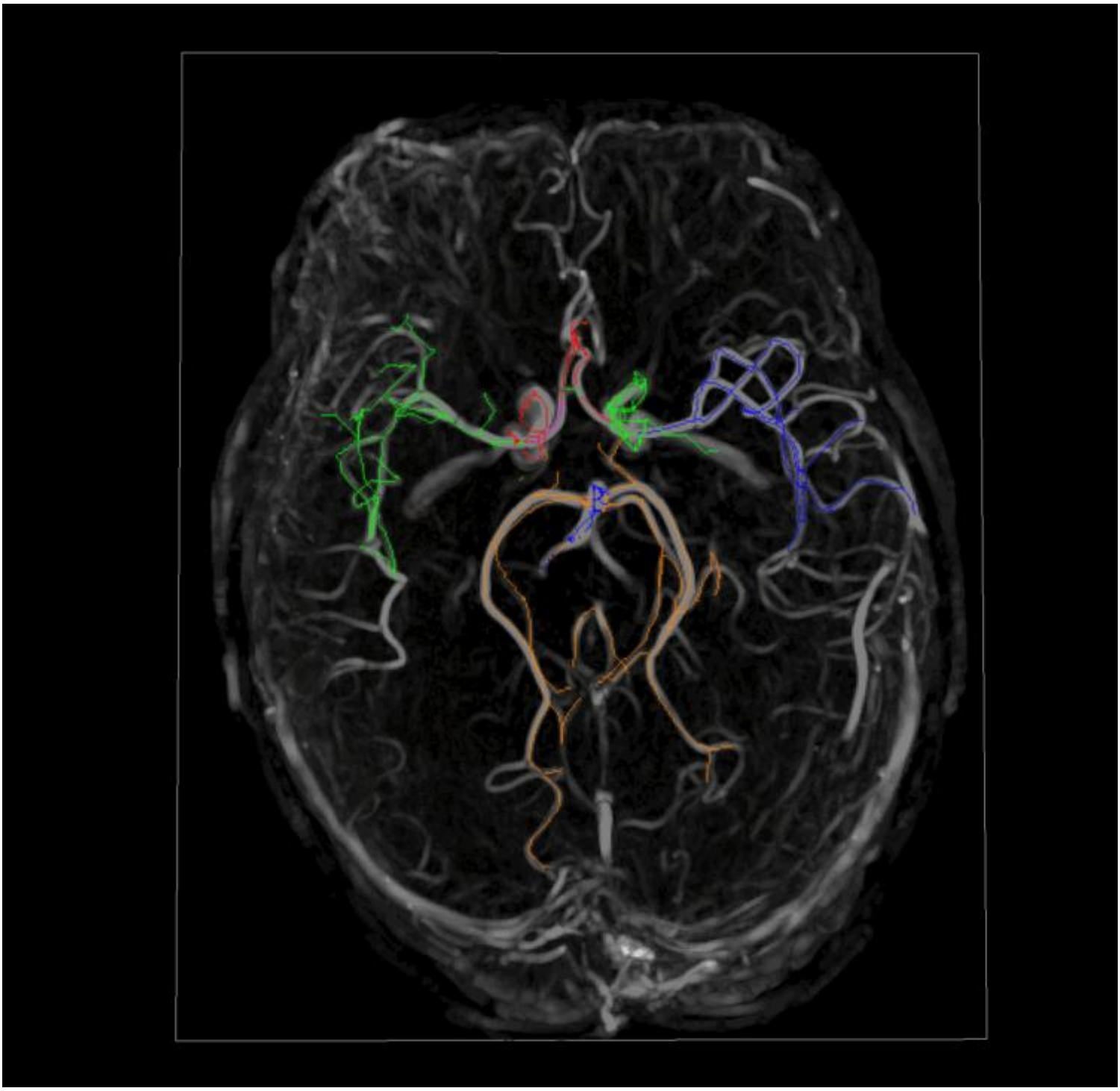


Figure 1. All big vessel labeled with different colors.

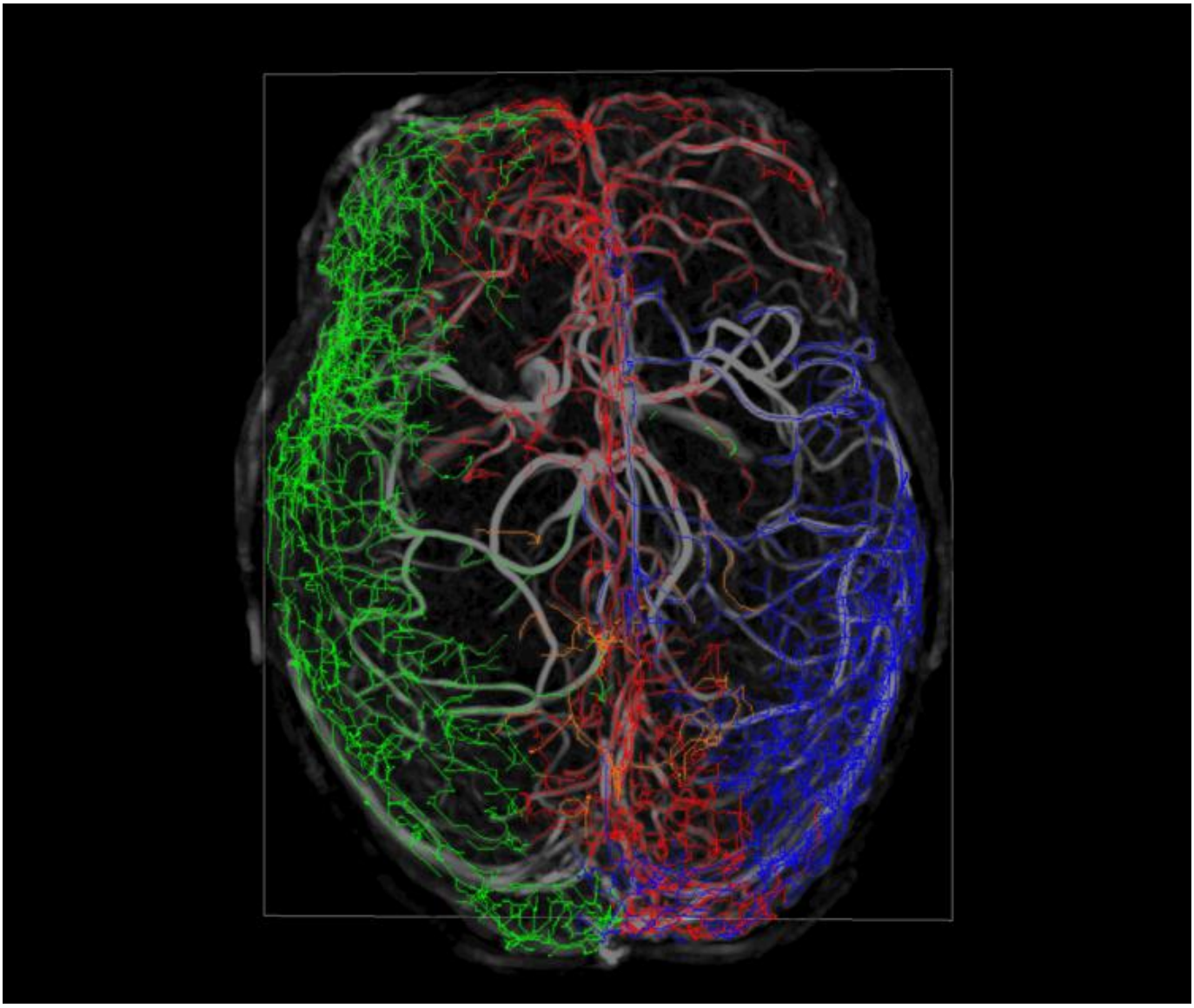


Figure 2. All segmented small vessel labeled with different colors.

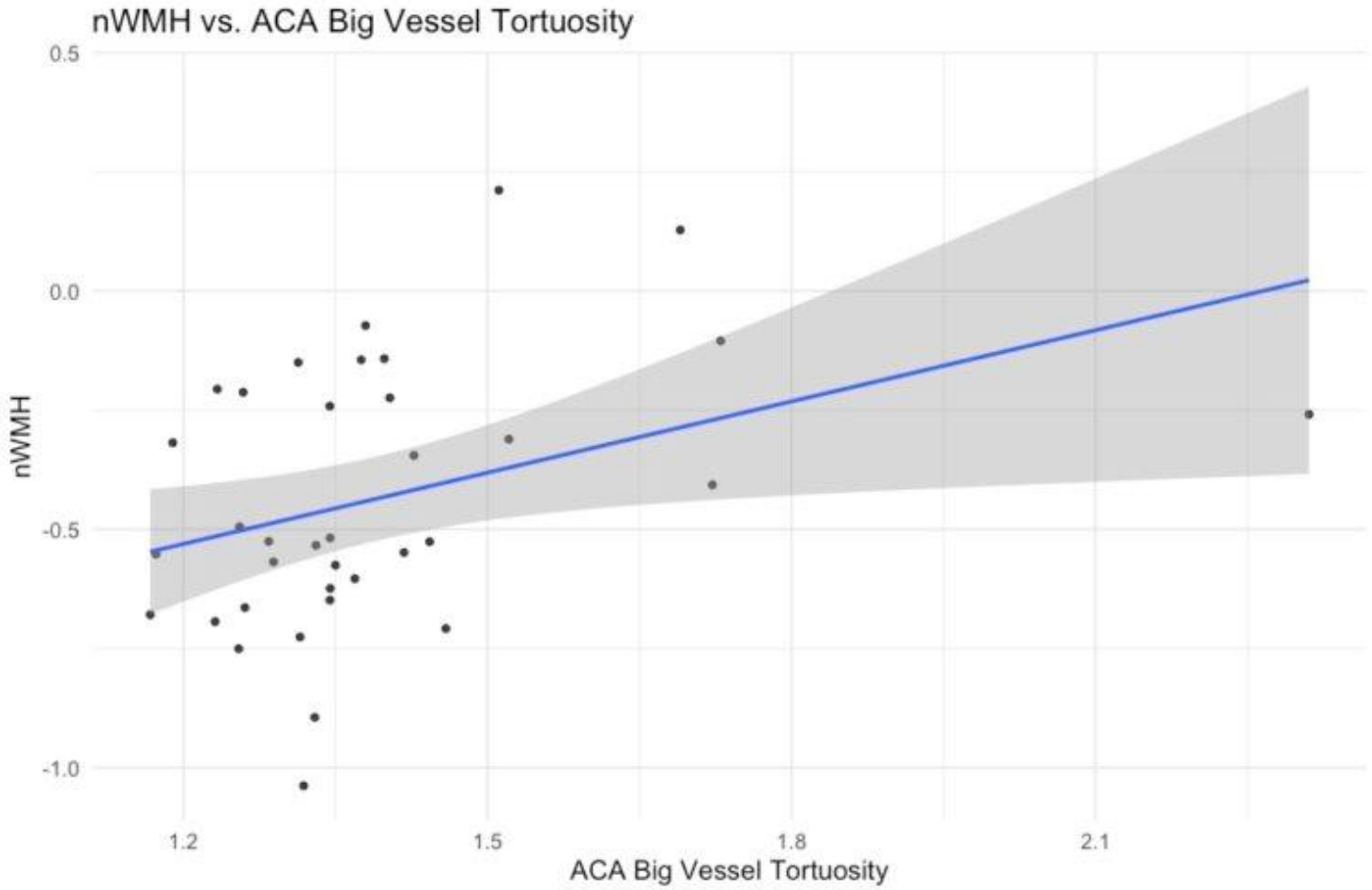


Figure 3. Regression between nWMH and ACA Big Vessel tortuosity

Keywords: Vessel Morphology, White Matter Hyperintensities, Aging.

123 Early ventral temporal tau burden marks functional vulnerability in aging

Jintao Sheng[1,2,3], Alexandra Trelle[2], Isha Sai[1,2], Christina Young[5,6], America Romero[7], Jennifer Park[8], Hillary Vossler[2], Kyan Younes[2], Guido Davidzon[4], Anthony Wagner[1,3], Elizabeth Mormino[2,3]

[1]*Department of Psychology, Stanford University, Stanford, CA, US*
[2]*Department of Neurology and Neurological Sciences, Stanford University School of Medicine, Stanford, CA, US*
[3]*Wu Tsai Neurosciences Institute, Stanford University, Stanford, CA, US*
[4]*Radiology, Stanford University, Stanford, CA, US*
[5]*Department of Radiology, University of California Davis, Davis, CA, US*
[6]*Department of Neurology, University of California, Davis, CA, US*
[7]*Department of Psychology, University of Oregon, Eugene, OR, US*
[8]*Department of Psychology, University of California, Berkeley, Berkeley, CA, US*

Objective: Ventral temporal cortex (VTC) is among the earliest neocortical sites to show tau accumulation in aging. The impact of focal tau in VTC on functions that support episodic memory, including the ability to maintain distinct responses to visual stimuli from different categories (i.e., neural selectivity), remains unclear.

Methods: This study included 103 cognitively unimpaired older adults (73.39±6.08 years; 59 females) from the Stanford Aging and Memory Study (SAMS) who underwent [^{18}F]PI-2620 tau-PET and fMRI during a word-picture (face/place) associative memory task (Figure 1A). Standardized uptake value ratios (SUVRs) were extracted from two subregions within VTC [fusiform face area (FFA) and parahippocampal place area (PPA)] and entorhinal cortex (ERC). Neural selectivity in the FFA (face-preferred) and PPA (place-preferred) was defined as the difference in univariate activation between preferred and non-preferred categories during encoding. Linear mixed-effects and regression models were used to examine the effects of interest while controlling for sex, education, and race, and for age when appropriate.

Results: Tau-PET SUVR was highest in ERC, followed by the FFA and PPA ($F_{2,200}$=221.632, p<0.001; Figure 1B). ERC tau was moderately correlated with FFA (b=0.288, p<0.001) and PPA tau (b=0.270, p<0.001), and SUVRs across all regions increased with age (bs=0.0075-0.0086, ps<0.01)(Figure 1C&D). FFA tau was marginally associated with reduced activation for both preferred and non-preferred categories (b=-1.217, p=0.089) in FFA and with lower, though non-significant, neural selectivity (b=-0.495, p=0.293)(Figure 2A&B). PPA and ERC tau exhibited negative but non-significant associations with functional measures in VTC (ps>0.05; Figure 2). SUVRs in ERC (b=-0.717, p=0.082) were negatively associated with memory, whereas FFA (β=–0.950, p = 0.175) and PPA SUVRs (β=–1.001, p=0.215) were not significant predictors (Figure 3).

Conclusions: These preliminary findings suggest that tau pathology and functional alterations co-localize in face-selective VTC regions and may exert distinct, dissociable influences on memory in aging.

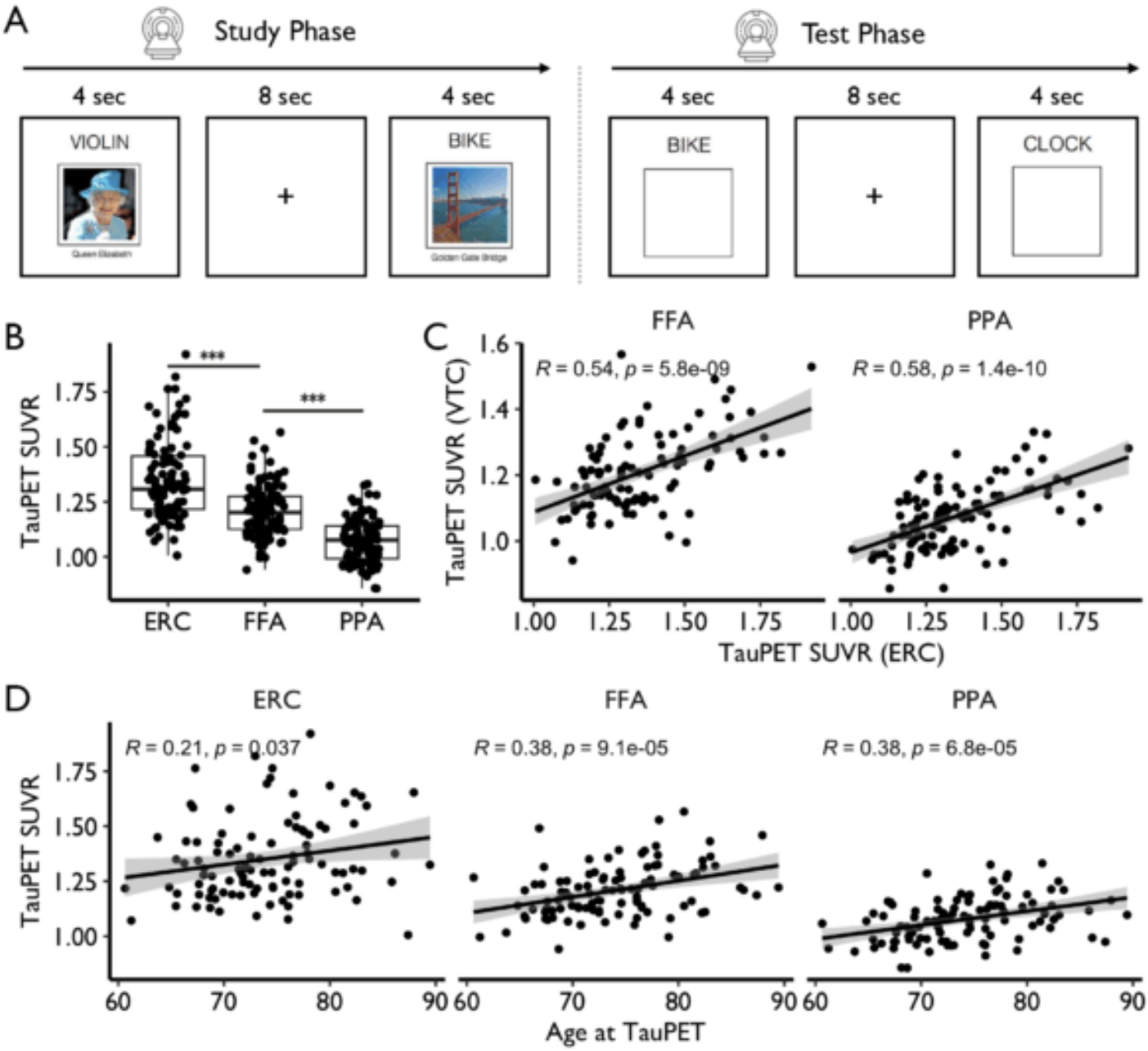


Figure 1. Regional tau-PET SUVRs in the VTC and ERC. (A) Associative memory paradigm. During fMRI scanning, participants intentionally encoded word-picture pairs (famous faces or places paired with nouns; Study phase) and later completed an associative cued-recall test (Test phase). **(B)** Boxplots show regional differences in tau-PET SUVRs, with the ERC exhibiting higher tau burden than the FFA and PPA, and FFA exhibiting higher tau than PPA. **(C)** Scatterplots illustrate positive associations between ERC tau and tau levels in the FFA and PPA. **(D)** Scatterplots show that regional tau-PET SUVRs increased with age across ERC, FFA, and PPA. *** $p < 0.001$; The reported R and p values are derived from the unadjusted data and are included to provide a visual reference for the direction and strength of associations prior to covariate adjustment. The beta coefficients reported in the main text were estimated while controlling for covariates such as sex, education, and race, and for age when appropriate.

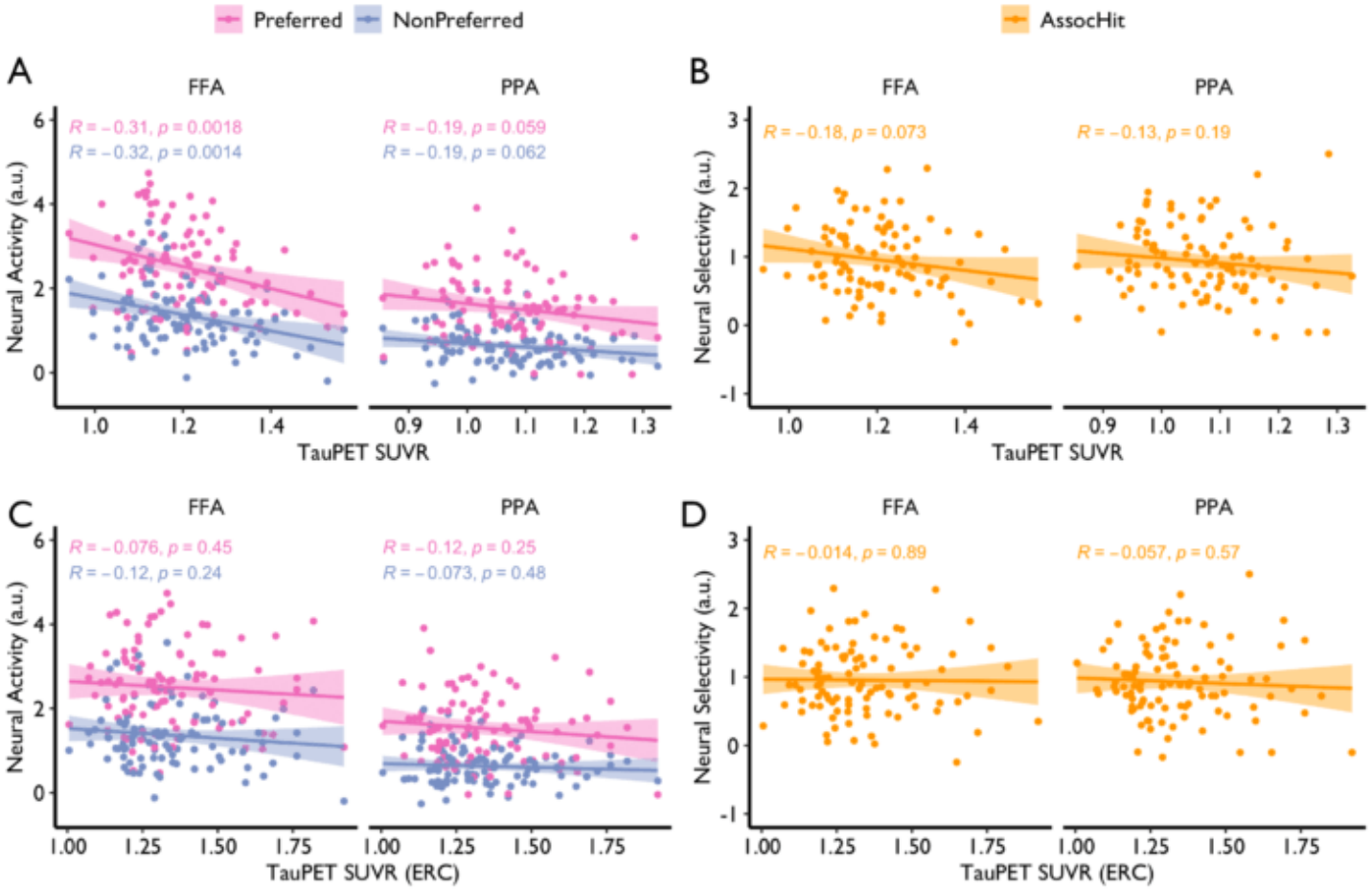


Figure 2. Focal tau pathology relates to neural activity and selectivity in the VTC. (A) Tau-PET SUVRs in the FFA were related to lower neural activity for both preferred and non-preferred categories during subsequent associative-hit trials, but not in the PPA. **(B)** Higher tau in FFA and PPA was associated with lower neural selectivity (preferred minus non-preferred category univariate activity), although these associations did not reach significance. **(C, D)** Scatterplots show ERC tau is not significantly associated with univariate activity or neural selectivity in FFA and PPA. The reported R and p values are based on unadjusted data and shown to illustrate the raw associations. The beta coefficients reported in the main text were estimated while controlling for age, sex, education, and race.

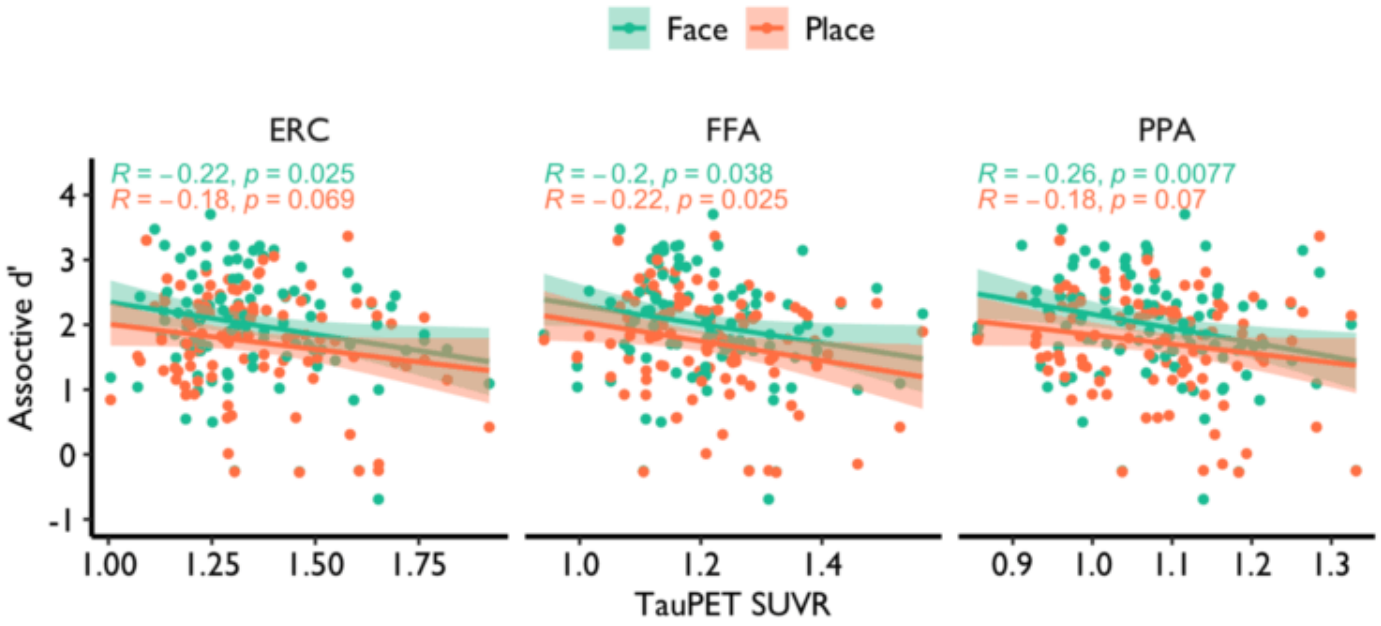


Figure 3. Associations between regional tau burden and associative memory. Scatterplots show negative associations between regional tau-PET SUVRs and associative memory across the ERC, FFA, and PPA. Green and orange represent associative memory for word-face pairs (Face) and word-place pairs (Place), respectively. The R and p values reported here were computed from the raw data without controlling for covariates and are presented to illustrate the overall pattern of associations. The beta coefficients reported in the main text were estimated while controlling for age, sex, education, and race.

Keywords: Ventral temporal cortex, tau-PET, fMRI, neural selectivity, early aging

124 Alignment of antemortem images to postmortem fixed hemibrains using standard neuroimaging tools

William Coath[1,2], Leah J Staruck Staruck[1,2], Finnuella J Carey[1,2], Elena R de Chavez[1,2], Crystal Karas[1,2], Eric E Abrahamson[3], Sanjay Asthana[1,2], Sterling Johnson[1,2], Milos D Ikonomovic[3], Jeffrey Nirschl[1,4], Tobey J Betthauser[1,2]

[1]*Wisconsin Alzheimer's Disease Research Center, University of Wisconsin School of Medicine and Public Health, Madison, WI, US*
[2]*Department of Medicine, University of Wisconsin-Madison School of Medicine and Public Health, Madison, WI, US*
[3]*Department of Neurology, School of Medicine, University of Pittsburgh, Pittsburgh, PA, US*
[4]*Department of Pathology and Laboratory Medicine, University of Wisconsin School of Medicine and Public Health, Madison, WI, US*

Background: Observational cohorts with longitudinal biomarker data, clinical characterization and brain donation programs represent a unique opportunity to elucidate pathologic drivers of biomarkers and clinical symptoms. Advances in precision tissue sampling and quantitative digital pathology coupled with automated image processing workflows typical of *in vivo* neuroimaging studies are needed to bridge the gap between neuropathology and *in vivo* biomarker findings. We investigated an SPM12-based process for registering antemortem images to fixed hemibrain ex-vivo MRI.

Methods: Brains were donated by five participants (1=unimpaired, 1=MCI, 3=dementia) from the Wisconsin Registry for Alzheimer's Prevention (WRAP) and Wisconsin ADRC that underwent antemortem MRI with some additional PET, biofluid and clinical assessment available. The left hemisphere was fixed in 10% neutral-buffered formalin and embedded in 3.5% agar prior to scanning. T1-weighted (0.5x0.5x0.7mm resolution) and T2-weighted (0.5x0.5x0.8mm) images were acquired on a 3T GE Magnus MRI scanner. Following the scan, the fixed brain was sliced into uniform ~4mm thick coronal tissue slabs, photographed and sampled. Images were processed with an automated pipeline for registration of antemortem to post-mortem images using basic operations (masking, origin re-setting) along with non-linear diffeomorphic pairwise registration in SPM12 (Figure 1). Available antemortem amyloid and tau-PET were transformed into ex-vivo MRI-space for visualization. Registration quality between antemortem T1w and postmortem images was visually assessed referencing anatomical landmarks.

Results: The SPM12 non-linear registration was able to account for within-person atrophy between the antemortem scan and autopsy and brain deformations that occurred after death with brain extraction and fixation (Figure 2A). Figure 2C shows the alignment of an [^{18}F]MK-6240 SUVR image, acquired 7 years before death, overlaid on ex-vivo T2w-MRI.

Conclusion: Antemortem images can be aligned to fixed hemibrain MRI using standard modules in SPM12. Work is ongoing to register antemortem and postmortem MRI to brain tissue slabs, allowing for spatially concordant radiopathologic comparisons.

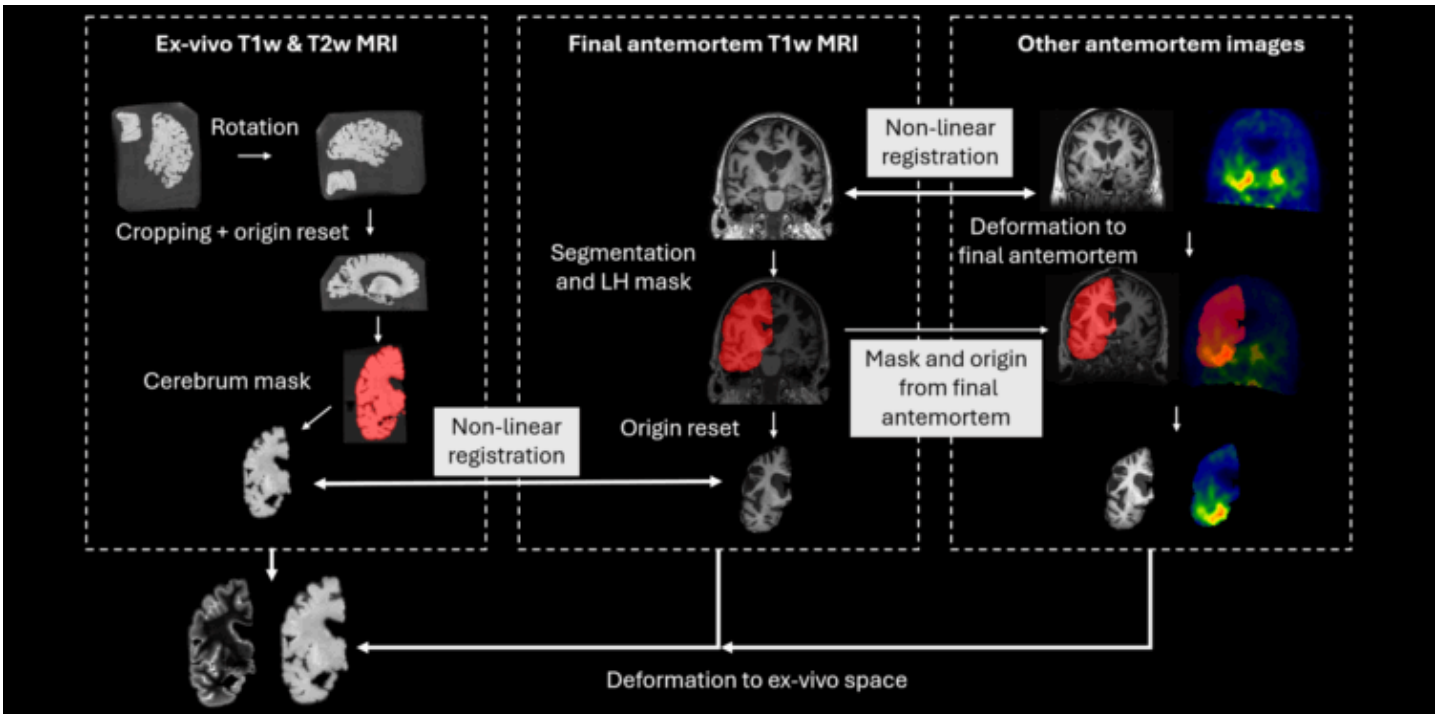


Figure 1. Schematic for preparation and registration steps to align antemortem images to ex-vivo hemibrain MRI using basic masking operations and SPM12 longitudinal registration. LH = left hemisphere.

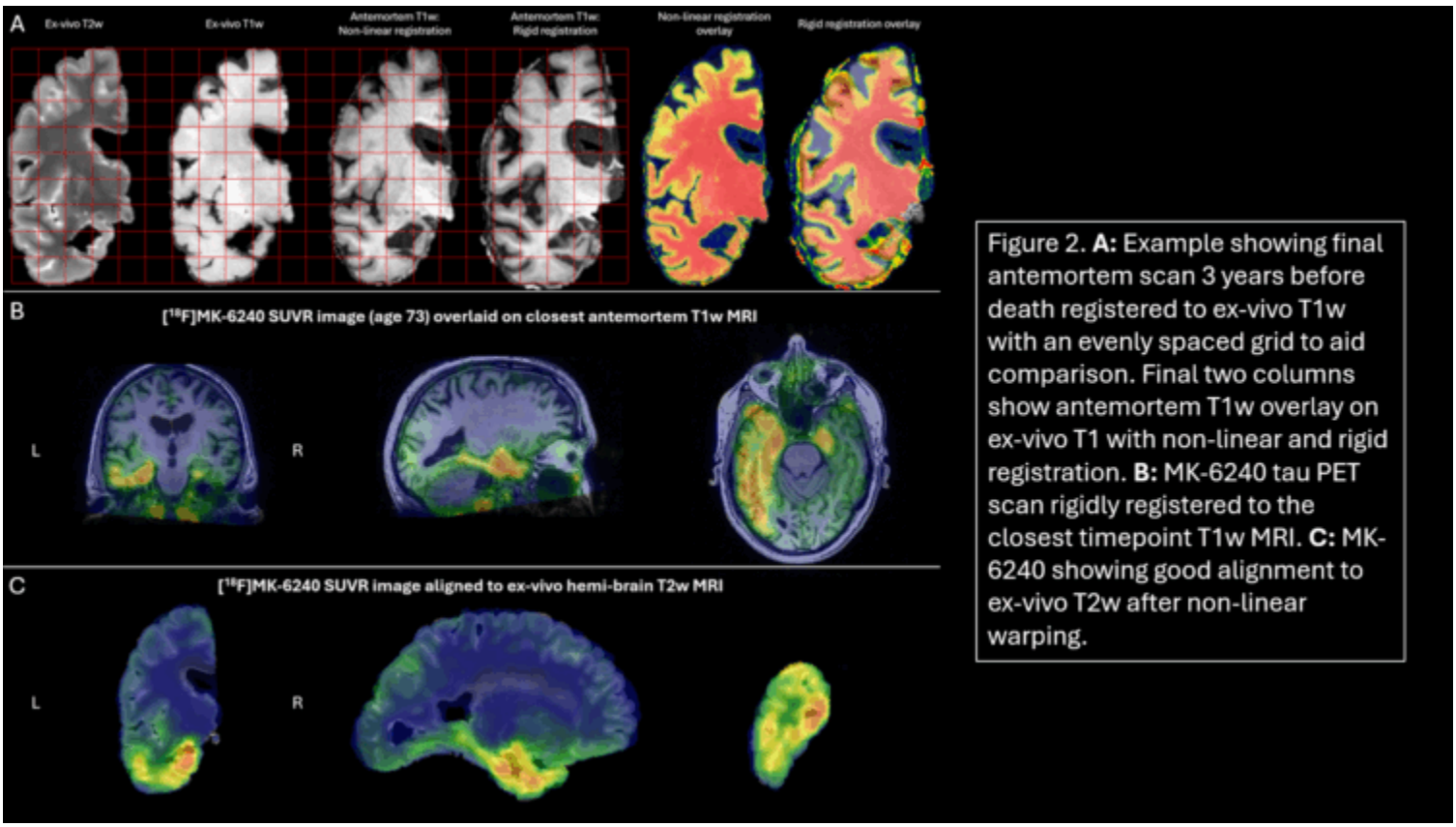


Figure 2. **A:** Example showing final antemortem scan 3 years before death registered to ex-vivo T1w with an evenly spaced grid to aid comparison. Final two columns show antemortem T1w overlay on ex-vivo T1 with non-linear and rigid registration. **B:** MK-6240 tau PET scan rigidly registered to the closest timepoint T1w MRI. **C:** MK-6240 showing good alignment to ex-vivo T2w after non-linear warping.

Keywords: Pathology, PET, tau, MRI, post-mortem

125 Towards a harmonized amyloid clock: centralized image processing and temporal modeling with multiple cohorts and tracers

William Coath[1,2], Hailey Bruzzone[1,2], Jacob Morse[1,2], Ruvini Navaratna[1,2,3], Angel Hammond[1,3], Leah Staruck[1,2], Simone Nowinski[1,2], Rose Palmer[1,2], Michael Kelley[1,2], Hayley Schwartz[1,2], Finnuella Carey[1,2], Tobey Betthauser[1,2]

[1]*Wisconsin Alzheimer's Disease Research Center, University of Wisconsin School of Medicine and Public Health, Madison, WI, US*
[2]*Department of Medicine, University of Wisconsin-Madison School of Medicine and Public Health, Madison, WI, US*
[3]*Center for Health Disparities Research, University of Wisconsin School of Medicine and Public Health, Madison, WI, US*

Background: Biomarker time-based dementia risk models are useful to communicate dementia risk and study mechanisms that lead to heterogeneity in AD. A key challenge is standardization of biomarker-based time estimates. We investigated image processing and temporal modeling strategies for combining PET scans from three cohorts with different amyloid tracers to create a common 'Amyloid clock'.

Methods: 4,523 amyloid PET and MRI scans (n=2,376 participants) from three cohorts (ADNI, OASIS, WISC (WRAP, WADRC)) using three tracers: [^{11}C]PiB, [18F]florbetapir (FBP), [18F]florbetaben (FBB) were processed centrally (Table 1). PET images were harmonized to 7mm using a frequency-domain analysis resolution estimation algorithm. Processing used SPM12 longitudinal MRI registration for consistent within-person ROI parcellation. SUVR from standard GAAIN ROIs were converted to Centiloids (whole cerebellum). Three approaches were tested using sampled iterative local approximation (SILA) with tracer-specific, cohort-specific, and pooled models. We evaluated differences between models visually and compared backwards prediction accuracy (RMSE), estimated amyloid onset age (EAOA; >20 CL) between methods with Wilcoxon tests and EAOA relative to midpoint onset age in observed converters using 10-fold cross-validation.

Results: Homogeneity of PET resolution estimates across cohorts increased following processing (Figure 1A). Amyloid trajectories from different models, cohorts and tracers largely overlapped between 20-100 CL (Figure 1B). RMSE was similar across modeling approaches and highest with FBP (Figure 2A). In A+ participants, the pooled model was most stable, producing fewer outliers (Figure 2B). No significant difference in EAOA was observed between models (Figure 2D). In observed converters (n=103) EAOA accuracy was highest for pooled model (RMSE=3.8, MAE=1.9, r=0.88, Figure 2C).

Conclusion: Initial results suggest centralized image processing with PET resolution matching and pooled temporal model training can provide harmonized amyloid time estimates across tracers and cohorts. This combined image processing and temporal modeling approach will enable study of the AD time course anchored to amyloid positivity.

Table 1. Participant characteristics.

Cohort		ADNI (n = 1019)			OASIS (n = 806)		WISC: WRAP & WADRC (n = 551)
Tracer		FBP	FBB	PiB	FBP	PiB	PiB
Longitudinal participant x tracer, n*		412	120	46	91	189	278
Mean (SD) timepoints		3.2 (1.2)	2.3 (0.4)	2.5 (0.6)	2.2 (0.4)	2.6 (0.8)	2.4 (0.6)
Amyloid positive, n (%)		221 (53.6)	51 (42.5)	33 (71.7)	22 (24.2)	51 (27.0)	90 (32.4)
Baseline age, mean (SD) years		73.1 (7.1)	71.6 (6.2)	74.8 (7.0)	69.4 (7.7)	65.9 (8.6)	66.4 (7.1)
Female Sex, n (%)		188 (45.6)	63 (52.5)	15 (32.6)	51 (56.0)	119 (63.0)	188 (67.6)
Baseline CDR-Global, n	**0**	199	74	11	82	180	228
	0.5	204	40	33	9	8	43
	1	8	6	2	0	1	1
	Missing	1	0	0	0	0	6

*Participants scanned with multiple tracers were treated as separate subjects per tracer, ensuring intra-subject trajectories were tracer specific.

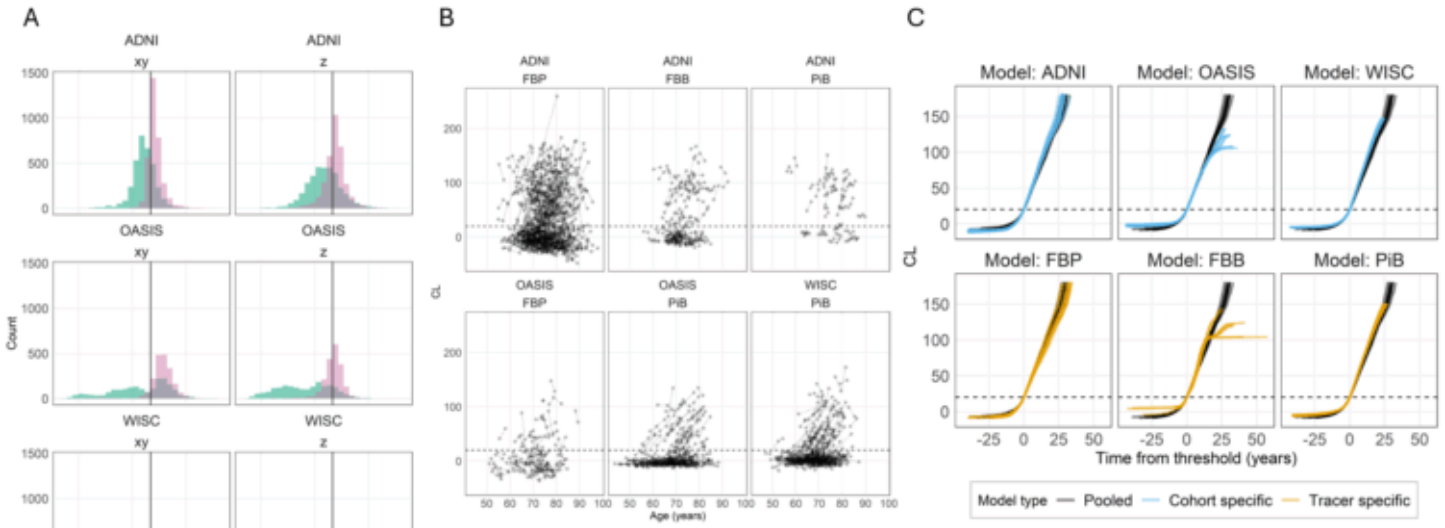
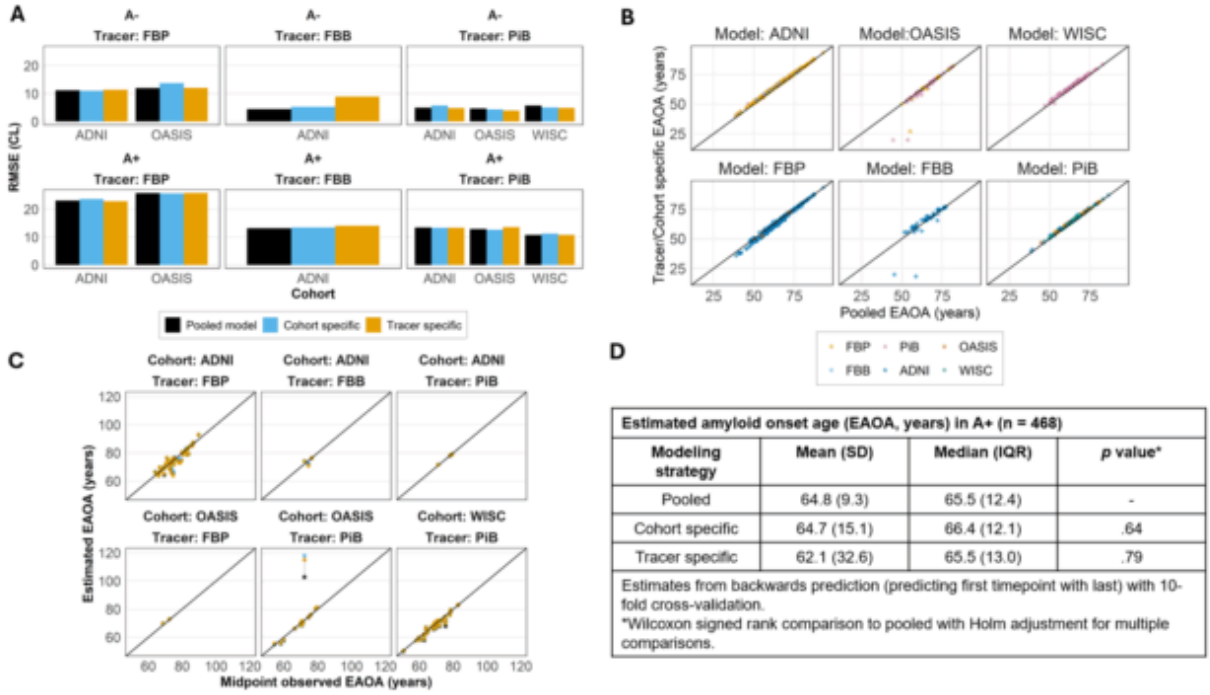


Figure 1. **A**: Spatial resolution estimates before and after differential smoothing of amyloid PET scans to 7mm full-width at half maximum (black line; 80th percentile of estimates from all scans). **B**: Spaghetti plots showing longitudinal data points, individual within-subject trajectories connected with lines. **C**: CL over time trajectories from sampled iterative local approximation (SILA) using the pooled (black, underlaid on each plot to aid comparison) and separate modeling strategies with cohort specific (blue; top row) and tracer specific (gold; bottom row) models. Models were trained using a 10-fold cross-validation scheme and trajectories trained using 9 folds are presented as separate lines on each plot. Dashed line represents the 20 CL positivity threshold. Trajectories using all strategies were similar between 20 and 100 CL, taking mean (SD) = 16.0 (2.5) years between these landmarks across all folds/models.



Estimated amyloid onset age (EAOA, years) in A+ (n = 468)			
Modeling strategy	**Mean (SD)**	**Median (IQR)**	***p* value***
Pooled	64.8 (9.3)	65.5 (12.4)	-
Cohort specific	64.7 (15.1)	66.4 (12.1)	.64
Tracer specific	62.1 (32.6)	65.5 (13.0)	.79
Estimates from backwards prediction (predicting first timepoint with last) with 10-fold cross-validation. *Wilcoxon signed rank comparison to pooled with Holm adjustment for multiple comparisons.			

Figure 2. **A**: Root mean squared error (RMSE) in Centiloids for using backwards prediction with cross-validation. **B**: Comparison of tracer and cohort specific vs pooled models for estimated amyloid onset age (EAOA) in amyloid positive individuals. Six outliers (four ADNI FBB, two OASIS PiB scans) were removed from the plot due to negative EAOA from tracer/cohort specific models – pooled model estimates were within 40-60-year range for these outliers. Solid line on panels B and C represents unity. **C**: For observed A- to A+ converters EAOA is plotted against midpoint accuracy for each model. Scans are connected with vertical lines. **D**: Summary statistics for EAOA in A+ individuals, no statistically significant difference in EAOA distributions was found between models .

Keywords: amyloid, PET, clock, time, risk

126 Cluster-based MK-6240 PET detects early neocortical temporal tau spread

Jackson Thompson[1], Alex Becker[1], Jessie Fanglu Fu[1,2], Michelle Farrell[1], Emma Thibault[1], Elliott Slade[1], Reisa Sperling[1], Julie Price[1,2], Keith Johnson[1]

[1]*Massachusetts General Hospital, Harvard Medical School, Boston, MA, US*
[2]*Athinoula A. Martinos Center for Biomedical Imaging, Charlestown, MA, US*

Background: Tau positron emission tomography (PET) analyses typically evaluate ligand binding as standardized uptake value ratios (SUVr) averaged over large anatomic regions-of-interest (ROI). We are developing an alternative approach that uses voxel-based identification of sources of binding that exceed a threshold and occur in contiguous clusters. We applied this voxel cluster approach to evaluate cross-sectional and longitudinal [^{18}F]MK-6240 data sampled from allocortical medial temporal lobe (MTL) and neocortical temporal lobe structures (NEO). We tested performance of alternative approaches in predicting NEO tau slope from baseline MTL.

Methods: 120 participants underwent baseline MR with Freesurfer parcellation, baseline PiB Aβ-PET, and up to 4 MK-6240 tau-PET (~6-month intervals). All analyses were performed in the left-hemisphere. Regional aggregates for MTL (entorhinal, parahippocampal, amygdala) and NEO (inferior temporal, fusiform) were evaluated using tau SUVr thresholds derived from PiB- individuals (N=80; MTL: mean+1SD=0.919; NEO: mean+2SD=1.15). Suprathreshold voxels were grouped into 4D clusters (spatially contiguous within time or occupying the same location across adjacent timepoints) (Figure1). Total binding (TB) at each timepoint was defined as the sum of SUVr over cluster voxels. Linear mixed models were used to assess NEO SUVr over time as a function of baseline MTL TB or MTL SUVr with Aβ and time.

Results: 4D-clustering yielded longitudinally coherent regions. The timexAβxMTL TB interaction showed a significant association with greater NEO SUVr. In the complementary model replacing MTL TB with MTL SUVr, the interaction was also significant, and lower AIC favored the SUVr model.

Conclusions: A spatiotemporal clustering framework with a "total binding" metric predicts the rise in neocortical tau alongside Aβ, but this method is under development and does not outperform traditional regional SUVr methods in this sample. Future directions will include threshold adjustments, alternative methods of defining longitudinal clusters, and other head-to-head comparisons with regional metrics.

Characteristic	Overall N = 120	PiB- N = 80	PiB+ N = 40	p-value
Diagnosis	CU: 103, MCI: 13, AD: 4	CU: 75, MCI: 4, AD: 1	CU: 28, MCI: 9, AD: 3	-
Age	68 (10) [37–87]	66 (10) [37–84]	72 (9) [52–87]	0.002
Years of Education	16.85 (2.62) [12.00–20.00]	16.73 (2.65) [12.00–20.00]	17.03 (2.62) [12.00–20.00]	0.5
Biological Sex (Female)	69 (56%)	45 (56%)	23 (58%)	0.8
MTL SUVr	0.98 (0.47) [0.52–3.68]	0.81 (0.18) [0.52–1.68]	1.31 (0.66) [0.74–3.68]	<0.001
MTL Cluster TB	925 (1,100) [11–7,075]	518 (504) [11–3,190]	1,737 (1,471) [51–7,075]	<0.001
NEO SUVr	1.12 (0.53) [0.69–4.77]	0.97 (0.11) [0.69–1.37]	1.43 (0.83) [0.75–4.77]	<0.001
NEO Cluster TB	3,197 (4,363) [36–28,457]	1,871 (1,165) [36–7,916]	5,849 (6,671) [456–28,457]	<0.001
Amyloid (FLR DVR)	1.22 (0.31) [0.96–2.12]	1.04 (0.04) [0.96–1.14]	1.60 (0.27) [1.16–2.12]	<0.001
Amyloid (CL)	19 (33) [-9–113]	0 (4) [-9–11]	59 (28) [13–113]	<0.001
# Tau Scans	2.68 (0.92) [1.00–4.00]	2.59 (0.94) [1.00–4.00]	2.85 (0.86) [1.00–4.00]	0.12
Time between first and last tau scan (years)	1.38 (1.07) [0.00–4.29]	1.25 (1.05) [0.00–4.29]	1.62 (1.06) [0.00–3.55]	0.080

Table 1. Demographic and imaging characteristics stratified by amyloid status. Values are presented as mean (SD) [range] or n (%). P-values reflect group comparisons between *PiB−* and *PiB+* participants using Wilcoxon rank-sum or Pearson's chi-squared tests, as appropriate. PiB+ was defined as PiB FLR DVR > 1.15. The overall sample included 120 participants from the Harvard Aging Brain Study 2 (80 PiB−; 40 PiB+). Diagnosis indicates if participants have a clinical diagnosis of mild cognitive impairment (MCI) or Alzheimer's disease (AD), or otherwise cognitively unimpaired (CU). PiB+ participants were significantly older than PiB− participants ($p = 0.002$), with no group differences in sex or years of education. SUVr in the composite regions (MTL SUVr, NEO ROI SUVr) and the sum of SUVr in the cluster (total binding, TB) were substantially greater in PiB+ participants ($p < 0.001$).

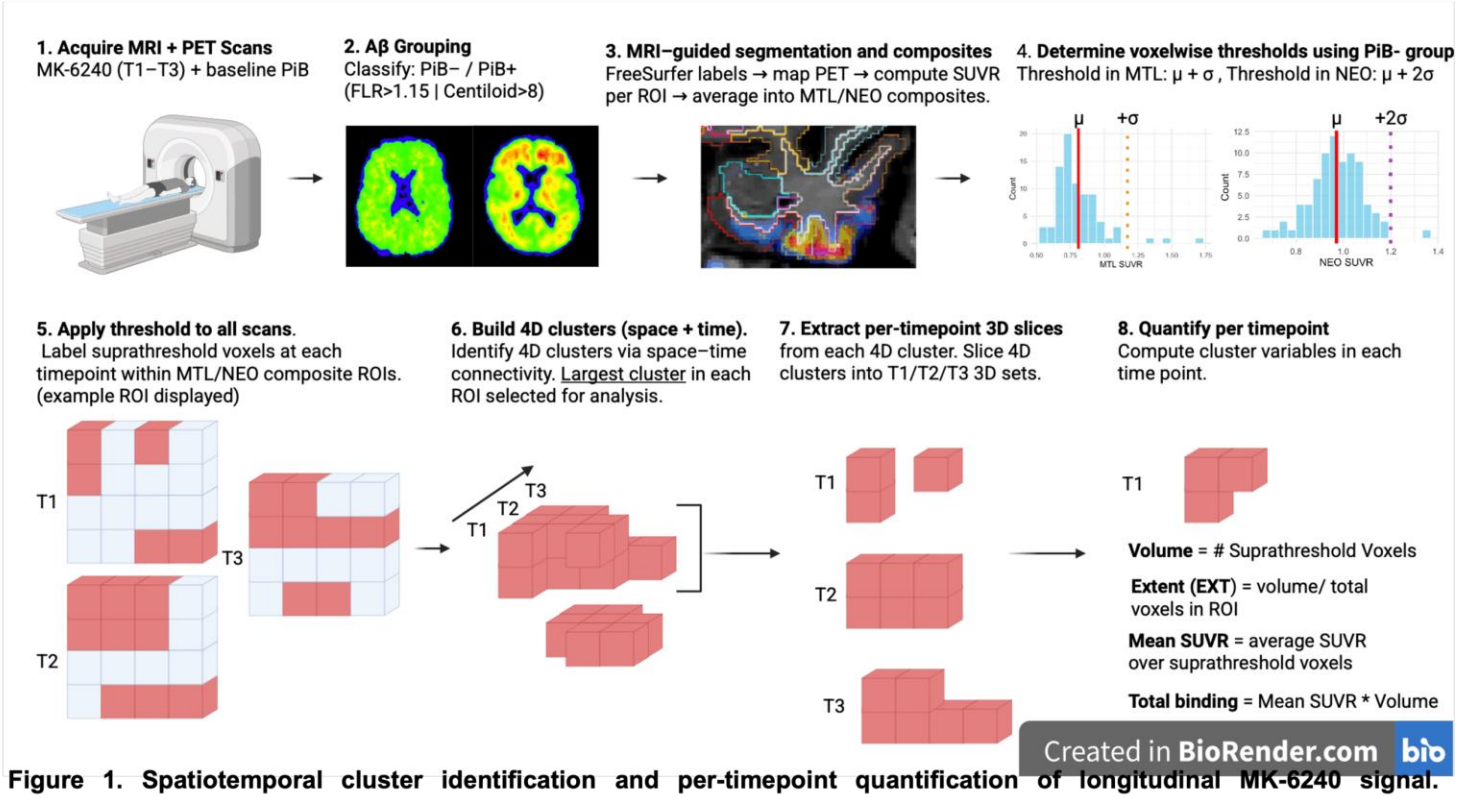
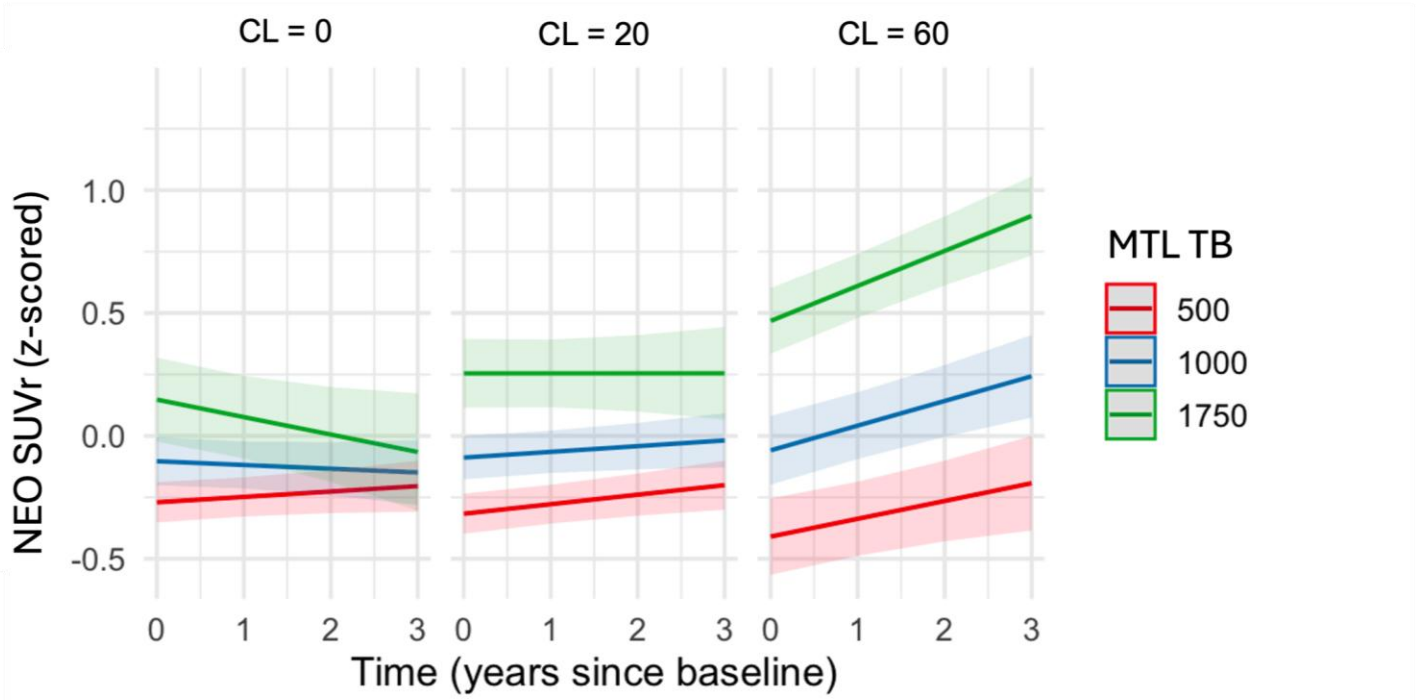


Figure 1. Spatiotemporal cluster identification and per-timepoint quantification of longitudinal MK-6240 signal. (1) Each participant underwent at least three longitudinal MK-6240 tau PET scans (~6 months apart; T1–T3) and one baseline PiB amyloid PET scan. (2) Participants were classified as PiB– or PiB+ based on FLR DVR > 1.15 or Centiloid > 8. (3) T1-weighted structural MRI was processed with FreeSurfer to obtain automated cortical and subcortical segmentations. Regional SUVRs were computed by mapping MK-6240 PET to each subject's MRI space and averaging within segmentation-defined **composites**: medial temporal lobe (MTL; entorhinal, parahippocampal, amygdala) and neocortical (NEO; inferior temporal, fusiform). (4) Within each composite, a voxelwise threshold for cluster detection was set to mean + 1SD (MTL) and mean + 2 SD (NEO) of SUVRs computed across all voxels in PiB– individuals; (5) voxels exceeding this value were designated suprathreshold. (6) Suprathreshold voxels were then grouped into four-dimensional (x, y, z, time) clusters using spatiotemporal connectivity: a suprathreshold voxel was included if it was spatially contiguous with another suprathreshold voxel within the same timepoint, or at the same spatial location as a suprathreshold voxel in an adjacent timepoint. After identifying each 4D cluster, (7) we isolated its 3D suprathreshold voxels at each timepoint and computed the cluster's volume, mean SUVR, and total binding separately for T1, T2, and T3.



Outcome	Model	β	SE	p	AIC
NEO SUVr	t × FLR × **MTL TB**	0.0785	0.0122	<0.001	107.0
NEO SUVr	t × FLR × **MTL SUVr**	0.0800	0.0126	<0.001	100.8

Figure 2. Neocortical tau trajectories from the MTL cluster model with comparison to an MTL SUVr model. Linear mixed effects model with random intercepts displayed in the table above, not included is the correction of age and APOE ε4 status, and all inputs are z-scored. Panels display model-predicted NEO SUVr (z-scored) over time (years since baseline) at representative centeloid (CL) values, conditioning on three levels of baseline MTL total binding (TB); ribbons are 95% CIs. The table summarizes the three-way interaction and model fit for two alternative specifications with the same outcome (NEO SUVr). Both interactions are significant and directionally consistent; lower AIC favors the SUVr model in this sample, while the figure illustrates the TB model to emphasize the spatiotemporal 4D–cluster approach.

Keywords: tau, cluster, MK-6240, SUVr, MTL

127 Gaussian smoothing and partial volume correction modify relationships of tau burden with biological variables in longitudinal multi-site studies of 18F-Flortaucipir PET

Weiquan Luo[1], Charles Laymon[1], Suzanne Baker[2], Ann Cohen[1], Victor Villemagne[1], Brian Lopresti[1], Howard Aizenstein[1], Dana Tudorascu[1], Davneet Minhas[1]

[1]*University of Pittsburgh, Pittsburgh, PA, US*
[2]*Molecular Biophysics and Integrated Bioimaging, Lawrence Berkeley National Laboratory, Berkeley, CA, US*

Introduction: In multi-site studies of tau PET, scanner-specific Gaussian smoothing reduces inter-scanner variability but increases partial volume spill-over contamination between neighboring regions. Here, we hypothesize that Gaussian smoothing and partial volume correction (PVC) modify the relationship of biological variables of interest (age, sex, Ab status) with tau burden in longitudinal multi-site multi-scanner studies of ^{18}F-Flortaucipir (FTP), which exhibits age- and sex- related off-target binding.

Method: Native-resolution FTP images (Raw) from 487 ADNI participants with up to 6-timepoint longitudinal imaging were included in analyses (Table 1). Image-processing methods evaluated were: (1) smoothing of PET data to an effective resolution of 8 mm FWHM (SMO) and (2) tau-specific PVC (Baker et al, 2017).

SUVR outcomes were extracted for all methods from composite Braak regions. A linear mixed model with subject as random intercept was used to regress regional SUVR on age and sex for FTP outcomes from each image-processing pipeline separately. Significances of model coefficients (Type-III ANOVA) were evaluated across groups stratified by Ab status (+/-) and cognitive status (cognitively unimpaired [CU] versus impaired [CI]). An advanced mixed model incorporating outcomes from all image-processing pipelines was developed via stepwise procedures (LRT) to test for pipeline interactions with age, sex, and amyloid status separately.

Result: For the CI-Ab+ group, Gaussian smoothing attenuated and even eliminated age and sex relationships with FTP SUVR in early Braak regions, which were significant with Raw and PVC image-processing pipelines (Figure 1). Image-processing pipeline significantly interacted with age and Ab status for all Braak regions and with sex for Braak regions I & V in predicting FTP SUVR (Table 2).

Conclusion: Image-processing and harmonization methodology modifies the apparent relationship between FTP SUVR and age, sex, and amyloid status. Care should be taken to identify the most appropriate methods of analysis in multi-site tau PET longitudinal studies.

Table 1: Demographic with amyloid status differentiation by Biological factors.

	Group		
	Aβ-	Aβ+	p-value*
Age at baseline, Mean (SD)	72.5 (7.4)	74.3 (7.4)	0.008
Sex, N (%**)			0.836
Female	143 (50.4)	105 (51.7)	
Male	141 (49.6)	98 (48.3)	
APOE4 positivity, N (%**)			<0.001
Non-APOE4 carrier	206 (72.5)	70 (34.5)	
APOE4 carrier	78 (27.5)	133 (65.5)	
Diagnosis, N (%**)			<0.001
Cognitively unimpaired [CU]	186 (65.5)	84 (41.4)	
Subjective Memory Concern [SMC]	8 (2.8)	11 (5.4)	
Early Mild Cognitive Impairment [EMCI]	16 (5.6)	12 (5.9)	
Late Mild Cognitive Impairment [LMCI]	12 (4.2)	6 (3.0)	
Mild Cognitive Impairment [MCI]	54 (19.0)	59 (29.1)	
Alzheimer's Disease [AD]	8 (2.8)	31 (15.3)	

*p-values is calculated using Welch two sample t-test for age at baseline differs between amyloid groups and using chi-square test for testing the propotion of Sex, APOE4 positivity, and diagnosis group differs between Amyloid group.

**calcluated within amyloid status group

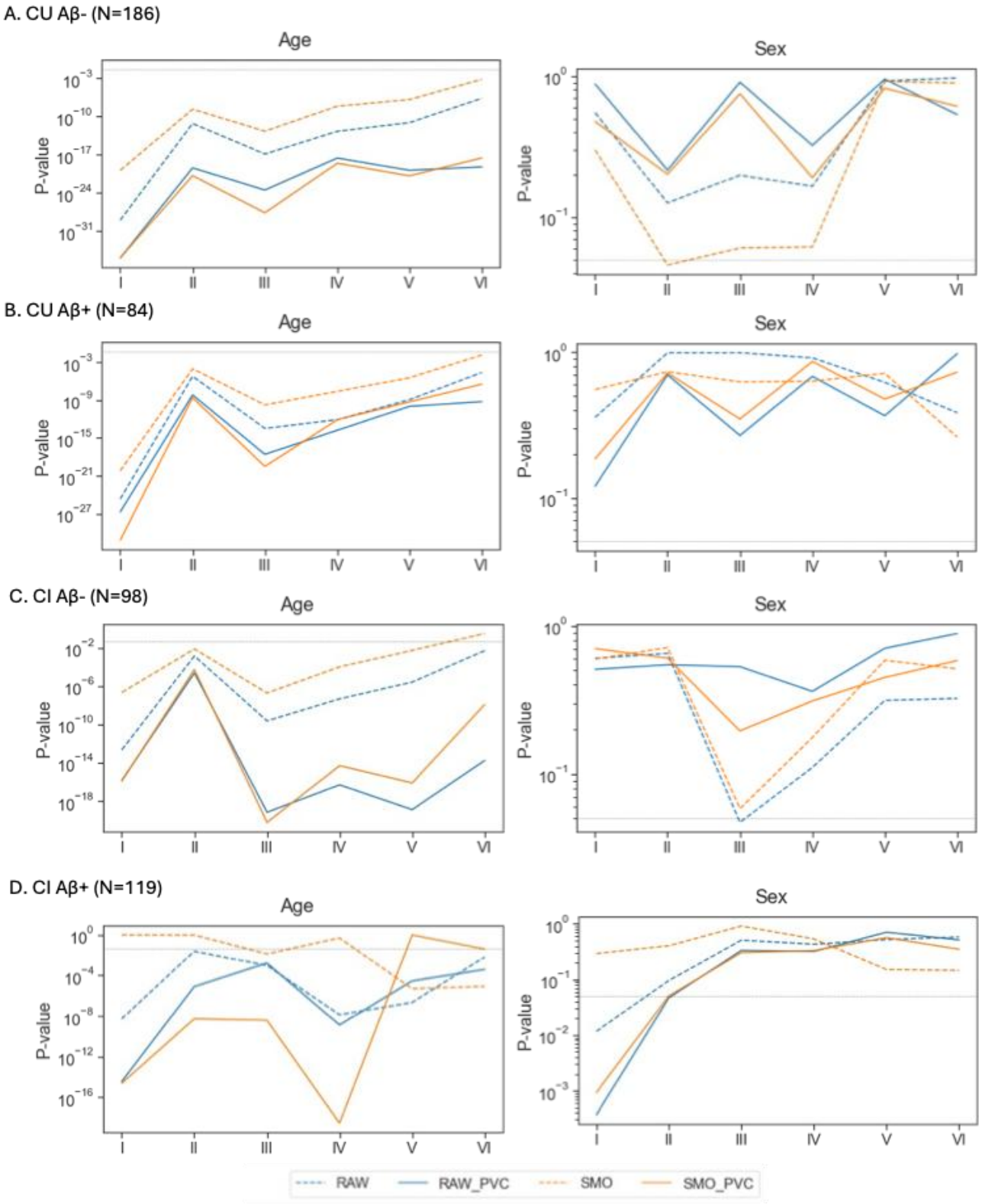


Figure 1: P-value of age and sex coefficient using Type-III ANOVA in linear mixed models: SUVR~ Age + Sex + (1 | Subject) with stratification by cognitive status (CN vs CI) and Aβ status (+ vs -) groups. The horizontal line signifies a significance level of p-value=0.05 (lower is more significant). Compared to RAW, PVC increase the significance of age effect except at Braak III&V in CI Aβ+ group, whereas SMO reduce the significance of age effect except at Braak V&VI in CI Aβ+ group. Within CI group, SMO changes age effect to insignificance at Aβ- Braak VI and Aβ+ Braak I,&II&IV. SMO increase sex effect significance for CN Aβ- group, leading changes to be significant at Braak II. Inversely, SMO reduce the significance of sex effect for CI group except for late region in Aβ+ group, leading change to be insignificant at Braak1 in Aβ+ group.

Table 2: Coefficients and standard errors extracted from linear mixed effect models, including subject as random intercept, with interactions between pipeline and biological variables including age, sex and amyloid status. P-values for fixed effects were obtained from Type III ANOVA F-tests. Post-hoc pairwise comparisons between pipeline levels were performed using t-tests of estimated marginal means, comparing each level to the RAW reference and adjusting for multiple testing via the Holm–Bonferroni method. Coefficients are colored according to p-value (adjusted): red ($p > 0.05$), blue ($0.01 < p < 0.05$) and green ($p < 0.01$). (A) Pipeline-age interaction are significant for all Braak regions. (B) Pipeline-sex interaction is significant only for Braak I and Braak V. (C) Pipeline-amyloid interaction is significant for all Braak regions.

A. Pipeline-Age interaction

Variable, Level	Braak I	Braak II	Braak III	Braak IV	Braak V	Braak VI
(Intercept)	0.145 (0.141)	0.640 (0.080)	0.205 (0.125)	0.439 (0.101)	0.289 (0.128)	0.682 (0.088)
Pipeline (ref = RAW)						
SMO	0.116 (0.073)	0.062 (0.039)	0.058 (0.062)	0.076 (0.049)	0.093 (0.065)	0.125 (0.048)
RAW PVC	-0.475 (0.073)	-0.213 (0.039)	-0.071 (0.062)	-0.075 (0.049)	0.066 (0.065)	-0.122 (0.048)
SMO PVC	-0.551 (0.073)	-0.212 (0.039)	-0.050 (0.062)	0.006 (0.049)	0.234 (0.065)	-0.020 (0.048)
Age	0.015 (0.002)	0.009 (0.001)	0.014 (0.002)	0.011 (0.001)	0.012 (0.002)	0.006 (0.001)
Sex (ref = female)	0.418 (0.176)	0.347 (0.101)	0.416 (0.157)	0.310 (0.127)	0.373 (0.161)	0.027 (0.110)
Amyloid status (ref: -)	-0.780 (0.183)	-0.352 (0.105)	-0.934 (0.165)	-1.079 (0.133)	-0.545 (0.168)	-0.022 (0.114)
Pipeline:Age						
SMO:Age	-0.002 (0.001)	-0.001 (0.001)	-0.001 (0.001)	-0.002 (0.001)	-0.002 (0.001)	-0.002 (0.001)
RAW PVC:Age	0.009 (0.001)	0.004 (0.001)	0.003 (0.001)	0.003 (0.001)	0.001 (0.001)	0.003 (0.001)
SMO PVC:Age	0.011 (0.001)	0.004 (0.001)	0.003 (0.001)	0.002 (0.001)	-0.000 (0.001)	0.001 (0.001)
Age:Sex	-0.006 (0.002)	-0.005 (0.001)	-0.005 (0.002)	-0.004 (0.002)	-0.005 (0.002)	-0.000 (0.001)
Age:Amyloid Status	0.015 (0.002)	0.007 (0.001)	0.016 (0.002)	0.018 (0.002)	0.011 (0.002)	0.002 (0.001)

B. Pipeline-Sex interaction

level	Braak I	Braak II	Braak III	Braak IV	Braak V	Braak VI
(Intercept)	-0.183 (0.136)	0.514 (0.077)	0.128 (0.120)	0.387 (0.097)	0.314 (0.122)	0.648 (0.084)
Pipeline (ref = RAW)						
SMO	-0.076 (0.010)	-0.027 (0.006)	-0.044 (0.009)	-0.049 (0.007)	-0.045 (0.009)	-0.029 (0.007)
RAW PVC	0.240 (0.010)	0.073 (0.006)	0.130 (0.009)	0.127 (0.007)	0.159 (0.009)	0.079 (0.007)
SMO PVC	0.265 (0.010)	0.097 (0.006)	0.160 (0.009)	0.137 (0.007)	0.179 (0.009)	0.068 (0.007)
Age	0.019 (0.002)	0.011 (0.001)	0.015 (0.002)	0.012 (0.001)	0.011 (0.002)	0.006 (0.001)
Sex (ref = female)	0.427 (0.179)	0.342 (0.102)	0.414 (0.158)	0.303 (0.128)	0.355 (0.161)	0.023 (0.110)
Amyloid status (ref: -)	-0.745 (0.186)	-0.342 (0.106)	-0.928 (0.165)	-1.073 (0.134)	-0.545 (0.168)	-0.016 (0.114)
Pipeline:Sex						
SMO:Sex	0.008 (0.015)	0.008 (0.008)	0.004 (0.012)	0.001 (0.010)	-0.000 (0.013)	0.003 (0.010)
RAW PVC:Sex	-0.042 (0.015)	0.007 (0.008)	-0.008 (0.012)	0.011 (0.010)	0.028 (0.013)	0.002 (0.010)
SMO PVC:Sex	-0.011 (0.015)	0.010 (0.008)	0.010 (0.012)	0.021 (0.010)	0.045 (0.013)	0.017 (0.010)
Age:Sex	-0.006 (0.002)	-0.005 (0.001)	-0.005 (0.002)	-0.004 (0.002)	-0.005 (0.002)	-0.000 (0.001)
Age:Amyloid Status	0.015 (0.002)	0.007 (0.001)	0.016 (0.002)	0.017 (0.002)	0.011 (0.002)	0.002 (0.001)

C. Pipeline-Amyloid interaction

level	Braak I	Braak II	Braak III	Braak IV	Braak V	Braak VI
(Intercept)	-0.150 (0.130)	0.526 (0.076)	0.157 (0.115)	0.407 (0.094)	0.340 (0.119)	0.656 (0.084)
Pipeline (ref = RAW)						
SMO	-0.051 (0.009)	-0.020 (0.005)	-0.029 (0.008)	-0.038 (0.006)	-0.037 (0.008)	-0.028 (0.006)
RAW PVC	0.123 (0.009)	0.046 (0.005)	0.048 (0.008)	0.075 (0.006)	0.105 (0.008)	0.061 (0.006)
SMO PVC	0.161 (0.009)	0.066 (0.005)	0.084 (0.008)	0.093 (0.006)	0.130 (0.008)	0.056 (0.006)
Age	0.019 (0.002)	0.011 (0.001)	0.015 (0.002)	0.012 (0.001)	0.011 (0.002)	0.006 (0.001)
Sex (ref = female)	0.422 (0.172)	0.347 (0.100)	0.412 (0.152)	0.303 (0.124)	0.358 (0.157)	0.027 (0.110)
Amyloid status (ref: -)	-0.922 (0.179)	-0.391 (0.105)	-1.091 (0.159)	-1.182 (0.130)	-0.678 (0.165)	-0.043 (0.114)
Pipeline						
SMO:Amyloid Status	-0.048 (0.014)	-0.007 (0.008)	-0.028 (0.012)	-0.023 (0.010)	-0.018 (0.013)	0.000 (0.010)
RAW PVC:Amyloid Status	0.224 (0.014)	0.070 (0.008)	0.181 (0.012)	0.132 (0.010)	0.154 (0.013)	0.045 (0.010)
SMO PVC:Amyloid Status	0.228 (0.014)	0.081 (0.008)	0.186 (0.012)	0.124 (0.010)	0.163 (0.013)	0.048 (0.010)
Age:Sex	-0.006 (0.002)	-0.005 (0.001)	-0.005 (0.002)	-0.004 (0.002)	-0.005 (0.002)	-0.000 (0.001)
Age:Amyloid Status	0.016 (0.002)	0.007 (0.001)	0.017 (0.002)	0.018 (0.002)	0.011 (0.002)	0.002 (0.001)

Keywords: PET, tau, flortaucipir, smoothing, partial volume correction

128 No detectable association between BDNF Val66Met and hippocampal volume or regional tau PET in ADNI after propensity score matching and ComBat harmonization

Yushui Han[1], Davneet Minhas[2], Charles Laymon[2,3], Victor Villemagne[4], Dana Tudorascu[1,4,5]

[1]*Intelligent Systems Program, University of Pittsburgh, Pittsburgh, PA, US*
[2]*Department of Radiology, University of Pittsburgh, Pittsburgh, PA, US*
[3]*Department of Bioengineering, University of Pittsburgh, Pittsburgh, PA, US*
[4]*Department of Psychiatry, University of Pittsburgh School of Medicine, Pittsburgh, PA, US*
[5]*Department of Biostatistics, University of Pittsburgh, Pittsburgh, PA, US*

Background: Brain-derived neurotrophic factor (BDNF) Val66Met (rs6265) reduces activity-dependent BDNF release and has been linked to reduced hippocampal resilience. Imaging genetics results in sporadic AD are mixed, with some reports of associations in amyloid-positive (A+) subsamples but many null findings. We tested rs6265 associations with MRI and tau PET at baseline in ADNI.

Methods: We used ADNI participants with rs6265 genotypes, baseline T1 MRI (FreeSurfer v6.0; intracranial-volume–adjusted hippocampal volume) and baseline ^18F-flortaucipir PET preprocessed per ADNI conventions (6-mm smoothing; region-based voxelwise PVC). SUVRs used inferior cerebellar gray; the meta-temporal composite combined entorhinal, inferior/middle temporal, fusiform, and temporal pole ROIs. Amyloid positivity was defined by baseline Centiloid (CL) ≥20. Within the A+ subset, we used 1:1 nearest-neighbor propensity-score matching (logit PS; caliper 0.2 SD) to balance withMet and noMet on age, sex, education, and APOE4. Regional measures were harmonized with neuroCombat while preserving age, sex, diagnosis, and APOE4. Primary outcomes were hippocampal volume and a Box–Cox–motivated transform of tau to better approximate normality and stabilize variance. Associations were estimated with linear models adjusted for age, sex, education, APOE4, and diagnosis, with sensitivity models additionally adjusting for continuous CL.

Results: In A+ matched participants (Table 1), covariate balance was good (median |SMD|=0.047; max |SMD|=0.083). rs6265 showed no association with hippocampal volume (β=139.0, 95% CI −184.1 to 462.2; p=0.395). Using the transformed tau outcome, rs6265 was not significant in the matched A+ set (β=0.037, −0.036 to 0.109; p=0.320) and remained non-significant after additional Centiloid adjustment (β=0.060, −0.002 to 0.123; p=0.056). Estimates within CN, MCI, and AD strata were small with confidence intervals spanning zero.

Conclusions: In ADNI amyloid-positive participants, after propensity-score matching and harmonization, BDNF Val66Met shows no detectable association with hippocampal volume or transformed meta-temporal tau at

baseline. Any rs6265 effects in sporadic AD are likely small or context dependent.

Table 1. Demographic and clinical characteristics of the amyloid-positive matched cohort (withMet vs noMet; N=120).

	noMet (N=60)	withMet (N=60)	Overall (N=120)
Diagnosis			
AD	10 (16.7%)	11 (18.3%)	21 (17.5%)
CN	4 (6.7%)	8 (13.3%)	12 (10.0%)
MCI	46 (76.7%)	41 (68.3%)	87 (72.5%)
APOE4 (ε4 allele count)			
0 alleles	20 (33.3%)	19 (31.7%)	39 (32.5%)
1 allele	30 (50.0%)	31 (51.7%)	61 (50.8%)
2 alleles	10 (16.7%)	10 (16.7%)	20 (16.7%)
Age (years)			
Mean (SD)	73.6 (7.35)	73.3 (7.63)	73.5 (7.46)
Median [Min, Max]	74.3 [55.3, 89.1]	73.5 [56.0, 89.2]	73.8 [55.3, 89.2]
Sex			
Female	31 (51.7%)	36 (60.0%)	67 (55.8%)
Male	29 (48.3%)	24 (40.0%)	53 (44.2%)
Education (years)			
Mean (SD)	16.7 (2.24)	16.5 (2.49)	16.6 (2.36)
Median [Min, Max]	17.0 [12.0, 20.0]	16.0 [12.0, 20.0]	16.0 [12.0, 20.0]

Keywords: BDNF Val66Met (rs6265), tau PET, hippocampal volume, ADNI, ComBat harmonization

129 Centiloid and SUVR amyloid harmonization techniques comparisons for head-to-head unequally spaced data

Yushui Han[1], Brian Lopresti[2], Pierrick Bourgea[3], Charles Laymon[2,4], Victor Villemagne[5], Ahmad Tafti[1], Davneet Minhas[2], Dana Tudorascu[1,5,6]

[1]*Intelligent Systems Program, University of Pittsburgh, Pittsburgh, PA, US*
[2]*Department of Radiology, University of Pittsburgh, Pittsburgh, PA, US*
[3]*Biomedical Informatics Group, CSIRO eHealth Research Centre, Brisbane, Australia*
[4]*Department of Bioengineering, University of Pittsburgh, Pittsburgh, PA, US*
[5]*Department of Psychiatry, University of Pittsburgh School of Medicine, Pittsburgh, PA, US*
[6]*Department of Biostatistics, University of Pittsburgh, Pittsburgh, PA, US*

Background: Scanner differences can bias amyloid SUVRs and the derived Centiloid (CL) values, complicating data pooling and use of universal thresholds. LongCombat (LC) and statistical and Machine Learning (ML) calibrators can be used for multiple and single-feature approaches to reduce inter-scanner bias while preserving ordering. Herein, we investigated the performance of LC on ROI SUVRs and ML on CL features. Since CL is a single scalar, LC is not appropriate.

Methods: We analyzed head-to-head PET data from 67 participants scanned on two scanners (HR+ and mCT) with a mean inter-scan interval of 2.0 years (Table 1). We harmonized SUVRs with LongComBat, modeling inter-scan interval (years) and subject as covariates, and quantified cross-scanner agreement by root mean square error (RMSE) and time-adjusted Bland–Altman limits of agreement (LoA) residualized for inter-scan interval. For CL, we compared two single-feature harmonization paradigms: (i) symmetric pooling via quantile regression and (ii) asymmetric reference calibration via isotonic regression (HR+→mCT). Performance was assessed against mCT as reference using RMSE, residual bias (mean difference) and SD of differences. Cross-scanner agreement was quantified by Pearson correlation between HR+ and mCT (SUVR per ROI; CL per subject).

Table 1. Participant demographics and scan characteristics by scanner (Biograph mCT vs HR+, head-to-head cohort, N=67).

	Biograph mCT (n=67)	HR+ (n=67)
Age: mean (SD)	77.0 (4.76)	74.2 (4.87)
Education: mean (SD)	15.6 (2.67)	15.6 (2.67)
Centiloid (mean, SD)	7.0 (21.13)	9.6 (21.86)
Time gap between scanners (years, mean, SD)	-2.0 (2.29)	-2.0 (2.29)
Race: count (%)		
African American	*19 (28.4%)*	*19 (28.4%)*
Caucasian	*48 (71.6%)*	*48 (71.6%)*
ApoE4: count (%)		
ApoE4 Carrier	*16 (23.9%)*	*16 (23.9%)*
Not ApoE4 Carrier	*51 (76.1%)*	*51 (76.1%)*
Sex: count (%)		
Female	*46 (68.7%)*	*46 (68.7%)*
Male	*21 (31.3%)*	*21 (31.3%)*
PIB status: count (%)		
neg	*55 (82.1%)*	*55 (82.1%)*
pos	*12 (17.9%)*	*12 (17.9%)*

Results: Across ROI SUVRs, median RMSE = 0.1259 (raw) vs 0.1275 (post), time-adjusted LoA width unchanged and ROI differences were small (e.g., Precuneus 0.1305→0.1331; Lateral Temporal 0.0934→0.0927). Cross-scanner correlation was unchanged (median r = 0.909 pre vs 0.900 post).

For CL, quantile regression yielded RMSE = 4.22, MAE = 3.00, SD_diff = 4.20, r = 0.915 and bias = 0.68 while isotonic regression achieved RMSE = 5.16, MAE = 3.52, SD_diff = 5.20, r = 0.969 and bias ≈ 0.

Conclusion: In this paired two-scanner study, LongComBat harmonization for SUVR did not perform well. For CL harmonization, quantile regression yielded the lowest error, while isotonic provided higher correlation with near-zero bias.

Keywords: amyloid PET, Centiloid, SUVR, LongComBat harmonization, quantile regression

130 Plasma amyloid beta 42/40 modifies the associations between MRI biomarkers and subsequent cognitive impairment: a neuroimaging-wide longitudinal study in the BLSA

Tugce Duran[1], Murat Bilgel[1], Yang An[1], Sridhar Kandala[1], Christos Davatzikos[2], Bennett Landman[3], Guray Erus[2], Luigi Ferrucci[1], Abhay Moghekar[4], Keenan Walker[1], Susan Resnick[1]

[1]*National Institute on Aging, Baltimore, MD, US*
[2]*University of Pennsylvania, Philadelphia, PA, US*
[3]*Vanderbilt University, Nashville, TN, US*
[4]*Johns Hopkins University, Baltimore, MD, US*

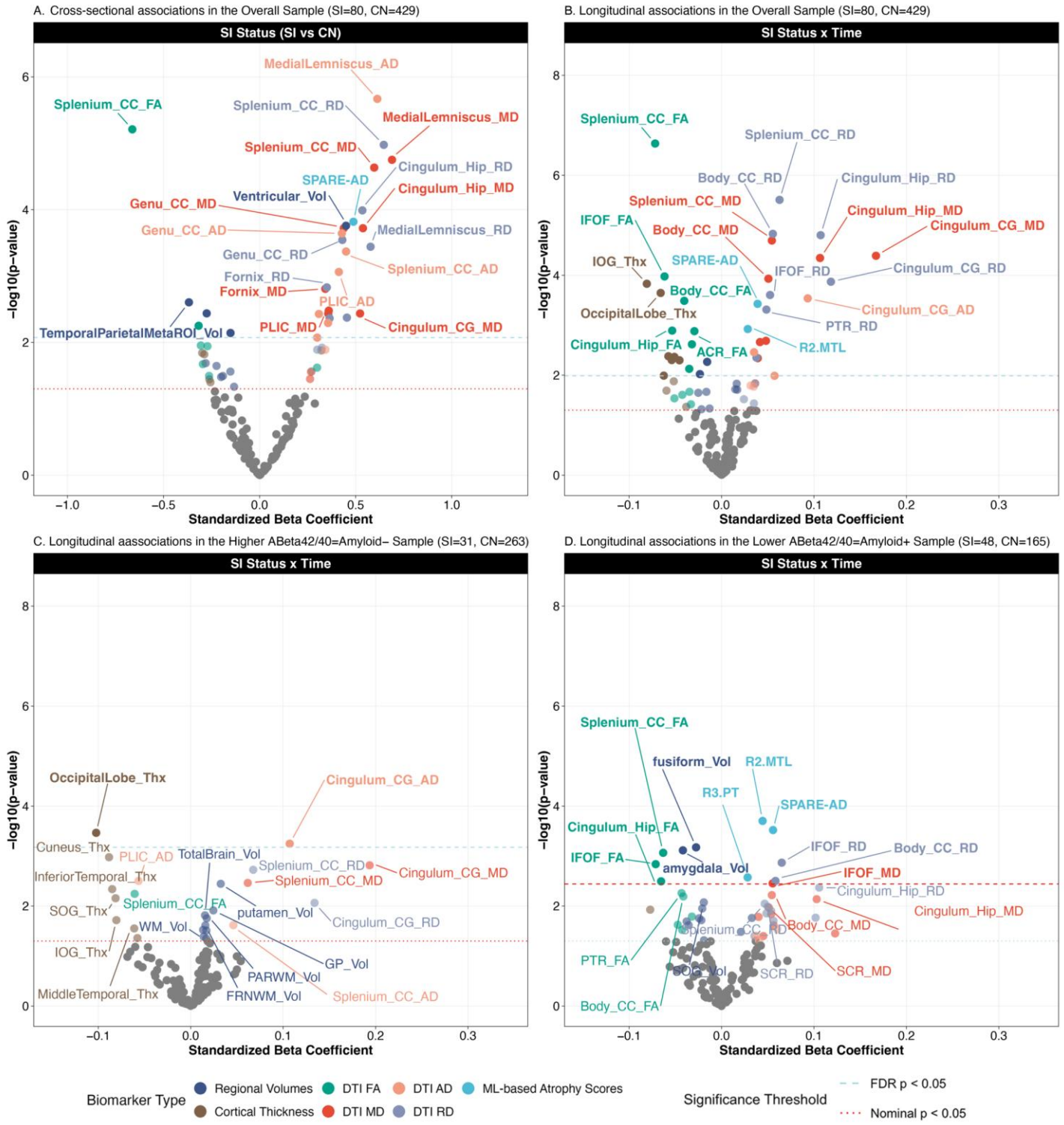
Background: Blood-based amyloid beta (Aβ) enables more accessible, CSF/PET-concordant diagnostics for Alzheimer's disease research. However, the extent to which MRI trajectories are strongly associated with subsequent cognitive impairment (SI) within plasma Aβ strata remains unclear.

Objective: To identify longitudinal MRI biomarkers distinguishing SI among older adults with higher vs lower plasma Aβ burden.

Methods: We analyzed 509 Baltimore Longitudinal Study of Aging (BLSA) participants aged ≥50 who were cognitively normal (CN) at baseline and had longitudinal cognitive assessments and 3T MRI. Brain macrostructure was quantified from T1-weighted images (cortical thickness, regional volumes, and Alzheimer's-related atrophy pattern scores); white matter (WM) microstructure was assessed with diffusion tensor imaging (DTI). A total of 154 MRI biomarkers were examined. Baseline plasma Aβ42/40 defined amyloid burden strata using a cutoff value of 0.05259 (by ROC analysis), optimized for predicting amyloid PET positivity. Over a median 4.6-year follow-up, 80 individuals developed SI. We examined associations between cognitive status (SI vs CN-stable) and longitudinal MRI biomarkers, adjusting for confounders and stratified by plasma Aβ42/40 status.

Results: Across the overall cohort, SI was associated with greater longitudinal decline on standardized DTI measures, most prominently within the corpus callosum, cingulum bundle, and inferior fronto-occipital fasciculus (**Figure 1**). Stratification by plasma Aβ42/40 revealed distinct MRI signatures: In Aβ+ individuals, temporal lobe volume loss and Alzheimer's-related atrophy scores (SPARE-AD and R2 MTL indices) showed stronger associations with SI than in CN-stable (Aβ+) individuals. In contrast, within the Aβ- group, only occipital thinning and increased diffusivity in the cingulate gyrus of the cingulum were most significantly associated with SI.

Conclusions: Longitudinal MRI provides amyloid-contextualized prognostic information. Incorporating plasma Aβ to capture MRI signatures may enhance risk stratification and screening for amyloid-targeted trials.



Volcano plots displaying cross-sectional and longitudinal associations between SI and neuroimaging biomarkers for the overall and plasma Aβ42/40 sample.

Keywords: plasma Aβ42/40, cortical thickness, regional volumes, diffusion tensor imaging, ML-based atrophy pattern scores

131 High-resolution NAV template using the Siemens Biograph Vision

Pierrick Bourgeat[1], Christopher Rowe[2], Ishara Paranawithana[1,2], Azadeh Feizpour[2], Kun Huang[2], Victor Villemagne[3], Jurgen Fripp[1], Vincent Dore[1,2]

[1]*Commonwealth Scientific and Industrial Research Organisation, Herston, Australia*
[2]*Austin Health, Heidelberg, Australia*
[3]*University of Pittsburgh, Pittsburgh, PA, US*

Background: MR-less PET quantification pipelines, such as CapAIBL, tend to be more sensitive to scanner changes due to their higher reliance on the PET scan appearance during spatial normalisation. We investigated if a high-resolution NAV adaptive template could be optimised to match new scans resolution, improving concordance with standard SPM quantification across scanners. Additionally, we investigated the impact of using a robust means (discarding top/bottom 15%) to reduce scanner effects, compared to standard means.

Method: 207 cognitively unimpaired participants from AIBL+ADNeT were imaged on the Siemens Biograph Vision using NAV, with 160 Aβ- (CL<20) and 43 Aβ+. All scans were spatially normalised using MR-based CapAIBL. The means of the Aβ- and Aβ+ were used to compute new negative and positive templates (Fig1). 558 NAV scans (excluding those used to build the template) from 5 scanners, were quantified using standard SPM pipeline and CapAIBL. For each scan, an optimiser was used to define the weight between the Aβ- and Aβ+ template, to best match the pattern of Aβ before non-rigid registration (standard CapAIBL pipeline). Additionally, the optimiser was used to smooth the high-resolution template to match target scan resolution, before non-rigid registration. Standard and robust means for CL calculation were compared. The standard adaptive PIB template was compared to the high-resolution NAV template with and without resolution matching. The impact of scanner was assessed using ANCOVA.

Results: In all scenarios, using robust means increased variability due to scanners, compared to SPM. The high-resolution NAV template increased agreement and reduced bias compared to SPM both with and without resolution matching (Fig2), but only resolution matching led to a non-significant contribution of scanner in ANCOVA intercept.

Conclusions: Standard mean reduces variability due to different scanners and should be preferred. High-resolution NAV adaptive template can further reduce variability due to differences in scanner resolutions.

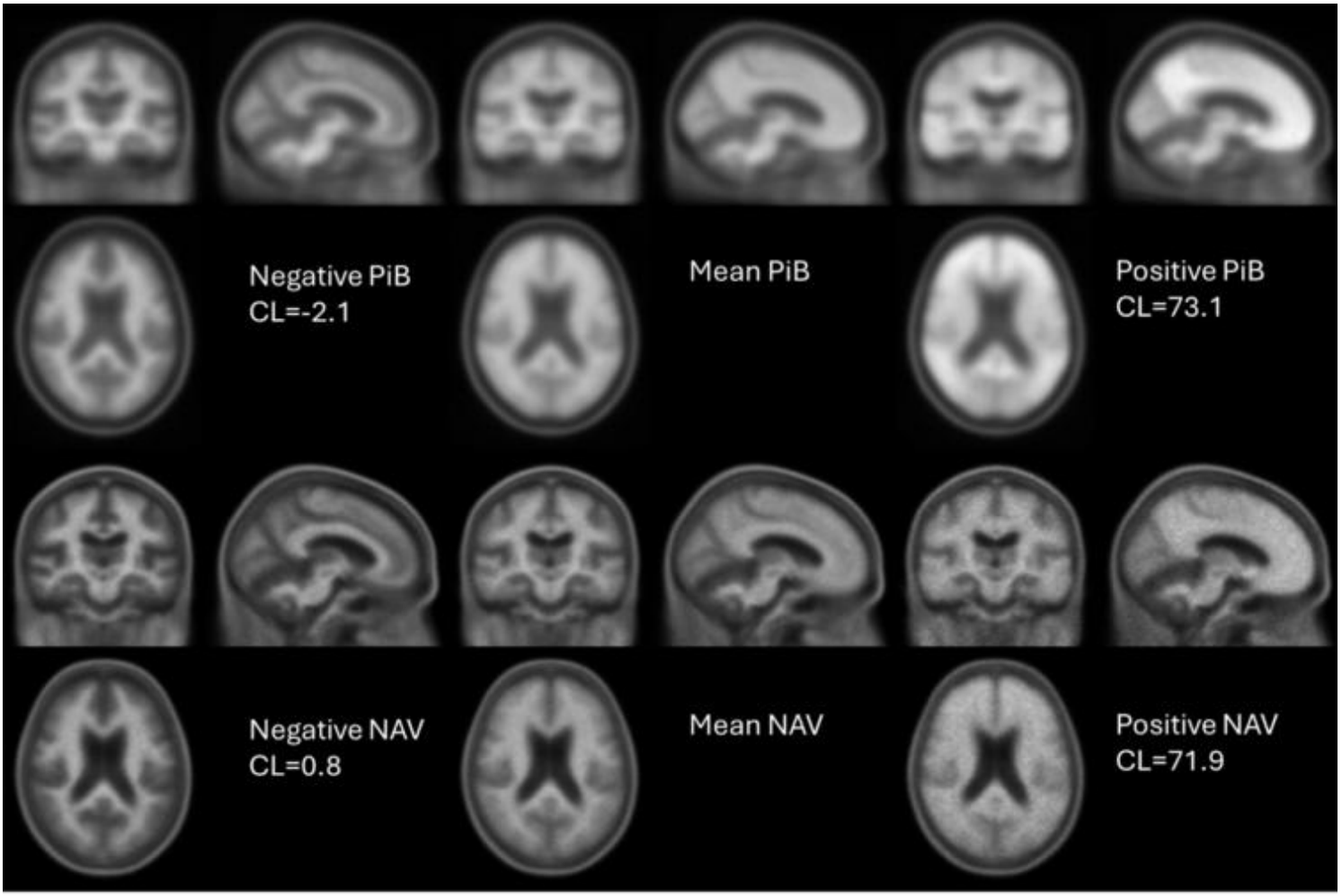


Fig 1. Top row: Standard PiB adaptive template used in CapAIBL: negative, mean and positive templates. Bottom row: New high-resolution NAV adaptive template: negative, mean and positive templates

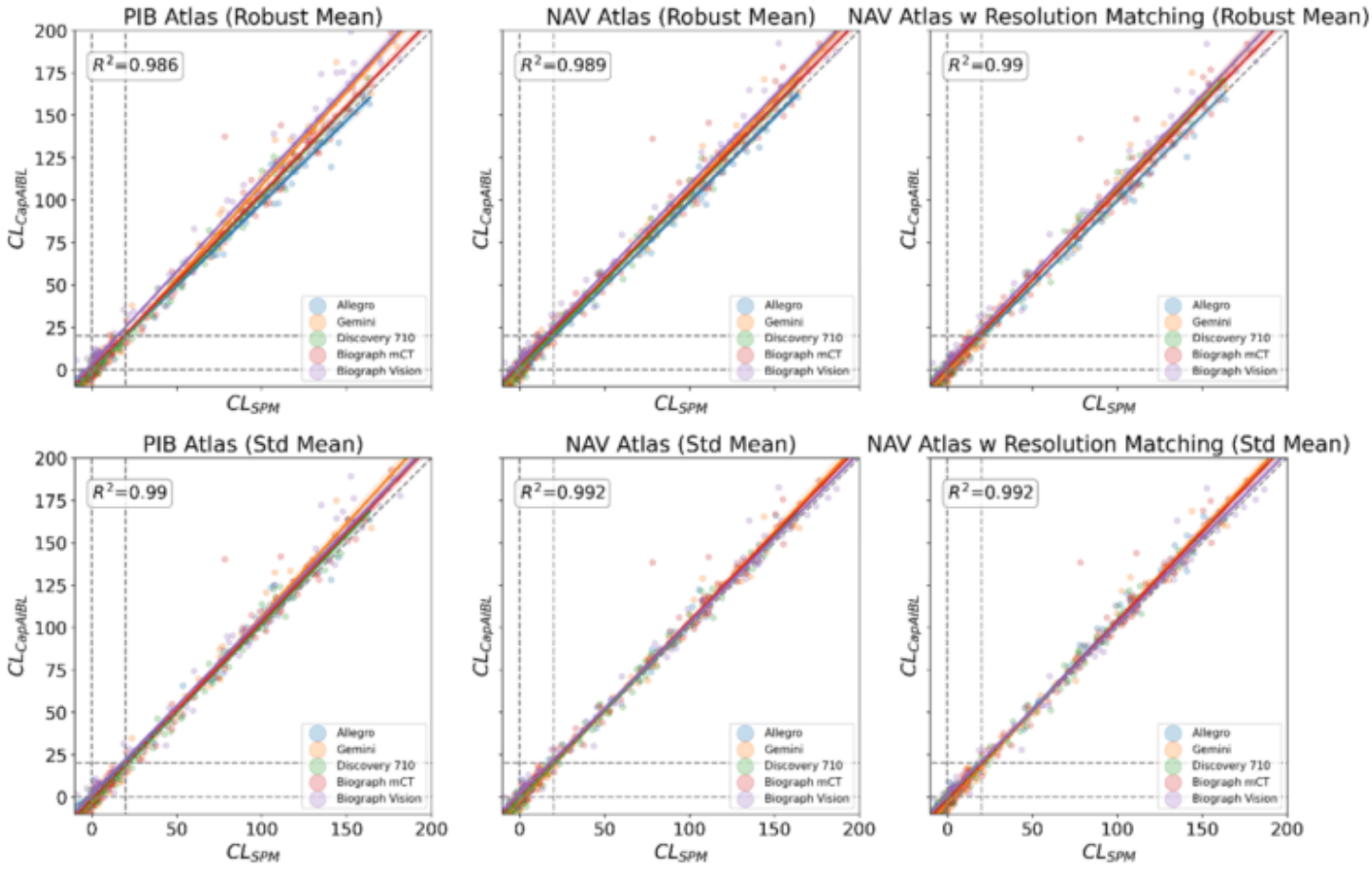


Figure 2. Comparison between SPM and CapAIBL quantification on NAV scans acquired on 5 different scanners, using robust means (top row) and standard means (bottom row). First column shows the results when using our standard PIB template, middle column is using the high-resolution NAV template, right column is using the high-resolution NAV template with resolution matching.

Keywords: Centiloid, NAV

132 Higher clinical throughput quantitative amyloid-β PET using abbreviated acquisition windows

Ishara Paranawithana[1,2], Ashley G. Gillman[4], Pierrick Bourgeat[4], Jurgen Fripp[4], Victor L. Villemagne[5], Graeme O'Keefe[2], Kun Huang[2], Tammie Benzinger[6], Pamela LaMontagne[7], John C. Morris[6], Vincent Doré[1,2], Christopher C. Rowe[2]

[1]*The Australian e-Health Research Centre, Commonwealth Scientific and Industrial Research Organisation, Melbourne, Australia*
[2]*Department of Molecular Imaging & Therapy, Austin Health, Melbourne, Australia*
[3]*The Australian e-Health Research Centre, Commonwealth Scientific and Industrial Research Organisation, Brisbane, Australia*
[4]*Department of Psychiatry, University of Pittsburgh, Pittsburgh, PA, US*
[5]*Department of Neurology, Washington University School of Medicine, St. Louis, MO, US*
[6]*Department of Radiology, Washington University School of Medicine, St. Louis, MO, US*
[7]*Florey Institute of Neuroscience and Mental Health, The University of Melbourne, Parkville, Australia*

Background: Anti-Aβ monoclonal antibody treatments for Alzheimer's disease have significantly increased demand for clinical Aβ PET imaging. To meet this need, enhancing clinical throughput of Aβ PET imaging is essential. This study assessed the feasibility of reducing uptake and scan times for Aβ PET using earlier and shortened acquisitions of ^{18}F-florbetapir (FBP), ^{11}C-Pittsburgh Compound B (PiB), and ^{18}F-NAV4694 (NAV), while maintaining Centiloid (CL) accuracy.

Methods: Dynamic PET data from 454 FBP scans (OASIS-3), 266 PiB scans (AIBL and OASIS-3) and 38 NAV scans (AIBL) were rebinned into three abbreviated windows: 50-60, 40-50, and 30-40 minutes post-injection. CL values were computed using the CapAIBL PET-only pipeline. CL mapping between abbreviated and standard (50-70 minutes) windows was evaluated via linear regression. Bland-Altman analysis evaluated the relationship between residual error and Aβ burden (DVR). CL values were recalibrated for timing bias using linear fit parameters, and accuracy was quantified by mean absolute error (MAE) and 95th percentile error range compared to the standard window.

Results: CL values from all abbreviated windows showed strong linear correlation with the standard window (R^2>0.95, shown in Figure 1-3 for FBP, PiB and NAV respectively), though correlation and accuracy declined with earlier windows. Bland-Altman analysis showed residual error was uncorrelated with the Aβ burden. With recalibrated CL, FBP at 40-50 minutes yielded 3.3 CL MAE (95% < 8.8 CL), PiB at 30-40 minutes yielded 2.8 CL MAE (95% < 8.0 CL), and NAV at 30-40 minutes yielded 2.7 CL MAE (95% < 6.5 CL).

Conclusion: Abbreviated Aβ PET protocols, FBP at 40-50 minutes, PiB and NAV at 30-40 minutes are feasible with recalibrated CL, introducing errors comparable to previously reported test-retest variability. These protocols enable up to 50% scan time and 20% (FBP) and 40% (NAV) uptake time reductions, offering a scalable solution to meet rising clinical demand.

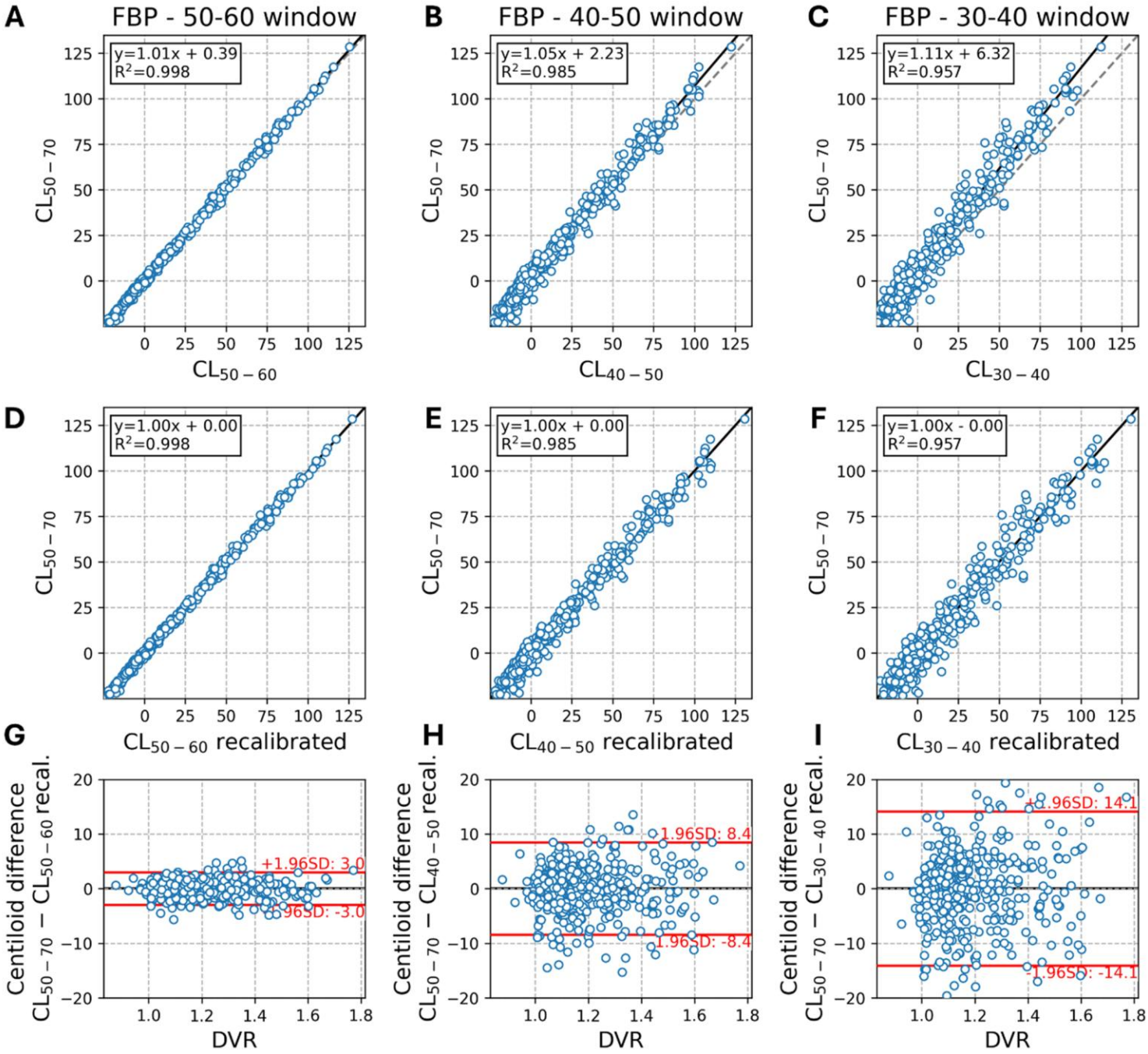


Figure 1: Scatter plots in the top panels show CL of FBP for shortened windows at (A) 50-60 minutes, (B) 40-50 minutes and (C) 30-40 minutes to the standard window. Scatter plots in the middle panels (D-F) show the mapping between recalibrated CL of abbreviated windows and CL of the standard window. The Bland-Altman plots (G-I) depict fit residuals by scan DVR values for the same shortened windows.

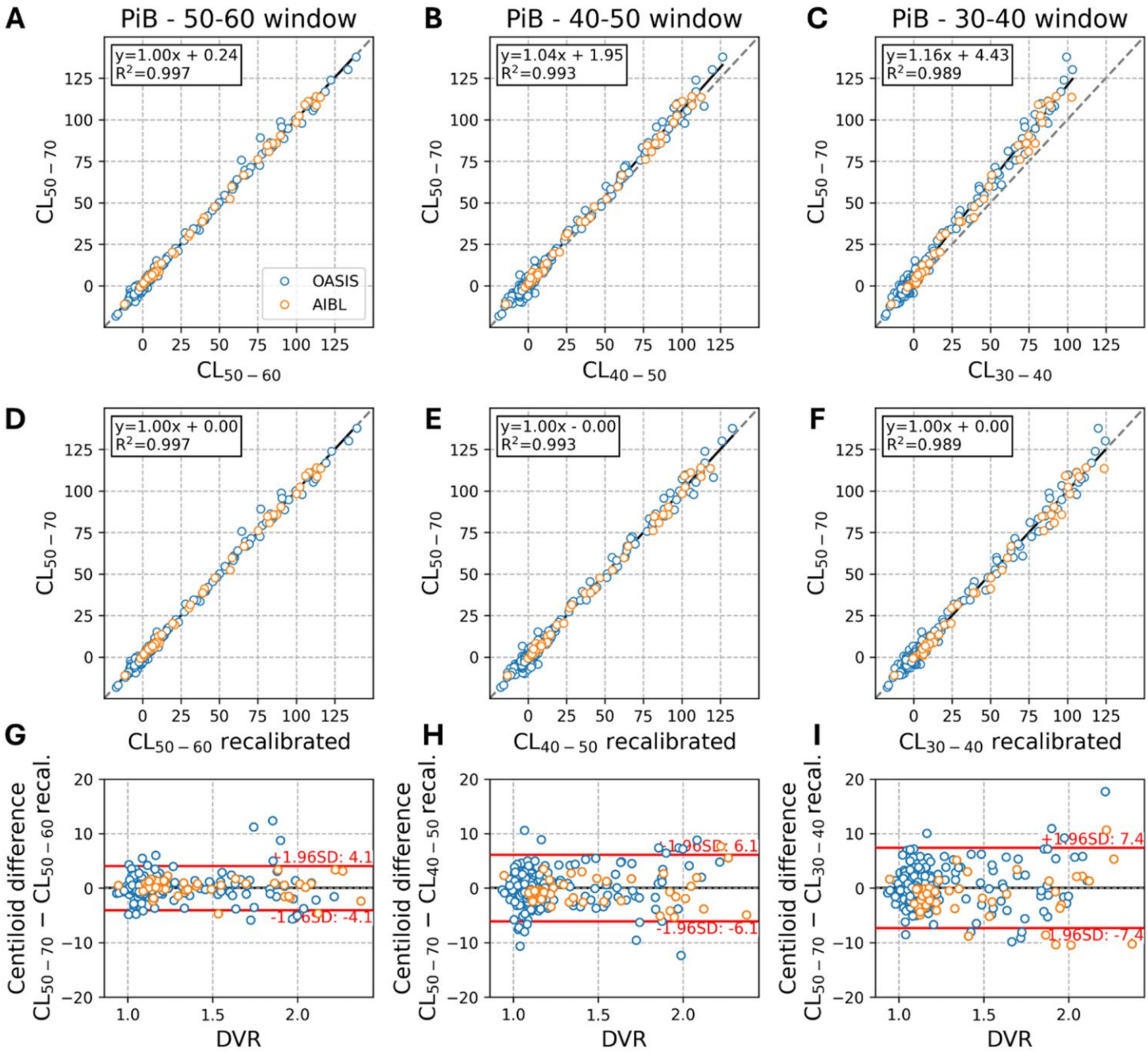


Figure 2: Scatter plots in the top panels show CL mapping of PiB for shortened windows at (A) 50-60 minutes, (B) 40-50 minutes and (C) 30-40 minutes to the standard window. Scatter plots in the middle panels (D-F) show the mapping between recalibrated CL of abbreviated windows and CL of the standard window. Bland-Altman plots (G-I) depict fit residuals by scan DVR values for the same shortened windows. The data points are color-coded based on the dataset: OASIS-3 in blue and AIBL in orange.

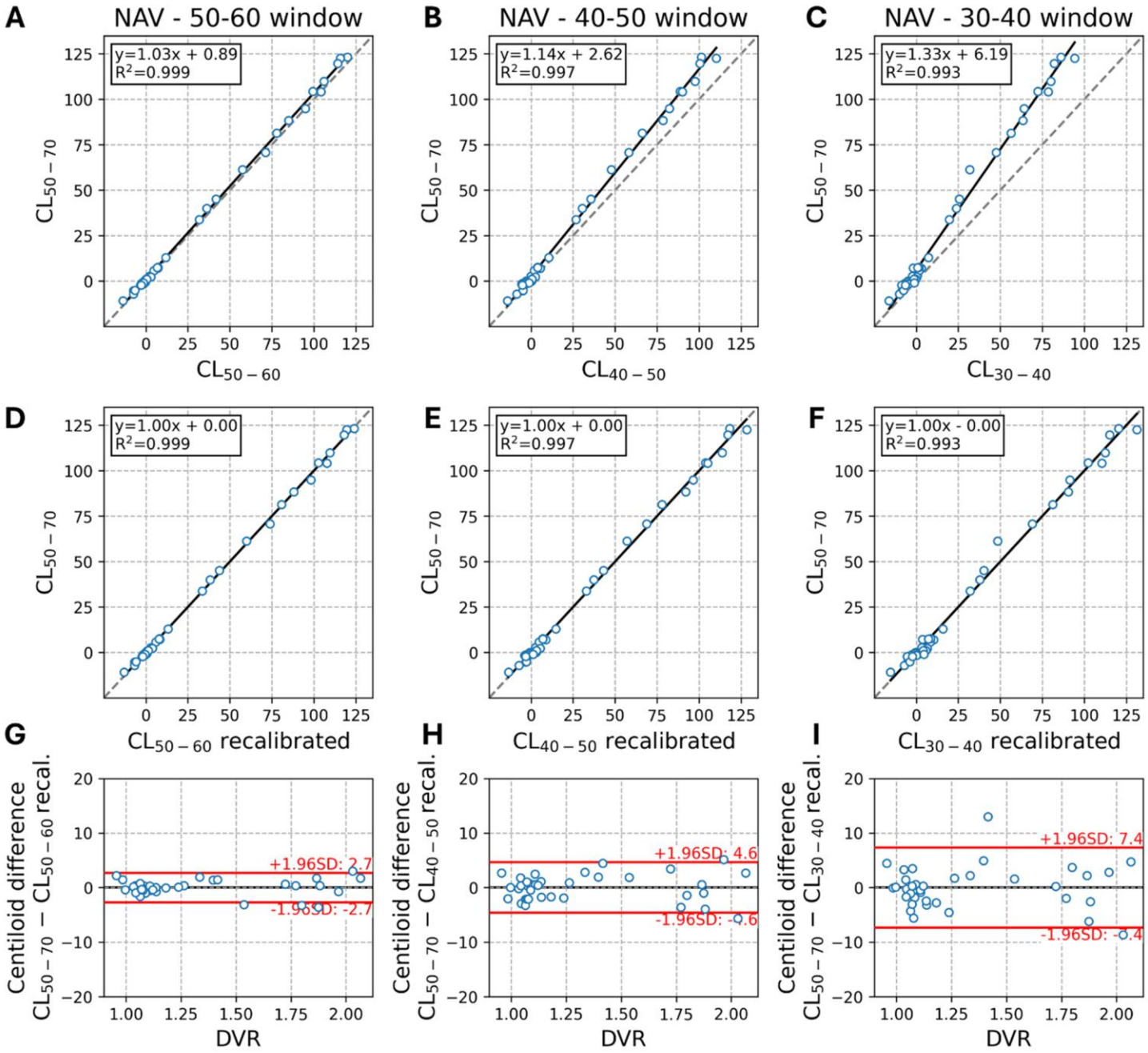


Figure 3: Scatter plots in the top panels show CL mapping of NAV for shortened windows at (A) 50-60 minutes, (B) 40-50 minutes and (C) 30-40 minutes (right) to the standard window. Scatter plots in the middle panels (D-F) show the mapping between recalibrated CL of abbreviated windows and CL of the standard window. Bland-Altman plots (G-I) depict fit residuals by scan DVR values for the same shortened windows.

Keywords: positron emission tomography, amyloid-β, PET quantification, distribution volume ratio, clinical throughput

133 Tracer-specific effects of hormone replacement therapy on age-related tau accumulation

Cécile Tissot[1], Wenhan Shi[2], Hsin-Yeh Tsai[1], Samira Maboudian[2], Corrina Fonseca[2], Nesrine Rahmouni[3], Firoza Lussier[4], Joseph Therriault[3], Lydia Trudel[3], Arthur Cassa Macedo[3], Jenna Stevenson[3], Bruna Bellaver[4], Pamela Ferreira[4], Guilherme Povala[4], Brian Gordon[5], Belen Pascual[6], Val Lowe[7], David Soleimani-Meigooni[8], Hwamee Oh[9], William Klunk[4], Pedro Rosa-Neto[3,10], William Jagust[1,2], Rachel Buckley[11], Tharick Pascoal[4], Suzanne Baker[1]

[1]*Lawrence Berkeley National Laboratory, Berkeley, CA, US*
[2]*University of California Berkeley, Berkeley, CA, US*
[3]*McGill University, Montreal, QC, Canada*
[4]*University of Pittsburgh, Pittsburgh, PA, US*
[5]*Washington University in Saint-Louis, Saint Louis, MO, US*
[6]*Houston Methodist, Houston, TX, US*
[7]*Mayo Clinic, Rochester, MN, US*
[8]*University of California San Francisco, San Francisco, CA, US*
[9]*Brown University, Providence, RI, US*
[10]*University of Texas Southwestern, Dallas, TX, US*
[11]*Massachussets General Hospital, Boston, MA, US*

Background: Hormone replacement therapy (HRT) has been associated with lower tau accumulation in Alzheimer's disease (AD). Here, we compared [^{18}F]FTP and [^{18}F]MK6240 accumulation in cognitively unimpaired (CU) individuals with no amyloid pathology (Aβ-) across age and sex, focusing on the potential influence of HRT.

Methods: We included 273 CU Aβ- individuals (149 females (F), 124 males (M)) from the HEAD study who underwent both [^{18}F]FTP and [^{18}F]MK6240 tau-PET scans and completed a reproductive health questionnaire. Fifty-two females reported undergoing HRT (Figure1). We examined group differences in tau-PET retention across Braak I and meta-temporal regions of interest (ROI) and assessed associations between brain region retention and age within each group (females with HRT, females without HRT, and males).

Results: There were no significant group differences in [^{18}F]FTP or [^{18}F]MK6240 retention in Braak I and meta-temporal ROI (Figure2). However, age was significantly associated with higher Braak I retention in females without HRT and in males for both tracers, while no significant correlation was observed in females who underwent HRT. In the meta-temporal ROI, age was significantly associated with tracer retention for all groups with [^{18}F]FTP, but only for females without HRT with [^{18}F]MK6240 (Figure3).

Discussion: Our findings suggest that hormone replacement therapy (HRT) may influence age-related tau accumulation in cognitively unimpaired, amyloid-negative individuals. Both [^{18}F]FTP and [^{18}F]MK6240 showed significant Braak I signal with age in females without HRT and in males, whereas females with HRT showed no significant correlation, indicating a potential protective effect. In the meta-temporal ROI, [^{18}F]FTP revealed consistent age associations across all groups, while [^{18}F]MK6240 was significant only in females without HRT, reflecting tracer-dependent sensitivity to early tau spread. Overall retention did not differ significantly between groups, suggesting HRT effects might be region-specific and age-dependent. These results highlight that reproductive hormone exposure may modulate early tau accumulation.

Figure1: Demographics

	F HRT (N=52)	F no HRT (N=97)	M (N=124)	P-value
Age (mean (SD))	66.29 (8.7)	63.77 (7.7)	68.28 (7.6)	<0.001
[^{18}F]FTP Braak I (mean(SD))	1.12 (0.1)	1.11 (0.1)	1.14 (0.1)	0.284
[^{18}F]MK6240 Braak I (mean(SD))	1.07 (0.2)	1.04 (0.2)	1.07 (0.2)	0.0865
[^{18}F]FTP Metatemp (mean(SD))	1.18 (0.1)	1.16 (0.1)	1.17 (0.1)	0.171
[^{18}F]MK6240 MetaTemp (mean(SD))	1.06 (0.1)	1.05 (0.1)	1.03 (0.1)	0.118

Figure2: Boxplots showing SUVR in Braak I and meta-temporal ROI

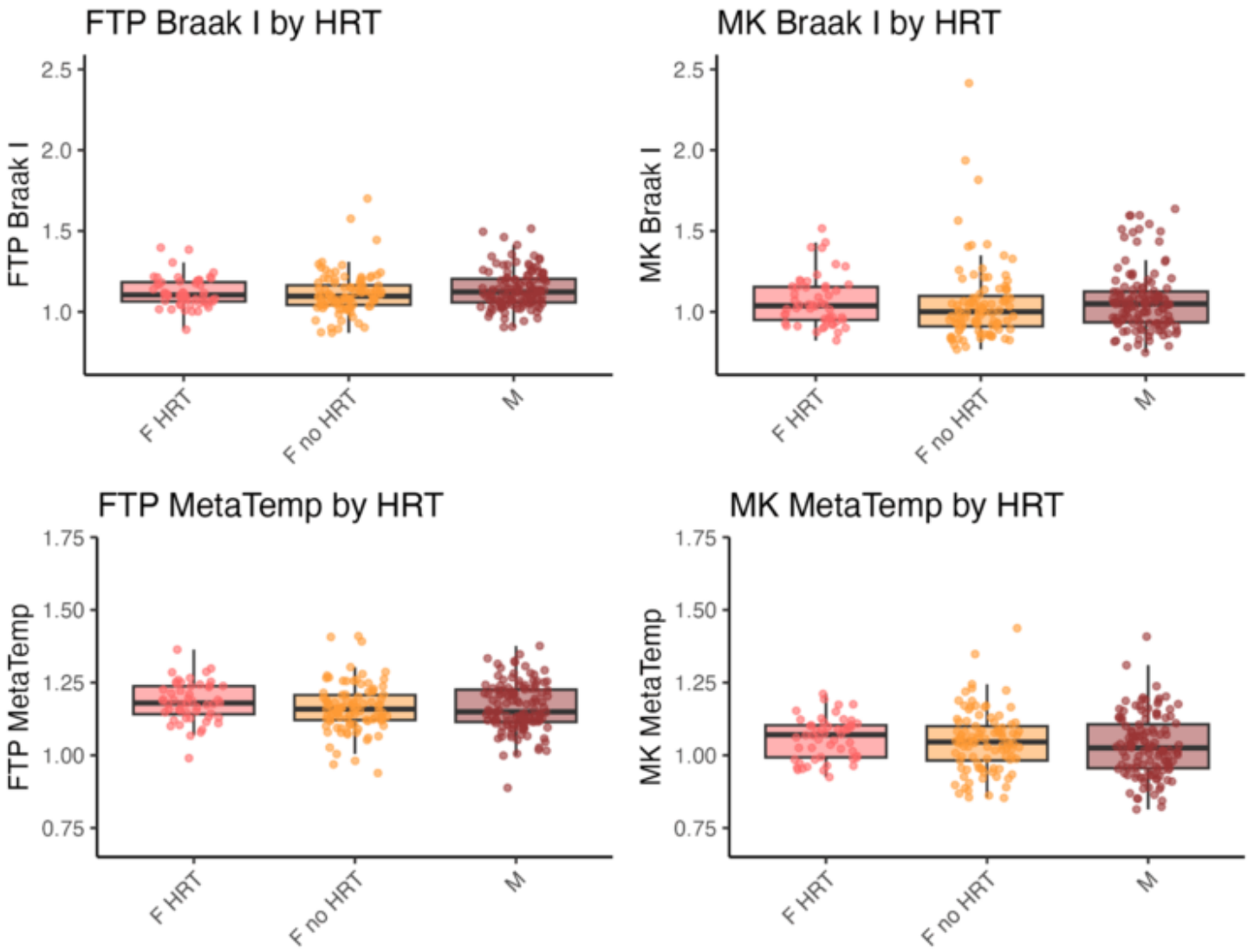
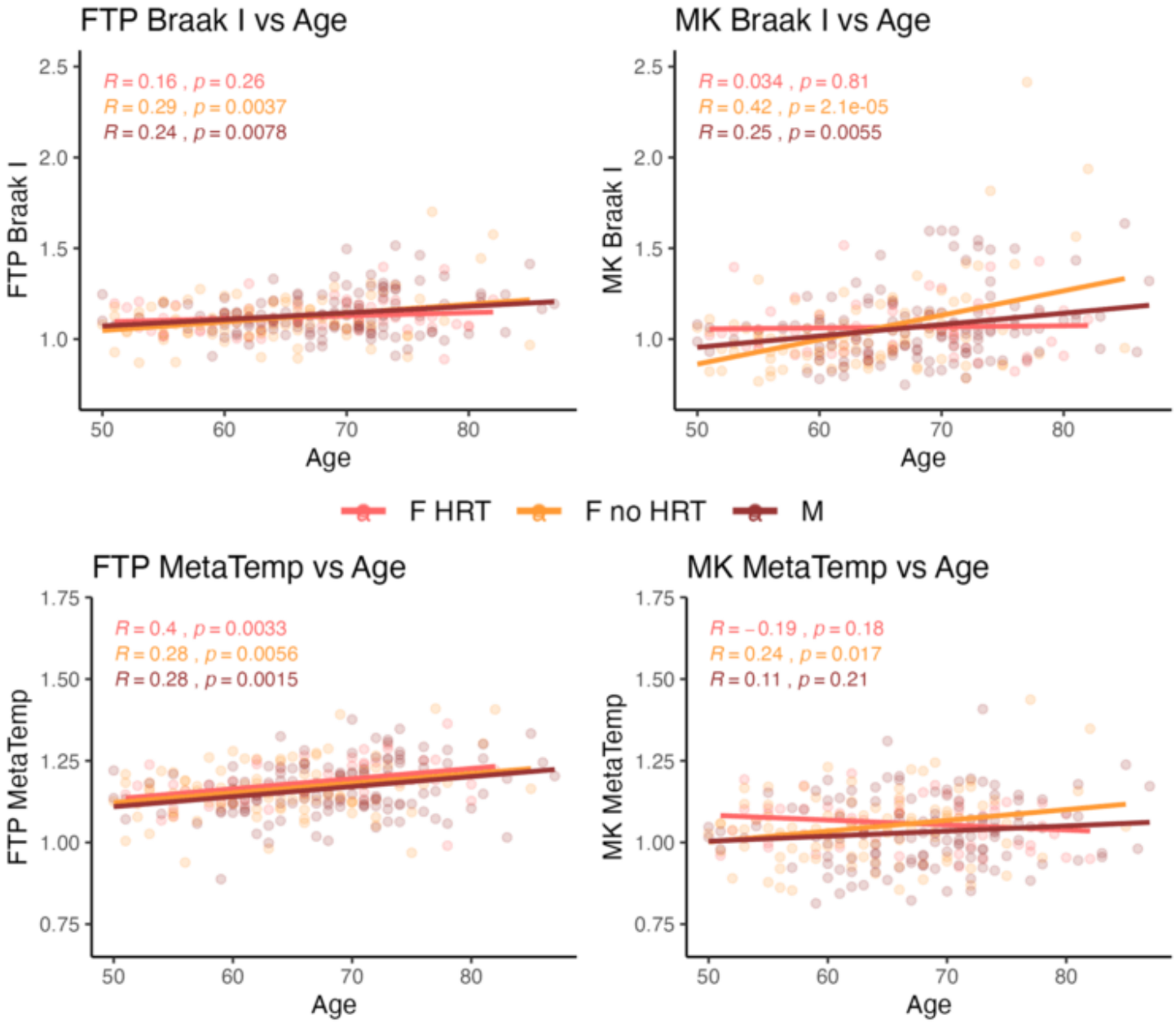


Figure3: Association with age



Keywords: early tau, tracer comparison, hormonal replacement therapy

134 Cognitive and age-related differences in low-tau individuals assessed with [18F]FTP and [18F]MK6240

Cécile Tissot[1], Aadi Shankar[2], Hsin-Yeh Tsai[1], Nesrine Rahmouni[3], Firoza Lussier[4], Joseph Therriault[3], Lydia Trudel[3], Arthur Cassa Macedo[3], Jenna Stevenson[3], Bruna Bellaver[4], Pamela Ferreira[4], Guilherme Povala[4], Brian Gordon[5], Belen Pascual[6], Val Lowe[7], David Soleimani-Meigooni[8], Hwamee Oh[9], William Klunk[4], Pedro Rosa-Neto[3,10], William Jagust[1,2], Susan Landau[2], Tharick Pascoal[4], Suzanne Baker[1]

[1]*Lawrence Berkeley National Laboratory, Berkeley, CA, US*
[2]*University of California Berkeley, Berkeley, CA, US*
[3]*McGill University, Montreal, QC, Canada*
[4]*University of Pittsburgh, Pittsburgh, PA, US*
[5]*Washington University in Saint-Louis, Saint Louis, MO, US*
[6]*Houston Methodist, Houston, TX, US*
[7]*Mayo Clinic, Rochester, MN, US*
[8]*University of California San Francisco, San Francisco, CA, US*
[9]*Brown University, Providence, RI, US*
[10]*University of Texas Southwestern, Dallas, TX, US*

Background: [18F]FTP and [18F]MK6240 enable in vivo quantification of tau pathology in Alzheimer's disease (AD) but differ in binding properties. Although highly correlated across the full dynamic range, tracers present weaker correlation at early tau levels. Accurately measuring early tau deposition is crucial, therefore we aimed to explored the relationship of low tau signal with cognition.

Methods: We analyzed 511 participants from the HEAD study (376 cognitively unimpaired older adults (CUO) and 135 cognitively impaired (CI; mild cognitive impairment (MCI) and AD)) who underwent [18F]FTP and [18F]MK6240 tau-PET scans processed with the same pipeline, using the inferior cerebellar grey as the reference region. Only participants with meta-temporal SUVR < 1.5 for both tracers were included. Median SUVR values classified individuals into four groups: lowFTP/lowMK, highFTP/highMK, and two discrepant groups (lowFTP/highMK, highFTP/lowMK). Group differences in demographics and cognition were assessed.

Results: Aβ- participants were more likely to be lowFTP/lowMK, while Aβ+ were predominantly highFTP/highMK. [18F]FTP signal increased with age, whereas [18F]MK6240 showed no clear age effect. Across cognitive tests, such as MINT, Trail B, and Animals, lowFTP/lowMK participants generally outperformed highFTP/highMK participants. Specific additional contrasts emerged: in MINT, highFTP/lowMK performed better than highFTP/highMK; in Trail B, lowFTP/lowMK outperformed highFTP/lowMK; in Animals, lowFTP/lowMK differed from highFTP/lowMK and lowFTP/highMK from highFTP/highMK.

Discussion: Low-tau individuals show variable patterns of [18F]FTP and [18F]MK6240 uptake, with cognitive performance differences linked to tracer-specific signals. Low tau on both tracers is associated with preserved cognition, whereas elevated tau corresponds to cognitive impairment. [18F]FTP shows age-related increases and group differences, but these differences lack a clear pattern, highlighting variability in early tau distribution. In contrast, [18F]MK6240 does not display a strong age effect. These findings underscore the importance of considering tracer-specific characteristics when assessing subtle tau-related cognitive changes, particularly in the context of early tau accumulation.

Figure1: Association between [^{18}F]FTP and [^{18}F]MK6240

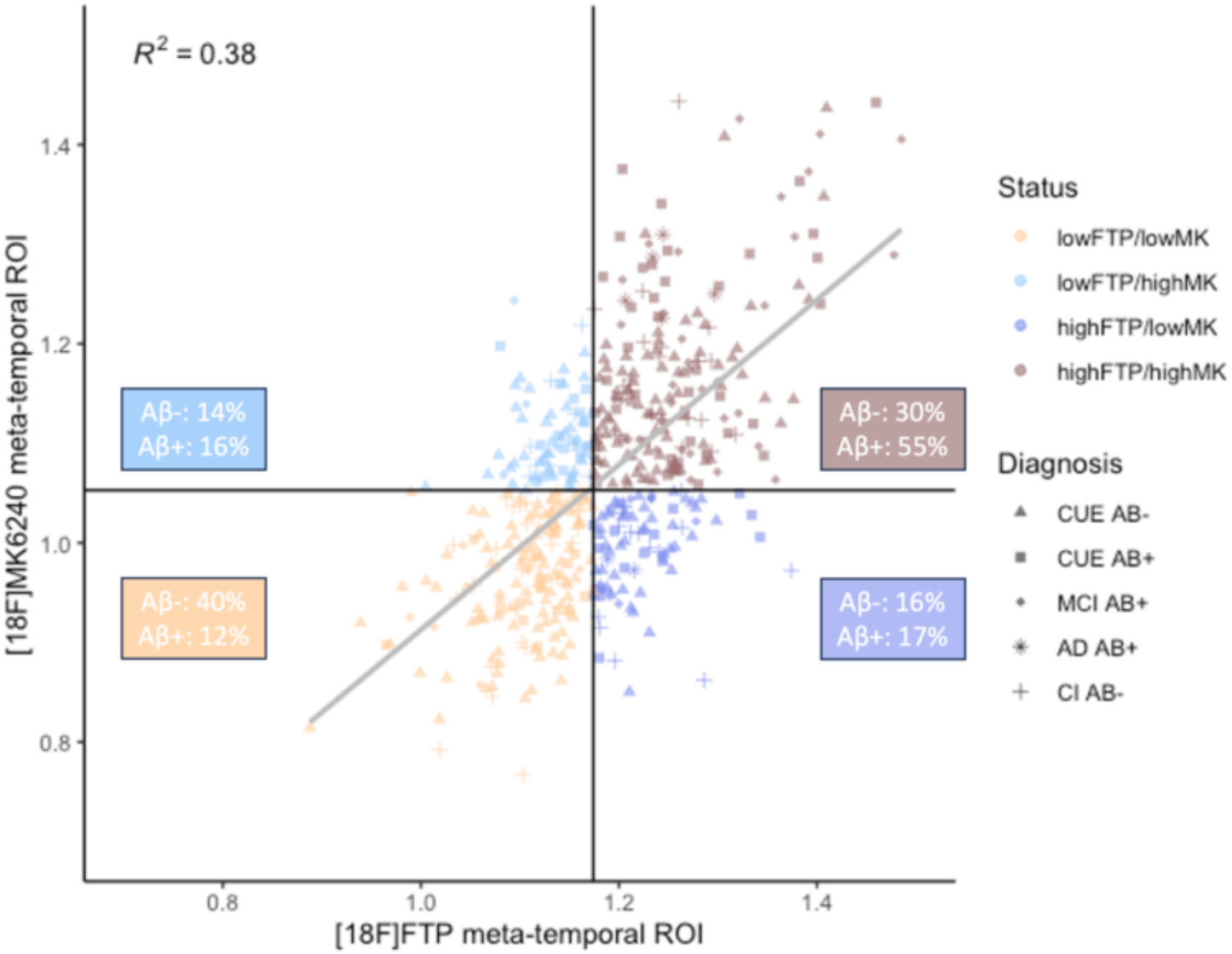


Figure2: Boxplot of age based on status groups

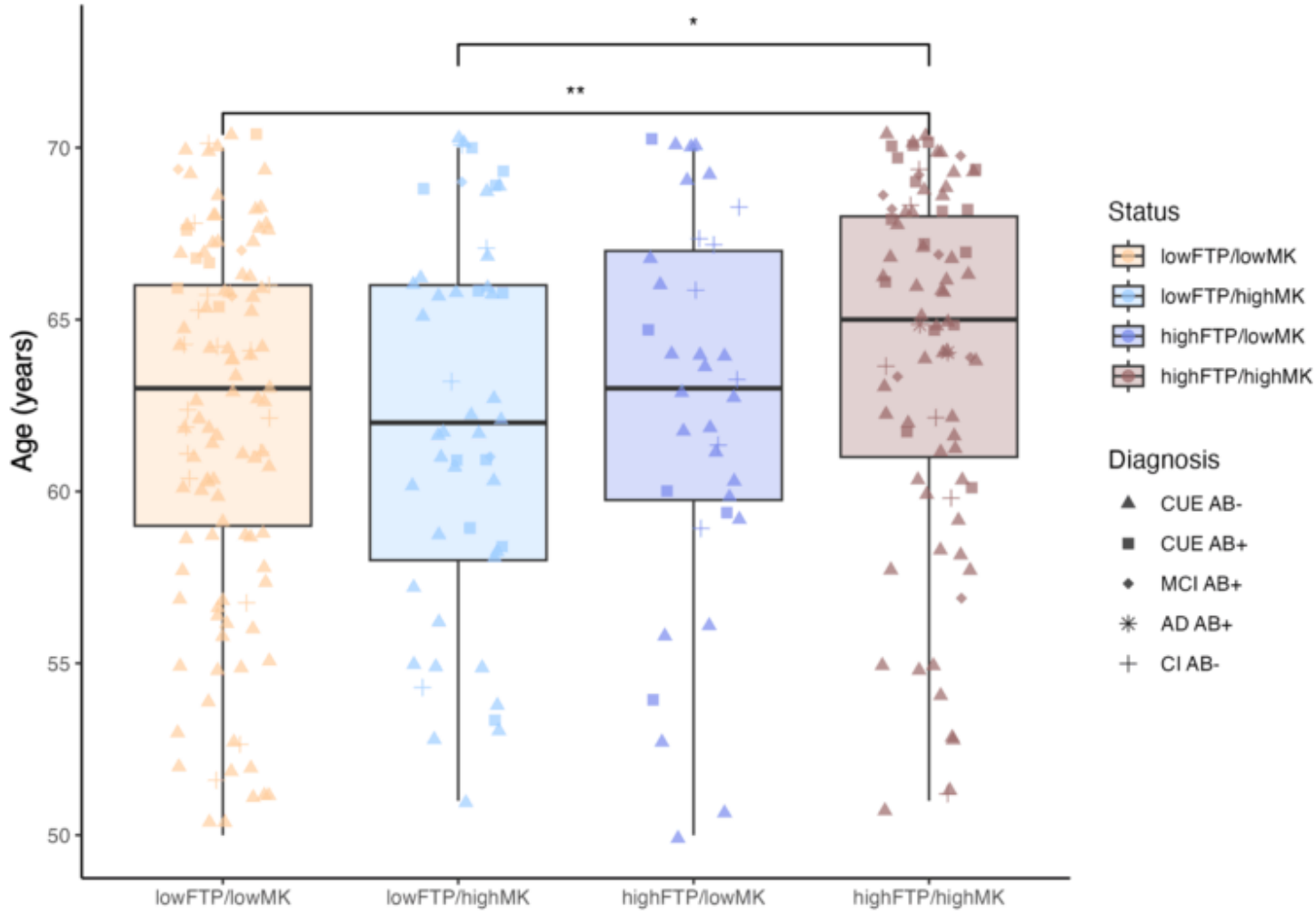
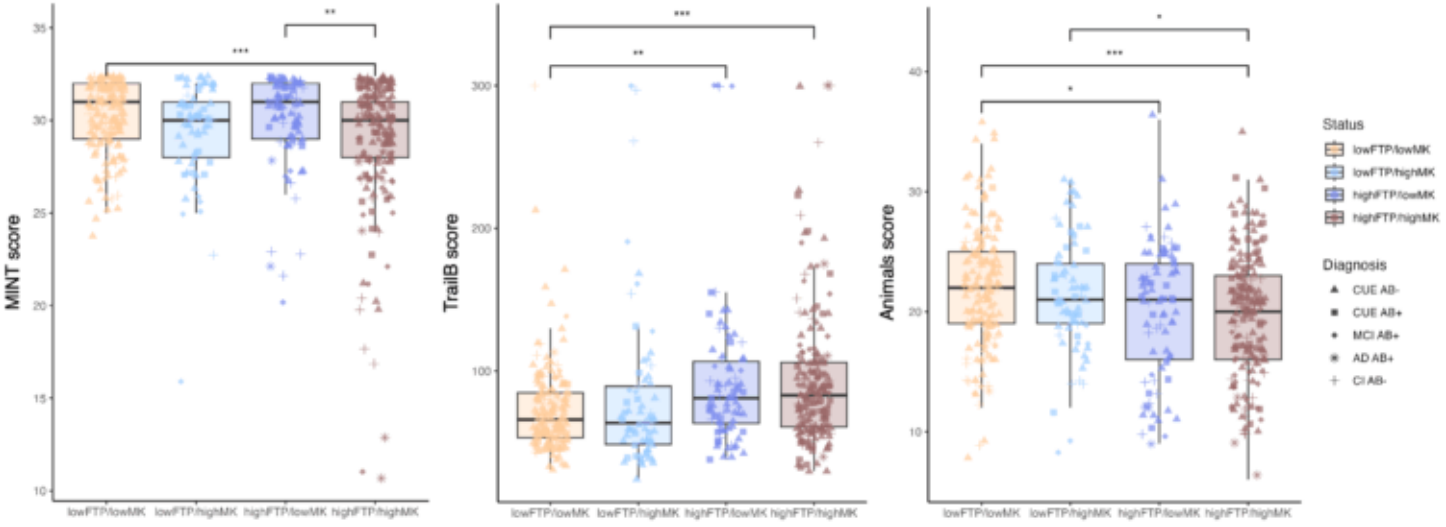


Figure3: Boxplot of age based on cognitive scores



Keywords: low tau, tracer comparison, cognition, age effect

135 Integration of network analysis of the plasma proteome with Alzheimer's disease neuroimaging outcomes in an African American cohort

Cheyenne Hurst[1], Lindsey Kuchenbecker[1], Michael Heckman[1], Thuy Nguyen[1], Heidi Casellas[1], Katie Sotelo[1], Christopher Shwarz[1], Matthew Senjem[1], Manoj Jain[1], John Lucas[1], Floyd Willis[1], Nilufer Ertekin-Taner[1], Neill Graff-Radford[1], Kejal Kantarci[1], Val Lowe[1], Christian Lachner[1], Gregory Day[1], Minerva Carrasquillo[1]

[1]*Mayo Clinic, Jacksonville, FL, US*

Background: Blood-based biomarkers offer accessibility to population-scale screening for early detection of Alzheimer's disease (AD). This pilot study evaluates the utility of network analysis to characterize the relationship between positron emission tomography (PET) outcomes and biological signatures which could serve as blood-based biomarkers.

Methods: This study included Mayo Clinic Alzheimer's Disease Research Center African American (AA) participants for whom we had previously obtained SomaScan7k untargeted plasma proteome measurements, and who underwent amyloid-PET (Pittsburgh compound B, n=38) and tau-PET (flourtaucipir, n=47) scans within 2 years of collection of blood utilized for the plasma proteome measurements. Weighted gene co-expression network analysis (WGCNA) was performed on the plasma proteome. The resulting co-expression module eigenprotein values were tested for associations with amyloid-PET (centiloids) and tau-PET (temporal meta-ROI SUVR) using biweight midcorrelation. Gene-set and cell-type enrichment analyses were conducted to characterize the biological pathways and cell-types represented by modules significantly associated with PET outcomes. Preservation and overrepresentation analyses were performed to evaluate the overlap of PET-associated modules with those previously shown by our group to associate with clinical diagnosis of AD dementia in a larger AA cohort (n=323).

Results: We observed significant correlations of module eigenproteins with amyloid-PET, tau-PET, cognition and AD diagnosis. Notably, module M13 eigenprotein values were correlated with decreased amyloid and tau burden and better cognitive outcomes, suggesting a protective effect of proteins in this module. Importantly, the majority of modules identified were significantly represented in a proteome network constructed from a larger cohort, supporting potential replicability in larger sample sizes.

Conclusion: Our pilot study supports the utility of a network-based strategy to characterize and prioritize key biological pathways and proteins detectable in blood that are altered in AD and correspond to pathological brain changes captured by neuroimaging. Future work is necessary to expand and replicate findings in larger, independent cohorts.

Keywords: Alzheimer's disease; proteome; biomarker

137 MK6240 and Flortaucipir Braak staging agreement in a head-to-head cohort

Andreia Rocha[1], Carolina Soares[1], Emma Ruppert[1], Marina Medeiros[1], Bruna Bellaver[1], Guilherme Povala[1], Pamela Ferreira[1], Guilherme Bauer-Negrini[1], Firoza Lussier[1], Dana Tudorascu[1], Joseph Masdeu[2], David Soleimani-Meigooni[3], Juan Fortea[4], Val Lowe[5], Hwamee Oh[6], Belen Pascual[2], Brian Gordon[7], Pedro Rosa-Neto[8], Suzanne Baker[9], Tharick Pascoal[1]

[1]*University of Pittsburgh, Pittsburgh, PA 15206-3561, PA, US*
[2]*Houston Methodist Research Institute, Houston, TX, US*
[3]*University of California San Francisco, San Francisco, CA, US*
[4]*Hospital de la Santa Creu i Sant Pau, Barcelona, Spain*
[5]*Mayo Clinic, Rochester, MN, US*
[6]*Brown University, Providence, RI, US*
[7]*Washington University in St. Louis, St. Louis, MO, US*
[8]*McGill University, Montreal, QC, Canada*
[9]*Lawrence Berkeley National Laboratory, Berkeley, CA, US*

Background: Braak staging is a widely used framework for classifying AD tau neuropathological progression. Although adapted for tau-PET imaging, tracer-specific differences may lead to inconsistent staging. The agreement of Braak staging across different tracers has not yet been assessed. This study directly compares Braak staging between the two most extensively used tau-PET tracers—Flortaucipir and MK6240— in a head-to-head study.

Methods: We assessed 644 participants (332 Aβ-, 312 Aβ+; mean age 69 ± 8.4 years) who underwent MK6240 and Flortaucipir PET, MRI, Aβ-PET, and clinical evaluations. Aβ+ participants (Centiloid ≥ 10) were classified into seven (0–VI) and four-stage (0, I–II, III–IV, V–VI) Braak staging frameworks. Tracer-specific positivity cut-offs were defined as mean + 2SD from the CU Aβ– reference group (≤ 65 years, Centiloid <10). Braak stage concordance was assessed between tracers, and discordant cases were visually inspected for off-target binding.

Results: Group-level Braak stage distributions were broadly similar between tracers, though MK6240 identified a higher proportion of positive cases and consistently more individuals at advanced Braak stages. Using the four-stage framework, MK6240 classified 30% of Aβ+ individuals as Braak 0 compared to 41% with Flortaucipir, and 29% as Braak V–VI compared to 22% (Fig1). However, when compared at the individual level, only ~60% of Aβ+ participants shared the same stage in both tracers. Among discordant cases, 89% had higher Braak stages on MK6240, while 11% were higher on Flortaucipir (Fig2). Visual inspection indicated that Flortaucipir elevations were related to off-target uptake, whereas most MK6240 elevations corresponded to binding consistent with AD tau pathology (Fig3).

Conclusion: Despite similar group-level distributions, individual-level Braak staging showed substantial discordance (~40%), with MK6240 frequently assigning higher stages. These findings suggest MK6240 may capture tau deposition earlier along the AD-continuum, leading to a systematic tendency to classify the same individuals at higher Braak stages than Flortaucipir.

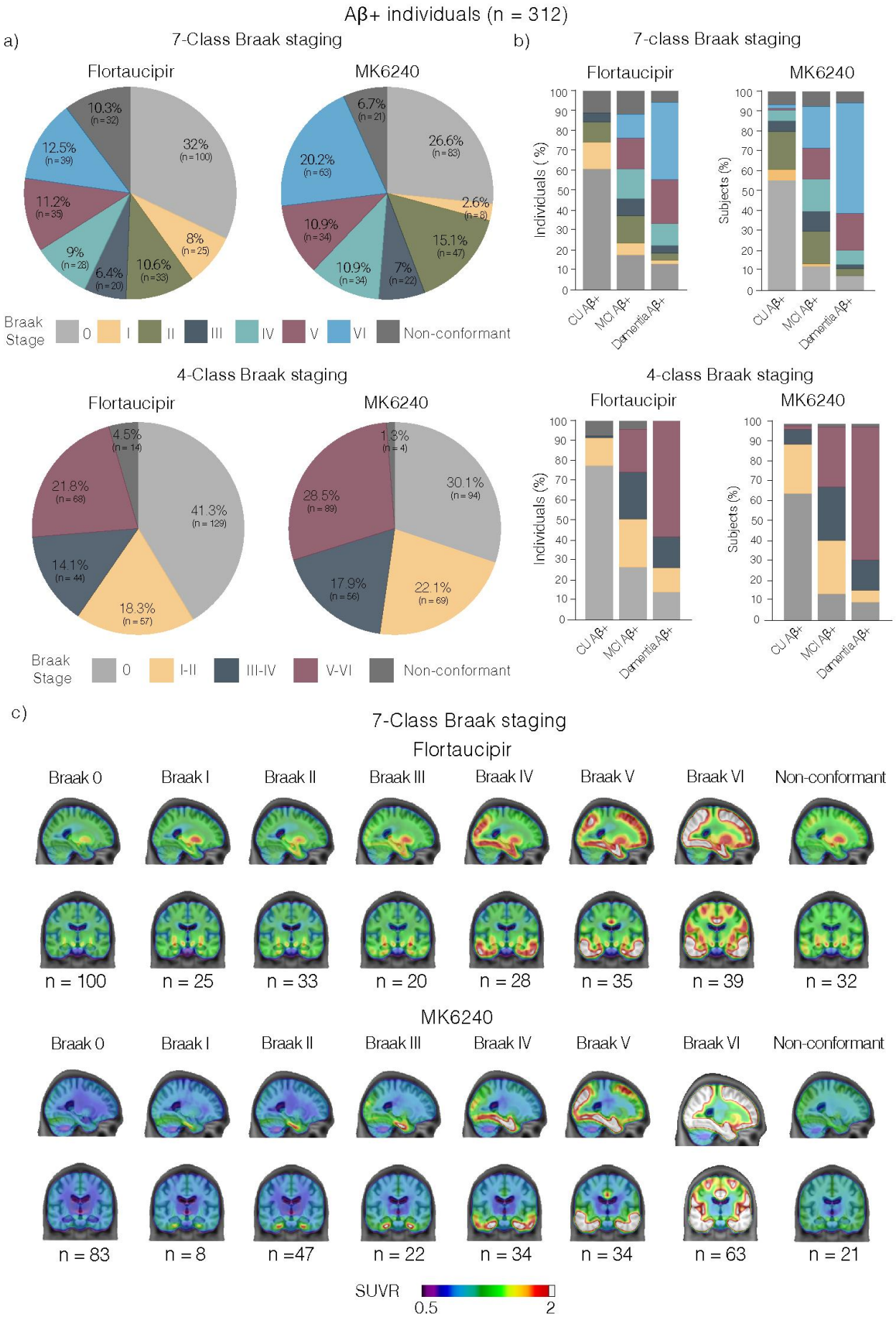


Fig1. Flortaucipir and MK6240 Braak stage distribuition in Aβ+ individuals. (a-b) Braak stage proportions by tracer and clinical group using the 7-class (top) and 4-class frameworks (bottom). (c) Mean SUVR images for individuals classified at each Braak stage using the 7-class framework. Braak stage cut-offs were defined as mean + 2.0 SD from the CU Aβ– (Centiloid < 10) middle-aged adults (age <65 years) group for each tracer.

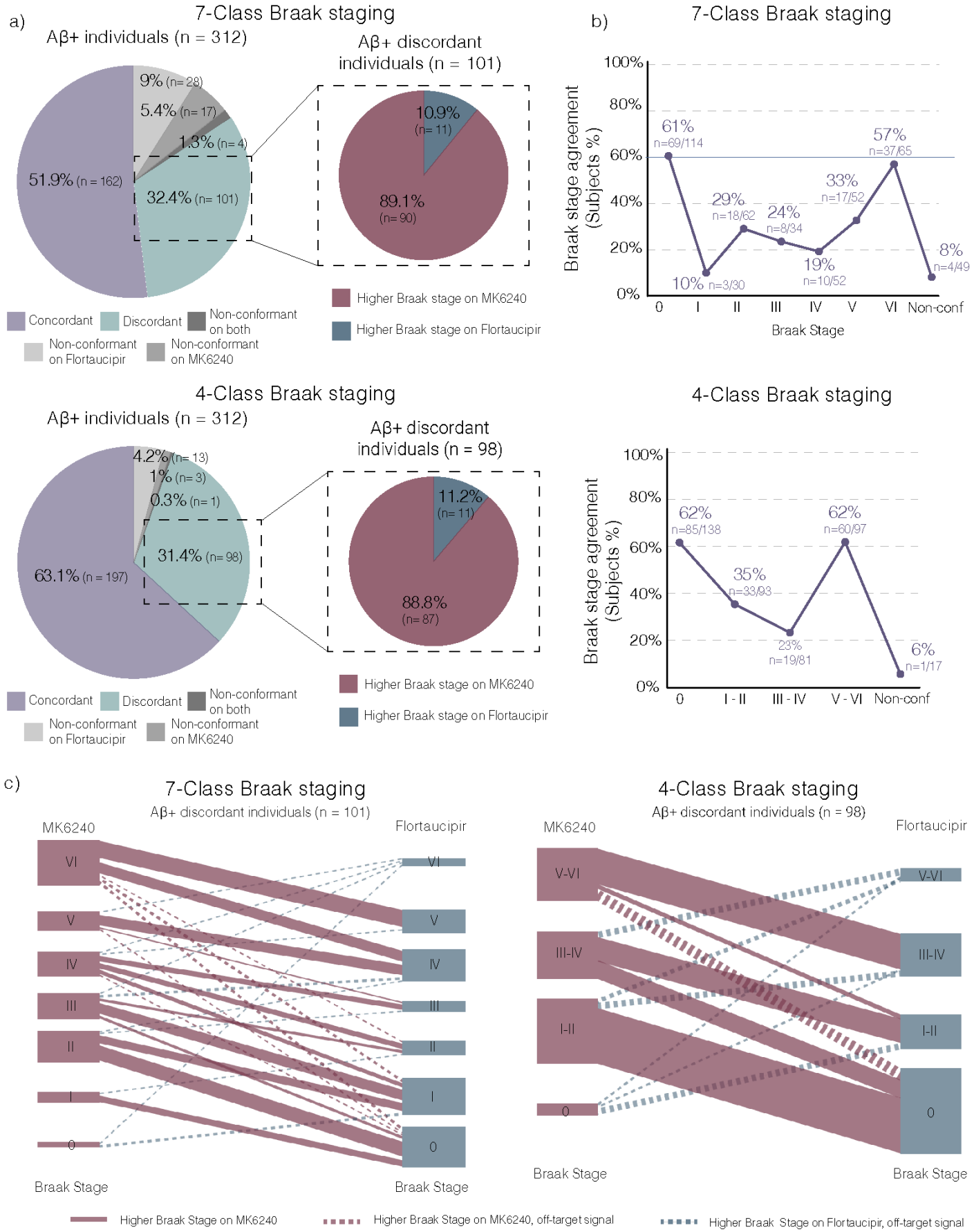


Fig2. Braak staging concordance between MK6240 and Flortaucipir in Aβ+ individuals. (a) Pie charts show the proportion of concordant, discordant, and non-conformant cases (left) and, among discordant cases, those with higher Braak stages on each tracer (right). (b) Stage-wise agreement rates between tracers. (c) Discordant cases alluvial plots illustrating stage shifts across tracers; cases on which discordance reflects off-target signal are represented as dotted lines. Non-conformant = not follow the hierarchical Braak ordering.

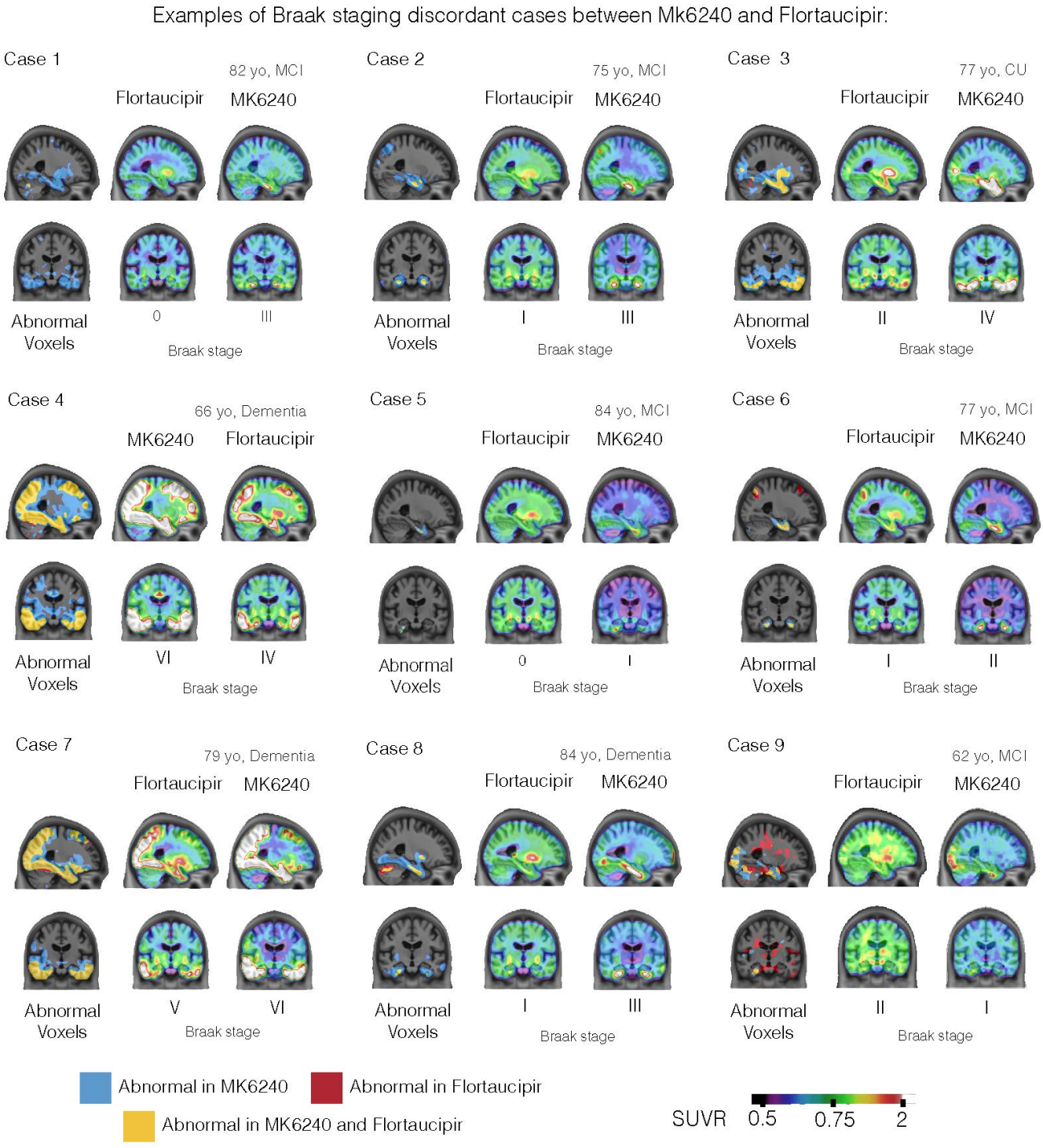


Fig3. Braak staging discordant cases between MK6240 and Flortaucipir. Abnormal voxel maps and SUVR images from nine Braak stage discordant cases. Abnormal voxels cut-offs were defined as mean + 2.0 SD the from CU Aβ– (Centiloid < 10) middle-aged adults (age <65 years) group by tracer for each voxel.

Keywords: Tau, Braak stage, MK6240, Flortaucipir

138 Comparing neuropathologic and tau-PET Braak staging across clinical progression using MK6240 and flortaucipir

Andreia Rocha[1], Hailey Bruzzone[2], Emma Ruppert[1], Marina Medeiros[1], Carolina Soares[1], Bruna Bellaver[1], Guilherme Povala[1], Pamela Ferreira[1], Firoza Lussier[1], Joseph Masdeu[3], David Soleimani-Meigooni[4], Juan Fortea[5], Val Lowe[6], Hwamee Oh[7], Belen Pascual[3], Brian Gordon[8], Pedro Rosa-Neto[9], Suzanne Baker[10], Sterling Johnson[2], Jeffrey Evelhoch[11], Tobey Betthauser[2], Tharick Pascoal[1]

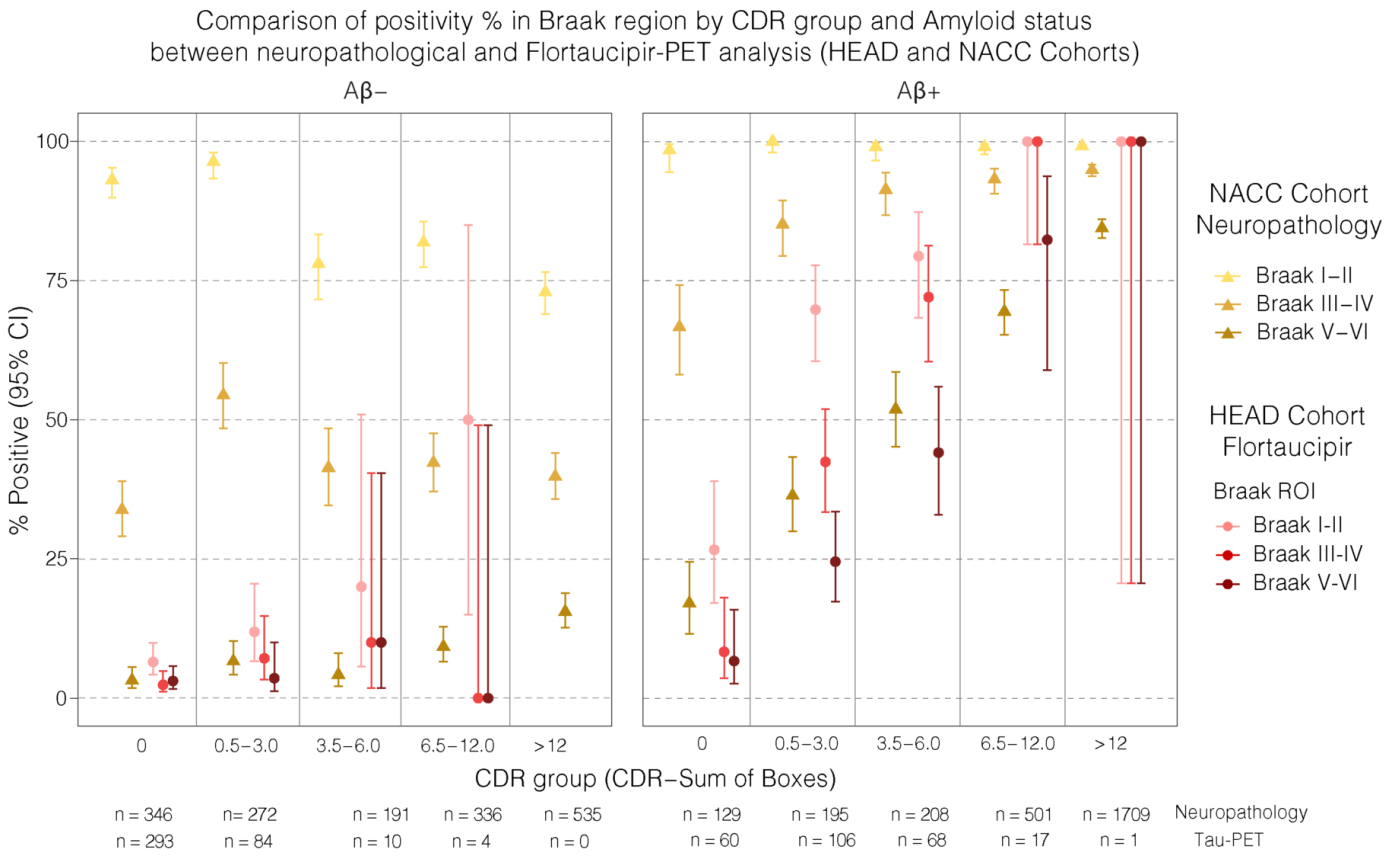
[1]*University of Pittsburgh, Pittsburgh, PA 15206-3561, PA, US*
[2]*University of Wisconsin-Madison, Madison, TX, US*
[3]*Houston Methodist Research Institute, Houston, TX, US*
[4]*University of California San Francisco, San Francisco, CA, US*
[5]*Hospital de la Santa Creu i Sant Pau, Barcelona, MN, Spain*
[6]*Mayo Clinic, Rochester, MN, US*
[7]*Brown University, Providence, RI, US*
[8]*Washington University in St. Louis, St. Louis, MO, US*
[9]*McGill University, Montreal, QC, Canada*
[10]*Lawrence Berkeley National Laboratory, Berkeley, CA, US*
[11]*JLEvelhoch Consulting LLC, Wayne, PA, US*

Background: Braak staging was originally developed in neuropathology to describe the hierarchical spread of neurofibrillary tangles. Translating this framework to in-vivo imaging remains challenging, as PET and neuropathology differ in sensitivity and measurement context. In addition, tau tracers have distinct binding properties, further complicating direct comparisons. Studies comparing Braak staging across neuropathology and imaging are scarce. Here, we used CDR-SB as a clinical anchor to indirectly compare Braak-stage positivity between neuropathology (NACC-cohort) and tau-PET (MK6240 and Flortaucipir) from the HEAD-cohort.

Methods: Two independent cohorts were analyzed. Neuropathological data from the National Alzheimer's Coordinating Center (NACC; *n*=4,422) included Braak stage, CERAD, and CDR-SB. In-vivo PET data from the HEAD cohort (*n*=644) included tau-PET (head-to-head MK6240 and Flortaucipir), amyloid-PET, and CDR-SB. Amyloid positivity was defined as CERAD≥2 for neuropathology and ≥24 Centiloids for PET. Tau-PET Braak positivity was defined as mean + 2SD from the CU Aβ- group. Group differences in regional tau positivity were assessed using chi-square or Fisher's exact tests with Benjamini–Hochberg correction.

Results: Across CDR-SB groups, neuropathology showed higher Braak-stage positivity than both tracers. Significant proportional differences ($p<0.05$) were observed for Braak I–IV across most CDR-SB groups(Fig1,2). MK6240 showed fewer significant discrepancies and smaller odds-ratio gaps relative to neuropathology than Flortaucipir, particularly in the CDR 0–3 range. When stratified by Centiloid levels, both tracers exhibited increased tau positivity with rising amyloid burden(Fig3). Notably, MK6240 demonstrated a higher frequency of tau positivity across Braak stages, with more pronounced differences in stages I–II within the intermediate Centiloid range (25–55)($p<0.05$).

Conclusion: Both tracers underestimated Braak stage positivity frequency compared with neuropathology; however, MK6240 more closely mirrored neuropathologic patterns, particularly in early and intermediate stages. Centiloid stratification suggested that MK6240 detects a higher frequency of tau positivity predominantly within the intermediate amyloid burden range, reinforcing its sensitivity to early AD-related tau pathology.

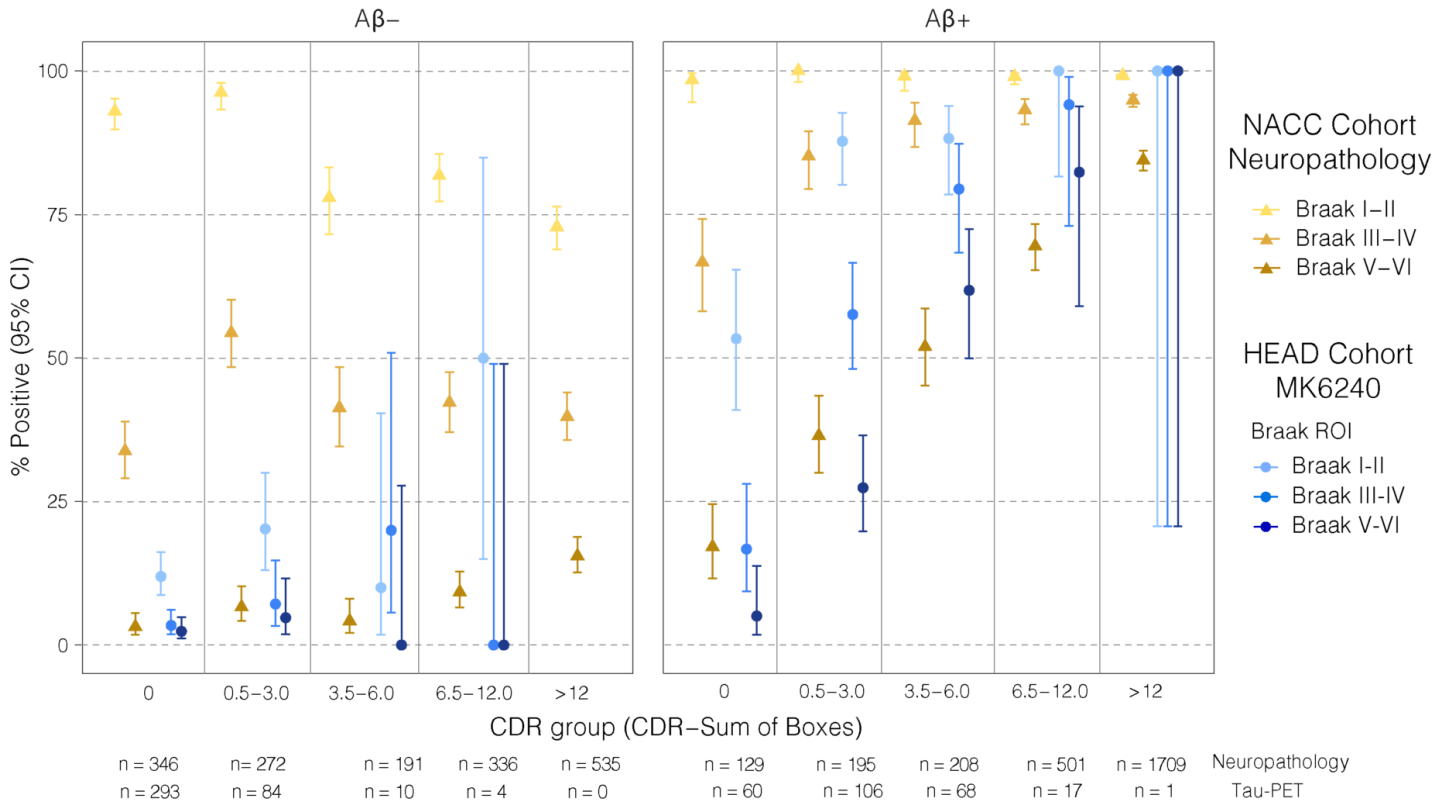


Differences between neuropathology and AV1451 PET positivity.

CDR Group	Stage	Test type	Odds Ratio	Higher Odds Group	p value	p adj BH	Sig	n PET	n NP
Aβ-									
0	I-II	Chi -square	0.01	Neuropathology	3.56e -105	1.07e -103	*	293	346
	III -IV	Chi -square	0.05	Neuropathology	3.81e -23	2.86e -22	*	293	346
	V-VI	Chi -square	0.97	Neuropathology	1	1		293	346
0.5 –3	I-II	Chi -square	0.01	Neuropathology	4.2e -56	6.3e -55	*	84	272
	III -IV	Chi -square	0.07	Neuropathology	5.59e -14	2.39e -13	*	84	272
	V-VI	Fisher	0.59	Neuropathology	0.429	0.643		84	272
3.5 –6	I-II	Fisher	0.08	Neuropathology	0.000274	0.000747	*	10	191
	III -IV	Fisher	0.22	Neuropathology	0.0538	0.124		10	191
	V-VI	Fisher	3.41	PET	0.374	0.624		10	191
6.5 –12	I-II	Fisher	0.22	Neuropathology	0.158	0.296		4	336
	III -IV	Fisher	0.15	Neuropathology	0.143	0.286		4	336
	V-VI	Fisher	1.08	PET	1	1		4	336
>12	I-II	Fisher	NA	Neuropathology	1	1		0	535
	III -IV	Fisher	NA	PET	1	1		0	535
	V-VI	Fisher	NA	PET	1	1		0	535
Aβ+									
0	I-II	Fisher	0.01	Neuropathology	5.17e -27	5.17e -26	*	60	129
	III -IV	Chi -square	0.05	Neuropathology	2.58e -13	9.67e -13	*	60	129
	V-VI	Fisher	0.38	Neuropathology	0.0689	0.148		60	129
0.5 –3	I-II	Fisher	0.01	Neuropathology	9.28e -17	5.57e -16	*	106	195
	III -IV	Chi -square	0.13	Neuropathology	3.13e -14	1.57e -13	*	106	195
	V-VI	Chi -square	0.57	Neuropathology	0.048	0.12		106	195
3.5 –6	I-II	Fisher	0.05	Neuropathology	7.89e -08	2.63e -07	*	68	208
	III -IV	Chi -square	0.25	Neuropathology	0.000119	0.000358	*	68	208
	V-VI	Chi -square	0.73	Neuropathology	0.328	0.579		68	208
6.5 –12	I-II	Fisher	0.39	Neuropathology	1	1		17	501
	III -IV	Fisher	2.58	PET	0.618	0.883		17	501
	V-VI	Fisher	1.82	PET	0.419	0.643		17	501
>12	I-II	Fisher	0.03	Neuropathology	1	1		1	1709
	III -IV	Fisher	0.16	Neuropathology	1	1		1	1709
	V-VI	Fisher	0.55	Neuropathology	1	1		1	1709

Adjusted p-values (p_adj) use the Benjamini–Hochberg correction within amyloid/CDR subgroups.
Sig (*) = adjusted p < 0.05. NP = Neuropathology

Fig 1. Comparing Neuropathologic and Flortaucipir-PET Braak Staging Across CDR-SB groups
Bar plots display the proportion of tau-positive individuals (95% Wilson CI) in Braak I–II, III–IV, and V–VI regions. The table reports chi-square or Fisher's exact tests with Benjamini–Hochberg correction. Amyloid status was defined by CERAD for neurpathology (0/1 = A−, 2/3 = A+) and by Centiloid for PET (CL >= 24 = A+). PET Braak stage cut-offs were defined as mean + 2.0 SD from the CU Aβ− middle-aged adults (age <65 years) group. Only participants with available CDR-SB data acquired at least one year before death were included in the neuropathological analysis (n = 4,422). PET Braak discordant cases excluded (n = 644).



Differences between neuropathology and MK6240 PET positivity

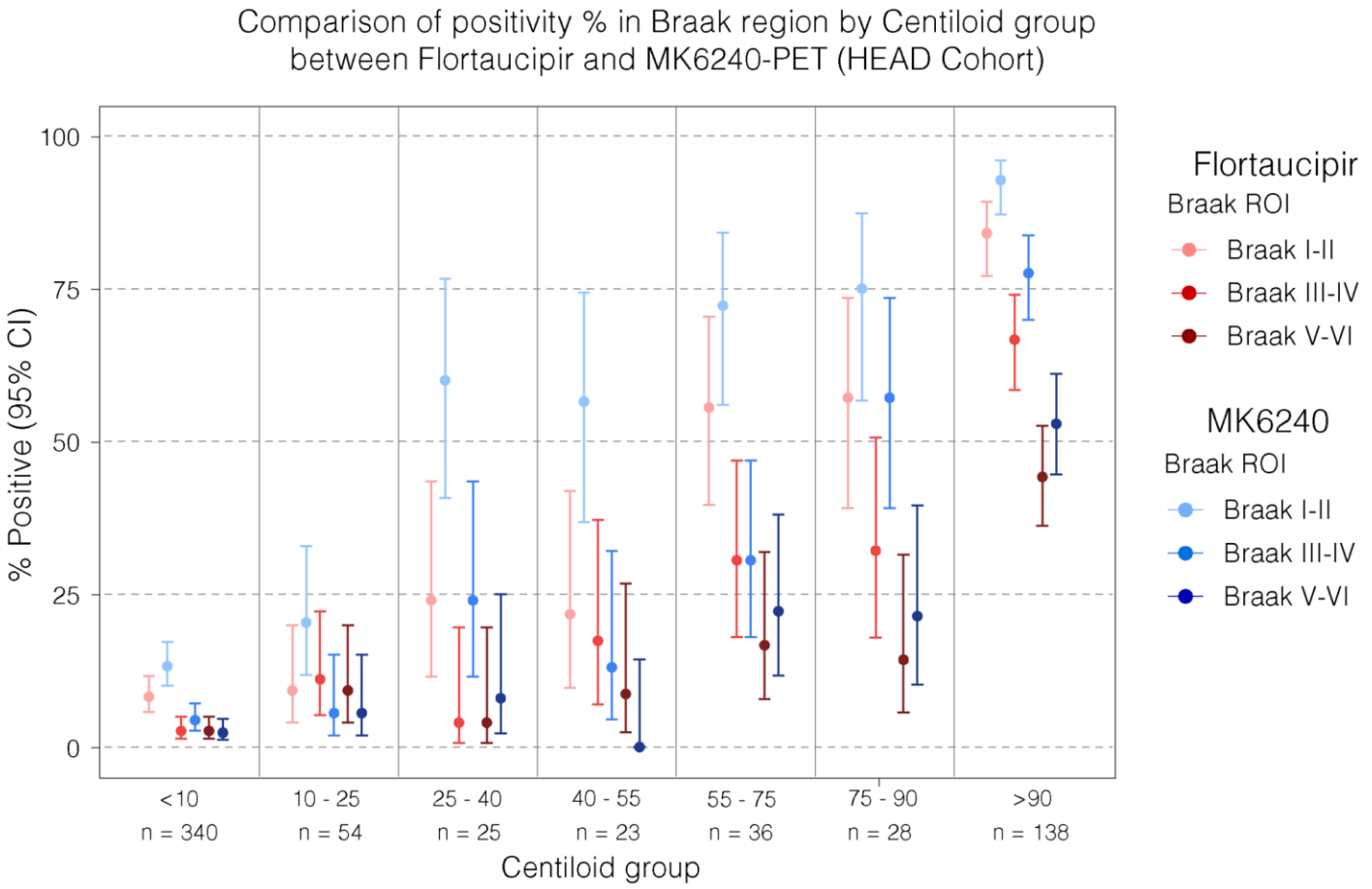
CDR Group	Stage	Test type	Odds Ratio	Higher Odds Group	p value	p adj BH	Sig	n PET	n NP
Aβ-									
0	I-II	Chi-square	0.01	Neuropathology	2.29e-93	6.86e-92	*	293	346
	III-IV	Chi-square	0.07	Neuropathology	2.17e-21	2.17e-20	*	293	346
	V-VI	Chi-square	0.76	Neuropathology	0.718	1		293	346
0.5−3	I-II	Chi-square	0.01	Neuropathology	1.28e-48	1.93e-47	*	84	272
	III-IV	Chi-square	0.07	Neuropathology	5.59e-14	3.35e-13	*	84	272
	V-VI	Fisher	0.77	Neuropathology	0.795	1		84	272
3.5−6	I-II	Fisher	0.04	Neuropathology	1.99e-05	6.62e-05	*	10	191
	III-IV	Fisher	0.42	Neuropathology	0.321	0.567		10	191
	V-VI	Fisher	1.03	PET	1	1		10	191
6.5−12	I-II	Fisher	0.22	Neuropathology	0.158	0.315		4	336
	III-IV	Fisher	0.15	Neuropathology	0.143	0.307		4	336
	V-VI	Fisher	1.08	PET	1	1		4	336
>12	I-II	Fisher	NA	Neuropathology	1	1		0	535
	III-IV	Fisher	NA	PET	1	1		0	535
	V-VI	Fisher	NA	PET	1	1		0	535
Aβ+									
0	I-II	Fisher	0.01	Neuropathology	1.34e-14	1e-13	*	60	129
	III-IV	Chi-square	0.05	Neuropathology	4.27e-10	2.13e-09	*	60	129
	V-VI	Fisher	0.38	Neuropathology	0.0221	0.0553		60	129
0.5−3	I-II	Fisher	0.01	Neuropathology	7.74e-07	2.9e-06	*	106	195
	III-IV	Chi-square	0.13	Neuropathology	2.37e-07	1.01e-06	*	106	195
	V-VI	Chi-square	0.57	Neuropathology	0.143	0.307		106	195
3.5−6	I-II	Fisher	0.05	Neuropathology	0.000283	0.000849	*	68	208
	III-IV	Chi-square	0.25	Neuropathology	0.0143	0.0389	*	68	208
	V-VI	Chi-square	0.73	PET	0.203	0.38		68	208
6.5−12	I-II	Fisher	0.39	Neuropathology	1	1		17	501
	III-IV	Fisher	2.58	Neuropathology	1	1		17	501
	V-VI	Fisher	1.82	PET	0.419	0.699		17	501
>12	I-II	Fisher	0.03	Neuropathology	1	1		1	1709
	III-IV	Fisher	0.16	Neuropathology	1	1		1	1709
	V-VI	Fisher	0.55	Neuropathology	1	1		1	1709

Adjusted p-values (p_adj) use the Benjamini–Hochberg correction within amyloid/CDR subgroups.

Sig (*) = adjusted p < 0.05. NP = Neuropathology

Fig 2. Comparing Neuropathologic and MK6240-PET Braak Staging Across CDR-SB groups

Bar plots display the proportion of tau-positive individuals (95% Wilson CI) in Braak I–II, III–IV, and V–VI regions. The table reports chi-square or Fisher's exact tests with Benjamini–Hochberg correction. Amyloid status was defined by CERAD for neurpathology (0/1 = A−, 2/3 = A+) and by Centiloid for PET (CL >= 24 = A+). PET Braak stage cut-offs were defined as mean + 2.0 SD from the CU Aβ− middle-aged adults (age <65 years) group. Only participants with available CDR-SB data acquired at least one year before death were included in the neuropathological analysis (n = 4,422). PET Braak discordant cases excluded (n = 644).



Differences between MK6240 and AV1451 PET positivity across Centiloid groups

Centiloid Group	Stage	Test type	p value	p adj BH	Higher Odds Tracer	Sig	n
<10	I–II	Chi -square	0.0352	0.106	MK6240		340
	III–IV	Chi -square	0.212	0.319	MK6240		340
	V–VI	Chi -square	0.806	0.806	AV1451		340
10–25	I–II	Chi -square	0.104	0.312	MK6240		51
	III–IV	Chi -square	0.489	0.716	AV1451		51
	V–VI	Fisher	0.716	0.716	AV1451		51
25–40	I–II	Chi -square	0.0099	0.0297	MK6240	*	45
	III–IV	Chi -square	0.0983	0.147	MK6240		45
	V–VI	Fisher	1.000	1.000	MK6240		45
40–55	I–II	Chi -square	0.0157	0.0470	MK6240	*	52
	III–IV	Chi -square	1.000	1.000	AV1451		52
	V–VI	Chi -square	0.489	0.733	AV1451		52
55–75	I–II	Chi -square	0.141	0.423	MK6240		52
	III–IV	Chi -square	1.000	1.000	Equal		52
	V–VI	Chi -square	0.551	0.827	MK6240		52

Adjusted p-values (p_adj) use the Benjamini–Hochberg correction within centiloid subgroups.
Sig (*) = adjusted $p < 0.05$.

Fig 3. Comparing MK6240 and Flortaucipir-PET Braak Staging Across Centiloid groups
Bar plots display the proportion of tau-positive individuals (95% Wilson CI) in Braak I–II, III–IV, and V–VI regions. The table reports chi-square or Fisher's exact tests with Benjamini–Hochberg correction. PET Braak stage cut-offs were defined as mean + 2.0 SD from the CU Aβ– middle-aged adults (age <65 years) group. Braak discordant cases excluded (n = 644).

Keywords: Tau, Braak staging, Neuropathology, Flortaucipir, MK6240

139 Predictors of data exclusion in MR-dependent imaging analyses of Alzheimer's disease

Shaney Flores[1], Jalen Scott[1], Ruijin Lu[1], Yi Su[2], Sarah Keefe[1], T. Hunter Smith[1], Russ Hornbeck[1], Nicole McKay[1], Jeremy Strain[1], Ashlee Simmons[1], Kaitlyn Dombrowski[1], Jacqueline Rizzo[1], Hope Shimony[1], Randall Bateman[1], Ganesh Babulal[1], Susan Landau[3], William Jagust[3], David Wolk[4], Jim Lah[5], Carey Gleason[6], Sterling Johnson[6], Erik Roberson[7], Reisa Sperling[8], Keith Johnson[8], John Morris[1], Chengjie Xiong[1], Brian Gordon[1], Tammie Benzinger[1]

[1]*Washington University School of Medicine, St. Louis, MO, US*
[2]*Banner Alzheimer's Institute, Phoenix, AZ, US*
[3]*Henry Wills Neuroscience Institute, Berkeley, CA, US*
[4]*University of Pennsylvania Perelman School of Medicine, Philadelphia, PA, US*
[5]*Emory University School of Medicine, Atlanta, GA, US*
[6]*Wisconsin Alzheimer's Disease Research Center, Madison, WI, US*
[7]*University of Alabama at Birmingham, Birmingham, AL, US*
[8]*Massachusetts General Hospital, Charlestown, MA, US*

Introduction: Quantifying β-amyloid (Aβ) accrual in Alzheimer's disease with *in vivo* PET typically requires contemporaneous structural MRI to define regions of interest (ROI). But when MRI is not acquired or if an acquired MRI is deemed unsuitable for ROI delineation due to excessive motion or comorbid pathology, the Aβ PET is excluded in MR-dependent analyses. Such exclusions could potentially limit study generalizability. We investigated participant features predicting data exclusion and further validated an existing MR-free PET pipeline to quantify this missing data.

Methods: Imaging, clinical, cognitive, and sociodemographic data were aggregated for 2082 individuals in a multi-site cohort. Participants were classified into two groups: those with usable MRI and those with either no MRI or whose MRI failed FreeSurfer segmentation (missing MRI/failed FS). Global cortical Centiloids (CL) derived using the FreeSurfer-based PET Unified Pipeline and the MR-free PET pipeline. Agreement between MR-dependent and MR-free CLs was examined using intra-class correlations. Differences between those with usable MRI and missing MRI/failed FS were assessed with Welch t-tests and Fisher's exact tests for continuous and categorical variables, respectively. Features predicting data exclusion were assessed with logistic regressions controlling for age, Clinical Dementia RatingÒ (CDR) status, and sex.

Results: MR-free and MR-dependent CLs were comparable for three widely used Aβ PET tracers (Figure 1; 11C-PiB: ICC=0.971 [0.929,0.0984], p<0.001; 18F-florbetapir: ICC=0.937 [0.800,0.971], p<0.001; 18F-florbetaben: ICC=0.965 [0.712,0.989], p<0.001). Approximately 19.5% of our cohort would have been excluded in a MR-dependent analysis. Excluded participants exhibited greater clinical and cognitive impairment (MMSE: t(126.50)=-4.513, p<0.001; Knight PACC: t(128.32)=-4.885, p<0.001), depressive symptomology (t(144.94)=2.925, p=0.004), and cerebrovascular comorbidities (Table 1). These features were significant predictors of data exclusion due to failed FS (Table 2).

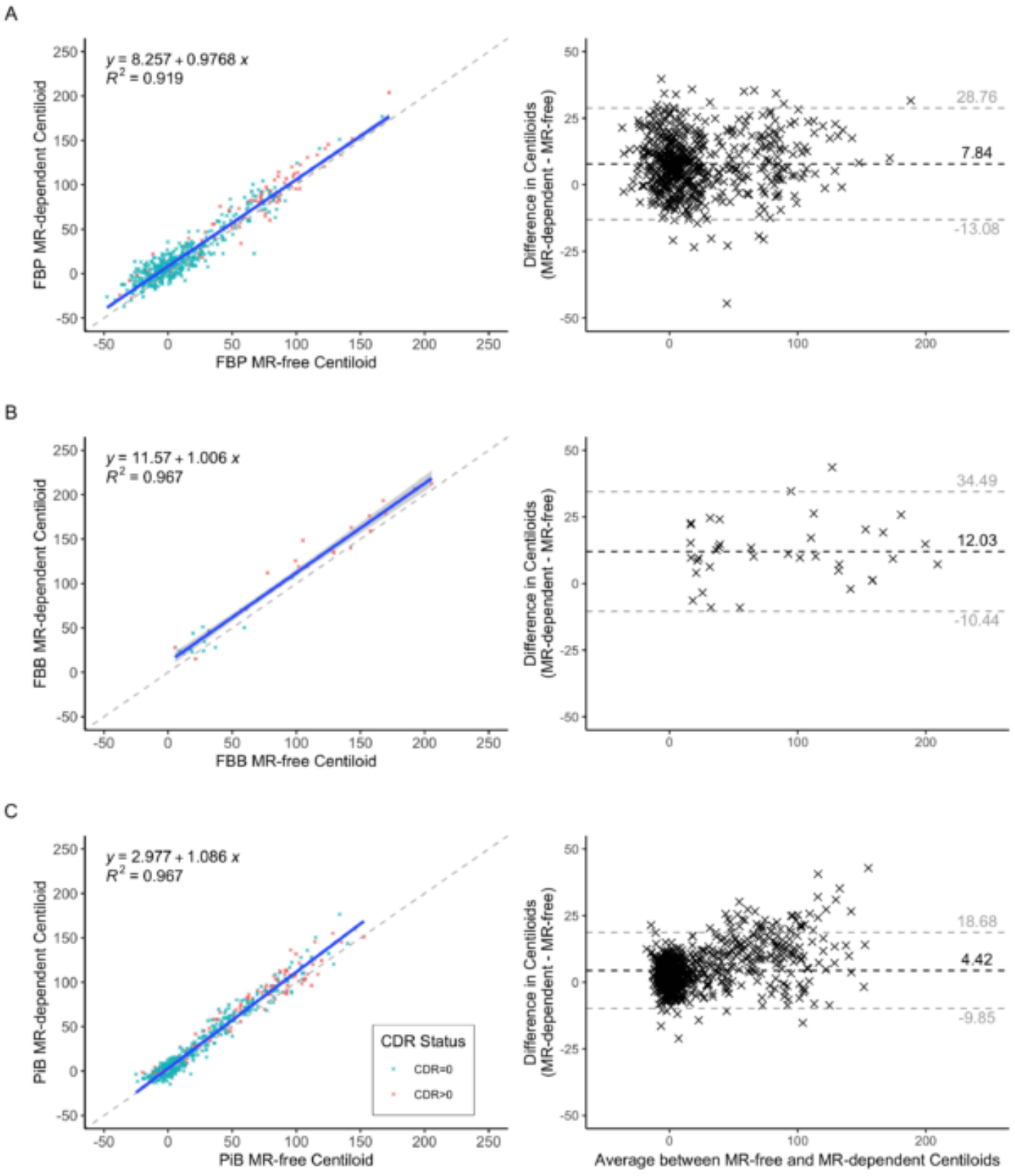


Figure 1. Regression and Bland-Altman plots comparing MR-dependent Centiloids (CL) and MR-free CLs for the amyloid tracers (A) 18F-florbetapir, (B) 18F-florbetaben, and (C) 11C-Pittsburgh Compound B.

Table 1. Characteristics of Cohort at Baseline

	N	Missing MRI/Failed FS (406)[1]	Usable MRI (1676)[1]	*p*-value[2]
Sex	1,869			**0.003**
female		147 (14%)	910 (86%)	
male		154 (19%)	658 (81%)	
Age	1,915	72.7 (8.9)	70.0 (8.5)	**<0.001**
Race	2,057			**0.015**
White		287 (18%)	1,298 (82%)	
Black/African American		107 (24%)	339 (76%)	
Asian		3 (20%)	12 (80%)	
American Indian or Alaska Native		4 (36%)	7 (64%)	
Ethnicity	1,937			>0.999
Non-Hispanic		357 (19%)	1,566 (81%)	
Hispanic or Latino		2 (14%)	12 (86%)	
Highest Education Achieved	1,807			**<0.001**
High School or Less		62 (20%)	243 (80%)	
Associate/Technical Schools		32 (12%)	226 (88%)	
Bachelor's		49 (9.9%)	447 (90%)	
Graduate		107 (14%)	641 (86%)	
CDR Global	1,711			**<0.001**
CDR=0		119 (9.0%)	1,196 (91%)	
CDR=0.5		79 (25%)	242 (75%)	
CDR>0.5		26 (35%)	49 (65%)	
MMSE	1,306	27.2 (3.2)	28.6 (2.2)	**<0.001**
Knight Preclinical Cognitive Composite	1,287	-0.7 (1.0)	-0.2 (0.8)	**<0.001**
ApoE Status	722			**0.023**
e4		82 (33%)	166 (67%)	
non-e4		118 (25%)	356 (75%)	
Body Mass Index	1,491	26.6 (20.9)	27.9 (9.2)	0.362
Geriatric Depression Scale	1,250	2.0 (2.7)	1.3 (1.8)	**0.004**
MR-free PET Centiloid	2,082	29.6 (43.5)	20.9 (37.1)	**<0.001**
WMH Volume (mm^3)	1,040	3.6 (0.6)	3.2 (0.6)	**<0.001**
Framingham 10-year CVD Risk	867	17.4 (3.5)	15.6 (4.5)	**<0.001**
Area Depreviation Index	941	46.9 (24.1)	43.9 (24.7)	0.182
Large Infarcts	621			**0.021**
Absent		55 (9.0%)	559 (91%)	
Present		3 (43%)	4 (57%)	
Small Infarcts	621			0.642
Absent		56 (9.2%)	550 (91%)	
Present		2 (13%)	13 (87%)	
Microbleeds	621			**<0.001**
Absent		44 (7.7%)	529 (92%)	
Present		14 (29%)	34 (71%)	

[1] n (%); Mean (SD)
[2] Fisher's exact test; Welch Two Sample t-test
Abbreviation: MMSE = Mini-Mental State Examination, WMH = White Matter Hyperintensity, CVD = Cardiovascular Disease

Table 2. Predictors for Failed MRI Segmentations

	N	B	OR (95% CI)	SE	z	*p*-value
Binarized Race	1,618					0.683
White			—	—	—	
Non-White		0.103	1.108 (0.666, 1.777)	0.249	0.411	
Education Level	1,628					0.127
4 year college or higher			—	—	—	
Less than 4 year college		0.294	1.341 (0.918, 1.945)	0.191	1.537	
MMSE	1,280	-0.092	0.912 (0.844, 0.989)	0.040	-2.300	**0.026**
Knight Preclinical Cognitive Composite	1,259	-0.326	0.722 (0.542, 0.961)	0.146	-2.239	**0.026**
ApoE Status	552					0.152
non-e4			—	—	—	
e4		0.413	1.512 (0.857, 2.636)	0.286	1.447	
Body Mass Index	1,389	-0.005	0.995 (0.982, 1.013)	0.007	-0.671	0.530
Geriatric Depression Scale	1,222	0.121	1.128 (1.029, 1.232)	0.046	2.648	**0.011**
MR-free PET Centiloid	1,631	0.003	1.003 (0.998, 1.007)	0.002	1.196	0.235
WMH Volume (mm^3)	863	0.566	1.761 (1.128, 2.770)	0.229	2.474	**0.013**
Framingham 10-year CVD Risk	862	0.033	1.034 (0.955, 1.118)	0.040	0.831	0.407
Area Depreviation Index	815	0.001	1.001 (0.990, 1.012)	0.006	0.214	0.830
Large Infarcts	607					**0.020**
Absent			—	—	—	
Present		2.114	8.285 (1.448, 42.46)	0.832	2.540	
Small Infarcts	607					0.699
Absent			—	—	—	
Present		0.318	1.375 (0.204, 5.448)	0.798	0.399	
Microbleeds	607					**<0.001**
Absent			—	—	—	
Present		1.458	4.296 (2.035, 8.737)	0.369	3.947	

Abbreviations: CI = Confidence Interval, MMSE = Mini-Mental State Examination, WMH = White Matter Hyperintensity, CVD = Cardiovascular Disease, OR = Odds Ratio, SE = Standard Error

Discussion: Data exclusion in imaging studies is not entirely random. MR-free PET quantification methods offer an alternative that may enhance the generalizability of imaging study results.

Keywords: MR-free PET, data exclusion, amyloid PET

140 Brain network architecture shapes the pattern of tau-induced neuronal dysfunction in Alzheimer's disease, while tau load drives local damage

Lukas Frontzkowski[1,5], Sebastian Roemer-Cassiano[1,4], Johannes Gnörich[5], Anna Dewenter[1], Anna Steward[1], Zeyu Zhu[1], Madleen Klonowski[1], Fabian Hirsch[1], Davina Biel[1,3], Carla Palleis[4], Günter Höglinger[2,4,6], Matthias Brendel[2,5,6], Nicolai Franzmeier[1,2,3]

[1]*Institute for Stroke and Dementia Research (ISD), LMU University Hospital, Ludwig-Maximilians-University (LMU), Munich, Germany*
[2]*Munich Cluster for Systems Neurology (SyNergy), Munich, Germany*
[3]*University of Gothenburg, The Sahlgrenska Academy, Institute of Neuroscience and Physiology, Department of Psychiatry and Neurochemistry, Gothenburg, Sweden*
[4]*Department of Neurology, LMU University Hospital, Ludwig-Maximilians-University (LMU), Munich, Germany*
[5]*Department of Nuclear Medicine, LMU University Hospital, Ludwig-Maximilians-University (LMU), Munich, Germany*
[6]*German Center for Neurodegenerative Diseases (DZNE), Munich, Germany*

Objectives: Tau pathology in Alzheimer's disease (AD) follows a connectome-based propagation pattern that mirrors the brain's network architecture. Neuronal dysfunction often exceeds beyond tau affected brain regions, but it remains unclear how tau shapes downstream neuronal dysfunction. Therefore, we aimed to combine tau-PET, perfusion-PET and functional connectivity to investigate the relationship between network architecture, tau burden and neuronal dysfunction.

Methods: We included 140 Aβ-positive individuals across the AD continuum and used dynamic 0-60min [^{18}F]PI-2620 tau-PET to compute standardized uptake value ratios (SUVR) and leveraged kinetic modeling to compute perfusion (R1) measures as proxy for neuronal dysfunction (Fig. 1A/B). Tau-PET epicenters were defined as top 5% of regions with highest SUVRs. A normative resting-state fMRI-based connectome from 66 amyloid and tau negative healthy controls was used to assess connectivity-based distance to tau-PET epicenters.

Results: Within patients, tau deposition patterns showed only a weak association with the spatial pattern of neuronal dysfunction, while connectivity-based distance to tau-PET epicenters was strongly linked to the spatial pattern of neuronal dysfunction (Cohen's d: 0.35 vs 0.91, Fig.2A). In contrast, the absolute levels of local neuronal dysfunction were strongly associated with local tau burden (Fig.2C) while tau-PET epicenters based-connectivity predicted hypoperfusion levels only in early AD disease stages with low global tau burden (Fig.2B), indicative of an early-stage diaschisis-like dysconnection. Lastly, we observed that hypoperfusion mediated the association between tau-PET and MMSE (Fig.3), suggesting that tau induces cognitive decline by triggering neuronal dysfunction.

Conclusions: Our findings add mechanistic insight into a network-based model of neuronal dysfunction in AD, wherein the connectivity of tau epicenters shape the brain-wide pattern of neuronal dysfunction while the amount of local tau burden determines the degree of damage that triggers cognitive deficits. This dual framework advances our understanding of how tau pathology drives cognitive decline in AD.

Figure 1: Group average PI-2620 SUVR and R1 patterns

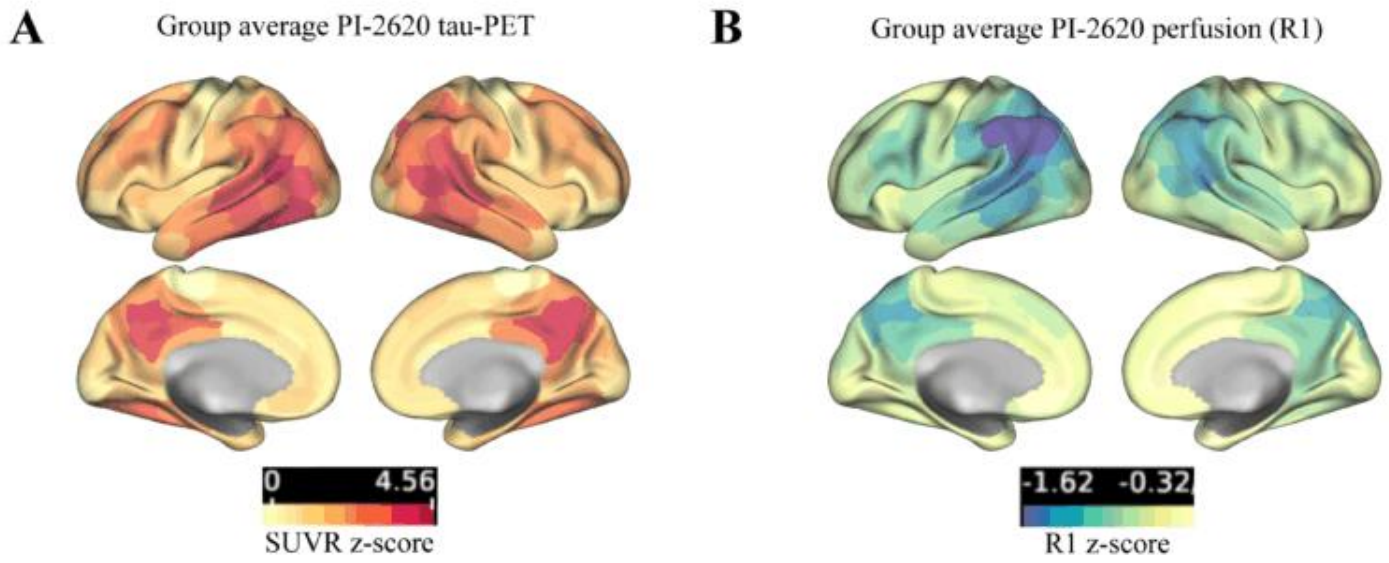


Figure 2: Association between network architecture, tau burden and neuronal dysfunction

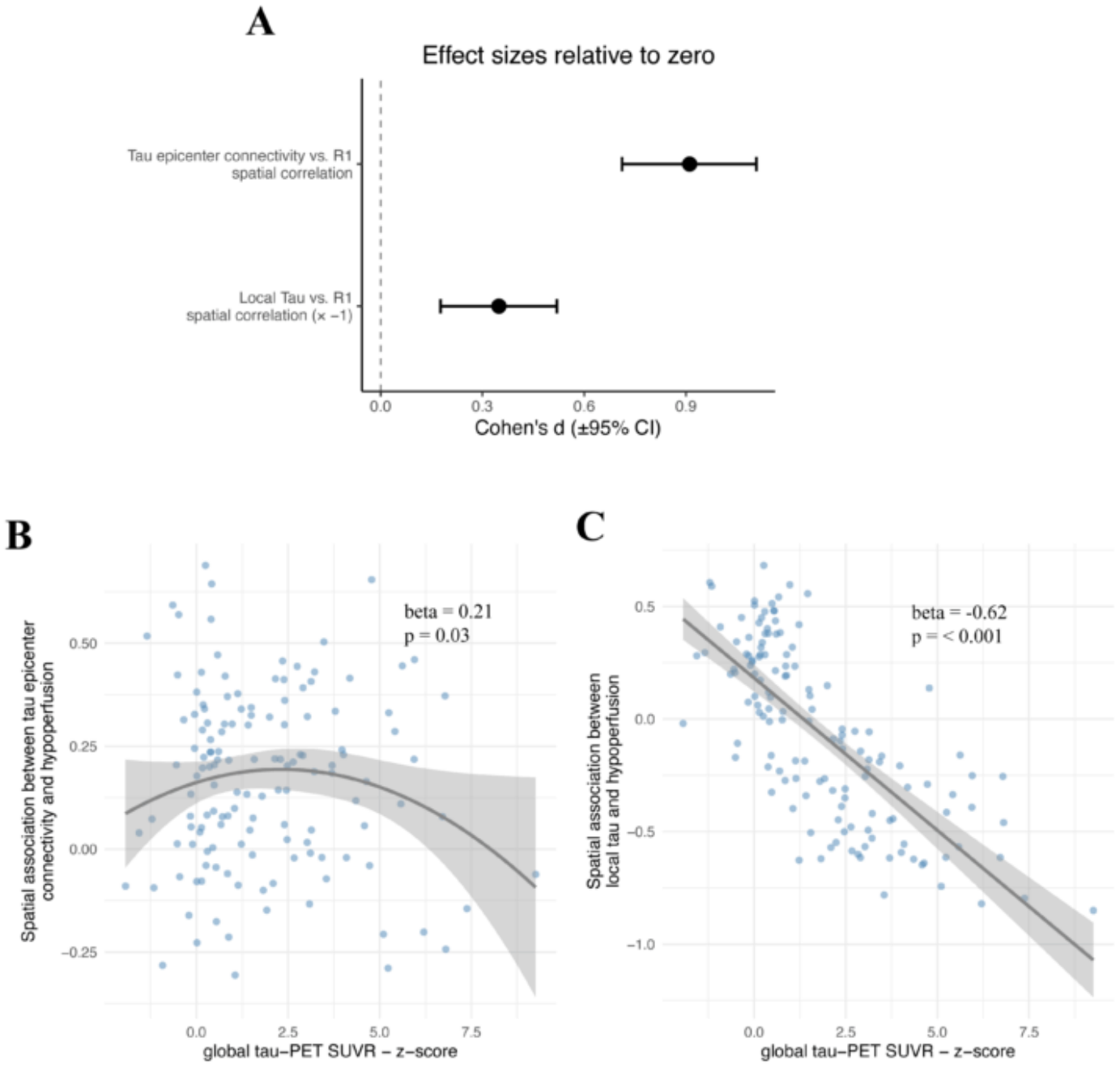
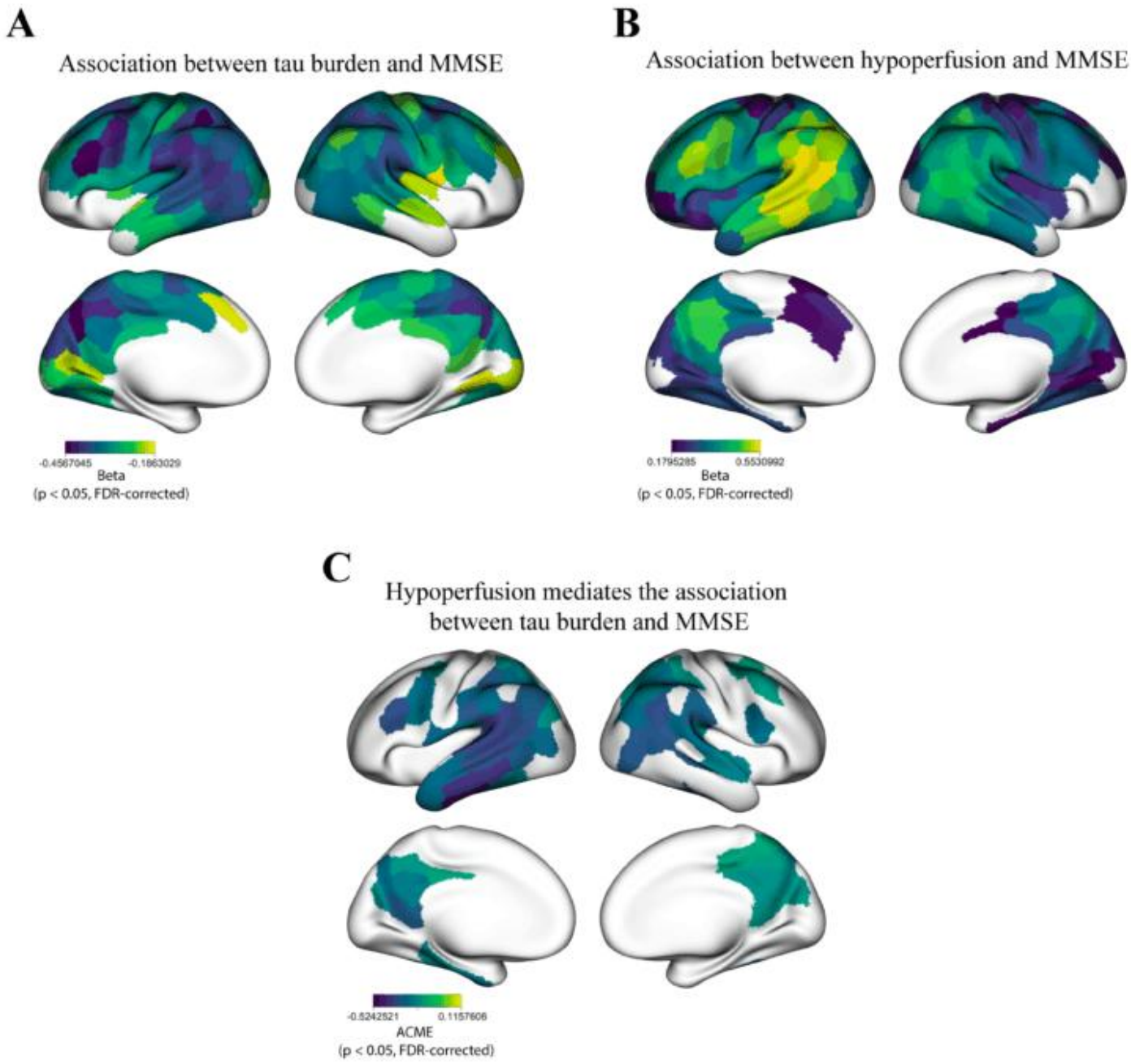


Figure 3: Hypoperfusion mediates the association between tau pathology and cognitive decline



Keywords: Tau, Neuronal dysfunction, PI-2620, Alzheimer's disease

141 Cortical thickness and female sex confer resilience to tau-related cognitive decline: A large multi-cohort study

Stuart Mitchell

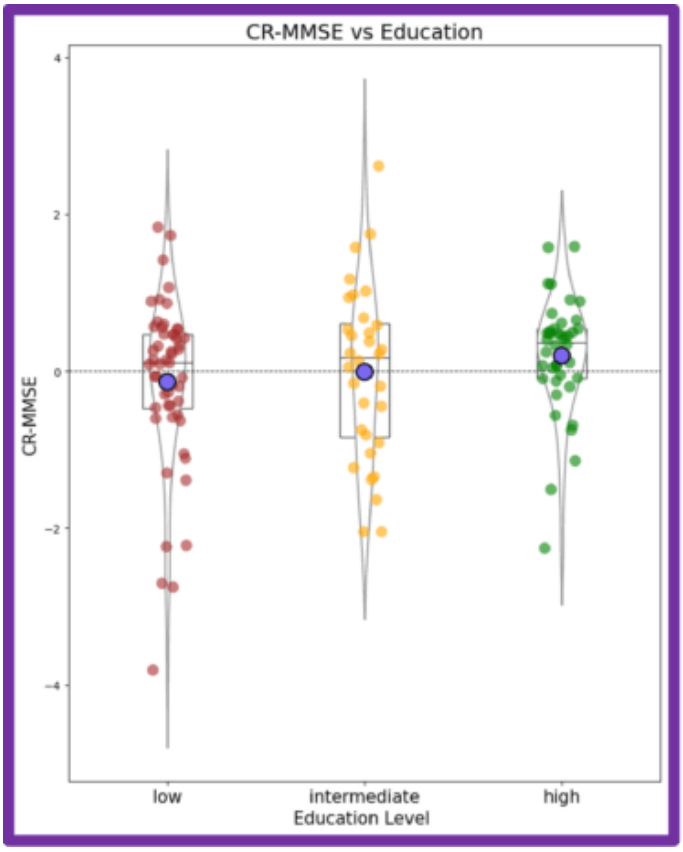
[1]McGill University, Translational Neuroimaging Lab, Montreal, QC, Canada

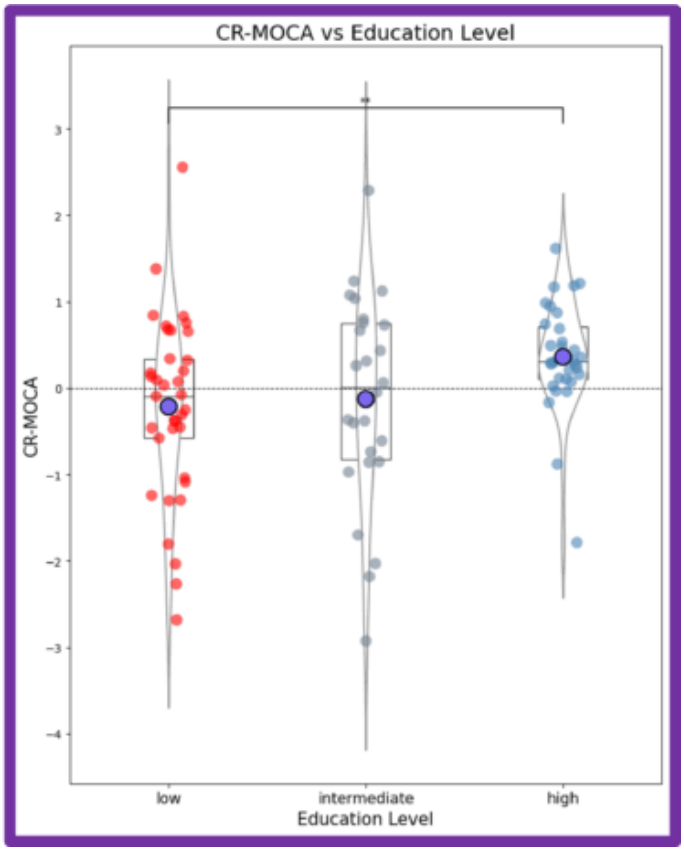
Background: Brain and cognitive resilience (BR, CR) reflect the capacity to preserve neural integrity and cognitive performance despite accumulating tau pathology in Alzheimer's disease (AD). Tau burden, quantified using [18F]MK-6240 and [18F]AV-1451 standardized uptake value ratios (SUVR), provides a sensitive measure of neurofibrillary tangle deposition and enables quantitative modeling of resilience mechanisms. This study aimed to evaluate the contribution of tau-PET SUVR metrics to resilience models, compare their predictive power across cognitive measures, and characterize interactions among tau pathology, cortical integrity, and cognitive decline across independent cohorts.

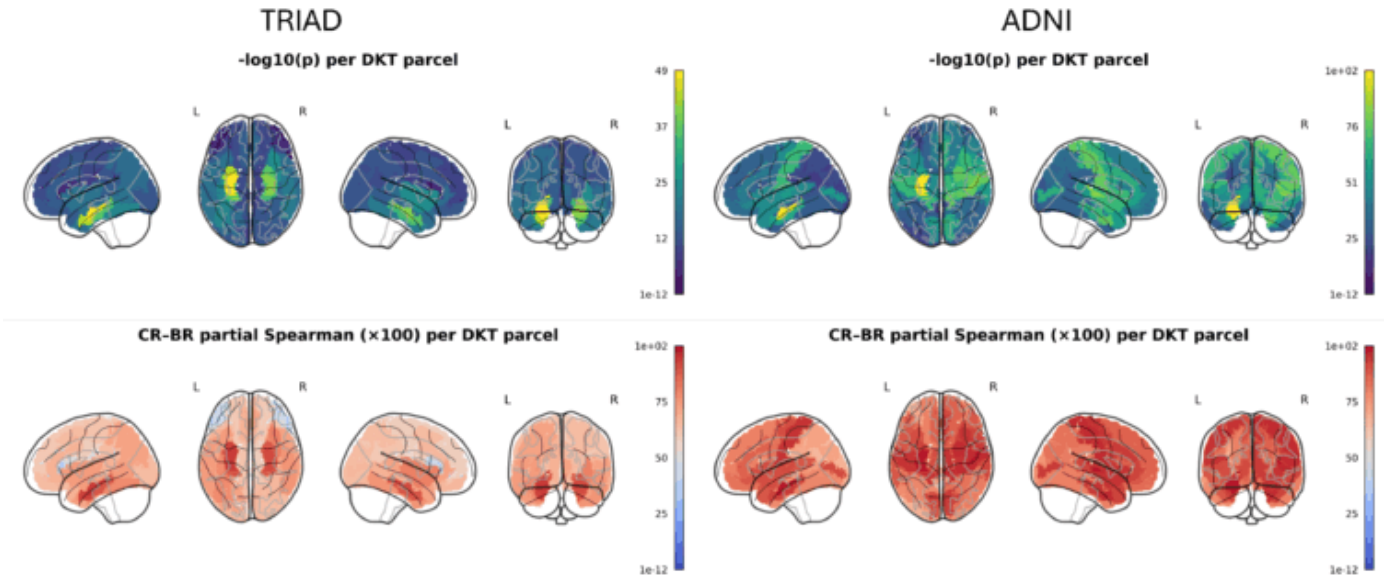
Methods: We analyzed 285 amyloid-β–positive participants from the TRIAD and ADNI cohorts (mean age = 68.7 ± 8.2 years; MCI + AD) who underwent [18F]MK-6240 or [18F]AV-1451 PET and cognitive testing. Cortical thickness served as a proxy for brain resilience. Associations among tau SUVR, cognition, and resilience factors (sex, education, APOE genotype, and white matter hyperintensities) were assessed using linear regression and partial Spearman correlations, controlling for age and education. Replication was conducted in ADNI using identical analytic pipelines.

Results: MCI participants demonstrated relative cognitive resilience despite comparable tau burden, while females exhibited greater brain resilience in SUVR–cortical thickness associations (stβ = –0.227, P = 0.0156), suggesting structural protection against tau-related neurodegeneration. Compared with education, MoCA more sensitively captured cognitive resilience than MMSE, supporting its value for early detection. Glass-brain analyses revealed convergent BR–CR patterns across the cortex, with strongest effects in early tau-accumulating regions (entorhinal, inferior temporal, and posterior cingulate cortices). Findings were replicated in ADNI.

Conclusion: Cortical thickness and tau aggregation may act as synergistic biomarkers of resilience in AD. Female sex and preserved cortical integrity emerge as key protective factors against tau-related cognitive decline. These findings support resilience as a quantifiable, cross-cohort construct for precision prognostication and targeted intervention.







Keywords: Alzheimers, tau, cognitive resilience, brain resilience, PET Imaging

142 Structure-guided design of 18F-FD4—a PET tracer of α-synuclein fibrils

Cong Liu[1], Dan Li[2], Jian Wang[3], Chuantao Zuo[4], Li Tan[1], Jiang Bian[2], Roger Fan[5], Qing Liang[5,6]

[1]*Interdisciplinary Research Center of Biology and Chemistry, Shanghai Institute of Organic Chemistry, Chinese Academy of Sciences, Shanghai, CN*
[2]*Shanghai Jiao Tong University, Shanghai, CN*
[3]*Department of Neurology, Huashan Hospital, Shanghai, CN*
[4]*Department of Nuclear Medicine, Huashan Hospital, Shanghai, CN*
[5]*Synusight Biotech (Shanghai) Co., Ltd., Shanghai, CN*
[6]*IRAD Bio LLC, Philadelphia, PA, US*

Parkinson's disease (PD) and related synucleinopathies are defined by the pathological aggregation of α-synuclein (α-syn) fibrils, a central hallmark of disease progression. Non-invasive visualization of α-syn pathology is critically needed to enable early diagnosis, patient stratification, and therapeutic monitoring. However, effective α-syn PET tracers—especially those capable of reliably detecting pathology in PD—remain unavailable. High-resolution cryo-EM structures have revealed precise ligand-binding sites on α-syn fibril polymorphs, providing a structural foundation for rational tracer design. Leveraging these insights, we applied a structure-guided design paradigm to develop 18F-FD4, a novel PET tracer with optimized affinity and selectivity for pathological α-syn fibrils.

We hypothesize that 18F-FD4, through structure-based optimization, will demonstrate superior binding specificity and affinity to α-syn aggregates, enabling accurate in vivo visualization of synucleinopathies.

Lead compounds were initially identified via structure-based high-throughput screening, then refined through iterative structure-guided design to yield FD4. Binding specificity was confirmed through radioligand binding, autoradiography, and immunofluorescence assays. In vivo PET imaging in rodent and marmoset models demonstrated robust visualization of α-syn pathology. Furthermore, investigator-initiated clinical trials (IIT) in PD and Multiple System Atrophy (MSA) patients validated FD4's translational capability as a clinically applicable α-syn PET tracer. By enabling in vivo imaging of α-syn pathology, 18F-FD4 could transform the diagnostic paradigm of PD, facilitating earlier and more precise diagnosis as well as objective assessment of therapeutic efficacy.

Next, multicenter and longitudinal IIT studies will be expanded, complemented by cross-validation against established biomarkers such as Serum Amyloid A (SAA). Parallel IND filings in China and the United States will support initiation of regulatory-grade clinical studies.

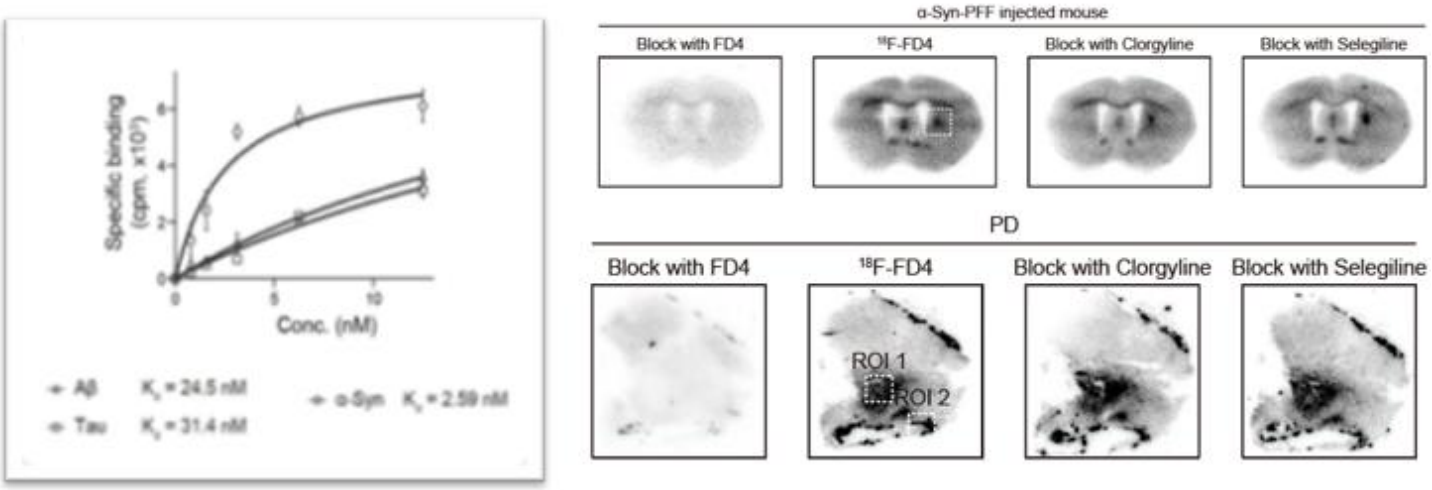


Fig 1. Binding affinity of 18F-FD4 to α-syn, Aβ, and Tau PFFs measured by radioligand binding assays, and autoradiographic labeling of α-syn PFF-injected mouse and PD patient brain slices.

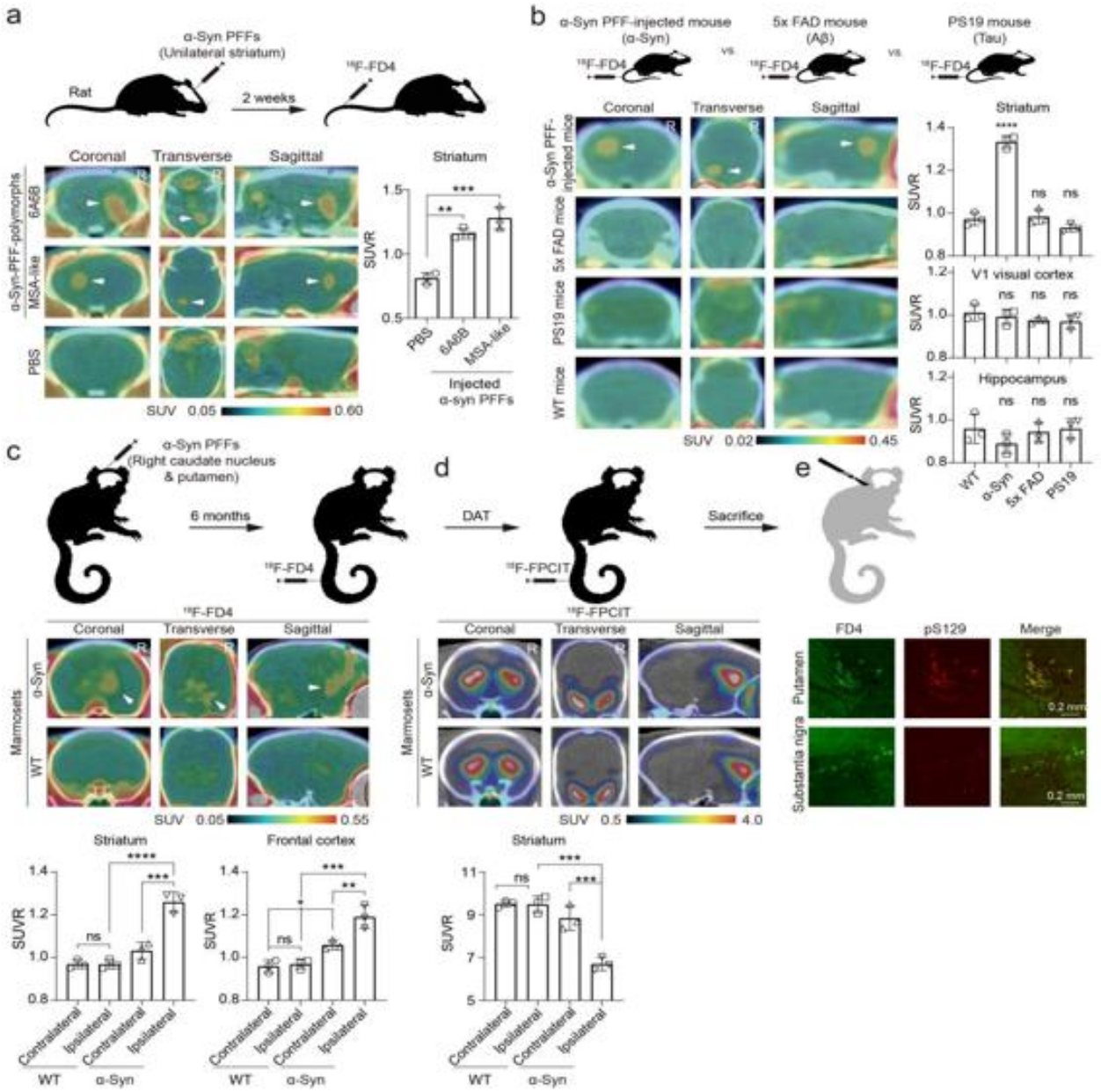


Fig 2. In vivo PET imaging of α-syn aggregates in rodent and marmoset brains using tracer 18F-FD4.

Keywords: α-synuclein, PET imaging, Parkinson's disease

143 NULISAseq CNS proteomic signatures of astrocytic reactivity in Alzheimer's disease

Ruyu Shi[1,3], Xuemei Zeng[1,2,3], Wasiu G. Balogun[1,2,3], Marissa F. Farinas[1,2,3], Brian J. Lopresti[1,3], Alexandra Gogola[4], Milos Ikonomovic[3,5,6], Howard Aizenstein[1,3], Victor L. Villemagne[1,3], Ann D. Cohen[1,3], Thomas K. Karikari[1,2,3]

[1]*Department of Psychiatry, School of Medicine, University of Pittsburgh, Pittsburgh, PA, US*
[2]*Biofluid Biomarker Laboratory, Western Psychiatric Hospital, University of Pittsburgh Medical Center, Pittsburgh, PA, US*
[3]*Alzheimer's Disease Research Center, University of Pittsburgh, Pittsburgh, PA, US*
[4]*Department of Radiology, University of Pittsburgh, Pittsburgh, PA, US*
[5]*Department of Neurology, University of Pittsburgh, Pittsburgh, PA, US*
[6]*Geriatric Research Education and Clinical Center, VA Pittsburgh HS, Pittsburgh, PA, US*

Objectives: Neuroinflammation involving reactive astrogliosis is increasingly recognized as a central pathological mechanism in Alzheimer's disease (AD). The NULISAseq CNS Disease Panel is a highly sensitive, multiplexed proteomic assay, with several of its blood-based biomarkers showing strong associations with Aβ pathology. However, its utility in monitoring astrocytic activation in blood remains unexplored. In this study, we investigated the relationship between NULISAseq biomarkers in plasma and reactive astrogliosis measured by the PET tracer [18F]SMBT-1, that binds to monoamine oxidase-B (MAO-B) overexpressed in reactive astrocytes. Our goal was to evaluate the potential of NULISAseq biomarkers for monitoring reactive astrogliosis in patients' plasma samples.

Methods: Participants from the INflammation ROIes in Aging and Alzheimer's disease Study (INROAADS) underwent blood collection, [11C]PiB and [18F]SMBT-1 PET imaging. Plasma samples were analyzed using the NULISAseq CNS Disease Panel 120 on an ArgoHT.

Results: Among 85 participants (51.8% female; 89.4% self-identified as non-Hispanic White, aged 68.1 ± 7.4 years, 16.5% Aβ PET-positive [59.4 ± 35.8 Centiloids]), 21 plasma proteins showed significant correlation with global Aβ burden on PET (Spearman $p < 0.05$, 29% FDR). The most significant biomarkers included APOE4, phosphorylated tau (p-tau217, p-tau231, and p-tau181), Aβ42, and several cytokines. In contrast, only three proteins-NPTX2, IL-12p70, and IL-16-were nominally associated with [18F]SMBT-1 retention in the precuneus, a region vulnerable to early Aβ deposition. Positive association with NPTX2 at early stages may reflect a protective effect to preserve synaptic integrity, while negative associations with IL-12p70 and IL-16 could indicate a different kind of reactive astrocytes.

Conclusions: The NULISAseq CNS panel more effectively captures Aβ pathology than reactive astrocytes assessed by SMBT-1 during the early stages of AD. This highlights the need for novel plasma biomarkers capable of monitoring reactive astrocytosis across the AD spectrum.

Keywords: NULISAseq CNS panel, [18F]SMBT-1 PET, Plasma biomarkers, Reactive astrocytes, Alzheimer's disease

144 High p-tau217 levels nullify the slower cognitive progression in younger older adults

Ruyu Shi[1,2], Lamia T. Choity[1,2,3], Shayna T. Brodman[1,2,3], Xuemei Zeng[1,2,3], Rebecca A. Deek[4], Jeremy Gu[1,2,3], Marissa F. Farinas[1,2,3], Michel N. Nafash[1,2,3], Annie Bedison[5], Rocco B. Mercurio[6], Cristy Matan[7], Alexandra Gogola[7], Julia Kofler[2,8], Dana L. Tudorascu[1,2], Neelesh K. Nadkarni[2,9], Howard J. Aizenstein[1,2], Elizabeth Shaaban[2,6], Jennifer Lingler[2,10], Tharick A. Pascoal[1,2,11], Victor L. Villemagne[1,2], Sarah B. Berman[2,11], Robert A. Sweet[1,2], Beth E. Snitz[2,11], Milos D. Ikonomovic[2,11,12], Ann D. Cohen[1,2], M. Ilyas Kamboh[2,5,6], Oscar I. Lopez[2,11], Thomas K. Karikari[1,2,3]

[1]*Department of Psychiatry, School of Medicine, University of Pittsburgh, Pittsburgh, PA, US*
[2]*Alzheimer's Disease Research Center, University of Pittsburgh, Pittsburgh, PA, US*
[3]*Biofluid Biomarker Laboratory, Western Psychiatric Hospital, University of Pittsburgh Medical Center, Pittsburgh, PA, US*
[4]*Department of Biostatistics and Health Data Science, School of Public Health, University of Pittsburgh, Pittsburgh, PA, US*
[5]*Department of Human Genetics, School of Public Health, University of Pittsburgh, Pittsburgh, PA, US*
[6]*Department of Epidemiology, School of Public Health, University of Pittsburgh, Pittsburgh, PA, US*
[7]*Department of Radiology, School of Medicine, University of Pittsburgh, Pittsburgh, PA, US*
[8]*Department of Pathology, University of Pittsburgh, Pittsburgh, PA, US*
[9]*Division of Geriatric Medicine, School of Medicine, University of Pittsburgh, Pittsburgh, PA, US*
[10]*Department of Health and Community Systems, School of Nursing, University of Pittsburgh, Pittsburgh, PA, US*
[11]*Department of Neurology, University of Pittsburgh, Pittsburgh, PA, US*
[12]*Geriatric Research Education and Clinical Center, VA Pittsburgh Healthcare System, Pittsburgh, PA, US*

Background: Plasma p-tau217 is a key biomarker for Alzheimer's Disease (AD), strongly associated with amyloid pathology and faster cognitive decline. While younger age typically progresses slower, how age modifies p-tau217's effect remains unclear. Addressing this gap may improve risk prediction.

Method: Participants from the University of Pittsburgh Alzheimer's Disease Research Center with plasma p-tau217 and Clinical Dementia Rating (CDR-GS) were followed up to 29 years (median 3.0 [IQR 1.0-5.0]). A subset (n=334) underwent amyloid-PET. Plasma p-tau217 was quantified by ALZpath p-tau217 assay. Cox proportional hazards models, adjusted for sex, APOE4 carrier and baseline clinical diagnosis, were used to examine the association between p-tau217 and progression risk, defined as an increase in CDR-GS during follow-up. Kaplan-Meier curves were used for visualization.

Result: Among 3742 individuals (aged 73.4 years [IQR66.1-79.0]; 59.9% female; 90.6% self-identified non-Hispanic White), high p-tau217 (≥0.695pg/mL, single-cutoff) and older age (≥70 years) independently predicted faster progression (HR 1.8[1.6-2.0] and 1.2[1.1-1.4]). Using dual-cutoff (0.615pg/mL; 0.951pg/mL), intermediate and high p-tau217 showed HRs of 1.6(1.3-1.8) and 2.0(1.7-2.4). Age significantly modified association between p-tau217 and progression (p<0.0001). Among younger individuals, high p-tau217 shows a greater hazard (HR 2.0[1.5-2.6], single-cutoff) and shorter median survival (2.2 vs 13.5 years for low p-tau217). In older individuals, the corresponding HR was 1.6(1.4-1.9), with median survival of 2.9 vs 5.8 years. Applying dual-cutoff approach revealed dose-response pattern. Among younger participants, intermediate p-tau217 showed a moderately elevated hazard (HR 1.7[1.2-2.5]; median 4.5 vs 14.9 years for low p-tau217), whereas high levels showed the strongest effect (HR 2.4[1.7-3.2]). In older adults, the trend was consistent though attenuated. Median survival did not differ between younger and older individuals with high p-tau217 under either cutoff approach.

Conclusion: High or intermediate p-tau217 negates the protective effect of youth on progression, highlighting early p-tau217 screening among younger adults to enable timely AD interventions.

Keywords: p-tau217, age interaction, cognitive progression, Azheimer's disease, risk prediction

Podium Session

KEYNOTE: Integrated Proteomics for Target and Biomarker Discovery in Alzheimer's Disease

Wednesday, January 14, 2026		
11:35 am - 12:05 am	Keynote: Integrated proteomics for target and biomarker discovery in Alzheimer's disease	**Nick Seyfried**, Emory University, Atlanta, GA, USA

Integrated Proteomics for Target and Biomarker Discovery in Alzheimer's Disease

Eric B. Dammer1,5, Erik C.B Johnson2,5 Aleksandra M. Wojtas1,5, Joshna Gadhavi1,5, Saima Rathore3,5 Anantharaman Shantaraman1,5, Qi Guo1,5, Rafi Haque2,5, Kathleen E. Carter2,5, Caroline M. Watson1,2,5, Lingyan Ping2,5, Duc M. Duong1,5, Yona Levites4,5, Todd E. Golde4,5, James J. Lah2,5, Lenora Higginbotham2,5, Allan I. Levey2,5 and Nicholas T. Seyfried1,2,5

1Department of Biochemistry, Emory University School of Medicine, Atlanta, GA, USA
2Department of Neurology, Emory University School of Medicine, Atlanta, GA, USA
3Department of Biomedical Informatics, Emory University School of Medicine, Atlanta, GA, USA
4Department of Department of Pharmacology and Chemical Biology, Emory University School of Medicine, Atlanta, GA, USA
5Center for Neurodegenerative Disease, Emory University School of Medicine, Atlanta, GA, USA

The proteome is the "executioner" of the effects of aging, genetics, the environment, and other risk factors that cause human disease. In Alzheimer's disease (AD), amyloid-beta (Aβ) and Tau were identified with classical biochemical methods, enabling breakthroughs from discovery as proteins directly altered in AD pathology. We hypothesize the AD proteome undoubtedly contains many other proteins that play key roles in the initiation and progression of AD. To further our understanding of AD pathophysiology and to identify new targets for early intervention, we employed unbiased large-scale quantitative proteomic methods utilizing high-resolution mass spectrometry platforms. To date, we have analyzed over 2000 individual brain tissues from multiple regions, quantifying nearly 9,000 proteins per sample. Systems biology approaches have enabled us to resolve modules or communities of proteins that correlate strongly with clinical, neuroimaging and pathological AD phenotypes. These modules reflect key mechanisms linked to impaired synaptic, vascular, metabolic and glial function. These comprehensive brain proteomic datasets linked to AD and other neurodegenerative diseases are then integrated with the cerebrospinal fluid (CSF) and plasma proteome profiles in AD patients to prioritize brain-based biomarkers in humans for the diagnosis, staging and therapeutic response to treatment.

Wednesday, January 14, 2026 - 01:10 pm - 02:40 pm

Podium Session

SESSION VIII: Moderators and co-pathologies

CHAIRS:

Annie Cohen, *University of Pittsburgh, Pittsburgh, PA, USA*

Trey Hedden, *Icahn School of Medicine at Mount Sinai, New York, NY, USA*

Wednesday, January 14, 2026			
01:10 pm – 02:40 pm	**Podium Presentation**	**Authors**	**Presenters**
01:15 pm – 01:30 pm	Investigating the role of socioeconomic status on AD biomarker relationships	Ovaici | Mindt | Okonkwo | Miller | Baker | Snyder | O'Bryant | Braskie | Harrison | Chadwick | Chao | Jagust | Weiner | Landau	**Nazanin Ovaici**, University of California, Berkeley, Berkeley, CA, US
01:30 pm – 01:45 pm	Blood LDL cholesterol synergistically amplifies tau pathology and cognitive outcome in an APOE4-dependent manner	Wang | Ossenkoppele | Collins | Burnham | Sims | Hansson | Mintun | Lu	**Tina Wang**, Eli Lilly and Company, Indianapolis, IN, US
01:45 pm – 02:00 pm	Mismatch between tau burden and cognitive domain performance identifies sub-groups with specific co-pathologies	Brown | Mundada | Liu | McGrew | Nasrallah | Das | Mechanic-Hamilton | Yushkevich | Wolk	**Christopher Brown**, Department of Neurology, University of Pennsylvania, Philadelphia, PA, US
02:00 pm – 02:15 pm	Characterizing the brain-wide atrophy pattern of LATE-NC-associated hippocampal sclerosis: an imaging-pathologic association study	Grothe | Zhang | López-González | Sánchez-Juan | Rábano | Silva-Rodríguez	**Michel Grothe**, Reina Sofia Alzheimer Center, CIEN Foundation, Spain

Investigating the role of socioeconomic status on AD biomarker relationships

Nazanin Ovaici[1], Monica Mindt[2,3], Ozioma Okonkwo[4], Melanie Miller[5,6], Laura Baker[7], Heather Snyder[8], Sid O'Bryant[9], Meredith Braskie[10], Theresa Harrison[1], Trevor Chadwick[1], Yishu Chao[1], William Jagust[1], Michael Weiner[5,6], Susan Landau[1]

[1]*University of California, Berkeley, Berkeley, CA, US*
[2]*Fordham University, Bronx, NY, US*
[3]*Icahn School of Medicine at Mount Sinai, New York, NY, US*
[4]*University of Wisconsin School of Medicine and Public Health, Madison, WI, US*
[5]*University of California, San Francisco, San Francisco, CA, US*
[6]*Northern California Institute for Research and Education, San Francisco, CA, US*
[7]*Wake Forest University School of Medicine, Winston-Salem, NC, US*
[8]*Alzheimer's Association, Chicago, IL, US*
[9]*The University of North Texas Health Science Center, Fort Worth, TX, US*
[10]*Keck School of Medicine of the University of Southern California, Los Angeles, CA, US*

Background: Low socioeconomic status (SES) individuals are underrepresented in Alzheimer's disease (AD) research cohorts despite comprising a large segment of the U.S. older adult population. Here, we examined relationships between SES and measures of AD progression across three cohorts with varying proportions of high/low SES individuals.

Method: We included participants with available amyloid (CL) and tau PET (entorhinal and meta-temporal) measures, socioeconomic status (SES) assessed with the Hollingshead Two-Factor Index calculated using occupation complexity rank and education, and Area Deprivation Index (ADI) scores from the Alzheimer's Disease Neuroimaging Initiative (ADNI; N=611), the Imaging substudy of the U.S. Study to Protect Brain Health Through Lifestyle Intervention to Reduce Risk (US POINTER; N=880), and the Health & Aging Brain Study-Health Disparities (HABS-HD; N=1035). In each cohort, we compared the demographic, clinical and biomarker characteristics of low (Hollingshead ≥ 47) versus high SES participants (Hollingshead<47), and tested SES as a moderator of amyloid-tau relationships, controlling for age, sex, and ApoE4.

Results: Across all cohorts, lower SES participants (ADNI: 11%, POINTER: 15%, HABS-HD: 27%) had higher ADI, and lower MMSE, and were more likely to be impaired (Table). There was no main effect of the SES group on amyloid or tau in any cohort. However, for a given CL value, low SES individuals had disproportionately higher tau than their high SES counterparts across cohorts (Figure), though this effect was not consistent across impaired/unimpaired groups, entorhinal/meta-temporal regions, and cohorts, perhaps due to sample size limitations.

Conclusion: Despite overall limited representation of low SES individuals, we observed a pattern of disproportionately higher tau for a given degree of amyloid burden across three multisite cohorts with heterogeneous sociodemographic characteristics. SES may capture multidimensional social and health-related factors that influence AD biomarker progression.

Characteristic	ADNI			POINTER			HABS-HD		
	High SES ≤ 47, 543 (89%)[1]	Low SES > 47, 68 (11%)[1]	p-value[2,3]	High SES ≤ 47, 747 (85%)[1]	Low SES > 47, 133 (15%)[1]	p-value[2,3]	High SES ≤ 47, 1035 (73%)[1]	Low SES > 47, 389 (27%)[1]	p-value[2,3]
Age	71 ± 7	70 ± 8	0.15	68.5 ± 5.2	68.0 ± 5.5	0.3	67 ± 9	65 ± 8	<0.001***
Sex			0.2			<0.001***			0.4
F	310 (57%)	45 (66%)		433 (58%)	111 (83%)		627 (61%)	226 (58%)	
M	233 (43%)	23 (34%)		314 (42%)	22 (17%)		408 (39%)	163 (42%)	
Education (years)	16.95 ± 2.21	13.76 ± 1.73	<0.001***	16.38 ± 2.07	13.55 ± 1.44	<0.001***	15.6 ± 2.5	10.1 ± 3.7	<0.001***
APOE ε4 Carrier	176 (37%)	18 (30%)	0.3	237 (32%)	32 (24%)	0.084	303 (31%)	90 (25%)	0.042*
Diagnosis			0.2			<0.001***			<0.001***
Impaired	184 (34%)	28 (41%)		32 (4.3%)	15 (11%)		248 (24%)	142 (37%)	
Unimpaired	359 (66%)	40 (59%)		715 (96%)	118 (89%)		787 (76%)	247 (63%)	
Race			0.004**			0.026*			<0.001***
Asian	26 (4.9%)	1 (1.5%)		25 (3.4%)	3 (2.3%)		0 (0%)	0 (0%)	
Black	83 (16%)	24 (35%)		99 (13%)	25 (19%)		341 (33%)	97 (25%)	
Other	15 (2.8%)	2 (2.9%)		48 (6.4%)	12 (9.0%)		19 (1.8%)	5 (1.3%)	
White	369 (69%)	38 (56%)		524 (70%)	77 (58%)		490 (47%)	54 (14%)	
White (Hispanic)	41 (7.7%)	3 (4.4%)		49 (6.6%)	16 (12%)		185 (18%)	233 (60%)	
Amyloid Status			0.8			>0.9			0.13
Amyloid Neg	344 (64%)	44 (66%)		530 (71%)	94 (71%)		812 (79%)	320 (82%)	
Amyloid Pos	194 (36%)	23 (34%)		217 (29%)	39 (29%)		220 (21%)	69 (18%)	
Meta Temporal SUVr	1.24 ± 0.22	1.28 ± 0.34	0.6	1.06 ± 0.14	1.07 ± 0.19	0.6	1.38 ± 0.19	1.37 ± 0.24	0.051
Entorhinal SUVr	1.22 ± 0.23	1.24 ± 0.30	0.6	1.10 ± 0.27	1.13 ± 0.38	0.9	1.15 ± 0.15	1.16 ± 0.19	0.7
CDR sum of boxes	0.59 ± 1.12	0.96 ± 1.62	0.081	0.17 ± 0.31	0.28 ± 0.39	0.001**	0.45 ± 1.34	0.96 ± 1.97	<0.001***
MMSE	28.55 ± 1.95	27.40 ± 3.04	<0.001***	28.84 ± 1.26	28.53 ± 1.51	0.038*	28.28 ± 2.19	25.85 ± 3.60	<0.001***
ADI National	34 ± 25	50 ± 29	<0.001***	32 ± 21	45 ± 23	<0.001***	50 ± 25	72 ± 23	<0.001***

[1] Mean ± SD; n (%)

[2] Wilcoxon rank sum test; Pearson's Chi-squared test; Fisher's exact test

[3] *p<0.05; **p<0.01; ***p<0.001

Table. Participant characteristics by SES for each cohort (ADNI, POINTER, and HABS-HD). Low SES individuals had lower education, higher ADI, and lower MMSE scores compared to high SES individuals, but tau and amyloid status did not differ.

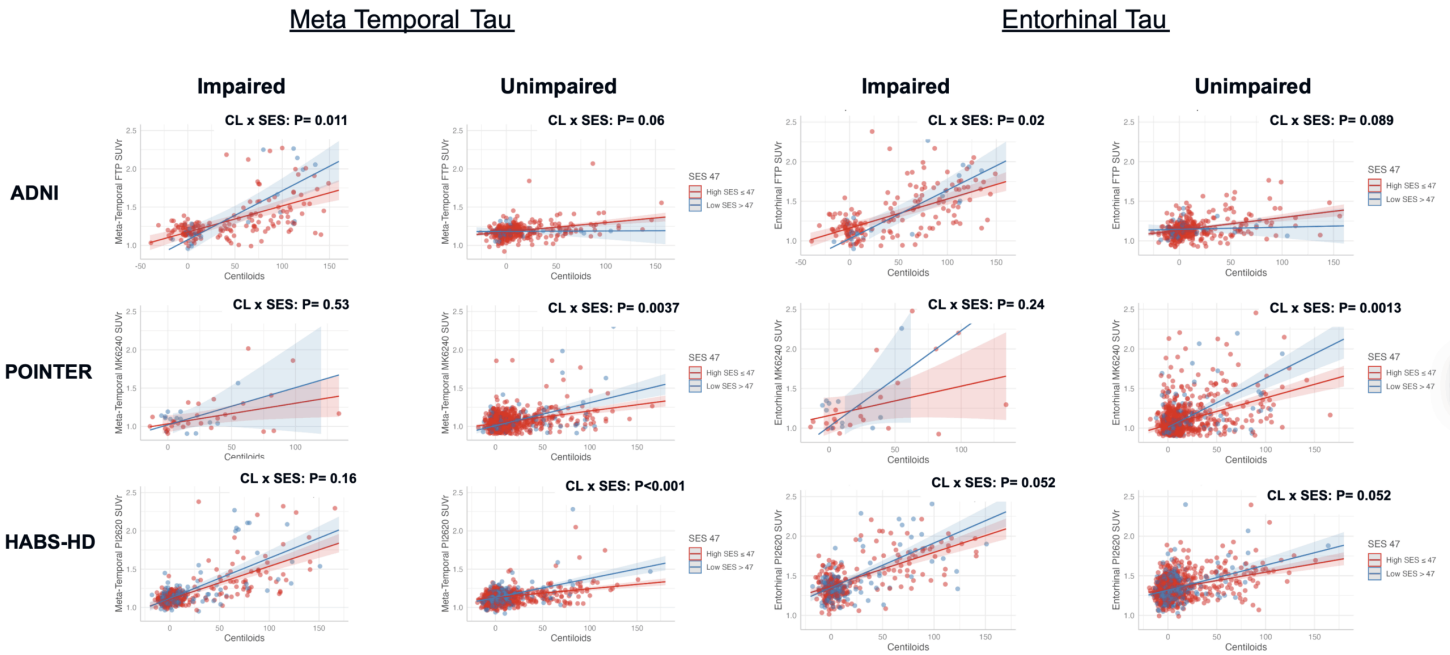


Figure. Meta-temporal and entorhinal tau was assessed using different tracers for each cohort (FTP in ADNI; MK62640 in POINTER; PI2620 in HABS-HD) relative to CL for high/low SES individuals, separately for impaired/unimpaired groups, controlling for age, sex, and APOE4. SES X CL interactions were observed for some comparisons such that low SES participants had higher tau for a given level of amyloid burden (CL) in ADNI impaired (meta-temporal, entorhinal), POINTER unimpaired (meta-temporal, entorhinal), and HABS-HD unimpaired (meta-temporal) groups.

Keywords: Socioeconomic Status (SES), Amyloid PET, Tau PET

Blood LDL cholesterol synergistically amplifies tau pathology and cognitive outcome in an APOE4-dependent manner

Tina Wang[1], Rik Ossenkoppele[1], Emily Collins[1], Samantha Burnham[1], John Sims[1], Oskar Hansson[1], Mark Mintun[1], Ming Lu[1]

[1]*Eli Lilly and Company, Indianapolis, IN, US*

Background: Elevated low-density lipoprotein cholesterol (LDL-C) concentrations have been implicated to increase Alzheimer's disease (AD) risk. APOE4, the strongest genetic risk factor for sporadic AD, plays a critical role in regulating brain lipid metabolism. Emerging research suggested that LDL-C may modulate relationships between amyloid-β (Aβ) and tau pathology, revealing the potential impact of cholesterol dysregulation in AD. Here, we investigate whether LDL-C interacts with AD biomarkers to predict pathological and cognitive outcomes, and whether this synergistic amplification is modulated by APOE4 carriage status.

Methods: Cross-sectional analyses were performed in 995 individuals from the Health and Aging Brain Study: Health Disparities (HABS-HD) cohort. Participants underwent APOE genotyping, Aβ ([^{18}F]Florbetaben) and tau ([^{18}F]PI-2620) PET imaging, plasma p-tau217 testing (Simoa Advantage PLUS, Quanterix), LDL-C measurements and cognitive assessments including Mini-Mental State Examination (MMSE) and Clinical Dementia Rating Sum of Boxes (CDR-SB). Multivariate regression models with interaction terms tested LDL-C × biomarker effects on outcomes, adjusted for age, sex and BMI. Analyses were stratified by APOE4 carriage status with false discovery rate (FDR) correction.

Results: Statistically significant synergistic effects were observed primarily in APOE4 carriers (N=339), who overall exhibited higher Aβ PET SUVr and plasma p-tau217 concentrations (Table 1). In APOE4 carriers, LDL-C×p-tau217 interactions substantially amplified adverse outcomes including elevated tau PET SUVr in the lateral parietal region ($p<0.0001$) and worsened cognitive performance ($p=0.0002$). Additionally, LDL-C also interacted with Aβ PET, significantly predicting lateral parietal tau PET SUVr ($p=0.01$) and MMSE ($p<0.0001$) (Fig. 1A). Multiplicative models incorporating interaction terms explained 1-8% additional variances ($\Delta R^2 = 0.011$-0.081) beyond additive models and yielded larger effect sizes (10-66%) (Fig. 1B).

Conclusion: Our findings suggest that peripheral cholesterol levels amplify pathological and cognitive outcomes through synergistic interactions with AD core biomarkers. This underscores the importance of further investigating lipid metabolism as a potential modulator of AD progression.

Table 1. Demographics and baseline cohort characteristics

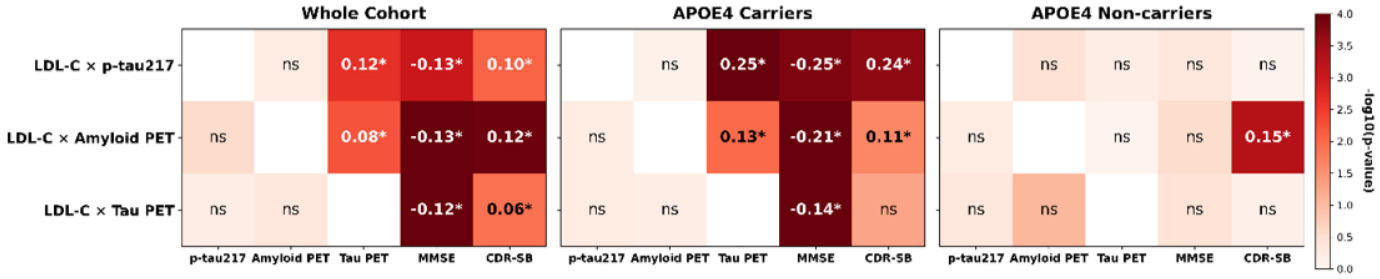
Sample Size	Whole cohort N= 995	APOE4 Carrier N= 339	APOE4 Non-Carrier N= 656	
Demographics				
Age, years	63.7 ± 8.2	63.0 ± 7.6	64.0 ± 8.4	ns
Sex, Female (%)	60.3%	59.3%	60.8%	ns
Race (%)	White: 48.0% Black: 50.8% More than one: 1.2%	White: 38.1% Black: 60.5% More than one: 1.5%	White: 53.2% Black: 45.7% More than one: 1.1%	**<0.001**
Ethnicity, Not Hispanic (%)	76.6%	82.6%	73.5%	**0.002**
Education, years	14.4 ± 3.3	14.4 ± 3.0	14.4 ± 3.4	ns
Clinical Characteristics				
MMSE	27.6 ± 2.7	27.7 ± 3.0	27.6 ± 2.5	ns
CDR-SB	0.57 ± 1.4	0.67 ± 1.6	0.52 ± 1.3	ns
Cardiovascular Risk Factors				
LDL-C (mg/dL)	99.9 ± 34.7	101.7± 34.2	99.0 ± 34.9	ns
BMI (kg/m2)	31.6 ± 7.3	31.7 ± 7.2	31.6 ± 7.4	ns
Hypertension, n (%)	545 (54.8%)	190 (56.0%)	355 (54.1%)	ns
Diabetes, n (%)	223 (22.4%)	78 (23.0%)	145 (22.1%)	ns
Hyperlipidemia, n (%)	478 (48.0%)	180 (53.1%)	298 (45.4%)	**0.026**
Stroke, n (%)	85 (8.5%)	35 (10.3%)	50 (7.6%)	ns
Current/Former Smoker, n (%)	399 (40.1%)	133 (39.2%)	266 (40.5%)	ns
Alzheimer's Disease Biomarkers				
Amyloid PET Global SUVr	1.031 ± 0.144	1.069 ± 0.182	1.012 ± 0.115	**<0.001**
Amyloid PET Positivity, A+ (%)	17.4%	26.5%	12.7%	**<0.001**
Tau PET Lateral Parietal SUVr	1.012 ± 0.121	1.025 ± 0.158	1.005 ± 0.096	ns
Plasma p-tau217 (pg/mL)	0.39 ± 0.36	0.48 ± 0.44	0.35 ± 0.30	**<0.001**

Statistical comparisons between APOE4 carriers and non-carriers employed independent t-tests or Mann-Whitney U tests for continuous demographic and clinical variables, depending on distributional assumptions, and chi-square (χ^2) tests for categorical variables. Amyloid PET positivity was assigned based on [^{18}F]Florbetaben global SUVr. *MMSE = Mini-Mental State Examination, CDR-SB = Clinical Dementia Rating Sum of Boxes, BMI = Body Mass Index, SUVr = standardized uptake value ratio. ns = not significant.*

Figure 1. LDL-C synergistically amplifies AD pathological and cognitive outcome

A. LDL-C × AD biomarker interactions across cohort stratifications

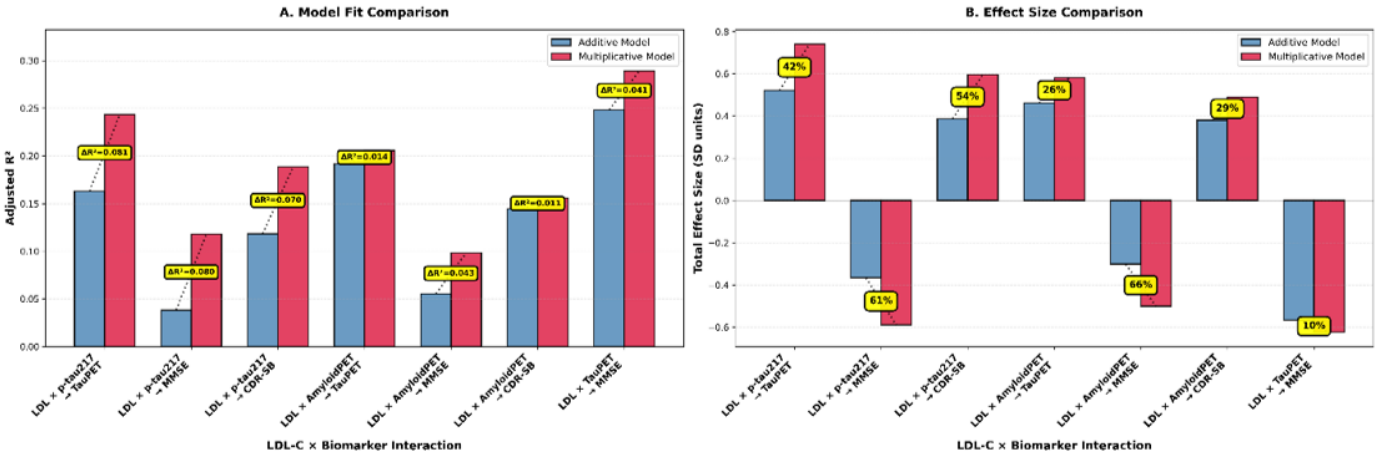
Three-panel heatmaps display statistical results from linear regression models fitted as ***Outcome ~ LDL-C + Biomarker + LDL-C × Biomarker + Age + Sex + BMI***. In each cell, the value represents standardized coefficients (β) of the LDL-C × AD biomarker interaction, and color shows significance level in -log10 scale. *Biomarker measurements (p-tau217, amyloid PET and tau PET) were log-transformed to correct for right-skewness, all variables were subsequently z-scored for standardization. FDR correction (Benjamini-Hochberg) applied within each panel to control for multiple comparisons across models. ns = not significant.*



B. Comparison of multiplicative vs. additive models in APOE4 carriers, for models with statistically significant interaction (q < 0.05)

Bar plots compare model fit and effect size between additive and multiplicative models. The difference between models quantifies the synergistic contribution beyond additive effects (highlighted in yellow: *left: ΔAdj R^2 shows model fit improvement; right: % shows synergy magnitude*).

```
Additive Model (Blue bars): Outcome ~ LDL-C + Biomarker + Age + Sex + BMI
                            Total effect size = β_LDL-C + β_Biomarker
Multiplicative Model (Red bars): Outcome ~ LDL-C + Biomarker + LDL-C × Biomarker + Age + Sex + BMI
                                 Total effect size = β_LDL-C + β_Biomarker + β_Interaction
```



Keywords: Alzheimer's disease, Lipid metabolism, APOE

Mismatch between tau burden and cognitive domain performance identifies sub-groups with specific co-pathologies

Christopher Brown[1], Nidhi Mundada[2], Xueying Liu[2], Emily McGrew[1], Ilya Nasrallah[3], Sandhitsu Das[1], Dawn Mechanic-Hamilton[1], Paul Yushkevich[3], David Wolk[1]

[1]*Department of Neurology, University of Pennsylvania, Philadelphia, PA, US*
[2]*Department of Bioengineering, University of Pennsylvania, Philadelphia, PA, US*
[3]*Department of Radiology, University of Pennsylvania, Philadelphia, PA, US*

Introduction: Dissociation between clinical impairment and tau burden has been highlighted in the Alzheimer's Association workgroup guidelines for diagnosis and staging of Alzheimer's disease and has recently been shown to reflect underlying co-pathologies. We sought to test whether mismatch between tau burden and multiple cognitive domain scores could identify patterns of tau-cognitive mismatch that reflect the presence of specific co-pathologies.

Methods: We used Tau-PET and cognitive scores from the Phenotype Harmonization Consortium to generate mismatch models using ADNI data and then applied these models to NACC data. Tau burden was quantified using a PET-only implementation of Tau-MaX, a summary metric of global tau burden. Composite domain scores for memory, executive function, and language were measures of cognition. Linear regression defined canonical tau-cognition relationships, and standardized residuals of ±0.6 were used to classify individuals as vulnerable or resilient for each domain before grouping individuals based on prescribed clinical patterns of vulnerability and resilience (Table 1).

Results: In ADNI, markers of specific co-pathologies mapped onto tau-cognitive mismatch phenotypes with lower ERC/PHC ratio (LATE signature) in the amnestic vulnerable group, higher white matter hyperintensities (vascular signature) in the non-amnestic vulnerable group, and greater rate of αSynuclein positivity by seeding amplification assay in the global vulnerable group (Figure 1). Using model-identified groups in NACC, we evaluated differential longitudinal change in cognitive domains between mismatch groups against time relative to tau onset estimated using SILA (Figure 2). Vulnerable groups showed domain-specific cognitive decline prior to the estimated time of tau onset, further implicating non-AD pathology in these groups.

Conclusion: These findings further highlight the utility of tau-clinical mismatch for identifying those with likely co-pathology and diverging clinical trajectories. These models could be particularly useful for examining the effects of disease-modifying therapies in the presence of co-pathology and providing more individualized estimates of expected clinical trajectories.

Table 1.

	Memory	Executive	Language	ADNI N	NACC N
Amnestic Resilient	↑	↔	↔ or ↑	40 (9.9%)	145 (12.1%)
Non-Amnestic Resilient	↔	↔ or ↑	↑ or ↔	58 (14.4%)	193 (16.2%)
Global Resilient	↑	↑	↑	49 (12.1%)	163 (13.6%)
Canonical	↔	↔	↔	74 (18.3%)	147 (12.3%)
Global Vulnerable	↓	↓	↓	49 (12.1%)	165 (13.8%)
Non-Amnestic Vulnerable	↔	↓ or ↔	↔ or ↓	71 (17.6%)	241 (20.2%)
Amnestic Vulnerable	↓	↔	↔ or ↓	63 (15.6%)	141 (11.8%)

↑ Standardized Residual (SR) > 0.6, ↓ SR < -0.6, ↔ -0.6 ≤ SR ≤ 0.6

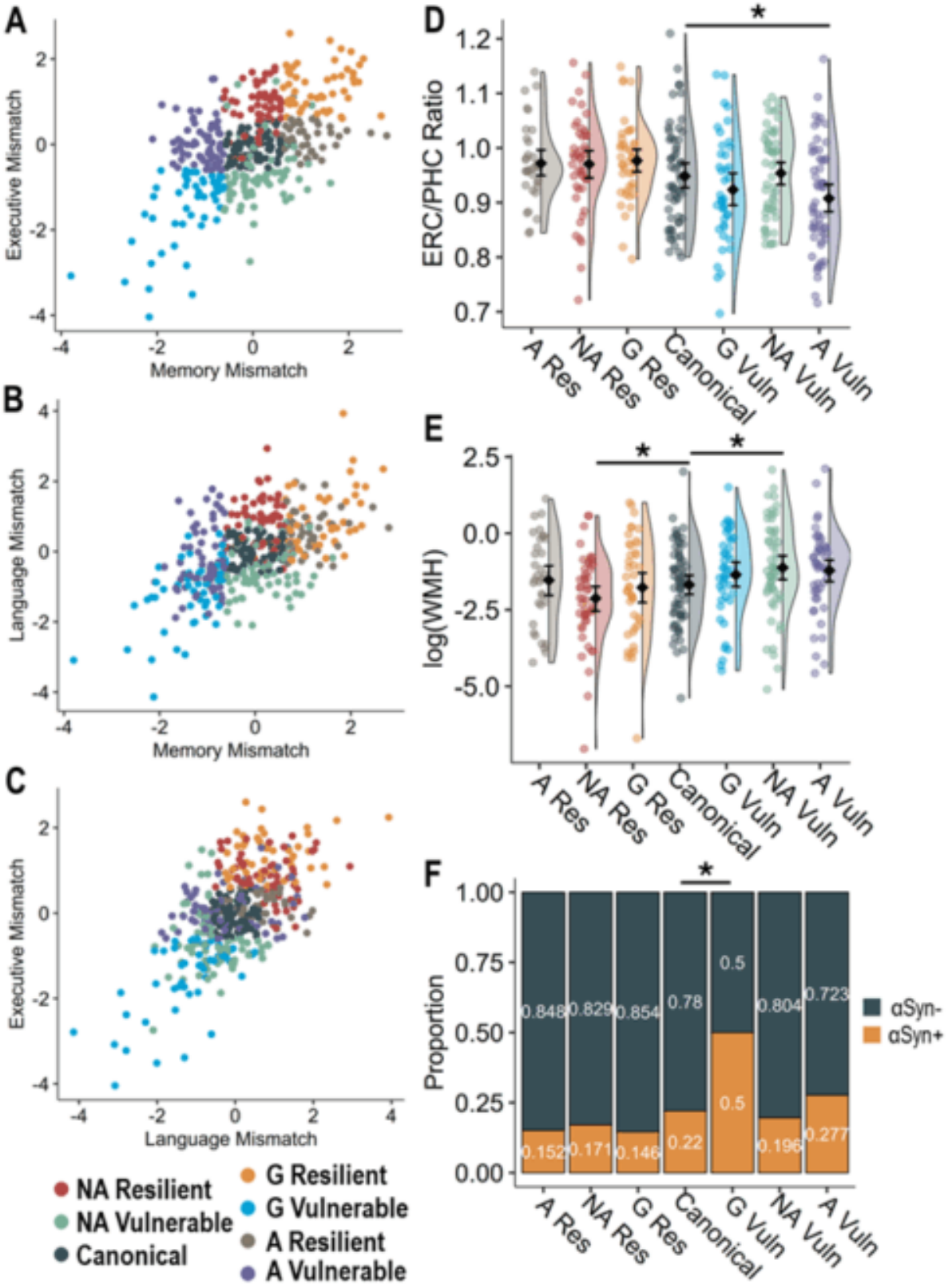


Figure 1. A-C: Mismatch residual between tau and each cognitive domain plotted against each other with points colored by the clinical mismatch group. **D:** ERC/PHC ratio, which is reduced in LATE, plotted across mismatch groups. **E:** WMH volume normalized for intracranial volume and log-transformed plotted across mismatch groups. **D-E:** Diamonds represent group mean with error bars representing 95% confidence interval of mean. **F:** Proportion of αSynuclein positivity across mismatch groups. **D-F:** Comparisons performed against the canonical group as reference, *p < 0.05. **A-F:** A: Amnestic, NA: Non-Amnestic, G: Global, Res: Resilient, Vuln: Vulnerable

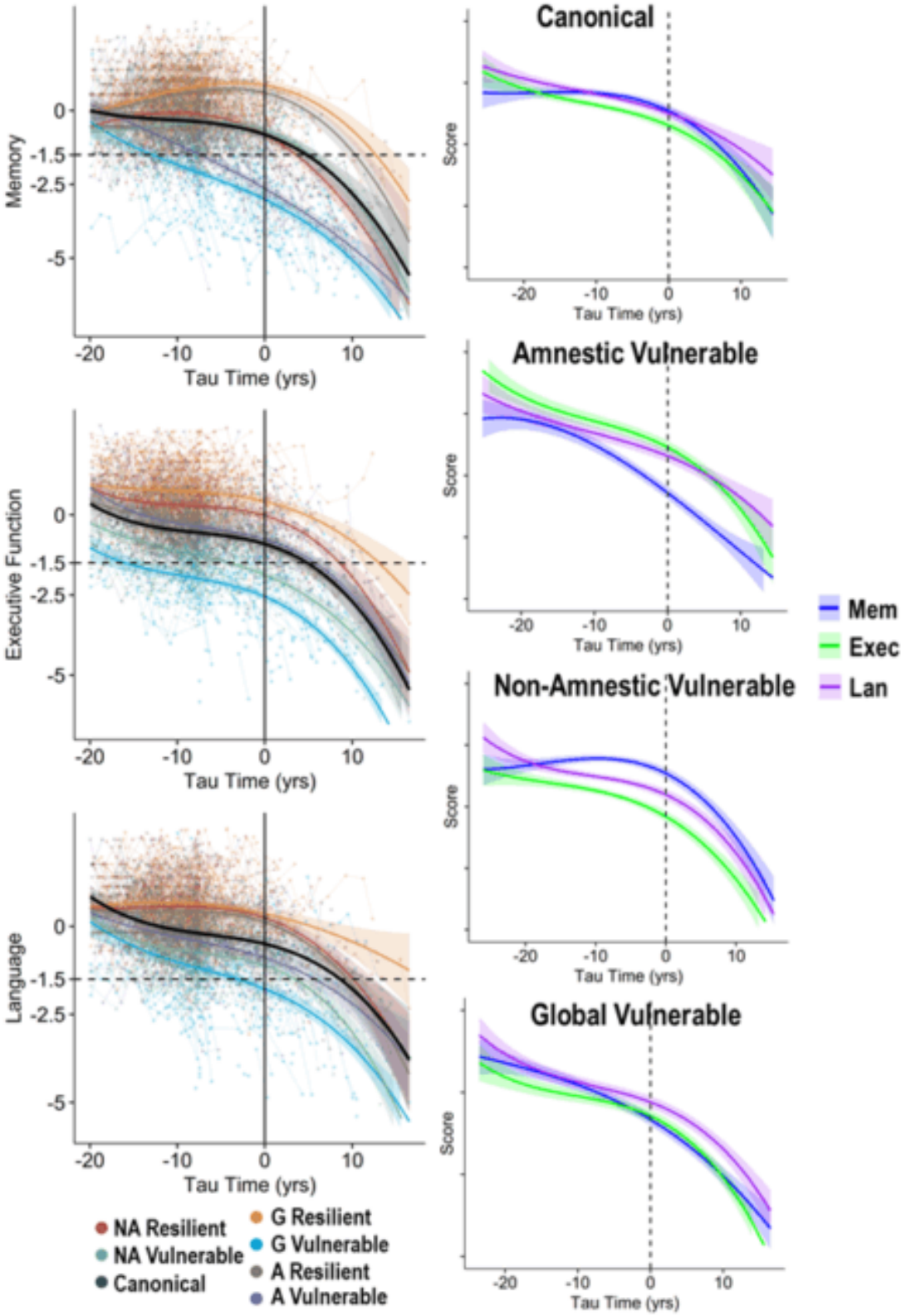


Figure 2. Longitudinal cognitive trajectories in NACC. Left: Longitudinal cognitive trajectories are shown for each mismatch group for each cognitive domain using b-spine linear mixed-models with time converted to time from SILA-estimated tau onset (vertical line). Standard deviations below unimpaired Aβ- mean are shown on y-axis with -1.5 SD considered the point of abnormality (dashed line). **Right:** Change in each cognitive domain shown for canonical and vulnerable sub-groups with dashed line showing the time of estimated tau onset. **Both:** Vulnerable domains/groups decline prior to tau onset, while other domains/groups decline after tau onset.

Keywords: Tau PET, cognition, TDP-43, alpha-synuclein, co-pathology

Characterizing the brain-wide atrophy pattern of LATE-NC-associated hippocampal sclerosis: an imaging-pathologic association study

Michel J. Grothe[1], Linda Zhang[1], Francisco J. López-González[1], Pascual Sánchez-Juan[1], Alberto Rábano[1], Jesús Silva-Rodríguez[1]

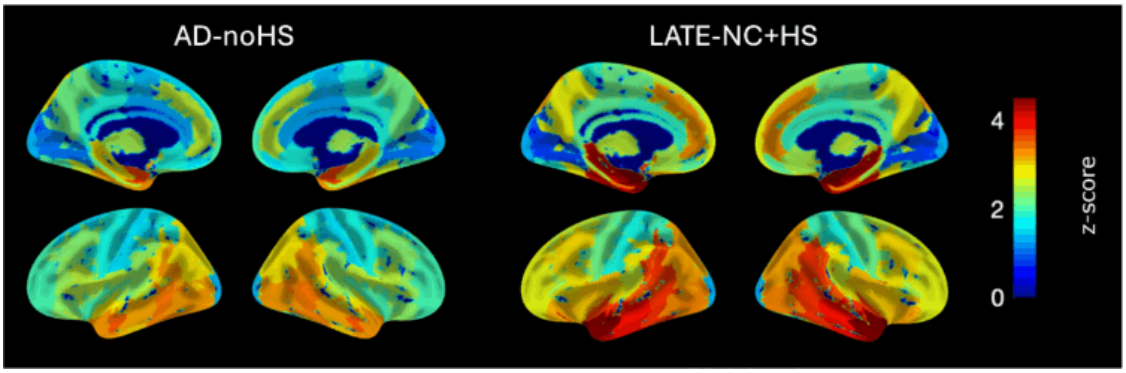
[1]*Reina Sofia Alzheimer Center, CIEN Foundation, Madrid, Spain*

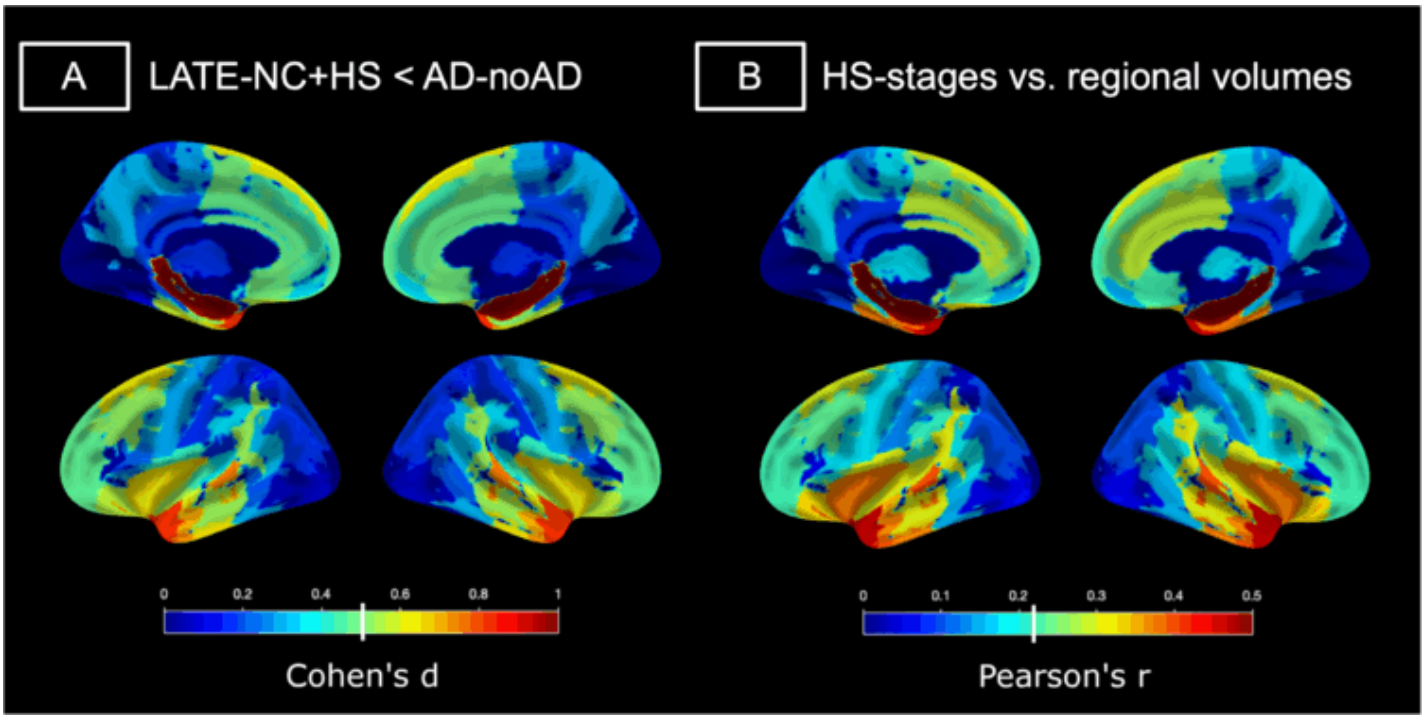
Background: Limbic age-related TDP-43 encephalopathy neuropathologic change (LATE-NC) is often comorbid to Alzheimer's disease neuropathologic change (ADNC) and it is linked to hippocampal sclerosis (HS), which contributes to amnestic deficits independently of AD. Previous imaging-pathologic association studies have described severe hippocampal atrophy in HS, but the brain-wide atrophy pattern of LATE-NC-associated HS remains to be characterized in more detail.

Methods: We studied 84 amnestic dementia patients from our brain bank cohort, who underwent detailed neuropathologic assessment at autopsy and had quality-controlled ante-mortem 3T-MRI available (MRI-to-death interval: 3.0±3.0 years). Neuropathologic evaluation included standard assessments of ADNC and LATE-NC, and HS was assessed using a novel pathologic staging scheme considering four consecutive stages of HS severity. MRI data was processed in CAT12/SPM12 to extract gray matter volumes of 52 atlas-defined brain regions. Regional volumes were compared to normative data of 1032 healthy elderly controls from the same scanner.

Results: Compared to controls, LATE-NC/HS cases (N=30) and those with typical AD without HS (AD-noHS; N=47) showed similar overall patterns of temporo-parietal atrophy (Fig-1). However, compared to AD-noHS, LATE-NC/HS cases had significantly more pronounced medial temporal lobe atrophy, but also of more extended areas of the paralimbic cortex, including the temporal pole, insula, and orbitofrontal cortex (Fig-2A). Incorporating this extended set of brain regions into a multi-regional classification model improved group separation over and above using hippocampal volume alone (AUC=0.82 vs 0.78). A largely identical HS-associated temporo-limbic atrophy pattern was observed when correlating the pathologic staging scheme of HS severity with regional brain volumes across all autopsy cases (Fig-2).

Conclusions: LATE-NC-associated hippocampal sclerosis is linked to an in-vivo atrophy pattern on MRI that extends well beyond the hippocampus and includes several temporo-limbic cortical areas known to accumulate TDP-43 pathology in LATE-NC. This signature could help to improve clinical detection of this pathologic condition in-vivo.





Keywords: Limbic-predominant age-related TDP-43 encephalopathy, hippocampal sclerosis, Alzheimer's disease, MRI, autopsy

Wednesday, January 14, 2026 - 02:40 pm - 02:45 pm

Podium Session

B3 - B: Short Poster Presentations

Wednesday, January 14, 2026			
02:40 pm – 02:45 pm	Title	Authors	Presenter
Board # 107	**Perivascular spaces: Predictors of longitudinal amyloid, tau, cerebrovascular biomarkers?**	Low | Gunter | Hu | Raghavan | Przybelski | Schwarz | Kantarci | Lowe | Graff-Radford | Petersen | Jack | Vemuri	**Audrey Low**, Mayo Clinic, Rochester, MN, USA
Board # 115	**Preliminary associations of plasma phosphorylated tau217 with regional tau deposition and accumulation in medial temporal and neocortical regions**	Pintucci | Thibault | Farrell | Yang | Chhatwal | Properzi | Becker | Price | Sperling | Johnson	**Eva Pintucci**, Massachusetts General Hospital, Harvard Medical School, Boston, MA, USA
Board # 99	**Intermediate blood-based biomarker status clarified by PET and CSF in cognitively impaired individuals**	Ziontz | Blazhenets | Lin | Landau | Shaw | Dage | Hammers | Eloyan | Koeppe | Carillo | Dickerson | Rabinovici | La Joie	**Jacob Ziontz**, University of California, San Francisco, San Francisco, CA, USA

Wednesday, January 14, 2026 - 03:45 pm - 05:30 pm

Podium Session

SESSION IX: Therapeutics: Anti-abeta and anti-tau effects

CHAIR:

***Christopher Van Dyck**, Yale University, New Haven, CT, USA*

Wednesday, January 14, 2026			
03:45 pm – 05:30 pm	**Podium Presentation**	**Authors**	**Presenter**
03:50 pm – 04:05 pm	Tau pathology interferes with amyloid removal by gantenerumab	Tonietto | Silvestri | Belousov | Kulic | Smith | Klein	**Matteo Tonietto**, Research and Early Development (pRED), Hoffmann-La Roche, Basel, Switzerland
04:05 pm – 04:20 pm	Clinical and PET outcomes following Aβ-targeting therapies in sporadic early-onset Alzheimer's disease: Trial emulation using the LEADS cohort	Chiotis | Eloyan | Kirby | Blazhenets | Maiti | Lin | Thangarajah | Touroutoglou | Hammers | Carrillo | Dickerson | Apostolova | Rabinovici | La Joie	**Konstantinos Chiotis**, University of California San Francisco, San Francisco, CA, US
04:20 pm – 04:35 pm	Tau positron emission tomography data from the open-label extension study of TOGETHER: a double-blind, placebo-controlled Phase II study of bepranemab in prodromal–mild Alzheimer's disease (AD)	Mercier | Byrnes | Rebollo Mesa | Buchanan | Van Den Steen | Van Tricht | Taiyari | Famodimu | Bloemers | Shimizu | Massow | Barton | Mann | Maguire	**Joël Mercier**, UCB, Braine-l'Alleud, Belgium
04:35 pm – 04:50 pm	Cortical laminar and Aβ species-specific correspondence between antemortem Aβ-PET and postmortem pathology in aducanumab-treated Alzheimer's disease	Boon | Burkett | Moloney | Piura | Hinkle | Rothberg | Petersen | Dickson | Reichard | Nguyen | Graff-Radford | Knopman | Graff-Radford | Lowe | Murray	**Baayla Boon**, Department of Neuroscience, Mayo Clinic, Jacksonville, FL, US
04:50 pm – 05:05 pm	In vivo and post-mortem evidence of downstream pathophysiologic effects of treatment-related amyloid clearance	Brown | Robinson | Das | McGrew | Nasrallah | Irwin | Yushkevich | Lee | Wolk	**David Wolk**, Department of Neurology, University of Pennsylvania, Philadelphia, PA, US

Tau pathology interferes with amyloid removal by gantenerumab

Matteo Tonietto[1], Erica Silvestri[1,2], Anton Belousov[3], Luka Kulic[1], Janice Smith[4], Gregory Klein[1]

[1]*Research and Early Development (pRED), Hoffmann-La Roche, Basel, Switzerland*
[2]*A4P Consulting Ltd, Sandwich, UK*
[3]*Roche Products Ltd, Basel, Switzerland*
[4]*Roche Products Ltd, Welwyn Garden City, UK*

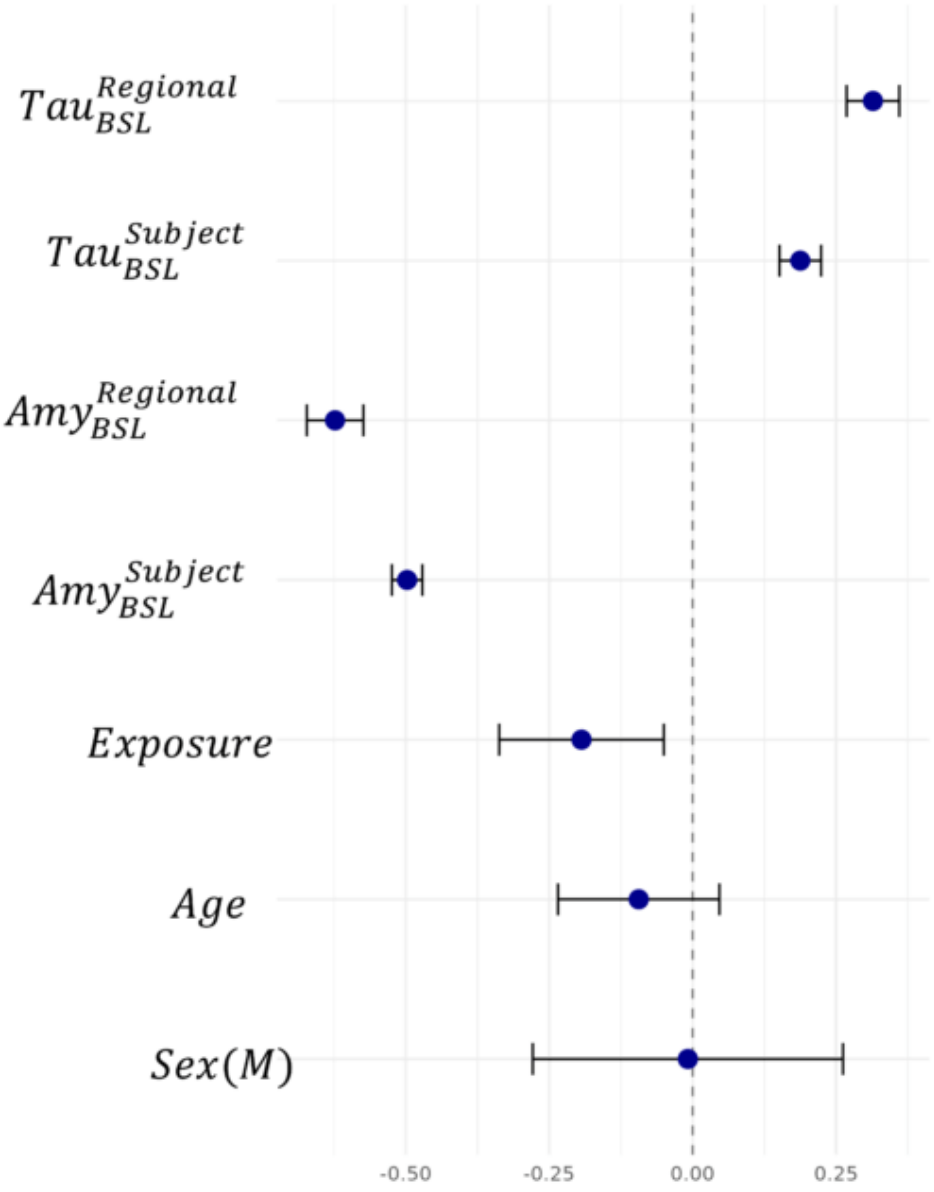
Introduction: Gantenerumab is a monoclonal antibody targeting aggregated forms of amyloid-beta. The phase III GRADUATE investigational studies aimed to assess the efficacy and safety of gantenerumab in early AD. Lower baseline amyloid and younger age have been associated with lower amyloid removal across amyloid-targeting immunotherapies (Hayato PSP-2022; Barkhof ADPD-2023; Battioui ADPD-2024). This study investigated whether the presence of baseline tau also influenced amyloid removal by gantenerumab.

Methods: Thirty-eight participants from the active arm of the GRADUATE studies who had baseline [18F]-GTP1 tau PET, and baseline and end of study (i.e. week 116) amyloid PET (either [18F]-florbetaben or [18F]-flutemetamol) were included in this analysis. Brain regions were segmented with Freesurfer. Regional amyloid SUVRs were converted into regional centiloids using regionally derived equations. Regional tau SUVRs were Z-scored using an external cohort of 15 cognitively unimpaired, amyloid-beta negative individuals imaged with [18F]-GTP1. To isolate regional- from subject-specific tau effect, baseline tau readout was decomposed into a regional-specific average and a subject-specific deviation. The same approach was used for baseline amyloid readout. Linear mixed-effects model was used to assess the relationship between amyloid removal and regional-/subject-specific tau components, while adjusting for baseline amyloid, age, sex, and drug exposure.

Results: Both regional- and subject-specific tau components displayed significant association with amyloid removal (Figure 1), implying that regions with higher baseline tau had lower amyloid removal (Figure 2A), and that within the same region, participants with higher tau levels displayed less amyloid removal (Figure 2B-E). This relationship appeared non-linear, suggesting the effect of tau is only evident after a certain pathological threshold. Images of a participant with an asymmetric tau deposition and spatially consistent amyloid removal are shown in Figure 3.

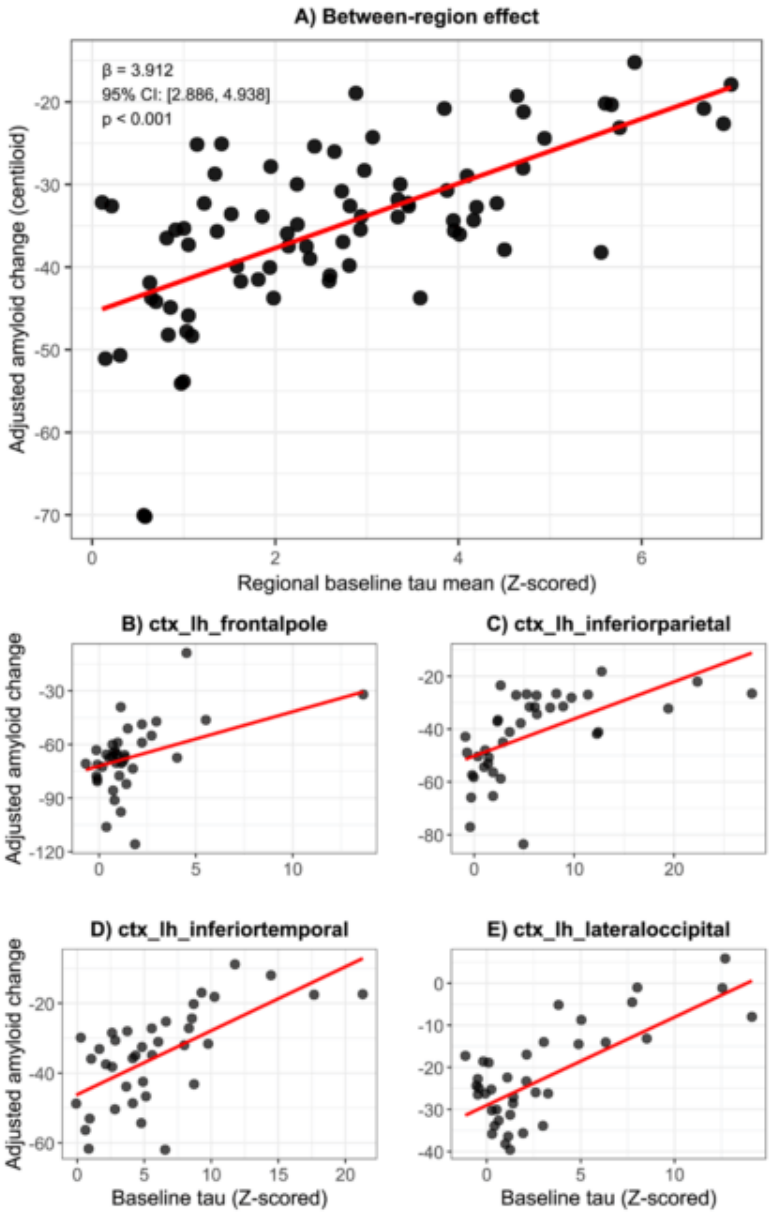
Conclusion: Baseline tau pathology strongly influences amyloid removal by gantenerumab. Further research is necessary to clarify if this is a gantenerumab-specific or class-wide effect.

Figure 1: Factors explaining amyloid reduction at w116



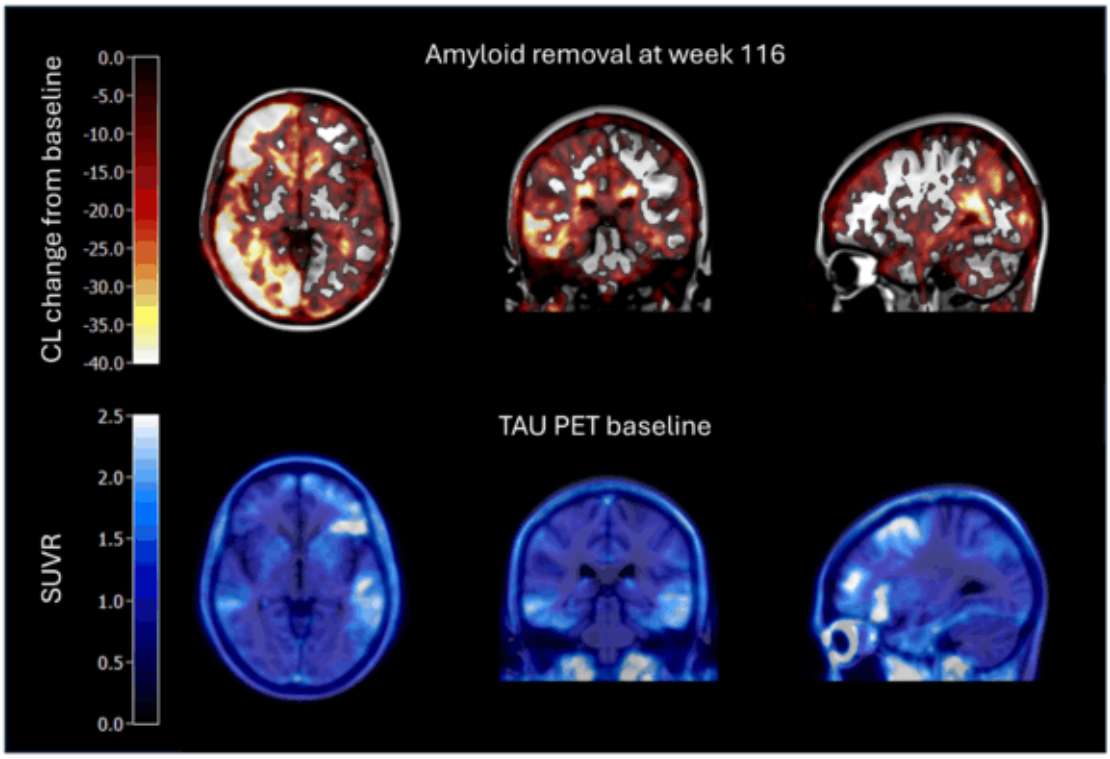
Standardized coefficients of the fixed effects from the linear mixed-effects model (point estimates with 95% confidence intervals). Both higher regional- and subject-level baseline tau load show significant association with lower amyloid removal.

Figure 2: Relationship between baseline tau and amyloid removal



Panel A displays the regional-specific effect, plotting regional mean baseline tau against the model-adjusted mean amyloid change from baseline, where each point represents a distinct brain region. Panels B-E show the subject-specific effect in four representative cortical areas. In these plots, each point represents an individual participant, showing their baseline tau level against their adjusted amyloid change. The red line in all panels represents the linear mixed-model fit.

Figure 3: participant with asymmetric tau deposition



A case example illustrating the spatial relationship between baseline tau and subsequent amyloid removal with gantenerumab. The bottom panel shows the baseline tau-PET scan with asymmetric tau deposition (brighter areas). The top panel shows little amyloid removal at week 116 in the same cortical regions with the highest baseline tau signal.

Keywords: Tau PET, Gantenerumab, anti-amyloid

Clinical and PET outcomes following Aβ-targeting therapies in sporadic early-onset Alzheimer's disease: Trial emulation using the LEADS cohort

Konstantinos Chiotis[1,2], Ani Eloyan[3], Kala Kirby[4], Ganna Blazhenets[1], Piyush Maiti[1], Zoe Lin[1], Maryanne Thangarajah[3], Alexandra Touroutoglou[5], Dustin Hammers[4], Maria Carrillo[6], Bradford Dickerson[5], Liana Apostolova[4], Gil Rabinovici[1], Renaud La Joie[1]

[1]*University of California San Francisco, San Francisco, CA, US*
[2]*Karolinska Institutet & Karolinska University Hospital, Stockholm, Sweden*
[3]*Brown University, Providence, RI, US*
[4]*Indiana University School of Medicine, Indianapolis, IN, US*
[5]*Massachusetts General Hospital & Harvard Medical School, Boston, MA, US*
[6]*Alzheimer's Association, Chicago, IL, US*

Objective: Trial data on Aβ-targeting therapy in early-onset Alzheimer's disease (EOAD) remain limited. Using Longitudinal Early-Onset Alzheimer's Study (LEADS) data, we examined whether treatment initiation was associated with inflection points in biomarker and clinical trajectories.

Method: We identified 31 participants with sporadic EOAD who had received Aβ-targeting therapies, and had both pre- and post-treatment LEADS visits (Table 1). In a target-trial emulation design, each treated participant was matched 1:2 to untreated participants by age, sex, APOE, clinical stage, amyloid and tau PET, CDR global, CDR-SB, and MoCA. For each untreated match, the treated participant's treatment start defined pseudo–time zero. Piecewise mixed-effects models estimated pre- and post-treatment slopes for amyloid and tau PET, and CDR-SB (Fig. 1A).

Table 1. Clinical characteristics of participants at the pretreatment visit

	Characteristics	Treated, n = 31 [1]	Untreated, n = 62 [1]	p-value [2]
General	Age in years	60 (56, 63)	59 (57, 63)	0.7
	Gender, female	25 (81%)	39 (63%)	0.13
	APOE ε4 carriers			0.8
	Heterozygotes	9 (29%)	6 (19%)	
	Homozygotes	6 (19%)	10 (16%)	
Clinical	Clinical stage at baseline			0.6
	MCI	12 (39%)	19 (31%)	
	Dementia	19 (61%)	43 (69%)	
	CDR global			0.2
	0	1 (3.2%)	1 (1.6%)	
	0.5	18 (58%)	46 (74%)	
	1	12 (39%)	15 (24%)	
	CDR-SB	3.5 (2.0, 4.5)	3.0 (2.0, 4.0)	0.6
	MoCA score	18 (14, 22)	18 (15, 21)	0.8
PET	Centiloids (^{18}F-florbetaben)	100 (85, 112)	99 (79, 115)	0.6
	Universal CenTauR SUVR (^{18}F-flortaucipir)	2.44 (1.93, 2.83)	2.43 (2.03, 2.78)	0.9
Treatment	Treatment duration in months	10.5 (7.4, 17.0)		-
	Treatment agent			-
	Aducanumab	3		
	Lecanemab	27		
	Aduc. -> Lecanemab	1		

[1] Median (Q1, Q3); n (%), [2] Kruskal-Wallis tests for continuous variables, Wilcoxon rank-sum tests for ordinal variables, and Chi-square tests for nominal variables.

Result: Before treatment, amyloid-PET averaged 96±3 Centiloids with a flat, non-significant slope (Fig. 1B). In untreated participants, slopes remained unchanged after time zero. After treatment initiation, treated participants showed a significant decline of −34.0±2.9 Centiloids/year ($p<0.001$) versus untreated, with reductions predominantly in frontotemporal-parietal areas and the basal ganglia (Fig. 2A). Pre-treatment, tau-PET was elevated (2.41±0.09 SUVR), mainly in temporoparietal areas, and increased significantly in widespread neocortical areas (+0.09±0.02 SUVR/year; $p<0.001$). No post-treatment slope differences in tau PET were observed between groups (Fig. 1C, 2B). Before treatment, CDR-SB averaged 3.4 (SE 0.3) and worsened by +0.5±0.1 units/year ($p<0.001$); after time zero, deterioration accelerated in untreated participants (Δ=+1.5±0.3 units/year; $p<0.001$), but was significantly slower in treated relative to untreated participants (Δ-from-Δ=−0.9±0.3 units/year; $p<0.001$) (Fig. 1D).

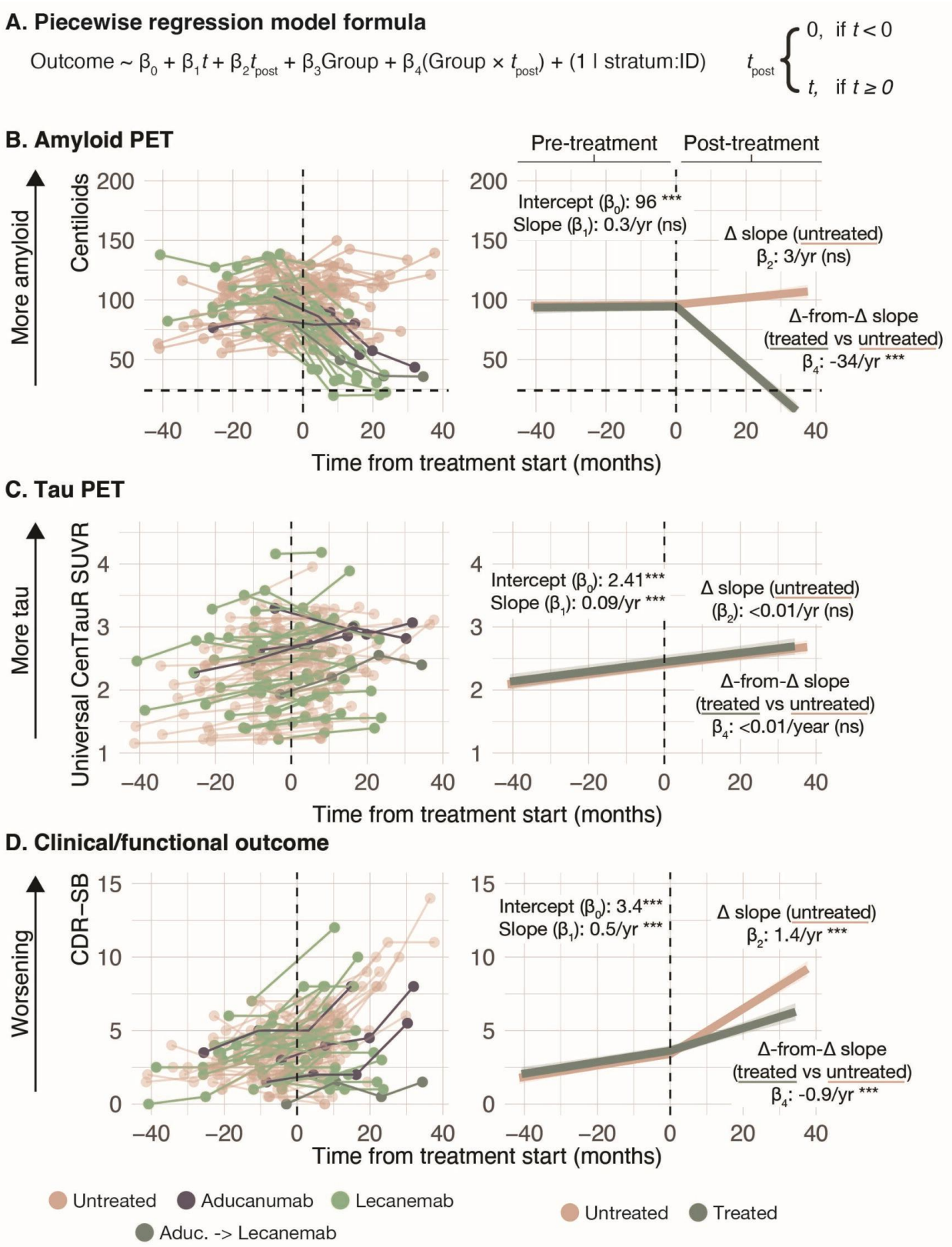


Figure 1. Longitudinal trajectories and model-estimated parameters from piecewise mixed-effects models. The plots show individual trajectories aligned to treatment initiation. Intercepts (β_0) represent values at treatment start, pre-treatment slopes (β_1) indicate annualized change before treatment, β_2 captures post-time-zero slope change in untreated participants, and β_4 represents the Δ-from-Δ slope (difference in post-treatment slope between treated and untreated participants).

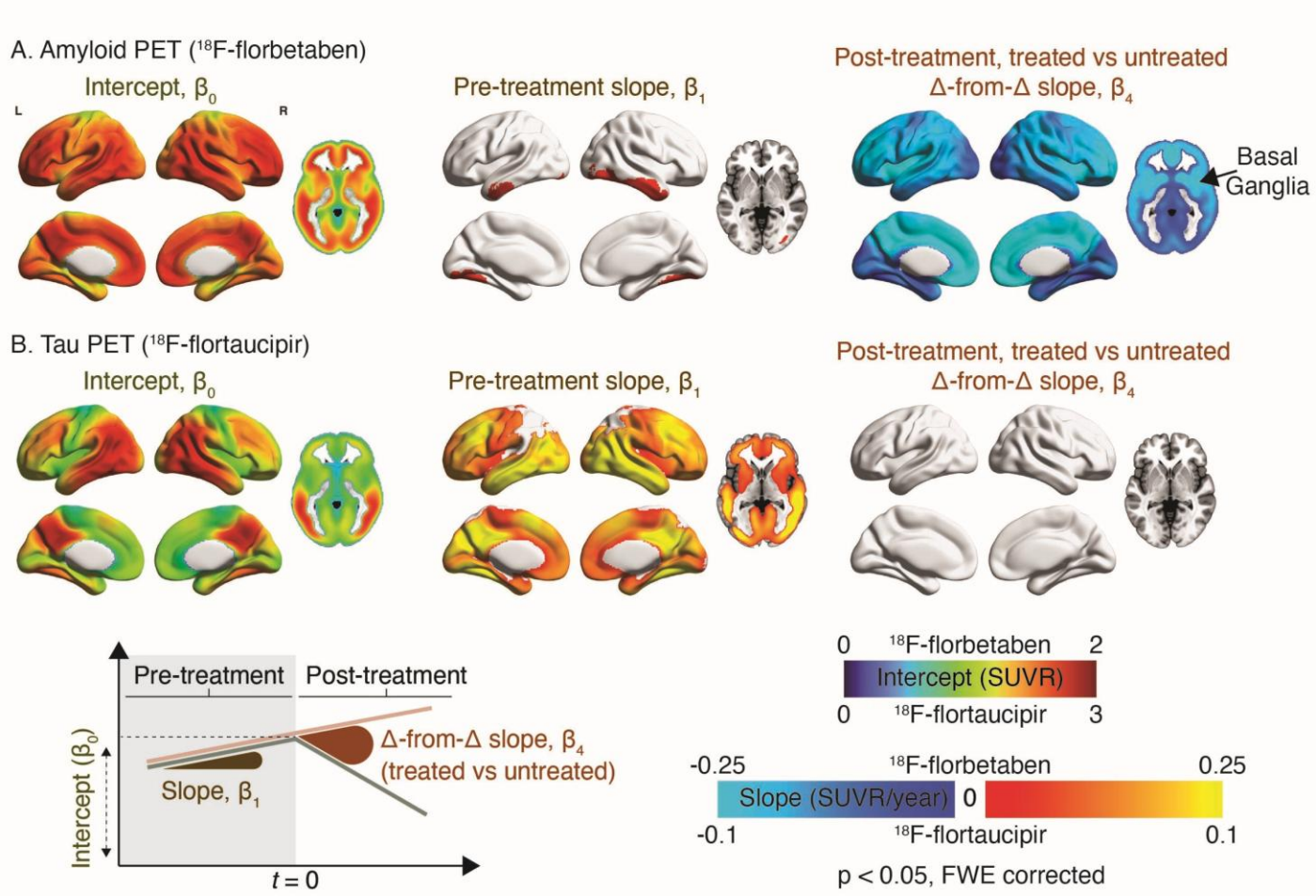


Figure 2. Voxel-wise parameter estimates from piecewise mixed-effects models. Intercepts (β_0) reflect baseline tracer uptake (SUVR) at the pretreatment time point; pre-treatment slopes (β_1) indicate annualized change before treatment; and Δ-from-Δ slopes (β_4) capture post-treatment slope differences between treated and untreated participants.

Conclusion: In this EOAD cohort, our emulated-trial analysis captured—in treated patients—amyloid clearance rates comparable to late-onset Alzheimer's disease trials, with no change in tau trajectories and without the acceleration of CDR-SB decline that was seen among untreated participants. The amyloid clearance displayed regional variation requiring further investigation. These findings support the feasibility of real-world, biomarker-based observational studies to assess treatment effects.

Keywords: amyloid PET, tau PET, lecanemab, aducanumab, early onset Alzheimer's disease

Tau positron emission tomography data from the open-label extension study of TOGETHER: a double-blind, placebo-controlled Phase II study of bepranemab in prodromal–mild Alzheimer's disease (AD)

Joël Mercier[1], William Byrnes[2], Irene Rebollo Mesa[3], Tim Buchanan[1], Bart Van Den Steen[1], Hans Van Tricht[4], Katie Taiyari[5], Omobola Famodimu[6], Jos Bloemers[7], Saori Shimizu[8], Ute Massow[9], Matthew Barton[2], Joanne Mann[5], Ralph Maguire[1]

[1]*UCB, Braine-l'Alleud, Belgium*
[2]*UCB, Raleigh, NC, US*
[3]*UCB, Madrid, Spain*
[4]*UCB, Anderlecht, Belgium*
[5]*UCB, Slough, UK*
[6]*UCB, Oakville, ON, Canada*
[7]*UCB, Breda, The Netherlands*
[8]*UCB, Brussels, Belgium*
[9]*UCB, Monheim am Rhein, Germany*

Background: Bepranemab is a tau mid-region-targeting IgG4 monoclonal antibody. TOGETHER (NCT04867616), a Phase II double-blind, randomized study, investigated efficacy, safety and tolerability of bepranemab in prodromal–mild AD. Previously presented data indicated a clinical benefit with bepranemab; differences were noted in clinical outcomes and tau imaging, favoring bepranemab. We report tau imaging data from the open-label extension (OLE) period.

Methods: Following the 80-week double-blind period, participants entered the 48-week OLE period, receiving bepranemab (45/90 mg/kg, intravenously Q4W). Participants receiving bepranemab during the double-blind period continued the same dose; placebo participants were re-randomized 1:1 to 45 or 90 mg/kg bepranemab. Tau PET at OLE Baseline coincided with the Week 80 scan of the double-blind period. Scans were conducted at Week 128, relative to Baseline in the double-blind period. Change from Baseline (CfB) for tau PET was calculated from Baseline of both periods.

Results: Table 1 shows CfB in the whole cortical grey region during double-blind and OLE periods. Mean increases from double-blind Baseline were slightly higher in the bepranemab 45 mg/kg previous placebo group versus the ongoing group. Less pronounced changes were observed in the Jack temporal meta-region.

Table 1: CfB in indices of tau burden (WCGR)

	Bepranemab 45 mg/kg (previous placebo) n=63	**Bepranemab 45 mg/kg ongoing n=131**	**Bepranemab 90 mg/kg (previous placebo) n=64**	**Bepranemab 90 mg/kg ongoing n=129**
Double-blind period: CfB to Week 80				
n	51	107	51	115
Mean (SD)	0.0981 (0.1058)	0.0531 (0.0897)	0.0971 (0.1077)	0.0615 (0.0926)
OLE period: CfB to Week 128				
n	53	103	46	115
Mean (SD)	0.0223 (0.0936)	0.0246 (0.0779)	0.0221 (0.0713)	0.0371 (0.0972)

CfB, change from Baseline; OLE, open-label extension SD, standard deviation; WCGR, whole cortical grey region.

Conclusion: Bepranemab treatment effect on tau accumulation was consistent in double-blind and OLE periods; results suggest continuous treatment with bepranemab may slow tau accumulation.

Keywords: Tau imaging, Bepranemab, Alzheimer's disease, Open-label extension study

Cortical laminar and Aβ species-specific correspondence between antemortem Aβ-PET and postmortem pathology in aducanumab-treated Alzheimer's disease

Baayla Boon[1,2], Brian Burkett[3], Christina Moloney[3], Yoav Piura[4], Kelly Hinkle[1], Darren Rothberg[1], Ronald Petersen[5], Dennis Dickson[1,6], R Reichard[7], Aivi Nguyen[7], Jonathan Graff-Radford[5], David Knopman[5], Neill Graff-Radford[4], Val Lowe[3], Melissa Murray[1,6]

[1]*Department of Neuroscience, Mayo Clinic, Jacksonville, FL, US*
[2]*Department of Neurology, Alzheimer Center Amsterdam, Amsterdam UMC, Amsterdam, The Netherlands*
[3]*Department of Radiology, Mayo Clinic, Rochester, MN, US*
[4]*Department of Neurology, Mayo Clinic, Jacksonville, FL, US*
[5]*Department of Neurology, Mayo Clinic, Rochester, MN, US*
[6]*Department of Laboratory Medicine and Pathology, Mayo Clinic, Jacksonville, MN, US*
[7]*Department of Laboratory Medicine and Pathology, Mayo Clinic, Rochester, MN, US*

Background: We observed a mismatch between apparent "clearance" on amyloid-β (Aβ)-PET and residual pathology in a small autopsy series of aducanumab-treated Alzheimer's disease (AD) participants who underwent ante-mortem PET with florbetapir. In two participants, PET scans showed near complete clearance, yet tissue contained Aβ in deeper cortical layers. These findings raise the question whether PET signal reductions truly reflect uniform cortical clearance or are biased toward specific layers and Aβ species.

Methods: We analyzed ante-mortem Aβ-PET and postmortem pathology in five aducanumab-treated AD participants. Global Aβ PET burden was quantified from regional florbetapir SUVr values as Centiloids from the last scan prior to death. Quantitative pathology was obtained by multiplex immunofluorescence for Aβaa1-8, AβN3pE, Aβ40, and Aβ42 across cortical layers I and I-VI in middle frontal, fusiform, parahippocampal, and visual cortices. Robust regression tested associations between global Centiloid and global Aβ pathology. Regional correlations were performed between left-hemisphere SUVr or SUV and region-matched pathology. Two-compartment "depth kernels" (layer I vs layers I-VI) were derived to estimate laminar weighting of PET signal.

Results: Global Centiloid values strongly predicted Aβ42 pathology (β=0.023 ±0.006, t=3.86, residual SE=0.23). Longer PET-to-death intervals also modestly increased Aβ42 burden (β=0.067 ±0.026), consistent with ongoing accumulation. Regionally, florbetapir SUVr correlated most strongly with Aβ42 all-layer pathology in mid-frontal (ρ=0.9, p=0.08), fusiform (ρ=0.9, p=0.08), and parahippocampal cortex (ρ=0.8, p=0.13) and least in visual cortex (ρ=0.4, p=0.75). Depth-kernel modeling indicated that ~40% of PET signal derived from layer I and ~60% from deeper laminae, suggesting proportional laminar contributions without a superficial bias.

Conclusion: In this small autopsy cohort, Aβ-PET signal corresponded closely with both global and laminar Aβ42 but no other Aβ species. These findings demonstrate that PET reductions reflect cortical Aβ changes across depth, supporting Aβ-PET as a quantitative marker of total cortical Aβ42 burden rather than surface-confined pathology.

Keywords: florbetapir, neuropathology, amyloid-beta, immunofluorescence

In vivo and post-mortem evidence of downstream pathophysiologic effects of treatment-related amyloid clearance

Christopher Brown[1], John Robinson[2], Sandhitsu Das[1], Emily McGrew[1], Ilya Nasrallah[3], David Irwin[1], Paul Yushkevich[3], Edward Lee[2], David Wolk[1]

[1]*Department of Neurology, University of Pennsylvania, Philadelphia, PA, US*
[2]*Department of Pathology and Laboratory Medicine, University of Pennsylvania, Philadelphia, PA, US*
[3]*Department of Radiology, Philadelphia, PA, US*

We present *in vivo* and autopsy findings from an individual who received ~2.5 years of aducanumab therapy. At baseline, they had significant amyloid burden with diffuse cortical binding (Centiloid (CL)=139). They had three total episodes of asymptomatic ARIA-E involving portions of bilateral occipital lobes and left parietal lobe. They stopped treatment after 3 years (~2.5 years of amyloid targeting therapy (ATT) after accounting for pauses) due to a possible infusion reaction and remained Aβ+ on final PET (CL=33). They died five years after stopping treatment and autopsy results from the right hemisphere are presented (Figure 1). There was partial amyloid clearance with absence of amyloid in superficial cortical layers. In addition, several neocortical gyral crests exhibited near complete clearance of amyloid plaques, while sulcal depths showed greater residual amyloid. The right occipital region involved in the ARIA-E episode had near complete amyloid clearance. Of note, amyloid-cleared regions showed minimal tau pathology, including both dystrophic neurites or neurofibrillary tangles, as well as decreased astrocytic and microglial reactivity. Review of *in vivo* amyloid PET recapitulated this clearance pattern and MK6240 Tau-PET obtained 1 year after completing therapy mirrored the reduced tau burden in regions showing amyloid clearance (Figure 2). Regions with greater amyloid clearance showed minimal atrophy over 6 years, while those with residual amyloid showed a faster rate of atrophy compared to all baseline Aβ+ regions (Figure 3). Post-mortem MRI and additional MRI-histological investigation will be completed in the coming weeks to further explore the relationship between *in vivo* findings and histology. Together the findings in this patient suggest that amyloid clearance differs anatomically with preference for superficial layers and near complete amyloid clearance in a subset of neocortical gyri. Moreover, regions exhibiting amyloid clearance may be protected from downstream tau and neurodegeneration, even several years after treatment cessation.

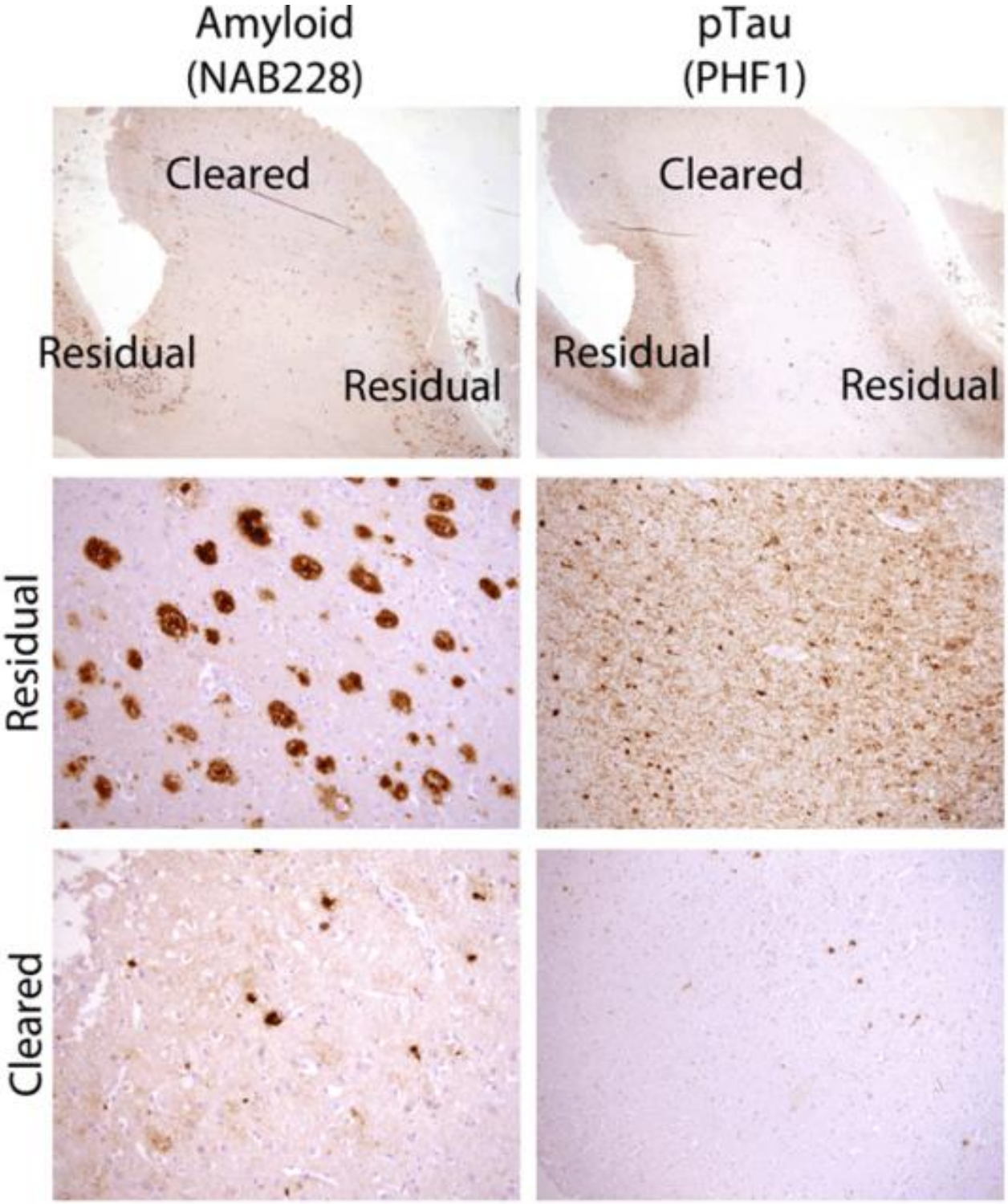


Figure 1. Autopsy Findings 8 years after starting ATT. NAB228 staining for amyloid plaques (left) and PHF1 staining for phosphorylated tau (right) shown at 10x (top) and 100x (middle and bottom) magnification. Top: Areas with near complete absence of amyloid plaques and phosphorylated tau (Cleared) and adjacent regions with residual amyloid plaques and tau deposition (Residual). Middle: Areas with residual plaques show dense neuritic tau and neurofibrillary tangles. Bottom: Cleared regions show minimal amyloid burden with some residual diffuse plaques and dense pericapillary staining. These regions show profound reduction in both neuritic tau and neurofibrillary tangles.

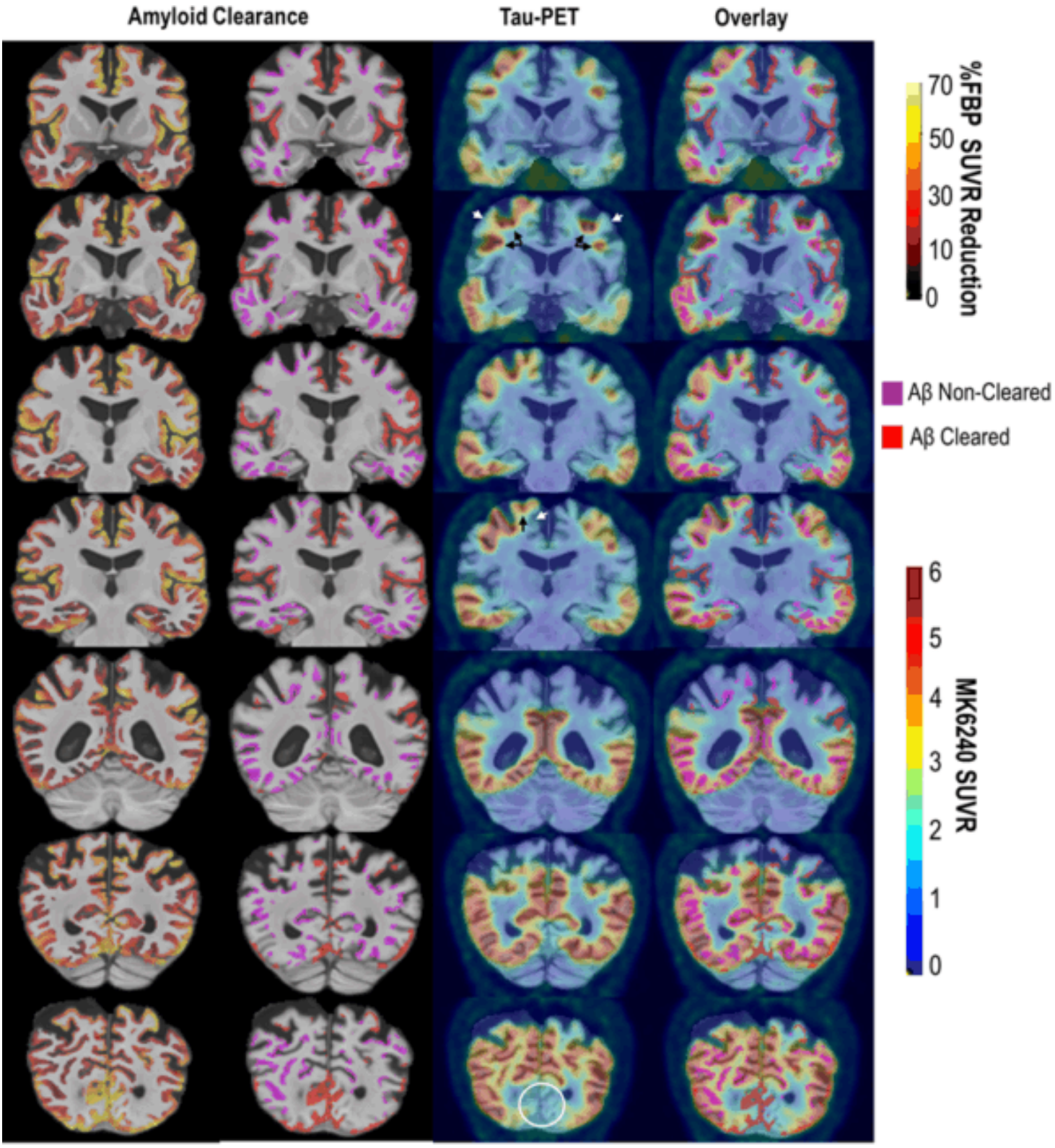


Figure 2. Left panels: Percent amyloid clearance in baseline Aβ+ regions (left) with top quartile of amyloid reduction (red) and lowest quartile of amyloid reduction (purple) after 3 years of amyloid targeting therapy (ATT) overlaid on T1 single-subject template brain. There is a pattern of greater clearance of gyral crests compared to sulcal depths and in superficial layers compared to deep layers. **Right panels:** MK6240 Tau-PET obtained 4 years after ATT start with patchy areas of absent tau burden (white arrows and circle) surrounded by adjacent regions with high burden (black arrows), closely corresponding to amyloid clearance patterns. Overlay of amyloid clearance masks on Tau PET (right).

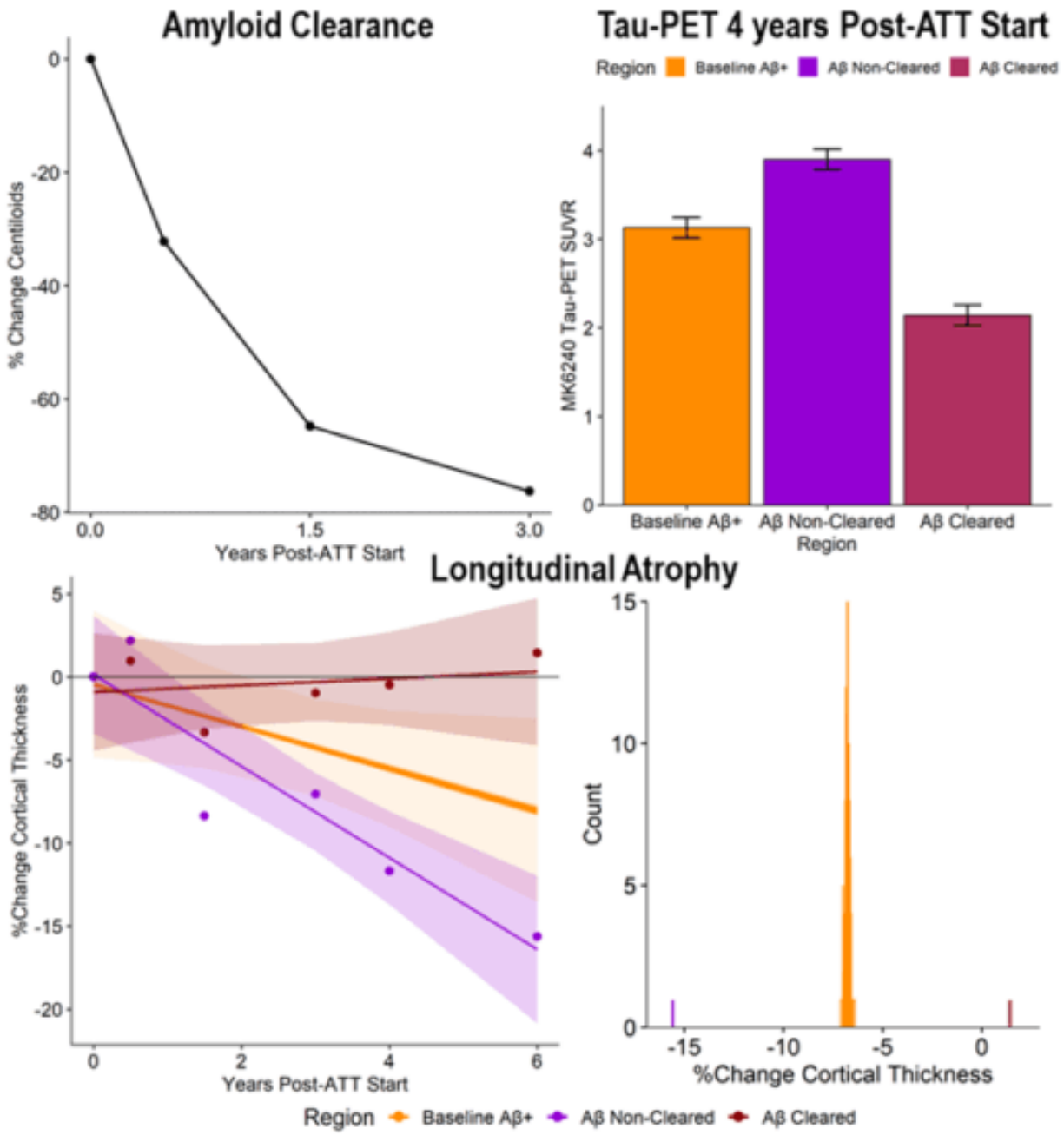


Figure 3. Top Left: Reduction in Centiloids with amyloid targeting therapy with modest reduction in early treatment and more robust clearance after 1.5-3 years, although remained positive at treatment conclusion (CL = 33.1). **Top Right:** MK6240 Tau-PET SUVR in all regions that were Aβ+ at baseline, in the lowest quartile of clearance (Aβ non-cleared), and in the highest quartile of clearance (Aβ cleared) obtained 4 years after ATT start with lower SUVR in cleared compared to non-cleared and all Aβ+ regions. Error bars ± 5 S.D. generated using 500 permutations randomly sampling 25% of voxels from the baseline Aβ+ mask. **Bottom:** Longitudinal %change in cortical thickness in all Aβ+ regions, low clearance, and high clearance regions showing minimal change in regions with high amyloid clearance and typical atrophy progression in regions with lower amyloid clearance. Data for all Aβ+ regions were generated using 500 permutations of randomly selecting 25% of all Aβ+ voxels at baseline with slopes from each permutation shown on bottom left and distribution of %change in cortical thickness at Year 6 shown on the bottom right

Keywords: amyloid targeting therapy, Tau-PET, Amyloid-PET, atrophy, neuropathology

HAI 2026 IS MADE POSSIBLE THROUGH GRANTS AND SPONSORSHIP FROM THE FOLLOWING ORGANIZATIONS:

DIAMOND ELITE

PALLADIUM

GOLD

SILVER/ SCHOLARSHIP

SILVER

BRONZE

ALZHEIMER'S® ASSOCIATION

LANTHEUS™

Lilly A MEDICINE COMPANY

Eisai

ENIGMA BIOMEDICAL GROUP

Biogen

Bristol Myers Squibb™

Johnson & Johnson

MERCK

RAINWATER Charitable Foundation

XingImaging Radiopharmaceutical Production and PET Acquisition

abbvie

ALAMAR BIOSCIENCES

GE HealthCare